

# A NEW ERA IN SPACE TRANSPORTATION

PROCEEDINGS OF THE XXVIIth INTERNATIONAL  
ASTRONAUTICAL CONGRESS, ANAHEIM, 10 - 16 OCTOBER 1976

*Edited by*

L. G. NAPOLITANO

*Istituto di Aerodinamica, Universita di Napoli, Naples*



PERGAMON PRESS

OXFORD · NEW YORK · TORONTO · SYDNEY · PARIS · FRANKFURT

U.K.	Pergamon Press Ltd., Headington Hill Hall, Oxford OX3 0BW, England
U.S.A.	Pergamon Press Inc., Maxwell House, Fairview Park, Elmsford, New York 10523, U.S.A.
CANADA	Pergamon of Canada Ltd., 75 The East Mall, Toronto, Ontario, Canada
AUSTRALIA	Pergamon Press (Aust.) Pty. Ltd., 19a Boundary Street, Rushcutters Bay, N.S.W. 2011, Australia
FRANCE	Pergamon Press SARL, 24 rue des Ecoles, 75240 Paris Cedex 05, France
WEST GERMANY	Pergamon Press GmbH, 6242 Kronberg-Taunus, Pferdstrasse 1, West Germany

---

Copyright © 1977 Pergamon Press Ltd.

*All Rights Reserved. No part of this publication may be reproduced, stored in a retrieval system or transmitted in any form or by any means: electronic, electrostatic, magnetic tape, mechanical, photocopying, recording or otherwise, without permission in writing from the publishers*

First edition 1977

**Library of Congress Cataloging in Publication Data**

International Astronautical Congress, 27th, Anaheim,

Calif., 1976.

A new era of space transportation.

1. Astronautics--Congresses. 2. Space vehicles--  
Congresses. 1. Napolitano, Luigi G. II. Title.  
TL787.1443 1976 629.4 77-2886  
ISBN 0-08-021710-9

*In order to make this volume available as economically and rapidly as possible the authors' typescripts have been reproduced in their original form. This method unfortunately has its typographical limitations but it is hoped that they in no way distract the reader.*

*Printed in Great Britain by William Clowes & Sons, Limited  
London, Beccles and Colchester*

## PREFACE

This book offers a selection of papers presented at the 27th International Astronautical Congress, held in Anaheim in October 1976, and together with a special issue of *Acta Astronautica* constitutes the Proceedings of that Meeting.

The book continues a series started in 1970, its title reflecting the Congress's main theme and, as always, is aimed at presenting a factual cross section of Astronautical Research in the world and indicating the trends of such researches.

It is not surprising, therefore, that the Spacelab and the Shuttle permeate these proceedings throughout its four parts and the reader should appreciate both the depth of coverage and the variety of different perspectives from which the problems are seen.

Similarly, to properly reflect a well-established trend, books in this series give progressively greater relevance to applications.

Progresses in Space Sciences and Technology lead to an increasing number of applications directly addressed to the solution of man's problems on earth, to improve the dynamics of man's interactions with his environment, to help him in his struggle against calamities, to alleviate or overcome disadvantages and restrictions deriving from non-uniform distribution and/or availability of earth resources. A significant panoramic view is offered by this book.

The book is divided into four parts.

The first part, devoted to the theme sessions, contains the 7th IAF invited lecture and gives a comprehensive look at the USA and ESA future programs related to the new era of space transportation.

The second part contains papers falling in the classical areas of Engineering and Life Sciences which have always had the IAF Congresses as their preferred international forum: Astrodynamics, Bioastronautics, Fluid Dynamics, Materials and Structures, Propulsion. Fluid Dynamics of Planetary Atmospheres and Laser Uses in Propulsion exemplify the spirit with which such classical areas have been addressed.

The third part is devoted to Space Technology and Space Systems. Besides the already mentioned papers related to Spacelab and the Transportation System, noteworthy attention is being given to balloon platforms.

The last part is devoted to applications, telecommunication (a by-now classical application), remote sensing of earth resources (a second runner), material processing in space (the latest addition to the family).

In closing I would like to thank the authors for their valuable contributions, the Session Chairmen for their most effective help in making the selection and Pergamon Press for their cooperation in making the book come out almost in record time.

L.G. NAPOLITANO

# A NEW ERA OF SPACE TRANSPORTATION

James C. Fletcher

*Administrator, National Aeronautics and Space Administration*

Good morning and welcome to all of you. I am delighted to be here and to be able to greet colleagues from so many nations.

Since the Space Age began many of us have succumbed to a use that sounds like hyperbole. Not only our own public affairs writers but also the independent press is given to words such as "awesome" and "incredible" to describe a new success in space endeavor. But I am obliged to say that the very theme and title of this Congress places us, in the context of time and progress, at a startling phase of human experience. Fifteen years ago, the theme would have been something like "The New Era of Space Exploration". Today, it is space transportation. In less than two decades, an inevitably short period of time, we have closed the book of science fiction and have reached a point of pragmatically assessing the uses of outer space as a benefit to all peoples of the world. We are about to enter an era, founded on the experiences of Apollo, Skylab, and the Apollo/Soyuz mission, which will be characterized in many instances by a displacement of the interface between the experimenter and his experiment from the control center on the ground to the laboratory in orbit—and this laboratory will be accessible to everyone.

A lingering few still ask space officials in many countries, "Why go into space?" We are far beyond the classic retort of the mountain climber, "Because it is there."

The answer is that we have entered a new world. The visionary Galileo could peer at places with his telescope and dream of man's ascent to other bodies in our solar system. We have already been there. And in reaching out to other worlds, we have discovered ways to enrich our own.

Utilizing space technology, we are expanding the precious gift of knowledge and are realizing economic applications unthought of in the span of a young man's life today. We have achieved enormous efficiency in world communications at a much lower cost. We have a better understanding and control of the environment and resources of the planet Earth. We have discovered and will exploit new energy sources, at a critical time in the technical acceleration of the world. We have expanded an understanding of life and science in the Universe.

But for all these achievements, you are well aware that we are all under severe economic constraints. The world economy is under similar pressures. To continue and enhance space exploration and usage, we must lower the cost of our programs through better management of limited resources and through concentrated international cooperation. I believe that a primary tool for this purpose is the Space Transportation System using the Space Shuttle. I am sure that most of you have seen pictures

or read articles about this spacecraft that resembles an aircraft. The Shuttle will be a low-cost, reliable and reusable launch system and you will hear a good deal about it in the course of this Congress. The first model of the Space Shuttle was rolled out in California just last month and will be test-flying, with follow-up vehicles, through the rest of the 1970s. I hope that many of you will take advantage of the field trip to Palmdale and the Rockwell International plant to see Orbiter 1 on October 13.

In 1980 the Shuttle will become fully operational and all through the next decade Shuttles will be placed into orbit. The scientists and technicians aboard will perform countless experiments, from studies of the Sun to the examination of Earth resources. At the conclusion of each mission, lasting from 7 days to as long as 30 days, the spacecraft makes its reentry and lands very much like a conventional airliner. This program is truly the début of genuine space transportation. Never before in the history of space flight has man had an opportunity like this: He can interact with his experiment while he is flying with it in space and later refly it on a subsequent shuttle flight after perfecting it.

I want to emphasize that the Shuttle is the work of many nations, and will provide opportunities for space participation for all the nations of the world. We have to remember that space technology has made the world smaller and all that we derive from it can be used to better the world.

The Shuttle system is an international enterprise. The initial payload will be the Spacelab, being developed by the European Space Agency at a cost roughly approaching 500 million of our dollars. Along with ESA's contribution, there is the Canadian development of an essential Remote Manipulator System for the Shuttle and there are additional joint efforts for new programs such as flight of a space telescope; other countries will submit their innovations and ideas. We have already received flight requests from twelve countries to conduct fifty-eight experiments and they are under review. Like music space has no boundaries.

The Shuttle will mean a new frequency of and access to space flights at low, fixed cost for all users. It will engender new capabilities in applications, material processing and science for near Earth orbit payloads and with manned missions using Spacelab as a focal point. Although the crews—the pilot-astronauts and mission specialists—will have to meet rigid physical and mental standards, the passengers can qualify with normal good health. That means that after a short training period, a variety of experts—astronomers, geologists and environmentalists—will make up the passenger manifest.

There may be men with gray beards, women, experts speaking in a wide variety of accents—a cross-section of nations—working in the unique ambience of space.

Some of you scientists listening here today will, I'm sure, experience the thrill of space flight.

The spacecraft, with its retractable claw, will not only deploy but also retrieve satellites. And the constant trips into orbit as man finds congenial his presence in space, will naturally facilitate the creation of structures stationed between Earth and Sun, manned orbiting satellites, and the eventual colonization of space.

As an overriding purpose, the Shuttle project will give us more sophisticated and more advanced space science to build upon the rapidly growing fund of knowledge about our universe. This will add to the things we have learned from unmanned deep space exploration, such as the Viking missions to Mars.

Consider what we have learned so far from our sister planet:

1. The approximately 4000 images from the orbiter have revealed details of extensive effects of tectonic activity and weathering.
2. Images and thermal data indicate that the North polar cap is water ice. Estimates based on these observations are that, on a proportional basis, there may be as much water on Mars as on Earth.
3. Results from the biology experiments, if obtained on Earth samples, would indicate the presence of living organisms. However, these results are not readily interpretable because of a highly active surface chemistry which is not fully understood at this time.
4. No organic compounds have been detected by the GCMS, but these data are confounded by the release of large volumes of water, presumed to come from hydrated salts, on heating the soil samples.
5. The ratio  $^{36}\text{Ar}/^{40}\text{Ar}$  suggests that the atmosphere may have been 10 or more times as dense as at present. Ten or more times the present density would have permitted the existence of large volumes of flowing water evidenced by channels and eroded features not unlike portions of the Western United States.

Thus a wealth of information is being gleaned about the course Earth might be taking and what might be done to preserve humankind.

But above all in these findings, invaluable to the scientific world, lies the ultimate value of such exploration—its impact on how people view themselves and the Universe around them. James Michener put it in these words: "...when you move out to a planet which is a creation comparable to our own and which has similar propensities and possibilities, then you are moving into a whole new orbit of speculation. The realization that in these very days, we are getting information from the threshold of our particular galaxy, and information which we can then apply to the billionth galaxy in farthest space, is to me an overwhelming experience...."

Space transportation offers more spectacular opportunities than man has ever experienced.

We are just beginning to realize the full potential of the Space Shuttle and I would like to in-

vite each and every one of you to help us reach out and grasp the near boundless potential of space. Many opportunities were developed and explained in an extensive NASA study call *Outlook for Space*, published just this year. To survey the principal themes in that study will demonstrate the prospect of space dramatically. They show that as we lower costs and heighten opportunities for access to space, combining our efforts through international accord, we will be able to pursue countless objectives.

Today, conventional launch services are not altogether satisfactory, in good part because costs have not been held to estimates and in fact have escalated steadily. In the Shuttle era we will make significant changes. Launch contracts will be for a firm, fixed price, set at the time of contracting, and the launch will be guaranteed. Should a launch failure occur, another launch will be provided without charge and NASA is prepared today to engage in fixed price contract negotiations for Shuttle launches in the 1980-81 time frame at the general price levels we have indicated to potential users.

Because we are still bound to Earth, *Outlook for Space* concentrates on the activities that are responsive to basic human needs. The most basic human need is food. And the study highlights the production and management of food and forestry resources. Consider, if you will, the progress already being made in that area. NASA has in operation two earth resources satellites called Landsats. They are in alternating synchronous orbit, about 500 nautical miles high. Each Landsat makes a complete orbit of the Earth every 103 minutes and each completes fourteen orbits each day. Each satellite, therefore, is able to scan the entire Earth every 18 days.

Crop management by satellites will tell the farmer much that he could never learn from just walking across his fields. Landsat information can tell him how his crops compare with those in other parts of his nation, his state, or even the world. Thus, for instance, he will be able to make better decisions on how to harvest his crops—whether to harvest for grain, for silage, or for pasturing.

By satellite, we are informed of our environment and can take steps toward the analysis and protection of it. Even deep space exploration renders aid, as in the case of Viking. Dust storms on Mars supply information on the future effects of smoke and especially pollution in our own atmosphere. And a study of Martian storms, where the weather-making mechanism is relatively simple because of the lack of oceans, can contribute heavily to an understanding of Earth's weather, thus to weather prediction and possibly to future weather control. Thereby, the space program can be a major factor in the protection of life and property.

In the area of communications, it is a nightly occurrence to hear a television news report say, "This story is via satellite." Today, it is as familiar as hearing your home telephone ring. But communications via satellite is only 10 years old. World telecommunications, for what it accomplishes, is one of the most inexpensive commodities in our society. And surpassing all others, this is an international accomplishment. Most of the nineteen launches from the Kennedy Space Center this year carry communications payloads. A number of them are not American. For example, Indonesia, a nation with little industry, yet with the world's fourth largest

population, joined the exclusive club of domestic communications satellite owners last July.

We are actively employing space technology for science and commerce in countless ways: from heart pacemakers to miniaturized calculators, digital watches, video tape storage and retrieval systems—all were direct products of space programs.

In a scant 15 years, the world has developed a deeper understanding of the composition and dynamics of this tiny globe that we inhabit. We do not know if we are alone as living beings in this galaxy, but both science and the humanities have been given invaluable gifts in the search for an answer to that puzzle. Above all, it has allied us as peoples of this planet who stand on the threshold of a new world.

Consider, also, the extraterrestrial activities and studies which are responsive to the human intellect and the need to study and understand:

the nature of the universe,  
the origins and fate of matter,  
the life cycle of the Sun and stars,  
the evolution of the solar system,  
the origins and future of life.

Our space achievements, as I have pointed out, have occurred over a very short time span. The Industrial Revolution lasted much longer, as did the period of remarkable political revolution that preceded it. It has been just 50 years since Dr. Robert Goddard, an unknown physics professor, launched his tiny liquid propellant rocket for a flight of a few seconds on a remote farm in New England. But rocketry

lay fallow for a long time afterwards, and then accelerated in the last few decades.

It is obvious that nations will have to pool their resources, their talents and their labors in the undertaking of space because no single country could mount the kind of expensive and massive program we envision for the future. We have taken some major first steps or we would not be gathered here. Every passing day sees the cohesion and cooperation of national aspiration in the greatest adventure of mankind. The prospects for the world's future are both stimulating and wondrous—but they are within our reach if we make the effort.

The spirit that formed the International Astronautical Federation, which underlies the body and relevant laws of the United Nations, which is manifest in Intelsat, the Apollo-Soyuz mission, Space-lab and many other instances of cooperation in space, is real and productive—we are all in pursuit, for the generations to come, of mutual objectives.

I can assure you that we here in the United States are doing what we can to reduce costs while increasing reliability. The primary instrument is the Space Transportation System. I recommend that in planning future conferences, congresses and colloquia, you solicit, develop and report upon ways and means of insuring easy access to space and simpler ways to benefit from this easy access, not that lower costs of space uses and space systems are ends in themselves but that unique and demanding opportunities will arise as a result of the availability of such systems. Let us go forward to pursue those opportunities together, developed and less-developed countries alike, in the New Era of Space Transportation.

# A NEW ERA OF SPACE TRANSPORTATION-FUTURE PROGRAMS

John F. Yardley

*Associate Administrator, Office of Space Flight, National Aeronautics and Space Administration  
Washington, D.C.*

## Abstract

The current status of and future plans for manned space flight activities in the United States of America is summarized. The Space Transportation System (STS), (Space Shuttle, Spacelab and Upper Stages) is described from both a systems and operations viewpoint. Future plans leading to permanent occupancy of space, are highlighted, including concepts for a Space Construction Base, Advanced Transportation Systems and Space Industrialization initiatives.

## I. Introduction

Whenever improved transportation has been implemented - wheeled vehicles, ocean going ships, motorized conveyances, or aircraft - the standard of living all over the world has risen sharply. The United States has a long history of transportation devices and is still ardently pursuing improvements in all areas - and one more in addition. That one is economical space transportation. Transportation to and from space so that exploration, scientific experimentation, commercial processing, and a large variety of beneficial satellite and manned laboratory investigations can continue and expand. All this for a cost considerably lower than using today's expendable boosters. The United States is developing the means of getting to and from low earth orbit and a spaceborne upper stage to achieve high energy orbits when necessary. An important part of this transportation system is being developed in Europe. The European efforts which are centered around the manned laboratory - Spacelab are addressed in some detail in other papers at this conference.

Activities we are now performing in space and the knowledge we have gained about the earth from spacecraft missions have provided us with benefits of immense value. The Space Transportation System (STS) (Figure 1) is being developed to lower the cost of space operations and provide the flexibility required for present and future payloads. This chart shows the three basic building blocks for this future space system: the Space Shuttle, Spacelab and the Upper Stage.

## II. The Space Shuttle

The Space Shuttle (Figure 2) is the principal element of the STS. It will carry out regular round trips from earth to space during the coming decades. Designed to lower the cost of transporting a variety of spacecraft to and from earth

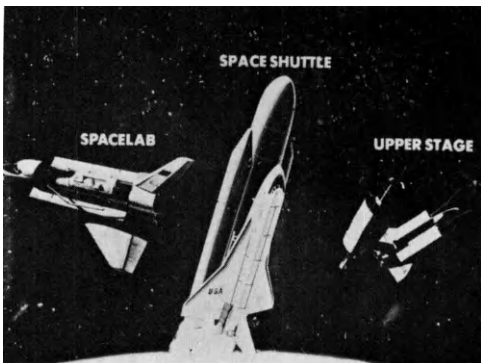


Figure 1. Space Transportation System (STS)

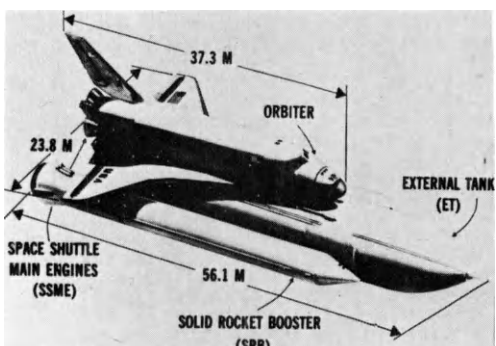


Figure 2. Space Shuttle

orbit, the Shuttle will allow a variety of experiments, investigations, and space applications to be accomplished. The Shuttle will be versatile, dependable, and reusable. It will lower launch costs and will lower the cost of future space payloads. During the 1980's sixty flights per year are forecast to satisfy the various government, academic, industrial, and international sponsors who wish to take advantage of these Shuttle capabilities. In addition to performing currently planned space tasks, the Shuttle will be used for new and as yet unknown space missions.

The basic mission of the Space Shuttle will be the placement of satellites in earth orbit (Figure 3). Up to 29,500 kilograms (65,000 pounds) of payloads can be carried to low earth orbit. A flight might be used for only one specific spacecraft or for a number of satellites where volume and weight permit. Such multiple cargo missions will provide each user with a cost sharing advantage. For a placement mission the satellite or satellites can be serviced, checked out, and deployed from the payload bay into the desired orbit. The cabin of the orbiter will serve as both a working and living area in which the crew will function in a shirtsleeve atmosphere. In addition to the Commander, Pilot and Mission Specialist, up to four payload specialists can also be carried.

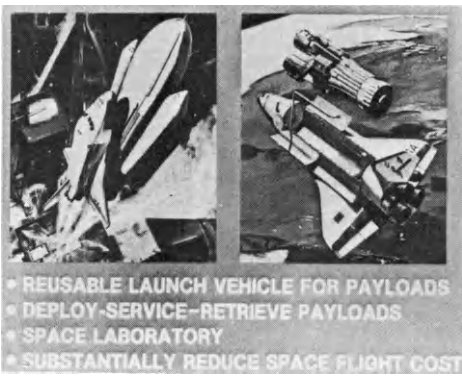


Figure 3. Space Shuttle Missions

On some placement missions, a spacecraft launched on a previous mission will be retrieved and returned to earth for refurbishment and reuse. It may also be launched empty to rendezvous with and recover a previously placed satellite. Or the Shuttle may be used to service, update, or repair an orbiting satellite. The recovery and servicing capabilities provided by the Shuttle are new and unique features which will substantially reduce satellite design and production costs.

Mission durations are nominally about seven days or less but missions up to 30 days can also be accommodated with the orbiter. For these missions many extra features can be provided for the payloads. They include electrical energy sources, thermal controls to maintain desired temperatures, a stabilized platform capability, communication links, contamination control, structural attachments, and add-on kits for extended duration missions.

#### Space Shuttle Orbiter

A month ago this country rolled out the first reusable spaceship - Orbiter 101 (Figure 4). The President has named this new spacecraft ENTERPRISE. This picture shows this first orbiter at the

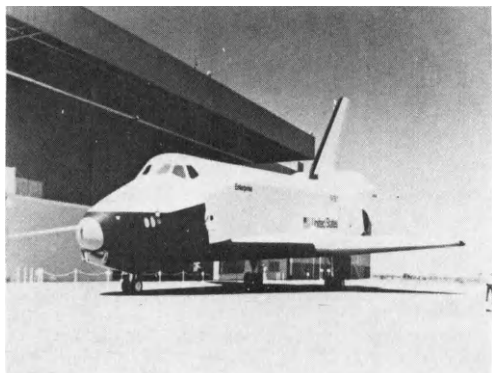


Figure 4. Space Shuttle Orbiter 101

Rockwell assembly plant in Palmdale, California. This vehicle will have additional equipment installed, be checked out and used in the approach and landing tests next year in 1977 at the Dryden Flight Research Center. The second orbiter, number 102, is now being fabricated. It will be used in the first manned orbital flight in 1979.

#### Space Shuttle Main Engines

The Space Shuttle Orbiter utilizes a cluster of three high chamber pressure hydrogen/oxygen engines, each with a 2100 kilonewtons (470,000 pounds) vacuum thrust level. This engine (Figure 5) is based on maximum utilization of existing technologies. However, it represents a major advancement in propulsion since it will include several advances in the state-of-the-art, such as long life and the ability to throttle the thrust level over a wide range. It is the first large liquid fuel rocket engine designed to be reusable and to require minimum maintenance between flights. The main engine will be computer controlled to insure performance at high temperatures and pressures without exceeding the allowable limits. Performance has been increased by using a two stage power cycle with a high expansion ratio nozzle. Three development engines have already been delivered to our National Space Technology Laboratories for propulsion testing. We have completed over 100 tests on these engines and achieved 95% of rated power.

#### Space Shuttle External Tank

The external tank (Figure 6) contains the liquid propellants for the Space Shuttle main engines. Liquid hydrogen is the fuel and liquid oxygen is the oxidizing agent. At lift-off it will contain about 700,000 kilograms (1.56 million pounds) of propellant. The external tank is the only major part of the Space Transportation System that is expendable and therefore, special efforts are being made to achieve low unit cost production.

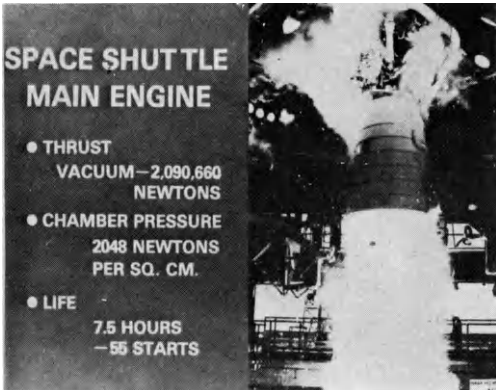
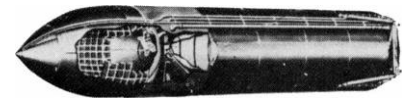


Figure 5. Space Shuttle Main Engine

At our Michoud Assembly Facility all major tank and assembly tools have been installed and assembly of ground test hardware has begun. Fabrication and assembly has also been initiated on the development tanks which will be used for propulsion tests at the National Space Technology Laboratories next year.



LENGTH (m)	47.2
DIAMETER (m)	8.4
CONTROL WEIGHT (kg)	34.0 K
PROPELLANTS (kg)	709 K
LIQUID O <sub>2</sub> (kg)	607 K
LIQUID H <sub>2</sub>	102 K

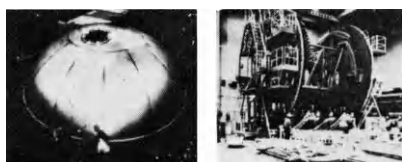


Figure 6. Space Shuttle External Tank

#### Space Shuttle Solid Rocket Booster

Along with the orbiter main propulsion system, two solid rocket boosters (Figure 7) provide the thrust required for lift-off. They are attached to the external tank. During parallel burn with the main engines each one will provide almost 12 million newtons (2.7 million pounds) of thrust at sea level. Each booster, which is 3.7 meters (146 inches) in diameter and 45.5 meters (149 ft.) in length, is detached from the external tank after use and is dropped by parachute into the ocean for recovery, refurbishment, and reuse.

Subcontractors have initiated manufacture, heat treatment, and machining of development motor case segments. Two full scale prototype motor nozzle flex bearings have been manufactured

and testing is proceeding. Booster subsystems development is progressing very well, i.e., parachutes, forward and aft skirts, nose cap assembly, and the thrust vector control subsystems are on schedule.

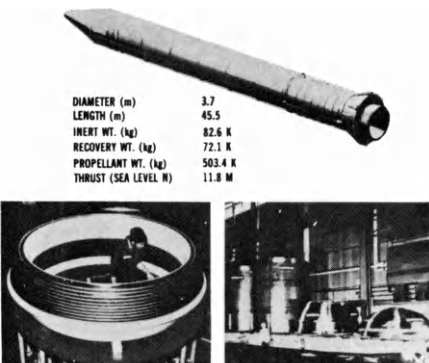


Figure 7. Space Shuttle Solid Rocket Booster

#### III. Spacelab

Spacelab and the status of its development in Europe is addressed in other papers at this conference. However, I would like to say that Spacelab is a fundamental part of the STS. It will complement the Shuttle by allowing scientists and technicians to perform experiments in a laboratory like environment on orbit, very much like the Skylab missions. The difference will be that Spacelab is reusable, can be flown in many different configurations and thereby will be less expensive to operate and will permit the conduct of a wide variety of experiments which can evolve from mission to mission.

As the hardware I have shown indicates, the program is well on its way toward meeting its objective to produce an operational Space Shuttle by 1980 - a system which will provide routine, lower cost space transportation.

#### IV. Upper Stages

The Upper Stages are essential elements of the Space Transportation System (STS). These stages deploy the payloads into the higher energy orbits not attainable by the Shuttle alone. Two upper stages are presently envisioned: The Interim Upper Stage (IUS) and the Spinning Solid Upper Stage (SSUS).

#### Interim Upper Stage

The Interim Upper Stage (Figure 8) under development by the DOD, will be a solid propellant, three axis stabilized expendable vehicle system designed to place up to 2,270 kilograms (5,000 pounds) into geosynchronous orbit. The IUS is

primarily a two-stage system for the earth orbital delivery mission. Three and four stage IUS configurations are planned for NASA's deep space missions. The IUS is being designed to accommodate those payloads projected by NASA, DOD and others to occur during the early Shuttle operational era.

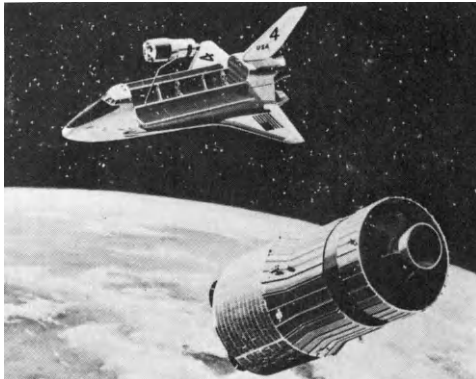


Figure 8. Interim Upper Stage (IUS)

#### Spinning Solid Upper Stage

The Spinning Solid Upper Stage (Figure 9) is an important element of the STS to assure the least possible delivery cost for all users of space. Its primary purpose is to put relatively small payloads (500 to 1200 kilograms) into geosynchronous orbit. The Spinning Solid Upper Stage system consists of a solid rocket stage used as the perigee kick motor; the airborne support equipment (ASE) and the ground support equipment (GSE). The ASE, which includes a cradle and spin table and deployment device, will be reusable from flight to flight. A costly navigation-guidance system is not required since the orbiter will provide a pre-determined position and attitude for accurate placement of SSUS/spaceship into the geosynchronous transfer orbit. The spacecraft apogee kick motor (AKM) will then be employed for the final insertion maneuver into the desired geosynchronous position. The low cost, simple SSUS will offer flight operations and vehicle integration/interfaces that are comparable to those experienced today by expendable launch vehicles spacecraft.

Tentative agreement with COMSAT and Ford-Aeronautronics for Intelsat V launches has been made that include SSUS performance, operating procedures, and schedules. A flight to demonstrate the SSUS system is planned for late 1979. Two SSUS sizes are planned: one to accommodate the Atlas-Centaur class spacecraft (e.g., Intelsat V) and one to accommodate the Delta class spacecraft.

Both upper stages discussed will provide a large enhancement of our space operations capability when employed with the Space Shuttle in 1980.



Figure 9. Spinning Solid Upper Stage (SSUS)

#### V. Space Transportation System Operations

As the development activities of the Space Transportation System continue to progress, we have directed an increasing proportion of our efforts towards planning and establishing the operational organization policies and procedures to be utilized with the STS System. This includes such activities as user development, mission planning, launch operations, flight operations, payload integration, and the development of financial plans including user charge policies.

The basis for operational planning in the decade of the '80's is the STS Traffic Model which is shown in Figure 10. Efforts are constantly under way to determine the latest STS utilization plans with particular emphasis on operations during the early years.

Requirements for, and definition of multi-use mission support equipment have been initiated. This is a class of ground and flight hardware providing interfaces between payloads and elements of the Space Transportation System (STS) which can be furnished more economically from a standard equipment inventory rather than by individual payload users.

Flight operations planning is well under way as are crew training and simulation planning and development of data processing requirements. The present complement of 20 pilots and 9 scientist astronauts will be insufficient to fly the planned 60 flights per year flight schedule even though it is anticipated each pilot would fly up to 6 flights per year and each Mission Specialist would fly 1-3 missions per year depending upon the complexity of the mission. Therefore, NASA has recently announced opportunities for additional pilots and mission specialists; actual selection and appointment into NASA will not be made until 1978. Guidelines are also being developed for selection and training of payload specialists.

Operational cost data have now been developed,

and baselines have been established to support the anticipated traffic as projected by the NASA STS traffic model.

During the past months a number of studies were undertaken to determine the STS operating costs and to establish user charges for STS flights. Each class of user will pay a fair share for use of the Shuttle based on the amount of capability used and an equal price for equal services provided to users.

For the normal Shuttle user, the policy provides a competitive price (compared to expendable launch vehicles) as well as a firm fixed price to the user in the early years of Shuttle operations. The fixed price, which will be adjusted for the years after 1984, allows the user to plan his payload transition to the Shuttle with assurance that there will be no subsequent cost incurrence.

Non-standard services will carry specific additional charges, some of which may be negotiated on a case by case basis. Non-standard services include such things as additional stay time on orbit, special mission or flight planning, accelerated priority or short notice launch services, cancellation of a scheduled launch by the user and other factors that are expected to arise as users enter the system.

In addition to the standard and optional services, the STS user charge policy contains features that are only achievable with a reusable launch system like the Space Shuttle. Because the system is manned and is capable of a safe flight abort, a guaranteed single reflight can be provided at a relatively insignificant additional cost to the user if the Shuttle fails to deliver the user's payload to the contracted Shuttle orbit. Additional optional guarantees may be provided for upper stages.

Due to the large Shuttle cargo bay (18 meters long by 5 meters dia.), there will be flights which may not use its full capacity in either volume or weight. This will make it possible to fly small payloads on a "space available" basis. If these small payloads are self-contained, i.e., they do not require Shuttle services other than transportation to orbit, then a very special price can be offered to the user. This low price will tend to encourage universities, research institutes and other developers of small experiments to utilize space for advanced research and applications projects while the cost to NASA for carrying their small payloads is very low.

In summary, the policies for the three classes of user charges recovers all NASA out-of-pocket costs for user flights during the initial phase (through FY 1983) of STS Operations. They provide for recovery of total operations costs for all users missions over the twelve year span of operations. The policy should provide incentives to users for early transition from expendable launch vehicles to the Space Shuttle and this early transition provides significant savings in

space transportation.

#### NATIONAL STS TRAFFIC MODEL SINGLE PAD AT WTR (USERS)

PLAN A		FY 80 81 82 83 84 85 86 87 88 89 90 91 92 TOTAL											
ETR													
NASA	1	8	13	15	25	21	26	22	23	23	24	8	225
US GOVT	-	1	-	-	-	-	-	-	-	-	-	4	8
US COML	-	2	1	3	5	6	8	3	9	7	8	4	1
FOREIGN	1	1	-	5	3	4	4	5	5	8	7	8	2
ODO	1	1	7	5	6	8	7	6	8	5	7	8	71
SUBTOTAL	3	13	21	28	34	43	38	40	45	42	48	43	11407
ABORTS	-	1	2	3	3	1	4	2	1	3	1	3	24
TOTAL ETR	3	14	23	31	37	44	42	42	48	45	47	46	11431
WTR													
NASA	2	3	5	4	5	5	4	8	8	2	42		
US GOVT	1	1	2	3	2	4	2	4	2	1	1	22	
US COML	-	1	-	1	-	2	-	1	1	-	5		
FOREIGN	1	1	1	2	3	2	2	1	1	1	1	14	
ODO	1	5	8	5	3	6	5	3	4	1	1	38	
SUBTOTAL	5	11	13	16	13	19	13	15	14	4	122		
ABORTS	-	1	1	1	1	-	1	1	1	-	7		
TOTAL WTR	5	12	14	16	14	19	14	16	15	4	129		
TOTAL SHUTTLE OPS	3	14	23	36	49	58	58	56	65	59	63	61	15560

Figure 10. Space Transportation System (STS) Traffic Model

#### VI. Future Planning

I would like to address some of the future planning activities now being pursued by NASA.

Our primary long term objectives for the future are centered about the achievement of permanent occupancy and limited self-sufficiency in space. The next major stepping stone in the accomplishment of permanent occupancy in space is the Space Station. The main objective of this effort is to provide long duration occupancy of near earth space and to extend manned capabilities achieved by the STS to higher altitudes including geosynchronous orbits.

Our future planning activities include studies of Space Stations. I envision such a system as a relatively large, modular, manned base in low or synchronous orbit which would be used to perform a wide variety of public service, commercial, and scientific functions. Such a permanent station would provide the opportunity to establish bases where fabrication, erection and deployment of large structures for a great number of new missions could take place. Also, many missions such as space manufacturing, the processing of pharmaceuticals and the formation of unique materials such as precision glasses and high performance metals can be achieved using such a permanent station.

In addition, advanced transportation systems are being studied, both to improve the Space Shuttle and complement it.

#### Space Construction Base

NASA has conducted studies of Earth Orbiting Space Station concepts for several years. These early studies emphasized a theme of "laboratory in orbit", wherein a collection of experiments or applications were brought together within a Space Station with man operating to conduct experiments,

perform maintenance, reconfigure equipment, and manage all activity.

While this space laboratory theme continues to be important, recent studies have made it clear that it is now timely to expand this theme and place primary emphasis on a "Space Construction Base" concept. I see an orbiting Space Construction Base being utilized in the following typical ways: (a) as a central work station for the fabrication, assembly, and testing of large structures, (b) as an orbiting depot for launch, retrieval, maintenance, and refueling of propulsive vehicles, (c) as an operations center for conducting retrieval, maintenance, upgrading, and redeployment of earth-orbiting spacecraft, and (d) as a central base for the conduct of research, industrial, and public service functions.

These typical uses of a Space Construction Base will require, in varying degrees, the capability to fabricate large structural systems on orbit. This on-orbit fabrication capability is seen as being required for solar power collection and transmission, large scale communications systems, and for earth resources, environmental and climate observations. At present, we see no basic limitation to the size of structures that can be erected in space. Concepts of space construction are shown in Figure 11 where the Shuttle orbiter is serving as the base for the fabrication of a relatively small antenna and in Figure 12 where construction of a space solar power satellite is being performed from a Space Construction Base. Systems utilizing very large antennas can greatly extend the present capabilities of communications and navigation schemes. If, for example, a large multi-beam antenna of several hundred meters diameter were placed in orbit along with the required power generating equipment and other sub-systems, then the ground equipment could be greatly simplified. A ground receiver of the "wrist watch size" is entirely feasible with the resultant opportunity for great proliferation of ground stations working with a small number of satellites.

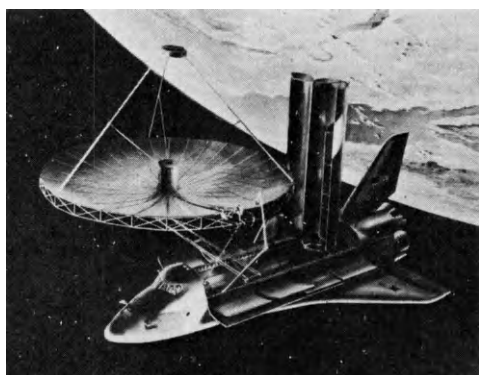


Figure 11. Fabrication in Space - Shuttle Supported



Figure 12. Fabrication in Space - Space Construction Base Supported

Similar systems for global low-cost navigation, electronic mail, diplomatic hot-lines, world-wide TV broadcast, holographic teleconferencing, intrusion detection, anti-collision radar and other new concepts are practical.

The Space Construction Base is being planned to permit growth from an initial concept shown here (Figure 13) where the base is shown being serviced by the Shuttle Orbiter to much larger, more complex systems (Figure 14) required to more fully realize the benefits of space.

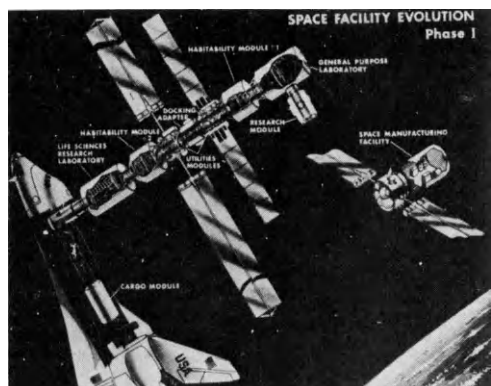


Figure 13. Space Construction Base - Initial Concept

#### Advanced Transportation Concepts

In parallel with Space Construction Base studies we are investigating advanced transportation concepts. These concepts include continuing efforts to reduce the cost of Shuttle operations and increase the flexibility and effectiveness of the system. Beyond the Shuttle, there are needs for extending manned operations to geosynchronous

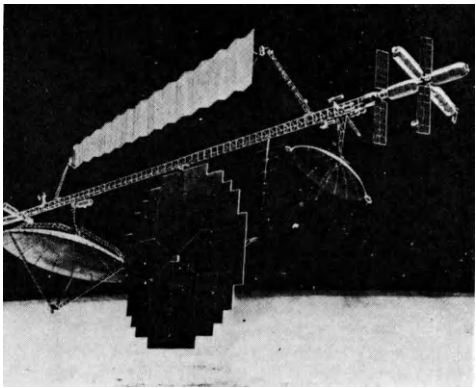


Figure 14. Space Construction Base - Growth Concept

orbits and beyond and to provide lower cost cargo transportation to both low and high orbits.

Currently, the Interim Upper Stage provides the capability to deploy automated payloads to high orbits. Studies have been made of a reusable Space Tug which could not only deploy payloads but ultimately retrieve satellites thus providing additional system capabilities and cost savings.

We are also studying a Manned Orbital Transfer Vehicle (Figure 15) which could perform the functions of the Space Tug and would extend man's utility from low altitude Shuttle mission orbits to geosynchronous altitude. The MOTV is required for many of the complex activities involving construction and maintenance at high altitude.

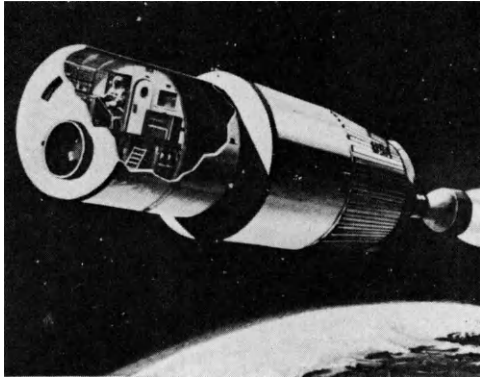


Figure 15. Manned Orbital Transfer Vehicle (MOTV) Concept

Further, for cargo transport to high orbits we are looking at concepts of a Solar Electric Propulsion Stage (SEPS)(Figure 16). SEPS will augment the STS capability to allow the performance of a variety of missions both in near Earth and in interplanetary regions of space.

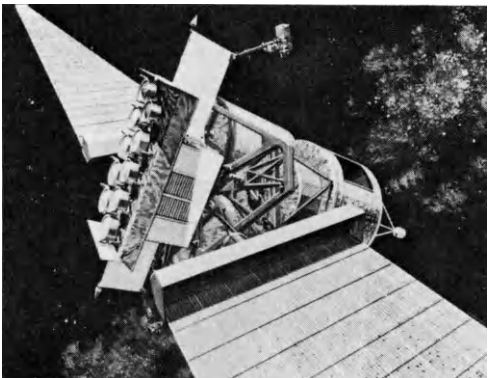


Figure 16. Solar Electric Propulsion Stage (SEPS)

Lastly, in the area of future transportation systems we are studying the requirements and design of a Heavy Lift Launch Vehicle (HLLV) for deploying very large payloads into low earth orbit. This type of vehicle appears to be required for the fabrication of very large, heavy structures for communication, solar energy collection, as well as for other very large structures. Figure 17 shows a concept of a Shuttle-derived HLLV wherein a large cargo module is substituted for the orbiter. Other concepts, including fully reusable systems will continue to be studied.



Figure 17. Heavy Lift Launch Vehicle (HLLV)

### Space Industrialization

Intrinsic to NASA's Space Construction Base Theme is the concept of Space Industrialization. By Space Industrialization we mean the use of space to produce a salable/profitable product or service which companies are willing to pay for.

It is only recent that we have begun to tap the unique attributes of space that make it amenable to industrialization. Experiments performed on Skylab and the Apollo-Soyuz mission have demonstrated that the near weightlessness and vacuum of space allows the manufacturing of materials which could have significant economic and health care value on earth.

Communication, weather, and navigation satellites have begun to make use of the overview attribute of space. The absence of atmospheric interference permits terrestrial and stellar observations with unparalleled clarity. The ease with which excess heat energy can be disposed in space may prove in the future to be of great importance in light of the potential Earth-bound thermal pollution problem. Another significant feature of space is long duration, stable flight whereby the operating lifetime of a spacecraft is limited only by our ingenuity in making systems available over long periods.

Space Industrialization through the exploitation of these attributes of space has the potential of great benefit to mankind. The Skylab and Apollo-Soyuz experiments were just the very meager beginning. The ability to fabricate large structures in space due to the near weightlessness environment will permit the use of large communication and energy collection systems. The existence of a near perfect vacuum and the absence of gravitational effects will permit the manufacturing in space of materials with significant commercial value. The virtually uninterrupted solar energy available in space has tremendous potential for collection and transmission to the ground and may be a vital part of our efforts in supplying the world's energy needs.

Taken collectively, the prospects for space industrialization are almost staggering in their breadth and depth. I believe that most of the things we've talked about in a summary sense here today are inevitable -- these things will happen.

### VII. Summary

To summarize, it is clear to me that we are entering an era in man's spaceflight history which will be characterized by lower cost, routine space transportation which will form a solid foundation for the permanent occupancy and industrialization of space. The roll-out of the first Space Shuttle Orbiter last month is a symbol of our progress and anticipation.

The Spacelab, being developed by our European colleagues, is an important element of the Space

Transportation System and will support the conduct of low cost and repeatable scientific and applications experiments.

In addition, Canada is developing the remote manipulator system to be used with the Shuttle orbiter for handling payloads in space.

To complement the Shuttle in the placement of various classes of payloads in high altitude orbits, we are developing the Interim Upper Stage and the Spinning Solid Upper Stage.

For the future the STS will be the backbone of our efforts. The goal of permanent occupancy and self-sufficiency in space must, if it is to be attained, be preceded by an STS-compatible Space Construction Base. Concurrently, advanced transportation systems must be pursued to extend man's utility outward. With an operational Space Station and complementary transportation systems the boundless opportunities for the Industrialization of Space will be within our grasp.

The challenge to us as a world community is vast but the potential rewards demand that we pursue our goals in space aggressively. Let us do so.

## NEW ERA OF SPACE TRANSPORTATION - FUTURE PROGRAMMES

Roy Gibson

*Director General, European Space Agency, 114, Avenue Charles de Gaulle, 92522 - Neuilly-sur-Seine, France*

The European Space Agency is grateful for this opportunity to explain, before such a distinguished audience, something of its future programmes. You will, I hope, permit me, before talking of the future, to tell you something of the present and a little of the - relevant - past.

The Convention which gave effect to the European Space Agency - ESA - had 11 Western European signatories by the end of 1975, which was the time allowed for Member States of the European Space Conference to become members of the new Agency. Ratification of the Convention has already been completed in some Member States and the process is still continuing in others. It is reasonable to assume that by mid-1977 all States will have ratified the Convention and the Agency will then legally exist - at present we owe our legal existence to the old ESRO Convention. I mention this not because I believe that many of you are at all interested in such legal niceties, but because the process of ratification is the consecration in individual countries of the collective political will Ministers demonstrated when they signed the ESA Convention eighteen months ago.

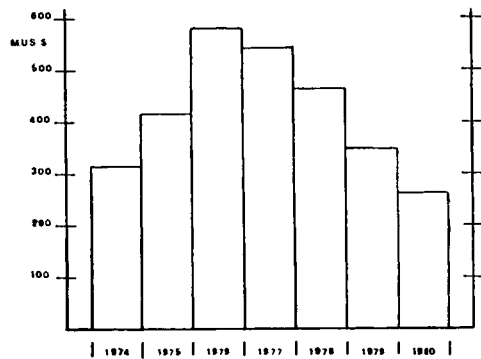
As most of you know, ESA did not have to start from zero, it inherited the installations of the two European space organisations which it replaced, and notably the two principal establishments of ESRO:

- the technical centre (ESTEC) in Noordwijk, Holland; and
- the operations centre (ESOC) in Darmstadt, Federal Republic of Germany.

ESA inherited also a space programme, or, more precisely, a series of programmes, most of which were the issue of Ministerial agreements: the so-called "package deals". No-one would wish to pretend that this inheritance was planned as a well-balanced whole, compatible with Europe's financial possibilities. If you will accept the metaphor, the new Agency at its inception had much in common with the boa-constrictor who has swallowed a pig. To continue the metaphor, we are quite sure that we can ultimately digest what we have undertaken, but the process of digestion takes time and is not without problems.

The ESA approved programmes necessitated a budget in 1976 of 450 million accounting units - that is 580 million U.S. dollars. That represented, in constant prices, an increase of 40% over 1975 and 85% over 1974. Moreover, it was announced already in 1975 that this level must be maintained in 1977, unless programmes were to be cut or seriously delayed. The annual expenditure for approved programmes therefore looks as follows:

**ESA EXPENDITURE FOR APPROVED PROGRAMMES**



This clearly shows the bulge, and also highlights the need for early programme decisions, in order to avoid a repetition of the dreaded "go-stop-go" syndrome. This period of peak expenditure now coincides with an unfavourable economic climate, and quite naturally Ministries of Finance all over Europe are avid for economies. The most alluring areas for cuts are inevitably the relatively small sums intended for the preparation of future programmes - the seed corn of ESA, if you will - and the Agency will be hard put to defend them in the coming budgetary discussions. But defend them we must, if Europe is to transform its somewhat haphazard collection of programmes into the coherent programme Ministers envisaged when they created the Agency. It seems obvious that ESA cannot in the next few years expect Member States to maintain their contributions at the present level, but, as I hope to show you as I review with you the constituent parts of our programme, it would be crippling if our cruising

altitude for the next five or so years were to be reduced by more than 15-20% from the present peak.

I should like to start this review by looking at ESA's scientific programme. This is the oldest of ESA's activities, ESRG was in fact created exclusively for the scientists - but it became eclipsed in the course of the 70s by the application satellite programmes. In the first "package deal" it was agreed to reserve at least 27 MAU (approximately 35 M dollars at 1976 exchange rates) annually for the scientific programme (with contributions from Member States based on the gross national product), but this floor rapidly became regarded as a ceiling. The amount is frankly too small to support a meaningful scientific programme, but the Agency nevertheless has a number of interesting scientific projects on the stocks in addition to the eight scientific satellites which have already been launched:

- GEOS - due for launch next year, will be devoted to magnetospheric research. It is Europe's first superclean satellite in the magnetic, electric and electromagnetic regimes.
- ISEE-B - also due for launch in 1977 - is a joint programme with NASA, formerly known as the International Magnetospheric Explorer. There are three spacecraft involved: A and C to be provided by NASA and B by ESA.
- IUE - the International Ultra-violet Explorer, is principally a project between NASA and the U.K. Science Research Council, but ESA has a contribution in the form of the deployable solar cell array, and the design, construction and operation of a ground station near Madrid for use by European astronomers.
- EXOSAT - the European X-Ray Observatory Satellite, is our latest approved scientific programme. The main development contract will be awarded before the end of 1976.

And the future? In spite of the general financial situation, there are signs that it will prove possible to increase very slightly the amount of money for the scientific programme. But in any event, the next ESA scientific project is to be selected before the end of 1976. I should like to note in passing that over the past year we have put a lot of effort into re-structuring our scientific advisory structure in order to be sure that the Agency was receiving advice from the broadest band of European

scientists. The process is not completed, but I should like to think that we have opened our windows, so to say, to all European scientists who can profit from space techniques.

For organisational purposes, ESA group meteorological satellites together with the scientific programme. For the present we are limited to next year's launch of our METEOSAT spacecraft, which is Europe's contribution to the Global Atmospheric Research Program (GARP), but there is reason to believe that European meteorologists will find METEOSAT of sufficient value to want at least to fly the second flight unit.

In this connection I should like here to mention a general problem which has been increasingly concerning the Agency over the past few years - responsibility for operational systems. The game is known by a variety of names, but it comes down to this: in Europe the development of application satellites is usually financed by the ministry responsible for space - Ministry of Research or Ministry of Technology. The actual users - the departments of meteorology, civil aviation or telecommunications - are, of course, intimately involved in defining the system, but they do not pay. This enviable situation cannot, however, continue indefinitely, and even before the launch of the experimental system it is necessary to talk to the users about the operational follow-on and its funding. Not unnaturally, they would prefer that the financing continue as before, and then begins a negotiation which varies from Member State to Member State in order to determine where the development subsidy should end. Equally important is the effort required to organise these users into an entity capable - both organisationally and juridically - of accepting responsibility for the operational phase.

The ESA Convention permits the Agency to play a role in operational phases, but obviously this can only be done in cooperation with the user organisation, for the Agency has no pretensions to a competence in these various specialist areas.

ESA's communications satellite programmes form the base of our applications activities, and cover three areas:

- the European Communications Satellite (ECS) programme: the aim of which is to provide by 1980 an operational satellite system to meet the needs of the telecommunications administrations of our Member States;
- the maritime satellite programme (MAROTS); and

- the air traffic control satellite (AEROSAT), a programme undertaken in collaboration with the United States and Canada.

There is no time today to go into the details of these three programmes - each has its importance and its complications. I should like rather to look at them as a group and to project a little into the future. ESA's aim has been, with the minimum investment, to keep abreast of the satellite communications technology. It is premature to judge whether or not we have been successful; the most one can say is that our technological developments are not without interest outside Europe and that our Member States, in spite of the prevailing poverty, seem inclined to invest further in these programmes. My personal view is that the next twelve months will see a significant extension to ESA's communications and maritime programmes. Without minimising the importance of our regional communications programme, I personally find the maritime programme the most exciting: European countries participating in our MAROTS programme own around 36 per cent of the world's shipping tonnage, and it needs no great effort of imagination to understand their interest in the establishment of a global operational maritime communication system. I remember this time last year John Johnson of COMSAT GENERAL in an intervention at Monte Carlo castigating the Europeans for not preparing themselves for cooperation with the U.S. in this field. Since then we have slowly eased our arthritic bones into action, and I am hopeful that ere long Europe will be ready to move ahead.

It is tempting to say that this reference to U.S. exasperation with Europe brings us naturally to Spacelab, but this would be to caricature the situation somewhat. It is true that our way of tackling this important programme bears little resemblance to the way in which NASA would have done it, but this is not necessarily wholly negative. The programme is in reasonably good shape. Although in such an audience it is scarcely necessary, let me briefly recall that Spacelab is Europe's contribution to the U.S. Space Transportation System. Spacelab consists of two elements: a pressurised module which provides a laboratory with a "shirt-sleeve environment", and an unpressurised pallet. The size of both module and pallet can be varied to suit the particular payload. This contribution is scheduled to cost Europe around 400 million US dollars, and it constitutes the real determination of ESA to break into manned space flight and to participate as pioneers in the development and exploitation of this exciting new space venture.

One should not underestimate the political importance of this European gesture; the relevant governmental agreements - which tend to be forgotten in the heat of hardware development - lay stress on the fact that this common venture is to be considered as the first step in a continuing space cooperation between ESA and NASA - a collaboration which, I need hardly add, is in no way exclusive or monopolistic. Plans for the utilisation of Spacelab are now gaining momentum. Our start was not as rapid as I had hoped, but the possibilities of Spacelab are now beginning to be understood. In parallel with this necessary period of, may I call it public information, we have created a skeleton infrastructure to assist European experimenters.

The final - and some may say contradictory - part of ESA's programme is provided by the ARIANE launcher. There is little doubt that the European acceptance of this programme had its roots in political rather than technological soil, but I should like here clearly to say how important we now consider this programme to be for ESA. The development is in good order, and the Agency is in the course of proposing to Member States the first slice of the operational phase, for no-one in his right mind would accept to develop such an instrument if it were not intended for production and use. I believe that the Agency's capacity to put into geostationary orbit, from the French-built and ESA-maintained launch site at Kourou, a satellite of more than 900 kg, will be of interest to a wide circle of spacecraft constructors - not only in Europe. Our present calculations indicate, moreover, that ESA launchings can be financially attractive. The first ARIANE test flight takes place in June 1979, and truly operational flights can commence from the first quarter of 1980.

My feeling is that it is in the area of remote sensing that ESA is likely to expand in the coming years. We have already made a modest start in coordinating European ground station activities, benefiting, as do so many of us, from the generous availability of NASA satellites. Lack of funds is likely to prevent any spectacular burst of activity in Europe, but in my view a European remote sensing satellite is nearer to reality than we suspected a year or so ago. But let me be clear, ESA is not an Agency which is chasing new programmes indiscriminately; I am resolutely determined not to propose the use of our overburdened taxpayers' money, unless and until we can be sure that the envisaged programme makes good, economic, sense for the end-user.

This, in capsule form, is ESA - past, present and immediate future. With our

financial concerns, our efforts to streamline management, to define a forward-looking industrial policy, we perhaps appear to have lost something of the glamour of "Space", as it was ten or so years ago. But what are ten or even twenty years in trying to obtain a perspective? I have recently been re-reading Macaulay's History of England (one has the right, even as an international civil servant, to remember one's origins from time to time), and I found under the year 1660, a reference to the poet Dryden's reactions to the exciting scientific discoveries of that period.

Macaulay, with his elegant, but acid-tipped pen, wrote:

"Dryden, with more zeal than knowledge, foretold things which neither he nor anybody else understood".

The Royal Society, he predicted, would soon lead us to the extreme verge of the globe and there delight us with a better view of the moon. Although the august Society no doubt played a role, it was left to others to realise Dryden's fumbling yearnings in the stanza from *Annus Mirabilis* 164:

"Then we upon the globe's last  
verge shall go,  
And view the ocean leaning on  
the sky;  
From thence our rolling  
neighbours we shall know,  
And on the lunar world  
securely pry."

Amid the complicated economic trade-off studies which are now part and parcel of our profession, I like to think that there is still room for a little of this mysticism - a dose of inspiration now and then is good for the most serious of us.

# OPTIMIZATION OF SPACE TRAJECTORIES

C. Marchal

Office National d'Etudes et de Recherches Aérospace—ONERA  
92320 Châtillon—France

## Résumé

L'optimisation des trajectoires spatiales est l'un des facteurs qui ont donné naissance aux théories modernes d'optimisation et aux méthodes numériques correspondantes (utilisées aujourd'hui bien au delà du domaine spatial). L'analyse complète des transferts optimaux de durée indifférente entre orbites képlériennes est en bonne voie, mais il n'en est pas de même dans les autres cas surtout à cause des difficultés liées aux arcs singuliers. L'optimisation stochastique n'est pas encore aussi développée et reste très difficile.

## Abstract

Optimization of space trajectories is the major factor in the birth of modern theories of optimization and of corresponding numerical methods (used to-day in all domains). The case of optimal time-free transfers between Keplerian orbits in a central field is on the way to be completely investigated, but the other cases remain difficult especially because of the different kinds of singular arcs. Stochastic optimization is much less investigated and remains very difficult.

### 1. Introduction

Space travel is one of the oldest dream of mankind and optimization of trajectories in space goes back to 1925 when Hohmann<sup>(1)</sup> determined the optimal transfer orbits between two planets : the famous "cotangential orbits" used during the "Hohmann planetary windows" which come back at regular intervals of time : 19 months for Venus, 26 months for Mars, etc ... However very naturally the number of papers on these questions remain small and mostly on theoretical subjects until the beginning of the space era (see for instance Contensou<sup>(2)</sup>, Bliss<sup>(3)</sup>, Lawden<sup>(4-6)</sup>).

Since then the problem has literally exploded into all directions for two major reasons : A) the problem can be put in a simple and clear way with easy models, the equations are accurate and simpler than in other fields of application. B) the price of astronautics is so large that any saving is welcomed. It has led to many optimization theories<sup>(7 - 11)</sup> and to the development of various numerical methods<sup>(12)</sup>. These numerical methods are more or less strongly related to the optimization theories, very general at the beginning they suffered from a lack of convergence and from an inability to deal with the various constraints met in optimization of space trajectories (forbidden zones, singularities, etc ...), they have been remarkably improved and exceed to day the domain of space optimization ; they are, for instance, able to deal with partial

differential equations and are used henceforth for a great number of problems in all branches of science and industry.

On the other hand the optimization theories have led to the discovery of surprising phenomena concerning the singularities even in very simple cases such as in the "Fuller problem"<sup>(13 - 14)</sup>. The existence of intermediate thrust arcs, switches, singular arcs, chattering arcs of the two kinds, etc ... lead to very complicated solutions which are certainly related to the complexity of biological phenomena since biology is full of optimization process ...

### 2. Formulation of the problem

Problems of optimization of space trajectories, i.e. problems of ascents into orbit, escapes, captures, transfers, rendez-vous, etc ... are generally deterministic and can be summarized as follow : a given space vehicle with known performances faces a given space mission out of the atmosphere ; there are generally many possible ways to realize that mission and we want to do it through the maximisation or the minimization of some performance index (time, mass, cost, etc ...). For instance a rocket R is on a given circular orbit  $O_1$  in a central field (fig.1) and it must go to a given upper circular orbit  $O_2$  with the smallest loss of propellant (the final time can be either fixed or free).

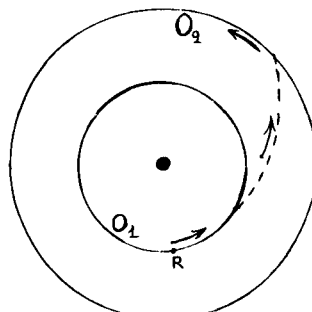


Fig. 1 - Example of a space mission.

### 3. Propulsion systems

We see immediately that an essential element of the optimization is the propulsion system of the

space vehicle of interest ; most studies only consider one of the two following propulsion systems :

A) The "high thrust rockets" or more precisely the rockets for which the largest mass flow rate corresponds to the largest exhaust velocity (chemical propulsion, nuclear rockets, etc ...). These rockets lead generally to "bang-bang trajectories" with a succession of coasting arcs and thrusting arcs of maximum thrust ; however there exist singular cases with "intermediate thrust arcs" the prototype of which is the "Lawden's spiral" (15).

B) The "low thrust rockets" or more precisely the rockets with an imposed exhaust power and without limitation on the exhaust velocity (nucleo-electric propulsion). These rockets lead to solutions with a continuous application of the thrust and a continuously variable exhaust velocity.

If the propulsion system is either fixed or only function of the mass (multi-stage rocket) and if  $\bar{a}$  is the artificial acceleration due to the thrusters, the performance index can be chosen equal to the "characteristic velocity" in the case A, i.e. to  $C_f = \int_{t_0}^{t_f} \|\bar{J}\| dt$  and it can be chosen equal to  $J_f = \int_{t_0}^{t_f} \bar{a}^2 dt$  in the case B. These quantities are monotonic and decreasing functions of the mass of the space vehicle of interest.

Some people have studied particular propulsion systems, see for instance the references (16-19) with either system of mixed type (16 - 17) or a couple of both systems (18) or systems with some impulses of imposed magnitude (19), they lead to some composite solutions, (note that the impulsive case is only a limit of the high thrust case : the exhaust velocity is given and there is no limit on the mass flow rate).

I never notice an optimization study with an other type of propulsion system, such as for instance a solar sail, but they certainly exist !

#### 4. On deterministic optimization theories

For a very short summary of the optimization theories (2-11, 20-22) let us use a parameter of description  $t$  (usually the time) and a state vector  $\vec{X}$  related to all other parameters of interest.

The velocity  $\vec{V}$  of  $\vec{X}$  can be chosen at will by some control  $\vec{u}$  in a maneuverability domain  $D$  function of  $\vec{X}$  and  $t$  :

$$d\vec{X}/dt = \vec{V} \in D(\vec{X}, t) \quad (1)$$

or :

$$\vec{V} = f(\vec{X}, \vec{u}, t) ; \text{ with } \vec{u} \in D(\vec{X}, t) = \text{control domain} \quad (2)$$

and with of course :

$$D(\vec{X}, t) = f[\vec{X}, \vec{D}(\vec{X}, t), t] \quad (3)$$

An admissible trajectory  $\vec{X}(t)$  is an absolutely continuous function  $\vec{X}$  of  $t$  verifying (1)

almost always. We will say that the admissible trajectory  $\vec{X}(t)$  "connects" its terminal points  $(\vec{X}_0, t_0)$  and  $(\vec{X}_f, t_f)$  and we will call it "extremal trajectory" if exist unconnectable couples in any vicinity of the couple  $(\vec{X}_0, t_0), (\vec{X}_f, t_f)$ .

An optimization problem is generally the research of the admissible trajectory  $\vec{X}(t)$  leading from  $\vec{X}_0, t_0$  to  $\vec{X}_f, t_f$  and maximizing some performance index  $I(\vec{X}_0, t_0, \vec{X}_f, t_f)$  under various conditions on terminal points (for instance  $\vec{X}_0, t_0$  and  $t_f$  are given,  $\vec{X}_f$  is free and to optimize). Note that if  $I$  is also related to some integral taken along  $\vec{X}(t)$  we can come back to the above problem (called "Mayer problem") if we include in  $\vec{X}$  a supplementary parameter related to the integral. Also note that the optimal solution of an optimization problem is usually an "extremal trajectory", but it is another admissible trajectory when the maximum of  $I(\vec{X}_0, t_0, \vec{X}_f, t_f)$  is inside the attainable domain.

Let us now define an adjoint vector  $\vec{P}$  (or Pontryagin's vector) and let us write the Hamiltonian  $H$  :

$$H = \vec{P} \cdot \vec{V} \quad (4)$$

The "Generalized Hamiltonian"  $H^*$  will be defined by :

$$H^* = \sup_{\vec{V} \in D(\vec{X}, t)} \vec{P} \cdot \vec{V} \quad (5)$$

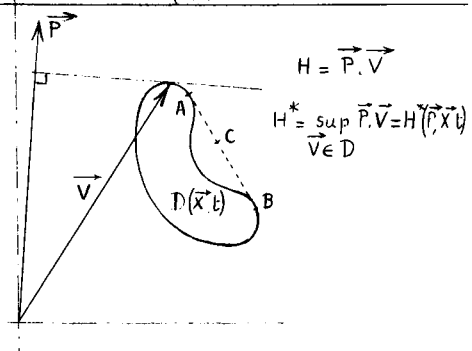


Fig. 2 - The adjoint vector  $\vec{P}$ , the maneuverability domain  $D$  and the generalized Hamiltonian  $H^*$ .

that is, if we prefer to use the control  $\vec{u}$  :

$$H^* = \sup_{\vec{u} \in D(\vec{X}, t)} [\vec{P} \cdot \vec{V}(\vec{X}, \vec{u}, t)] \quad (6)$$

$H^*$  is then a function of  $\vec{P}$ ,  $\vec{X}$  and  $t$  and, under proper conditions of continuity (10, 22), essentially the Lipschitz character of  $H^*$  with respect to  $\vec{P}$  and  $\vec{X}$ , the optimization theories lead to :

To each extremal trajectory  $\vec{X}(t)$  can be associated a non-zero absolutely continuous adjoint function  $\vec{P}(t)$  verifying :

A) Along  $[\vec{P}(t), \vec{X}(t)]$  at points where  $H^*(\vec{P}, \vec{X}, t)$  is continuously differentiable in terms of  $\vec{P}$  and  $\vec{X}$ :

$$\frac{d\vec{X}}{dt} = \frac{\partial H^*(\vec{P}, \vec{X}, t)}{\partial \vec{P}}; \quad \frac{d\vec{P}}{dt} = \frac{\partial H^*(\vec{P}, \vec{X}, t)}{\partial \vec{X}} \quad \text{almost always} \quad (7)$$

B) At the other points we need the convex hull  $D_H(\vec{P}, \vec{X}, t)$  of local gradient vectors  $\partial H^*/\partial(\vec{P}, \vec{X})$  obtained at points  $\vec{P} + \delta\vec{P}, \vec{X} + \delta\vec{X}$ ,  $t$  where  $\delta\vec{P}$  and  $\delta\vec{X}$  are infinitely small and the equations (7) are generalized into :

$$\left[ \frac{d\vec{X}}{dt}; -\frac{d\vec{P}}{dt} \right] \in D_H(\vec{P}, \vec{X}, t) \quad \text{almost always} \quad (8)$$

(7) and (8) imply the "condition of the maximum", i.e. if we take account of (5) :

$$\vec{P}(t), \vec{V}(t) = H^*[\vec{P}(t), \vec{X}(t), t] \quad \text{almost always.}$$

For "ordinary extremals of Pontryagin" and "singular extremals of type 1" (21) only exists one independant adjoint function  $\vec{P}(t)$  and, to the first order, the "neighbouring connectable couples"  $(\vec{X}_o + \delta\vec{X}_o, t_o + \delta t_o), (\vec{X}_f + \delta\vec{X}_f, t_f + \delta t_f)$  fill the half-space defined by :

$$\vec{P}_o \delta\vec{X}_o - H_o^* \delta t_o \geq \vec{P}_f \delta\vec{X}_f - H_f^* \delta t_f \quad (9)$$

Since the performance index  $I$  to maximise is, by construction, a function of  $\vec{X}_o, t_o, \vec{X}_f, t_f$  the inequation (9) leads to obvious "necessary conditions of optimality" or "first order conditions of optimality" or "transversality conditions"; for instance if  $t_o$  and  $t_f$  are given,  $\vec{X}_o$  and  $\vec{X}_f$  being free these conditions are :

$$\vec{P}_o = -\frac{\partial I}{\partial \vec{X}_o}; \quad \vec{P}_f = \frac{\partial I}{\partial \vec{X}_f} \quad (10)$$

These optimization theories have been improved and completed in order to allow to take account of discontinuities, forbidden zones, etc ... they have led to various "second-order conditions of optimality" (23) the simplest being the "Generalized Legendre - Clebsch condition" for singular arcs (24 - 25). In the best cases, these new conditions lead to the conclusion of local optimality.

Some sufficient conditions of absolute optimality exist but are difficult to apply (see for instance the survey paper (23) and its references 28 to 40).

## 5. On numerical methods

The simplicity of equations (7) has led to an obvious numerical method (10, 31). If  $\vec{X}_o, t_o$  are given we can choose an arbitrary adjoint initial vector  $\vec{P}_o$  and integrate (7) from  $t_o$  to  $t_f$ ; the final values  $\vec{P}_f, \vec{X}_f$  don't satisfy in general the transversality conditions but a step by step improvement of  $\vec{P}_o$  can lead to the desired result.

However that simple method suffer from an extreme instability of  $\vec{P}_f, \vec{X}_f$  in terms of  $\vec{P}_o$ ,

especially in singular cases (when (8) is used) and people have been led to more converging methods such as the methods of gradient, steepest ascent, second variation, conjugate gradient, epsilon technique, etc ... (see for instance (20, 27, 30, 54, 55) and the survey paper (12) with its 147 references). These methodes starts from an admissible trajectory  $\vec{X}(t)$  and improve it step by step until the optimum, various techniques allow them to take account of the different types of constraints.

## 6. Space case

In the case of a space vehicle the state vector  $\vec{X}$  is generally composed of :

A) the position of the vehicle defined by the radius vector  $\vec{r}$ ;

B) the velocity  $\vec{V}$  of the vehicle ;

C) the mass  $m$  of the vehicle or some equivalent function such as the present characteristic velocity  $C(t) = \int_{t_0}^t \|\vec{v}(\theta)\| d\theta$  in the case of a "high thrust rocket" of above section 3 or the corresponding parameter  $J(t) = \int_{t_0}^t \vec{v}^2(\theta) d\theta$  for a "low thrust rocket". With the corresponding adjoint parameters  $\vec{P}_r, \vec{P}_v, p_c, p_j$  and in a given gravitational field  $\vec{g}(\vec{r}, t)$  the Hamiltonian of the problem is either :

$$H = \vec{P}_r \cdot \vec{V} + \vec{P}_v \cdot (\vec{g} + \vec{\sigma}) + p_c \vec{v} \quad (11) \quad \text{(for "high thrust rockets")}$$

or :

$$H = \vec{P}_r \cdot \vec{V} + \vec{P}_v \cdot (\vec{g} + \vec{\sigma}) + p_j \vec{v}^2 \quad (12) \quad \text{(for "low thrust rockets")}$$

The artificial acceleration  $\vec{\sigma}$  due to the thrusters represents the control and hence the maximisation of  $H$  with respect to  $\vec{\sigma}$  leads to the following generalized Hamiltonians :

A) For "high thrust rockets" :

$$H^* = \vec{P}_r \cdot \vec{V} + \vec{P}_v \cdot (\vec{g} + \sup \{ 0, (p_v + p_c) \vec{v}_{max} \}); \text{ with } \begin{cases} p_v + p_c > 0 \Rightarrow \vec{\sigma} = \vec{\sigma}_{max} \\ p_v + p_c < 0 \Rightarrow \vec{\sigma} = \vec{0} \\ p_v + p_c = 0 \Rightarrow 0 \leq \vec{\sigma} \leq \vec{\sigma}_{max} \end{cases} \quad (13)$$

The maximum acceleration  $\vec{\sigma}_{max}$  is generally only a function of the present mass  $m$  (or the present characteristic velocity  $C(t)$ ) and the extremal trajectories are generally "bang-bang" with either zero or full thrust. However some intermediate thrust arcs exist (15, 65, 68 - 70) with  $p_v + p_c = 0$  along the arc.

B) For "low thrust rockets"

$$H = \vec{P}_r \cdot \vec{V} + \vec{P}_v \cdot \vec{g} - p_j \frac{\vec{v}}{2p_j}; \text{ with } p_j < 0 \text{ and } \vec{\sigma} = \frac{\vec{P}_v}{2p_j} \quad (14)$$

In both cases the control  $\vec{\sigma}$  is parallel to  $\vec{P}_v$  and into the same direction, for that reason that essential vector  $\vec{P}_v$  has been called "primer vector" by Lawden (11).

The differential equations (7) lead to various integrals of motion along extremal trajec-

tories (32 - 33) :

- 1- If the gravitational field  $\vec{g}(\vec{r}, t)$  has a spherical symmetry (as in a central field :  $\vec{g} = -\mu \vec{r}/r^3$ ) there is for both cases (13) and (14) the integral :

$$\vec{A} = \vec{r} \times \vec{p}_r + \vec{V} \times \vec{p}_V = \text{constant vector} \quad (15)$$

- 2- If  $H^*$  is independant of  $t$  (hence  $\vec{g}(\vec{r}, t) = \vec{g}(\vec{r})$ ) it is a constant along extremal trajectories.

- 3- In the case (14)  $p_r$  is constant and if furthermore  $\vec{g} = -\mu \vec{r}/r^3$  (central field) there is a last integral of motion :

$$K = 3H^*t + \vec{V} \cdot \vec{p}_V - 2\vec{r} \cdot \vec{p}_r + 5J p_r \quad (16)$$

In the case (13) the corresponding integral of motion is :

$$K = 3H^*t + \vec{V} \cdot \vec{p}_V - 2\vec{r} \cdot \vec{p}_r + C p_c \quad (17)$$

but it is valid only for coasting arcs ( $p_r + p_c < 0, J=0$ ) for singular arcs ( $p_r + p_c = 0$ ) and also for a very particular case : the "impulsive case" in which  $T_{\text{maximum}}$  is infinite and which implies for all time  $p_r + p_c < 0$  and  $p_c = \text{constant} < 0$ .

It seems that no other general integral of motion exists (32 - 33) but at least the equations (7) can be integrated completely along a coasting arc of a central field, i.e. along an elliptic or hyperbolic Keplerian arc ; it leads to :

$$\begin{aligned} \vec{p}_V &= \lambda_1 \vec{V} + \lambda_2 \vec{x} \cdot \vec{r} + (\vec{r} \times \vec{V}) \lambda_3 + \vec{r} \times (\vec{V} \times \lambda_3) + \lambda_4 (\vec{r}^2 - 2\mu/r) \\ \vec{p}_r &= -\frac{d\vec{p}_r}{dt} = \lambda_1 \mu \frac{\vec{r}}{r^3} + \vec{V} \times \lambda_2 + \vec{V} \times (\lambda_3 \times \vec{V}) + \mu \vec{r} \times (\vec{r} \times \lambda_3) + \lambda_4 (\sqrt{3} \mu \vec{r}) \quad (18) \\ p_c &= \text{constant} \end{aligned}$$

$\lambda_2, \lambda_3$  being two constant vectors and

$\lambda_1, \lambda_4$  two constants.

$$H^* = \lambda_4 (V^2 - 2\mu/r)$$

$$\vec{A} = (\vec{r} \times \vec{V}) \times \lambda_2 + [\vec{V} \times (\vec{r}^2 \times \vec{V}) - \mu \frac{\vec{r}}{r^3}] \times \lambda_3 - \lambda_4 \vec{r} \times \vec{V}$$

$$K = \lambda_4 (V^2 - 2\mu/r) - \lambda_2 (\vec{r} \times \vec{V}) + C p_c$$

## 7. Analytical versus numerical results

From a general point of view the most interesting results are the analytical ones, indeed there are numerous numerical studies but they generally deal with a particular mission with all its constraints and it is difficult to obtain a general idea from these results. However it is fair to recognize that :

A) The numerical studies have introduced new ideas such as the discontinuities of the adjoint vector at the boundaries of forbidden zones.

B) Analytical results are sometimes very restricted and their extension, their refinement, their verification need the help of numerical researches : these analytico-numerical studies are the most fruitful (for instance the excellent analytico-numerical study of Small (41) improves and extends the analytical paper (42) in many ways ... and corrects my errors on the size of the zones of one-impulse and three-impulse transfers : the calculation of a curve point by point is generally better than any analytical development).

Let us do a brief survey.

A) "Low thrust rockets" is a central field. The infinitesimal transfers and rendez-vous have been obtained to the first order. It is also the case (through an averaging technique) for transfers and for rendez-vous of very long duration with then a very large number of revolutions (34-35). During these missions the average energy of the space vehicle, per unit of mass, is a quadratic function of the time (see also the survey paper (36) with its references 80 - 83, 137 - 152 and 214).

B) "High thrust rockets"

For these rockets the first classification of studies of optimal trajectories is related to the magnitude of maximum thrust : either that maximum thrust is finite or it is infinite (possibility of impulses).

The finite thrust case gives relatively few analytical results. For instance (42) the replacement of an impulse by the corresponding optimal thrust arc of maximum thrust can be done with a loss of second order (except for impulses at terminal instants) : in a central field, if  $\Delta t$  is the duration of the maximum thrust arc and  $T$  the duration of circular revolution at the altitude of the impulse, then the relative loss of characteristic velocity is smaller than  $\pi^2 \Delta t^2 / 6T^2$ .

That small difference between impulses and maximum thrust arcs is one of the two main interest of the studies of impulsive cases, the other interest being of course the mathematical simplicity of impulses in comparison of thrust arcs.

For these two major reasons the number of studies of optimal impulsive trajectories is very large, see for instance the five survey papers (36-40).

Optimal impulsive trajectories can be classified into many ways :

A) With respect to the field of attraction : arbitrary field, zero field, constant field, central field, transfers in the many problem, approximation of the "activity spheres" etc ...

B) With respect to the type of the mission : ascent into orbit, escape, capture, transfer (i.e. to go from a given initial orbit to a given final orbit), rendez-vous (i.e. to reach a given space vehicle along the final orbit), transfers between ellipses or between hyperbolae in a central field, etc ...

C) With respect to the mathematical properties of the mission : finite or infinitesimal transfers or rendez-vous ; time-free, time limited, time fixed, minimum time mission, etc ... A major distinction lies between the deterministic and the stochastic missions, however these last ones - generally on mid-course corrections - are rather rare, we will see them in section 9. Another mathematical property is the existence of singular arcs of various types, intermediate thrust arcs, chattering arcs of the two kinds, etc ... (see for instance (48) and the five survey papers (14, 44-47).

### 7.1 - Time free transfers between Keplerian elliptic orbits

The most studied case of impulsive trajectories is the time-free transfer between Keplerian elliptic orbits in a central field, in which a major simplification occurs : instead of the seven components of the state-vector used in the above section 6 :  $\tau$ ,  $V$ ,  $C$  it is possible to use only five components. Indeed we can use as state-vector the five first orbital elements, the last one (the position along the orbit) can be chosen at will since Keplerian elliptic motions are periodical and since the time is free : that element becomes a control parameter. On the other hand the characteristic velocity  $C$  can be chosen as parameter of description instead of the time  $t$  that can be ignored.

In this problem the optimal solutions are always impulsive (51) and use only elliptic or parabolic velocities. A particular type of optimal solutions is the bi-parabolic transfer (fig. 3) :

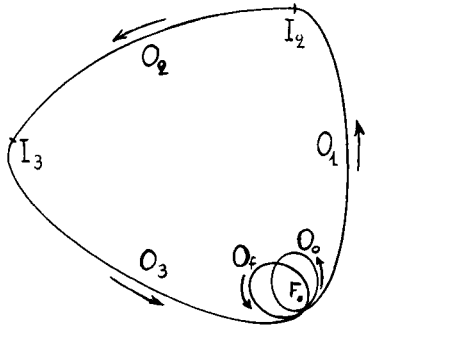


Fig. 3 - The bi-parabolic transfer

A) A tangential accelerative impulse at perigee leads to the parabola or the very elongated ellipse  $O_1$ .

B) Infinitely small impulses at  $I_2$  and  $I_3$  lead to the parabola or the very elongated ellipse  $O_3$  of proper orientation.

C) A tangential decelerative impulse at the perigee leads to the final orbit  $O_2$ . Of course these bi-parabolic transfers are optimal only between distant orbits (for instance when the angle between the two orbital planes is larger than  $60.185^\circ$  and/or when the ratio of the two perigee radius is larger than 11.938).

The optimal solutions are also known between near circular close orbits (52-53), between coplanar orbits (41) between "coaxial orbits" (50) (also called "co-apsidal orbits" : they have the same "line of apsides" which is the straight line joining perigee and apogee). All these solutions, when they are not of bi-parabolic type, have at most three impulses and it is possible to demonstrate that it is also the case between non-circular close orbits and between elliptic orbits the eccentricity of one of which is close to one. It seems that this general result remain true between arbitrary Keplerian elliptic orbits.

The coaxial or "co-apsidal" case is simple : all impulses occur on the line of apsides either at perigee or at apogee and lie in the local horizontal plane, they don't change the line of apsides which is thus also the line of nodes.

The optimal transfers between circular orbits are a particular case of coaxial transfers, they lead to the results drawn in figure 4 in terms of the radius ratio and the angle between the two orbital planes. In usual cases (for instance : ascent from a parking orbit to a geostationary orbit) the optimal transfer has generally two-impulses, but between equal circles it has three-impulses.

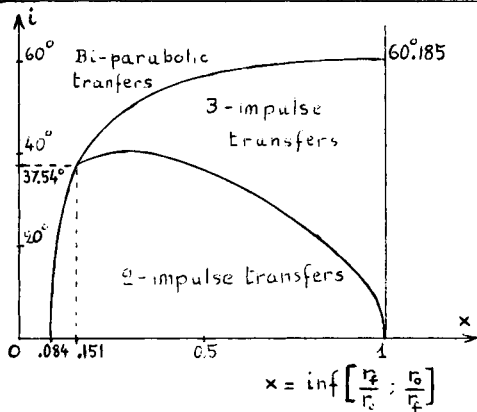


Fig. 4 - Optimal time-free transfers between circular Keplerian orbits in terms of the radius ratio ( $r_f/r_o$ ) and the inclination  $i$

Let us note that an impulse can always be decomposed into smaller impulses done at the same point at an interval of one revolution ; the impulses can thus be approximated as nearly as desired by several maximum thrust arcs and arbitrary rendez-vous can be obtained for the characteristic velocity of the corresponding transfer.

Finally the general solution of optimal time-free transfers between Keplerian elliptic

orbits remains unknown, but at least the optimal succession of impulses, i.e. the "switching conditions" are known in closed form (49) and thus are implicitly known all optimal time-free two-impulse transfers between Keplerian elliptic orbits.

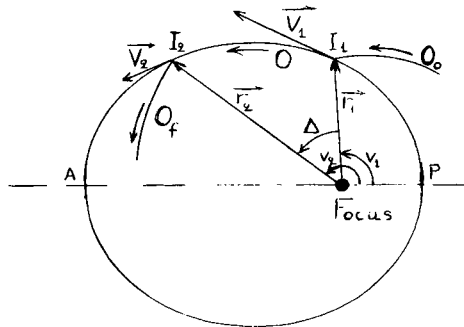


Fig. 5 - Two-impulse optimal transfer between the orbits  $O_0$  and  $O_f$

$$e = \text{excentricity of the intermediate orbit } O \quad (20)$$

The relations between the direction cosines  $S_1, T_1, W_1, S_2, T_2, W_2$  and the elements  $v_1, v_2, e$  are :

$$\begin{aligned} & \theta^3(T_2 - T_1)(S_1 + S_2)^2 + \theta^2(S_1 + S_2)[3 - 2S_1^2 - 2S_2^2 - 3T_1T_2 - W_1W_2] + \\ & + \theta[2T_2 - 2T_1 - T_1S_1^2 + 3T_2S_2^2 - 3T_2S_1^2 + T_2S_2^2] + \\ & + [S_1 + S_2][1 - 2S_1^2 - 2S_2^2 + 3S_1S_2 - T_1T_2 - W_1W_2] = 0 \end{aligned} \quad (21)$$

$$1 + e \cos v_1 = \frac{(1 - \cos \Delta)[1 - 2S_2^2 - S_1S_2 + \theta T_2(S_1 + S_2)]}{1 + \sin \Delta(S_1T_2 - S_2T_1) - \cos \Delta(S_1S_2 + T_1T_2) - W_1W_2} \quad (22)$$

and :

$$1 + e \cos v_2 = \frac{(1 - \cos \Delta)[1 - 2S_1^2 - S_1S_2 - \theta T_1(S_1 + S_2)]}{1 + \sin \Delta(S_1T_2 - S_2T_1) - \cos \Delta(S_1S_2 + T_1T_2) - W_1W_2} \quad (23)$$

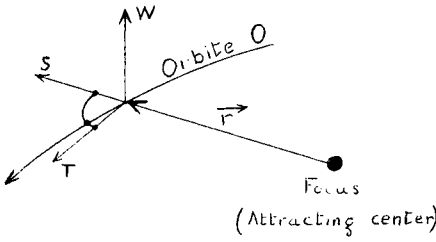


Fig. 6 - The radial, circumferential and normal components of the local frame of reference of the orbit  $O$ .

In the plane case, i.e. when  $W_1 = W_2 = 0$ , it is possible to put  $S_1 = \sin \Psi_1, T_1 = \cos \Psi_1$ ;  $S_2 = \sin \Psi_2, T_2 = \cos \Psi_2$  and the above relation (21) is simplified into :

$$\cos(\Psi_1 + \Psi_2) = \frac{\sin \Delta - \theta \cos \Delta \cdot \tan(\Psi_2 - \Psi_1)}{\sin \Delta + (3 + \cos \Delta) \tan(\Psi_2 - \Psi_1)} \quad (24)$$

and the denominator of (22) and (23) is then equal to  $1 - \cos(\Delta + \Psi_1 - \Psi_2)$ .

These relations allow to built examples of optimal switches in terms of two parameters in the plane case and four parameters in the general case (plus the usual parameters of scale and orientation). The radius and velocity vectors  $\vec{r}_1$  and  $\vec{v}_1$  at  $I_1$  and also  $\vec{r}_2$  and  $\vec{v}_2$  at  $I_2$  are easily deduced from  $e, v_1$  and  $v_2$ ; the primer vectors  $\vec{p}_{v_1}$  and  $\vec{p}_{v_2}$  defined in section 6 can be chosen equal to the unit vectors  $(S_1, T_1, W_1)$  and  $(S_2, T_2, W_2)$  of the direction of impulses (it implies  $F_C = -1$ ) and the vectors  $\vec{r}_{v_1}$  and  $\vec{r}_{v_2}$  can be deduced from the conditions of optimal time-free transfers between Keplerian elliptic orbits :

$$H^* = 0 = \vec{p}_{v_1} \cdot \vec{V}_1 - \mu S_1 r_1^{-2} = \vec{p}_{v_2} \cdot \vec{V}_2 - \mu S_2 r_2^{-2} \quad (25)$$

$$\vec{p}_{v_1} \cdot \vec{p}_{v_2} = \vec{p}_{v_2} \cdot \vec{p}_{v_1} = 0 \quad (26)$$

$$\vec{A} = \vec{r}_1 \times \vec{p}_{v_1} + \vec{V}_1 \times \vec{p}_{v_1} = \vec{r}_2 \times \vec{p}_{v_2} + \vec{V}_2 \times \vec{p}_{v_2} \quad (27)$$

Let us consider an intermediate orbit  $O$  between the impulses at  $I_1$  and  $I_2$  and leading optimally from the initial orbit  $O_0$  to the final orbit  $O_f$  (figure 5); let us call  $S_1, T_1, W_1$  and  $S_2, T_2, W_2$  the direction cosines of the two impulses in the local frame of reference of the orbit  $O$  ( $S$  being the radial component,  $T$  the circumferential component and  $W$  the normal component : see figure 6), finally let us call  $v_1$  and  $v_2$  the true anomalies of  $I_1$  and  $I_2$  along  $O$  (figure 5) and let us put :

$$\Delta = v_2 - v_1 \quad ; \quad \theta = \tan(\Delta/2) \quad (19)$$

It remains to satisfy 2 conditions :

A) The condition of optimal direction of switch :  $T_1 \cdot (1 + e \cos v_1) > T_2 \cdot (1 + e \cos v_2)$  which is equivalent to  $\vec{V}_1 \cdot \vec{P}_{V1} > \vec{V}_2 \cdot \vec{P}_{V2}$

B) The condition  $P_V + P_C \leq 0$  all along the intermediate orbit 0 (that condition, related to the conditions (26) and to the expression (18) with  $\lambda_4 = 0$ , can also be expressed as  $P_{V1} \leq 1$  all along 0 if we choose  $P_C = -1$ , that is  $\vec{P}_{V1} = (S_1, T_1, W_1)$  and  $\vec{P}_{V2} = (S_2, T_2, W_2)$ ).

If the condition  $P_V + P_C \leq 0$  is satisfied at all points of the orbit 0, except  $I_1$  and  $I_2$ , where  $P_V + P_C = 0$ , the transfer of the figure 5 is optimal provided that the impulses at  $I_1$  and  $I_2$  be sufficiently small.

Hence the major elements of optimal time-free transfers between elliptic Keplerian orbits are already known and many particular cases, coplanar, coaxial, etc ... are completely investigated. It would be useful (but certainly hard) to complete the investigation and in particular to verify the "no four finite impulses" assumption. However it is surprising to note that some apparently less simple cases lead to simpler solutions, for instance if we consider a Vinti potential (56), that is a potential due to two fixed equal masses in symmetrical complex positions (a good approximation of the oblateness of the Earth) and if we exclude the small central sphere of radius equal to the distance of the two masses, then the optimal time-free transfers between two arbitrary bounded orbits are very similar to the above transfers between "coaxial orbits" : the optimal transfers are impulsive and all non infinitesimal impulses lie in the local horizontal plane and occur either at perigee or at apogee when these points cross the line of equatorial nodes.

#### 7.2 - Time-free transfers between Keplerian hyperbolic orbits

Between Keplerian hyperbolic orbits the optimal transfer is simple but unrealistic when the attracting mass is a point mass (the solutions require somme passages infinitely close to the center of mass : see the six-impulse transfer of the reference (37)). If we consider an attracting sphere with a finite radius the problem becomes realistic (57 - 58) and the optimal solutions are always plane and impulsive, they have never more than two non-infinitesimal impulses ; they are of twelve different types nine of them with a grazing passage at the boundary of the planet. That problem can be considered as solved (58) as long as no atmospheric braking is used and the economy of characteristic velocity is at most two times the escape velocity from the planet.

#### 7.3 - The other motions in a central field

Other motions in a central field : ascent into orbit, escape, capture, time fixed transfers, etc ... have been the subject of very few general analytical studies (for instance (57, 47, 53, 59)) and their results are less interesting because :

A) The planet intersect many orbits and the above simplification for elliptic orbits (the position along the orbit considered as a control

parameter) cannot be done even in a time-free case.

B) The impulsive approximation is not so good as in the case of transfers : an ascent into orbit require a powerful initial thrust phase for which the impulsive approximation is only of the first order and not of the second (that approximation lead in general to optimal trajectories with 2, 3 or 4 impulses).

C) The presence of the atmosphere modify completely the optimization of the initial phase of an ascent, on the other hand various atmospheric brakings can be used at descent, it extends very much the field of research.

D) For escape and capture the time-free hypothesis lead generally to optimal maneuvers of infinite duration, even in realistic problems, hence that simplification cannot be done.

For all these reasons the usual simplifications necessary for analytical studies are generally unrealistics and thus the most interesting studies of these motions are the numerical ones especially for the direct escape and for the ascent into orbit (see for instance the survey paper (36) and its references 153 - 187 ).

#### 7.4 - Non central field : the assumption of activity spheres

If we consider the zero-field and the constant field as particular cases of a Newtonian central field (60 - 64) the optimization studies in non Newtonian central fields are rather rare. There are some special studies (for instance the  $\mu/r^n$  field in (65)) but it is of course the n-body problem - transfers between planets - that attracts most people since Hohmann (1) out of the domain of the simple Newtonian central field.

The complexity of n-body motion and the multiplicity of attracting forces exerted on the space vehicle let very few place for analytical studies and give the first place to a great variety of very sophisticated numerical studies generally related to real space missions. These missions present the general characters of Hohmann transfers, they have short maximum thrust arcs in the vicinity of planets separated by long coasting arcs in interplanetary space, with sometimes a small midcourse correction due to the various inaccuracies and errors.

Some particular missions such as that of the "grand tour" use the successive force field of the planets to jump optimally from planet to planet, their elaboration represent a masterpiece of numerical study.

However let us note two interesting analytico-numerical studies :

A) A study oriented toward the influence of departure and arrival dates (66)

B) A time-free study oriented toward the influence of eccentricities and inclinations of planetary orbits (67). Both studies use the usual approximation of activity sphere (also called mean sphere of influence) and lead to two-impulse or three-impulse trajectories. The second study show that the influence of eccentricities is small but

that of inclinations is large.

### 8. The singular arcs

The Lawden spiral (15) is the first known singular arc, its non-optimality was demonstrated by Robbins (68). Since then numerous people have studied these arcs (see for instance the references (13, 20, 24, 48, 51, 65, 68 - 70) and especially the five survey papers (14, 44 - 47).

The singular arcs are of three types :

A) The "intermediate thrust arcs" obtained for "high thrust rockets" when in equation (13) the quantity  $\frac{1}{2}v^2 + \frac{1}{2}P_c$  remains for a while equal to zero ( $\frac{d}{dt}$  can be chosen in order to satisfy that condition). The Lawden spiral (15) is the prototype of these arcs, it is non optimal but some other intermediate thrust arcs are optimal such as the "reversible arc" (23, 48, 69).

More generally these arcs are obtained when it is necessary to use a velocity corresponding to a point as C in above figure 2 on a straight line or a cylindrical surface of the maneuverability domain : the Pontryagin conditions cannot give directly the optimal control.

Various generalization of these arcs exist (for instance when the point C belongs to a triangle of the surface of the maneuverability domain) and their optimality is obtained by various tests (23), the most known being the Kelley-Contensou test (24 - 25) also called "Generalized Legendre - Clebsch condition".

B) The "chattering arcs of the first kind". Let us look again at point C in figure 2. If the true shape of the maneuverability domain is the full line it is impossible to use C directly but it is possible to approximate it by a "chattering" between A and B (for instance if the acceleration  $\frac{d}{dt}$  of (13) can only be chosen equal to either 0 or  $\frac{d}{dt}_{max}$ , an alternate use of 0 and  $\frac{d}{dt}_{max}$  allow to approximate an intermediate thrust arc).

That singularity seem rather artificial and it is overcome by the convention of "relaxation of the control" (equivalent to the "convexisation" of the maneuverability domain) however in some cases the relaxation is not physically possible (70) and furthermore chattering and relaxation are not always equivalent (reference (14) page 444).

C) The "chattering arcs of the second kind". These arcs are not a mathematical singularity as the above chattering arcs, they are concrete and appear in problems as simple as the "Fuller problem" (13) : minimize  $\int_{t_0}^{t_f} x^2 dt$

for given  $x_0, x'_0, t_0$  and  $t_f$ ,  
the function  $x(t)$  being limited by  $|x''| \leq 1$   
(with  $x'' = \frac{d^2x}{dt^2}$ ). If  $t_f$  is sufficiently large, for instance if  $x_0 = 2$  ;  
 $x'_0 = -2$  and  $t_f > t_0 + 3.4304$ , the function  $x(t)$  ends by the singular arc (of "intermediate thrust" type) :  $x \equiv 0$  between  $t_0 + 3.4304$  and  $t_f$  ; before the instant  $t_0 + 3.4304$  there are an infinite number of switches between  $x'' = +1$  and  $x'' = -1$ , the switching instants being disposed in a geometrical progression

converging at  $t_0 + 3.4304$  (reference (14) page 446).

That surprising phenomenon is called "chattering of the second kind" and appears before the beginning and after the end of usual intermediate thrust arcs (reference (48) page 471) and more generally before and after the usual singular arcs as soon as the test of the "Generalized Legendre-Clebsch condition" require more than three differentiations.

These chattering arcs can be of an extraordinary complexity (14), they allow intermediate thrust arcs to be part of general transfers or rendez-vous (and not only of very particular transfers or rendez-vous), when initial and final conditions are sufficiently near to the conditions of the intermediate thrust arc, but, as we have already note in section 7.1, there is neither intermediate thrust arc nor chattering arc in the optimal time-free transfers or rendez-vous between elliptic Keplerian orbits.

### 9. Stochastic optimization

Stochasticity appears in optimization of space trajectories through the problem of mid-course corrections due to all the unavoidable inaccuracies met all along the way :

A) Inaccuracies due to surface forces : air drag, winds, radiation pressure from the Sun or the Earth, solar wind, meteoritic effects.

B) Inaccuracies due to gravitational forces : complexity and variations of the Earth potential, errors on masses, shapes and motions of outer bodies, relativistic effects.

C) Possible magnetic or electric effects.

D) Errors on measure of distances, times, velocities ; errors on the (variable) position of observatories, on light propagation, on set of axes (motions of equator and ecliptic).

E) Errors on rocket performances (thrust, orientation, etc ...).

F) Mathematical errors in the integration of equations of motion.

For all these reasons it is necessary to correct the trajectories from time to time ; however the complexity of stochastic optimization, even for linear quadratic systems (43, 71) and the small gain it gives for usual space trajectories lead to very few analytical studies of these phenomena, see for instance the reference (72).

### Conclusion

Optimization of space trajectories has initiated the modern theories of optimization and has led to always better and better numerical methods used to-day in all kind of optimization problems. It has also led to the discovery of surprising phenomena related to the singularities and leading to solutions of an extreme complexity. Being free of these singularities the optimal time-free transfers between Keplerian orbits are on the way to be completely investigated but it

would also be interesting to improve the knowledge of singularities and that of stochastic optimization and, if possible, to relate them to the complexity of biological phenomena in which optimization is so fundamental.

#### References

- It is impossible to give all the references related to optimization of space trajectories (more than one thousand !). So are only presented references of major importance or of historical interest or -as example- related to some interesting particular point and especially a serie of survey papers in the different fields of the subject.
1. W. Hohmann - "Die Erreichbarkeit der Himmelskörper". Oldenburg, Munich (1925) - "The attainability of heavenly bodies". NASA Technical translation F. 44 (1960).
  2. P. Contensou - "Note sur la cinématique générale du mobile dirigé". Communication à l'Association Technique, Maritime et Aéronautique, Vol. 45, n° 836 (1946).
  3. G.A. Bliss - "Lectures on the calculus of variations". The University of Chicago Press, Ch. VII - Chicago (1946).
  4. D.F. Lawden - "Minimal trajectories". Journal of the British Interplanetary Society, 9, p. 179 - 186 (July 1950).
  5. D.F. Lawden - "Minimal rocket trajectories". Jet propulsion 23, 360 - 367 and 382 (1953).
  6. D.F. Lawden - "Fundamentals of space navigation". Journal of the British Interplanetary Society, 13, 87 - 101 (1954).
  7. P. Contensou - "Etude théorique des trajectoires optimales dans un champ de gravitation. Application au cas d'un centre d'attraction unique". Astronautica Acta VIII, fasc. 2-3 (1962).
  8. J.V. Breakwell - "The optimization of trajectories". S.I.A.M. Journal, 7, p. 215 - 247 (1959).
  9. D.F. Lawden - "Interplanetary rocket trajectories". Advances in Space Science and Technology, edited by F.I. Ordway (Academic Press N.Y.), Vol. 1 (1960).
  10. L.S. Pontryagin - V.G. Boltyanskii - R.V. Gamkrelidze - E.F. Mishchenko - "The Mathematical Theory of Optimal Processes". Interscience Publishers, John Wiley and Sons, Inc. New-York (1962).
  11. D.F. Lawden - "Optimal trajectories for space navigation". Butterworths Mathematical Texts, Butterworths London (1963).
  12. A. Miele - "Survey paper - Recent Advances in Gradient Algorithms for Optimal Control Problems". Journal of Optimization Theory and Applications - Vol. 17, n° 5/6 (1975).
  13. A.T. Fuller - "An optimum Non-linear Control System". Paper presented at the IFAC Congress, Moscow, USSR (1961).
  14. C. Marchal - "Survey paper - Chattering arcs and chattering controls". Journal of Optimization Theory and Applications. Vol. 11, n° 5 (1973).
  15. D.F. Lawden - "Optimal intermediate-thrust arcs in a gravitational field". Astronautica Acta 8, p. 106 - 123 (1962).
  16. G. Leitmann - "Optimization techniques". Academic Press - New-York - New-York (1962).
  17. J.P. Marec - "Transferts optimaux entre orbites elliptiques proches". Thèse de Doctorat - Faculté des Sciences de Paris, n° A0 1610 (1967).
  18. T.N. Edelbaum - "The use of high-and-low-thrust propulsion in combination for space missions". Journal of Astronautical Sciences, 9, 58 - 59 (1962).
  19. G.A. Hazelrigg - R.G. Brusch - W.L. Sachs - "Optimal space trajectories with delta-velocity constraints". Proceedings of the 21st International Astronautical Congress - North Holland (1971).
  20. G. Leitmann - "Topics in optimization - Mathematics in Science and Engineering". Vol. 31, Academic Press, New-York (1967).
  21. C. Marchal - "Theoretical research in deterministic optimization". ONERA Publication, n° 139 (1971).
  22. C. Marchal - "The bi-canonical systems" in "Techniques of Optimization". A.V. Balakrishnan Editor, p. 211 - 228 - Academic Press - New-York and London (1972).
  23. C. Marchal - "Survey paper - second order tests in optimization theories". Journal of Optimization Theory and Applications, Vol. 15, n° 6 (June 1975).
  24. H.J. Kelley - "A second variation test for singular extremals". AIAA Journal, Vol. 2, n° 8 (1964).

25. P. Contensou - "Conditions d'optimalité pour les domaines de manœuvrabilité à frontière semi-affine". Proceedings of the second colloquium on methods of optimization (Novosibirsk 1968). Edited by N.N. Moiseev, Springer-Verlag, Berlin, Germany (1970).
26. H.J. Kelley - "Method of gradients" in "Optimization Techniques" edited by G. Leitmann, Academic Press, New-York (1962).
27. A.E. Jr. Bryson - W.F. Denham - "A steepest ascent method for solving optimum programming problems". Journal of Applied Mechanics, Vol. 84, n° 3 (1962).
28. H.J. Kelley - R.E. Kopp - H.G. Moyer - "A trajectory optimization technique based upon the theory of the second variation". AIAA Preprint 63-415 (August 1963).
29. J.V. Breakwell - J.L. Speyer - A.E. Bryson - "Optimization and control of non linear systems using the second variation". SIAM Journal 1 - 193 - 223 (1963).
30. B. Fraeijs de Veubeke - "The second variation test with algebraic and differential constraints". Advanced problems and methods for space flight optimization. Fraeijs de Veubeke Editor, Pergamon, p. 189 - 217 (1969).
31. C.F. Price - "An indirect numerical method based on offset vectors for obtaining solutions to optimum control problems". Proceedings of the 18th Congress of the International Astronautical Federation. Belgrade (1967).
32. S. Pines - "Constants of the motion for optimum thrust trajectories in a central force field". AIAA Journal, 2, p. 2010 (1964).
33. T.N. Edelbaum - S. Pines - "The fifth and sixth integrals for optimum rocket trajectories in a central field". AIAA/AAS Astrodynamics Conference. Princeton, New-Jersey, August 20 - 22 (1969).
34. T.N. Edelbaum - "Optimum power-limited orbit transfer in strong gravity fields". AIAA - Journal 3, p. 921 - 925 (1965).
35. J.P. Marec - N.X. Vinh - "Transferts optimaux à puissance limitée entre orbites elliptiques quelconques". Paper presented at the 27 th International Astronautical Congress Anaheim. 11 - 16 Octobre (1976).
36. C. Marchal - J.P. Marec - C.B. Winn - Survey paper - "Synthesis of the analytical results on optimal transfers between Keplerian orbits".
- Paper presented at the 18th International Astronautical Congress - Belgrade - 25 - 29 Septembre (1967). Also ONERA tiré à part n° 515 (1967).
37. T.N. Edelbaum - Survey paper - "How many impulses ?" Paper 66-7 AIAA (1966) ; Astronautics and Aeronautics, Vol. 5, n° 11, 64 - 69 (1967).
38. C. Marchal - Survey paper - "Synthesis of the analytical results on optimal transfers between Keplerian orbits (time-free case)". T.P. ONERA n° 482 (1967) - Also in "Advanced problems and methods for space flight optimization". B. Fraeijs de Veubeke Editor. Pergamon Press. (1969).
39. D.J. Bell - Survey paper - "Optimal space trajectories a review of published work". The aeronautical journal of the royal aeronautical society, vol. 72, p. 141 (February 1968).
40. F.W. Gobetz - J.R. Doll - Survey paper - "A survey of impulsive trajectories". AIAA Journal, Vol. 7, n° 5, p. 801 - 834 (1969).
41. H.W. Small - "Minimum fuel time-free transfer between elliptic orbits". Dissertation - Stanford University (August 1972).
42. C. Marchal - "Transferts optimaux entre orbites elliptiques (durée indifférente)". Thèse de doctorat, AO 1609, Faculté des Sciences de Paris (1967).
43. Masanao Aoki - "Optimization of stochastic systems. Topics in discrete-time systems". Academic Press - New-York - London (1967).
44. D.H. Jacobson - Survey paper on singular arcs - IEEE Trans. Automatic control 16, p. 651 (1971).
45. R. Gabasov - F.M. Kirillova - V.A. Strochko - Survey paper on singular arcs - Autom. remote control 32, 689, 857, 1013 (1971).
46. R. Gabasov - F.M. Kirillova - Survey paper - "High order necessary conditions for optimality". SIAM Journal of Control, vol. 10, p. 127 (1972).
47. D.J. Bell - Survey paper - "Singular problems in optimal control - a survey". Int. Journal of Control - Vol. 21 n° 2, p. 319 - 331 (1975).
- 47.1 J.B. Jones - "Optimal rendez-vous in the neighbourhood of a circular orbit". Paper No AAS-75-061 AAS/AIAA Astrodynamics Specialist Conference - Nassau (1975).

48. J.V. Breakwell - J.F. Dixon - "Minimum fuel rocket trajectories involving intermediate thrust arcs". Journal of Optimization Theory and Applications. Vol. 17, n° 5/6 (1975).
49. C. Marchal - "The optimal transfer problem between Keplerian orbits : the switching conditions in explicit form". La Recherche Aérospatiale, n° 1, p. 7 - 15 (1971).
50. C.B. Winn - "Minimum fuel transfers between coaxial orbits, both coplanar and non-coplanar" Stanford University, Center for Systems Research, Sudaar 305 (March 1967).
51. C. Marchal - "Généralisation tridimensionnelle et étude de l'optimalité des arcs à poussée intermédiaire de Lawden (dans un champ newtonien)". La Recherche Aérospatiale, n° 123 (1968).
52. J.V. Breakwell - "Minimum impulse transfer between a circular orbit and a nearby non-coplanar elliptic orbit". Advanced problems and methods for space flight optimization. B. Fraeijis de Veubeke Editor. Pergamon Press, p. 255 - 274 (1969).
53. J.P. Marec - "Rendez-vous impulsionnels optimaux de longue durée entre orbites quasi-circulaires proches coplanaires ou non". Advanced problems and methods for space flight optimization. B. Fraeijis de Veubeke Editor. Pergamon Press, p. 227 - 254 (1969).
54. A.V. Balakrishnan - L.W. Neustadt - "Computing methods in optimization problems". Academic Press. New-York - London (1964).
55. L.A. Zadeh - A.V. Balakrishnan - L.W. Neustadt - "Computing methods in optimization problems II". Academic press - New-York - London (1969).
56. J.P. Vinti - "Theory of an Accurate Intermediate Orbit for Satellite Astronomy". Journal of Research of the National Bureau of Standards - B Mathematics and Mathematical Physics, Vol. 65 B, n° 3, p. 169 - 201 (1961).
57. F.W. Gobetz - "Optimum transfer between hyperbolic asymptotes". AIAA Journal 1, p. 2034 - 2041 (1963).
58. J.M. Walton - "Optimum transfer between asymptotes about a planet of finite size". Ph.D. Thesis. Department of aerospace engineering science ; University of Colorado, Boulder, Colorado (May 1973).
59. C. Marchal - "Optimisation de la phase exté-atmosphérique de la montée en orbite". La Recherche Aérospatiale n° 116, 118 (1967) et n° 122 (1968) - ONERA - tiré à part n° 560 (1968).
60. D.B. Langmuir - "Low thrust flight : constant exhaust velocity in field-free space". Space technology, chapter 9 (John Wiley and Sons) (1959).
61. T.C. Tsu - "Requirements of interstellar flight". Astronautica Acta VI, p. 247 - 255 (1960).
62. V.K. Isaev - "Le principe du maximum de L.S. Pontryagin et la programmation optimale de la poussée d'une fusée". Revue russe : Automatisme et télémechanique, tome 22, n° 8 (1961).
63. D.F. Spencer - L.D. Jaffe - "Feasibility of interstellar travel". Astronautica Acta, IX, 49 - 58 (1963).
64. G.M. Anderson - P.L. Falb - A.C. Robinson - "One dimensional minimum-time rendez-vous for a thrust limited rocket". AIAA Journal, 5, p. 1017 - 1019 (1967).
65. A.R. Archenti - N.X. Vinh - "Intermediate thrust arcs and their optimality in a central, time invariant force field". Journal of optimization theory and applications, Vol. II, n° 3, p. 293 - 304 (1973).
66. J.P. Peltier - "Contribution numérique à l'étude des rendez-vous optimaux entre planètes massives". Note technique ONERA n° 167 (1970).
67. J.P. Gravier - "Absolute optimum and two-impulse optimal interplanetary transfers with applications to Earth-Mars and Earth-Venus", University of Colorado, Ph.D.Thesis (1970). Also (with Mr Culp) : "Optimal impulsive transfers between real planetary orbits". J.O.T.A. Vol. 15, n° 5, p.587-604 (1975).
68. H.M. Robbins - "Optimality of intermediate thrust arcs of rocket trajectories". AIAA Journal, Vol. 3, p.1094-1098 (1965).
69. A. Archenti - C. Marchal - "Intégration numérique des arcs à poussée intermédiaire de Lawden et étude de leur optimalité (dans un champ newtonien central)", 21<sup>e</sup> Congrès Int. d'Astronautique, Constance, Allemagne (1970) - tiré à part ONERA n° 869 (1970).
70. A. Archenti - J.P. Marec - "On the optimality of Contensou's singular alternating arcs in the optimal transfer problem". J.O.T.A. Vol. 8, n° 1 (1971).
71. C.Aumasson - "Processus aléatoires à commande et applications à l'optimisation stochastique". publication ONERA n° 141 (1972).
72. H. Erzberger - "Application of Kalman filtering to error correction of inertial navigators". NASA technical note D-3874 (February 1967).

# JOINT INFLIGHT BIOMEDICAL EXPERIMENTS PERFORMED DURING THE ASTP SPACEFLIGHT

Gerald R. Taylor, \*Thomas D. Rogers, Margaret E. Brower and Kathryn Kropf

NASA/Johnson Space Center, Houston, TX

\*Northrop Services, Inc., Houston, TX, USA

## Abstract

Two joint inflight biomedical experiments were conducted during the unique Apollo-Soyuz Test Project (ASTP) spaceflight. One experiment evaluated rhythmicity of spore production of *Streptomyces levoris*. The other evaluated components of the infectious disease process by measuring alteration in: (1) the composition of the microbial population inhabiting USA and USSR crewmembers and spacecraft; (2) the ability of each crewmember's defense mechanism to resist infection; and (3) the ability of certain microorganisms to originate infections. These two experiments are described and the major results discussed.

## I. Introduction

In July 1975, a unique spaceflight in which the American "Apollo" and the Soviet "Soyuz" spacecrafts joined together in Earth Orbit. During this historic adventure, a group of five scientific experiments were conducted jointly by members of the Apollo and Soyuz crews(1). Two of these studies were biological and are described in this report.

## II. Evaluation of Spaceflight Factors on the Rhythmicity of Spore Production of *Streptomyces levoris*

### IIa. Introduction

The filamentous bacterium, *Streptomyces* (*Actinomyces* in the USSR) *levoris* Kras was provided from a stock isolated and characterized at the Institute of Biophysics, Puschino, USSR. This microorganism was chosen because, under appropriate conditions, a growing colony will alternate between the production of vegetative cells (mycelia) and the production of spores with predictable rhythmicity(2). It is possible to macroscopically observe the formation of concentric rings of spores and observe any alterations in the periodicity or morphological character of each new ring. For this experiment, four cultures (four separate colonies) were prepared and launched from the Baykonur launch site in the Soviet Union. Likewise, four cultures were prepared in Houston, Texas and launched in the Apollo Spacecraft from Cape Kennedy, Florida, USA. Growth of the two sets of test specimens was controlled so that each set was out of phase with the other by exactly 12 hours. During the period when Apollo and Soyuz were linked together in Earth Orbit, two cultures from each craft were transferred to the other. Therefore, two original and two exchanged cultures were recovered from each spacecraft. Each colony was photographed every 12 hours from the time of culture selection until seven to ten days after return from spaceflight so that any alteration in the growth pattern could be accurately observed(3). Additionally, radiation

detectors were provided so that if point alterations occurred, the possibility of radiation-induced damage could be evaluated.

### IIb. Methods and Materials

Cultures of *S. levoris* were initiated by single-point inoculation of spores on agar-based medium in 60 x 5 mm Petri dishes six days preceding the spaceflight. Phasing of the vegetative and spore production cycle was accomplished in both the USA and the USSR by using a 12-hour light-dark period from 0900 hours to 2100 hours local time. The light-dark cycle was maintained until the cultures were selected for the experiment and placed in the flight devices four days after inoculation. Two cultures of *S. levoris*, each contained in a 60 x 5 mm Petri dish, were placed in each flight device (Fig. 1). Two flight devices (four cultures) were prepared for launch in the Apollo spacecraft and two identical devices with matching cultures were prepared as ground controls in the USA. A similar procedure was followed with Soyuz-launched cultures. The main body of each device consisted of separable halves that were composed of anodized aluminum. A protective glass, fitted with a biologically nonreactive siliconized rubber ring, was inserted beneath the movable lid in the top half of each device. This glass served as a protective cover and permitted observation and photography of the cultures. The bottom of the device, which included the Petri dishes with cultures, spacing rings around the dishes, and siliconized rubber rings below the dishes, was fitted with the top half of the device to complete the assembly. These components of the experiment device are shown in Fig. 2. Radiation detectors of Lexan and cellulose acetate were placed beneath each Petri dish as well as in the movable lid. A dried agar film containing T4Br<sup>+</sup> bacteriophage was also placed under radiation detectors and the Petri dishes of each device.

Following assembly of the devices launched in the Apollo, both the flight and control cultures were placed in a portable incubator and maintained at 27°C during transport to the launch site. The control cultures were maintained in the incubator during the entire course of the experiment. Following recovery, the flight specimens were again placed in the portable incubator and maintained at 27°C until termination of the experiment. A similar procedure was followed by both laboratories.

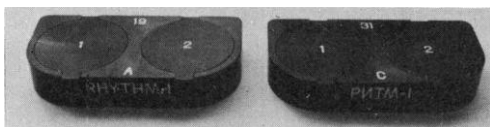


Fig. 1. Example of flight devices.

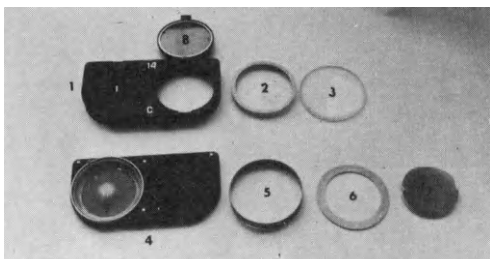


Fig. 2. Photograph of the components of a flight device.

- (1) Upper half of the device with movable covers.
- (2) Siliconized rubber ring, fits around protective glass.
- (3) Protective glass rings, which are inserted into upper half of device, serve to protect specimen in Petri dish.
- (4) Bottom half of the device.
- (5) Metal spacing ring.
- (6) Siliconized rubber washer, fits in well of lower half.
- (7) Radiation detector, placed in bottom of the device under Petri dish.
- (8) Radiation detector in movable cover.
- (9) Petri dish and specimen.

Photography of the specimens was initiated at the time the cultures were assembled in the flight devices. Both control and flight specimens were photographed at 12 hour ( $\pm 3$  hours) intervals until termination of the experiment. A Nikon 35 mm camera equipped with a 55 mm lens (F 2.8) and adapted with a special framing device to facilitate focusing was used for photography. This visual documentation was used to provide a comparative basis for growth analyses<sup>(3)</sup>.

### IIC. Results and Discussion

Cultures were initiated for the experiment in both the USA and the USSR on 9 July 1975. At the respective launch times on 15 July, the rate of vegetative growth and the subsequent spore ring development (biorhythm) was different. The difference in growth rate and frequency between the two sets of cultures continued throughout the experiment. The total number of spore rings formed by the control and flight cultures at the end of each of the three periods are shown in Table 1. Since there was a three day difference between the American and Soviet inflight timelines, the average growth rate per day for each culture during each experiment period is also shown. This latter value provides a more uniform basis of comparison between cultures.

The controls cultured in the USA grew at the same rate when compared with each other within a given time period, with the exception of number 2

of A-25, which exhibited a slight decrease in growth rate during the postflight period (see Table 1). During the preflight period, the flight cultures (A-19 and A-22) exhibited growth rates identical to the controls. At the end of the inflight period, the flight specimens showed a noticeable difference in the growth rate and frequency.

Table 1 Growth rate of *Streptomyces levoris* during ASTP

Source	Status	Device	Culture	Preflight period		Inflight <sup>1</sup> period		Postflight <sup>2</sup> period	
				Number of rings	Growth rate <sup>3</sup>	Number of rings	Growth rate	Number of rings	Growth rate
USA	Control	A-24	1	4.0	1.0	9.5	0.61	13.0	0.44
			2	4.0	1.0	9.5	0.61	13.0	0.44
	Flight	A-25	1	4.0	1.0	9.5	0.61	13.0	0.44
		A-25	2	4.0	1.0	9.5	0.61	12.5	0.38
	Flight	A-22	1	4.0	1.0	8.0	0.4	12.0	0.5
		A-22	2	4.0	1.0	10.0	0.66	15.0	0.63
USSR	Control	C-35	1	3.0	0.75	6.1	0.52	9.5	0.31
		C-35	2	3.0	0.75	6.1	0.53	9.3	0.29
	Flight	C-36	1	2.0	0.5	6.0	0.67	9.2	0.29
		C-36	2	2.0	0.5	6.2	0.7	11.5	0.48
	Flight	C-31	1	3.0	0.75	5.0	0.33	9.3	0.39
		C-31	2	2.8	0.7	4.8	0.33	8.5	0.33
	Flight	C-12 <sup>6</sup>	1	2.5	0.63	7.3	0.53	10.3	0.38
		C-12 <sup>6</sup>	2	2.3	0.58	6.3	0.44	9.2	0.36

1. USA inflight period - 15 July to 24 July; USSR inflight period - 15 July to 21 July.

2. USA postflight period - 24 July to 1 Aug.; USSR inflight period 21 July to 1 Aug.

3. Total number of rings at the end of each period.

4. Number of spore rings formed per day during each period.

5. Exchanged from Apollo to Soyuz on 17 July.

6. Exchanged from Soyuz to Apollo on 17 July.

The temperature profile in the Apollo spacecraft is shown in Fig. 3. Even though this reduced and variable temperature would cause a decreased growth rate, this factor alone does not explain the differences observed in the flight cultures during the inflight period. The growth rate of the inflight cultures would have decreased uniformly if temperature were the only factor involved. One or more physical factors of spaceflight (weightlessness, magnetic field forces, and possible solar effects) appear to have invoked various effects on the growth rate periodicity since the spaceflight cultures exhibited different types of growth patterns and biorhythms. Some of the more apparent differences are: (1) Increased growth rate of number 2 of A-22 which grew more rapidly during spaceflight and at a reduced temperature than did the other spaceflight cultures or the controls. (2) Differences in reduced growth rate of spaceflight cultures even though they were at the same temperature (number 1 of A-22 as compared with number 2 of A-22, number 1 of C-12 as compared to number 2 of C-12). (3) Differences between the flight cultures of each group (A-22, A-19 and C-31, C-12) even though it is difficult to directly compare since A-19 and C-12 were exchanged during spaceflight.

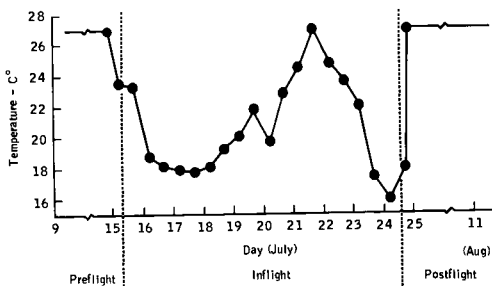


Fig. 3. Apollo temperature profile during ASTP

Spore ring morphology during the inflight period was distinct and in general, exhibited no alteration of growth pattern. Spores failed to form in two distinct areas of the last inflight spore ring of number 1 of A-19 (see Fig. 4). At first, it was suspected that this void area in the spore ring would be the result of the radiation effects, however, in a postflight radiation experiment study where *Streptomyces* cultures were subjected to Neon ions with radiation ranges of 100-10,000 rads, not a single aberration of this nature was observed. No other explanation for this type of aberration is suggested at this time, especially in view of the fact that a number of variables are known to have been involved when comparing the spaceflight cultures with each other or with ground controls(4). Spore ring offsets and subsequent spiral ring formation (Fig. 5) also occurred during the spaceflight period in number 2 of A-22. Similar offsets and spirals were observed in the ground controls.

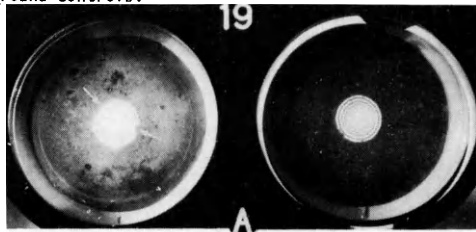


Fig. 4. Photograph of cultures of A-9 showing the last inflight spore ring where spores failed to form (indicated by arrows).

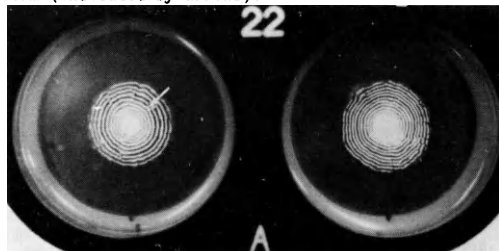


Fig. 5. Examples of offsets and spiral spore rings developed inflight.

Unusual double spore rings were formed during the immediate postflight period in cultures A-19 and number 2 of C-31 (Fig. 6-7). Although it may be coincidental, it is also possible that the dynamics of physical forces related to reentry and landing of Soyuz may have attributed to the growth pattern aberrations. The subsequent spore rings in the cultures developed in a normal pattern. This type of aberration was not observed in the specimens recovered from Apollo. Postflight subculturing of the USA and the USSR control and spaceflight cultures revealed little or no difference in the growth rates or spore ring formation when grown on the standard culture medium.

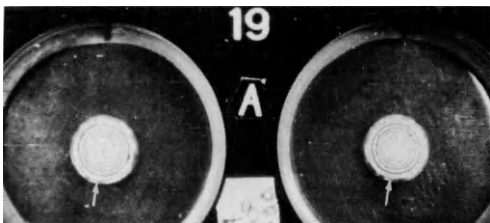


Fig. 6. Double spore rings formed during the immediate postflight period in A-19.



Fig. 7. Double spore rings formed during the immediate postflight period in number 2 of C-31.

Prior to inoculation of cultures for the spaceflight experiment, an attempt was made to standardize procedures and components of the nutritional medium, however, specific chemicals were not obtained from the same sources in all cases. The differences in growth rate observed between the two sets of cultures (USA and USSR initiated cultures) was probably due to a slight difference in the medium rather than an inherent biorhythm difference between the source cultures for the experiment.

Preliminary examination using scanning electron microscopy revealed an irregular and elongated spore morphology in some portion of both of the flight cultures when compared with the controls (see Fig. 8). Spores of number 2 of A-22 exhibited a greater deviation from the normal spore morphology than did any of the other spaceflight cultures (see Fig. 9); however, spores which formed during the postflight period appeared similar to those of the controls. Investigations are in process to determine if this abnormal spore morphology will appear in subculture.

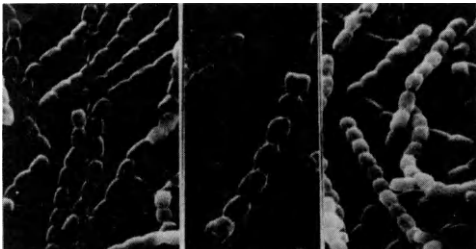


Fig. 8. Scanning electron microscope photographs of representative control spores.

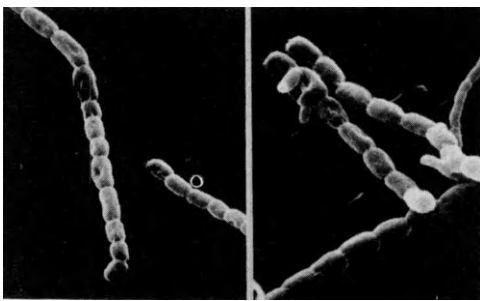


Fig. 9. Scanning electron microscope photographs of irregular and elongated spores from spore rings found inflight in number 2 of A-22.

#### IId. Conclusion

There is an ordered oscillation of cellular events which is visibly manifest in *S. levoris* and which results in the intrinsic rhythm of the vegetative and spore phases. This experiment was conducted in an attempt to evaluate the stability, or instability, of this intrinsic rhythm during short-term spaceflight. Although differences were observed in the biorhythm of the test species during spaceflight, the differences were not uniform. Accordingly, the resulting data were not suitable for statistical analysis (as is often the case with spaceflight experiments). Largely because of the variations in growth rate, it was not possible to demonstrate that the time phase shift affected the biorhythm in the exchanged spaceflight specimens.

It is important to keep in mind that variations in temperature, nutritional medium components, and light conditions could have perturbed the results. It appears that the single most variable factor was a lack of temperature control during spaceflight. Although the general temperature profile can be repeated on subcultures under laboratory conditions, the influences of weightlessness, and other unique spaceflight factors (such as HZE radiation, launch vibration, and recovery shock) can not be simultaneously reconstructed.

The results obtained from this experiment

indicate that spaceflight did effect the biorhythm of *S. levoris* vegetative and spore stages. However, because of the interaction of certain uncontrolled and irreproducible variables, the magnitude of such an effect cannot be accurately determined.

### III. Microbial Exchange Experiment

#### IIIa. Introduction

The Microbial Exchange Experiment was designed to monitor the microbial load of the five flight and five backup crewmembers of the Apollo and Soyuz spacecraft and to evaluate the status of certain components of the immune mechanism of each individual. In addition, selected inner surfaces of both spacecraft were periodically sampled for microorganisms.

To accomplish this objective, the normal auto-flora and immunocompetence level of each crewmember was established before flight through repeated sampling and analyses. Therefore, quantitative and qualitative change occurring during or after flight could be measured and evaluated, and instances of intercrew transfer of marker organisms could be identified. At the same time, certain immunological parameters of the blood and saliva of each crewmember were studied to determine if there were postflight changes in the ability of the individual to resist infection. The monitoring of two crews, which differed microbiologically and immunologically, provided a unique opportunity to study inflight cross-contamination patterns. Since the two ASTP crews came from widely different geographical and ecological areas, it was possible to identify specific, naturally occurring, marker microorganisms for detailed analysis. Only the microbial monitoring portion of this experiment is reviewed in this communication.

#### IIIB. Methods and Materials

Specimens for microbiological analysis were recovered from each of the 10 sample collection sites outlined in Table 2. Samples were collected from all 10 crewmembers (three Apollo and two Soyuz flight personnel; three Apollo and two Soyuz backup astronauts) at five different times the last 45 days before flight so that preflight baselines could be established. Analysis of additional specimens collected during the flight and immediately after return of the subjects from space provided the comparative information required to evaluate the effect of the ASTP mission on the medically important microorganisms carried by each crewmember.

Inflight samples, consisting of the first six areas outlined in Table 2 were obtained from all five flight crewmembers between 77:40 and 78:30 Soyuz ground-elapsed time. For this set of samples, the specially developed sample collection device illustrated in Fig. 10 was employed. This device consisted of a cotton-tipped teflon swab on a capillary tube which contained conservative fluid to keep the microorganisms alive. This conservative fluid was selected following extensive experimentation conducted jointly by American and

Soviet investigators. Each swab was housed within an air-tight case to prevent desiccation.

Table 2. ASTP crew sample collection sites.

SAMPLE DESIGNATION	AREA SAMPLED
HAIR	20 CM <sup>2</sup> AREA OF HAIR (AND SCALP) ON TOP OF HEAD
EARS	RIGHT AND LEFT EXTERNAL AUDITORY CANALS WITH TWO REVOLUTIONS OF EACH SWAB IN EACH EAR CANAL
NECK	20 CM <sup>2</sup> BELOW HAIRLINE AT BASE OF NECK
NARES	INTERNAL AREA OF BOTH NOSTRILS
THROAT SWAB	SURFACES OF TONSILS AND POSTERIOR PHARYNGEAL VAULT
HANDS	20 CM <sup>2</sup> ON RIGHT AND LEFT PALMS
AXILLAE	20 CM <sup>2</sup> BELOW HAIR AREA ON EACH SIDE
GROIN	5 CM STRIP FROM REAR TO FRONT ON RIGHT AND LEFT INGUINAL AREA BETWEEN LEGS
TOES	AREA BETWEEN THE TWO SMALLEST TOES OF EACH FOOT
GARGLE	10 CM <sup>2</sup> PHOSPHATE BUFFER USED AS GARGLE AND WASHED THROUGH ORAL CAVITY THREE TIMES

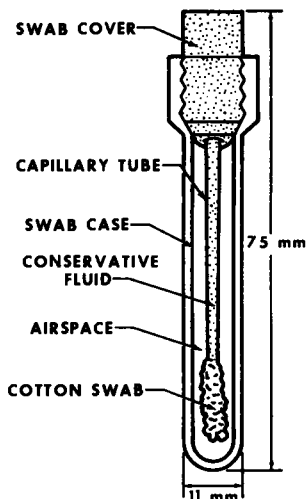


Fig. 10. Inflight sample collection device.

The contents of each swab and each gargle were serially diluted under aseptic conditions and subsequently inoculated onto the surfaces of appropriate nutrient media. Following incubation, the resulting aerobic bacterial colonies were evaluated with suitable biochemical techniques. Medically important microorganisms were identified and quantitated. Analyses of Apollo crewmember samples were conducted at the NASA laboratories in Houston, Texas whereas evaluations of specimens from Soyuz crewmembers were conducted at the Institute of Biomedical Problems of the USSR Ministry of Health in Moscow. Although these studies were conducted individually, a common methodology was used to ensure comparability of data<sup>(5)</sup>,

### IIIc. Results and Discussions

The number of viable bacterial cells recovered from the skin sites of all five flight crewmembers was determined and is illustrated in Fig. 11. These data show no significant differences between subjects, indicating that Apollo and Soyuz crewmembers retained about the same microbial load on their skin in spite of the geographical and cultural differences involved. The data in Fig. 11 also show that the values obtained immediately after spaceflight were within the preflight range, demonstrating that the population of aerobic bacteria (measured in terms of total viable cells) inhabiting the integumentary surfaces was stable following spaceflight.

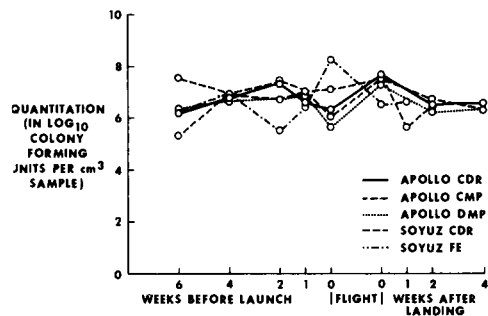


Fig. 11. Number of aerobic bacterial cells in skin samples from ASTP crewmembers.

Analyses of the bacterial load recovered from the nasal and oral cavities of ASTP crewmembers were likewise determined and are presented in Figures 12 and 13 respectively. The upper respiratory tract samples obtained from cosmonauts yielded counts that were generally lower and more variable than those obtained from astronaut specimens. Even with this variability, the resulting data show that the spaceflight had no demonstrable effect on the total bacterial load recovered from the oral and nasal cavities.

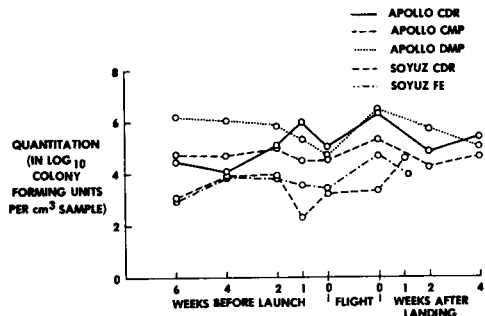


Fig. 12. Number of aerobic bacterial cells in nasal cavity samples from ASTP crewmembers

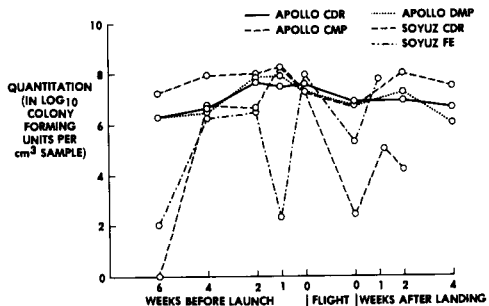


Fig. 13. Number of aerobic bacterial cells in oral cavity samples from ASTP crewmembers.

Analysis of samples obtained within the Apollo and Soyuz spacecraft before, during, and after flight resulted in the data illustrated in Fig. 14. Most sampled areas were not sterile before flight and thus afforded a potential source of contamination to the crew. Contamination within the Soyuz spacecraft was increased (by one order of magnitude) the day of return from spaceflight, a response similar to those previously reported for other spaceflights (6,7,8). Contamination within the Apollo craft was measurably decreased after the flight. This situation was probably the result of prolonged contact of the sampled surfaces to a dinitrogen tetroxide-nitrous oxide gas mixture which had inadvertently entered the spacecraft during the landing procedure. It is important to note that this toxic gas affected the contamination level of spacecraft surfaces but did not measurably influence the astronaut autoflora. This occurred because the autoflora components were better protected from outside effectors and had a significantly shorter contact time with the toxic gas.

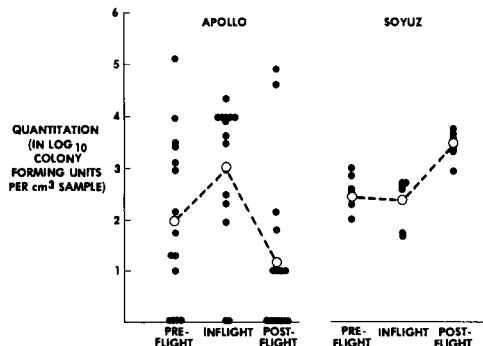


Fig. 14. Number of aerobic bacterial cells on spacecraft internal surfaces (ASTP mission).

A number of different microbes which occur normally in the intestinal tract, or are associated with intestinal infection, are placed in the enteric group of microorganisms. The normally occurring members of this group are generally considered of potential medical importance when recovered repeatedly, or in large numbers, from sites other than the lower digestive tract. It has previously been reported (9,10) that the Gram-negative rod component of the autoflora could change during or following confinement in a closed environment, and that this change could result in "dysbacteriosis," such as a flooding of the oral cavity with a particular species. However, when considered as a unit, the quantitation of Gram-negative rods recovered from ASTP crew-members was too variable to establish any flight-affected alteration. This is to be expected because these species are mostly transient to the human body rather than being true members of the autoflora (except in the lower gastrointestinal tract which was not evaluated in this study). There was, however, an increase in the number (incidence) of cosmonaut body sites from which Gram-negative rods were recovered upon return from spaceflight. This spreading of bacteria to previously uncontaminated sites probably resulted from the altered hygiene regimen employed aboard the Soyuz spacecraft.

Of the Gram-negative rods recovered, only members of the genus Haemophilus are indigenous to the human autoflora, being continually present in the oral cavity. Therefore, it is possible to evaluate changes only with these microorganisms. The data illustrated in Fig. 15 show that there was a quantitative decrease in the recovery of Haemophilus in both prime and backup crewmembers immediately preceding the flight. This decrease coincides with the preflight maintenance of these subjects in protective isolation, a procedure which has been shown to minimize the probability of preflight and inflight infections in previous spaceflights (6,11). The load of Haemophilus cells in the oral cavity of all three of the flight astronauts was significantly reduced during the flight but remained constant in the nonflight control group. This demonstrates a decrease in the relative importance to the autoflora of these potential pathogens during spaceflight.

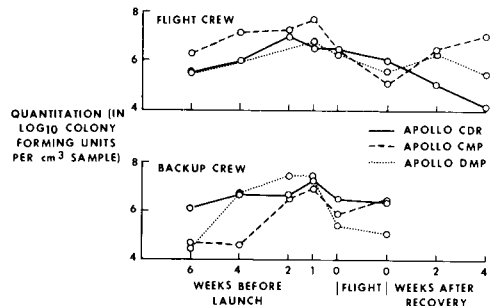


Fig. 15. Number of Haemophilus cells in oral cavity samples from ASTP astronauts.

None of the observations above support the view that Gram-negative rods undergo unfavorable dysbacteriotic changes following spaceflight. Therefore, those few instances where such changes have been reported should be considered to be coincidental with, and not a function of, spaceflight.

*Candida albicans*, which has long been recognized as a normal component of the indigenous auto-flora of man, has frequently been recovered from the crewmembers of previous spaceflights and spaceflights and space simulation missions<sup>(1,2,13,14)</sup>. Because this species has been identified as the causative agent for serious oral cavity disease, its presence in the mouth of ASTP crewmembers was carefully monitored. *C. albicans* was carried by the Apollo Command Module Pilot and the Apollo Docking Module Pilot before flight and was transferred to the Apollo Commander during the ASTP mission. No such transfer occurred with the Apollo, although this species was routinely carried in the mouth of the backup Apollo Command Module Pilot. Among the Soyuz cosmonaut population, *C. albicans* was recovered only from the prime Flight Engineer 33 and 15 days before launch, and therefore was not considered of medical importance during the flight.

Although *Staphylococcus aureus* microorganisms are not uncommon skin and nasal contaminants, all strains are potential pathogens. The results of several spaceflight-simulation studies have suggested increases in the toxigenic activity, virulence, or pathogenicity of this species with stressful confinement of the human host<sup>(9,10,15)</sup>. The recovery of strains of *S. aureus* from the 10 ASTP crewmembers is presented in Table 3. These data show that each crewmember carried a different strain, each of which is expressed as a numbered bacteriophage type. Type 52, 52A, 80, 81 was carried by the Apollo Prime Docking Module Pilot and was transferred to the Apollo Prime Commander during flight. There was no transfer demonstrated between crews.

Table 3 *Staphylococcus aureus* strains carried by ASTP crewmembers.

CREW	FLIGHT STATUS	POSITION	QUANTITATION		PREDOMINANT BACTERIOPHAGE TYPE CARRIED
			PREFLIGHT MEAN	POSTFLIGHT	
APOLLO	FLIGHT	ACOR	3.04	1.95	NOT TYPABLE
		CMP	2.06	0	53.83A.85
		OMP	1.10	1.30	52.52A.80.81
	BACKUP	ACDR	1.85	0	3A.3C
		CMP	3.80	3.86	56.71
		DMP	3.23	4.83	29.53.54.75.79.80
SOYUZ	FLIGHT	SCDR	2.82	3.36	53.54.80.81
		FE	3.15	4.85	6.42D.42E.47.53.81
	BACKUP	SCDR	2.27	...	6.53.75.85
		FE	2.48	...	52.53

QUANTIFICATIONS GIVEN AS LOG<sub>10</sub> COLONY FORMING UNITS PER cm<sup>3</sup> SAMPLE.

A postflight increase in the incidence of *S. aureus* has previously been reported<sup>(10)</sup>. This could not occur during the ASTP mission because of the universal presence of this species before flight. However, there was a measurable increase in the number of *S. aureus* cells recovered from prime Soyuz crewmembers immediately after the flight. Although recovery incidence and quantitation of this medically important species was unusually high, no disease events were reported.

Several authors have warned that returning space travelers may experience a "Microbial Shock" and may respond negatively to renewed contact with potentially pathogenic microorganisms which were absent in the spaceflight environment<sup>(16,17,18)</sup>. These warnings were based on the assumption that contact with potential pathogens during spaceflight would be very limited, resulting in a reduction of immunocompetence. However, there was no demonstrable decrease in the incidence of medically important microorganisms recovered from the ASTP crewmembers on recovery day, a finding which supports earlier reported results. Accordingly, there were no postflight disease events reported. Therefore, neither the proposed simplification of the population of medically important microorganisms, nor the theorized postflight microbial shock, could be supported by the results of this study.

#### Acknowledgment

The authors wish to thank the laboratory personnel of Northrop Services, Inc., Houston, TX without whose technical expertise these studies could not have been accomplished. The cooperative assistance of I. G. Akoev and his staff at the Institute of Biophysics at Pushchino and S. N. Zaloguev and his staff at the Institute of Biomedical Problems, Ministry of Health, Moscow, USSR, is also greatfully acknowledged.

#### References

- (1) Giuli, R. T., "Summary of Scientific Results," In: Apollo-Soyuz Test Project Preliminary Science Report, NASA Document TMX-58173, Lyndon B. Johnson Space Center, February 1976, pp. 1-1 through 1-4.
- (2) Akoev, I. G., Saveliev, and Akhamadieva, H. K., "Preliminary data on the Apollo-Soyuz Test Project Experiment Zone-Forming Fungi-Biorhythm," COSPAR, Life Sciences and Space Research XV, in press, 1976.
- (3) Rogers, T. D., Taylor, G. R., and Brower, M. E., "Zone-Forming Fungi Experiment MA-147." In: Apollo-Soyuz Test Project Preliminary Science Report, NASA Document, TMX-58173, February 1976, pp. 15-1 through 5-12.
- (4) Rogers, T. D., Brower, M. E., and Taylor, G. R., "Growth Rate Periodicity of *Streptomyces levoris* During Spaceflight." Life Sciences and Space Research. In press, 1976.
- (5) Taylor, G. R. and Zaloguev, S. N., "Methods for Microbiological and Immunological Studies of Spaceflight Crews," TMX-48185, NASA, Lyndon B. Johnson Space Center, Houston, TX, in press, 1976.

- (6) Ferguson, J. K. Taylor, G. R., and Mieszkuc, B. J., "Microbial Investigation." In: Biomedical Results of Apollo, NASA Special Publication SP-368, pp. 83-103, 1975.
- (7) Taylor, G. R., "Apollo 14 Microbial Analyses" NASA TMX-58094. November 1972.
- (8) Taylor, G. R. "Apollo 14 Microbiology," Annual Reviews of Microbiology 40, 1974, pp. 23-400.
- (9) Nefedov, Yu. G., et al., "Microbiological and Immunological Aspects of Extended Manned Space-flights," Life Sciences and Space Research, Akademie-Verlag, Berlin, Vol. 9, pp. 11-16.
- (10) Shilov, V. M., et al., "Changes in the Microflora of Man During Long-Term Confinement," Life Sciences and Space Research, Akademie-Verlag, Berlin, Vol. 9, 1971, pp. 43-49.
- (11) Taylor, G. R., "Recovery of Medically Important Microorganisms from Apollo Astronauts," Aerospace Medicine, Vol. 45, August 1974, pp. 804-828.
- (12) Taylor, G.R., Henney, M. R., and Ellis, H.L., "Changes in the Fungal Autoflora of Apollo Astronauts," Applied Microbiology, Vol. 26, November 1972, pp. 803-813.
- (13) Zaloquev, S. N., Shinkarvera, M.M., and Utkina, T. G., "State of Automicroflora of Skin Tissue and Certain Natural Immunity Indices in the Astronauts," Kosmicheskaya Biologiya i Meditsina, Vol. 4, 1970, pp. 54-59.
- (14) Zaloquev, S.N., Utkina, T. G., and Shinkareva, M.M., "The Microflora of the Human Integument During Prolonged Confinement," Life Sciences and Space Research, Vol. 9, 1971, pp. 55-59.
- (15) Chukhlovia, P. B., Ostrovmov, P. B., and Ivanova, S. P., "Development of Staphylococcal Infections in Human Subjects Under the Influence of Some Spaceflight Factors," Kosmicheskaya Biologiya i Meditsina, Vol. 5, 1971, pp. 61-65.
- (16) Berry, C. A., "Summary of Medical Experience in the Apollo 7 through 11 Manned Spaceflights," Aerospace Medicine, Vol. 41, May 1970, pp. 500-519.
- (17) Luckey, T.D., "Potential Microbic Shock in Manned Aerospace Systems," Aerospace Medicine, Vol. 37, 1966, pp. 1223-1228.
- (18) Spizizen, J., "Microbiological Problems of Manned Spaceflight," Life Sciences and Space Research, Akademie-Verlag, Berlin, Vol. 9, 1971, pp. 65-68.

# PROBLEMS OF CREATING CLOSED BIOLOGICAL LIFE SUPPORT SYSTEMS

I. I. Gitelson, I. A. Terskov, B. G. Kovrov, G. M. Lisovsky and F. Ya. Sidko

*The USSR Academy of Sciences, USSR*

## Abstract

The experiment lasting half a year was with a crew of 3 men. The recovery of  $O_2$  and water was accomplished through photosynthetic process. A part of wheat and vegetables was also produced in the system. All the processes were controlled by the crewmen. The result obtained established beyond question that a small closed ecosystem is quite feasible. The possibility of biological systems to support the life through closed substance turnover is their great advantage which should be realized at the coming stage of manned space activity. Solution obtained with developed ecosystems will find applications in the Earth as an important problem today concerning the protection of the Earth's large ecosystem from contamination by waste products.

The idea of creating closed substance turnover on board a spacecraft first introduced by K.E.Tsiolkovsky and analyzed theoretically in the works of Mayers, Violetta, Nichiporovich, Shepelev and others after the first manned space flight has been confirmed experimentally.

At the XIX, XX, XXIY, XXY IAF Congresses we reported various stages of the development of an experimental ecological life support system.

It was a research and developmental effort oriented primarily toward the establishment of metabolic balance between man's oxidative processes and plant's regenerative processes. Different variants of this system including continuous culture of microalgae (chlorella), high plants (continuous flow culture), and the combination of these has been developed.

The recent experiment lasting half a year was performed with a crew of 3 men. The recovery of oxygen from atmospheric  $CO_2$  and that of wash and potable water was

accomplished in the system through photosynthetic regenerative process. A certain amount of grain and vegetables was also produced in the system. All the processes were controlled by men who inhabited the system.

The result obtained established beyond question that a small steadily-operating essentially closed system of substance turnover involving man is quite feasible.

That's why at present some problems of further development of biological life support systems should be considered.

The major problem is to improve the degree of metabolic closure of the ecosystem. The solution to this problem lies in minimizing a share of food provisions stored. A large amount of food products must be produced in the system.

In the present experimental ecosystem all food provisions consisted primarily of a menu of traditional food which was obtained in the non-traditional way. The problem to be solved is to introduce into a menu non-traditional food products. These will include certain higher plant species and parts of edible plants which are not commonly used as food and biosynthetic products of unicellular organisms.

All known food ingredients can be reproduced by microbial biosynthesis. However as indicated by studies such biomass will not be digested in a proper way as intestinal peptidases have limited ability to attack it. The possibility of introducing into a menu products of microbial synthesis will arise when the mechanism responsible for this limited digestion is disclosed.

Another major problem is to guarantee the stability of artificial small ecosystems in which ecological mechanism of large natural cenosis stabilization do not work. Instabilities of small

artificial ecosystems are brought about about by biological and technological reasons. The first ones include a) endogenous factors, i.e. metabolic instability is due to changes in genetic programme of the main links of the ecosystem caused by mutation and selection processes; exogenous factors, i.e. invasion and division of foreign genomes causing biosynthetic processes to deviate from the preset program and the balance exchange in the system.

At present these instabilities are mainly due to the lack of advanced and effective technology as modern equipment unlike living organisms is not capable of self-reconstruction. Thus a major bio-engineering task is to develop technology which is nearly as reliable as living components of an artificial ecosystem.

Instabilities due to endogenous factors more than once predicted by Odum and Cook were not observed in our experiment. As concluded from an analysis in small artificial ecosystems like continuous flow culture effective are stabilization mechanism like autoselection and autostabilization. Division of accompanying microbial flora and viruses may greatly contribute to destabilization of the system. Experiments lasting to 6 month did not show any significant changes in the test environment caused by bacterial infection, but a balance of accompanying microbial flora was not achieved either. Evolution of microbial flora is a factor which creates a threat to the existance of the system. Principles of ecological control of this non-functional but inevitable component of the ecosystem should be developed.

Another pressing problem is that of maintaining optimal environment for man. The advantage of artificial biological systems over physical chemical ones is that in artificial biological systems as well as in natural ecosystems environment is regenerated by biological factors (Shepelev). Now when the possibility of environment regeneration in artificial

ecosystems has been proved one should define quantitatively and more precisely the term "optimal environment for man" the maintenance of which is the aim of an ecosystem. In order that life support systems be economic with relation to size weight and power requirements the environmental parameters are usually fixed. However numerous physiological and psychological data tend to indicate that optimal environment for man is that which is rhythmically fluctuating. Therefore it is necessary to find out optimum characteristics of environmental parameters fluctuations and to develop ecosystems which are capable of simulating such fluctuations.

Another problem is that of determining the fields of applicability of artificial ecosystems employing biological substance turnover.

With an energy and weight approach currently used in the space technology biological systems can be as good as physical chemical ones.

But at the present stage of space research the energy-weight criterion can not be regarded as sufficient. New means of space transportation will permit long-duration manned space flights and long term manned activity in space and in other planets. The problem then arises is that of protecting space environment and cosmic bodies from contamination by waste products. It is of importance primarily because in known planets biological substance turnover which could consume waste products does not occur. The possibility of biological systems to support the normal functioning of the organism through closed substance turnover is their great advantage which should be realized at the coming stage of space research. Solution obtained with developed model ecosystems based on closed substance turnover will find a wide application in the Earth as an important problem today concerning the protection of the Earth's large ecosystem is to develop such technology which would make it possible to avoid industrial wastes.

# THE MAGNETOSPHERE

C. T. Russell

*Institute of Geophysics and Planetary Physics, University of California, Los Angeles,  
Los Angeles, California 90024*

## Abstract

The terrestrial magnetic field shields the earth from the supersonic wind of the expanding solar atmosphere, forming a cavity called the magnetosphere. Since the velocity of the solar wind is supersonic, a detached shock wave stands in front of this cavity. The flow past the cavity is viscous, drawing the field lines back into a long tail. In this paper we review briefly the nature of the magnetosphere, the outstanding problem areas in this field, and what space missions are needed to attack these problems.

## I. Introduction

Although this paper is scheduled for a session on flight in planetary atmospheres, we will first address the question of the flight of a planetary atmosphere. The planet in question is the earth and its atmosphere will be taken to include its ionized as well as neutral constituents and its shielding magnetic field. After a rather general description of the flight of the terrestrial magnetosphere, we will describe some of the outstanding scientific problems in this discipline, those which may require new missions in the late 70's and earlier 80's for their solution. Finally we discuss what some of these flights in our planetary magnetospheres might be.

## II. Magnetospheric Aerodynamics

### The Cavity

The hot, highly ionized upper atmosphere of the sun, the solar corona, is continually expanding outwards, becoming supersonic beyond about 30 solar radii. This supersonic solar wind confines the terrestrial magnetic field to a cavity with a roughly hemispherical forward end having a radius of curvature of about 10 earth radii, and a long tail about 50 earth radii in diameter extending far past the orbit of the moon in the antisolar direction. We call this cavity the magnetosphere. Figure 1 shows a sketch of the noon-midnight meridian cross-section of the cavity.

The magnetosphere very efficiently shields the earth from the solar wind. Less than 1 percent of the incident energy of the solar wind enters the magnetosphere. Magnetospheric physicists devote most of their efforts to studying the leakage of mass, momentum and energy into the magnetosphere and its consequent effects on the terrestrial environment.

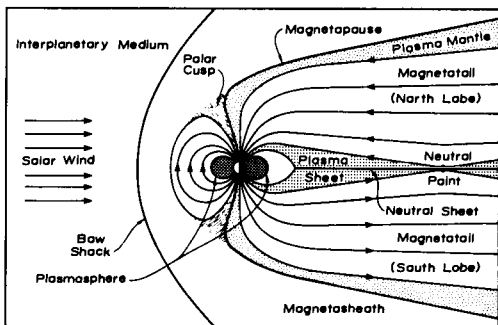


Figure 1. Noon-Midnight Meridian of Terrestrial Magnetosphere

In front of the cavity a bow shock forms, even though there are no particle-particle collisions in the classical sense. The role of collisions is replaced by plasma waves which heat and scatter the electrons and ions of the solar wind.

### Drag and Lift

The interaction of the solar wind with the magnetosphere is in many ways analogous to the flow of hypersonic gas over a blunt object in a wind tunnel. The drag can be computed from the pressure distribution over the boundary surface. There are two sources of drag in ordinary gas dynamics: wave drag and viscous drag. Wave drag is associated with supersonic flow and provides the power to maintain the entropy increase across the bow shock. The viscous drag is due to a component of stress on the boundary itself and is produced in a thin boundary layer. In a magnetized plasma, both normal and tangential Maxwell stresses act in addition to the usual viscous stress. The relative importance of these viscous stresses and their dependence on solar wind conditions is currently one of the most active areas of magnetospheric research and we defer discussion of this topic to a later section.

The wave drag is about an order of magnitude greater than the viscous drag(1). Its strength depends on the shape of the magnetopause, the Mach number of the solar wind, and the specific heat ratio of the plasma(2). Theoretical estimates range from 0.4 to  $3.0 \times 10^7$  N(1-3). Within observational uncertainties the observed drag agrees with theory(4).

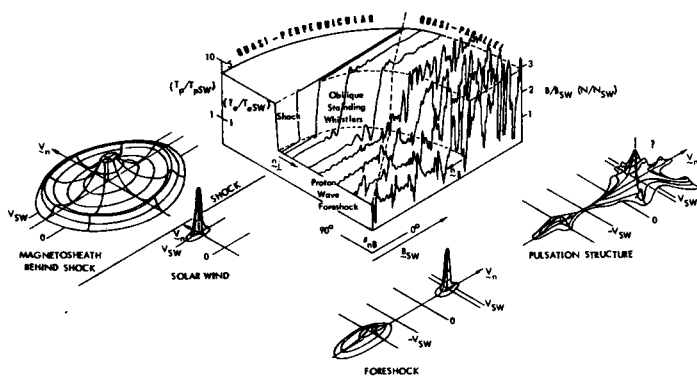


**Figure 2. Schematic Representation of Plasma Distribution Functions and Magnetic Field Profiles as a Function of the Direction of the Magnetic Field Relative to the Shock Normal.**

The magnetosphere has lift both in the east-west and north-south directions. The east-west lift was first treated in references (5) and (6) and later confirmed in (4). The north-south lift is related to the tilt of the dipole axis into the solar wind. It is northward in winter when the north pole points away from the sun(4).

#### The Bow Shock

Despite the fact that the solar wind is collisionless in the classical sense, it behaves in many ways like a fluid. When it intersects the earth's magnetosphere a standing shock wave forms which deflects and heats the solar wind in much the same way air is deflected and heated around a blunt object in supersonic flight. One important difference is that the velocity of wave propagation in the solar wind is anisotropic. Thus, the bow shock structure varies with position along the curved shock front. The anisotropy is controlled by the direction of the solar wind magnetic field. As illustrated in Figure 2, the shock structure is quite smooth for an upstream magnetic field lying in the shock plane (quasi-perpendicular) and quite irregular for fields lying along the shock normal(7).

The shock structure also depends on the Mach number and on the ratio of the magnetic energy density to thermal energy density(8). When both these quantities are small the shock front is termed laminar and when both are high it is called turbulent. The appearance of magnetic profiles through the shock is as suggested by this nomenclature.

Although the morphology of the earth's bow shock is moderately well understood, the detailed physical processes by which plasma waves heat and scatter the solar wind particles is not well understood and will be the subject of much investigation in future years.

#### The Magnetosheath

The region of post shock flow surrounding the magnetosphere is called the magnetosheath. For the macroscopic properties of the flow the gas dynamic analogue works quite well. Again plasma waves act in place of collisions in the ordinary sense and the medium acts as a collisional fluid. Figure 3 shows a gas dynamic calculation of the stream lines and Mach lines for the flow of the solar wind past the magnetosphere(9). This macroscopic behavior is well understood. Of interest in the magnetosheath at present is how energy is coupled to the magnetosphere. For example, one question is whether waves generated ahead of the bow shock be amplified through the shock and be convected against the magnetosphere causing the earth's magnetic field to resonate.

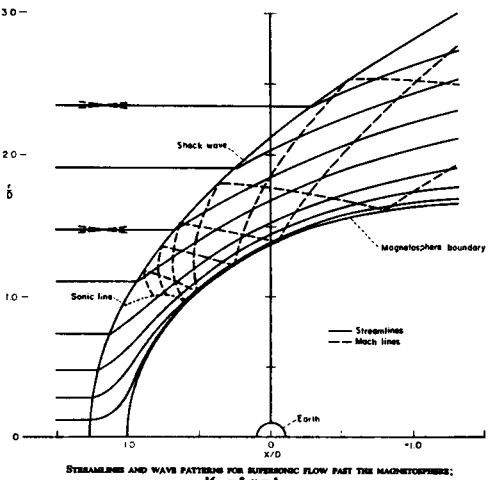


**Figure 3.**

### III. Momentum Transfer

If the boundary of the magnetosphere, the magnetopause, were impermeable to the solar wind flow yet permitted momentum transfer across the boundary, and if the earth did not rotate, we would expect the plasma in the earth's magnetosphere, to move along the streamlines sketched in Figure 4(10). (The effect of the earth's rotation would be to skew the streamlines and destroy the symmetry of the flow.) Such a magnetosphere is called a closed magnetosphere. In this model all terrestrial magnetic field lines cross the surface of the earth twice. Throughout the 1960's, this was the most widely held model. The Kelvin-Helmholtz instability, i.e., the wind over water instability, was believed to be responsible for the momentum transfer(11).

The closed magnetospheric model however does not explain many phenomena in magnetospheric physics. The competing model the open magnetosphere,(12) was much more successful in explaining these phenomena, especially the appearance of energetic solar flare particles over the polar caps, and the auroral zone phenomenon known as a substorm which will be discussed in more detail in the next section. In the open model, the solar wind and magnetospheric plasmas interpenetrate. When this occurs one can trace some magnetic field lines from the surface of the earth (by following a compass in three dimensions) and end up in the solar wind and never return to earth. These field lines are called open field lines and they occur over the polar caps. The process by which the plasma leaves the closed field lines and joins with the solar wind or vice versa is called merging. The plasma leaves closed field lines near local noon (the top of Figure 4) and drifts onto closed lines near local midnight. Thus, the open model alters the streamlines of Figure 4 mainly by having the flow cross the boundary and having the antisunward flow take place in the magnetosheath.

Although there can be no doubt now that the magnetosphere is open, it should be obvious that the mechanisms for momentum transfer that were proposed for the closed magnetosphere will also work in the open magnetosphere and at times may dominate in the momentum transfer. The newest discovery in the magnetosphere is the entry layer(13, 14, 15) a region in which solar wind plasma is streaming across closed field lines. This flow of plasma across a magnetic field is an magnetohydrodynamic generator which causes currents to flow down the magnetic field lines and through the ionosphere(16). The ionospheric currents, provide the load on the generator and pull on the ionospheric plasma. In other words the field-aligned current system and its closure currents transmit the stress from the solar wind to the ionosphere. The decelerated solar wind plasma contributes to the nighttime plasma sheet.

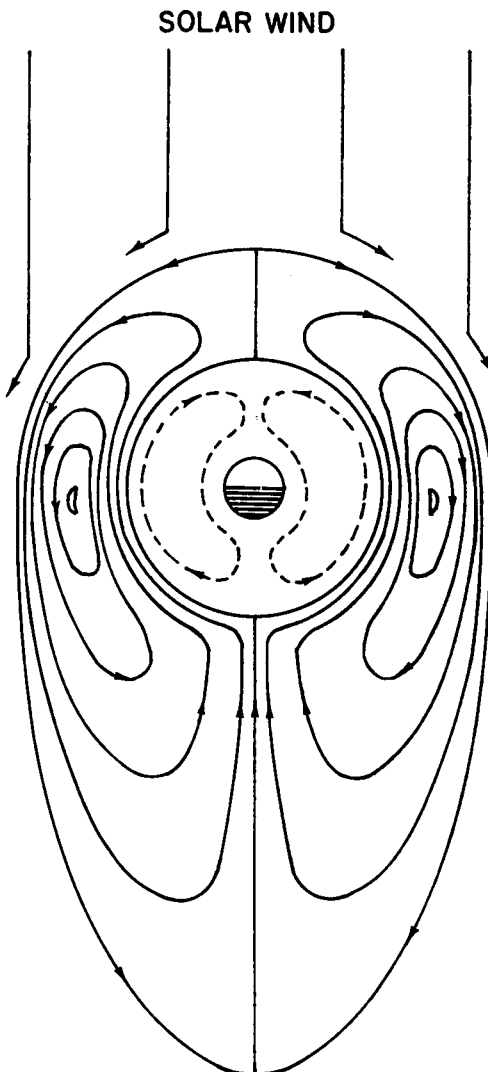


Figure 4. Convection Pattern in Closed Magnetosphere

### IV. Magnetospheric Dynamics

The magnetic field measured on the surface of the earth is due to sources within the earth which change slowly over millennia and sources above the neutral atmosphere, in the ionosphere, in the magnetosphere, in the magnetotail and on the magnetopause which can change significantly on times of minutes to hours. These latter currents produce effects typically 0.1% to 1% of the earth's main field although in the auroral zone the effects may at extreme times approach 10% of the main field.

### Geomagnetic Storms

The first work on the dynamics of the earth's outer magnetic field began in the last century with the study of what we now call geomagnetic storms and with the correlation of auroral occurrences with magnetic field changes. During geomagnetic storms there is often, but not always, a sudden increase in the ground level magnetic field and then a less rapid but much stronger depression in the field strength lasting sometimes many days. The cause of the sudden increase in the field strength is now known to be an increase in the strength of the solar wind and the consequent compression of the magnetosphere. The decrease in the field strength occurs when the momentum transfer rate increases leading to energization of particles in the magnetosphere. The field strength recovery occurs as these energized particles are lost upon collision with the neutral atmosphere(17).

### Aurora

If the rate of loss of energy of the magnetospheric particles to the atmosphere is great enough, emissions in the upper atmosphere, the aurora, can be seen from the ground. Usually the loss rate is great enough only at high northerly and southerly latitudes in the so-called auroral zones. However, on occasion aurora have been seen as far south as Mexico City and Singapore. In the auroral zone, aurora may be seen on almost any clear night.

During the International Geophysical Year, 1957-58, fish-eye-lens cameras were stationed throughout the auroral oval to photograph the night sky continuously. After much labor, it was shown that aurora occurred almost continuously around the auroral oval from noon to midnight and back, and that auroral phenomena underwent repeated sequences of events every night and sometimes many times on a single night(18). These sequences were called substorms.

Now such a study would be much simpler because we have satellite photos of the aurora which confirm most of the findings of the all-sky camera network. However, as yet the satellite data cannot completely replace the ground data because it is available only once every 90 minutes and because the present pictures are not optimized for auroral studies.

### Substorms

As mentioned above, the auroral displays are an indication of energy deposition in the upper atmosphere and these occur periodically in a sequence of events known as a substorm. The substorm has other than auroral manifestations. It can be observed by its characteristic perturbations in ground based magnetograms. It is associated with characteristic deformations of the magnetosphere. Since energy is re-

leased from the magnetosphere episodically in substorms, and since the magnetosphere is not an infinite reservoir of energy, it would seem natural that the magnetosphere would have a period of energy storage or "growth" before the energy deposition(19). However, this postulate led to one of the longest controversies in magnetospheric studies. It is clear from recent studies that the period of enhanced momentum transfer to the magnetosphere precedes the substorm onset by 1 to 2 hours. The energy stored in the magnetosphere often waits for an external trigger to initiate its release. This release may be a solar wind pressure increase or a lessening of the tangential stress of the solar wind(20, 21).

### V. Magnetosphere - Atmosphere Coupling

In the preceding discussion we have stressed principally the coupling of the solar wind with the magnetosphere and only touched on two of the coupling processes of the magnetosphere with the atmosphere: field-aligned current systems and auroral precipitation of energetic particles. The coupling of the magnetosphere with the atmosphere as illustrated in Figure 5, is now beginning to receive much attention from the scientific community and promises to be the subject of many future studies. Three general areas of great interest are: the relation of field-aligned currents to auroral forms; the acceleration processes of the auroral precipitation; and sun-weather relationships.

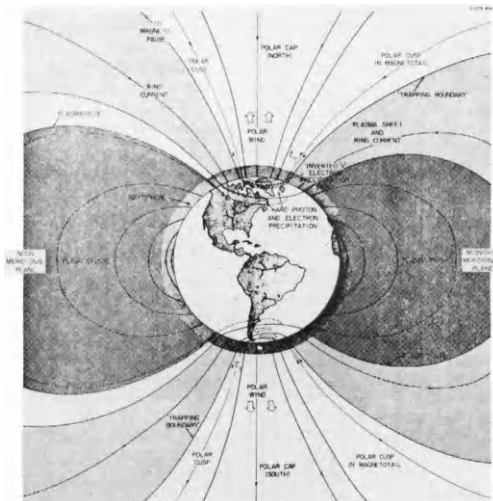


Figure 5. Morphology of the Inner Magnetosphere

### Field-Aligned Currents

Currents flowing along field lines are a ubiquitous feature of the auroral oval. They are seen at essentially all local times and can extend over many hundreds of kilometers in latitude. As observed on polar-orbiting spacecraft, these currents exhibit much structure. We do not know whether this structure is temporal or spatial. Aurora often show strong brightness fluctuations, and they can move rapidly, but they also bend and fold. With single point measurements such as those we have from present-day spacecraft, the best we can do is to assume that the currents are time stationary and flow in planar sheets. Very probably the currents also exhibit motion and spatial structure. In order to unfold this behavior we require simultaneous multipoint measurements of the magnetic field and particles population on overflights of the auroral oval accompanied by multispectral imaging of the auroral forms. Such a problem seems ideally suited to the Shuttle launched Spacelab which will have the ability to carry a comprehensive payload of imagers, and particles and fields instruments as well as to launch and monitor a cluster of subsatellites surrounding the Spacelab.

### Auroral Acceleration Processes

Charged particles are accelerated or decelerated when they move in the direction of an electric field, that is experience a drop in electric potential. In a magnetized plasma an electric field imposed at right angles to the magnetic field will cause the electrons and ions to drift together perpendicular to both the electric and magnetic field. The radial gradient in the magnetosphere and the curvature of field lines can cause energetic, or hot, particles to drift through potential drops but these processes do not energize the cold particles.

Electric fields parallel to the magnetic fields would at first appear to be the obvious mechanism for accelerating low energy particles. However, it was long thought that the high mobility of charged particles along field lines would soon neutralize any potential difference along a field line. This mobility, though, can be reduced by plasma wave turbulence. One possible scenario takes place in a magnetic flux tube carrying current from the ionosphere to the magnetosphere. The magnetospheric plasma can sustain only so much current density and the current becomes unstable to plasma wave turbulence which limits the current density. However, a current passing through a resistive medium must experience a potential drop. Electrons encountering this resistive upward flowing current will then be accelerated downwards causing an auroral arc at the bottom of the flux tube.

This mechanism is not the only one for creating parallel electric fields, but it illustrates the possible close interrelationship of various auroral processes and the need to study them simultaneously. One way to probe such electric fields is with artificial electron and ion beams. Such beams would also permit the study of current instability processes. Again Spacelab with its ability to carry large comprehensive payloads into space is an ideal platform for these investigations.

### Sun-Weather Relationships

The effect of man's technology on the delicate balance of the ozone layer is at present the subject of much debate. In all the noise and confusion, it is generally overlooked that the ozone layer can be destroyed from above as well as below. Solar particle events also deplete the ozone layer(22). Thus, although there is little energy in the particle eflux from the sun when compared to the output of light, solar activity may act to modulate the energy received by the surface of the earth. Thus, studies of the response of the middle and upper ionosphere to solar and magnetospheric activity are of high importance for future investigations.

## VI. Future Needs

Magnetospheric research with satellites has now been in progress for over 15 years and the exploratory phase is over. We now know the qualitative characteristics of all the plasma regimes surrounding the earth. What remains is to study quantitative characteristics and determine which physical mechanisms are operative. Two restrictions on our ability to solve these problems in the past were the availability of only single point measurements in space and the inability to alter the characteristics of the medium, that is, to do a controlled experiment.

### Multipoint Measurements

Simultaneous measurements at a variety of positions throughout the magnetosphere are essential for understanding how it works. Measurements in the solar wind are necessary when data are being gathered in the magnetosphere to provide the boundary conditions need to understand the observed magnetospheric response. Data in the magnetosphere are similarly necessary to provide the magnetospheric context for ground based observations. Since the magnetospheric plasma and its boundaries are constantly in motion dual closely-spaced spacecraft measurements are necessary to turn observed time profiles into spatial profiles.

Such a coordinated program is now well into the planning stage and partially executed at present. This program is the International Magnetospheric Study scheduled for 1976-1978. At present ground

based programs are being initiated and presently operable satellites being used to monitor the magnetosphere and solar wind. In 1977 and 1978, a new generation of magnetospheric spacecraft will be launched: GEOS, an European spacecraft, into geosynchronous orbit; ISEE A/B, a cooperative European-US dual satellite mission, into highly elliptical orbit with apogee at 23 earth radii; and ISEE-C into a heliocentric halo orbit around the sun-earth Lagrangian point(23).

While these missions cover the outer magnetosphere and solar wind-magnetosphere interaction, they provide little data on magnetosphere-atmosphere coupling. A dual satellite mission called Electrodynamic Explorer is planned to probe this region. These satellites will be in quite different orbits, one in a circular polar at an altitude of about 400 km and one in an elliptical polar orbit with apogee about 4 earth radii.

Finally, as we noted above, Space Shuttle will provide an opportunity to fly a network of detectors in low altitude orbit. We must await the outcome of the IMS to determine whether such a cluster of detectors is also necessary for probing the remaining problems in the outer magnetosphere.

#### Active Experimentation

Until recently we were unable to perform classical experiments in the magnetosphere, i.e., introduce a perturbation into the system and watch its response. Our studies consisted of passive observations, waiting until a phenomenon occurred and then trying to understand it. Recently, rocket-launched payloads have fired electron and ion beams into the magnetosphere, and released ion clouds in the ionosphere. Ground based transmitters have been used to heat the ionosphere and interact with the trapped Van Allen belt radiation. These are true experiments and provide excellent testbeds of theory. In the future we wish to perform such experiments in orbit where flight-time is not so short and where an operations plan has time to evolve in response to initial findings.

#### VII. Concluding Remarks

There is no shortage of scientific work to be done in the area of magnetospheric studies, even though much has been learned over the last decade and a half. In fact, it is because of these pioneering efforts, that our present objectives are so well defined. Many of these objectives can be readily attacked using Shuttle launched Spacelabs; others will require the use of free flyers, in particular multispacecraft missions. These measurements will be of interest not just to the magnetospheric physicist but also to atmospheric and plasma physicists and to the man on the street. For not only are these problems of intense scientific in-

terest, they are also of practical concern. Magnetospheric disturbances affect communication, can disrupt power transmission and accelerate pipeline corrosion and may even perturb our weather systems.

#### VIII. Acknowledgments

The National Aeronautics and Space Administration provided support for the preparation of this review under Research Grant NGR 05-007-004.

#### IX. References

1. G.L. Siscoe. A Unified Treatment of Magnetospheric Dynamics with Applications to Geomagnetic Storms. *Planetary Space Sciences*, Vol. 14, 1966, p947.
2. M. Dryer and G.R. Heckman. On the Hypersonic Analogue as Applied to Planetary Interaction with the Solar Plasma. *Planetary Space Science*, Vol. 15, 1967, p515.
3. M. Dryer and R. Faye-Petersen. Magnetogasdynamics Boundary Condition for Self-consistent Solution to Closed Magnetosphere. *AIAA Journal*, Vol. 4, 1966, p246.
4. J.P. Schieldge and G.L. Siscoe, An Empirical Determination of Aerodynamic Factors for the Magnetosphere. *Cosmic Electrodynamics*, Vol. 2, 1971, p141.
5. J.G. Roederer, P.J. Coleman, Jr., W.D. Cummings and M.F. Robbins. Determination of Magnetospheric Parameters from Magnetic Field Measurements at Synchronous Orbit. *Transactions of American Geophysical Union*, Vol. 49, 1968, p227.
6. W.D. Cummings, P.J. Coleman, Jr., and G.L. Siscoe. The Quiet Day Magnetic Field at ATS 1. *Journal of Geophysical Research*, Vol. 76, 1971, p926.
7. E.W. Greenstadt. Phenomenology of the Earth's Bow Shock System: A Summary Description of Experimental Results in "Magnetospheric Particles and Fields" (edited by B.M. McCormac) Reidel Publ. Co., Dordrecht, Holland, 1976.
8. M. Dobrowolny and V. Formisano. The Structure of the Earth's Bow Shock. *Rev. Nuovo Cim.*, Vol. 3, 1973, p419.
9. J.R. Spreiter, A.L. Summers and A.Y. Alksne. Hydromagnetic Flow Around the Magnetosphere. *Planetary Space Science*, Vol. 14, 1966, p223.
10. W.I. Axford and C.O. Hines. A Unifying Theory of High Latitude Geophysical Phenomena and Geomagnetic

- Storms. Canadian Journal of Physics, Vol. 39, 1961, p1433.
11. D.J. Southwood. The Hydromagnetic Stability of the Magnetospheric Boundary. Planetary Space Science, Vol. 16, 1968, p587.
12. J.W. Dungey. Interplanetary Magnetic Field and the Auroral Zones. Physical Review Letters, Vol. 6, 1961, p47.
13. G. Paschmann, G. Haerendel, N. Sckopke, H. Rosenbauer and P.C. Hedgecock. Plasma and Magnetic Field Characteristics of the Distant Polar Cusp Near Local Noon: The Entry Layer. Journal of Geophysical Research, Vol. 81, 1976, p2883.
14. N.U. Crooker. Explorer 33 Entry Layer Observations. Journal of Geophysical Research, Vol. 81, 1976, Submitted.
15. T.E. Eastman, E.W. Hones, Jr., S.J. Bame and J.R. Asbridge. The Magnetospheric Boundary Layer: Site of Plasma, Momentum and Energy Transfer from the Magnetosheath into the Magnetosphere. Geophysical Research Letters, Vol. 3, 1976, Submitted.
16. P.J. Coleman, Jr., A Model of the Geomagnetic Cavity. Radiac Science, Vol. 6, p321.
17. R.K. Burton, R.L. McPherron and C.T. Russell. An Empirical Relationship Between Interplanetary Conditions and Dst. Journal of Geophysical Research, Vol. 80, 1975, p4204.
18. S.-I. Akasofu. Polar and Magnetic Substorms. D. Reidel, Dordrecht, Holland, 1968.
19. R.L. McPherron, Growth Phase of Magnetospheric Substorms. Journal of Geophysical Research, Vol. 75, 1970, p5592.
20. C.T. Russell. Reconnection, in "Proceedings of International Symposium on Solar-Terrestrial Physics", NOAA, Boulder, Colorado, 1976.
21. M.N. Caan, R.L. McPherron and C.T. Russell, in preparation, 1976.
22. G.C. Reid, I.S.A. Isaksen, T.E. Holzer and P.J. Grutzen. Influences of Ancient Solar Proton Events on the Evolution of Life. Nature, Vol. 259, January 22, 1976, p177.
23. C.T. Russell. The IMS Satellite Program: Scientific Objectives. in "The Scientific Satellite Program During the International Magnetospheric Study" (edited by K. Knott and B. Battrick), Pergamon Press, Dordrecht, Holland, 1976, p9.

# THE PARTICIPATION OF THE EUROPEAN SPACE AGENCY IN ATMOSPHERIC AND MAGNETOSPHERIC RESEARCH

D. Edgar Page

*European Space Agency, ESTEC, Domeinweg, Noordwijk, The Netherlands*

## Abstract

Five spacecraft of the European Space Agency have carried instruments to study the earth's magnetosphere. Selected results on magnetic field configuration, boundary plasma layers and solar particle entry to the magnetosphere are reviewed. The 1977-79 missions of GEOS (the first purely scientific geostationary spacecraft) and of the ISEE A, B and C ESA/NASA co-operation (resolving space-time ambiguities) will be described. Results from the highly successful ESRO 4 atmospheric neutral mass spectrometer will be presented - in particular the relationships between the neutral atmosphere and geomagnetic activity. Possible ESA atmospheric science contributions to early Spacelab payloads will be outlined.

## I. Selected results from ESA's Magnetospheric Programme.

Five of the eight ESRO/ESA spacecraft have carried experiments which studied the magnetosphere of the earth. A few of the interesting recent results have been selected for presentation.

- the magnetopause - where plasma pressure was balanced by dipole magnetic field pressure. No plasma penetrated across the magnetopause. The bulk of satellite data collected to date has supported that picture but most of this data has been obtained at low geomagnetic latitudes. HEOS-2 has, however, with its plasma experiment (Max Planck Institute, Garching) and its magnetometer (Imperial College, London) detected at higher latitudes layers of clearly directed plasma flow, earthward of positions normally identified as the magnetopause.

## The Plasma Mantle<sup>1</sup>

The first such layer detected and called the Plasma Mantle by the HEOS-2 experimenters can be seen in Figure 1. In this layer plasma is found inside the magnetopause and flowing from the polar cusp down the earth's magnetotail with velocities between 100 and 200 km/sec. This flow speed is always slower than plasma speeds in the adjacent magnetosheath. The plasma mantle, found to be present in more than 70% of spacecraft passes through the region, varies greatly in width having thickness up

Table 1:

ESRO/ESA Scientific Spacecraft

	<u>Launch Date</u>	<u>End of useful life</u>	<u>Mission</u>
ESRO II	May 1968	May 1971	Cosmic rays, solar X-rays.
ESRO-IA	October 1968	June 1970	Auroral and Polar Cap phenomena, ionosphere.
ESRO-IB	October 1969	November 1969	As ESRO-IA.
HEOS-1	December 1968	October 1975	Solar wind, interplanetary magnetic field, bow shock.
HEOS-2	January 1972	August 1974	Polar magnetosphere, neutral point, interplanetary medium.
TD-1	March 1972	May 1974	Astronomy (UV, X- and $\gamma$ -ray).
ESRO-4	November 1972	April 1974	Neutral atmosphere, ionosphere, auroral particles.
COS-B	August 1975	-	Cosmic Gamma Radiation.

The HEOS-2 satellite launched in January 1972 operated till its re-entry in August 1974 through regions of the polar magnetosphere where no spacecraft had previously gone. It has discovered several completely unexpected features which are just beginning to be understood.

The gross shape of the magnetosphere, a dipole magnetic field compressed by the solar wind plasma, has been remarkably well explained by fluid dynamics. In the calculations the plasma flow has been assumed to stop completely at a position

to about  $4R_E$ . This thickness does not appear to vary significantly with position or with the state of the magnetosphere as indicated by the geomagnetic disturbance index  $K_p$ .

It would appear that the thickness of the mantle depends on the direction of the interplanetary magnetic field (Figure 2.). When the field has a southward component, i.e.  $B_z$  is negative, then the mantle has maximum thickness.<sup>2</sup>

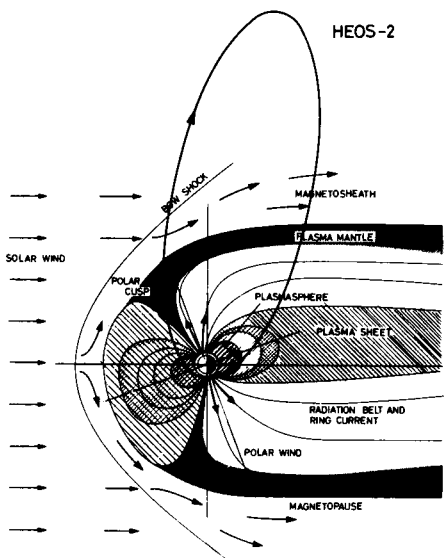


Figure 1. The HEOS-2 orbit through identified regions of the magnetosphere.

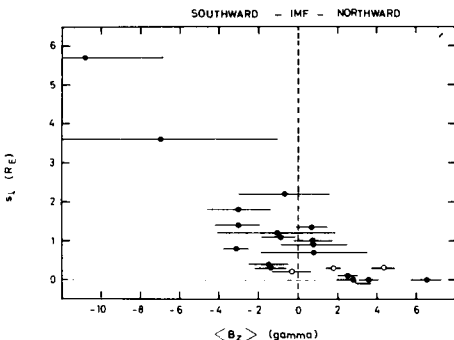


Figure 2. When  $B_z$  is negative (i.e. the interplanetary magnetic field points south) then the plasma mantle is thickest.

### The Entry Layer

A region which is apparently related to the Plasma Mantle is the Entry Layer. This region again is one where polar wind plasma seems to have crossed the magnetopause.

The entry layer is located on day side field lines just inside the magnetopause (see Figure 3). It is contiguous to both the polar cusp and the plasma mantle and the data suggest that this region is the

"port of entry" of solar wind plasma into the front magnetosphere.

The plasma density and temperature in the entry layer exhibit values similar to those observed in the adjacent magnetosheath. The main difference lies in the proton flow characteristics. Flow velocities in the entry layer are highly variable (temporal and/or spatial) and usually substantially lower than just outside the magnetopause. Changes of the flow speed between  $<60 \text{ km s}^{-1}$  and  $>200 \text{ km s}^{-1}$  are as common as changes of the direction by  $180^\circ$ . The flow direction is generally aligned with the magnetic-field direction, and is either Sunward or anti-Sunward. The typical thickness of the entry layer is of the order of  $1 R_E$ . The outer boundary of the layer usually coincides with a strong rotation of the magnetic field which is interpreted as the magnetopause. The inner boundary overlaps slightly with the outer boundary of the hot, trapped ("ring current") plasma.

In the entry layer, the magnetic-field magnitude often fluctuates strongly, as in the magnetosheath, but the direction is generally more stable and is consistent with an orientation expected in a closed magnetosphere. However, the field is systematically distorted out of the local meridional plane into a direction that indicates a transfer of momentum from the penetrating magnetosheath plasma to the field.

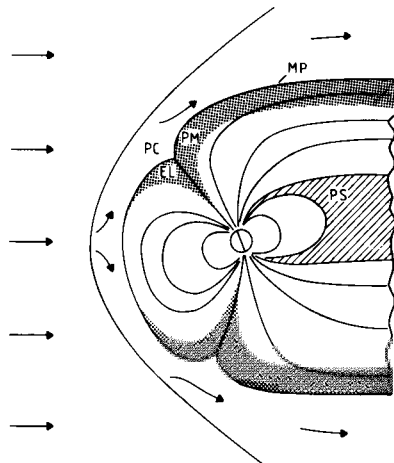


Figure 3. Illustrating the relative positions of the Entry Layer (EL) and the Plasma Mantle (PM). MP is the magnetopause, PC the polar cusp and PS the plasma sheet.

### A Neutral Point in the Dayside Magnetosphere?

One of the interesting questions asked prior to the launch of HEOS-2 was: Is there a neutral point at the high-latitude magnetopause separating the closed field lines of the dayside magnetosphere from the open field lines of the magnetotail? Magnetic-field and plasma data obtained from the potential neutral-point region for two years have been carefully analysed, but the answer is still open.

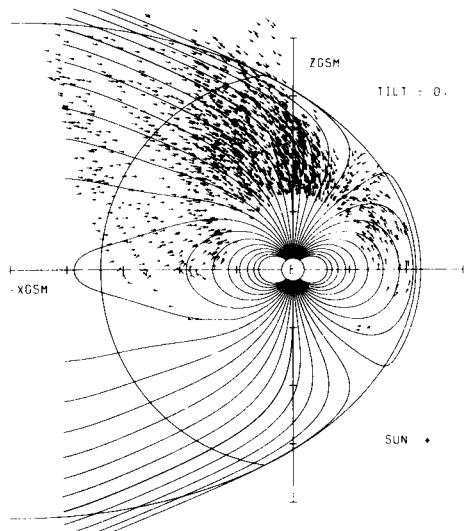


Figure 4. The magnetospheric field directly measured by HEOS-2. The polar cusp position is clear and the neutral point should be in the same region.

On some outbound passes, HEOS-2 encountered deep minima in  $|B|$  of 1-4% near the magnetopause. These minima did not coincide precisely with the first sharp turn of the magnetic field vector, which was identified as a transit through the magnetopause, but were located slightly further outwards. In none of these cases were the internal and external orientations of  $B$  sufficiently anti-parallel to enable the minima to be related to an annihilation of opposing fields. Instead, they could be explained by strong diamagnetic effects that are frequently found near the magnetopause. Their occurrence is not restricted to this region since similar events are found elsewhere in the magnetosheath. The temporal resolution of the plasma measurements is not sufficient to demonstrate the accompanying changes in the plasma pressure. One can therefore conclude that the experimenters have not yet found in their data the clear signature of a neutral point, i.e. a transit from a radial to a tangential orientation of  $B$  just inside the magnetopause,

accompanied by a strong depression of the field strength.

Figure 4 is a plot of the magnetic field vectors actually measured by the HEOS-2 magnetometer<sup>4</sup>. It is easy to identify where the neutral point is supposed to be. It is, however, clearly much more difficult to catch the measurement.

### Solar Particle Entry to the Earth's Polar Caps 5.6

Results from the HEOS-1 and HEOS-2 spacecraft - and from several U.S. spacecraft - in interplanetary space have been combined with simultaneous results from the ESRO-1 and ESRO-2 spacecraft orbiting close to the earth in order to study how solar particles travel from interplanetary space to the polar caps of the earth. At the polar caps these solar particles arrive in rather strange spatial patterns causing ionospheric and radio disturbance over wide regions. For high energies above about 100 MeV reasonable explanations appear to have been found. The solar particles depending on their anisotropy in interplanetary space and the direction of the interplanetary field impact on a particular zone of the earth's magnetotail. From there they take a particular route along the tail field lines to the polar cap of the earth.

Unfortunately the link from interplanetary space to the polar cap has been provided by calculation only in which assumptions are necessary. Directional measurements of such high energy particles in the tail has not been possible because of the very low fluxes involved. At lower energies of a few MeV where there are enough particles for sensible measurements the picture becomes very unclear. On no occasion has a majority of the particles been detected moving along the magnetotail toward the earth's polar caps.

### II. ESA's Magnetospheric Projects for the International Magnetospheric Study 1976-1979

ESA will make a major contribution to the International Magnetospheric Study (IMS) with its GEOS satellite and its contribution to the joint ESA/NASA ISEE (International Sun Earth Explorer) project.

#### GEOS

GEOS is a sophisticated and purely scientific geostationary spacecraft due to be launched in April 1977. Details of the payload are given in Table 2. It will be possible to move the spacecraft in longitude so that it can be on magnetic field lines which join the earth close to the Scandinavian ground observatories or on field lines coming down close to Iceland. The ground stations in Iceland are magnetically conjugate to Japanese stations in the Antarctic and joint studies are planned.

Table 2 GEOS Experiments

Exp. No.	Measurement	Technique	Experimenter from
S300	AC-magnetic fields up to 30 kHz DC/AC electric fields and plasma resonances up to 80 kHz mutual and self-impedance	Search-coil mag-netometer Electric aerials Emission and reception of VLF signals	CRPE, Yssy-les-Moulineaux, France, Space Science Dept., ESTEC, Holland, Danish Space Research Institute, Lyngby
S302	Study of thermal plasma	2 electrostatic analysers	Mullard Space Science Lab., Dorking, UK
S303	Composition, energy spectra & angular distribution of plasma particles	Combined electrostatic and magnetic analyser	University of Bern, Switzerland, and Max Planck Institute, Garching, Germany
S310	Pitch-angle distribution of electrons and protons in the 0.2-20 keV energy range	10 electrostatic analysers	Kiruna Geophysical Observatory, Kiruna, Sweden
S321	Pitch-angle distribution for electrons (20- 300 keV) and protons (20 keV-2 MeV)	Magnetic deflect-ion system followed by solid-state detectors	Max Planck Institute, Lindau, Germany
S329	DC electric field and grad $ B $	Tracing of electron beam over one or more gyrations	Max Planck Institute, Garching, Germany
S331	DC and ULF magnetic field	Fluxgate mag-netometer	University of Rome, Italy

A particularly interesting technical problem has been the coating of the space-craft solar cells with a good conductor to prevent high voltages developing between the sunlit and dark sides of the space-craft.

#### ISEE

The ISEE mission consists of three spacecraft. ISEE-C will sit at a libration point between the earth and sun in order to provide continuous monitoring of interplanetary parameters at a position where such measurements are undisturbed by the presence of the earth. ISEE-A and B will be launched together and orbit as a pair out to an apogee of  $22 R_E$  and close to the equatorial plane of the earth. A major problem in magnetospheric research till now has been the sorting out of spatial from time variations. With a single satellite this was near impossible and major advances are expected using the pair. The ISEE-A and B spacecraft will then study the behaviour of magnetospheric features in response to the interplanetary changes simultaneously monitored by ISEE-C.

ISEE-A carries 13 experiments, ISEE-B 8, and ISEE-C 12 experiments. Launch of ISEE-A and B is scheduled for September 1977 and ISEE-C about nine months later. ISEE-B is built by ESA, ISEE-A and C by NASA. Each spacecraft carries both European and American experiments.

#### III. Atmospheric Results from ESRO 4

##### Spacecraft and Scientific Instrument Parameters

The ESRO 4 satellite with a perfectly operating tape recorder collected a wealth of atmospheric and ionospheric data between launch on 22 November, 1972, and re-entry on April 15, 1974. The satellite with an inclination of  $91^\circ$ , apogee around 1,200 km and perigee around 250 km was spin stabilised. The spin axis was re-oriented from time to time by means of a magneto-torquer so that the varied demands of the scientific instruments could be met.

Here we are interested in three of the five experiments carried.

S80 a gas-analyser from the University of Bonn, used an antechamber, an electron impact ion source, a monopole analysing field and a triple current detection system to record neutral atmospheric constituents in the mass range 1-44 atomic masses. For this experiment the magneto-torquer was particularly important so that the orifice of the instrument could be aligned with the velocity vector of the spacecraft.

S45 from University College, London, used a boom-mounted Langmuir probe to identify positive ions and another smaller probe to obtain electron density, temperature and spacecraft potential.

S94 from Kiruna Geophysical Observatory used electrostatic analysers followed by channeltrons to monitor low energy charged particles and Geiger counters for electrons >44 keV. Here we concentrate on 0.21 keV and >44 keV electrons.

#### The Helium(He) and Argon(Ar) Bulges 7

It has been known for a few years that He densities are very much higher over the winter pole of the earth than over the summer pole. Measurement of the effect is thought to be very useful as a tracer of transport processes in the upper atmosphere. However, the actual ratio of winter to summer He is critically dependent on altitude, mean solar activity and the instantaneous geomagnetic activity. ESRO 4 results indicate a winter to summer ratio of 20 measured at 270 km in December, 1972.

One of the first things looked for by ESRO 4 was a summer Argon bulge corresponding to the winter Helium bulge. And it has been found. Because He is lighter and Ar is heavier than the mean molecular mass of thermospheric air, it was to be expected that they would respond in opposite ways to many dynamical processes such as changes in turbopause altitude and vertical winds. (The turbopause (or homopause) at around 120 km marks the height above which atmospheric constituents move freely with very long mean free paths and settle out in response to gravity and temperature. The heaviest and least mobile remain at low altitudes while the lightest like He reach greater heights. Below 120 km mixing takes place so that the proportion of any constituent present cannot be taken as a measure of height.) At 270 km altitude the summer Ar density was found to be 10 times higher than the winter density. It was also found that Ar densities showed very large increases with increases in K<sub>p</sub>, an index of geomagnetic disturbance.

It would seem that while the winter He bulge is controlled by atmospheric dynamics the summer Ar bulge is probably temperature controlled.

#### The Ratio of Atomic Oxygen to Molecular Nitrogen O/N<sub>2</sub> and Its Relationship to Geomagnetic Activity

For an altitude of 250 km and quiet geomagnetic conditions the ratio of O/N<sub>2</sub> was derived during the period December 1972-December 1973. The results are shown in Figure 5 for winter and summer periods. The amplitude of the seasonal variation is significantly larger than was predicted from ionospheric observations.

A particularly interesting result has been the observation that the ratio O/N<sub>2</sub> changed in step with f<sub>oF2</sub>, the critical frequency of the F2 layer as measured by ground-based ionosondes. (see Figure 6.).

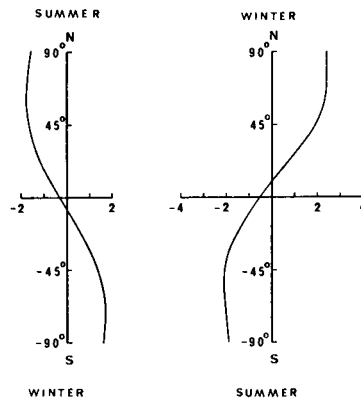


Figure 5. The ratio of oxygen to molecular nitrogen (O/N<sub>2</sub>) at 250 km altitude and for quiet geomagnetic conditions, December 1972-December 1973.

As geomagnetic activity increased both ratios decreased. The correlation between ionospheric storms, as measured by f<sub>oF2</sub>, and magnetic storms, indicated by K<sub>p</sub>, has not been particularly good. It seems very significant that the correlation between changes in the neutral atmosphere, as indicated by the O/N<sub>2</sub> ratio, and f<sub>oF2</sub> ionospheric changes is much better.

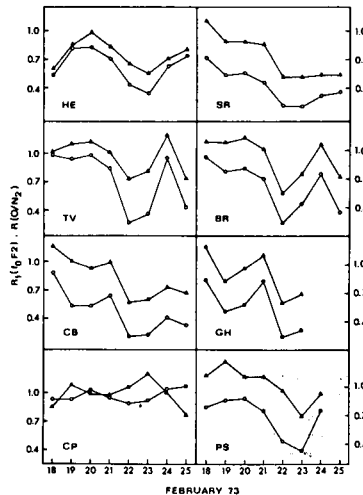


Figure 6. Changes in f<sub>oF2</sub> compared with simultaneous changes in the ratio O/N<sub>2</sub> as observed at eight ionosonde stations, February 18-25, 1973.

The result indicates how important a role the neutral atmosphere plays in determining ionospheric behaviour. It would seem too that the connection between magnetic storms and ionospheric storms is an indirect one.

#### Spatial Structure of Storms in the Atmosphere

The result that foF2 and the ratio O/N2 change in step is particularly useful in studying the extent of atmospheric disturbances. A single satellite passing through an atmospheric feature finds it difficult or impossible to separate time and spatial effects. However, clearly a very powerful tool exists if direct measurements in the atmosphere are combined with a ground network of stations which can indicate storm onset times at a variety of locations.

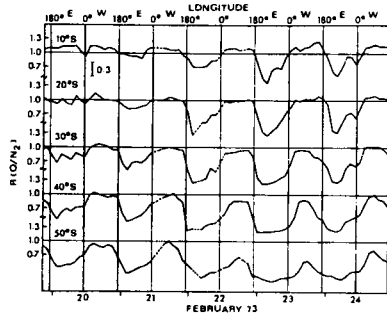


Figure 7. Changes in the ratio O/N2 at different geographical locations during February 20-24, 1973. Note the steep boundary at about 180°E.

A period of geomagnetic storminess in February, 1973, has been studied using combined ionosonde and ESRO 4 measurements. These measurements indicate not only latitudinal structure but perhaps more surprisingly a complicated longitudinal structure of disturbances in the upper atmosphere. In the particular case studied, a strong depression of the O/N2 ratio developed and persisted for several consecutive days above the Australian-African area. It has a remarkably sharp eastern boundary at about 180°E geographic longitude (see Figure 7.). This mid-latitude disturbance zone was distinctly separated from strongly disturbed regions simultaneously existing at higher latitudes. How these distinct regions with sharp boundaries are created and maintained has been speculated upon but satisfactory explanations are still missing.

#### Thermospheric Neutral Gas Heating and Related Plasma and Energetic charged Particle Phenomena at High Latitudes during Geomagnetic Disturbances

For this study the results of three of the ESRO 4 experiments were combined. The S80 neutral gas analyser provided Ar, N2, O and He densities, the S45 experiment gave ion composition (in particular for O<sup>+</sup>) and the S94 experiment provided data from its 0.21 and >44 keV electron detectors.

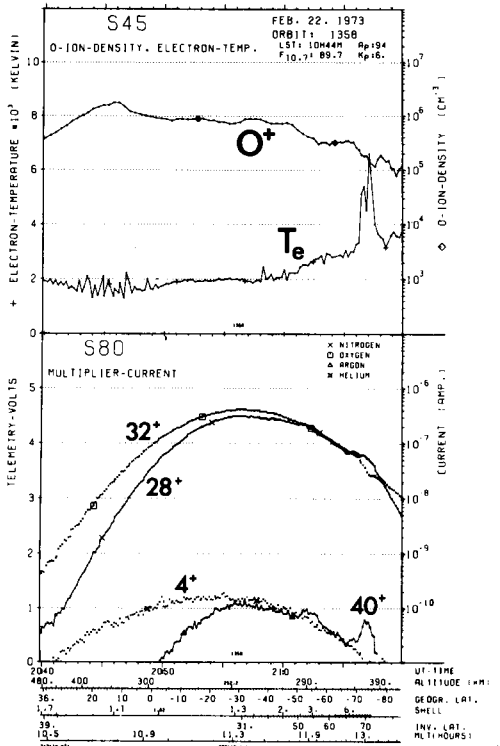


Figure 8. An orbit of ESRO 4. February 22, 1973. The top part of the figure displays Oxygen ion concentration and electron temperature. The bottom part gives the concentration of Helium (4), Nitrogen (28), Oxygen (32) and Argon (40). The kinks in the curves at the position of the magnetospheric polar cusp are evident.

Following the onset of geomagnetic activity three main regions of neutral atmospheric disturbance have been identified. These are:

- At heights around 250 km and over the poles the density ratio O/N<sub>2</sub> varies from around 7:1 in quiet conditions to about 1:1 when K<sub>p</sub> reaches values of about 5. By "over the poles" is meant in this case the zone extending from around 65° invariant latitude on the night side to about 50° invariant latitude on the day side.
- On the night side the N<sub>2</sub> density is enhanced in a belt extending from about 50 to 80° invariant latitude. This region corresponds closely with the region in which >44 keV electrons were being dumped into the atmosphere.
- The day side region at latitudes around 70 to 80° invariant latitude frequently shows a narrow band of N<sub>2</sub> enhancement. Coincident with this N<sub>2</sub> enhancement there are generally peaks in Ar density and in electron temperature, T<sub>e</sub>, and a trough in the oxygen ion density, n(O<sup>+</sup>). The effect is shown in Figure 8 where the peaks are immediately evident toward the right side of the diagram.

#### Global Changes of Composition in the Thermosphere during Geomagnetic Disturbances

The results already presented indicate clearly that there are spatially limited neutral atmospheric responses to geomagnetic activity. An attempt has been made to establish a global pattern for these responses.

The oppositely directed variations of Argon and of Helium have already been described in relation to seasonal "bulges" over the poles. It has been found that at high and mid latitudes Ar and N<sub>2</sub> increase in phase with K<sub>p</sub> while He decreases in antiphase and O changes very little. Such behaviour is illustrated in Figure 9 for an analysis carried out at 280 km altitude during an intense magnetic storm.

If then a long period of sustained geomagnetic activity - rather than a short intense burst - is analysed results similar to those in Figure 10 are found. At middle latitudes (and the same applies to high latitudes) illustrated in the top part of the figure, Ar and N<sub>2</sub> show a 24-hour periodicity having maxima at the highest geomagnetic latitudes. He and O on the other hand show minimum densities at the highest geomagnetic latitudes. (In the event of an intense storm such as in Figure 9 these regular periodicities are swamped by the response to the large K<sub>p</sub> changes.) The lower part of Figure 10 indicates that in equatorial regions the periodic (i.e. latitudinal) variation has more or less disappeared.

The experimenters have concluded that the observations can be explained by assuming that the temperature at 280 km increases with geomagnetic latitude and that this change in temperature T is accompanied by

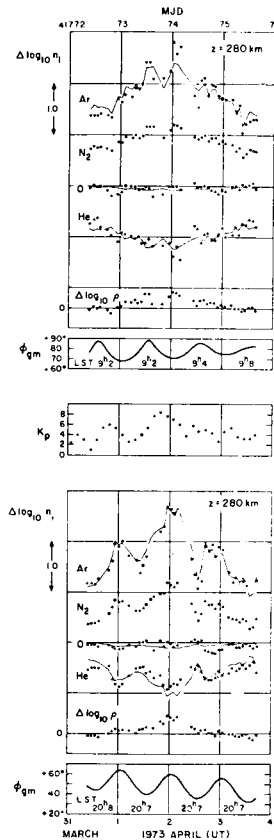
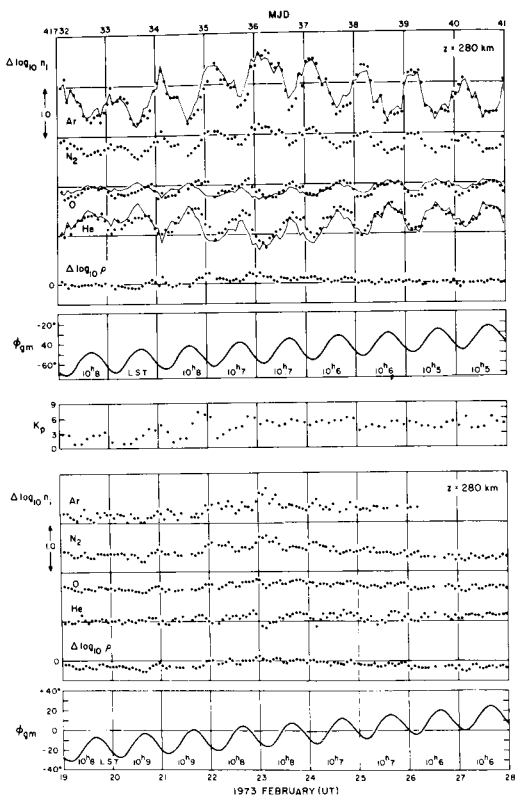


Figure 9. Response of Argon, Nitrogen, Oxygen and Helium at 280 km to intense changes in geomagnetic disturbance as measured by K<sub>p</sub>. Top part of the figure is for high geomagnetic latitudes ( $\phi_{gm}$ ) and bottom part for middle latitudes. The light and heavy constituents vary in antiphase.

a change in the height  $Z_H$  of the homopause (also called the turbopause). During periods of sustained geomagnetic activity  $dZ_H/dT$  is about 50 metres per degree Kelvin (m/°K) and maximum temperature is reached near the magnetic pole. During transient storms, however,  $dZ_H/dT$  is closer to 30 m/°K and the maximum temperature seems to be at the auroral zones. This lower value of  $dZ_H/dT$  required to fit the observations during transient storms indicates that the homopause reacts rather slowly to geomagnetic activity, reaching a steady height only after 2 or 3 days. The regime in equatorial latitudes appears to be completely different. There all four atmospheric constituents Ar, N<sub>2</sub>, O and He vary in phase following K<sub>p</sub> changes with a



**Figure 10.** Response during sustained geomagnetic activity. The top part shows middle latitude and the bottom low latitudes. See text for explanation.

lag of about 8 hours. Since the lag is much smaller at higher latitudes the observations suggest that a density wave proceeds from higher latitudes toward the equator.

#### IV. ESA's Participation in Atmospheric and Magnetospheric Spacelab Payloads

Until recently ESA has thought about atmospheric and magnetospheric research from Spacelab in the framework of the AMPS (Atmosphere Magnetosphere Plasmas in Space) study and of the opportunities provided by the first spacelab payload (FSLP) which will not be primarily geared toward science.

The future of AMPS seems a little unclear at present. In relation to AMPS ESA has studied a Lidar facility and sub-satellites. The intention was that these ESA contributions to the payload would make possible a joint NASA/ESA payload in which data from all instruments was avail-

able to all those scientists contributing any part.

More recently the Lidar facility and supporting or indeed competing passive atmospheric sounding experimental packages have been studied in the context of what was available on the FSLP.

#### Sub-satellites

The possibility of ejecting, controlling and recovering very simple sub-satellites from Spacelab has been studied in a preliminary way. Sub-satellites are very attractive to many potential Spacelab experimenters in that they make it possible to carry out experiments sufficiently distant from the chemical and electromagnetic interferences which seem likely close to the main laboratory. For atmospheric and magnetospheric experimenters there are the additional attractions of sorting out spatial from temporal changes by using two or more sub-satellites and the possibility of using signals transmitted between satellites, or from satellite to Spacelab, in order to study the properties of the intervening medium.

Both free flying and tethered satellites have been examined. The biggest problem - unless the sub-satellite is made with an expensive and sophisticated propellant system - would seem to be the atmospheric drag. For typical drag and mass values it would seem to be near impossible to maintain a simple 7-day sub-satellite mission at altitudes much below 300 km. And of course much of the desired atmospheric data lies well below these altitudes.

#### Passive Sounding Experiments

Passive sounding experiments from Spacelab can be divided into two main classes. Vertical sounders look down at the earth to monitor radiation back scattered and reflected from the atmosphere and line emissions produced in atmospheric atomic or molecular transitions. Limb sounders look from the position of Spacelab past the earth's limb and essentially horizontally through a large amount of atmosphere and generally in the direction of the setting or rising sun. The absorption of sunlight in various atmospheric path lengths is studied. The earth's limb can be used for occultation measurements. When the sun has set atmospheric emissions can still be studied.

Vertical sounding can provide height resolutions of 10 km and horizontal resolution of 25 km. Limb scanning can provide height resolution of 2 km but the horizontal resolution is not better than about 200 km.

Atmospheric emissions of interest appear in all wavelengths from the ultra-violet through the visible to the infra red and microwave region. The techniques required have been highly developed by spectroscop-

Table 3 Package A

Instrument	Spectral Region	Mode of Operation
Microwave Radiometer (2m x 1m antenna)	118 GHz ( $O_2$ ) 184 GHz ( $O_3$ ) 183 GHz ( $H_2O$ ) 115 or 230 GHz (CO)	Limb-sounder (Emission)
Gas Correlation Radiometer (PMR)	2-15 $\mu m$	Limb-sounder (Emission) (LOS $\perp$ VV)
UV-NIR Spectrometer	UV-NIR	Limb-sounder (Emission)
IR Filter Radiometer (cooled)	67 and 147 $\mu m$	Limb-sounder (Emission)
Fabry-Perot Interferometer	UV-NIR	Limb-sounder (Emission)

Table 4 Attitude Requirements

Operating Mode	Absolute attitude measurement accuracy	Stabilisation during measurement period (typically a few seconds)
<u>Limb-scanner</u>		
-Emission	~ 0.03° roll ~ 1° pitch ~ 1° yaw	0.005° roll 0.25° pitch > 1° yaw
-Absorption	As above	As above
-Wind determination (to 3 m/s)	~ 0.03° roll ~ 0.02° pitch ~ 0.02° yaw	0.005° roll ~ 0.02° pitch ~ 0.02° yaw
<u>Vertical sounders</u>		
	~ 1° roll and pitch > 1° yaw	~ 1° roll and pitch > 1° yaw

ists over many years. Consequently the studies dealt mainly with which set of atmospheric questions should be attacked at any one time and how the required instruments could be packaged. Three model payloads were studied on the basis of certain scientific objectives.

Package A was for the measurement of temperature and composition in the mesosphere and lower thermosphere (70-140 km). This carried five experiments which weighed 320 kg.

Package B was for the measurement of temperature and composition (including aerosols and ozone) in the stratosphere and mesosphere (15-70 km). This carried six experiments totalling 245 kg.

Package C was for measurement of the motion field (50-140 km). This carried three experiments weighing 270 kg.

As illustration the composition of Package A is given in Table 3. The various attitude requirements deemed necessary are given in Table 4.

It is clear that because of the large number of experiment choices available a highly flexible system can be put together to comply with the various technical constraints and still attain the main scientific objectives.

#### The Lidar

The LIDAR is a LIght-raDAR in which a laser beam is employed. As with a normal radar, distances are measured by recording the delay of the return signal. Atmospheric constituents can be differentiated because of their differing abilities to return the transmitted signal. The principal techniques being considered are those of backscattering by resonant and non-resonant

processes, and those of differential absorption. Thus composition at various atmospheric depths below Spacelab can be measured.

ESA planned to develop the transmitting and receiving optical systems as a central and reusable facility. A variety of lasers

and detectors of the return signal should be developed by contributing experimenters in pursuit of a particular measurement.

The system performance foreseen for measuring atmospheric sodium is given in Table 5 while Table 6 details the requirements for Aerosol measurements.

Table 5 Sodium Measurements - System Performance

<u>Laser</u>					<u>Receiver</u>						
Primary Pulse Energy	Efficiency	Pulse Repetition Rate	Power Input	Transmitted Pulse Energy	Photo-multiplier Efficiency	Filter Efficiency	Other Losses	Overall Optical Efficiency	Electron Counts per second for layer peak	Latitude resolution (10% accuracy)	
<u>Case (a)</u>											
1J	0.002	1 s <sup>-1</sup>	500W	0.5J	0.2	0.2	0.5	0.02	230	<1°	
<u>Case (b)</u>											
0.3J	0.01	20 s <sup>-1</sup>	600W	0.011J	0.2	0.2	0.5	0.02	92	<1°	

Table 6 Aerosol Measurements - System Performance

Height	Backscatter Coefficient	Pulse Energy	Pulse Repetition Rate	Power Input	Receiver Efficiency				Electron counts per second	Resolution for 10% accuracy
					Photomultiplier	Filter	Other	Overall		
Troposphere (5 km)	8.0 × 10 <sup>-9</sup> (cm ster) <sup>-1</sup>	0.3 J	20	600 W	0.02	0.5	0.5	0.005	2900	300 m
Stratosphere - large aerosol concentration (15 km)	2.4 × 10 <sup>-10</sup> (cm ster) <sup>-1</sup>	0.3 J	20	600 W	0.02	0.5	0.5	0.005	86	10 km
Stratosphere - small aerosol concentration (15 km)	2.4 × 10 <sup>-11</sup> (cm ster) <sup>-1</sup>	0.3 J	20	600 W	0.02	0.5	0.5	0.005	9	100 km

### References

1. Paschmann, G., H. Grünwaldt, M. D. Montgomery, H. Rosenbauer and N. Sckopke. Plasma observations in the high latitude magnetosphere. in Correlated Interplanetary and Magnetospheric Observations, edited by D. E. Page, pp. 249-253. D. Reidel Publ. Co., Dordrecht, Netherlands, 1974.
2. Sckopke, N., G. Paschmann, H. Rosenbauer and D. H. Fairfield. Influence of the Interplanetary Magnetic Field on the Occurrence and Thickness of the Plasma Mantle. J. Geophys. Res. 81,
3. Paschmann, G., G. Haerendel, N. Sckopke, H. Rosenbauer and P. C. Hedgecock. Plasma and Magnetic field characteristics of the Distant Polar Cusp near Local Noon: The Entry Layer. J. Geophys. Res. 81, 2883-2899, 1976.
4. Hedgecock, P. C., Private Communication.
5. Durney, A. C., G. E. Morfill and J. J. Quenby. Entry of high energy solar protons into the distant geomagnetic tail. J. Geophys. Res. 77, 3345-3360, 1972.

2687-2700, 1976.

6. Domingo, V., D. E. Page and K.-P. Wenzel. Measurements of solar protons in the near earth magnetotail. in Correlated Interplanetary and Magnetospheric Observations, edited by D. E. Page, pp. 507-519, D. Reidel Publ. Co., Dordrecht, Netherlands, 1974.
7. Von Zahn, U.. Early Aeronomy results from the satellite ESRO 4. in Atmospheres of Earth and the Planets, edited by B. M. McCormac, pp. 133-157, D. Reidel Publ. Co., Dordrecht, Netherlands, 1975.
8. Raitt, W. J., U. von Zahn and P. Christoffersen. A comparison of thermospheric neutral gas heating and related Thermal and Energetic Plasma Phenomena at High Latitudes during Geomagnetic Disturbances. *J. Geophys. Res.* 80, 2277-2288, 1975.
9. Jacchia, L. G., J. W. Slowey and U. von Zahn. Latitudinal changes of Composition in the Disturbed Thermosphere from ESRO 4 measurements. *J. Geophys. Res.* 81, 36-42, 1976.

# DYNAMICS AND THERMAL STRUCTURE OF PLANETARY ATMOSPHERES

R. E. Dickinson

*Climate Project, National Center for Atmospheric Research, Boulder, Colorado, U.S.A.*

## Abstract

A fruitful approach to studying the planetary atmospheres is the comparison of the similarities and differences between them. The terrestrial atmosphere has been the most extensively studied of these. Its comparison with those of other planets provides a comprehensive understanding of the dynamics of planetary atmospheres in general. This paper considers the processes occurring in the earth's atmosphere and compares them with like processes in other atmospheres to suggest what similarities and differences are to be expected. We attempt to answer several questions: i.e. 1) What features have already been discovered by planetary probes or earth-based observations? 2) What further discoveries are anticipated considering our likely observational capabilities? 3) What further understanding of our atmosphere is likely to result from future studies of planetary atmospheres?

## I. Introduction

A recurrent theme of the planetary exploration program has been that by looking at other planets we learn more about earth. Sometimes scientists who would prefer to have more support for studying earth directly may wonder about the cost effectiveness of such an approach. It is certainly very difficult to quantify the value of the scientific excitement and deep insights into the nature of physical processes and thus the benefits that the studies of other planetary atmospheres provide to studies of the earth's own atmosphere. Yet it is not difficult for scientists as myself, mostly concerned with the earth's atmosphere, to see that the understanding gained from consideration of the atmospheres of other planets is profoundly influencing our perceptions of terrestrial processes.

As indicated by the title of this paper, I shall be emphasizing here the dynamics and thermal structure of planetary atmospheres. Of the many complicated processes that occur in the earth's atmosphere, these are perhaps most central. Attempts at understanding them theoretically soon lead to the necessity of coping with all the other most important physical processes in the system such as absorption of solar radiation, infrared radiative transfer, formation of clouds, and so on. The earth's atmosphere and its interactions with terrestrial surface processes must be studied as a whole to achieve the most useful if not deepest understanding. This is a lesson but reinforced by consideration of the atmospheres of other planets. Hence, the underlying theme of this paper will be not only the better understanding of terrestrial atmospheric processes we gain by studying planetary atmospheres, but also the essential unity of all these processes. To limit

somewhat my scope, I shall restrict myself here to explicit consideration of only the best known planetary atmospheres, those of Venus, Mars, and Jupiter.

The excitement and awe engendered by looking at what we now know or think we know about these atmospheres is indeed great. In particular, we have found: On Mars, vast global dust storms, enveloping a very dry planet, which is locked in such a severe ice age that much of its atmosphere is now frozen in polar ice caps but which may in the distant past have had ample atmosphere to support an active hydrological cycle and flowing rivers. Venus with an atmosphere 100 times as massive as that of earth and with a surface temperature of 900°K, but which in the distant past may have supported oceans and appeared like a tropical earth, before it was cooked by a brightening sun and the run-away greenhouse effect. There exist on all the planets global cloud patterns controlling the structure of atmospheric temperatures and winds and strange brews of photo-chemical reactions that turn out to have some remarkable similarities to reactions now known to occur in the earth's stratosphere. Jupiter appears as a massive planet which rotates more than twice as fast as earth, and at the level of visible clouds has a strongly zonal wind system exhibiting fastest winds at the equator. Venus hardly rotates at all but also, remarkably enough, has a zonal wind system stronger than any on earth at the top of its cloud deck. On Mars, cyclonic storms develop from the baroclinic instability of zonal winds driven by mass flows off a sublimating polar cap. These zonal winds couple to strong temperature variations driven by the thermal contrast between the frozen CO<sub>2</sub> cap and bare rock warmed by hot solar rays. All of the planetary atmospheres have interesting thermospheres and ionospheres, topped by cavities shielding the highest layers from solar wind, which in the case of Jupiter is controlled by a massive internally generated planetary magnetic field, in the case of Venus merely by the hydromagnetics of the solar wind impinging directly on the magnetosphere.

Basic scientific questions relating to dynamics and thermal structure are easily identified. The planets as a result of their geometry are differentially heated by incoming solar radiation. What sort of motion systems originate from the day-to-night and pole-to-equator heating contrasts? How do these motion systems redistribute this heat, what horizontal temperature contrasts result from the balance between radiative energy sources and hydrodynamic transport?

Scientists studying the earth's climate are becoming increasingly cognizant of the major role clouds and aerosols play in establishing a planetary heat balance through their scattering and absorption of solar radiation and their large infrared opacities. Not only do clouds strongly modify dynamic and thermal processes, but their distribution in turn depends in an essential

\*The National Center for Atmospheric Research is sponsored by the National Science Foundation.

fashion on dynamic and thermal processes. The closely coupled feedbacks between the radiative effects of clouds and dynamic-thermal processes also characterizes the atmospheres of Venus and Jupiter, and to a lesser but not entirely insignificant extent, Mars. Somewhat analogous feedback processes occur in the tenuous atmosphere layers high above the levels of cloud formation, but with a major role played by chemical composition rather than clouds.

It is not possible here to look in detail at more than a small number of the specific examples of the interplay between questions, theory and observation that characterizes the present studies of planetary atmospheres. I shall concentrate on the wind and thermal structure as now revealed by observations and theory and reluctantly say but little about the closely coupled questions of cloud and chemical structure or how any of the atmospheres may have differed in the geological past.

## II. Thermal Structure

The thermal structure of a planetary atmosphere can be inferred in many ways because many observable processes are linked to the atmospheric temperatures. One of the most powerful observational techniques has been to look at the outgoing infrared radiation. The emission of infrared radiation used for sensing of a planetary atmosphere also determines the infrared cooling of the atmosphere—one major consideration in understanding atmospheric thermal and dynamic processes. It is the strong Planck function temperature dependence of infrared radiation emission which is responsible, on the one hand, for its usefulness in measuring temperatures and on the other hand for its importance in the physical processes determining temperature. In terrestrial meteorology, temperature sensing from infrared emission has developed over the last decade into one of the major observational tools.

Two recent observational studies of atmospheric temperatures of Mars and Jupiter from infrared emission are especially notable for the usefulness of their data to dynamical studies. The first of these, using an infrared spectrometer on Mariner 9, mapped the diurnal and vertical structure of Martian atmospheric temperatures during the maximum and declining phases of the global dust storm of 1971. An example of this data<sup>1</sup> is shown in Fig. 1. Such results have stimulated several theoretical-diagnostic studies of diurnal and meridional winds on Mars (e.g. <sup>2,3,4,5,6</sup>) which have attempted not only to evaluate the nature of global Martian wind systems but also to determine what surface wind components might be responsible for raising the dust.

Observations of the decay of the dust effects indicate the dependence of the atmospheric temperatures on the dust heating and the strength of the upper level winds which hold up the dust. Fig. 2<sup>5</sup> shows the decay of the 0.3 mb (30 km above surface) temperature as observed and inferred from a simple heating model. From such data, it is concluded that the dust settled out of the atmosphere on a 60 day time scale, and that during the decay period transport by winds kept the highest dust from settling out much faster in its free molecular

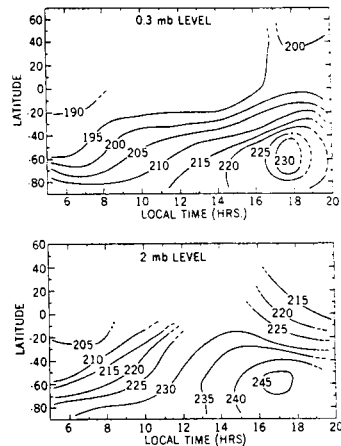


Fig. 1 Mars temperatures during duststorm.

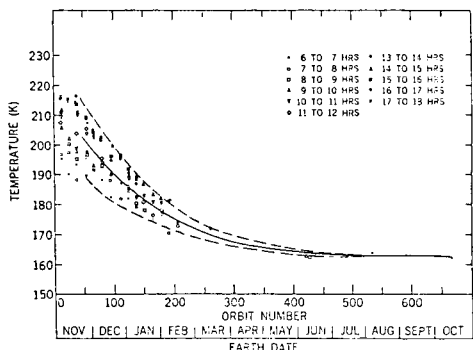


Fig. 2 Decay of temperature after duststorm.

flow gravitational falling than did the dust in the lower layers.

Although many of the gross features of the dusty and nondusty Martian atmosphere are now understood, we are still far from the desired goal of deriving these from first principles such as the incoming solar radiation and observed surface features. One possible first step in that direction would be to study the global mean planet-atmosphere heat balances by means of a radiative-convective climate model. Such models are now actively being used for studying the relative sensitivity of the earth's climate to various possible perturbing elements from volcanic dust to chlorofluoromethanes. A fundamental question with regard to Mars that could be answered with such an approach is the importance of the residual dust for the planetary heat balance during nondust-storm conditions. We know from the Viking landing that there is enough residual dust to make the Martian sky red. Does this dust also make the Martian atmosphere much warmer and thermally more

stable at all times than it would be without any dust? One approach to this question would be to determine for example, whether the observed quiet time temperatures, as indicated by the right side of Fig. 2, are explicable without dust, or alternatively whether a plausible amount of residual dust could explain any significant differences.

The possible effect of dust and other aerosol particles on the earth's climate is now of considerable concern and attention. Additional study of the effects of Martian aerosol might provide fresh insights into the terrestrial problem. Such a calculation of the Martian global heat balance demands great care in including all the significant infrared absorption and emission bands of carbon dioxide, but I hope to be able to do it with computer models I previously developed for Venus.

Fig. 3 illustrates the results of a now somewhat old such modeling calculation as applied to the atmosphere of Venus above cloud level.<sup>7</sup> This picture has been somewhat modified by more recent calculations<sup>8</sup> but is still qualitatively correct. Observational temperature profiles were obtained in the lower stratosphere of Venus by the Mariner 5 occultation experiment. These indicate that my calculated temperature dropoff below 75 km is probably too rapid. I would expect such an error from the large heating effect now known to originate from the observed haze layers<sup>9</sup> which must be added to our calculation before it can be regarded as physically complete. Infrared measurements of the temperature of the stratosphere and mesosphere of Venus will first be attempted on the Venus Pioneer orbiter mission using methods described by Taylor and Houghton.<sup>10</sup> The near agreement between the observed and calculated level of peak ionosphere indicates that our average calculated temperature from the lower stratosphere to the level of the ionosphere cannot be much in error. The thermosphere temperatures shown here, on the other hand, are warmer than those suggested by the currently most popular interpretations of ionosphere and hydrogen Lyman- $\alpha$  airglow lapse rates. The colder temperatures can be modeled if more of the heat deposited by extreme ultraviolet solar radiation channels into infrared airglow than assumed for the calculation shown here.<sup>8</sup>

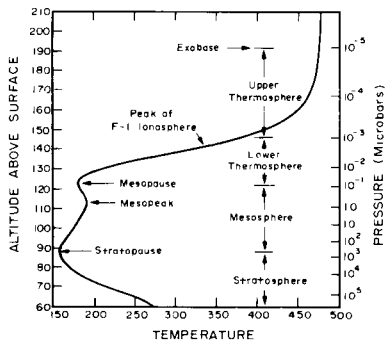


Fig. 3 Venus temperatures above cloud level.

### III. Relationships between Thermal and Dynamic Processes on Jupiter

In the past, many theories of dynamic processes on Jupiter (e.g. the presence of the great red spot) turned out to be quite sensitive to the largely unknown vertical temperature gradients. This difficulty is now considerably less severe. Fig. 4 shows the average vertical temperature structure inferred by Orton<sup>11,12</sup> from a combination of the angular dependence of 20 and 45  $\mu\text{m}$  thermal radiation as seen by the recent Pioneer 10 flyby and earth based infrared observations. Estimates of pole-to-equator and zone-to-belt temperature contrasts are also important constraints on dynamic models.

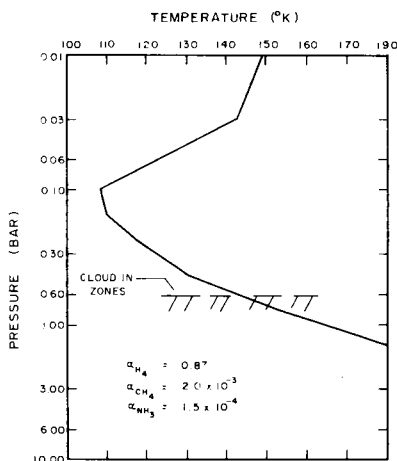


Fig. 4 Jupiter temperatures from IR observations.

The observed pole-to-equator temperature contrast of a few degrees or less is remarkably less than that seen on Earth. The explanation of its smallness should increase our understanding of planetary heat transport processes in both atmospheres. It is questionable whether the balance between the pole-to-equator solar heating difference and large-scale horizontal transports, as is dominant in the terrestrial atmosphere, could produce such a small difference. Rather, the explanation may be connected with the large internal heat source of Jupiter. The Jovian atmosphere is observed to emit twice as much total infrared energy as the amount of solar energy it absorbs, so that it must be heated as much by convection carrying heat up from below its visible layers as by the sun. The internal heat source is likely to be spherically symmetric, and result in essentially no horizontal temperature variation at lower levels. If so, any temperature variations in the upper layers would lead to latitudinal differences in the vertical temperature gradient. Vertical convective heat transport is sensitive to vertical temperature gradients. Possibly this negative

feedback is able to remove any horizontal temperature variations of more than a few degrees at the levels where observations are possible.<sup>13</sup>

The most spectacular and longest recognized visual features in the Jovian atmosphere are the "zones" and "belts." They are the 10 or more white (zones) and brown (belts) regions that circle the planet in a pattern nearly symmetric about the axis of planetary rotation. This banded structure has long been believed to represent cloud structure, and differential velocities of small scale features have been used to measure atmospheric motion. Past attempts to explain the belted structure have involved instability of the larger-scale zonal wind systems that would originate from the pole-to-equator difference in solar heating. This explanation is the basis of our current understanding of terrestrial wind systems. Thus the question was to explain in terms of planetary parameters such as radius, gravity, and rotation rate, why Earth should respond to the differential solar heating by development of longitudinal waves, cyclonic storms etc. whereas, in contrast, the analogous disturbances in the atmosphere of Jupiter are largely zonally symmetric. Recently, however, some further new and promising insights have evolved from theoretical and observational results. It appears from the planetary chemical models of Lewis<sup>14</sup> that water or ice clouds form (with varying amounts of ammonia dissolved in them) between the 1 and 100 bar pressure levels. Furthermore, the latent heat released in the formation of these clouds would be sufficient to significantly warm the atmosphere. It is tempting to interpret the observed banded structure as a consequence of the manner in which moist convection organizes itself at the level of water cloud formation.<sup>15</sup> The zones are believed to be high level ammonia clouds whereas the belts are interpreted as a lower, hence warmer, cloud deck lying below the ammonia clouds. Consequently, less total infrared radiation should originate from the higher and colder zone clouds than the warmer and lower belt clouds as is observed. Such a picture is consistent with large-scale upward motion in the zones and downward motion in the belts. Clouds form on Earth where moisture is carried upward because temperature decreases with altitude whereas the amount of water vapor that air can hold without the water condensing out decreases rapidly with temperature. The same arguments apply to water or other condensable species on Jupiter.

Because of Jupiter's rapid rotation, its zonal winds must be in geostrophic balance with pole-equator pressure gradients. The strongest eastward winds are on the equatorward side of belts and strongest westward winds on the poleward side of belts. This implies the belts are of relatively low pressure compared to the zones at the same altitude. The atmosphere at some deeper level is presumably in near uniform rotation. If so, the average temperature between that level and the observed clouds must be warmer in the zones than in the belts.<sup>16</sup> Remarkably enough, this is opposite to the temperature contrast observed at levels above the clouds<sup>11</sup> where temperatures have been derived from the Pioneer 10 observations.

Zones warm below and cold above, would be precisely the signature that would be expected if the upward motion of the zones were driven by

latent heat release below the visible clouds. By way of analogy, we can look at the terrestrial tropics where the troposphere is extensively warmed by latent heat release whereas the overlying lower stratosphere is cooled by the overshooting of upward vertical motion above the level of cloud formation and latent heat release. In the absence of condensation, regions of rising motion would necessarily be cooler than sinking regions at all levels where the lapse rate is subadiabatic. It is only possible to model the belts and zones with dry convection if there is a significantly superadiabatic lapse rate, and this may not be possible for realistic conditions.<sup>17</sup> Thus, it may be difficult to explain the latitudinal variations of the observed cloud motions without there being water clouds formed.

The reasons why Jovian rainfall should occur in banded structures is still far from understood. Yet it is interesting to speculate that both the latent heating and the effect of clouds on radiative energy transfer are important components of this process. The only theoretical model yet proposed for the formation of banded water clouds<sup>15</sup> requires to achieve the banded structure, variations in net radiative heating to correlate positively with the corresponding temperature variations, opposite to that expected for a dry atmosphere. By better understanding the Jovian hydrological cycle and cloud-radiation interactions we should improve our understanding of these important processes in the earth's atmosphere.

#### IV. Mysterious Planetary Winds on Venus

Venus as seen from Earth is like Jupiter completely shrouded by clouds. Clouds on Venus extend up to pressures only a few hundreds of an atmosphere, that is into the stable lower stratosphere region shown in Fig. 3. The terrestrial stratosphere has an aerosol layer consisting largely of concentrated sulphuric acid droplets. Remarkably enough, concentrated sulphuric acid droplets of 1μ radius are the only known particles that would satisfy most of the optical constraints for Venus clouds as derived from observations on Earth. There must be, however, at least one further aerosol component of smaller concentration, possibly mixed in with some of the sulphuric acid particles, to account for the observed large absorptivity of the clouds in the ultraviolet.

The ultraviolet absorber is patchy and, therefore, useful as a tracer for winds. Observations of these patches show them to rotate in the retrograde (westward) direction, essentially about the planetary axis, with a 4 to 5 day period, much faster than the 243 day retrograde period of the planetary surface. Before the presence of these winds was realized it was believed that such strong zonal winds could only arise as a result of processes on a rapidly rotating planet. Because of the relative ease with which these winds are deduced and their surprising nature, there has been many recent theoretical efforts attempting to explain them.

Two somewhat different approaches to such an explanation may be attempted. First, it is interesting to understand how such a wind system might

originate from an atmosphere corotating with the planet. For this to happen, the angular momentum of the winds must be provided by some means. Most of the models that have been proposed involve the organization of day-night convection into tilted patterns. Schubert and colleagues<sup>18</sup> have emphasized the tilting of the convection resulting from motion of a heating source and lags with height due to finite conductivity. Thompson<sup>19</sup> suggested that tilting of stream lines could originate from interaction between the solar driven convection cell and vertical shears in the zonal winds. Another approach emphasizes the excitation of internal gravity waves by a moving heat source in a stably stratified fluid.<sup>20,21,22</sup> These export momentum from the heating region in the direction of the motion of the heat source. The solar heating pattern rotates prograde relative to the atmosphere so this effect would generate winds in the observed direction. If internal gravity waves were excited, weak winds in the opposite direction would be expected above and below the heated region where the extracted momentum was redeposited. All these approaches just discussed involve only east-west motions. Other suggestions<sup>23,24</sup> have emphasized the role of north-south overturning in spinning up zonal winds. Presumably, only a physically realistic realistic 3-dimensional model (such as being developed by Young and Pollack<sup>25</sup>) will be able to establish the relative importance of the individual simple mechanisms. There is no reason to expect that the atmosphere ever corotated with the planet, so a better approach might be to start with the observed zonal winds and see what is necessary for the present winds to represent a stable configuration. This approach, however, is hindered by almost total lack of knowledge as to the winds above and below cloud level. Even at cloud level, recent observations (e.g.<sup>26</sup>) show the winds to vary by more than  $\pm 50\%$  so a steady picture is probably inappropriate.

Current realistic models of the Venus cloud level large-scale circulation include the large contributions of the clouds to absorption of solar radiation and infrared opacity. However, the

converse question as to the role of the large-scale circulation on the formation and maintenance of the clouds has not yet been addressed. If, as likely, formation of cloud particles depends on upward motions, the nightside and polar clouds should have originated earlier near the subsolar point and be undergoing some degree of dissipation.

The circulation regions at pressures several orders of magnitude higher or lower than Venus cloud level are equally important and interesting but more difficult to observe. The primary observational information on lower atmosphere circulation comes from the Venera 4, 7, and 8 probes<sup>27</sup> which shows the winds are indeed maximum near cloud level and decrease to a few meters sec<sup>-1</sup> or less near the surface. Much order of magnitude information on the circulation of the lower Venus atmosphere has been gained by simple theoretical arguments involving scale analyses and a parameterized dynamic model<sup>28</sup>. Our understanding of this region is expected to greatly increase in the next few years in the light of anticipated observations from the 1978 Pioneer probes and further development of realistic 3-dimensional numerical models.

The observational information on dynamic and thermal processes at the higher levels of the Venus atmosphere above 100 km, i.e. the mesosphere and thermosphere, is now scant but tantalizing. I have been developing over the past several years a comprehensive dynamic model of this region to interpret observed features and to infer other features that have not yet been measured. I do not know how to extend the stratospheric zonal winds up into this region so they are assumed, if present, to have a negligible effect. Otherwise, the model is as realistic as possible. It includes in great detail all the significant solar and infrared heating processes, and calculates not only winds, pressures, and temperatures, but also the relative concentrations of CO<sub>2</sub>, CO and O in a self-consistent fashion. Fig. 5 shows the calculated circulation<sup>29</sup> from dayside to nightside. The left frame shows horizontal winds in m sec<sup>-1</sup>

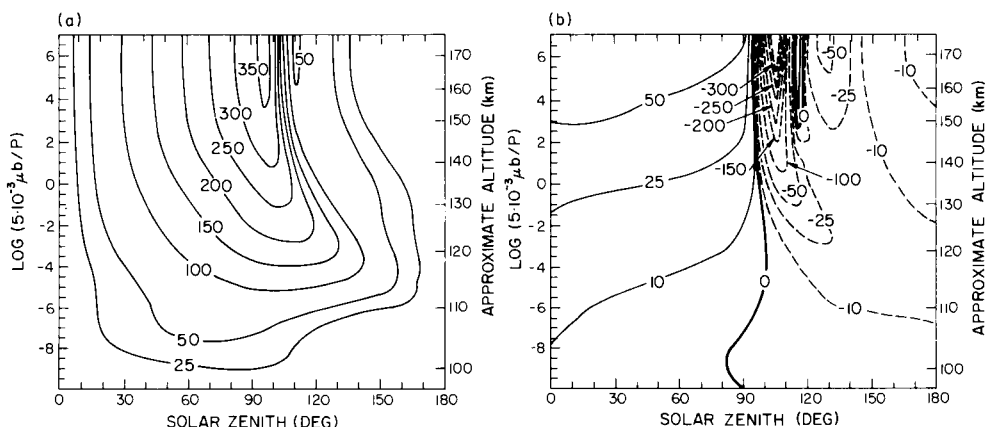


Fig. 5 Venus thermosphere motions (see text).

The maximum winds occur at highest levels just to the nightside of the terminator. They are four times as strong as the earlier discussed stratospheric zonal winds. The vertical motions in the right frame are in  $\text{cm sec}^{-1}$ . There are uniformly upward on the dayside but with most of the downflow occurs near the terminator on the nightside, where the horizontal winds rapidly decelerate. This peculiar behavior results from a build up on the night-side of the lighter gases, atomic oxygen and carbon monoxide. These species are produced on the dayside by photodissociation and transported downward on the nightside by the motions shown. At stratospheric levels, the CO and O encounter vigorous photochemical processes that are able to restore them back to  $\text{CO}_2$ . The dayside concentrations of O produced by the model are consistent with values inferred from ionospheric models. The latter reproduce past ionospheric observations. The 1978 Pioneer orbiter should be able to determine the validity of this picture by establishing the day-to-night variations of composition and temperature of the Venus thermosphere.

### V. Conclusions

On the basis of various examples I have discussed above, it can be concluded that planetary probes and earth based observations have revealed a wealth of fundamental physical processes operating in planetary atmospheres. Much progress has been made in modeling and interpreting these processes. Both observational and theoretical information is expected to rapidly further evolve in the next decade. The excitement and physical insights engendered by planetary exploration will surely have further profound impacts on the understanding of our own atmosphere, especially in the areas I have emphasized in this paper.

### References

1. Hanel, R., Conrath, B., Hovis, W., Kunde, V., Lowman, P., Maguire, W., Pearl, J., Pirraglia, J., Prabhakara, C., Schlachman, B., Levin, G., Straat, P., and Burke, T., Investigation of the Martian environment by infrared spectroscopy on Mariner 9, *Icarus*, 17, 423-442 (1972).
2. Leovy, C. B., Zurek, R. W., Pollack, J. B., Mechanisms for Mars dust storms, *J. Atmos. Sci.*, 30, 749-762 (1973).
3. Pirraglia, J. A., and Conrath, B. J., Martian tidal pressure and wind fields obtained from the Mariner 9 infrared spectroscopy experiment, *J. Atmos. Sci.*, 31, 318-329 (1974).
4. Pirraglia, J. A., Polar symmetric flow of a viscous compressible atmosphere: An application to Mars, *J. Atmos. Sci.*, 32, 60-72 (1975).
5. Conrath, B. J., Thermal structure of the Martian atmosphere during the dissipation of the dust storm of 1971, *Icarus*, 24, 36-46 (1975).
6. Zurek, R. W., Diurnal tide in the Martian atmosphere, *J. Atmos. Sci.*, 33, 322-337 (1976).
7. Dickinson, R. E., Infrared radiative heating and cooling in the Venusian mesosphere. I: Global mean radiative equilibrium, *J. Atmos. Sci.*, 29, 1531-1556 (1972).
8. Dickinson, R. E., Venus mesosphere and thermosphere temperature structure. I: Global mean radiative and conductive equilibrium, *Icarus*, 27, 479-493 (1976).
9. Lacis, A. A., Cloud structure and heating rates in the atmosphere of Venus, *J. Atmos. Sci.*, 32, 1107-1124 (1975).
10. Houghton, J. T., and Taylor, F. W., On remote sounding of the upper atmosphere of Venus, *J. Atmos. Sci.*, 32, 620-629 (1975).
11. Orton, G. S., The thermal structure of Jupiter. I: Implications of Pioneer 10 infrared radiometer data, *Icarus*, 26, 125-141 (1975a).
12. Orton, G. S., The thermal structure of Jupiter. II: Observations and analysis of 8-14 micron radiation, *Icarus*, 26, 142-158 (1975b).
13. Ingersoll, A. P., The meteorology of Jupiter, *Sci. Amer.*, 234, 46-56 (1976).
14. Lewis, J. S., The clouds of Jupiter and the  $\text{NH}_3\text{-H}_2\text{O}$  and  $\text{NH}_3\text{-H}_2\text{S}$  systems, *Icarus*, 10, 365-378 (1969).
15. Barcilon, A., and Gierasch, P., A moist, Hadley cell model for Jupiter's cloud bands, *J. Atmos. Sci.*, 27, 550-560 (1970).
16. Ingersoll, A. P., and Cuzzi, J. N., Dynamics of Jupiter's cloud bands, *J. Atmos. Sci.*, 26, 981-985 (1969).
17. Williams, G. P., and Robinson, J. B., Dynamics of a convectively unstable atmosphere: Jupiter? *J. Atmos. Sci.*, 30, 684-717 (1973).
18. Schubert, G., and Young, R. E., The 4-day Venus circulation driven by periodic thermal forcing, *J. Atmos. Sci.*, 27, 523-528 (1970).
19. Thompson, R., Venus's general circulation is a merry-go-round, *J. Atmos. Sci.*, 27, 1107 (1970).
20. Fels, S. B., and Lindzen, R. S., The interaction of thermally excited gravity waves with mean flows, *Geophys. Fluid Dyn.*, 6, 149-191 (1974).
21. Ramanathan, V., and Cess, R. D., An analysis of the strong zonal circulation within the stratosphere of Venus, *Icarus*, 25, 89-103 (1975).
22. Plumb, R. A., Momentum transport by the thermal tide in the stratosphere of Venus, *Quart. J. R. Met. Soc.*, 101, 763-776 (1975).
23. Leovy, C., Rotation of the upper atmosphere of Venus, *J. Atmos. Sci.*, 30, 1218-1220 (1973).

24. Gierasch, P., Meridional circulation and the maintenance of the Venus atmospheric rotation, *J. Atmos. Sci.*, 32, 1038-1044 (1975).
25. Pollack, J. B., and Young, R., Calculations of the radiative and dynamical state of the Venus atmosphere, *J. Atmos. Sci.*, 32, 1025-1037 (1975).
26. Traub, W., and Carleton, N., Spectroscopic observations of winds on Venus, *J. Atmos. Sci.*, 32, 1045-1059 (1975).
27. Marov, M., Avduevsky, V., Kerzhanovich, V., Rozhdestvensky, M., Borodin, N., and Ryabov, O., Venera 8: Measurements of temperature, pressure, and wind velocity on the illuminated side of Venus, *J. Atmos. Sci.*, 30, 1210-1214 (1973).
28. Stone, P., The structure and circulation of the deep Venus atmosphere, *J. Atmos. Sci.*, 31, 1681-1690 (1974).
29. Dickinson, R. E., and Ridley, E. C., Venus mesosphere and thermosphere temperature structure. II: Day-night variations, *Icarus*, submitted for publication (1976).

# MATERIALS AND PROCESSES FOR SHUTTLE ENGINE, EXTERNAL TANK, AND SOLID ROCKET BOOSTER

R. J. Schwighamer

*Marshall Space Flight Center, Alabama 35812*

## Abstract

The Space Shuttle will provide a low cost delivery system for Earth orbital payloads by amortizing launch costs through system reusability. The Shuttle flight system is composed of the Orbiter, an External Tank (ET)\* that contains the ascent propellant to be used by the Space Shuttle Main Engines (SSME)\*\*, and two Solid Rocket Boosters (SRB)\*\*\*. The ET is expended on each launch; the Orbiter and SRB's are reusable. It is the requirement for reuse which poses the exciting new materials and processes challenges in the development of the Space Shuttle. This paper deals with the materials and processes for the SSME, the ET, and the SRB. A brief description of the Space Shuttle and the mission profile is given. The Shuttle configuration is then described with emphasis on the SSME, ET, and SRB. The materials selection, tracking, and control system used to assure reliability and to minimize cost is described, and salient features and challenges in materials and processes associated with the SSME, ET, and SRB are subsequently discussed.

## Introduction

The accomplishments of the Space Program have been possible primarily because of the availability of highly reliable expendable launch vehicles and non-reusable spacecraft. However, the next generation space transportation system, the Space Shuttle, will provide a low cost delivery system for Earth orbital payloads by amortizing launch costs through system reusability. It is the reuse requirement which poses the exciting new materials and processes challenges in the development of the Space Shuttle.

The integrated Space Shuttle vehicle consists of the Orbiter, the External Tank (ET), and two Solid Rocket Boosters (SRB). The propulsive system for the Orbiter is composed of three 470,000 lb (vacuum thrust), reusable, high performance throttleable rocket engines burning liquid hydrogen ( $\text{LH}_2$ ) and liquid oxygen (LOX), and referred to as the Space Shuttle Main Engines (SSME). The reusable Orbiter can deliver into orbit single or multiple payloads of up to 65,000 lb, with cargo bay capacity of 60 by 15 ft.

The ET contains the ascent propellant to be used by the SSME's and is the only major flight structure intended to be expendable. The SRB's provide thrust augmentation during the initial phases of the launch, up to a velocity of approximately 4600 ft/sec, and are

\*Contractor — Martin Marietta Corporation. \*\*Contractor — Rocketyne Division of Rockwell International.

\*\*\*Contractors — Thiokol Corporation and MacDonnell Douglas Corporation.

recoverable by means of large parachutes. The combined sea level thrust of SSME's and SRB's is approximately 6.25 million lb.

A brief scenario of a future Space Shuttle mission is as follows: The mission begins with the installation of the mission payload into the Orbiter payload bay. The SSME's and SRB's will fire in parallel for liftoff. The two SRB's are jettisoned after burnout and are recovered after parachuting into the ocean. The ET is then jettisoned before the Orbiter has attained orbit. An orbital maneuvering system is then used for orbital insertion, orbit change, rendezvous, and the subsequent deorbiting thrust to return to Earth.

Payload bay doors in the Orbiter can be opened, allowing payload exposure or capture of any orbiting object if that is a requisite. After orbital operations of 7 days (30 days with additional consumables), deorbit and reentry into the Earth's atmosphere at a high angle of attack occur. At low altitude, the Orbiter then planes into horizontal flight for a typical high-performance type aircraft landing at approximately 185 kt nominal. A 2-week ground turn-around is the approximate goal for reuse of the Orbiter.

This paper deals with the materials and processes for the Space Shuttle elements, SSME, ET and SRB, for which the George C. Marshall Space Flight Center (MSFC) has management and development responsibility. The detailed treatment of these major Space Shuttle elements begins with an overview of the materials selection, tracking and control system employed by MSFC to provide that cohesiveness across these Shuttle elements so necessary to guarantee materials and processes uniformity with minimum cost, minimum documentation redundancy, and high reliability. A discussion of management information and control of Shuttle element materials and a detailed independent treatment of the salient features and challenges in materials and processes associated with SSME's, the ET, and the SRB's follow.

## Materials Control for SSME, ET, and SRB

Past experience has shown conclusively that a good materials control program is necessary to optimize reliability and minimize cost. Extensive experience with materials in the Redstone, Jupiter, Juno II, Saturn, and Skylab Programs has demonstrated conclusively the necessity to control the materials and associated processing used in critical space vehicle service. The

ability to know all the materials in the system and to recall this information on demand is equally important. A fact all too frequently overlooked by nonaerospace critics of meticulous materials control is simply that the final commitment to Shuttle liftoff is irrevocable. There is no turning around on the runway, no last minute opportunity to change one's mind; things have to work right the first time on the Shuttle. We believe this is within the state-of-the-art, primarily through the establishment of the proper disciplinary controls at the outset (early in the preliminary requirements/design cycle).

An effective materials control system must accomplish the following tasks:

1. Identify materials and processes
  2. Identify materials usages
  3. Identify, evaluate, and eliminate materials dependent hazards.\*
  4. Provide for waivers or deviations to materials and processes specifications, through the aegis of a Materials Application and Evaluation Board (MAEB).
  5. Document all materials and processes decisions and associated rationale.
  6. Provide for information retrieval.

In the execution of this responsibility, some specific materials properties and characteristics are of special concern:

1. Material environmental compatibility:
    - a. Compatibility with LOX or gaseous oxygen (GOX)
    - b. Propellant compatibility
    - c. Gaseous hydrogen ( $\text{CH}_2$ ) embrittlement
    - d. Hydraulic fluids/pressurization gases
    - e. Coolant compatibility
  2. Flammability (air)
  3. Toxicity (as related to production, or use, considering combustion, pyrolysis, etc.)
  4. Corrosion and stress corrosion
  5. Vacuum outgassing and contamination
  6. Age/life
  7. Properties and characterization.

The fundamental method by which materials are selected, tracked, and finally controlled at MSFC can be seen in

the Materials Control Logic Diagram (Fig. 1). Note that waivers/deviations are submitted in triplicate by the contractor via a Materials Usage Agreement (MUA). MUA's requiring action by the MAEB are acted on by the Board in real time. Some potential waivers/deviations to the materials specifications are resolved without submittal to the Board when it can be shown that there really is no departure from specifications. Such an MUA is withdrawn by the contractor involved through mutual agreement. Only authentic MUAs are logged and tracked by the system. In actual practice, only very rarely does an MUA ever progress farther through the logic network than the output of the MAEB to the project manager and thence to the contractor. Because the project manager has representation on the MAEB, the Board decision has been invariably final.

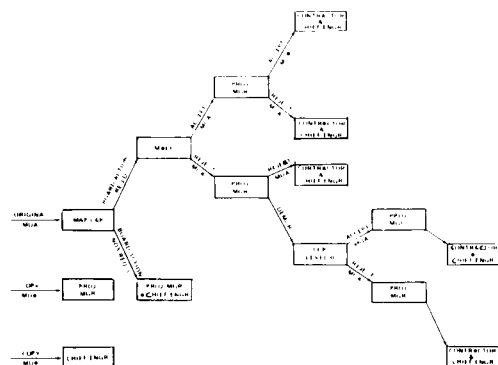


Figure 1. Materials control logic diagram.

This system is employed at MSFC in the management of materials control for SRB, ET, and SSME. The adoption of a uniform system has already proved invaluable by providing concrete assurance and tangible proof that materials requirements are met, and uniformity and equitability of materials excellence are being maintained across the three Shuttle elements. Also, the system quite naturally fosters cross-fertilization and greatly enhances the systems material compatibility aspect.

To the casual observer, the structural method of control previously described may seem inordinate when superficially contemplated. However, the enormous variety of materials with their multitudinous stringent environmental requirements such as high pressures and temperatures, LOX and GOX compatibility, GH<sub>3</sub> compatibility, and a host of other integrated and synergistic influences necessitates an orderly, disciplined method of materials control. And nowhere in the three aforementioned Shuttle elements are the challenges in materials development more crucial or more evident than in the SSME.

\* A material dependent hazard is defined as an occurrence that places either a person, the mission, or vehicle itself in jeopardy.

## SSME Materials and Processes

The SSME is a reusable high performance liquid propellant rocket engine with variable thrust. Three SSME's are used to power the Orbiter, each burning approximately 8 min from launch through the vehicle boost period. Each SSME employs a staged combustion cycle to power the turbopumps and utilizes high combustion chamber pressure. The staged combustion cycle features partial propellant combustion first in the pre-burners at high pressure and relatively low temperature, then subsequently the propellants are completely combusted at high temperature and high pressure in the main chamber, before expanding through the high-area-ratio-nozzle. Figure 2 shows typical pressures, temperature, and propellant flow rates used.

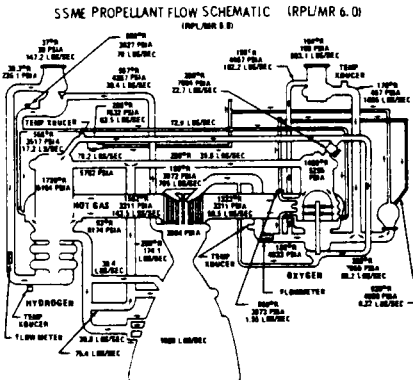


Figure 2. SSME propellant flow schematic.

The hydrogen fuel cools all combustion devices which are contacted by high temperature combustion products. The engine is controlled by an electronic controller which automatically performs the checkout, start, main-stage, and engine shutdown functions. For flight, the three orbiter SSME's operate in parallel with the SRB's during launch and then continue to burn until just before injection after SRB separation. Each of the engines operates at a mixture ratio (LOX/LH<sub>2</sub>) of 6:1 and a chamber pressure of approximately 3000 psia to produce a sea level thrust of 375,000 lb and a vacuum thrust of 470,000 lb with a fixed nozzle area ratio of 77.5:1. The engines are throttleable over a thrust range of 50 to 109 percent of the design thrust level. The throttleability feature allows a higher thrust level during liftoff and during the initial ascent period, and also provides the capability to limit Orbiter acceleration to 3 g's during the final period of the ascent. The engines are gimbaled to provide roll, pitch, and yaw control during the Orbiter boost phase. The engine gimbal angle capability is approximately  $\pm 10.5^\circ$  of pitch and  $\pm 8.5^\circ$  of yaw control.

The aspects of reusability and the high engine operating pressures and temperatures are prime techni-

cal drivers in the engine design and provide the bulk of the technical challenges associated with the engine development. The following are of considerable importance to the ultimate success of the engine:

1. Hydrogen environment embrittlement (HEE)
2. LOX/GOx compatibility
3. Stress corrosion cracking (SCC)
4. Hydraulic fluid testing and qualification.

More than 50 different alloys are used in construction of the SSME, many of them well established in the Aerospace Industry. However some of the alloys are relatively new, with less accumulated backlog of experience, especially in the high pressure hydrogen environment. Table 1 gives examples of the type materials used and the related applications.

Table 1. Space Shuttle Main Engine Metallic Materials

Material	Applications
Inconel 617S	Alloys, manifolds, structural shells, bellows, valves, springs
Inconel 625	Face plates, valves, acoustic mass, spark plug adaptors
René 41	Bolts, screws
K-MONEL®	Turbopump stators and rotors, housing covers
MAR-M26 (DS)	Turbine blades
MAR-M26 (CC)	Turbine Nozzles
Wasaloy	Disc shafts
140C stainless steel	Thrust bearings, valve seats
2024 Aluminum	Reliner rings
Tons + 50 Aluminum	Valve housings, diffuser assemblies
NARCOV-Z	Thrust chamber liner
7075-T73	Pneumatic console housing
ARMCO 21-6-9	Spark plug housing, flow straighteners
Kovar	Adapters
Beryllium Copper	Bearing Assemblies
Ti-6Al-4V-2SN	Gimbal bearing and ring
Ti-6Al-4V	Actuator static manifolds
Ti-5Al-2-5 cu	Impellers, valves
Silvers-cu	Seals
304H	Injector elements, filters, connectors, assemblies
Narloy A	Baffles, ASI insert
Havens 188	Embossed element sleeve, ASI nozzle, mounting flange rings, shells, flanges, brackets
317 CRES	Mixer tube plate, plenum rings
A-286	Coolant tubes, baffle element sleeves, nuts, washers, solenoid valve, body shafts
Inconel 903	Transition rings, IEEE protection, strut ring, turbine shell, bellows housing, diffusers, transfer tube, sleeve assembly
321 CRES	Flowmeter sleeves, and hubs
mon-76	Seal mounting plate, burst diaphragm
Falloy	Springs
Inconel X-750	Seals
Alloy 713 LC	Nozzle turbine casting
Rastello B	Pump housing cartridges
902 CRES	Recessers, shims, and pins

## Hydrogen Environment Embrittlement

Many of the iron, nickel, and cobalt-based alloys are adversely affected by high pressure hydrogen in terms of reduced ductility, tensile strength, low cycle fatigue life, and increased crack growth rates when used in applications involving plastic strain.

Inexplicably and often, HEE effects do prove to be more pronounced at room temperature than at either higher or lower temperature. The graph of notch strength versus temperature for electroformed nickel shown in Figure 3 gives graphic evidence of this fact. An appreciable amount of electroformed nickel is used in the SSME.

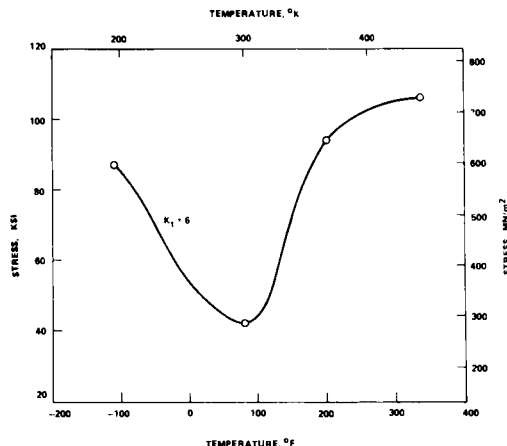


Figure 3. Notched strength versus temperature for EF nickel in 1200 psi H<sub>2</sub>.

The electroforming process has been developed to a high degree of perfection and is used extensively as a process to fabricate and bond SSME structural members. In fact, electrodeposited (ED) nickel is used to close out the NARLOY Z main combustion chamber liner; therefore, ED nickel resistance to HEE is of prime concern. The solution to the embrittlement problem in this instance proved to be the use of an ED copper coating process to protect the nickel.

Table 2 gives a compilation of notched strength data accumulated from work done by Pratt and Whitney, Rocketdyne Division of Rockwell International and the MSFC. In general, HEE appears in the presence of relatively high purity hydrogen and is more pronounced at room temperature and high pressure, is not time dependent, and disappears with no after effects upon removal of the hydrogen environment (provided there was no plastic strain while in the environment). The increased effect of HEE at high pressure, mentioned earlier, is clearly depicted in a comparison of two materials used extensively in the SSME. Incoloy 903 is a corrosion and heat resistant age-hardenable iron-nickel-base alloy, while Inconel 718 is a wrought, age-hardenable nickel-base alloy. Figure 4 shows the

Table 2. Relative Resistance to Hydrogen Embrittlement  
Notched Strength Ratio (H<sub>2</sub>/He) for Various Alloys in  
Hydrogen at Room Temperature

Alloy	$K_t$	Pressure ksi	Ratio H <sub>2</sub> /He
250 Maraging	✓	10	0.12
410	✓	10	0.22
1042 (Q&T)	✓	10	0.22
17.7 PH (TH 1050)	✓	10	0.23
HP 9-1-20	✓	10	0.24
H-11	✓	10	0.25
Inconel N-750	6.3	7	0.26
Rene 11	✓	10	0.27
ED Nickel	✓	10	0.31
4140	✓	10	0.40
Inconel 718	✓	10	0.46
MP 35N	6.3	10	0.50
440 C	✓	10	0.50
Ti-6 Al-4 V (Sta)	✓	10	0.58
Monel 400	6.3	7	0.65
D 979 Stainless	6.3	7	0.69
Nickel 270	✓	10	0.70
CG 27 Stainless	6.3	7	0.72
A 515-G70	✓	10	0.73
HY 100	✓	10	0.73
A 372-IV	✓	10	0.74
1042 (Normalized)	✓	10	0.75
Inconel 625	✓	5	0.76
A517-F (T-1)	✓	10	0.77
A 533-B	✓	10	0.78
Ti-6 Al-4 V (Ann.)	✓	10	0.79
1020	✓	10	0.79
HY 80	✓	10	0.80
Inconel 706	6.3	7	0.80
Ti-5 Al-2.5 Sn ELI	✓	10	0.81
Armco Iron	✓	10	0.86
304	✓	10	0.87
321	✓	5	0.87
Hastelloy X	✓	5	0.87
305	✓	10	0.89
Astroloy	✓	5	0.90
347	✓	5	0.91
Haynes 188	6.3	7	0.92
304 N	6.3	15	0.93
310	✓	10	0.93
Be-Cu (Alloy 25)	✓	10	0.93
RA 330	6.3	7	0.95
A-286	✓	10	0.97
21-6-9	6.3	7	0.97
7075-T73	✓	10	0.98
6061-T6	✓	10	1.00
OFHC Copper	✓	10	1.00
316	✓	10	1.00
Incoloy 903	✓	5	1.00

relative performance of these two alloys with regard to crack growth rate at various stress intensities and at room temperature (highest temperature susceptibility). Note that the iron base alloy 903, in this instance, show far less pressure dependency than the nickel base alloy 718; therefore, it does not generally require the coating and protective overlay of a material such as Incoloy 88. The design strategy to avoid the debilitating effects of GH<sub>2</sub> embrittlement has been to:

1. Use nonsusceptible materials where possible
2. Avoid plastic strain (notches, sharp fillets, etc.)
3. Use appropriate processes to provide an overlay or coating of nonsusceptible material.

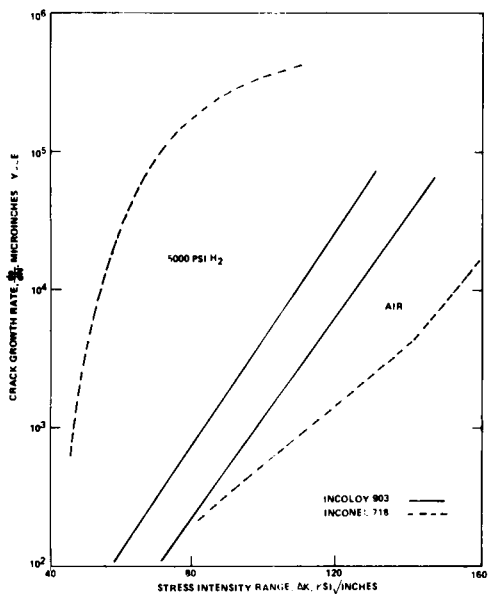


Figure 4. Crack growth rate,  $da/dN$ , versus stress intensity range,  $\Delta K$ , for Incoloy 903 and Inconel 718 in air and 5000 psi hydrogen at room temperature with a 9-minute load time cycle (simulated SSME cycle)

Although the basic embrittlement mechanism is by no means well understood, ways and means of circumventing its harmful effects on material properties have been devised. This is done frequently by appropriate coating or plating operations in the manufacturing processes and by the other design stratagem previously noted, i.e., keeping design stresses low enough to avoid plastic strain.

#### LOX/GOX Compatibility

LOX/GOX materials compatibility has been a persistent specter in rocket propulsion systems since the beginning. The recorded history of LOX/GOX material compatibility testing at MSFC dates back to the mid-50's when Lucas and Riehl<sup>1</sup> at the Army Ballistic Missile Agency developed an instrument for acquisition of impact sensitivity data for use by designers then designing the first Saturn space vehicles. At that time, an impact sensitivity specification called MSFC-SPEC-106 was also developed which, together with its successors, has been the primary LOX/GOX materials compatibility regulatory means employed during the design of the Saturn vehicles. The Apollo 13 incident was the crucial happening in NASA which pointed up the urgent requirement for further research on LOX/GOX compatibility at high pressure. In that event, a Teflon-fueled LOX/GOX fire in the No. 2 supercritical O<sub>2</sub> tank caused tank rupture in the CSM of the Apollo 13 approximately 55 hr after liftoff, while enroute to the moon. The extensive failure investigations subsequently conducted gave some

unprecedented insight into the next generation of problems to be solved in the operation of the even higher pressure LOX/GOX systems used on SSME.<sup>2</sup> This insight led directly to the development of a 10,000 psia (68.94 MN/m<sup>2</sup>) tester built to MSFC specified requirements by the Rocketdyne Division of Rockwell International.<sup>3</sup> This tester incorporated many new features such as the balanced striker, oscilloscope and digital monitoring of plummet velocity, material reaction via photocell flash, load cell response (measuring energy to the sample) and sample temperature and cell pressure.

In developing materials LOX/GOX compatibility design data, the high pressures used in the SSME have necessitated a departure from the previous low pressure criterion of "go-no go." That is, in some applications, materials tested at the high anticipated-use pressures do not meet the former straightforward low pressure impact sensitivity criterion of 10 kg m energy delivered to the test specimen. It has been necessary to evaluate the materials' LOX/GOX threshold energy density rate ( $E^*$ ) at representative use pressure, temperature, and material thickness. Further, the threshold energy density rate is then used to determine a figure of merit by dividing the  $E^*$  by the energy density rate reasonably attainable in the component in question. This gives one a "figure of merit" on which to judge the application, but it is not precisely correct to refer to this number as a safety factor. I consider the term "safety factor" in the commonly used structural design context as inappropriate to describe the calculated figure of merit, since there cannot be that same degree of precision in the absolute magnitude of the figure of merit number. Materials, metallic and nonmetallic, are assessed on this basis for the critical very high pressure and temperature applications. In certain special cases, effects such as adiabatic compression and cavitation are also taken into account.

Figure 5 shows the precise decision logic used in the accurate determination of a material threshold energy. This is then convertible into the energy density rate parameter  $E^*$  by knowing the test specimen modulus and the plummet deceleration rate. For reference purposes the standard 10 kg m drop in a standard tester equates to an  $E^*$  of approximately  $2.4 \times 10^6$  ft-lb/in.<sup>2</sup>/sec.

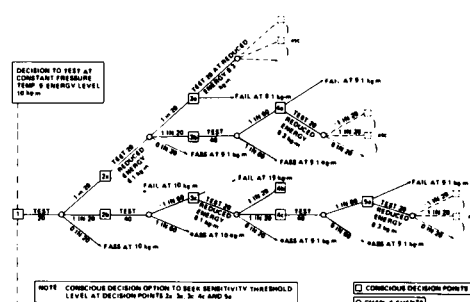


Figure 5. Decision logic diagram for LOX/GOX impact sensitivity threshold determination.

Table 3 shows some of the recent test data relating effects of high pressure and material thickness to impact threshold sensitivity energy for some of the more important nonmetallic materials used in the SSME. These data show an increased sensitivity with increasing pressure, and decreased sensitivity with increased material thickness. Both results are explainable on the basis of increased energy density per unit time. As noted earlier, if the rate of energy absorption is a variable, then  $E^*$  will increase or decrease accordingly, a factor which must ultimately be accounted for in analyzing components using the factor of merit calculation method.

**Table 3. Effects of Pressure and Material Thickness on Impact Threshold Sensitivity Energy for Selected Nonmetallic Materials in LOX**

Material	Thickness (in)	Pressure (psia)	Threshold Energy (kg m)
CTFF	0.053	1500	10
CTFE	0.050	8800	< 6
CTFE	0.125	8800	<10
PTFE	0.050	1500	10
PTFE	0.050	5500	9
PTFE	0.050	8800	8
PTFE Glass	0.100	300	10
PTFE Glass	0.100	5200	3
15 PTFE Glass	0.050	1500	10
15 PTFE Glass	0.050	8800	5
Mineral Filled PTFE	0.062	1500	10
Mineral Filled PTFE	0.062	5000	> 6
FEP	0.050	1500	10
FEP	0.050	8800	6
FEP	0.125	9000	10

Other test data indicate that almost all the metallic materials used in the SSME are insensitive to the 10 kg m energy level in either LOX or GOX at pressures up to at least 8,000 psi and at the anticipated use temperatures. So, the high pressure effect on LOX/GOX sensitivity has been carefully explored for the range of applications anticipated in the SSME, and workable solutions have been developed accordingly.

#### Stress Corrosion Cracking

In past space vehicle and engine development programs, one of the most insidious problems has been stress corrosion cracking (SCC) of certain alloys. The insidious aspects of SCC has to do with the propensity for the cracking to progress undetected inside holes,

under attachments, and at other virtually uninspectable locations where the combined action of corrosion and static tensile stress conspired to produce brittle fracture. Nearly all metal systems extensively used in aerospace vehicle design contain one or more alloys susceptible to SCC in some environment. Unfortunately, the higher the strength, the greater the susceptibility to SCC. Like the siren Lorelei, the lure and enticement of superior strength seemingly continue to bewitch designers into the selection of SCC susceptible alloys, in spite of the attendant risk.

In full recognition of this inherent tendency, Design Criteria for Controlling Stress Corrosion Cracking, MSFC Document (10M33107B), was prepared at the Marshall Center<sup>4</sup> to clearly define and control the use of alloys with respect to SCC. This is the controlling SCC document not only for the SSME development but for the ET and the SRB as well. The document is so written to group alloys into three main categories, or tables:

1. Alloys with high resistance to SCC
2. Alloys with moderate resistance to SCC
3. Alloys with low resistance to SCC.

Not all alloys will be found in these tables, since only materials are listed for which there is a statistically meaningful body of SCC data available. The use of materials other than those listed requires appropriate substantiating data before any use is permitted, and then only through the submittal and approval of an MUA. In spite of a sustained effort to purge susceptible materials entirely from the system, one inevitably finds a few isolated cases where a specific property is so crucial in that specific application, that SCC must be eliminated by some other stratagem and a susceptible material must be used. When such a case of dire necessity to use a SCC susceptible material arises, an MUA must be submitted with the following information:

1. Combination of all tensile service stresses (sustained structural, assembly, handling, etc.), when additive, must be less than the threshold stress for SCC.
2. Component is hermetically sealed or totally immersed in nonmoisture-bearing oil in a sealed system.

Only a very few examples come to mind where SCC susceptible alloys must be used, the most notable being the use of 440C steel in bearings where there is a requirement for high hardness and where the wear characteristics of the material are superior to any other contender. Occasionally, a precipitation hardening alloy must be used where high temperature heat treatment processes cannot be employed. In such cases, adequate precautions must be taken to prevent excessively high assembly or use stresses, and to protect the material from moisture or other aggressive media. The list of parent materials with high resistance to SCC at ambient temperature, in or around salt water (alternate immersion), is quite impressive (Table 4). Weldments present a more difficult problem, and data are not as

Table 4. Alloys with High Resistance to Stress Corrosion Cracking

Steel and Nickel Alloys			
Alloy	Condition	Alloy	Condition
Carbon Steel (1000 Series)	Below 180 ksi YS	PH 13-8 MO Stainless Steel	H1000 and above
Low Alloy Steel (4130, 4340, D6AC, etc.)	Below 180 ksi YS	15-5 PH Stainless Steel	H1000 and above
Music Wire (ASTM 228)	Cold drawn	PH 14-8 Stainless Steel	CH900 and SR 11950 and above
HY-80 Steel	Quenched and tempered	PH 15-7 MO Stainless Steel	CH900
HY-130 Steel	Quenched and tempered	17-7 PH Stainless Steel	CH900
HY-140 Steel	Quenched and tempered	Hastelloy C	All
1095 Spring Steel	Quenched and tempered	Hastelloy X	All
300 Series Stainless Steel (Unsensitized) <sup>a</sup>	All	Incoloy 901	All
21-6-9 Stainless Steel	All	Incoloy 903	All
Carpenter 20 CB Stainless Steel	All	Inconel 718	All
Carpenter 20 CB-3 Stainless Steel	All	Inconel X-750	All
A286 Stainless Steel	All	Ni-SPAN-C 902	All
AM350 Stainless Steel	SCT 1000 and above	Rene <sup>f</sup> 41	All
AM355 Stainless Steel	SCT 1000 and above	Unitemp 212	All
ALMAR 362 Stainless Steel	H1000 and above	Waspaloy	All
Custom 455 Stainless Steel	H1000 and above		
Aluminum Alloys			
Wrought <sup>b</sup>		Cast	
Alloy	Condition	Alloy <sup>f</sup>	Condition
1000 Series	All	319.0, A319.0	As cast
2011	T8	333.0, A333.0	As cast
2024	T6 <sup>c</sup> T8 <sup>d</sup>	355.0, C355.0	T6
2219	T6, T8	356.0, A356.0	All
3000 Series	All	357.0	All
4032	T6	B358.0 (tens-50)	All
5000 Series	All <sup>e</sup>	359.0	All
6000 Series	All	380.0, A380.0	As cast
7075	T73	A612.0, C612.0	As cast
7475	T73	514.0 (214)	As cast
		518.0 (218)	As cast
		535.0 (Almag 35)	As cast
Miscellaneous Alloys			
Wrought		Cast	
Alloy	Condition	Alloy	Condition
Beryllium, S-200C	Annealed	Magnesium, ZK51A	All
HS 25 (L605)	All		
HS 188	All		
MP35N	All		
Titanium, 6Al-4V	All		
Titanium, 13V-11Cr-3Al	All		
Magnesium, M1A	All		
Magnesium, LA141	All		
Magnesium, LAZ933	All		

a. Including weldments of 304L, 316L, 321 and 347.

b. Mechanically stress relieved (TX5X or TX5XX) where possible; including weldments of the weldable alloys.

c. Except plate and forgings which have low resistance.

d. Except forgings which have low resistance and plate which has moderate resistance.

e. High magnesium content alloys 5456, 5083, and 5086 should be used only in controlled tempers for resistance to SCC and exfoliation; these alloys are not recommended for high temperature application (150°F and above).

f. The former designation is shown in parenthesis when significantly different.

extensive in this case, although there are good data for aluminum alloys and selected stainless steels in the 300 series.

Unlike the Lorelei, I do not propose to entice the reader-designer by printing in this paper the list of moderate and highly susceptible alloys. Those with legitimate justification will no doubt acquire, or already have, a copy of the MSFC 10M33107B document. In the SSME, predominantly non-SCC-susceptible materials have been used, but where departures have been absolutely necessary, then the previously noted use criteria have been relied upon.

#### SSME Hydraulic Fluid Mil-H-83282

As can be seen in Figure 2, the higher operating pressures in the SSME have been accompanied by higher operating temperatures as well. The requirement for higher operating engine temperatures and reusability, and safety consideration prompted a critical assessment of the old standby hydraulic fluid (Mil-H-5606) used so successfully in the Saturn program, which was straight hydrocarbon material. Coincidentally, a "new" fluid, Mil-H-83282, a synthetic hydrocarbon, was under development by the DOD, reportedly for use as a more fire resistant, high temperature replacement for the older fluid. Properties data for the Mil-H-83282 fluid were gathered and assessed for SSME and Shuttle Orbiter applicability, and it became apparent that the fluid could not, at that time, be considered completely characterized for use in the SSME hydraulic system, especially in four specific areas:

1. Lubricity
2. Corrosion and stress corrosion
3. Elastomer and seal compatibility
4. Sustained operation in the 275° to 300°F range.

Subsequently, test data showed that the Mil-H-83282 fluid was superior to the Mil-H-5606 fluid with regard to lubricity, especially under high pressure load conditions. Extensive corrosion testing revealed negligible weight loss from metallic samples in air and in a nitrogen atmosphere blanket environment around the fluid in which the samples were immersed. Testing of soft goods such as Buna N and Viton revealed that Buna N withstood a temperature of 212°F for 1 year quite well, and the Viton retained good properties for 180 days at a temperature of 300°F, a temperature much higher than any anticipated for use in the SSME. In testing for oxidation characteristics at 275° to 300°F, it became apparent that the Mil-H-83282 fluid was much less affected when the fluid was deaerated and operated in a sealed system. Under these conditions, the fluid performed quite well at 275°F operating temperature with virtually no degradation of properties.

A comparison of pertinent properties of the older Mil-H-5606 material and the newer Mil-H-83282 material can be seen in Table 5. Particularly noteworthy from a

safety viewpoint are the favorable flash point, fire point, and autoignition temperature.

Table 5. Typical Properties of Hydraulic Fluids

	Mil-H-5606	Mil-H-83282
KINEMATIC VISCOSITY, CPS		
At 300°F	2.36	1.89
At -10°F	188	2100
FLASH POINT, °F	209	410
FIRE POINT, °F	230	495
AUTOIGNITION, °F	460	640
POUR POINT, °F	-75	-85
SPECIFIC GRAVITY, gm/cm³	0.8681	0.8433
RUBBER SWELL, %		
72 hr at 275°F	—	11.7
BULK MODULUS ISOTHERMAL SECANT, PSI		
at 4000 psig	212,000	236,000
BULK MODULUS ADIABATIC, PSIG		
500-3000 at 75°F	260,700	265,000
500-3000 at 275°F	200,900	182,000
SPECIFIC HEAT		
At 100°F	0.465	0.499
At 300°F	0.590	0.598
Thermal Conductivity, BTU hr/ft² °F ft		
At 100°F	0.079	0.097
At 300°F	0.076	0.096
VAPOR PRESSURE ASTM, ISOTERMOSE, MM		
At 100°F	0.6	0.6
At 300°F	56.0	7.8
VACUUM EXPOSURE		
7 days at $2.5 \times 10^{-4}$ torr		
WEIGHT LOSS, %	89.7	8.9
RESIDUE	Tacky	Oily
4-BALL TEST DATA, MM		
1 KG LOAD	0.20	0.15
10 KG LOAD	0.25	0.24
40 KG LOAD	0.63	0.37

#### SSME Processing in General

The SSME is fabricated and assembled largely by welding and brazing of the wrought and cast components. Extensive and unique use of electron beam welding techniques is evident, but gas tungsten arc (TIG) welding is also used. Inertia welding is used to weld the oxidizer "posts" into the main injector body. The brazed assemblies are predominantly furnace brazed in a hydrogen environment, using noble-metal braze alloys to join Inconels 625/718, A-286, and Haynes 188. Overlays or surface barriers to hydrogen are provided by gold and copper platings of only 0.002 in. thickness, and Incolloys 88 and 903 are used extensively in the form of weld bead overlays. The corrosion and heat resistant age-hardenable iron-nickel-base alloy Incoloy 903 is used extensively because of its low thermal expansion, low elastic modulus, high strength, and resistance to HEE. Inconel 718, a vacuum melted austenitic precipitation hardened nickel-chromium base superalloy with excellent corrosion resistance, is also used extensively and is overlaid largely with the Incoloy 903 during processing to provide protection for HEE where temperatures above approximately -100°F are expected, or where strains greater than approximately 0.5 percent will exist. Unquestionably, the manufacturing of the SSME represents one of the most challenging opportunities currently existing in the field of aerospace hardware.

## ET Materials and Processes

The ET contains all the propellants supplied to the Orbiter main engines (LOX and LH<sub>2</sub>). The fluid controls and valves for the main propulsion system are located in the Orbiter to reduce recurring costs. Antivortex and slosh baffles are mounted in the oxidizer tank to minimize liquid residuals and to damp fluid motion. The ET is 28 by 155 ft and weighs 73,881 lb empty. It is currently planned for the ET to contain approximately 1.5 million lb of propellant. The forward LOX tank holds 1.3 million lb of LOX and the volumetrically larger rear tank holds 0.2 million lb of LH<sub>2</sub>. The ET system is the only expendable element of the Space Shuttle and is jettisoned after the Orbiter has consumed the required fuel before achieving orbital velocity. The ET breaks up as it tumbles back through the atmosphere into an ocean impact area. The ET weight at main engine cutoff (MECO) is 78,807 lb (dry weight plus residual propellants) as presently planned. The materials and processes required to fabricate this unique "drop tank" will now be discussed in some detail.

## ET Welding and Fracture Mechanics

The ET is primarily a welded structure, fabricated predominantly of aluminum alloy 2219. Saturn space vehicle manufacturing experience has been invaluable in providing the insight required to assure better weld quality with less repairs. Indeed, that experience plus the diligent weld materials properties and characterization work conducted in parallel, coupled with the coming-of-age and general acceptance of fracture mechanics, has laid the ground work for deliberate, calculable quality level, and optimization of manufacturing cost in the fabrication of the ET. The evolution of the current ET design and manufacturing philosophy is a lucid example of one of the salient characteristics of the aerospace industry — learning by, and building on, past experience thereby greatly enhancing future designs.

Capitalizing heavily on the past beneficial experiences with aluminum alloy 2219 on Saturn space vehicles, a large portion of the ET is composed of that alloy. Aluminum alloy 2024 is used also with due consideration given in the tank design to the somewhat reduced notched/unnotched tensile strength ratio at cryogenic temperatures, and non-stress corrosion cracking susceptible tempera and material forms of 2024 alloy have been used almost exclusively. Table 6 shows the major metallic materials used in the ET together with the appropriate applications. The materials selected and the associated processing have been strongly influenced by previous Saturn experience and by the early decision to capitalize on the accumulated fracture mechanics knowledge and experience.

Many of the Saturn V welds in 2219 alloy were made in a horizontal position, a condition which aids and abets the formation of weld porosity by entrapment of oxides and gas. A comprehensive analysis of accumulated weld data near the end of the Saturn Program in the late 1960's indicated that the major contributor to welding problems had indeed been weld porosity. As a consequence, a detailed study was initiated with the objective

**Table 6. Space Shuttle External Tank Metallic Materials**

Material	Applications
A356	Lighting, rad
2024 <sup>a</sup>	Tank baffle webs, stiffeners, angles and stringers, ring frames, chords, frame stabilizers, skin and stringers, panels, buttstraps and flanges
2219	Tank and ogive gores, fittings, T-rings, tank band panels, legs, ring frames, caps, covers, fittings, longerons, frame stabilizers, thrust panels, struts, channels, crossbeams, bulkheads, brackets, stiffeners, and braces
6061	Nose cap skins, frames and doublers
6063	Skin and stringer panels
7075 <sup>b</sup>	Panel I-beams, longerons, ring frames, beam chords, webs, stiffeners, bulkheads, thrust fittings and struts
TiAl-2.5 Sn	Strut fittings, spindle housings, and tank fittings
Inconel 718	Spindles
MIL-S-22499B	Shims
T-5648A	Tie plates

a. Design allows for reduced notch unnotched tensile strength ratio at cryogenic temperatures and some small application of moderately SCC susceptible TiAl plate, based on short transverse stresses being below SCC threshold stress.

b. Alloy is not used in any application at temperature colder than -200° F in recognition of reduced notch-to-unnotched tensile strength below -200° F and is used either in non-SCC susceptible temps or in applications where short transverse stress is below the SCC threshold stress.

of determining very precisely the true nature of weld strength degradation as a result of weld porosity for a wide range of conditions.<sup>5</sup> The results of this extensive investigation are best shown in Figure 6. Here we see statistical proof that the percentage of accumulative pore area in the cross-sectional plane of the test specimen bears a very strong linear relationship with the ultimate tensile strength. In fact, the relationship is so pronounced it is cardinal, having a linear regression correlation coefficient ( $\gamma$ ) which exceeded -0.900, with the square of the correlation coefficient being in excess of 0.81. It should be noted, however, that the results of this analysis would not be appropriate for severe linear, or string, porosity. The results do apply to discrete porosity, however, which almost always predominates. To capitalize on this knowledge and the prior welding experience, two important changes were made for the ET:

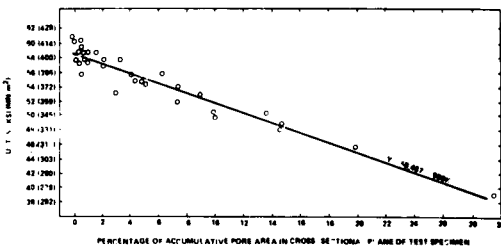


**Figure 6. Cryogenic, -320°F (-196°C), ultimate tensile strength of flush bead TIG weldments in alloy 2219-T87, 0.250 in. (0.635 cm) plate, versus percentage of accumulative area in porosity in cross-sectional plane.**

1. Porosity limits were relaxed.

2. Excellent welding tooling, designed to utilize down-hand welding, was developed, thereby, greatly minimizing the incidence of porosity.

The Martin Marietta Corporation at the NASA Michoud Plant in New Orleans has designed and is using some of the most rigid and highest precision aluminum welding tooling ever used in any aerospace program; preliminary results already show the wisdom of the above noted changes.

Figure 7 shows the ET LH<sub>2</sub> barrel trim-and-weld fixture and gives graphic evidence of the design consideration given to rigid positive tooling. Note that the welding of the barrel section longitudinal weld is done in the inside, down-hand position at the 6 o'clock location. This fixture trims the edges of the eight skin panels per barrel section to be welded. The barrel is rotated in a horizontal position to index each seam sequentially under the weld head, located on the bottom inside of the assembly.

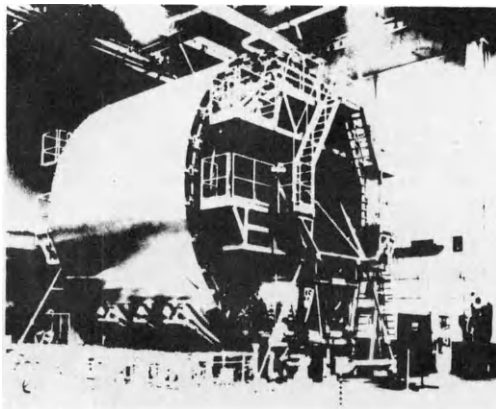


Figure 7. LH<sub>2</sub> barrel trim-and-weld fixture.

The "opportunity cost" of the noted tooling pales into insignificance when the full advantage of the new welding approach is realized. This effects tremendous savings in subsequent radiographic inspection costs. It is intended to radiograph all welds during the Design Development Test and Evaluation period, involving six ET's. Subsequently, only fracture critical welds will be radiographed. For the purposes of this discussion, a fracture critical weld is defined as one in which the critical flaw size is less than the thru-weld cross section thickness. The statistical validity of this approach will be verified by a careful analysis of the 100 percent radiographic results during the development phase, involving the fabrication of the first six tanks, before the production tanks are begun.

The fracture mechanics testing approach employed on ET consists of precracking appropriate specimens and then proof-stressing them to the point where

penetration, or fracture, is imminent. The specimens are then cycled under operating conditions (stress and temperature profile) to simulate actual operating conditions and proof factor being evaluated. Specimens pass the test when they survive 12 operating cycles; the design requirement is three cycles with a scatter factor of four. Design and verification test requirements for the ET overall structure are 1.40 safety factor on ultimate and 1.50 safety factor on ultimate for pressure vessels with a scatter factor of four.

The fracture mechanics approach has also resulted in the "grading" of welds. Twenty-one grades of welds have been established, each of which has an associated allowable defect length for a single defect. For pressure vessel welds, defect lengths are not to exceed  $1.8 t$  (where  $t$  is the material thickness of the thinnest member being joined). This stratagem approaches the maximum manufacturing leeway permissible and minimizes the cost and tank weight without compromising ultimate reliability.

#### ET Thermal Protection System (TPS) Considerations

The ET TPS is designed to maintain the primary structure and its subsystem components within design temperature limits during prelaunch and ascent phases. It currently consists primarily of two types of sprayable material to meet a variety of mission and surface application conditions. One protects primarily by insulating and the other by ablating. Although both TPS materials used on the ET are sprayable, both can be used pre-molded for certain applications such as closeouts. The TPS system also includes the use of phenolic insulator blocks and cryopumped argon-jacketed feed and recirculation lines. Prior to launch, the TPS maintains consistent LOX and LH<sub>2</sub> boiloff rates within the vent valve capabilities, helps loading accuracy and propellant density, minimizes air liquification and ice formation on the LH<sub>2</sub> tank, and insures LOX and LH<sub>2</sub> specified temperatures on the Orbiter surface. During ascent, the TPS maintains the primary structure and subsystem components within the design temperature limits and it minimizes unusable LH<sub>2</sub>. The types, areas, and thicknesses of the TPS materials are based primarily on worst-case environments which can only be encountered in the case of an abort-once-around condition.

The Shuttle ET TPS flight environment is a more severe one than the Saturn V stages experienced; temperatures in general are higher. Saturn V foam insulation was a polyurethane material, while the ET foam is a fluorocarbon-blown-rigid polyisocyanurate foam. This foam compares favorably with polyurethane foam regarding density and thermal conductivity, and although tensile strength is somewhat less, the polyisocyanurate foam can withstand greater heating and greater aerodynamic shear and has superior thermal stability. The foam is entirely cryo-strain compatible. A chromate inhibited epoxy primer is applied over the Iridite coated 2219 material before spraying the foam. The foam is net-spray applied (no machining to contour) at  $125 \pm 5^\circ\text{F}$  and at a maximum relative humidity of 60 percent. A silicone cover coat is then used to cover the net-sprayed foam. The spraying of the foam insulation is carried out under

very carefully controlled process conditions. Figure 8 shows the "processing feasibility box" developed by extensive processing testing. This chart gives the permissible limits of temperature and humidity of successful spray application of the polyisocyanurate foam to the ET. The processing facility at the plant in Michoud, New Orleans, has been designed to maintain processing conditions well inside the feasibility box noted in Figure 7.

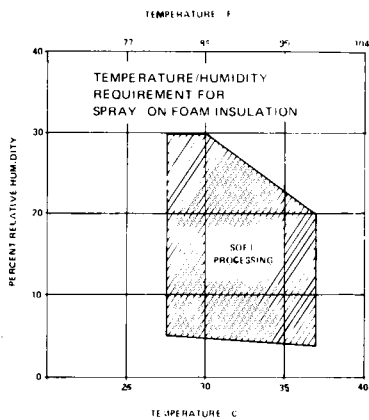


Figure 8. SOFI facility capability at Michoud assembly facility.

Above a heat flux of approximately  $6 \text{ Btu}/\text{ft}^2/\text{sec}$ , a more dense, ablating type material is required. Shock impingement resulting from interference contours causes interference heating in certain specific areas. While spray foam predominantly covers the forward LOX tank, the intertank structure and the aft hydrogen tank, there is a requirement for the ablative type material on the nose cap, the ET-to-Orbiter attachments, the external LOX and LH<sub>2</sub> tank tray cabling, under the external GOX and LOX lines, and on the intertank where the Orbiter shock wave impinges. The sprayable ablative material, SLA 561S, has a silicone resin matrix with low and high density fillers according to function, consisting of cork and silica microspheres and microballoons, and silica glass fibers and carbon powder. Table 7 gives the properties of the primary and alternate spray foam, and also properties of the prime ablative candidate. The ablative material is applied to the Iridized surfaces which have been previously prepared with a chromate/epoxy corrosion protective coating, a silicone primer, and a polysiloxane adhesive coating. The ablative can be sprayed, or molded, and adhesively bonded in place as noted earlier. The external surfaces of the applied ablative are sealed with a spray-applied silicone coating. The spray foam insulation and the ablative material are nonstructural from an overall load carrying point of view, but both are designed and fabricated to withstand the aero/thermal and induced load stresses without impairing their thermal efficiency.

Table 7. ET/TPS Materials

Type	Polyisocyanurate Foam No. 1	Polyisocyanurate Foam No. 2	Ablator-Filled Silicone
Density (lb ft <sup>-3</sup> )	2.3-0.3	2.3-0.3	1.7 - 2
Form	Spray	Spray	Sheet Spray
Thermal Conductivity K Btu-In. hr-ft <sup>-2</sup> °F <sup>-1</sup>	0.15	0.15	0.50
Heat Flux (Btu ft <sup>-2</sup> sec <sup>-1</sup> ) Radiant	10	(8-10)	
Aeroshear	6-8	(6-8)	20
Coefficient Expansion F (Temperature Range °F) (0 to +200)	$7 \cdot 10^{-5}$	$7 \cdot 10^{-5}$ (0 to +200)	$0.95 - 10^{-5}$ (-200 to +200)
Flatwise Tensile Strength (psi) -300°F	35-60	(24-45)	460-600
75°F	40-70	30-55	35-55
300°F	(20-40) <sup>a</sup>	(15-35)	(30-45) <sup>a</sup>
500°F			(20-35) <sup>a</sup>

a. Data range estimated

#### SRB Materials and Processes

The SRB element of the Space Shuttle is composed of six subsystems: the Solid Rocket Motor (SRM), the structural subsystem, the thrust vector control (TVC) subsystem, the mechanical and ordnance equipment subsystem, the recovery subsystem containing the mechanical and parachute equipment, and the electrical subsystem including the range safety system. All elements except the nose cap and separation motors are intended to be reusable and are recovered via pilot, drogue, and main chutes.

The SRM is the primary propulsive element, providing impulse and TVC from ignition to SRB staging. The SRM consists essentially of a lined, insulated, segmented weldless D6AC steel rocket motor case loaded with TP-H1148 propellant which is a composite type solid propellant formulated of polybutadiene acrylic acid acrylonitrile terpolymer binder (PBAN), ammonium perchlorate, and aluminum powder, with a small amount of iron oxide burning rate catalyst. An ignition system, initiators, igniter, movable nozzle, raceway, and instrumentation are other essential parts of the SRB.

Performance interchangeability and replaceability between a flight set of SRM's for the SRB can be maintained by matching the burning rates of motor segments cast in matched pairs from the same propellant lot. The sea level thrust of the SRM will be 2.65 million lb. The propellant grain design is performance tailored, consisting of a forward segment with an 11-point star and transitioning into a cylindrical perforated configuration in the cylindrical portion of the segment, two identically configured center segments that are tapered cylindrical perforated and an aft segment with a dual taper cylindrical perforated configuration. Figure 9 gives SRB subsystem and propellant configuration detailed information.

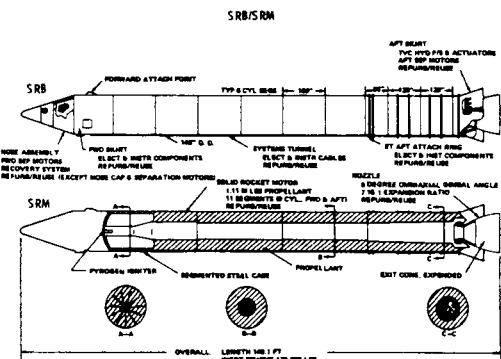


Figure 9. SRB/SRM.

The 11-point star configuration in the forward segment produces high level liftoff thrust until burnout of the star sliver, within approximately 52 sec. Burning of the cylindrical perforated configurations continues until thrust decay due to burnout of the aft-most portion of the aft segment. A linear 10 sec thrust decay is achieved by the programmed burnout of slivers in all four segments.

The insulation used in the chamber, the propellant relief flaps, and the forward inhibitors are asbestos-silica-filled nitrile butadiene rubber (NBR). The aft inhibitor insulation material is an asbestos-filled carboxyl terminated polybutadiene polymer (HC polymer). The inhibitors typically are designed to prevent ignition and burning of the propellant grain in a direction perpendicular to the inhibitor surface. The case liner material is an asbestos-filled CTPB polymer (UF-2137).

The SRM nozzle is a convergent divergent movable design containing an aft pivot point flexible bearing as the gimbal mechanism. This type of bearing has been used previously in the Poseidon missile; however, the SRM nozzle and flexible bearing are larger than any others in current use.

Throughout the design and development of the SRB, recovery and reuse have been the prime design drivers. A number of new situations never before faced by aerospace designers have arisen. In fact in the areas of recovery and reuse of subsystems, the engineering shop talk has been frequently more reminiscent of a Navy shipyard or a dockside marina, with frequent discussions on estuarine corrosion, splash zone corrosion, salt water enhanced crack growth, and a host of other marine related considerations. Even the ravages of marine biological attack had to be considered because under conducive conditions some undesirable forms of biological attachment can begin within hours. As a consequence, materials were selected very carefully. Table 8 presents a wide range of metallic materials and associated applications which are used in the SRB.

The driving impetus of reusability provided many of the unique challenges. A few of the more salient materials and processes challenges and resolutions to those challenges will now be discussed.

#### Engineering to Prevent Corrosion

One of the most seemingly incongruous intentions in the whole Shuttle element recovery scheme is the idea of dropping the steel/aluminum SRB's in the ocean, and then subsequently reusing them. The D6AC steel used in the motor case elements is a medium carbon (0.42 to 0.48 percent), low alloy ultra-high strength steel, which is electric furnace air melted and remelted by the vacuum consumable electrode process (denoted by the addition of "C" to the D6AC designation). The rusting of unprotected D6AC steel in salt water is rapid and uniformly aggressive. Although the selection of D6AC for the SRM motor case was sound from a design and an econometrics point of view, it placed much responsibility on the corrosion engineer. Weekend sailors and others well acquainted with the aggressiveness of the marine environment can comprehend the full significance of recovery from the ocean, refurbishment, and reuse of the SRB's.

In the corrosion engineering assessment of the SRB, several marine environments were considered: atmosphere, splash zone, tidal zone, and immersed condition. The many corrosion tests conducted were designed to evaluate potential materials under the aggressive conditions expected in the use-recovery-refurbish-reuse cycle of the SRB. In the corrosion testing, factors affecting corrosivity in seawater such as biological activity, oxygen availability, water temperature, water velocity, salinity, and pH were considered. Specific forms of corrosion considered in the design of the corrosion protective materials arrangements included galvanic corrosion, crevice corrosion, pitting corrosion, impingement corrosion, and cavitation corrosion. Only the first three forms of corrosion are considered important in the SRB application because the recovery towing speeds are relatively low.

Bare D6AC steel corrosion is controlled largely by the reaction at the cathode, while bare 2219 aluminum corrosion rate is influenced primarily by the formation of a passive oxide film. The practical implications of this behavior are that the bare D6AC will exhibit high corrosion rates in the splash zone where O<sub>2</sub> is plentiful, and bare 2219 aluminum will be especially susceptible to crevice corrosion and pitting in stagnant seawater conditions because the formation of the protective oxide is impeded by the limited availability of O<sub>2</sub>. The latter effect is sometimes referred to as a differential aeration cell effect. The presence of copper in the 2219 aluminum alloy also enhances the probability of pitting due to the availability of heavy metal ions. Obviously good surface protection is mandatory.

In recognition of these challenging corrosion engineering requirements, a comprehensive series of tests was accomplished between February 1972 and July 1976 in the Gulf of Mexico and in the Atlantic Ocean

**Table 8. Space Shuttle SRB Metallic Materials**

Material	Application	Material	Application
2219 2419	Systems tunnel Forward skirt Aft skirt Frustum structural assembly Forward ordnance ring Forward skirt Aft skirt	5052 Aluminum 1100 Aluminum Al. Shim Stock	Systems tunnel Aft ring Forward skirt Systems tunnel Pendant assembly towing
2024	Nose cap	Alclad	Frustum structural assembly Nose cap
6061	Data capsule assembly Pendant assembly Frustum - secondary structure Forward ordnance ring Forward skirt - cable	Inconel	Pendant assembly towing Forward skirt Aft ring
A 286	Pendant assembly Data capsule assembly Systems tunnel Nose cap Frustum structural assembly Forward ordnance ring Forward skirt Aft skirt Aft ring	MP 35N 18-8 CRES Steel Wire, QQ-W-470 CRES Wire, MIL-W-46071S D6AC Steel, Roll Forged	Frustum structural assembly Forward skirt Aft skirt Forward skirt Systems tunnel Aft skirt
300 series steel	Data capsule assembly Frustum structural assembly Forward skirt Systems tunnel	Forged Carbon Steel, Zinc Coating (NAS 1053-04-16 modified)	Pendant assembly towing
174 PH H1025	Data capsule assembly	Brass, Cadmium Plated (MS 20230BPS2 modified)	Pendant assembly towing
13~PH H1000	Aft skirt	Expanded Polystyrene Foam per MIL-P-40619, Class 2, Grade A,	Frustum flotation blocks
4340	Systems tunnel Aft ring	Formed by the Expansion and Fusion of Polystyrene Beads	

in the vicinity of Cape Canaveral. Table 9 depicts the Canaveral location, some of the test materials and protective coatings, and one of the test modes. In addition to these tests, flowing seawater and alternate immersion tests were conducted. The results give confidence that adequate protection can be provided the SRB's, sufficient to allow the schedule 20 uses per SRM case segment and 40 uses for the SRB structure. Based on these results, the following protective coatings and TPS material appear most probable for use at this time:

**Forward SRB/ET attach fitting-2219 Al and aft ET attach ring-4340 steel:**

**Primer** Zinc Sele #9334 (Rustoleum)  
2 part epoxy-polyamide, converted resin (90% zinc in dried film)

**Topcoat** #9392 white epoxy polyamide, 47% titanium dioxide pigment (Rustoleum)

**2219 aluminum skirts:**

**Surface Treatment** Alodine 1200 conversion coating

**Primer** Bostik/Finch #463-6-3, 2 component epoxy-amine calcium chromate inhibited

**Topcoat** Bostik/Finch Cat-A-Lac Epoxy #443-3-1 epoxy-amine, titanium dioxide pigment

**SRB TPS:**

**Coalesing Agent** Epoxy-modified polyurethane resin, Crest 7344

**MXSA\*** Composition: BJO micro-balloon (phenolic) and glass eocoshperes, chopped and milled glass fibers, end capped Epoxy-polyurethane resin, Crest 7119 accelerator, methylene chloride and perchloroethylene thinner, Bentone 27 suspension agent with ethyl alcohol activator.

**Topcoat** White pigmented butadiene/styrene with methylene chloride/perchloroethylene solvent.

\* Marshall Experimental Spray-on Ablator

**Table 9. Ocean Environment SRB Materials Tests**

Date	Location	Materials	Coatings	Sealants	Test Mode
1. Feb. 1972	Gulf (7 days)	<ul style="list-style-type: none"> <li>• 2219-T8</li> <li>• Inconel 718</li> <li>• Ti-6Al-4V</li> <li>• Couples of above</li> </ul>	Bare; epoxy; anodize; alodine Bare	None	Rack and tower
2. July 1972	Gulf (24 and 72 hr)	<ul style="list-style-type: none"> <li>• D6AC</li> <li>• 4130</li> <li>• 1S-Ni Maraging</li> <li>• HY-140</li> <li>• 2219-T87</li> <li>• 6061-T6</li> </ul>	Bare and epoxy zinc rich Bare Epoxy chromate Epoxy chromate Epoxy chromate Epoxy chromate	None	3 and 12 mile tower
3. Feb. 1974	Gulf (5 days and 100 days)	<ul style="list-style-type: none"> <li>• HY-140</li> <li>• 2219-T87</li> </ul>	(1) Bare; (2) galvanized; (3) galvanized - epoxy zinc; (4) galvanized - epoxy zinc - silicone sealant Bare; epoxy		12 mile tower
4. Sept. 1975	Canaveral (7 days ocean + 3 Banana River)	<ul style="list-style-type: none"> <li>• 2219-T87</li> <li>• 7075-T651</li> <li>• D6AC</li> <li>• Couples of above with 7 polysulfide and 1 silicone</li> <li>• Clevis joint specimens</li> </ul>	Bare; epoxy chromate Bare; epoxy chromate Bare; epoxy zinc rich		Rock at splash level
			D6AC and 2219-T87 Bare; corrosion preventative coating		Rock at splash level
5. July 1976	Canaveral ITB Test (7 days ocean - 3 days Banana River)	<ul style="list-style-type: none"> <li>• D6AC</li> <li>• 2219</li> <li>• 7075</li> <li>• Insulations           <ol style="list-style-type: none"> <li>1. MNSA sprayed</li> <li>2. Silicone, bonded</li> <li>3. Cork, bonded</li> </ol> <li>• Clevis joint - painted with preservative and retainer band</li> </li></ul>	Epoxy zinc rich Epoxy chromate		Floated 80 immersed

The ability of these coatings to provide adequate protection is of paramount importance, as is shown in the next section on stress corrosion.

#### The Stress Corrosion Ogre and Fracture Toughness

As noted earlier, D6AC steel corrodes relatively readily. Not unexpectedly, it is also susceptible to SCC, having a sustained tensile stress threshold of one-half the yield strength, or approximately 90 ksi, as determined by 3.5 percent sodium chloride solution alternate immersion tests. In actual use, the SRB could be subjected to sustained tensile stresses due to assembly, storage or handling peculiarities, and wind loads on the launch pads, but estimation of these stresses indicates that the aggregate will be well below the threshold stress of 90 ksi. Hence, there is no reasonable probability that environmentally initiated SCC of the type previously encountered in certain aluminum alloy launch vehicles will occur. However, the possibility of environmentally enhanced growth of preexisting flaws must then be given serious consideration.

Preexisting flaws in the D6AC steel will be sought out by meticulous application of ultrasonic and magnetic particle inspection of raw materials, forgings, and machined case segments. Further, each case segment

will be proof tested before each use, and magnetic particle inspection will be used before and after proof. The flaw detection capability is approximately 0.100 by 0.050 in. with a probability of detection .915 at a confidence level of 99 percent. Tests on an actual clevis joint which joins the case segments have verified this capability. By this means, flaws which have the propensity to grow to critical dimensions (size where unstable propagation results) will be detected before hand. The critical flaw size is a function of stress and the fracture toughness,  $K_{Ic}$ , of the D6AC material. The SRM case segments will be heat treated to a  $K_{Ic}$  of at least  $90 \text{ ksi} \sqrt{\text{in.}}$ . However, should a flaw with the potential to grow critical during the very next use-cycle of the case go undetected, it will be found during the hydroproof of the case segment.

The flaw detection system is almost foolproof — except for one possibility, i.e., the possibility of environmentally enhanced flaw growth after hydroproof in the subsequent period of storage, handling, pad time, and the relatively short flight service period. To assess the implications of this relatively long term, environmentally enhanced, flaw growth possibility, a knowledge of  $K_{Isc}$  is required — the fracture toughness of the D6AC material in the presence of a SCC environment. Analysis and

testing are in progress to insure that either flaw sizes acceptable on the basis of  $K_{1c}$  (benign environment) do not grow to critical size due to the presence of a SCC environment, or that if smaller flaw sizes must be detected, they can be.

For the vast majority of the SRB structural elements, the amount by which the proof stress exceeds the operating stress provides sufficient margin for only subcritical flaw growth; that is, no flaw surviving proof can subsequently grow to fracture critical size either before or during the flight. But four specific areas are receiving special attention: clevis joints, case membrane at aft end side toward ET/SRB attach point, the forward and aft "Y" joint, and the membrane of the forward and aft closures. To exonerate these areas, new precise data on  $K_{1sc}$  are being developed using authentic SRM materials which are heat treated according to the exact SRM schedule to be used for the flight vehicle. These data are being used in conjunction with special measured data on manufacturing stresses, assembly stresses, and calculated wind loading stresses to determine what improvement in flaw size detection, if any, will be required in these four areas where proof test alone is inadequate, regarding the slight possibility of environmentally enhanced flaw growth. The fracture toughness in a stress corrosion environment is appreciably lower than the standard benign environment fracture toughness, or  $K_{1c}$ . Values for D6AC  $K_{1sc}$  can be found in the

literature ranging from 16 to 30 ksi  $\sqrt{\text{in}}$ . As noted previously, analysis and preliminary data indicate that nondestructive evaluation techniques which will allow the detection of the even smaller flaw sizes associated with  $K_{1sc}$  values in the low end of the range can be applied should that prove necessary. The determination of the role of the SCC environmentally induced flaw growth is a precaution not previously considered with "one-shot" solid rocket cases. The requirement for reuse makes the  $K_{1sc}$  assessment necessary. It is important, however, to remember that for environmentally enhanced flaw growth to occur in the first place a breakdown in the protective coatings must occur. As noted in the discussion of engineering to prevent corrosion, excellent sacrificial, tenacious coatings have been prescribed for use on the D6AC, and the probability for inadvertent exposure to the corrosive environment is low. However, in any case no stone has been left unturned to assure sustained adequate fracture toughness throughout the life cycle of the SRB.

#### In Situ Corrosion Protection Verification — The Integrated Test Bed

As noted earlier, the requirement for economical reuse has been the predominant influence in the selection of materials for the SRB. This has been most apparent in the case of materials selection for corrosion protection. As noted in the earlier discussion entitled "Engineering to Prevent Corrosion," a number of sample material tests were completed during the period of February 1972 through July 1976 in the Gulf of Mexico and in the Atlantic Ocean. Various metal alloy and protective coating specimens were tested under a variety

of exposure conditions designed to run the gamut of expected SRB exposure conditions.

The results of these preliminary tests determined the material selections for the integrated test bed (ITB). The ITB is an almost-full-scale (10 by 8 ft) simulation of the 12 ft diameter SRB frustum, which has been prepared using the currently most promising candidate materials. The prime ablator material MXSA, and backup cork and silicone materials were used as were zinc rich primer coating topcoats. A modified styrene butadiene rubber coating material with a carbon black pigment and one with a titanium dioxide white pigment were tested. This material has promise for use as a moisture resistant overcoat for the MXSA ablator material and also as a "cummerbund" around the clevis joint elements of the solid motor case segments. The clevis joint requires the cummerbund overlay to prevent seawater from entering the clevis joint where corrosion could continue even after the SRB had been removed from the sea. An earlier design concept envisioned a 7 in. wide cummerbund of ethylene-propylene rubber, spanning the parting line of the joint, held in place by a circumferential stainless steel retainer strap at each end of the cummerbund. The current concept consists of a modified styrene butadiene material either painted or sprayed over the clevis joint. This material was proven in the ITB tests to be completely watertight and can be cleanly stripped from the joint with only moderate effort.

Interior frustum floatation foam and methods of quick removal of floatation foam were also tested in the ITB test. Figure 10 shows the ITB being taken under tow in the Atlantic Ocean off Cape Canaveral. The results of the ITB test have been excellent, and it is evident that the materials used in the ITB test now constitute a baseline set of materials adequate for environmental protection during recovery and for the refurbishment activity. In actual use, the ablative material will have to be removed during the refurbishment activity; therefore, some inordinately tenacious materials and coating combinations had to be eliminated from consideration. The MXSA ablator material can be readily removed by a "Hydro Laser" machine which employs a 5000 to 7000 psi jet of water to remove the material. Because of the associated adhesives and softeners, some other materials (e.g. silicone) are extremely difficult to remove by Hydro Laser.

Open ocean and Banana River exposure were provided in the ITB test series. As a result of this exposure considerable biological attachment was evident on the test bed. When a metal or other surface is first immersed in seawater, a biological slime develops in a matter of a few hours. This slime is a prerequisite to the attraction and attachment of sessile fouling organisms which, once attached, rapidly transform to the mature form and become immobile. The initial supposition that the relatively short periods of exposure during recovery would constitute inadequate time for biological growth to begin has not proved accurate. Special cleaning techniques are being developed to strip the SRB of slime and the embryonic fouling organisms. Even if the exposure time has only allowed the formation of the prerequisite slime, the slime itself is highly hygroscopic and retains

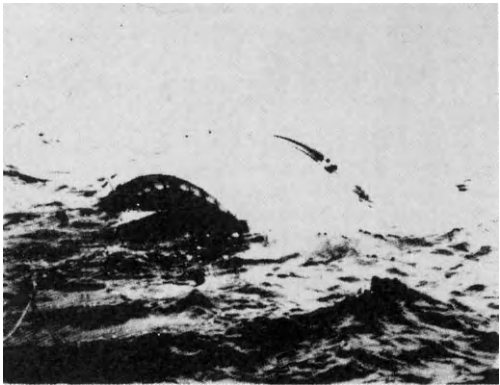


Figure 10. The integrated test bed (ITB) which simulates the SRM frustum, being taken under tow in the Atlantic Ocean off Cape Canaveral.

a high percentage of moisture and salt when an object is removed from the water. This aids and abets general corrosion of the metallic materials. The SRB will experience optimum corrosion conditions for steel and aluminum, but at different times, in the recovery sequence. In the splash zone and open sea, steel corrosion will be enhanced due to the oxygen rich environment which provides ready depolarization of the cathode and greatly aids local action corrosion. Aluminum, however, rapidly builds a protective passive film or layer in the presence of abundant oxygen, but in areas such as bays, estuaries, and rivers the corrosion of aluminum is accelerated where the oxygen supply to the metal may be restricted. These factors have all been considered in the design and selection of materials for the recoverable SRB. Noteworthy accomplishments have not been confined to design alone. Some outstanding processing improvements have been incorporated in the SRB development; an example is presented in the next section.

#### 2219 Aluminum Processing Breakthrough

The SRB aft skirt and forward frustum design utilizes 2219 aluminum alloy in the T87 heat treated temper. These SRB elements are composed of forgings, extruded shapes, and heavy plates which are machine milled into pocketed or ribbed patterns. These components are subsequently welded together to comprise the large rigid structures (Fig. 9). The forward frustum is just aft of the nose cap and part of the nose assembly and the aft skirt can be seen all the way aft.

The aft skirt in particular has a high strength requirement to survive the parachute plunge into the ocean, stern first. The momentum of this plunge will carry the aft end of the SRB to a depth of 80 ft. This water entry requires a skirt structure of rigid construction, and the associated loads are the predominant design driver. Further, as noted earlier, the structural parts of the SRB must allow 40 uses. To provide the many reuses required, the aft skirt design became very sturdy and required welding of heavy 2219 sections. This

prospect caused no little concern about welding distortion, residual stresses, and lowering of strength due to the effect of welding thick sections.

As a result, a test program was initiated in which 2219-T37 aluminum alloy was welded and then restrained aged to the T87 temper by heat aging at 350°F for 18 hr. The results were quite spectacular. Weld distortion was virtually eliminated, yield and ultimate strength were typically improved approximately 10 percent and 20 percent, respectively, and the consistency of improved properties over a wide range of material thicknesses was quite remarkable. Figure 11 shows a typical stress-strain curve for 3/4 in. TIG welded aluminum plate, as-welded and welded and aged at 350°F for 18 hr. The dramatic improvement in properties is readily apparent. The fact that the welded and aged stress strain curve for 1/4 in., and 1/2 in. material practically coincides with the welded and aged curve for 3/4 in. material is significant. This shows the efficacy of the weld and restrain age technique in acquiring uniformly high and consistent properties throughout the entire skirt structure. By restraining the welded structure to the designed contour during the heat aging cycle, nearly all weld distortion can be removed. It naturally follows then, that the welded assembly fabricated by this method has very low residual stresses and is easy to produce to specified tolerances. This is important for good fit-up of mating parts, which in turn guarantees low assembly stresses. The sum total of this material/process innovation greatly improves the service life of the SRB aft skirt and the forward frustum, both of which experience the water impact loads associated with ocean recovery.

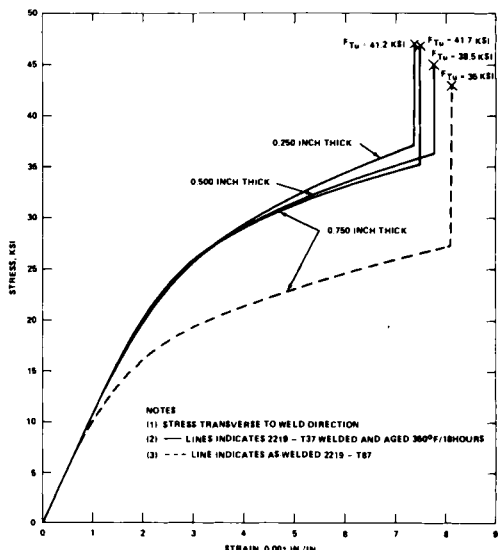


Figure 11. Typical stress-strain curves of 2219 aluminum plate, 3/4 in. thick, weldments (TIG process).

### SRB Thermal Protection System

The thermal environment to which the SRB will be exposed in flight requires that a portion of the surface be covered with a high temperature ablator material. A typical heat flux/aeroshear level of approximately 12 Btu/ft<sup>2</sup>-sec must be withstood. In 1972, MSFC undertook the development of a material to meet the SRB requirements. MXSA, a room temperature curing ablator material which is sprayable through standard commercially available spray guns and pumps, evolved. In the interest of expediency in processing, an elevated temperature cure was also developed ( $150^{\circ} \pm 10^{\circ}$  F for 4 hr). The general composition is as previously noted under SRB TPS-MXSA.

The application of the ablative material to the SRB is baselined as an automated process. The SRB segment to be sprayed will be attached to a turntable, permitting a controlled rate of ablator material application. During spraying, the rotational speed of the turntable, the vertical speed of the spray gun, and the output of the spray equipment are synchronized so that the deposited ablator material is of the required uniform thickness. The surface of the cured insulation exhibits a fibrous overspray (haystack) appearance with a coarse texture that can easily be removed by brushing with a stiff brush. The surface can also be abraded to contour, if necessary. The final operation consists of the application of sealant or topcoat (composition as noted previously).

In the search for the specialized MXSA material, cost of material and applied cost weighed heavily. In the testing domain, vibro-acoustic/thermal and aeroshear tests were an essential part of the materials characterization effort. Other candidate materials were also

considered; Table 10 gives pertinent properties of some alternate materials. While the MXSA material currently has the highest level of maturity and characterization, the option to select one of the alternate materials in the event of any unforeseen impediment still remains.

### Summary

Previous launch vehicles have been highly reliable and expendable; however, the Space Shuttle will provide a highly reliable, low cost, reusable launch vehicle system. Reusability, through amortization, lowers the cost. At the same time, reusability has proved to be the prime design driver. To attain the objectives of reusability and low cost, materials and processes selection and tracking are key ingredients which are controlled in the development program. The development of the high performance, variable thrust SSME has challenged the designers and materials engineers particularly in the areas of hydrogen environment embrittlement (HEE), LOX/GOX compatibility and stress corrosion cracking (SCC). From these areas, a wide variety of successful materials and process applications have resulted. New data on HEE, LOX/GOX compatibility, and SCC have evolved, which have potential use in a wide variety of applications outside the aerospace field. In the design and manufacture of the ET, significant improvement in 2219 weld quality and reduction in radiographic requirements are being effected. This is primarily the result of the excellent MMC weld tooling and extensive weld porosity testing and weld properties determinations carried out at the MSFC during the late 60's and early 70's. The recoverable SRB provides an impressive challenge to the corrosion engineer, a challenge which is being met successfully through extensive in-situ marine testing. The test effort on the one remaining consideration in the total fracture

Table 10. SRB/TPS Materials

Type	MXSA Filled Epoxy-Urethane	Silicone Sponge	Cork	Silicone Foam	Filled Silicone
Density. (lb/ft <sup>3</sup> )	$17 \pm 2$	$17 \pm 1$	$30 \pm 2$	$17 \pm 2$	$17 \pm 2$
Form	Spray	Sheet	Sheet	Spray	Sheet/spray
Thermal Conductivity K Btu-in./hr-ft <sup>2</sup> -°F	0.55	0.49	0.65	0.54	0.50
Heat Flux/Aeroshear Btu/ft <sup>2</sup> -sec	13	>13	13	—	>20
Coefficient Expansion/°F (Temperature Range °F)	$1.5 \times 10^{-5}$ <sup>a</sup> (-200 to +200)	$14.8 \times 10^{-5}$ (-150 to +650)	$2.8 \times 10^{-5}$ (-65 to +425)	$0.71 \times 10^{-5}$ (-13 to +302)	$0.98 \times 10^{-5}$ (-200 to +200)
Flatwise Tensile Strength (psi) -300°F	(420-500) <sup>a</sup>	86	(420) <sup>a</sup>	192	460-600
75°F	220-260	24	(90) <sup>a</sup>	26	35-55
300°F	(90-120) <sup>a</sup>	16	(16) <sup>a</sup>	15	(30-45) <sup>a</sup>
500°F	TBD	11	(10) <sup>a</sup>	7	(20-35) <sup>a</sup>

a. Data extrapolated

control picture for the SRB, the possibility of environmentally enhanced growth of pre-existing flaws, is well in hand and is not expected to present any difficulty. New techniques of welding and aging the SRB 2219 forward frustum and aft skirt have shown significant improvements in weld properties, with greatly reduced distortion; the soon-to-be-commercialized MXSA TPS material for SRB promises to provide appropriate thermal protection and ease of refurbishment. In general, the materials and processes associated with the SSME, ET, and SRB development have evolved and progressed in an orderly manner, accompanied by evolution of significant technological data. From the current chronological vantage point, it appears certain that the materials and processes will indeed be equal to the challenging development of the SSME, ET, and SRB.

#### References

1. Lucas, W. R. and Richl, W. A.: An Instrument for the Determination of Impact Sensitivity of Materials in Contact with Liquid Oxygen. MSFC, ASTM Bulletin No. 244, February 1960, pp. 29-34.
2. Schwinghamer, R. J.: Impact Sensitivity of Materials in Contact with Liquid and Gaseous Oxygen at High Pressure. Proceedings, Symposium on Oxygen Compressors and Pumps, Compressed Gas Association, Inc., Atlanta, November 9-11, 1971.
3. Schwinghamer, R. F. and Key, C. F.: High Pressure Oxygen Test Evaluations. MSFC, NASA TM X-64899, November 29, 1974.
4. Herring, H. W. and Franklin, D. B.: Design Criteria for Controlling Stress Corrosion Cracking. MSFC, Document 10M33107B, June 11, 1970.
5. Lovoy, C. V.: Effects of Porosity on Weld-Joint Tensile Strength of Aluminum Alloys, MSFC, NASA TM X-64933, September 1974.

# EXPANDABLE STRUCTURES FOR SPACECRAFT

Karl O. Brauer

*Senior Chief Research Officer, Council for Scientific and Industrial Research, Cheverny 330,  
La Montagne, Pretoria 0184, South Africa*

## Abstract

Various types of expandable structures and their advantageous utilization in spacecraft are described in this paper. Special features of some of these expandable structures are their suitability for stowage in a relatively small volume, and for quick and reliable deployment, and furthermore, their excellent rigidity in deployed condition, and their low weight. Ideal applications of expandable structures, as for example, to large solar arrays, stabilization booms for satellites, shaft and truss antennae, truss booms, manipulating arms, landing gear struts, airlocks, decelerators, recovery systems, landing impact attenuators, and flotation systems are presented and their characteristic features are explained. The major types of expandable structures, such as mechanically deployable structures, inflatable structures, chemically-rigidized cloth structures, stiffened and unstiffened cloth structures are shown and typical applications and performance data are presented. Concluding, recommendations for optimum utilization of various special types of expandable structures for future spacecraft are made.

## I. Introduction

Numerous important tasks of space missions can best be accomplished by utilizing expandable structures, which can be stowed in a small volume within the spacecraft and can be deployed within a very short time and also provide the advantageous features of high rigidity, low weight and the ability to withstand extreme space environmental conditions. Expandable structures have been used very successfully in passive communication satellites, antennae, stabilization booms, solar arrays, spacecraft landing struts, and in recovery, landing and flotation systems.

Based on the vast experience gained with these systems, greatly improved expandable structures have been and are being developed for applications to large antennae, solar arrays, manipulating arms, airlocks, rescue vehicles and recovery systems.

## II. Types of Expandable Structures

The major types of expandable structures for spacecraft applications are:

- Mechanically deployable structures
- Inflatable structures
- Chemically-rigidized cloth structures
- Stiffened cloth structures
- Unstiffened cloth structures

## III. Mechanically Deployable Structures

The major mechanically deployable structures are categorized as:

- Storable tubular extendible shaft systems
- Spring-loaded systems
- Telescoping systems
- Unfolding systems

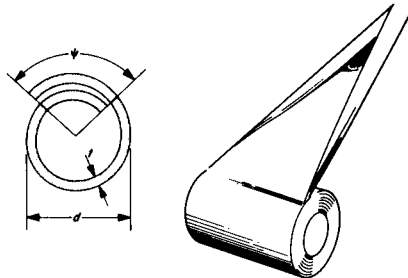
## Storable Tubular Extendible Shaft Systems

Storable tubular extendible members (STEM) find ideal applications as gravity gradient booms, antenna array extension booms, magnetometer booms, vehicle despin devices, transponder booms, solar panel extension booms, astronaut attachment systems, and altitude sensing devices.

A storable tubular extendible member is a flat strip of resilient spring material which, when unwound from a storage spool, in extended condition, assumes a tubular shape of high strength. When coiled in the flattened condition on a spool, it can be stored in a small volume. To prevent introduction of permanent strain in the metal strip, the spool diameter is chosen such that the elastic limit of the material is not exceeded when coiled. All materials with a high ratio of yield strength to modulus of elasticity can be used for storable extendible members. Beryllium copper and stainless steel are most commonly used. Tubular extendible members can be deployed by their inherent strain energy, or if retraction capability is required, a manual or motor drive mechanism is used. Extension speeds vary from 0,15 to 4,57 m/sec for self-extended units, and from 0,02 to 0,46 m/sec for motorized units.

The three basic configurations of tubular extendible members are the overlapped storable tubular extendible member (STEM), the BI-STEM, and the helically-wound shafts. The element of the overlapped

storable tubular extendible member (STEM) consists of a single tape formed into cylindrical shape such that the edges of the metal strip overlap approximately  $160^\circ$  (see Fig. 1).<sup>1</sup>



The Storable Tubular Extendible Shaft Principle (STEM)

Fig. 1

The element of the BI-STEM consists of two tapes each formed into an open circular section such that each tape circumscribes an angle of approximately  $330^\circ$ . One tape is then placed inside the other, so that the tapes are diametrically opposed, thus forming the basic BI-STEM element (see Fig. 2).

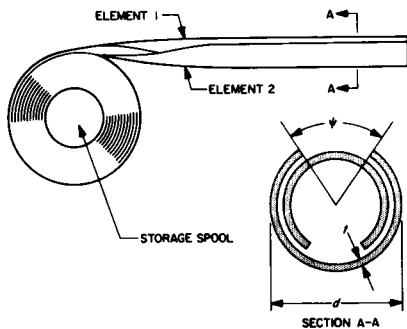


Fig. 2 The BI-STEM Principle

The advantages provided by the BI-STEM are:

- Reduction in package size, resulting in unit weight reduction
- Improved inherent straightness
- Deletion of longitudinal curvature in the ploy region, which is inherent with the overlapped tubular member (STEM)
- Improved strength and stability in the ploy region
- Improved structural damping characteristics
- Increased bending and torsional strength.

Critical bending moments, compressive strength properties and natural frequencies of both types of extendible members

are presented in the diagrams Fig. 3, Fig. 4, and Fig. 5.<sup>2</sup>

**CRITICAL BENDING MOMENT,  $M_{cr}$  PER ELEMENT (ft.lb.)**

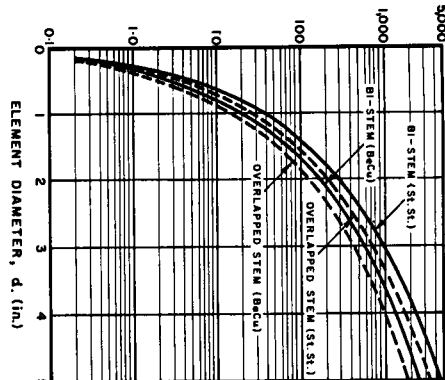


Fig. 3 TYPICAL VALUES FOR CRITICAL BENDING MOMENT

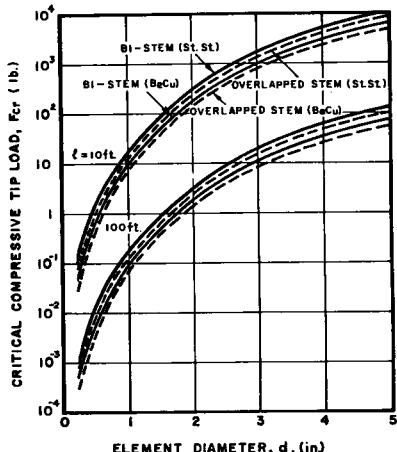


Fig. 4 TYPICAL COMPRESSIVE STRENGTH

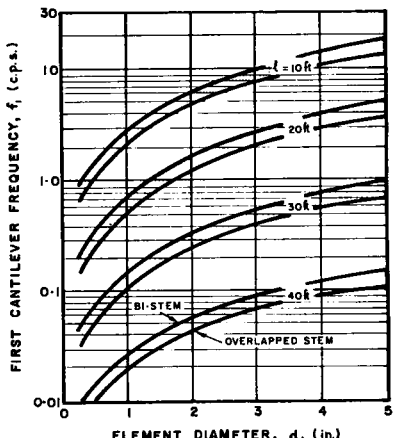
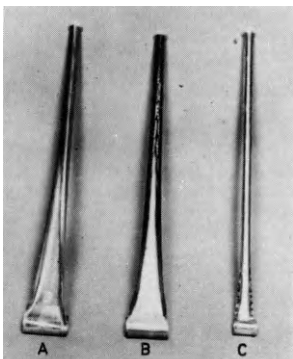


Fig. 5 NATURAL FREQUENCY

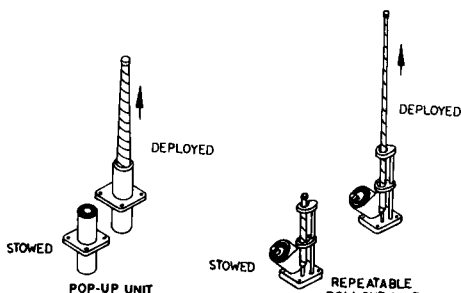
Greatly increased torsional and bending strengths are obtained in simple overlapped tubular extendible members (STEM) and also in BI-STEM with tab-slot connections of the tape edges, such as the edge-lock or hingelock interlocking seams (see Fig. 6)



**TUBULAR EXTENDIBLE ELEMENTS**  
A. OVERLAP TYPE  
B. EDGELOCK TYPE  
C. HINGELOCK TYPE

Fig. 6

The third configuration are helically-wound shafts. They are formed by releasing an angularly pre-stressed metal strip from a storage drum. The basic types of helically-wound shafts are one-shot pop-up shafts and repeatable roll-out shafts (see Fig. 7)



**HELICALLY-WOUND EXTENDIBLE SHAFTS**

Fig. 7

Tubular extendible shafts respond to the thermal energy incident from the Sun with a degree of bending that caused a significant impairment of pointing accuracy. To eliminate this effect of solar irradiation, a passive control scheme consisting of a hole pattern in the shafts and a thermal coating has been developed.

The advantageous feature of very low weight is demonstrated by a 70-ft long helically-wound extendible shaft which

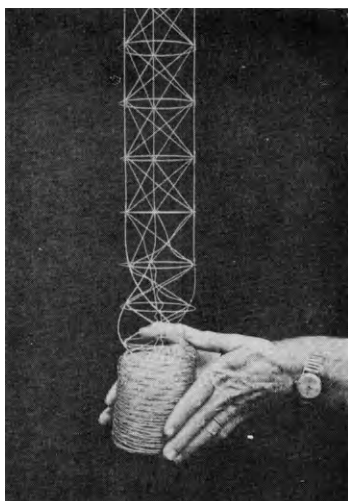
weighs only 0.4 lbs.

Two extendible shafts, each 33 ft long, are used as planetary radio astronomy and plasma wave antennae on the Mariner Jupiter/Saturn 1977 spacecraft.<sup>5</sup>

Recent developments in extendible boom technology have demonstrated that it is feasible to extend 750 ft long booms which are sufficiently straight and rigid. Extendible booms of this size, measuring 1500 ft from tip to tip, were used on the Radio Astronomy Explorer (RAE) space- craft.<sup>4</sup>

#### Spring-loaded Systems

An ideal example for a spring-loaded system is a truss boom, a linear lattice structure, which is automatically deployed from and retracted into a compact stowage volume. The ratio of the retracted length to the deployed length of this boom is typically 1 : 50. The automatically deploying boom has continuous longeron members that are elastically coiled when in stowed configuration (see Fig. 8)<sup>6</sup>



**Automatically Deploying Truss Boom**  
Fig. 8

On the Mariner Jupiter/Saturn 1977 spacecraft, an extendible truss boom is utilized to carry four magnetometer sensors. This truss boom extends automatically to a length of 43 ft. The deployment rate is controlled to avoid shock loads, and the extended boom is locked in place to avoid undesirable dynamic behavior during maneuvers. The truss, which consists of thin fiberglass epoxy, is restrained by phosphor-bronze cables when extended and can be spirally collapsed to a 2.3 ft long stowed condition. The boom mass

amounts to 5.3 lbs. The strict requirements that extended booms of this kind must be extremely rigid and well damped to avoid unstable interactions with the spacecraft attitude control subsystem are met by these extendible truss booms.<sup>5</sup>

The spring-loaded principle is also utilized in a special type of geodesic truss antenna (see Fig. 9).<sup>7</sup>

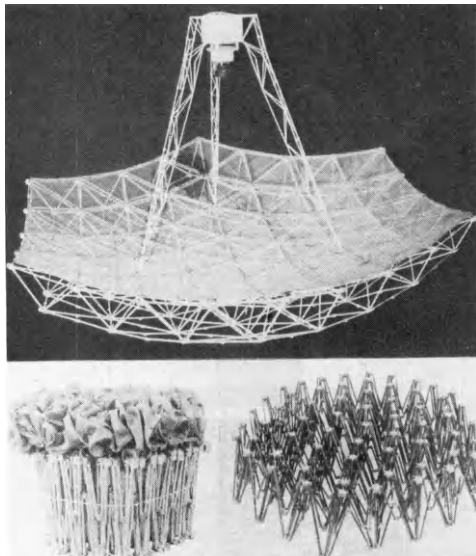


Fig. 9 Expandable Truss Antenna

The deployment force for the folded antenna is provided by spring-loaded center joints. The advantages of this truss concept are excellent stowage characteristics, structural rigidity, and resistance to thermal distortion. Furthermore, it provides the high natural frequency necessary for compatibility with the attitude control systems of large spacecraft.

The truss elements of this antenna are made from perforated tubing. Surprisingly low is the weight of this truss-mesh reflector, only 0.10 lb/sq.ft antenna aperture. The ideal stowage features of this 180-ft diameter antenna are demonstrated by a stowage envelope diameter of 10 ft.

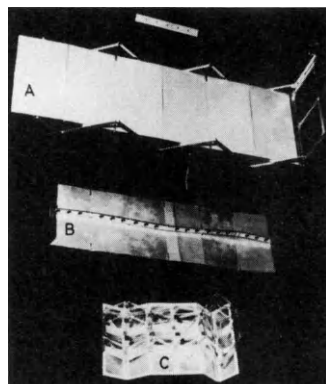
#### Telescoping Systems

The main applications of telescoping structures are shock absorbers in landing gear struts and crew couch supports, extendible manipulating arms, antennae, and long shafts for experiment equipment. Telescoping structures have been used successfully in the Surveyor, Apollo and in the Lunar Module, and they have also been applied to the Viking Mars Lander.<sup>8, 9</sup>

When telescoping structures are to be considered for use as containers or shelters, the disadvantageous fact is to be taken into account that their weight amounts to approximately 1.4 times the weight of rigid cylinders. Telescoping structures have the additional disadvantage that their leakage possibility is considerably greater than that of non-telescoping structures.

#### Unfolding Systems

Unfolding systems are used for deployment of large antennae, solar arrays, spacecraft landing struts, and similar large, bulky structures. For deployment of such large structures, the scissors linkage technique, the center folding beam technique and the folding box beam technique are frequently used (see Fig. 10).<sup>4</sup>



PANEL DEPLOYMENT TECHNIQUES  
A. SCISSORS LINKAGE TECHNIQUE  
B. CENTER FOLDING BEAM TECHNIQUE  
C. FOLDING BOX BEAM TECHNIQUE

Fig. 10

The scissors linkage technique was, for example, used successfully for deployment and support of the large solar arrays of Skylab.

On the Communications Technology Satellite (CTS), twin solar power arrays, measuring 21.5 x 4.3 ft each, are stowed during launch, transfer orbit and synchronous drift orbit in a flat, folded configuration between two honeycomb panels on either side of the spacecraft. On command from Earth, protective covers are blown off by pyrotechnic devices, and each array pops out 30 in., and support arms lock into place. The deployment is continued by a central drive mechanism, utilizing tubular extendible members until full extension, where a tensioning mechanism records a nominal tension of 5 lbs (see Fig. 11).

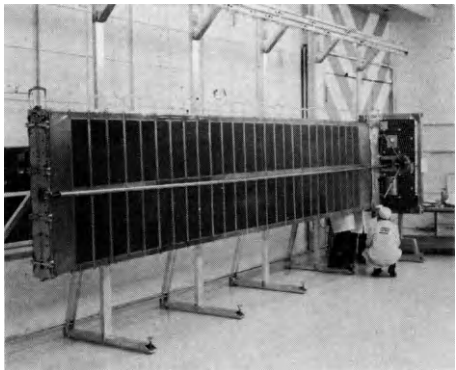


Fig. 11 CTS Solar Array

Another remarkable application of unfolding structures is the large, light-weight solar cell array system for a solar electric propulsion stage (SEPS) being developed for NASA. The array consists of 41 flexible fold-up panels and measures 105 x 14 ft when fully deployed. It can be retracted either fully or partially to meet various operating conditions in space. For example, full retraction would be required when docking the propulsion system to a payload, or for stowing it in the Space Shuttle Orbiter if it is being returned to Earth for refurbishment. Partial retraction might be required for protection from solar radiation flares while limited power output is required. 10

#### IV. Inflatable Structures

The requirements of small stowage volume, low weight and high efficiency are ideally met by inflatable structures, which are utilized in flotation systems for sea recovery of spacecraft, test vehicles and boosters, and also in some decelerator systems for space recovery. The low weight and small size of flotation systems is impressively demonstrated by a typical system having a ratio of flotation bag weight to provided buoyancy of 1 : 420.

The experience gained from aluminized Mylar spheres, such as the Echo satellite, has led to the development of substantially improved materials and structures of high strength and low weight. An astronomy probe balloon made from an improved Mylar scrim polyester fabric, which is an order of magnitude stronger than the previously used materials, was successfully utilized for exploration of the clouds around Venus. These improved materials provide the advantage that they do not become brittle at tropopause temperatures. Balloons used for astronomy experiments offer the advantage over rocket-powered spacecraft of a much higher payload capability (5000 lbs versus 150 lbs) and that

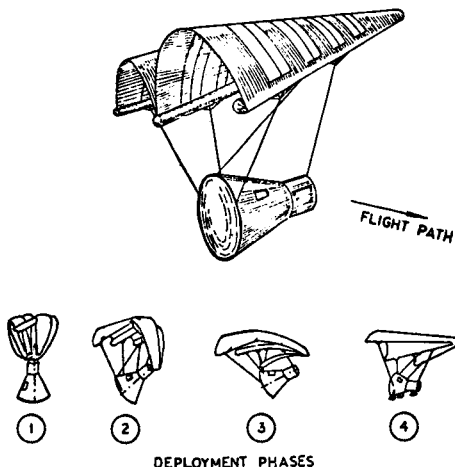
they can stay near maximum altitude longer than rockets (several hours versus 4-5 minutes).

New materials, such as Keflar, new fabrication techniques, for example, tri-axial weave, and new coating and laminating configurations are being investigated to determine their suitability for withstanding extreme space environmental conditions for long duration. The optimum materials are planned to be used for fabrication of a 45,000 cu.ft high-altitude balloon for astronomy experiments. 11

An interesting example of an inflatable structure is a spherical personnel rescue enclosure, which is under construction for the Space Shuttle. The rescue enclosure is planned to be utilized for transferring non-astronaut passengers to a rescue vehicle in case of emergency. Since passengers will not be equipped with the expensive space suits that are now being considered for the Shuttle, they could zip themselves along with an oxygen bottle into the rescue enclosure for transfer to a space rescue vehicle. With the passenger inside, the spherical enclosure would be inflated to its full 34-in. diameter with oxygen from the Shuttle system, with the oxygen bottle providing supplementary air, if needed. The present configuration of the rescue enclosure consists of a urethane bladder, Keflar restraint fabric, a thermal protective cover similar to that of the Shuttle pressure suit, a small Lexan window and provisions for plug-in communications. The enclosure may be towed to the rescue vehicle by an astronaut, or transferred from the Shuttle to the rescue vehicle by means of a clothes-line-type transfer system similar to that used by vessels at sea. 12. 13

Typical spacecraft recovery devices utilizing inflatable structures are inflated flexible wings, ballutes and paraloons. Flexible wings provide the advantage that their weight, volume, stowage and deployment characteristics are potentially as good as those of conventional parachutes, but additionally provide a stable and controllable glide with performance adequate for landing spacecraft, boosters, cargo, and personnel. A typical inflatable flexible wing has a triangular planform and consists of a layer of cloth attached to two inflatable swept-back leading edges and an inflatable keel spar, forming two lobes to the canopy. A typical wing is inflated with nitrogen gas to 20 psi pressure within 20 seconds (see Fig. 12). 14

This flexible wing, developed for a 6000-lb manned spacecraft, has a wing loading of 6 lbs/sq.ft, an inflated volume of 600 cu.ft, and a stowed volume of only 12 cu.ft.



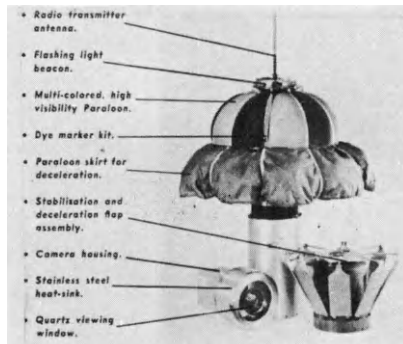
**INFLATABLE FLEXIBLE WING FOR RECOVERY OF MANNED SPACECRAFT**

Fig. 12

During spaceflight, the wing is stowed in harmonica-fold condition in a canister attached to the aft end of the spacecraft. Prior to the recovery phase, the canister is released from the vehicle, and the wing is deployed and inflated from a gas bottle in the spacecraft. The wing apex inflation fitting contains a quick-disconnect mechanism, which is activated on completion of the inflation to permit the wing to move above the spacecraft, which is then suspended by load and control cables. The spacecraft is equipped with extendible landing skids for landing on land, rather than on water. This wing has a glide ratio  $L/D = 3.5$  and a glide angle of 25 degrees. Its touchdown speed is about 42 knots, which corresponds to a lift coefficient slightly less than maximum.

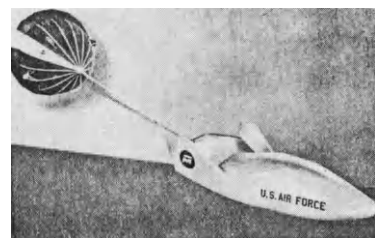
As a non-steerable inflatable decelerator, the paraloop, consisting of a balloon and a decelerator skirt, has been developed. Paraloops have been used for recovery of camera capsules in the Atlas, Titan and Saturn/Apollo programs and have provided valuable information with regard to staging, motor ignition, fuel consumption, and flight control (see Fig. 13).<sup>16</sup>

A similar decelerator is the ballute, a combination of balloon and parachute, which was developed as a high-altitude, high-speed recovery device for unmanned spacecraft at Mach 10. In the recovery system of the PRIME SV-5 re-entry vehicle, a ballute was ideally used as drogue. The recovery system with a 47-ft diameter parachute provided a terminal descent rate of 26 ft/sec for the 900-lb spacecraft (see Fig. 14).<sup>15</sup>



**Paraloop for Camera Capsule Recovery**

Fig. 13



**Ballute used as Drogue  
for SV-5 Lifting-Body Vehicle**

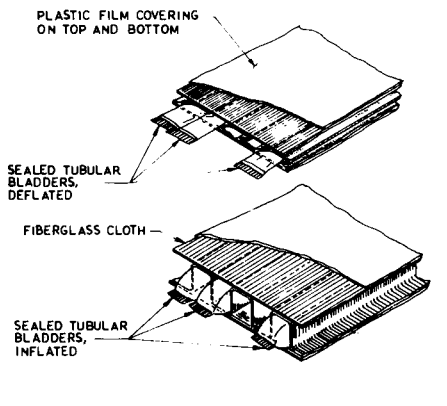
Fig. 14

#### V. Chemically-Rigidized Cloth Structures

Chemically-rigidized inflated cloth structures have been developed to provide a certain desired stiffness and to reduce the danger of damage by penetration by micro-meteoroids or other objects. Rigidizing of flexible structures is usually accomplished by release of subliming materials which rigidize the system by plasticizer boil-off. A relatively good load-carrying capability is obtained in rigidized structures. Rigidization techniques can be applied to a great variety of space structures. The chemically-rigidized structure can consist of an expandable self-rigidizing honeycomb or truss core, or it can be a foamed-in-place rigidized membrane. On a strength-to-weight basis, the optimum rigidized structure is an expandable honeycomb. For a cylindrical structure, a very efficient core configuration is the corrugated type of core, where the corrugations run circumferentially around the cylinder. For protection against damage from micro-meteoroids, a double-wall sandwich structure is of great advantage. A suitable resin system for pre-impregnating the core is urethane resin, cured to a B-stage. Good results were obtained with water vapor with a

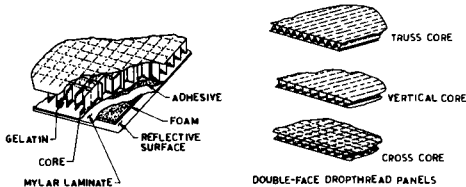
small amount of amine as catalyst to inflate the core flutes and to rigidize the structure. To prevent system failures, the effects of temperature on the rate of rigidization and on the strength of the selected fibrous reinforced structures must be predetermined. Polyurethane foams developed for high vacuum applications have been produced as rigidizing materials in a vacuum of  $10^{-6}$  Torr and have been tested under space environmental conditions for 770 hours.

The rigidized honeycomb construction offers the advantage of high compression strength, great stiffness and low weight. A typical concept of a rigidizing technique for a double-wall structure is shown in the following example (see Fig. 15). 17



RIGIDIZING TECHNIQUE FOR DOUBLE-WALL STRUCTURE  
Fig. 15

Three self-rigidizing core structures are presented in Fig. 16. 18



SELF-RIGIDIZING CORE STRUCTURES FOR SPACE APPLICATIONS  
Fig. 16

Good results were obtained by tests with gelatin (amino acid) as rigidizing material for expandable structures. Gelatin has the advantageous characteristics that it exhibits high tensile strength and high modulus of elasticity values and that it is highly resistant to ultraviolet radiation. The gelatin/fabric ratio has been optimized for maximum strength-to-weight characteristics. For maximum tensile strength to weight, the optimum

gelatin content is 15 percent of the total composite weight.

Test specimens consisting of eight plies of Type 181 fiberglass fabric, rigidized and cured with gelatin under 1,000 psi pressure at a temperature of 275° F for one hour have a flexural strength of 65,000 psi, a flexural modulus of  $3.2 \times 10^6$  psi, and tensile properties of approximately the same values. 18

## VI. Stiffened Cloth Structures

Stiffened cloth structures are mainly used in flexible wings and in airlocks. Stiffened flexible wings, having a small tapered rigid leading edge, offer the advantage over inflatable flexible wings of a substantially higher lift-to-drag ratio. With cylindrical-type flexible wings, stiffened with a rigid leading edge, lift-to-drag ratios up to 17.0, as compared to an L/D value of only 3.5 of inflatable wings, have been achieved. Disadvantageous features of stiffened flexible wings are greater stowage volume and greater complexity in packaging and deployment.

A flexible wing with rigid leading edges, used for recovery of a high-altitude rocket test vehicle of a weight of 165 lbs, has a span of 10.7 ft and a wing area of 40 sq.ft. During launch and rocket flight, the wing with its hinged leading edge members is stored in a long cylindrical container mounted on top of the rocket vehicle. To deploy the wing, the container is opened and separated from the vehicle, and the rigid leading edge members are spread out by a hydraulic cylinder system. 19

A good example for stiffened cloth structures is an accordion-style airlock developed for Spacelab flights on Space Shuttle missions in the 1980s. The airlock consists of a pressurized tunnel which will connect the Space Shuttle Orbiter with the forward end of the Spacelab to provide a passageway for crew members. The tunnel has an inside diameter of 4 ft, and it can be extended from a length of 2 ft to 14 ft 8 in. The circular shape is kept by steel rings, and steel cables are used to extend and compress the airlock. The airtight bladder consists of layers of aluminum foil, Kapton film and nylon cloth. To protect the airlock against meteoroid impact damage, the outside is covered with a spongy meteoroid shield and nylon cloth. 20

Extensive tests, including underwater tests using neutral buoyancy techniques to simulate zero "g" condition, which were conducted with 7 ft long airlocks, have provided valuable data and experience for this new airlock development. 21

## VII. Unstiffened Cloth Structures

In the category of unstiffened cloth structures, all-flexible parawings and parafoils are to be listed. In recent years, extensive research, development and testing in this special field of deceleration systems have provided valuable results. Both the all-flexible parawing and the parafoil are controllable and thus, make land landing of spacecraft at selected sites possible.

All-flexible parawings, as compared with conventional parachutes, offer not only the advantage of steerability, but also of a lower packaging volume. All-flexible wings are packaged and deployed similar to parachutes, but for the same rate of descent, they require only one tenth as much fabric area. A parachute with a wing loading of  $W/S = 0.1 \text{ lb/ft}^2$  has approximately the same vertical velocity as an all-flexible parawing with a wing loading of  $W/S = 1.0 \text{ lb/ft}^2$ .

All-flexible wings have no stiffening or inflatable members, but the surface of the lobes has a compound curvature which holds its aerodynamic shape with a minimum of reinforcement of the edges. The advantages of this type of wing are that it is of simple design, easy to stow, its areas of local heating are very small, and it does not require an inflation system, which results in a low system weight and high reliability (see Fig. 17).

In the course of the development and testing of an all-flexible parawing for recovery of a 15,000 lb vehicle, a two-keel wing configuration proved to be superior over a one-keel type in terms of its maximum L/D glide capability. This parawing had a keel length of 72 ft, a wing span of 111 ft, a canopy area of 4000  $\text{ft}^2$ , and an L/D glide ratio of 2.5 - 2.75. By employing a multi-stage reefing system, the deployment loads could be maintained at a level of 3.0-3.5 G's. The weight of this parawing, made from 2.25 oz/yd<sup>2</sup> low-permeability nylon sailcloth, was 530 lbs, and its packed volume was 11.75  $\text{ft}^3$ . 22

Land-landing of reusable spacecraft is currently of interest for future space missions. The combination of a steerable lifting body vehicle in the hypersonic phase of the re-entry trajectory and a parawing that can be deployed in the subsonic and landing phases could possibly provide a land-landing system which may offer great advantages.

A unique type of flexible wing is the ram-air inflated parafoil wing, consisting of an upper and a lower nylon cloth surface which are connected by vertical webs forming chordwise channels which are open at the leading edge. The ram-air inflated

open cells between both surfaces provide the required rigidity for this airfoil-shaped wing. Pennants are distributed along the bottom surface to which the suspension lines are attached. These pennants serve to distribute the aerodynamic forces to the suspension lines, to partially channel the flow into a two-dimensional flow pattern which improves the aerodynamic efficiency and reduces tip losses, and to provide side area which aids in obtaining directional flight stability. Glide ratios L/D = 1.5-2.4 have been achieved with parafoil wings. 23

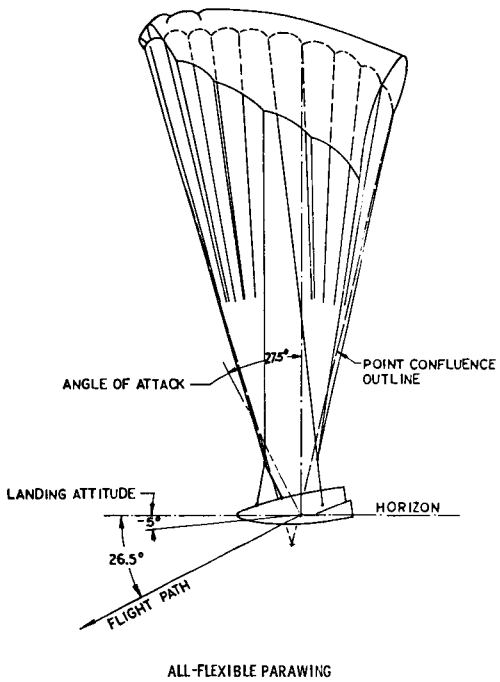


Fig. 17

## VIII. Future Applications of Expandable Structures

Within a few years from now, the era of large space stations and of the Space Shuttle and the Space Tug will begin. At the same time, it can be expected that the energy shortages on earth will lead to the development of very large space solar power stations. Expandable structures will find ideal applications in these important space projects, and it can be predicted that these large space station can be built only by utilizing expandable structures.

For one project of a space solar power

station, a transmitter support structure, to be erected from 2700 sixty-foot core cubes spanning about 1000 meters, is being planned. Collapsed-truss structural members for this project are to be transported by the Space Shuttle, and the first structure cubes are to be erected utilizing the Shuttle's manipulator.

Another interesting future project is a 200-meter diameter dual-polarization parabolic antenna for a radio-astronomy telescope to be assembled in space from 50-ft long telescoping beams which are to be transported in compressed condition. These beams would be extended outward in a spoke-like configuration. A wire-mesh screen would then be stretched over a wire support and attached to the spokes by a crew in EVA. <sup>24</sup>

Methods and tooling to be used in the assembly of such large space structures are being developed. A data base from the repairs performed on the vacated orbiting Skylab workshop has been provided for these development efforts. Extensive simulation exercises and studies have led to the conclusions that large space structures can be packaged, transported and assembled in space within a reasonable time, utilizing expandable structures.

#### References

1. J.D. MacNaughton, H.N. Weyman, and E. Groskopfs, "The BI-STEM - A New Technique in Unfurtable Structures", 2nd aerospace mechanism Symposium, Santa Clara, Calif., May 1967.
2. "STEM, Design and Performance", Astro Research Corp., Carpinteria, Cal., 1976
3. "Introducing the Hunter Stacer, AMETEK/Hunter Spring, Bulletin S-101.
4. "Large Space Structures", Fairchild Hiller Corporation.
5. L.N. Dumas, "Mechanical Engineering in Spacecraft Design: Art or Science?", John Orr Memorial Lecture, The South African Mechanical Engineer, Vol. 25, Oct. 1975, p. 299-315.
6. "Astromasts for Space Applications", Astro Research Corp., Santa Barbara, Calif.
7. J.A. Fager, "Erectable Antenna Applications", General Dynamics/Convair, San Diego, Calif.
8. "CTS Launch News", SPAR Aerospace Products Ltd., Toronto, 16 Jan. 1976.
9. "SPAR tests flexible solar array for CTS", SPAR Aerospace Products Ltd., Toronto.
10. "Space Agency Plans to Build Large, Light Solar Cell Array", Aviation Week & Space Technology, 15 Sep. 1975, p. 23
11. G.P. Durney, "Balloon Material Development", ILC Industries, Inc., Dover, Delaware, 1975.
12. "Shuttle Suit to offer Improved Mobility", Aviation Week & Space Technology, 5 Apr. 1976, p. 59.
13. "NASA's Rescue Ball", Time, 19 April 1976, p. 45.
14. F.M. Rogallo, "Flexible Wing Research and Development", Symposium on Retardation and Recovery, Dayton, Ohio, 1962.
15. "The Expandable Deployables, Recovery Systems", Goodyear Aerospace Corp.
16. "Recoverable Camera Capsule", Cook Electric, Tech Center Division, Bulletin 4-1-1.
17. L.J. Boler, "Lightweight Packagable Structural Materials for the Exploration of Space", AIAA Paper A66-28016.
18. S. Schwartz, "Space Rigidization Techniques for Expandable Structures", Hughes Material Technology Department.
19. E. Wieland, "Zur Bergung von Raumfahrzeugen mit flexiblen Tragflächen (Paragleiter)", Raumfahrtforschung, DGLR, Band 9, Heft 2, 1965, p. 53-60.
20. "Accordion-style Rubber Airlock", Design News, 19 May 1975.
21. F.W. Forbes, "Progress Report on the Do 21 Expandable Airlock Experiment for the S-IVB Workshop", 19th IAF Congress, New York, 1968, SD 49.
22. J.H. Moeller and E.M. Linhart, "Parawing Technology for Spacecart Land Landing, a Progress Report, Journal of Aircraft, Vol. 8, No. 12, Dec. 1971, p. 1016-1021.
23. J.D. Nicolaides, R.J. Speelman III, and G.L.C. Menard, "A Review of Para-Foil Applications", Journal of Aircraft, Sep.-Oct. 1970, p. 423-431.
24. T. Hagler, "Building Large Structures in Space", Astronautics & Aeronautics, May 1976, p. 56-61.

# PROPULSION BY LASER ENERGY TRANSMISSION

## (Considerations to Selected Problems)

R. E. Lo\*

*DFVLR - Institute of Chemical Rocket Propulsion, Hardthausen-Lampoldshausen,  
Federal Republic of Germany*

### Abstract

The rewards of laser propulsion are substantial payload gains for missions with high velocity increment. Laser-assisted chemical propulsion is an effective means to reduce required laser powers. Payload gains of this new mode of propulsion can be calculated as functions of ratio of laser power to chemical power, structural mass fraction and velocity increment. Payload mass fraction can be optimized for minimum laser power requirement. Deep space missions require very high laser power and/or very small beam divergence. For near-earth missions, the simultaneous input of laser- and solar-power is worthwhile and can be optimized.

### I. Mission Considerations

When a spacecraft receives its propulsive energy by laser- or other energy-transmission from the outside, a gain over chemical propulsion systems can only be obtained, if the effective exhaust velocity is increased above chemically achievable values. The mass of the energy transmitted is zero for all practical purposes and the on-board propellant mass would have to be the same for a given propulsion requirement  $\Delta V$  and a given exhaust velocity, whether it contains chemical energy or not. For this reason, all missions requiring larger than chemical exhaust velocities are the only candidates of real interest for laser-propulsion. However, many of these missions require also large absolute amounts of power. Typical examples are

- single-stage-to-orbit missions
- two-way tug missions servicing geostationary orbit
- fast perigee-apogee delivery of payloads.

Therefore, aside of pure laser-propulsion with chemically inert propellants, mixed mode laser-assisted chemical propulsion should be considered as an effective means to reduce required laser power. If the take-off mass  $M_O$  of a spacecraft is simply split into payload  $M_n$ , structural mass  $M_s$  and propellant mass  $M_p$

$$M_O = M_n + M_s + M_p \quad (1)$$

$$\frac{M_n}{M_O} = \alpha \quad (2)$$

$$\frac{M_s}{M_O} = \beta \quad (3)$$

the basic Ziolkowsky equation

$$\Delta V = c \cdot \ln \frac{1}{\alpha + \beta} \quad (4)$$

shows (see Fig. 1) that perigee-apogee missions with a typical  $\Delta V$  of 4000 m/s and in particular single-stage-to-orbit missions ( $\Delta V$  about 10.000 m/s) suffer from a very steep decrease of the payload mass fraction with  $c$ .

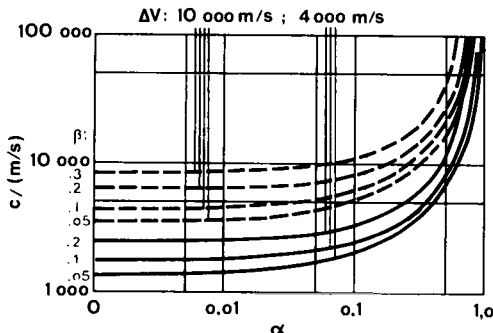


Fig. 1 Required minimum exhaust velocities  $c$  as functions of payload mass fraction  $\alpha$  with structural factor  $\beta$  as parameter, for single-stage-to-orbit ( $\Delta V = 10.000$  m/s) and perigee-apogee ( $\Delta V = 4000$  m/s) missions.

Single-stage-to-orbit propulsion with 1 to 5% of payload is in the tantalizing region of marginal feasibility with exhaust velocities of 4500 to 5000 m/s, if structural factors  $\beta$  of 0.1 or better can be obtained. This may be the example, where some additional beamed energy may make all the difference between tiny payload fractions of uncertain feasibility and commercially interesting percentages. Total exhaust jet power  $P$  would thus have to consist of a chemical and a laser contribution

\* Director, Member AIAA, DGLR, HOG

$P_{Ch}$  and  $P_L$ :

$$P = P_{Ch} + P_L \quad (5)$$

Its absolute value depends upon thrust  $F$  or massflow rate  $\dot{m}$  which, in turn, are determined by the chosen vehicle acceleration  $g$ :

$$P = 0.5 \dot{m} c^2 \quad (6)$$

$$F = \dot{m} c \quad (7)$$

$$P = 0.5 F \cdot c = \frac{F \cdot \Delta V}{2 \ln \frac{1}{\alpha+\beta}} \quad (8)$$

$$F = g M_0 = \frac{g M_0}{\alpha} \quad (9)$$

$$F = \frac{g M_0}{\alpha} \cdot \frac{\Delta V}{\ln \frac{1}{\alpha+\beta}} \quad (10)$$

$$P_{Ch} = 0.5 \cdot \dot{m} c_{Ch}^2 \quad (11)$$

$$P_L = 0.5 \cdot \dot{m} \cdot C_L^2 \quad (12)$$

Due to equation (5),  $C_L$  is not the difference between necessary exhaust velocity  $c$  and the chemically achievable one  $c_{Ch}$ , but

$$C_L = \sqrt{c^2 - \frac{C_{Ch}^2}{c}} \quad (13)$$

Therefore

$$P_L = 0.5 \cdot F \cdot \left( c - \frac{C_{Ch}^2}{c} \right) \quad (14)$$

and similarly

$$P_{Ch} = 0.5 \cdot F \cdot \frac{C_{Ch}^2}{c} \quad (15)$$

$$P_{Ch} = \frac{g M_0}{2\alpha} \cdot \frac{C_{Ch}^2}{\Delta V} \cdot \ln \frac{1}{\alpha+\beta} \quad (16)$$

$$P_L = \frac{g M_0}{2\alpha} \left( \frac{\Delta V}{\ln \frac{1}{\alpha+\beta}} - \frac{C_{Ch}^2}{\Delta V} \cdot \ln \frac{1}{\alpha+\beta} \right) \quad (17)$$

The necessary ratio of laser- to chemical power can thus be expressed as a function of the desired  $\alpha$  at a given  $\Delta V$  for values of  $\beta$  and  $C_{Ch}$  as they are achievable:

$$\pi = \frac{P_L}{P_{Ch}} = \left( \frac{1}{\ln \frac{1}{\alpha+\beta}} \cdot \frac{\Delta V}{C_{Ch}} \right)^2 - 1 \quad (18)$$

In Fig. 2, the combined sum of payload and structural mass fractions is plotted over the mission propulsion requirement  $\Delta V$  in multiples of available chemical exhaust velocity. Since  $C_{Ch}$  has to be considered in the range of 3000 to 5000 m/s, the value of  $\Delta V/C_{Ch}$  is in the range of

- 0.1 for attitude control
- 1.0 for perigee-apogee missions
- 2.0 to 3.0 for single-stage-to-orbit and two-way trips.

For any given structural factor  $\beta$ , the gain in payload fraction  $\alpha$  is obviously increasing with  $\pi$ .

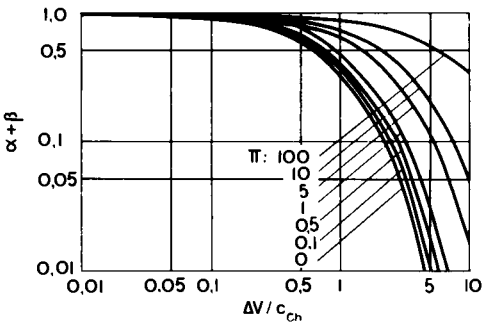


Fig. 2 Achievable dry-mass fractions  $\alpha + \beta$  as a function of propulsion requirement  $\Delta V$  over chemical exhaust velocity  $C_{Ch}$ , with ratio  $\pi$  of laser-to-chemical power as parameter.

For a given  $\pi$  it increases dramatically with  $\Delta V/C_{Ch}$ . No significant gain is obtained for low energy missions. On the other hand, additional laser-power of 10 to 50% of chemical power may raise the fraction available for masses other than propellants from 0.1 with zero payload to feasible values.

This can more clearly be shown if payload gain in terms of % of pure chemical propulsion is calculated as a function of  $\pi$  and  $\Delta V/C_{Ch}$ :

$$\Delta\alpha[\%] = f(\pi, \Delta V/C_{Ch}) = \frac{100 \alpha (\pi=\pi)}{\alpha (\pi=0)} \quad (19)$$

Fig. 3 shows how this gain increases with  $\pi$ . It is only for high energy missions that the gain exceeds 50 to 100% even for small  $\pi$ . Vehicles with heavier structures gain more than lighter ones. For example, payload fraction  $\alpha$  of a  $\beta = 0.1$  single-stage-to-orbit vehicle could be increased from 3.5% of  $M_0$  by a factor of 4 up to 14.3% by adding once again the amount of chemical power with beamed energy. With  $\beta = 0.2$ , such a vehicle has no positive payload ( $\alpha$  is then - 6.5%). With  $\pi = 1$ , it carries 4.3% of payload.

Fig. 4 shows  $\Delta\alpha$  as a function of  $\beta$ : for high energy missions payload gain increases steeply with  $\beta$ .

Therefore, it may be concluded that the application of beamed energy is worthwhile only in missions with large  $\Delta V$ , with ratios  $\Delta V/C_{Ch}$  above 1. Single-stage-to-orbit missions are considered as an example in the

next chapter, however, very similar results could be obtained for a two-way tug. Most of the mathematical relations derived hold for any  $\Delta V$ .

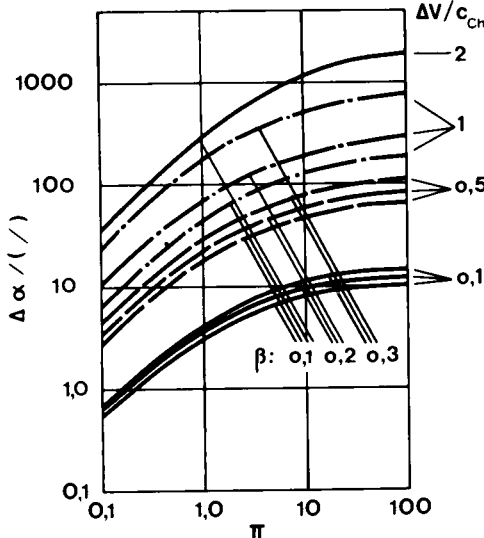


Fig. 3 Payload increase  $\Delta\alpha$  in percents as a function of laser-assistance ratio  $\Pi = P_L/P_{Ch}$ , with  $\beta$  and  $\Delta V/C_{Ch}$  as parameters.

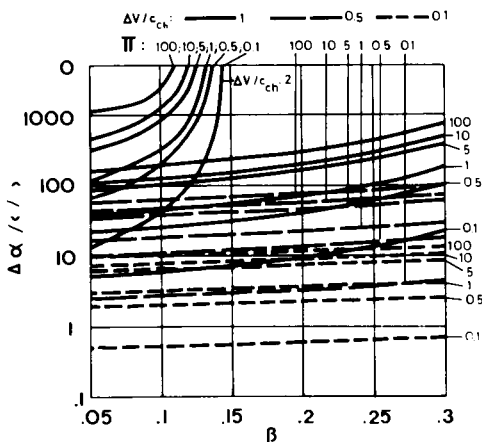


Fig. 4 Payload increase  $\Delta\alpha$  in percents as a function of structural factor  $\beta$ , with  $\Delta V/C_{Ch}$  and laser assistance ratio  $\Pi$  as parameters.

## II. Laser-Assisted Single-Stage-to-Orbit Vehicles

Such vehicles fall under two restrictions:

- laser power limited design
- $\beta$  limited design.

The following Table 1 gives the values for a single-stage-to-orbit vehicle with  $\beta$  and  $M_n$  a little better than the present space shuttle design (for Table 1, see Page 4).

The following conclusions can be drawn from the results:

- Lifting of 30 t of payload into orbit is not a question of megawatts, as they may be available within several years, it is a question of gigawatts.
- If, however, gigawatts are available, even a small contribution to chemical power has dramatic effects on vehicle size: with little more than 5.5 GW it can be reduced by a factor of more than 21!
- There is a region, where vehicle mass is a very sensitive function of laser power. It is very much worthwhile to get into this region: in the present example, an increase of 0.26 GW from 5.52 to 5.78 will result in a further vehicle mass reduction by another factor of almost 3!
- At larger laser-powers, their application becomes temperature limited. If 10.000 m/s are considered as maximum achievable exhaust velocity (corresponding to chamber temperatures of 6000-7000 K), no more than 5.6 GW can be applied (assuming total conversion).
- Total power requirement goes through a minimum, while laser-power does not, since in this particular case  $\beta$  is marginal.

Let us consider the question of minimum power requirement as a function of payload mass fraction  $\alpha$ . It is well known, that such a minimum exists for any thrust  $F$ , propulsion requirement  $\Delta V$  and structural factor  $\beta$ . However, at available exit velocities,  $\alpha$  has to be kept far below optimum values, while on the other hand chemical power has no upper limit.

From equation (10) we derive:

$$\frac{dP}{d\alpha} = \frac{gM_n}{\alpha} \cdot \frac{\Delta V}{\ln \frac{1}{\alpha+\beta}} \left( \frac{1}{(\alpha+\beta) \ln \frac{1}{\alpha+\beta}} \right) - \frac{1}{\alpha}, \quad (20)$$

$$\frac{dP}{d\alpha} (\alpha) = \frac{1}{2} \cdot F(\alpha) \cdot c(\alpha) \cdot f(\alpha) \quad (21)$$

$$\frac{dP}{d\alpha} = 0 ! \quad (22)$$

$$\alpha - (\alpha+\beta) \ln \frac{1}{\alpha+\beta} = 0 ! \quad (23)$$

Table 1

Data of laser-assisted chemical single-stage-to-orbit vehicles as a function of ratio  $\pi$  of laser-power  $P_L$  to chemical power  $P_{Ch}$ . There is in all cases a payload of 30.000 kg, structural factor  $\beta$  of 0.13, chemical exhaust velocity of 5000 m/s, take-off acceleration of 1.2 g and  $\Delta V$  of 10.000 m/s ( $t_b$  = thrust time)

$\pi$	0	0.1	0.5	1	5	10	100
$\alpha$	0.00533	0.01854	0.06534	0.1131	0.3120	0.4172	0.6895
$M_O$ [t]	5622.9	1618.4	495.1	265.2	96.16	71.92	43.51
$M_S$ [t]	731.0	210.4	59.7	34.5	12.50	9.35	5.66
$M_P$ [t]	4861.9	1378.0	369.4	200.7	53.66	32.57	7.85
$F$ [ $10^4$ N]	6619	1905	540.5	312.2	113.2	84.7	51.2
$c$ [m/s]	5000	5244	6114	7071	12247	16583	50249
$\dot{m}$ [kg/s]	13239	3633	882.6	441.5	92.43	51.05	10.19
$t_b$ [J]	367	379	418	455	580	638	770
$P$ [GW]	165.5	49.95	16.55	11.04	6.932	7.019	12.865
$P_{Ch}$ [GW]	165.5	45.41	11.03	5.52	1.155	0.638	0.1274
$P_L$ [GW]	0	4.54	5.51	5.52	5.777	6.381	12.7380

Table 2

Payload mass fraction  $\alpha_{min}$  for minimum total power requirement as function of structural factor  $\beta$ .

$\beta$	0	0.05	0.10	0.15	0.20	0.25	0.30	0.35	0.5	0.7	0.9	1.0
$\alpha_{min}$	0.3679	0.3650	0.3577	0.3474	0.3347	0.3203	0.3044	0.2872	0.2298	0.1435	0.0493	0.0

Numerical solution of equation (23) results in the minimum values for  $\alpha$  shown in Table 2.

This minimum can, of course, easily be understood in terms of masses (see Fig. 6): power requirement increases at low values of  $\alpha$ , due to raising  $M_O$ , at high values of  $\alpha$  it increases due to decreasing propellant mass with accordingly increasing exhaust velocity requirements.

With a constant chemical contribution to power in laser-assisted chemical propulsion there, too, should be minima for required laser power.

Differentiation of equation (17) gives:

$$\frac{dP_L}{d\alpha} = \frac{gMn}{2\alpha} \left[ \frac{1}{\alpha+\beta} \left( \frac{\Delta V}{\ln^2 \frac{1}{\alpha+\beta}} + \frac{C_{Ch}^2}{\Delta V} \right) - \frac{1}{\alpha} \left( \frac{\Delta V}{\ln \frac{1}{\alpha+\beta}} - \frac{C_{Ch}^2}{\Delta V} \ln \frac{1}{\alpha+\beta} \right) \right] \quad (24)$$

$$\frac{1}{\alpha} \left( \frac{\Delta V}{\ln \frac{1}{\alpha+\beta}} - \frac{C_{Ch}^2}{\Delta V} \ln \frac{1}{\alpha+\beta} \right)$$

$$\alpha_{min} = f(\Delta V, C_{Ch}, \beta) \quad (25)$$

An analytical expression in the form of equation (25) cannot be obtained by setting the factors of equation (24) equal to zero. However, numerical solution of equation (24) or (17) gives the desired answers (Fig. 5).

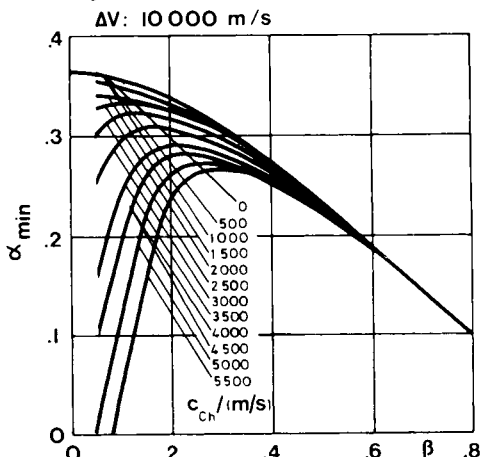


Fig. 5 Payload mass fraction  $\alpha_{min}$  for minimum required laser power as a function of structural factor  $\beta$  with  $C_{Ch}$  as parameter.

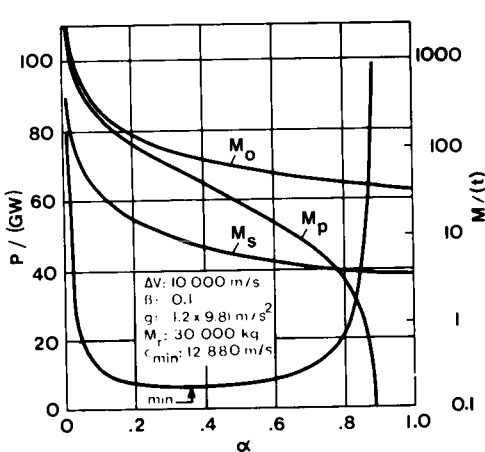


Fig. 6 Total power requirement  $P$  of exhaust gases as a function of payload mass fraction  $\alpha$ . Total mass  $M_0$ , structural mass  $M_s$  and propellant mass  $M_p$  also as functions of  $\alpha$ .  $C_{min}$  cannot be achieved chemically. Power for  $C = 4500 \text{ m/s}$  is 95 GW at  $\alpha = 0.0084$ .

For a  $\Delta V = 10.000 \text{ m/s}$  single-stage-to-orbit mission, the results are shown in Fig. 6. From these, minimum required laser-power results with payload and acceleration as additional parameters.

Equation (14) may be rewritten as follows:

$$P_{L,min} = \frac{gM_0}{2\alpha_{min}} \cdot (c - \frac{C_{Ch}^2}{c}) \quad (26)$$

$$P_{L,min} = \frac{gM_0}{2\alpha_{min}} \cdot P_L' = \frac{F}{2} \cdot P_L' \quad (27)$$

$$P_L'_{min} = c - \frac{C_{Ch}^2}{c} = \frac{\Delta V}{\ln \frac{1}{\alpha_{min} + \beta}} \quad (28)$$

$$- \frac{C_{Ch}^2}{\Delta V} \cdot \ln \frac{1}{\alpha_{min} + \beta}$$

$P_L'$  being the equivalent laser-exhaust velocity. Plotted as a function of  $\alpha_{min}$  with  $C_{Ch}$  and  $\beta$  as parameters (see Fig. 7), it delivers the required minimum laser power for any thrust level (chosen according to equation (27) after selection of acceleration and payload along with fixed  $\alpha_{min}$ , the latter being determined by  $\Delta V$ ,  $C_{Ch}$  and  $\beta$ ).

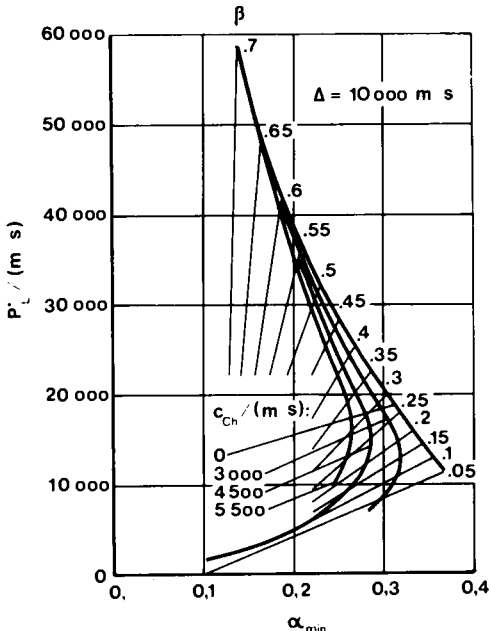


Fig. 7 Required equivalent laser induced exhaust velocity as defined by equation (27) as a function of  $\alpha_{min}$  with  $C_{Ch}$  and  $\beta$  as parameters.

As Fig. 7 shows, no  $\alpha_{min}$  occurs where a line of constant  $C_{Ch}$  does not cross a particular line of constant  $\beta$ . Below a certain  $\beta$  laser power simply decreases with decreasing  $\alpha$ . This is always the case, when  $C_{Ch}$  alone is close to being sufficient for a particular mission, as in the example of Table 1. This is made more obvious by considering another sample case.

A single-stage-to-orbit ( $\Delta V = 10.000 \text{ m/s}$ ) vehicle providing a chemical exhaust velocity of  $C_{Ch} = 4500 \text{ m/s}$  cannot be built with structural factors  $\beta$  above 0.10837. In this case, it has precisely zero payload. To design it with any other values of the sum  $\alpha + \beta$  requires additional beamed power. The situation is depicted in Fig. 8.

$P_L$  is plotted over  $\alpha$ , with  $\beta$  as parameter. All values of  $\beta$  above 0.1 show minima at  $\alpha$  values between 0.1 and 0.3. For very low values of  $\alpha$ ,  $P_L$  again decreases monotonously with  $\alpha$  (not shown in Fig. 7). However, vehicles with very light construction ( $\beta$  below 0.10837) require smoothly raising amounts of laser power if  $\alpha$  increases beyond values where  $\alpha + \beta$  equals 0.10837.

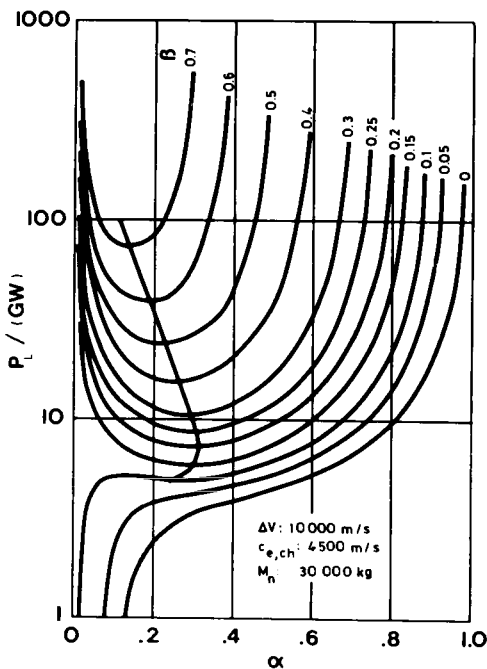


Fig. 8 Additional laser power required for a single-stage-to-orbit vehicle as a function of payload mass fraction  $\alpha$ , with structural factor  $\beta$  as parameter.

The  $P_L$  lines of constant  $\beta$  in Fig. 8 are very flat in the vicinity of this critical value. This again reflects the fact found in the example of Table 1: in these regions a small increase in  $P_L$  results in a dramatic increase of possible payload mass-fractions  $\alpha$ .

In closing the present considerations of laser-assisted chemical propulsion, it should be mentioned that, of course, all  $P_L$  values considered here are effective values as they must show up in the kinetic energy of the exhaust gases. Laser power to be transmitted from the base power station  $P_{L,\text{bas}}$  has to be larger according to transmission and conversion efficiencies  $n_T$  and  $n_C$ , which normally will together be below 0.5:

$$P_L = n_T \cdot n_C \cdot P_{L,\text{bas}} \quad (29)$$

### III. Transmission Considerations

Even in the case of short distance laser power transmission to ascending launch vehicles or to spacecraft in low-earth orbits beam divergence, tracking and jitter may be well beyond present-day technology. The situation is gravely worsened if transmission to geosynchronous orbits, over lunar or interplanetary distances is considered.

Due to beam divergence, power density is diluted by the square of the transmission distance. Since direct conversion to propulsive power requires large total amounts of energy per second, which may not be feasible with power-limited laser energy sources, indirect conversion by means of solar panels might be of interest. This, as another advantage, offers the opportunity of making use of the solar radiation as additional energy source, with which to compete any laser will have trouble over larger distances. Electric power from the panels could then be converted to thrust with ion- or plasma engines.

Let us assume the existence of a laser-power base in low earth orbit, such that its distance from the sun is essentially 1 AU (taken to be  $1,496 \cdot 10^{11} \text{m}$ ). The base emits a conical laser beam with divergence angle  $\epsilon$ . The cross-sectional area of the beam at any distance from the laser source  $D_L$  will then be:

$$A = D_L^2 \pi \operatorname{tg}^2 \frac{\epsilon}{2}. \quad (30)$$

If the laser has a power  $E_0$  at the source, its intensity will then diminish with  $D_L$ :

$$I_L = \frac{E_0}{D_L^2 \pi \operatorname{tg}^2 \frac{\epsilon}{2}} \quad (31)$$

On the other hand, the solar intensity at 1 AU is  $k_0$ .  $k_0 = 1,3146 \cdot 10^3 \text{ W/m}^2$ .

The local solar intensity at any distance  $D_S$  from the sun is

$$I_S = k_0 \left( \frac{AU}{D_S} \right)^2 \quad [\text{W/m}^2]. \quad (32)$$

The ratio of laser to solar intensity is therefore:

$$\frac{I_L}{I_S} = \left( \frac{D_S}{D_L} \right)^2 \cdot \frac{1}{AU^2 \pi \operatorname{tg}^2 \frac{\epsilon}{2}} \cdot \frac{E_0}{k_0} \quad (33)$$

The solar panel shall be a planarian surface of area  $A$  and radius  $r$  (not necessarily determined by equation (30)). The angle between this surface and the line of sight to the laser base be  $\alpha$ , the angle with the line of sight to the sun  $\beta$ , so that the angle  $\delta$  between the two lines is the difference

$$\delta = \alpha - \beta. \quad (34)$$

The effective areas of the panel surface are then the projection upon a plane perpendicular to the respective lines of sight:

$$A_L = r^2 \pi \sin \alpha \quad (35)$$

$$A_S = r^2 \pi \sin \beta \quad (36)$$

since

$$\begin{aligned}\sin \beta &= \sin (\alpha + \delta) = \sin \alpha \cos \delta + \\ &+ \cos \alpha \sin \delta\end{aligned}\quad (37)$$

$$I_s = r^2 \pi (\sin \alpha \cos \delta + \cos \alpha \sin \delta). \quad (38)$$

If laser beam divergence satisfies equation (30), the laser power received by the panel is

$$I_L = \frac{E_0}{D_L^2 \pi \operatorname{tg}^2 \frac{\varepsilon}{2}} \cdot r^2 \pi \sin \alpha \quad (39)$$

while from the sun it receives

$$\begin{aligned}I_s &= k_o \left( \frac{AU}{D_s} \right)^2 r^2 \pi (\sin \alpha \cos \delta + \\ &+ \cos \alpha \sin \delta).\end{aligned}\quad (40)$$

Panel center, laser base and sun form a triangle with sides  $D_L$ ,  $AU$  and  $D_s$ , the angle  $\delta$  formed by  $D_L$  and  $D_s$ . Therefore

$$AU^2 = D_L^2 + D_s^2 - 2 D_L D_s \cos \delta \quad (41)$$

$$\cos \delta = \frac{D_L^2 + D_s^2 - AU^2}{2 D_L D_s} \quad (42)$$

with the following abbreviations

$$K_1 = k_o \left( \frac{AU}{D_s} \right)^2 r^2 \pi \quad (43)$$

$$K_2 = \frac{D_L^2 + D_s^2 - AU^2}{2 D_L D_s} \quad (44)$$

$$K_3 = \operatorname{sinarc} \cos \frac{D_L^2 + D_s^2 - AU^2}{2 D_L D_s} \quad (45)$$

$$K_4 = \frac{E_0}{D_L^2 \pi \operatorname{tg}^2 \frac{\varepsilon}{2}} \cdot r^2 \pi \quad (46)$$

the total power received by the panel becomes the following function of  $\alpha$ :

$$\begin{aligned}I_{\text{tot}} &= I_L + I_s = \\ &= (K_1 K_2 + K_4) \sin \alpha + K_1 K_3 \cos \alpha.\end{aligned}\quad (47)$$

Before studying the influence of  $\alpha$ , let us consider power and beam divergence requirements as a function of distance.

For the simple case of the panel bearing spacecraft being in the direction opposite to the sun (that is, the angle  $\phi$  between the line of sight from base to sun and from base to spacecraft is 180 degrees), the following results are obtained. It is

further assumed that the panel has a size given by local laser beam diameter and that the center line of the beam goes through the panel center.  $\varepsilon$  is measured in fractions of one degree

#### a) Case of a $10^3$ W laser.

Fig. 9 plots  $I_{\text{tot}}$  as a function of  $D_L$  for this moderate size laser, with beam divergence  $\varepsilon$  as parameter. Under the optimistic assumption of a pointing accuracy and beam divergence as low as  $10^{-5}$  ( $= 0.036$  seconds!) being feasible, this laser contributes substantially to solar power only below 30.000 km distance.

Its influence at all distances beyond the earth-moon distance is negligible even if  $\varepsilon$  is decreased by another order of magnitude.

Such a small laser is therefore of any interest only in the immediate vicinity of the earth, and might assist operations of spacecraft within the shadow cone of the earth.

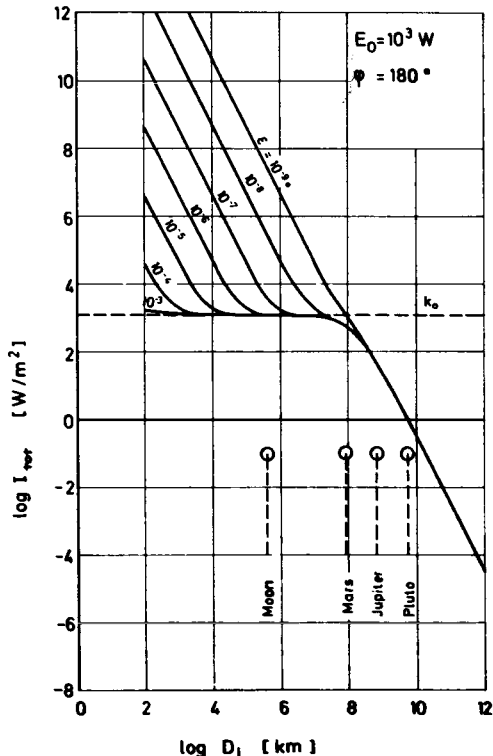


Fig. 9 Total energy input of a solar panel for a kW-laser as a function of distance and beam divergence.

b) Case of a  $10^6$  W laser.

Fig. 10: this laser is without any influence beyond lunar distances with  $\epsilon = 10^{-5}$ . However, it might power electrical tugs to and from geosynchronous orbit even with larger beam divergence.

It is a true but unrealistic statement that this laser, with  $10^{-9}$  degrees beam divergence could produce an illumination intensity equal to one solar constant  $k_0$  as far as the distance of Uranus. With equal pointing accuracy, the panel area required would have a diameter of 50 m. An electrical engine with a specific impuls of 2000 s and a total panel- and engine-efficiency of 20% could produce a thrust of 20 N with a propellant consumption of 1 g/s.

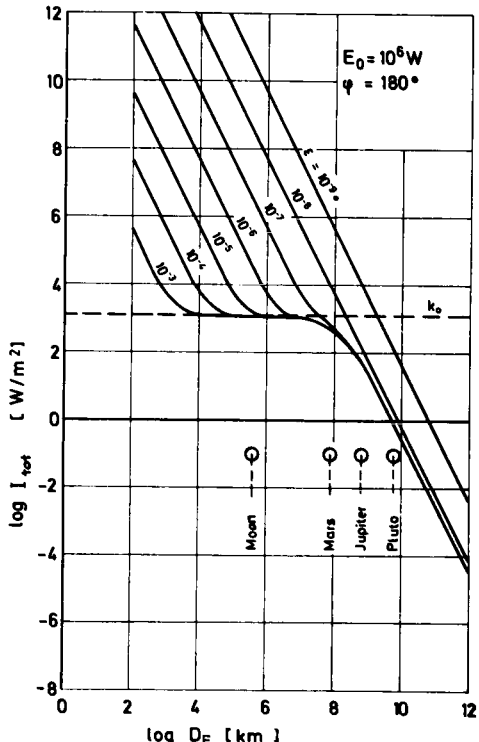


Fig. 10 Total energy input of a solar panel for a MW-laser as a function of distance and beam divergence.

c) Case of a  $10^9$  W laser.

Fig. 11: for all  $\epsilon$  greater than  $10^{-3}$  degrees, the power intensity beyond lunar distance is essentially  $k_0$ , before it decreases below the level short of Mars due to decreas-

ing solar intensity. It would require  $10^{-6}$  degrees to keep power level at 1  $k_0$  up to Mars. Jupiter distance requires  $10^{-7}$  degrees, Pluto  $10^{-8}$ .

Required panel diameter at Jupiter distance (and  $10^{-7}$  degrees) is 1358 m. An electrical engine could - under the same assumptions as mentioned above - produce a thrust of 2000 N at a mass flow rate of 106 g/s.

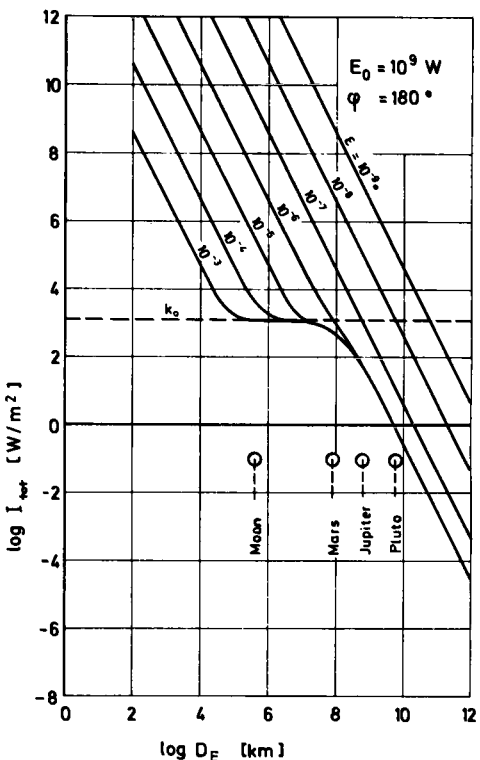


Fig. 11 Total energy input of a solar panel for a GW-Laser as a function of distance and beam divergence.

As the above examples clearly demonstrate, the use of lasers over planetary distances is completely unfeasible. If these cases were  $\epsilon$ -limited, the situation becomes swiftly power-limited when more realistic divergence angles are assumed.

With  $\epsilon = 1$  second ( $2.78 \cdot 10^{-4}$  degrees), it takes 3.56 GW to produce the local solar intensity at the distance of the moon, 64 200 GW for Mars in opposition and 516 000 for Pluto.

Since energy distribution across a laser beam as well as beam divergence are govern-

ed by optical laws, including non-linear effects, none of the split-second divergence angles considered above might ever become feasible. As Table 3 shows, it takes again multi-gigawatt lasers to produce 1  $k_o$  only at the distance of the moon, if an  $\alpha$  of  $1.67 \cdot 10^{-2}$  degrees (1 minute) is assumed:

Table 3

Range of lasers with power  $E_0$  to produce 1  $k_o$  intensity.

$E_0$ (W)	$10^6$	$10^7$	$10^8$	$10^9$	$12,2880 \cdot 10^9$
$D_L$ (km)	107	338	1070	3383	384.000

Therefore, once again, laser-powered propulsion will be restricted to short distances. At such distances, if indirect conversion is used rather than directly laser-powered engines, the simultaneous use of solar light is most rewarding. (For direct conversion propulsion, the additional use of chemical power at appropriate  $\Delta V/C_{Ch}$ -missions leads to moderate laser power requirements. See previous chapter).

Turning back to equation (47) we find:

$$\frac{dE_{tot}}{d\alpha} = (K_1 K_2 + K_4) \cos \alpha - K_1 K_3 \sin \alpha \quad (48)$$

$$\alpha_{max} = \text{arc} \operatorname{tg} \frac{K_1 K_2 + K_4}{K_1 K_3} \quad (49)$$

$\alpha_{max}$  being the angle between panel surface and line of sight to the laser base for obtaining maximum combined solar and laser energy input.

Although equation (49) is valid for any value of the constants, the optimization of  $\alpha$  at moderate laser powers is worthwhile only at rather short distances.

Fig. 12 shows the result for a 1000 W laser with  $\epsilon = 10^{-6}$  (which again is unrealistic, but the result is quite typical): for all distances above 40.000 km, the panel has always to be turned towards the sun. It is a question of payload gain or thrust-to-weight gain, whether the required amount of attitude control pays off.

#### IV. Conclusion

Laser propulsion is worthwhile for high  $\Delta V$  missions only. With limited laser power, laser-assisted chemical propulsion can lead to very high payload gains over purely chemical propulsion. This would require the use of chemical propellant combinations rather than inert materials. Long-range laser propulsion requires very low beam divergence angles. Laser propul-

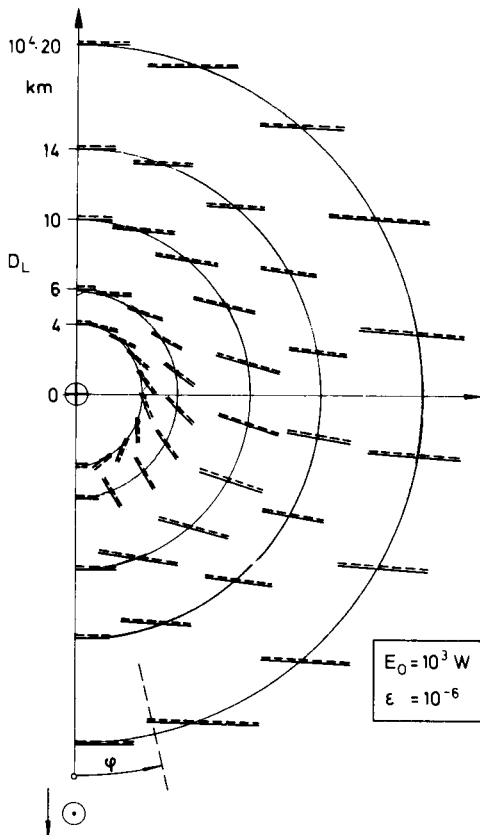


Fig. 12 Orientations of a solar panel optimized for maximum total energy input of solar power and a kw-laser as a function of distance  $D_L$  to laser base and angle  $\phi$  between the lines of sight from laser base to sun and spacecraft. Dotted line means the blind side of the panel. Length of line indicates relative panel diameter.

sion will therefore have to be confined to near-earth missions. Two-way tugs and single-stage-to-orbit shuttles are attractive candidates.

However, these and other missions are up to several orders of magnitude beyond present-day technology in one or several of the following areas:

- laser power output
- mirror materials for very high intensity energy fluxes
- solar panels for very high intensity energy fluxes
- pointing accuracy
- jitter reduction
- beam divergence angle.

However, it is hoped that the arguments presented above contribute to the conviction shared by many scientists not afraid of looking into a somewhat more distant future, that laser propulsion is a rewarding field for further studies.

# LASER PROPULSION

C. Selph and W. Horning

*Air Force Rocket Propulsion Laboratory, Edwards AFB, CA 93523*

## Abstract

The concept of projecting a high energy laser beam into a rocket in flight for propulsion purposes offers the possibility for a major increase in specific impulse over conventional chemical systems. Some of the payoffs and problems associated with this concept are examined. The design of a suitable converter for the laser energy presents many problems not faced in the design of conventional systems. The various types of proposed energy converters are discussed, including energy coupling mechanisms, and working fluid considerations. Laser propulsion bears some resemblances to solar thermal propulsion, and some comparisons are offered between these two concepts.

## I. Introduction

Of all the applications that have been proposed for high power lasers, few can challenge their capabilities so thoroughly as the concept of using lasers as primary energy sources for rocket propulsion. The jet power contained in the exhausts of chemical rockets ranges from tens of kilowatts for small altitude control engines to terawatts in large boosters such as the Saturn V. Projection distances may range from kilometers during the early phases of earth launch to tens of thousands of kilometers to reach a thruster at geosynchronous altitude. Thus it is seen that the propulsion application is in fact a manifold of applications embracing a variety of requirements. Somewhere between the trivial and the Herculean may lie a job that is harder or more costly to do in a conventional way than with lasers, and is significant enough to justify the large development costs. Much of the AFRL effort to date has been connected with the search for such a mission or missions. It consists of the analysis of a number of propulsion missions within the context of both laser propulsion and competing chemical propulsion and solar propulsion forms. And we are attempting to identify needed technology, with an emphasis on the problems of coupling a laser beam into the working fluid of a rocket chamber. Out of all this will come a decision as to whether it is timely to invest AFRL resources in experimental studies in this area, and also what direction those studies should take. This paper will highlight our efforts to describe potential propellants, working fluids, and coupling mechanisms.

For present purposes we take the laser propelled rocket to be a heat engine. It accepts radiant energy beamed from some remote beam generating plant and uses it to heat propellant to a high temperature.

The resulting working fluid is expanded through a conventional nozzle to produce thrust. Alternate schemes to generate thrust more directly via the pressure of the laser light on the vehicle, or less directly through the intermediate conversion of laser energy to electricity are not considered.

## II. The Likely Missions

Whatever advantage laser propulsion might offer with respect to a chemical rocket will arise from a supposed advantage in specific impulse,  $I_{sp}$ . The simplest expression demonstrating the importance of  $I_{sp}$  is the familiar "boost velocity" equation,  $m_i/m_f = \exp(AV/I_{sp} g.)$ , where  $m_i$  is the initial vehicle mass,  $m_f$  is the final vehicle mass, and  $AV$  is a velocity increment added by the rocket. This exponential relationship is celebrated in some of the greatest marvels of modern times - a rocket 35 stories high, an assembly building that dwarfs the pyramids. In spite of the grandeur of these accomplishments, we would select a more modest approach if we could. Or looking at it from the other end, given a new approach to high  $I_{sp}$ , we are led to examine the grandly applications to appreciate its virtues. By far the greatest mission which is commonly done is the lifting of payloads from the earth's surface to low earth orbit, a maneuver requiring about 9000 m/sec of velocity; and it was in this context that laser propulsion was first mentioned, Ref 1. Despite the dramatic appeal of this mission, it is an arduous case due to the enormous power levels required, and we can afford to defer it until the laser concept has demonstrated itself in a more limited setting.

More likely candidates begin with the vehicle already in low earth orbit. Requirements exist to change orbital altitude or plane, or the satellites' position in the orbit; also to maintain orbital parameters against the perturbing effects of drag and a non-spherical gravity field.

Figure 1 shows one of the more demanding cases, that of lifting a payload to geosynchronous orbit; or, more demanding yet, retrieving a payload from geosynchronous orbit. This orbit is intrinsically important and forms the major motive for the development of the Space Tug as companion to the Space Shuttle. The essential maneuvers consist of a burn of about 2500 m/sec to enter an elongated transfer orbit, and a circularization burn at apogee of about 1850 m/sec. The same velocity increments are needed for the return trip. The two 2500 m/sec increments take place in low earth orbit, and are relatively accessible to an earth based laser transmitter.

Furthermore a strategy exists for reducing the power needed by dividing the velocity increment into smaller bits, each put in with a burn on a successive circuit. The two 1850 m/sec increments must take place at geosynchronous distance and make extreme demands upon the optics if laser propulsion is used.

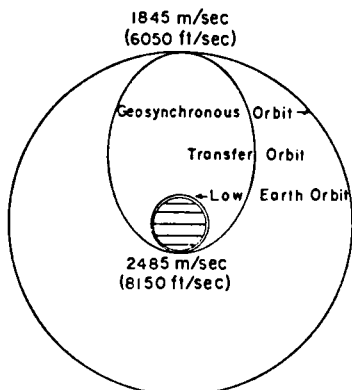


Fig. 1. Maneuvers for geosynchronous missions.

Two studies have been made of this mission, Ref 2 and 3, and they made different assumptions about the apogee thrusting maneuver. Ref 3 assumed chemical propulsion for the high altitude maneuver and escaped with a mere seven meter concentrator for the low altitude thrusting maneuvers. Ref 2 used laser propulsion for all maneuvers, and paid the price - a 50 meter concentrator aboard the vehicle and a similar mirror at the laser. The object of this boldness shows in an approximate way in Fig 2, which graphs the ratio of total initial vehicle non-payload mass to the payload mass as a function of velocity increment. The top curve is for an Isp of 470 sec and corresponds to an advanced O<sub>2</sub>/H<sub>2</sub> chemical stage. The bottom curve is for an assumed laser driven stage with Isp 1000 sec. A lower stage mass fraction was assumed for the laser propelled vehicle to allow for lower density propellant and extra mass for the collector.

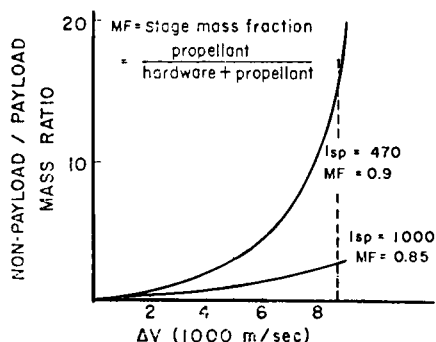


Fig. 2. Mass ratio improvement.

The difference between the curves is an advantage that is directly translatable into savings in launch costs to get the vehicles into low earth orbit.

Although these savings are considerable, Ref 3 found that a large number of missions would be required to amortize the R&D costs associated with the development of laser propulsion technology. Furthermore the savings could be rapidly dissipated if there are significant additional refurbishment costs associated with the greater hardware mass of the laser propelled vehicle. The energy costs to operate the laser were found to have a surprisingly minor impact, assuming an electric discharge laser operating at 30% efficiency and use of commercial power.

While the laser power levels to accomplish the mission are far less than those needed for earth launch, they are nevertheless impressive. Even when the thrusting periods were stretched out over 28 days, a laser power of over 100 megawatts was calculated (Ref 3) to lift useful (6000 lb) payloads. This is due to the very short thrusting period when the vehicle is within range of the laser. This is only about a minute per revolution when the perigee altitude is 100 nautical miles. The available thrusting time may be more than an order of magnitude greater for a space based laser with a similar orbital track, and so Ref 3 also considered this possibility. Whereas the laser power required was reduced to about ten megawatts, the economic motive completely disappeared. The cost of transporting laser reactants to orbit exceeded the propellant savings gained at the laser propelled rocket. It is probable that a space based laser using a closed cycle concept and nuclear or solar energy would overcome this problem and generate a net cost advantage. This, however, is regarded as a rather distant technological prospect and has not been examined in detail.

### III. Propellant Considerations

In laser propulsion the rate of energy delivery is not fixed by the rate of on-board propellant consumption, or the energetics of any particular chemical propellant combination. Thus the successful insertion of externally generated energy into the propulsion fluid is not constrained within the usual bounds of chamber temperature and resulting specific impulse. Working fluids may be selected for optimum expansion characteristics without regard to needs for higher molecular weight oxidizer, which again translates into a potential specific impulse advantage.

Fig 3 shows the specific impulse available for a variety of working fluids as a function of plenum temperature. These correspond to an assumed chemical equilibrium condition in the chamber and compositions which shift in the nozzle to maintain chemical equilibrium during an assumed isentropic one-dimensional expansion. A rather low chamber pressure of 50 psia was selected due to concern over high heat fluxes that would exist in the higher temperature ranges covered. The high area ratio chosen produces a low pressure at the exit to offset the low chamber pressure - and restricts the usefulness of the calculation to space, or at least upper stage application. The flame temperatures covered range from values that are low by chemical standards to values that cannot be obtained chemically. The upper temperature bounds were generously chosen with hardware limitations in mind, rather than by assumed limitations on heating. Reactants were selected primarily for low molecular weight.

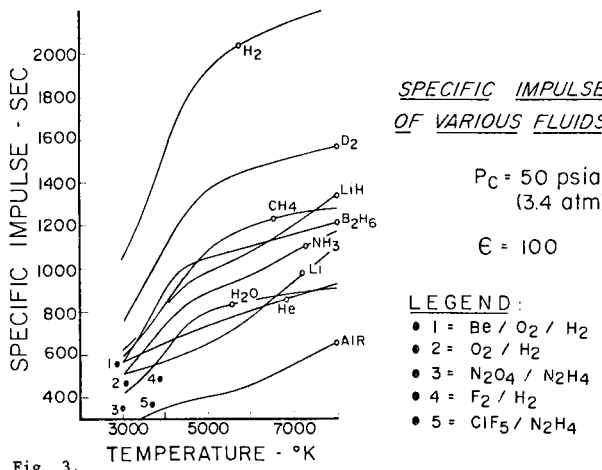


Fig. 3.

The most obvious conclusion from Fig 3 is that the specific impulse for hydrogen considerably exceeds that of all other fuels, as might be expected. It reaches a specific impulse over 1000 seconds at rather modest temperatures; and it appears that specific impulse values of 1800-2000 seconds can be obtained with temperatures that do not greatly exceed today's hotter chemical combinations.

Interest in other substances must be based on other considerations, such as improved propellant density and storage and handling characteristics. Most of the other propellants are themselves hydrogen-bearing compounds. An important conclusion from these lower curves is that it is possible to obtain specific impulse over 1000 seconds without elemental hydrogen, and without exceeding flame temperatures that have already been successfully handled.

There is a surprising amount of structure and a variety to the curves, including concave upwards, concave downwards, and more complex shapes. The simplest theory has specific impulse related to temperature by a simple square root function,  $I_{sp} \propto T_c^{1/2}$ . The observed structure arises primarily from changes in molecular weight with temperature, as molecules dissociate and condensable vaporize. The curve for lithium is curious. Over much of the range it is lower than helium, as is expected in light of the relative atomic weights of helium and vapor lithium. Above 6200° K the lithium curve is higher, which turns out to be due to ionization. There is a large partial pressure of free electrons which lowers the average molecular weight. Lithium hydride shares this characteristic; and is, unexpectedly, the best performer (except for H<sub>2</sub>) at the highest temperature calculated. Over a broad range from 4800° - 7500° methane is the highest. The generally high performance of diborane, and its space storability make it attractive.

The effect of changes in molecular weight in magnifying the effect of changes in temperature is a significant feature, and is most responsible for the rapid rise in specific impulse up to about 4500° K. Many of the fuels have a "knee" in this vicinity which diminishes the return on higher temperatures.

Also plotted on the graph are five characteristic chemical systems. Included are the Be/O<sub>2</sub>/H<sub>2</sub> system,

with the highest known Isp with stable propellants, H<sub>2</sub>F<sub>2</sub>, H<sub>2</sub>/O<sub>2</sub>, and two storable systems, N<sub>2</sub>O<sub>4</sub>/N<sub>2</sub>H<sub>4</sub> and ClF<sub>5</sub>/N<sub>2</sub>H<sub>4</sub>. The specific impulse is lower as a rule at any given temperature than in the selected beam powered systems. The difficulty lies in the lack of an oxidizer element with atomic weight to match the low values of unoxidized systems.

#### IV. Laser Coupling

There are a variety of useful photon energy conversion methods based on the generation of electric energy, such as photovoltaic and thermionic emission. In the propulsion context these methods are characterized by a very high mass per unit of thrust. The simplest way conceptually of using the energy is to introduce the beam directly into a chamber through a window and thermalize a working fluid. This is by far the least massive thruster, and is furthermore a potentially very efficient conversion method. The method places an additional constraint on the working fluid, however, since it must be made opaque at the frequency of the laser. Several possible ways of accomplishing this have been described, Ref 3 and 4. The major characteristics of these coupling techniques are discussed below.

#### Inverse Bremsstrahlung

One of the most important possible coupling mechanisms is inverse Bremsstrahlung, which is applicable to working fluids that are hot enough for significant ionization. The free electrons in such a gas are caused to oscillate by the varying electric field of any transmitted electro-magnetic beam. The oscillation is itself a conservative process for an isolated electron and removes no energy from the radiation. But in the working gas the electrons undergo inelastic collisions with atoms, molecules, and ions and thereby lose energy which ultimately is supplied from the radiation field. The result is that the gas becomes absorptive towards the radiation. Inverse Bremsstrahlung absorption takes place along with an opposing process, Bremsstrahlung radiation, and they both share the characteristic of being continuous with respect to wavelength. One of the attractive features of the inverse Bremsstrahlung mechanism is its relative insensitivity to

wavelength. It may be proposed to couple with the radiation from several of the current high energy lasers. It is particularly suited to CO<sub>2</sub> lasers, but there is a drop off in absorption coefficient at shorter wavelengths which will make it difficult to use at HF laser wavelengths and probably DF as well. This mechanism has no high temperature limit. As will be seen later it is unique in this respect, since the other known coupling techniques cease to operate at various upper temperature bounds. It also has disadvantages. Thermal ionization does have low temperature bounds. Seeding with some easily ionized substance such as cesium is a practical necessity. Because of the high molecular weights of suitable seedants compared with hydrogen, they can cause significant loss of specific impulse even at relatively low partial pressures. Another possible problem with this coupling mechanism is that the absorption coefficient is temperature sensitive, which creates the possibility for instabilities due to laser supported combustion waves. The loss of coupling efficiency is extreme below about 3000°K, even with easily ionized seedants; and at room temperature there is no coupling offered by this mechanism. This necessitates some alternate mechanism for "igniting" the working gas and raising it to a sufficient temperature for inverse Bremsstrahlung to take over. Finally it may be mentioned that the use of ionizable seedants that may condense out complicates the problem of keeping windows through the chamber wall clean.

#### Particulate Absorption

Laser energy may also be coupled to the working fluid by seeding it with light-absorbing particulate matter. The particles are heated above the gas temperature and then thermally conduct to it. The absorption coefficient depends upon the material and can also be wavelength dependent. However, for elemental materials, such as carbon, and tungsten it will generally have a smooth spectral variation and will offer means for absorbing over a wide range of wavelengths. Unlike the inverse Bremsstrahlung mechanism, particulate absorption is little dependent upon temperature. It will operate in a cold gas and thus offers a mechanism for "igniting" it. Furthermore, it should have little tendency to generate instabilities in the working gas. There is a high temperature limit, however, based upon the disappearance of the condensed phase due to vaporization and/or chemical reaction. The normal boiling point of graphite is about 3800°K. It also undergoes reactions to form various hydrocarbon species, such as C<sub>2</sub>H and C<sub>2</sub>H<sub>2</sub>, and these would limit the temperature of the methane system discussed earlier to about 3400°K. The particulate boron formed in the diborane system would survive to about 3900°K. Among materials which might be separately introduced into the working fluid, tungsten is particularly attractive, based on its high boiling point (above 5900°K) and the lack of high temperature stable hydrides. In addition to high temperature limitations arising from disappearance of the particles, this absorption technique suffers from the possibilities of contaminating the window, and from the complexities of the seedant device. Also there is the possibility for introducing large radiation loads on the hardware due to reflection and scattering of the incident laser beam. Finally, by analogy with experience with conventional metallized solid propellants, we may expect some performance losses due to lags in transporting heat from the solids to the gas, and in transporting momentum from the gas to the solid.

#### Molecular Absorption

Radiation may be absorbed directly by appropriate molecules in the working gas undergoing transitions to higher vibrational-rotational energy states. The energy thus stored becomes useable heat for the working fluid when the molecule "relaxes" back to the lower vibrational level, and passes its energy to the translational modes of the gas. There are a number of criteria which the absorbing molecule must satisfy. Because the vibrational energy levels of molecules are quantized, the absorption takes place at discrete wavelengths, and it is essential that each of the spectral lines produced by the laser be provided with a matching absorption line in the working fluid. Otherwise the energy in the line will be wasted, perhaps in a hardware damaging way. It is also necessary that the molecule be capable of rapidly releasing its vibrational energy to the translational modes of the working gas. And it is necessary that the molecule survive the high temperature environment of the working gas without dissociating.

The molecular absorption coupling technique has a number of potential advantages. The absorption coefficient is not usually a strong function of temperature and coupling is possible with a cold gas. Thus a separate ignition technique is unnecessary. Because the molecules are in vapor form they avoid the problem of contaminating the window. The most obvious molecules to propose for this purpose are the molecules that are used to produce the laser radiation itself. Thus attention is focussed upon HF, DF, CO, and CO<sub>2</sub>. This strategy almost guarantees a strong correlation between the emitted lines of the laser and the absorbed lines of the working fluid. But the strategy is not completely reliable, as is shown by the case with CO<sub>2</sub>. Cold CO<sub>2</sub> does not effectively absorb CO<sub>2</sub> laser radiation. This is because the cold gas contains almost no molecules at the elevated vibrational level represented by the terminal laser level of a CO<sub>2</sub> laser. Furthermore the CO<sub>2</sub> laser is based upon a transition with a relatively low transition probability. So the absorption line is similarly weak, even when the absorbing gas is heated to help populate the appropriate lower level. Finally, CO<sub>2</sub> is ineffective at useful chamber temperatures due to its tendency to dissociate. The dissociation occurs at quite low temperatures because CO<sub>2</sub> is a high oxidation state of carbon in a very reducing environment (mostly H<sub>2</sub> in the usual laser coupled rocket). The great stability of the reduced form, CO, is also a factor at work.

Carbon monoxide on the other hand appears to be very promising as an absorber of CO laser radiation. CO is the most stable molecule in nature and remains intact to temperatures over 6000°K. Ref 5 considered the use of CO in the context of laser coupling, and found satisfactory absorption for two CO laser lines chosen for calculation. A difficulty with CO is the slow kinetics for the conversion of vibrational to translational energy. Ref 5 goes on to suggest the catalysis of this conversion by the introduction of iron atoms via an iron carbonyl dopant. Perhaps the most serious question relative to the use of CO as a coupling molecule is the laser itself. CO lasers have poor atmospheric propagation characteristics, at least in the lines that carry the most power. This objection, of course, is not unique to CO, but is shared in full measure by HF lasers, and to a lesser extent by CO<sub>2</sub> lasers.

The coupling molecule of choice for an HF laser is likely to be HF, and for a DF laser, DF. Although HF is not as stable thermally as CO, it is nevertheless very stable and its high temperature dissociation is largely suppressed by the great amount of hydrogen present. Useable concentrations may be maintained to temperatures up to 5000°K. To stabilize DF it would be necessary to add significant amounts of D<sub>2</sub> to the propellant. The molecule of choice for CO<sub>2</sub> lasers is less obvious. The difficulty in using CO<sub>2</sub> as an absorber has already been mentioned. We have conducted a search of diatomic molecules which absorb near 10.6 microns and which possess strong chemical bonds. Diatomics are usually more thermally stable than more complicated structures, and the stabilizing effect of a strong bond needs little elaboration. The most interesting molecules found were the vapors of two refractory oxides TaO and ZrO. Chemical equilibrium calculations showed that these molecules are relatively stable to 4500 to 5000°K. Their high molecular weights are a disadvantage to the Isp of the working fluid. ZrO has the lower molecular weight of the two. Furthermore the small spacings of its rotational line structure offer hope that pressure broadening effects can smear the absorption band into a virtual continuum. This would relieve the need for exact correspondence with the laser lines. A lower molecular weight molecule, AlO, also absorbs in the CO<sub>2</sub> region, but its weaker bond was found to cause dissociation at relatively uninteresting temperatures. In the course of these calculations we found that gaseous H<sub>2</sub>O persists to temperatures that rival those of ZrO at a given weight percent of doping. This was surprising, since its bonds are no stronger than those of AlO, and it suffers the further disadvantage of being triatomic. Further study reminds us that water is a hydrogen bearing compound, and gains stability from the large amount of hydrogen present to drive the dissociation in the reverse direction. This finding is potentially significant since water, with its wealth of vibrational modes, absorbs over a wide range of frequencies. It is especially strong near the CO<sub>2</sub> lines, but has absorptions at all the high power IR laser wavelengths (although they are not strong at DF wavelengths). Furthermore the close spacings of its rotational lines makes it easier for pressure broadening to smear the absorption into a continuum, and reduces the need for exact line matching.

#### Heat Exchanger

There is no necessary reason why the absorbing material must be carried as part of the flow. The laser beam may be impinged on a fixed solid surface which heats up and then conducts to the working fluid. Gas heating by hot walls is, of course, a thoroughly familiar process; but one that has been overlooked, or perhaps dismissed in most of the thinking that has gone into the laser propulsion area. Its limitations in an extreme temperature process are obvious. We have already observed limitations on the highest temperature that can be obtained with several absorption techniques, due to vaporization or dissociation. Clearly the heat exchanger technique will be the most limited in this respect. But it also has some advantages that make it worthwhile to explore just what level of performance it might be capable of. Like particulate absorption it works at essentially all wavelengths, and also when the working gas is initially cold. Unlike particulate absorption, it does not contaminate the working fluid with solid products that can settle onto optical surfaces.

Ordinarily a heat exchanger used in a thermal engine is also a pressure vessel. Its operating temperature is limited not only by the melting of the wall, but by its progressive loss of strength at temperatures far less than the melting point. It is very difficult to avoid this characteristic when the heat source is a hot combustion gas, such as is the case in the boiler for a steam turbine. When the heat source is a highly directional electromagnetic beam, however, it becomes possible to get the energy inside the pressure vessel through a cooled window. So we will borrow this much from the usual description of a laser thruster. Once inside, the beam falls on a material which is heated to high temperatures, but one which does not simultaneously have to withstand pressure differentials. If other significant loads are absent it should be possible to heat the absorber to within one or two hundred degrees of its melting point.

The prescription for the heat exchanger would call for a cellular or porous structure mode of a refractory material, such as tungsten. The essential characteristic is a high surface area for the absorption of light and for the conduction of heat to the working fluid. An example is shown in Fig 4. Note that the laser beam falls on one face and penetrates the interior in a series of reflections and absorptions. Hydrogen is introduced on the opposite face and flows through the heated structure. It resembles a countercurrent heat exchanger in that the hydrogen contacts the hottest surfaces as it exits. The flowing hydrogen creates a "dynamic insulation" effect which maintains the inlet face at a cooler temperature, minimizing heat losses. A thruster design employing such a heat absorber-exchanger is suggested in Fig 5. The laser beam enters through a window in the front and falls on the inner surface of a conically shaped absorber which lines the rear of the thruster. Except for a small flow to cool the window, the hydrogen enters through the absorber. Note that the forward section contains an uncooled refractory liner which runs hot to minimize heat losses. The pressure vessel itself is regeneratively cooled.

The most characteristic part of the thruster is the heat absorber-exchanger, so it is natural to ask if such a structure is feasible, and if so what its performance capabilities might be. Ref 6 claims that a structure of the type needed was in fact built under the nuclear rocket program during the late 1950s. The dimensions provided in Fig 4 are taken from Ref 6. In the original application the tungsten foil contained a nuclear fuel in the form of uranium dioxide. Such elements did not evaporate or corrode after running for hours at 3300°K while flowing hydrogen. And they proved highly resistant to thermal shock.

Based largely on fabrication arguments the design was eventually abandoned in favor of more conventional graphite reactor designs. So the ultimate feasibility remains a moot point.

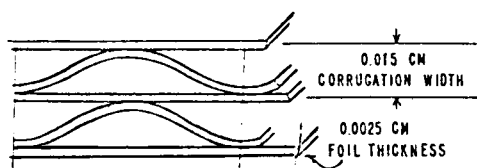


Fig. 4. Heat exchanger-absorber.

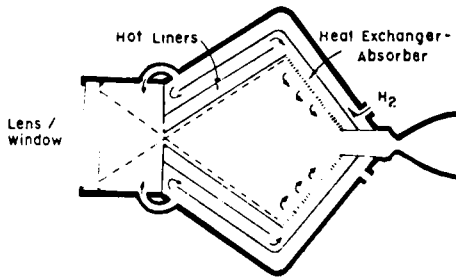


Fig. 5. Thruster using heat exchanger-absorber.

The power handling limitations for such a design are set by the gas side heat flow resistance. The calculation is sensitive to the surface area assumed to be actively heated by the laser flux. For rough estimation purposes we assumed the laser flux to penetrate effectively into the interior about 20 corrugation widths, or 0.3 cm. At a temperature differential of 100°K between the surface and the gas, the power handling capability is about 16 kw per square cm of frontal area. A megawatt of laser power could thus be absorbed and transmitted via an absorber 8 cm on a side weighing less than half a kilogram. The specific impulse for an absorber temperature of 3300°K is found from Fig 3 to be just over 1100 seconds, and the thrust is about 165 newtons (37 pound). By using a delta T of 300 degrees the thrust may be tripled with less than 100 sec specific impulse loss.

#### V. Systems Considerations

A variety of coupling techniques have been outlined, and there are as yet no hard criteria for eliminating any of them. Each has its own collection of advantages and disadvantages. Some of the issues may be sharpened by standing back further from the thruster and looking at the vehicle as a whole. At this point I will borrow some concepts from the literature. Fig 6 shows a laser propelled vehicle from Ref 2, designed to lift payloads from low earth orbit to geosynchronous orbit. It features a very large collector-concentrator mirror because of the intent to collect the beam over great distances - essentially from earth's surface to geosynchronous altitude. The mirror is located on the vehicle centerline and can rotate about a transverse axis to face a laser beam in almost any direction. And it can do this without affecting the vehicle center of gravity. Subsequent optical elements are all much smaller and operate on the concentrated beam. There is a secondary mirror which reflects the light to a beam-splitter which in turn sends half the beam in each direction to the two outrigger engines through the tubular rotation axis of the main concentrator. After the second reflection the beam is essentially a pencil of light, which can be directed as needed. The ability to form such narrow beams is, of course, a hallmark of laser light. But there is a caution - the built-in coherence of the beam must be preserved through the use of accurately configured optics. And this includes the main collector. Considerable weight will be required to stiffen the mirror so that it can maintain its figure, even if it can be built to the necessary tolerance in the first place.

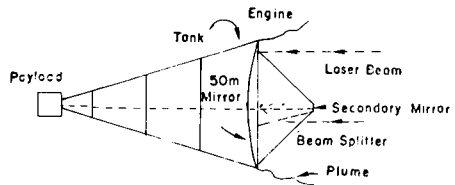


Fig. 6. Laser propelled transfer vehicle (*Phaser*).

There must also be concern over the number of operations on the concentrated beam. Each reflection is a source of loss and a potential point of failure given the enormous fluxes. With highly reflective surface and active cooling, these concentrated beams may be successfully handled without destruction. But the best of surfaces degrade with time, and this might occur very rapidly around an engine spewing dirty exhaust. To be sure, the engines face rearward, but this will give small reassurance to anyone who has seen the plume from an engine at altitude. The plume is quite able to turn corners and bathe the forward hemisphere. Ref 3 has considered these problems and elected to place both the engine and the main concentrator on the same axis. As shown in Fig 7, the concentrator face directly into the thruster and needs no interposing secondary optics. The only optical element that operates on the concentrated beam is the thruster window itself. The need for a precision surface on the concentrator is greatly reduced. The main areas of awkwardness are associated with the need for a very large flat mirror to accommodate laser beams from different directions to the concentrator. The flat must be larger than the concentrator, and indeed considerably larger if the beam comes much from the rear. The need for a hole in the center is a drawback. In either design the beam must be concentrated at least once to allow it to pass into the chamber. So the concern for extreme cleanliness in the optics remains. Although it is difficult to judge the extent of the problem, a preference must be stated for coupling techniques which do not rely upon condensed or condensable materials in the working fluid, i.e., molecular absorption and the heat absorber-exchanger.

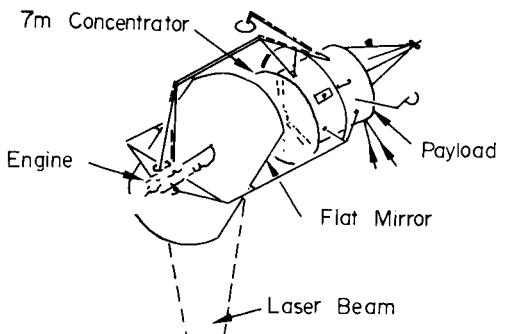


Fig. 7. Laser propelled transfer vehicle (*TRW*).

For his original publication in the area, Minovitch chose a provocative title, "Reactorless Nuclear Propulsion - The Laser Rocket". In a similar spirit, I will fit an epigram over my final subject:

#### VI. Laserless Laser Propulsion - The Solar Rocket

Though he missed the title, Minovitch made the connection in Ref 2. In contemplating the oversized mirror he had diagrammed for long distance collection of laser beams, he realized that it intercepted 2.6 megawatts of solar flux. He suggested using the concentrated solar flux when laser beams were not available. Solar thermal rockets, of course, have been described conceptually in the prior literature, Ref 7. But the invitation to comparison can no longer be avoided. Laser propulsion was already in the position of defending itself from attack from two directions - The high thrust, low Isp chemical systems, and the low thrust, high Isp electric systems. Although it is more often compared to chemical propulsion, until very large lasers become available, it more accurately fills a niche between the two. It must now be suggested that the same general niche is occupied by solar thermal propulsion.

The idea that a common system might be capable of operating in either mode is an interesting thought. We looked briefly at some constraints that might arise from such a wedding. In one case the beam is local, intense, coherent, and has a handful of discrete frequencies, usually in the infrared. In the other case the beam is nonlocal, dilute, much less coherent, and covers a broad, nearly continuous spectrum that peaks in the visible.

For a given collector size the solar thruster will be ten to a hundred times lower in thrust, depending upon the distance to the laser and its assumed power. The mission implications of this disparity are at least partially offset by the high availability of sunlight and the probable sporadic availability of laser light due to line of sight limitations. But there remains a disparity in the scale of the thrusters.

Theoretically the possible temperatures approach that of the surface of the sun. Practically the temperature will be much less than this due to materials limits, radiation losses, and the heat carried away by the working fluid. If a windowed chamber is assumed, corresponding to the usual plan of a laser rocket, the materials limitations are alleviated. Some of the coupling mechanisms for lasers are not appropriate for solar flux, however; inverse Bremsstrahlung is relatively ineffective at visible wavelengths, as is molecular absorption. Particulate absorption is feasible. However, if the problem of maintaining clean windows and mirrors cannot be solved, then the only remaining coupling mechanism common to both laser and solar rockets is the heat absorber-exchanger device. Attractive values of specific impulse are possible with hydrogen using this approach; but among the other "clean" fuels, only ammonia shows a performance advantage over chemical systems - and a small advantage at that. We may expect that any solar rocket will be forced to use hydrogen to show a meaningful advantage.

Because of its much reduced coherence, the spot sizes to which sunlight may be focussed are much larger. Furthermore the concentrated beam can not be readily projected in narrow beams. As a conse-

quence the solar rocket requires a low F number concentrator closely coupled to the thruster, along the lines of Fig 7.

The window problem is also different, and in some ways more difficult. The window must transmit well over a broad range of wavelengths, particularly in the visible, and including the near UV. Most of the common IR window materials extend well into and even through the visible spectrum, but only a few go far enough into the UV to safely pass this component. It might be necessary to absorb damaging frequencies before the concentration is accomplished. Because of the short focal length of the concentrator the window will see rays from a wide solid angle, and specular reflection at the window surfaces will become a greater source of energy loss.

#### VII. Conclusions

Laser propulsion offers a potential way of circumventing the Isp limitations of chemical rockets through higher temperatures and particularly through lower molecular weight working fluids. For earth based lasers, line of sight restrictions reduce thrusting time severely and drive the required laser powers into the range of 100 megawatts for useful orbit raising missions. Space based lasers would reduce this problem, but are not economically feasible using open cycle laser concepts. Although more distant technologically closed cycle space based lasers using nuclear or solar energy sources offer the greatest promise. The technology which must be developed in support of laser propulsion remains in a speculative state. A number of techniques exist for coupling the energy into the working fluid, including inverse Bremsstrahlung absorption, particulate absorption, molecular absorption, and heat absorber-exchangers. Based on the importance of maintaining the window and the external optics in a clean condition, a preference exists for molecular absorption, which needs no condensed or condensable materials in the flow. Enforcing a clean gas criterion would also eliminate the use of metal hydrides and unoxidized hydro carbons, and severely limit options for storable propellants. A major new technology must be developed in support of laser propulsion, whose costs must be amortized over a period of time by cost savings that are associated with the higher Isp. Whether a convincing economic justification exists is a matter still under study. In addition to chemical rockets, and electric thrusters, the laser rocket must be compared with solar thermal rockets projected to the same level of development. Although it is possible that a combined laser/solar rocket may be possible, initial studies indicate that important performance compromises may be required, especially to the operation of the laser rocket mode.

#### VIII. References

1. Kantrowitz, A., "Propulsion to Orbit by Ground-based Lasers", *Astronautics and Aeronautics*, Vol 10, No 5, 74-75, May 1972.
2. Minovitch, M. A., "Performance Analysis of A Laser Propelled Interorbital Transfer Vehicle," NASA CR-134966, Final Report, Contract NAS3-18536, Phaser Telepropulsion, Inc., Feb 1976.

3. Huberman, M. et al., "Investigation of Beamed Energy Concepts for Propulsion", Final Technical Report, RPL Contract F04611-76-C-0003, TRW, Oct 1976.
4. Caledonia, G. E., Wu, P. K. S. and Pirri, A. N. "Radiant Energy Absorption Studies for Laser Propulsion", NASA CR 134809, Final Report Contract NAS3-18528, Physical Sciences, Inc, Mar 1975.
5. Caledonia, G. E., "Conversion of Laser Energy", *Second NASA Conference on Laser Energy Conversion*, NASA SP-395, Jan 27-28, 1975.
6. Kingsbury, D., "Atomic Rockets", *Science Fact Dept. Analog Science Fiction*, Dec 1975.
7. Ehricke, K. A., "Perspective and Systems Engineering of Manned Planetary Flight," *Space Shuttles and Interplanetary Missions*, AAS Advances in the Astronautical Sciences, Vol 28, 1970.

# SPACE SHUTTLE MAIN PROPULSION SYSTEM

Charles C. Wood

*Chief Engineer, Shuttle Main Propulsion System, National Aeronautics and Space Administration, Marshall Space Flight Center, Alabama*

## Abstract

The Space Shuttle Main Propulsion System provides the impulse to transfer the reusable Orbiter of the Space Shuttle Transportation system and its payload from earth to earth orbit. Both cryogenic and solid rocket propulsion systems are utilized. The selected systems are characterized by (1) reusability wherever possible to reduce program cost, (2) design pressures, and other important design parameters, for the liquid propellant engine significantly higher than past programs for increased performance, and (3) advanced materials and manufacturing processes to withstand the extreme environments. The approaches for solution of these varied problems are emphasized.

## L. Introduction

The Space Shuttle is a reusable transportation system that will substantially reduce the cost of earth orbital operations while improving operational capabilities and flexibility. The system will be able to deliver payloads of up to 30,910 kg (65,000 lb.) to orbit and return to earth with 14,545 kg (32,000 lb.) of payload, a capability unavailable with current expendable launch vehicles.

The Shuttle Main Propulsion System thrusts the Orbiter from earth to earth orbit. Both cryogenic and solid rocket propulsion systems are utilized. Total thrust is tailored to limit acceleration (for crew comfort) and dynamic pressure (to limit loads). Three major elements comprise the Shuttle Main Propulsion System: (1) the Orbiter which contains three Space Shuttle Main Engines, portions of the propellant feed, pressurization and loading systems, the thrust vector control system, and major control elements; (2) the External Tank which contains hydrogen and oxygen propellants, propellant feed system lines connecting tankage to the Orbiter, a portion of the pressurization and loading systems and a minimum of controls and valves; and (3) two Solid Rocket Boosters, each comprising of a solid rocket motor, forward and aft structures, a thrust vector control system, a separation and recovery system and electronics (Figure 1).

The liquid and the solid systems are ignited on the ground and burn in parallel during the initial flight phase. Both liquid and solid propellant nozzles are gimbaled for thrust vector control. The two Solid Rocket Boosters burn out approximately 125 seconds after liftoff at an altitude of

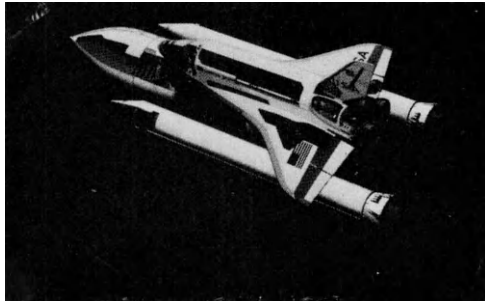


Figure 1 Space Shuttle

approximately 46 km (25 nautical miles) and are separated from the shuttle which continues toward orbit. The expended Solid Rocket Boosters fall in an arc and are decelerated by aerodynamic drag and parachutes prior to entering the ocean, where they are subsequently recovered for refurbishment and reuse (Figure 2). The Shuttle Orbiter's three main liquid propellant engines continue to burn for approximately 350 seconds beyond separation of the Solid Rocket Boosters. Immediately following main engine shutdown and prior to orbital insertion, the External Tank is separated. The Orbiter is then inserted into an elliptical orbit 110 x 184 km (60 x 100 nautical miles) by the Orbital Maneuvering System. The External Tank impacts in a selected remote ocean area. It is expendable and is not recovered for reuse as are the Solid Rocket Boosters. After orbital mission completion the Orbiter returns to earth in a non-propulsive mode for subsequent reuse.

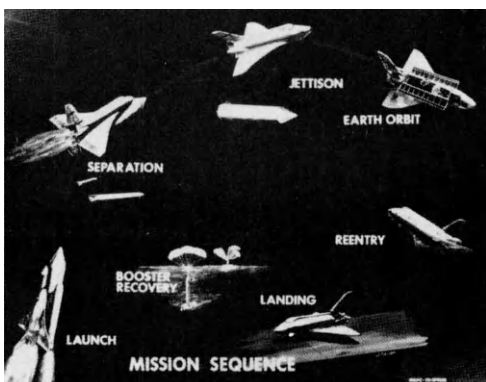


Figure 2 Mission Sequence

The planned high flight density extending over a great number of years emphasizes minimal operating cost. For that reason all elements of the vehicle except for the External Tank have been designed for reuse. To be consistent with this philosophy, the Shuttle main propulsion system is designed to maximize use of existing technology as well as existing hardware while minimizing the cost of components located on the expendable external tank. However, one should not conclude the Shuttle main propulsion systems are void of design and technological advancements. System requirements and reusability severely tax hardware design in many areas and necessitate advanced design, material, and manufacturing approaches. This is particularly true in the Space Shuttle Main Engine which will be emphasized in this paper.

## II. Performance and Design Requirements

The performance requirements for the Space Shuttle propulsion system (Table I) were derived to maximize overall Shuttle vehicle performance while limiting acceleration and vehicle loads.

## III. Solid Rocket Booster

The Solid Rocket Booster propulsion system complements the liquid propulsion system and provides the major thrust required for vehicle lift off.  $12.7 \times 10^6$  N ( $2.86 \times 10^6$  lbf) and a total

vacuum impulse of approximately  $12.9 \times 10^8$  Ns ( $2.9 \times 10^8$  lbf-sec) per booster during the first 122 seconds of vehicle flight. Thrust vector control capability in conjunction with the liquid engines is also provided until burnout of the booster. The solid rocket motor is the principal propulsion element of the booster. The solid rocket propulsion system represents the minimum cost and simplest approach known for the stated functions and can be designed and constructed within an existing technology base. An unprecedented requirement, twenty reuses of the hardware, is placed on the solid rocket propulsion system, but this is recognized as an advanced engineering consideration as contrasted to a technological advancement. This entails deceleration by aerodynamic drag on the booster followed by parachute deployment, impact in sea water at vertical and horizontal velocities up to 26 m/s (85 ft/sec) and 13.7 m/s (45 ft/sec) respectively and a maximum of fourteen days exposure to the corrosive environment. The booster is reoriented from the stable vertical flotation mode to a horizontal orientation and towed by ship for several hundred miles. Finally, the booster is washed down and protected for shipment to Utah where it is refurbished. Other unique requirements compared to previous programs are closer tolerances about a complex thrust time curve during ignition, main-stage (action), and tail off. The Solid Rocket Motor (SRM), Figure 3, is 3.71 m (146 in.) in diameter, 38.1 m (125 ft.) in length, has a mass

Table I Significant Performance and Design Requirements

Shuttle Vehicle:

Lift Off Thrust to Weight Ratio	1.5
Maximum Dynamic Pressure N/cm <sup>2</sup>	3.1 (650 PSF)
Maximum Vehicle Acceleration (g)	3

Parameter	International Units		English Units	
	Solid	Liquid	Solid	Liquid
Thrust/engine (N)	$12.7 \times 10^6$	$2.09 \times 10^6$	(lbf)	$2.86 \times 10^6$
Thrust variation (%)	Fig. 4	50-109	(%)	Fig. 4
Specific impulse (Ns/kg)	529.6	919.5	(lbf-sec)	262.2
			lbm	455.2
Total vacuum impulse (Ns)	$25.8 \times 10^8$	$31.1 \times 10^8$	(lbf-sec)	$5.8 \times 10^8$
Maximum inert mass (kg)	-	33680 ET		-
	66000	2881 SSME	(lbm)	145,000
Minimum propellant mass (kg)	$0.503 \times 10^6$	$0.745 \times 10^6$	(lbm)	$1.106 \times 10^6$
Control authority (deg)	+8	+6.8	(deg)	+8
Thrust differential between motors (N)	$1.335 \times 10^6$	(ignition)	(lbf)	300,000
Maximum impulse imbalance between motors (Ns)	$3.16 \times 10^6$	(tailoff)	(lbf)	710,000
	$20 \times 10^6$	-	(lbf-sec)	$4.5 \times 10^6$
Reuse	20	55 starts		20
Minimum Life (hr)	-	7.5	(hr)	-
			55 starts	7.5

of 568,000 kg (1.25 million pounds) and will produce a thrust versus time trace as shown in Figure 4. Pertinent design requirements for the motor are tabulated in Table 1. The motor case, propellant and nozzle are discussed in some detail in following paragraphs. Other motor subsystems such as the ignition system, propellant liner, insulation, etc. are less affected by Shuttle peculiar requirements.

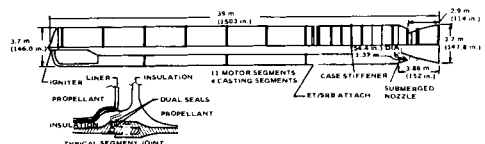


Figure 3 Solid Rocket Motor Design

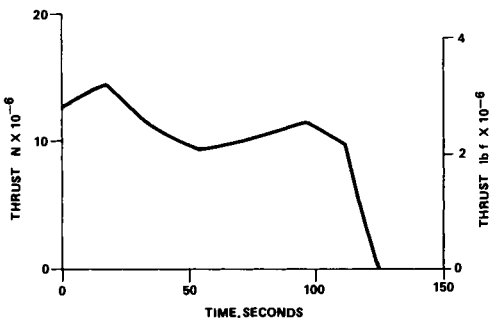


Figure 4 Solid Booster Vacuum Thrust

Motor components and subsystems are integrated into a systems test configuration. Whenever possible, the components will be qualified prior to systems tests. Four development and three qualification motor firings are planned within a 19 month period with the first motor firing planned for May 1977 and the first flight in 1979.

#### Motor Case:

The segmented SRM case is roll formed from D6AC steel. The case is weld free and consists of 11 manufacturing segments, with 5 different designs. These 11 segments will be assembled to form 4 propellant casting segments.

<u>Item</u>	<u>Quantity Required</u>
Forward Case Closure	1
Cylindrical Case Segment	6
Attach Case Segment	1
Stiffness Case Segment	2
Aft Case Closure	1

The configuration and number of case segments were selected so that welds could be eliminated

and existing proven roll forming and machining capability could be used. Ribs are located on the attach segment for attachment to the External Tank and on the stiffener segments for the additional stiffness required during water impact. These ribs are integrally formed during case roll forming and machining operations. Case segments are joined using clevis type joints and pins whose successful use has been demonstrated in previous programs (Figure 3).

The reuse requirement introduces in addition to normal strength criteria a minimum fracture toughness requirement, a design requirement for water tight joints and a durable protective coating. A  $K_{IC} \geq 99,000 \frac{N}{\sqrt{cm^2}} \sqrt{cm} (90,000 \frac{psi}{\sqrt{in}} \sqrt{in})$  for heat treated D6AC steel will provide the required fracture toughness and although easily obtainable independently, becomes difficult without compromising the usual minimum strength criteria. An extensive heat treatment development test program utilizing an existing Titan vehicle case to simulate mass and a number of well instrumented test plates strategically located about the case was conducted in the planned production heat treating facility. An optimum procedure was selected after a number of tests and an extensive test program was then conducted for statistical evaluation. With the selected procedures all design requirements can be met; however, margins are small, necessitating careful quality control. Initial case segments for the Space Shuttle have only recently been successfully heat treated. The direct quench process was selected; it uses an Austenizing temperature of  $1152^\circ K (1615^\circ F)$  followed by a direct salt quench at  $436^\circ K (325^\circ F)$  and two oven temper cycles of  $861^\circ K (1090^\circ F)$  for final temper.

A two part epoxy polyimide coating plus a segment joint protective device is used for motor case external protection from all preflight environments, all flight phases including re-entry, two weeks exposure to salt water, and the preliminary refurbish cycle including shipment by rail to Utah. The coating is then removed and replaced preparatory to reuse of the case. At Kennedy Space Center, prior to shipment to Utah for refurbishment, the case is disassembled into casting segments (4 segments versus 11 individual segments) and exposed surfaces are cleaned. The watertight segment joint cover must be effective or many of these highly finished machined joints would be exposed to the detrimental effects of salt water for approximately four weeks. Development programs have successfully proved the coating and the refurbishment procedure.

#### Propellant:

The propellant is a polybutadiene acrylic acid-acrylonitrile terpolymer binder (PBAN), ammonium perchlorate (AP), aluminum formulation with a small amount of burning rate catalyst added to achieve the desired propellant burning

rate. The propellant as well as the case insulation and liner have been used extensively. The simplicity of the formulation, which contains only four major ingredients, assures reproducible propellant ballistic and mechanical properties. The projected propellant vacuum specific impulse of 530 Ns/kg (262.2 lbf-sec/lbm) is based upon data projection from previous large motor programs. Availability, experience, performance, and cost are all criteria which are readily met with the formulation.

The propellant grain is carefully shaped to control thrust during liftoff and later flight phases to achieve structural load compatibility with Shuttle hardware (Figure 5). An eleven-point star configuration grain is provided in the forward portion of the forward segment to provide the desired high initial thrust level while the grain configurations in the remainder of the motor segments are tapered cylindrical perforate designs (CP). Thrust decay from approximately 18 to 50 seconds results from burnout of the star whereas the progressive thrust characteristic between approximately 50 and 100 seconds is produced by the CP configuration. The thrust decay required to limit vehicle acceleration to  $29.4 \text{ m/sec}^2$  (3g) between approximately 100 and 115 seconds is achieved by burning out the aftmost portion of the aft segment.

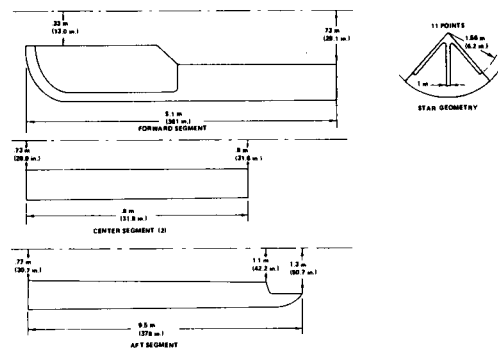


Figure 5 SRM Propellant Grain Design

Thrust differential between two SRM's during all flight phases must be minimized to reduce vehicle control requirements. Because of critical aspects associated with SRM separation from the Shuttle vehicle, thrust and total impulse differentials are of particular importance during thrust decay at shutdown. The principal variable which affects thrust differential between motors and which can practically be controlled is propellant burn rate. Several steps are being taken to minimize differences in propellant burn rate: (1) mixing several single batches of new materials, (2) two identical motor segments will be cast simultaneously and used on the different motors

of the same Shuttle vehicle, and (3) propellant from multiple propellant mixers will be cast alternately into simultaneous segment castings.

#### Nozzle:

A conventional movable converging-diverging nozzle having a throat diameter of 137 cm (54 inches), expansion ratio of 7.16 to 1 and an omnidirectional deflection capability of  $\pm 8$  degrees has been selected, Figure 6. The nozzle design incorporates two piece construction to facilitate shipment and a linear shaped charge to separate the exit cone aft of the field splice and actuator attach location to reduce re-entry aerodynamics resonance and loads resulting from water impact since the motor aft end initially impacts the water. The nozzle upstream of the throat and part of the exit cone are submerged in the motor case to minimize weight and cost and to reduce motor length. The diverging portion of the nozzle is contoured to achieve maximum performance efficiency. The design utilizes state of the art materials for internal parts of the nozzle, carbon cloth phenolic in the nose, throat and forward portions of nozzle where the gas environment is most severe and silica cloth phenolic in the aft portions of the nozzle. For gimbaling, the nozzle incorporates a flex bearing which consists of ten alternating layers of D6AC steel shims and natural rubber elastomeric pads. Bearing refurbishment is planned after the tenth flight with metal parts to be reused. A snubbing device incorporated in the design permits vectoring of the nozzle but limits bearing loading during water impact.

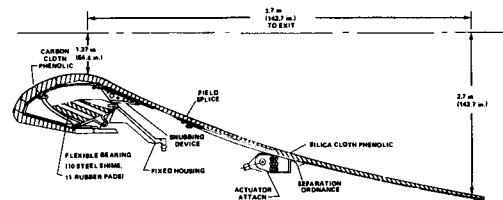


Figure 6 Nozzle Design

Subscale flexible bearing tests have been conducted to further characterize selected materials and to obtain data for finalizing full scale bearing manufacturing processes and process testing. Subscale bearings have performed the flight duty cycle, and fatigue testing has been conducted. Two full scale development bearings have been manufactured using tooling and processes developed from the subscale programs. Extensive testing in a bearing test fixture will be conducted to integrate nozzle performance with the thrust vector control system.

#### IV. Liquid Propulsion System

The liquid propulsion system for the Space Shuttle is located in both the External Tank which is expendable after each flight and the Orbiter which is reusable. Although the propulsion system is located in two distinct hardware elements provided by different contractors and emphasis in design differs between the two elements, the design must be totally compatible. Since the External Tank (ET) is expended in each flight, four hundred and forty-five tanks must be procured to support the planned shuttle missions, thus cost per copy is of paramount importance toward achieving projected operational flight cost. The Orbiter is planned for reuse, and only a limited number will be procured, thus, minimum weight and reuse with minimum preflight service become important considerations along with cost.

Every effort has been made to design the liquid propulsion system within today's state of the art technologies. The Apollo program established an extensive data base in analytical procedures, hardware design practices, manufacturing practices, and development techniques, all of which are directly applicable and are being used. The major area where Apollo developed technology is deficient is related to the reuse requirements, thus special new efforts are required.

The requirements placed on the liquid propulsion system by the program and the engine are rigid but in most cases are not unique. The systems designed to satisfy these requirements are shown schematically in Figure 7 and in diagram form for the External Tank and Orbiter in Figures 8 and 9 respectively. Forward in the ET is the liquid oxygen tank with a capability of 608,000 kg (1,337,558 lbm) of LO<sub>2</sub> and aft is the liquid hydrogen tank containing 102,000 kg (224,458 lbm) of LH<sub>2</sub>. The ET is 8.53 m (28 feet) in diameter and 47.2 m (155 feet) in length. The three Orbiter located Space Shuttle Main Engines are fed from the External Tank through disconnects mounted at the aft end of the External Tank.

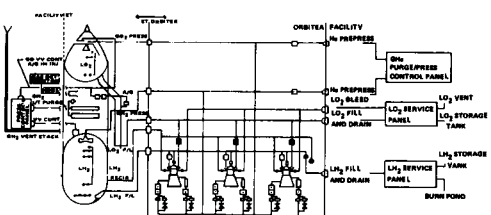


Figure 7 Liquid Propulsion System Schematic

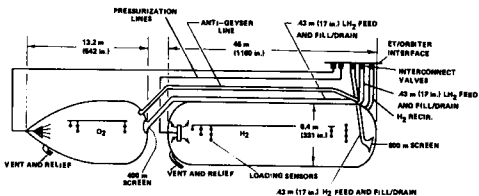


Figure 8 External Tank Propulsion System

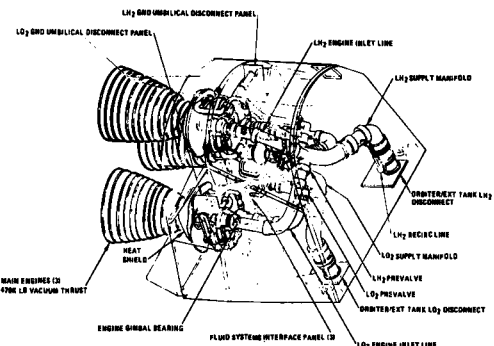


Figure 9 Orbiter Main Propulsion System

The Shuttle must be capable of launch within two hours of notification. The initiation of this time period is the start of propellant loading for both propellants. The ET propellant tanks are filled through the Orbiter feedlines. Fill rates are varied as predetermined point level sensors are covered, the final fill rate compensates for steady state boiloff.

#### Propellant Delivery:

Propellants are delivered from the tank to the engines through tank mounted screens into foam insulated 43.2 cm (17 inch) diameter lines with vacuum jacketed flex joints and through ET/Orbiter disconnects to vacuum jacketed lines and vacuum jacketed manifolds in the aft compartment of the Orbiter where the lines divide into three individual 30.5 cm (12 inch) vacuum jacketed engine feedlines for both fuel and oxidizer. The engines have a cleanliness requirement for the propellant system to avoid blockage of passages critical to proper engine operation. Critical particle sizes have been established as 800 and 400 microns for the oxidizer and fuel systems respectively, thus tank outlet screens are sized accordingly. Feedlines downstream from screens are assembled with special procedures producing clean room like conditions. The oxidizer feedline has a parallel "antigeyser" line which, by natural convection, sets up a flow loop to maintain subcooled LOX in the line during prelaunch. Facility supplied helium is available for injection

into the 10.2 cm (4 in.) "antigeyser" line to insure noninterruption of flow and to eliminate potential geysering. Oxygen is bled overboard from the feedline through the engine bleed valves to chill the oxidizer side of each engine and to have available, at engine start command, subcooled propellant at the pump inlet. At the same time and for the same purposes, liquid hydrogen is pumped through the feedlines, engine liquid hydrogen pumps, and back to the propellant tank by small Orbiter mounted electrically driven pumps provided specifically for this purpose. The hydrogen tank propellant ducting is unique for a booster vehicle in that a "siphon" from the tank is used rather than the conventional outlet and ducting which would require extensive structural support and thermal protection. The liquid oxygen tank aft end and propellant duct inlet have been carefully shaped to minimize propellant residuals. Vapor detectors located in the bottom of the hydrogen tank and in the 43.2 cm (17 in.) diameter oxygen feedline downstream of the ET/Orbiter interconnect valve are optimally located to shutdown the engines and minimize system liquid residuals for missions requiring consumption of all available propellants. Costs are minimized by using identical line contours and diameters for oxidizer and fuel, and by constructing the oxidizer outlet and fuel "siphon" with the same manufacturing techniques. Some other cost saving features in the design are standardization of line designs, use of cast elbows contrasted to the usual machined forgings, and Argon back filled annuli rather than conventional vacuum jacketed flex joints.

#### Propellant Pressurization:

Propellant tanks are pressurized three minutes prior to launch with facility supplied gaseous helium. After the engines are ignited, gaseous hydrogen and oxygen are supplied to the respective propellant tanks directly from the engines for H<sub>2</sub> and from a heat exchanger mounted in each engine for O<sub>2</sub>. Tank pressures are sensed in each propellant tank, and solenoid valves in the Orbiter are controlled for regulation of the manifolded pressurant gas flow from the three engines. Planned operational pressures within the two propellant tanks are shown in Figure 10. Adequate ullage pressure is not only required to satisfy pump suction pressure requirements but also to provide structural stability for the oxidizer and fuel tanks at lift off, when the asymmetrical thrust vectors from the engines and SRB's produce a compressive shear load in each tank. In addition, planned upper pressure limits minimize the tank structural requirements for pressure carrying capabilities which strongly influences ET weight. The nominal pressurant temperatures have been selected to minimize residuals while not exceeding the upper structural limits of the tank bulkhead material. An appropriately sized vent and relief valve is located in the forward end of each propellant tank to vent

gases during propellant loading and for relief from overpressure.

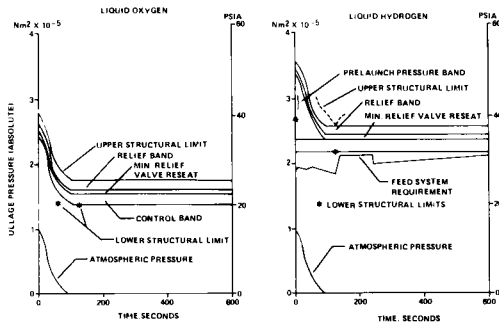


Figure 10 Shuttle Propellant Tank Pressures

The philosophy of minimizing cost is also evident in the pressurization system wherein the high cost components such as heat exchangers, control valves, logic control system and check valves are contained in the reusable Orbiter whereas the passive and less expensive components are located in the expendable External Tank. It was cost effective to locate the vent and relief valves on the expendable ET, since otherwise, larger vent valves would be required, vent lines would have to cross over from Orbiter to ET to interface with the umbilicals, and the large vent lines and disconnects would be thrown away with each tank. Use of common hydrogen and oxygen vent and relief valve bodies helps minimize cost with the selected concept.

#### Propellant Delivery Dynamics:

The natural frequency of the Shuttle vehicle structure and the propulsion system have been carefully evaluated. The first and second mode structural frequencies are 2.0-2.4 hertz, while the propulsion system frequency is 2.4 hertz. Even though the modes couple, the gains are stable, but without adequate margin. It was recognized that the consequences of such coupling could be far more serious than were the effects on prior vehicle configurations, thus, to preclude the possibility of longitudinal structural-propulsion coupling, a passive suppressor has been designed into each engine and integrated into the propulsion system. The effect is to reduce the feed system frequency to 1.8 hertz. The design is dictated by the wide range of feed system pressures encountered by the suppressors in the course of the mission. The suppressors, one per engine, which are located between the low and high pressure oxidizer pumps of the engine, are charged initially with facility helium and continuously during flight with vaporized oxidizer from the heat exchangers. Excessive suppressor

pressurant is discharged into the 43.2 cm (17 in.) diameter LOX feedline immediately downstream from the ET/Orbiter disconnect valve. Extreme care must be exercised to assure that the liquid/gas interfaces of the suppressors are not broken to preclude pressurant gases short circuiting the suppressors and allow pressurant to be pumped directly into the ducting upstream of the high pressure pumps.

#### System Testing:

The selected design makes maximum use of analytical and hardware design and development techniques used in previous programs. Thus, propulsion system testing is minimized. Components are qualified, then integrated into a system for the first time in the Main Propulsion Test Article (MPTA) which consists of flight-type propellant tanks, feed and pressurization systems and three flight-type engines. While there is an "antigeysers" test planned prior to MPTA, the flow and thermal characteristics of the feedlines, liquid residuals, pressurant requirements, propellant loading accuracy, and propellant thermal stratification will not be tested prior to MPTA. Previous programs are relied upon for experience in these areas. Fourteen tests commencing in December 1977 are planned over a one year time period to thoroughly explore the propulsion system's operating characteristics and performance limitations. This test series will end five months before first flight of the Shuttle vehicle. The first flight vehicle will undergo a short Flight Readiness Firing at Kennedy Space Center; data will be evaluated, and the flight vehicle will be launched to orbit in 1979.

#### V. Space Shuttle Main Engine

Much is required of the Space Shuttle Main Engine to fulfill the Shuttle mission goals. High performance, minimum weight, compact arrangement, and long life are all extremely important. To achieve these goals, it was necessary that hydrogen and oxygen be selected as propellants. Operational pressures which are significantly greater than used in previous rocket engine programs were necessary. The most efficient cycle considered practical to develop was selected to approach as closely as possible the maximum theoretical specific impulse of 947 Ns/kg (468.8 lbf-sec/lbm). Advanced materials and manufacturing processes were also required in number of areas.

The selected staged combustion cycle is of utmost importance and is shown in Figure 11 along with the gas generator cycle. The gas generator cycle was used for the hydrogen and oxygen J-2 engine developed for the Apollo program. The J-2 engine delivered a vacuum specific impulse of 860 Ns/kg (425 lbf-sec/lbm) and had a combustion chamber pressure of 538 N/cm<sup>2</sup> (780 psi). The staged combustion cycle wherein pumps are driven

by partially burned fuel from a preburner and all propellants exit the system through the combustion chamber was selected for the Space Shuttle Main Engine (SSME). The cycle was optimized for a chamber pressure of 2070 N/cm<sup>2</sup> (3000 psi) which requires the oxidizer pump to generate in excess of 5245 N/cm<sup>2</sup> (7600 psi). The development engine has the potential to meet all requirements depicted in Section II which includes a vacuum specific impulse of 919.5 Ns/kg (455.2 lbf-sec/lbm), vacuum rated power level thrust of  $2.09 \times 10^6$  N (470,000 lb) at a mixture ratio of six parts by mass of O<sub>2</sub> to one part H<sub>2</sub>, a throttling capability between 50 and 109 per cent of rated thrust and an engine life of 7.5 hours which is to include 55 starts.

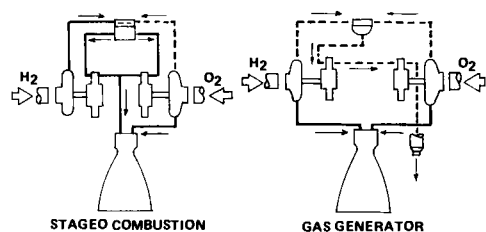


Figure 11 Engine Cycles

The engine design and characteristic parameters are shown on Figures 12 through 14. In this engine all the propellants are burned and expanded through the main combustion chamber nozzle. The engine utilizes two turbopumps in each propellant feed system to assure adequate head rise to operate the two preburners. Each of these preburners mixes and burns the propellants at high pressure and relatively low temperature to provide a fuel rich gas which is used to drive the high pressure turbopump turbines. This fuel rich gas then passes through the main injector into the main combustion chamber where it is mixed with liquid oxygen, burned at high pressure and temperature, and expanded through the high area ratio nozzle. The hydrogen fuel is used to cool all combustion devices directly exposed to high temperature combustion products. An electronic engine controller automatically performs checkout, start, mainstage throttling and engine shutdown functions. Easy accessibility of line replaceable components and the use of internal inspection for parts in critical components are provided to aid maintainability.

While the SSME design is dependent upon advanced design concepts, advanced materials, innovative design approaches or advanced manufacturing methods, or a combination, in virtually every subsystem of the engine, the most prominent advances are judged to be in the turbomachinery, main combustion chamber, and engine controller. These subsystems will be discussed in detail to illustrate the technology level the engine must achieve.

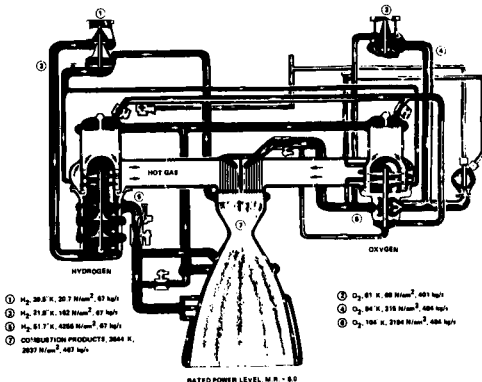


Figure 12 SSME Propellant Flow Schematic

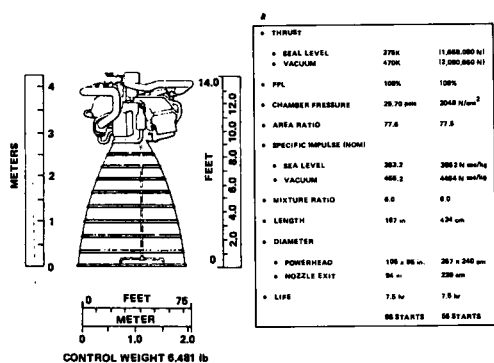


Figure 13 SSME Characteristics

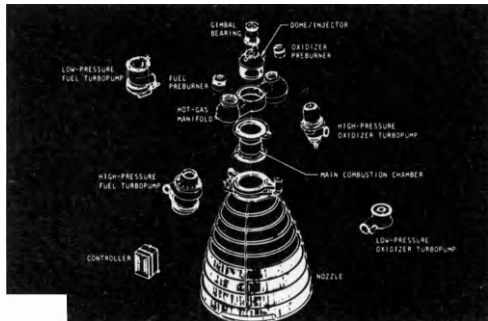


Figure 14 SSME Major Components

#### Turbopumps:

The high-chamber pressure and staged-combustion cycle of the Space Shuttle Main Engine, coupled with the criticality of weight and low

propellant tank pressure, impose unique constraints on the design of the turbomachinery required to deliver propellants from the vehicle tanks to the engine. The importance of the pumps and turbines operating at high efficiency to minimize the pump discharge pressures is illustrated in Figure 15 where fuel pump discharge pressure required to produce a 2070 N/cm<sup>2</sup> (3000 psi) rocket engine chamber pressure is plotted as a function of the average of all pump and turbine efficiencies. A comparison of the required operational pressures and the turbomachinery power density for the SSME and several prior operational engines is shown on Figures 16 and 17. High discharge pressures, speeds and horsepower requirements combined with low weight have resulted in significant advances in power density.

PUMP OUTLET PRESSURE, PSIA

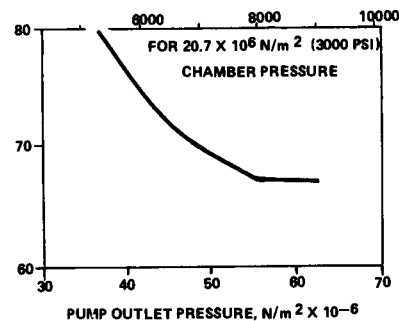


Figure 15 Pressure Requirement Versus Average Turbo Pump Efficiency

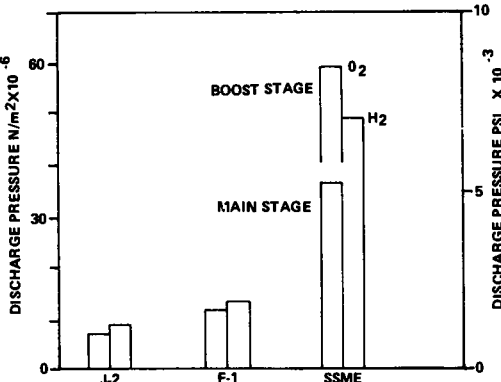


Figure 16 Summary of Pump Discharge Pressures

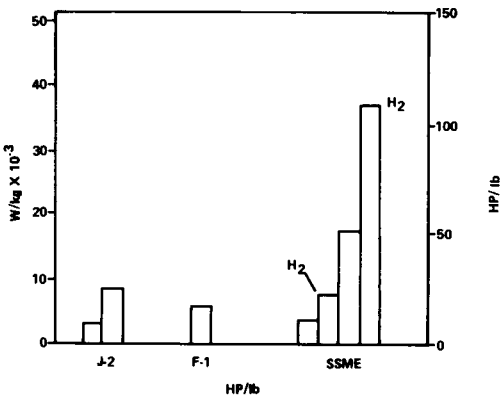


Figure 17 Turbo Machinery Power Density

To achieve the high efficiencies required with minimum weight, the pumping function is divided among four turbopumps, a low pressure and a high pressure pump for each propellant. The relatively low weights of the high pressure pumps considering the flow rates and discharge pressures are achieved by eliminating the requirement that the pumps operate at low net positive suction pressure (NPSP), low NPSP operation is achieved by the low pressure pumps upstream of the high pressure pumps. The low pressure oxidizer and fuel pumps are axial flow-type operating at low speed to provide sufficient pressure to preclude cavitation at the inlet of the high pressure pumps. The high pressure fuel pump is a three stage centrifugal flow-type pump operating at 35,000 rpm with  $4278 \text{ N/cm}^2$  (6200 psi) discharge pressure supplying hydrogen to the main chamber, nozzle coolant circuit, and high pressure turbopump preburners. The high pressure oxidizer pump consists of two centrifugal-type pumps on a common shaft. The main pump supplies the main chamber inputs, low pressure pump drive turbine, and the preburner pump (second pump); it operates at 29,000 rpm and  $3174 \text{ N/cm}^2$  (4600 psi) discharge pressure. The preburner (second) pump supplies the fuel and oxidizer preburners and operates at 29,000 rpm and  $5244 \text{ N/cm}^2$  (7600 psi) discharge pressure.

To perform the complete pumping cycle with single oxidizer and fuel pumps would force a compromise between the low speeds needed for the inlet condition and high speeds required for increased pressure resulting in a weight penalty and turbomachinery complexity. A large weight saving is achieved in the high pressure oxidizer turbopump through the use of a single inlet that feeds a double-entry centrifugal impeller. Since each entry handles half the flow, the impeller eye is smaller and the impeller speed is higher than could be obtained with a single-entry impeller. Another important feature in the high pressure turbomachinery design is that of control over the

location of the rotating member within the turbopump. Over a period of time, many new techniques in balance position systems have been utilized to keep the rotors properly positioned within the machinery during start transient and mainstage operation to preclude overloading bearings and rubbing critical parts.

Development testing was planned to be done, to an unprecedented extent, at the engine system level. Thus, the test program was structured for essentially simultaneous testing of a prototype engine (the Interim System Test Bed) and the components such as main combustion chamber, nozzle, turbopumps, POGO suppressor, valves, preburners, etc. A number of development difficulties have been experienced in both subsystem and system level testing; however, these are characteristic of a development program at this state of maturity.

#### Main Combustion Chamber:

The primary functions of the main combustion chamber are: to contain the burning main propellant; to accelerate the combusted gases to sonic velocity; and to supersonically expand them to an area ratio of 5:1. These combustion products are then expanded to 77:1 by the nozzle. The main combustion chamber operates at approximately  $2070 \text{ N/cm}^2$  (3000 psi) chamber pressure utilizing oxygen and hydrogen propellants burning at  $3311^\circ\text{K}$  ( $5500^\circ\text{F}$ ). It consists of a regeneratively cooled wall exposed to the hot gases and an external structure. Approximately 25 per cent of the total hydrogen flow is used for cooling. The exiting hydrogen is used to drive the low pressure hydrogen turbopump and is then used to cool the preburners, hot gas manifold, main injector faces and combustion stability aids prior to being transferred to the main injector for combustion.

Major considerations in the combustion chamber design are materials, fabrication techniques, life, cooling and performance. In selecting the design approach, technologies in each of these areas were evaluated and applied to the SSME design. The selected design is unique in all aspects relative to currently operational engines. The regenerative cooling is achieved by passing hydrogen through a slotted liner that has an electroform close out.

The heat flux in the combustion chamber is a function of combustion pressure and combustion chamber geometry. The heat flux in the SSME chamber throat is shown on Figure 18 along with values for some previous operational engines. Previous operational engines used steel tubular construction for the combustion chamber; however, the heat flux was less than 1/3 that of the SSME design requirement. Regenerative cooling of the high heat fluxes with nontubular-wall combustion chambers had been established by numerous programs conducted during the 60's with linear

segments and heat fluxes as high as  $1.2 \times 10^8 \text{ W/m}^2$  ( $72 \text{ BTU/in}^2 \text{ sec}$ ). This and related work in fabrication and materials technology served as the basis for the SSME chamber design.

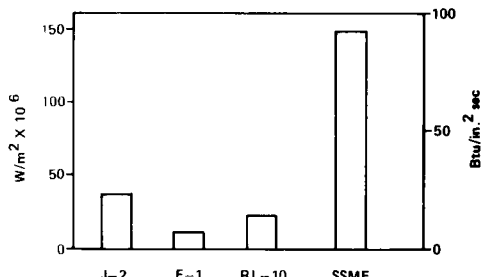


Figure 18 Throat Heat Flux

The extremely high heat transfer rates dictated that the coolant passages be configured for maximum thermal efficiency. Thus a rectangular channel geometry which possesses a maximum two dimensional heat transfer fin effect was selected. A high thermal conductivity material was required for minimum wall temperature and minimum thermal strain. Maximum cycle life demanded a high-ductility material.

To meet these demanding requirements, a Rocketdyne developed material, Narloy Z, which is a combination of 96% copper, 3.6% silver and .4% zirconium centrifugally cast to maintain uniformity is used for the SSME combustion chamber. Three hundred and ninety cooling channels are milled into the chamber by a computer controlled milling machine, Figure 19. Channels are closed out by an electroforming process that deposits a 0.13 mm (.005 inch) thickness copper barrier, followed by a nickel closeout of varying thickness over the coolant channels. The thin copper barrier is to protect the nickel from hydrogen embrittlement. This electroformed closeout structure contains the coolant hydrogen at  $4830 \text{ N/cm}^2$  (7000 psi) internal pressure. The design is compatible with 3 per cent local strain, a requirement necessary for achieving engine life. The channel width, depth, and thickness of the wall between the combustion products and hydrogen coolants are varied along the length of the combustor to achieve a heat transfer rate that keeps the wall temperature from exceeding approximately  $811^\circ\text{K}$  ( $1000^\circ\text{F}$ ). The external jacket is inconel 718 designed to accept the high chamber pressure and external loads imparted by nozzle thrust, gimbaling, and side loads.

Development tests of the full scale main combustion chamber have been conducted. For these tests the subsystem performed as expected and no major difficulties have developed. Tests were conducted initially at the subsystem level in a pressure fed system. Subsequently, a total of

ninety-three tests for two engines and an accumulated test duration of 600 seconds with a maximum test length of 65 seconds have been conducted with the pump fed system. All ninety-three of the pump fed tests have been conducted at or below eighty-five per cent of engine rated power level and without the flight nozzle.

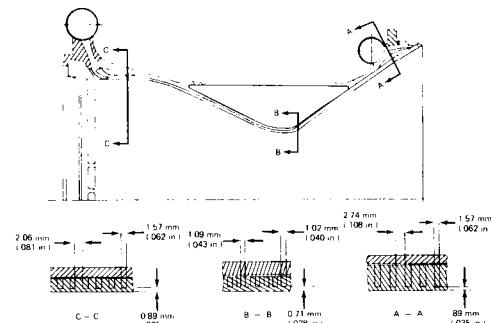


Figure 19 Main Combustion Chamber Construction

A 178,000 N (40,000 lbf) thrust model pressure fed engine was designed to acquire early test experience with the main combustion chamber design. Two of these model engines have been constructed and tested during the past eighteen months. The principal goal was to acquire cycle life data to evaluate the design, materials, and manufacturing approaches selected for the main chamber. Appropriate dimensions on the 178,000 N engine were scaled as necessary for validation of internal parameters of the full scale combustion chamber. One hundred sixty-four tests have been conducted on the two engines, with one engine accumulating 55 tests (cycles) and the other accumulating 109 tests (cycles) prior to critical failure of metal in the liner. The maximum load/strain conditions occur during the startup and shutdown, transient periods thus the tests were of short duration (approximately 3 seconds) to evaluate the design under the worst load conditions. Metalurgical examinations of the two test engines are currently being made.

#### Engine Control:

The combination of high combustion pressure and temperature in the SSME requires oxygen and hydrogen pump discharge pressures of approximately  $5245 \text{ N/cm}^2$  (7600 psi) and  $4278 \text{ N/cm}^2$  (6200 psi) respectively. The engine contains these high pressures during operation with the temperature in the turbine approaching  $1033^\circ\text{K}$  ( $1400^\circ\text{F}$ ) while the main combustion chamber temperature exceeds  $3311^\circ\text{K}$  ( $5500^\circ\text{F}$ ). The combination of high pressure and temperature necessitates careful control of the engine to avoid exceeding operational limits based on the engine life requirements.

This is the function of an engine mounted controller containing dual digital computers.

The engine controller, Figure 20, receives commands from the vehicle and responds by sending commands to engine valves. Valve responses are monitored by position sensors on all propellant valves. A total of 68 sensors are located on the engine to measure temperature, shaft speed, pressure, flow rate and acceleration. These sensors monitor operating conditions and transmit data to the computer for computation of engine mixture ratio and for comparison to the vehicle initiated thrust commands. If the engine strays or drifts, error signals are generated and valve commands are given to bring the engine to the correct operating conditions. The sensors also provide data during the programmed prestart engine checkout phase to determine engine start readiness. The controller also requests and transmits data to the vehicle through the engine interface unit.

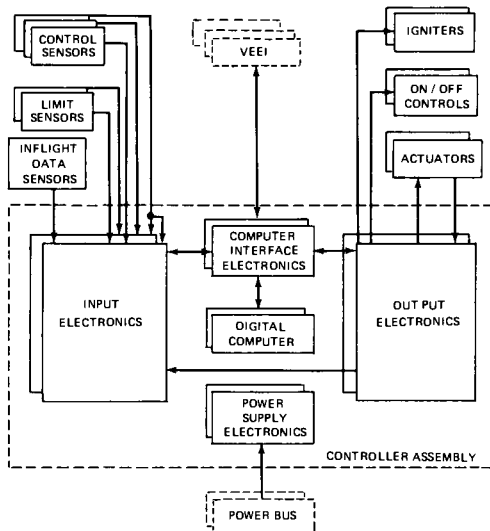


Figure 20 Controller Organization

The controller operates five control valves through dual redundant servovalves. The principal control is exercised on the two preburner oxidizer valves for the control of thrust and mixture ratio. The remaining three valves are main fuel, main oxidizer, and coolant control which are adjusted to improve the engine balance. The complete electrical redundancy is augmented by a pneumatic shutdown system thus providing a fail-operational, fail-safe system.

The J-2 engine utilized an electrical control system for sequencing in operating limits, start, and shutdown. Valve rates and positions were not

controlled. The J-2 controller was, in effect, a switch selector and signal conditioner and was significantly less complex than is the SSME controller.

Engine testing has demonstrated that the SSME control system is capable of meeting its design requirements. The control system is providing repeatable starts and shutdowns as well as throttling during mainstage operation.

#### VI. Main Propulsion System Development Status Summary

The Space Shuttle Main Propulsion System design has been established. Critical Design Reviews for the SSME and the ET have been successfully completed with Reviews for the SRB and Orbiter to be completed within the next few months. Development testing of the SSME at both component and engine system level has been underway for a number of months and is proceeding satisfactorily as is development testing at the component and subsystem level for the Orbiter, ET and SRB. Major hardware deliveries for all propulsion system elements will occur during the first and second quarter of 1977 to support initial system level testing for the SRB in May 1977 and in December 1977 for the liquid Propulsion System. Characteristic of a complex development of this type, engineering difficulties frequently occur, however at this stage in development of the Shuttle propulsion system, no delays are anticipated in the initiation of system level testing in 1977 nor the first manned flight planned for 1979.

# SUPERVISED EXPERIMENTAL AND MODEL ROCKETRY; THE 8th SAFETY IN YOUTH ROCKET EXPERIMENTS (SYRE) SESSION

G. S. James

*National Science Foundation, Washington, D.C. (USA)*  
Chairman of the SYRE Study Group of the IAF

The SYRE session at the IAF Congress provides teachers and rocket club supervisors an annual forum for discussing the youth rocketry and science motivation programs in their countries. The session at the 27th IAF Congress in Anaheim had as its theme, Supervised Experimental and Model Rocketry.

Because of the American Bicentennial, the program covered a spectrum of activities in the United States ranging from an educator-supervised high school model rocket program, to university-level model rocket and experimental rocket activities, to a historic memoir on the establishment of model rocketry, to a slide presentation on the most extensive extra-curricular supervised experimental rocketry program for students in the U.S., and concluded with a report outlining opportunities for students to fly their own payloads aboard government sounding rockets, aircraft, and spacecraft.

On display during the session was a poster: "SPACE TRANSPORTATION - THE FUTURE FOR YOUTH OF THE TRICENTENNIAL ERA -1776/2076," part of the cargo flown aboard the RRI ROCKETPOST 76/37 vehicle launched in Nevada, on September 5, 1976, with the endorsement of the Nevada Bicentennial Commission, to announce the youth-oriented sessions at this Congress. Cosmonaut Vitali I. Sevastjanov was presented with one of the postcards, during the Congress, from this 3.5-mile-high flight.

SYRE endeavors to facilitate information exchange between educators involved in youth rocketry and science motivation programs and educators wishing to initiate such activities. Space limitations necessitate that the seven papers of this session be presented in summary rather than full text. However, the names and addresses of individuals and programs have been retained whenever possible. If additional information or photocopies of particular full papers from this session are desired please contact the SYRE Chairman c/o IAF, 250 Rue Saint-Jacques, 75005 Paris, France.

## A BICENTENNIAL SALUTE WITH MODEL ROCKETS BY SECONDARY STUDENTS

B.P. Preece, Melbourne High School, Melbourne, Florida, USA (76-240)

Early in the year students at Melbourne High School suggested that the annual rocket firings of the physics and physical science classes, during May, be made into a Bicentennial Salute by firing 200 rockets. Students thought this would be a great idea...a welcome change from the usual pattern in which the time available limited each student to only one firing (ref 1).

Melbourne High School offers a nongraded program which provides for different rates and means for progressing toward achievement of educational goals. To provide for more individualization of instruction, a multiphase class structure has been established. The students who participated in this Bicentennial Salute were members of four science phases as follows: Physical Science for students who need more emphasis on basic skills; Project Physics for average students; Physics I for extremely well prepared students; and Research in the Physical Sciences for students who assume responsibility for their own learning. These four phases made it necessary for the teacher to consider the following limitations in planning the rocket firing program:

- (1) The skills of the 100 students involved varied greatly not only in science knowledge but also in reading and vocabulary, in mechanical abilities and in expertise in organizing and carrying out group activities;
- (2) The time available for preparations and firings could not extend beyond

five or six days of class time; and (3) The system developed would have to consist of equipment that could be understood and operated by all the students involved.

Student's discussion first centered around what would be the best ways to save time in firings. All agreed that the operation which took the most time was putting each individual rocket on the pad and making connections to it; therefore, the most likely way to save time would be to install on the pad at one time as many rockets as possible. Only a switch would need to be turned or a plug changed to put power from one rocket to another.

The physical size of the pad had to provide sufficient room for students to prepare rockets on the pad without interfering with each other. Experimentation showed that students need a minimum of 25 to 30 cm. The pad also had to be both easy to carry from classroom to range and easy to set up, especially since all phases would use it. Five positions would require a pad 1.5 m long and this was considered a maximum. The pad itself was envisioned as a wooden saw horse on which welding rods were fastened as guides. Because in previous firings malfunctioning rockets often had been blown around the range by gusting winds, the teacher required a minimum distance of 17 m between pad and control or instrumentation. (Mrs. Preece's full paper discusses in detail the electrical requirements for the system and the multiple launcher designed and constructed by the Research Class).

Each class had prepared for the firings by selecting its Launch Director; by checking weight and balance of its rockets; and by signing the rocket safety code. Each class also had divided into groups assigned specific initial launch functions, such as range safety, tracking, launch pad preparations, and launching. These groups had prepared check lists of jobs each function would involve and had described these functions to their classmates. Each Launch Director assigned the order of rotation to groups in his class so that all would have an opportunity to perform each launch function during the course of the firings. Throughout the entire time the teacher maintained the role of an observer who acted only when student safety was involved.

The first period physics class (students in the average science level) on the first firing day collected its rockets and engines, the Research Class launch system, and other equipment and rushed out to fire. Because none of the students had copied down the system or instructions from the classroom blackboard, these students spent most of the period trying to set up the system. They prepared and armed five rockets, all of which eventually checked good on TEST. But not a single rocket would take off when FIRE was pushed. They blamed everything except their own lack of information and finally had to give up at the end of the class period and return everything to the room.

Second and fourth periods were physical science classes for students whose knowledge of science, as indicated on standardized tests used in the school system, was below the fiftieth percentile. Most of these scores were the result of either student's lack of previous motivation to fully utilize opportunities for science study or of their fifth to sixth school-year reading level. Because only two or three students in each class had previously been involved at all in launching rockets one of the Research Class students assisted the classes in setting up the launch system. By the time the range was ready and the students were in their assigned range positions, there was only time to fire the two or three rockets that went off on the first launch attempt.

Third period was the teacher's planning period and so contained only two independent study students and a lab assistant. Two of these had fired rockets previously, so the three of them managed to fire four rockets and collect all necessary data during their first and only day of operations.

The students in the fifth period physics class were considered to have the highest level of science and math knowledge of all the physics classes. A number of them brought in tracking equipment. Will brought a five-position launch pad made merely of a long board on which he had installed flattened tin cans as flame deflectors underneath the launch rods. The Research Class system could not work with this bare pad but fortunately Brenda designed and constructed herself one that would. hers was the only launch system other than the one built by the Research Class.

This class now proceeded to set up for firing nine rockets at the same time--five with the Research Class system and four with their classmates' equipment. After the Range Safety Officer declared the range clear, an attempt was made to fire in order each of the nine rockets. Then power to the range was dis-

connected and owners of the remaining rockets tried quickly to determine and repair the problems before the next firing of that round. Since the launch group for each firing round consisted of the owners of the rockets on the pad, each of whom wanted to fire his or her own rocket, it was necessary to lift off most of the nine rockets before groups rotated their range functions. If, after three attempts, some of the original nine rockets still refused to fly, the owners were asked to take them off the pad for repairs and flight on another day. During this first day on the range, time spent in setting up the range and equipment limited the number of firings to about one round of nine.

When the Research Class had its turn to fire its own rockets, the students launched a few rockets with their own system and a few with the system of Brenda and Will. When they had fired all the seven engines they had, they felt that they had satisfactorily completed their requirements. They then volunteered to let the other classes use the remainder of their firing quota.

During the remaining three days of firings, the twelve students in the first period physics class used both launch systems, worked rapidly and obviously effectively, and actually launched 91% of the class quota of 32 of the 200 Bicentennial Salute rockets (See Table I). This high rate of success appears related to several factors concerning the students themselves: over half the students had previously fired rockets on their own; nearly half the students had taken one or more years of electricity or electronics classes; almost all male students enjoyed mechanical tinkering with cars, cameras, motors and etc.; the three girls in the class were all unusually active participants who were often dominant leaders in class activities.

Both physical science classes used only the Research Class launching system. They showed little interest in learning any more about the system than was necessary to launch their rockets. They were quite satisfied to watch others' rockets fly. About half the students cooperated willingly in gathering data although all the students did participate.

The second period class launched 27% of its quota of 45 firings and the fourth period class only 24% of its quota of 42 firings. The quotas of rocket launches were based in large part on class enrollment. By May in these classes, perhaps only 75% to 80% of the students enrolled were actually attending class. This, coupled with the few rockets built, accounted for the low percentage of firings.

Some of the data collected by these physical science classes appeared to be in error when the two-dimension graphical determination of maximum altitude was attempted, for maximum altitudes of 25 to 20 meters were read from graphs which should have given at least two or three times that. Errors in reading the correct angles from the protractors of the altiscope were responsible as the protractors had double scales.

The fifth period physics class of thirty students was given a quota of 60 of the 200 launches. This meant that every rocket would have to be fired twice. They got off only 67% or 40 launches, and nine of these were in the final attempt at a "barrage" launch.

A considerable amount of time could have been saved had students not rotated range function groups. But for this to be a useful activity, students need to get more from the launches than just to watch rockets fly. And it surely is a lot more fun when each student gets to fire his own rocket.

"Barrage" firing and the multiple-position pads both save range time, but even together they probably would not have made it possible to fire 200 rockets in the time available. Too large a proportion of the 55-minute class periods was spent in moving equipment to and from the range and setting it up for use; two-hour or longer class periods would have resulted in much more than twice as much effective time on the range.

Finally, if the "barrage" firing is not counted in, the number of rockets (29) launched by twelve students in first period was very nearly the same as the number of rockets (31) launched by thirty students in fifth period. This seems to indicate that the equipment used was more of a factor in determining the number of rockets launched than the number of students involved.

Table I Class Launch Quotas & Results for Bicentennial Salute of 200 Model Rockets

Class Period	No. of Students	No. Rockets To Be Fired	No. Rockets Fired	% of Quota Fired	% of Total Rockets Fired
1	12	32	29	91	27.8
2	22	45	12	27	11.4
3	3	0	4	400	3.8
4	19	42	10	24	9.5
5	30	60	40	67	38.0
6	4	21	10	47	9.5
TOTALS	90	200	105	52	100.0

In the final analysis, 105 of the planned 200 rockets were actually launched for the Bicentennial Salute. All the other goals were fully accomplished. The Research Class designed the rocket firing experiment and passed on to the other classes instructions in enough detail to enable those students to build rockets, everyone of which met the established criteria; to construct and successfully operate range equipment, interconnecting it where necessary to get working systems; to observe range safety precautions so that there was not even an "almost" mishap; to collect data and correctly use it for graphical or mathematical analysis of the launches; and to work together effectively in groups to accomplish scientific objectives.

All the students had so much fun it was hard for them to realize they were really saluting the Bicentennial with SCIENCE IN ACTION!

THE FORMATIVE YEARS OF MODEL ROCKETRY, 1957-1962; A PERSONAL MEMOIR  
G. Harry Stine, Phoenix, Arizona, USA (76-241).

Model rocketry was a fortuitous synthesis of three technologies: (a) the ancient art of pyrotechnics, (b) model aeronautics, and (c) professional aeronautics and rocketry. Although all three of these technologies existed in forms sophisticated enough to permit the development of model rocketry prior to 1957, and although many individuals had made partial synthesis before that time, a social need of sufficient magnitude did not exist prior to late 1957. Sputnik-I provided the impetus that created the social need for model rocketry. Fortunately for millions of young people, the technical elements responded to the prod of social need to create model rocketry as we know it today.

The world's first true model rocketeer is Orville H. Carlisle, a self-taught merchant. Orville's hobby is pyrotechnics. He is one of the outstanding amateur pyrotechnists in the United States today. He is a member of the Committee on Pyrotechnics of the National Fire Protection Association because of his extensive practical knowledge of pyrotechnics.

Robert Carlisle, his brother, also played a decisive role in the development of model rocketry. He is a former naval aviator and an ardent builder of flying scale model aircraft. In the early 1950's, he began giving lecture demonstrations about the history of flight using line-controlled model airplanes. He asked Orville to make a small rocket that could be used to show the future of flight into space.

Orville and Robert Carlisle combined the art of pyrotechnics with the technology of model aeronautics. This produced the first true model rocket. By 1954 with Robert's help, Orville had developed the "Rock-A-Chute Mark I" using model airplane construction techniques and materials. It used a plastic parachute to bring the entire model gently back to the ground. It was propelled by a paper-cased, replaceable solid propellant rocket motor. On August 30, 1954, Orville filed for U.S. patent on the elements of his system. On July 1, 1958, U.S. Patent Number 2,841,084 was granted to Orville Carlisle.

One element remained to be added before model rocketry as we know it was born: the techniques of professional aeronautics and rocketry.

In 1952, fresh out of Colorado College with a B.A. in physics, I went to work as a civilian scientist at White Sands Proving Ground, New Mexico. I learned

about rocket motors as Chief of the Controls and Instruments Section of the Propulsion Branch testing both solid and liquid propellant rocket motors for the U.S. Army. In 1955, I went to work for the U.S. Naval Ordnance Missile Test Facility at White Sands as head of the Range Operations Division and Navy Flight Safety Engineer. Thus, I became intimately familiar with flight operations and safety of rockets such as the Viking and Aerobee.

I also found myself talking to youth groups visiting the proving ground. Thus I became acutely aware of the youth rocketry problem, as it was known in those days. The youth rocketry problem revolved around a series of knotty questions. How do you tell a teen-ager how to correctly and safely mix toxic chemicals to obtain highly explosive rocket propellants? How do you instruct them concerning the loading of these propellants into rocket airframes? George S. James and others were hard at work trying to get answers to these questions and others that were involved as well.

One of my responses to the urgency of the youth rocketry problem was to devote one of my *Mechanix Illustrated* articles to the safety rules practiced by the professionals with some safety rules for amateur rocketry that I derived from them. It was entitled, "The World's Safest Business," and it appeared in the February 1957 issue.

On January 28, 1957, I received a letter from Orville Carlisle telling me of his model rocket developments and offering to send me some samples to try out. I accepted his offer with some trepidation because, although I was intensely interested, I was also somewhat skeptical of non-professional rocket experiments and development by that time.

On February 5, 1957, Railway Express delivered to my home in Las Cruces, New Mexico, a large box. Carlisle had sent me three built-up Mark II Rock-A-Chute models, and three unassembled Mark II's in "kit form." He included several dozen replaceable solid propellant model rocket motors 1/2-inch in diameter and 2-1/4 inches long. I assembled the two launch pads that Carlisle had sent along in the shipment. I read the instructions carefully. Then I took one of the built-up Mark II models, packed the parachute, installed a motor, and took it with a launch pad into the middle of a 400-acre cotton field. I set everything up, lit the fuse (we had not yet developed electrical ignition) and ran about 20 yards back.

What I saw in that New Mexico cotton field on that bright morning in February 1957 has now been repeated more than 100 million times in the United States alone since that day. The Mark II Rock-A-Chute took off with a woosh, leaving a thin trail of grey smoke. It climbed to about 250 feet and ejected a bright red plastic parachute. The whole assembly wafted gently back to the ground. I picked it up, took it home, installed a new motor, and repacked the parachute. I went over into the cotton field and flew it again. It was a repeat performance. So was the next flight. And the next flight. And the next flight.

I realized that ignition by means of a standard safety fuse was very "unprofessional." Carlisle and I independently developed electric ignition for model rocket motors in early March 1957; our letters to each other describing in detail how to do it crossed in the mails. Carlisle told me how to make multi-staged model rockets and sent some specially-loaded lower stage booster motors for me to try. I conducted some primitive static tests of the Carlisle motors, running them through a series of environmental stress tests as well. In no case did these little motors fail to work properly. And I could not get them to undergo spontaneous ignition under any condition that might normally be expected to occur. I was greatly impressed. It was difficult to believe that a shoe store owner from Nebraska had achieved the fabled nine-nines reliability that we professionals strove for but rarely achieved at White Sands.

Here was the obvious answer to the youth rocketry problem! Extend the field of model aviation into the space age. Market model rocketry through the hobby trade. Put the models out in kit form. Get someone with pyrotechnic experience to make the model rocket motors, thus eliminating one of the most hazardous aspects of rocketry: propellant handling. Put every bit of professional astronautics and rocketry technique, safety, and charisma into model rocketry as possible. Make it a legitimate hobby alongside model railroading, model boating, and model aviation.

I left Las Cruces in August 1957 and moved my family to Littleton, Colorado, where I went to work on advanced projects for the Martin Company. I had just

started to get things unpacked in our new home when Sputnik-I went into orbit on October 4, 1957. That day was the turning point for model rocketry. Without Sputnik, model rocketry would never have developed. Sputnik fired the imaginations of young people all over America. The youth rocketry problem became serious as thousands of young people began to make and fly their own rockets. And we were almost ready with the model rocket to satisfy that desire in safety.

Sputnik also allowed me to devote my full time to model rocketry. To make a long story short, I was fired by the Martin Company on October 5, 1957 for telling United Press that the Soviets had used their ICBM as a launch vehicle (which they had), that Sputnik meant that the entire United States was open to nuclear ICBM attack (which it still is), and that the United States was not first in space because we did not have a serious space program (which we did not under the Eisenhower administration).

At just about that moment, my article on Carlisle's model rockets appeared in the October 1957 issue of *Mechanix Illustrated* magazine. Carlisle was deluged by over 10,000 letters within weeks. He had to return over \$5000 in cash that had been sent to him by readers who wanted to buy those model rockets and motors right away. It hurt to return that money, but we weren't ready to ship model rockets yet. MMI was officially chartered as a Colorado corporation on October 10, 1957 by my college friend attorney, Robert S. Appel. The response to the magazine article was so overwhelming that it convinced us that there was indeed a market for model rockets. We needed to satisfy that market.

An interesting facet of model rocketry revolves around a visit to Brown Manufacturing Company by Carlisle and me on October 22, 1957. Lawrence Brown told us, "I can make your lifting charges for your rockets the same size as Carlisle's, but I would have to order special tubes and make special fittings for my loading machines. I roll my own tubes here for my fireworks. I could make your lifting charges much cheaper if I could use the same tube that I use for my Buzz Bomb Helicopter firework." Brown's firework tube was 2.75 inches long and 0.69 inches in diameter. We settled on this size for our model rocket motors because they would be cheaper to make with existing tube supplies and production tooling. These bigger motors had more thrust but Brown could tailor the amount of propellant to provide the total impulse we wanted. Today, nearly twenty years later, the worldwide standard model rocket motor casing is 2.75 inches long (70 mm) and 0.69 inches in diameter (18 mm). On that October day in 1957, we had unknowingly established an inviolable standard. Every model rocket motor manufacturer who came along later had to make model rocket motors that would fit into existing kits and models, except for some of the larger models and motors that did not follow this standard. Fully 99% of all model rocket motors made and used since 1957 have been the "standard" 18 x 70 millimeter size that was established on the basis of an existing firework!

It became obvious to me in November 1957 that the youth rocketry problem would not be totally solved just because MMI made safe, workable model rockets available in hobby shops and by direct mail to anyone who wanted them. Something else was needed. That "something else" turned out to be, upon careful analysis, a non-profit educational organization to publicize and promote safety rules, establish and enforce standards, establish communication between model rocketeers, and eventually set up competition and record-setting activities. Every hobby and sport has such an organization. Model rocketry needed to have one also. On December 7, 1957, the Model Missile Association was granted a charter as a non-profit organization in the State of Colorado, thanks again to my attorney friend, Robert S. Appel who never took a single penny for all the work he did for this non-profit organization.

Because of the confusion between MMI and MMA, the name of the MMA was officially changed to the National Association of Rocketry (NAR) on October 25, 1958 although we began operating as the NAR several months earlier. Taking a cue from the American Rocket Society, upon whose By-Laws we patterned the MMA/NAR By-Laws in the first place, we set up a local chartered Section organization within the NAR. The first NAR Section was the Mile-High Section in Denver, chartered on September 18, 1958 and composed of the old MMI Flight Test Crew. Peak City Section under Bill Roe in Colorado Springs was chartered shortly thereafter.

In the meantime, there was action in the model rocket industry as well. Brown was having difficulty making the quantity of model motors we needed; his efforts to meet the quantity problem forced him into a quality problem. The quality control required for model rocket motors and the reliability re-

quirements were far beyond anything previously experienced by the fireworks industry.

The solution walked through the front door. On a hot July day in 1958, a young man with a crew cut and rimless glasses walked into MMI. "I'm Vernon Estes. I don't know who is making your rocket motors for you, but I can and will make them better and cheaper." When I asked him what his background was, he told me that he built garages for a living and his father was in the wholesale fireworks business. When I asked him how he was going to make model rocket motors for us, he said, "I'll learn how to do it." And he did.

In the chilly fall and frigid winter of 1958-1959, Vern Estes designed, built tested, and worked the bugs out, and put into production the world's first fully automatic model rocket motor manufacturing machine, dubbed "Mabel." It produced a complete model rocket motor every five seconds. The first production model rocket motor popped out of Mabel on January 20, 1959. Estes' model rocket motors were much superior to anything that we had had before. The NAR was invited to participate in the First World Congress of Flight in Las Vegas, Nevada on April 12-18, 1959. The Air Force Association picked up the tabs for the hotel rooms. Our NAR model rocket demonstrations appeared on nationwide NBC television. I was introduced to Jacqueline Cochran, the famous aviatrix who was then President of the National Aeronautic Association and the Federation Aeronautique Internationale. When Jacqueline Cochran later made a trip to Denver, Del Hitch and I gave her a full briefing on model rocketry, the NAR, and model rocketry competition. Because of Jacqueline Cochran, model rocketry was later introduced into the Federation Aeronautique Internationale as an international aerospace sport.

But we were just beginning to get started in model rocketry competition in the NAR. The world's first model rocket competition was flown on May 16, 1959 at Green Mountain Proving Ground with the NAR Mile-High Section pitted against the NAR Peak City Section. We felt it was time to attempt to hold a national meet. Maybe we would not get any model rocketeers from outside the State of Colorado for the first one (we didn't), but we would advertise the competition to all NAR members and accept entries from any NAR member. The First National Association of Rocketry Annual Meet (NARAM-1) was held at Hogback Rocket Range on July 16-19, 1959. I was contest director. There were 24 contestants. Norman G. Mains, Jr. won the title of National Champion with 26 contest points.

In July 1960, an NAR team from Mile-High and Peak City Sections flew model rockets at the 1960 Boy Scout Jamboree. On September 20, 1960, I made a presentation on model rocketry before Colonel Russell G. Pinsky and his staff at United States Air Force Headquarters in the Pentagon, pointing out that model rocketry would make an excellent addition to the USAF special services hobby program along with model aviation. On July 3, 1961, the USAF published a letter to all commands endorsing model rocketry as a worthwhile activity for USAF personnel and dependents and naming the NAR as the USAF-approved organization for model rocketry. The NAR Safety Code became mandatory for all non-military USAF rocket activities. The first USAF model rocketry competition was held at Langley Air Force Base, Virginia on July 16, 1961 to choose a USAF team to participate in NARAM-3 in Denver. Leading the USAF Team was Captain Bryant A. Thompson, later to become Vice President of the NAR.

NARAM-3 took place at Hogback Rocket Range near Denver on August 17-21, 1961 with J. Delano Hitch as contest director. It was the first true national competition, drawing 67 contestants from as far away as the East Coast. NARAM-3 saw the introduction of a whole new area of model rocketry: boost gliders. These are either rocket-propelled gliders or glide-recovered rockets, depending upon their design. The first successful boost-glider was developed by Vern Estes and John Schutz, and it was demonstrated in flight many times at NARAM-3.

On November 24, 1962 in Paris, France, the 51-nation Federation Aeronautique Internationale (FAI) officially recognized model rocketry as an international aerospace sport following my presentation to the Commission Internationale de l'Aeromodelisme. A model rocketry subcommittee was formed to write the international competition rules. I was elected the first Chairman of that Subcommittee and served as such until 1973.

Thus, in the first five years of its existence, the field of model rocketry grew from Orville H. Carlisle's basement in Norfolk, Nebraska to a world-wide aerospace sport. The model rocket industry was on firm ground with the two major firms of 1976, Estes Industries, Inc., and Centuri Engineering

Company, producing a growing number of high quality products for a growing market. The market itself had started in the hobby industry, shifted to direct mail marketing, and had just started to re-enter the hobby industry again in 1962. The NAR had been formed and forged into a truly national educational organization for the hobby and sport. Four national meets had been conducted under nationally-available rules. Sections of the NAR had been formed and chartered from California to Connecticut. The first national model rocket records had been established and exceeded, and these had been recognized by the National Aeronautic Association. Recognition was beginning to come to model rocketry from prominent national organizations.

One final thing needs to be said about the formative years of model rocketry. There was no accident more serious than a minor finger burn during this period; there were no deaths or serious injuries as a result of model rocketry; there was no property damage as a result of model rocketry. This outstanding safety record established during the raw beginnings of the hobby has continued to this day. Yes, there have been burned fingers and a couple of grass fires, but nothing more serious. The number of incidents resulting from mis-use of model rocket products has been surprisingly low, and even these have not been of serious nature.

In essence, model rocketry as it is known today in the United States and Canada, and "space modelling" as it is known around the world, had its firm foundations laid in the first five years of its existence, thanks to the fortuitous synthesis of pyrotechnics, model aeronautics, and astronautics and thanks to a continuing belief that people, young and old, want to experiment with rockets that are safe and that really work.

By 1962, there was still much work to be done. But model rocketry was with us to stay.

(In his full paper, Mr. Stine also discusses the contributions of the following individuals to the establishment of model rocketry: Arthur H. Ballah, Gabriel J. Brilliante, Manning Butterworth, Robert Daly, Gene Dickerson, Mrs. Vern Estes, William Gore, Grant R. Gray, William G. Haggard, Andrew G. Halye, Charles S. Hans, J. Delano Hitch, Melvin O. Johnson, Donald Z. Kauth, William L. Kauth, Richard D. Keller, Albert G. Kniele, Albert G. Lewis, Norman G. Mains, Richard L. Mayes; R. Gilbert Moore, Russel G. Nichols, Leroy E. Piester, David Post, James Post, John S. Roe, Lawrence Saunders, Robert A. Smith, Mrs. Harry Stein, Menford L. Sutton, Alden Tombaugh, Captain Vernon Van Vonderen, Nathan Wagner, and Irving R. Waite).

#### MODEL ROCKET ENGINE TESTING AT OHIO STATE UNIVERSITY

G.M. Gregorek, Ohio State University, Columbus, Ohio, USA (76-242)

At the 24th IAF Congress in Baku, in 1973, Dr. G.M. Gregorek, a member of SYRE and Chairman of the Standards and Testing Committee of the National Association of Rocketry, presented a paper, (ref 2), advocating the development of international model rocket engine testing standards. Subsequently, his paper at the 26th Congress in Lisbon, in 1975, (ref 3), described some of the results of testing model rocket engines from various countries. This year, his paper, accompanied by a 16 mm film, discusses some of the problems of these tests and the equipment used to obtain the data at the static model rocket engine test facility of the Aeronautical and Astronautical Research Laboratory of the Ohio State University used for these tests.

The experiments are conducted with the aid of undergraduate Aero-Astro Engineering students and serve as teaching methods for experimental techniques and data reduction methods applicable to rocket engine testing. The author is greatly indebted to Mr. Craig L. Streett and Mr. George Pantalos for their great contributions to this program.

Engine thrust vs time curves are obtained on a simple beam measuring device, using a four active strain gauge bridge circuit as a measuring element. The electrical signal from the bridge is stored as a function of time on a disc and then processed by a small digital computer after the engine test. The stored data can be displayed on a cathode ray tube for a quick look and then plotted by an X-Y plotter for a hard copy. This short term delay procedure is superior to the earlier method used at the Laboratory of plotting the signal from the strain gauge bridge directly through the recorder in "real-time." The older method suffered at times from recorder response, when the pen of the recorder could not follow very rapid thrust variations. The present disc equipment accepts thrust-time data with millisecond response and plays this data back to the recorder after the test at a slow (e.g. 10 second) pace. The

thrust-time data is integrated for total impulse and time averaged to find the average thrust level.

Calibration of the strain gauge element is performed prior to every test series and several times during the test program. The calibration procedure simply requires known weights to be placed on the beam at the engine location and the electrical output recorded. Four weights are used and a straight line fit through the data by the method of least squares. Linearity of the thrust stand is better than  $\pm 1\%$  in the test range. The time signal is provided by the computer system and time is known within  $\pm 0.001$  seconds.

Using the Ohio State facilities, model rocket engines constructed in five countries were tested. Unfortunately, there is no easy method for obtaining engines from various countries, as yet. This severely limits the scope of any testing program and the statistical validity upon which the results can be based. This exchange of engines is another area in which members of the IAF may contribute to international cooperation. With the reservation that the test data are representative of engine performance of the various types, and the understanding that sufficient numbers of each type were unavailable for a true statistical sample of performance, the test data from engines of five countries are offered as a first step toward the exchange of model rocket engine static test performance information in Table II (reproduced from paper 75-088).

The classification of the engines in the table follows the standards set by the Federation Aeronautique International (FAI), the world aerospace record keeping agency. Fortunately, the desire for world-class competition in Space Modeling has resulted in the FAI establishing certain rocket engine classes and standards of performance which the engine manufacturers in the various countries follow. The major criterion is the total impulse. Class I engines have up to 5 Newton seconds (Ns) total impulse; Class II engines have from 5.01 to 10.0 Ns total impulse; and Class III engines have from 10.1 to 40.00 Ns. Total thrust, average thrust, and delay time prior to ejection charge ignition are other descriptive terms used to classify the model rocket engines. There are not standards set for size of engines, and as shown in the

Table II - Description and Static Performance Summary of Model Rocket Engines

Country	Engine Mfg.	Dia. (mm)	Length (mm)	Loaded Weight (g)	Burnout Weight (g)	$I_t$ (Ns)	$t_b$ (s)	$T_p$ (N)	$T_{ave}$ (N)	$I_{sp}$ (s)	Remarks
<b>Class I</b>											
Czech	ZVS	18	63	22.8	10.5	5.23	1.45	10	3.6	60	
Poland	CHEMA	20	49	16.4	8.6	4.21	0.80	12	5.3	54	- Port Burner
U.S.A.	AVI	13	56	9.5	2.2	2.70	1.30	5	2.1	37	- Mini-engine
Yugoslavia	GORADZE	18	55	13.9	8.0	4.18	1.10	12	3.8	71	
<b>Class II</b>											
Czech	ZVS	18	63	22.8	10.5	7.50	2.0	7.6	3.8	61	- Black Powder
Czech	ZVS	18	60	24.5	13.8	9.35	0.7	24.0	13.4	88	- Composite Prop.
Poland	CHEMA	20	70	25.4	9.3	9.42	0.8	23.6	11.8	59	- Port Burner
U.S.A.	AVI	18	69	22.9	10.3	8.61	1.4	13.0	6.1	68	
<b>Class III</b>											
Czech	ZVS	18	80	34.8	16.3	17.12	1.3	25.6	13.2	93	- Composite Prop.
U.S.A.	AVI	18	69	29.6	8.6	11.0	1.9	12.5	5.8	69	
U.S.A.	Estes	24	70	43.9	19.0	18.5	1.8	25.0	10.3	74	
U.S.A.	FSI	21	95	43.0	21.0	13.1	1.8	31.8	7.3	60	
<b>Other Engines</b>											
U.S.A.	AVI Micro	9	38	3.1	1.3	0.83	1.1	1.8	0.75	46	
U.S.A.	FSI F-100	27	150	113.4	51.5	40.40	0.8	96.0	51.0	65	- Port Burner
U.S.A.	FSI F-7	27	150	118.0	58.4	51.90	9.5	17.0	54.6	87	- End Burner
German	HELD	15	95	—	9.4	5.50	2.8	8.5	2.0	—	Only Engine Available

table, the engine diameters and lengths vary considerably. Neither are limits placed on the types of propellants used - except that they must be safe, of course. However, cost has usually resulted in some derivative of black powder being used. Composite propellants have been used for special cases and two such engines from Czechoslovakia are shown in the table to illustrate these high performance engines. Listed in the table are the total impulse,  $I_T$ , in Newton seconds (Ns); the burn time  $t_b$ , in seconds (s); the peak thrust,  $T_p$ , and average thrust,  $T_{ave}$ , in Newtons (N); and the estimate of specific impulse,  $T_{sp}$ , in seconds. The specific impulse is an estimate since it was not possible to remove the delay train from all the engines. Thus, the difference between the loaded weight and the burnout weight includes the weight of the delay charge. This leads to specific impulse values slightly lower than the true value. The generally accepted values for black powder performance were obtained, ranging from 50 to 80 seconds. The Czechoslovakian engines with the composite propellants show values approaching 100 seconds.

ROCKET RESEARCH INSTITUTE TEST FACILITIES AND FLIGHT VEHICLES  
AVAILABLE FOR YOUTH ROCKETRY PROGRAMS  
C. Piper, III, Rocket Research Institute, Inc., Glendale,  
California, USA (76-245)

During the past two decades, the Rocket Research Institute, Inc., has made its facilities and technical resources available to high school and college students engaged in experimental and model rocket activities (refs 4-13). These activities include the design, construction, and evaluation of student built rocket motors, payloads, and flight vehicles. This paper describes the present RRI facilities and the various rocket motors and vehicles developed for supervised student projects.

The Rocket Research Institute, Inc., is a non-profit consulting organization staffed by professionally employed individuals who volunteer their services to guide the development of safe and effective youth motivation and education programs related to the space sciences. The RRI, Inc., is an Institutional member of the International Astronautical Federation and maintains its headquarters in Glendale, California, 91208.

Youth activities are organized under the Institute's National Rocket Safety Registry (NRSR) program whose purpose is to help provide guidance; in cooperation with industry, government agencies, educators, and parents; for supervision of safe student space-science study and training programs. The NRSR, initially called the National Registry of Student Rocketeers, was established in December, 1957, by the Institute's Board of Trustees. The NRSR program, a free service, not an organization, surveys the spectrum of supervised student rocketry from primary-level through post-graduate university projects. The Program is managed by the Eastern Operations Office of the RRI, Inc., P.O. Box 7122, Washington, D.C. 20044.

The Institute firmly believes that programs in supervised experimental rocketry can only be undertaken if the three factors of competent guidance, professionally designed equipment, and proper safety facilities are available. Consequently, the RRI maintains a professionally designed and supervised static test site, the Perkins Rocket Safety Test Center, near Sacramento, California, and an experimental rocket flight range is operated by the Institute at the Smoke Creek Desert, near Gerlach, Nevada. Activities at these test sites are supervised by the RRI, Inc., Western Operations Office, P.O. Box 373, Fair Oaks, California.

Much volunteer time and effort have been expended in developing the Perkins Rocket Safety Test Center. The use of the land on which the PRSTC is located is donated by the family of the late Dr. John Craig, a prominent Sacramento County physician, who felt that student experimental rocket activities could be educationally redeeming if they were conducted in a proper place with qualified supervision. Here students have the facilities available for mixing propellants, fueling motors, and conducting instrumented static test firing of motors prior to assembly of the flight vehicle. Special storage facilities are also available for loaded motors and other explosive-pyrotechnic materials related to each specific program. RRI personnel supervise all facets of each operation to assure that proper safety precautions and standards are adhered to at all times. Both solid and liquid test facilities are available at PRSTC.

Three test stands are available for static testing (see Table III). Test Stand Number One, located approximately 30 feet from the control room, is used for testing liquid rocket engines with thrusts up to 5,000 pounds. The stand is

separated from the control room by a 15 foot thick earth wall and equipped with space for tankage and area for mounting gauges and transducers. The engine is contained within a concrete test cell which can be cooled with water. A flame trough extends from the stand to a burn-off pond about 75 feet away. On this stand, several projects utilizing student built units have been tested. Data derived from the testing of an Atlas Vernier rocket engine, a small regeneratively cooled unit, has led to the development of an ablative thrust chamber. Burning liquid oxygen/kerosene, the engine develops a thrust of 1,000 pounds and has proven its reliability through repeated testing in runs lasting up to 40 seconds.

Test Stand Number Two is located 50 feet from the control room. This stand is used exclusively for testing solid rocket motors. Motors up to 10 inches in diameter and up to 6 feet in length can be accommodated by this stand. The stand consists of a concrete slab 5 feet by 7 feet with 4 foot high revetments on two sides. The motor is held in the horizontal position by a support stand which allows only one degree of freedom, thus allowing the motor to push directly against the load cell. This stand has a rated capacity of 15,000 pounds thrust. Stand Two also exhausts into the same pond as Stand Number One. Both of these stands were constructed by the RRI.

Test Stand Number Three was constructed and donated to the RRI by Truax Engineering Corporation for the purpose of testing large steam powered rocket motors (ref 14). One of these rocket motors was eventually used by dare-devil Evil Kineval in his "Snake River Canyon Jump." The stand is currently being modified for testing of flight configuration liquid rocket systems. Motors with thrusts up to 10,000 pounds can be tested on this stand with a considerable safety margin. A unique feature of this stand is that it can be operated in either the horizontal or vertical position.

A five foot high earth embankment surrounds the test stand area at PRSTC. As with Test Stand Number Three, the labor for this safety wall was donated by Truax Engineering. Between these three stands, virtually any student built system likely to exist in the present or near future can be tested safely with relative ease.

Operations at the PRSTC are conducted from inside a buried, steel reinforced, concrete block house. The block house is divided into two sections; one for the control room, and one for the observation room. Firing circuits and instrumentation are housed within the control room, while space for spectators and miscellaneous equipment occupy the observation half of the building. Viewing of the tests is possible by direct observation through a large periscope in the control room and on closed circuit television monitors located throughout the building.

Instrumentation at the PRSTC consists of several multichannel recording oscilloscopes. Amplifiers and preamps allow the use of both strain gauge and potentiometer type transducers. An X-Y plotter and a high speed electronic counter are also available as optional equipment. Data collection is made as redundant as possible through the use of test gauges as well as electronic pressure transducers. During test, cameras, mounted on the roof of the block house, photograph the gauges. Videotape is also used but is generally not as reliable. With the photographic back-up system, even if the chart recorders malfunction, all the data will not be lost.

Currently a new static test instrumentation system is under development, the heart of which is an Intel 8080 (R) based micro-computer; the main duties of which will be digital data acquisition and real time data processing.

The Institute presently has three propellant mixers; two remote mixers for Micrograin and Plastisol type propellants, and the third a thermostatically controlled manual mixer for GALCIT type propellants. All mixers are operated electrically and are located in a special area of the PRSTC specifically set aside for this activity. The Micrograin mixer is capable of mixing up to 50 pounds, while the GALCIT mixer can handle up to 95 pound batches. The mixer for Plastisol type propellants can handle 15 pounds at a time.

After motors have been loaded, they are stored in a special magazine designed to maintain a high level of security. The magazine has been approved and specifically licensed by the U.S. Treasury Department's Alcohol, Firearms, Tobacco Division (AFT) as well as the local governmental agencies.

Arrangements for utilizing facilities at PRSTC can be arranged by writing any of the RRI, Inc., offices listed in the introduction of this paper. An RRI

staff member will be assigned to assist in preparing whatever is needed to complete the project. The Institute, of course, reserves the right to carefully screen and reject any project or projects which are considered to be of an unsafe, unrealistic, or politically motivated nature.

The second RRI test facility is located in an area of northwestern Nevada known as the Smoke Creek Desert. It is here that all RRI flight tests are conducted. The remoteness and almost total absence of vegetation makes this one of the most ideal locations for flight testing anywhere in the United States and, because of its size (approximately 300 square miles), the range can safely accommodate virtually any size student constructed vehicle. Because the Smoke Creek Desert is located outside most of the major air traffic routes, permission from the Federal Aviation Administration (FAA) can be obtained for flight vehicle launches.

Rockets can be launched in any of three directions. The major downrange leg of the range is 32 miles long, while the other two legs are 10 and 15 miles respectively. Flight vehicles with altitude capabilities in excess of 150,000 feet can be flown at the range, although 60,000 feet is the current altitude record. Due to its remoteness, there are no permanent facilities available at the range. All equipment is transported to the site as it is required, and generally several days in advance of any test. Most field trip participants camp at the test site because it generally consumes too much time driving to and from the nearest town with suitable accommodations.

The desert test site is divided up into several smaller areas. The first is the encampment area where sleeping, eating, and other non-rocket related activities occur. Most participants stay in this area. The second area is the rocket assembly area. It is here that rockets are stored, uncrated, assembled and transported to the launch area. Electric lighting and electric power are provided for both of these areas by a trailer mounted 5 Kw generator. The launch area consists of two to three portable zero length launchers. Since most flight vehicles launched at the SCDFR are of a high thrust to weight ratio, rail type launchers are usually not used. They are, however, available should their use be warranted. The firing control center is located approximately one half mile from the launch area. During a launching, all operations are controlled from this location. Spectators occupy a trench 6 feet deep by thirty feet long at the control center.

Tracking sites are located at three different locations at the range. One is one mile from the launch area, while the others are located at distances of five and ten miles. Tracking is usually done by optical methods with the aid of pyrotechnics attached to the flight vehicle. An experimental radar tracking system is currently under development. Small portable generators and battery banks provide whatever electricity is required at these sites.

Recovery of the rocket and its payload is accomplished by receiving data from the tracking sites and plotting the impact point on a plotting board. Because the alkali flat on which the flight range is located is dry during most of the year, it is usually possible to drive vehicles directly to the point of impact. In some instances, aircraft have been used in the search for payloads due to the ideal landing conditions on the lake bed during dry months of the year.

Data recording at the site is handled on an individual case basis. Since every payload is different, experimenters usually bring their own equipment. The Institute's present flight instrumentation program is to design and construct a standard payload section that includes the necessary internal structure for mounting printed circuit boards and transducers, a standard power system and a transmitter receiver antenna unit. The power supply has already been designed, constructed, and successfully flight tested three times. The unit consists of a 400 hz inverter running off a single 1.2 volt nickel cadmium cell. The output transformer is custom wound to supply any voltage required. The design of a transmitter receiver antenna system uses a transistorized stripline; a L band (1.2 Ghz) transmitter, S band (2.4 Ghz) receiver and antenna duplex unit which will feed a single omnidirectional antenna array. Tracking will be possible by using the receiver-transmitter as a doppler transponder.

For serious scientific payload work it is absolutely essential that the propulsion system of the flight vehicle be as reliable as possible. It was for this reason that, in 1967, the RRI undertook the development of a highly reliable, moderately high performance solid propellant rocket motor. The motor, designated RR-1, was designed and constructed using surplus military

5-inch diameter rocket motor casings (refs 15 & 16). Up to this time the RRI has flown 55 of these units with only 2 motor failures, which occurred early in the flight test program due to igniter malfunctions. In addition to the BR-1 series motor, the Institute has two other units available for use in student payload programs; the BR-2 motor, higher in thrust than the BR-1; and the SR-1, a relatively low thrust sustainer unit. The characteristics of these propulsion units are summarized in Table IV.

Because all of these motors are made from the same surplus rocket casings, it is relatively simple to couple them together in any combination to form a multi-stage vehicle. So far a BR-2/BR-1 two stage vehicle has reached an altitude of 60,000 feet carrying a 20 pound payload. By adding a SR-1 third stage, computer predictions indicate that it would be possible to send a student payload to altitudes in excess of 150,000. Performance characteristics of these RRI flight vehicles are presented in Table V.

The availability of the RRI series of high performance rocket motors allows the experimenter, who is interested predominately in electronics and payload construction, to concentrate his or her efforts on problems other than the propulsion system. It also eliminates the initial expense of "tooling up" to produce the propulsion systems and developing proper safety facilities which a group of students and their supervisors would encounter if they were to develop systems of similar performance.

The Institute usually manufactures motors at the Perkins Rocket Safety Test Center in lots of 5 to 10 motors at a time to reduce costs. After being loaded with propellant, the motors are inspected for flaws in the propellant grains. After acceptance, the motors are painted, stenciled and packed in special wooden shipping and storage cases. These cases accompany the motors from the magazine to the Smoke Creek Desert Flight Range and are stenciled with appropriate markings in order to comply with Department of Transportation shipping regulations.

Individuals or groups interested in using any of the motors described to fly payloads at the SCDFR or in using any of the PRSTC facilities should contact the Rocket Research Institute, Inc., at the addresses mentioned in the introduction to this paper. These facilities serve a definite need in the extra-curricular educational options available to students and teachers in science motivation activities. The Institute looks forward to hearing from you.

Safety and education have always been of paramount importance in developing all RRI programs, past and present. The primary goal of the Rocket Research Institute, Inc., has been to have the proper static and flight test facilities where students and educators could evaluate the performance of their rocket, flight vehicle, and payload projects. We are well on the way to accomplishing this goal.

TABLE III - PRSTC TEST STAND CAPACITIES

Test Stand	Thrust Capacity	Function	Max Motor Capacity		Motor Test Position
			Diameter	Length	
1	5,000 lbs.	Liquid	10.0 in.	30.0 in.	Horizontal
	22,000 nt.		25.4 cm.	76.2 c.m.	
2	15,000 lbs.	Solid	10.0 in.	72.0 in.	Horizontal
	66,500 nt.		25.4 cm.	182.0 cm.	
3	10,000 lbs.	Solid & Liquid Flight Configuration	36.0 in.	96.0 in.	Vertical or Horizontal
	44,300 nt.		92.0 cm.	244.0 cm.	

TABLE IV - ROCKET MOTORS USED IN RRI/NRSR  
SUPERVISED STUDENT PAYLOAD PROGRAMS

Motor*	Thrust	Duration	Diameter	Length	Empty Weight	Propellant Weight	Loaded Weight
BR-2	6,700 lbs.	1.15 sec.	5.0 in.	64.0 in.	62.0 lbs	40.4 lbs.	105.0 lbs.
	29,800 nt.		12.7 cm.	162.6 cm.	28.2 kg.	18.2 kg.	46.5 kg.
BR-1	4,700 lbs.	.7 sec.	5.0 in.	33.5 in.	45.4 lbs.	21.1 lbs.	66.5 lbs.
	21,000 nt.		12.7 cm.	85.0 cm.	20.5 kg.	9.5 kg.	30.0 kg.
SR-1 MR-1	350 lbs.	8.5 sec.	5.0 in.	22.0 in.	26.0 lbs.	15.0 lbs.	41.0 lbs
	1,550 nt.		12.7 cm.	56.0 cm.	11.8 kg.	6.8 kg.	18.6 kg.

\*All above motors use GALCIT 61-c as propellant (Isp 186 sec.)

TABLE V - PERFORMANCE OF TYPICAL FLIGHT VEHICLES\*  
USED IN RRI/NRSR  
SUPERVISED STUDENT PAYLOAD PROGRAMS

Vehicle	Total Vehicle Weight	Payload Weight	Launch Angle	Maximum Altitude
BR-1	96.0 lbs.	20.0 lbs	85°	25,000 ft.
	43.5 kg.	9.1 kg.		8,230 m.
BR-2	135.0 lbs.	20.0 lbs.	85°	23,000 ft.
	61.2 kg.	9.1 kg.		10,500 m.
SR-1	70.0 lbs.	20.0 lbs.	85°	24,000 ft.
	31.7 kg.	9.1 kg.		7,900 m.
Two Stage BR-2 Booster BR-1 Sustainer	250.0 lbs.	20.0 lbs.	85°	75,000 ft.
	113.0 kg.	9.1 kg.		24,700 m.
Three Stage BR-2 Booster BR-1 2nd Stage SR-1 3rd Stage	300.0 lbs.	20.1 lbs.	95°	125,000 ft.
	136.0 kg.	9.1 kg.		41,100 m.

\*Values tabulated are based on actual data and extrapolated performance from 67 flight tests and from computer predictions.

**STATUS REVIEW OF THE LIQUID ROCKET STATIC TEST RANGE AT IOWA  
STATE UNIVERSITY**  
R.F. Brodsky, Iowa State University, Ames, Iowa, USA (76-243)

The planning of this facility was first reported on by the author at the 24th IAF Congress in Baku in 1973 (refs 17&18). Since that time, much progress has been made and several realities have been faced. To date, four test firings in the water expulsion mode have been at least partially successful; the last (May 1976) being completely successful in that all ten data channels monitored (9 pressure and 1 thrust) have behaved as anticipated. All firings have been completely successful from the safety and environmental standpoint.

The purpose of this program, jointly undertaken by the Aerospace Engineering Department of Iowa State University and supported by NASA Goddard Space Flight Center, was to provide undergraduate students with practical experience in liquid rocketry; to permit the conduct of research in rocket engine technology; and to provide an information center to assist similar efforts at other universities. To this end, NASA provided Aerobee 170 rocket engines, test tankage, ancillary hardware, documentation, and technical advice. For its part, Iowa State agreed to provide a facility, integrate engine firings into the normal propulsion course and laboratory curriculum, utilize the faculty for graduate research as required, and to demonstrate/assist/advise other educational institutions interested in initiating similar programs.

The Aerobee sustainer propulsion system consists of a pressure fed (helium) liquid bipropellant (hypergolic) rocket engine with a regeneratively fuel cooled thrust chamber assembly approximately 19 cm in diameter and 46 cm long. The propellants are inhibited red fuming nitric acid oxidizer and a fuel mixture of 65% aniline and 35% furfuryl alcohol. With normal tankage, running time is approximately one minute. Sea level thrust is 1830 N at a chamber pressure of 22.3 bar, yielding a specific impulse of approximately 200 sec. The initial plan was to mount the system components on a movable cart to facilitate "indoor" maintenance, preparation, and water expulsion firing; while hot firings would occur in an adjacent outdoor concrete block safety igloo. The ultimate facility plan includes many special safety features involved with security; test warning lights and signs; deluge water systems; personnel safety systems and devices; propellant storage, conditioning and handling features, a safety door, remote observation systems; as well as site preparations and public relations planning with nearby (500 meters) residential neighbors. In addition, University-approved environmental impact and safety plans were required to be implemented prior to hot firing.

At the present time, the installation has been only partially completed. The static thrust stand cart is safely operative and instrumentation is complete. Water expulsion firing demonstrations and lectures have been integrated into our laboratory course sequence. The environmental impact report (ref 19), has been completed but is not yet approved. Completion of the final safety plan is being held in abeyance pending our decision on further progress.

The Aerobee water expulsion experiment is one of four programs in the Aerospace Engineering Laboratory course Aero. E. 373. This one credit course is taken during the spring quarter of the Junior year and meets once a week for a three hour period. Two of these meeting periods are assigned to the Aerobee water expulsion problem.

The primary purpose of this laboratory problem is to provide practical experience with a rocket engine which is currently in service. The students receive valuable "hands-on" experience which is directly related to classroom lectures in propulsion, fluid mechanics, instrumentation, etc. By operating in the water expulsion mode, most of the dangers associated with a "live" firing are eliminated, but the actual flow rates and pressure drops are retained.

During the first laboratory period, the students are introduced to the Aerobee rocket system and are given the instructions for the laboratory problem. The history, characteristics, and operation of the rocket are discussed. Individual components of the Aerobee rocket system are examined by the students and their operation is described in detail. These components include: thrust chamber; main propellant valve; pressure regulator; check valve; burst diaphragms; squib valves; solenoid valves; quick disconnects; and pressure transducers. Some of these components, such as the thrust chamber, have been "cut-away" while others have been disassembled for better understanding by the students. The properties and hazards of the propellants are discussed.

The checkout procedure which includes a pressure leak test is explained to the students with the aid of a flow diagram of the Aerobee rocket system. And

finally, the firing sequence is described and a videotape of a previous water expulsion test is shown.

At the end of the first laboratory period, the students are assigned the problem of analytically predicting the thrust which will be achieved during the water expulsion test. In order to predict the thrust (for a given chamber pressure), it is necessary to make a number of simplifying assumptions. The students are required to list all assumptions which they make in their analysis. This provides one of the more important educational aspects of this exercise. During the firing, the thrust is measured experimentally so that a comparison can be made between the student's theoretical prediction and the actual test.

The water expulsion test is conducted during the second laboratory period. The actual preparation and checkout of the rocket is performed by a technician in the interval between the two laboratory periods. However, the students aid the laboratory instructor in calibrating the pressure transducers and load cell immediately prior to the test. During the firing, thrust is recorded in the central control room along with the following pressures: helium tank pressure; regulator pressure; fuel tank pressure; oxidizer tank pressure; fuel line pressure; oxidizer line pressure; fuel jacket inlet pressure; fuel jacket outlet pressure; and chamber pressure. Students monitor the instrumentation in the control room while viewing the firing via a closed circuit TV system. Immediately following the test, the measured thrusts and chamber pressures are given to the students for comparison with their predictions.

The program has been presented to students in the Spring of 1975 and 1976, and was preceded by two trial runs during the summer of 1974. These latter tests were supervised by engineers of the Liquid Rocket Company of the Aerojet-General Corporation, the engine manufacturer and the NASA Goddard's contractor for Aerobee Sounding Rocket System and Launch Operations. Instrumentation, located in the modified bunder "catacomb," measured strategic pressures and thrust and monitored valve operations. The firing sequence was initiated utilizing a special firing panel, with suitable safety interlocks. Readings were recorded by strip chart recording at 50 mm/sec speed. Run times were of the order of 12 seconds utilizing special sub-scale tankage. The peak db noise level perceived in the immediate area of the engine was approximately 110. Thrust measured in the water expulsion mode was about 890 N. Initial helium tank pressure was 105 bars. Water charges simulating the propellants were metered to assure correct ullage in the propellant tanks. All channels were pre-calibrated, and calibrations were checked after the run. Following firing, the complete system is dismantled, inspected, and dried. Prior to re-assembly, new sets of burst diaphragms are installed. All firings have been at least partially successful; the last (May 1976) being completely successful in that all 10 data channels monitored behaved as anticipated. Measured and predicted pressure drops showed reasonable agreement, although calculated vs. measured thrust agreement was poor. It is believed that, in this case, more elegant theory must be utilized to obtain more accurate thrust values. The firings to date have indicated no adverse environmental effects.

The main concern of the environmental impact report, based on normal "live" operation, off-design operation modes, and catastrophic failure modes are: (1) noise, affecting test personnel and observers, and neighboring installations; (2) air quality, predominantly involving exhaust gas composition and disposal; and (3) Propellant disposal, both from normal operation and from spills or catastrophic occurrences (ref 19). Water expulsion testing has not presented any observable problems. Most of the peripheral noise generated is absorbed within the high bay room area of the facility, so that classroom work in the other portion of the building is not disrupted. The facility site is located in a remote non-contiguous portion of the campus at one end of a building which is presently also employed for classrooms and automotive laboratories by the Industrial Education Department. The firing cannot be heard by personnel within the ERDA Research Reactor complex (400 m), and the noise is barely discernable outdoors in the residential area (500 m). Test operational personnel employ ear guards, while student observers are asked to manually close their ears.

The report, however, addresses itself exclusively to live firing situations, and, here noise predictions are difficult to construct due to lack of applicable data. A report covering noise generation by many NASA launch and sounding rocket systems in situ at their launch bases, (ref 20), provided the extremal data listed in reference 19. Although the values are believed to be an order of magnitude (i.e., a decade in db) high, as flat plain terrain with no blocking was assumed, they are sufficiently high to indicate that proper notice of impending firings must be given to those affected. The environ-

mental impact report does not indicate any other serious problems, if proper design attention is paid to handle propellant spills and waste.

It was the ISU Aerospace Department's original plan to proceed at best possible pace to move into a hot firing mode of operation. Since Baku, several factors have lead to second thoughts: (1) The University Physical Plant Department estimates a \$15-20,000 expenditure would be required to convert the present facility into the specified live firing complex mentioned earlier; (2) Two proposals to complete the facility have been made to the National Science Foundation for Undergraduate Scientific Equipment grants, but, to date, neither has been funded. Concern about student safety appears to be a major area of negativism. NASA headquarters organizations (Sounding Rocket Program and Educational Activities offices) have been approached. Again, due to higher priorities, no help has as yet been forthcoming; and (3) The Aerobee Sounding Rocket program is gradually (after 30 years of extra-ordinarily successful work-horse operations) being phased out in favor of newer vehicles. In particular, the problems of the future supply of the special burst diaphragms and the high quality propellants is in question. Although NASA has promised help on these matters within their capabilities and constraints, a heavy financial facility improvement investment is "chancy."

In retrospect, the water expulsion firing problem as now conducted, achieves many of our educational goals. The students become familiar with the actual hardware and procedures associated with the firing of a pressure-fed bi-propellant rocket engine system. Factors lacking, besides the excitement and interest generated by a live firing, are experience in the proper handling and transfer of toxic and "dangerous" propellants, and the ability to make temperature, noise, and exhaust gas measurements, etc. On a graduate level, where we hoped research in simplified sounding rocket thrust vector control systems, combustion instability, injector design, etc., could be conducted under funded contracts or grants, such aims could not be realized. The cost of an individual water expulsion experiment, considering technician time, materials, and helium is roughly \$800; unquestionably live firings would be more expensive, as well as adding environmental and safety precautions to the trade-off matrix.

The present department position on this question is one of "wait and see." Should an obvious research need arise; should we receive encouragement from an agency with funds to help us; or if a well-suited new grant program appears, we will clearly press for facility completion. In the meantime, we believe that we have accomplished several of our and NASA's main goals, and have evolved a somewhat unique educational program that provides much insight and practical experience for all of our students. A color movie depicting the May 1976 firing, a black and white videotape and various slides and pictures of pre- and in-test situations are available on loan from the author.

PROGRESS REPORT ON DEVELOPMENT OF A LIQUID MONOPROPELLANT SOUNDING  
ROCKET AT STATE UNIVERSITY OF NEW YORK (SUNY), BUFFALO  
P. Ramsden, Bell Aerospace Textron, Division of Textron Inc.,  
Buffalo, New York, USA (76-244)

At the 22nd IAF Congress in Brussels, a design of a simple sounding rocket was proposed for development by student groups (ref 21). The vehicle has a structure consisting of a single piece of aluminum alloy tube and the propulsion system uses the liquid monopropellant, propyl nitrate. The technical approach was dictated by safety and reliability requirements which were further discussed in a paper at the 24th IAF Congress in Baku (ref 22).

The basic requirement of the design was to provide aerospace engineering students with practical design and development experience and yet retain the goal of a useful end product. A strong emphasis has been placed on achieving high reliability goals at each phase of development of the components.

Because the purpose of the vehicle is educational, the design evolves to one which is very different from that which would result from a normal commercial design team working to a performance specification. The effect is to produce a very simple basic design of vehicle, but one which is large in relation to its performance.

Since 1971 further studies have been made and practical development has begun at the University of New York at Buffalo. An injector and combustion chamber have been designed and manufactured. The test stand has been designed and tests will be started during the coming academic year. The immediate objectives are to develop a reliable ignition system and to measure performance.

In the academic year 1974-1975 a student group at SUNYAB (State University of New York at Buffalo) made studies which confirmed the feasibility and educational value of the rocket vehicle, which they named "SUBSTAR." A prototype injector and burst disc were made and tested (ref 23). A second group of students took up the project in 1975-76. Up to the present time they have designed and constructed a test chamber and injector for starting tests and performance measurements (ref 24).

The liquid monopropellant propyl nitrate has been chosen for primary propulsion. Solid propellants were avoided because of expensive development and inflexible operation. Liquid bipropellants were avoided because of the unpleasant properties of oxidizers. Also because it requires only one tank, the liquid monopropellant simplifies the structure of the vehicle and the fluid feed system. The basis of the vehicle structure is a single length of aluminum alloy tube 6 inches in diameter. This tube has a pressure closure at the forward end and a pressure bulkhead near the aft end to separate the tank section from the combustion chamber. The extreme aft end of the tube has a closure which incorporates the propulsion nozzle and supports the fins.

The expulsion system operates by simple blowdown. The tank will be filled about 60% full of propellant, the remaining space being pressurized with nitrogen prior to launch. In order to speed up the start sequence, the tank will be prepressurized to 200 lb/in<sup>2</sup> during the vehicle preparation; final pressurization is part of the start sequence immediately prior to launch. At launch, the vehicle will have a tank pressure of approximately 1000 lb/in<sup>2</sup> and a combustion pressure of 600 lb/in<sup>2</sup>. At all-burnt the tank pressure will be down to 300 lb/in<sup>2</sup> with the combustion pressure (and hence thrust) correspondingly reduced.

In order to avoid control valves in the vehicle itself, it is proposed to initiate the start sequence from the igniter. The sequence of events is as follows: (1) Fire igniter; (2) Sense combustion chamber pressure rise and use this pressure to trigger the tank pressurization system; (3) When the tank/combustion pressure is 250 lb/in<sup>2</sup> the burst disc ruptures allowing propellant into the chamber; (4) When the tank pressure reaches 1000 lb/in<sup>2</sup>, withdraw the pressurizing probe; and (5) If at this time there is correct thrust, release the vehicle for launch. This procedure constitutes a fully interlocked starting sequence using pressure signals for the interlocks. Hence the locks can be direct mechanical types without electrical links.

The flight propulsion system requires an injector which will pass 3.2 lb/sec at 400 lb/in<sup>2</sup> and which has good atomization at all pressures down to less than 100 lb/in<sup>2</sup> differential so that good combustion can be maintained to the end of blowdown. The swirl atomizer type of injector was chosen for its good atomization and, to keep the cost low, a design having only three or four large atomizers is planned.

During 1974-75 a prototype atomizer was made and tested. Subsequently five more were tested to assure a design with acceptable flow rate and cone angle. The variables investigated were number of tangential holes and shape of the swirl chamber. The final version has four tangential holes and passes a flow of 0.9 lb/sec at 400 lb/in<sup>2</sup>. This design will be used in the first test firings, though with some modification to the propellant feed to eliminate stagnant pockets. The concern is for the consequences of heat soak back from the combustion chamber, particularly after shutdown. Although the possibility of explosions is not great, the design incorporates separate feed tubes to each tangential hole so that there is no possibility of any low fluid velocities in regions of high heat flux. An aluminum burst disc was developed in 1975 to have a burst pressure of 250 lb/in<sup>2</sup>. The test disc had a spread in burst pressure of + 30 lb/in<sup>2</sup>, which is acceptable. However, before the discs are used in a flight-type firing sequence a large batch of discs will be made and actual mean and standard deviation of burst pressure evaluated. This work has low priority because the discs will not be used in the initial test program.

The design of the firing test rig and its instrumentation depend very much on the location available for conduct of the test. Ideally the tests would be conducted in a place where the basic supporting services like water and electrical power are available, but no such site could be found. Of course, suitable test sites do exist; the principal obstacle to their use is the question of accident liability. Owners are generally not willing to take any risk on a project like this which they do not fully understand and do not directly control. The only solution possible, then, is to conduct the test in a remote place, making all the equipment, instrumentation and power supplies portable. Fortunately, the University at Buffalo owns sufficient land, yet undeveloped and sufficiently far from public highways and buildings to make this solution

a convenient one. A van-mounted electrical generator is available to supply power for operation of valves, preheater and instrumentation. Another vehicle will be used to carry the instrumentation and serve as control center. These vehicles will be parked at a safe distance from the firing bay, out of direct line-of-sight and viewing the test through a large mirror.

The firing stand itself consists of three parts as follows: (1) The safety wall, forming a three-sided bay with open top, constructed of sandbags or a supported earth bank; (2) The anchor frame, comprising deflector plate and structural beams built into the safety wall; and (3) A plate to carry the test chamber, control valves and tank. The first two items will remain on site, the third will be portable so that the experiment can be set up in the laboratory, where major checkout operations like leak checks and flow tests will be performed. This is an important safety feature. Where some assembly of fluid systems has to be completed on site, in relative discomfort, the risk of errors and contamination is much greater.

(In his full text, Mr. Ramsden describes the program for 1976-77 which will include the four phase initial firing tests which have the objective of obtaining experience in the firing procedures through laboratory flow tests and preheat and firing tests at the test site. He also discusses the design of the flight injector following obtaining performance data from the firing tests and the design of the pyrotecnic igniter for the flight program).

The success of the 1976-77 program will pave the way for design of the whole flight propulsion system in the following year, 1978. A detailed time scale has not been worked out, because experience has shown that the progress possible depends too much on individual students who choose to take up the project. To use current jargon, the program must be people-oriented rather than time schedule oriented. It is necessary to have a clear view of the tasks which need to be completed before the vehicle can fly. Beyond that, the program needs to be very flexible, so that a student can choose a work package to suit his particular interest and talents. Obviously, this process runs the risk of bottlenecks when necessary but unexciting tasks remain undone. However, it is expected that when this happens, either the final goal or some exciting intermediate one will be sufficiently close for good publicity to get the work done. Good management by permanent staff who can ensure continuity will see the project through to a successful conclusion.

PIGGY-BACK STUDENT PAYLOADS ON LARGE SOUNDING ROCKETS  
R.G. Moore, Thiokol Astronut Plant, Ogden, Utah, USA (76-246)

It is the purpose of this paper to call attention to the steadily increasing opportunities for "hands-on" participation by young people in the exciting field of aeronautical and astronautical exploration. The other papers in this session deal with the involvement of young people in development and testing of rockets, per se. This paper will deal with student development of scientific and engineering experiment packages for flight in sounding rockets, aircraft and spacecraft.

On January 15, 1976, a Terrier-Malemute sounding rocket was launched from NASA's Wallops Flight Center, Virginia, on a combined Sandia Laboratories/NASA Goddard Space Flight Center engineering test flight. Tucked inconspicuously away in one corner of the 40-cm diameter, 230-cm long, 160-kg Sandia payload was a 5 cm x 10 cm x 15 cm experiment package, which contained, among other things, a 60-gm digital watch and a pair of alkaline "AA" cells. The pulse train from the watch's one-per-second LED firing circuit was connected to a spare subcarrier oscillator in one of the three telemetry transmitters carried on-board the vehicle.

The objective of the experiment was to measure the shift in frequency, if any, in the basic time standard of the watch under the acceleration and deceleration forces to which it would be subject during the rocket vehicle's thrusting, atmospheric exiting and re-entry phases, and under the zero gravity conditions it would experience during the exo-atmospheric coasting phase of the rocket's flight. The experiment was carried out by the Utah Section of the American Institute of Aeronautics and Astronautics on behalf of three North Ogden, Utah, junior high school students, John Lundstedt, Bruce Moore, and Doug Fulmer. The watch was donated by the President of the Greater Ogden Chamber of Commerce, Mr. Dee Brockman.

After reducing the telemetry and radar data from the flight, the boys determined that no measurable shift in watch oscillator frequency had occurred over the longitudinal acceleration range from -5 g's to +24 g's and they

further found that the exposure to zero g conditions for eight minutes had likewise no measurable effect on the oscillator frequency. They therefore concluded that a digital time standard would be a likely candidate to replace the electro-mechanical timing devices traditionally utilized for programming purposes in sounding rockets. The experiment was a trophy winner at the local and regional junior high school bicentennial science fairs, and it won the 1976 aerospace award of the Utah Civil Air Patrol.

During two weeks of April of 1975, a seventeen-year-old Beverly Hills, California, high school student named David Paige flew a series of sorties aboard the NASA Galileo II, a Convair 990 flying laboratory jet aircraft, from Alaska to Greenland, making photographs in polarized light for the purpose of discriminating between clouds and snow, and between ice floes and water, by remote sensing techniques. David earned his seat aboard the aircraft by submitting the winning scientific proposal in a competition conducted by Mike Donahoe, Educational Programs Officer at NASA's Ames Research Center. David's classmates at Beverly Hills High School donated the money for his subsistence at Eielson Air Force Base in Alaska and Thule Air Force Base in Greenland during his tour. Edward Smith, President of the California State Science Teacher's Association was David's faculty advisor for this experiment.

For the past fifteen years, Project OSCAR, Inc., the Radio Amateur Satellite Corporation (AMSAT), and the American Radio Relay League (ARRL) have cooperated to provide satellites that can be used for amateur radio communication and experimentation by suitably equipped amateur radio stations throughout the world. The well-known Orbiting Satellite Carrying Amateur Radio (OSCAR) series of satellites is the product of this cooperation. Funding for these internationally designed and built satellites has come from member dues and donations, and transportation to orbit has been supplied on a space-available no-cost basis by the U.S. Airforce and NASA. Of the seven satellites launched in this series, AMSAT-OSCAR 6 and AMSAT-OSCAR 7 are still operational and in daily international use. A curriculum supplement has been developed for classroom use of these satellites, with emphasis on space science, physics, mathematics, astronomy, communications and electronics by educators at the Talcott Mountain Science Center for ARRL and AMSAT.

During 1972, NASA Headquarters conducted a nationwide competition for student experiments to be carried aboard the Skylab Orbital Workshop. Twenty-five experiments in all were selected, nineteen of which actually flew. These experiments were placed in orbit on May 14, 1973 and were serviced at various times over the next nine months by Skylab 2, 3, and 4 crews. Results from the student experiments will soon be made available in a report being published by NASA's Marshall Space Flight Center.

Now to the future. The AIAA has made tentative arrangements with NASA's Goddard Space Flight Center to fly selected student scientific and engineering experiments, on a space-available, non-interference basis, on NASA sounding rockets from the Wallops Flight Center in Virginia, the White Sands Missile Range in New Mexico, and, where indicated by the nature of the experiment, from sites in other parts of the globe. Proposals should be directed to: Director of Student Activities, American Institute of Aeronautics and Astronautics, 1290 Avenue of the Americas, New York, N.Y. 10019. The AIAA will communicate with the Section of the AIAA located near the student and with appropriate universities engaged in sounding rocket research in the general field of the proposed project for advice and assistance in carrying out the experiment.

NASA's Ames Research Center may consider follow-on student experiments for the Galileo II aircraft, if sufficiently worthwhile proposals are submitted. Proposals should be directed to Mr. B. Michael Donahoe, Educational Programs Officer, Ames Research Center, National Aeronautics and Space Administration, Mountain View, California 94035.

AMSAT is planning an ambitious new experiment, in which a spacecraft will be placed in a highly elliptical orbit, with its apogee located 36,000 km above the North Pole, so as to permit amateur communications for a period of several hours per day between any two points in the northern hemisphere. AMSAT will supply not only the basic spacecraft, but the kick stage as well. Dr. Perry Klein, AMSAT's President, and Mr. Jan King, AMSAT-OSCAR Spacecraft Project Manager, are considering the incorporation of student-supplied instruments into some of the spacecraft for conducting experiments in magnetospheric physics and astronomy. Inquiries and proposals should be sent to the Radio Amateur Satellite Corporation, P.O. Box 27, Washington, D.C. 20044.

As a follow-on to its highly successful Skylab Student Project, NASA, with the enthusiastic support from the Federation of Americans Supporting Science and Technology (FAAST), is now considering a program to solicit student proposals for experiments to be flown on the Space Shuttle Orbiter. Selections will be made in both a high school category and a college and university category. Proposals in a broad spectrum of science and engineering will be encouraged. The coordinator for the high school program is Mr. Robert Tiemann, Educational Programs Division, NASA, Washington, D.C. 20546. Coordinator for the college and university program is Mr. Charles Carter, Office of University Affairs, NASA, Washington, D.C. 20546.

As should be clearly evident from the foregoing, opportunities for student scientific and engineering experimentation in aeronautics and astronautics are plentiful and increasing. The day may not be impossibly far off for Apollo Astronaut Harrison Schmitt's University in Space to become a reality. After all, if the Galileo II can serve as a flying laboratory for the gifted student, can the Enterprise be far behind?

#### REFERENCES

1. B.P. Preece and T. Treger, "Is it Safe for Underachievers to Fire Rockets?" Paper 74-072, XXVth Congress, International Astronautical Federation, Amsterdam, 5 October 1974.
2. G.M. Gregorek, "International Model Rocket Engine Standards," in Space Activity, Impact on Science and Technology; Proceedings of the XXIVth International Astronautical Congress (Oxford & New York: Pergamon Press, 1976), pp. 407-408.
3. G.M. Gregorek, "International Model Rocket Static Tests," Paper 75-088, XXVI Congress, International Astronautical Federation, Lisbon, 27 September 1975.
4. G.S. James, "The Rocket Research Institute and the International Geophysical Year," Fusées et Recherche Aéronautique, vol. 2, no. 2, (May 1957). pp. 125-131.
5. J. W. Salter, G.S. James, and D. Starrett "A Liquid Propellant Rocket for Group Training," Paper 438-57, American Rocket Society Semi-Annual Meeting, San Francisco, California, 10-13 June 1957.
6. "Diagram of SPARK I Propulsion System," Aviation Week, 8 July 1957, p. 84.
7. A.J. Zaehringer, "Propulsion Engineering; Now a Rocket Engine for Students," Missiles and Rockets, September 1957, p. 89.
8. "Rocket Researchers Registering Students," Aviation Week, 27 January 1958, p. 85.
9. G.S. James, D.L. Scharosch, and R.K. James, Student Rocket Activities, A Guide for Teachers to Supplement the Film Strip, Don't Build That Rocket Alone, Contract No. NAS 7-347, for the NASA Western Support Office, prepared by the National Rocket Safety Registry Program, RRI, Inc., Glendale, California, Current Edition, 1966.
10. J. Brown, "Sacramento Rocketry Students Avoid Use of Word "Amateur" at Test Center," The Sacramento Bee, 10 September 1967.
11. "Young Rocket Builders Hard at Work on Project," Aerojet Booster, Northern Edition, 29 January 1968, p. 4.
12. "W. Blum, "Youth Blasts Off," Sunday Examiner and Chronicle, California Living Section (San Francisco), 20 October 1968, pp. 26-27.
13. G.S. James, L.M. Pearce, D.E. Cantey, R. Woolf, D.F. Mika, and C. Piper, "Rocket Industry Cooperation with Supervised Youth Rocketry Programs," in Organizing Space Activities for World Needs, ed. E.A. Steinhoff (Oxford & New York: Pergamon Press, 1971), pp. 399-428.
14. R.C. Truax, "Hot Water Rockets, Development and Applications," in Proceedings of the XXth International Astronautical Congress, eds. M. Lunc, P. Contensou, G.N. Doboshin, and W.F. Hilton, (Oxford, New York and Warsaw: Pergamon Press and PWN-Polish Scientific Publishers, 1972), pp. 971-984.

15. See pp. 419-427 of Reference 13.
16. G.S. James, C. Piper, J. Billheimer, and J. Christensen, "The BR-1 Rocket for the Safe Supervised Launching of Student Payloads," in Astronautical Research 1971, eds. L.G. Napolitano, P. Contensou, and W.F. Hilton, (Dordrecht & Boston: D. Reidel, 1973), pp. 515-519.
17. R.F. Brodsky, "A University Liquid Rocket Static Test Range," Iowa State University Engineering Research Institute preprint ERI-73183, Ames, Iowa, August 1973.
18. R.F. Brodsky, "A University Liquid Rocket Static Test Range," in Space Activity, Impact on Science and Technology; Proceedings of the XXIVth International Astronautical Congress, (Oxford & New York: Pergamon Press, 1976), pp. 401-404.
19. F.J. Kurtenback, Environmental Impact Statement for the Iowa State University Liquid Rocket Static Firing Facility, Ames, Iowa, June 1975.
20. Final Environmental Impact Statement, NASA, Office of Space Science, Sounding Rocket Program, Washington, D.C., July 1973.
21. P. Ramsden, "A Simple Sounding Rocket for Educational Purposes," in Astronautical Research 1971, eds. L.G. Napolitano, P. Contensou, and W.F. Hilton, (Dordrecht & Boston: D. Reidel, 1973). pp. 503-506.
22. P. Ramsden, "Rocket Vehicle Safety During Development and Operational Use," in Space Activity, Impact on Science and Technology, Proceedings of the XXIVth International Astronautical Congress, (Oxford & New York: Pergamon Press, 1976), pp. 395-398.
23. J. R. Wood, "Project SUBSTAR: An Educational Student Rocket Program," AIAA Northeast Regional Conference, Rutgers University, April 1975.
24. M. J. Pazden and J.E. Ayer, "The Design of a Liquid Propellant Rocket Engine," Student Project, State University of New York at Buffalo, April 1976.

# MODERN TRANSPONDER TECHNOLOGY FOR BASELINE DESIGNS OF DATA PROCESSING AND SWITCHING COMMUNICATION SATELLITES

C. Louis Cuccia

Aeronutronic Ford, 3939 Fabian Way, Palo Alto, California

## Abstract

Heavy route communication satellites for the 1980's will employ spot-beam down-links to key communication switching centers and will process and route information transmitted up-link on-board the satellite to the antennas for transmission to various destinations. Such a satellite will function as a "switch board in the sky" and will primarily use time-multiplexed signal techniques such as TDMA in combination with switched transponders or switched beams to perform the routing functions. Many concepts have been developed during the last decade for ways that a SS-TDMA satellite can be switched, including on-board translation, on-board regeneration and store and forward modes of operation. This paper will review the types of SS-TDMA switching satellite systems proposed and the new component technologies which can now make these satellites technologically possible.

## Introduction

As pointed out in 1974 by W. Schmidt<sup>(1)</sup>, "for satellite communications in the 1980's, there is a strong trend toward wide band communications packages utilizing a multiplicity of high power beams ... a disadvantage, however, is the burden this technology places on the interconnection flexibility of the satellite".

This paper addresses the new advances in technology which now make possible serious consideration of advanced switching multiple-beam satellite designs using new supporting technological development, based on actual experimental results with high-performance hardware. Table 1 lists the subsystems and components and the alternative approaches which form the building blocks of multiple-beam satellites; the principle candidate technologies in areas of Table 1 will be the subject of discussions in the paragraphs to follow. Table 1 lists the widest possible range of subsystems, from antennas to switches to modulators, etc. It is significant that many of these subsystems represent developments which in many cases did not even exist as other than concepts as recently as only three years ago.

The technological design of the switched multiple beam communication satellite is therefore a true product of the most recent thinking and innovation - worldwide - in the late 1970's and provides the logical springboard to the high capacity communication satellites required in the 1980's.

## SS-TDMA Satellites

Many conferences and publications<sup>(1)-(8)</sup> during the last decade have dealt with the various aspects of satellite-switched TDMA (SS-TDMA) satellites. This effort has resulted in bringing into focus the techniques of on-board switching of TDMA bursts to interconnect and route time multiplexed signals between a variety of users illuminated by the

various beams. Information routing, now common practice in terrestrial communications, will enable the SS-TDMA satellite to provide a logical solution to the fulfillment of future needs in national and worldwide communications.

Fig. 1 shows a basic SS-TDMA satellite system illustrating the use of isolated beams to a variety of users. On-board routing via a switch matrix is employed to provide an interconnect between these users. Fig. 2 shows a detail of one version of this system by Schmidt and Cooperman<sup>(2)</sup> which shows the use of a matrix system which serves to interconnect a set of receivers and transmitters. This concept provides for dedicated antennas to specific areas and yields a suitable system solution for the recent discussions on SS-TDMA by G. Dill, et al.<sup>(7)</sup> at ICC-76 where he showed how an 8 x 8 matrix switch could serve a system involving 11 satellite beams comprising two spot beams at 11/14 GHz using right hand circular polarization, five zone beams and one global beam using left hand circular polarization in the 4/6 GHz spectrum, and two zone beams and one global beam using right hand circular polarization in the 4/6 GHz spectrum. In his paper, Dill pointed out how a hypothetical Atlantic primary satellite launched in 1985 could use three 80 MHz slots operated in the SS-TDMA mode to accommodate the traffic requirements to the end of 1993.

As Intelsat with Comsat Labs were planning future designs to meet the needs of the late 1980's and 1990's, other satellite users were also developing concepts and technologies for multiple beam information-routing or beam steering satellites.

Lincoln Laboratories had already made major advances in multiple beam antennas using multiple feed lens antennas; this later formed the basis of innovative designs of DSCS III which was postulated for using multiple beam antennas providing around 20 transmit beams and 60 receive beams. Recently at the MTT International Microwave Symposium in Cherry Hill, N.J., Dr. D. Reudink of Bell Telephone Laboratories discussed a hypothetical hybrid switched-beam and switched-transponder system for serving more than a hundred isolated areas. The SS-TDMA transponder and antenna concept of Reudink is shown in Fig. 3.

Many technological developments were initiated to make these various SS-TDMA or steered-beam satellites possible. In addition to the new technologies which were being developed by the burgeoning telecommunications industry (FET's, QPSK, modems, etc.) and the development of TDMA hardware in many parts of the world for international (Intelsat) and domestic (Telesat) use, specific SS-TDMA building blocks have now been brought to a significant point of realization. These include lens antennas, switching matrices, space-paramps, space qualified FET's and solid state power amplifiers from Intelsat via Comsat Labs; lens antennas and power TWTs from the Air Force Space and Missile Support Organization (SAMSO), matrix switching and transponder component developments via KDD in Japan,

and from BTL, many new developments, including multiple feed antennas, multi-level TWTA, matrix switches and near-gigabit TDMA circuitry. This paper will highlight these developments and other innovative subsystems which advance the practicability of a SS-TDMA multiple beam communication satellite.

#### Types of SS-TDMA Satellites

In 1974, W. Schmidt<sup>(5)</sup> succinctly described the types and modes of SS-TDMA communication satellites which can be built according to three distinct types, i.e.:

- Transponder switched
- Antenna beam switched
- Hybrid transponder and antenna beam switched

Transponder-switched TDMA uses fixed beam antennas, and in what is essentially a preassigned arrangement, uses a matrix switch to interconnect the various receive and transmit antennas. The beam-switched TDMA, on the other hand, makes use of one or more multiple beam antennas whose beams can be quickly redirected; in a more advanced mode, power sharing between various transmit beams can be altered depending on the amount of traffic or the link architecture involved. In a hybrid system, both transponder and beam switching are employed. The Reudink concept of Fig. 3 is an example of this hybrid system with the antenna structures shown designed for beam steering based on action of the co-phase and conjugate circuits.

Spatial frequency reuse provided by a multiple beam satellite can be stated in terms of "conservation of footprint flux" in order to optimally provide satellite radiated power to only the area or user desired instead of dispersing satellite power, in much the same way that a global beam illuminates ocean areas where no earth terminals are involved, ultimately requiring a higher earth terminal G/T (and therefore cost) to serve user areas. The hybrid SS-TDMA with control of effective radiated power from each of the various transmit beams is a direct answer to the conservation of footprint flux.

The SS-TDMA satellite can operate in two modes of operation: (1) translating SS-TDMA, and (2) regenerative SS-TDMA. In translating SS-TDMA, the incoming signals are not demodulated but retained in modulated carrier form to be rerouted to desired antennas via the microwave matrix switch. The regenerative SS-TDMA satellite, originally proposed by K. Nosaka and T. Muratani<sup>(3)</sup> provides for on-board demodulation and remodulation to correct for intersymbol interference introduced in the uplink, particularly when the uplink is power limited due to low earth terminal power, low satellite G/T or when extremely high data rates and satellite transponder bandwidth make the energy per bit minimal. The regenerative SS-TDMA satellite then provides two alternative species: (1) one in which the demod-remod function is used primarily to correct for uplink intersymbol interference and also to provide a point to permit the introduction of on-board data processing, store and forward, or additional information such as a TDMA start-of-frame synchronizing pulse. This species would use a microwave frequency matrix switch following the demod-remod, and (2) one in which each incoming carrier is demodulated, additional data introduced

or store and forward instituted; the various de-modulated and reformatted data streams are then rerouted via an LSI logic switch matrix to various modulators which drive the directive antenna complexes. This mode is illustrated in one form by Fig. 3.

#### The SS-TDMA Link

The effectiveness of SS-TDMA satellite to handle data must be determined from a consideration of the entire link in which all data filters, rf filters, nonlinear devices such as TWTA and solid state power amplifiers contribute bandwidth limiting in the case of the filters and AM-to-PM and AM-to-AM conversion in the case of the nonlinear devices. These considerations include the modulators and up-link hardware and the downlink and demodulators of each earth terminal in addition to the satellite transponder.

In the translating transponder version of a SS-TDMA satellite, considerations of the modulation technique; i.e., BPSK, QPSK, SQPSK, or FM-CPSK (FFSK) are made with the extent of bandwidth limiting BT where when BT = 2, the entire main lobe of, say, a QPSK spectrum exactly fits the filter passband, and the AM-to-PM and AM-to-AM factors based on the modeling of an actual TWI or solid state amplifier including choice of operating point on the power-in to power-out curve. Many scientists have studied this link model in the U.S., Japan, and Europe. Table 2 includes some results<sup>(10-11)</sup> summarizing system  $E_b/N_0$  degradation from theory for two choices of TWI (Hughes 261-H) operating point for the heavily band-limited case (BT = 1) and the non-band-limited case (BT = 2) for the faces above listed modulation techniques. It is evident that link degradation from one to three dB can be expected for the non-band-limited case, and that for bandwidth limiting, only FM-CPSK (FFSK) avoids rapid deterioration of link signal to noise ratio with increase in band-limiting.

Normally, down links are link margin limited with the up link less margin limited but contributing significant link degradation by the HPA noise, intermodulation distortion and AM-to-PM conversion. However, plans to move to the 20/30 GHz frequency bands with the availability of 2.5 GHz bandwidths now introduces the probability of significant technical problems in providing a viable up-link for the translating SS-TDMA satellite. Accordingly, J. Chiao and F. Chethik<sup>(12)</sup> have modeled the link of a QPSK and FFSK satellite system for both the translating and regenerative repeater modes of operation. Table 3 and Fig. 3 are derived from their work, and while their model is very conservative and even pessimistic since it does not optimize the point of backoff of the TWI, their results provide very key and pertinent comparisons between translating and regenerative links:

- For low uplink  $E_b/N_0$  in the 10 dB range, the translating repeater system is limited to very poor bit error rate performance, poorer than  $10^{-3}$ . This is not surprising since a perfect link with no SNR degradation factors and an uplink  $E_b/N_0$  of 10 dB would not exceed  $10^{-5}$  bit error rate.
- For low uplink  $E_b/N_0 = 10$  dB, the translating repeater restores the link BER capability to the  $10^{-4}$  to  $10^{-6}$  range, even with a down-link  $E_b/N_0$  of 10 dB, depending on the

amount of intersymbol interference experienced in both links.

- For larger uplink  $E_b/N_0 = 16$  dB, then it is the downlink  $E_b/N_0$  which limits the system BER performance.
- For uplink and downlink  $E_b/N_0$  values which are not severely BER-limiting, the regenerative repeater offers 2-5 dB improvement in system performance. However, this improvement is optimum for theoretical equipment and other considerations in the demod-remod process may make it difficult to achieve any improvement at all.
- The regenerative repeater is more tolerant of intersymbol interference than the translating repeater which implies a larger dynamic range and provides a better coherency for demodulation.

#### Multi-Beam Spacecraft Antennas

The early architects<sup>(1)-(4)</sup> of SS-TDMA satellites discussed primarily switched transponders using switch matrices to interconnect various antennas of a spacecraft antenna "farm" since the art of multi-beam antenna had not yet been developed. Many have now been reduced to actual operating hardware. These paragraphs will review the principle multi-beam antenna achievements based on the antenna types listed in Table 4.

Such multiple beam antennas provide the vital function of providing at least 30 dB isolation between beams. This would be virtually impossible with a standard parabolic antenna with multiple horns at its focal point due to the blockage problem. They also provide means to simultaneously provide space diversity, polarization diversity, variable beam shape, and directive beam movement.

Figs. 4 through 8 show the variety of multi-beam antennas which have been developed by a variety of companies in the U.S. The constrained lens of Fig. 4 provides ray-paths constrained by an RF transmission line interconnecting small pickup and reradiating elements. This system was designed by W. Scott and C. C. Han of Aeronutronic Ford under contract to Comsat Labs for 4/6 GHz. They designed a lens five feet in diameter with five foot focal length using 396 TEM transmission line cards in the TEM lens and used a 19-element feed cluster which could be connected in with a 7-way (6 GHz) or 13-way (4 GHz) power divider. For a beam scan over the earth's FOV (0 to 8.6°), the equivalent on earth side lobes remained below -30 dB.

The waveguide lens antenna pioneered at Lincoln Laboratories by Dion and Ricardi<sup>(13)</sup> and shown in Fig. 5 has been the subject of intensive investigative effort at Aeronutronic Ford, G.E., Lockheed, Hughes, at X-band (7/8 GHz) due to the impending development of the DSCS III satellite. In the Aeronutronic Ford antenna, the lens is a matrix of square hollow metallic waveguides forming a metallic "egg crate" structure in a 46 inch diameter using 1528 waveguide cells. This lens antenna has a usable bandwidth of 5.5% and was excited by a 61-feed array, and nulls of 20 dB could be produced between adjacent beams.

The mechanism of gain is not as apparent in a lens antenna as it is in a large aperture reflector antenna. The various horn feeds illuminate a portion of one side of the lens which then focuses this energy into a discrete beam in which gain is derived. In the Aeronutronic Ford 4/6 GHz TEM lens antenna, above, 19-20 dB gain was readily obtained with an earth coverage beam, with correspondingly increased gain for smaller footprints yielding in excess of 25 dB gain for a zone footprint and in excess of 30 dB for a spot footprint.

Multiple-feed horns illuminating a single parabolic reflector for multibeam operation, with avoidance of the blockage caused deterioration of adjacent beam isolation, have lately been given considerable consideration. Fig. 6 shows a simple offset fed multiple beam antenna which will be used by Aeronutronic Ford for Intelsat V. This antenna requires considerably tighter control of individual shaped beams necessary to maintain low axial ratios (under 0.75 dB) to achieve at least 27 dB isolation between beams. Aeronutronic Ford has built a 9-GHz (3 ft. diameter) scale model of this C-band antenna. Phase and amplitudes for the 48-horn feed array used were determined by computer optimization to yield the desired coverage pattern.

Fig. 7 shows a multibeam reflector antenna using a novel means of minimizing blockage devised by Turrin of BTL wherein he extended the feed-horns through holes in an auxiliary plane reflector thus eliminating most of the support and feed network structures from the blockage region. His design was for a spherical reflector accommodating six simultaneous beams pointing within a 13° area to cover ground terminals from Hawaii to Puerto Rico for use at 20 and 30 GHz.

The phased array, too, has been the subject of significant effort in development for spacecraft following the outstanding development of ground-commanded spacecraft adaptive antenna arrays by J. Smith and P. Sielman of AIL (ITC, 1973). Recently, Hughes designed a multibeam purpose Armed Forces satellite (SAMSO TR No. 74-71) to position 10 to 30 simultaneous beams anywhere on earth from synchronous altitudes. This array was designed for 91 elements in a 5-foot diameter with 2 degree beamwidth and 40 dB gain on axis. The array was designed to use 10-watt TWT beam and to use FET amplifiers at each receive element. This design estimated that a 10-beam 5-foot array with a prime power requirement of 45 kw would weigh over 700 pounds and provide a net radiated power of only 100 watts.

#### Spacecraft G/T and LNA

Spacecraft sensitivity is dependent upon its Figure of Merit G/T which relates the antenna gain  $G$  in dB to the system noise temperature  $T$  in dB which is derived from the antenna noise temperature which is largely the earth temperature since the antenna is illuminated by the warm earth, i.e.,  $\approx 330^{\circ}\text{K}$ , plus the feed or feeder losses, plus the receiver noise temperature. The antenna gains will range from 30 to 40 dB depending on spot size and frequency, the feeder loss can be a matter of a few tenths of a dB ( $7^{\circ}\text{K}$  per 0.1 dB loss) but can be large for a feeder network, and the receiver noise temperature will be dependent on the LNA (low noise amplifier)<sup>(17)-(21)</sup> which can range from as low as  $50^{\circ}\text{K}$  in C-band to  $300\text{-}400^{\circ}\text{K}$  in Ka-band for a paramp;

from 2.5 to 6 dB noise figure for a FET amplifier; and from 3.5 dB to 8 dB for a TDA. If a mixer is used, then the system noise figure will be determined by the mixer conversion loss (3.5 dB to 6 dB) plus the noise figure of the transponder post amplifier (2.5-6 dB). Thus, it is evident that the G/T which determines the received C/N in the spacecraft and therefore its sensitivity, will not be grossly influenced by the use of FET's, TDA's or even Schottky barrier mixers with 3.5 dB conversion loss operating into a 3 dB noise figure post amplifier. However, the paramp(17)-(18) with its 1-2 dB noise figure capability will provide almost a 3-5 dB improvement in G/T which can yield substantial increase in data capacity or reduction in required earth terminal EIRP.

The TDA, despite problems experienced in early Intelsat satellites has been the LNA work horse of more modern communication satellites and will be used as the 6 GHz and 15 GHz LNA's by Aeronutronic Ford in Intelsat V. The FET is becoming a prominent contender for spacecraft low noise mixer post-amplifiers and IF amplifiers and is used in the Canadian CTS satellite at 12 GHz<sup>(21)</sup> and will be used as the first IF amplifier stage at 2.5-5 GHz for the 30/18 GHz transponders being built in the Japan Communication Satellite (CS) by Aeronutronic Ford.

The spacecraft paramp - once the butt of scorn and ridicule as a modern "Peck's bad boy" when klystron pumps were used, has become a very stable spacecraft device thanks to the use of Gunn diode pumps in the 50-60 GHz range with MTBF's far in excess of 100,000 hrs. This bore out the early inspiration and effort of the late Pio Dalla Mura of NASA GSFC who funded numerous spacecraft paramp developments at 14 GHz, including the AIL paramp of Fig. 11 which was designed by Kramer, Leeper and Whelehan and which provides a noise temperature as low as 120°K. Along with this development came the development of a 14 GHz paramp with a 300°K noise figure at GTE Telecommunications in Italy by Dr. F. Ambrosio<sup>(19)</sup> which is presently flying in the Canadian CTS.

The FET LNA can be expected to play a prominent role as the partner to the feed horn of a multiple feed beam forming network to offset the ravages of feeder loss on G/T. Also the FET noise temperature can be greatly reduced by cooling to low ambient temperatures. C. Leichti has reduced the noise figure of a 12 GHz FET amplifier from 5.5 dB to 2 dB by cooling the FET amplifier to 40°K.

In the space environment, it may become expedient to mount the FET amplifier directly on the feed horn under a sun shield and use a small infrared Cassegrain antenna to radiate FET amplifier heat into space to create a 90-100°K environment which will make the FET amplifier almost the equivalent of an uncooled paramp in noise temperature performance.

#### The SS-TDMA Switch-Matrix Systems

After the various received signals are amplified by the satellite receivers, then the three modes of operation represented in Fig. 12 provide alternatives to SS-TDMA design. Fig. 12 shows how each receiver is connected to a port of the microwave matrix switch to be routed to the appropriate trans-

mitter. This follows from the Schmidt/Cooperman system of Fig. 2. Figures 12b and 12c, involve demodulation of each received carrier; in Fig. 12b, the demodulated data directly remodulates a carrier with the regenerated carrier then applied to its port of a microwave matrix switch for its routing; this arrangement provides the basic advantages of a regenerative transponder over the translating transponder of Fig. 12a.

The circuit of Fig. 12c involves routing the demodulated data to an appropriate remodulation/transmitter complex using a baseband matrix switch. This system not only provides the advantages of data regeneration, but also allows the uses of certain matrix switch and modulator technologies which can materially contribute to overall SS-TDMA switched-beam satellite design and which will be discussed in the following paragraphs.

#### Demodulator - Remodulator Circuits

Modern digital terrestrial radio repeaters use the technique of demodulation, regeneration and remodulation of QPSK data streams. These repeaters operate at data rates from 40 Mb/s in Canada to 120 Mb/s in Great Britain, to 274 Mb/s in the U.S., to 405 Mb/s in Japan. These repeaters are for continuous QPSK transmission and demonstrate the reliability of the demod-remod function in remote and often inaccessible locations. Of special interest is the 800 Mb/s QPSK repeater for the Japan mm-wave guided waveguide system which was designed for highly reliable operation by S. Seki and Dr. K. Myauchi of the Japan NTT-ECL.

For burst transmission of QPSK the problems of demodulation and remodulation are compounded by the need to resynchronize the carrier phase and data clock during each burst period. This has led to a wealth of innovation due originally to the impetus of the Comsat-led developments for the Intelsat TDMA requirements, and more recently, for the domestic TDMA system developed for Canada by Telstar. Also long term requirements by AT&T have led to the funding of efforts at TRW to study the problems of extremely high data rate TDMA in a routing system.

Fig. 13 shows a basic spacecraft QPSK demodulator-remodulator (demod-remod) following the Nosaka-Muratai PSK approach. This circuit includes carrier reconstruction, clock recovery, decoding and encoding, and branch and insert points in which data processing or bit insertion can be accomplished.

Most subsystems of the demod-remod of Fig. 13 are now fairly well known but the carrier reconstruction loop bears critical discussion because each burst will require carrier reconstruction indigenous to that burst for QPSK demodulation. Phase locked loop carrier reconstruction loops designed for continuous wave QPSK transmission are difficult to use for burst transmission due to residual phase error, resulting in a unique area of technology which has been developed for burst QPSK carrier reconstruction for TDMA using a 60-bit word length QPSK reference phase in a preamble preceding the burst.

The reference phase transmission can be used to produce a reference carrier by each of several techniques. One is to use a X4 multiplier circuit as shown in Figures 14 and 15 in association with

a ringing or very high Q tank circuit to develop the reference carrier. The ingenious tracking filter of Fig. 16, following the multiplier, is an advanced version of this circuit which was developed by S. Yokoyama, et al., at NEC in Japan and which is used in the TELSAT TDMA.

Fig. 17 shows yet another type of reference carrier generator using a non-PLO (phase lock oscillator) using a back-to-back demodulator and remodulator which was developed by Gardiner, Lopriore, and Lundquist at ESTEC in Holland for use with the OTS satellite TDMA systems.

Other methods are being developed for synchronization, including the use of unique pseudo-random code words in the preamble for DCPSK detection by Dr. B. Ekstrom of AEG-Telefunken, the use of an RF PSK regenerator as shown in Fig. 18 by M. Hata in Japan, and the total elimination of preambles for carrier synchronization at near 1-Gbps rate and the use of the technique of determining the time location of the first bit in each burst and readjusting oscillator phase depending on whether slippage or advance-in-time has occurred.

#### Switch Matrix Technology

Schmidt and Cooperman provided first concepts<sup>(2)</sup> in 1973 of a transponder switched satellite using a switch matrix from their work at Comsat Labs. This was followed by Mr. Cooperman funding a 16x16 switch matrix development<sup>(29)</sup> to Thomson-CSF and a distribution control unit<sup>(31)</sup> to Intertechniques, both in France. At the same time, work was started on an 8x8 switch matrix in Japan at KDD and Fujitsu by M. Yamaguchi. In the U.S., BTL funded a switch matrix at TRW as a part of AT&T advanced planning for future satellite design and a significant switch matrix technology developed.

Actually, switches in spacecraft are by no means new. Aeronutronic Ford has logged hundreds of thousands of hours of operation in space of special SP2T and SP4T PIN diode switches to despin the UHF antenna of the SMS satellites and as power switches for the S-band antenna feed of the ATS-6 satellite. Table 6 lists the characteristics of the ATS-6 switches.

Two types of switch matrix circuits, capable of providing 50 dB isolation, will be described here; the matrix switch using Wilkinson splitter-combiner circuits (Fig. 1) following the work of Rozec and Assal<sup>(29)</sup> and the B-element rearrangeable switch matrix of Yamaguchi, et al.,<sup>(31-32)</sup>. Both use PIN diodes, represent advanced switch design, use microwave integrated circuit techniques, and have been designed for redundancy operation. The paper by Dr. T. Muratani<sup>(9)</sup> is particularly noteworthy in dealing with the redundancy problem.

The splitter-combiner switch matrix of Fig. 19 interconnects sets of splitters and combiners to provide the capability of interconnecting any one of N inputs to N outputs. The power splitters and combiners can use Wilkinson techniques, shown in Fig. 20 since each splitter handles the same signal to its output ports, while the combiner will only have one signal input at a time.

The splitter-divider circuit shows one circuit developed by Aeronutronic Ford using the PIN diode switch complex of Fig. 20. This circuit is easily

adaptable to MIC techniques and requires only 0-20 mA per PIN diode to provide the connection or isolation required.

Fig. 22 shows the PIN diode switch developed by X. Rozec using two PIN diodes as shunt elements in a low-pass filter arrangement. This switch provides both controllable insertion losses and control of LP filter cutoff frequency which develops the 50 dB isolation required when the switch is off. It responds to 0 to 6 volts applied to a driver.

The overall switch matrix of Rozec and Assal was a box with 16 inputs and 16 outputs, had a small size 10.5 x 12.1 x 12.1 cm, had a light weight, 2.3 kg, low power consumption of 8.5 watts, and had a switching speed of less than 50 ns with less than 5 ns of jitter. This switch matrix had 256 switches designed for a 500 MHz band centered at 3.95 GHz, had a transmission loss between 25.6 and 28.8 dB and RF isolation in the off mode greater than 50 dB.

As pointed out in Table 7, other switching devices can be used. Of special interest is the doubly balanced modulator switch of Fig. 23 which uses a "quad" of Schottky barrier diodes with isolation of 40-50 dB (Fig. 24) with zero voltage bias or 2-3 dB transmission loss with either 0.7 or -0.7 volt applied to the diodes. Such a switch follows from extensive mixer developments with high reliability and is basically self-redundant. Fig. 25 shows a high Ku-band MIC switch using a 3-dB hybrid with PIN diodes developed for Aeronutronic Ford illustrating present 18 GHz switch technology.

Fig. 26 shows the KDD switch matrix using B-element switches which, as shown in Figures 27 and 28, provide transmission in either of two states. Fig. 28 shows the MIC realization of a B-element switch using 8 PIN diodes which provided 14 dB transmission loss and 40 dB isolation loss over the 3.7-4.2 GHz band.

Figures 29 and 30 show a baseband logic type of B-element switch using gates which, using ECL type gates, could switch in 1-nanosecond times and could ultimately be configured in a switch matrix with LSI techniques.

#### Microwave Vs Baseband Switch Matrix

The question of microwave switch matrix versus baseband switch matrix does not have a simple solution and brings in considerations of overall satellite transponder design. These considerations involve:

- Weight of the switch matrix
- Number of interconnects
- Type of switch driver circuit
- Type of transmitter

The weight of the Rozec/Assal microwave switch matrix is around 10 pounds exclusive of the DCU. It is evident that if the number of accesses is to increase to 50 to 100 as suggested by Dr. Reudink, then the weight considerations of size and weight of the microwave switch matrix will make it increasingly unattractive when compared to the far more miniature LSI baseband matrix whose number of interconnects do not seriously impact on size and weight.

For a simple translating SS-TDMA transponder using the Dill model with less than 16 antenna beams, particularly without regeneration, the microwave matrix switch approach is far more practical than the baseband switch matrix approach. However, if the SS-TDMA satellite must handle, say 50 data signals, with directed beams and with changes in the mix of power between the various transmit beams, then the baseband switch matrix approach offers the attractive flexibility or choice of alternative modulator and power-amplifier techniques, some of which are shown in Fig. 31. These include the use of a low power QPSK modulator followed by a power amplifier such as a TWTA or an IMPATT diode or a power QPSK modulator driven by a high power carrier source.

A hidden consideration which is not normally discussed when describing a microwave switch is the driver circuit which interconnects the logic control or data circuits and the switching diode or diodes. This driver is sometimes a more significant design problem than the switch itself since it must not only handle the voltage translation from the applied logic voltages to the required diode voltage, but must handle the surges of diode current experienced during the switching operation without ringing, over shoot, or deterioration of rise time or fall time.

In a SS-TDMA system using a baseband logic switch matrix, the switch driver is eliminated since only logic-to-logic voltages are required (emitter coupled logic voltages are between -0.5v and -1.5v); but the overall power consumption of the microwave switch matrix with its driver circuits can be much larger than that required for an all baseband logic and distribution system.

Other advantages of the baseband LSI switch matrix include the possibility of introducing processing and branch/insert functions into the switch, including locally generated data, preambles, and pulse stuffing.

#### QPSK Modulators

Figures 32 through 35 show the basic types of QPSK modulators<sup>(33-37)</sup> used in worldwide telecommunications today. Whereas this paper discusses primarily QPSK techniques, it is to be emphasized that BPSK, 8-QPSK and FFSK are derivatives using the same basic device technologies.

Fig. 32 shows an integrated circuit type of PSK modulator using two PIN diodes which essentially switches between the 0° and 180° ports of a hybrid coupler and π/2 delay line. This circuit was developed by NEC for 4 GHz digital radio systems.

Dr. Carl Ryan of Motorola<sup>(37)</sup> developed a gigabit rate QPSK modulator of the serial type (Fig. 35) using a 90° hybrid with one gigabit bipolar logic IC's as a SP2T logic switch for the 0-90° PSK modulator using essentially the circuit of Fig. 32, and an exclusive OR circuit as the 180° PSK modulator. The residual amplitude modulation (~0.5 dB) of the exclusive OR circuit was solved by Dr. Ryan by using a gate connected as a limiter. The switching functions were accomplished in 0.25 ns. This QPSK modulator, operating at 800 MHz made ideal use of entirely integrated circuit logic without requiring drivers.

Figure 33 shows the doubly balanced PSK modulator using quad-diode Schottky barrier diodes. This 4-diode modulator is identical in construction to the doubly balanced mixer used for frequencies from below one MHz to at least 20 GHz in integrated circuit form. The writer has used an Aertech Ortho-Star (trademark) Ku-band doubly balanced mixer similar to that of Fig. 33, at 20 GHz with excellent results. For PSK operation, the doubly balanced modulator is optimized for exact phase length (0, 180°) and minimal amplitude modulation (less than 0.1 dB), and interport isolation instead of the conversion loss requirements of mixer applications. Such modulators are very inexpensive and from VHF (70 MHz) to C-band, are available in packages suitable for inclusion in micro-strip circuits. They operate at low power, with output levels around -10 dBm and require post amplification.

The waveguide path length modulator of Fig. 34 was given considerable attention at the millimeter waves in the early 1970's by Cuccia and Spilker<sup>(33)</sup> of Aeronutronic Ford and extensive work was done at Bell Telephone Laboratories by Clemeson, Kurakawa and others (BSTJ, Nov. 1971) and at the Hughes EDD, by Kuno, English and Chang (MTT Microwave Symposium, 1972) and data rates in the gigabit per second range were obtained at that time. The work of Dr. Kuno was of particular interest since he was one of the first to report the use of an injection-locked IMPATT oscillator following the PSK modulator, to increase output power with a locking gain-bandwidth product of 6 GHz level; see Fig. 35. The work at BTL was also significant since it demonstrated that a PIN diode could switch a waveguide PSK modulator in less than a nanosecond (0.8 ns).

In 1972, Y. Ito, et al., of Fujitsu<sup>(34)</sup> described a serial QPSK modulator for the 19.7-21 GHz band for 400 Mbps operation using special GaAs Schottky barrier diodes instead of PIN diodes and using unique MIC technology. The MIC in a waveguide is composed of two half divided waveguides; a rectangular waveguide is half divided at the center in parallel to the E-field of the TE<sub>10</sub> mode. At the interface of the divided waveguides, a carrier plate is placed on which MIC substrates are mounted. The carrier has two stepped slots for input/output. The stepped slot, near the waveguide flange acts as a double ridged waveguide. In the final narrow slot, the slot mode acts as a transformation between the waveguide and the TEM mode in the MIC. The return loss and the insertion loss from the WR-51 waveguide to the 50-ohm microstrip (based on 0.6 mm thick ferrite/alumina substrate) are more than 25 dB and less than 0.05 dB over a 20% bandwidth in the K-band respectively.

The Fujitsu QPSK modulator had an output of 10 dBm and was followed by a two-stage IMPATT diode amplifier to provide an output of 22 dBm.

The 100 mw power level availability from the IMPATT diode amplifier of 1972 has given way to at least a 10-watt to 30-watt technology at C-band to a 1-2 watt technology at 20 GHz as shown in Table 9, which is available for space applications.

The use of 28 dBm IMPATT amplifiers designed by Comsat Labs, using RCA and NEC diodes, for the centimeter wave beacons at 19.04 GHz and 28.5 GHz now operating in space on COMSTAR makes available

to the SS-TDMA satellite design actual operating experience of solid state diode amplifiers. Actually, a variety of solid state diode amplifiers (38-41) are now in use in terrestrial radio line-of-sight systems in various parts of the world as listed in Table 10 and a mounting history of operation and reliability under critical terrestrial revenue-oriented conditions is building up a catalog of availability which is certain to impact on space communications.

Within the near future, the output power levels of IMPATT and READ diode amplifiers will approach those of the equivalent TWTA listed in Table 8, particularly by using multiple-diode and hybrid-coupled amplifier arrangements. The low efficiencies (10 to 20%) of the semiconductor oscillator/amplifiers remain a major disadvantage to the solid state amplifiers as compared to the space-type TWT amplifiers which, with dual collectors, are now giving 40-45% efficiencies at high gain. However, elimination of the TWTA power supply with its impact on TWT efficiency reducing it by 80-85%, and the elimination of its major contribution to weight is a great plus for the solid state amplifier.

Recently Y. Takayama and Y. Higo of NEC have disclosed<sup>(36)</sup> the development of a high power QPSK PIN diode waveguide type modulator with 4-watt output at 3.8 GHz which was capable of operating at rates of 60 Mbps. This power QPSK modulator had a total insertion loss of 0.8 dB and an RF switching time of 5 nanoseconds. This unusually low loss in an art which has usually measured from 2 to 3 dB insertion loss, confirms calculations made by W. Schlosser and K. Kurokawa in 1972 and makes such 4-level power phase modulators exceptionally attractive for space applications following a very high efficiency carrier source. In order to obtain the high power level, special high-power driver for the PIN diodes was developed using PNP-type and NPN-type transistors in complementary operation with collectors connected to each other and emitters grounded. Saturation of the driver transistors which would have greatly reduced speed was prevented by connecting Schottky barrier diodes between each transistor's collector and base.

#### Transmitter Alternatives

In addition to the transmitter alternatives shown in Fig. 31, Figures 36 through 40 show interesting additional alternatives which have special application to SS-TDMA beam switched or power-level controlled satellites.

Figure 36 shows one embodiment of an concept originally proposed by W. Schmidt<sup>(5)</sup> in which he speculated on the replacement of a multiplicity of heavy TWTA's with a "high powered oscillator with outputs to the multiple digital modulators". In Fig. 36, the common power source could comprise a high power, high efficiency linear electron tube oscillator or even return to the consideration of cylindrical types of devices such as an amplitron or a magnetron with their efficiency capability in the 60 to 80% range, assuming that the long life now common in the use of pulsed magnetrons for airborne weather radar could be guaranteed for space applications and where the normal "back bombardment" of such devices would not be a limiting factor.

The power divider of Fig. 36 is an established technology for multiple horn feeder arrays to be discussed later in this paper (Fig. 43) and can be commanded to vary or distribute power levels to the various output ports within a few microseconds using latching ferrite techniques.

The power QPSK modulators have been discussed above, and a high power capability (4-10 watts) up into K-band coupled with very low modulator RF loss (~1 dB) would make such a system attractive particularly in a very broad band SS-TDMA satellite which was built for routing in a single channel performing the function of a cross-bar switch in space, (i.e., full 2.5 GHz band in the 20/30 GHz range for 2 Gbps QPSK carriers).

Fig. 37 shows another variant of the Schmidt approach to single carrier source operation. This system uses a low power carrier source, low power modulators and two-collector TWTA whose input levels are controlled by ground-commanded variable attenuators. The feature of this system is the unique quality of the 2-collector TWT. Unlike the one-collector TWT whose efficiency drastically reduces with power-level backoff from saturation, the two-collector TWT, as indicated in Fig. 38, largely retains its high efficiency for significant changes in output power level (44° to 40% for a power change from saturation to 4 dB backoff potential). Thus, this system with its high TWTA gain (~55 dB) presents a very viable approach to the Schmidt concept.

Figure 39 shows the circuit of the recent Fujitsu 8 GHz FET power amplifier which provides over 2 watts of linear operation with over 25% efficiency. Such devices which can be increased to the 10-watt level by hybrid coupling individual amplifiers, are also candidate transmitter amplifiers which can be used to either increase QPSK modulator power, or operate as a variable power output amplifier without drastic change in high efficiency. Improved AM-to-PM conversion characteristics of the FET power amplifier (not shown) can partially offset the reduction in efficiency by reducing the link SNR degradation now caused by the TWT AM-to-PM conversion and in essence, contributing the equivalent of as much as a 1.5-2 dB increase satellite effective radiated power.

#### Linearization of Transmitter Amplifiers

The quest for improved linearization of the transmitter amplifiers has led to some interesting circuits which either reduce the need for excessive TWTA power backoff from saturation or reduce the intermodulation product generation. The linearization of the TWT has been the subject of much attention since the pioneering work by Siedel at Bell Telephone Laboratories. Recently (EASCON-74), P. Bakken of Elab, Norway, disclosed the feed-forward circuit for a two-tube linearized TWT amplifier, shown in Fig. 41, in which a portion of the input signals are fed forward and combined with the outputs of the TWT to subtract from the distortion caused by nonlinearity. This circuit demonstrated that the TWT backoff may be reduced by from 2 to 4 dB, depending on the linearity requirement. Also, from Europe have come two other outstanding assaults on amplifier nonlinearity. At ESTEC, J. Berretta, R. Cough, and J. Guijarro disclosed (Microwave Journal, July 1975) a linearization system for an L-band power transistor

amplifier. Also D. Lombard and P. Dri Reau of CNET, France, at Kyoto, Japan, 1975 (Dig-Sat-Con) noted that a shunt PIN diode has an opposite AM-to-PM conversion characteristic than a TWT, and used one at the HPA TWT input with significant reduction in distortion. Another approach to linearization leading to the suppression of intermodulation products and reduced backoff is the use of Butler matrices as input and output circuits to the TWT as shown in Fig. 42. This circuit, by W. Sandrin of Comsat Labs (Comsat Tech. Rev., Fall 1974), provides an approach capable of doubling the overall DC-to-RF efficiency for a 12-channel transponder and also provides a system for re-apportioning output power among the various channels.

#### New Carrier Sources

The low power carrier sources of SS-TDMA, and the local oscillators (LO) of communication satellites are undergoing significant technological advances. The historic method of developing L.O. power has been the use of VHF X-tal oscillator driven transistor amplifier-frequency multiplexers which have demonstrated an excellent history of reliability in space. However, four new "direct frequency" source approaches are now in development; one is the cavity-stabilized FET oscillator which gives excellent promise of stability and low phase noise at X-band and above, using high Q graphite-epoxy cavities or dielectric cavities, and the surface acoustic wave (SAW) filter<sup>(45-46)</sup> which, as a very narrow band stable filter at S-band, can provide excellent equivalence of an X-tal filter at these microwave frequencies and yield stable low-phase-noise carrier signals which can be multiplied to the desired higher frequency. High speed transferred electron logic devices (TEL)<sup>(47-48)</sup> are now in development with speeds suitable for gigabit data rate signal processing, making possible frequency synthesizer circuits for carrier and LO signal generation in association with a SAW or FET oscillator. The third approach is the Gunn diode oscillator with its low phase noise and basic long life operation as exhibited by the pumps of many paramps, and the fourth is the single-drift or double-drift IMPATT which provides power levels as high as 1-watt to millimeter frequencies well above 50 GHz.

#### SS-TDMA Transponder Concept

Fig. 43 now introduces a transponder which includes both transponder switching and beam switching according to the original Schmidt concept and includes many of the multiple-user concepts recently introduced by Dr. Reudink. This transponder includes all feeds, feeder networks, beamforming networks, and signal summation systems as a part of the transponder, rather than utilizing the historic precedent of separating the antenna system from the RF transponder system. Only in the joining of the antenna and feeder system and receive/switch/transmitter system can the system requirements of such a satellite be realistically addressed.

Many of the basic RF and baseband elements of the system of Fig. 43 have been discussed in the preceding sections, which have already introduced the basic multi-beam structures, but not the beam-forming networks which will be discussed in their many varieties in the paragraphs to follow. These beam-forming networks include the new technologies of coherent and noncoherent carrier variable power dividers or combiners and coherent and noncoherent

multiple-signal splitters or summation networks.

Following the SS-TDMA system of Fig. 43, the various multiple feed horns are connected to a beam forming network made up of variable power dividers (VPD's) as shown in Fig. 44 (for a transmit-beam) providing either a point at which the received beam power is produced, or at which the transmit power is applied. It is a characteristic of lens antennas, as compared to phased arrays, that the beams can be formed and moved by changing the power levels of the carrier energy applied to or received from the various horns as compared to the need for phase shift networks to develop receive or transmit beams in phased arrays. Figures 45 and 46 show the use of a multiplicity of feed clusters to produce independent beams from the lens, and Fig. 47 shows the measured versus calculated 4.9 GHz pattern of the TEM lens of Fig. 46 with a 7-element feed of an actual lens antenna developed by Aeronutronic Ford for Comsat Labs.

#### Variable Power Combiners/Dividers for Coherent Signals

The SS-TDMA satellite of Fig. 43, using multibeam antennas, must perform the function of dividing or combining a multiplicity of carriers at various points in the system, with variable amounts of power applied to both the beam-forming network itself and to the various elements of each beam-forming network.

Any divider circuit is for a single carrier. All signals appearing at its output ports are coherent. The divider circuit consists of cascaded dividers comprising either quadrature hybrid splitters or Wilkinson splitters, each of which splits its input signal to provide two output signals with each output signal 3 dB down from input power level. Negligible power appears in the hybrid circuit load or the Wilkinson strap resistor. The principal technology addressed here is one of variable control of power level between divider or splitter outputs.

The combiner circuit, on the other hand, is sensitive to coherency or noncoherency between applied signals. If a Wilkinson type of quadrature hybrid combining circuit is used, then two noncoherent signals applied to each hybrid combining circuit result in each signal losing 3 dB of signal power to the combiner load, thus giving rise to the term "lossy combiner". This loss is unacceptable in the combining circuits of feeder matrices of multibeam antennas since it severely reduces sensitivity in the receive system, or reduces carrier power in the transmit system. Thus, this section will discuss combiners for only coherent identical carriers. As in the case for the divider or splitter circuits, the point of interest is in the technology of varying the power levels between output ports; i.e., the BFN feeding the various transmit horns. Combiners for non-coherent dissimilar carriers will be discussed in the next section.

Fig. 48 shows the basic circuit of a beam-forming network using variable power dividers (VPD's). This network has eight input (or output) ports. The variable power divider art which has been discussed in detail by Dr. E. W. Matthews<sup>(15)</sup> encompasses both mechanical, solid state and

ferrite devices and can handle power levels up to hundreds of watts.

Figure 49 shows a simple mechanical VPD which consists of an H-plane movable vane in a waveguide Y-junction and is essentially mismatched at all ports. Figure 50 shows the circuit approach, using one or more 4-port hybrids to maintain a match condition at all ports for all VPD settings which can be adjusted so that each of two outputs (or inputs) can split the applied power to any ratio desired.

The VPD circuit of Fig. 50 uses four reflecting phase shifters (RPS) at the junctions of two of the quadrature hybrids. Fig. 51 shows the basic varactor type reflection phase shifter used with the VPD of Fig. 50 as the basic variable power splitter between the L-band antennas of the electronically despun phased array of the synchronous meteorological satellite (SMS) made by Aeronutronic Ford and operating in synchronous orbit for more than a year and a half. These varactor type VPD's have the characteristics of Fig. 52 and Table 11 and handle RF power levels in the 2 to 5 watt range. Other embodiments of the RPS using up to 4 varactors, can handle up to 10 watts of power with variable power change capability of less than a microsecond although such speed was not required or designed for the SMS satellite.

Fig. 53 shows the circuit of a latching ferrite variable power divider (VPD) using an approach pioneered by Dr. Pippin of Electromagnetic Sciences in Atlanta, Ga. This VPD can handle up to hundreds of watts with characteristics similar to those shown in Fig. 54 and Table 12. 8-GHz VPD's of the latching ferrite, obtained from Electromagnetic Sciences for evaluation in a DSCS III engineering model lens antenna system had set and switching speeds of around 6 microseconds.

The varactor and ferrite VPD networks both have the significant features of very low loss per VPD stage (0.25 dB). If the beam forming network (BFN) is to include many stages of VPD's, as shown in Fig. 44, then approximately one ohm or more of loss to each horn may not be acceptable due to critical G/T or EIRP requirements and it may be necessary to include FET LNA's in each horn of the receive cluster, or FET or IMPATT diode power amplifiers directly in the feed horns of the transmit cluster.

#### High Power Combiner/Summing Networks

In a SS-TDMA transponder, it may be required to combine or divide carriers at fairly high power levels without requiring variable power control which would be performed by driving VPD circuits; i.e., the post-modulator VPD and  $\Sigma$  circuits of the transmit portion of the SS-TDMA system of Fig. 43. Recent developments in switches, combiners and semiconductor devices disclosed in recent publications and at the MTT International Microwave Conferences (IMC) of 1974 and 1975 have provided many attractive candidates for this technology in SS-TDMA satellites.

Fig. 55 shows an adaptation of the familiar Wilkinson dividers/combiners disclosed by U. Gysel (50) which avoids the problems of power handling capacity of the chip resistors used to cross strap the output ports. The resistor heat sinking normally limits the Wilkinson combiner to less than 100 watts.

Gysel provided a method of using external loads and ease in control of imbalance between output ports which provides power handling capability well into the kilowatt range.

The use of quadrature hybrids is, of course, a well known method of combining signals but its applicability to combining power amplifiers is slowly gaining acceptance. The paralleling of two TWTA using hybrids is used in many ground terminal amplifiers to increase transmitted power; its use in space was accomplished with two C-band TWTA in ATS-6 and engineers of the Thomson-CSF company in Paris have combined the outputs of two 20-watt 11-GHz space type TWT to obtain almost 40 watts output power at these frequencies.

In 1965, J. Kuno and D. English<sup>(51)</sup> of Hughes EDD carried the amplifier combining technique a step further at 60 GHz when they used a set of equivalent quadrature hybrids to combine the outputs of six IMPATT amplifiers to obtain 1 watt total output power with 22 dB of gain, a technique which may become very attractive to spacecraft designers as a more reliable alternative to a single stage IMPATT diode using a multiple diode structure.

#### High Power Combining of Carriers of Different Frequency

The even-odd multiplexer for combining carriers from various channels into a single output port may be difficult to use in a SS-TDMA multiple beam satellite because of the need for spatial combining using coupled horns and the possible need of rotary joints in a spinner type satellite. The spatial combining will very likely not be compatible with the complex beam forming networks required of a multiple-beam SS-TDMA satellite.

One of the newest developments in the multiplexer-combining art is the contiguous band multiplexer which can be built in a variety of forms. One approach, shown in Fig. 57, uses the quadrature hybrid approach in which sets of two quadrature hybrids coupled by two filters having the frequency of the required channel are connected in series. This approach has long been used in ground terminals and the technique was employed by R. Gruner and A. Williams<sup>(52)</sup> of Comsat Labs in the design of the unattended terminal multi-tube transmitter. This approach was also used by C. Coiner, also of Comsat Labs, using suspended-substrate stripline to build a 3.7-4.2 GHz band splitter multiplexer using all microstrip techniques including filters, in a structure ideally suited for spacecraft use.

Another development in contiguous band filters was realized by Dr. S. Cohn using singly terminated filters based on original designs first discussed by Dr. Cohn in the 1950's at SRI. These designs were brought to hardware status by John Bowes<sup>(53)</sup> of Aeronutronic Ford for the C-band multiplexer of Intelsat V and further developed in graphite epoxy materials. The filter art, following the innovative developments by Dr's. Atia and Williams of Comsat Labs<sup>(54)</sup> on dual mode elliptic function filters, Dr's. Rhodes and R. Levy in linear phase filters<sup>(55)</sup> and V. O'Donovan and S. Kallianteris<sup>(56)</sup> in Canada on Com Dev C-band graphite epoxy filters for RCA Satcom and 11 GHz filters for CTS is providing a

constant succession of innovations in the combining of carriers of different frequencies at a single output port with minimum loss and group delay distortion, minimum guard bands, and significant break-throughs in weight reduction.

#### High Power Switch Combiners for Burst Carriers

Combining various TDMA carrier bursts which are routed from different input ports to a single output port is a logical extension of the technology of the cylindrical scanning phased array antenna art which, in reverse, has required switching of one input to a large number of output ports of the cylindrical array.

Fig. 58 shows the basic requirements of a SS-TDMA burst combiner where a succession of bursts of known position in time pass into a commutating PIN diode switch to a single output. The commutating PIN diode switch can be simple NPST PIN power handling multi-throw switch made up of series and shunt PIN diodes arranged to fan out from a central hub representing the sum point, to a number of input ports on a circular periphery. The switch driver is programmed in response to a clock and timing signal to turn each "spoke PIN diode" on in succession. Such multi-throw PIN diode switches are available for various power levels from Alpha Industries and Microwave Associates, both in the Massachusetts Boston area, and were described in principle in Microwave Associates Micronotes Vol. 11, No. 3, August 1974. In 1974, H. Malone, et al.,<sup>(57)</sup> of Motorola described yet another approach to a high power (greater than half kilowatt) PIN diode switch matrix consisting of a single pole, fifty-six throw matrix which had around 1.8 dB insertion loss at 4.5 GHz. This switch used arrays of submatrices starting with a single input and seven outputs, each output driving a matrix with eight outputs.

The Malone approach of fanning submatrices makes attractive a recent SPST switch development by P. Bakeman and A. Armstrong<sup>(58)</sup> who built the N-diode PIN diode matrix for waveguide applications shown in Fig. 59, which was capable of switching 250 watts of CW power in 50 ns.

A switch device which may have application in the far future provided development is continued is a high power amplifying switch which can directly switch high burst carrier power to different antennas. This device is the electron bombardment semiconductor (EBS) switch amplifier<sup>(49)</sup> of Fig. 60 which was developed by A. Silzars, D. Bates of Watkins Johnson, and A. Ballonoff of Signetics Corporation. This device uses an electron beam in vacuum which is amplified by a traveling wave structure and deflected to either of one or more semiconductor diode collectors. Such an electron tube designed as a signal processor is capable of switching with subnanosecond on-off times and very large on-off ratios. Such devices have been built for 50 watts of linear RF output over the DC-to-300 MHz frequency range and show analytically predicted capability of being developed into the microwave frequency range with a DC-to-4000 MHz bandwidth capable of handling hundreds of watts.

#### Integrated Horn-FET Amplifiers for Receive and Transmit

The technological approach to integrating a low noise FET amplifier with each receive horn and a power FET amplifier with each transmit which was mentioned earlier has a variety of advantages relative to each function. The receive beam forming network of VPD's for a large array of horns may have overall loss which would seriously limit G/T and thereby the data handling capacity of multi-beam SS-TDMA satellites. An FET amplifier with waveguide input represents an established technique now used in the small earth terminal recently procured by Alaska from Amplica Co. of Westlake Village, Ca. Providing the first 15 dB of gain at each receiver horn with a 4-6 dB noise figure will enhance the satellite sensitivity provided that the phase characteristics of each FET amplifier are matched.

The FET amplifier is not the only viable candidate for low noise device usage with each receiver horn. In 1973, Y. Konishi, et al., of the NHR Technical Research Laboratories in Japan developed a 12-GHz low noise converter of low cost and high sensitivity for use in the ground terminal of a TV broadcast satellite. This converter used a planar card suitable for inclusion in the waveguide horn; this card included a 12-GHz bandpass filter, a Schottky barrier diode mount, a local oscillator frequency bandpass filter, a Gunn diode local oscillator and an output at 420 MHz. This card, shown in Fig. 61, provided a 3.5 dB conversion loss and a 4.5 dB noise figure into 2 dB N.F., IF.

The use of an FET power amplifier (or IMPATT diode amplifier) at each transmit feed horn at, say, the 1-watt level per amplifier can be used to provide the primary EIRP producing amplification in addition to making up for VPD loss. A cluster of FET amplifier/feed horn arrangements, operated with each amplifier responsive to driving power controlled by the VPD can produce, in aggregate, the equivalent of using a higher power TWT or Impatt diode amplifier to drive the input to the VPD. If one of the FET amplifiers fails a catastrophic failure of the beam EIRP will not be experienced.

#### Conclusion - A Satellite Concept

The final reckoning of the technological feasibility of an SS-TDMA transponder/beam switched communication satellite using VPD controlled multiple beam lens antennas is whether or not such a satellite can be built with practical size and weight.

Recent proposal consideration by Aeronutronic Ford of the design of the proposed X-band DSCS III satellite provided a unique design vehicle for an entire satellite design and to design and test waveguide lens multi-beam antennas complete with latched ferrite VPD's for that satellite. In addition, our experience included the successful operation of varactor VPD switching of the electronically despun SMS satellite antenna and experience with a 4 GHz TEM lens antenna designed for Comsat Labs which was successfully tested.

Fig. 62 shows this basic satellite concept using 3-axis stabilization, two transmit multi-beam antennas (MBA's) and one receive MBA. Fig. 63 shows

the sketch of the waveguide lens and 61 horn feed array which was actually built and tested. It was significant that the weight of MBA's weighed less than 130 pounds for the receive MBA and less than 75 pounds for each transmit MBA. These weights included 17.5 pounds and 70 pounds for the receive MBA's lens and BFN/feed array respectively while the transmit MBA's lens and BFN/feed array weighed only 14.2 and 32.5 pounds respectively.

Thus, the multi-beam lens antenna for transponder/beam switched SS-TDMA is believed to be highly technologically viable, provided that the feed weight, which forms the major weight increment of the antenna can be accommodated in the overall weight budget of the satellite. Consideration of suggested weight budgets of large 3-axis satellites such as Intelsat V and the proposed DSACS III suggests that the antenna/feed weight will comprise approximately 5% of the entire satellite weight. Then as much as 75-80% of this antenna system weight for a multi-beam antenna system used in such a satellite may be required for the feed and feeder system; i.e., around 120 pounds for a satellite weighing 3500 pounds. This type of weight budget is in line with the C-band and X-band multiple-beam antenna and feeder systems already designed by Scott, Luh and Matthews<sup>(60)</sup>. However, specific satellite requirements must be considered, in addition to the employment of weight saving techniques such as the use of graphite epoxy or equivalent light weight materials for feed and feeder structures to arrive at a proper determination of just how many feeder systems can be used.

Scott, Luh and Matthews have considered an additional case which will impact on both satellite radiated power in certain beams, and on the design and weight of the feed system itself; i.e., when two beams overlap. For this situation, an additional source of loss is encountered since a particular feed element or horn may have to be shared with the two overlapping beams. If this feed horn is, say, surrounded by six beams whose centers surround it, then its available power may have to be shared six ways resulting in an inherent power loss to each beam. Fortunately, the outer elements would probably not all be shared, but a source of potential loss could exist in a number of overlapping beams which could result in potential inherent losses as great as several dB.

A drastic reduction in feeder loss may be possible by using commutating switches. A concept using this approach was suggested by Scott, Luh, and Matthews in the beam-forming switch-matrix shown in Figure 64. The commutating switch-matrix could be built to benefit from extensive miniaturization using microstrip feeder and switch circuits which would reduce both size and also weight when compared to equivalent waveguide circuitry.

Technological basis for such feeder circuits is already an accomplished fact in the Intelsat IVA where a team of Hughes engineers headed by F. Taormina designed TEM squarax transmission line feeder networks for the 19 horns for east coverage used in that satellite.

#### Acknowledgements

The author wishes to acknowledge significant guidance from his colleagues at Aerofusonic Ford;

i.e., Mr. William Scott and Dr. E. W. Matthews on multi-beam antennas and feeder networks, Mr. Richard Davies, Dr. L. Valdes and Dr. J. Chiao on regenerative repeaters and switch matrices, and Mr. Henry Hyams and Mr. John D. Bowes on many aspects of satellite transponder design. The author also wishes to thank Mr. David Jarett of TRW for many hours of discussion of related switching satellite concepts, particularly with regard to the switch matrix; to Mr. Sidney Metzger of Comsat who shared some advanced concepts with the author relative to beam switching and power-distribution in SS-TDMA satellites; and to Dr. K. Myauchi, Mr. S. Seki, and Mr. H. Ishio of Japan NTT's ECL for sharing the details of many of the technology achievements in high speed QPSK transmission developed for the Japanese mm-wave guided waveguide system.

### References

- (1) W. Schmidt, "An On-Board Switched Multiple Access System for Millimeter Wave Satellites", 1969 Intelsat/IEEE Conference on Digital Satellite Communications, London, England.
- (2) W. Schmidt and R. Cooperman, "A Satellite Switched SDMA/TDMA System for a Wideband Multibeam Satellite", 1973 ICC-73, Seattle, Washington.
- (3) K. Nosaka and T. Muratani, "A New Satellite Transponder with Regenerative Repeater and Higher Order DPSK for TDMA/SDMA System", Proc. of Second International Conference on Digital Satellite Communications, Paris, 1972.
- (4) J. Puente, W. Schmidt, A. Werth, "Multiple Access Techniques for Commercial Satellites", Proc. IEEE, Feb. 1961, Vol. 59, No. 2.
- (5) W. Schmidt, "Satellite Switched TDMA; Transponder Switched or Beam Switched", AIAA 5th Communication Satellite Systems Conference, Los Angeles, 1974, AIAA Paper No. 74-460.
- (6) D. Reudink, "Problems and Challenges in Satellite Communications Frequency Reuse Antennas and Components", 1976 IEEE-MTT-S International Microwave Symposium, Cherry Hill, N.J.
- (7) G. Dill, "Application of SS-TDMA in a Channelized Satellite", Conference Record, ICC 76, June 16, Philadelphia, Pa.
- (8) T. Muratani, "Satellite-Switched Time-Domain Multiple Access", EASCON-74, 189.
- (9) C. L. Cuccia and W. Lee, "PSK and QPSK Modulation and Demodulation in Digital Satellite-to-Ground Links", Communications Satellite Technology, Vol. 33. Edited by P. Bargellini, MIT Press, 1974.
- (10) H. Chan, D. Taylor, S. Haykin, "A Comparative Study of Digital Modulation Techniques for Single Carrier Satellite Communications", Intelsat/IECE/ITE Third International Conf. on Digital Satellite Communications, Nov. 11-13, Kyoto, Japan, 1975.
- (11) C. L. Cuccia and R. Davies, "Optimum Adjacent Channel Design Considerations for a Communication Satellite Carrying Both FDMA and TDMA", ICC-76, June 14-16, Philadelphia, Pa.
- (12) J. Chiao and F. Chethik, "Satellite Repeater Study", Canadian Communications and Power Conference, Montreal, Canada, Oct. 21, 22, 1976.
- (13) A. Dion and L. Ricardi, "A Variable-Coverage Satellite Antenna System", Proc. IEEE, Feb. 1971.
- (14) E. Matthews, W. Scott, C. Han, "Advances in Multiple Beam Satellite Antenna Technology", ICC 76, Philadelphia, Pa.
- (15) E. Matthews, "Variable Power Dividers in Satellite Systems", 1976 IEEE-MTT-S International Microwave Symposium, Cherry Hill, N.J.
- (16) E. Binz and D. Waines, "Satellite Multibeam Antenna Concept", AIAA/CASI, 6th Communications Satellite Systems Conference, Montreal, Canada, AIAA Paper No. 76-251.
- (17) K. Tsukamoto and R. Hayashi, "Receiving Part of Satellite Borne Millimeter Wave Transponder", 1975 IEEE-MTT-S International Microwave Symposium, Palo Alto, Ca., May 12.
- (18) E. Kramer, J. Leeper, J. Whelehan, "Ku-Band Spacecraft Parametric Amplifier", 1973 IEEE-MTT-S International Microwave Symposium, Chicago, Ill.
- (19) A. DiAmbrosio, "A Ku-Band Uncooled Parametric Amplifier for Spacecraft Application", First European Microwave Conference 1973, Brighton, England.
- (20) C. Liechti, "Microwave Field-Effect Transistors", IEEE Trans. MTT, June 1976.
- (21) D. James, R. Douville, R. Breithaupt, A. Van Koughnett, "A 12 GHz Field-Effect Transistor Amplifier for Communications Satellite Applications", European Microwave Conference, Hamburg, 1975.
- (22) N. Fukuta, K. Suyama, H. Suzuki, Y. Nakayama, H. Ishikawa, "X-Band GaAs Schottky Barrier Power FET with a High Drain-Source Breakdown Voltage", ISSCC-76, Philadelphia, Feb. 1976.
- (23) F. Gardiner, "Rapid Synchronization: Carrier and Clock Recovery for High Speed Digital Communications", MSN, Feb/Mar 1976.
- (24) Y. Matsuo, S. Sugimoto, S. Yokoyama, "A Study on Carrier and Bit-Timing Recovery for Ultra-High Speed PSK-TDMA Systems", Telecommunications Numeriques Per Satellite Equipment, AMRT p-277.
- (25) S. Yokoyama, K. Kato, T. Noguchi, N. Kusama, S. Otani, "The Design of a PSK Modem for the Telsat TDMA System", ICC-75.
- (26) L. Lundquist, M. Lopriore, F. Gardner, "Transmission of a 4 $\phi$ -Phase Shift Keyed Time Division Multiple Access Over Satellite Channels", IEEE Trans-Comm, Sept. 1974.
- (27) C. L. Cuccia, "Microwave QPSK Demodulator Techniques of the Receiver Front End", 1975 IEEE-MTT-S International Microwave Symposium, May 1975, Palo Alto, Ca.
- (28) M. Hata, T. Ohita, S. Ohwaku, H. Honda, "A New Direct Regenerative Technique for PCM-PSK Microwave System", ICC-70-CP-297-COM.
- (29) X. Rozec and F. Assal, "Microwave Switch Matrix for Communication Satellites", ICC-76, Philadelphia, Pa.
- (30) R. Cooperman and T. Dobyns, "A Distribution Control Unit for Satellite Switched Communications", International Telemetry Conf., Los Angeles, Oct. 1972.

- (31) Y. Ito and M. Kyogoku, "SDMA On-Board Switching System Using Rearrangeable Multi-Stage Network", IEE International Conf. Sat. Comm. System Tech, April 1975.
- (32) M. Yamaguchi, Y. Ito, M. Kyogoku, "4 GHz 8 x 8 Switch Matrix for SDMA System", 1975 IEEE-MTT-S International Microwave Conf., Palo Alto, Ca.
- (33) O. Cuccia and J. Spilker, Jr., "Component and System Aspects of 200 Mbps BPSK V-Band Data Communications", NAECON Record, 1971, Dayton, Ohio.
- (34) Y. Ito, H. Yunoki, H. Komizo, J. Dodo, "K-Band Integrated Microstrip Modulator and Mixer in Waveguide for High Speed PCM Radio", ISSCC-72, Feb. 17, 1972, Philadelphia, Pa.
- (35) W. Schlosser and K. Kurokawa, "Insertion Loss of 4-Level Phase Switch", IEEE Trans. MTT, Sept. 1972.
- (36) Y. Kakayama and Y. Higo, "3.8 GHz 4-Watt PSK Modulator Using PIN Diodes", NEC Research and Development", April/July 1975.
- (37) C. Ryan, "Bipolar IC's for Microwave Signal Processing", 1975 IEEE-MTT-S International Microwave Conference, Palo Alto, Ca.
- (38) U. S. Berger, "Impatt Amplifiers in Bell System Microwave Systems", NTC-74.
- (39) I. Tatsuguchi and J. Gewartowski, "10-W 6-GHz GaAs Impatt Amplifier for Microwave Radio Systems", ISSCC 75, Philadelphia, Pa.
- (40) R. Lee, U. Gysel, D. Parker, "High Power C-Band Multiple Impatt Diode Amplifiers", IEEE Trans MTT, May 1976.
- (41) M. Harris, W. Tsai, S. Paik, "C-Band Solid State TWT Replacement", 1975 IEEE-MTT-S International Microwave Symposium, Palo Alto, Ca.
- (42) K. Kurita and K. Morita, "Microwave MesFet Mixers", IEEE Trans. MTT, June 1976, MTT-24.
- (43) S. Komaki, O. Kurita, T. Memita, "GaAs MesFet Regenerator for Phase Shift Keying Signals at the Carrier Frequency", IEEE Trans. MTT, June 1976, MTT-24.
- (44) J. Maines and E. Paige, "Surface Acoustic Wave Devices for Signal Processing Applications", Proc. IEEE, May 1976.
- (45) R. Hays and C. Hartman, "Surface Acoustic Wave Devices for Communications", Proc. IEEE, May 1976.
- (46) R. Weglein, "SAW Chirp Filter Performances Above 1 GHz", Proc. IEEE, May 1976.
- (47) H. Yanai and T. Ikoma, "Recent Development of Transferred Electron Logic Devices in Japan", IEEE-MTT-S 1976 International Microwave Conference, Cherry Hill, N.J., June 15.
- (48) L. Upadhyayula, R. Smith, J. Wilhelm, S. Jolly, and J. Paczkowski, "Transferred Electron Logic (TELDS) for Gigabit Rate Signal Processing", IEEE-MTT-S 1976 International Microwave Conf., Cherry Hill, N.J., June 15.
- (49) A. Silzars, D. Bates, A. Ballonoff, "Electron Bombarded Semiconductor Devices", Proc. IEEE, Vol. 62, August 1974.

(References continued on Page 28)

TABLE 1 APPLICABLE TECHNOLOGIES TO SS-TDMA SATELLITE	
SUBSYSTEM	ALTERNATIVES/CANDIDATES
TYPES OF MODULATORS	BPSK, QPSK, SQPSK, FM-CPSK (FFSK)
MULTI-BEAM ANTENNA	REFRACTIVE LENS, CONSTRAINED LENS, MULTIPLE HORN - SINGLE REFLECTOR, MULTIPLE HORN - MULTIPLE REFLECTOR
LNA	PARAMP, TDA, FET AMPLIFIERS, FET MIXER, SCHOTTKY BARRIER MIXER, BIPOLEAR AMPLIFIER
RECEIVERS	TRANSLATING REGENERATING <ul style="list-style-type: none"> <li>• RF REGENERATOR AT CARRIER FREQ.</li> <li>• X4 RINGING CIRCUIT CARRIER RECONSTRUCTION</li> <li>• GARDINER DEMOD-REMOD</li> <li>• STORE AND FORWARD</li> <li>• USE OF FEC</li> </ul>
MATRICES	MICROWAVE MATRIX <ul style="list-style-type: none"> <li>• SWITCH - DISTRIBUTOR CIRCUITS</li> <li>• B-ELEMENT REARRANGEABLE CIRCUIT</li> <li>• DEVICES FOR SWITCHES <ul style="list-style-type: none"> <li>• PIN DIODE</li> <li>• SCHOTTKY BARRIER DIODES</li> <li>• VARACTOR DIODE</li> <li>• FET</li> </ul> </li> </ul> BASEBAND MATRIX <ul style="list-style-type: none"> <li>• IC LOGIC ELEMENTS</li> <li>• USE OF LSI</li> <li>• GUNN LOGIC ELEMENTS</li> </ul>
QPSK MODULATOR	LOW POWER DOUBLY-BALANCED MODULATOR WAVEGUIDE PATH-LENGTH MODULATOR PARALLEL 0-180° PSK MODULATORS SERIAL 0-90°, 0-180° PSK MODULATORS
TRANSMITTERS	TWTA - ONE COLLECTOR - TWO COLLECTOR QPSK MODULATOR + TWTA QPSK MODULATOR + IMPATT AMP. POWER QPSK MODULATOR
VARIABLE POWER DIVIDERS (UPD)	VARACTOR DIODE REFLECTION PHASE SHIFTER LATCHING FARADAY-ROTATOR FERRITE PHASE SHIFTER MECHANICAL
LOCAL OSC.	VHF X-TAL OSC + MULTIPLIER STABILIZED GUNN OSCILLATOR SAW OSCILLATOR + MULTIPLIER FET CAVITY STABILIZED OSC.
FILTERS	ELLYPTIC FUNCTION, DUAL-MODE FILTER TSCHEBYCHEV FILTER CONTIGUOUS BAND MULTIPLEXER GRAPHITE EPOXY CONSTRUCTION

TABLE 3  
BIT ERROR RATE COMPARISONS OF TRANSLATING AND REGENERATIVE QPSK

UPLINK $(E_b/N_o)_u$	10 dB				16 dB			
VOLTAGE RATIO OF INTERSYMBOL INTERFERENCE I TO CARRIER I/C =	UPLINK $\alpha_u = 0$ DLINK $\alpha_d = 0$	UPLINK $\alpha_u = 0.2$ DLINK $\alpha_d = 0.2$	UPLINK $\alpha_u = 0$ DLINK $\alpha_d = 0$	UPLINK $\alpha_u = 0.2$ DLINK $\alpha_d = 0.2$				
DLINK $E_b/N_o$	10 dB	16 dB	10 dB	16 dB	10 dB	16 dB	10 dB	16 dB
TRANSLATING QPSK BER	$3 \cdot 10^{-2}$	$2 \cdot 10^{-3}$	$7 \cdot 10^{-2}$	$1 \cdot 10^{-2}$	$10^{-3}$	$5 \cdot 10^{-8}$	$2 \cdot 10^{-2}$	$10^{-4}$
REGENERATIVE QPSK BER	$10^{-5}$	$3 \cdot 10^{-6}$	$10^{-3}$	$2 \cdot 10^{-4}$	$5 \cdot 10^{-6}$	$10^{-18}$	$5 \cdot 10^{-4}$	$5 \cdot 10^{-9}$

TABLE 2 SYSTEM $E_b/N_o$ DEGRADATION FROM THEORY			
MODULATION TECHNIQUES	BT = 2	BT = 1.6	BT = 1
I:	BPSK	3.2	
	QPSK	2.9	
	SQPSK	2.9	
	FM-CPSK	1.3	
II:	BPSK	1.5	1.8
	QPSK	1.3	2.5
	SQPSK	0.4	1.0
	FM-CFSK	0.8	1.0
I. L. Lamin; TWT 3 dB into saturation AM/PM 3.5° dB, BER = $10^{-5}$			
II. H. Chan, D. Taylor, S. Haykin; 1 dB backoff for Hughes 261-H			

TABLE 5 NOISE PERFORMANCE OF CANDIDATE SPACECRAFT LNA				
TYPE AMPLIFIER	NOISE TEMPERATURES ( $^{\circ}\text{K}$ )/ FACTORS (dB)			
	6	8	14.25	28
UNCOOLED PARAMP	$50^{\circ}\text{K}$ - $75^{\circ}\text{K}$	$75^{\circ}\text{K}$ - $100^{\circ}\text{K}$	$120^{\circ}\text{K}$ - $300^{\circ}\text{K}$	$250^{\circ}\text{K}$ - $400^{\circ}\text{K}$
TDA	3.7	4.0	6.0	8.0
FET	2.5	3.5	5.0	---
BI-POLAR TRANSISTOR	5.0	---	---	---

TABLE 4 MULTIBEAM SPACECRAFT ANTENNAS	
TYPE	CHARACTERISTICS
MULTIBEAM REFRACTIVE LENS ANTENNA	REQUIRES SOLID DIELECTRIC LENS. NOT APPLICABLE UNTIL LIGHT-WEIGHT LOW LOSS MATERIAL IS DEVELOPED.
MULTIBEAM CONSTRAINED LENS ANTENNA • IEM • WAVEGUIDE	SPACE-FED ARRAY; EXCELLENT ISOLATION BETWEEN BEAMS. DESIGNED FOR C-BAND DESIGNED FOR X-BAND AND ABOVE
MULTIBEAM REFLECTOR ANTENNA • SIMPLE OFFSET • DUAL OFFSET	DESIGN SIMPLICITY; USED IN INTELSAT IV-A AND WILL BE USED IN INTELSAT V. REDUCES BLOCKAGE AND SIDELOBE LEVELS REDUCTION IN SIZE OF ARRAY
MULTIBEAM PHASED ARRAY ANTENNA	WEIGHT AND COMPLEXITY INCREASE WITH NUMBER OF ELEMENTS.

	SP4T ACHIEVED	SP2T ACHIEVED
INSERTION LOSS TRANSMIT RECEIVE	.4 dB .4 dB	.3 dB .3 dB
ISOLATION TRANSMIT RECEIVE	>20 dB >20 dB	>20 dB >20 dB
MAXIMUM HOLDING POWER	<900 ma	<300 ma
MINIMUM BANDWIDTH TRANSMIT	NO MEASURABLE ROLLOFF	NO MEASURABLE ROLLOFF
RECEIVE	NO MEASURABLE ROLLOFF	NO MEASURABLE ROLLOFF
POWER HANDLING	>30 w	>30 w
VSWR TRANSMIT RECEIVE	1.3 1.3	1.3 1.3
TEMPERATURE	-30°C to +50°C	-30°C to +50°C
WEIGHT	.65 lb.	0.5 lb.

DEVICE		FREQUENCY (GHz)			
		4 TO 6	7 TO 8	12	18 TO 20
GUNN DIODE AMP		25 dBm VARIAN	1 WATT HUGHES	27 dBm VARIAN	17 dBm VARIAN
IMPATT DIODE AMP		15.8 WATTS SRI  10 WATTS BTL	4 WATTS HUGHES  3 WATTS H-P	0.5 WATT FUJITSU  13 WATTS G&E BRADLEY  4 WATTS HUGHES  3.5 WATTS BTL	1.2 WATTS HITACHI  1 WATT AERO-FORD  28 dBm COMSAT LABS
READ DIODE AMP		10 WATTS RAYTHEON			
AVALANCHE DIODE AMP		2 WATTS RAYTHEON	1 WATT RAYTHEON	1 WATT RAYTHEON	
FET AMP		3 WATTS FUJITSU	2.5 WATTS FUJITSU  1 WATT T.I., HUGHES		
BIPOLAR TRANSISTOR AMP		7 WATTS CLASS C  1 WATT CLASS A	1.5 WATTS T.I.		

TABLE 7 TYPES OF SWITCHING DEVICES		
TYPE	SWITCHING SPEED CAPABILITY	SWITCHING VOLTAGE OR CURRENT
PIN DIODE SWITCH		DEPENDS ON POWER LEVEL
• SERIES • SHUNT • LP FILTER WITH SWITCHED f <sub>C</sub>	1-5 ns 0.8 ns 35 ns	0 - 10-100 mA 0 - 10-100 mA 0 - 5 mA
VARACTOR DIODE SHUNT LP FILTER SWITCH	1-10 ns	NOT SUITABLE AS A DIRECT ON-OFF SWITCH DEVICE. SWITCHES BY TUNING. -20V TO +1V
SCHOTTKY DIODE QUAD SWITCH	700 ps	HEART OF DOUBLY BALANCED MODULATORS. -0.7 TO +0.7V
FET SWITCH	100 ps	CAN BE DESIGNED TO SWITCH WITH STANDARD LOGIC VOLTAGE DIFFERENCES OF 1 VOLT. -2V TO +2V

TWTA POWER OUTPUT RANGE	FREQUENCY (GHz)			
	4	7	12	18
4-8W	HUGHES NEC	HUGHES		HUGHES NEC
8-15W	TELEFUNKEN AEG		HUGHES THOMSON CSF	HUGHES
15-40W		HUGHES W.J.	THOMSON CSF TELEFUNKEN	
100-200W		HUGHES LITTON		
500-1000W		SIEMENS TELEFUNKEN AEG		

TABLE 10  
NEW SOLID STATE RF POWER SYSTEMS

TYPE	FREQ.	CIRCUIT	POWER OUTPUT	APPLICATION
UP-CONVERTER	INPUT: 2 GHz OUTPUT: 36-38 GHz	VARACTOR UP-CONVERTER UTILIZING 100 mW DRIVE POWER.	10 mW	NAVY
FM PHASE LOCK POWER AMPLIFIER	11 GHz	A VARACTOR TUNED GUNN OSC. PHASE LOCKED TO AN FM SIGNAL. OSCILLATOR OUTPUT DRIVES IMPATT AMPLIFIER.	1 WATT	LOS
C-BAND TWT REPLACEMENT	5.9-6.4 GHz	CASCADED GUNN, IMPATT AND READ DIODE OSCILLATORS.	10 WATTS	LOS
FET POWER AMP	8 GHz	CASCADED FET AMPLIFIERS.	2 WATTS	EXPERIMENTAL
FM MM-WAVE RADIO	38 GHz	GUNN DIODE, DIRECT-FM MODULATOR WITH AFC CIRCUIT.	20 mW	MULTI-CHANNEL VIDEO
HIGH SPEED DIGITAL LOS RADIO	20 GHz	FOUR-PHASE WAVEGUIDE PATH LENGTH SERIAL TYPE QPSK MODULATOR DRIVING A READ-TYPE IMPATT DIODE INJECTION LOCKING AMPLIFIER.	200 mW	400 Mb/s 20 GHz LOS RADIO REPEATER
LOS RADIO POWER AMP	6 GHz	1-WATT SILICON IMPATT DIODE AMP WITH 20 dB GAIN AND 52 dB NOISE FIGURE.	1 WATT	SHORT-HAUL COMMON CARRIER
HIGH CAPACITY FM RADIO LINKS	4 GHz	SIX STAGE 7-WATT BIPOLAR TRANSISTOR AMPLIFIER WITH 30 dB GAIN AND GAIN FLAT TO 0.5 dB WITHIN A BANDWIDTH OF 7.5%.	7 WATTS	1800-CHANNEL TDFM/FM RADIO RELAY
HIGH CAPACITY FM RADIO LINKS	6 GHz	UTILIZES A 2 GHz POWER AMPLIFIER WITH 14 WATT OUTPUT DRIVING A STEP RECOVERY DIODE MULTIPLEXER (X3) WITH 40% CONVERSION EFFICIENCY.	5 WATTS	TWT REPLACEMENT FOR FM MICROWAVE REPEATER

TABLE 11 MEASURED X-BAND VPD CHARACTERISTICS		
CHARACTERISTIC	FERRITE PHASE-SHIFT	FARADAY ROTATION
FREQUENCY BAND (GHz)	7.25 - 7.75	7.25 - 7.75
CONTROL TYPE	PULSED LATCHING	CURRENT DRIVE
INSERTION LOSS (MAXIMUM)	0.3 dB	0.25 dB
ISOLATION (MINIMUM)	30 dB	25 dB
PHASE VARIATION	$\pm 3^\circ$	$\pm 3^\circ$
WEIGHT	12 OZ.	12 OZ.
MAXIMUM DRIVE POWER	PULSED	0.5 WATTS
MAXIMUM RF POWER	100 WATTS	100 WATTS
INTERMODULATOR PRODUCTS (MAX. FIFTH ORDER, WITH 27-WATT CARRIERS)	-104 dBm	-123 dBm

TABLE 12 ELECTRICAL CHARACTERISTICS OF SMS-VPD	
FREQUENCY BANDS:	1687 AND 2029 $\pm$ 20 MHz
DIODE TYPE:	VARIAN VAT-71, 6 pf VARACTOR 60-VOLT BREAKDOWN, 150 GHz CUTOFF
CONTROL VOLTAGE:	-10 TO -40 VOLTS
POWER LEVEL:	5 WATTS cw
TYPICAL INSERTION LOSS:	1.1 dB MAX.
TYPICAL ISOLATION:	20 dB MIN.
PHASE VARIATION WITH SETTING:	$\pm 3^\circ$

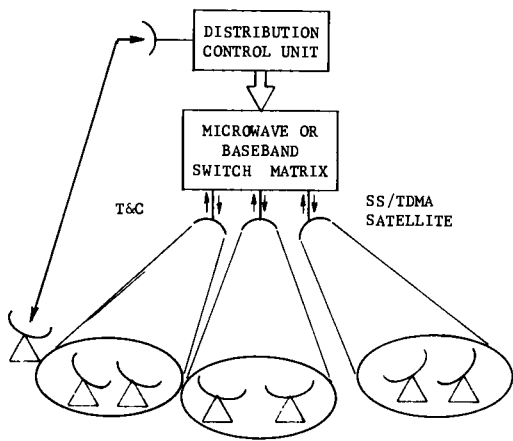


Fig. 1A Basic Satellite  
Switched TDMA (SS-TDMA)  
System

Fig. 1B Transponder  
Switched TDMA  
(After Schmidt  
and Cooperman)

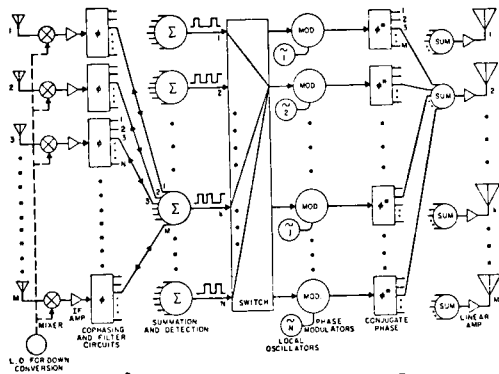
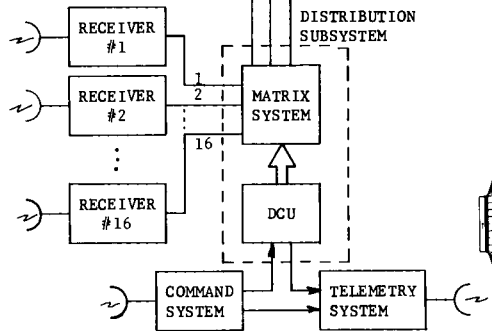


Fig. 2 Block Diagram of a Multi-Beam  
Switched Satellite (by D. Reudink)

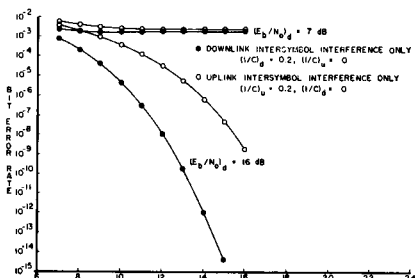


Fig. 3 BER Comparison of Regenerated  
QPSK Between Up-Link-Only and  
Down-Link-Only Intersymbol  
Interference

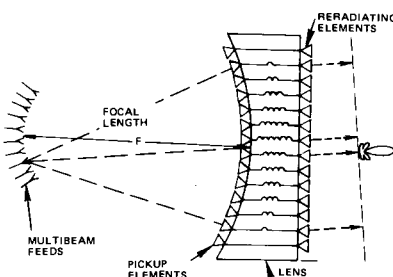


Fig. 4 Constrained Lens

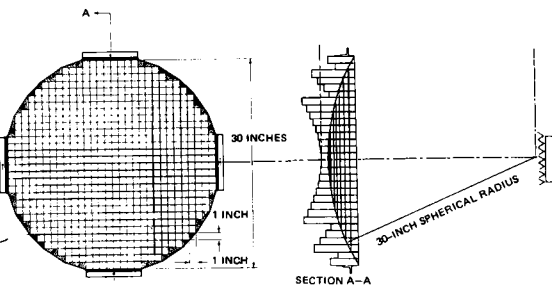


Fig. 5 LES-7 Experimental Waveguide Lens  
Antenna Design (After Dion and  
Ricardi)

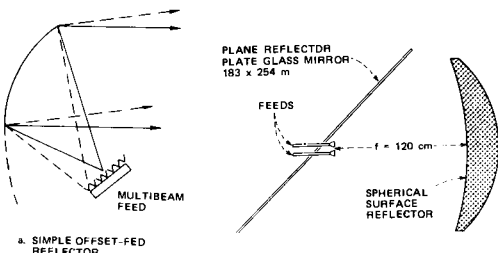


Fig. 6 Simple Offset-  
Fed Multiple Beam Feed  
and Reflector

Fig. 7 Turrin Type  
Multiple Feed Antenna  
System

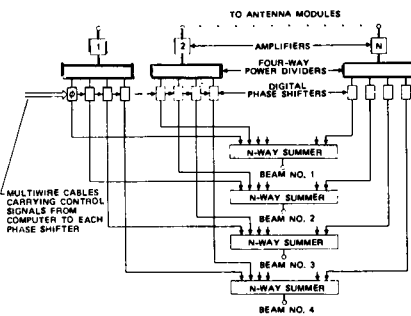
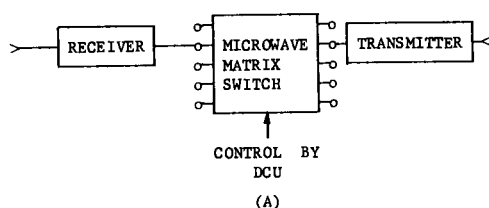
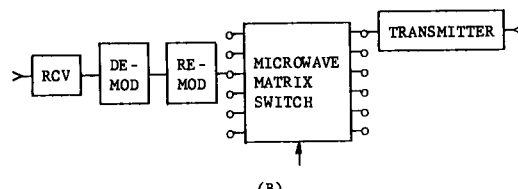


Fig. 8 Four Beam Phased Array



(A)



(B)

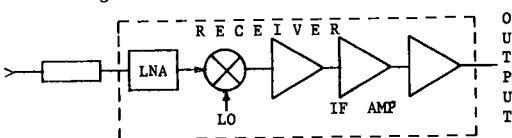
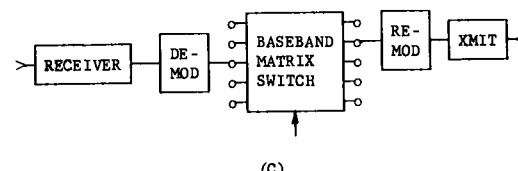


Fig. 10 Typical FET Amplifier



(C)

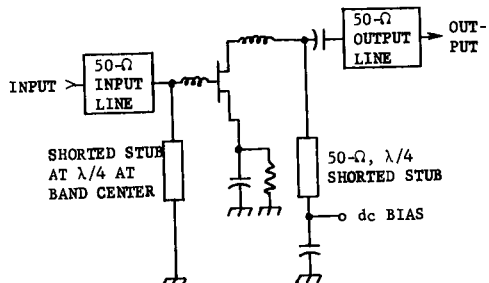


Fig. 11 Circuit Diagram of AIL 15 GHz Paramp For Spacecraft Applications

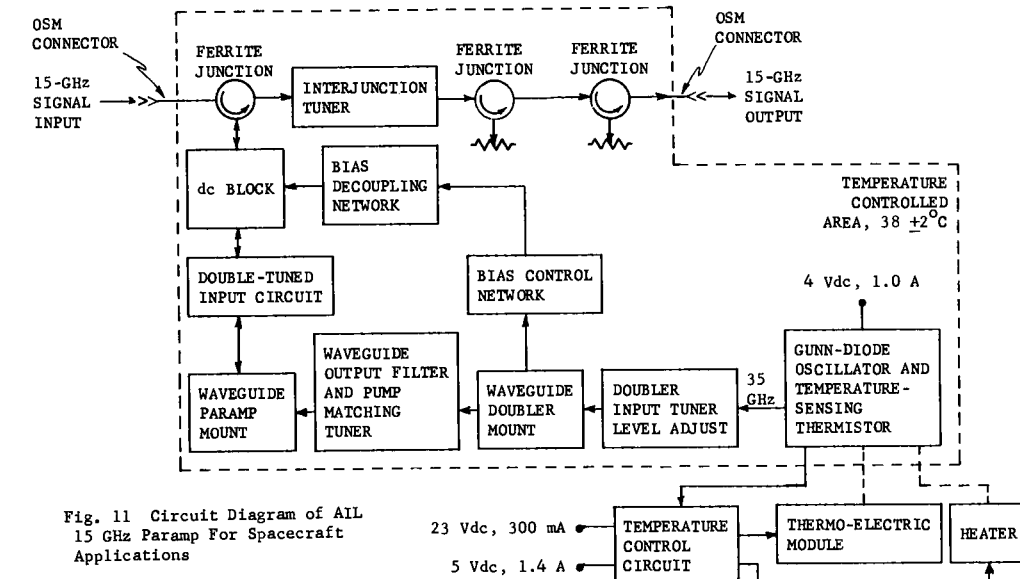


Fig. 12 Three Types of SS-TDMA Switch-Matrix Systems - (a) Translating Switched Transponder, (b) Regenerative Microwave Switched Transponder, and (c) Regenerative Baseband Switched Transponder

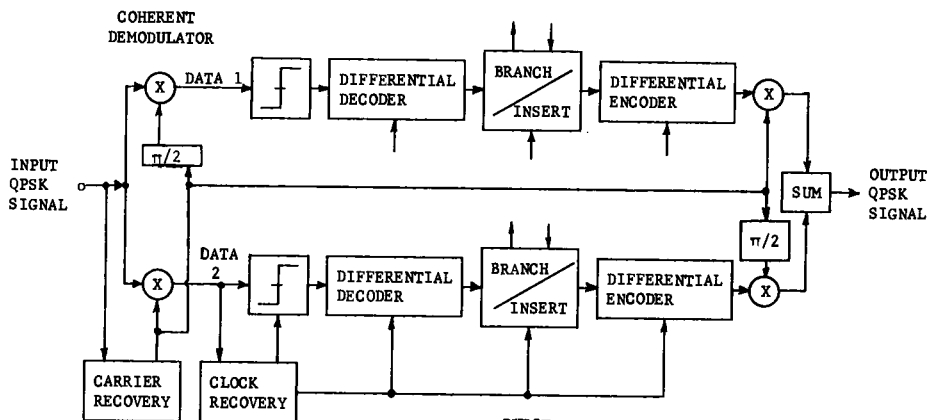


Fig. 13 Basic Demodulator-Remodulator Regenerator System

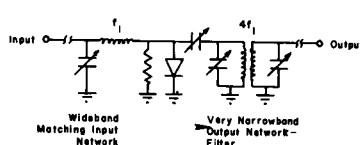


Fig. 14 X4 Multiplexer Using Step Recovery Diode

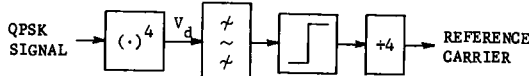


Fig. 15 Carrier Recovery Circuit Using X4 Multiplier

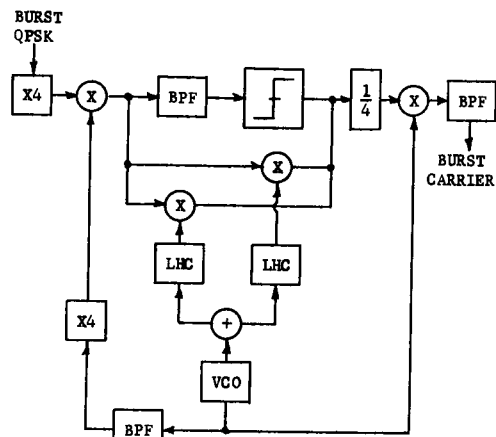
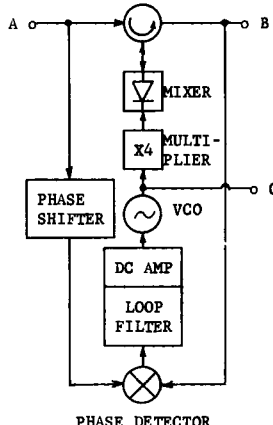


Fig. 16 Carrier Recovery Circuit Using Tracking Filter Following the X4 Multiplier



A = QPSK SOURCE  
B = REGENERATED OUTPUT SIGNAL  
C = SYNCHRONIZED CARRIER OUTPUT

Fig. 18 PSK Regenerator

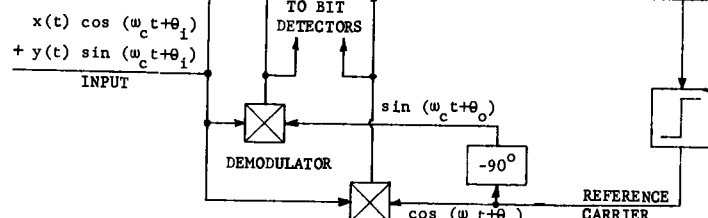


Fig. 17 Gardiner Type Demod-Remod

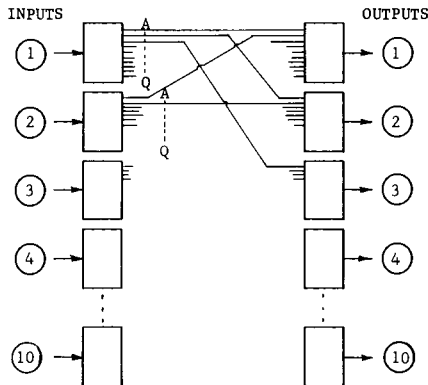


Fig. 19 Matrix Switch Using Splitter Combiner Circuits

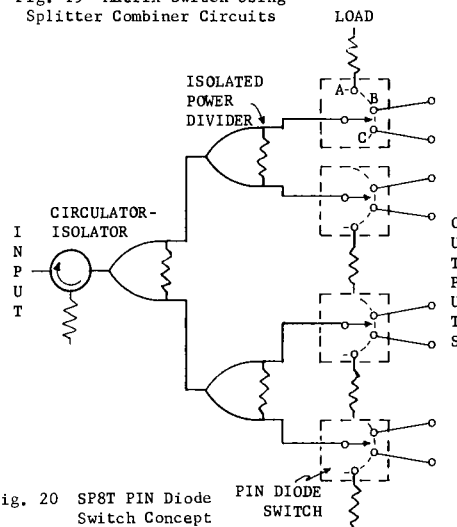


Fig. 20 SP8T PIN Diode Switch Concept

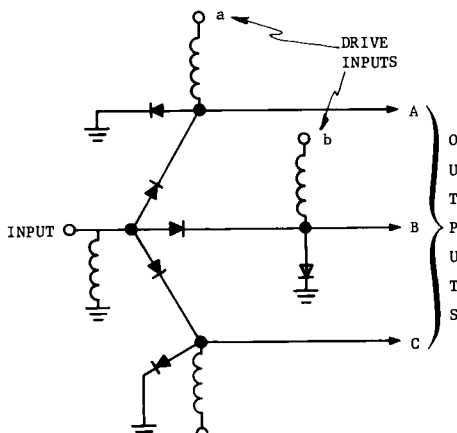


Fig. 21 PIN Diode Switch of Fig. 20

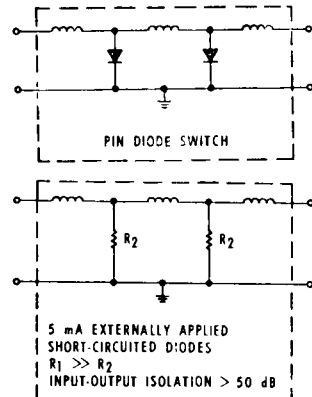


Fig. 22 PIN Diode Switch by X. Rozec and F. Assal

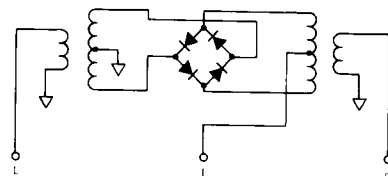


Fig. 23 Doubly Balanced Modulator Switch Using Shottky Barrier Diodes

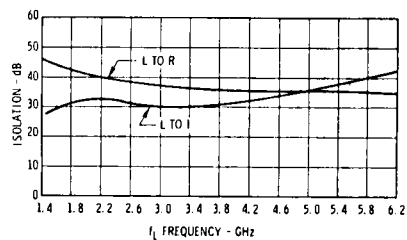


Fig. 24 Isolation of Switch of Fig. 23

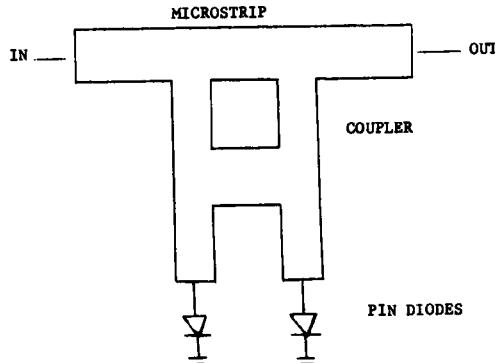


Fig. 25 PIN Diode Switch Using Hybrid Coupler

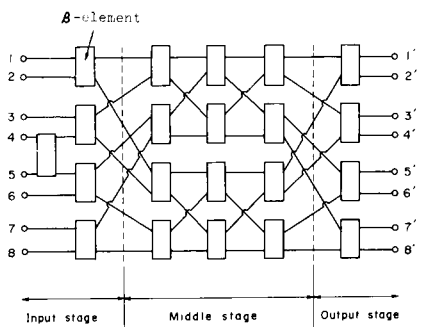


Fig. 26 Rearrangeable Multi-Stage Matrix Using B-Elements Developed at KDD Laboratories in Japan

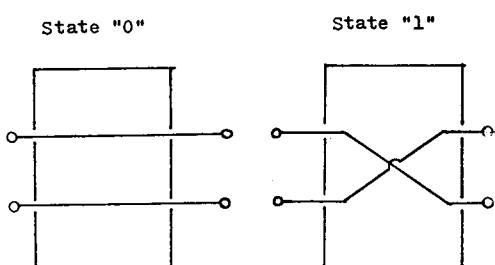


Fig. 27 Function of B-Element Switch

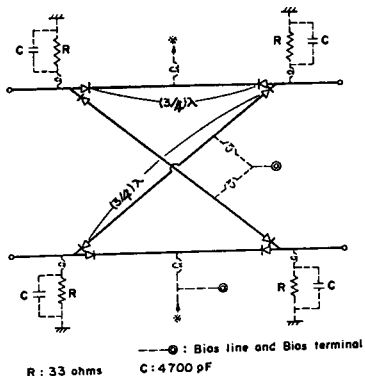


Fig. 28 B-Element Circuit Showing PIN Diodes and Bias System

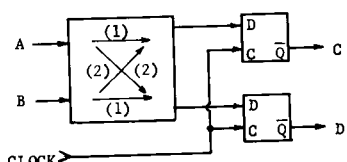


Fig. 29 Logic Type B-Element Switch

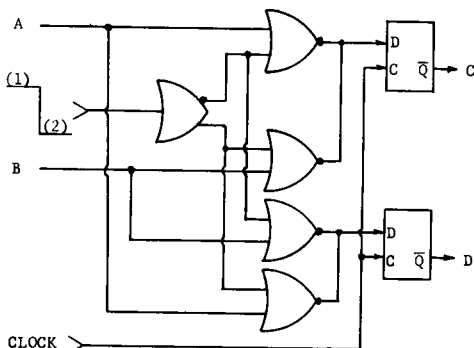
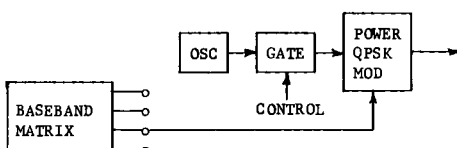
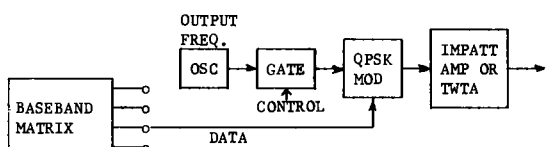
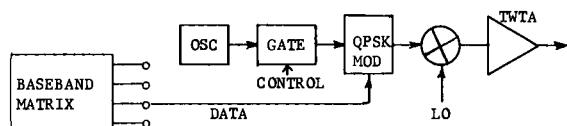
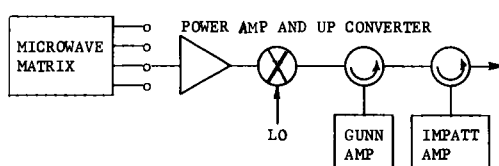
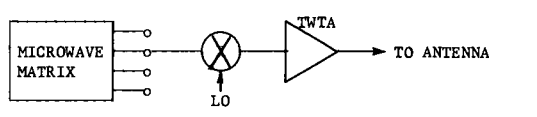


Fig. 30 Logic B-Element Switch Using Gates



**Fig. 31** Five Types of Transmitters Using Microwave and Baseband Matrices. The Baseband Matrix provides data streams to QPSK modulators in the output circuits.

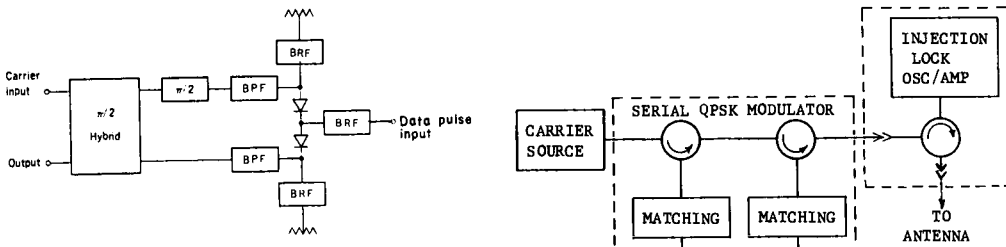


Fig. 32 Two-Diode Switch Type of PSK Modulator

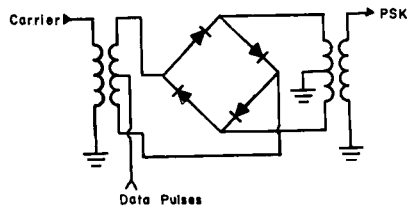


Fig. 33 Doubly-Balanced PSK Modulator

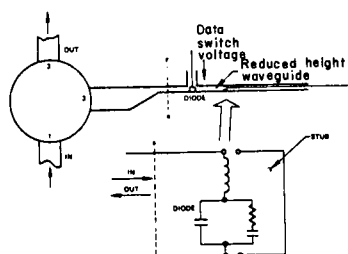


Fig. 34 Diode Switched Path Length Waveguide PSK Modulator

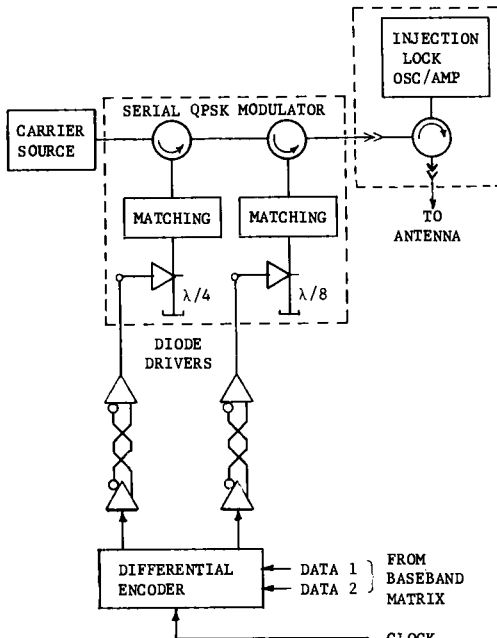


Fig. 35 Serial QPSK Modulator Followed by Injection-Locked Power Diode Amplifier. This output circuit is used in many terrestrial microwave systems.

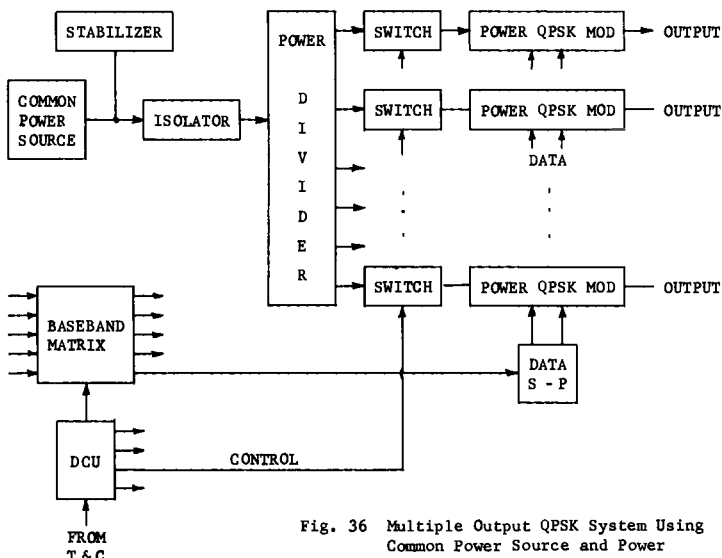


Fig. 36 Multiple Output QPSK System Using Common Power Source and Power QPSK Modulators

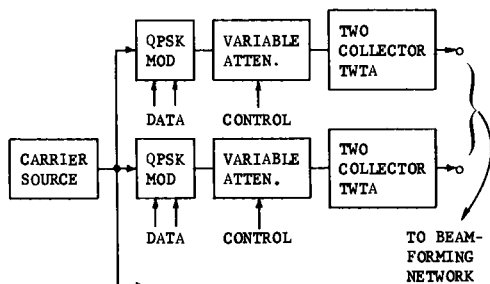


Fig. 37 Common Carrier Source System Using Two-Collector TWTA and Variable Output Carrier Level Control for High Efficiency

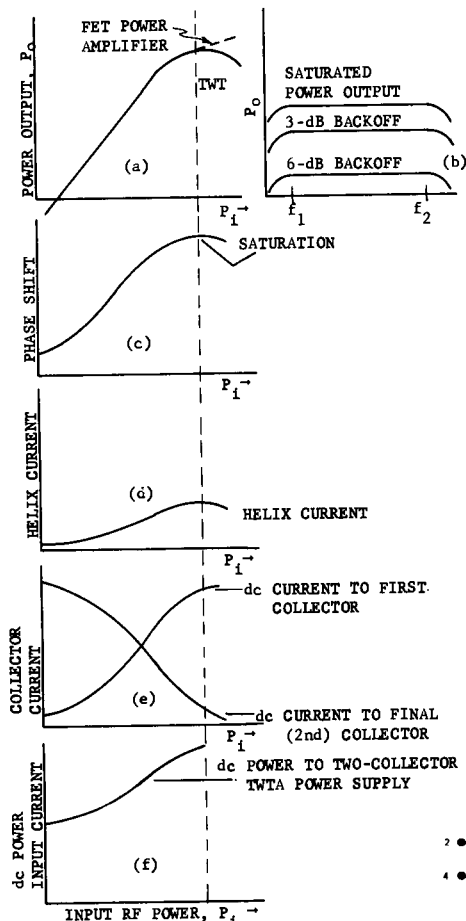


Fig. 38 Pertinent Characteristics of Two-Collector TWTA as a Function of Input RF Power Level

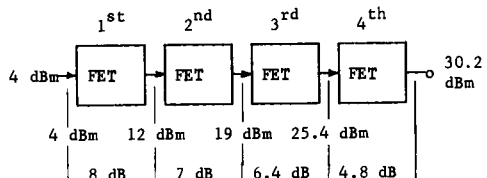


Fig. 39 X-Band FET Power Amplifier Developed by Fujitsu Ltd.

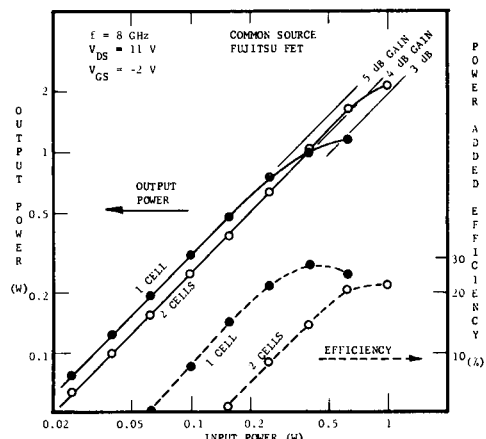


Fig. 40 Recent Output Power Achievement with FET's by Fujitsu Ltd.

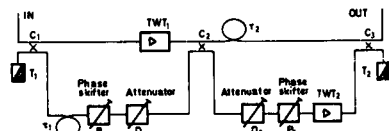


Fig. 41 Feed Forward Linearized TWT Amplifier by Bakken

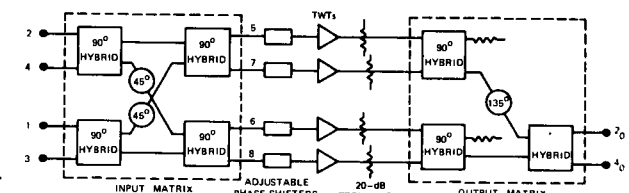


Fig. 42 Butler Matrix Transponder for Significant Suppression of IM Products Due to TWT Nonlinearity by W. Sandrin of Comsat Labs

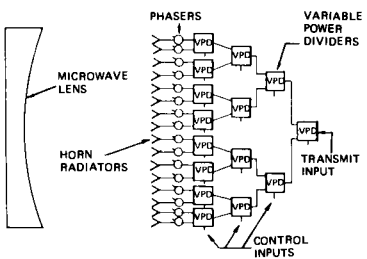


Fig. 44 Transmit Beam Forming Network Using Variable Power Dividers and Phasers

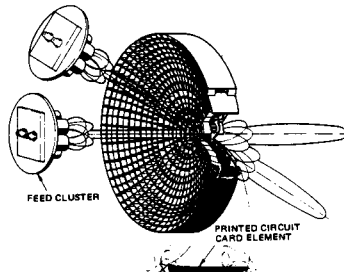


Fig. 46 Printed Circuit Card TEM Lens and Feed Clusters After Scott and Han

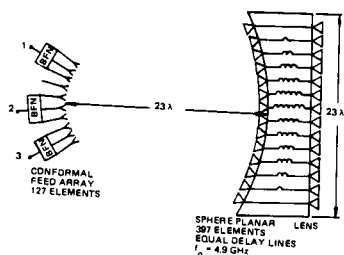


Fig. 45 Multi-Beam TEM Lens System Using Multiple Feed Arrays and Beam Forming Networks

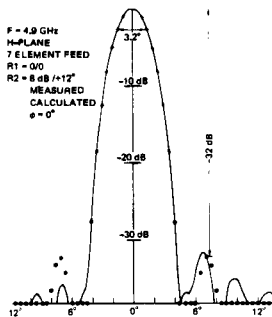


Fig. 47 Measured vs Calculated 4.9 GHz Pattern of TEM Lens with 7-Element Feed Cluster (On Axis)

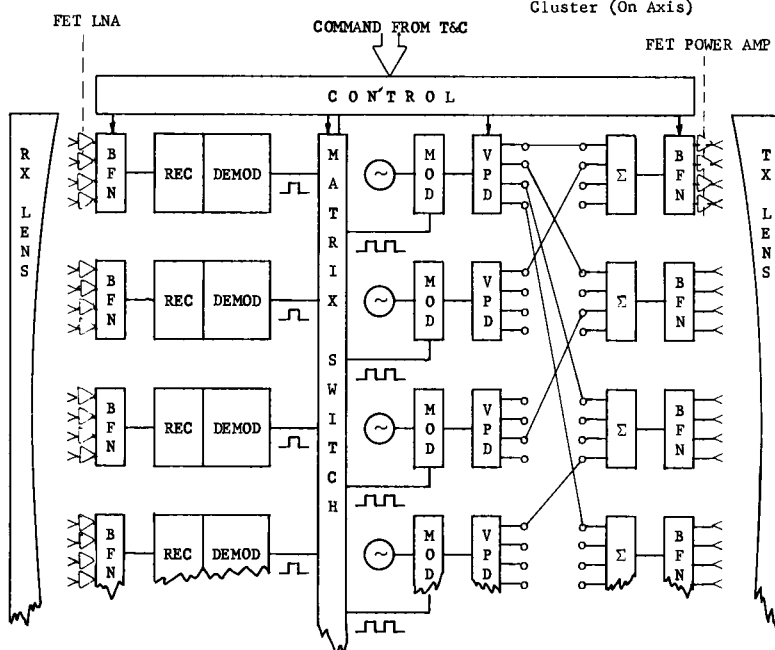


Fig. 43 Concept of Beam Switched SS-TDMA Transponder Using Beam Forming Networks with VPD's and Lenses

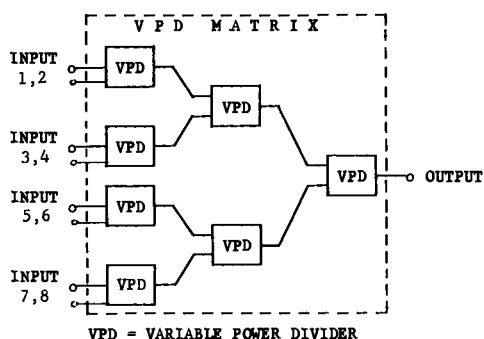


Fig. 48 VPD Matrix for Eight Inputs Combining to a Single Output

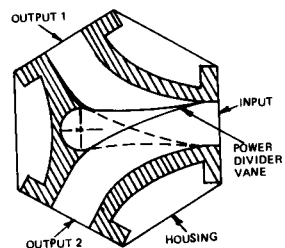
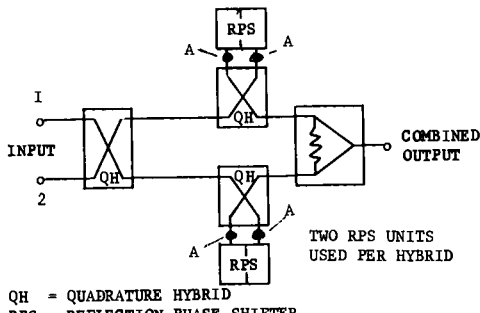


Fig. 49 Mechanical VPD



QH = QUADRATURE HYBRID  
RPS = REFLECTION PHASE SHIFTER

Fig. 50 Quad-Hybrid Coupled VPD  
Using Reflection Phase Shifters

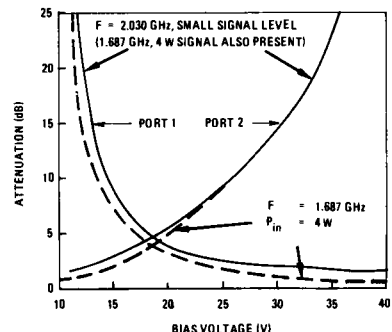


Fig. 52 Power Division Characteristics of Variable Power Divider of Figs. 50, 51 Used in SMS

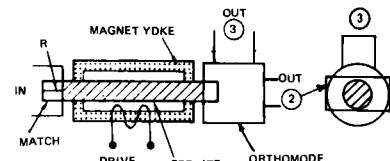


Fig. 53 Latching Faraday - Rotator VPD

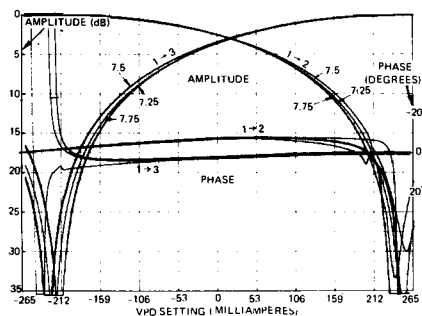


Fig. 54 VPD Characteristics of One Type of Faraday Rotator VPD

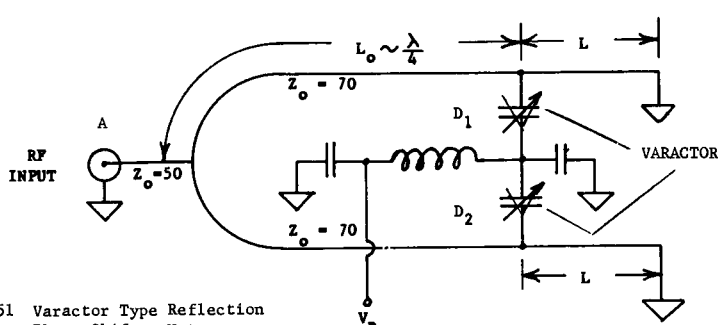


Fig. 51 Varactor Type Reflection Phase Shifter Unit

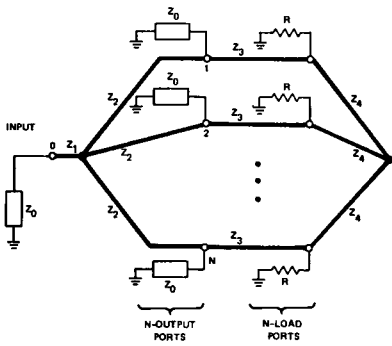


Fig. 55 N-Way Power Divider/Combiner for High Power Applications by U. Gyser of SRI

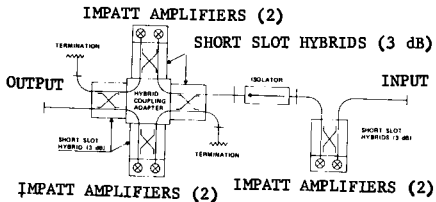


Fig. 56 Impatt Amplifier Combining Circuit after H. Kuno and D. English of Hughes EDD

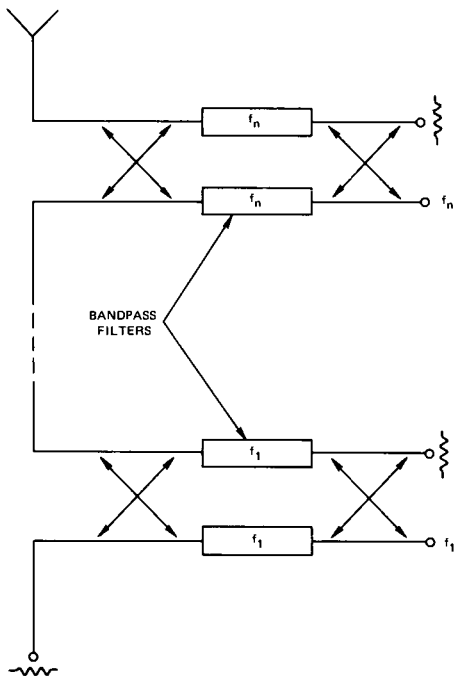


Fig. 57 Quadrature-Hybrid Coupled Contiguous Band Multiplexer

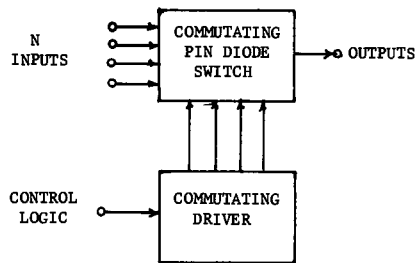


Fig. 58 Commutating N-Input PIN Diode Switch

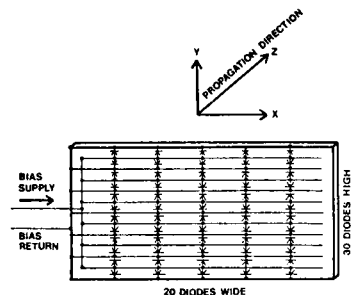


Fig. 59 The PIN Diode Matrix of an N-Diode High Power Microwave Switch for Multi-Throw Waveguide Switching

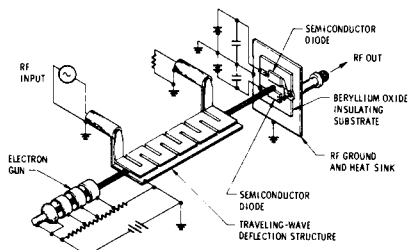


Fig. 60 Electron Bombardment Semiconductor Switch/ Amplifier

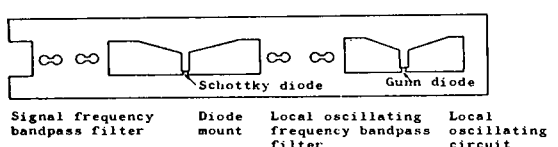


Fig. 61 12-GHz Mixer-Converter Mounted on a Planar Circuit for Use in a Receiving Waveguide Horn, After Y. Konishi, et al., of NHK Labs, Japan

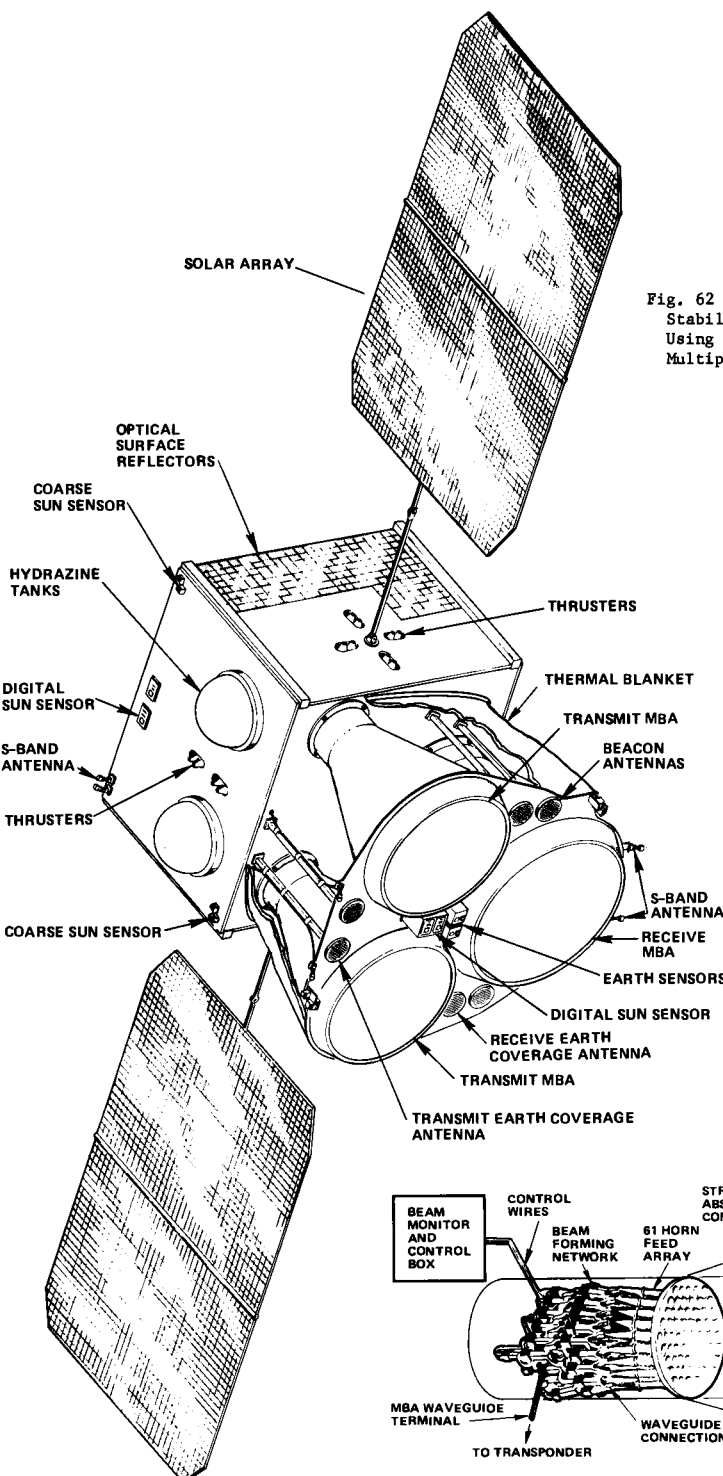


Fig. 62 Design Concept of a 3-Axis  
Stabilized Communication Satellite  
Using Two Transmit and One Receive  
Multiple Beam Antennas (MBA)

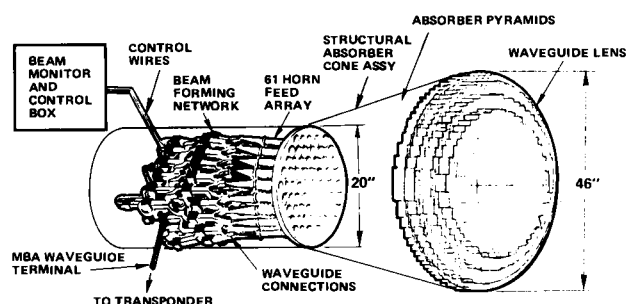


Fig. 63 Multiple Beam  
Antenna Using Wave-  
Guide Lens and 61 Horn  
Feed Array and Beam  
Forming Network

References (continued)

- (50) U. Gysel, "A New Way Power Divider/Combiner Suitable for High Power Applications", IEEE-MTT-S, 1975 International Microwave Symposium, Palo Alto, Ca.
- (51) H. Kuno, D. English, "Millimeter Wave Power Amplifier and Combiner", IEEE-MTT-S 1975 International Microwave Conference, Palo Alto, Ca.
- (52) R. Gruner and A. Williams, "A Low-Loss Multiplexer for Satellite Earth Terminals", Comsat Technical Review, Spring 1975.
- (53) C. L. Cuccia, J. B. Bowes, "Bandpass Filters: Vital Elements in Efficient MW Communication Spectrum Usage", Microwave System News, August/September 1976.
- (54) A. Atia and A. Williams, "Non-Minimum Phase Optimum Amplitude Bandpass Waveguide Filters", IEEE Trans. MTT-22, 1974.
- (55) R. Levy, "Linear Phase Filters and the Demise of External Equalization", Microwave System News, August/September 1976.
- (56) V. O'Donovan and S. Kallianteris, AIAA Paper 96-292, Montreal 1976.
- (57) H. Malone, M. Matson, P. Kennedy, "High Power PIN Diode Switch Matrix", IEEE-MTT 1974 International Microwave Symposium, Atlanta, Ga.
- (58) P. Bakeman, A. Armstrong, "Fast High Power Octave Bandwidth X-Band Waveguide Microwave Switch", IEEE-MTT 1976 International Microwave Symposium, Cherry Hill, N.J.
- (59) Y. Konishi, K. Uenakada, N. Yazawa, N. Hoshino, "Proposed SHF FM Receiver for Satellite Broadcasting", ICC-73, Seattle, Washington.
- (60) W. Scott, H. Luh, and E. Matthews, "Design Tradeoffs for Multibeam Antennas in Communication Satellites", ICC-76, June 14, 1976, Philadelphia, Pa.
- (61) F. Taormina, D. McCarty, T. Crail, D. Nakatani, "Intelsat IVA Communications Antenna Frequency Reuse through Spatial Isolation", ICC-76, June 14, 1976, Philadelphia, Pa.

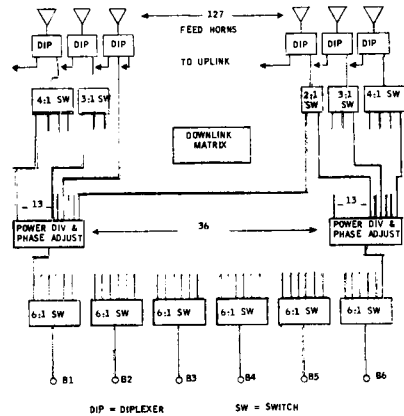


Fig. 64 Switched Feeder Network Concept by Scott, Luh and Matthews

# AN EXPOSITION OF ADVANCED LARGE AREA SPACECRAFT SOLAR ARRAY TECHNOLOGY

Larry G. Chidester

*Lockheed Missiles & Space Co., Inc, Sunnyvale, California USA*

## Abstract

Silicon solar arrays have provided the energy source for virtually all space satellites with orbital lifetimes greater than 30 days. The first experimental solar panels were orbited in 1958 and as early as 1961 large area solar arrays providing up to 1 kilowatt were qualified and used on classified programs. This paper will review the large area solar array development progress at Lockheed including the 100 kilowatt space station solar array and provide an up to date progress report on the newest United States large area lightweight solar array which is being developed for the NASA Solar Electric Propulsion (SEP) Spacecraft. The 25 kilowatt SEP solar array is approximately 4 meters wide and 65 meters long.

## Introduction

Recent studies by the Aerospace Corporation,<sup>1</sup> NASA,<sup>2,3</sup> and Boeing Aircraft<sup>4</sup> have identified over 100 space missions planned for the 1980 to 2000 time period which would require electrical power sources in the range of 25 kilowatts to 5 megawatts. Solar arrays have been the primary power source for virtually all long life spacecraft and most mission planners feel they will continue to be used over the next 20 years. Therefore, a great amount of interest centers around the challenge to build, test, and fly large area lightweight solar arrays. This paper summarizes the solar array development work at Lockheed Missiles & Space Co., Inc., where the two major NASA large area solar array technology programs have been conducted.

## Background

The solar cell utilizing the photovoltaic effect was invented in 1954. Arrays of solar cells were first used in space experiments in 1958 and by 1961 solar arrays large enough to generate over 1 kilowatt of electrical power were in use on classified spacecraft. To date over 14,000 square meters of solar cells have been used to power United States satellites. The largest power system flown was on Skylab<sup>5</sup> which had two separate area arrays (1) the Orbital Workshop (OWS) array consisting of two 56-square-meters wings and (2) the Apollo Telescope Mount (ATM) wing consisting of four 28-square meters wings. One wing of the OWS array was torn off during ascent; however, the remaining OWS wing and the ATM wings provided over 18 kilowatts of power to the Skylab spacecraft. Figure 1 shows the Skylab vehicle which includes the OWS and ATM arrays. The solar arrays on Skylab represented the 1969 state of the art of rigid solar panel design, but their 3600 kilogram weight made it obvious that if larger arrays were needed they must be lighter in weight. As a result, when the Manned Space Station Program was being configured in 1969 lightweight flexible solar arrays were selected for that application.

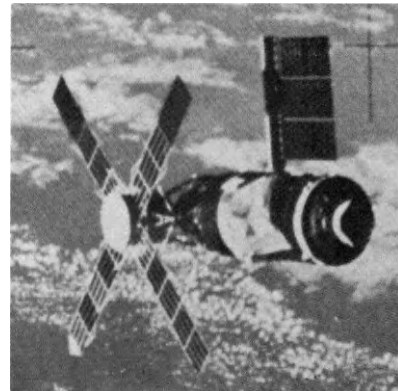


Figure 1 NASA Skylab Vehicle with Orbital Workshop and Apollo Telescope Solar Arrays

## Rigid Solar Panel Development 1961-1976

Large area solar arrays such as those shown in Figure 2 were used on Lockheed satellites as early as 1961. Although solar cell efficiency at that time was only 8 percent, these array system provided up to 2 kilowatts. Rigid solar panels built up typically on aluminum or nonmetallic honeycomb structures have been used on all United States missions using solar arrays. Each mission has defined a unique set of launch and orbital environmental conditions which resulted in a very specific solar array design. This wide range of missions has resulted in an equally wide variety of rigid solar panel designs. Figure 3 illustrates the different types of rigid solar panels developed at Lockheed. The standard method of measuring solar array performance is in watts per kilogram (W/kg). In all numbers quoted in this text for W/kg the entire structure to support the array assembly and the mechanism to extend and initially position the array are included in the mass. On this basis, the newest, lightest weight rigid solar array (developed at LMSC), will provide 30 W/kg at 25 deg C, compared with the 7 W/kg provided by the Skylab arrays. Although this is a significant improvement it is still much too heavy and bulky for very large solar arrays.

## Flexible Lightweight Solar Array Development

Flexible lightweight solar array design was initiated in the early sixties; however, no flexible solar array was tested in orbit until 1971. That array was the Hughes Aircraft "Flexible Rolled-up Solar Array" (FRUSA) which was flown as an experiment in the Air Force Space Test Program vehicle 71-2. The two 1.7-meter by 5-meter solar panels extended from a central 20 cm diameter storage



- 8 PANELS PER WING
- 8 WINGS FLOWN
- PANEL CONSTRUCTION:  
CAST MAGNESIUM GRIDS IN MAGNESIUM FRAME
- EXTENSION MECHANISM:  
PANTOGRAPH  
ROTATING SLIDER CRANK
- RATE CONTROL:  
ONE VISCOUS DAMPED LINEAR ACTUATOR
- FIXED WING
- ASCENT RESTRAINT:  
PANEL'S EDGE CLAMPED TO FRAME  
PRELOADED VIA TORQUE TUBE
- GROUND TEST TECHNIQUE:  
HORIZONTAL OVERHEAD TRACK

Figure 2 Large Area Solar Arrays Used in 1961

drum and provided 1.5 kilowatts with a total weight of 113 kg. Considering our previous method of comparing arrays, this unit provided approximately 45 W/kg. Figure 4 is an illustration of the 71-2 vehicle with the FRUSA extended. This array used conventional solar cell assemblies which were attached with adhesives to a fiberglass cloth substrate. It should be pointed out that this array development was started in the early 1960's and did not represent the newest technology in flexible array design when it was flight tested.

In 1968 NASA had initiated the Manned Space Station Program which required a 25 kilowatt power source. In low earth orbit operation (where earth shade and battery charge efficiency had to be considered) this requirement became a 100 kilowatt normal incident output solar array. Nuclear sources were first considered and then abandoned in favor of solar arrays. Even so, the photo-voltaic array technology for this application was questionable and as a result a new solar array study program was initiated by NASA to determine exactly what technology was available and to develop the required new technology. This Space Station Solar Array Technology Program (Aug 1970-Dec 1972) was performed by Lockheed (NAS9-11039) under the direction of NASA Johnson Spacecraft Center (JSC). It contained the following major phases:

1. Technology Evaluation (Blue Book)<sup>6</sup>
2. Design and Analysis (Red Book)<sup>7</sup>
3. Fabrication and Test (White Book)<sup>8</sup>

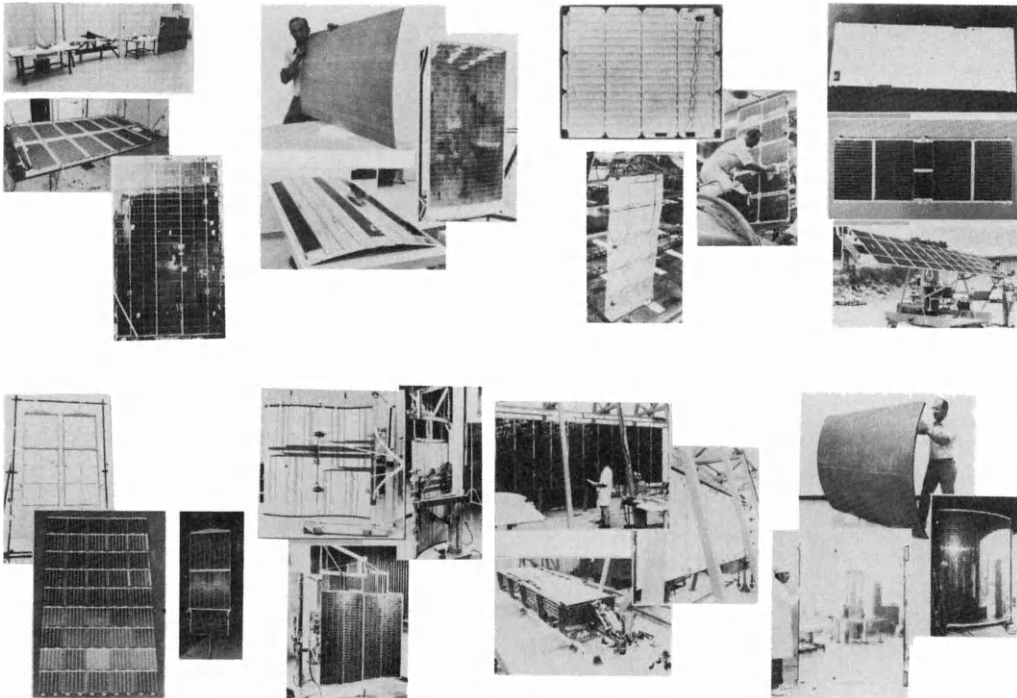
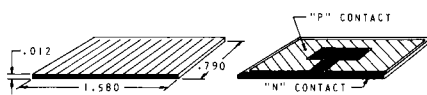
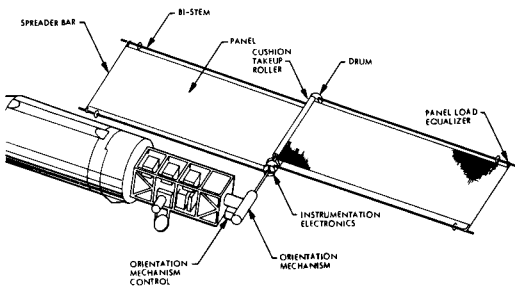


Figure 3 Rigid Solar Panel Developments Since 1965



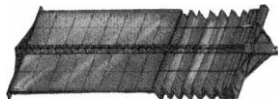
- Development (by Astro-Research Corporation) of a high strength extendible beam structure which would extend and retract the array. This was the only structure known which could be fully loaded at incremental points of extension.

FRUSA FLIGHT WEIGHTS	
Subsystem	Weight, lb
Orientation	
Orientation mechanism and electronics	74.17
Filter	.50
Subsystem total	77.67
Solar array	
Solar array panel	34.00
Array cushion, fuel and drive	34.20
Storage mechanism	32.60
Subsystem total	69.80
Power conditioning and storage	
Battery/charge controllers	42.46
Power converter	.31
Subsystem total	60.77
Basic FRUSA system total	208.24
Instrumentation	
Solar cell electronics unit	7.80
Load limit for 1 g load	77.13
Mic. sensors, conditioners, etc.	39.60
Subsystem total	39.53
Total experimental weight	247.77

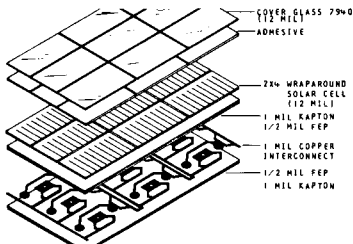
Figure 4 FRUSA Solar Array

This first large area flexible array technology program provided many significant results including:

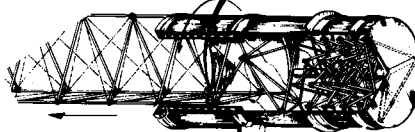
- Development (by Lockheed) of the flat-fold retractable array concept.



- Development (by Lockheed) of a lightweight blanket concept using Kapton material and incorporating printed circuitry, eliminating the need to use adhesives to mount cells to the blanket.



- Development (by Spectrolab and OCLI) of wrap-around contact solar cells, eliminating interconnect bends and allowing use of mass production techniques for soldering or welding.



- Development (by Ball Brothers) of a 1.5-meter diameter, 2-axis drive system and power transfer assembly which would orient each 50 kilowatt wing independently and transfer the 100 kilowatts of power into the Space Station.



The total array assembly weighed 2720 kilograms (minus the drive and slip ring assy) resulting in an output of 37 W/kg. The conservative weight of the space station solar array resulted from using 300 micron thick solar cell and 300 micron thick coverglasses which were the only high production cells available at that time. Also this array had to be designed to withstand 1-g loads for occasions when the space station was spun up for gravity oriented experiments. Figure 5 is a sketch of the 100 kilowatt wing deployment sequence and Figure 6 shows the full scale 9.1 meter by 31 meter quadrant (25 kilowatt) of the array that was fabricated and extension/retraction tested. Unfortunately, the United States space station program was delayed in favor of the Space Shuttle development so that further development and flight qualification of this array did not occur.

The need for large area lightweight arrays was still evident, however, and in 1974 NASA MSFC awarded Lockheed a contract (NAS8-30315) to develop a 66 W/kg design for the Solar Electric Propulsion (SEP Stage). This program, summarized in the remaining portion of this paper, will result in fabrication and test of one wing of a 25 kilowatt SEP solar array system.

#### SEP Vehicle Background

Solar electric propulsion, or the use of ion engines to provide spacecraft motive power, is considered critical to future interplanetary exploration. Ion engines need large amounts of electrical power and here again solar arrays have been selected as the primary power

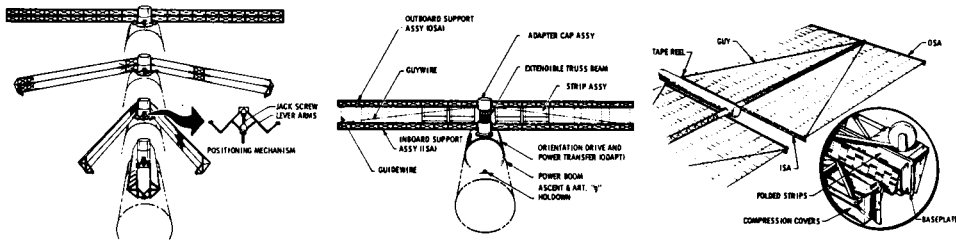


Figure 5 Deployment Sequence of 100 Kilowatt Space Station Solar Array

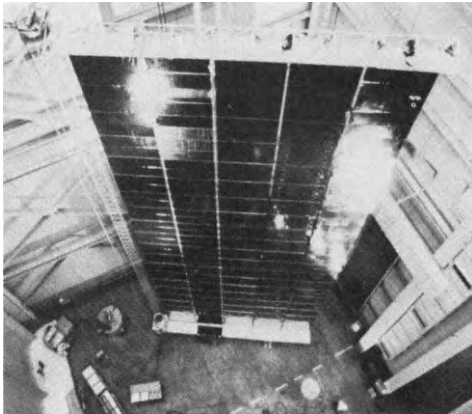


Figure 6 100 Kilowatt Space Station Solar Array Quadrant

source for this mission. Figure 7 is a sketch showing the SEP vehicle as it was envisioned in NASA studies by Rockwell International and also showing details of the SEP solar array wing as they are defined by the baseline design of the Lockheed study for MSFC (NAS8-31352). The SEP vehicle studies were stopped in 1975; however, SEP-related activities such as the array technology program, the ion engine technology program, and the SEP payload utilization study<sup>4</sup> were continued. That overall vehicle program has been restarted by NASA and will be in full swing by 1978. Typical missions planned for the SEP spacecraft will include: Flora Rendezvous - 500 days, Tempel Rendezvous - 800 days, 1987 Earth-Earth Flyby - 760 days, Mercury Orbiter - 500 days, 1985 Jupiter Flyby - 950 days, and Geosynchronous Tug - 3 to 6 years.

#### SEP Solar Array Study\*

The schedule of key milestones for the SEP solar array study is shown in Figure 8. The program objectives are: to develop a detail design of a 25 kilowatts array that will operate from 0.3 to 6.0 astronomical units (AU) and weigh no more than 380 kilograms, to perform a test program

demonstrating technological readiness for development and fabrication of the SEP solar array, and to fabricate and test a full scale 12.5 kilowatt array wing. The dominant design requirements of this array are shown below in Table 1.

Table 1 Dominant design requirements

- Operation between 0.3 to 6.0 AU
- Withstand Shuttle launch and reentry environments
- Operation in free space and in the earth's radiation environments with specified allowable degradation
- Power availability of 25 kilowatts BOL and 21 kilowatts EOL after performing typical SEP missions
- Full deployment, full retraction, to and from one intermediate deployment position
- Weight limit of 380 kilograms (66 W/kg)
- $V_{oc} \leq 420 \text{ Vdc}$ ,  $V_{mp} > 200 \text{ Vdc}$

#### Mechanical Design

Details of the array mechanical design are shown in Figures 9 and 10. The components include the 32 meter mast, a solar cell blanket 31 meters by 4 meters, an ascent support containment box, a preload cover, and a blanket tension/guide wire system.

The mast is a continuous longeron, collable lattice structure that can be extended or retracted from its storage canister to full length or any intermediate length. The mast provides a preload force to the array container locking levers of 533N (120 lb) at the start of extension and at the end of retraction. In the fully extended position it supports a 93.3N (21 lb) tip load offset 15.24 cm (6 inches) from a flat side of the mast triangular cross section. AEC-Able Engineering Co., of Goleta, Calif., is doing the initial development work on this mast.

The array blanket consists of 41 panels that are hinged together with a fiberglass cloth piano hinge and a fiber-glass/epoxy hinge pin. A graphite/epoxy intermediate tension bar has a hinge-half that allows it to be attached to the hinge between two panels at any point over the blanket length.

The array containment box cover and floor are clamped together to compress and support the array blanket

\*All of the data on the SEP Solar Array Technology Program was made available by Mr. R. V. Elms, who is the Lockheed Program Manager.

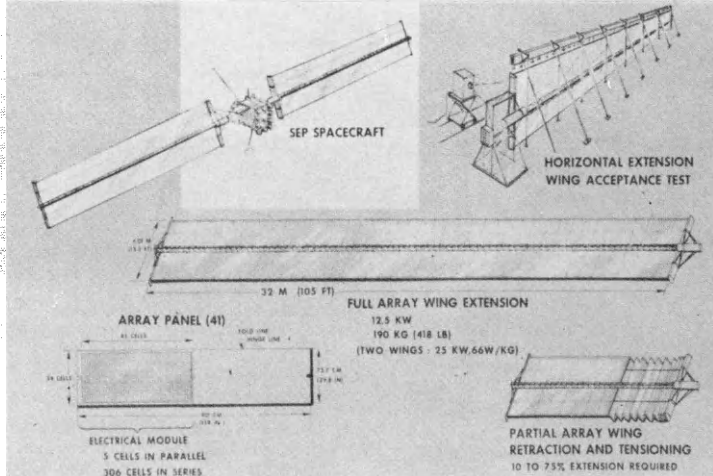


Figure 7 SEP Vehicle Showing Details of the 25 Kilowatt Solar Array

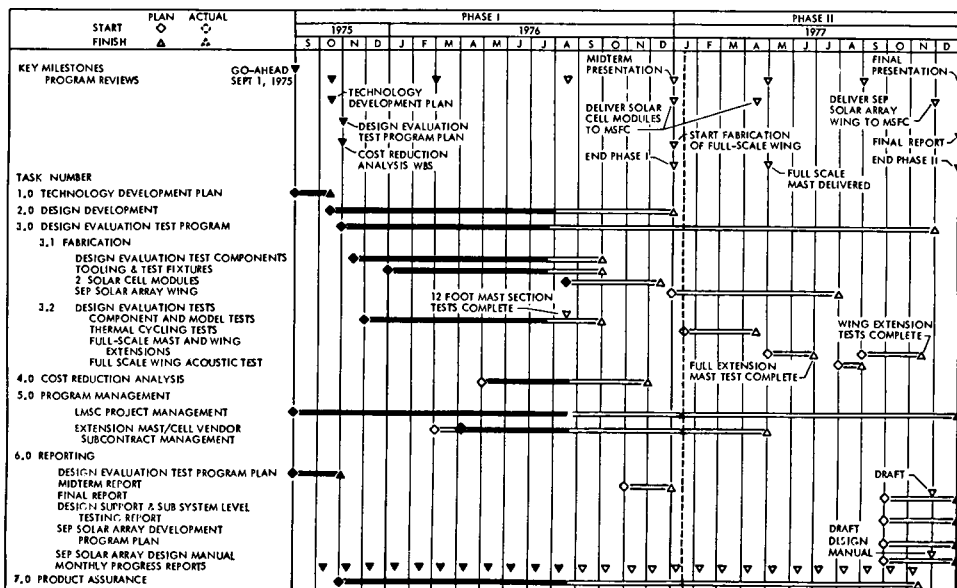


Figure 8 SEP Solar Array Schedule

during Shuttle launch and reentry. The box cover and floor are honeycomb assemblies with graphite/epoxy face sheets and perforated aluminum cores. The box floor and two thin skins form the main triangular beam for module torsional and bending stiffness. The mast is supported for the ascent period by the containment box with two fittings and four graphite/epoxy struts.

The blanket tension and guide wire systems are negotiator powered. The guide cables provide location control for the unextended blanket during array extension. The intermediate tension and bottom tension cables provide the

required blanket tension that in concert with the mast stiffness controls extended array natural vibration frequency.

## **Electrical Design**

The components and elements of the array electrical system are listed in Table 2. A wraparound electrode solar cell assembly is welded to the integral printed circuit interconnect. A 2 ohm-cm base resistivity cell is used since it does not drop off in power under high illumination intensity as much as a 10 ohm-cm cell and its

Table 2 Electrical design

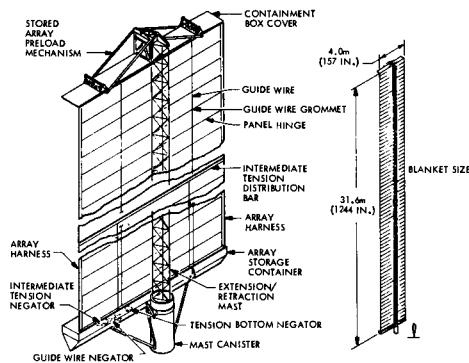


Figure 9 SEP Solar Array Mechanical Design

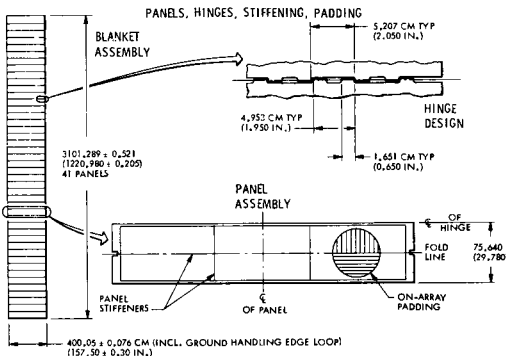


Figure 10 SEP Solar Array Blanket Design

higher initial specific power also provides a lighter array design.

The array harness is mounted on the back of the solar array blanket at the two long edges. The harness uses flat cable conductor (FCC) and 3 mil thick aluminum conductors of widths in the range of 0.050 to 0.25 in. to control voltage drops. Electrical joints are made to the copper busing in the panels in an area. There are no solar cells in front of the harness and the cell temperatures are not influenced by the harness.

The electrical modules are 30 in. x 80 in. for ease of fabrication and illumination testing. Two modules are joined together to form 30 in. x 160 in. panels as the array blanket is assembled. The array wing weights are shown in Table 3.

Substrate	
Material	1/2 mil Kapton with 1/2 mil adhesive, two sheets
Interconnect Bonding method	1 oz copper, 20% area Parallel-gap welding
Solar Cells	
Type	Wraparound, wraparound violet or helios alternative
Metallization	Passivated Ag-Pd-Ti or equivalent
Surface required for welding	≤150 nanometers RMS
Base resistivity	2 ohm-cm
Contact thickness	3 to 8 microns
Size	2 x 4 cm
Thickness	8 mil
Cell Cover	
Material	Fused silica, ceria glass alternative
Coatings	AR, blue filter
Adhesive	Refined Sylgard 182 (DC93-500)
Thickness	6 mil
Panel Electrical Design	
Voltage	125V nom at 1 AU, 50°C
Module configuration	Two per panel
Feeder Harness	
Type	Flat conductor cable
Conductor	Aluminum

Table 3 Array wing weight summary

	kg
Mast	32.04
Guidewire, Intermediate Tension	3.57
Full Tension Mechanisms	
Tension Transfer	0.08
Mast Tip Fitting	0.69
Cover Assembly	10.40
Container	4.20
Triangular Beam	8.35
Support Struts	1.55
Solar Cell Blanket	113.65
Array Harness	5.59
Miscellaneous Nuts and Bolts	0.90
Total	184.11
Required Weight	190.00
Solar Cell Blanket	113.65
Leaders and Tension Bars	1.38
Panel (41)	112.27
Substrate W/Padding	0.531
Solar Cells (3060)	1.171
Cover Adhesive (3060)	0.130
Cover Slide (3060)	0.845
Hinge (2)	0.058
Hinge Pin (1)	0.003
Total	2.738

The weldable solar cell assembly supplier, Spectrolab, Inc., has developed an 8 mil wraparound contact  $2 \times 4$  cm cell design providing 11.4 percent average covered efficiency with a 6 mil fused silica cover (350 nm UV cut-on filter). The first 20 cells of 4800 have been delivered to LMSC for electrical and weldability evaluation. A solar cell voltage change from 0.165V to 0.75V is seen at the root of the array over the AU range of 0.3 to 6.0. This is for a radiation degraded cell and includes the effect of changing electrical harness voltage drop values with temperature. Since this represents a factor of 4.5 it necessitates changing the number of electrical modules in series by switching to provide the required 200V to 400V input to the vehicle as follows:

	0.3 to 0.75 AU	0.75 to 3.1 AU	3.1 to 6.0 AU
Electrical Modules in series (306 cells in series in a module)	4	2	1

The predicted array power reduction ( $P/P_0$ ) versus sun distance is shown in Figure 11. This is in effect changing the array illumination from 11 suns to 1/36 sun. At the 0.3 AU distance the array must be inclined to the incident sunlight to reduce operating temperatures to the acceptable limit of 150 deg C.

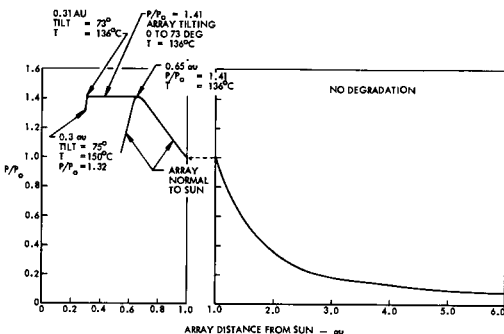


Figure 11 Ratio of SEP Solar Array Power From 0.3 AU to 6.0 AU

#### Solar Array Testing

An SEP solar array materials evaluation program is being conducted by NASA-MSFC to evaluate candidate array system materials for stability under UV and particle irradiation environments.

The overall SEP array test program at Lockheed is shown in Table 4.

Table 4 SEP array test program summary

#### Fabrication Evaluation Testing

- Flexible Substrate Module Fabrication
- Numerical Control Weld Station Tests
- Aluminum FCC Harness Joints to Copper Bus
- Composite Materials Fabrication Tests
- Extension Mast High Temperature Materials

#### Design Support Evaluation Tests

- Substrate Tensile, Tear, and Creep Tests
- Thermal Control Tests
- Cell Joint Bonding Tests
- Thermal Cycling Tests
- Solar Cell Performance Tests
- UV Testing
- Blanket and Harness Folding at Temp Extremes
- Array Harness Fatigue Test
- On-Array Padding Vibration Test
- Tension and Guide Wire Mechanical Test
- Extension Mast Component Tests

#### Zero-Gravity Operation Testing

- SEPS Root Section Model Tests
- Aircraft Zero-Gravity Simulation Test

#### Full-Scale Hardware Testing

- Full-Scale Mast Structural Tests
- Full-Scale Wing Acoustic Tests
- Full-Scale Wing Extension Tests

#### NDT Testing

- Small 155 Cell Module Tests
- Full-Scale Electrical Module Tests

#### Zero-Gravity Array Fold-Up Testing

A significant area for technology demonstration in the SEP solar array program is the proper folding of the proposed flat fold flexible array blanket during retraction in a zero-gravity environment. The fold line of the array panels must move outward from the plane of the extended array blanket when blanket tension is released. The two tensioned guide cables behind the array blanket and running through grommets at the panel hinge lines tend to prevent the panel fold lines from folding in the wrong direction. If the blanket is completely flexible, the orientation of the fold-lines in the retracted array configuration is not predictable with high confidence.

Panel stiffening in the form of lightweight composite ribs is added to the array panels. This stiffening increases the influence that the two taut guide cables have in a direction across the width of panels on both the hinge lines and the foldlines.

Two candidate test methods, neutral buoyancy testing and aircraft zero-gravity simulation, were evaluated and the aircraft zero-gravity trajectory test was selected as providing a better dynamic simulation at design array retraction rates. The test configuration is shown in Figure 12. One zero-gravity parabola will be used to extend the model blanket (full scale width and short length) and one will be used to retract the model blanket. During the test sequence the amount of panel stiffening will be reduced until an operable minimum weight configuration is defined. The test sequence requires 12 parabolas nominally.

#### Full-Scale Hardware Tests

The full-scale mast and SEP solar array wing will be extended in 1-g to evaluate the hardware against the assembly design requirements to the maximum extent possible. The full-scale wing assembly will also be exposed to the mission acoustic noise environment to validate the solar cell blanket preload and padding protection design.

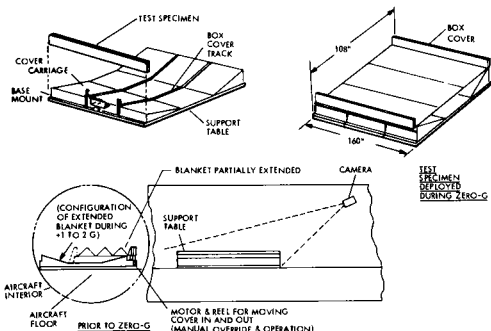


Figure 12 Aircraft Zero-Gravity Test Configuration

The evaluation of SEP solar array wing extension acceptance test methods was completed. The recommended method is the horizontal-vertical configuration shown in Figure 7. The major advantages of this method are:

1. Limited impact on the flight design panel hardware.
2. Limited handling stress placed on the solar cell connections during the acceptance test.
3. Ease of access to both the front and back of the extended solar array blanket, as well as the extension mast.

#### NDT Development Testing

The development of practical and effective nondestructive test methods for the evaluation of parallel gap welding of solar cell joints and array modules is required to ensure hardware quality for the large area SEP solar array. The cell joint NDT techniques to be used include the RDI infrared microscope and the Van Zetti Thermal Sensor (Weld Temperature Monitor). Large area panels can be tested by IR scanning of mounted array panels through which current is forced. Dark I-V testing of large area panels will also be evaluated for application to launch base checks following transportation and/or storage.

#### Space Shuttle Flight Test

The SEP solar array described above has been identified by NASA as one of the Shuttle flight experiments to demonstrate array performance and deployment of large area structures in space.

#### Summary

Solar photovoltaics continue to be favored over nuclear sources for 1980-2000 space missions. Rigid substrate solar arrays have been improved in performance significantly but still are limited to producing in the range of 30 W/kg. Lightweight flexible solar arrays have been qualified in orbital flight which produce 45 W/kg and studies where prototypes were fabricated will produce 66 W/kg. Improvements in solar cell efficiency and radiation resistant qualities are projected to occur before 1985 that will allow silicon photovoltaic array designs producing 200 W/kg.

#### References

1. Study of Commonality of Space Vehicle Applications for Future National Needs; Aerospace Corporation Report ATR-75 (7365)-1, March 1975.
2. "Outlook For Space," NASA Report SP-386, 387, January 1976.
3. "Critical Areas Satellite Power System Concepts," NASA/JSC Report WPJSC 10873, July 1975.
4. "Payload Utilization of the SEPS Vehicle" (PLUS) Study by Boeing Aircraft Corp. for NASA MSFC, Contract No. NAS8-31444.
5. J. Bruno, "ATM Solar Cell Module Performance Testing," 4th Intersociety Energy Conversion Engineering Conference Proceedings, September 22-26, 1969.
6. LMSC, "First Topical Report, Space Station Solar Array Program," LMSC-A981486, December 1970.
7. LMSC, "Second Topical Report, Space Station Solar Array Program," LMSC-A995719, November 1971.
8. LMSC, "Third Topical Report, Space Station Solar Array Program," LMSC-D153526, September 1972.
9. G. F. Turner, "Electric Power Systems for Space - A Progress Report," AIAA Astronautics and Aeronautics Publication, December 1975.
10. R. V. Elms, et al, "SEPS Solar Array Design and Technology Evaluation," AIAA 11th Electric Propulsion Conference Proceedings, March 1975.
11. R. V. Elms, et al, "SEP Solar Array Technology Development," 11th IECEC Conference Proceedings, September 1976.

# URANIUM ZIRCONIUM HYDRIDE REACTOR SPACE POWER SYSTEMS

James H. Van Osdol, Wallace B. Thomson and Owen S. Merrill\*

*Atomics International, Division of Rockwell International, Canoga Park, California 91304*

*\*Energy Research and Development Administration, Washington, D.C.*

## Abstract

A brief summary of the characteristics of unmanned 10 to 75 kW zirconium hydride reactor space power systems is presented. The power conversion types considered are Brayton, organic Rankine, Stirling, and thermoelectric. Design and performance data for each of the systems is presented at selected power levels as well as parametric information which includes total system weight, radiator area and system size as a function of power level. The systems utilize deployable waste heat rejection radiators which not only result in compact launch configurations, but also yield light-weight systems.

The Brayton, organic Rankine, and thermoelectric systems represent near-to-intermediate term technologies. Of these systems, the Brayton system is the smallest and has the lowest mass. These area and mass advantages are offset somewhat by the considerably lower operating temperature of the organic Rankine systems. While not yet developed to an equivalent technology status, Stirling systems represent attractive possibilities for future applications. They are significantly lower in mass and smaller than the Brayton systems.

## INTRODUCTION

Zirconium hydride ( $ZrH_2$ ) reactor power systems have been under active development since 1957. Since then, over \$300 million has been invested in development efforts. In 1965, the only U. S. reactor system ever tested in space, the SNAP 10A system, was launched into a 700 nautical mile earth orbit. This test proved that a reactor power system could be safely placed in orbit without compromising launch or mission operations. The power system successfully started up in orbit on command and operated flawlessly although the mission was prematurely terminated by a failure in the spacecraft. Since that time, there have been continuing development programs which have resulted in substantial improvements in power system efficiency, mass, and size. As a result, there has been increased interest in reactor systems by potential users of high-power space systems, and consequently, a system engineering study was recently conducted to establish the characteristics of unmanned space power systems in the power range of 10 to 75 kW.\* As is described in this paper, system specific masses and areas and system efficiencies of 24 g/W,  $1.5 \text{ m}^2/\text{kW}$ , and 26.5%, respectively, are achievable at 75 kW. This is indeed a significant step forward considering that the SNAP 10A system had a specific mass of 863 g/W, its efficiency was less than 2%, and it had a specific radiator area of  $12.3 \text{ m}^2/\text{kW}$ .

## POWER SYSTEMS DESCRIPTION

The zirconium hydride reactor, shown in Figure 1, is a thermal reactor. The fuel is 10 wt %, fully enriched uranium, and 90 wt % zirconium,

\*Unless otherwise noted, power is electrical power throughout this paper.

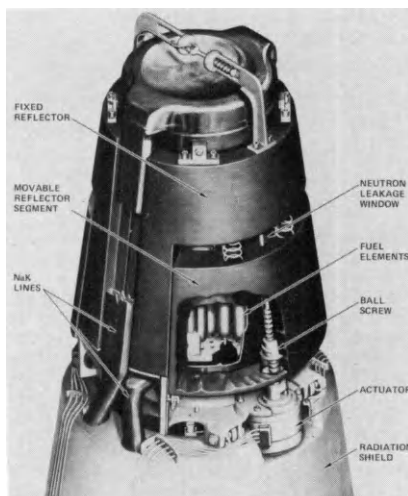


Figure 1. ZrH Reactor System

hydrided to contain approximately as much hydrogen as room temperature water. The fuel is contained in Hastelloy X cladding. The inside surface of the cladding is coated with a ceramic to retard hydrogen leakage from the element at operating temperature. The exterior surface of the cladding has spiral fins which promote coolant mixing within the core and also provide positive spacing between elements, which are arranged in a hexagonal pattern within the core. Core cylinder diameters are typically in the 20 to 40 cm range

and lengths vary from 30 to 50 cm. Liquid metal NaK flows through the core between fuel elements and delivers heat to the power conversion unit (PCU). An actuator-ball screw drive system positions the movable neutron reflector segment to permit the appropriate neutron leakage to occur through the reflector window, thereby providing the desired operating temperature and power. Reflector thicknesses range from 5 to 10 cm.

Table I shows the guidelines used in the systems' designs. System characteristics were determined at power levels of 10, 25, 50, and 75 kW, for Brayton, organic Rankine, and Stirling systems. Thermoelectric (TE) systems were only considered at 10 and 25 kW because their weights were excessive at higher powers. Radiation levels to the payload of  $10^{13}$  nvt neutrons and  $10^7$  rads gamma rays were selected as being consistent with the radiation hardness of solid state components and circuitry.

TABLE I

SYSTEM DESIGN GUIDELINES

Power Requirements	10, 25, 50, and 75 kW
Power Conversion Unit Types	Brayton Organic Rankine Stirling Thermoelectric
Power System Life	7 years
Radiation Levels at Base of System	
Neutrons	$10^{13}$ nvt
Gamma rays	$10^7$ rads
Orbit	Geosynchronous
Launch Vehicle	Shuttle plus upper stage

The configurations of all four power system types are essentially as shown in Figures 2 and 3. Systems of other configurations can be utilized if they are more compatible with the particular mission and spacecraft concept under study. Figure 2 shows an organic Rankine system in the compact, launch configuration. The reactor and shield are mounted atop the conical portion of the all aluminum radiator, which houses and supports the PCU. The cylindrical radiator sections only support their own mass during launch and are, therefore, very light weight. The radiator sections are interconnected by metallic, flexible lines, and utilize an organic heat transfer fluid. Once a satisfactory orbit is achieved, a mechanism deploys the system as shown in Figure 3.

All four system types have a NaK primary loop, as shown typically in Figure 4 for a Brayton system, which delivers heat to the PCU. The Brayton, Stirling, and TE systems all use coolers to transfer waste heat from the PCU to the radiator loop. The organic Rankine systems are direct cycle, however, using the organic working fluid in the radiator.

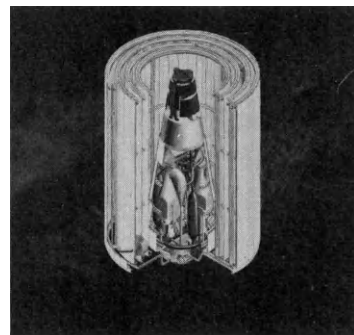


Figure 2. Typical Zirconium Hydride Reactor Space Power System Launch Configuration

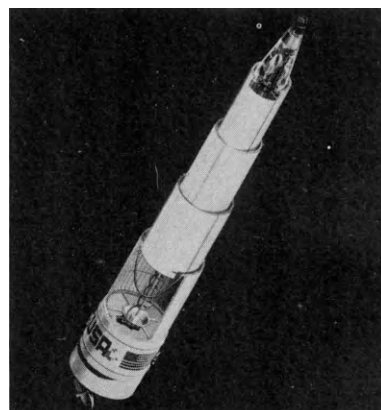


Figure 3. Typical Zirconium Hydride Reactor Space Power System

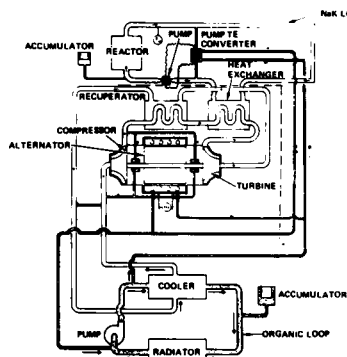


Figure 4. Reactor-Brayton (System Schematic)

## SYSTEM OPTIMIZATION

Parametric PCU data were obtained from AiResearch (Brayton), Sundstrand (organic Rankine), and Mechanical Technology, Inc. (Stirling). Data previously obtained from Westinghouse on their tubular modules were used for the TE systems. The data obtained were PCU efficiency, mass, and size as a function of radiator average temperature for a fixed hot side temperature. Figures 5 and 6 are examples of this data. The efficiencies are in the 35 to 50% range for the Stirling PCU, Brayton 10 to 25%, organic Rankine 10 to 20%, and TE 6 to 7%. The Brayton PCU mass increases with increasing temperature, as shown in Figure 6, because gas density is decreasing, resulting in larger, heavier heat transfer components. Organic Rankine system mass decreases with increasing temperature because higher temperature corresponds to higher turbine back pressure, higher vapor density, and smaller heat transfer components. Because 90% of the Stirling PCU weight is in the linear alternator and because the alternator weight is insensitive to radiator temperature, the PCU weight was considered to be independent of cold side temperature.

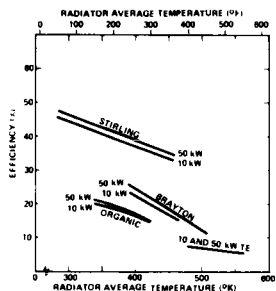


Figure 5. Power Conversion Unit Efficiency

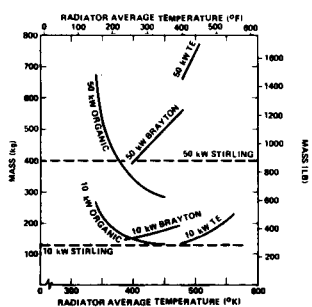


Figure 6. Power Conversion Unit Mass

The parametric efficiency data were used as input to establish overall system efficiency and performance as a function of radiator temperature. Component requirements were then established at each radiator temperature and components sized to meet the requirements. These component characteristics were used to establish total system mass curves, which along with radiator area and other factors, was used to select the reference system design points.

Figures 7 and 8 are examples of how total system mass and area vary with radiator average temperature. The Brayton and organic Rankine masses show the same trend as the PCU mass curves. The other major components in the systems are the reactor, heat transfer equipment, and the radiator. As radiator temperature increases, the reactor and heat transfer equipment masses increase, but radiator mass decreases. Radiator area decreases with increasing temperature until the minimum area point is reached. Over the temperature ranges studied, only the Brayton system exhibited a true minimum. In this case, the reference system was selected at a slightly larger area than minimum in order to realize a mass reduction. The organic Rankine and Stirling systems smallest area and lowest mass occurred at the maximum temperatures investigated. The TE system mass was approximately 4100 kg at 50 kW and, consequently, was excluded from further consideration at 50 and 75 kW. Similar systems characteristic curves were prepared at the other power levels and reference system designs were selected.

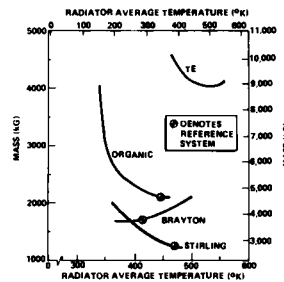


Figure 7. 50 kW Systems Mass

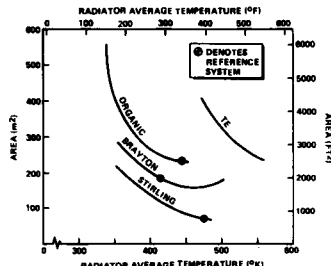


Figure 8. 50 kW Systems Radiator Area

## REFERENCE SYSTEMS

Tables II and III show characteristics and mass summaries for 50 kW systems. Reactor outlet temperature for the Stirling and Brayton systems was limited to 977°K by reactor fuel peak temperature limits. The organic Rankine reactor outlet temperature is dictated by organic fluid degradation in the boiler. Although not shown on the table, the TE systems at 10 and 25 kW had reactor outlet temperatures of 922°K. At higher temperatures, degradation in the TE modules offsets any system gains. The radiator area is smallest for the Stirling system followed in order by Brayton and organic Rankine.

As Table III shows, the Stirling also has the lowest mass at 1177 kg. The masses of the reactor, liquid metal components, heat rejection loop components and radiator are all the lowest for the most efficient system. A trend in shield mass cannot be discerned because: (1) as reactor power increases, shield mass goes up, (2) as the radiator area goes up, the separation distances grows and shield mass goes down. These two trends are off-setting and hide any obvious overall trend.

Figure 9 shows the deployed configurations of the three 50 kW systems. The Stirling, Brayton, and organic Rankine systems have 3, 6, and 7 radiator sections, respectively.

Figures 10 and 11, and Table IV show system mass, radiator area, and geometry as a function of power level for all four systems. The organic Rankine system mass starts to increase more steeply above 55 kW because of the increasing weight of heat transfer components, piping, and radiator. Tables V and VI show the specific mass and radiator area, respectively, of each system at the power levels studied.

Figure 11 shows that above 50 kW, radiator area increases more rapidly with increasing power. At 50 kW, the specific areas are 1.4, 3.7, and 4.6 m<sup>2</sup>/kW for the Stirling, Brayton, and organic Rankine systems, respectively.

Table IV shows power systems maximum diameter, launch length, and deployed length as a function of power for all four system types. Some discontinuities appear as the power level changes because of the use of different numbers of radiator sections.

TABLE II  
50 kWe SYSTEMS CHARACTERISTICS

	Brayton	Organic Rankine	Stirling
<b>Power, kW</b>			
Gross Electrical	52	52	52
Net Electrical	50	50	50
Reactor Thermal	255	439	189
<b>Efficiency, %</b>			
System	19.6	11.4	26.5
PCU	22.4	13.0	34.0
<b>Temperatures, °K (°F)</b>			
Reactor Outlet	977 (1300)	700 (800)	977 (1300)
Turbine or Heater Inlet	961 (1270)	644 (700)	977 (1300)
Radiator Average	413 (285)	447 (345)	475 (395)
<b>Flowrates, kg/s (lb/s)</b>			
Primary Loop	5.2 (11.5)	8.8 (19.4)	3.9 (8.5)
Working Fluid	2.5 (5.4)	0.95 (2.1)	-
Heat Rejection Loop	0.9 (2.1)	3.4 (7.4)	1.2 (2.6)
<b>Pressure Drop, Pascal × 10<sup>4</sup> (psi)</b>			
Primary Loop	1.0 (1.5)	1.0 (1.5)	0.8 (1.2)
Heat Rejection Loop	55.2 (80)	51.7 (75)	51.7 (75)
<b>Radiator Area, m<sup>2</sup> (ft<sup>2</sup>)</b>	186 (2000)	232 (2500)	68.7 (740)
<b>Total Mass, kg (lb)</b>	1709 (3767)	2037 (4488)	1179 (2596)
<b>System Size, m (ft)</b>			
Launch Height	4.6 (15.3)	4.7 (15.5)	4.7 (15.7)
Deployed Height	24.7 (82.3)	30.5 (101.6)	13.2 (44)
Diameter	3.2 (10.6)	3.7 (12.3)	2.2 (7.3)
<b>Number of Radiator Sections</b>	6	7	3

TABLE III  
50 kWe SYSTEMS MASS SUMMARY  
kg (lb)

	Brayton	Organic Rankine	Stirling
Reactor	267 (587)	309 (680)	255 (561)
Shield	75 (165)	74 (163)	79 (174)
Liquid Metal Components	185 (406)	279 (615)	114 (252)
Power Conversion Unit	412 (906)	213 (470)	399 (880)
Heat Rejection Loop Components	109 (239)	181 (398)	71 (156)
Radiator-Structure	623 (1374)	937 (2064)	236 (521)
Electrical	41 (90)	44 (98)	23 (52)
Total	1712 (3767)	2037 (4488)	1177 (2596)

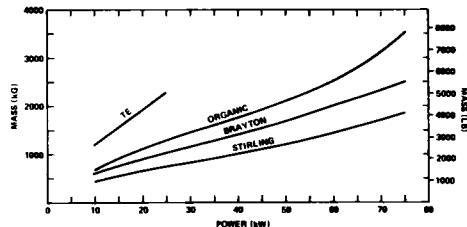


Figure 10. Power Systems Mass

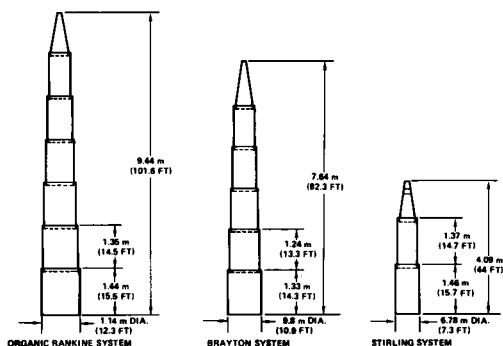


Figure 9. 50 kW Systems - Deployed Configuration

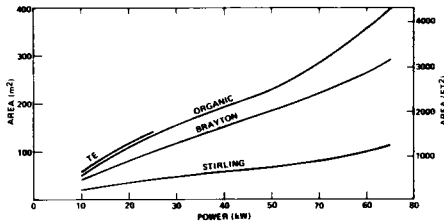


Figure 11. Power Systems Radiator Area

TABLE IV  
SYSTEM GEOMETRY

Power (kW)	Dimensions (m)											
	Brayton			Organic Rankine			Stirling			TE		
	D*	L <sub>L</sub> †	L <sub>D</sub> ‡	D	L <sub>L</sub>	L <sub>D</sub>	D	L <sub>L</sub>	L <sub>D</sub>	D	L <sub>L</sub>	L <sub>D</sub>
10	2.0	3.4	8.7	1.7	4.6	11.6	1.4	5.0	5.0	2	4.7	125
25	2.5	4.6	17.3	2.5	5.0	24.4	2.1	4.3	10.5	3.2	5.6	20.9
50	3.2	4.6	24.7	3.7	4.7	30.5	2.2	4.7	13.2			
75	3.7	5.3	34.2	4.0	6.0	44.9	3.0	5.1	17.4			

\*Maximum Diameter

†Launch Length

‡Deployed Length

TABLE V  
SYSTEMS SPECIFIC MASS  
(g/W)

System	10 kW	25 kW	50 kW	75 kW
Brayton	63.1	43.5	34.2	33.7
Organic Rankine	68.3	53.8	40.7	46.4
Stirling	48.4	31.2	23.6	24.4
Thermoelectric	105.0	94.4	-	-

TABLE VI  
SYSTEMS SPECIFIC AREA  
(m<sup>2</sup>/kW)

System	10 kW	25 kW	50 kW	75 kW
Brayton	4.0	4.1	3.7	3.9
Organic Rankine	5.0	5.5	4.6	5.3
Stirling	1.8	1.9	1.4	1.5
Thermoelectric	5.8	6.0	-	-

#### SUMMARY AND CONCLUSIONS

Zirconium hydride reactor space power systems possess several key attributes for unmanned space missions requiring tens of kilowatts of electric power. They are reasonably compact in the launch configuration and will be compatible with the shut-

tle volume and mass constraints with most space-craft configurations. Since the systems are essentially nonradioactive prior to operation in space, they present minimum safety concerns during prelaunch, launch, and orbit injection phases as was demonstrated during the SNAP 10A flight test program. Post operation safety problems are greatly minimized in orbits having lifetimes long enough to permit the reactor to decay to extremely low levels of radioactivity (altitudes >400 nautical miles).

Of the near-to-intermediate term technology systems, i.e., the Brayton, organic Rankine, and TE, the Brayton system is the smallest and has the lowest specific mass. While not yet developed to an equivalent technology status, the Stirling systems represent attractive possibilities for future development. Stirling systems will be especially advantageous at power levels at 75 kW and beyond.

In conclusion, the zirconium hydride reactor program and power conversion system programs have provided the U. S. with a substantial technology base for high-power, space nuclear systems. The capabilities and limitations of most components and subsystems are well understood and the reactor space systems are ready for application.

#### ACKNOWLEDGMENTS

The authors wish to express their gratitude to James McCormick (AiResearch), Earl Krueger (Sundstrand), and Bruce Goldwater (MTI) who provided the power conversion unit parametric information. The contributions of William Willcox, Milton Goodman, and William Perrin of Atomics International, who did the systems analysis and design, are also greatly appreciated.

# MODULAR SOLAR ENERGY SYSTEMS FOR FUTURE SPACE LABORATORIES

J. Rath and E. F. Schmidt

AEG - Telefunken Hamburg-Wedel, W. - Germany

## Abstract

Future space laboratories require large lightweight solar arrays in the multi-kilowatt range. The basic requirements for solar arrays for future missions and the optimum methods for their realization are described. Three basic candidate concepts are discussed and analysed: semi-flexible foldable arrays, flexible fold-out and roll-out arrays. The flexible roll-out solar array DORA, designed for a 9 kW-mission and presently built at AEG-Telefunken for qualification tests, is described in detail. This system is designed as a basic unit to be modularly integrated to cover the power demand of communication satellites up to extremely high power systems like space stations. A first and attractive application of the present DORA-array is proposed for advanced Space Lab missions with the purpose to increase the Space Lab power capability significantly.

The presentation of the paper will be followed by a film showing DORA during deployment tests.

## I. Introduction

Since 1958, when the U.S. satellite Vanguard I was launched into orbit, solar arrays have demonstrated their excellent performance in supplying the space craft loads with electrical energy.

Complex mission requirements and an increasing power demand for communication satellites and for space stations up to 100 kW, where photovoltaic systems are clearly favored over nuclear systems, have accelerated the development of lightweight solar array concepts and new technologies for the components in the late 1960's. In addition to the continuing design advancements the following major technological improvements were introduced in the past several years:

- high-efficiency solar cells
- welding technique for solar cell interconnection
- reinforced Kapton substrates
- carbon fibre technology for structural elements.

These improvements promise that solar arrays will remain the dominant power source for long-life missions well beyond the 1980's.

Solar arrays with an output power up

to some 100 W can be directly attached to the spacecraft outer-surface. Representatives of satellites with "body mounted solar arrays" are:

- Intelsat IV , min. power 540 W
- Sunprohe HELIOS, min. power 260 W

Due to limited payload volume and mass restrictions advanced solar array configurations had to be developed which were capable of generating electrical power in the kilowatt range. These new types of solar generators are characterized by large flat structures (rigid, semi-flexible or flexible) that are covered almost completely with solar cells. During transportation into orbit the solar array structures are stowed and fixed to the spacecraft walls, thus providing minimum storage volume. After achieving the final orbit the structures are deployed to form large size arrays. In most cases the deployed arrays are continuously oriented to the sun in order to maximize the array power output.

The largest solar array that has been flown up to now on a communication satellite is the flexible foldable array of the Canadian Communications Technology Satellite (CTS), which was successfully launched in January 1976. This array generates a power output of 1.3 kW at beginning of life<sup>1,2</sup>. Skylab, which was launched in May, 1973, for an eight-months mission, was equipped with two solar arrays with a maximum power output of 18 kW, introducing solar arrays in the U.S. for manned missions. This mission together with the similar USSR SALYUT-program and the joint US/USSR APOLLO/SOYUS-program demonstrated impressively that solar array systems will play an important role in the design and operation of future space programs like communication satellites, free-flying space labs, and automated or manned space laboratories.

## II. Requirements for future Solar Array Systems

Manned space programs of the coming decades will differ significantly from present and past programs creating different requirements for the power source. The difference is mainly caused by the new reusable space transportation systems the Space Shuttle and Space Tug type systems. The Shuttle, combined with a Space Lab, will allow to fly low-earth-orbit missions of nominally 7 days duration

which are extendible up to 30 days. Presently more than 220 Space Lab missions are planned for 1980-1991. A survey of the expected evolution of space laboratory programs is shown Fig. 1.

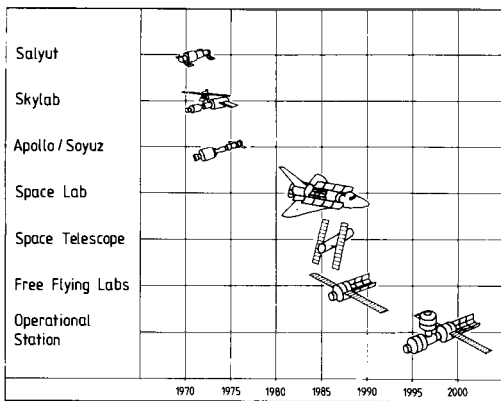


Fig. 1 Evolution of space laboratory programs

Space Lab missions will be followed by manned and automated free-flying Space Labs with mission times up to 60 days. After completion of its mission the free-flyers are flown back to earth to be refurbished, retrofitted and flown again.

The last step of this evolution will consequently be the integration of medium and large space stations from standardized modules to house the crews that will operate and maintain the stations. The operation time of these stations will be several years. Throughout this phase of future space activities also automated scientific and communication satellites will be launched, powered with advanced solar arrays.

The technical requirements of power systems for future space laboratories must be governed by the following major constraints:

- low cost
- low packing volume
- high power/weight ratio

Cost factor will become much more important than in the past because the ratio of power system cost to the cost of the total system will rapidly increase with increasing power demand. In addition in communication satellite systems maximum profit rather than minimum costs is the dominant factor: advanced solar arrays offer reduced weight and increased life time thus allowing for greater communication capacity which leads to a revenue potential of 1 to 2 Mill. \$ for each kg of saved weight.

Low packing volume and high power/weight ratio will be the limiting constraints with regard to the launcher the latter factor having a major influence on transportation cost.

These major constraints together with constraints imposed by the mission profile of future space laboratories lead to solar array specific requirements which shall be discussed here and which are summarized in Table 1.

Present solar array technology has been designed for solitary and long-life missions with mission times up to 10 years and for severe environmental conditions with temperature extremes from + 200° C to - 200° C, and high particle and UV-radiation.

Future space laboratories will be reusable for multi-missions and require power systems that are reusable also. The solar array must therefore be deployable and retractable to be flown back to earth together with the space laboratory. Especially for manned space laboratories deployment and retraction of the array must be

Tab. 1 Basic design characteristics and requirements for future solar array systems

Design Characteristic/Requirement	Methods for Realization
<ul style="list-style-type: none"> <li>• Reuseability of flight hardware</li> </ul>	<ul style="list-style-type: none"> <li>• Deployable and retractable arrays</li> <li>• Deployable to intermediate configuration</li> <li>• Quick and simple check-out for subsequent flights</li> <li>• Quick refurbishment and/or replacement of defective sections</li> <li>• Provisions for manual operation in orbit</li> </ul>
<ul style="list-style-type: none"> <li>• No undesired interaction solar array/spacecraft</li> </ul>	<ul style="list-style-type: none"> <li>• Partial or total retraction during maneuvers</li> </ul>
<ul style="list-style-type: none"> <li>• Low cost hardware</li> <li>• Reliable integration and replacement of hardware units</li> <li>• Maintainability</li> <li>• Growth capability and adaptability to different missions</li> <li>• Few spare units</li> </ul>	<ul style="list-style-type: none"> <li>• Modular design</li> </ul>

possible by remote command and manually to minimize the risk for the crew in case of severe array malfunction.

Deployment should also be possible to intermediate configurations in order to adapt the array power to the actual load profile. By this means the power conditioning system can be simplified and the same solar array can be flown on different missions with differing power requirements. Furthermore, partial deployment would avoid subjecting the unused portion of the array to degradational effects.

The preparation of a flown array for new missions will require an intensive and thorough check-out. Since nondestructive inspections (visual, electrical) will not detect all flight-induced degradation, new check-out methods will have to be established. The array, for example, will have small test sections, representative of the complete array, to be subjected to destructive tests indicating a possible degradation. Provisions will also have to be made in the design to allow for simple and quick replacement and refurbishment of unacceptably degraded or damaged sections.

Although the next generation of advanced SPACE LABS will only fly relatively short missions the technology must be adequate for long lifetimes since multi-mission operation will accumulate to long overall mission times. On the other hand, near-future arrays will be the fore-runners of those for space stations that will operate continuously in orbit for several years.

A particular problem area of large lightweight solar arrays is their partial interaction with the attitude control system of the space laboratory, specifically during maneuvers. This interaction can be reduced by partial or total retraction of the array. Sequential retraction and re-extension cycles could also prevent problems of seizure of moving parts following long periods of inactivity in vacuum, e.g. hinges, gears, bearings, etc.

Modular design will be the concept to reduce manufacturing costs to economic limits. The solar array is a matrix arrangement of essentially identical parallel-connected subarrays - solar cell strings or groups of strings - and is predestined by its nature to follow this concept.

Modularization in the production line will produce array subsections of identical size and characteristics, using automated and highly reproducible manufacturing techniques. These subsections will be integrated to solar panel assemblies (SPA) of standard configuration. Depending on the final solar array design these assemblies will have an area of approx.  $1-2 \text{ m}^2$  which are easy to handle during inspection, integration, and refurbishment. The design of these assem-

blies must primarily be directed to simple and reliable mechanical and electrical integration.

A versatile modular concept need not necessarily be the optimum design from a specific mission point of view but will be optimum for a wide range of application. Growth capability and adaptability of one basic design to different mission requirements is the leading argument for this concept.

### III. Lightweight Solar Arrays - Present Status

Three basic concepts for lightweight solar arrays in the kW-range are presently developed, see Fig. 2:

- semi-flexible arrays
- flexible fold-out arrays
- flexible roll-out arrays

Representatives of these concepts will be described and their suitability as solar energy systems for future space laboratories will be discussed.

Power outputs of the arrays are given for beginning of life (BOL) conditions, since high energy particle degradation for space laboratories will be small compared to long missions of communication satellites in synchronous orbit.

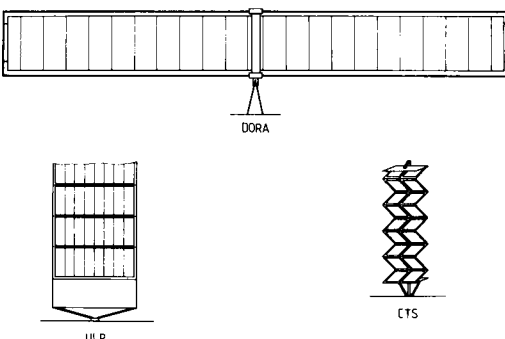


Fig. 2 Wing configuration of semi-flexible (ULP), flexible fold-out (CTS) and flexible roll-out (DORA) solar arrays

#### The Semi-flexible Ultralight Solar Array (ULP)

The ULP-system consists of two wings with a variable number of identical and inter-changeable semi-flexible panels,  $1.1 \times 3.2 \text{ m}^2$  each. They are interconnected and deployed by a spring-actuated mechanism with a closed cable-loop to enforce simultaneous unfolding of all panels. The inboard panel which is connected to the

yoke, is left blank to provide a safe distance from the spacecraft for avoidance of cell shadowing.<sup>4</sup>

The panels consist of a rigid carbon fibre composite frame to which a flexible pretensioned Kapton blanket is attached.

Each blanket is covered with 3600 high efficiency solar cells (HEC) of  $2 \times 4 \text{ cm}^2$  size which are electrically interconnected by automated RC-welding and which are bonded directly to the blanket. The complete development and manufacturing of the blankets to be integrated into the frame is performed by AEG-Tfk.

Vibration amplitudes of the blanket during launch are limited by thin carbon fibre rods running across the blanket and fixed to the frame.

Adaption to different power requirements shall be achieved by changing the number of panels up to 15 per wing. Retractability of the array is presently not foreseen but could be achieved with design changes.

#### The Flexible Fold-out CTS-Array

The Canadian CTS, successfully launched in Jan. 1976, is equipped with the largest solar array ever flown on a communication satellite. The two solar array blankets, designed and manufactured at AEG-Telefunken, generate a BOL-power of 1.3 kW. At the end of its two-years mission in synchronous orbit, the power output will be 1 kW.

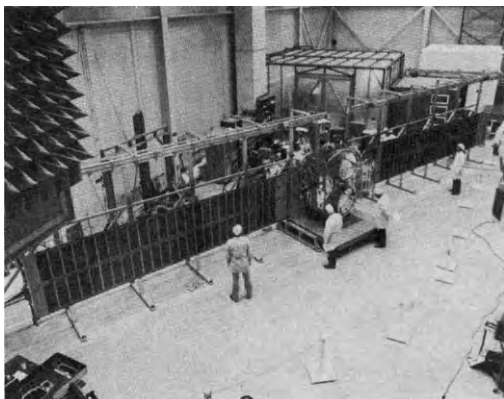


Fig. 3 Deployed flexible fold-out CTS solar array

The CTS array is a flexible fold-out array consisting of two identical wings which are mounted on the north and south walls of the spacecraft. Each wing has an area of  $6.5 \text{ m} \times 1.3 \text{ m} = 8.5 \text{ m}^2$  and is subdivided into 30 foldable panels, 26 of which are covered with 12,636 solar cells

of  $2 \times 2 \text{ cm}^2$  size.

The modular design of the CTS array is shown in figure 3. Each wing is composed of 8 SPA's which are mechanically integrated by means of a piano-type hinge joint. The flat cable wiring system on the front side is located at the edges and in the centre of the blanket. Electrical integration of adjacent SPA's is done by prefolded flat cable pieces which are soldered to lands in the SPA wiring.

The  $200 \mu\text{m}$  thick solar cells, covered with  $100 \mu\text{m}$  thick cerium doped microsheet cover glasses, are interconnected by an automatic parallel-gap welding process after having been automatically matched into electrical categories. The flexible substrate to which the cells are bonded consists of a  $25 \mu\text{m}$  thick Kapton foil which is reinforced on the cell side with a  $35 \mu\text{m}$  thick glass fibre layer.

In the transfer orbit the array is folded between an inboard pallet and an outboard pressure plate. During stowed configuration the cells are protected by thin foam interleaves which remain at the pallet during deployment. Each blanket is deployed-fold by fold to prevent denting - by a single BI-STEM boom.

The CTS has a potential growth capability up to approx. 3 kW. However, making the system retractable would require basic redesign and would make the system more complex.

#### The Flexible Roll-Up Solar Array (FRUSA)

Up to now FRUSA is the only roll-up array that has been flown. In the frame of an orbital flight test program FRUSA was launched in Oct. 1971, together with other subsystems, for a successful six months mission.

The flown array configuration generated an electrical power output of 1.5 kW. The system consists of one stowage drum onto which two solar array blankets are rolled in the stowed configuration. Adjacent solar array blanket layers are separated by embossed Kapton interlayers. In orbit the stowage drum is released from the spacecraft and swung out by  $90^\circ$ . In this position the two blankets are rolled off the drum by means of two BI-STEM deployment actuators which are located at both ends of the drum. During blanket roll-out the Kapton interlayers are simultaneously rolled onto two separate cushioning drums.

The FRUSA test program has demonstrated that roll-up solar arrays are capable of many deployment and retraction cycles in vacuum. During flight ten retraction/re-extension cycles were run, two cycles during eclipse period.

Roll-out concepts have a growth potential exceeding 20 kW without general de-

sign changes. For this power class merely the drum length and blanket width have to be increased. The array wing configuration will then consist of two separate drum/blanket systems side-by-side (double-H-configuration).

Table 2 shows an overall comparison of the different rigid and flexible solar array concepts including the AEG-Telefunken DORA concept which is discussed in the next paragraph.

Tab. 2: Comparison of different semi-flexible and flexible solar array concepts

Manuf. (Design- nation)	Power (BOL) kW	Mass incl. Hold-down& Deployment Mechanism kg	Power/ Mass (BOL) W/kg	Array size $m^2$	Array Characteristics	Design Status	Ref
SNIAS	2.5	71.4	35	29.2	fold-out of flexible Kapton substrate with multi-link pantograph deployment mechanism from Alhoneycomb stowage box.	Dev.-model	5 6
SPAR/AEG (CTS)	1.3	39.3	33	17	fold-out of flex. Kapton substrate with single BI-STEM boom, stowed during launch between pressure plate and pallet	Flight model launched 1976	1 2
MBB/AEG (ULP)	2	45	45	19.8	panels of 3 $m^2$ size each, rigid carbon fibre composite frame with pretensioned flexible solar cell blanket of reinforced Kapton	Dev.-model	4
Hughes (FRUSA)	1.5	32	47	16	two solar cell blankets rolled off one common storage drum by BI-STEMS. One wing flown for 6 months flight test	Flight model launched 1971	7
AEG (DORA)	9	171	53	86	one qual.-wing being manufactured, two solar cell blankets rolled off one common storage drum. Carbon fibre epoxy drum and deployment mechanism.	Qual.-model	8 9

#### IV. The Double Roll-Out Solar Array DORA

The development of the present large-area DORA started late 1973. Preceding development programs of a 5  $m^2$  single roll-out solar array ROSA and of a 10  $m^2$  DORA form the basis of the present design. Additionally, numerous design elements of the CTS solar array have been introduced to the present design.

The current development program is divided into three phases of approx. one year duration. The objectives of the three phases are:

- Phase 1 (1974) : Development of array components
- Phase 2 (1975) : Development of a functional model
- Phase 3 (1976) : Development and manufacturing of one qualifyable generator wing.

The array is designed for a power output of 7 kW at 100 V at the end of a 5-years satellite mission in geostationary orbit. It's BOL power is 9 kW. Furthermore the design was governed by the following major requirements:

- minimum stowage volume
- maximum power/mass ratio
- roll-off and roll-up capability

The configuration of the 9 kW DORA is shown in Fig. 4. During launch and in the transfer orbit the solar array is fixed to two opposite walls of the spacecraft body by a holdown and release mechanism. In this stowed configuration the four array blankets are rolled onto two separate stowage drums. To protect the solar cells against damage during launch adjacent blanket layers are separated by a foam interlayer. The dimensions of the stowed wing are:

length: 2.85 m  
width: 0.90 m  
height: 0.45 m

In the final orbit both wings are released from the spacecraft and deployed by means of a swing-out mechanism in such a way that the stowage drums are turned by 90° relative to their stowed position and are locked in an distance of 1.5 m from the spacecraft.

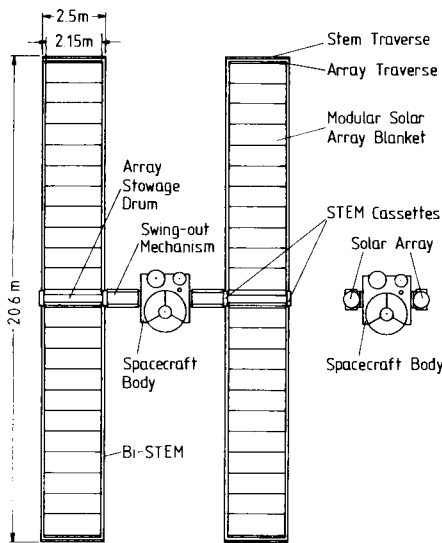


Fig. 4 9 kW DORA in deployed and stowed configuration

In order to achieve a high stiffness at a very low weight the swing-out mechanism, drums, and central tube are essentially made of carbon fibre reinforced plastic. The necessary mechanical force to initiate the swing-out operation is provided by spiral springs, see fig. 5.

Swing-out operation is followed by the deployment of the two wings, consisting of four solar array blankets. The deployment mechanism of each wing consists of two double-spool STEM\*-cassettes at the drum ends in which the four BI-STEMMS are stored before extension. The inboard cassette, called master unit, is motor driven and is connected to the outboard cassette, called slave unit, by a torque tube to synchronize boom deployment. The tips of the STEM-booms are pairwise connected by STEM-traverses. Thus, a pair of booms, a traverse and the array stowage drum form the supporting frame of the blanket.

On one side the blankets are attached to the array stowage drum, on the other side they are fixed to array traverses. The array traverses are fastened to the STEM-traverses by means of a wire-loop running in guide-rolls to compensate different boom lengths to ensure a homogeneous tension distribution over the width of the blanket. Pretensioning of the blanket during and after deployment is achieved by a tensator spring device inside the stowage drum, which applies a constant force of 30 N/m to the blanket.

\*) STEM = Storable Tubular Extendible Members

The flexible substrate, to which the solar cells and the wiring is bonded, is

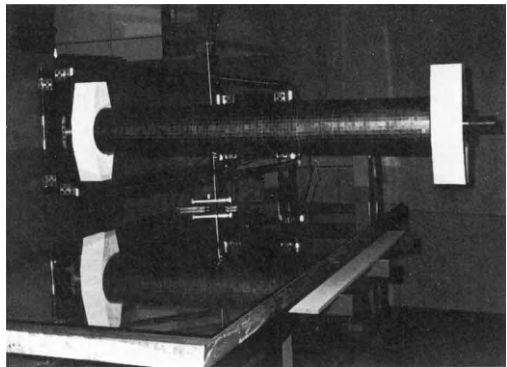


Fig. 5 DORA swing-out mechanism in partially deployed configuration

made of a 50  $\mu\text{m}$  thick, reinforced Kapton foil. For reasons of

- economic manufacturing
- simple replacement
- adaptability of the array for different power ranges

the blanket is built up of standardized SPA's. Each blanket consists of

- one blank traverse assembly, which is fixed to the array traverses
- 11 identical power SPA's, to which the solar cells and the wiring is bonded .
- one blank drum assembly, attached to the stowage drum and equipped with a flexible wiring system on its rear side to interconnect the power assemblies with the harness inside the stowage drum.

The dimension of the power SPA's are 2.15 m x 0.84 m. Each of them is covered with 2080 solar cells of 20 mm x 40 mm dimensions. The electrical layout is realized by solar cell modules of identical dimensions and characteristics: each module is a matrix arrangement of 8 (parallel) x 26 (series) = 208 solar cells. The meander shaped series connection of 10 modules forms an electrical string to provide the required 100 V operation voltage. This layout, with a printed circuit on the blanket's rear side, has a packing density of 91,6 %. The specific mass of the power SPA's with 200  $\mu\text{m}$  thick solar cells and 100  $\mu\text{m}$  thick cover glasses is 1.07 kg/m<sup>2</sup>.

A large number of technological features that were successfully introduced by AEG-Telefunken in the field of solar arrays are used in the present DORA layout. They are summarized in Table 3.

The present DORA configuration, based on standard 200  $\mu\text{m}$  thick solar cells with an output of 62 mW/cm<sup>2</sup> cell, is summarized by the characteristics in Table 4.

The present DORA is shown in Fig. 6.

**Tab. 3 Utilization of space qualified technologies from AEG-Telefunken for DORA**

	ESRO IV	HELIOS	ETCS	GEOS	IUE	OTS/MAROTS	ISEE-B	DORA
SOLAR CELL								
TiO <sub>x</sub> -Ar-Coating								
Passivated Contacts								
Multifinger Grid								
Weldable Contacts								
200 µm Thickness								
COVER GLASS								
Cerium Doped Material								
Compl. Covered Surface								
Conductive Coating								
MODULE / GENERATOR								
Automated Welding Technique								
Vacuum Bonding								
Single Cell Replacement								
Flexible Blanket Substrate								
Carbon Fibre Technology for Struct Elements								

**Tab. 4 Main technical characteristics of DORA**

Power output (BOL)	9 kW
Area of deployed blankets	86 m <sup>2</sup>
Total mass	171 kg
Specific power output	53 W/kg
Mass breakdown in %	
Blankets	46.8
Stowage drums	15.3
Central tubes	2.8
STEM-cassettes	24.5
Traverses	2.9
Wiring	0.4
Swing-out mechanism	5.8
Hold-down mechanism	1.5



**Fig. 6 Double roll-out solar array DORA**

With minor design changes and by adding one additional drum/blanket system to each wing (double-H configuration), the power capability of DORA can easily be increased to 20 kW. As can be seen from Figure 7 which shows the analyzed relative increase of power/mass for the FRUSA system, DORA will arrive at a specific power output of about 61 W/kg in the 20 kW power range.

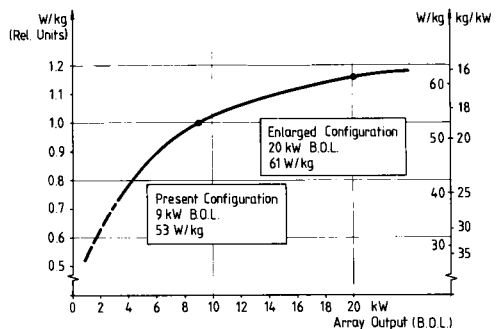


**Fig. 7 Increase of power/mass ratio for DORA with increasing array output**

Additional power gain will be achieved by using high efficient (HEC) or black (BC) solar cells. Table 5 shows the influence of different solar cell types on the DORA power output.

**Tab. 5 Influence of different solar cell types on the DORA power output (BOL)**

Cell Type (thickness)	Cell Output (mW/cm <sup>2</sup> )	Present Config. (kW)	Growth Capability (kW)
standard (200 µm)	15.5	9.0	20
standard (350 µm)	16.25	9.4	20.9
HEC (200 µm)	16.5	9.6	21.3
HEC (350 µm)	17.5	10.2	22.7
BC (200 µm)	19-20	11-11.6	24.6-25.8

Of special interest are 350 µm thick solar cells, because their power output, compared with 200 µm thick cells, is higher and in addition not degraded in a low orbit environment. Furthermore these cells can be manufactured more economically than thin cells and it has to be decided from an overall systems point of view whether their increased mass is justified by more efficiency and reduced manufacturing cost.

With respect to its power capability the present DORA configuration represents a design optimization for different space missions like communication satellites as

well as for advanced Space Labs and space stations. Due to its modular design it can be easily adapted in relatively short time to specific power profiles and can also be utilized as 25 kW power units for future space stations in the 100 kW power range.

#### V. Future Activities

In order to improve solar power systems for their future application one of the planned Space Lab missions should be chosen to subject available solar array hardware to *in situ* tests in orbit. For this reason a corresponding proposal has been made which is attractive in three respects:

1. Using the Space Lab as a test platform for large solar arrays would allow to run orbit tests in a realistic environment that cannot be adequately simulated on earth like vacuum, zero-g condition, and radiation at the same time.
2. During this mission the solar array power can be made available to run additional or excessive power consuming experiments which presently exceed the power capability of the Space Lab.
3. Electrical power from the test array will allow to study experimentally a microwave power-line from satellite to earth.

Table 5 summarizes the major elements of the proposed orbit test program and shows the advantages of orbit tests compared to ground simulation tests.

The electrical power available in Space Lab for experiments is presently limited to 5.2 kW maximum average, depending on the flight configuration of the specific mission. It can be seen from table 6 that the proposed operation of one DORA qualification wing will increase the electrical capability of Space Lab by a factor of two. The additional power supply of DORA could assist to improve the conditions for Space Lab experimenters significantly. DORA would allow to operate excessive power consuming experiments and would permit increased operation time.

Space power station concepts have been born out of the need for new power sources for mankind. The purpose of these large energy satellites is to convert sun light into electrical energy and to transmit the generated energy to earth by means of a microwave beam. The power capability of these power stations will be in the range of 5 to 10 GW.

Although these systems are still in the conceptual phase, several key technological problem areas will have to be investigated in the near future. One of these areas is electrical energy transport by means of microwaves from space to earth.

Tab. 6 Orbit tests with 4.5 kW DORA-array

Test	Remark
<b>1. Mechanical/Dynamic Tests</b>	
1.1 Deployment and retraction cycles	Vacuum: no air damping Zero-g: no influence of gravitation-compensation device
1.2 Dynamic characteristics of deployed array (moment of inertia, Eigen-frequencies vs. blanket pretension).	Undisturbed interaction of blanket and attitude control
1.3 Thermal induced deflection (form-stability)	No influence of boundary effects as in TV-chambers
1.4 Mechanical stress distribution in flexible blanket	Zero-g: no influence of gravitational forces
<b>2. Electrical/Thermal Tests</b>	
2.1 Electrical performance under different orbit conditions	Undisturbed radiation environment
2.2 Temperature profiles under different orbit conditions	Undisturbed radiation environment

Tab. 7 Power and energy capability of Space Lab

Flight Configuration	Available Power		Available Energy for 7-days Mission
	Average	Peak	
Module only	4.0 kW	9.0 kW	422 kWh
Module + Palette	3.8 kW	8.8 kW	392 kWh
Palette only	5.2 kW	10.0 kW	609 kWh
DORA-Wing	4.5 kW	4.5 kW	750 kWh 3250 kWh*

(\* for 30-days mission)

First approaches have already been made when JPL established an experimental microwave power-line over a distance of 1.5 km in 1975.

More realistic experiments could be performed with the Space Lab provided that sufficient electrical power can be made available on board. In contrast to terrestrial tests a power-line from spacecraft to earth has to pass the total atmosphere of the earth. Absorption, refraction, and scattering of the power beam could be measured under realistic conditions. The test results will be a valuable basis to review the economic and technical feasibility of future power stations in space. Solar array power on board of future space laboratories will help to realize these necessary experiments.

#### VI. Conclusion

The coming decade will usher in a new era of space utilization featuring high-power satellites as well as free-flying space laboratories and space stations, both manned and unmanned. The development has already begun.

Several system concepts of large-area arrays offer a potential growth capability needed for such future missions. Especially the double roll-out solar array DORA, presently developed at AEG-Telefunken, is capable of satisfying the demand for light-weight arrays with a range of application from communication satellites to near-future high power space stations. The excellent performance of this type of array has been demonstrated by FRUSA under real space conditions.

The implementation of solar arrays for advanced Space Lab missions has been shown to be an attractive approach for providing Space Lab with additional power and for performing Space Lab-based test programs for solar arrays which will provide additional experience in order to improve present solar power systems for future space stations.

#### References

1. R. Buhs, Layout and Technology of the CTS Solar Array Blanket, Proceedings of the 10th Photovoltaic Specialists Conference, Palo Alto, Nov. 1973.
2. S.S. Sachdev, E. Quittner, J.D. Graham, The CTS Deployable Solar Array System, International Conference on Photovoltaic Power Generation, Hamburg, Sept. 1974.
3. P.E. Glaser, The Future of Power from the Sun, Proceedings IECEC, 1968.
4. D.E. Koelle, H.v. Bassewitz, The Ultra-light Solar Array (ULP) for Future Communications Satellites, AIAA/CASI 6th Communications Satellite Systems Conference, Montreal, Apr. 76.
5. G. Barkats, Development of Flexible, Fold-out Solar Array, Proceedings of International Congress "The Sun in the Service of Mankind", Paris, July 1973.
6. F. Fremy and D. Lorans, Development of a Flexible, Fold-out Solar Array, International Conference on Photovoltaic Power Generation, Hamburg, Sept. 1974.
7. G. Wolff, Oriented Flexible Rolled-up Solar-Array, Proceedings of AIAA 3rd Communications Satellite Systems Conference, Los Angeles, April 1970.
8. S. Karius, D. Rüsch, Roll-out Solar Arrays for High Power Application, Proceedings of International Congress "The Sun in the Service of Mankind", Paris, July 1973.
9. G. Gohrbandt, S. Karius, E.F. Schmidt, Spacecraft Power Systems in the Kilowatt Range, Proceedings of the XXVIIth I.A.F. Congress, Lisbon, Sept. 1975.

\* sponsored by the German Ministry of Research and Technology.

# PHOTOVOLTAIC AND THERMAL ENERGY CONVERSION FOR SOLAR POWER SATELLITE

G. F. von Tiesenhausen\*

*G. C. Marshall Space Flight Center, NASA, Huntsville, Alabama, USA*

## Abstract

A systems-oriented technical overview of present candidate solar power satellite baseline concepts is given including preliminary ground rules, assumptions, and specifications used in present system studies. Various critical system elements and required research and development activities are described. Data on expected performance, economics, state of the art, and cost are presented. Present results indicate a potential economic feasibility of solar power satellites by the end of this century.

## Introduction

Solar Power Satellites (SPS) are a potential future source of terrestrial energy. SPS constitute a challenge to the arts of engineering and management with regard to analysis of a total system and the involved critical technology development areas. Coverage of all considerations and problem areas and their solutions exceed the scope of this paper. A list of references is attached covering most areas studied to date. This paper summarizes the most important aspects of present investigations.

## Objectives

The objective of National Aeronautics and Space Administration (NASA) efforts is generation of reliable information on economic and technical viability of SPS concepts.

## General SPS Characteristics

Utilization of solar energy in near Earth space uses the average flow of energy of  $1.338 \text{ kW/m}^2$  from the Sun. This compares favorably with equivalent ground-based solar energy utilization (Figure 1). SPS, therefore, are characterized by large area structures able to intercept large quantities of solar energy flow for photovoltaic or thermal conversion to electricity.

2.45 GHz microwaves are considered for use in transmission of space converted solar energy to Earth. Requirement of specific, fixed sites on the ground for collection and rectification of the transmitted energy requires SPS to be in geosynchronous orbit at a 22,300 km distance. (Sun-synchronous SPS coupled with a geosynchronous relay station will be studied in the near future.)

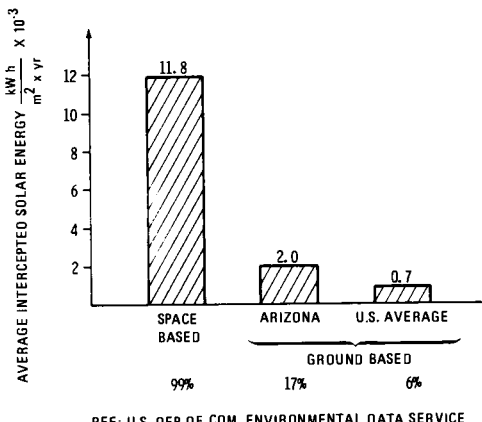


Figure 1. Space and Ground Based Solar Energy Interception

## Early Work

The possibility of SPS as a potential new source of terrestrial energy was first postulated, analyzed, and published by Dr. P. E. Glaser in 1968 and patented in 1973<sup>1,2,3</sup> (Figure 2). In 1970 J. G. Gavin and J. Mockovciak, Jr. initiated extensive analytical work within their company.<sup>4</sup> G. R. Woodcock and G. T. Patha analyzed the first thermal conversion system for SPS in 1972 and subsequent years.<sup>5</sup>

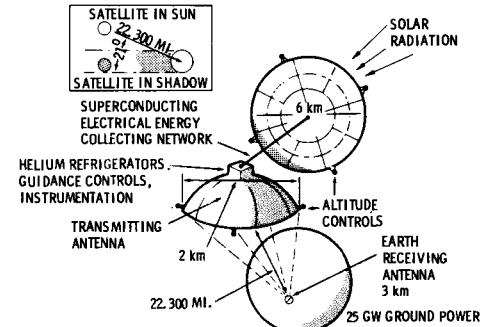


Figure 2. Concept of Satellite System for Solar Power Generation<sup>2</sup>

\* Assistant Director, Payload Studies Office, Program Development

The first NASA sponsored study efforts on SPS were completed in February 1974. The results indicated that SPS appeared feasible and merit further studies.

#### Present Efforts

Four major overall systems analysis efforts are in progress at present within NASA and NASA's industrial partners. Each effort covers different system and subsystem options. In addition, critical technology areas such as microwave high power transmission, large space structures and associated in-orbit production and assembly operations, and advanced heavy lift launch and space transportation systems receive thorough analytical and, in some areas, experimental efforts.

#### Basic Guidelines and Assumptions

All present efforts draw from past and related current industry and NASA efforts.<sup>6-17</sup>

The following basic guidelines and assumptions are used in present system efforts:

- Provide electric power for commercial utilization within the United States.

- Power output of the associated individual ground installations is baselined at 5 GW or 10 GW each at 60 Hz.

- The SPS will be located in geostationary orbit, with power transfer by a microwave link.

- The technology levels used will be those available for subscale orbital demonstration 5 years prior to operational use.

- Overall system lifetime will be 30 years with maintenance.

- Maximum microwave power level at beam center is 20 to 25 mW cm<sup>-2</sup> and drops to 0.1 mW cm<sup>-2</sup> at the rim of the receiving antenna area.

- Primary evaluation criteria will be cost per kW h of the power distributed on the ground, and impacts and benefits of the SPS.

- All costs are to be recovered from operational revenues.

At MSFC the following assumptions are made:

- The expansion rate of the United States electric power generation rate will be 4.5 percent per year.

- The fraction of the total capacity provided by satellite power will be:

- 10 years after initial operational satellite installation, 10 percent

- 20 years after initial operational satellite installation, 25 percent.

These guidelines and assumptions are being updated and modified as studies progress.

#### System Definition

The following system options are presently under study:

<u>Energy Source</u>	<u>Energy Converter</u>
Solar	Photovoltaic Array
Solar	<ul style="list-style-type: none"><li>• Direct and Radiation</li><li>Thermionic</li><li>Cooled</li><li>• Liquid Cooled</li></ul>
Solar	Closed Brayton Cycle
Solar	Cascaded Thermionic/Closed Brayton Cycle
Nuclear	Thermionic
Nuclear	Closed Brayton Cycle

Data currently available on the two nuclear energy source options are insufficient for inclusion in this paper.

Various SPS concepts and configurations for the options have been proposed and studied by industry and NASA (Figures 3 through 6 show a few examples). A well defined set of subprogram areas is common to all concepts; however, significant differences exist in the emphasis of these subprograms.

#### Basic Building Blocks and Efficiency Chains

Any SPS consists of the following main building blocks (Figure 7):

- Solar Energy Collection and Conversion
- Energy Distribution within Satellite
- Energy Transmission to Earth
- Ground Reception and Distribution.

Present study efforts are penetrating into increasing depths in these building blocks. The basic building blocks indicate the flow of energy from interception in space to the user. The resulting efficiency chain is shown in some detail in Figure 8. The range in

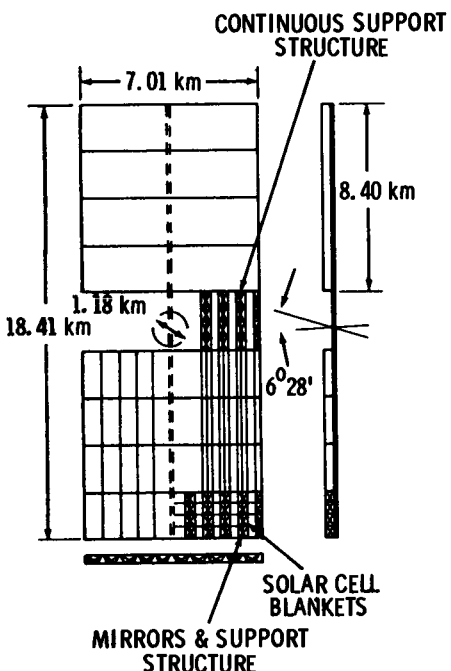


Figure 3. The 10,000 MW Satellite Solar Power Station

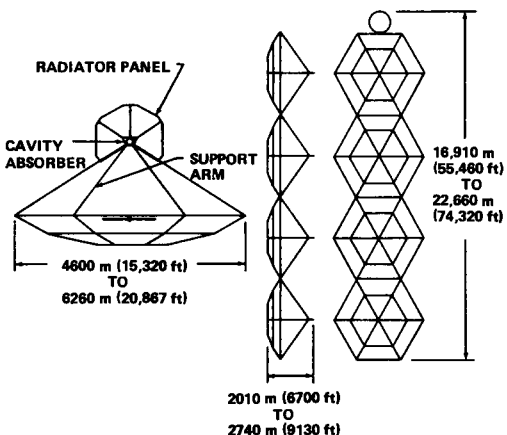


Figure 4. Thermal Conversion, Solar Power Satellite

efficiencies indicates the present uncertainty regarding expected performance of the various chain elements.

#### System Reference Options

Two reference system options, one based on photovoltaic and one on thermal solar energy conversion, have been selected for indepth definition. Both options use the same microwave power transmission system to

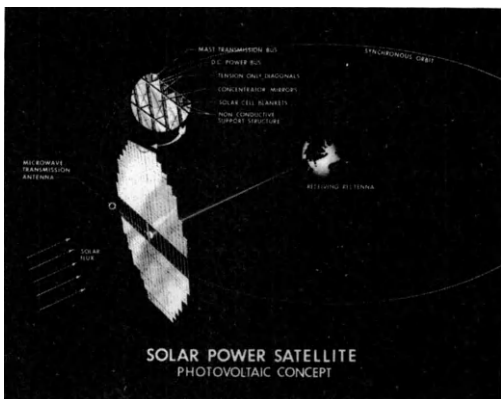


Figure 5. Solar Power Satellite, Photovoltaic Concept

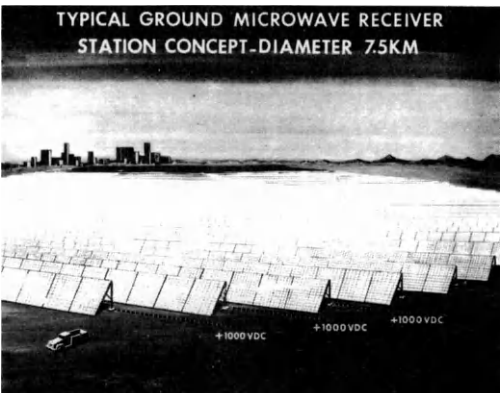


Figure 6. Typical Ground Microwave Receiver Station Concept, Diameter 7.5 km

the ground. Summary data on presently studied solar power satellite versions are shown in Table 1.

Photovoltaic System. The power conversion subsystem of photovoltaic SPS consists of the following major characteristic elements:

<u>Element</u>	<u>Directed Present Efforts</u>
• Solar Cells and Blankets	• Technology Advancement
• Concentrators	• Weight/Cost Studies
• Power Distribution	• Weight Optimization, Voltage and Current Selection

The system's mass and cost are highly dependent on the cell blanket area and, therefore, on the efficiency and cost of the cells.

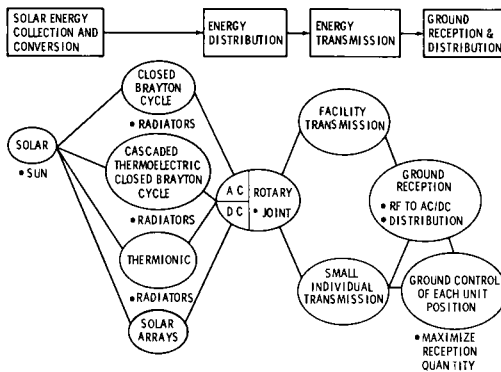


Figure 7. SPS Basic Building Blocks

The present reference system is based on single crystal silicon cells, and a variety of alternatives is also being investigated.

To establish viable photovoltaic SPS system boundaries, required solar array characteristics have been established. On-going and planned technology efforts follow a multipronged approach toward a minimum cost solar array (Figures 9 and 10). Efforts are underway to arrive at an optimum compromise between often conflicting goals.

Another approach toward cost reduction is solar energy concentration on a reduced size solar array. Considering all involved parameters, a concentration factor of 2 is used in the reference system (Figure 11). The design approach for concentration is shown in Figure 12.

**Thermal Electric System.** The power conversion subsystem of a thermal electric SPS consists of the following major characteristic elements:

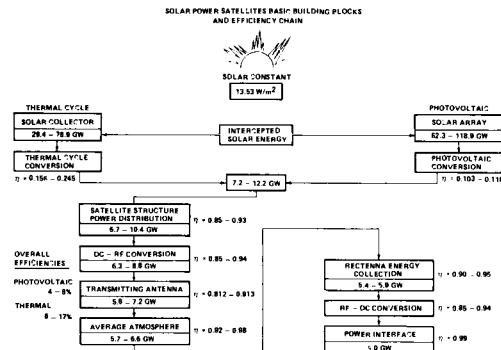


Figure 8. SPS Basic Building Blocks and Efficiency Chain

Table 1: Summary data on presently studied SPS (discounted dollars, 7.5%)<sup>8,9</sup>

ITEM	CONVERSION CONCEPT		BRAYTON	CASCADeD THERMIONIC BRAYTON	PHOTOVOLTAIC
	DIRECT RADIATION COOLED	LIQUID COOLED			
MASS ( $\text{kg} \times 10^6$ )	151	190	151	130	34
SIZE ( $\text{km}^2$ )	102	90	70	54	129
DDT & E (\$B)	44	51	59	56	50
UNIT COST (\$B)	18	21	26	23	14
OPER. COST (\$B/SAT)	0.36	0.45	0.36	0.33	0.35
REVENUE (\$B/SAT)	2	2	2	2	2
ENERGY PRODUCTION COST (MILS/kW h)	39	47	50	44	27
EFFICIENCIES (%) DC-DC CONVERSION			58		58
TOTAL			22		11.3
12.8					6.6
OPER. FREQUENCY			2.45 GHz		
LIFE			30 YEARS		
GROUND POWER			10 GW		

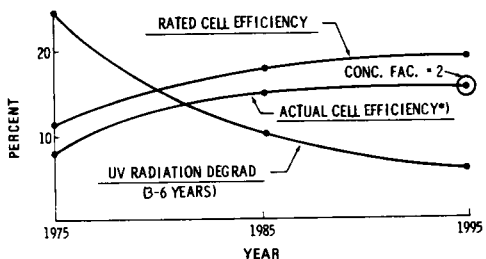


Figure 9. Projected Solar Array Characteristics  
(Single Crystal Silicon)

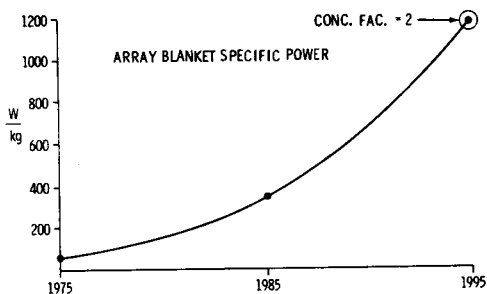


Figure 10. Projected Solar Array Characteristics  
(Single Crystal Silicon)

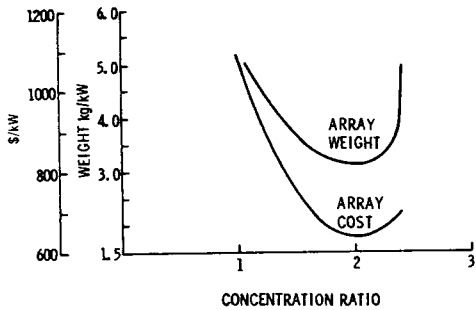


Figure 11. Concentration Ratio Trades

Present reference systems are based on thermionic Brayton and combined thermionic/Brayton energy conversion. Summary data on solar thermal conversion systems presently being studied are presented in Table 2.

#### Subprogram Areas

The following SPS subprogram areas are principal to the fundamental feasibility of the concepts.

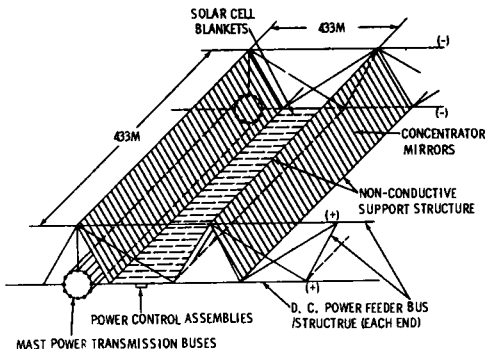


Figure 12. Solar Array Configuration (One of 792 Structural Modules)

#### System Analysis and Engineering

No in-depth effort in this area has previously been done covering the total system. The quantity and complexity of system elements require a systems model which is presently being generated. Presently recognized SPS program elements can be categorized as in Table 3. These elements are being analyzed, optimized, and integrated. Technology requirements are generated.

#### Transportation

**Heavy Lift Launch Vehicle (HLLV).** With solar power satellite masses between approximately 100 and  $200 \times 10^6$  kg, HLLV payload ranges between 0.225 and  $2.25 \times 10^6$  kg are being studied. Cost sensitivity makes this area critical. The cost goal for transportation to low Earth orbit is approximately \$40 to \$100 per kg payload.

**Orbital Transfer Vehicle.** Masses of approximately  $10^8$  kg must be transferred from low to geosynchronous orbit. These vehicles will require refueling and will perform docking with the large masses. The characteristics of these masses must be integrated into the vehicle's overall control system. Logistic support for these vehicles must be defined.

#### Large Area Space Structures

Solar power satellites typically have large, thin, low density structures on the order of  $10^7$  to  $10^8$  m<sup>2</sup> area with an average density of approximately 1 g/m<sup>2</sup> over large parts of the satellite (Figure 13). This dictates special requirements on structural design optimization and materials. The combined and complex mechanical and thermal load effects on the structure require analysis with the latest analytical methods.

#### Attitude Control and Station Keeping

Little information is available to date on control techniques for large space structures with a large number of sensors and actuators distributed over a highly flexible

Table 2. Summary data on solar thermal conversion systems

ENERGY CONVERSION	ELECTRIC ENERGY GENERATED	DC-AC CONVERSION	AC-DC CONVERSION (ROTARY TRANSF.)	ACTIVE COOLING	WORKING FLUID
THERMIONIC - DIRECT RADIATION COOLED		20 kV (ROTARY CONVERTER)			
THERMIONIC - ACTIVELY COOLED	64 V - DC		20 KV		
BRAYTON CYCLE	50 KV - AC	382 KV TRANSFORMER		No K	Xe/He (m = 8)
THERMIONIC BRAYTON CYCLE	64 V - DC 50 KV - AC	50 KV (ROTARY CONVERTER)			
RANKINE	NO DATA AVAILABLE YET				LIQUID METAL

Table 3. Program Elements

13 PROGRAMS	233 ACTIVITIES AND OPERATIONS
48 PROJECTS	29 FACILITIES
124 SYSTEMS	1 REAL ESTATE
122 SUBSYSTEMS	

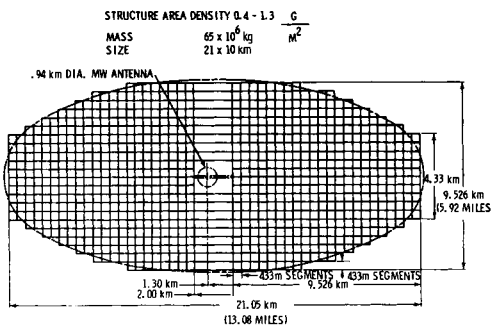


Figure 13. SPS Structure

structure. The stringent requirements for pointing accuracy of the solar energy collectors, and particularly of the microwave antenna with minimum expenditures of propellants, require major advancements in technology and analysis methods.

#### Operations

The full utilization of HLLV requires maximum payload density (Figure 14). The shipment of raw material for structures such as roll stock, etc. is the present approach toward this requirement. Mass production of structural elements in space is consequently required. Subsequent assembly of these elements and the alignment, checkout, maintenance, and repair are critical operations to be performed. Many operations may be automated. Performance standards of man and machine have to be generated, and equipment and facilities developed with local transportation of man and cargo. Ground operations are expected to be extensive at launch sites and at the rectenna areas.

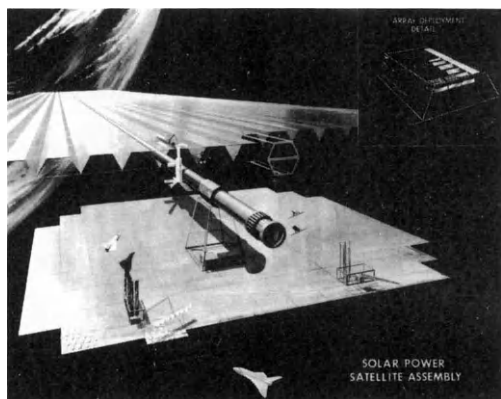


Figure 14. SPS Assembly

#### Power Conversion

Photovoltaic Conversion. Besides transportation the next major critical area is solar energy conversion. The photovoltaic energy conversion system needs major advancement in a number of characteristics.

The following parameters must be improved and optimized:

- Rated and actual cell efficiency
- UV radiation degradation
- Array power per unit of area, rated and actual
- Array blanket specific weight.

The following developments are required for economic and technical feasibility:

- Blanket fabrication needs automation.
- 30-year life requires encapsulation and resistance to radiation damage.

- Present beginning-of-life efficiencies of 12 to 14 percent must be increased.

- Investigation of alternate photovoltaic devices is required (e.g. Gallium Arsenide, multivertical P/N junction cells).

Present efforts concentrate on

- Efficiency prediction (present prediction 17.5 to 20 percent).
- Thermal analysis (optimum concentration ratio).
- Radiation degradation.

**Thermal Conversion.** A major development area in the thermal conversion system is the thermal radiator subsystem. Sizes up to  $2 \times 10^7 \text{ m}^2$  are required. Thin alloy tubings (Haynes 188) or equivalent need testing for long life behavior (creep stress) possibly using liquid metal (NaK) as working fluid.

Tradeoffs between Brayton, Rankine, and thermionic conversion are in progress. Past work has limited applicability to SPS requirements. A few major goals are indicated in Figure 15.

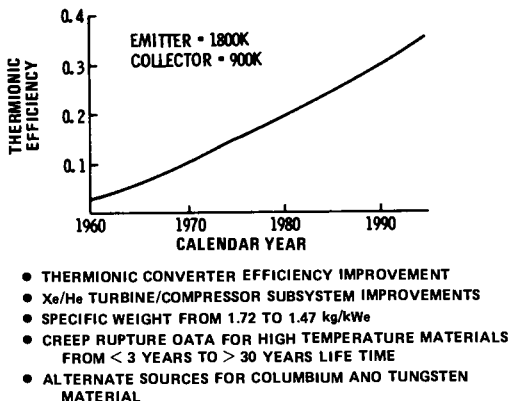


Figure 15. Thermal Solar Electric Conversion Goals

**High Voltage — Plasma Interactions.** The possible exposure of high voltage surfaces requires consideration of possible interactions between high voltage surfaces and the space plasma such as the current flows between surfaces at different voltages immersed in the space plasma, the charge stored on surfaces (i.e. spacecraft charging), and plasma initiated discharges. An understanding and an account of these interactions and their impact on the high voltage, high power subsystem performance must exist. A critical need exists for experimental data on plasma interaction at high power and high voltage.

**Power Processing.** Experimental data are needed on power processing elements in space environment in the 40 kV range combined with much higher power levels than currently required. These elements are a significant factor in overall SPS mass and cost. Characteristics of integrated regulation into solar arrays are unknown. System with combined lightweight, high efficiency, and long life have not been verified.

#### Microwave Power Transmission

Detail cost, performance and total efficiency are as yet unknown. DC-RF conversion, transmission phase control, and wave guides are major systems sizing factors and require development. SPS systems require combined high efficiency, long life, low RFI output and phase stability. Data are needed on applicable phase reference distribution systems, wave guide materials, and tolerances. Optimum transmitting antenna structures require definition. Present and expected overall efficiencies are shown in Figure 16.

#### Environmental Effects

Environmental effects of SPS operations are categorized in Figure 17. This includes the effects of the environment on the Satellite operations and of the satellite operations on the environment. Information is needed on the following:

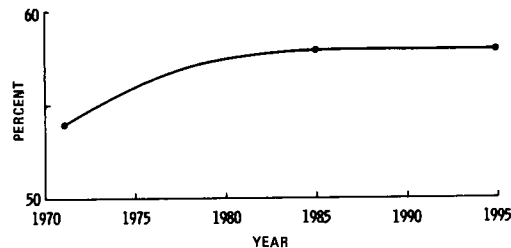


Figure 16. Microwave Efficiency (DC-DC)

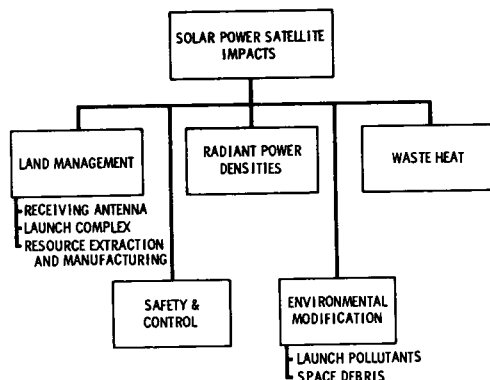


Figure 17. Environmental Effects of SPS Operations

- Atmospheric models (3-dimensional)
- Allowable radiation doses for microwaves (Figure 18)
- Ionospheric interactions with microwave beam
- Radiation limitation on orbital construction crews
- Lifetime limitation on materials
- Biological effects of microwave beam
- Effects of transportation system pollutants.

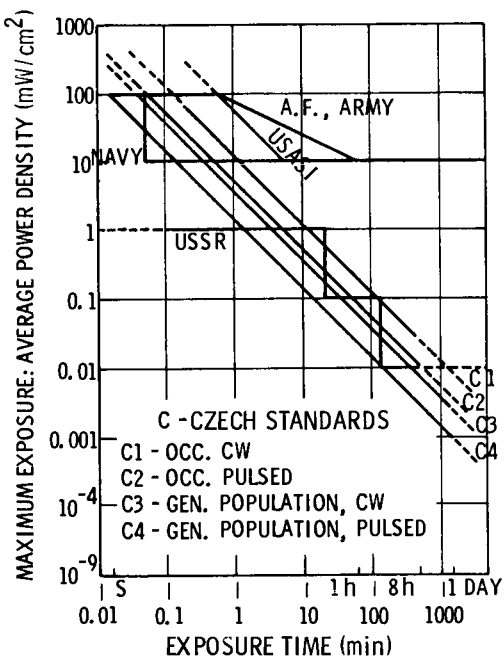


Figure 18. Microwave Exposure Standards<sup>9</sup>

The potential collision probability of SPS under construction and in operation with space debris (Figure 19) requires study.

#### Management

SPS systems consist of a large number of closely interrelated internal system elements and operations. Simultaneously, SPS activities have close relations to other related NASA activities (Space Station, Space Transportation, etc.). This requires application of central management of the program elements (Table 3).

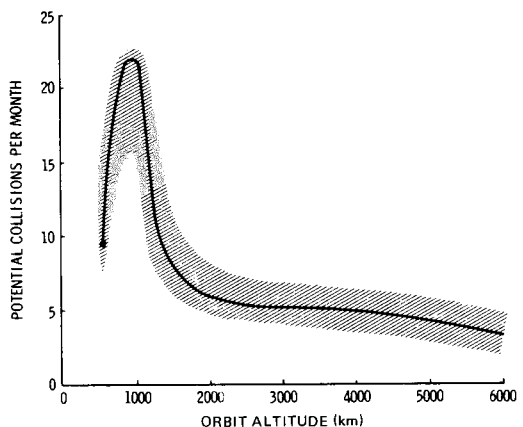


Figure 19. SPS Orbit Transfer/Assembly Orbit Issue: Potential Collision Frequency

#### Economic Analysis Method

No practical economic analysis methodology existed that enabled comparison of SPS and conventional terrestrial power plants due to vast character differences. The following development steps are being implemented:

- Methodology for comparative economic analysis of electric generation systems
- Computation of economically justifiable SPS cost including payback analysis.

Also, a development and unit cost risk analysis is being prepared.

#### Utility Interface

A lack of understanding exists concerning the effects of interfacing substantially larger electric power sources than presently in operation like SPS with existing power grids. The effects of bi-annual blackout periods during the equinoxes on the interface are unknown. Successful discussions between NASA and major electric power suppliers have started.

#### Study Findings to Date

The findings of present intensive but uncompleted studies are in the early tentative stages. These findings indicate that the SPS concepts show sufficient promise of feasibility and practicality in justifying continued in-depth and detailed investigations coupled with exploratory technology experimentation.

#### Economical and Technical Findings

The following technology and operations development areas need to be investigated for an adequate SPS assessment decision (Table 4). Major economic findings are:

Table 4. Critical Technology and Operations Development Areas

SYSTEM ANALYSIS AND ENGINEERING	CONCENTRATION & ABSORPTION
UTILITY INTERFACE	TERMAL-ELECTRIC CONVERSION
HEAVY LIFT LAUNCH VEHICLE	DISTRIBUTION
ORBITAL TRANSFER VEHICLE	HIGH VOLTAGE - PLASMA EFFECTS
LARGE SPACE STRUCTURES	POWER PROCESSING
MATERIALS	MICROWAVE POWER TRANSMISSION
ASSEMBLY AND FABRICATION	DC - RF CONVERSION
THERMAL CONTROL	PHASE CONTROL
ATTITUDE CONTROL & STATUS KEEPING	WAVEGUIDES
OPERATIONS, LOGISTICS, SUPPORT	RF - DC CONVERSION
SOLAR ENERGY CONVERSION	ENVIRONMENTAL EFFECTS
PHOTOVOLTAIC CONVERSION	RF INTERFERENCE
SILICON	BIOLOGICAL EFFECTS OF MW
OTHERS	ATMOSPHERIC EFFECTS
THERMAL CONVERSION	LAUNCH POLLUTANTS

- SPS may be cost effective compared to terrestrial systems by 1995.

- If SPS cover 10 percent or more of the projected US installed generation capacity at a terrestrial power generation cost of 35 mils/kW h, the development costs may be amortized.

Significant economic benefits can be realized if relative social and environmental cost of terrestrial systems are included in the comparison with solar power satellites.

#### Operational Fundings

Potential economic advantages are indicated in two space operational areas:

- a. Satellite Assembly — A great economic advantage is indicated in low Earth orbital assembly; however, environmental and technical problems are more severe at that location.

#### Pro LEO Assembly

- Considerably less overall transportation requirements
- Quick return to ground

#### Pro GSO Assembly

- No degradation of solar panels in transit
- No construction energy storage
- Less attitude control and station keeping propellants
- Less thermal stress
- Low collision damage

- b. Structural beam fabrication in space will allow high payload packing density (flat stock, etc.).

#### Impacts and Benefits

**Impacts.** Very preliminary and incomplete impact assessments have been performed to date. The impact categories being investigated are shown in Figure 20. A few selected findings are:

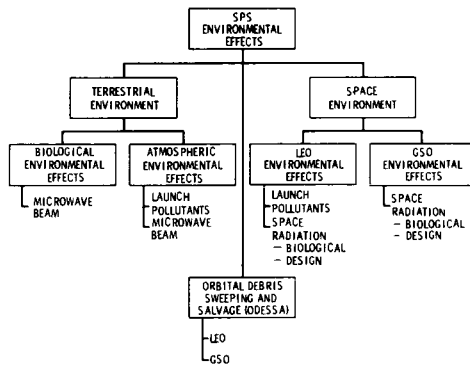


Figure 20. SPS Environmental Effects

- A better definition of land usage for the rectenna.

- 10 to 15 percent of the rectified microwave power will be waste heat; this is substantially less than from conventional power production.

**Benefits.** A program as shown in Figure 21 would provide approximately 25 percent of the newly installed electric generating capacity at the turn of the century or 10 percent of the total.

Such a program, if viable, would contribute to domestic and potentially exportable supplies of clean energy.

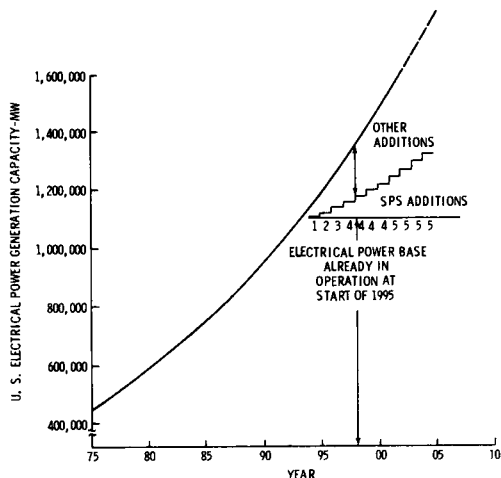


Figure 21. Mid-trend Forecast of U.S. Electrical Energy Consumption

### Outlook

Present estimates indicate that a time period between now and the end of this decade is required before a decision can be made to engage into specific, large scale technology advancement for a preferred concept. In the future there will be a continuation and increase in efforts in total system analysis and exploratory work in primary technology areas.

Efforts will also continue in related system elements such as transportation systems, space stations, and space teleoperators. Continued efforts over several years will permit realistic cost and economical assessments of the SPS concept. To date, no principal obstacle has been found that would render the concepts unfeasible. This is encouraging and progress toward a potentially ultimate source of terrestrial energy is foreseeable.

### References

7. NASA CR-134886, "Microwave Power Transmission System Studies," December 1975 (NAS3-17835).
8. Econ, Inc., Grumman, Arthur D. Little, Inc., Raytheon Company, Aerospace Corp, "Space-Based Solar Power Conversion and Delivery Systems Study." Interim Summary Report, March 1976 (NAS8-31308).
9. Boeing Aerospace Company, "Space-Based Conversion and Power Relay Systems — Preliminary Analysis of Alternate Systems," April 14, 1976 (NAS8-31628).
10. Martin Marietta, "Orbital Assembly and Maintenance Study — Final Report," August 1975.
11. Jet Propulsion Laboratory, Quarterly Reviews, "Comparative Assessment Orbital and Terrestrial Central Power Systems."
12. Greenblat, E. J., "Electrical Energy Costs from Future Generating Systems," Econ, Inc., May 1975.
13. Greenblat, E. J., "Some Further Discussions on the Economic Comparison of Future Electric Power Generation and Transmission Systems," Econ, Inc., April 1975.
14. Hatsopoulos, G. N., and Huffman, F. N., "The Growth of Thermionic Energy Conversion" Tenth Intersociety Energy Conversion Conference, August 1975.
15. Lundholm, J. G., "NASA Thermionic Converter Research and Technology Program" 10th IECEC Proceedings, August 1975.
16. MSFC Solar Power Satellite Study Team, NASA Internal Documentation, June 1976.
17. JSC Solar Power Satellite Study Team, NASA Internal Documentation, June 1976.

# SATELLITE POWER SYSTEMS FOR LARGE-SCALE POWER GENERATION

Gordon R. Woodcock

*Boeing Aerospace Company, Seattle, Washington*

## ABSTRACT

The feasibility of commercial electric power derived from solar power satellites is primarily an economic question. There is little doubt that such systems would work from the technical standpoint. Efficiency levels needed for economic feasibility represent a considerable technical challenge. Minimizing system cost is therefore the principal design objective. A complete space solar power system includes four principal elements: power generation, power transmission and reception, space transportation, and support systems. These represent roughly 30%, 20%, 40%, and 10%, respectively, of the system recurring cost in a typical case. Several options exist for each system element; at the current state of knowledge clear selections of preferred options cannot be made. Interdependency of the system elements and options is very important in selecting and defining a best overall system. Development of a space solar power system would be a major challenge, similar in some respects to development of any other major new technology for large scale energy production. A typical program would progress through basic technology demonstrations, pilot plant phases, and full scale development. The development issues are somewhat different than those for most other new energy technologies; these differences are discussed in the paper. A brief economic outlook is also provided.

## INTRODUCTION

In the past few years the world has become widely aware of a trend discussed in futurology literature for some time - the depletion of the natural resources that are the basis for industrial civilization. Alternatives exist for many of these in the form of substitute materials. In the case of energy, there is no substitute. Energy itself can, however, be derived from many potential sources. With the traditional sources of coal and oil becoming finite in the practical sense of contemporary long range planning, the search for non-traditional, non-depletable sources has been considerably intensified in the past few years. Several options exist, including nuclear energy in the form of plutonium breeders and thermonuclear fusion, and various forms of solar energy. Solar energy has the advantage that it is available in enormous quantities in a potentially usable, nonpolluting form. The production of energy is not required. Solar energy has the severe disadvantage that its availability is in a very diffuse state. The design of collection and utilization systems that can acquire industrially significant amounts and supply it in a usable form, i.e. continuously available electricity, has yet to be proven on a large scale.

One approach to improving the intensity of solar energy at the collector and essentially eliminating the intermittency problem was originally proposed by Dr. Peter Glaser in about 1968. This proposal was to place the solar collector in space in a continuously illuminated orbit, transmitting the collected power to Earth by radio waves. This solution has been regarded by most analysts of the energy problem as not worthy of serious investigation. Pollard, for example,

recently characterized the construction of solar power satellites as "such a monumental task that it was not likely to be undertaken". We are used to thinking of anything involving space flight as exotic, extraordinary, and above all, expensive. Clearly, the placement in space of power systems for large scale industrial and commercial use seems at first blush to be preposterous. It is the purpose of this paper to show why it is not, and to outline some of the things that need to be done to find out if solar power from space is practical.

## CONCEPTS AND OPTIONS

A complete satellite power system must include means for collecting solar energy, converting it to a transmittable form, producing an efficient beam, efficiently receiving the beam and converting it to electricity, and in addition must include means of constructing these system elements and placing them in operation. Accordingly, it is convenient for purposes of analysis and discussion to divide the system into four major categories:

- o Power conversion and onboard distribution system
- o Power transmission and reception system
- o Space transportation systems
- o Construction and operational support systems.

Several options exist in each of these areas. In this paper we will not try to be exhaustive in describing options, but will cover the more prominent ones in each area. Technical characteristics, issues, and cost indicators will be briefly discussed.

The overall concept of the solar power satellite is shown in Figure 1. A large satellite is to be placed in a geostationary orbit 36 000 km above the Earth's equator. There it will be continuously illuminated by sunlight at an average intensity of 1 353 kw/m<sup>2</sup> except for brief shadow periods at certain times of

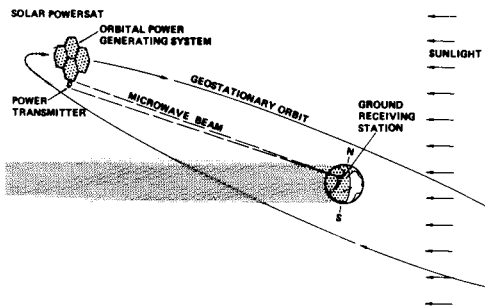


Figure 1: Solar Power Satellite Concept

year. The power conversion system is attached to the power transmission system by a rotating joint so that the former can continuously face the sun while the latter continuously faces the Earth. The power transmission system converts the onboard power, supplied as electricity, to a beam transmitted to the Earth. There it is received and re-converted, by an antenna farm, to electricity for distribution to users. The amount of power to be supplied in a usable form at the Earth terminal from one such satellite would be on the order of 5 000 to 10 000 megawatts. Accordingly, a complete satellite system for energy supply would consist of a number of individual satellites and Earth terminals, depending on the total amount of electricity to be supplied from this source. The total present electrical generating capacity in the United States, for example, is equal to about 45 satellites of 10 000 megawatt capacity.

#### Power Conversion Systems

Sunlight can be converted into electricity by quantum devices or by thermal cycles. The former extract the energy available in discrete solar light quanta directly as electrons in excited states that in turn deliver electrical energy to a load. Thermal cycles first extract the light energy as heat on a macroscopic scale and then utilize a heat engine to directly or indirectly convert the heat energy into electrical energy. A quantum device is not limited (in the macroscopic sense) by the second law of thermodynamics, and therefore need not be operated with large temperature differences. Heat engines are limited by the second law, and therefore, in the space environment where all energy must arrive at and leave the system by radiation, have

certain intrinsic properties derivable only from the second law and from the Stefan-Boltzmann law for thermal radiation.

A space solar heat engine can be represented as a device that collects and concentrates solar light, converts it to heat, processes the heat energy, and rejects unusable heat energy by radiation. This concept is shown in Figure 2 along with the results of applying the physical laws noted above. Surprisingly, the

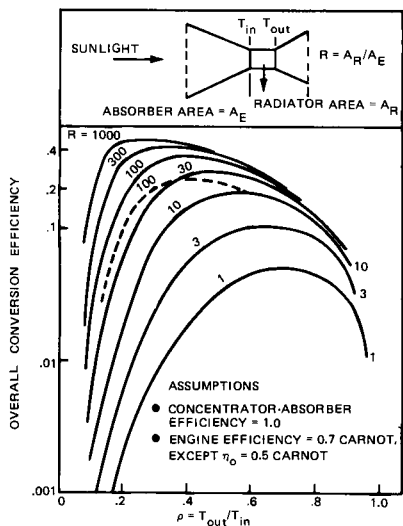


Figure 2: Heat Engines Require Large Radiator

efficiency of a space solar heat engine does not depend on solar light concentration ratio, but only on heat rejection area ratio and temperature ratio across the cycle. The area  $A_e$  may be thought of as the area of a cavity absorber, and the area  $A_r$  as the radiator area. If the ratio  $R$  is small, high efficiency cannot be obtained. With small  $R$ , a significant fraction of the heat flows through the cycle and is processed only when the temperature ratio limits processing efficiency (Second Law of Thermodynamics) to very low values. Thus heat engines can be efficient only when the radiator area is large by comparison to the heat absorber area. Because thermal radiators are quite massive by comparison to concentrators, this leads in practice to thermal engine space solar cycles previously analyzed by Boeing includes a ratio  $R$  on the order of 300, a ratio  $\rho$  on the order of .35, a concentration ratio of about 1500, and a cycle thermal efficiency of about 40%. The result of reducing the fraction of Carnot efficiency attainable from .7 to .5 is also shown; these values are representative of mechanical and

thermionic systems, respectively. Because the thermionic systems do not involve significant mechanical stresses and therefore can operate at higher temperatures, and because the optimal value of  $\rho$  tends to be higher, they achieve significant reductions in radiator area that compensate for reduction in overall efficiency and are roughly mass-competitive with the mechanical engines. They require, however, still higher concentration ratios and are in a very early state of development by comparison to mechanical cycles. The preferred mechanical cycles appear to be Brayton (gas turbine) and Rankine (two-phase liquid/vapor) cycles. Most of the space solar power analyses have assumed Brayton cycles, but a definitive trade-off needs to be accomplished before a final selection is made.

Although solar cells are not limited by the second law of thermodynamics, they have other limitations that make a determination of preference between thermal and photovoltaic conversion difficult. They are limited to conversion efficiencies roughly half those of practical heat engine cycles. They are made from high purity materials that are in some instances relatively rare. (Silicon, the basic ingredient of the most common variety of solar cell, is one of the most plentiful substances on Earth.) They operate best

with relatively little solar light concentration, resulting in a major power distribution problem, and a satellite that is almost entirely electrically active. In their favor are the facts that they are simple devices that integrate into simple systems that are easy to analyse.

In summary, the photovoltaic versus thermal issue can be characterized as (1) simple systems made from simple devices requiring high purity and exotic manufacturing techniques that must produce enormous numbers of small devices, and comparatively low conversion efficiencies, in contrast to (2) complex systems made from complex devices which, however, are today used for large-scale energy conversion, have higher conversion efficiency, and process large quantities of power per device.

The characteristics of the power conversion system largely determine the appearance of the satellites. Figures 3 and 4 illustrate typical photovoltaic and Brayton engine satellites. The photovoltaic configuration shown results from minimizing power distribution losses. It is basically a planar design with silicon solar cell blankets used at a solar concentration ratio of 2. Flat concentrator surfaces of plastic film are employed. The Brayton configuration employs a concentration ratio of about 1500, with concentrator structures

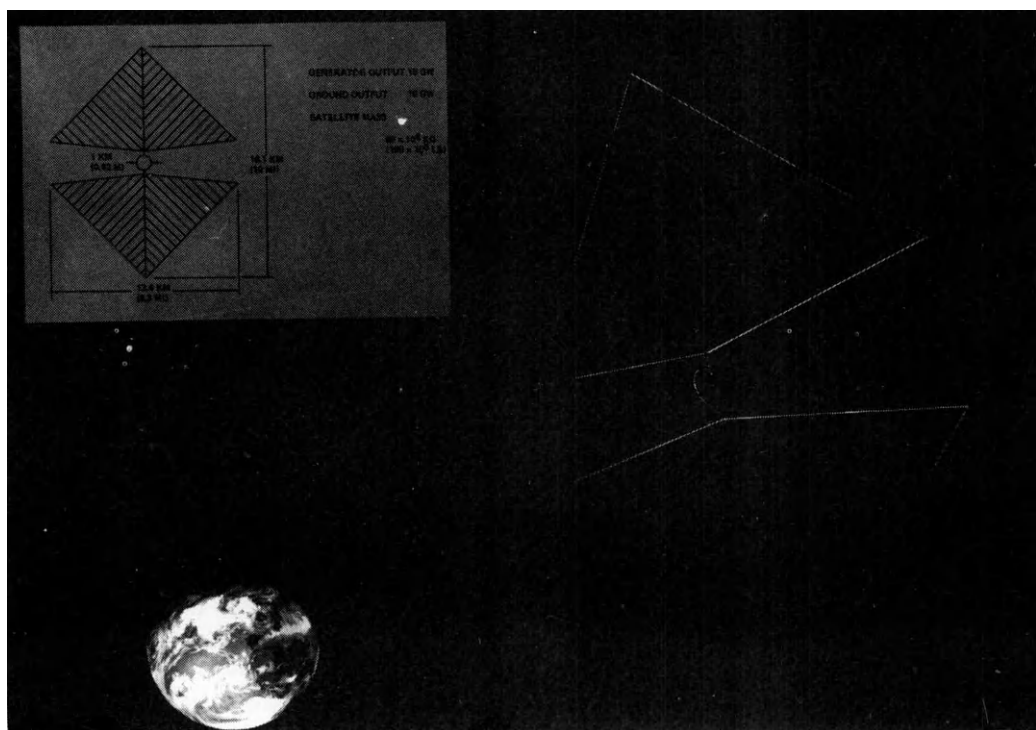
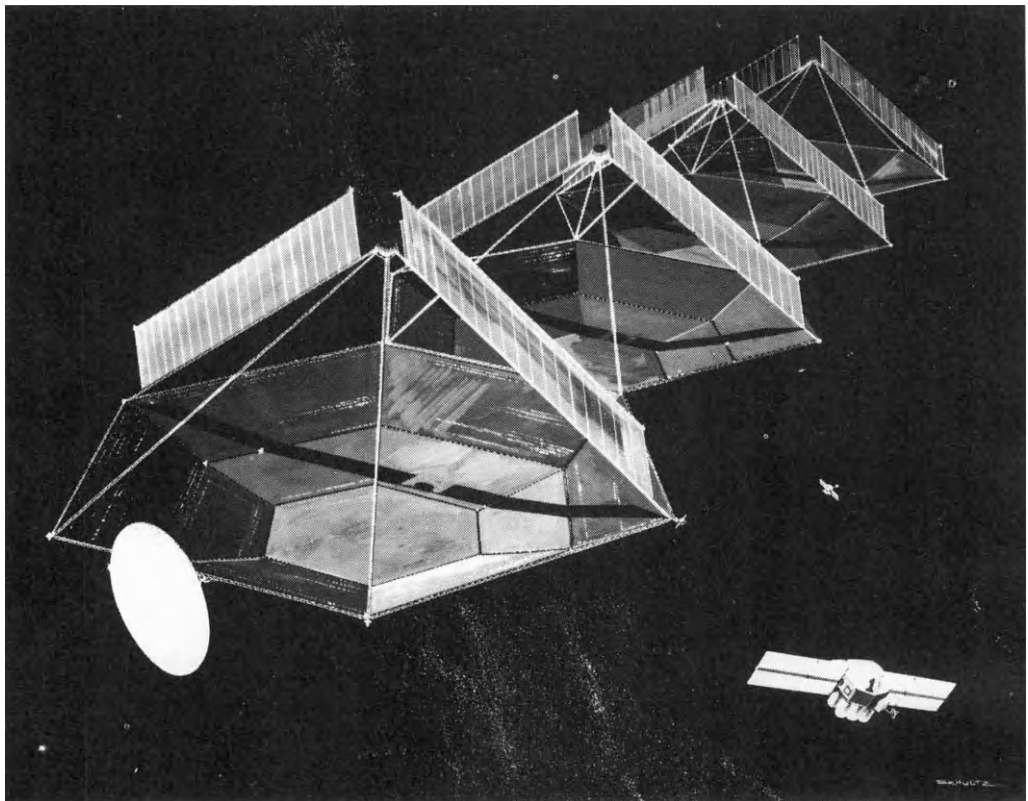
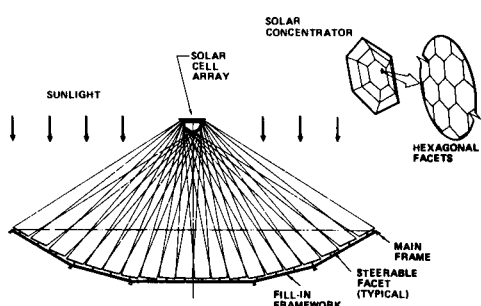


Figure 3: Photovoltaic SPS Concept (Boeing IR&D)



*Figure 4: Thermal Concentrator SPS Concept (Gregory, 11th IECEC)*

that approximate a paraboloid. Individual heliostats, about 10 000 in number, tile each dish. A pointing system steers each heliostat to compensate for attitude control errors and structural deformations. The heliostat concept is diagrammed in Figure 5. Turbomachine sets are clustered around the cavity absorber, 14 per absorber, as shown in Figure 6. Heat is rejected from the thermal cycle by large space radiators wrapped around the cavities



*Figure 5: Faceted Concentrator Individual Steerable Facets Direct Solar Images Into Solar Cell Array*

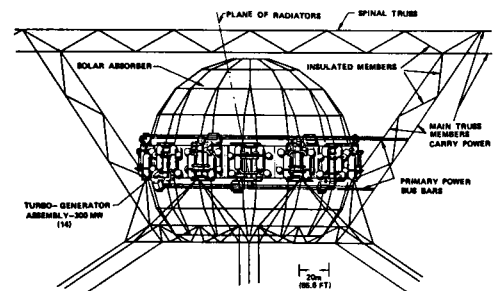


*Figure 6: Cavity Assembly*

in halo fashion, as shown in Figure 7. The mass of either of these options is estimated as approximately 100 000 metric tons including the microwave power transmission system. The solar flux interception area of the Brayton satellite is about 50 km<sup>2</sup>, and the area of the photovoltaic satellite is about twice that. These satellites are as large as a small city in area extent and have average mass per unit area of 1 to 2 kg/m<sup>2</sup>, about equivalent to a few layers of aluminum

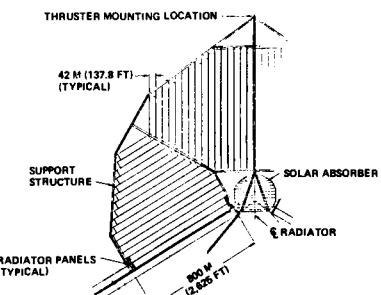


Figure 7: Radiator System, Solar Thermionic Liquid Cooled Power Satellite

foil. The capture of such enormous areas of sunlight with so little material is possible only in space.

The cost of the Brayton system was estimated by a high-level cost model recently published by Dix and Riddell [1]. This cost correlation was shown by the authors noted to apply well to such diverse systems as aircraft, automobiles, and ships. Converted to 1976 dollars and metric units, the Dix-Riddell correlation is expressed by

$$C = (1230m + 1800p)N^{-33}$$

where  $m$  is system mass in metric tons,  $p$  is installed power in kilowatts, and  $N$  is the number of units procured. A system of 100 SPS satellites is predicted to cost about \$700 per kilowatt of capacity expressed in terms of useful ground output, based on a power transmission efficiency of 60%. By the nature of the correlation, this cost does not include space transportation, space construction, or the ground-based power receiving antenna.

The Dix-Riddell correlation does not appear to be applicable to photovoltaic systems. A cost value can be estimated based on application of learning concepts to today's solar cell array costs and the very high production required for an SPS program. The result, about \$1100/kwe, is probably conservative, since learning effects do not account for radical changes in production techniques; such techniques may be developed for solar cells by developmental programs now being funded by ERDA. Other possibilities for reducing the cost of photovoltaic SPS's include the use of thin film cell systems, and the use of gallium arsenide cells. The latter are somewhat more efficient than silicon and can be used at higher concentration ratios, reducing the quantity of cells required. Cost forecasts for gallium arsenide cells in large production are not presently available.

#### Power Transmission Systems

Lasers and microwaves have been proposed as means of transmission of SPS-derived energy

to Earth. The present state of laser technology, however, leads to serious drawbacks that do not seem likely to be eliminated by technology advance. Two of the principal drawbacks are: (1) The conversion efficiency of electrical energy to laser light at the satellite is not likely to exceed 30%; The reconversion of light energy to electricity at the ground is not likely to exceed 40%; The overall efficiency of energy transmission by laser will probably not exceed 15%. (By comparison, efficiencies possible with microwaves may exceed 60%.) End-to-end efficiency has a major effect on system economics as is shown in Figure 8. (2) The laser beam would almost certainly be extremely dangerous.

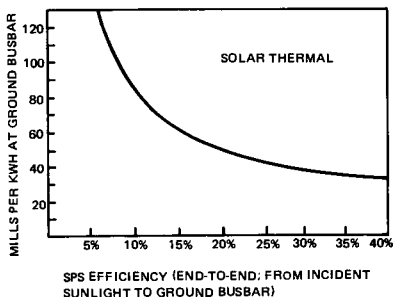


Figure 8: Power Cost vs. System Efficiency

For these reasons our attention has been directed to microwave power transmission without further consideration of lasers. The microwave system, in addition to efficiency, provides a beam that can be made safe.

Power transmission efficiency includes several elements: DC to RF conversion, beam forming and radiation efficiency, beam reception efficiency, and RF to DC conversion efficiency. A complete end-to-end efficiency analysis must also include electrical power distribution losses on the satellite and at the ground receiving station. Tests and analyses indicate that either amplitron or klystron tubes can exceed 85% efficiency in DC to RF conversion. Similar studies have indicated that RF to DC conversion efficiencies can approach 90% using the "rectenna" concept originated by Brown at Raytheon. Therefore, efficiency of beam forming, radiation, and reception are the major issues.

High efficiency radiative energy transfer is foreign to our experience. We are used to dealing with RF systems wherein only a very small fraction of the radiated energy is intercepted by the receiver. In a system designed to transfer data, it is more economical to provide plenty of radiated power and get by with less antenna efficiency. To economically transfer power, however, antenna design cannot be compromised.

There are many detailed references on SPS power transmission [2,3,4 are representative]. They indicate that radiation, beam forming, and interception combined efficiency can readily exceed 90%; a system cost optimization might compromise this slightly. Theory and experience with high performance radar systems provides the basis for performance goals for the SPS power transmission antennas. The antenna on the satellite must approach 90 db directivity. This leads to an antenna size of approximately one kilometer, considering the selected RF frequency of 2.45 GHz (the industrial microwave band) and the approximately 38 000 km transmission distance.

One of the principal issues in power transmission is exposure of the public to microwave energy fluxes. The flux in the center of the beam will be on the order of 20 mw/cm<sup>2</sup>, about twice the current US public exposure standard (far below a lethal level). Standards applicable to the SPS may be set considerably lower. It does not appear to be cost effective to intercept energy below about 1 mw/cm<sup>2</sup> flux density. This leads to the idea of an

exclusion area around the receiving site as illustrated in Figure 9. The rectenna is about 7X10 km in this picture. Most of the studies of SPS power transmission have used antenna patterns that generate sidelobes about 25 db below the beam central strength. It is quite likely that continuous exposure standards will be set lower than this sidelobe strength. It has therefore been supposed that the exclusion area might have to encompass the first or second sidelobes and hence be 20 to 40 km across. However, better antenna patterns are possible. Figure 10 shows that sidelobes can be suppressed to at least 40 db, resulting in sidelobe strengths below the lowest public microwave exposure standards (Czech) now in use. The result is a slight enlargement of the main beam, but enough improvement in system efficiency occurs to more than pay for the larger rectenna.

Costs previously quoted for power generation systems are believed sufficient to cover the space segment of the power transmission system, in that the mass data input to the cost correlations included the space antenna mass. The ground antenna,



Figure 9: SPS Power Receiving Antenna

however, is not included. Preliminary estimates of the ground antenna cost have been in the vicinity of \$200/kwe.

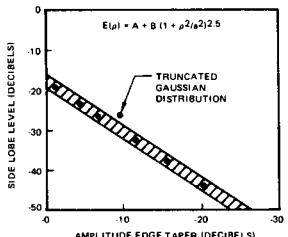


Figure 10: Side Lobe Levels Resulting From Various Taylor Series Tapers

#### Transportation and Construction

The SPS concept calls for great extrapolations of past experience in space transportation and space construction. Freighter vehicle (HLLV - Heavy Lift Launch Vehicle) traffic to low Earth orbit could well reach ten flights per day; construction of things in space the size of small cities is entirely outside human

experience. In fact, the only construction jobs ever carried out in space were the Skylab sunshades and the repair of a fender on the Apollo lunar surface vehicle. However, the space environment offers unique advantages of minimal environmental loads (no wind, almost no gravity forces on structure) and may be ideal for construction of the large devices needed to utilize solar power on a significant scale.

In a recent paper [5], we discussed the transportation options and showed that transportation costs for SPS's can probably be reduced to acceptable levels. A typical SPS scenario involves installation in orbit of 30 to 40 Gw of capacity annually, translating to 300 000 to 400 000 metric tons of SPS hardware delivered to geosynchronous orbit per year. This represents thousands of times more space transportation traffic than occurs today. At these high traffic rates, classes of vehicles not practical at today's traffic rates become attractive. Completely reusable launch systems capable of placing 200 metric tons or more in orbit per flight have been defined by studies [6]. Figure 11 shows one of several concepts analyzed. This class of vehicle shows promise of

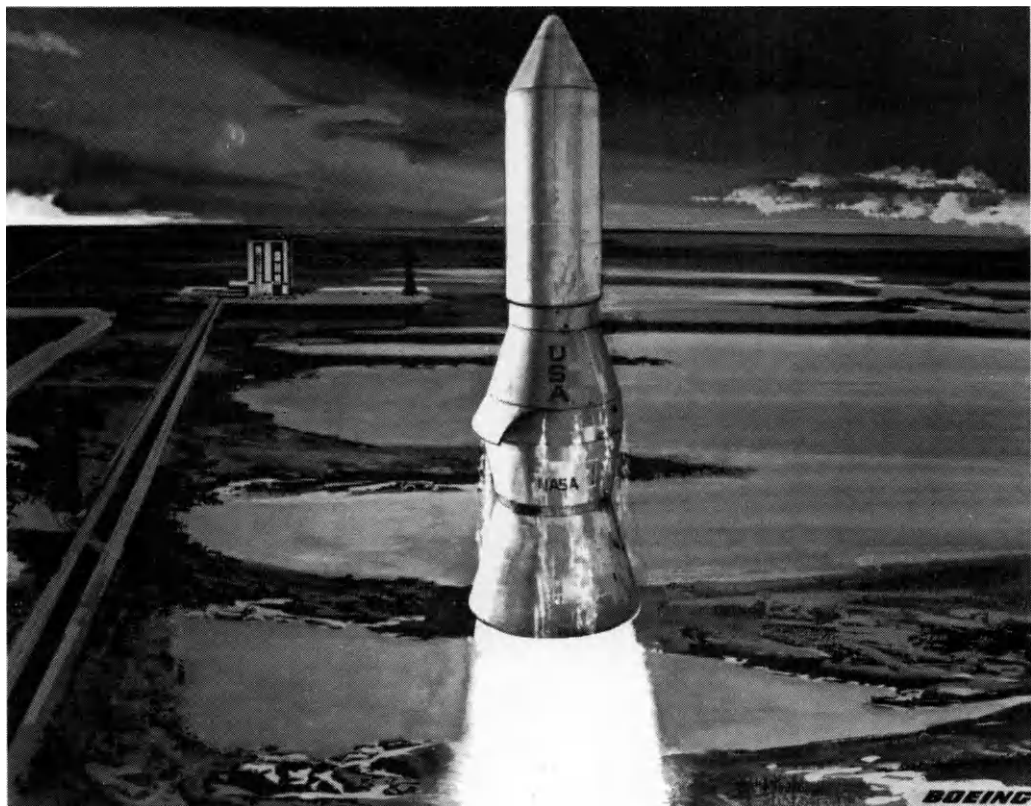


Figure 11: Heavy-Lift Launch Vehicle

attaining transportation costs in the vicinity of \$30 per kilogram delivered to low Earth orbit; about three times the cost of the propellant required to operate the vehicle.

Advanced orbit transfer systems will be able to accomplish delivery from low orbit to geosynchronous orbit relatively efficiently, yielding total transportation costs of about \$75 per kilogram. One of the more promising concepts is the use of the power output capability of the satellite, or a module thereof, to drive an electric propulsion system for orbit transfer. The electric propulsion hardware would be installed on the satellite module in a manner similar to that illustrated in Figure 12. Transfers would require several months at the low thrust levels achievable. The use of high thrust chemical rocket systems, delivering SPS hardware as inert payloads to geosynchronous orbit for construction, is estimated to be somewhat more expensive. This avoids complicating the satellite design and allows rapid transfers of less than one day. The total costs of transportation by these two modes including all launches to low Earth orbit are estimated as about \$750 and \$1100 per kilowatt electric, respectively.

Construction operations could be carried out either in low or geosynchronous orbits

If the self powered electric propulsion transfer mode is adopted at least some low orbit assembly is required. Preliminary studies of construction operations have been made. They indicate that some hundreds of construction personnel will be needed to construct one SPS in one year. These studies have assumed that SPS hardware is prefabricated on the ground to the extent possible considering launch vehicle payload mass and volume capability limits. Figure 13 is a typical concept of an SPS construction base. Large "space cranes" are used to move the hardware to the work stations and to perform the installations. These devices include a pressurized crew cab and employ crew-directed remote manipulators similar to those used in undersea operations. Because of the large size of the SPS hardware, the manipulators provide a scale-up of motion to augment the crewman's capability.

Preliminary cost estimates that have been made for space construction are equivalent to \$100 - \$150 per kilowatt of ground output. Projections of space construction techniques and productivity, however, involve major extrapolations of existing space experience.

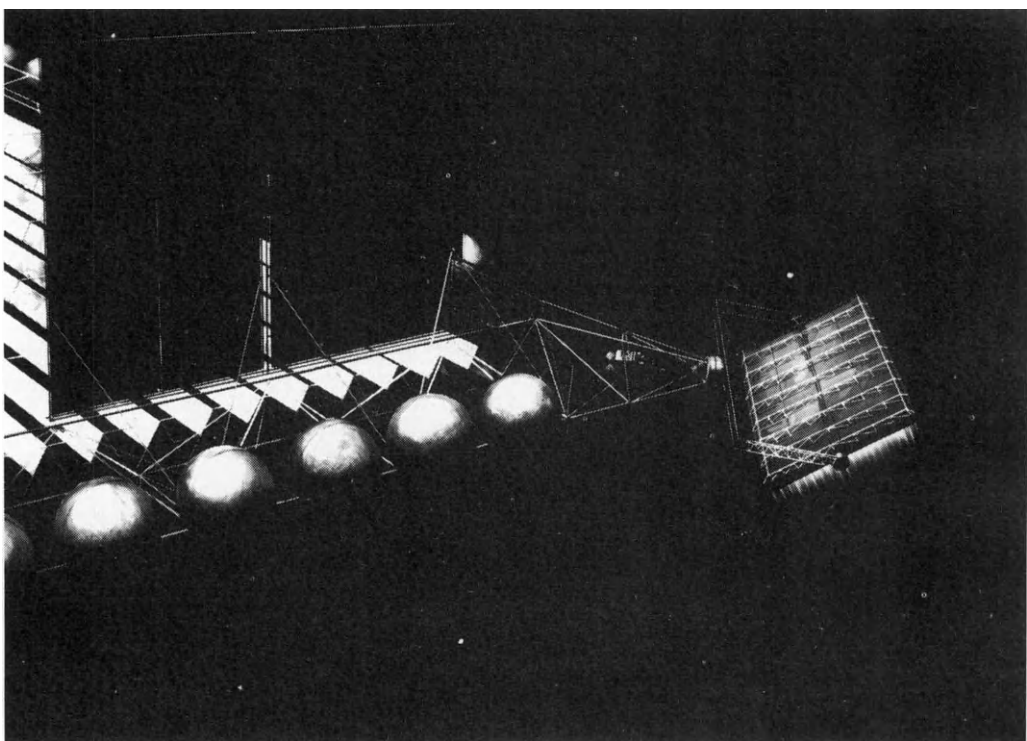


Figure 12: Electric Propulsion Installed on SPS Module

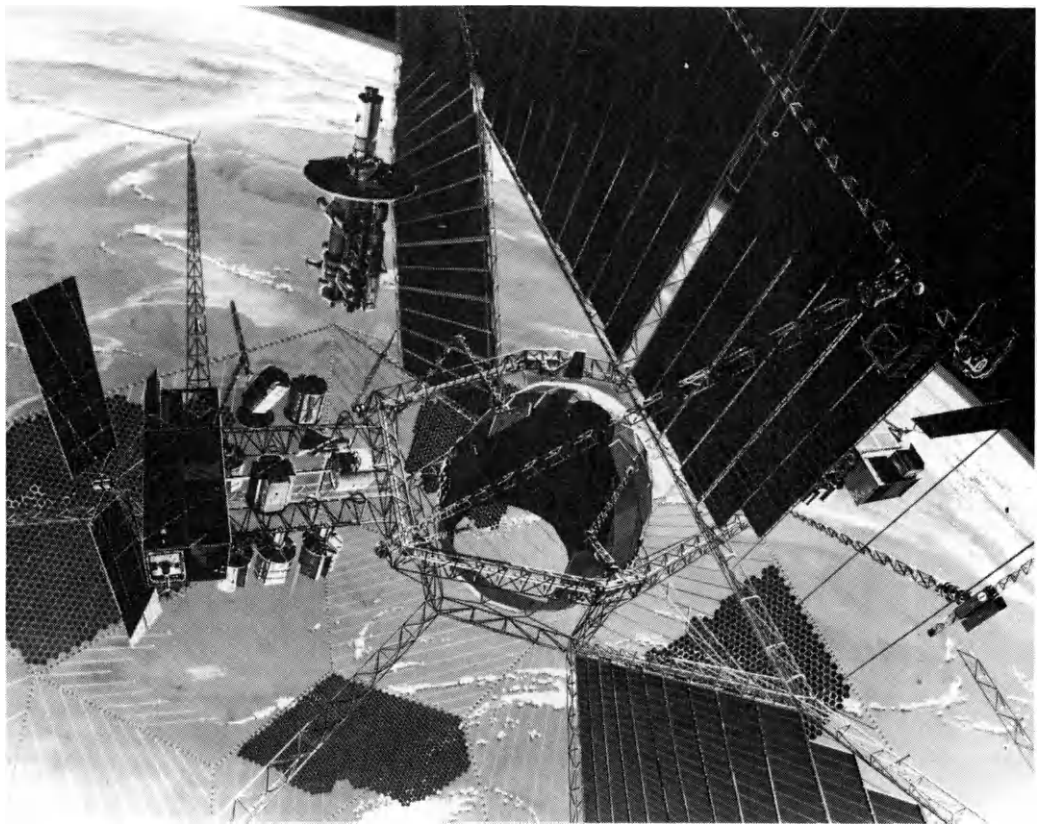


Figure 13: SPS Construction Base Concept

#### THE SPS AS AN OPERATIONAL SYSTEM

Even if reasonable costs for SPS's can be achieved, we must still address the question of their operational suitability. Comparatively little work has been done in this area. The two principal issues are the satellite availability achievable and the large amount of power, 5 Gw (5 000 megawatts) or more, produced by each ground receiving antenna. Some SPS concepts employ two antennas per satellite, resulting in 10-Gw SPS's but 5-Gw antennas and beams.

SPS's will be highly redundant in almost all aspects, incorporating dozens of turbomachines or billions of solar cells, redundant conductors and switchgear, and thousands to millions of RF generators on the antenna. Functions that could shut down an entire SPS, such as the rotary joint between the power generation and antenna systems, can also be made redundant so that the entire system has no single failure modes that can result in a complete outage. Preliminary estimates of failure rates of the redundant elements do indicate the need for system maintenance. If this

maintenance is provided on a reasonably regular schedule, each SPS should normally be able to operate at more than 90% capacity. Attainment of availability on the order of 95% should be possible. Occultations by the Earth's shadow and by nearby SPS's account for somewhat less than 1% outage, the remainder being allocated to occasional instances when shutdown of an entire satellite is needed for maintenance reasons or occurs inadvertently.

Maintenance of the systems may be desirable on a more or less continuous basis. Because of the large number of system elements, e.g. thousands of RF tubes, the expected failure/replacement rates may be on the order of several per month. If continuous maintenance is employed, the power output will be maximized and the total work required is no different than for less frequent maintenance. Because of the desirability of working on the systems while they are operating (with only local shutdown around the area requiring service), the use of remote manipulators is probably indicated for safety reasons. Preliminary estimates are that the maintenance requirement will not have a major impact on

power cost. A crew of 25 people could be supported at each 5-Gw SPS at an equivalent power cost on the order of 3 mills (\$.003) per kwh.

Typical plants currently coming on line are roughly 1 Gw each, compared to 5 Gw for an SPS. The larger a plant, the more severe the impact on the power grid in the event of an outage. The reason that such large amounts of power are desirable for each antenna is that the antenna system must be of the size described earlier regardless of the amount of power transmitted, if good efficiency is to be achieved. The upper limit for power per antenna may be set by ionosphere heating. A provisional limit to central beam flux density of 23 mw/cm<sup>2</sup> has been used in recent studies. This value is, of course, subject to experimental confirmation. A recent publication by Drummond[7] suggests much lower values based on a theory of thermal plasma instabilities, but other experts[8] believe that these, even if they occur, will not present a serious problem.

The first few SPS's placed in orbit would undoubtedly be completely backed up by alternate energy sources as has been true with the introduction of other new technology energy systems. With achievement of 95% availability, a system of 10 SPS's needs four in reserve, i.e. six that can be depended on, to achieve .9999 system availability. A system of 100 (at 5 Gw each, about equal to current U.S. generating capacity) needs 13 in reserve to achieve the same system availability. Thus the problem of the large size of each SPS can be alleviated by the collective operation of a system of SPS's such that any satellite can drive any rectenna. The larger the number of units in the system, the smaller the fraction that must be reserve capacity. This leads to the concept of a national grid. It is greatly facilitated by the wireless nature of the power transmission; transfer of loads over thousands of miles with no additional loss could be achieved simply by shifting the microwave beams. (During the shift, the beam would of course be shut off to avoid public exposure hazards.)

#### DEVELOPMENT ISSUES

The three most significant technical issues for SPS appear to be microwave propagation, ionosphere heating, and space construction. The principle of microwave power transmission has been demonstrated over short ranges by JPL and Raytheon. There remain the concerns about actual propagation effects in the ionosphere and space plasmas. Two experiments appear appropriate. The first is a microwave interferometer spacecraft in geosynchronous orbit. Such a spacecraft, operating at low RF power levels, could simulate the operation of the highly directive transmission system and measure any disturbing effects introduced by the unperturbed ionosphere. The size of such a

spacecraft would probably permit launch by the space shuttle and IUS. Figure 14 shows a concept of the interferometer spacecraft, including a shuttle payload bay deployment sequence. Ionosphere heating could be simulated from the ground by using the Arecibo radio telescope antenna with a transmitter power level of several megawatts. Measurements of the resulting effects would determine the beam strength limits that could be used without deleterious ionosphere modifications. A variety of experiments have been proposed to use the shuttle in low Earth orbit to demonstrate and develop construction techniques. All of the critical procedures could be developed and preliminary measures of productivity acquired.

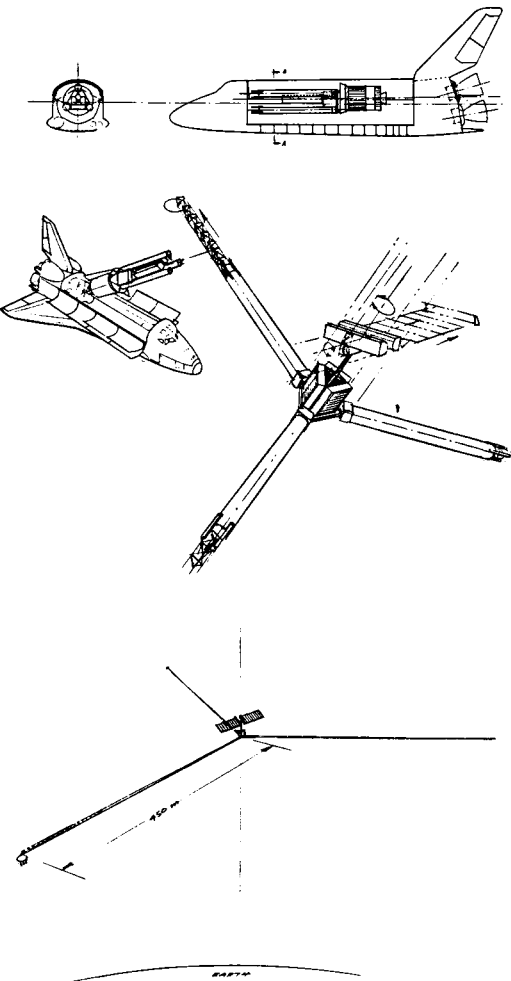


Figure 14: Interferometer Spacecraft Concept

Beyond these critical areas, most of the other issues are in the realm of engineering development. These developments may be more demanding than the feasibility experiments described, probably requiring continuously-manned space stations, e.g. to build a pilot plant SPS. There are of course significant cost uncertainties associated with these engineering development issues. But the selection of those that need to precede full-scale SPS development is a matter of tradeoff of demonstration cost versus reduction in financial risk of deferring the development. These tradeoffs have not been conducted; it is therefore somewhat premature to speculate as to specifics of an entire SPS development program.

The ranges of costs previously discussed, when combined with a range of capital charges from 0.12 to 0.15 and a range of (capacity achieved)x(availability) of 0.6 to 0.9, result in a predicted range of power cost from about 25 to about 75 mills per kilowatt hour. This range is too large to make firm statements about the economic attractiveness of SPS; at the low end it is quite attractive and at the high end, probably not. However, studies presently in prospect should reduce the uncertainty and increase the system definition to a level that judgements as to the attractiveness of the concept can be made. It is the author's view, after having been involved in SPS studies for several years, that we will be able to develop confidence that the lower to middle of the range of costs is attainable.

#### REFERENCES

- (1) Dix, D. M., & Riddell, F. R., "Projecting Cost-Performance Tradeoffs for Military Vehicles". *Astronautics & Aeronautics*, Sept 1976.
- (2) "Microwave Power Transmission System Studies", NASA CR-134886, (Raytheon), Dec 1975
- (3) Dickinson, R. M., "Evaluation of a Microwave High-Power Reception - Conversion Array for Wireless Power Transmission", JPL TM33-741, Sept 1975
- (4) JSC Inhouse Study, "Initial Technical, Environmental, And Economic Evaluation of Space Solar Power Concepts", JSC-11568, Aug 1976
- (5) Woodcock & Davis, "Transportation Options For Solar Power Satellites", 11th IECEC, Sept 1976
- (6) Morgan, et. al., "Systems Concepts for STS-Derived Heavy Lift Launch Vehicles", (Boeing), Contract NAS9-14710, 1976
- (7) Drummond & Drummond, "Derivation of a Low-Cost Satellite Power System", 11th IECEC, Sept 1976
- (8) Private Communication, Perkins & Nalos

# SPACE AND ENERGY

Ivan Bekey

*The Aerospace Corporation, El Segundo, California*

## Abstract

Potential contributions of space to energy-related activities are discussed. Advanced concepts presented include worldwide energy distribution to substation-sized users using low-altitude space reflectors; powering large numbers of large aircraft worldwide using laser beams reflected from space mirror complexes; providing night illumination via sunlight-reflecting space mirrors; fine-scale power programming and monitoring in transmission networks by monitoring millions of network points from space; prevention of undetected hijacking of nuclear reactor fuels by space tracking of signals from tagging transmitters on all such materials; and disposal of nuclear power plant radioactive wastes in space.

## I. Introduction

Technological advances expected during the next 25 years will make an almost limitless number of space systems of dramatic performance possible. Many of these space systems will be able to contribute either in a primary or in supporting roles to energy-related activities. In this paper, a number of such advanced space system concepts are briefly presented. These concepts are drawn from a much longer list identified in the course of a NASA study contract\* with The Aerospace Corporation on which the author and Dr. Harris Mayer were the study director and principal collaborator respectively. Some of the concepts have been previously known, while it is believed that others are original. In addition to future space concept identification, the intent of the NASA contract was to derive the needs for orbital transportation and operational support space facilities which would be required by the entire set of concepts.

The objectives of this paper are to show examples of the breadth of possible contributions of future space systems to the generation, distribution, and control of energy; the search for resources and control of pollution; and the disposal of some waste by-products. The concepts presented are not advocated by the author, The Aerospace Corporation, or by NASA. They have had the benefit of only very preliminary analysis, and the numbers should only be viewed as illustrative of the generic concepts. Further, no claim is made that any of them are preferred over terrestrial or other space approaches, or that benefits to society will accrue with their use. They are simply advanced as candidates for serious investigation, believing them to be potentially useful.

The specific space concepts presented here will depend on the ability of advanced technology to exploit the most fundamental characteristics

of space: the absence of gravitational forces, the benign environment, the availability of abundant and free energy, the vantage point due to satellite altitude, and the essentially continuous motion without requiring additional propulsion.

The absence of gravity will allow the construction of very large structures, reflectors, optics, and antennas making possible beam power transmission and energy reflection with beam spreads so small that power transmission over orbital ranges will be possible, with capture of most of the energy by practically sized structures. The motion and vantage point of observing satellites in low orbit around the earth will allow the continuing search for new energy sources. Lasers in space will allow great finesse in aiding pollution control and resource search. Space itself could be utilized as a sink to permanently dispose of radioactive and toxic materials. New communication concepts will make possible real-time monitoring and control of an extremely large number of points on energy distribution networks, which will allow fine-scale real-time power programming. Communication satellites could help allay the growing fears of nuclear blackmail or terrorism by continuously locating and tracking each item of nuclear material or fuel in real-time anywhere in the world. Laser beams could even be used to deliver energy to aircraft in flight.

These concepts are discussed in two major categories. The first category includes concepts which utilize relatively low-risk extensions of today's technology, which could become operational in the 1980-1990 time period, and which represent no operational hazards. The second category includes relatively high-risk and far-term concepts which could not become operational until the 1990-2000 time frame or even later, which require an unprecedented scale of operations in space, which require large advances in technology, which have some degree of hazards associated with their operation, or which have some combination of such features.

This paper will not treat in detail the solar-energy power plants in space, since they comprise the primary subject being discussed in this session by other speakers. Likewise, point-to-point microwave power relay, and sunlight reflection for the purposes of illumination enhancement on earth are only briefly treated.

## II. Near-Term Concepts (1980-1990)

### Nuclear Materials Location

The nuclear electric power industry in the USA is estimated to grow<sup>1</sup> from  $3 \times 10^{10}$  W in 1975 to  $5 \times 10^{11}$  W in 1993. There are projected to be in excess of 500 light-water-nuclear reactors in

\* NASW-2727, Study of the Commonality of Space Vehicle Applications to Future National Needs, NASA, Office of Space Flight, 1975. This contract was conceived and directed by Capt. R. F. Freitag, assisted by Mr. Fred S. Roberts.

operation, including 150 reactors using mixed-oxide fuels. The new fuel for the reactors, the spent fuel assemblies, and plutonium compounds will have to be shipped between fuel fabrication plants, enrichment plants, reprocessing plants, storage sites, and the reactors themselves. Diversion or hijacking of these materials at any point in the cycle by terrorists for blackmail purposes is a real and growing concern, not only within the USA but also in equivalent programs worldwide.

In the USA it is estimated that in 1993, 10,000 metric tons of spent fuel will be transported in 4700 shipments; 15,000 tons of new fuel rods in 700 shipments; 1000 tons of radioactive waste in 320 shipments; and 600 tons of plutonium compounds in 400 shipments. These materials are now and will continue to be shipped via train or truck, and though encased in thick-walled massive shipping casks, could be intercepted and hijacked by well coordinated terrorists. Though the Nuclear Regulatory Commission has in effect a system of safeguards to detect and prevent diversion in fixed facilities and to a more limited extent in transit, public fears (and perhaps one or more such real incidents) may severely limit the growth of the nuclear power industry.

The visibility gained from space could be used to advantage to track all the fuel element assemblies, casks, or packages continuously, identifying and locating each one in real time. This tracking would be all-weather, 24 hours, unaffected by location, and not subject to undetected tampering, destruction, or hijacking of the material. Though the mere detection of such acts is not sufficient to prevent loss of the material, the instant awareness would allow rapid and accurate use of guard forces to minimize the loss, as well as help in acting as a deterrent.

The ideal concept would "tag" each element of nuclear materials in such a way that the material itself emits signals which are detectable and recognizable at long range. Lacking that, the next best solution would be to "tag" each fuel element assembly or cask with a small microwave transmitter which would send unique coded signals continuously from the moment it is "tagged" in the factory until deactivated on return for reprocessing or at the receiving site. The signals from all packages would be received by communications satellites and retransmitted to a ground control center where each assembly or cask would be continuously identified and its location continuously computed. In case of attempted hijacking, diversion, or tampering, automatic alarms would be sounded enabling security forces to take immediate and accurate action. This technique could be an adjunct to or replacement of the safeguard techniques currently in use.

In this concept, illustrated in Fig. 1, each fuel rod assembly, cask, or package would be "tagged" with a unique, pseudo-random coded signal. The tagging transmitter could be associated with an individual assembly of rods, or with a cask, the three main requirements being that tampering with the active elements or contents be detected and transmitted in real time, the transmitter be so located as to have a minimal effect on fuel utility, and that silencing or

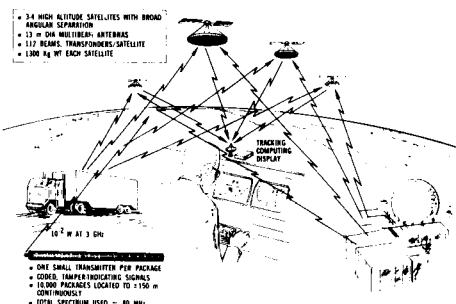


Figure 1. Nuclear Fuel Location

spoofing the transmitter itself would be detected. The transmitted microwave signal would be continuously emitted and propagated through shipping containers, vehicles, and buildings by ensuring their proper construction or by using proper transponders in their roof or case.

The transmitters would radiate identification data, and retransmission of their codes by three or four transponding satellites would allow ground computation of their location using the time-difference-of-arrival of the signals as transponded. Three satellites would allow latitude, longitude, and identity data to be derived, while use of four satellites would add altitude to the above data.

This data would be computed sequentially or in parallel for each element, and displayed on visual as well as printed records at one or more control centers essentially in real time. Automatic alarms would be sounded in the event that the signal from any fuel element or assembly:

1. goes off the air
2. shows an altered code
3. indicates tamper with the element/assembly
4. indicates tamper with the transmitter
5. deviates more than 150 m from a filed route plan in any direction
6. other abnormality is detected.

The technique is equally applicable to tracking assemblies of new or spent fuel rods, casks containing those assemblies, plutonium compound packages, or any other toxic or dangerous materials. A particular example for tagging fuel element assemblies is discussed briefly below.

Many variations are possible for devising the tagging transmitters. For maximum security of fuel rod assemblies, the tagging transmitters could consist of microminiaturized vacuum-tube electronics, which probably could withstand the heat and radiation environment to which the assembly will be exposed. A small klystron transmitter operating in the 1000 MHz microwave region would be used to radiate through a number of cavity-backed slot antennas to achieve a non-directional pattern. The transmitter would be modulated with a pseudo-random code unique to each fuel element, which could be changed upon reprocessing or at more frequent intervals as desired. The transmitter package would be

attached to the fuel element assembly with adequate separation that no sensible decrease of reactor reactivity results. The integrity of the entire case of the transmitter and the fuel rods could be sensed by an acoustic wave or other intrusion sensor integral with the "tag" which would signal attempts to disable, disconnect, or destroy the transmitter, and attempts to remove the fuel. The reflected power in the antennas would also be sensed in order to detect attempts at shielding the transmitter. The coded signal would be pseudo-random so that even very sophisticated would-be thieves would not be able to simply replicate the code while silencing the real transmitter.

For less severe threats, the transmitters could be detached from the rod assemblies while they are in use inside the pressure vessel in a reactor, while for more severe threats, and to guard against diversion by inside personnel, the transmitters could be continuously attached to and integral with the rod assemblies, even while inside a reactor. Thus, the transmitters would have to survive the operating environment, though they would not have to transmit signals to space while inside a reactor, it being sufficient to receive the transmissions when the reactor pressure vessel is opened.

In a very similar way, smaller, more conventional all-solid-state transmitter tag units could be attached to the casks or cases within which the rods or plutonium compounds are shipped, eliminating the problems of survival in a radiation environment, but at some reduction in security.

The signal radiated from the fuel package transmitter would have to pass through some obstacles on its way to the satellite receivers. Whether the units are in a depot building, factory, truck, or other transportation vehicles, the walls or containers would have to be fairly transparent to the frequency of the transmitters. Such "radiation transparency" could readily be assured in new construction by avoiding solid metal wall vehicles, and properly designing reinforced structures to allow sufficiently large mesh sizes such that the waves can pass through -- this would generally mean avoiding metallic meshes with spacing less than 15 cm. The transmissions would then readily pass through several feet of concrete with attenuation less than several db. It would, of course, not be possible to radiate through the steel pressure vessel of an operating reactor, though there really would be no need for such a capability.

The use of existing buildings, transportation vehicles, or shipping casks which do not possess the above features would require either their modification (cutting slots or windows in their walls) or the installation of external small transponders with a small antenna inside to pick up the fuel package signal, and a small antenna on the outside for transmissions to space. Such transponding units could be similar to units already in use, could readily incorporate tamper alarm circuitry, and have battery power for autonomous operation in case of power disruption.

Four satellites would be required to locate the fuel elements in three dimensions (longitude,

latitude, and altitude). The satellites would form a constellation with wide angular separation such that each satellite would receive the signal from each fuel element transmitter at a slightly different time. The signals received at each satellite would be retransmitted to a ground computation and control station, where the differences in arrival time would be detected and used for location computations. Code recognition would serve for identification of each element.

Low transmitted powers would be required in order to allow for small element "tag" sizes. The signals could further be attenuated by walls and structures, and would arrive at the satellites much weaker than signals from current satellite communication terminals, which possess large antennas and powerful transmitters. As a consequence, the satellite receiving antenna would have to be large, and the signal bandwidth very restricted to compensate for the weak signals.

A preliminary design has indicated that a near-geostationary satellite with 14-m diameter antenna, operating in the 1000-MHz band would be adequate. The footprint of the antenna beam would be about 350 km in diameter, and so multiple beams would have to be used to cover the entire country. An extension to worldwide use would require five constellations of four satellites each, and more beams per satellite.

Each satellite would form 116 beams, each by a separate horn coupled to one common lens structure. The horns would be connected to 116 receivers, whose output would be amplified, combined, and transmitted to the ground on one of the beams. About 10,000 channels would be needed to accommodate the simultaneous signals from all the anticipated shipments in the year 1993. An uplink bandwidth of 40 MHz would suffice, taking into account the frequency reuse capabilities of the antenna and presuming that no more than 10 percent of the total transmitters would be concentrated in any one of the 116 beams at any one time. A 40-MHz bandwidth would also be needed for the downlink from all four satellites to the control center. Both of these bandwidths could be reduced significantly by proper code and circuit design.

The satellites would be very similar to communications satellites already in orbit or programmed to fly in the early 1980's. The ground control center equipment is likewise similar to many in existence. The tagging transmitters appear to be a straightforward application of well understood design techniques.

Each fuel package would generate a 10 bit/sec unique pseudo-random coded signal which would be used for identification, superimposed on a cyclically repeating 100 kbit/sec code, the time of arrival of the latter pulses being used for location determination to an accuracy of 150 m. The ground receiving station would have 20,000 parallel code generators and integrators for identification and tracking. All the circuits would be constructed with large-scale integrated microcircuits to form a compact data processor.

The above concept could materially contribute to maintaining nuclear safeguards worldwide. The technology is relatively straightforward

extrapolation of today's techniques, and flight articles could be available in the early 1980's.

#### Resource Assessment

##### General Earth Observations

The advent of earth-resources satellites in low-altitude orbits has already had significant impact in energy-related areas, contributing in resources search, power plant pollution control, and other areas. Technology available now could allow equivalent performance from synchronous equatorial orbit, with an increase in both optical sizes and numbers of detectors by two orders of magnitude. Such performance would then feature continuous visibility with no loss in resolution -- an advantage in power plant effluent or pollution control. Thus, a few satellites at synchronous altitude could perform the same function as today's satellites in low orbit, but cover all points in the globe almost simultaneously.

Alternatively, advanced technology could be used to improve the performance of low-altitude satellites beyond that achieved today. Figure 2 illustrates one such approach, which is essentially a larger, radar- and laser-equipped version of the current Landsat earth-resources satellites, operating in a 500-nmi sun-synchronous orbit. This concept, featuring high-resolution multispectral imaging and all-weather mapping of the surface, would serve resource search, pollution identification, forest management, crop prediction, insect-infestation monitoring, drought diagnosis, and the like. It would make optical observations with a 2-m telescope with beam splitters that feed detectors in different spectral regions from 0.4 to 4  $\mu\text{m}$ , and it would use mosaic charge-coupled devices containing millions of detectors in the focal plane, obtaining high resolution, high area coverage rate, and flexible preprocessing at the same time. Active laser illumination of selected scenes would extend the optical observation period to 24 hours a day. The system would further use a synthetic aperture high power radar to obtain high-resolution all-weather imaging of swaths on either side of the satellite ground track.

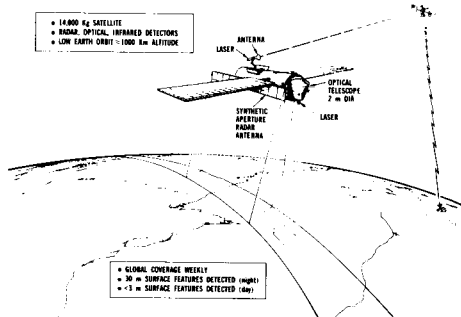


Figure 2. Advanced Resources/  
Pollution Detection

The satellite would obtain resolutions of 3 to 30 m in the visible, IR, and microwave spectrums. Because of the large-aperture optics

and the high-power radar, this satellite would have high raw power requirements (12 kW), and be large (3 by 20 m) and heavy (14,000 kg). Although an order of magnitude heavier than current Landsats, it could be easily placed in orbit and serviced by the Space Shuttle. It would be considered a low-risk near-term (1985) system concept.

The advent of such all-weather, 24-hour, high-resolution earth-observing satellites could greatly increase the energy industry's ability to search out resources, site its plants, predict its available supply, and control its effluent pollution.

##### Fine-Grain Laser Measurements

In contrast to the images obtainable from even advanced observatories such as in the previous concept, pulsed or continuous-wave lasers in space could be used with finesse far exceeding simple imaging. For example, gaseous effluents from power plants could be monitored by two laser beams projected from a satellite and retrodirected by corner reflectors in the path of the effluent. The frequency of one laser beam would be chosen in the absorption band of the molecule being monitored, while the frequency of the other beam would be located outside the band. The ratio of the intensities of the signals returned to the satellite would measure the amount of effluent in the beam path.

While such measurements could be made with laser systems at each plant, in the space concept a single laser could serve all plants with similar effluent located in a hemisphere, and three lasers could provide global service coverage. Pushed both by scientific interest and the promise of technical applications such as the above, laser technology is expanding rapidly today, and will probably continue to do so. It is a good bet that lasers of almost any desired characteristic will be available for space applications in the 1980-2000 period. Their real strong points are that their wavelength, phase front, beamwidth, and pulse length can be finely tailored so as to elicit only the desired molecular response -- rejecting all others, and the energy applied only where wanted and when needed.

Another application of space lasers with direct benefit to the energy industry would take advantage of extremely short pulse laser radar. Mode-locked lasers are now available that give a regular series of picosecond-wide pulses separated by 10-nsec intervals. Individual pulses can be isolated from the pulse train. Single detectors and streak cameras are also available with picosecond time resolution to measure the short laser pulses. Combined with such detectors, the pulsed lasers operating in a ranging-radar mode could result in range resolutions of 0.3 mm.

This capability leads to a concept for measuring the water level at many places along a river system, including its fine tributaries, to aid water level measurements, flow control, and resource prediction which could be very useful in the hydroelectric power industry. The concept is illustrated in Fig. 3. A fixed and a floating corner reflector (or the equivalent on the shore) would be placed at each measuring point in the stream, fashioned so that the float can only move

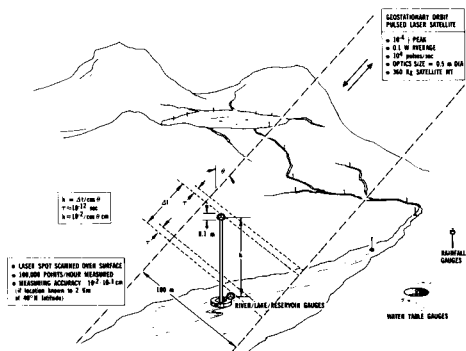


Figure 3. Precise Water Level Measurement

vertically with respect to the fixed reflector. A geostationary satellite would scan the terrain in a programmed fashion with its picosecond-pulsed laser. The difference in time of arrival of pulses reflected back to the satellite from the pairs of fixed and floating corner reflectors would readily indicate the water level to an accuracy of between  $10^{-2}$  and  $10^{-1}$  cm. The laser would generate  $10^{-4}$  J per pulse, but its long-time average power would only be  $10^{-1}$  W, a fairly small laser even by today's standards.

The laser beam would be projected through 0.5-m optics, which would result in a 100-m spot being illuminated from synchronous equatorial orbit. The beam would be swept in a raster scan over the area of interest, the USA in the illustration, and the relative water level measured in over 100,000 instrumented points each hour. The accuracy of the measurement could be significantly improved by a design in which one corner reflector would not see the satellite directly, but instead would receive and reflect back some fraction of the light illuminating the other reflector. Then the time difference in the returns to the satellite would translate into twice the distance between reflectors with no trigonometric factors to degrade accuracy.

The satellite in this application would be small and weigh only 360 kg. It could easily be put in synchronous orbit. The telescope systems are available now, and though the laser and picosecond detectors are still only laboratory devices, could probably be developed and orbited in 1985 at low risk.

The measurements of laser transit times between reflectors could, of course, be made without a satellite by having individual lasers at each station and recording the data locally (or collecting it via communications satellite). But the space platform would make it possible to use just one laser with one calibration on one satellite per hemisphere. With the satellite laser, the ground installations could be made simple and inexpensive, consisting of passive corner reflectors.

With a very similar satellite, laser corner reflectors used as survey markers could be placed quite accurately in a coordinate system centered on the satellite. The round-trip time

of the laser pulse would give the distance between the satellite and a survey marker. The angular coordinates would be obtained to good accuracy ( $10^{-6}$  rad) from the pointing of the laser beam, and could be improved by the use of a long-base-line laser interferometer on the spacecraft. Effects of the atmosphere could be corrected by using three different laser frequencies. With this system, markers could be placed by helicopter in wild territory and then surveyed accurately by the laser satellite. As many as a million markers could be surveyed or resurveyed in a day, with impact on oil prospecting and drilling operations.

In these and other ways space lasers could contribute to energy-related activities in the next 10-20 years.

#### Network Monitoring

The coverage and visibility obtainable from satellites, especially those in geostationary orbit would enable communications contact with extremely large numbers of earth terminals provided that the satellites are made deliberately large and complex, thus allowing the using terminals to be small, cheap, lightweight, and proliferated by the millions. If only small amounts of information are to be collected from each sensor/user, then a data collection system with extremely large access capability would result.

One application of relevance to the power industry would be the simultaneous monitoring of an extremely large number of points in the power distribution networks, measuring for example, voltage, current, power, power factor, energy flow, harmonic content, etc. This information would be collected by a large communications satellite, and relayed to one or more control centers, and it could be used for fine-scale as well as gross power programming, power sharing, greatly detailed distribution control, and even direct readout of the detailed energy consumption of every residential and commercial user in the USA.

An example of the concept, illustrated in Fig. 4, would make use of very low power ( $3 \times 10^{-5}$  W average, 2.5 W peak) pulsed microwave transponders operating at 1 GHz. The small, self-contained units would consist of one microcircuit chip, a battery, and a crossed dipole stub antenna, which could be produced extremely cheaply in mass production, probably costing less than \$10 each.

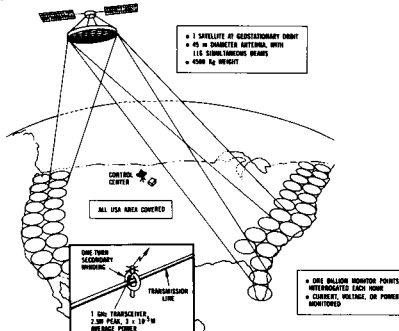


Figure 4. Energy Monitor

Each transponder would periodically or on demand receive a short digital interrogation from the satellite, and transmit a short coded message containing the unit identification code and the value of the measured parameter at the time of interrogation. The interrogation would consist of a 30-bit addressee code, specifying the unique unit out of  $10^9$  units. The unit response, upon code match, would consist of its 30-bit identifying code followed by, say, a 10-bit message -- specifying a measured quantity to 0.1 percent.

The signals would be received by a communications satellite with 45-m diameter multibeam antenna outfitted with 116 simultaneous receive and transmit beams. These beams would cover the entire USA land area. Each beam would feed a 1000-channel processing receiver, each channel being 10-kHz wide and accommodating a 3-kHz information bandwidth, such that  $3 \times 10^{-4}$  sec long pulses would be accommodated.

The total time for an interrogation would therefore be 10 msec while the response time from each unit would be 15 msec. Allowing 25 msec processing time, 50 msec should be sufficient for an interrogate-reply cycle. Thus the number of units which could be interrogated/reply each 50 msec would be equal to the number of channels times the number of beams, about  $10^5$ . The number of units sampled each hour could therefore be  $7 \times 10^8$ , a truly enormous number.

The total spectrum required by each beam would be the number of channels times the channel bandwidth, or about 10 MHz. The isolation between beams would allow three to five such 10-MHz bands to serve an arbitrarily large number of beams, so that 30 to 50 MHz would suffice for the total channel occupancy. The sum total information could be sent to a central processing site using one high microwave or laser link to carry 1000-MHz bandwidth, or each beam area could include one processing site, with a more modest 10-MHz bandwidth capability each.

The truly enormous number of points which could be sampled ( $7 \times 10^8$  per hour) would result in an unprecedented ability to control the energy network, fine-tuning the distribution of energy. Automatic consumption controls could be established at the individual user level, and automatic billing for consumption instituted. Detail hour-by-hour consumption plots could be made available to all for energy conservation efforts.

All components of this concept could be constructed with current technology and be operating within 10 years. The investment could well be readily recovered through more efficient operations or user charges.

#### Night Illumination

Concepts for providing nighttime illumination to the earth by reflecting sunlight energy using large thin-film reflectors in orbit have been known since the early 1960's and analyzed by NASA and others. More recently, Dr. Kraft Ehricke also discussed the concept in the context of general space industrialization.<sup>3</sup> Since the concept is treated in detail elsewhere in this session, it will only be briefly reviewed here.

In contrast to applications that require high-quality optical telescopes, in this application the chief requirement is for extremely large optical surfaces of relatively poor quality that simply reflect lots of light. The optical surface could be constructed of a very thin membrane of plastic, metallized on one surface, and stretched by some structure to form very-large-area but lightweight reflectors. A typical concept is illustrated in Fig. 5.

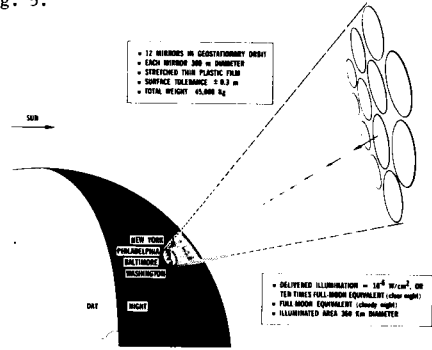


Figure 5. Night Illuminator

A number of large plane reflectors in synchronous orbit would reflect a 360-km diameter image of the Sun onto the Earth. The image brightness would depend on the area of the reflectors. The 12 mirrors, each about 300 m in diameter, would result in an energy density of about  $10^{-6} \text{ W/cm}^2$ , equivalent to a brightness of ten times full moonlight delivered on a cloudless night. That is about the same level as the night illumination standards in residential areas between light poles. The presence of cloud cover would probably not reduce the brightness much below that equivalent to full moonlight, since clouds scatter more than absorb light. The large area covered would be evenly illuminated, and the level of light could be modulated or programmed to match the need. This type of space reflector also could provide emergency illumination to disaster and blackout areas.

The mirrors could be very coarse by optical standards, with surface tolerance of one part in 1000, since the beam spread could be as much as 0.1 deg. The satellite cluster, each member of which would be a three-axis stabilized tensioned sheet of aluminized mylar film, would weigh about 45,000 kg. That would require the Shuttle, a large tug, and/or a solar-electric stage for transportation and deployment in final orbit.

The size of reflector involved probably requires an orbital demonstration, even though no great technological risk is anticipated. Although a Westinghouse study<sup>2</sup> indicates that the use of reflected light from space might save energy and reduce service and maintenance cost for street illumination, it would also raise a number of environmental and societal questions. Great increases in the size of the reflectors could provide greatly increased energy density on the ground -- and might be large enough to increase crop productivity in some marginal yield regions.<sup>3</sup>

### III. Far-Term Concepts (1990-2000+)

#### Nuclear Waste Disposal

Nuclear power plants produce undesired radioactive nuclides in addition to the desired generation of electrical energy. Approximately one ton of fission products and one-sixth ton of actinides result from the operation of a 1000-MW electrical power station for one year. Although in 1970 only 2 percent of the electrical power of the United States was produced by nuclear plants, and only  $0.3 \times 10^{12}$  W electric capacity existed, by the year 2000, the projected capacity will be five times as great, fully one-half of it being nuclear. The management of the radioactive wastes produced by the power reactors will be a problem, growing in magnitude from the present handling of 5 tons per year of radio nuclides to an estimated 4500 tons per year at the end of this century. Moreover, other countries as well as the USA plan to expand their reactor capacity rapidly. Since contamination from radio-nuclides would not necessarily be confined within national boundaries, control of reactor wastes is a worldwide necessity.

At present, high level radioactive wastes are stored in liquid form in large tanks and in solid form, encapsulated, and then protected in concrete blocks. Serious proposals have been made to store concentrated wastes in insoluble ceramics or glasses in deep mines, in which the high level wastes would be isolated and kept in recoverable form, and the lower level wastes diluted and dispersed in non-recoverable form. There have also been suggestions for non-recoverable disposal of the high level wastes in salt domes or in cavities in silicate rock formations. Since in both cases the radioactive heat released would result in a fused mixture of waste products and substrate, questions have been raised about the stability of the formations over geological periods.

To permanently preclude contamination on earth, studies performed by NASA<sup>5</sup>, Batelle<sup>6</sup>, and suggestions by others<sup>7</sup> have treated the disposal of reactor wastes in space. In the simplest form of this concept, illustrated in Fig. 6, the concentrated reactor wastes from fuel element reprocessing plants would be placed aboard a large rocket and sent into an earth escape solar orbit, solar system escape orbit, or even into a solar capture orbit. Because of the high cost of space operations, it would not be wise to put the entire burden of reactor waste management on a space system, but rather to use space disposal methods as a complement to earth control methods. Therefore, the waste radio-isotopes would be separated into three fractions, the first fraction consisting of those isotopes which decay into stable nuclides on a short enough time scale that, when stored on earth for a few years they would reach a harmless level of activity. The second fraction would consist of those radio-isotopes of such long half life and low energy release that they could be safely placed in salt domes, cavities, or mines without disturbing the geological equilibrium of the formation. Only the remaining fraction with nuclides of intermediary half life, 1 to 100 years, plus some special long lived isotope (in all about 20 percent of the mass of fissile material used up) would then be disposed of in space.

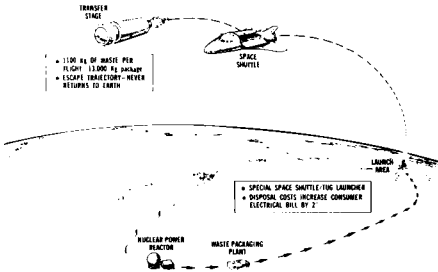


Figure 6. Nuclear Waste Disposal

Space disposal of the reactor wastes would require a continual schedule of launches. The reusable Space Shuttle with modification for unmanned operation would boost the waste package into low earth orbit. Then an upper stage would carry the package plus auxiliary equipment for hazard control to earth or solar system escape velocity. Orbit for solar capture would not be necessary. The total weight of a loaded escape stage is estimated at 30 metric tons of which about 1 metric ton would be radio-nuclides. The packages could be designed with the radioactive oxides incorporated into copper matrix, surrounded by copper radiation shields. They would thus have good thermal conductivity for cooling during transit and boost.

Of many hazards in the operation, the most severe would be fires or explosions on the launch pad, and unplanned reentry. Design requirements on the waste packages would have to ensure their survival without breakup. Recovery after reentry of the packages, whether on land or in water, could be aided by the use of thermal detectors for location, since the packages would be intense sources of heat. Recovery in space by rescue spacecraft would also be feasible. Reliability in operation would have to be achieved by a very careful stepwise engineering development program with extensive test experience obtained with inert or short-lived simulated waste packages, since breakup of even a single package would have disastrous effects.

The concept illustrated disposes of 1.1 metric tons of waste per flight at a cost of about 430 million dollars, equivalent to about 0.3 to 0.6 mills/kW-hr of nuclear power plant-produced electricity. This represents an increase of only about 2 percent of the average consumer's electricity bill. Of the 500 tons of wastes per year expected to be produced by the year 2000, only about 16 percent would be disposed in space, requiring some 80 flights/year. This launch rate could readily be supported by the required date.

This concept for permanent disposal of the most troublesome radioisotopes resulting from fission reactor power plants could significantly reduce some of the fears associated with reactors for power production.

### Energy Generation/Delivery

Large space systems can be utilized for the generation and delivery of energy to the surface of the earth. Among the concepts treated comprehensively by other authors in this session are concepts which employ photovoltaic solar cells to generate DC, with subsequent conversion into microwaves, the microwave beam being projected to the earth from synchronous altitude and intercepted by a rectenna; a concept which uses a concentrator of solar energy which supplies heat input to a Brayton cycle thermal converter, the electricity then being used to power the same kind of microwave generator as in the photovoltaic concept; and a third concept which uses a nuclear source to provide the heat with a Brayton cycle generator or a Magnetohydrodynamic generator for furnishing the electricity to the same kind of microwave generator. Extensive studies are currently being performed by NASA on the advantages and disadvantages of each, and their ability to compete economically with ground-based thermal, solar, nuclear, or hydroelectric power generation systems.

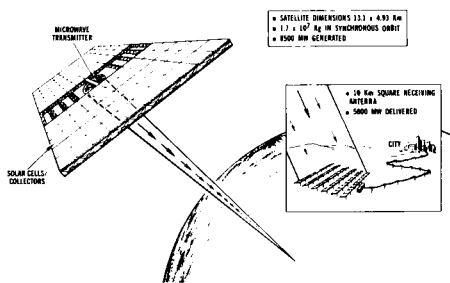


Figure 7. Solar Power Delivery Satellite

A brief overview is presented of the large solar voltaic space power station concept originated by Glaser et al.,<sup>8</sup> illustrated in Fig. 7. A solar cell complex measuring about 13 x 5 km would power microwave generators operating in the 3-GHz band assembled into a 1-km diameter phased array antenna. The antenna would be gimbaled so that the solar array and the antenna can be simultaneously pointed toward the sun and earth respectively as the satellite orbits in geostationary orbit. The microwave beam would be intercepted, detected, and rectified by an antenna structure on the ground approximately 10 km across. The system would deliver 5000 MW. Weight estimates currently range from 17 to 90 million kg. Estimates for the R&D cost average about 50 billion dollars. With operating costs in the 1000-1500 dollars per kilowatt delivered, the R&D would be amortized with 100 to 150 satellites on-line -- a truly impressive undertaking since the satellites would be fabricated and assembled in orbit.

The peak energy density in the center of the microwave beam would be about 20 mW/cm<sup>2</sup>, which could pose a small but finite hazard to populated areas in the event of failure of the

beam-pointing technique. In any form such concepts entail a long-term undertaking of very large proportions and unprecedented engineering difficulties. For the above reasons it must be considered high risk, but of very high potential value.

Such projects could well be the vanguard of industrial use of space and in order to be feasible, would require the development and operation of larger boosters than the Space Shuttle, large orbit-transfer stage, and assembly and maintenance bases in orbit.

### Energy Distribution

Space is an ideal medium for the distribution of electrical energy utilizing beam power transmission since space allows the propagation of the energy with no attenuation, and allows the construction of large transmission and/or reception terminals, forming beams of very small angular subtense such that energy may be received at long ranges with high efficiency. Two major options for power distribution using microwaves will be addressed, followed by options which utilize laser beams.

### Microwave Point-to-Point Power Transmission

The first concept described is one in which orbiting reflectors are utilized as a means of point-to-point microwave energy transmission. Systems of this type have been described in the literature primarily by Dr. Krafft Ehricke.<sup>9</sup> These concepts, as illustrated in Fig. 8, involve the transmission of large amounts of electrical power in trunking circuits which could enable transcontinental power transmission of receivers on the dark side of the earth to be powered from transmitters on the sunlit side. In this concept, DC power is converted to microwave energy and radiated to space utilizing a phased array transmitter and antenna-feed assembly very similar to that discussed under energy delivery for the solar-power space station with microwave transmission. The 8 GW microwave beam so generated would be reflected from an essentially passive planar structure in geostationary orbit, and received in a dipole/diode array "rectenna" also very similar in concept (if not identical to) that envisioned for solar-power transmission.

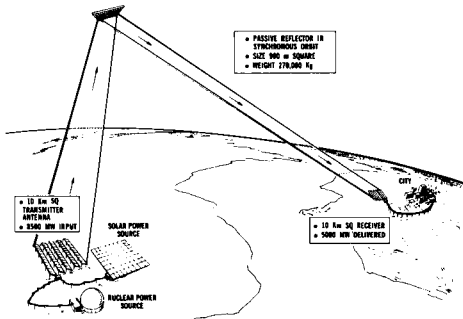


Figure 8. Power Relay Satellite

The reflecting satellite must of necessity maintain flatness over the reflecting surface to

about 1/20 of a wavelength to assure a coherent wavefront. A simple reflecting structure such as a mesh can be used, and the bulk of the orbital weight arises from the structural and mechanical systems required to assure surface flatness. An electrical equivalent for controlling the phase-front without requiring a single large structure or high mechanical surface tolerances has been suggested by the author.<sup>10</sup> A reflector of 1000-m diameter in synchronous-equatorial orbit is required in order to collimate a beam over double synchronous ranges to a beam divergence such that a rectenna diameter of approximately 10 km across captures most of the energy (beam divergence of  $10^{-4}$  rad).

Systems of this type are characterized by their energy transfer between only two points on the earth, and one reflector must be used for each source-sink pair. In order to maximize the utilization of the reflectors, very large amounts of energy must be transferred over each circuit. Dr. Ehrcke points out that the economic cross-over point between use of surface transmission lines and the power relay satellite depends on the basis used for comparison, with cross-over points varying between 1000 km to over 5000 km.<sup>3</sup> Thus, the power relay satellite will probably be most useful for very long range or transoceanic power transmission.

#### Microwave Network Power Distribution

An ideal power distribution technique would allow highly flexible inter-connection of a number of power sources with a very large number of substation-sized user distribution points, would have low losses not dependent on path length in the links, would use the same design equipment for all the links, and would minimize land area required and environmental impacts. A system concept for microwave energy distribution utilizing phased-array reflectors in space has been conceived which may approach some of the above goals.

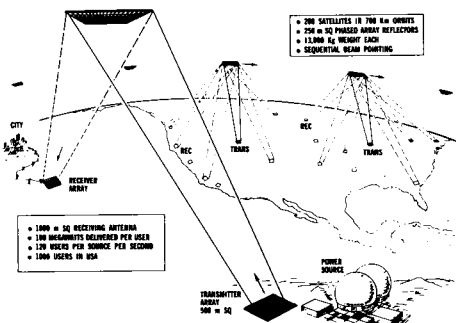


Figure 9. Energy Distribution

In this concept, illustrated in Fig. 9, a large number of phase-controlled reflectors would be placed in low orbit, each satellite reflecting microwave energy transmitted from one source to 120 user areas in rapid sequence, with the connectivity flexibly changed by program. The angle of reflection (in two dimensions) of the

microwave phased-array reflectors would be controlled and varied to point the beam at the user rectennas in rapid sequence. The rapidly pulsating power would be filtered by synchronous or passive techniques at each substation. Changing the relative duration of the illumination cycle to the user antennas would allow highly flexible power-programming, obtaining flexibility of power interconnection approaching that of radio communications. Power could be supplied to growing or new communities within the USA from resource-rich areas in remote regions. The same satellites, being in low orbit, could also be used by other nations for their domestic power distribution without affecting USA distribution. Developing nations could thus depend mostly or entirely on space relay for power, and bypass building the transmission line networks currently used worldwide by industrialized nations for lack of choice.

The concept illustrated is sized to deliver an average of 100 MW to each of 1000 user areas in the USA from eight sources in the USA, each transmitting 12 GW of power. Two hundred satellites would be needed so that an average of eight satellites would be seen over the USA at any one time, each satellite supplying power to 120 user areas. Proportionate numbers of sources and users could be interconnected in other nations around the globe simultaneously by utilizing the satellites not over the USA (which number 192 out of the 200).

The power supplied to any one user from a relay satellite would consist of power pulses of 12-GW peak, lasting about 0.13 msec, and repeated 60 times/sec. The average power would thus be 100 MW, and the pulses would occur with the correct periodicity to supply 60-Hz networks by use of a proper synchronous or static filter.

The power generated by each station and reflected by each satellite would consist of interrupted continuous-wave microwave power, with 7200 pulses of 12 GW each occurring each second. A power interruption interval of  $0.8 \times 10^{-6}$  sec would allow the delay shifters in the satellite phased-array reflector to be set to the values corresponding to the proper reflection angle for the next user, allow for only properly formed beams to be reflected, and yet would result in less than 1 percent energy loss.

Use of antenna sizes of 500 m for the source transmitter, 250 m for the satellite reflectors, and 1150 m for the user receiving array, and orbital altitudes of 700 km would allow the system to function with distances between source and user of 2000 km maximum, utilize low attenuation transmissions at 3 GHz, and yet allow fast enough beam steering and switching such that the 120 users could be supplied sequentially each second.

The average power density at the center of the ground rectennas would be less than  $7.6 \text{ mW/cm}^2$ . The provision of an exclusion area fence of three beam diameters total (3.5 km) would ensure that CW or transient radiation densities outside the fence would be less than  $0.8 \text{ mW/cm}^2$  average, which is probably a safe exposure level. Radio interference could be all but eliminated by a metallic fence 30 m high surrounding each

transmitter antenna at a distance of 100 to 200 m from its periphery.

Beam pointing would be accomplished by a combination of preprogrammed steering and retrodirection of coherent but spectrally distant pilot signals originating in the user receiving antennas. Override sensors surrounding the rectenna would command turnoff of the beam in case of failure of the retrodirection equipment.

The satellites for such a system would consist of  $250 \times 250$  m phased array antennas, passive except for the phase or time-delay control mechanisms and the attitude control devices. The satellites would probably weigh about 15,000 kg each and require orbital assembly and servicing. They could be constructed as conventional trusses, holding the reflection array components flat for phase coherence, or use individually stationkept antenna subelements and phase control of the assembly for coherent phase-front generation, a technique suggested by the author.<sup>10</sup> The arrays would consist of horns connected to terminations through commandable phase-delay or time-delay units, the latter being preferred as the antenna bandwidth would be thus maximized.

The Space Shuttle and specialized orbital support equipment for assembly, initialization, servicing, and reconfiguration in orbit would suffice for the space portion of this concept. About 130 launches would be required to establish an active constellation of 200 satellites in low orbit at various low orbit inclinations.

The magnitude of the undertaking, and the small but finite hazards associated with failure of the beam-pointing devices, dictates that this be considered a high-risk and far-term concept though of high potential value. Ultimately, in the very far future, the power could be generated in space and delivered to the users directly, utilizing fewer but larger phase-controlled antennas at higher altitude.

#### Laser-Powered Aircraft

Power transmission through space utilizing laser beams can utilize structures smaller than microwave structures by four to five orders of magnitude. Laser power transmission through space could be used for supplying energy to satellites by impinging on their solar cells, at a much higher flux density than possible by capture of sunlight. Smaller size arrays would thus be possible resulting in economies in weight and cost of the satellites. Laser transmission of power could also be utilized for supplying the energy required for expulsion of propulsive "fuel" mass, and thus utilized for reducing the mass required for propulsion of rockets. The laser energy could be supplied by surface lasers of very large size, and time-shared to serve many boosters and space vehicles. This concept, of course, has been advanced by Dr. Kantrowitz of AVCO.<sup>11</sup> Although the potential gains are significant, since the Isp of the propulsion system could be large, the vehicle still would have to provide its own mass for reaction.

Another speculative concept in this class is very tentatively offered as one of many alternatives to provide propulsive energy for large

commercial jet aircraft, which currently require about 10 percent of all the petroleum used for transportation in the USA. This concept, illustrated in Fig. 10, is intended to avoid the need for carrying fuel aboard large aircraft.<sup>10</sup> It envisions the use of laser beams generated on the ground and reflected by space mirrors to aircraft in flight. The energy would be collected by an optical collector on the upper surface of the aircraft and focused into the heating chambers of "jet" engines. The laser-beam energy, rather than combustion of hydrocarbon fuel, would heat the inlet air. The aircraft would carry some jet fuel for operation under thick cloud cover, typically in some takeoff and landing situations.

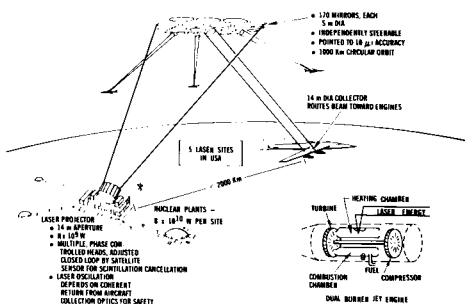


Figure 10. Aircraft Laser Beam Powering

The concept requires a number of ground laser stations, both for geometrical coverage and to assure cloud-free paths to the complexes of low-orbit space mirrors for a large fraction of the time. Alternatively, space-based laser stations could be used. In principle, most of the current aircraft fuel load could be replaced by payload and, also in principle, the aircraft could fly an arbitrarily long time and have global range.

The energy required by a large commercial subsonic transport is the fuel-equivalent of 10 to 50 MW. Assuming a year-2000 fleet of 2000 such aircraft operation at about 1/3 duty cycle, the total power required is about  $4 \times 10^{10}$  W. To minimize the optical sizes involved, the space mirrors would be placed in low orbits, say 1000 km, and 100 to 200 clusters of mirrors placed in varying orbits. Hence an average of five clusters would be in view of the USA at any time illuminated by five laser stations located in geographically diverse locations. The required redundancy to assure continuous laser paths to the satellites in the face of adverse weather could require as many as 15 laser station installations, but only five power sources and five lasers would need be active at any one time.

Each cluster of space mirrors would contain 170 independently steered mirrors of 5-m diameter each, with the cluster being illuminated by one or a cluster of lasers at each laser station. The optical collecting aperture on the upper surface of aircraft would be 14 m in diameter, and allow operation at 2000-km range from the laser. The energy would be routed to the engines and focused into very small volumes inside heating chambers,

where the large energy density would cause air breakdown and almost total absorption in the air, heating it very rapidly, and expelling it at high velocity through the turbines for propulsion.

The power densities going through the atmosphere would be low enough to avoid breakdown. The power density at the satellite mirrors would be about  $300 \text{ W/cm}^2$ , a very tolerable number for highly reflective and cooled mirrors; and  $40 \text{ W/cm}^2$  at the aircraft collector. If focused into four 0.3-mm spots in the engines, the power density would be  $1.6 \times 10^{10} \text{ W/cm}^2$ , causing sure air breakdown and total absorption of the beam energy.

The beams would be pointed by a combination of mechanical and phase-front steering using mechanical mirror orientation responsive to signals from energy sensors placed around the aircraft optical collector, and coherent feedback into the laser oscillator itself using a retro-director on the aircraft collector. Thus, beam tracking of the aircraft collector could be essentially assured, since should the mechanical pointing system fail, the lack of beam feedback will make laser oscillations impossible.

Optimistic estimates place the overall energy efficiency (heat energy in the heating chamber to nuclear energy used to power the lasers) at about 10 percent. Therefore, the total energy required to power each laser station would be  $4 \times 10^{11} \text{ W}$ , a major fraction of the entire electrical needs of the USA today. However, preliminary calculations indicate that operating costs for the laser-powered aircraft (assuming nuclear power sources) would break-even with operating costs using jet fuel, should the cost of fuel reach \$0.50 per gallon, a likely occurrence in the near future. The investment cost in the lasers and sources, however, would be comparable to that already sunk in the power industry, or \$160 billion, based on cost of plants at \$1 per installed watt.

The space-mirror complex should be viewed as an energy common carrier, with the energy supplied either from the ground or from space, manipulated and directed in the desired patterns in space. The energy common carrier could thus be utilized to power large aircraft by all nations. The generation and transmission via laser beams of the huge quantities of energy assumed in this concept greatly outstrips the capabilities of today's technology. In principle, however, the laser techniques required are known.

The large and complex satellites would probably require assembly, initialization, and servicing, and space transportation systems of greater payload weight and volume capacity than the Space Shuttle and Tug. The concept involves high risk because of the potential burn danger on the ground should the laser beam wander off the aircraft collector as a result of cumulative failures or deliberate misuse; as well as due to the very advanced technology required for all elements of the system.

Even allowing projections of today's technology, other methods of saving petroleum fuel or

developing substitutes could well be preferable to this concept. Having ample nuclear energy, the USA could synthesize jet fuel from coal and water at better energy efficiency than in this laser initiative. Nevertheless, "far out" ideas such as this one merit continuing examination.

#### IV. Conclusions

Space systems can offer unique advantages to the support of earth-bound energy activities, as well as generate, delivery, and distribute energy in a large scale. Many of the concepts presented in this paper require very similar space transportation and orbital support facilities, including low-earth orbit boosters, orbit transfer stages, orbital assembly and maintenance yards and depots, and test devices. The industrial and commercial use of space on an increasing scale can bring some of these advantages to bear, and the option to construct and operate these and other satellite concepts needs to be protected by ensuring the availability of such orbital support and transportation devices, since they will probably be needed regardless of the exact form and makeup of the future space program.

It must be stated in reminder that none of the space concepts presented in this paper are advocated by the author, The Aerospace Corporation, or by NASA, but rather are advanced so that economic benefit studies and detailed system definition can proceed to evaluate them against the alternatives, be they terrestrial or space-based. The only points truly advocated in this article are that space has the potential to benefit energy-related activities; and that even though satellites will have to become larger, more complex, and more highly competent than today's satellites in order to provide the required services, that the benefits may make such increases not only desirable but mandatory.

#### V. References

1. Projected Plutonium Recycle Industry, Draft GESMO, Vol 2, Ch 3; WASH-1327, August 1974.
2. A. C. Buckingham and H. M. Watson, The Uses of Orbiting Reflectors, Westinghouse Electric Corporation, AIAA 4th Meeting, October 1967.
3. Krafft A. Ehricke, Space Industrial Productivity - New Options for the Future, Presentation Record to the Committee on Science and Technology, Hearings on Future Space Programs, July 1975.
4. Siting of Fuel Reprocessing Plants and Waste Management Facilities, Oak Ridge National Laboratory Report ORNL-4451, July 1971.
5. Space Systems for the 1980's, Vol. VI: Nuclear Waste Disposal, The Aerospace Corporation, ATR-72(7259-01)-1, September 1971.
6. High Level Radioactive Waste Management Alternatives, Batelle Memorial Institute, BNML-1900, May 1974.
7. Renee Miller, Thinking Hypersonic, Astrodynamics and Aeronautics, August, 1971.
8. P. Glaser, et.al., Feasibility Study of a Satellite Solar Power Station, NTIS, U.S. Dept. of Commerce, February 1974.

9. Kraft A. Ehricke, The Power Relay Satellite, Rockwell International Report E-74-6-1, June 1974.
10. I. Bekey, H. Mayer, and M. Wolfe, Advanced Space System Concepts and Their Orbital Support Needs (1980-2000), The Aerospace Corporation, ATR-76(7365)-1, April 1975.
11. Kantrowitz, Propulsion to Orbit by Ground-Based Lasers, Astronautics and Aeronautics, May 1974.

# LONG DURATION BALLOON PLATFORM

A. Shipley and I. S. Smith

*National Scientific Balloon Facility\* Palestine, Texas*

## Abstract

With the development of large plastic balloons in the early 1950's the use of the balloon as a research tool has increased dramatically. "Zero-pressure" balloons, made of polyethylene materials, and using ballasting techniques to maintain level float have been capable of meeting most of the requirements until recent years. The demand for exposure periods of days, weeks, and months for many scientific experiments, however has prompted the development of large "super-pressure", globe circling, balloons capable of floating at a near constant altitude without ballasting. The work of the National Scientific Balloon Facility towards the development of a balloon vehicle that will accomplish the goal of sustaining a 250 Kg payload at 40 Km for 100 days is discussed.

## I. Introduction

With the advent of thin high quality plastic films in the 1950's, balloons have had an ever increasing roll as a means of lifting scientific payloads to near space altitudes. The balloon occupies a unique space between satellites and aircraft, offering a relatively cheap and efficient vehicle for conducting near space experiments. The balloon not only enables scientists to carry out research in such areas as infrared, x-ray, gamma-ray and ultra-violet astronomy, high energy physics, and atmospheric sciences, but the balloon also serves as a proof testing platform for future satellite packages. Although these are just a few balloon-borne experiments, the balloon has proven itself as an inexpensive, reliable, and stable platform for high altitude work.

The increased utilization of balloons has also increased the scientific requirements. This has required continuing advancements in vehicle development, telemetry, and telecommand capabilities to advance the state-of-the-art. The National Scientific Balloon Facility (NSBF) continually strives to achieve greater capabilities in such areas as payload size, float altitudes, and flight durations. The average payload size is 1000 Kg with payload sizes of up to 5000 Kg having been successfully flown, with requirements to fly 6,364 Kg to 24.5 Km. Float altitudes of approximately 45 Km and above are commonplace with a few flights achieving 49 Km and above. There are also requirements for light payloads at float altitudes of 55 Km. Of the three major areas of development, that of longer flight durations has had the highest priority in recent years. A major development program is currently being conducted at the NSBF under sponsor-

ship of the National Science Foundation (NSF). The goals of the program are to float a 250 Kg payload at 40 Km for periods of 60-100 days, with near-continuous data retrieval, and payload recovery at the completion of the flight.

## II. Long Duration Ballooning

### History

Surveys conducted by the NSBF of the scientific community have shown that nearly all balloon-borne scientific investigations could benefit from longer exposure at altitude. Cosmic dust collection, high energy and super heavy nuclei cosmic ray investigations, magnetospheric and gamma ray measurements all require long flights in order to obtain significant scientific information. In the past, the opportunities to observe rare cosmic phenomena from a balloon required considerable good fortune. Since present balloon systems allow an average time at float of only several hours, a great deal of information could be gained by extending the flight time. The polls taken of the scientific users revealed that a vehicle should be developed with the capability of supporting a 250 Kg payload at 40 Km for a minimum of 100 days duration.<sup>1</sup>

There are two basic techniques for extending the float duration of a balloon. One method is the use of the normally flown "natural shape" unpressurized balloon, or "zero-pressure balloon", utilizing its heavy lift capability to support a heavy ballast load. The "zero-pressure" balloon is vented to the atmosphere to valve off excess lifting gas to prevent over-pressurization of the balloon, thus requiring the dropping of ballast each night, (approximately 7% of the gross system's mass), to compensate for descent caused by the nighttime cooling of the gas. This type of balloon, which is currently being used for nearly all flights, has had extended float durations lasting 60-80 hours with one flight of over 120 hours. In the past two years, extended flight durations utilizing balloons of this type have been launched by the NSBF from Sicily, with recovery of the scientific payloads being made in the United States, as shown in Figure 1. Joint payloads of several countries (Great Britain, Italy, West Germany, France and the United States), weighing approximately 910 Kg achieved flight durations of over 100 hours, with float altitudes of approximately 40 Km, using automatic ballasting systems. This technique appears feasible for flights of 5-8 days but becomes unfeasible, due to large ballast requirements, for flights longer than this.

\* The National Scientific Balloon Facility is operated by the University Corporation for Atmospheric Research under sponsorship of the National Science Foundation.

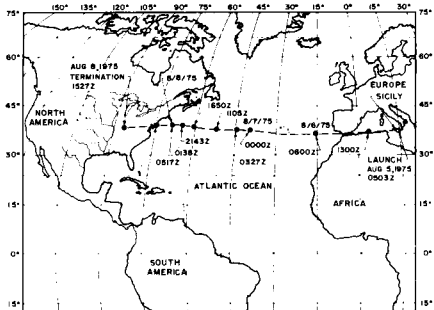


Figure 1. Typical Trajectory of a Trans-Atlantic Balloon Flight

The second method of achieving increased flight duration is to fly a pressurized balloon capable of withstanding high skin stresses caused by over-pressurization from warm daytime temperatures. The balloon must also maintain a slight nighttime overpressure during the much colder nighttime temperatures. This type of balloon is called a super-pressure balloon and floats at a constant density altitude. Over a thousand balloons of this type have been flown with some having flight durations of over 700 days. The large majority of these, however, were only a few meters in diameter. In January, 1973, from Toowoomba, Australia, a 68 Kg scientific experiment was launched by the NSBF. The 19.5 M diameter balloon floated at an altitude of 24 Km for 36 days. During its time at float, the balloon "orbited" the globe twice as illustrated in Figure 2, remaining between 22°S and 30°S latitude, with recovery of the scientific payload within 14 Km of the launch site after termination by radio command. The highly successful nature of this flight drew world-wide scientific interest and proved the feasibility of long duration scientific balloon flights.

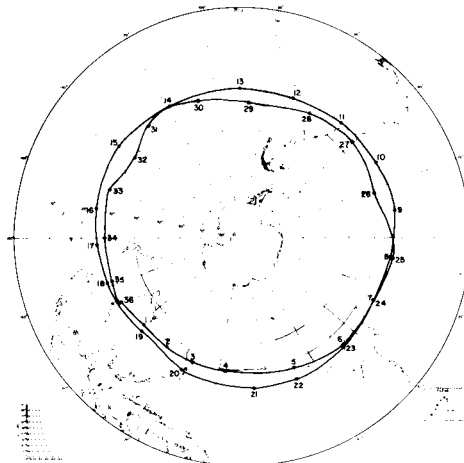


Figure 2. Flight Trajectory of Superpressure Flight 81-N.

#### Balloon Vehicle Design

A superpressure balloon can be defined as a closed cell vehicle which maintains a positive internal pressure throughout its lifetime at float. By proper selection of materials, the balloon very nearly becomes a constant volume process thus enabling the balloon and its payload to float at a constant density altitude. This contrasts significantly with the commonly used open cell polyethylene "zero-pressure" balloon. As the "zero-pressure" balloon vents its excess lifting gas at altitude, it changes volume thereby changing altitude when subjected to internal gas temperature changes. This reduction in volume can only be compensated for by dropping ballast to attain altitude. Internal gas temperatures of both balloons are controlled by the radiation input experienced by the balloon during its flight. This radiation input varies with changing cloud deck conditions, changing ground conditions, changing of the balloon film's radiometric properties due to ultra-violet (UV) degradation, and, of course, sunrise and sunset effects. In balloon design, all of these must be considered in the design so that the balloon is capable of surviving during its life at float.

There are several basic areas of studies which must be taken into account in designing a super-pressure long duration platform. Balloon shape, launch methods, manufacturing techniques, reliability/cost relationships, accessory designs, and material selection all play very important rolls in determining a balloon design. Materials selection, however, is the single most important factor that influences the balloon design process. Important factors influencing the materials selection are UV degradation, pinholing, toughness, radiometric properties, critical flaw and crack propagation, fabrication properties, and strength/weight/cost relationships. All of these factors influence the ultimate balloon size and weight requirements thus ultimately the overall cost as shown in Figure 3.

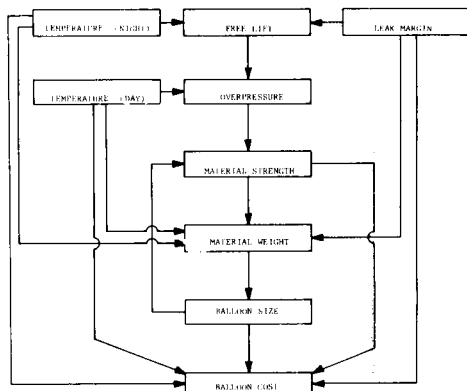


Figure 3. Balloon Design Relationships for a Long Duration Platform.

The optimum balloon configuration would have equal stresses in both of the principal directions over the entire surface. It would also have no stress concentrations such as payload attachment

fittings, inflation ducts, and seals. In other words, a very large soap bubble would be an optimum balloon design. However, man does not presently have the capability to blow a flawless 76 meter diameter bubble made of some strong, but thin, plastic film. Even if he did have this capability a problem still arises in that the payload must be attached in some manner to this bubble, and there must be provision made for putting inflation gas inside. This then defines several problem areas in the design and fabrication of a balloon.

Load introduction at the base introduces additional meridional stresses with nearly no circumferential stress in the extreme lower portion of the balloon. This additional meridional stress must be compensated for by increasing the meridional material strength. The balloon shape must also be designed so that a smooth transition occurs from the unbalanced loading near the base to balanced loading in the upper region of the balloon.

Stress concentrations such as inflation ports, fittings, tapes and manufacturing tolerances must also be taken into consideration during the design process. Proper reinforcements must be made so that no large stress concentrations develop around intentional cutouts in the balloon envelope or other existing discontinuities. Areas such as the end cap regions located at the top and base of the balloon must be carefully reinforced. Due to the balloon being fabricated from flat sheets of material and sealed together with special adhesive tapes, a large material build up would occur at the zenith and nadir of the balloon. Therefore to prevent large stress concentrations the tapes must be terminated at some distance short of the zenith and nadir, forming a large circular hole. A large circular piece of material is then sealed to the tapes thus forming a cap. All this requires meticulous care and observance of very close tolerances.

Both shape and materials therefore influence the manufacturing techniques required. Super-pressure balloon manufacturing technology has advanced steadily during the last decade to a point where smaller spheres (2-23 meter diameter) can be constructed on an extremely reliable basis. In developing a Long Duration Platform, full use of existing technology along with development of new technology, is being made to extend it to the fabrication of large diameter (61-92 M) balloons required to achieve the design goals.

#### Balloon Materials

There are two basic requirements that a candidate balloon material must meet in order to reach the required long duration goals. The material must have sufficient strength to withstand the large stresses developed in the balloon skin during the daytime heating of the gas. Secondly, the material stiffness should be such that little volume change occurs from daytime to nighttime, thus giving good altitude stability. In both cases, it is mandatory that the material not lose its structural integrity.

The first requirement specifies certain functional material properties that must be defined in the early stages of the material design and selection. The governing property is the equation for

the balloon skin stress which is given by the expression:

$$S = \frac{P R}{2} [F + (1+F) \frac{T_g - T_a}{T_a}] \quad (1)$$

where  $S$  is the strength in force/unit length,  $R$ , is the balloon radius,  $P$  the ambient pressure,  $F$  the free lift or excess lifting gas, and  $\frac{T_g - T_a}{T_a}$  is the

ratio of internal gas temperature to ambient temperature (super-temperature). For a given material; each parameter is interrelated. The strength to weight ratio governs the balloon size therefore balloon radius such that for a given payload and altitude, the higher strength to weight material will result in a smaller radius. The ratio term  $\frac{T_g - T_a}{T_a}$  is governed by the radiometric properties

of the material. The day and night gas temperatures,  $T_d$  and  $T_n$ , are determined by the effective  $\sigma_{\text{solar}}$  and  $\epsilon_{\text{IR}}$  values of the material. For a clear film, the effective  $\sigma$  and  $\epsilon$  values are calculated assuming the interior surface of the balloon emits and reflects diffusely, changing measured values.<sup>3</sup> Black ball temperatures along with albedo also significantly influence day and night temperatures as shown in Figure 4 which shows the internal nighttime gas temperatures for two identical balloons, one which overflew severe thunderstorm activity while the other was over clear skies. Thus, using nominal values for these inputs, average day and night gas temperatures can be calculated for various  $\sigma$  and  $\epsilon$  values of materials. By using the "worst possible case" values for these terms, the maximum daytime and minimum nighttime super-pressures can be obtained. These values then determine the amount of free lift,  $F$ , that is required. Not only does the material have to withstand these requirements but it must also have good critical flaw/crack propagation characteristics, good UV degradation resistance, and withstand the severe folding, creasing, and snapping of the material at launch and ascent to altitude.

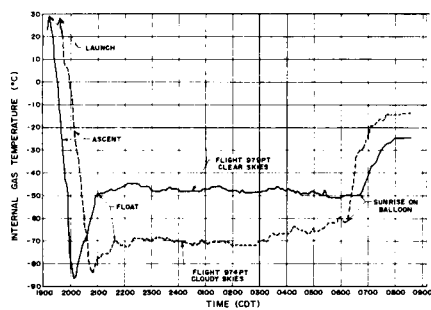


Figure 4. Comparison of Internal Gas Temperatures for Varying Radiation Inputs

The second requirement defines certain properties which must also be met by the material. Since the balloon is to have little day to night altitude excursion, this then specifies the material stiffness. For short term altitude excursions

(day to night), the elastic modulus ( $E_e t$ ) governs the magnitude which is found from:

$$E_e t \geq 75 P_a R (1 + F) (T_d - T_n) / \Delta Z^4 \quad (2)$$

where  $\Delta Z$  is the allowable altitude change, and  $T_d - T_n$  is the gas temperature change from day to night. Another term that causes long term variations (visco-elastic growth) is governed by the creep apparent modulus ( $\Delta E_c t$ ) by the following equation:

$$\Delta E_c t \leq 38 P_a R [(1+F) (T_d + T_n) - 2T_a] / \Delta Z^4 \quad (3)$$

Thus initial conditions can be defined for a material by defining these terms and then generating families of curves based on changing  $R$ ,  $T_d$ , and  $T_n$ .

Based on the two basic requirements, and the implications with each, several materials and materials combinations have been and are presently being tested and developed for possible use in long duration superpressure platform development. These materials are all laminations of polyethylene, nylon, and polyester films along with scrim materials of both Dacron and Kevlar yarn. Each materials combination defines a balloon size as illustrated in Figure 5.

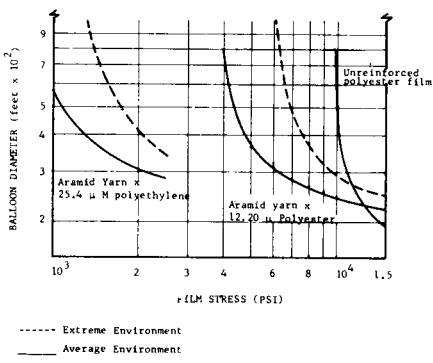


Figure 5. Balloon Size Comparison for Various Materials

There are basically two film combinations presently being pursued actively with others also being investigated. One material is a basic lamination of polyester to polyester with a thick layer of "soft" adhesive which gives the bi-laminated film better handling and pinholing characteristics than unlaminated film. The second type of material is a much thinner polyester lamination with a Kevlar yarn bonded to the film resulting in a lightweight high strength composite. This film, as illustrated in Figure 6, reduces the stresses in the film with the Kevlar yarns taking most of the load while the polyester film serves chiefly as a gas barrier. The low film stresses also give the composite film better flaw/crack propagation properties. It is presently felt that

crack growth and propagation is a very important design factor when selecting a balloon material for superpressure work. The critical crack length and stress is given by the following equation:

$$A_{cr} = \frac{1}{\pi} \left( \frac{K_{IC}}{\sigma_{cr}} \right)^2 - \frac{1}{2\pi} \left( \frac{K_{IC}}{\sigma_{ys}} \right)^2 \quad (4)$$

where  $A_{cr}$  is the critical crack length,  $K_{IC}$  is the fracture toughness,  $\sigma_{cr}$  is the critical stress, and  $\sigma_{ys}$  is the yield strength of the material.

Thus, by experimentally determining the fracture toughness ( $K_{IC}$ ), it is then possible to determine the size crack or magnitude of stress that will cause catastrophic crack propagation. For large balloons with surface areas of tens of thousands of square meters of material, the chances of a flawless balloon are extremely small. Thus, a material possessing good fracture toughness characteristics becomes mandatory. Recent test flights of large unreinforced polyester super-pressure balloons have shown that crack propagation may have been the primary cause for failure of at least two flights.

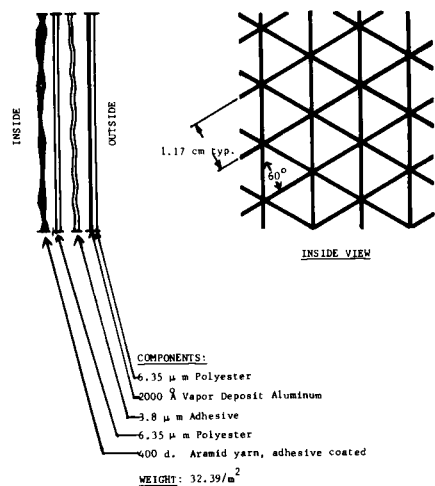


Figure 6. Selected Long Duration Platform Base-line Material

### III. Test Flights

During the past 4 years since the successful test flight of the superpressure balloon out of Australia, several larger unreinforced polyester balloons have been launched. During the fall of 1972 a 33.5 M diameter successfully supported a 68 Kg payload at 30.5 Km. During 1973, 1974, and 1975, one balloon was flown each spring turnaround in an attempt to support 150 Kg at 36.6 Km. Although not totally successful, due to accessory design problems, much was learned as to the probable cause of failure. Using the results obtained from the flights, a new type of adhesive was used to laminate the film and a new load attachment patch

design was used. The next balloon which was 38.9 M in diameter, was launched in the fall of 1975 and successfully supported 205 Kg at 30 Km. In May 1976, a 55 M diameter sphere was launched and successfully achieved a float altitude of 33 Km with a suspended load of 273 Kg. However, after several hours at float, further pressurization of the balloon resulted in a catastrophic balloon failure. The reason for failure appeared to be an inadequate seal at the inflation port. Each of the last three flights have been heavily instrumented with 122 - 168 channels of information being continuously transmitted to the computerized ground station. The measured parameters contained gas, film, and ambient air temperatures, skin strain, and forces in the load attachment that were being introduced into the balloon wall. This type and magnitude of data has never been previously acquired and has resulted in valuable knowledge of balloon dynamics.

#### IV. Future Plans

Future plans call for continuing with a series of intermediate size test flights, similarly instrumented, of both unreinforced polyester and polyester-Kevlar composites. These flights, starting with one in October 1976, will be to test the ultimate manufactured strength of the balloon. Information obtained from these flights will then be incorporated into larger balloon designs, and flights possibly from Sicily to the United States

during the summer of 1977. It is planned that the newly developed balloon vehicle will become an available vehicle for use by the scientific community by early 1978. One flight is being planned for launch out of Australia beginning in the winter of 1977.

#### References

1. Pavey, Michael S. and J. Snider; "Technical Proposal for Long Duration Platform Development" National Scientific Balloon Facility, Palestine, Texas, Revised 1974.
2. Pavey, Michael S., "Long Duration Scientific Ballooning Platform Development," AIAA Paper 75-1391, 1975.
3. Kreith, F. and J. F. Kreider; "Numerical Prediction of High Altitude Balloons," National Center for Atmospheric Research, Boulder, Colo., TN/STR-65, Revised, 1974.
4. Munson, J. B.; "Preliminary Design Report for the Long Duration Platform (LDP) Balloon," Sheldahl, Inc., Northfield, Minn. SER 0204, 1975.
5. Aerospace and Civil Engineering Departments; "Materials Science Notes and Laboratory Manual," Texas A & M University, College Station, Texas, Second Edition, 1972.

This material is based upon research supported by the National Science Foundation under Contract No. NSF-C760.

# SOME ASPECTS OF MULTIMISSION SPACECRAFT CARRIER MODERNIZATION

V. N. Novikov and D. N. Tscheverov

*Intercosmos Council, Moscow, USSR*

The wide use of space vehicles (SV) for the aims of science and national economy timely sets the task of making the multimission missile-carriers (M-C) for launching several types of SV. The question is also to fix the dates of M-C substitute and modernization using unified blocks and standard assembly units, because these are the actions which reduce considerably the costs on specific space missions and further the development and tests and increase the launch reliability.

The structure of a space system providing carrier's role is shown in Fig. 1. Since the composition of carriers specifies the technical capabilities of the space system as a whole, the task of choosing the M-C composition, dates of commissioning, change and modernization, requires dynamics analysis of the combined forming four upper-level subsystems.

- 2-Reentry module (RM)
- 3-Power plant (PP)
- 4-Reentry vehicle (RV)
- 5-Scientific instrumentation (SI)
- 6-Scientific equipment (SE)
- 7-Support system complex (SSC)

Fig. 1. Space system structure and communications.

As well as the process of system forming (see Fig. 2), the problem of putting into operation, substitution, unification and standardization has a solution of some dynamic iterative character. The primary decision as to the time of putting into operation and possible change, and the unification of blocks as well, is substantiated when forming technical requirements. In the light of technical proposals considered are the questions of modernization depth, block unification and unit standardization. After performing the project there appear specific offers on the change dates and modernization depth. Thus, the decision-making on the commission dates, change by a modernized or a new carrier, unification level and standardization appears to be a single process of carrier development at different stages of project elaboration, when the rate of information about an object is continuously increasing and the detailing of models up to the full-scale objects is growing.

The task of changing and modernizing the M-C of an ordinary space system (OSS), solved when forming technical requirements, is organically connected with planning and organization of works over the whole space system. While studying this task it is natural to be guided by a best decision which can be taken with regard to development of science and engineering. Such a decision provides that objects of the above-mentioned four levels have optimal meanings of the quantities control parameters  $\pi_{jik}$ , which are considered as independent variables.

The problems of planning the OSS development, including the questions of commission, substitution and unification, can be defined as follows: it is necessary to establish such a combination of control parameters when the effectiveness of the whole space system in the time interval is maximum:

$$W_{SC} = \max_{\pi_y} W_{jik} [\pi_{SV}, \pi_{MC}, \pi_{SC}, \pi_{TE}, \pi_{SI}, \pi_{GIC}, n, G^*, T^*, t_{ji}, m_j, m_{jik}, P_{jik}, W(\pi_w), C_{\Sigma}] \quad (1)$$

where  $\pi_{SV}$ ,  $\pi_{MC}$ ,  $\pi_{SC}$ —vectors of control parameters of the space vehicle, the carrier and the spacecraft;  $\pi_{TE}$ ,  $\pi_{SI}$  and  $\pi_{GIC}$ —vectors of parameters of the

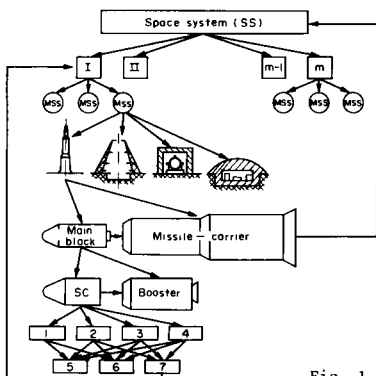


Fig. 1.

## I—subsystem

Ordinary space system (OSS), consisting of missile space system (MSS) with different spacecraft (C) and missile-carrier (MC)

## II—subsystem

Space missile complex (SMC), spacecraft (SC), launching installations (LI), technological equipment (TE), ground instrumentation control centre (GIC)

## III—subsystem

Space vehicle (SV), main block (MB) and missile-carrier (MC)

## IV—subsystem

Main block of spacecraft (MB), spacecraft (SC) and booster (B)

## V—subsystem

Blocks of spacecraft:

1-Trajectory device (TD)

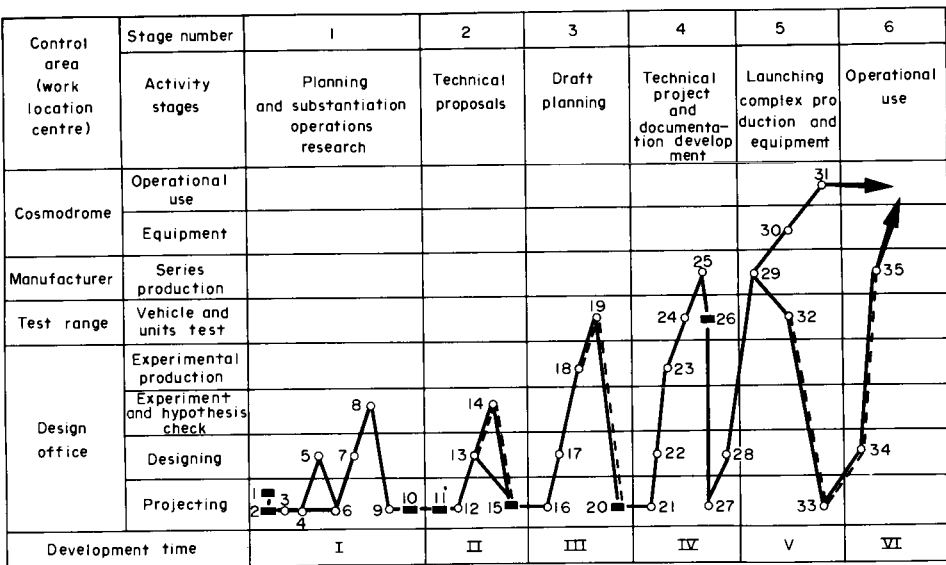


Fig. 2. The main control stages and areas in spacecraft creation process 0—focal points of substantiation, ■—decision making.

technological equipment, the start area installations and the flight control and information transmission;  $W(\Pi_0)$ —vector of parameters, which specify the mission of ordinary space systems;  $n$ —number of ordinary space systems (systems with identical carrier);  $G_{ij}$ —useful load, launched into the basic orbit of carriers of  $j$ -type;  $T_j$ —time, determined for OSS realization with a carrier of  $j$ -type ( $j = 1, \dots, n$ );  $j$ —number of types of carriers used in OSS;  $t_{ji}$ —time, assigned for the  $i$ -stage of  $j$ -system forming ( $i = 1, \dots, K$ );  $K$ —number of stages (including substitutions and modernizations);  $P_{ijk}$ —reliability of the  $x$ -subsystem on the  $i$ -stage ( $k = 1, \dots, P$ );  $P$ —number of alternatives, which reflect the modernization depth of the  $x$ -subsystem—number of measures with the  $j$ -system on the  $i$ -stage for  $k$ ;  $m_j$ —number of OSS subsystems, involved in the model under study, when observed are the limitation on expenditures  $C$ , the limitation in reliability  $P_{ijk} < 1$ , 0, elaboration period, to the time of beginning and finish of works, by service life, to technical parameters of objects and also for manpower and material resources.

In the capacity of parameters for the control vector of space vehicle considered are the type and the composition of equipment, the resolving power and other indexes of the SV units and instruments. Referred to the control parameters of SV carrier are the number of alternatives and variants of blocks, which form the system of carriers as well as their design parameters (the number of stages, the mass ratio and the thrust-to-weight ratio coefficient of the stages, the pressure in chambers and nozzle exit sections of the stages, the loading on the stage middle, etc.). To the control parameters of the space-craft we relate values which determine the flight program and others. To the control parameters of technological, starting and control-testing equipment we relate the alternatives of variants of

performing the objects and some of their parameters.

It is useful to study such a complicated closed-solution problem even in parametric space by way of dividing it into the main and ordinary ones. In this case:

all problems of forecasting are solved independently as problems of forecasting the load and also decisive parameters to the time of project realization;  
the main and ordinary problems are considered as individual;  
in every particular case on the base of studying a combination of particular and main tasks we can carry out an iterative study of general decision.

The main problems of divided planning of OSS development in general are given in Fig. 3.

After gaining some experience in studying of main and particular tasks it becomes possible to build a common research model by electronic computing machine. As an example, in Fig. 4 an algorithm of such generalized research is given. Here, from the input initial data unit (block 1) comes a request for missing information into the information-search system (block 2). In the forecasting unit (block 3) data are formed on loading and controlling parameters to the moment of program realization. In blocks 4 and 5, correspondingly, a convergence of iterative search is set up, and, depending on intermediate results, an insertion of new alternatives is made.

The search for a best decision can, for instance, be made in sequence of program (operations) realization:  $\Pi_1, \Pi_2, \Pi_3, \Pi_4, \Pi_5, \Pi_6, \Pi_7, \Pi_8, \Pi_9$ , when, at first, basing on forecast-operation  $\Pi_1$ —

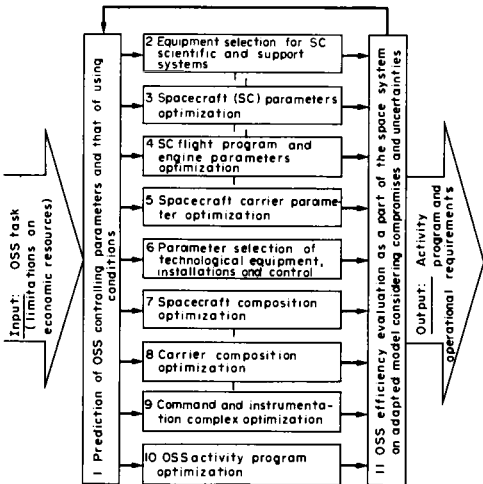


Fig. 3. Logical model of ordinary space system research.

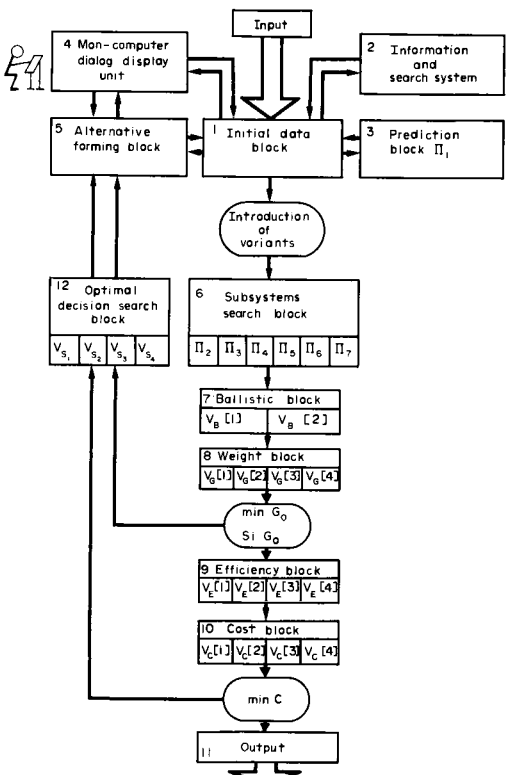


Fig. 4. Functional diagram of the systems generalized activity optimization.

the parameters of spacecraft, carrier and flight vehicle at large are found—operations  $\Pi_2$ ,  $\Pi_3$  and  $\Pi_4$ . Then, after realizing the operation  $\Pi_5$ , a search of optimal composition of an ordinary space system is made. Next comes the selection of optimal plan of works on OSS—the operation  $\Pi_6$ .

The search ends by specifying the parameters of carrier, spacecraft and objects of the complex—operations  $\Pi_2$ ,  $\Pi_3$  and  $\Pi_4$ . On the output enter the planning papers in accordance with the forecast time and task research (operation  $\Pi_7$ ). In the algorithm in order to specify the task and adapt the models of ballistic, weight, economic and effectiveness blocks there are two and four operating modules respectively. In each case, when realizing the operations, their own and the most suitable method of particular task optimal decision is used.

When exploring (1) the determination of a launcher's optimal commission time, its change by a modernized or a new one and of M-C unification alternatives appears to be a particular result of the parameter search  $\Pi_{MC}^{opt}$ . When the relations with others are fixed, the task can be reduced to a distribution of OSS complexing objects so that to ensure launching of required load into the base orbit in the course of definite service time  $T_{serv}$  with SS minimum cost expenses, when

$$C_{SC}^{(n)} (\Pi^{**}) = \min_{\Pi_{MC} \in \Pi^{**} eG} \left\{ \sum_{j=1}^n \sum_{i=1}^k \sum_{k=1}^m C_{ijk} [t_j, \Pi_{MC}, N_j, G_{SCj}(t_j)] \right\}; \quad (2)$$

$$G = \left\{ \Pi_{MC}; [G_{ULj}^*(\Pi_{MC}) - G_{SCj}(t_j)] \right\} \geq 0$$

where  $C_{ijk}$ —expenses on performing  $j$ -particular operation;  $n$ —number of particular operations, provided by different missile carrier;  $k$ —number of complexing types of delivery means (BM);  $m$ —number of means, ensuring task fulfillment (SV);  $G_{ULj}^*(\Pi_{MC})$ —payload weight, delivered into the base orbit;  $\Pi^{**}$  and  $\Pi_{MC}$ —control parameters of the distribution and of the carrier;  $t_j$ —carrier insertion time into the system;  $N_j$ —number of carriers required for performing  $j$ -operation;  $G_{SCj}(t_j)$ —spacecraft maximum weight to be brought at time  $t_j$  into the base orbit. The search  $\Pi_{MC}^{opt}$  is conducted on assumption that one type of missile-carrier (one OSS) is used for performing the  $j$ -operation in the definite interval of the expected load spectrum. The main composition of carriers with a different level of block unification and the time of their commission  $t_j$  are supposed to be preassigned. Some of them are planned to undergo an operation of filling-up the list based on parameter forecast and ballistic designing model according to concrete alternatives.

The analysis (2) shows that while reducing the number of carrier types the operating costs become less, thereby making it necessary to manufacture new ones and hence increasing the expenses on a space system. The impact of these contradictory factors, including expenses on completion of spacecraft, the launching of which will be executed by new M-C, liquidative assets and carrier cost reduction by the growth in number of one-type blocks and M-C, stipulates a rather sharply pronounced cost minimum on SS task fulfillment depending on carrier composition. Naturally, these regularities must be considered in forming (2).

In Fig. 5 is given an algorithm of carrier optimal composition determination from the list with an addition for a part of load spectrum. If the items of the list are fully known, the calculation is made without using the algorithm contour. In this case it is convenient to use recurrent dependence as a purpose function

$$c_{SS}^{(n)} = \min_{\substack{i_0 \leq i_m \\ i_0 + i_m}} [c_{SS}^{(n-1)} \min_{\substack{i_0 \leq i_{m-1} \\ i_0 + i_{m-1}}} + c_{OSS}^{(n)}] \quad (3)$$

where  $c_{SS}^{(n-1)}$ —expenditures on SS out of  $(n-1)$  OSS, carrying out the task in the interval of load network  $i_0 \leq i_m$ ;  $c_{OSS}^{(n)}$ —expenditures on  $n$ -OSS, carrying out the task in the interval of maximum loads (by  $G_{SCj}$ );  $i_0 - i_m$ —interval of SS load network.

Then the search of optimal decision can be organized by dynamic or some other method of non-linear programming. In determining the optimal composition of carriers from the list, when M-C have different commission dates, it is convenient to conduct the investigation using the recurrent expression.

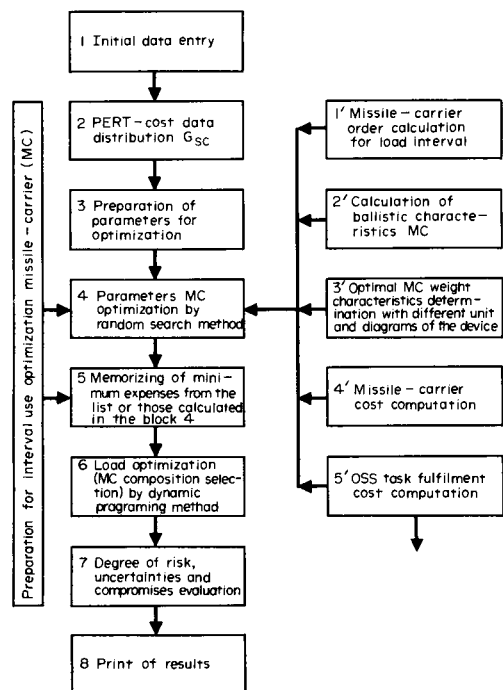


Fig. 5. Algorithm of optimizing the missile-carrier (MC) composition and its parameters.

$$c_{SS}^{(n, \bar{P}_K)} = \min \left\{ \left[ c_{SS}^{[(n-1), \bar{P}_{k-1}]} \right]_{\min_{i_0 \leq i_{m-1}}} + \left[ c_{OSS}^{(n, \bar{P}_{k-1})} \right]_{\min_{i_{m-1} \leq i_0}} \right\};$$

$$i_0 \leq i_m \leq n; i_{m-1}, t_{ij}, \bar{P}_K$$

$$c_{SC}(t_{ij}) \in G_{uLj}(t_{ij}) \quad (4)$$

where:  $c_{SS}^{[(n-1), \bar{P}_{k-1}]}$ —expenditures on space system which has M-C  $n-1$ , with a number of possible substitutions of each MC  $\bar{P}_{k-1} = P_{k-1}, \dots, P_1$ , used in the load interval  $i_0 \leq i_{m-1}$ ;  $t_{ij}$ —time of corresponding substitutions;  $c_{OSS}^{(n, \bar{P}_{k-1})}$ —costs on  $n$ -OSS with a number of possible substitutions  $\bar{P}_{k-n}$  used in the load interval  $i_{m-1} \leq i_m$ .

In exploring (4) on minimum a dynamic programming method can be used with the four cycles of sorting-out procedures in number of OSS- $n$ , load network, load network components inside the interval of system use out of  $(n-1)$  OSS and network components of change time by a modernized or new M-C.

When presenting technical proposals the task of change is solved together with assignment of OSS plan of works based on investigation of the process graph of system forming, the arcs of which show the stages (phases) of works over the main objects. If the graph arcs are presented by analytical relations, characterizing the change of reliability on boundaries of stages into functions of cost expenses, time and volume of measures, then it would be possible to find efficient dates, reliability on boundaries of stages and extent of measures (amount of tests, modernization levels, etc.) through the process stages for the OSS designed effectiveness in the course of serviceability with the minimum cost expenses on the system.

In this case the vector of decisive parameters  $\Pi(P_{ij}, t_{ij}, r_{ij})$  is set up, ensuring the minimum of expenses on ordinary space system, when

$$c_{OSS} = \min \left\{ \sum_{i=1}^h \sum_{j=1}^l K(t_{ij}) [c_{ij}(P_{ij}, t_{ij}, r_{ij}) + c_o] \right\}$$

$$P_{ij}, t_{ij}, r_{ij} \quad j \in \omega \quad (5)$$

where  $h$ —number of works stages,  $l$ —number of sub-stages (stage objects);  $\omega$ —great number of possible plans of OSS development,  $P_{ij}$ ,  $t_{ij}$ ,  $r_{ij}$ —process variables, respectively: reliability on boundaries of stages on the object, time and number of measures on plan improvement over  $j$ -object;  $K(t_{ij})$ —function, counting the time difference of expenses;  $c_o$ —expenses independent of  $P_{ij}$ ,  $t_{ij}$  and  $r_{ij}$ .

The most important task is to define dates of modernization and change for recent operating missile-carriers. In this case, in addition to the main factors defining the terms of putting into service, one should also refer: the reduction in reliability due to a long storage (without additional maintenance), the relatively high service expenses on old models, the reduction in effectiveness of task fulfillment owing to a rise of requirements to injection accuracy, reliability of life-support systems.

When taking a decision, also to be taken into account are the growing requirements for spacecraft weights and number of launches, carriers reserve, additional expenses due to their replenishment, expenses on new M-C, means paid back by realizing unused objects and those received after realizing the inventions and technical proposals in other spheres of production, normative allocations from capital investments, change of expenses on space system at large.

Owing to a large conservatism of means for a launching complex (LC) the possible levels of modernization depth can be defined by discrete cases of changes, such, for instance, as: M-C modernization without changing SV and LC; M-C modernization with a change of SV; M-C change together with SV at partial modernization of LC and others. Considering the above-mentioned regularities and peculiarities of substitutions it is possible to use as an aiming function the following dependence:

$$\begin{aligned}
 C_{OSS} = & \sum_{i=1}^n C'_{L_i} N_i (1+K) + \frac{C'_{ad_1} N}{(1-\alpha_1)} (1+K)^{\tau_i} \\
 & + \sum_{i=1}^n C'_{US_i} (N_i + N_{ad_i}) \tau_i + \sum_{i=1}^{n-1} C'_{LF_i} (1+K)^{\tau_i} \\
 & - \sum_{i=2}^n C'_{RJ_i} (1+K)^{\tau_i} + \sum_{i=2}^n C'_{NC_i} (\Delta t_i) (1+K)^{\tau_i} + \Delta C_{MC} (t_{MC}) \\
 N_i = & N_{re_i} + N_{ad_i}; T_i = T_{US} - \sum_{j=1}^{i-1} t_j; C_i = C_{MC_i} + C'_{LC_i}; \\
 & + \Delta C_{SS_i}
 \end{aligned} \tag{6}$$

where  $C'_{L_i}$ —cost of one launch (without carrier);  $C'_{ad_1}$ —means, spent on one launch with additional manufacturing of carriers (without carrier's cost);  $C'_{US_i}$ —service expenses, related to one launch;  $C'_{MC_i}$ —cost of one carrier;  $C'_{LC_i}$ —cost of launching complex, related to one launch;  $C'_{LF_i}$ —liquidative funds;  $C'_{RJ_i}$ —means, coming from other branches of industry at the expense of realizing the improvements on the carrier;  $C'_{NC_i}$ —expenses on commission of new carriers;  $\Delta C_{MC}$ —expenses on modernization of carriers;  $\Delta C_{SS}$ —change of expenses, related with general provision of works;  $N_{re_i}, N_{ad_i}$ —number of carriers manufactured (ready and additionally produced);  $\alpha$ —coefficient, counting the impact of production volume;  $t_i, n$ —time number of changes by a modernized or new M-C at the interval  $T_{US}$ .

In (6) for control parameters are taken the number of changes  $n$  terms of changes  $t_i$ , commission time of new models  $\Delta t_i$ .

The task is largely simplified, supposing that the commission time of new M-C and the expenses  $C(\Delta t_i)$  in each case are constant.

The algorithm block-diagram of task investigation at  $C(\Delta t_i) = \text{const}$  is given in Fig. 6. Here:  $j, i, l$ —operating variables;  $a_1, a_2$  and  $a_3$ —minimum numbers of change levels (modernization);  $G[1:m, 1:n]$ —cost massif of system transfer into a corresponding point of network (time-change depth)—ij;  $H[1:m, 1:n]$ —massif of storing the meanings of point coordinates from which a transition into a new one is conducted;

1-point of change in the matrix of expenses  $C_{ij}$ , to which corresponds optimal decision  $le_{ij}$ ;  $C_{ij}$ —launching cost, corresponding to time  $i$  and modernization depth  $l$  in the interval ie; F—launching cost without a change in the interval il.

The count process is illustrated by a picture table. At first from the point (1, 1) a step in time is being made onto the borderline  $i = 2$ , and for each level of changes the cost of task fulfilment by the system of the given level during  $\tau_i$  is determined. Then a transfer onto the borderline  $i = 3$  is made so as to minimize the cost of task fulfilment. In this manner the process is being repeated till the system reaches the borderline which corresponds the assigned service time  $T_{US}(i = m)$ . The computer then prints out the number of changes  $n_{opt}$ , terms and levels of changes, corresponding to the best path in space of the expense matrix  $C_{ij}$ .

In determining the dates of commission, substitution, modernization and unification the central place belongs to the question on adequacy of mathematical models which specify the aiming function and obviously the degree of risk in decision-making. In Fig. 7 is given the dependence for determining the expenses on OSS, having  $n$  modernizations and changes and ensuring the task fulfilment in the definite service period. However, the concrete recommendations could be given only for a definite M-C system.

To the common regularities can be referred the following:  
according to the growth of number and types of SV, launched into space, also grows the optimal number of M-C types ( $n_{opt}$ );  
the greater the cost of carriers  $C_{MC}$  and  $N$  in a definite interval of loads ( $G_{SC}$ ) is, the more the number of M-C of different capacity is required to put into service in the interval;  
the increase of reserve, reliability and the reduction of operating costs leads to a widening of SS carriers composition;  
modernization dates are shortened when commissioning new models;  
reliability level of components (blocks) considerably influences on quantitative estimations, related with M-C modernization and change, etc.

In conclusion, let us mention that because of uncertainties in realization it is expedient to investigate the whole spectrum of alternatives of OSS usage with regard to properties which defy mathematical description (prestige factors and others). Evidently, such investigation always needs final evaluation of authenticity of the results at a definite confidential probability.

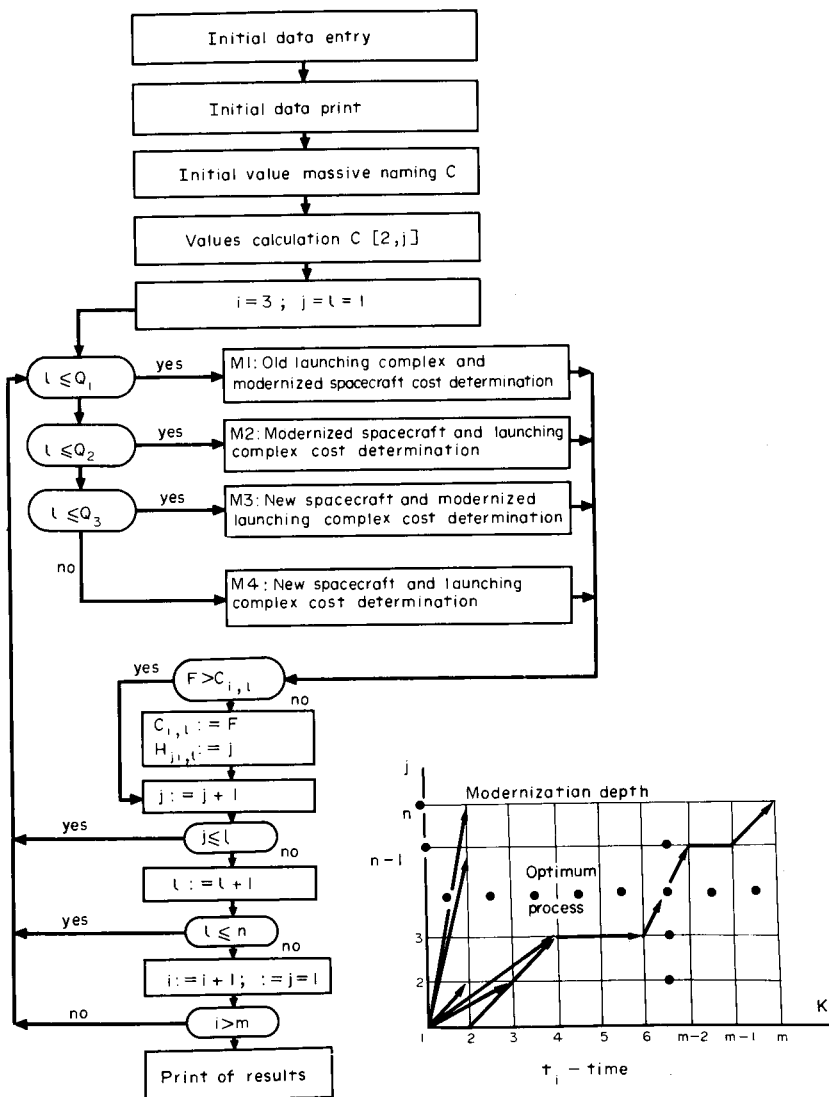


Fig. 6. The algorithm of determining the spacecraft optimal change time (modernization) and the search diagram of the best decision.

## REFERENCES

1. Booslenko, N. P., Kalashnikov, V. V. and Kovalenko, I. N. *Lectures on Theory of Complex Systems*, Moscow, Soviet Radio, 1973.
2. Quade, E. S. *Analysis of Complex Systems*, Moscow, Soviet Radio, 1969.
3. *Fundamentals of Operations Research for Military Equipment*, Chief Ed. J. V. Chuev, Moscow, Soviet Radio, 1965.
4. Piyavsky, S. A., Brusov, V. S. and Hvilon, E. A. *Multimission Spacecraft Parameters Optimization*, Mechanical Engineering, 1974.
5. Chuev, J. V. and Spehova, G. P. *Technical Tasks of Operations Research*, Moscow, Soviet Radio, 1971.
6. Chuev, J. V., Mikhailov, J. B. and Koozmin, V. I. *Forecasting of Process Quantitative Characteristics*, Moscow, Soviet Radio, 1975.

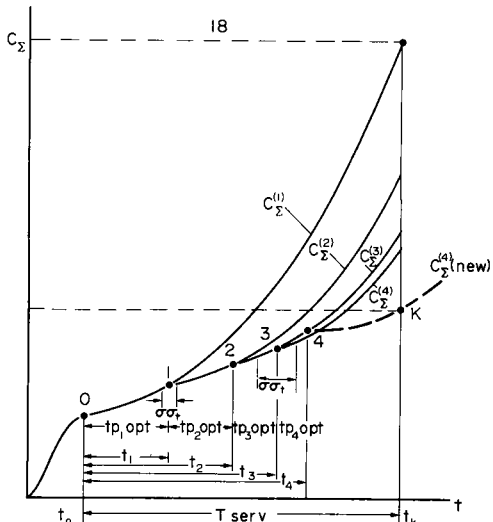


Fig. 7. Change of OSS total costs depending on service time.

- $C_{\Sigma}^{(1)}$ —OSS total costs with the carrier at  $t$ ;
- $C_{\Sigma}^{(2)}$ —the same by using an old carrier and one model of a modernization at  $t_1$ .
- $C_{\Sigma}^{(3)}$ —the same by using an old carrier and two modernizations at  $t_1$  and  $t_2$ ;
- $C_{\Sigma}^{(4)}$ —the same by using an old carrier and three modernizations at  $t_1$ ,  $t_2$  and  $t_3$ ;
- $C_{\Sigma(H)}^{(4)}$ —OSS total costs with a new carrier, by changing at  $t_4$ .

# ECNOMIC BENEFITS OF IMPROVED METEOROLOGICAL FORECASTS THE CONSTRUCTION INDUSTRY

R. K. Bhattacharyya and J. S. Greenberg

*ECON, Inc, Princeton, New Jersey*

## Abstract

Estimates have been made of the potential economic benefits that might accrue to a number of industries and to society as a result of optimal utilization of meteorological forecast improvements made possible by data obtained from synchronous satellites such as SMS/GOES, STORMSAT and SEOS. Their capabilities include a continuous and on-demand collection of meteorological and earth observation data. The reduction in type 1 and type 2 errors have been used to measure the improvements in forecasting meteorological events such as thunderstorms, snow storms, frost, temperature, etc., that are of relevance to the user concerned. The resulting economic benefits have been related to the cost reduction due to an improvement in the decision process on the part of the user regarding whether or not to take some specific protective or scheduling action against the possibility of a future adverse weather condition. Taking a protective action involves a cost with certainty, while not taking the action may lead to a loss due to the probable occurrence of adverse weather. This methodology of benefit estimation has been developed and then applied to a number of industries. The U.S. construction industry has been given special emphasis. For the remaining industries, only the final results are stated.

## I. Introduction

Since the launching of TIROS I in April 1960, the science of meteorology has been impacted by the introduction of global synoptic data provided by instrumented satellites. Concurrently, sophisticated numerical forecasting models have been developed embodying the state-of-the-art understanding of the physics of the atmosphere and oceans, and large-scale computer facilities have been acquired to provide meteorological forecasts using these models. In order to monitor the fleeting and meso-scale weather phenomena an experimental SMS/GOES was placed into a geosynchronous orbit and has been operating since 1974. With the increasing sophistication of space and related tech-

nology, efforts are now being focused on futuristic geosynchronous satellites like STORMSAT and SEOS. STORMSAT is planned to be equipped with an advanced atmospheric sounding and imaging radiometer (AASIR) to provide visual and infrared imagery with a resolution of 750 meters and 4.5 kilometers respectively. The plan for SEOS is to use a 150 centimeter telescope and achieve a much greater resolution than STORMSAT.

The impact of such high resolution measurement capabilities on the forecast of meteorological phenomena and consequent economic benefits has necessarily to be deferred for experimental verification until the launching of the futuristic satellites. With regard to the SMS/GOES satellite, various designed experiments are, at present, under consideration for the verification of resulting forecast improvements and economic benefits. In the absence of experimental results, a reasonable approach to economic benefit estimation is to conduct parametric analyses in terms of forecast capability. This allows specific numerical values of benefits to be obtained when the capabilities are experimentally confirmed. But more importantly, the parametric analysis provides insight into the economic value of achieving different levels of capability and as such can be used to assist in the planning of R&D programs and satellite configurations.

## II. Methodology

The benefits of a government investment in meteorological research and development are assumed to result from industries' (the producers) utilization of data provided by an operational system which is a direct outgrowth of the R&D efforts. It is anticipated that this will lead to cost reductions which in turn will lead to increased profits and/or a reduction in the price of related products and/or services. The analysis of the benefits resulting from a government expenditure can be assessed by considering Figures 1 and 2. Figure 1 illustrates supply and demand curves in terms of price and quantity where a quantity  $Q$  of a particular product or service will be sold at a price  $P$ . The consumers' surplus represents the maximum sum of money a consumer would be willing to pay for a given amount of a good, less the amount he actually pays ( $P$ ). The consumer surplus is the net benefit to consumers from consumption. The producers' surplus represents the net benefit or profit obtained by the

\* This paper is the result of work performed by ECON, Inc. supported by the Environmental Research Institute of Michigan and sponsored by NASA, Goddard Space Flight Center, Contract NAS5-20021.

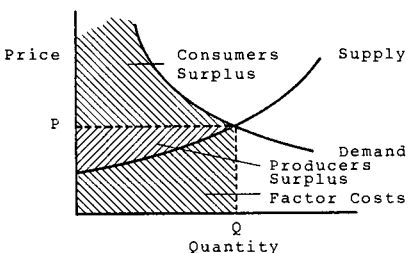


Figure 1. Supply/Demand/Benefit Relationship

suppliers. The factor costs represent payments made by the producers for materials and services and other expenses of production. The particular supply curve ( $S$ ) represents the marginal cost of the product or service when conventional or current meteorological forecasting capability data are incorporated into the production process. This results in the product or service price  $P$ . If, because of government funding, a technology and operational capability are developed which, through improved meteorological forecasting capability, results in reduced factor costs and leads to supply curve  $S'$  as illustrated in Figure 2, then there is an associated decrease in product or service cost to  $P'$ . The reduction of the cost of a product or service is deemed to confer a benefit on society and is measured by the cross-hatched area ABCD. This area depends upon the shape of the supply and demand curves and represents the change in consumers' and producers' surplus. Note that the benefits are obtained as a result of factor cost reductions. It is normally assumed that in the long-term, all displaced factors will seek and find their next best use.

Referring to Figure 2, it can be seen that the area ABCD, representing the increase in benefits, consists of the change

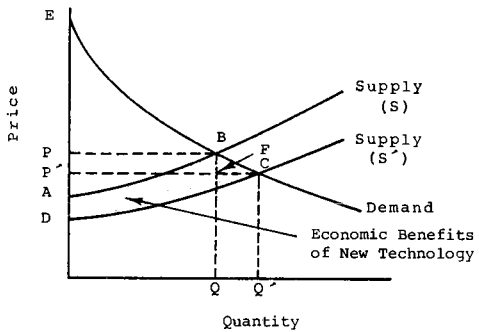


Figure 2. Impact of New Technology - Economic Benefits

in consumer surplus ( $PBCP' = ECP' - EBP$ ) plus the change in producer surplus ( $P'CD - PBA$ ). The change in consumer surplus consists, in turn, of two parts that are referred to as the equal capability benefits given by  $(P - P') \times Q$  and the added capability benefits as per the area  $BCF$ . Simply multiplying the quantity consumed by the price differential  $(P - P')$  yields a measure of the equal capability consumer surplus benefits; it does not include the added capability benefits and does not necessarily properly provide an accurate measure of the added public welfare resulting from the development of the new technology (because of the producers' surplus). When demand is inelastic, i.e.,  $|\epsilon| = 0$ ,<sup>\*</sup> there are no added capability benefits resulting from a price decrease. On the other extreme, when demand is perfectly elastic, i.e.,  $|\epsilon| \rightarrow \infty$ , the added capability benefits resulting from a price reduction become very large. Depending upon the values of  $\epsilon$  and the shape of the supply curves, it is clear that the added public welfare may differ from the increase in equal capability consumer surplus by a non-negligible amount.

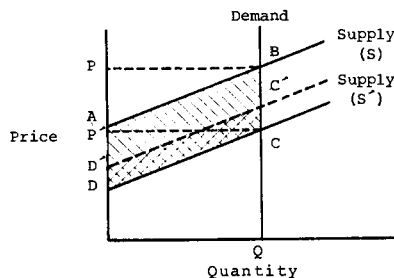


Figure 3. Supply/Demand Relationship Approximation

In the benefit analysis discussed in following paragraphs, a number of simplifying assumptions have been made. These are illustrated in Figure 3. The major assumption is that demand is inelastic, i.e.,  $|\epsilon| = 0$ , and therefore there are no added capability benefits resulting from price reductions. This is a conservative assumption which tends to lead to an understatement of benefits. The area ABCD represents the benefits attributable to the new technology (the shift in the supply curve from  $S$  to  $S'$ ). The benefits result from improvements in scheduling brought about by the efficient utilization

\* Elasticity,  $\epsilon$ , is defined as the percentage change in quantity divided by the percentage change in price:

$$\epsilon = \frac{P}{Q} \frac{dQ}{dP}$$

of improved meteorological forecasting data in the decision-making process. The scheduling improvements result in reductions in factor costs which may or may not be passed on to consumers; in either case, the benefits are given by the area ABCD. The assumption is that the factors which are no longer required will seek and find their next best use. This, however, may not necessarily be the case in the short-term since part of the cost savings may occur from intermittent and essentially random labor work hour reductions. When this occurs, it may not be possible, in the short-term, for the labor force to find its next best use. Thus, the situation may arise where part of the increase in producers' surplus occurs as a result of disbenefit to the workers. Again, to be conservative, when this occurs the benefits are computed as the area ABC'D', with the true benefits (in the short-term) being between the areas ABC'D' and ABCD. It might be argued, on the other hand, that workers so affected will ultimately renegotiate annual wage rates so as to earn the same annual wage (even though they are productively employed less) thus reducing the producers surplus to the area given by ABC'D'. It further might be argued that this added leisure time has an economic value with the area D'C'CD being an upper limit. In any event, to be on the conservative side, the area ABC'D' has been used as a measure of the economic benefits of society of improved meteorological forecasting.

The industry potential annual benefits are defined as the cost reduction, i.e., the savings that would result from the optimum utilization by the user community of meteorological forecasts of increased accuracy and reliability. Savings are computed as the difference between the cost of performing a specified task or application when forecasts of level x are available and when forecasts of level y are available. It is assumed that the forecasts are used in such a manner that the user undertakes that course of action which, for a given forecast capability, minimizes cost.

Many applications which have been considered were found to be quite similar, particularly with respect to the utilization of meteorological forecast data. These are applications where a decision-maker must choose between taking or not taking some specific protective action against a future unfavorable weather condition: taking the protective action involves some cost with certainty; not taking the protective action involves escaping that cost, but incurring a certain loss if the unfavorable weather condition does in fact occur.

Thus, a newspaper distributor who has a standard routine for distribution, can wrap his papers in plastic bags to protect them from rain. A storekeeper can tape his windows to protect them from a

threatening hurricane. A construction company can delay pouring concrete and release employees from work when thunderstorms are forecast. A farmer can delay spraying his crops given a forecast for heavy rain. A citrus grower can light smudge pots to protect his fruit from frost. Snow removal crews can be alerted and snow removal started earlier. Fishing fleets can be rescheduled when severe storms are forecast.

Consider the forecasts which might be provided to a decision-maker. For example, let  $y_1$  and  $y_2$  be forecasts of the occurrence or non-occurrence of a meteorological event; for example, storm or no storm. In the event that  $y_1$  is forecast, the event  $w_1$  or  $w_2$  may actually be observed. This is shown in Figure 4, where a two-by-two contingency array is illustrated. Frequently,  $\pi_{11}$  is referred to as the false alarm probability and  $\pi_{12}$  is referred to as the probability of miss. The significance of these two terms will become apparent. Suffice it to say at this point, that the economic benefits which may be achieved as a result of a new forecast capability are directly related to the probability of a false alarm and the probability of a miss. A false alarm occurs when, for example, clear weather occurs when a storm has been predicted. A miss occurs when, for example, a storm occurs when clear weather had been predicted.

A payoff function is defined in Figure 5 and illustrates the cost of taking actions (pursuing strategies)  $a_1$  and  $a_2$  in terms of the weather forecast.<sup>1,7</sup> Here  $a_1$  represents the "protect" action and  $a_2$  represents the "do not protect" action.

The decision-maker's problem is to determine the best course of action given a forecast of  $y_1$  or  $y_2$ . If the decision-maker receives forecast  $y_1$ , his expected cost if he chooses action  $a_1$  is  $C$ , while his expected cost if he chooses  $a_2$  is  $\pi_{11}L$ . Therefore, the choice of action given  $y_1$  (i.e.,  $a|y_1$ ) is:

$$a|y_1 = \begin{cases} a_1 & \text{if } C < \pi_{11}L \\ a_1 \text{ or } a_2 & \text{if } C = \pi_{11}L \\ a_2 & \text{if } C > \pi_{11}L \end{cases} \quad (1)$$

and the objective is to select that course of action depending upon the specific values of  $C$ ,  $L$  and  $\pi_{11}$ , such that

$$E(a|y_1) = \text{Min } (C, \pi_{11}L) \quad (2)$$

where  $E(a|y_1)$  is the expected cost given forecast  $y_1$ .

Similarly, when he receives forecast  $y_2$ , he chooses  $a_1$  or  $a_2$  depending on whether  $C$  or  $\pi_{12}L$  is smaller. Therefore,

		FORECAST	
		$y_1$ (storm)	$y_2$ (no storm)
OBSERVED	$w_1$ (storm)	$\pi_{11}$	$\pi_{12}$
	$w_2$ (no storm)	$\frac{\pi_{21}}{\pi_1}$	$\frac{\pi_{22}}{\pi_2}$
$\pi_1$ = Probability of forecast $y_1$ , the forecast of unfavorable weather (i.e. storm), $\pi_2$ = $1-\pi_1$ = Probability of forecast $y_2$ , the forecast of favorable weather (i.e., no storm), $\pi_{11}$ = The conditional probability of unfavorable weather ( $w_1$ ), given that forecast $y_1$ is made, $\pi_{21} = 1-\pi_{11}$ = The conditional probability of favorable weather ( $w_2$ ), given that forecast $y_1$ is made, $\pi_{12}$ = The conditional probability of unfavorable weather ( $w_1$ ), given that forecast $y_2$ is made, $\pi_{22} = 1-\pi_{12}$ = The conditional probability of favorable weather ( $w_2$ ), given that forecast $y_2$ is made.			

Figure 4. Two-by-Two Contingency Array

		WEATHER	
		$y_1 \& w_1$ (storm)	$y_2 \& w_2$ (no storm)
ACTION	$a_1$ (protect)	-C	-C <span style="float: right;">cost of protection</span>
	$a_2$ (no protect)	-L <span style="float: right;">loss</span>	0

Figure 5. Payoff Function

$$a|y_2 = \begin{cases} a_1 & \text{if } C < \pi_{12} L \\ a_1 \text{ or } a_2 & \text{if } C = \pi_{12} L \\ a_2 & \text{if } C > \pi_{12} L \end{cases} \quad (3)$$

and

$$E(a|y_2) = \min(C, \pi_{12} L) \quad (4)$$

The above equations determine the decision-maker's best decision rule, and the expected minimized cost for each of the two forecasts. The overall expected cost,  $E(C)$ , under the best decision rule is given by

$$E(C) = \pi_1 \min(C, \pi_{11} L) + \pi_2 \min(C, \pi_{12} L) \quad (5)$$

Potential saving,  $S$ , or industry benefit resulting from improved forecasts is therefore given by

$$S = \Delta E(C) = E_A(C) - E_B(C) \quad (6)$$

where  $E_A(C)$  and  $E_B(C)$  are the specific values of minimum expected cost resulting from system alternatives A and B where each alternative has associated with it

different values of the  $\pi_{ij}$  terms in the contingency array.

Equations (5) and (6) yield the industry expected costs and potential industry annual benefits, respectively, resulting from the best decision rule for a given capability level of forecast. The social benefits may differ since, in general, at least a portion of the industry savings will occur as the result of a loss to some other sector of the economy (for example, industry savings which result from wage reductions are offset by labor's loss of wages, assuming that labor cannot recoup, at least in the short-term, the lost wages by some other productive means or wages are renegotiated so as to maintain near or the same annual wage as before the introduction of the new technology).

To establish the expected social cost,  $E'(C)$ , under the best industry decision rule, Equation (5) can be restated as

$$E'(C) = \pi_1 [\min(C, \pi_{11} L) + K_1] + \pi_2 [\min(C, \pi_{12} L) + K_2] \quad (5A)$$

where

$$\begin{aligned} K_1 &= C' & \text{when } C \leq \pi_{11} L \\ K_1 &= \pi_{11} L' & \text{when } C > \pi_{11} L \\ K_2 &= C' & \text{when } C \leq \pi_{12} L \\ K_2 &= \pi_{12} L' & \text{when } C > \pi_{12} L \end{aligned}$$

$C'$  and  $L'$  are the losses or costs which are incurred by other segments of the economy when the optimum industry policy is pursued.

The expected potential annual social benefits are given by

$$E(B) = B = \Delta E'(C) = E'_A(C) - E'_B(C) \quad (6A)$$

where  $E'_A(C)$  and  $E'_B(C)$  are the specific values of expected social costs resulting from system alternatives A and B.

In general, the annual costs or expenses associated with weather phenomena can be considered in three parts, namely (1) expenses incurred on false alarm days; (2) expenses incurred on miss days; and (3) expenses incurred on correctly forecast days. A false alarm day signifies a day when a forecast for an adverse weather condition is made which, in reality, turns out to have favorable weather conditions. A miss day signifies a day when a forecast is made for favorable weather which, in reality, turns out to be adverse. A correctly forecast day is one where the event forecast actually occurs. It should be noted that when the forecast capability is perfect the total expense is associated with correctly forecast days. As the forecast capability degrades the expenses associated with false alarm and miss days increase, whereas those associated with correctly forecast days decrease. This is illustrated by the following equations.

$$\beta = N\pi'_{12} \quad (7)$$

$$\gamma = N - \beta \quad (8)$$

$$\alpha = n - \gamma = \gamma \left( \frac{1}{\pi_{11}} - 1 \right) \quad (9)$$

where

$\beta$  = number of miss days,

$N$  = number of adverse weather days which occur per year,

$\pi'_{12}$  = probability of favorable weather forecast, given that adverse weather is to occur in reality,

$\gamma$  = number of days of adverse weather occurrence which are forecast correctly,

$\alpha$  = number of false alarm days.

$n$  = number of days that adverse weather is forecast, and

$\pi_{11}$  = probability of adverse weather occurrence, given adverse weather forecast.

Note that  $\pi'_{12}$  differs from  $\pi_{12}$  which was previously defined as the probability of adverse weather occurrence, given a favorable weather forecast. This modification is necessary because data are available on the number of adverse weather occurrences in a year rather than on the total number of annual favorable weather forecasts.

In the following paragraphs, the economic benefits are evaluated in terms of the probabilities  $\pi_{11}$  and  $\pi'_{12}$ . As will be described, the different system alternatives, such as SMS/GOES, STORMSAT and SEOS, can be described in terms of estimated values for  $\pi_{11}$  and  $\pi'_{12}$  for different weather events and the resulting economic benefits established in terms of these probabilities, the number of events per year, the affected activities and their associated losses and cost of protection.

### III. Construction Industry

Over a period of at least the last fifteen years, the value associated with annual construction activities in the United States has typically been around 10% of the gross national product. In 1975, the value of new construction was approximately \$135 million.<sup>2</sup> Based upon the assumption that the expenses of the construction industry maintain a constant relationship with the nominal GNP, the estimated expense figures in the 1980's, when expressed in 1975 dollars are expected to be on the order of \$176 billion. The reason for choosing the 1980's is that the launching of futuristic satellites such as STORMSAT and SEOS can be expected in the 1980's.

The construction industry can be broadly classified into the following segments:<sup>3,4</sup>

1. Heavy construction: airport, dam, sewage, powerlines, utilities, etc.
2. General building: industrial, institutional, high-rise, apartment complex, etc.
3. Single family residential
4. Highways and bridges
5. Repair and maintenance

It has been reported<sup>5</sup> that out of the total volume of construction business, 14.2% is related to heavy construction, 33.75% to general building, 19.55% to single family residential, 7.5% to highways and bridges and 25% to repair and maintenance. Naturally, these five segments of construction are not equally sensitive to bad weather. Reference 6 gives a detailed description of these sensitivities. The breakdown of the total volume of \$176 billion on the five construction categories along with the incor-

Table 1. Estimated Volume of '80 Construction (Billion Dollars)						
Category	Volume	Weather Sensitive Portion				Total Sensitive Volume
		Perishable	Wages	Equipment	Overhead and Profit	
Residential	34.4	1.92	3.24	.14	4.28	9.58 (27.9%)
General	59.4	3.85	8.16	.44	5.34	17.79 (30%)
Highway etc.	13.2	1.33	3.26	1.55	1.45	9.59 (72.7%)
Heavy	25.0	3.75	6.25	5.0	5.0	20.00 (80%)
Repair and Maintenance	44.0	5.35	7.99	2.77	6.28	22.39 (50.9%)
TOTAL	176.0	18.2	28.9	9.9	22.35	79.35 (45%)

poration of their respective weather sensitivities is illustrated in Table 1.

The weather sensitive portion of the business has been divided into four categories: perishable material, wages, equipment and overhead and profit. The actual losses due to adverse weather, however, depend on the frequency of unfavorable weather occurrence, the forecast accuracy and the nature of the response of the construction industry to the weather forecast as reflected in its scheduling policy. Usually, the schedule for the day is drawn in the morning around 7:00 am.

Assuming that the weather condition observed early in the morning prevails for the rest of the morning, it is the forecast for the afternoon weather condition that is of critical importance at the time of drawing the schedule for the day. Hence an accurate six-hour forecast has a significant impact on the construction industry, and it is the six-hour forecast ability of the various satellites that has been considered in this study. Of course, longer range forecasts, if accurate, are usually of greater value because they allow a longer lead time for appropriate planning. However, at the moment there does not seem to be any definite knowledge regarding the extent of improvement in medium and long range forecasts that can be effected by data from satellites like SMS/GOES, STORMSAT and SEOS. Hence, this study has been restricted to the benefits associated with the improvement in six-hour forecasts.

#### IV. Cost Factors

The various weather phenomena that have an impact on construction activities include thunderstorm, snowstorm, very low and very high temperatures, high wind, dense fog, ground freeze, etc. A detailed breakdown of various construction activities and the degree to which they are

Table 2. Critical Limits of Weather Elements Having Significant Influence on Construction Operations						
Operation	Thunderstorm	Sleet & Snow	Operation	Thunderstorm	Sleet & Snow	
Surveying	L*	L	Waterproofing	M	M	
Demolition and clearing	M	M	Backfilling	M	M	
Temporary site work	M	M	Erecting structural steel	L	L	
Delivery of materials	M	M	Exterior carpentry	L	L	
Material stockpiling	L	L	Exterior masonry	L	L	
Site grading	M	M	External cladding	L	L	
Excavation	M	M	Installing metal siding	L	L	
Pile driving	M	M	Fireproofing	L	L	
Dredging	M	M	Roofing	L	L	
Erection of coffer dams	M	L	Cutting concrete pavement	M	M	
Forming	M	M	Trenching, installing pipe	M	M	
Emplacing reinforcing steel	M	M	Bituminous concrete pouring	M	L	
Quarrying	M	M	Installing windows and doors, glazing	L	L	
Delivery of pre-mixed concrete	M	L	Exterior painting	L	L	
Pouring concrete	M	L	Installation of culverts and incidental drainage	M	L	
Stripping and curing concrete	M	M	Landscaping	M	L	
Installing underground plumbing	M	M	Traffic protections	M	M	
			Paving	L	L	
			Fencing	M	M	

\*L indicates light; M indicates moderate

influenced by these meteorological phenomena are discussed in References 3 and 6. Part of this discussion is listed in Table 2 for ready reference.

It is evident from Table 2 that the actual impacts of thunderstorm and snow-storm are approximately the same. Of course, in winter there is the added problem of ground freeze. But that is an independent phenomenon in the sense that ground freeze does not imply snowstorm and vice versa. Hence, excluding the days when construction activities have to be held up due to ground freeze, the weather sensitive volume of the construction industry shown in Table 1 is, in an approximate sense, equally affected by either a thunderstorm or a snowstorm. This allows one to spread these weather sensitive volumes equally over the days constituting construction work on a per day basis, disregarding whether the working day belongs to summer or winter. Assuming uniformity in construction work throughout the country (approximately 3,022 thousand square miles), and assuming that on the average there are 250 working days of construction per year, the following results directly follow from Table 1:

$$R = \text{perishable raw material used per half day per square mile} = 18.2 \times 10^3 / [250 \times 2 \times 3,022 \times 10^3] = \$12.045$$

Similarly

$$E = \text{weather sensitive volume of equipment usage per half day per square mile} = \$6.552$$

$$P = \text{weather sensitive volume of overhead and profit per half day per square mile} = \$14.792$$

$$W = \text{weather sensitive volume of wages per half day per square mile} = \$19.126$$

The above cost factors are computed on a half day basis because, as explained earlier, it is the forecast for the afternoon made in the morning that is of relevance to this study. It follows from the above definitions that if the forecast for the afternoon as available in the morning is favorable thus prompting the regular work schedule, and if adverse weather occurs unexpectedly in the afternoon, the loss incurred by the construction company per square mile on that afternoon is  $R+E+P+W$ . This loss would have been zero if the afternoon weather conditions had been favorable and work continued according to schedule. On the other hand, if in response to an adverse weather forecast the decision is to suspend the work in the afternoon, the perishable material  $R$  can be saved. Further, in all probability the workers do not have to be paid for the whole four hours of the afternoon if advance notice can be given. The actual amount that the workers have to be paid under these circumstances depends on union

Table 3. Expense Function of Construction Industry Per Square Mile Per Half Day of Adverse Weather (Dollars)

Policy	Adverse Weather	Favorable Weather
Work	$R+E+W+P$	0
No Work	$P+E+W'$	$P+E+W'$

$$R = 12.045, E = 6.552, W = 19.126, P = 14.792$$

$$0 \leq W' \leq 9.563$$

contracts and has been found to vary anywhere between zero and two hours wages. Thus, the loss to the construction company under these circumstances will be  $E+P+W'$  where  $0 \leq W' \leq W/2$ . This loss, of course, will be the same as long as a no work decision is taken irrespective of whether the weather in the afternoon is adverse or not. The expense function matrix for the construction industry is presented in Table 3.

However, expenses to the society are somewhat different from the expenses incurred by the construction industry. This is partly because, as explained earlier, the savings that accrue to the construction company as a result of paying  $W'$  to the workers instead of  $W$  is negated by an equal amount of loss suffered by the workers on the assumption that they have no other alternative to be productive over those idle hours. To determine the loss to the society on a day when work is called off, the total earnings (i.e., the earnings of construction industry, the workers and the equipment rentals) on such a day have to be compared against the total earnings on a normal working day. On a normal working day, the construction company consumes  $R+W+E$  to generate a capital  $R+W+E+P$ . In other words, the construction company earns a profit  $P$ . The workers and equipment rentals earn  $W$  and  $E$  respectively. Thus the total earnings at the end of the day is  $P+W+E$ . In contrast, if work is called off, the value of  $P$  becomes zero. The company spends  $W+E$ , which is earned by the workers and equipment rentals. Hence the total earnings at the end of the day is zero. Thus, in comparison with a regular working day, the cost to the society is  $P+W+E$ . Hence, the expense function matrix for the society can be obtained if  $W'$  in Table 3 is replaced by  $W$ .

#### V. Optimal Decision

The scheduling decision that a construction company is faced with is whether or not to take any protective action in the face of an adverse weather forecast. Such protective actions can be varied in nature, the most critical one being whether to stop work. Accordingly, in this study the scope of protective actions has been narrowed down to the decision

that has to be made in the morning as to whether or not to work in the afternoon in the face of an adverse weather forecast for the afternoon. Referring to Equation (1), the values of C and L for the construction company as illustrated in Table 3 are  $P+E+W'$  ( $=30.907$ ) and  $R+E+W$  ( $=52.515$ ) respectively. Hence, if  $\pi_{11} > 0.589$ , it follows from Equation (1) that the optimal course of action for the construction company should be to stop work in the face of an adverse weather forecast. It can be similarly demonstrated that if  $\pi_{11} > 0.771$ , the optimal course of action for the benefit to the society is to stop work in the face of an adverse weather forecast.

The value of  $\pi_{11}$  corresponding to a six hour forecast is different for different levels of forecast capability associated with different satellite systems. Further the value of  $\pi_{11}$  is a function of the nature of the meteorological phenomenon in question, and the area over which the forecast is made. The same applies for  $\pi_{12}$ . Rough order of magnitude estimates for the values of  $\pi_{11}$  and  $\pi_{12}$  associated with a six-hour forecast of thunderstorm over a large area, and corresponding to various satellite capabilities have been obtained from NASA and are presented in Table 4. These estimates are not claimed to be precise, and are apt to be modified as greater knowledge is acquired regarding the interpretation of satellite data. The conventional capability in Table 4 refers to the forecast capability prior to the launching of SMS/GOES.

Table 4. Estimates of Six-Hour Forecast Capabilities for Thunderstorm Over Large Areas

Capability	$\pi_{11}$	$\pi_{12}$	
Conventional	0.65	0.2	$\pi_{11} = \text{Given a thunderstorm forecast, probability of thunderstorm occurrence}$
SMS/GOES	0.75	0.15	
STORMSAT	0.80	0.1	$\pi_{12} = \text{Given a thunderstorm occurrence, probability that forecast was for clear weather}$
SEOS	0.85	0.05	

It follows directly from Table 4 that the values of  $\pi_{11}$  corresponding to all the four capability levels are greater than 0.589. Hence, the decision to optimize the benefit to the construction industry in all the four cases is to stop work if adverse weather is forecast. However, for the benefit to the society the stop work decision is optimal only in the case of STORMSAT and SEOS, while under the conventional and the SMS/GOES systems, the optimal benefit to the society is obtained if the forecast is ignored and the regular schedule for work is adhered to. This is no surprise because the stopping of work inflicts more cost to the society than to the construction company. Hence, better forecast quality is needed before stopping work in the event of an adverse forecast becomes beneficial to the society. However, in

Table 5. Geographical Distribution of Miss and False Alarm (six-hour forecast)

# of Days of Thunderstorm Occurrence	Area (Square Miles)
$N_1 = 100$	$A_1 = 4,151$
$N_2 = 90$	$A_2 = 8,302$
$N_3 = 80$	$A_3 = 20,755$
$N_4 = 70$	$A_4 = 58,114$
$N_5 = 60$	$A_5 = 99,624$
$N_6 = 50$	$A_6 = 581,140$
$N_7 = 40$	$A_7 = 747,180$
$N_8 = 30$	$A_8 = 547,932$
$N_9 = 20$	$A_9 = 249,060$
$N_{10} = 10$	$A_{10} = 282,268$
$N_{11} = 5$	$A_{11} = 66,416$

a free enterprise system, it cannot be expected that the construction industry will be motivated more by benefit considerations for the society than by the profit considerations for the industry itself. Hence it has been assumed in this study that the optimal policy is the one that maximizes the benefit to the construction industry. The benefits to the construction industry as well as the benefits to the society associated with this optimal policy under different forecast capabilities are computed.

#### VI. Estimates of Benefits

Figure 6 depicts the geographical distribution of mean annual number of thunderstorm days in the mainland of the United States.<sup>8</sup> Table 5 is the corresponding description of the approximate areas of equi-thunderstorm zones.

The areas are denoted as  $A_1$  through  $A_{11}$ , and the corresponding number of days

Table 6. Annual Expenses and Savings in the 1980s to Construction Industry and Society (billions of 1975 dollars)

Capability	T'		$\Delta T$ W.r.t. Conventional		T	$\Delta T$ W.r.t. Conventional
	Upper	Lower	Upper	Lower		
Conventional	4.683	3.547	0	0	5.308	0
SMS/GOES	4.125	3.084	0.558	0.463	5.155	0.653
STORMSAT	3.860	2.822	0.823	0.725	4.886	0.922
SEOS	3.592	2.558	1.091	0.989	4.612	1.196

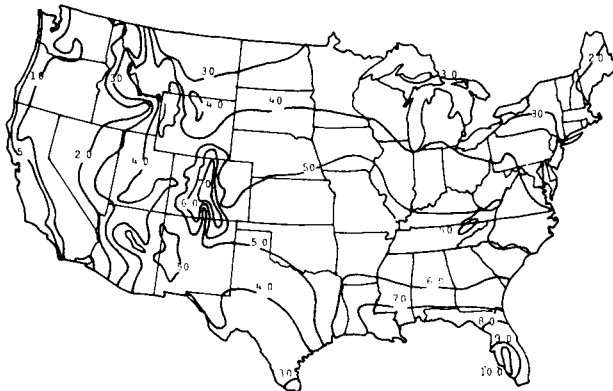


Figure 6. Geographical Distribution of Thunderstorms in Terms of Mean Annual Number of Storm Days (from Reference 10)

of thunderstorm per year are denoted as  $N_1$  through  $N_{11}$ .

In any area  $A_i$ , the number of false alarm days, the number of miss days and the number of correctly forecast thunderstorm days per year are given by Equations (10), (11) and (12) respectively, which follow directly from Equations (7), (8) and (9).

$$\alpha_i = N_i(1-\pi'_{12})(1-\pi_{11})/\pi_{11} \quad (10)$$

$$\beta_i = N_i \pi'_{12} \quad (11)$$

$$\gamma_i = N_i(1-\pi'_{12}) \quad (12)$$

From the expense matrix illustrated in Table 3, it directly follows that under the optimal decision for the construction industry,

$$J'_i = (\alpha_i + \gamma_i)(P+E+W) + \beta_i(R+E+W+P) \quad (13)$$

and

$$J_i = (\alpha_i + \gamma_i)(P+E+W) + \beta_i(R+E+W+P) \quad (14)$$

where  $J'_i$  and  $J_i$  represent the annual incremental expenses due to thunderstorm incurred by the construction industry and the society respectively per square mile area. The incremental expenses are measured relative to the usual expenses that are incurred on a regular working day under favorable weather conditions. Multiplying  $J'_i$  and  $J_i$  with the respective areas, the annual incremental expenses  $T'$  and  $T$  over the mainland of the United States incurred respectively by the construction industry and the society due to thunderstorm under the optimal decision rule are given by:

$$T' = [\pi'_{12}(R+E+W+P) + \frac{(P+E+W')(1-\pi'_{12})}{\pi_{11}}] \sum_{i=1}^{11} A_i N_i \quad (15)$$

and

$$T = [\pi'_{12}(R+E+W+P) + \frac{(P+E+W)(1-\pi'_{12})}{\pi_{11}}] \sum_{i=1}^{11} A_i N_i \quad (16)$$

Inserting the values of  $\pi_{11}$  and  $\pi'_{12}$  from Table 4,  $R$ ,  $E$ ,  $W$ ,  $P$  and  $W'$  from Table 3, and  $A_i$  and  $N_i$  from Table 5 into Equations (15) and (16), Table 6 results. The upper and the lower bounds on the values of  $T'$  and  $\Delta T'$  correspond to the two bounds on  $W'$  viz 0 and 9.563 as explained earlier. The values of  $\Delta T'$  and  $\Delta T$  are the estimates of benefits expected to accrue relative to the conventional forecast capabilities prior to the SMS/GOES launching.

#### VII. A Few Other Industries

The methodology illustrated above in relation to the construction industry has been applied to a wide range of industries. References 9 and 10 include the details on these studies. The main results are illustrated in Figure 7. In order to avoid clumsiness in presentation, the SEOS figures are omitted from this table.

#### VIII. Conclusion

The benefit figures developed in this paper are projected estimates for the 1980s expressed in terms of 1975 dollars. They indicate potential benefits that would be realizable only if all users implement their respective optimal strategies. A simplifying assumption has been made regarding the format of weather forecast, namely that the forecast consists of yes/no statements regarding the occurrence of weather events rather than their probability descriptions. The complicated decision rules and various options of protection that exist in real life have been simplified into a work/no work situation. The values of  $\pi_{11}$  and  $\pi'_{12}$  as illustrated

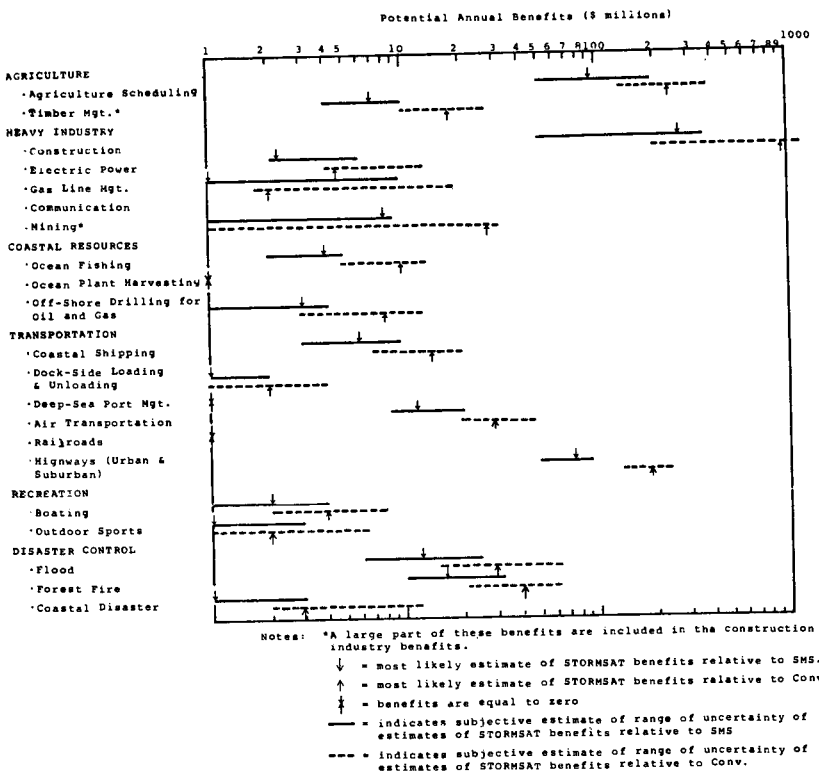


Figure 7. Summary of Potential Annual Benefits (\$ million) Including Most Likely Values and Subjective Estimates of Range and Uncertainty

in Table 4 are only approximate. As a result of all these simplifications, the numerical values illustrated in Table 6 and Figure 7 should only be considered as preliminary findings and indicative of rough order of magnitude.

The relative ranking of benefits among various industries, as illustrated in Table 7, does however, serve a useful purpose in establishing a guideline for further detailed case studies to be directed towards those industries where the expected benefits are relatively large.

3. Russo, Jr., John A., The Economic Impact of Weather on the Construction Industry of the United States, *Bulletin American Meteorology Society*, vol. 47, No. 12, December 1966.

4. Economic and Social Benefits of Weather Forecasting and Weather Related Programs, Operations Research, Inc., Technical Report #838, May 1974.

5. Weather and Construction Industry, U.S. Department of Commerce, Environmental Science Services Administration, Report #ESSA/P1 660013.

6. The Operational and Economic Impact of Weather on the Construction Industry of the United States, The Travelers Research Center, Final Report on Weather Bureau Contract Cwb-10948, March 1965.

7. Some Economic Benefits of a Synchronous Earth Observatory Satellite, Environmental Institute of Michigan and ECON, Inc., Technical Report #NASA-CR, ERIM 107400-3-F, September 1974.

#### References

1. Nelson, R.R., and Winter, Jr., S.G., A Case Study in the Economics of Information and Coordination: The Weather Forecasting System, *Quarterly Journal of Economics*, vol. LXXVIII, August 1964.
2. *Statistical Abstract of the United States - 1975*, U.S. Department of Commerce.

8. National Atlas of the United States of America
9. Economic Benefits of STORMSAT - An Initial Survey, ECON, Inc., Technical Report, NAS-5-20021, June 1975.
10. A Prospectus of Potential SEOS Economic Benefits, ECON, Inc., Technical Report, NAS-5-20940, June 1975.

# ATMOSPHERIC MODELS FOR SPACE SHUTTLE DESIGN

Clyde D. Martin

*Space Division, Rockwell International, Downey, California*

## Abstract

Atmospheric data in terms of models of individual elements such as wind, temperature, density, and precipitation must be considered in making decisions involving the planning, design, development, test, and operation of a major aerospace system. This paper discusses the atmospheric data elements and models that are of the greatest importance to the design of the Space Shuttle flight systems, the historical and philosophical reasons for the models developed for design of the Space Shuttle, the actual key atmospheric design criteria models selected for the Space Shuttle, and the sources of research data used in the models.

## Introduction

Atmospheric data models must be included in the planning, design, development, test, and operation of a major aerospace system. In many decisions, the atmospheric environment is an important factor; in some decisions, it is the dominant factor.

This paper describes those atmospheric data elements and models thereof that are of the greatest importance to the design of the Space Shuttle flight systems, the historical and philosophical reasons for the models developed for design of the Space Shuttle, and the actual key atmospheric design criteria models selected for the Space Shuttle. It also discusses sources of research data used in the models.

The paper is limited to a discussion of the use of atmospheric data for flight system design; test and operations support is omitted. Also omitted are space environment models of phenomena such as meteoroids, the ionosphere, and solar and cosmic radiation, which are also included in the design specification for the Space Shuttle natural environment.

## Atmospheric Data Used in Shuttle Design

Nearly all atmospheric elements are considered for some design aspect of the Space Shuttle. The key meteorological elements in the design of the flight systems are wind, turbulence, and the neutral-atmosphere parameters (pressure, temperature, and density). Other important atmospheric elements are precipitation, electrical potential, humidity, clouds/visibility, and sea state. Following is a brief discussion of these factors, with examples of engineering design application. Table I summarizes these elements and the design areas that they affect.

## Wind Data

Both wind speed and wind direction data are utilized in Space Shuttle design. The areas to which these data are applied are numerous, and both surface data and altitude profile representations are used. The following are among the key application areas: flight control system design, ground and flight structural load analyses, reference trajectory specification, ground activity (towing, transportation, etc.), ferry requirements, and support facilities.

## Turbulence

The relatively small-scale variations of the steady-state wind are also an important consideration in the design of the Space Shuttle. In particular, turbulence criteria models are required for flight control system design, ground and flight structural load analyses, and structural fatigue analyses.

## Neutral Atmospheres

The neutral-atmosphere data of greatest importance are temperature, density, and pressure. In some applications, models for a single element and/or a single altitude are required. Other applications require the realistic combination (hydrostatic and equation of state) of these key elements. The most important areas of application are flight control system design, structural loads, solid-fuel propulsion properties, thermal control and protection analysis, landing and stopping, external-tank icing, and reference, or nominal, trajectories.

## Precipitation

The frequency of occurrence and the durations of various rates of precipitation and the associated droplet sizes are data used in Shuttle design considerations of thermal protection system damage, runway grooving, and potential flight constraints, including the selection of an alternate landing site.

## Humidity

Humidity data are utilized in several areas of the Space Shuttle design, including analyses of external-tank icing probabilities, moisture in the graphite-epoxy payload bay doors and OMS pods, condensation in the mid fuselage, and window frosting/fogging.

Table I. Key Meteorological Elements and Application Areas in Space Shuttle Design

Wind	Turbulence	Neutral Atmospheres		
Flight control	Flight control	Flight control		
Structural loads	Structural loads	Structural loads		
Reference trajectories	Fatigue analyses	Propulsion (solid-fuel temperature)		
Ground activities (towing, transportation, etc.)	Ground activities	Thermal control, protection		
Ferry requirements		Landing & stopping studies		
Support facilities		Combined environments (external tank icing)		
		Reference trajectories		
Precipitation	Humidity	Electrical Potential	Sea State	Clouds/Visibility
TPS erosion	Icing (external tank & flight)	Stroke protection	Solid-rocket booster water entry	Photography
Flight constraints	Various subsystems	Static-charge flash	Solid-rocket booster float & tow	Landing
Runway grooving	Orbiter mid fuselage			

### Electrical Potential

Very severe lightning models are used for the Space Shuttle lightning protection criteria. Models are developed specially for a lightning stroke while the vehicle is in flight or on the ground and for static electrical flash.

### Sea State

Environmental models for sea state are exclusively associated with Space Shuttle solid-rocket booster (SRB) design analyses related to water entry and float and towback.

### Clouds/Visibility

Cloud and visibility data have applications in the Space Shuttle Program in the areas of test and operational in-flight photography, and descent and landing operations affected by icing and visual contact with the runway.

### General Atmospheric Design Criteria Models

The historical and philosophical basis for atmospheric design criteria model selection for aerospace vehicles includes the concept of design reference period\* relative to nominal, or mean, models for efficiency considerations and performance comparisons; extreme or seldom-exceeded models that ensure a low-risk (high-reliability) vehicle and minimum flight constraints; worst location, time, and altitude considerations; synthetic models for preliminary design; verification or design capability demonstration; different models for mission phases and altitude intervals; and specification and support documents. Each of these elements is covered in the following summary and briefly discussed below. These general concepts have been applied to the Shuttle design criteria specification.

### Basis of General Atmospheric Models for Design

<b>Probability Levels</b>	<ul style="list-style-type: none"> <li>• Mean values for nominal design and reference trajectories</li> <li>• Extreme or seldom-exceeded values for low-risk design or minimum constraints</li> </ul>
<b>Design Reference Period</b>	<ul style="list-style-type: none"> <li>• Annual or transitional-month values for reference trajectories</li> <li>• Worst-month values for low-risk design</li> </ul>
<b>Location Factor</b>	<ul style="list-style-type: none"> <li>• Worldwide or specific-location mean values for reference trajectories</li> <li>• Worst-location values for low-risk design</li> </ul>
<b>Altitude Factor</b>	<ul style="list-style-type: none"> <li>• Mean altitude or mean profile for reference trajectories</li> <li>• Worst-altitude or worst-profile values for low-risk design</li> </ul>

### Mean Models

Mean environmental models, sometimes referred to as reference or nominal models, are basic to the design of any

aerospace vehicle. The primary uses of such aids are as neutral-atmosphere models—to ensure a vehicle that will operate efficiently in the most frequently experienced atmospheric conditions and to provide a singular atmospheric model for the quotation of vehicle performance.

The most frequently experienced atmospheric conditions are best described by the average, or mean, values of the atmosphere, and mean values are usually selected for reference models. For worldwide operations throughout the year, mean models are frequently best fitted by midlatitude data for the transitional months of April and October.

### Low-Risk Design Models

Design of an aerospace vehicle must also ensure reliability in near-extreme or seldom-exceeded adverse conditions as well as efficiency in the atmospheric mean conditions. This is achieved by designing to seldom-exceeded adverse atmospheric conditions in order to provide low-risk probabilities under random flight requirements and/or low-constraint probabilities under non-random flight requirements.

The definition of *adverse conditions* depends on the vehicle or vehicle system. Nearly always, for example, only high winds are adverse. But in the case of temperature and other atmospheric conditions, either high or low temperatures may be adverse for different systems. Thus low-risk environmental models on both the high- and low-value side are required and for example, both the 5th and 95th percentile values are needed to evaluate the five-percent risk level for some atmospheric properties.

Additionally, such percentile values are normally specified for a design reference point such as a season or month. For example, five-percent risk values for high surface temperatures are specified for the adverse summer season (or a single representative month such as July, northern hemisphere). This may be expanded to quote the 5-percent high-temperature risk at the adverse time of day, such as 1400 local standard time, if the design application requires it.

The adverse, or design reference period, concept for low-risk design models is further expanded to the worst-location concept in cases where specific locations apply. A Shuttle example would be the launch phase, which is restricted to Kennedy Space Center (KSC) or Vandenberg Air Force Base (VAFB), and the design low-risk value would be applied to the most adverse design reference period data for either of these two locations.

Finally, adverse conditions should be biased to data for the single altitude and/or the associated altitude profile that is most important for each design problem. For example, many design cases exist for nearly vertical boost at the altitude of maximum dynamic pressure—10 to 14 kilometers.

### Synthetic and Design Demonstration Models

Because of the numerous atmospheric factors that affect the design of an aerospace vehicle, it is necessary in the preliminary design stage to select a very limited number of "synthetic" environmental models. These preliminary design models are based upon experience gained in the design and operation of previous vehicles. As the vehicle design develops, other unique problem areas will be identified, and these will require additional synthetic models that are consistent with the existing model.

Once the design is essentially completed by using the synthetic models, adequacy of the design must be analytically demonstrated for certain environmental conditions, such as wind and turbulence. This may be done by simulated flight through selected statistically representative combinations of atmospheric properties actually observed.

### Environmental Criteria Documents

The general environmental documents for aerospace vehicle development consist of broad guidelines of environmental data at various probability levels and for various geographical locations. These documents present environmental data that are divided into

\*The design reference period selected is dictated by the operational capability required for the aerospace vehicle system in terms of the expected mission(s). Depending on atmospheric element and design applications, this may be an annual, seasonal, monthly, daily, or hourly reference period (or combination thereof).

distinct sections for individual elements such as wind/turbulence, temperature, and humidity. The specification guideline data document used for Space Shuttle development is "Terrestrial Environment (Climatic) Criteria Guidelines for Use in Aerospace Vehicle Development,"<sup>1</sup> prepared by the Aerospace Environment Division of NASA's Marshall Space Flight Center. This document is occasionally augmented or revised as more recent data are received.

For a specific program, such as Shuttle, it is necessary to select risk probability levels and the associated environmental data. Because the Shuttle operational mission may be divided into well-defined phases and the atmospheric properties tend to be naturally divided into ground, boundary layer, and free-atmosphere intervals, it is appropriate to develop and to specify design criteria for mission phases and atmospheric intervals. For Shuttle, these phases are prelaunch ground, on-pad ground, lift-off, ascent/boost, orbital, descent, landing, and ferry. Thus for each atmospheric element, design criteria models are specified for each mission phase in which the element is considered to be a significant design factor. The document specifying such environmental design criteria for Shuttle is Appendix 10.10 of Volume X of "Shuttle System Specification."<sup>2</sup> "Space Shuttle Natural Environments Data Book,"<sup>3</sup> published by Rockwell International, expands the specification data of Appendix 10.10 through use of data in the NASA guideline document.

#### Atmospheric Models for Space Shuttle Design

A description of all the atmospheric models for Space Shuttle design is beyond the scope of this paper. For that reason, emphasis is placed on in-flight wind and turbulence models, and models such as ground winds/turbulence, neutral atmospheres, precipitation, temperature, and humidity are only briefly described.

#### Ground Winds (0 to 150 meters)

During the initial and intermediate phases of the Shuttle development cycle, a set of idealized, or synthetic, ground and in-flight wind models are used. The ground wind models are based upon conventional single-level ground wind observations and upon wind observations in instrumented towers. Some of the most important considerations of ground wind effects are the Von Kármán vortex shedding forces that result in lateral displacement of the vehicle and aerodynamic drag forces that result in base bending moments while the vehicle is on the pad, and vehicle drift and pitch and yaw plane angular accelerations during lift-off. Many other applications can be made in ground handling, vehicle towing, etc.

In the past, the basic treatment has been to statistically define the particular crucial aspects of the wind profile for a specified design reference period and risk of encounter. Typical considerations are where the vehicle is to operate, how long the vehicle is to be exposed, the consequences of vehicle constraints or vehicle loss, and the cost and engineering practicalities of the design criteria.

Table 2 gives an example of Shuttle ground wind design criteria, which are based on the above factors. Various risk levels and design reference period data for the worst launch-wind location—i.e., KSC—are given. Figure 1 presents the basic exposure time statistics for the reference altitude of 18.3 meters used in selecting the illustrated ground wind criteria. The profiles associated with the reference-level peak wind speed for the selected risk level are representative of the three-sigma profile shape. Thus, should the peak wind level occur, there is only a 0.135-percent chance that the peak wind will exceed the corresponding profile value at any other altitude. The steady-state wind speed values, which are representative of 10-minute mean wind speeds, are derived from the peak winds by the use of a representative gust factor.

The following equations, which represent the Shuttle ground wind design profiles, were developed by MSFC investigators<sup>2</sup>.

Peak wind speed profile values associated with the 18.3-meter-level wind speeds are given by

$$U(h) = U_{18.3} \left[ \frac{h}{18.3} \right]^{1.6(U_{18.3})^{-3/4}} \quad (1)$$

Table 2. Omnidirectional Ground Wind Models for Space Shuttle

Altitude (m)	Prelaunch, Launch, Landing HW/CW*		At Pad Unfueled**/Fueled†	
	SSW Speed (m/s)	Peak Wind Speed (m/s)	SSW Speed (m/s)	Peak Wind Speed (m/s)
10.0	9.8	15.8	21.7/14.5	34.7/23.1
18.3	11.7	17.7	24.7/16.7	37.1/25.2
30.5	13.4	19.5	27.2/18.8	39.1/27.1
61.0	16.1	22.1	31.0/21.9	42.1/30.1
91.4	17.9	23.9	33.3/24.3	44.0/31.6
121.9	19.2	25.2	35.1/25.4	45.4/33.0
152.4	20.3	26.2	36.5/26.6	46.5/34.0

HW/CW = head winds/crosswinds

SSW = steady-state winds

\*Five-percent risk, windiest one-hour exposure period, KSC, normal-wind operations

\*\*One-percent risk, windiest two-week exposure period, KSC, high-wind operations

†One-percent risk, windiest one-day exposure period, KSC, high-wind operations

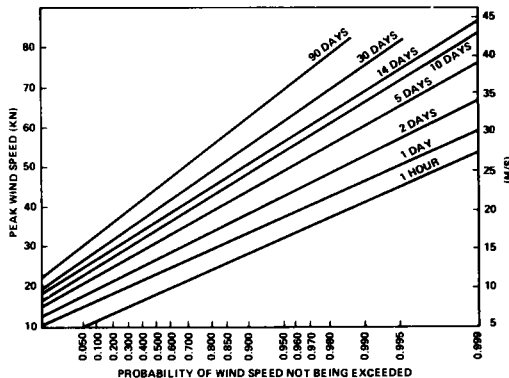


Figure 1. Cape Kennedy Peak Wind Speed for Windiest Reference Period Versus Probability for Several Exposure Periods (18.3-m Reference Level)

where  $U(h)$  is the peak wind speed at height  $h$  (in meters) above natural grade, and  $U_{18.3}$  is the peak wind speed at the 18.3-meter reference level (in m/s).

For the design steady-state ground wind profile,

$$\bar{U}(h) = U(h) \left[ 1 + \frac{(18.3/h)^{0.283} - 0.435e^{-0.2U_{18.3}}}{1.98 - 1.887e^{-0.2U_{18.3}}} \right]^{-1} \quad (2)$$

where  $U(h)$  is given by Equation 1.

#### In-Flight Wind Models

In-flight wind information for Shuttle design consists of directional synthetic wind speed profile data for selected launch azimuths, mean vector wind-profile biasing during boost, and measured profile samples for design demonstration.

#### Synthetic Wind Profile Envelopes

The synthetic wind profile, which is based upon wind data from conventional Rawinsonde observations, has long been used to present in-flight wind criteria and is well understood and generally employed in preliminary and intermediate design computations. This profile includes wind speed, wind shears (speed change with altitude), and gusts.

The synthetic wind profile provides a conditionalized wind shear/gust with respect to the given design wind speed. In Figure 2 is presented the synthetic scalar wind profile for the Shuttle

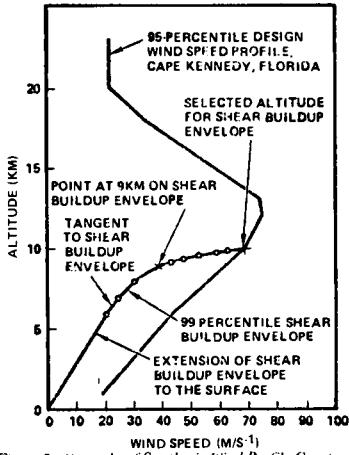


Figure 2. Example of Synthetic Wind Profile Construction.  
Without Addition of Gust

general launch design, with associated 99th-percentile wind shears and discrete gust applied to a reference altitude 95th-percentile speed profile for Cape Kennedy. Figure 3 shows an expanded-scale representation of the discrete gust, and Figure 4 presents the basic statistics used in selecting typical scalar synthetic profile design criteria.

#### Directional Steady-State Winds in Ascent

Since Shuttle will be launched only at KSC or VAFB and will have a limited number of launch headings, directional steady-state winds have also been specified for unique design reference mission launch headings, using wind statistics for the appropriate launch site. The specified directional wind design data are the five-percent risk envelopes for tail winds (TW), head winds (HW), left cross winds (LCW), and right cross winds (RCW), using the windiest monthly reference period concept. Shown in Table 3 are the specified directional wind components for appropriate Space Shuttle launch azimuths at KSC. Figures 5, 6, and 7 present examples of directional wind-speed envelope data that may be used to derive directional envelope values for any desired flight azimuth. These examples are for high-wind altitudes of 9 to 14 kilometers.

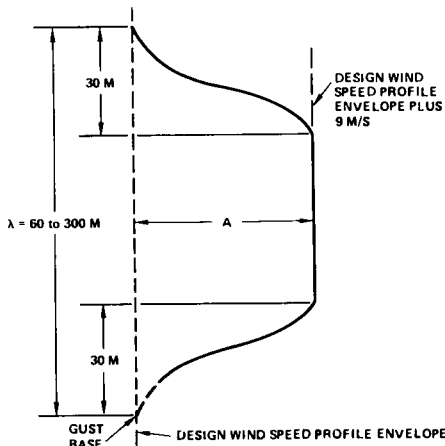


Figure 3. Relationship Between Discrete Gust and/or Embedded Jet Characteristics (Quasi-Square-Wave Shape) and the Design Wind Speed Profile Envelope

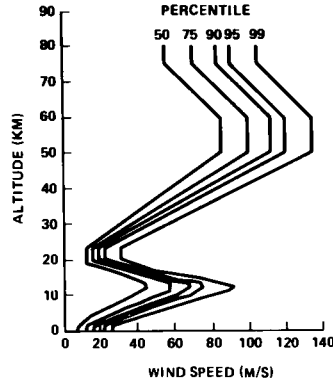


Figure 4. Scalar Wind Speed Steady-State Envelopes as Functions of Altitude for Various Probabilities for the Eastern Test Range

Table 3. Directional Wind-Speed Profile Envelopes (95th Percentile) for Selected Flight Azimuths

	PROBABILITY 50%	PROBABILITY 75%	PROBABILITY 90%	PROBABILITY 95%	PROBABILITY 99%	
ALTITUDE	SPEED	ALTITUDE	SPEED	ALTITUDE	SPEED	ALTITUDE
1	8	1	12	1	16	1
4	15	5	27	5	34	5
10	38	11	57	10	62	10
12	45	13	62	12	68	12
13	44	13	57	13	67	13
16	32	16	38	16	44	16
19	13	19	18	18	20	17
20	13	20	15	20	19	20
23	13	23	15	23	19	23
50	85	50	100	50	112	50
60	85	60	100	60	112	60
75	55	75	70	75	83	75
80	55	80	70	80	83	80

Table 3. Directional Wind-Speed Profile Envelopes (95th Percentile) for Selected Flight Azimuths

Altitude (km)	Eastern Test Range Flight Azimuth ( $\alpha$ )							
	$\alpha = 380^\circ$				$\alpha = 90^\circ$			
	Head Wind (m/s)	Tail Wind (m/s)	Right Cross Wind (m/s)	Left Cross Wind (m/s)	Head Wind (m/s)	Tail Wind (m/s)	Right Cross Wind (m/s)	Left Cross Wind (m/s)
1	12	15	11	13	12	16	13	10
2	11	19	10	17	11	21	13	10
3	10	23	8	20	10	25	14	11
4	9	26	7	24	9	30	16	11
5	10	30	7	28	9	36	18	12
6	11	35	7	31	10	42	19	14
7	11	40	8	35	10	48	21	16
8	12	44	8	39	11	54	23	18
9	13	49	8	44	11	60	24	20
10	14	54	9	50	13	65	26	22
11	17	59	10	55	15	70	28	25
12	19	59	12	56	17	72	28	28
13	22	57	13	54	19	70	27	25
14	21	51	12	48	17	63	24	22
15	18	45	10	43	15	56	21	19
16	15	39	9	37	14	48	18	17
17	12	33	9	32	12	41	15	14
18	12	28	11	26	13	34	12	11
19	12	22	13	20	16	27	9	8
20	14	16	15	15	19	20	8	8
23	14	16	15	15	19	20	8	8
40	30	60	37	59	45	78	27	14
50	44	90	55	67	62	95	38	11
58	47	95	65	77	76	112	41	20
60	47	95	65	77	76	112	41	29
75	20	60	32	55	20	30	26	10
80	20	60	32	55	20	30	26	10

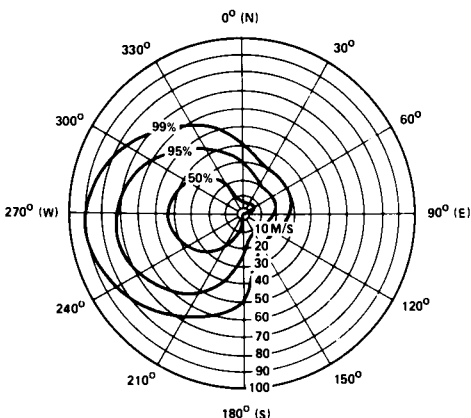


Figure 5. 10- to 14-Kilometer Altitude Layer at Cape Kennedy

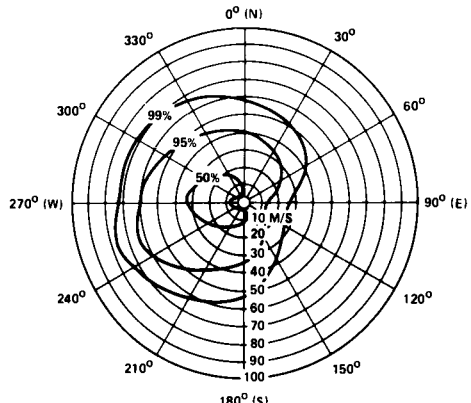


Figure 6. 9- to 13-Kilometer Altitude Layer at Edwards Air Force Base

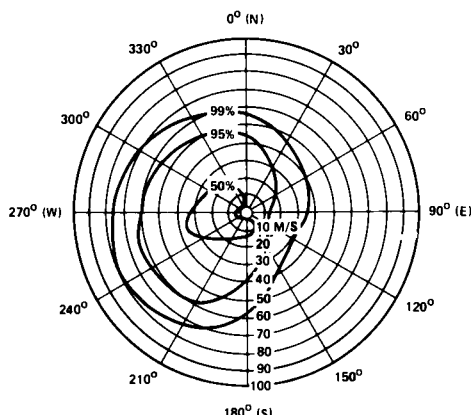


Figure 7. 9- to 13-Kilometer Altitude Layer at Vandenberg Air Force Base

#### Directional Wind-Speed Statistics

In some cases, it is desirable to bias the ascent trajectory in the vehicle pitch and yaw planes. For this event, the monthly vector mean winds at the location of launch are recommended for

Space Shuttle. The necessary wind statistics for the derivation of such biasing programs, which have been determined for each month at KSC and VAFB by personnel at MSFC, are illustrated for the windiest monthly reference period at VAFB (December) in Table 4.

Table 4. Design Directional Steady-State Wind Profile Parameters Between 27- and 1-Kilometer Levels, December, Vandenberg AFB

Altitude (km)	$\bar{u}$ (m/s <sup>-1</sup> )	$\bar{v}$ (m/s <sup>-1</sup> )	$s_u$ (m/s <sup>-1</sup> )	$s_v$ (m/s <sup>-1</sup> )	$r(u, v)$ (nondimensional)
0	0.33	-0.96	2.88	3.10	-0.4632
1	1.39	-2.33	4.60	6.95	-0.0455
2	4.00	-3.15	5.96	8.18	0.0494
3	7.02	-3.68	7.71	9.76	0.0939
4	9.92	-4.29	9.66	11.65	0.1008
5	12.44	-4.72	11.27	13.20	0.1619
6	14.63	-5.17	12.78	15.05	0.2405
7	16.84	-5.65	14.57	17.06	0.3057
8	18.98	-5.72	16.15	18.61	0.3564
9	21.06	-5.91	17.42	20.21	0.3768
10	23.04	-5.73	18.07	21.21	0.4026
11	24.60	-5.38	17.61	20.91	0.3793
12	24.91	-4.36	16.09	18.99	0.3987
13	24.24	-3.23	14.46	16.28	0.3938
14	22.52	-2.29	12.18	13.90	0.4196
15	20.21	-1.94	10.38	11.73	0.4205
16	17.03	-1.73	9.17	9.81	0.4241
17	13.85	-1.55	8.15	8.33	0.4530
18	10.21	-1.66	6.91	6.39	0.4977
19	6.98	-2.07	6.06	5.02	0.4693
20	4.62	-2.39	5.99	4.33	0.3912
21	2.63	-2.63	5.94	4.11	0.3041
22	1.17	-2.55	6.25	3.96	0.3503
23	0.32	-2.57	6.92	3.75	0.2671
24	0.13	-2.79	7.21	3.65	0.2404
25	-0.19	-2.59	7.75	3.59	0.3049
26	-0.01	-2.62	8.86	3.97	0.3413
27	0.76	-2.74	10.56	4.66	0.3790

The basic statistics for the derivation of directional, or vector, wind criteria may be seen in Table 4 to be the zonal component,  $u$ , and the meridional component,  $v$ , of the vector wind. The  $u$  and  $v$  components thus represent the wind components along and normal to the vehicle axis, respectively, for a flight azimuth  $\alpha = 90$  degrees clockwise from north.

For any flight azimuth,  $\alpha$ , the corresponding basic statistics become

$$\bar{u}_\alpha = \bar{u} \cos(90 - \alpha) + \bar{v} \sin(90 - \alpha) \quad (3)$$

$$\bar{v}_\alpha = \bar{v} \cos(90 - \alpha) - \bar{u} \sin(90 - \alpha) \quad (4)$$

$$s_{u\alpha} = \left[ s_u^2 \cos^2(90 - \alpha) + s_v^2 \sin^2(90 - \alpha) + 2r(u,v)s_u s_v \cos(90 - \alpha) \sin(90 - \alpha) \right]^{1/2} \quad (5)$$

$$s_{v\alpha} = \left[ s_v^2 \cos^2(90 - \alpha) + s_u^2 \sin^2(90 - \alpha) - 2r(u,v)s_u s_v \cos(90 - \alpha) \sin(90 - \alpha) \right]^{1/2} \quad (6)$$

The flight azimuth,  $\alpha$ , is in degrees clockwise from north and is the heading of the orbiter. The statistical parameters,  $\bar{u}$ ,  $\bar{v}$  and  $s_u$ ,  $s_v$ , and  $r(u,v)$ , are the means, standard deviations, and correlation coefficients, respectively. The coordinate system used produces a positive  $u$ -component tail wind, a negative  $u$ -component head wind, a positive  $v$ -component right-to-left cross wind, and a negative  $v$ -component left-to-right cross wind.

These statistics are also used to derive directional wind profiles for the Shuttle descent wind model of the altitude region between 27 kilometers and 1 kilometer. The Space Shuttle descent directional wind model is expressed in terms of the 99th-interpercentile range of the wind components through use of the following relationships:

$$u(\alpha) = \bar{u}_\alpha \pm 2.5758 s_{u\alpha} \quad (7)$$

$$v(\alpha) = \bar{v}_\alpha \pm 2.5758 s_{v\alpha} \quad (8)$$

Equations 6 and 7 produce four distinct wind profiles. The two  $u(\alpha)$  profiles bound the 99th-interpercentile range of wind components longitudinally with respect to the flight azimuth; the two  $v(\alpha)$  profiles bound the 99th-interpercentile range of wind components normal to the flight azimuth.

An example of model wind profiles for sectors, which include a range of azimuths at VAFB, derived by using the statistics of Table 4 is shown in Figure 8. These profiles are used in analyses of descents at VAFB. Similar data are derived for KSC descents by using the worst-month reference period statistics (February) for KSC.

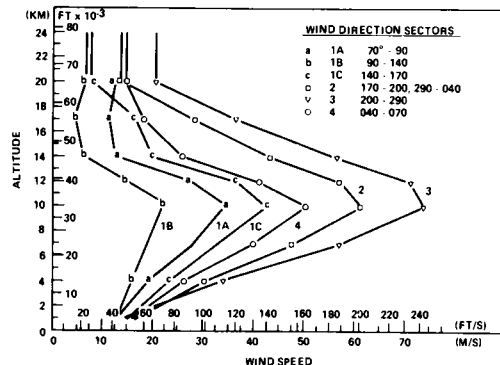


Figure 8. December Wind Profiles for Vandenberg Air Force Base

Another application of directional wind component statistics to Space Shuttle is the construction, at any altitude, of vector ellipses that contain a selected percentage of the wind vectors. Assuming that the wind components are bivariate normal distributions, the five statistical parameters may be used to determine the probability ellipse containing the design percentage of the wind vectors. These statistics are used in conjunction with the mean wind in wind biasing for Shuttle ascent trajectories. For example, dispersions from the mean vector wind (center of the ellipse) used for biasing may be determined by employing ellipses such as those illustrated in Figure 9. Further, monthly wind vector winds may be combined with the associated monthly solid-rocket booster temperatures to obtain realistic reference ascent trajectory data. Figure 10 presents such mean vector wind profile data for KSC, February, which were developed from the directional component wind statistics. The development of conditional statistics for

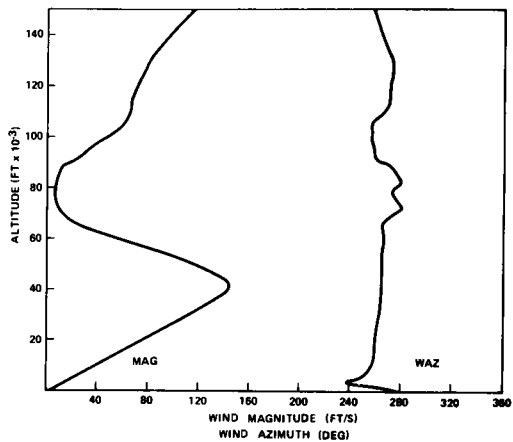


Figure 10. February Winds at Cape Kennedy

vector shears, which require the expansion of the basic statistics to include interlevel wind component parameters, is a recent development in this area.

#### Wind Shears

The current wind shears to be combined with the Shuttle directional steady-state wind profiles consist of tabular values of 99th-percentile shears versus steady-state wind speed. Different shear tables exist for each of the ascent/descent locations. The method of applying such shears at a selected reference altitude is shown in Figure 2, and an example of prescribed wind shears is presented in Table 5. Both buildup and backoff shears are illustrated.

#### Turbulence Models

Turbulence criteria, in the form of gust data, are specified for Space Shuttle for both ground (0 to 150 meters) levels and in-flight levels of ascent and descent. Gusts are defined as the sudden increases (or decreases) in wind speed and are stated with respect to the steady-state, or mean, wind speed.

Two distinct and independent types of gust model criteria are specified for Space Shuttle. The first is the so-called discrete gust model, in which a single large-amplitude gust is superimposed upon the steady-state wind. The discrete gust model includes a specification of gust magnitude, length, and shape. Different discrete gust models are specified for ground and in-flight phases. Figures 2 and 3 illustrate the design discrete gust model for vertical flight phases.

The second gust model used for Space Shuttle is the continuous, or spectral, type, which specifies the characteristics of the superposition of small-scale motions of random frequencies. Different spectral models are specified for the ground (boundary layer) and in-flight altitudes (above 300 meters). Gust criteria are applied directly to the design steady-state wind profiles; but if it is desirable to combine steady-state winds, wind shears, and gusts in flight, the design wind shears and/or gusts are reduced before being combined. This accounts for a correlation coefficient of less than unity between design shears and gusts.

The discrete gust model for vertical flight is illustrated in Figure 2. The spectral gust model for ascent has the following spectral density function:

$$E(k) = \frac{683.4 (4000k)^{1.62}}{1 + 0.0067(4000k)^{4.05}} \quad (9)$$

The spectrum  $E(k)$  is defined such that integration over the domain  $0 \leq k \leq \infty$  yields the variance of the turbulence.

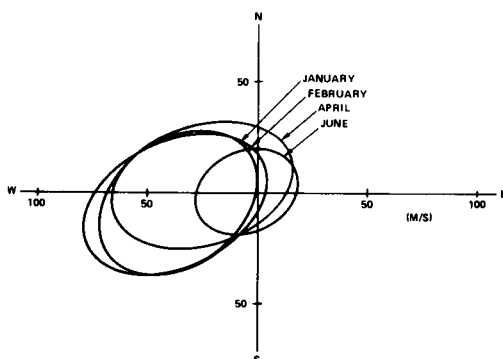


Figure 9. Eastern Test Range Wind Ellipses at 10 Kilometers (95th Percentile)

Table 5. Design Envelopes of 99th-Percentile Scalar Wind-Speed Change, 1- to 80-Kilometer Altitude Region, Eastern Test Range

Wind Speed at top of Altitude Layer (m/s)	Scales of Distance (m)									
	5000	4000	3000	2000	1000	800	600	400	200	100
Buildup										
≤ 90	65.6	59.5	52.3	43.5	34.0	29.0	23.8	17.9	11.2	6.8
80	60.4	55.5	49.7	42.0	32.7	27.7	22.7	17.0	10.6	6.5
70	56.0	51.7	47.0	40.4	31.2	26.6	21.8	16.4	10.1	6.2
60	51.3	48.5	44.5	38.6	30.0	25.6	21.1	15.8	9.8	6.0
50	46.5	45.0	41.2	36.5	28.5	24.4	20.0	15.0	9.2	5.7
40	38.5	37.7	36.8	34.9	26.5	22.6	18.5	13.8	8.6	5.3
30	28.0	27.5	26.5	24.5	20.8	17.8	14.5	10.8	6.7	4.1
20	17.6	17.3	16.6	15.8	14.6	12.5	10.2	7.2	4.7	2.9
Backoff										
≤ 90	77.5	74.4	68.0	59.3	42.6	36.4	29.7	22.4	13.8	8.5
80	71.0	68.0	63.8	56.0	40.5	34.7	28.5	21.4	13.2	8.1
70	63.5	61.0	57.9	52.0	38.8	33.1	27.0	20.3	12.5	7.7
60	56.0	54.7	52.3	47.4	36.0	31.0	25.3	18.9	11.7	7.2
50	47.5	47.0	46.2	43.8	33.0	28.3	23.2	17.5	10.7	6.6
40	39.0	38.0	37.0	35.3	29.5	25.3	20.6	15.5	9.6	5.9
30	30.6	30.0	29.4	16.9	22.6	19.4	15.8	11.9	7.3	4.5
20	18.0	17.5	16.7	15.7	14.2	12.2	9.9	7.5	4.6	2.8

For descent and landing phases with significant horizontal motion, the Shuttle orbiter spectra turbulence model is that of a Dryden spectral model with the following longitudinal (u), lateral (v), and vertical (w) density functions:

$$\text{longitudinal: } \phi_u(\Omega) = \sigma^2 \left( \frac{2L}{\pi} \right) \frac{1}{1 + (L\Omega)^2} \quad (10)$$

$$\text{lateral and vertical: } \phi_{v,w}(\Omega) = \sigma^2 \left( \frac{L}{\pi} \right) \frac{1 + 3(L\Omega)^2}{[1 + (L\Omega)^2]^2} \quad (11)$$

The design criteria are established by specifying values for the quantities  $\sigma$  and  $L$ , which denote the standard deviation and integral scale of the turbulence. The specified values of  $\sigma$  and  $L$  are functions of the atmospheric characteristics and the lifetime of exposure to turbulence.

#### Neutral-Atmosphere Models

Neutral-atmosphere models provide important design criteria for Space Shuttle. Mean, or reference, atmospheres, represented by mean atmospheric properties, are used in reference trajectory computations. Near-extreme or seldom-exceeded hot and cold atmospheres are used to compute dispersions from mean conditions and to provide vehicle system designs that will operate in adverse conditions. For Shuttle, the atmospheres of maximum interest are those of ascent and orbiter descent, near altitudes of maximum dynamic pressure and heating. The neutral atmospheres for Shuttle have been developed in the conventional manner of specifying a temperature profile and a surface pressure; then computing pressure values from the hydrostatic equilibrium equations; the general gas law is used to compute density values from the temperature and pressure values.

Since Shuttle ascent will be essentially vertical from KSC and VAFB, the ascent atmospheres of interest are limited to those launch sites. For test purposes, the atmospheres of Edwards Air Force Base are also of interest and have been developed.

Orbiter entry from 120 to 30 kilometers involves a significant horizontal trajectory, and the neutral atmospheres for a single location are inadequate. The preliminary design atmospheres incorporate the USSA'62 as the mean atmosphere, with dispersions therefrom based upon extreme density as a function of month and latitude versus altitude. Through the use of such data, density dispersions for any entry trajectory of altitude may be developed for any month.

The Four-D Global Reference Atmosphere (GRA)<sup>4</sup>—in which the term *four-D* refers to latitude, longitude, and altitude plus time—is a recent development in the area of neutral atmospheres. The GRA generates values for pressure, density, temperature, and wind, from surface levels to orbital altitudes. The computer program output includes monthly and annual mean values, quasi-biennial oscillations, and random perturbations, to simulate partially the variability about mean values due to synoptic, diurnal, planetary, and gravity wave variations. This model has been used to generate altitude profiles at a given location or atmospheric parameters along a simulated trajectory through the atmosphere. Figure 11 illustrates a GRA-profile output during the initial portion of a July, Mission 3 entry-and-return trajectory, while Figure 12 shows a GRA-generated monthly mean temperature profile for Cape Kennedy.

Table 6 summarizes the design neutral atmospheres for Shuttle.

#### Thermal Models

Numerous thermal models are required for Shuttle design, with emphasis on ground-level temperatures. Among these are

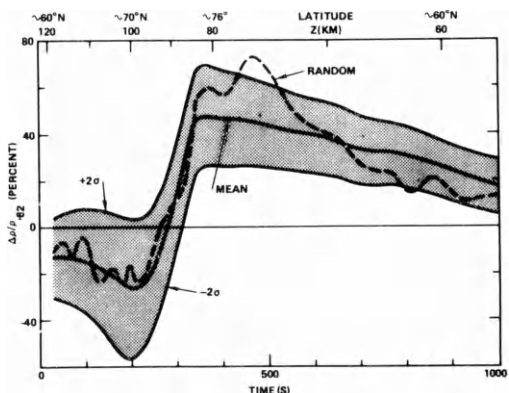


Figure 11. Density Along a July, Mission 3 Reentry and Return Trajectory

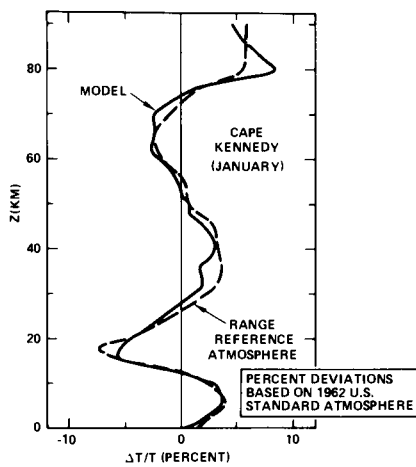


Figure 12. GRA-Generated January Mean Temperature for Cape Kennedy

statistical frequency distributions of temperature on an hourly, monthly, or annual basis at launch, test, and recovery sites, for applications such as runway heating of orbiter tires during landing, temperature and wind combinations conductive to ice formation on the external tank before lift-off, and solid-rocket motor (SRM) propellant temperatures which affect thrust. Figure 12 shows an example of hot thermal models at the 95th-percentile level at KSC that are used in various applications requiring high temperatures for varying time periods. VAFB is a cold site compared with KSC, and similar cold thermal models at the 5th-percentile level at VAFB are used. It should be noted that the seldom-exceeded hot SRM propellant temperatures referred to above are approximated by the 30-day average temperatures in Figure 13.

Table 7 presents the basic ground thermal environment design model for air temperature, solar radiation, and sky temperature limits.

#### Precipitation Models

Precipitation models for Shuttle design applications involve requirements for precipitation probabilities, rates, and total

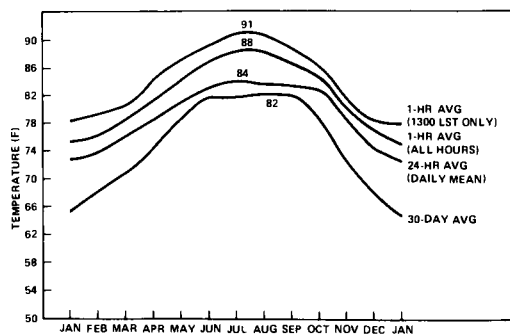


Figure 13. 95th-Percentile Values for Various Time Periods  
(Cape Kennedy)

Table 7. Ground Thermal Environment

Thermal Factor	Ferry Sites	Vertical Flight
Air temperature (F)		
Design high	103	99
Design low	20	31
<hr/>		
Sky temperature (F)		
Design high		50
Design low	-22	5
<hr/>		
Solar Radiation		
Time of Day	Design High	Design Low
0500	0	0.00
1100	363	1.64
1300		70
1400	363	1.64
2000	0	0.00
	Btu/ft <sup>2</sup> /hr	gm-cal/cm <sup>2</sup> /min
	Btu/ft <sup>2</sup> /hr	gm-cal/cm <sup>2</sup> /min

Table 6. Neutral Atmospheres for Space Shuttle

Mission Phase	Nominal or Reference Data	Extreme or Dispersion Data
Launch to orbit		
KSC	PRA'63	KHA'71, KCA'71
VAFB	VRA'71	VHA'73, VCA'73
Orbiter entry (90 to 30 km)	USSA'62, USSA'66	Tabular density extremes (for seasons, latitudes vs. altitude)
Orbiter entry (30 km to landing)		
KSC	PRA'63	KHA'71, KCA'71
VAFB	VRA'71	VHA'73, VCA'73
Special Analyses		
Approach and landing test(ALT)	EPA'75	EHA'75, ECA'75
Orbital flight test (OFT)	EPA'75	EHA'75, ECA'75
Worldwide entry analyses	4-D GRA	4-D GRA

#### Legend

- USSA'62 - U.S. Standard Atmosphere. 1962
- CIRA'65 - COSPAR International Reference Atmosphere. 1965
- USSA'66 - U.S. Standard Atmosphere Supplements. 1966
- PRA'63 - Kennedy/Patrick AFB Reference Atmosphere. 1963
- KHA'71 - Cape Kennedy Summer (Hot) Atmosphere. 1971
- KCA'71 - Cape Kennedy Winter (Cold) Atmosphere. 1971
- VRA'71 - Vandenberg AFB Reference Atmosphere. 1971
- VHA'73 - Vandenberg AFB Summer (Hot) Atmosphere. 1971
- VCA'73 - Vandenberg AFB Winter (Cold) Atmosphere. 1973
- ERA'75 - Edwards AFB Reference Atmosphere. 1975
- EHA'75 - Edwards AFB Summer (Hot) Atmosphere. 1975
- ECA'75 - Edwards AFB Winter (Cold) Atmosphere. 1975
- 4-D GRA - Four-Dimensional Global Reference Atmosphere

amounts. Among the design questions to which such data have been applied is the probability of rain and hail encounters during launch and descent. These encounters and probabilities are important for their potential impact on the orbiter's thermal protection system, requirements for and design of runway grooves for orbiter landings, and precipitation models for analyzing external-tank icing.

#### Electrical-Discharge Model

A very severe lightning discharge model is specified for Space Shuttle (Figure 14), with the objective of ensuring operations under conditions of triggered or other atmospheric electrical discharges during prelaunch, launch, and flight operations. A separate lightning protection criteria document has been prepared by a special Shuttle Lightning Protection Committee.<sup>5</sup>

#### Atmospheric Data Sources

The development of atmospheric design models depends upon meteorological data developed by numerous organizations in the form of basic conventional observations, climatological summaries, research observations and analyses, and environmental manuals. Various governmental agencies perform most of the tasks associated with these contributions.

For Space Shuttle, NASA has utilized the Aerospace Environment Division of the Marshall Space Flight Center to develop natural-environment design criteria for the Johnson Space Center's Space Shuttle Program Office. The USAF Air Weather Service and Rockwell International have also participated in this development. Table 8 illustrates the basic observations used.

Mention should be made of some atmospheric research activities that have made major contributions to Space Shuttle atmospheric design criteria. In particular, the research that led to the development of rockets and satellites as atmospheric probes has provided otherwise unaccessible observations; the development of nominal reference atmospheres such as the COSPAR Inter-

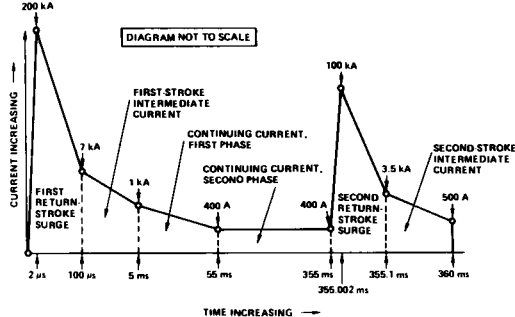


Figure 14. Diagrammatic Representation of a Very Severe Lightning Model

national Reference Atmosphere (CIRA), the Meteorological Rocket Network (MRN) Range Reference Atmospheres, and the U.S. Standard Atmospheres has contributed importantly to model atmospheric criteria; the JIMSPHERE balloon and improved radars have contributed significantly to improvements in in-flight turbulence criteria; and the Four-D Global Reference Atmosphere research has resulted in greater knowledge of atmospheric phenomena encountered along an entry trajectory. This extremely limited list of research projects should be considered only as a representative sampling, since any increase in knowledge of the atmosphere eventually leads to improved environmental design criteria. And improved criteria ensure more reliable aerospace vehicles and lower costs, by precluding the overdesign or underdesign that would result from inadequate knowledge of the atmosphere.

Table 8. Atmospheric Data Sources for Shuttle Design Models ( $P$ ,  $T$ ,  $\rho$ , Winds, Humidity, Weather, Visibility, Clouds, Sea State)

Conventional Observations	Climatological Data	Research/Special Observations
Surface Synoptic All elements Hourly, every 3 hours Standard locations	Surface Revised uniform summary of surface weather observations Surface climatological information Shuttle launch and entry locations NASA CR61342 NASA CR61319	Surface Special locations Special times Special elements (turbulence, etc.) Special equipment
Upper air to 27 km Synoptic Every 12 hours $P$ , $T$ , $\rho$ humidity, winds Balloons	Upper air to 27 km Revised uniform summary of Rawinsonde observations	Lower atmosphere Special locations, times, elements Special equipment/systems towers Fixed balloons, satellites
Upper air, 27 to 90 km MRN rockets	Upper air 27 to 90 km Data reports, meteorological rocket network firings	Upper air to 27 km Special locations, times, elements Special equipment Balloons Aircraft Satellites
		Upper air, 27 to 90 km Research rockets Satellites

#### References

1. *Terrestrial Environment (Climatic) Criteria Guidelines for use in Aerospace Vehicle Development, 1973 Revision*, ed. by G.E. Daniels. NASA TM X-64757 (July 1973).
2. *Natural Environment Design Requirements* Vol. X, Appendix 10.10 (Aug. 1975).
3. C.D. Martin. *Space Shuttle Natural Environments Data Book* SD 73-0025C (July 1976).
4. Justus, C.G. et al. *Four-D Global Reference Atmosphere*. NASA TM X-14871 (Sept. 1974).
5. *Space Shuttle Lightning Protection Criteria Document*. NASA JSC-07636 (1973).

#### Acknowledgment

The author acknowledges with appreciation the assistance of William W. Vaughan, of NASA's Marshall Space Flight Center, who reviewed the paper and made valuable suggestions for its improvement.

# SPACELAB NEW TOOL FOR RESEARCH AND INVESTIGATIONS IN SPACE

Roy Gibson and Douglas R. Lorc\*

*Director General, European Space Agency, Neuilly sur-Seine, France  
\*NASA Director of Spacelab Program, Washington, D.C., USA*

## Abstract

Spacelab was conceived to provide a ready access to space for a broad community of scientists and engineers. As an integral part of the Space Shuttle transportation system it will provide a platform for orbital experimentation that will permit radically new approaches to space exploration and exploitation. This unique ESA-NASA venture is described from the point of view of programme management, the concept, and what Spacelab has to offer the user. The operational aspects of Spacelab payloads, that permit considerable user involvement, are described and some typical applications of this new tool are presented.

## I. Introduction

In July 1980 Spacelab will be taken into low-Earth orbit by the Space Shuttle for an orbital mission that will last about seven days. This event will mark the culmination of a unique development programme and the start of a new era of space exploration. Spacelab is being developed in Europe, with European funds, as part of NASA's Space transportation system. Its introduction as an operational tool will revolutionize our approach to space activities since it embodies the principles of reusability and permits the experimenter to operate his (or her) equipment in a veritable space laboratory.

The Orbiter/Spacelab system (Figure 1) must be regarded as an entity that provides an orbital platform for experiments in a wide variety of scientific, applications and technological fields. Because of the design and operational intimacy of the two elements, Spacelab derives many of its merits from the Orbiter vehicle (e.g. basic resources, flight parameters, orientation) but must also conform to certain constraints imposed by it (e.g. dimensions, landing weight limitation, center of gravity restrictions).

The present concept of Spacelab is derived from previous studies performed by ESA and NASA on the most suitable means of meeting the many and varied needs of potential users of the Space Shuttle, from both sides of the Atlantic. As background, the major Spacelab objectives and principal programme requirements are presented in Figures 2 and 3 respectively. It is in keeping with the overall theme of this Congress that the attributes and modus operandi of Spacelab be presented, so that its potential as an international orbital facility be fully appreciated.

## II. Spacelab Programme

The European Space Agency (ESA), acting on behalf of its Member States, is responsible for

the design, development and manufacture of the Spacelab system. NASA provides technical support to the programme, as mutually agreed, and will be responsible for the operation of Spacelab as part of the Space Shuttle. The main hardware development contract has been assigned to a European industrial team led by the German company VFW-Fokker/ERNO as prime contractor. The management of such a joint venture, with its many interfaces and ramifications, presents a number of new and challenging problems. The management organization that has been established to ensure the fulfilment of the Spacelab programme is depicted in Figure 4. Spacelab Directorates have been set-up at ESA and NASA with the function of discharging each side's responsibilities. A joint Spacelab Working Group, containing representatives from ESA and NASA, co-ordinates top-level actions which affect the interests of both Agencies.

As we are now just four years from first flight, the Spacelab programme is near the peak of its definition and design activity with nearly 2000 persons actively involved in Europe. A summary schedule and some important milestones for the remaining part of the programme are given in Figure 5. The criticality of our present circumstances (at the time of writing) is evident from the fact that we are between two important milestones - Preliminary Design Review A and B. The latter review will lead to a go-ahead for final development activities with a frozen design baseline. The Critical Design and Qualification Review is another important milestone since it formally establishes the final production baseline for the Spacelab flight unit, ground hardware and related software. A fully functional engineering model will be provided to NASA by early 1979 and the flight unit will be delivered one year before the scheduled first flight. The summary schedule exhibits parallel subsystem and system development with maximum use is made of early test data obtained at subsystem unit level.

In accordance with the ESA-NASA Memorandum of Understanding on the Spacelab Programme, ESA undertakes to deliver the hardware and software items listed in Figure 6 and ensures that a follow-on production capability is preserved in Europe. Additionally, ESA will provide for preliminary integration of ESA-supported experiments that are destined for flight aboard Spacelab.

Concurrent with ESA's development and production activities NASA has been preparing the operational base needed to assume its role as Spacelab operator. This planning provides for NASA post delivery operations, encompassing such support activities as crew training, experiment

integration, experiment flight software, launch site operations, orbital operations and data acquisition and processing. In addition NASA will design and develop a limited number of components, such as the crew transfer tunnel, needed to interface the Spacelab with the Orbiter.

### III. Spacelab System

As a result of the intense activity in both ESA and NASA over the past year on design of the Spacelab, the system is emerging from its conceptual phases to a firm system configuration. In Figure 7 the three modes in which the Spacelab can be configured, namely the pressurized module mode, the pallet-only mode, and the combination pressurized module and pallet assembly are shown. These configurations, while used to indicate the range of flexibility of the system, by no means describe all of the possible configurations. In total, thirteen configurations of the Spacelab are possible. It is this flexibility to the user that underscores the meaning of the title of this paper, a tool for research and investigations in Space. Figure 8 displays the external features of both the pressurized module and the pallet. For pallet-only configurations, an "Igloo", a pressurized cylinder attached to a pallet, is provided for installation of certain subsystem hardware. Recent major changes that have been made to the system are a revised tunnel configuration, the new utility interfaces in which the utility bridges have been eliminated in favor of cable connections and a change in the igloo from a horizontal position. Moreover, the size of the igloo has been increased significantly both in diameter and in length.

The in-board profile of the pressurized module as it existed subsequent to PDR-A is shown in Figure 9. Certain changes have been made recently viz. increasing the size of the feed-throughs in the equipment racks and to certain avionics designs and airlock configurations. Figure 10 depicts the major elements of Spacelab and illustrates modular design which permits a wide range of flexibility in its utilization. This flexibility gives to Spacelab unique characteristics for the users. Three typical Spacelab configurations which illustrate this flexibility are shown in Figure 11.

In a survey paper of this nature, it is impossible to describe the subsystem design in any detail. For this reason only one illustration to describe the characteristics of the Spacelab subsystems is possible. These are described in Figure 12 where the characteristics of the major subsystems, namely the Air Revitalization System (ARS), the Command and Data Management System (CDMS), the Electrical Power Distribution System (EPDS), and the Environmental Control System (ECS) are displayed. Shown are the amounts of resources which are provided by Spacelab and the Orbiter. In all cases maximum use is made of Orbiter resources.

### IV. Spacelab Support to User

It has always been the intent of the Spacelab

programme that the developed concept would satisfy the needs of a broad community of users. This has been achieved by a prudent choice of Orbiter- and Spacelab- provided resources. Orbiter provisions for the Spacelab user are summarized in Figure 13. The Spacelab subsystems provide basic services for operating Spacelab itself and for its payload. Although a raw resource might be provided by the Orbiter, the Spacelab subsystem equipment ensures that the resource is conditioned so that it is available in a form compatible with the needs of the user. The total Spacelab capability for supporting user experimentation is summarized in Figure 14.

Consistent with meeting the major programme requirements, Spacelab is a build-to-cost project. Thus, in the course of the programme, particularly in the harsh light of meeting development schedules and a hardening financial environment, some reductions in requirements have had to be made. The net result has been the deletion of some Spacelab features that were foreseen during the more idealistic definition phase. These measures mean that the following items will not be delivered as part of the Spacelab programme - aft airlock, peaking battery and a second engineering model. It is stressed that some form of equivalent facility already exists on Spacelab and provisions in the design have been ensured to permit the future addition of any of the above items.

Reference to the services provided indicates that the user needs are satisfied by the system. Further, the CDMS capability has been improved considerably over the original concept, a capability for remote control of subsystems has been included in the concept, and a high rate data multiplexer has been added to ensure accommodation of simultaneous high rate data sources.

As part of Spacelab, a high precision Instrument Pointing Subsystem (IPS) is provided for orientation of scientific instruments for Earth, solar and astronomy experiments. The IPS, illustrated in Figure 15, employs the "inside-outside" principle so that the gimbal system does not restrict the diameter of the instrument to be pointed. Optical sensors, either located on the payload itself or on the body of the IPS, together with 3-axis gimbal system ensures high precision pointing accuracy and stability. Instruments of up to 5000 kg mass and 2m or greater in diameter can be pointed with arc sec accuracy. The IPS is now under development and delivery is scheduled for 1980. It is planned that the necessary integration and testing will be performed in time for the IPS to be included as part of the second Spacelab payload.

Apart from the physical and functional support provided to the user, it is the mode of preparation and operation of experiments that is a particularly attractive feature of Spacelab. In this context, the following points (summarized in Figure 16) should be cited.

- Reusability permits reflight of equipment in the same or modified form which, in turn, can lead to extended observation programmes; also the need for high reliability equipment is reduced.

- Manned attendance, if required, leads to the efficient performance of routine observations and the full exploitation of unexpected events.

- Spacelab provides a "shirt-sleeve" environment laboratory in space which, through the use of standard services (e.g. power, 19" racks), the large weight and volume available, and the relatively benign environment, can use Earth laboratory-type equipment.

- Men or women experimenters can be accommodated without the need for extensive astronaut-type training.

- Spacelab experiments may be performed in the module or directly exposed to space on the pallet and can be controlled from on-board or from the ground; the latter point means that groups of scientists may be involved with real time access to computers and data banks.

- Short experiment gestation times (i.e. time from conception of experiment to delivery of results) are involved; these are of the order of months rather than years normally associated with automatic satellites.

- The off-line integration and check-out of experiments, permissible because of the roll-out concept illustrated in Figure 17, means that experiment integration schedules may be optimized and leads to the assignment of active roles to the users throughout the complete experiment cycle.

- Mission flexibility through the modular design and the range of flight parameters provided by the Space Shuttle.

- The use of universal facilities (e.g. large furnace or telescope) developed on international funds by simple "behind-the-focus" type experiments.

- Relatively low cost experimentation resulting from shared launches, less constrained development and the use of universal facilities.

#### V. Relaxed Design Requirements for Experiments

Consistent with the intent to make experiment design as inexpensive as possible to the user, the Spacelab programme has adopted a policy of relaxed design requirements for experiments. These requirements have been established based on the experience gained on both sides of the ocean in both manned and automated spacecraft programmes. Table I shows the relatively benign environmental parameters such as shock, acoustics, vibration for Spacelab with which the experiment design must be compatible. In addition, the design of the racks, pallets, and remote acquisition units have been designed with the intent of making them as similar to ground-based equipment as possible. Standard single and double 19" racks are provided for the user with the remote acquisition units located in each rack providing up to 128 sensor terminals per RAU. In addition, every advantage to the on-board crew has been evaluated in terms of visibility, ease of operations and accessibility such that the payload specialist crew member will find his familiarization and learning process as simplified as possible. The Spacelab air circulation system will include provisions for contaminant control

within the pressurized module. In the area of materials control, an approach to materials has been incorporated which represents a significant contribution to reduce risk and cost to the user. Table II summarizes these material control requirements as they are presently defined.

Relaxed design however does not denote increased risk or reduced safety assurance for payloads. In this area both the NASA and ESA have taken major steps in the definition of and approval of a major safety policy for the space transportation system. The major elements of this document are contained in Table III.

#### VI. Operations

The major emphasis to date in the Spacelab programme has been to ensure that the design reflects the requirements necessary to serve the varied potential user community. More recently, considerable attention has been and is being given to planning the operational usage of Spacelab and the setting up of organizations for its use. It is intended that the mode of operation of Spacelab will lead to low cost utilization hence many new approaches will be adopted and some radical changes to past procedures (e.g. those associated with Apollo and Skylab) are anticipated. In particular, simplified management procedures, reduced documentation, and more direct involvement of the experimenter in the experiment cycle are foreseen. NASA and ESA are currently involved in preparation for a joint simulation of a Spacelab flight using a CV-990. This flight is planned for mid-1977 and it will exercise many of the simplified management, documentation and integration procedures to be adopted for Spacelab.

NASA has the major responsibility for the operation of Spacelab as part of the Space transportation system. Two essentially different aspects are evident - ground operations and flight operations. Ground operations involve the processing of the Spacelab elements and its experiment equipment up to the moment of launch and the post-flight handling of data. Flight operations refer to all the activities, both on-board and on-the-ground support, relevant to the execution of the on-orbit mission itself. The various elements of the two operational phases are depicted in Figure 18.

The principal activities involved in the ground operations are Spacelab refurbishment and configuration build-up, payload integration and payload specialist training. Four levels of Spacelab/Payload integration have been defined and are summarized in Figure 19. Levels I through III will normally be carried out at Kennedy Space Center (KSC) although, later in the programme, the Western Test Range (California) will be used as a launch site so that Level I procedures would be accomplished there. As regards Level IV experiment integration this can be done at the user site (e.g. university laboratory) or at a designated central facility, depending on the complexity of the operations involved.

In the US, the Marshall Space Flight Center has been assigned the responsibility for planning for Level IV integration for the early Spacelab flights. In Europe, ESA has established a special

team - SPICE (Spacelab Payload Integration and Co-ordination in Europe) - operating out of Porz-Wahn, Germany to perform a similar function for European experiments. Both organizations will support the experimenter throughout all phases of the experiment programme, including planning, technical advice, check-out, software and physical integration. Standard ground support equipment will be maintained for general use by the experimenters. Typical functions envisaged in support of the experimenter are depicted in Figure 20.

As regards flight operations, the Spacelab payload will be under the control of the NASA Payload Operations Control Center (POCC) whereas the Shuttle/Spacelab system will be controlled by the Space Transportation System (STS) Mission Control Center. The functions and support of these two facilities at the Johnson Space Center are illustrated in Figure 21. On-board and on-the-ground activities are involved. The on-board functions typically involve the flight of the Shuttle by the STS crew, extra vehicular activities, and operation of the experiments by the payload specialists. On-the-ground support includes mission management, data and communication control, and access to the on-board experiment equipment by experimenter teams - either directly or via the payload specialists. This real-time access is made possible by using the Tracking and Data Relay Satellite System (TDRSS) which is capable of transmitting data rates of up to 50 mbps.

To ensure a ready European experimenter involvement, ESA is currently evaluating the possibility of establishing a European Payload Operations Support Center (EPOSC). The concept is illustrated in Figure 22. Communication satellite links are proposed to connect the EPOSC with the POCC. Further, it is visualized that individual European experimenters could be linked by land lines to the EPOSC.

The acquisition and distribution of data generated by the experiments impacts both ground and flight operations. In this context, data refers to voice, video, digital, photographs and specimens that might be transferred to or from Spacelab. The data flow picture is presented in Figure 23 which also illustrates the principal elements involved. The data is available in real-time, delayed time or in a stored form. The TDRSS is a key element for down-link and up-link data transmission and domestic satellites are used for high-bit-rate data transfer from the TDRSS ground terminal via the NASCOM interface to the control centers. Transmitted and on-board stored data that is retrieved after landing will be delivered to the experimenters for analysis.

#### VII. Typical Applications

Spacelab users will be drawn from all disciplines of science, applications and technology. Investigations have shown that all the more conventional fields of space research and applications can benefit from the use of Spacelab (astronomy, magnetospheric physics, remote sensing, communications, etc.). It is expected that new areas that would gain from using Spacelab will be recognized as its operational life matures.

In general, the importance of Spacelab springs from the fact that large universal facilities (e.g. furnaces, telescopes, high power lasers) can be carried on-board that can be used by individual experimenters. The latter might originate from universities or government agencies and would provide detectors and specimens for use with the orbiting facilities. The large payload capabilities of Spacelab mean that simultaneous observations of a phenomenon, using a variety of techniques and instruments, can be employed.

It is visualized that Spacelab will find applications in all phases of space activities - pure research, development of instruments and technologies, methodology evaluation and the execution of operational programmes. In order to illustrate in a more definitive way the capability of the Spacelab to support research and experimentation on orbit, two typical payloads have been selected. The first of these refer to the Atmosphere, magnetosphere and Plasmas in Space (AMPS) mission and the second to a Space Processing mission. These are described in some detail to demonstrate the relationship between these missions and the Spacelab system.

The objectives of the AMPS missions are to conduct scientific experiments in the area of atmospheric physics, plasma physics and magnetospheric physics in an environment unachievable in ground-based laboratories. The AMPS laboratory consists of the Spacelab suitably instrumented on the pallet to take maximum advantage of the natural environment in which it is to be placed. Four primary areas of scientific interest have been defined. (1) Atmospheric Science, to provide a detailed quantitative understanding of the atmosphere of this planet and its interactions with the energy input from the sun, (2) Wave Phenomena experiments to obtain a much more detailed understanding of the propagation of electromagnetic waves through a plasma, (3) Plasma Interaction and Flow studies to evaluate the properties of plasma wakes and sheaths created by bodies travelling through a plasma and (4) Particle Interaction studies to determine the interactions of charged particles with the earth's electric and magnetic fields and with the ambient plasma in the ionosphere.

For the AMPS kind of mission it is essential that in the allotted seven-day mission time, an efficient use of free flying sub-satellites, deployable balloons, chemical releases and other supporting instruments will be utilized, as well as efficient planning and timing of these activities during the mission. Electron and ion accelerators mounted on the pallet are used to inject highly energetic particles at pre-determined angles to the geomagnetic field lines. An Artist's concept of a Spacelab AMPS payload is shown in Figure 24.

As regards the Space Processing mission, the overall objective is to study low-g processes and to produce samples in the fields of biology, metallurgy and chemistry. Various sub-element packages are carried on Spacelab to satisfy the needs of the various sub-disciplines. These sub-elements consist of (1) core, for general support and control (2) biological, for purification and separation of biological phenomena (3) general

purpose, for fundamental investigations in fluid flow (4) furnace, and (5) levitation, the latter two being for the evaluation of melting phenomena in metals and glasses and to perform basic metallurgical research.

These sub-elements and supporting equipment are accommodated by Spacelab in the large module plus two pallets configuration. The power, energy and heat rejection requirements for this payload exceed the basic resources provided by Spacelab. Hence, additional fuel cells and energy kits and a deployable radiator will be installed on the pallet. The lay-out of the various pieces of equipment comprising the Space Processing payload for Spacelab is shown in Figure 25.

#### VIII. Concluding Remarks

This paper has given a brief summary of the Spacelab system and its operation as an introduction to a new tool that will be available to an international community of users through the 1980's. More detailed information on Spacelab can be obtained through NASA or ESA. It is stressed that Spacelab will appeal to a variety of users through its inherent mission flexibility and its design in response to valid user requirements. The concept has been fixed, detailed design is well under way and hardware is being produced. The success of a co-operative ESA/NASA venture is being demonstrated. The ultimate success, however, will be to provide its use as an international orbital laboratory for the benefit of experimenters in all walks of science, applications and technology.

#### MAJOR SPACELAB PROGRAMME OBJECTIVES

- TO PROVIDE TO A LARGE MULTIDISCIPLINARY USER COMMUNITY A VERSATILE LABORATORY AND OBSERVATORY FACILITY
- TO REDUCE SIGNIFICANTLY BOTH THE TIME AND COST REQUIRED FOR SPACE EXPERIMENTATION
- TO MAKE DIRECT SPACE RESEARCH POSSIBLE FOR QUALIFIED SCIENTISTS AND ENGINEERS WITHOUT THE NEED OF FULL ASTRONAUT TRAINING

Figure 2.

#### PRINCIPAL SPACELAB PROGRAMME REQUIREMENTS

- PRE-DETERMINED FUNDING CEILING
- DELIVERY OF FLIGHT UNIT EARLY 1979, ENGINEERING MODEL EARLY 1979 TOGETHER WITH ASSOCIATED GROUND SUPPORT EQUIPMENT
- LOW OPERATIONS COSTS TO BE ENSURED
- USER FLEXIBILITY TO BE PRESERVED
- EXPERIMENT PAYLOAD WEIGHT 5000 TO 8000 KG
- PROVISION FOR FOLLOW-ON PRODUCTION
- FLIGHT DURATION 7 TO 30 DAYS
- DESIGN LIFE 50 REUSES OR 10 YEAR LIFETIME
- CREW OF 1 TO 4 PAYLOAD SPECIALISTS
- COMPATIBILITY WITH SPACE SHUTTLE

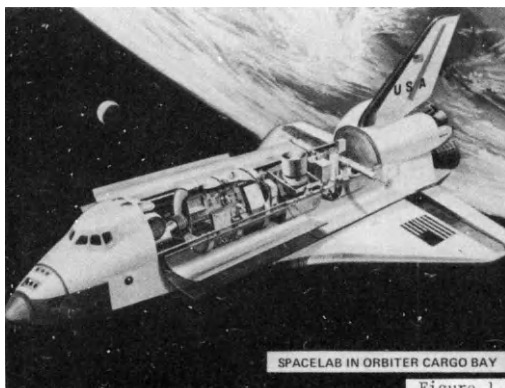


Figure 3.

#### SPACELAB PROGRAMME MANAGEMENT ORGANISATION

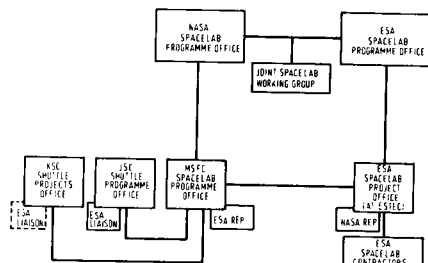


Figure 4.

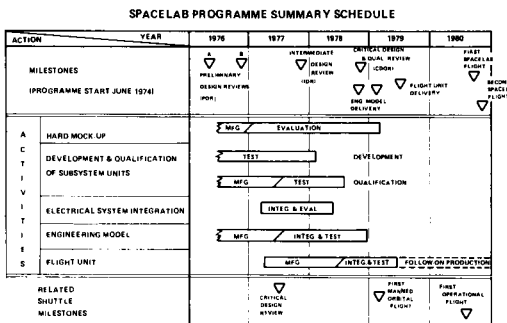


Figure 5.

**SPACELAB EXTERNAL DESIGN FEATURES**

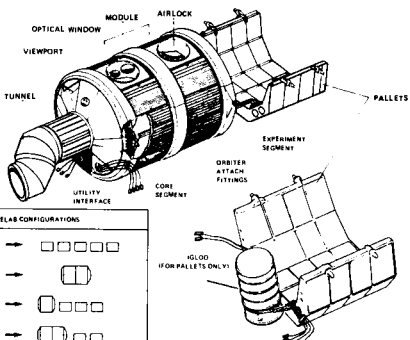


Figure 8.

**SPACELAB DELIVERABLES**

IN ACCORDANCE WITH THE MEMORANDUM OF UNDERSTANDING AND TO ENSURE A VIABLE SPACELAB OPERATIONAL PROGRAMME, ESA WILL DELIVER TO NASA THE FOLLOWING ITEMS OF SPACELAB EQUIPMENT AND SERVICES:

- ONE FLIGHT UNIT (BASIC MODULE, EXTENSION MODULE, SUBSYSTEMS, COMMON PAYLOAD SUPPORT EQUIPMENT)
- ENGINEERING MODEL
- INITIAL SPARES
- GROUND SUPPORT EQUIPMENT (2 SETS)
- SUPPORT SOFTWARE (NON-APPLICATIONS)
- DOCUMENTATION
- SUSTAINING ENGINEERING THROUGH FIRST 2 FLIGHTS
- PRELIMINARY INTEGRATION OF ESA-SUPPORTED EXPERIMENTS

Figure 6.

**SECTIONAL VIEWS OF SPACELAB MODULE**

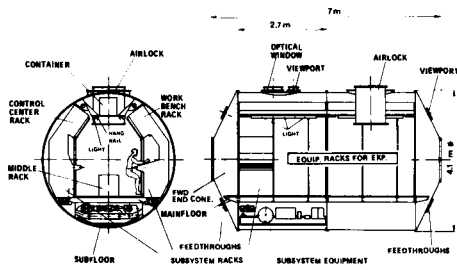


Figure 9.

**BASIC SPACELAB CONFIGURATIONS**

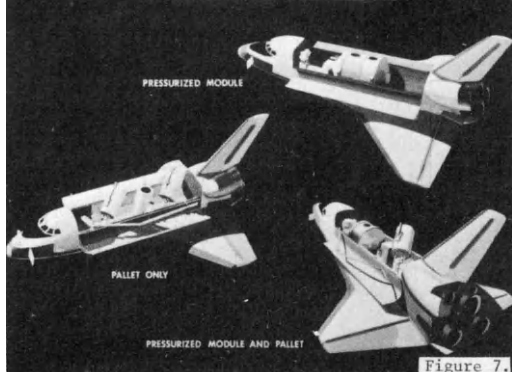


Figure 7.

**SPACELAB MOODULARITY APPROACH**

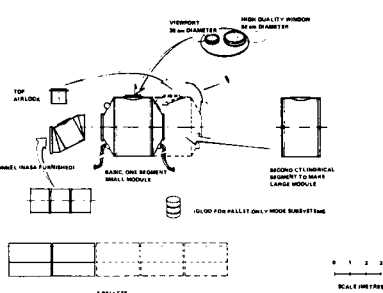


Figure 10.

#### THREE TYPICAL SPACELAB FLIGHT CONFIGURATIONS

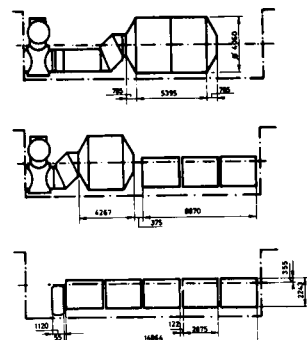


FIG. 11

## **CHARACTERISTICS OF MAJOR SPACELAB SUBSYSTEMS**

#### AIR REVITALIZATION SYSTEM (ARS)

- REGULATES ATMOSPHERE COMPOSITION AND PRESSURE (80% N<sub>2</sub>, 20% O<sub>2</sub>, 1.1 BAR, HUMIDITY-25% TO 70%)
  - MONITORS AND CONTROLS CONTAMINANTS INCLUDING CO<sub>2</sub>

#### **Thermal Control System (TCS)**

- CONTROLS AMBIENT TEMPERATURE (18°C TO 27°C)
  - REMOVES HEAT OUTPUT OF EXPERIMENTS, SUBSYSTEMS AND CREWMEN ( $\approx 8.5$  Kw)

## ELECTRICAL POWER AND DISTRIBUTION SYSTEM (EPDS)

- DISTRIBUTES 7.75 KW AVERAGE (±12 KW PEAK) OF ORBITER GENERATED POWER TO EXPERIMENTS AND SUBSYSTEMS
  - MAXIMUM ENERGY UP TO 2870 KWH (WITH WEIGHT PENALTIES)
  - VOLTAGES AVAILABLE - 284VDC, - 115/200 VAC 400 HZ

## **CONTROL AND DATA MANAGEMENT SYSTEM (CDMS)**

- COMPUTERS EXPERIMENTS/SUBSYSTEMS - 16 BIT WORD, 64X MEMORY, 360,000 OPS/SEC.
  - ALPHANUMERIC AND DISCRETE DISPLAYS
  - RECORD 32 MB/SEC DIGITAL AND 0.0 MHZ ANALOG
  - TELEMETER 50 MB/SEC DIGITAL OR 4.2 MHZ ANALOG

Figure 12.

## SPACE SHUTTLE PROVISIONS FOR SPACELAB USER

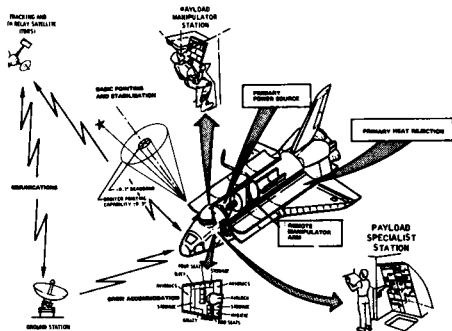


Figure 13.

SPACE LAB SERVICES FOR USERS

AVAILABLE TO USERS	CONFIGURATION	B600	B600	10 METER PALLET	INDEPENDENTLY SUPPORTED PALLET
	SINGLE MODULE + 3 METERS BASED				
<b>Payload weight</b> (kg)	5000	5000	8000	8000	8000
<b>VOLUME FOR EXPERIMENT EQUIPMENT</b> PRESSURIZED (m <sup>3</sup> )	1.0	22.2			-
NONPRESURIZED (NO OVERHANG)	98.8		187.4		97.1
<b>PALLET MOUNTING AREA</b> (m <sup>2</sup> )	81.3	-	85.7		53.9
<b>ELECTRICAL POWER (28 VOLTS DC)</b> 110/200 VOLTS AT 400 HZ AC					
AVERAGE (kW)	3 - 4	3 - 4	4 - 5		4 - 5
PEAK (kW)	8.0	8.0	10.0		10.0
ENERGY (kWh)	~400	~400	~800		~800
<b>EXP. SUPPORT COMPUTER</b> WITH CENTRAL PROCESSING UNIT		64 K CORE MEMORY OF 16 - 64 WORDS			
<b>DATA HANDLING</b> TRANSMISSION THROUGH ORBITER STORAGE DIGITAL DATA		320 000 OPERATIONS PER SEC.			
		UP TO 50 Mbps			
		UP TO 30 Mbps			

Figure 14.

## **INSTRUMENT POINTING SUBSYSTEM**

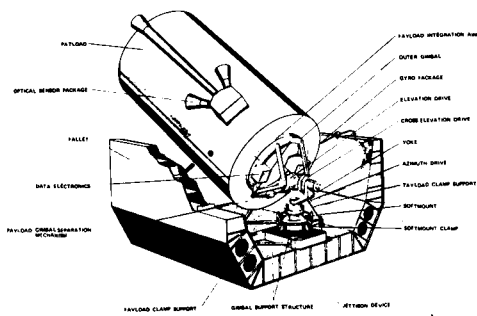


Figure 15.

#### **ADVANTAGEOUS FEATURES OF SPACELAB**

- REUSABILITY GIVING RISE TO EXTENDED OBSERVATION PROGRAMMES AND REDUCED NEED FOR HI-REL EQUIPMENT
  - DUAL ROLE - MANNED AND/OR AUTOMATIC EXPERIMENTS
  - AN EARTH-LIKE LABORATORY IN SPACE
  - EASY ACCESS TO SPACE FOR SCIENTISTS AND ENGINEERS
  - PARTICIPATION OF ON-GROUND USERS IN FLIGHT EXPERIMENTATION
  - SIMPLIFIED AND SHORTER EXPERIMENT CYCLES
  - OFF-LINE EXPERIMENT INTEGRATION AND INVOLVEMENT OF EXPERIMENTER
  - MISSION FLEXIBILITY
  - USE OF UNIVERSAL FACILITIES
  - RELATIVELY LOW COST

Figure 16.

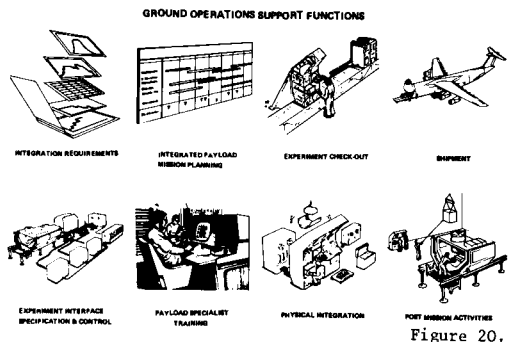
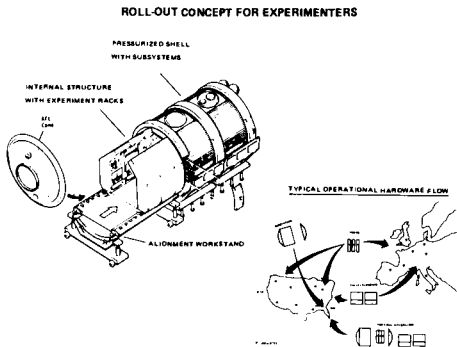


Figure 17.

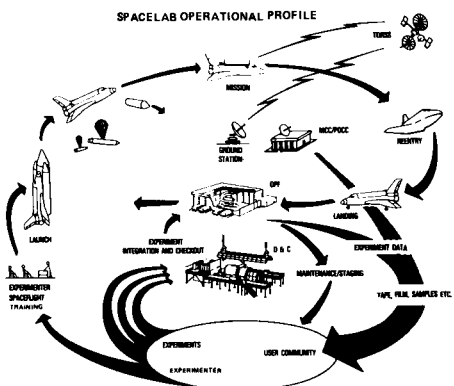


Figure 18.

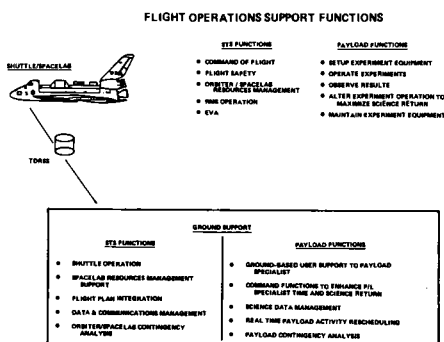


Figure 21.

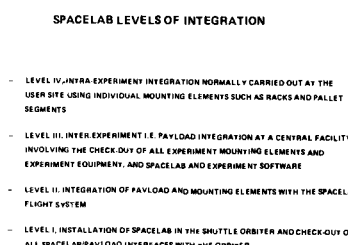


Figure 19.

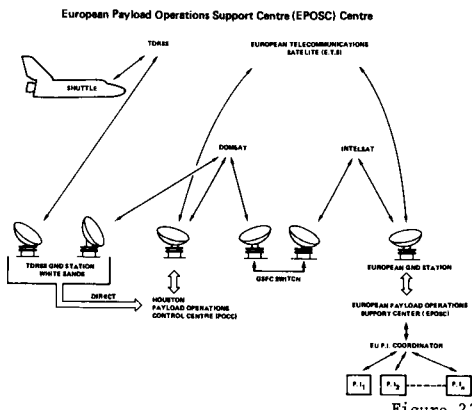


Figure 22.

OVERALL SPACELAB DATA FLOW

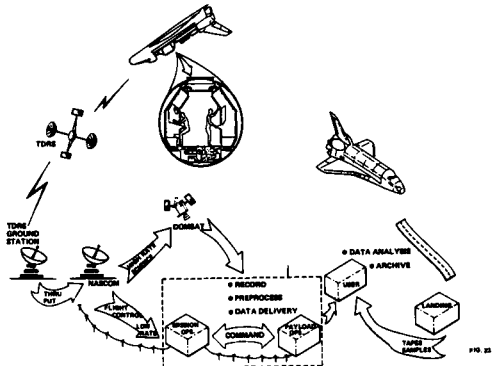


Figure 23.

TABLE I - PRINCIPAL ENVIRONMENT PARAMETERS

PARAMETER	APPROXIMATE VALUES
ACCELERATION	MAXIMUM $3g$ LINEAR ACCELERATION DURING ASCENT AND DESCENT, TYPICALLY $10^{-6} g$ ON ORBIT.
VIBRATION	140dB ACOUSTIC NOISE IN CARGO BAY (LAUNCH ONLY); 130dB ACOUSTIC NOISE INSIDE MODULE (LAUNCH ONLY). TYPICALLY $4g$ RANDOM VIBRATION INPUT TO EQUIPMENT IN RACKS IN THE MODULE.
THERMAL	INSIDE THE MODULE: EQUIPMENT COOLING THROUGH FORCED AIR IN THE RANGE 30 TO 40°C. CABIN AIR IN THE RANGE 10 TO 25°C (ADJUSTABLE). ON PALLET: EQUIPMENT COOLING BY COLD PLATES WITH TEMPERATURES IN THE RANGE 10 TO 40°C.
CONTAMINATION	ARISES FROM ORBITER, SPACELAB AND REQUIREMENTS. PRECAUTIONS WILL BE TAKEN IN DESIGN TO REDUCE LEVEL AS FAR AS PRACTICALLY POSSIBLE. DUMPS CAN BE PROGRAMMED.

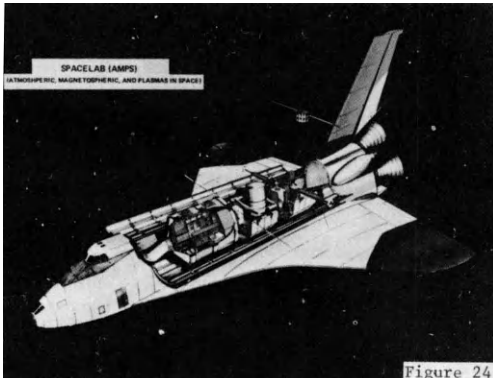


Figure 24.

TABLE II - MATERIALS CONTROLS REQUIREMENTS

ORBITER CAB IN ONLY:	FULL MATERIALS CONTROLS PER NHB 8860.1A "FLAMMABILITY, ODOR AND OFF-GASSING REQUIREMENTS AND TEST PROCEDURES FOR MATERIALS IN ENVIRONMENTS THAT SUPPORT COMBUSTION": SAFE HAVEN FOR RETREAT IN CASE OF EMERGENCY.
OFF-GASSING (APPLIES TO SPACELAB HABITABLE MODULE ONLY):	<ul style="list-style-type: none"> <li>- AVOID SIGNIFICANT OFF-GASSING MATERIALS;</li> <li>- MATERIALS SELECTION GUIDELINES AVAILABLE;</li> <li>- BLACK-BOX LEVEL OFF-GASSING TEST REQUIRED.</li> </ul>
FLAMMABILITY (APPLIES TO SPACELAB MODULE AND PAYLOAD BAY):	<ul style="list-style-type: none"> <li>- GOOD PRACTICES REQUIRED ON PROPAGATION PATHS AND SEPARATION FROM IGNITION SOURCES;</li> <li>- CONSIDERATION TO MINIMIZING USE OF FLAMMABLE MATERIALS;</li> <li>- MATERIALS SELECTION GUIDELINES AND ASSISTANCE AVAILABLE.</li> </ul>

SPACE PROCESSING PAYLOAD IN SPACELAB

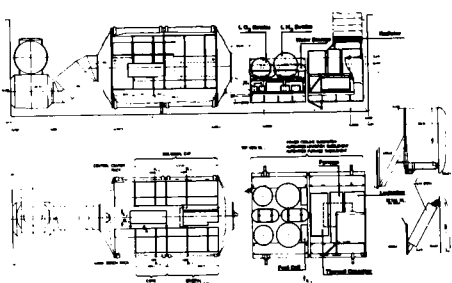


Figure 25.

TABLE III - COMMAND & CONTROL OF HAZARDOUS FUNCTIONS

- NO SINGLE HOUR FAILURE OR PROCEDURAL ERROR CAN CAUSE INADVERTENT OCCURRENCE OF POTENTIALLY HAZARDOUS FUNCTION.
- WHERE OPERATION RESULTS IN CATASTROPHIC CONDITION, NO TWO FAILURES OR PROCEDURAL ERRORS OR ANY TWO COMBINATIONS THEREOF CAN CAUSE INADVERTENT OPERATION. ARM AND EXECUTE ACTIONS REQUIRED - ALSO PROVISIONS TO RETURN TO SAFE CONDITION.
- MINIMUM DEPENDENCE ON ORBITER AND CREW FOR SAFING ACTIONS IS AN STS GOAL.
- HAZARDOUS SITUATIONS WHICH REQUIRE A RAPID RESPONSE PREFERABLY CORRECTED BY AUTOMATIC SYSTEMS WITHIN PAYLOAD DESIGN.
- THE LIMITED ORBITER CAPABILITY FOR DISPLAY AND SUBSEQUENT COMMAND OF PAYLOAD SAFETY PARAMETERS SHOULD BE USED ONLY WHEN ALTERNATE MEANS ARE NOT AVAILABLE TO REDUCE OR CONTROL THE HAZARD.
- WHEN THIS CAPABILITY IS USED, SUCH FUNCTIONS SHALL BE CAPABLE OF BEING TESTED FOR PROPER OPERATION.
- IMPLEMENTATION TO BE DETERMINED ON AN INDIVIDUAL PAYLOAD BASIS.

# TECHNOLOGICAL AND OPERATIONAL FEATURES OF THE ARAKS EXPERIMENT

Gilles Charles

*Head of the ARAKS Project, Centre National d'Etudes Spatiales, Toulouse, France*

## Abstract

The artificial injection of charged particles into the ionosphere and magnetosphere opens up a new line of research, providing an active method of investigation, in theory under controlled initial conditions.

These conditions cover the type, energy, incidence and intensity of the particles injected.

The French-Soviet Project ARAKS, i.e. : "Artificial Radiation and Aurora between Kerguelen and the Soviet Union", which involved the launching, on 26th January 1975 and 15th February 1975, of two ERIDAN sounding rockets from the temporary CNES Base on Kerguelen Islands, consisted in injecting 27 Kev 0.5 A and 15 Kev 1 A electrons by rocket-borne guns.

In agreement with the Soviet side, CNES has invited a Houston University team under NASA guidance to participate in the launching programme.

The project was a logical extension to passive rocket and satellite experiments, and went a long way towards providing a more thorough insight into the problems posed to the physics of ionized atmospheres.

It has also opened up new vistas to a deeper understanding of the scientific implications of the AMPS project.

The main scientific aims included :

- (i) Measurement and analysis of the waves generated by the electron beam injected into the ionosphere plasma.
- (ii) Investigation into the large scale ( $L = 3.6$ ) movement and drift of electrons.
- (iii) Research into electron scattering in the atmosphere.
- (iv) Study of the magnetic combination with artificial auroras produced in the Northern hemisphere (Arkhangelsk region in the Soviet Union).

After a brief look at the scientific objectives set and the characteristics of the relevant sensors, the report will try and sketch in all the trammels the project had to contend with.

The main stress will lie on a detailed sizing up of the task involved, and the technical answers we have found to meet it.

## I . Introduction

In application of June 30, 1966's agreement between the Government of the French Republic and the Government of the Socialist Soviet Republic on a cooperation programme to be conducted for the study and exploration of space for pacific purposes, the NATIONAL CENTER FOR SPACE RESEARCH and the INTERCOSMOS BOARD of the Soviet Union Academy of Sciences, carried out, from October 1974 to March 1975, a joint cooperation programme, called "ARAKS Project" (1) in compliance with the research programme on ionosphere, magnetosphere and plasma physics.

The said programme included the launching of two two-stage ERIDAN rockets from the Kerguelen Islands, completed by ground measurements at Kerguelen and in the Arkhangelsk region.

The organization of the launching campaign was conducted by the CNES with the logistic support of the French Austral and Antarctic Territory and the ground observations carried out in the Soviet Union INTERCOSMOS Board. Research scientists, i.e. French and Soviet Engineers and Technicians were members of the teams working on both French and Soviet Territory.

With the agreement of the Soviet side the CNES had invited a team from Houston University led by NASA to participate in the campaign.

The main participants in the Project are listed hereafter :

### FRANCE

The scientific experiments achieved by France had been placed under the responsibility of the following organizations :

- The Center for Research on Space Radiations Paul Sabatier University in Toulouse (CESR)
- The CNRS (National Center for Scientific Research) External Geophysics Laboratory - Paris VI University at Saint-Maur des Fossés (IGE)
- The CNRS Institute for Astrophysics in Paris (IAP)
- The CNRS Observatory of Haute Provence at Saint-Michel de Haute Provence (OHP)

Have also shared in the project :

- The Industrial National Company "Aérospatiale"
- The National Meteorology Office
- The Communications Center of the Ministry of Defence (SGDN)
- The Armaments Electronics Center (CELAIR)
- The Center for Research on Physics of the Earth and Planetary Environment (CRPE)
- The CNRS Space Astronomy Laboratory (LAS)
- The French Polar Expeditions
- The Laboratory for Theoretical Physics Polytechnic School
- The National Center for Studies on Telecommunications (CNET)

#### SOVIET UNION

- IKI Institute for Space Research USSR Academy of Sciences - Moscow
- IZMIRAN Institute for Research on Earth Magnetism, research on the Ionosphere and Waves Propagation - USSR Academy of Sciences - Moscow
- PATON Institute in Kiev for Electric Soldering - USSR Academy of Sciences
- KOURCHATOV INSTITUTE for Atomic Energy Moscow
- INSTITUTE for Electrodynamics in Kiev USSR Academy of Sciences
- PATON INSTITUTE Facilities for Experimental Manufacturing in Kiev - USSR Academy of Sciences
- Moscow Hydrometeorological Service
- IZMIRAN Geophysics Observatory at Arkhangelsk
- INSTITUTE for Polar Geophysics - USSR Academy of Sciences - APATITI
- KIEV State University
- LENINGRAD State University
- MORFLOT Shipping Company
- USSR Telecommunications Service
- AEROFLOT Company

#### II . Scientific Aims

The discovery in 1958 of the energetic particles radiation belts caught in the earth's magnetic field have been subjected to intensive research with a view to understanding the Earth space environment.

For instance, the aurora phenomena which take place in high latitude areas could thus be explained. It is almost certain today that these phenomena are created by

electrons precipitated into the atmosphere which consequently excite molecules and atoms.

The studies carried out with the help of space probes on the natural phenomena which develop in the ionosphere and in the magnetosphere where the solar activity plays a significant part, have stressed the wide complexity of said phenomena if we take into account the very extensive number of parameters to be measured.

That is why on the world level the idea prevailed to perform, and thus control, active experiments under the same initial conditions.

After HESS and WINCKLER's experiments (1) in the United States, France and Soviet Union undertook together the ARAKS active experiments programme. ZARNITSA's experiment (an electrons gun aboard MR12 Probe rocket) had already been performed by the Soviet side within ARAKS project framework. Said ARAKS programme aim was to inject energetic electrons into the ionosphere and into the magnetosphere. These injections were carried out by means of an electron accelerator airborne on ERIDAN probe rockets which reached an altitude of 200 km.s.

Two probe rockets were thus launched on the 26th of January 1975 and on the 15th of February 1975, from the temporary launching station of the CNES located in the COURBET peninsula of the Kerguelen Islands in the Indian Ocean 49° South Latitude and 70° East Longitude.

The electrons emitted by the accelerator are guided by the earth's magnetic field LORENTZ force. By the effect of said force, the electrons gain a helicoidal movement around a magnetic line of force. All of them follow the same line of force and reach over USSR, the "magnetic point" in conjunction with the electrons injection spot. The projection of said point on the Earth in the Northern Hemisphere is located south of Arkhangelsk region. It is in this region that the French/Soviet installations had been set up for the ground observations to be performed in the course of the two launching operations.

What happens to the electrons depends on the values of the pitch angle of beam and the magnetic field.

This is how a wide injection angle in the Southern Hemisphere, to "a magnetic mission" spot located at an altitude higher than that from which the collision effects of the atmosphere atoms on the electrons movement (about 100 km) can be disregarded.

The electrons then, guided by LORENTZ force, come back to Kerguelen but with a slight eastward drift due to the magnetic field gradient and to the curve of the force lines.

One of the rockets was consequently launched toward the magnetic East on February 15, 1975, with a view to studying this particular effect.

When the injection angle is narrow the mirror spot is located under the 100 km area and the electrons interact with the molecules and the atoms of the atmosphere ; in this case part of them is retrodiffused upwards through Columbian interactions with the atmosphere atoms and is sent back to Kerguelen.

The electron precipitation generates the following phenomena :

- 1 . a visible light emission and additional ionisation of the atmosphere building up an artificial aurora.
- 2 . "Bremstrahlung" X-rays emissions which can be compared with those observed during "magnetic storms".

The electron precipitation process can also take place over the Kerguelen : the electrons which precipitate have their origin in the electrons reflected in the Northern Hemisphere and the electrons emitted by the accelerator when the injection is carried out downwards.

The main aims of ARAKS experiment were the following :

- 1 . An analysis of the neutralizing process of the charge accumulated by the rocket.
- 2 . A study of the atmospheric retrodiffusion through an analysis of the angular and energetic dispersion of the retrodiffused electrons (2).
- 3 . A study of the longitude drift of the electrons back from the Northern Hemisphere (drift toward the magnetic East) (2).
- 4 . A study of the magnetic conjunction through a localization by the auroral effects of the impact spots of the electrons precipitated above USSR.
- 5 . A study of the beam/plasma interactions within the ionosphere and the magnetosphere. A study of the various types of waves emitted during such beam/plasma interactions.

The number of wave/particle interactions we can think of is most extensive.

Taking into account the developed theories it is nevertheless possible to classify the waves under three categories :

- a) The waves generated in the vicinity of the electron gun
  - . individual or spontaneous radiation : CERENKOV radiation

- . inducted radiation, unsteadiness
  - . waves born from neutralization
- b) The waves generated along the magnetic equator.
  - c) The waves generated at the moment when the particles penetrate into the ionosphere.

### III . Technical and operational implementation set up

#### III.1. Payloads

The payloads built by FRANCE have been launched by the French probe rockets ERIDAN (fig. 1 and 2).

Each payload consisted of two parts :

- ERIDAN payload where the following items had been installed :
  - . the soviet electron accelerator
  - . the soviet plasma source
  - . CESR particle counter (3)
  - . the particle counters built by the CESR (4) jointly with IKI
  - . the soviet IKI particle counter
  - . IKI potential measuring system
  - . the soviet radar responder
- The ejective propelled cone where had been installed :
  - . the wave experiments (5) et (6)
  - . LGE magnetic antenna
  - . TBF-LGE electric ball antenna
  - . HF-LGE electric antenna
  - . LGE ionic analyser counter (7)
  - . 2 CESR particle counter (3)
  - . IZMIRAN soviet spectrum experiment (6)

The payloads were fitted with 3 telemetry transmitters and with attitude restitution systems and also with various technological systems for operation and control.

#### III.2. Ground observations

At Kerguelan an overall implementation for geophysical ground measurements was set up (ionospheric probe, optical observations, riometers, fluxmeters, etc.).

In the Soviet Union three observation sites had been set up for the French and Soviet stations, namely :

KARPOGORY, NOVAYA - LAVELA and PATCHIKA

Soviet Union scientists operated aurora observation radars ; a YAK 40 aircraft was fitted with various observation systems.

France (CESR - OHP - IAP) set up at NOVOYA-LAVELA a French television station and a microchannel electron multiplier array picture intensification station at PATCHIKA (8).

### III.3. Logistic implementation

The CNES mobile station developed for the sounding rockets launching campaigns in Terre Adelie, Argentina, Island, Norway, Kerguelen, was operated. It consisted of mobile launching equipment summarily fitted up.

1.200 cubic meters of material (400 t.) were transported from France to Kerguelen. Three Soviet ships participated in the operation and also the TAAF ship "Marion Dufresne".

Two helicopters of the French Air Force assisted us in several helicopter operations.

Radio connections in real time were set up between USSR (Moscow and the region of Arkhangelsk) - PARIS - KERGUELEN

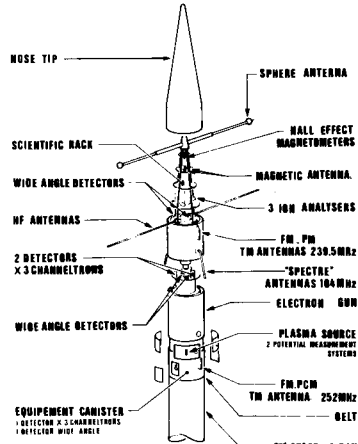


FIG.2 - PAYLOAD

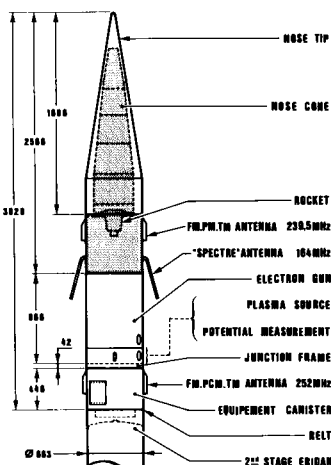


FIG.1 - PAYLOAD

The description of the project (experiments, payloads (9), various sub-systems) will be the subject of an article to be published in a special issue of "SPACE SCIENCE INSTRUMENTATION".

The first results were the subject of two conferences, one FRANCO/SOVIET on active experiments in the magnetosphere, held in May 1976 in Toulouse, and the other on active experiments in the magnetosphere plasmas, held in June 1976 in BOULDER (COSPAR working group).

This is the reason why the following report has been purposely restricted to some technical features which enabled us to meet the project requirements or mission analysis and payload testing levels.

### IV . Special technical features

In addition to the theoretical studies conducted by the various scientific groups, the latter were given assistance in computing the interception possibilities of the electron beam by the rocket. The beam ejected into the Southern Hemisphere is reflected under certain conditions into the Northern Hemisphere. It returns to the Southern Hemisphere with a drift to the

magnetic East. It was assumed that the reflection was flawless. A 15 to 27 Kev energy dispersal and also the specifications (10) of the unguided ERIDAN rocket and the wind patterns in Kerguelen as recorded over a 10 year period were taken into account.

The results of such a study showed up that the chances for intercepting the beam were small if we consider the use of unguided rockets showing a dispersal of about 35 Kms ( $1\sigma$ ) and even more considering the lack of measurements of the electric field in the Ionosphere before the launchings from Kerguelen.

If the results obtained by means of particle counters and (Monte Carlo method) calculations on the actual trajectories do not enable us to come to a final conclusion that the return beam was intercepted during the launching towards the magnetic East, it seems nevertheless that this objective will receive a negative answer.

#### IV.1.2. A study for setting up ground stations in USSR. Magnetic conjugated points Kerguelen/ Arkhangelsk Region

The artificial auroras generated in the Arkhangelsk Region were observed by means of various systems installed on the ground (optical systems-radars) and in flight on board a YAK 40.

With a view to setting up these stations and organizing the flight plan for both launchings (magnetic North and magnetic East), the conjugated magnetic points as estimated for ERIDAN nominal trajectories were calculated by applying several magnetic field models, such as : POGO 8/69, 8/71, GSFC 12/66, MAGNET 2 and OLSON PFITZER 1974.

The results were compared with the measurements obtained through the Soviet Radars (11).

#### IV.1.3. Remoteness of ejectable cones from electron accelerators

Do the waves generated by an electron beam within the magnetospheric plasma propagate at a great distance ? To answer this question the ejection cones, carrying the captors measuring the waves were moved away from the electron guns by means of a small powder propellant.

At  $t = HO + 70$  seconds, i.e. at about 79 kms, the separation between the two portions of the payload was performed by means of a hermetic oleopneumatic system. This system operates by displacement of an annular piston ; after two nitrogen bottles are burst, the piston displacement shears the calibrated bolts.

The experimenters had set a  $40 \text{ m.s}^{-1}$  speed increment.

The results are summarized on the following table and in figures 3 and 4 (12).

Launching Events	NORTHWARD Measured Speed increment in M/S	EASTWARD Measured Speed increment in M/S
$T = HO + 70 \text{ s}$ EJECTION CONE	Duration = 0,01 s $\Delta V = 2,47 \text{ m/s}$	Duration = 0,01 s $\Delta V = 2,30 \text{ m/s}$
$T = HO + 85 \text{ s}$ Minipropulsion thrust	Duration = 1,4 s $\Delta V = 36 \text{ m/s}$	Duration = 1,5 s $\Delta V = 38,8 \text{ m/s}$
$T = HO + 88 \text{ s}$ EJECTION CAP	Duration = 0,04 s $\Delta V = - 2,3 \text{ m/s}$	Duration = 0,04 s $\Delta V = - 2,84 \text{ m/s}$

#### DATA ON THE CONE TRAJECTORIES

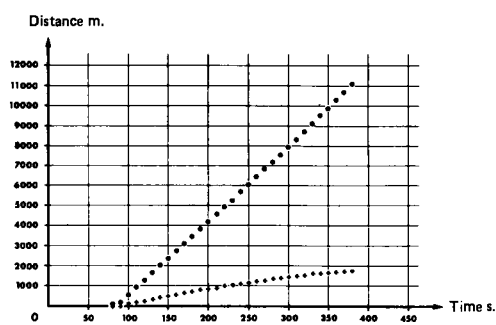


FIG.3 - ARAKS EAST : PARALLEL DISTANCE AND PERPENDICULAR DISTANCE IN RELATION TO THE MAGNETIC FIELD MEASURED FROM THE CONE

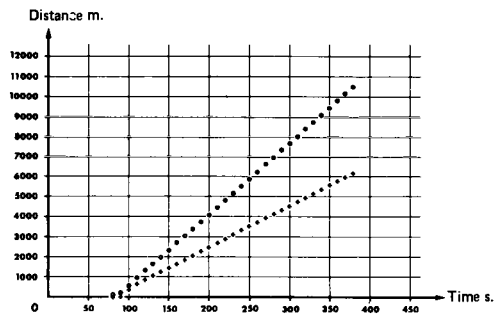


FIG.4 - ARAKS NORTH : PARALLEL DISTANCE AND PERPENDICULAR DISTANCE IN RELATION TO THE MAGNETIC FIELD MEASURED FROM THE CONE

The objective aimed at had been reached. To this end the following precautions had been taken.

- use of a propellant the powder of which had not been doped in order to minimize pollutants on the upper portion of the accelerator
- careful equilibration of the ejectable cones
- also careful lining up of the propellant along the main inertia axis of the cone
- separation of the cone from the accelerator along the main axis with a guidance system on the separation level and the upper portion of the accelerator.

The cones mutation angle before the antenna were pulled out was  $5^\circ$ , but at the end of the flight performance it reached  $19^\circ$  for the launching to the magnetic North and  $40^\circ$  for the launching to the magnetic East. This last high figure could be explained by a partial unfolding of the graphite ball antenna carried on struts made of fibre glass.

#### IV.1.4. Corrective actions on the ejectable cone dynamics to ensure the mechanical behaviour of the "waves experiment" antenna within the HF range.

One of the three captors of the ARAKS project "Waves" experiment is made of a linear bipole made up of two flexible extensible antenna. The study of the cone movement showed that the antennas mechanical behaviour was jeopardized. To solve this problem, the cone was fitted with a decoupling antenna meridian and a stretch yo-yo. The kinematic conditions reached in flight in the course of the launching proved that the actions so conducted were adequate as they made possible the success of the experiment (13).

##### IV.1.4.1. Stretch yo-yo

A large dispersal on the rolling speed when the HF antenna began to be deployed ( $2 \times 4$  m bipole) could consequently excite and bring the parallel antenna mode to resonance.

It is known that the dispersals on the final speed attained through thread yo-yos, and despite the care brought to the manufacture of such experiments, figure within the same range as the initial dispersals when the yo-yos were not in operation.

After looking into the problem and adequate testing, it was decided to use a stretch yo-yo.

The final rotation speed after the yo-yo had operated and the antennas had been deployed was equal to, or higher than 0.5

$t.s^{-1}$ . The scientific measuring operation lasted 2.56s.

The antenna parallel resonance mode was excited provided the  $Wz$  rotation was such as :  $0,7 \geq Wz \geq 0,8 t.s^{-1}$ .

The nominal value of the rotation speed, namely  $Wzo$ , was  $1,85 t.s^{-1}$ , taking into account the position of the rocket fins.

In fact the missiles spun at  $2,44 t.s^{-1}$  for one of them and  $2,24 t.s^{-1}$  for the other. By using a thread yo-yo, a final rotation speed  $Wzf = 0,79 t.s^{-1}$  for an initial speed of  $2,44 t.s^{-1}$  and  $Wzf = 0,72 t.s^{-1}$  for  $2,24 t.s^{-1}$ , would have been obtained.

The final figures would have been reached in the very middle of the antenna critical zone (figure 5).

The following figures were obtained with the stretch yo-yo :

$$Wzf = 0,57 t.s^{-1} \text{ for } Wzo = 2,44 t.s^{-1}$$

$$\text{and } Wzf = 0,58 t.s^{-1} \text{ for } Wzo = 2,224 t.s^{-1}$$

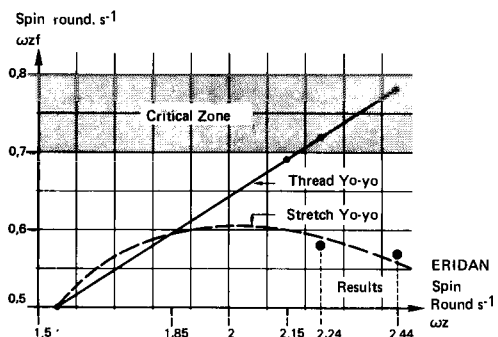


FIG.5 - COMPARISON BETWEEN THREAD YO-YO AND STRETCH YO-YO

##### IV.1.4.2. Ball joint suspensions

The antenna are made of two 4M. long, copperberyllium tapes, 5/100 mm in thickness. From the beginning of the deployment the antenna is cylinder-shaped.

The tape is stored in the unit itself which includes the electric motor. For each cone two packs were installed at  $180^\circ$ .

The volume of the rolled antenna in the unit is 10 x 10 x 5 cm and its weight : 1 kg.

The study of the dynamics of the ejectable cones and the calculations about antenna made it clear that in the meridian plan antenna might break.

It was therefore decided to decrease the excitations transmitted to the antenna, by installing the tape units on a pivoting system which allowed the displacements between the antenna and the cone in the meridian plan.

These systems operated satisfactorily and the resulting measures were valuable. It was the first time that the CNES developed such antenna units in France.

#### IV.2. Payload tests

All the tests conducted in the course of integration and reception of payload emphasized the two following items :

- radio electric tests of the ejection cones
- tests of the accelerators integrated in the ERIDAN payloads.

##### IV.2.1. The radio electric tests of the ejectable cones

For us the constraints imposed in the framework of a sounding rocket programme for space research are very different from

those imposed in the case of a satellite. Therefore EMI norms were not imposed in the development of ARAKS project. In addition with a view to cut down costs, standard equipments (telemetry, programmer, safety box, magnetometer...) were standard equipment and already available even before the project had been decided.

These tests have been difficult. In any event, whatsoever, perturbations are of two kinds :

- the captors (6) very sensitive, receives the natural radiations and a portion of the perturbations is therefore screened. A high performing shielded chamber is necessary.
- the telemetry emission must not be reflected by anything if flight conditions are to be simulated : it is therefore imperative to dispose of an anechoic chamber.

The signals processed through the various measuring sequences before starting the telemetry had dynamics reaching up to 80 db. The telemetry of IRIG-FM-PM type had a 36 db dynamic on channel 21 and 74 db on channel 3 : in fact the channel were used from 3 to 21 inclusively.

These tests were carried out in fairly quiet sites such as Chambon la Forêt Observatory (near Orleans) and in an anechoic chamber at the Armament Electronic Center of BRUZ near Rennes. To arrive at the following table and take pertaining actions, five overall tests were necessary (6).

#### COHABITATION TESTS

Places and Dates	Type of perturbation and level shown on the analysers in relation to noise					Actions taken
	Commutator Converter	Programmer Converter	VCO Telemetry	Fluxgate Magnetometer	Telemetry Emitters	
CHAMBON la FORET From March 10 to March 24, 1973	no test	50 dB	30 dB	60 dB	no test	CONECTIC shielding is adopted for the converters and oscillators. Further tests are prepared with a 0,2 mm shield thickness.
BRUZ From April 9 to April 20, 1973	20 dB	20 dB	10 dB	60 dB	elementary test	We assume CONECTIC thickness figures. We leave out the use of Flux gate Magnetometer and advise a Hall effect Magnetometer. We notice VHF perturbations on the large gain preamplifiers.
CHAMBON la FORET From March 25, to April 12, 1974	10 dB	20 dB	0 dB	-	no test	We can see that the residual perturbations after shielding are conduction perturbations and not direct radiation perturbations.
BRUZ From May 6 to May 24, 1974	10 dB	20 dB	0 dB	-	40 dB	We decide to stop feeding the programmer after propulsion. Filtering and shielding of all scientific modules is decided.
BRUZ From August 5 to August 9, 1974	0	0	0	-	10 dB	-

## V. CONCLUSIONS

To comply with ARAKS project, complex payload had to be set up.

Present sensitiveness of scientific captors and the use of active systems such as electrons accelerators, ionised gas sources on board of space vehicles raise difficult cohabitation problems. What is going on in the close environment of the source ? and thus of the payload ? It seems indeed that by making the sources from the captors, we succeed in minimizing the further away effects, reaching at the same time new scientific aims, such as, for instance, the study of the dynamics of an electron beam itself and its behaviour on a large scale.

Will the active experiments in the magnetosphere through electron beams become a large scale diagnostic technique? It pertains to the scientists to find the answer. Through the analysis of ARAKS project results and the difficulties which were met, the technician must be convinced that sounding rockets experiments deserve a specific attention in the field of tests. EMC norms should be included in the technical specifications, in order to realize scientific sensors and payloads for sounding rockets projects.

## REFERENCES

- 1 . The French Soviet "ARAKS" Experiment  
R. GENDRIN Space Science Reviews 15  
(1974) 905-931
- 2 . Objectifs et description d'une expérience active en fusée, mesures des particules dans l'expérience ARAKS par Henri REME  
Rapport CESR 73-359 Mars 1973  
Colloque Franco-Soviétique sur les points conjugués AUSSOIS - Mars 1973
- 3 . Apparatus for the study of artificially injected particules during the ARAKS Experiments. Electronics part CESR 76 - 584 Février 76  
H. BARTH, F. COTIN and H. REME  
Submitted for publication to Space Science Instrumentation
- 4 . New large angle detectors for low energy electrons. Electronics part CESR 76 588 Février 1976  
H. BARTH, F. COTIN, J.L. MEDALE and H. REME  
submitted for publication to Space Science Instrumentation
- 5 . Waves measurement in "ARAKS" experiment  
LGE  
J.Y. DELAHAYE, J. LAVERGNAT, R. NEY et J.F. KARCZEWSKI  
Submitted for publication to Space Science Instrumentation
- 6 . Mesure des ondes dans l'expérience ARAKS  
C. BERCY, J.J. BERTHELLIER, J.Y. DELAHAYE, G. GOGLY, J.F. KARCZEWSKI, J. LAVERGNAT, J.M. MOREAU, R. NEY, G. PENAZZI, M. PIRRE, J.C. REBOURG, F. SERRE - Partie française et G.A. GOUSSEVE, Ju.V. KOUCHNERESKI, V.V. MIGOLINE, S.A. POULINETZ - Partie Soviétique - Rapport interne LGE 15 septembre 1975
- 7 . Ion analysers for measurement of D.C. electric fields and ion temperature J.J. BERTHELLIER et M. PIRRE submitted for publication to Space Science Instrumentation
- 8 . Les expériences françaises, Mesures optiques du projet ARAKS dans la région d'Arkhangelsk - URSS.  
C.BARAT, M. FEHRENBACH, G. WEILL submitted for publication to Space Science Instrumentation
- 9 . The project ARAKS PAYLOADS  
G. CHARLES Toulouse Space Center - FRANCE  
V. DOKUKINE IZMIRAN - Academy of Sciences - URSS
10. AAIA 3rd Sounding Rocket Technology Conference Albuberque - New Mexico March 7-9, 1973 - A. REHRI and J.C. PENNANECK CNES  
Study of the influence of asymmetries on the flight behaviour of the sounding rocket
11. Symposium Franco-Soviétique - Expériences actives dans la magnétosphère - Toulouse 10-14 mai 1976  
Comparaison des données radar et des modèles de champ géomagnétique.  
Y. GERVAIS DE FAFOND, N.Y. IZHOVKINA, I.A. JOULINE, J.C. KOSIK, A.Kh. PYATSI H. REME, A. ST MARC, Uy.L. SREDLOV, M. V. USPENSKII et J.M. VIGO
12. Note technique CNES/75/489/DEXO/MT/ML 19 septembre 1975 ARAKS - Résultats d'attitude et de trajectoire - J.M. ROBERT
13. Projet ARAKS - Expériences "ondes"  
Actions correctrices sur la dynamique du cône éjectable pour assurer la tenue des antennes extensibles  
J. et J.J. RUNAVOT CNES - Pages 625 à 651  
Colloque international - Technologie des expériences spatiales Paris 26-30 mai 1975 - Document CNES

# THE INFORMATION SYSTEM OF PLANETARY VEHICLES AND MOTION SAFETY PROBLEMS

B. N. Petrov, Ye. V. Avotinsh, V. G. Grigoryev, A. L. Kemurdzhian,  
L. N. Lupichev, L. T. Panova, L. N. Polenov, and P. S. Semenov

*USSR Academy of Sciences, Moscow*

## Abstract

The creation of an effective on-board information system is a major problem for remote controlled and self-contained planetary vehicles.

The key functions of such a system are to collect and process topographic information needed for motion, to classify passable and impassable sections and to choose the motion path. It is expedient to construct the information system consisting of two subsystems - the far view subsystem and the close view subsystem. The paper outlines the range of problems solved by the close view subsystem, the main function of which is to ensure the vehicle's motion safety.

The vehicle's motion features linked with its stability, profile trafficability and bearing trafficability on the terrain are discussed. The authors also analyze the effect exerted on the vehicle's motion safety by the distortions of the prescribed motion due to the interaction between the driver and the surface. Motion distortion cases are illustrated by examples from the service of Lunokhod-1 and its terrestrial running mock-ups.

It is concluded from the specific features of the vehicle's motion that the close view information system should consist of three subsystems: the profile trafficability forecasting subsystem, the bearing trafficability forecasting subsystem and the on-board performance estimation subsystem.

The authors consider the elements of information needed to ensure the safety of the vehicle's motion, analyze some types of information sensors and the size of their visibility zones proceeding from the features of the vehicle's motion. This conclusion is made on the necessity of either to increase the visibility zone of information sensors to the limits guaranteeing safety or to control the zone of view by signals from the sensors of the on-board performance estimation subsystem.

Structural schemes of motion control with different degrees of automation on board the vehicle are considered, as well as the solution of the motion safety problems, in particular during the operation of Lunokhod-1.

## Introduction

The logic of space exploration has brought about the advent of automatic laboratories moving on the planetary surface and collecting scientific information without man's presence on board. As noted in<sup>1</sup>, by the motion control mode these mobile planetary laboratories are subdivided into remote controlled and autonomously controlled. The feasibility of creating the former was proved by the successful operation of Lunokhod-1 and Lunokhod-2. The necessity of designing the latter was widely discussed in a number of papers at the IFAC symposiums<sup>2,3,4,5</sup>. The success of solving the problem of ensuring the planetary vehicle's motion in the autonomous control mode depends above all on the creation of an effective and highly reliable on-board information system. The key function of this system is to ensure the vehicle's motion safety. The problem of designing an on-board information system is also topical for remote controlled planetary vehicles. The extension of its functions, as compared with the system used in Lunokhod-1, will enhance the reliability of motion in conditions, when it is difficult for the driver to discern obstacles, and will reduce the strain on him. The on-board information system for motion purposes should collect and promptly process topographic information, classify passable and impassable sections and choose the vehicle's path.

As mentioned earlier<sup>2,4</sup>, it is expedient to divide the region in which topographic information is obtained into two zones - the close view zone and the far view zone. The gist of this division is as follows. The reliability of topographic information is unequal for sections close to the vehicle and removed from it. On far-away sections some obstacles, for instance, due to the screening effect of the relief, are indiscernible from the vehicle. Information on soil can be obtained only in the close zone. However, to choose the optimum path of motion, information on terrain is needed both in the close vicinity to the vehicle and at the maximum possible distance from it. This is why it is reasonable to construct the topographic information system consisting of two parts - the far view system and the close view system. The length of the zone of obtaining information by this or that system is determined as a result of the analysis of the capacities of information sensors and the properties of the area of the vehicle's

planned operation. The vehicle's maneuvering depends on the fact from which system the information on the necessity of the maneuver is obtained. On the basis of information from the far view system the vehicle can execute extensive maneuvering while choosing the optimum path of motion. The maneuvering on the basis of information from the close view system is limited since it is connected with the bypassing of a dangerous obstacle which lies in the immediate proximity to the vehicle. Since the most reliable information on terrain can be obtained by the close view system the latter must solve the problems of ensuring the motion safety of the planetary vehicle.

The aim of the present paper is to outline the range of problems which must be solved by the on-board close view system. This is done on the basis of an analysis of the vehicle's ability to cope with various road situations. Besides, the structures of this system for planetary vehicles operating in the remote control mode and in the self-contained control mode are considered.

#### The Specific Features of the Planetary Vehicle's Motion on Terrain

The planetary vehicle's ability to move on terrain is determined by two factors: the trafficability by geometric formations of the relief (profile trafficability) and the trafficability linked with the physical properties of soil (bearing trafficability). To estimate the profile trafficability on the surface the real profile of the surface in the direction of the vehicle's motion should be determined, taking account of the limitations due to the vehicle's geometric characteristics. The vehicle's encounter with geometric formations exceeding the indexes of its profile trafficability may lead to the loss of the mobility or stability of the vehicle. The vehicle's mobility may be lost when its bottom bogs down in an obstacle, when the front (rear) part sticks into an obstacle, and so on. The loss of stability can be due to the surmounting of a counterescarp or a crater, the braking on the slope, the sticking into a jutting obstacle, etc.

In the stage of designing the planetary vehicle dangerous situations can be determined by estimating its mobility and stability. For this purpose a mathematical model describing the reaction of the planetary vehicle to external disturbances must be constructed. Using this model, after checking its correctness and accuracy on running mock-ups simulating the planetary vehicle, the problem of the vehicle's mobility and stability in the prescribed service conditions is solved. This method was applied to Lunokhod-1. Its mathematical model<sup>1</sup> was checked in tests of special running mock-ups in terrestrial conditions and in tests of the vehicle itself operating on the Moon's surface.

Fig. 1 summarizes the results of the motion of Lunokhod-1 and mock-ups across a crater 3 m in diameter.

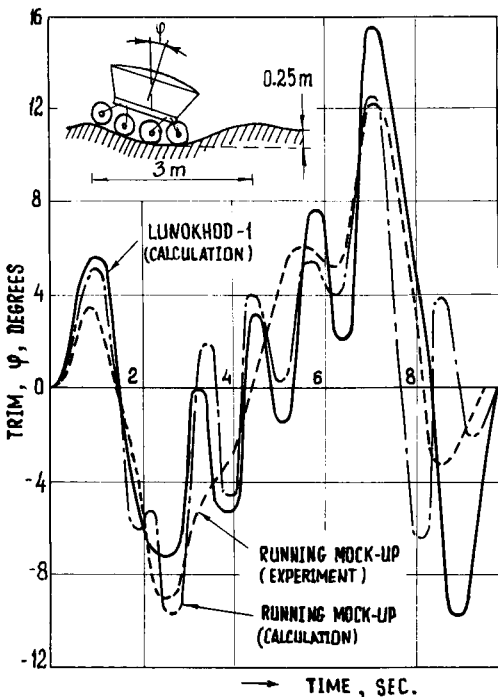


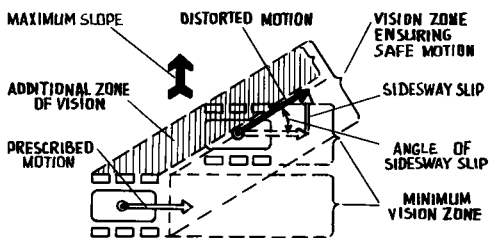
Fig. 1. Trim variations of Lunokhod-1 and the running mock-up when they surmounted a crater 3 m in diameter and 0.25 mm deep

Such craters were safe, as far as mobility and stability were concerned, since, when that crater was being surmounted, the trim of Lunokhod-1 did not exceed 15° while the angle of its tumbling was 45°.

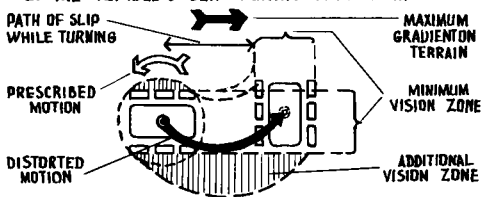
To appraise the vehicle's bearing trafficability the mechanical properties of soil (bearing strength) should be determined in the direction of its motion and also the vehicle's cohesion and traction capabilities with due account of existing limitations. The motion on the terrain section with low bearing strength or riding into it may lead, due to the sinkage of the chassis into soil, to the loss in the vehicle's mobility, or, if the geometry of the surface varies considerably, to the damage of the vehicle's bottom. Hence, the trafficability of the planetary vehicle should be determined from information on terrain in the direction of motion. However, the direction of the vehicle moving on the planetary surface is not always known exactly. An analysis of the vehicle's motion in diffi-

cult topographic conditions, tests of the vehicle's mock-ups and the operation of Lunokhod-1 and Lunokhod-2 show that in some cases the direction of motion does not coincide with the prescribed motion determined by commands ("straight motion," "spot turn"). As a result of the interaction of the vehicle's chassis with relief, sometimes the movement is distorted. Several types of distorted motion are schematically presented in Fig. 2.

#### A. THE VEHICLE'S SIDESWAY SLIP ON THE SLOPE



#### B. THE VEHICLE'S SLIP DURING SPOT TURN



#### C. THE VEHICLE TURNS ENCOUNTERING A STONE



Fig. 2. Schemes of the planetary vehicle's motion in various road conditions and viewing zones necessary for safe movement.

Fig. 2a shows the vehicle's sideways slip during straight motion on a rather abrupt slope on a surface having low bearing strength. Fig. 2b shows the shift of the vehicle's turning center during a spot turn in conditions similar to previous ones. If the vehicle is surmounting a stone, a crater crest or a ledge, it can turn to take a new course (see Fig. 2c).

In some cases, for instance, during the motion along a crater slope, both the lead and the sideways slip can take place simultaneously. Table 1 lists numerical characteristics of several cases of distorted

motion of the mock-ups of the planetary vehicle on the testing ground.

Table 1. The characteristics of distorted motion of Lunokhod and a mock-up

Distorted motion	Unit	Numerical value	of measure
The lead of Lunokhod-1 on a section with alternating slopes (per 10 m of the path)	degrees	5 to 6	
The slip of the Lunokhod mock-up on a slope with low bearing strength (the angle of the slope $30^\circ$ )	meters		
spot turn by $45^\circ$		1.3	
spot turn by $90^\circ$		2.5	
The turn of the Lunokhod mock-up while meeting single obstacles:	degrees		
riding over a stone (by one board) on a horizontal section		10 to 20	
riding over a crater rim at a sharp angle		5 to 15	

As evident from the Table, distortions may reach considerable values and essentially influence the vehicle's position on the surface. It can be concluded that the vehicle's motion safety can be ensured only if all factors determining its motion on terrain are taken into account.

These factors are profile trafficability, stability, bearing trafficability, distortion of prescribed motion.

Problems of the vehicle's motion safety should be tackled on special running mock-ups whose parameters are close to the corresponding parameters of the planetary vehicle under design. This will make it possible to simulate the specific features of the vehicle's motion on terrain during studies of motion safety problems depending on the degree to which the vehicle is self-contained.

The motion safety of Lunokhods 1 and 2 was studied with the help of such mock-ups moving on a special testing ground fitted out with an information-controlling complex. Studies were also made of the specific features of the motion of running mock-ups overcoming various kinds of profile obstacles and the surface sections with low bearing strength.

Table 2 compares some parameters of Lunokhod-1 and the running mock-ups with

the aid of which motion safety was investigated.

Table 2. Parameters of Lunokhod-1 and the running mock-up used for motion safety studies

Parameter	Unit of Measure	Luno-khod-1	Mock-up
Weight	N	1,270	1,750
Wheel base	m	1.7	1.7
Wheel spacing	m	1.6	1.6
The center of gravity height	m	0.835	0.835
Double rigidity of front (back) wheels	N/m	16,600	16,600
Double rigidity of middle wheels	N/m	7,000	7,000
The wheel's radial rigidity	N/m	250,000	250,000
Total damping coefficient	N·s/m	1,000	1,000
Moment of inertia with respect to the lateral axis passing through the center of gravity	kg·m <sup>2</sup>	290	290

As obvious from Table 2, the running mock-up parameters are close to Lunokhod-1 parameters. This made it possible to simulate in terrestrial conditions with the sufficient accuracy the specific features of the motion of Lunokhod-1 on the Moon. The accuracy of simulating the dynamics of the motion of Lunokhod-1 by angular oscillations is reflected in the curves represented in Fig. 1.

#### Specific Features of Constructing the Information System

It is reasonable to construct the vehicle's close view information system determining motion safety in the form of a complex consisting of three specialized subsystems:

the profile trafficability forecasting subsystem,  
the bearing trafficability forecasting subsystem,  
the on-board performance estimation subsystem.

Each subsystem solves the problem of discovering dangerous situations in the process of motion. It must be provided with appropriate information sensors and electronic circuits of processing information from its sensors, taking account of information coming from sensors of other subsystems. To ensure the vehicle's safety the subsystem must solve the problem of trafficability forecasting in the direction of motion. Fig. 3 presents the struc-

ture of information necessary for ensuring the vehicle's motion safety for each of the above-mentioned subsystems.

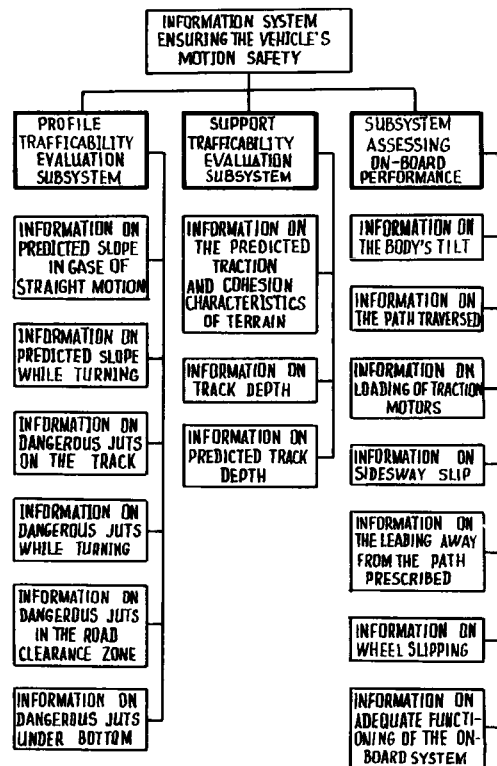


Fig. 3. Elements of information necessary to ensure the motion safety of the planetary vehicle

The greatest difficulties in designing the subsystems are associated with information sensors. In the profile trafficability estimation subsystem we can use as topographic information sensors both contact (mechanical feelers) and non-contact sensors. The latter (television systems, gamma-radar, laser radars, etc.) have some advantages over contact sensors: they bring more information, are more compact and do not interact with obstacles. However, unlike contact sensors, the readings of non-contact sensors depend to a great extent on service conditions which may be insufficiently known while the planetary vehicle is under design. For instance, the experience of the operation of Lunokhods 1 and 2 has demonstrated that in a number of cases television topographic information has not helped the driver discover some obstacles. For instance, cra-

ters on the slope in conditions of "the high sun" and obstacles before the vehicle which was closed by its shadow were not seen on the driver's television screen when the sun was behind the vehicle. If the planetary vehicle operates in conditions of dust storms on Mars the retention of design characteristics of sensors using optical systems can involve certain difficulties.

To obtain information on soil characteristics in the bearing trafficability forecasting subsystem contact (mechanical) devices are most effective. The principles of their operation are well known<sup>7</sup>. Lunokhods 1 and 2 had a device for estimating bearing trafficability. It contained a conic vane stamp<sup>7,8</sup>, with the aid of which the traction and cohesion properties of soil were determined. It is difficult to design a contact sensor measuring the properties of soil without the vehicle's stoppage. In addition to forecasting the traction and cohesion characteristics (bearing trafficability) of the surface on which the vehicle will move, the subsystem evaluating bearing trafficability must determine the depth of the trail formed by the chassis of the planetary vehicle and forecast the subsequent depth of the trail. This information is fed into the profile trafficability evaluation subsystem to correct the information on the predicted slope and dangerous obstacles under the bottom.

The subsystem estimating the on-board performance must generate information needed for the operation of other subsystems and ban the motion when the on-board systems reach values dangerous for the vehicle's normal operation (overloading of traction motors, the hazardous tilt of the vehicle's body, the risky sideways slip, dangerous skidding or wheel slide).

Subsystems ensuring motion safety must formulate the vehicle's performance in two terms: "motion admissible" and "motion inadmissible." In determining the operation zone of topographic information sensors the possibility of the vehicle's distorted motion should not be neglected.

Fig. 2 shows schemes of the vehicle's motion in various topographic conditions and zones of the operation of information sensors needed to ensure motion safety. As is seen from the schemes, the sensors' minimum viewing zone corresponding to the vehicle's width does not ensure its safe motion. In all cases of the vehicle's distorted motion shown here the motion zone is larger than the minimum viewing zone of information sensors. This incongruity can be abolished in two ways. First, through the expansion of the minimum viewing zone to the value ensuring the range of scanning the terrain with due account to the size of the possible risky zone (the standard width of viewing). This is reasonable when the scanning zone increases insignificantly (Fig. 2c). However, there is no need to expand the scanning zone to the value meeting the requirements of the schemes in Figs 2a and b.

This will reduce the vehicle's ability to move on terrain since an enlarged safe corridor will be needed for motion.

Second, through controlling the scanning zone of topographic information sensors. The viewing zone may be extended in the needed direction by the signal from the subsystem responsible for the estimation of on-board performance. The vision zone can be expanded by installing extra side sensors of relief switched on by information from the corresponding sensors of the subsystem estimating on-board performance (sideways slip, lead, etc.) Such are the main features of the vehicle's motion on the planetary surface and the range of problems which should be solved to secure its motion safety.

#### The Structure of the Motion Control System with Various Degrees of the Vehicle's Automation

As shown above, to ensure safe motion one should possess information presented in Fig. 3. This information must be contained in the vehicle's information system irrespective of the degree to which it is self-contained. The difference for vehicles which are self-contained to various degrees consists in the method of obtaining this information (either directly by the driver, or by special information sensors).

However, the obtaining of the necessary amount of information is determined by the performance of the information system. If information is incomplete, motion safety decreases. The extent of the decrease depends on the role of this or that element of information.

The structure of the information system and the motion control system is closely linked with the degree of the automation of solving the motion safety problem on board the vehicle. Fig. 4 presents three structural schemes of vehicles' motion control systems which are self-contained to different degrees.

In the remote controlled vehicle the crew is responsible for motion control.

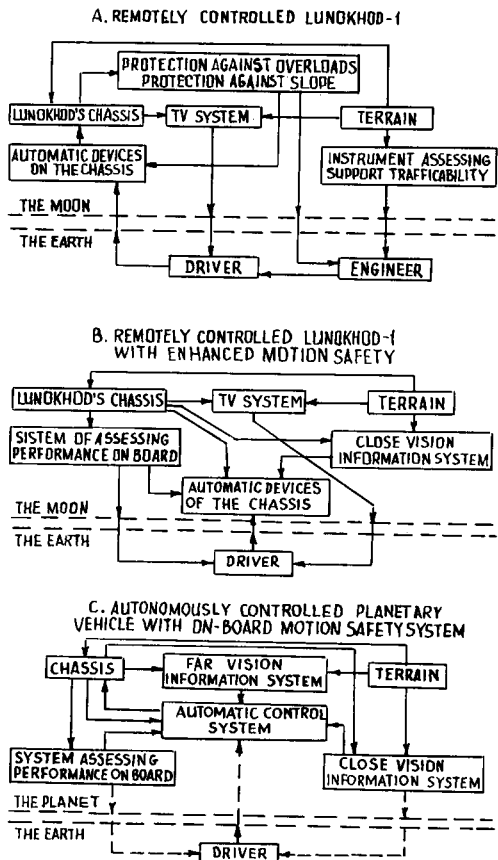


Fig. 4. Structural schemes of vehicles' motion control systems which are self-contained to a different degree

The problem of ensuring the motion safety of Lunokhod-1 was solved mainly by the driver (profile trafficability forecasting) and partly by the system assessing on-board performance (overloading of traction motors and the vehicle's dangerous tilt). Information for choosing the direction of motion and for assessing the ability to move came to the driver from the on-board television system. The safety of the motion of Lunokhod by the bearing trafficability crite-

tion was ensured by the driver through forecasting bearing trafficability and by the engineer through determining wheel slip. The driver predicted the vehicle's trafficability on the basis of a comparative analysis of television information on terrain and the results of processing by a group or the on-board engineer the data on measuring the mechanical properties of soil by the on-board instrument which appraised trafficability. These measurements were carried out when Lunokhod stopped to perform its operations. The quality of forecasting improved with the accumulation of topographic data and the driver's growing experience in comparing various information. With the further improvement of Lunokhod's remote control system it is reasonable to expand the functions performed by the on-board system by forecasting profile and bearing trafficability on board Lunokhod (Fig. 4B).

The driver should continue to carry out a general expert analysis of terrain to choose the direction of motion. This will enhance Lunokhod's motion safety, will raise the average speed of motion and reduce the intensity of the driver's work.

For the vehicle operating in the self-contained control mode the motion problems should be solved by an-board control system (Fig. 4C).

As evident from the schemes, with the development of an on-board topographic information system the flow of information to the ground-based control center diminishes.

#### Conclusions

1. The vehicle's motion safety depends on the completeness of topographic information from the on-board information system. The information should take into account all the specific features of the vehicle's motion, in particular the distortions of the path due to the interaction of the driver with the surface.

2. The structure of the information system depends on the fact how self-contained the vehicle is and what is the method of controlling its motion. It is rational to construct this system in the form of two subsystems - the close view subsystem and the farview subsystem which must solve the problems of profile and bearing trafficability forecasting and also problems of the vehicle's stability and performance.

### References

1. G. P. Katys, Information Systems of Research Vehicles, Energiya Publishers, Moscow, 1972
2. B. N. Petrov, V. Ye. Ishevsky, V. P. Panteleyev, G. I. Ulanov, Ye. I. Krinetsky, and G. N. Lebedev, Supply of a Space Experiment of Planetary Exploration With Information, Paper presented at the Sixth Symposium of IFAC, Yerevan, 1974
3. V. V. Solodovnikov, A. M. Dmitriyev, and Ye. I. Kuzin, Identification of the Situation in Controlling the Motion of a Self-Contained Vehicle, Paper presented at the Sixth Symposium of IFAC, Yerevan, 1974
4. B. N. Petrov, L. N. Lupichev, V. I. Agafonov, V. D. Vasiliyev, B. L. Kozlov, and I. V. Shamanov, The Problem of Controlling Self-Contained Mobile Planetary Complexes, Paper presented at the Sixth Symposium of IFAC, Yerevan, 1974
5. M. G. Bekker, Introduction to Terrain-Vehicle Systems, Ann Arbor, The University of Michigan Press
6. Lunokhod-1, a Mobile Laboratory on the Moon, Editor-in-Chief A. P. Vinogradov, USSR Academy of Sciences, Moscow, 1971
7. A. K. Leonovich, V. V. Gromov, et al., Studies into the Physical and Mechanical Properties of Lunar Soil on the Basis of an Analysis of the Soil Sample Brought by the Luna-20 Unmanned Station and of the Soil on the Path of the Motion of the Lunokhod-2 Self-Propelled Vehicle, Paper Presented at the XXIVth Congress of the International Astronautical Federation, 1973
8. A. L. Kemurdzhian, and L. N. Lupichev, Control of Self-Contained Mobile Planetary Complexes, Paper Presented at the eventh Symposium of IFAC
9. Ye. V. Avotinsh, A. K. Alexandrov, and F. P. Yakovlev, The Stability of the Motion of Vehicles at Reduced Gravity, Kosmicheskiye Issledovaniya (Cosmic Research), Issue 6, Vol. XI, 1973, Moscow

# MULTISPECTRAL AND STEREO IMAGING ON MARS

Elliott C. Levinthal\* and Friedrich O. Huck\*\*

\*Stanford University, Stanford, CA 94305, U.S.A.

\*\*Langley Research Center, Hampton, VA 23665, U.S.A.

In this paper we will discuss some of the general aspects of the Viking Lander Camera system (1,2), its design and function, illustrated with some results of its operation on Mars during the Viking Mission.

Figure 1 presents a view of a Viking Lander in a test facility. Its two turret-like cameras are separated by 0.8 m and view the surrounding terrain from a height of 1.3 m.

Figure 2 shows an outline drawing of the field of view of the cameras. A large segment of their view is obscured by the lander structure. Three reference test charts, of which each camera can view two, are used to calibrate the radiometric performance of the cameras. "Hard points" on the lander top, geometrically characterized before launch, are used to calibrate the cameras photogrammetric performance. The shaded area is accessible to the surface sampler which delivers samples to hoppers on the lander for biological and organic and inorganic chemical analysis.

The lander performs a roll maneuver (i.e., rotation about an axis parallel to the camera axis) during its final descent phase. The goal is to obtain morning and afternoon lighting of the sampler area, first from one direction and then from the other, to insure that all features in this area can be viewed at one time or another out of shadow.

Figure 3 presents a simplified cutaway view of the camera, which weighs 7.3 kg, and requires an average operating power of about 30 W.

The upper assembly, which contains an elevation scanning mirror, a lens, and photosensor array, rotates in azimuth during imaging. The lower assembly, which contains all signal processing and servo electronics, is bolted to the lander.

The narrow window entrance is usually stored behind a post to avoid unnecessary exposure to dust. The post contains two small tungsten filament light sources that permit the camera performance to be checked during the flight to Mars and on Mars to monitor the window transmittance for possible dust adhesion or abrasion. Carbon dioxide carried under pressure in a container inside the lander can be released on command through an orifice attached to the post, to blow dust off the window.

The camera has two windows. The outer window, not shown in Fig. 3, is hinged on one side and spring-loaded. Rotating the camera nearly  $360^{\circ}$  in a rapid slew mode, a lever can be forced against the side of the dust post with sufficient impact to release a catch on the outer window. A spring then moves this window out of the optical path. The outer window was intended to protect the inner window from gaseous condensation during the lander heat sterilization process prior to flight, and from dust contamination during the initial operations on Mars. It is intended to be released when there is evidence of optical attenuation. Light which passes through the window is reflected by a mirror that nods up and down to provide the elevation scanning. Image data are acquired only during the relatively slow upward motion. The reflected light is imaged by an achromatic triplet lens onto a photosensor array. The lens aperture diameter is 0.95 cm and the focal length is 5.37 cm.

Immediately below the lens is a shutter that can be moved over the lens to block light from reaching the photosensor array. The purpose is two-fold: to sample the photosensor-preamplifier dark current, which is stored for later subtraction from the signal current, and to permit calibration of the photosensor array with a small tungsten filament lamp located below the shutter.

The optical tunnel between the lens and the photosensor array contains a multiaperture baffle that is designed not only to reduce veiling glare but also to attenuate radio frequency interference from the lander antennas.

Figure 4 presents a view of the photosensor array. Its light-sensitive part is a miniature array of 12 silicon photodiodes. Four of the diodes are spaced at different distances from the lens providing electronic focus selection for high-resolution (black and white) imaging. Six of the other diodes are covered with optical filters for multispectral (color and near-infrared) imaging. Another diode is unfiltered and used for rapid surveys of the terrain, and one is covered with a red filter and used for viewing the sun directly. The aperture diameter for the high-resolution diodes is 0.04 mm to form an instantaneous field of view of  $0.04^{\circ}$ , and for the other diodes is 0.12 mm to form an instantaneous field of view of  $0.12^{\circ}$ . The geometric depth of field for these angular resolutions extends from 1.7 m to infinity, providing that the high resolution photodiode providing the best focus is selected within this range.

Camera operation is controlled by the lander computer. Control includes selection of photodiode, azimuth start and stop and elevation pointing angles, and imaging scanning modes. Upon receipt of clock pulses, the camera logic selects first engineering data (such as temperature) from various sources and then video data. Video data is passed through a 524-bit memory which converts the 75-percent mirror scanning efficiency to a 90-percent video data format efficiency. This process is repeated for each line scan in an image. Several different imaging modes can be commanded.

A high-resolution imaging mode is effected by video sampling every  $0.04^{\circ}$  during each  $20^{\circ}$  elevation line, and an equal azimuth stepping angle between line scans.

Similarly, a low-resolution (survey) imaging mode is effected by video sampling every  $0.12^{\circ}$  during each  $60^{\circ}$  elevation line, and an equal azimuth stepping angle between line scans.

Low-resolution multispectral imaging modes are available by alternately selecting three diodes for successive elevation scans and inhibiting the azimuth servo until three elevation scans have been completed. Usually triplets with blue, green and red or three infrared filters are chosen although other combinations are possible.

In addition, repeated line scans are effected by inhibiting the azimuth servo. This mode is used for radiometric measurements of atmospheric and surface features, and for observing variable features.

Data are acquired at either one of two rates: Synchronous with the lander data transmission rate of 16,000 bits per second to one of the two Viking orbiters as relay stations; or 250 bits per second directly to earth. Data acquired at either rate can also be stored on a lander tape recorder, permitting the cameras to be used during favorable imaging opportunities independent of data transmission periods.

Photosensor array responsivities are plotted in figure 5. The three spectral channels in the visual (0.4 to  $0.7\mu\text{m}$ ) region were selected to produce conventional color images, and the three channels in the near-infrared (0.7 to  $1.1\mu\text{m}$ ) were selected to detect reflectance minima near 0.95 mm due to  $\text{Fe}^{++}$  electronic transition absorption bands.

Photosensor array size and heat sterilization requirements dictated that interference-type filters be used. The filters have multiple order transmittance peaks, and are most readily made with narrow-band transmittances (about  $0.01\mu\text{m}$  for visible wavelength filters). Blocking of multiple order transmittance peaks for broader band transmittances (about 0.05 to  $0.1\mu\text{m}$ ) over the silicon photodiode responsivity range from 0.4 to  $1.1\mu\text{m}$  was only partially successful, and consequently some of the filters exhibit severe out-of-band leakage and a generally undesirable responsivity shape.

Dr. Stephen K. Park (3), of the Langley Research Center, has developed the computer processing software required to estimate spectral surface reflectance curves from the multispectral data. To do so, the output of each channel is expressed as a linear (integral) function of the unknown spectral reflectance and the known solar irradiance and camera responsivity. This produces six equations which can be used to determine the coefficients in a representation of the spectral reflectance as a linear combination of known basis functions. Spectral reflectance estimates are calibrated by repeated imaging of the 14 calibrated reflectance patches on each of the three reference test charts located on the lander. Figure 6 is a color image using only information from the internal calibration of the blue, green and red diodes to achieve color balance.

Limitations of data transmission required a trade-off scheme in the selection of a digital encoding between a large number of encoding levels to provide a wide dynamic range with small quantization intervals and a small number of encoding levels to obtain more images. This tradeoff led to the selection of 6-bit encoding (i.e., 64 quantization levels) with six commandable linear gains and 32 offsets as shown in Figure 7. Together these gains and offsets provide many choices between wide dynamic ranges with broad quantization intervals and narrow dynamic ranges with small quantization intervals. It was anticipated that the initial characterization of scene radiance may involve some trials and possible errors in selecting proper gains and offsets. The dynamic range for the first pictures could have been selected too narrow to encompass the scene radiance, or too wide to encode the scene radiance with enough quantization levels for adequate image quality (4). However, as the first lander pictures themselves prove, the initial gain selections were not only adequate to generally characterize the landing site but to provide us with a dramatically clear view of the terrain.

Figure 8 is the first image ever returned from the surface of Mars (5,6). It is a high-resolution ( $0.04^{\circ}$ ) picture of footpad number 3 and the adjacent surface initiated 25 seconds after touchdown. The large rock in the center is 10 cm across. In the first 75 lines of the picture, which took 15 seconds to acquire, there are a large number of fine bright striations in the image. These are the result of a turbulent cloud of fine dust raised by the lander's retro-rockets between the camera and surface region viewed. The dark vertical band appearing to the right of these striations is probably due to a shadow of a cloud of the dust raised by the landing.

The second image is shown in figure 9. It is a low resolution ( $0.12^{\circ}$ ) panorama consisting of 2500 scan lines. At this resolution an object 6 m in size subtends  $0.12^{\circ}$  (one picture element) at the nominal horizon. The apparent horizon sinusoid is an artifact of camera tilt. Figure 10 shows the use of another  $0.04^{\circ}$  diode designed to bring into focus objects such as the large 3 m wide, 1 m high rock 8 meters away. Figure 11 illustrates the use of another  $0.04^{\circ}$  diode bringing into focus the landscape extending out to the local horizon at about 150 m. The rescan mode is represented by the right part of figure 12. Left-right variability in this mode is shown in the lower right portion of the picture indicating motion of a shadow across the footpad during the rescan period.

The use of two cameras allows quantitative topographic information to be derived from stereo pairs of Lander camera images. This information is generated using software and hardware collaboratively developed by Dr. Sidney Liebes of the Stanford University Genetics Department and Mr. Arnold Schwartz of the Image Processing Laboratory of the Jet Propulsion Laboratory (7). The software is a set of application programs called RANGER.

The hardware, an interactive stereo station shown in figure 13, consists of two specially developed monitors with provision for precision rotation of the cathode ray tube yoke.

RANGER runs on an IPL IBM 360/65 computer, and requires support from a PDP-11 mini-computer, and a RAMTEK random access solid state memory device. The Stanford interactive stereo station is required for the efficient processing of stereo data, particularly the development of topographic profiles.

It is possible, using the contour mode of RANGER, to interactively generate a profile representing the intersection of a selectable mathematically specified surface with the relief of Mars perceived in a stereo image pair.

The principle of operation of the contour mode is as follows. An arbitrary surface is mathematically defined in a Lander Aligned Coordinate System (LACS). For example, the surface may be oriented parallel to the top deck of the Lander and located 1.3 meters below the nominal height of the optical reference points within the cameras. As a trackball is rotated the computer moves a dot cursor in one-to-one fashion in the graphics overlay plane that is superimposed on the left camera image and displayed on the left monitor. If at any given instant the pointing direction for the dot cursor is directed below the horizon to a negative value of left camera elevation, the ray associated with that pointing direction for the left camera will intersect the above specified mathematical plane at a calculable three-space point. The computer, which samples the trackball position many times each second, promptly calculates the LACS coordinates of the instantaneous location of the three-space point, computes the right camera azimuth and elevation values associated with the three-space point, and projects a dot cursor at the evaluated right camera values of azimuth and elevation onto the graphics overlay plane superimposed on the right camera image displayed on the right monitor.

The photogrammetrist/operator will now see when looking into the stereo viewer, in addition to the Martian relief, an overlaid three-space cursor (representing the visually fused individual but mutually constrained dots overlaying the left and right images) which will be constrained to lie on the mathematically specified surface. By rotating the trackball, the operator can cause the three-space mark to move freely over the defined surface, but he will be unable to move it off the surface.

If he wishes to generate a profile representing the intersection of the defined surface with the relief, he moves the three-space cursor along the defined surface to a starting point along the intersection of the surface with the perceived Martian relief, issues a command indicating that he is ready to start generating a profile, and then moves the three-space cursor along his perception of the intersection of the defined surface with the Martian relief. As the trackball is rotated, a data set of specified granularity is generated.

The RANGER operator is able to provide support for sample acquisition by orienting the profile plane so that it contains the vertical axis about which the sample arm articulates when its azimuth is varied. The

vertical profiles, generated at prospective commanded azimuths for the arm, reveal the topography beneath the arm and through the prospective site.

Figure 14, a stereo pair, illustrates a vertical profiling session to define the topography of a site near Lander 2. A graphics formatting program has been written to output arm specific vertical profiles. Figure 15 is an example of the graphic output used to determine the suitability of a site for sample acquisition (9).

Other modes of contouring and ranging are possible. The accuracy is limited by the stereo base, the resolution of the camera picture elements and the geometric calibration.

Finally, to help determine the desirability as well as the safety of possible sample sites we use both radiometric and photogrammetric information for each picture element to combine high resolution pictures with low resolution color pictures of the same area. The resulting high resolution color image is shown in figure 16. (in black and white)

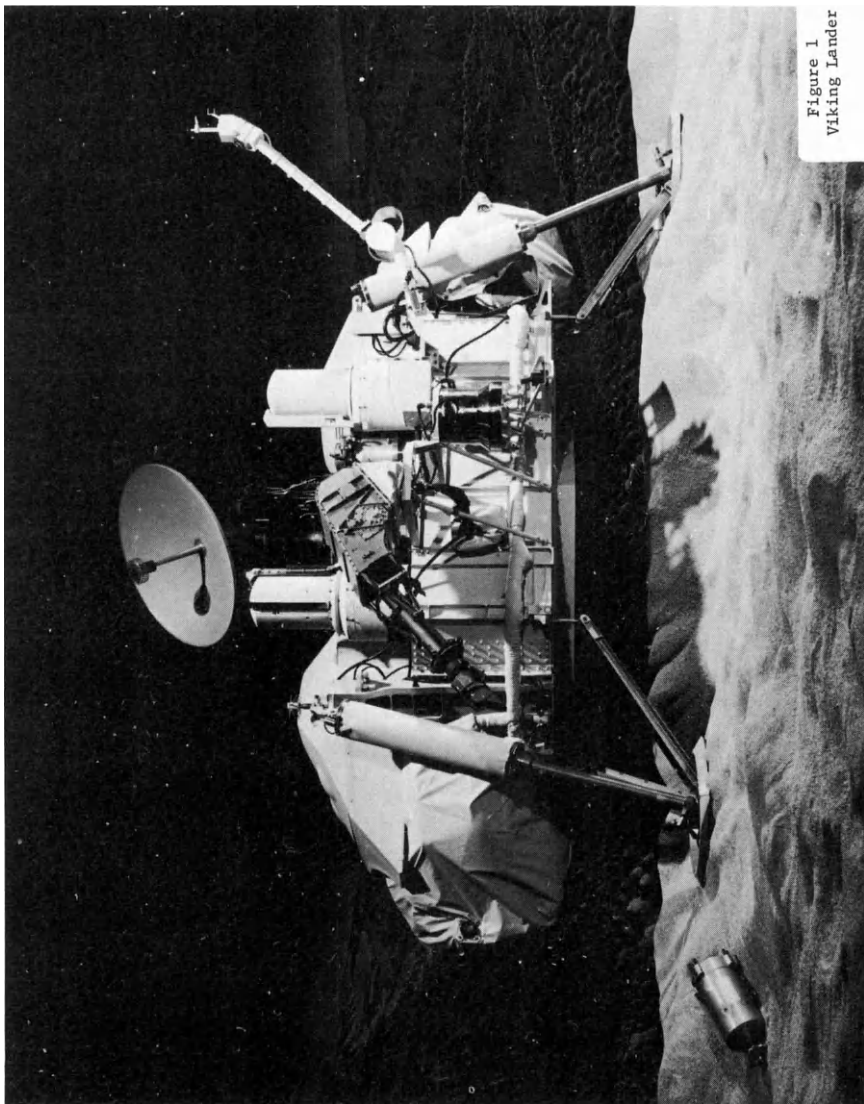
#### REFERENCES

1. T. A. Mutch, A. B. Binder, F. O. Huck, E. C. Levinthal, E. C. Morris, C. Sagan, A. T. Young, *Icarus* 16, 92(1972).
2. F. O. Huck, H. F. McCall, W. R. Patterson, G. R. Taylor, *Space Sci. Instrum.* 1, 189(1975).
3. S. K. Park and F. O. Huck: A Spectral Reflectance Estimation Technique for the Viking Lander Camera Multispectral Data, NASA TND-8292(1976).
4. F. O. Huck and S. D. Wall: Image Quality Prediction: An Aid to the Viking Lander Imaging Investigation on Mars, *Appl. Opt.* 15, 1748(1976).

The following two articles give details of the observations of Mars with the Lander Cameras:

5. T. A. Mutch, A. B. Binder, F. O. Huck, E. C. Levinthal, S. Liebes, Jr., E. C. Morris, W. R. Patterson, J. B. Pollack, C. Sagan, G. R. Taylor, *Science* 193, 791(1976).
6. T. A. Mutch, R. E. Arvidson, A. B. Binder, F. O. Huck, E. C. Levinthal, S. Liebes, Jr., E. C. Morris, D. Nummedal, J. B. Pollack, C. Sagan, *Science* 194, 87(1976).
7. Paper to be presented: Liebes and Schwartz, "Mars Viking '75 Lander Interactive Computerized Video Photogrammetry", FEB 1977 Meeting American Society of Photogrammetry.
8. R. W. Shorthill, H. J. Moore, II., R. F. Scott, R. E. Hutton, S. Liebes, Jr., C. R. Spitzer, *Science* 194, 91(1976).

Figure 1  
Viking Lander



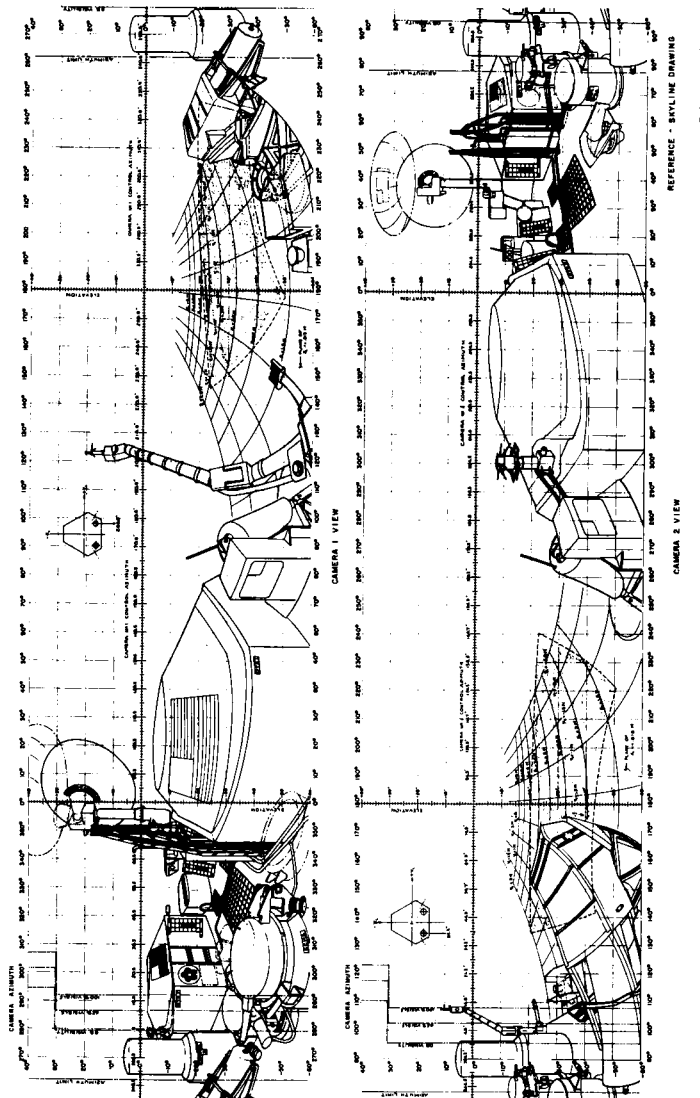


Figure 2  
Field of View  
of Cameras

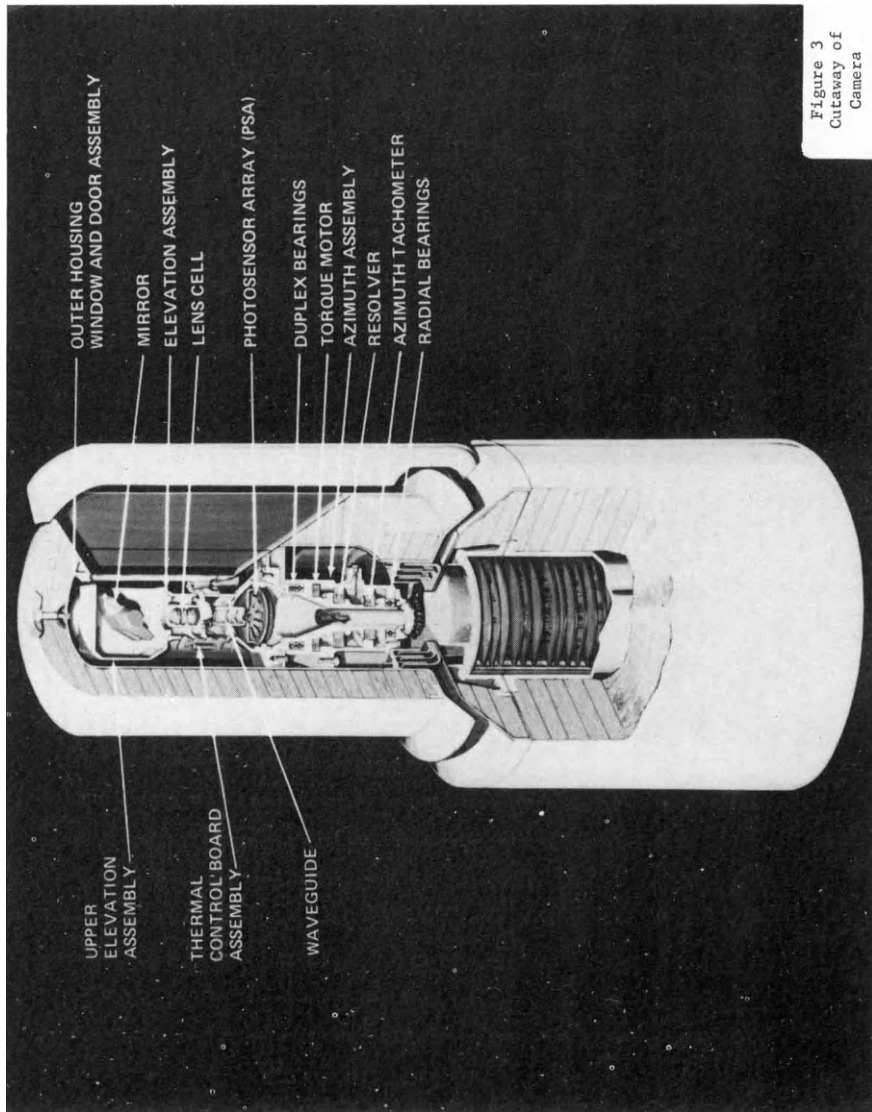


Figure 3  
Cutaway of  
Camera

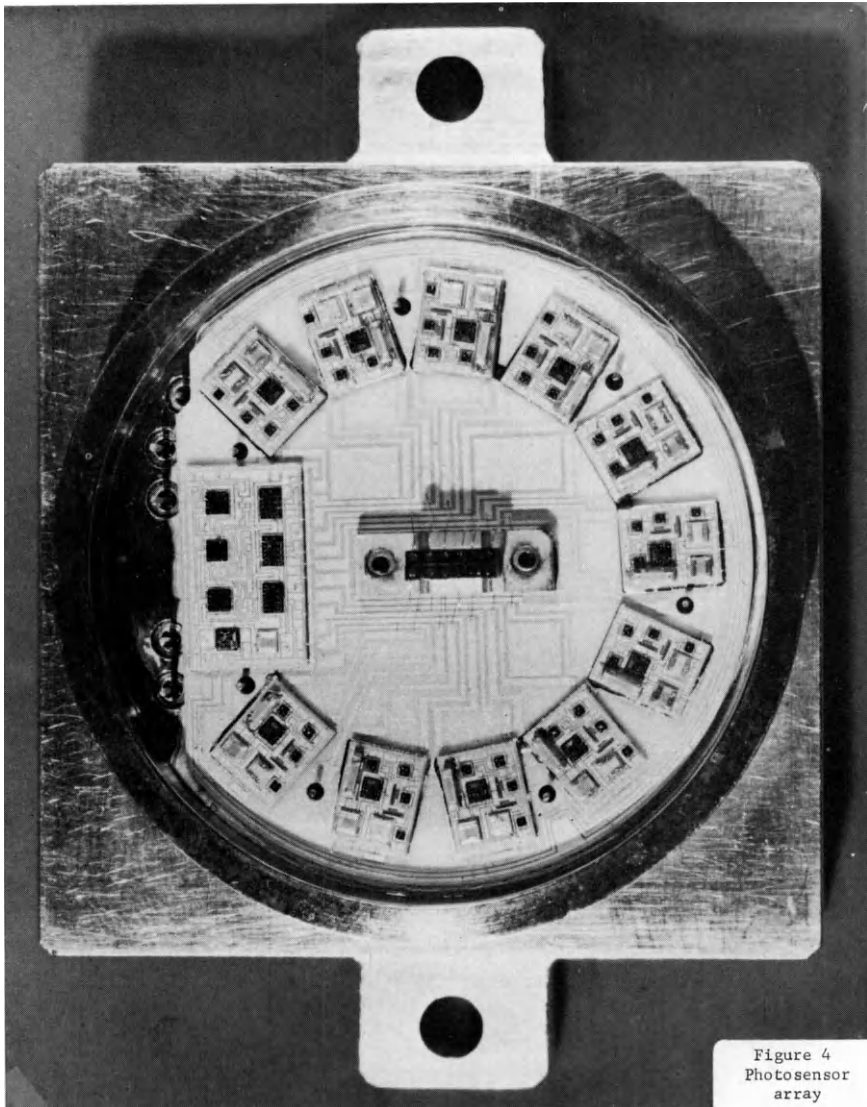
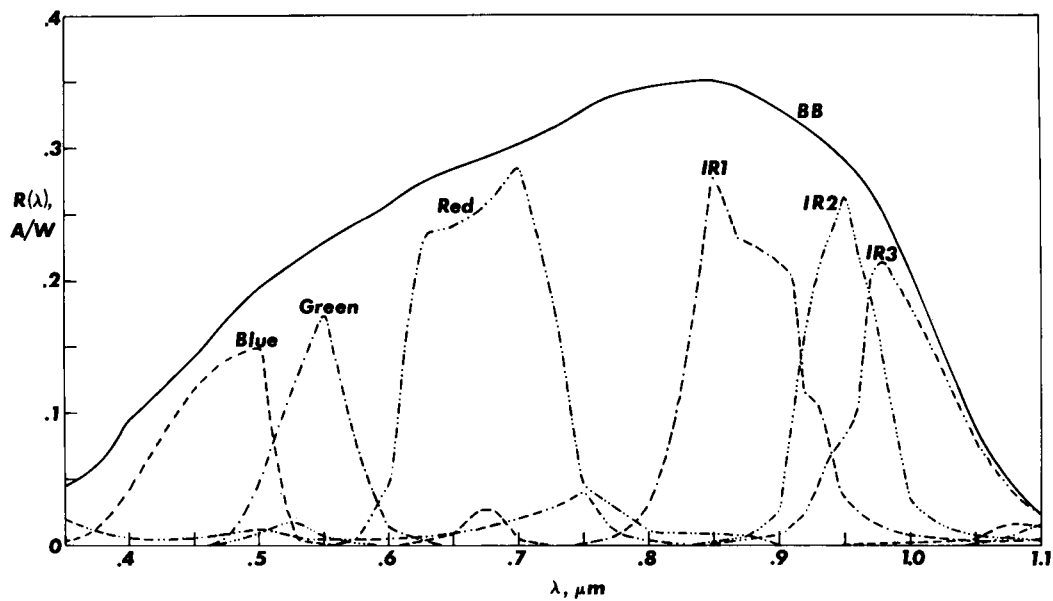


Figure 4  
Photosensor  
array



## Spectral responsivities of photosensor array.

Figure 5  
Spectral Respon-  
sivities of  
Photosensor array

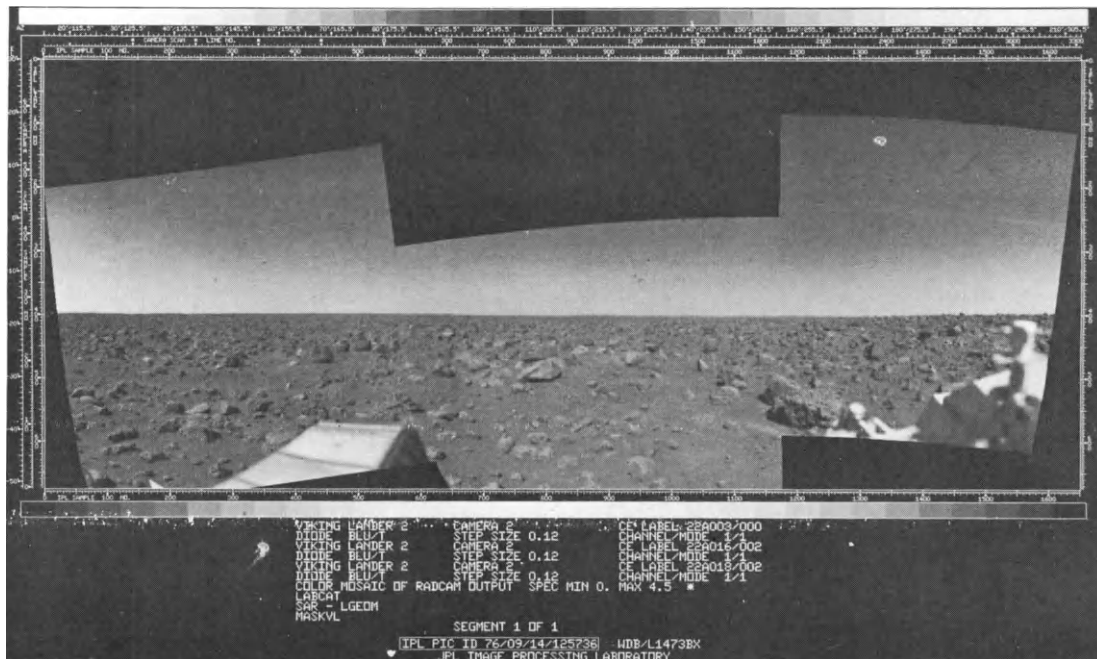


Figure 6  
Lander 2  
Color Mosaic

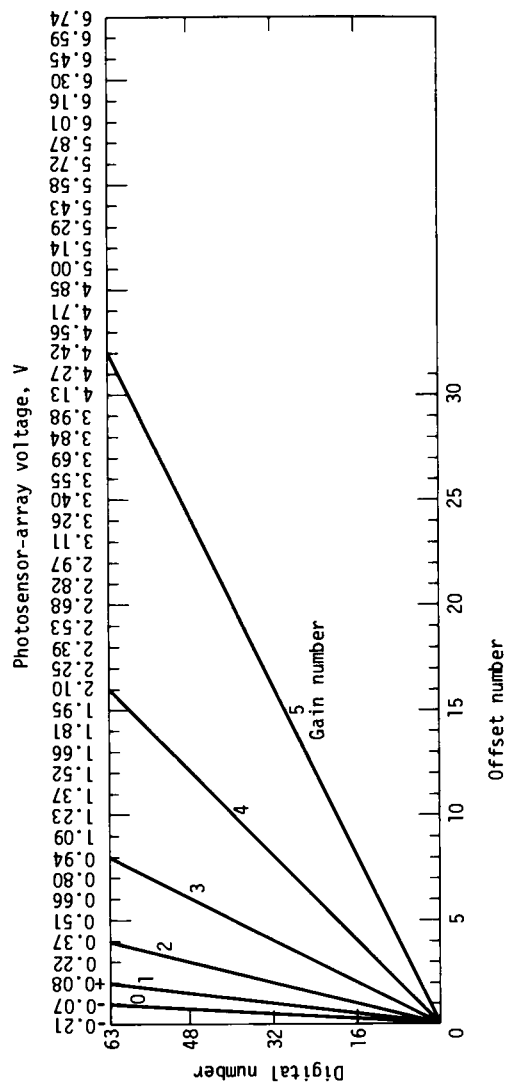


Figure 7  
Camera Gains  
and Offsets

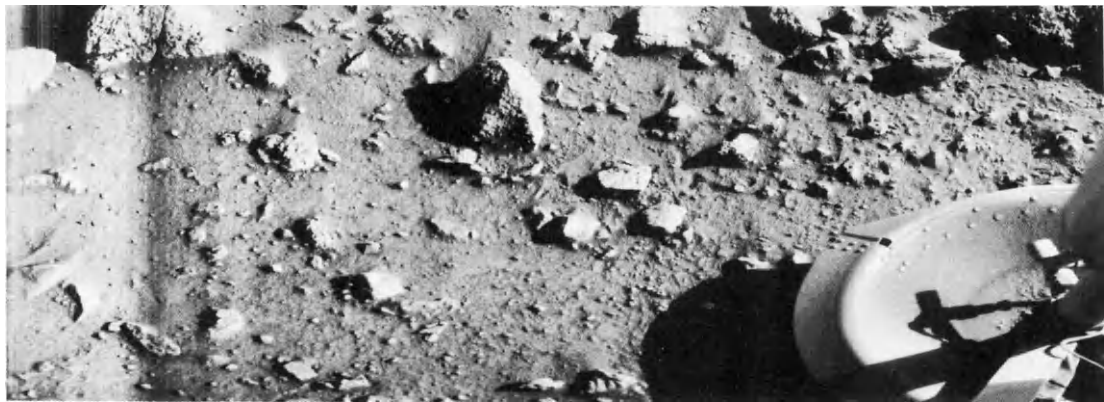


PHOTO CAPTION

Viking 1-44  
P 17053 (Sol 0)  
July 20, 1976

This is the first photograph ever taken on the surface of the planet Mars. It was obtained by Viking 1 just minutes after the spacecraft landed successfully early today. The center of the image is about 1.4 meters (five feet) from Viking Lander camera #2. We see both rocks and finely granulated material--sand or dust. Many of the small foreground rocks are flat with angular facets. Several larger rocks exhibit irregular surfaces with pits and the large rock at top left shows intersecting linear cracks. Extending from that rock toward the camera is a vertical linear dark band which may be due to a one-minute partial obscuration of the landscape due to clouds or dust intervening between the sun and the surface. Associated with several of the rocks are apparent signs of wind transport of granular material. The large rock in the center is about 10 centimeters (4 inches) across and shows three rough facets. To its lower right is a rock near a smooth portion of the Martian surface probably composed of very fine-grained material. It is possible that the rock was moved during Viking 1 descent maneuvers, revealing the finer-grained basement substratum; or that the fine-grained material has accumulated adjacent to the rock. There are a number of other furrows and depressions and places with fine-grained material elsewhere in the picture. At right is a portion of footpad #3. Small quantities of fine grained sand and dust are seen at the center of the footpad near the strut and were deposited at landing. The shadow to the left of the footpad clearly exhibits detail, due to scattering of light either from the Martian atmosphere or from the spacecraft, observable because the Martian sky scatters light into shadowed areas.

Figure 8  
BBL Diode 1st  
Picture  
Lander I Footpad

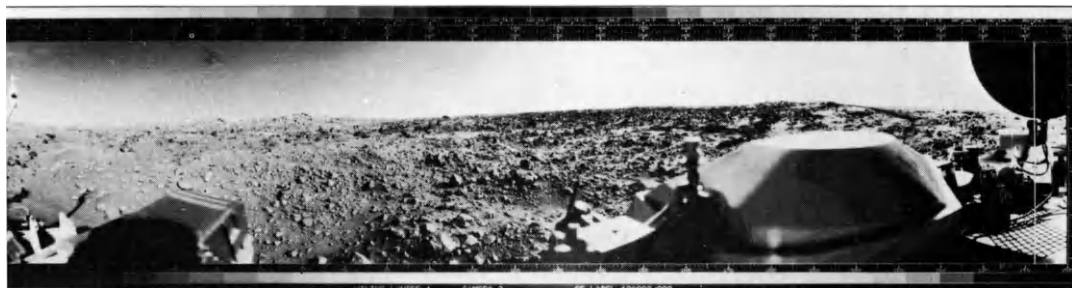


PHOTO CAPTION

P-17045AA (Sol 0)  
July 20, 1976

First panoramic view by Viking 1 from the surface of Mars. The out-of-focus spacecraft component toward left center is the housing for the Viking sample arm, which is not yet deployed. Parallel lines in the sky are an artifact and are not real features. However, the change of brightness from horizon towards zenith and towards the right (west) is accurately reflected in this picture, taken in late Martian afternoon. At the horizon to the left is a plateau-like prominence much brighter than the foreground material between the rocks. The horizon features are approximately three kilometers (1.8 miles) away. At left is a collection of fine-grained material reminiscent of sand dunes. The dark sinuous markings in left foreground are of unknown origin. Some unidentified shapes can be perceived on the hilly eminence at the horizon towards left center. The horizontal cloud stratum can be made out halfway from the horizon to the top of the picture.

At the center is seen the low-gain antenna for receipt of commands from the Earth. The projections on or near the horizon may represent the rims distant impact craters. In right foreground are color charts for Lander camera calibration, a mirror for the Viking magnetic properties experiment and part of a grid on the top of the Lander body. At upper right is the high-gain dish antenna for direct communication between landed spacecraft and Earth. Toward the right edge is an array of smooth fine-grained material which shows some hint of ripple structure and may be the beginning of a large dune field off to the right of the picture, which joins with dunes seen at the top left in this 300° panoramic view. Some of the rocks appear to be undercut on one side and partially buried by drifting sand on the other.

Figure 9  
Survey Mode  
Panorama  
Lander I

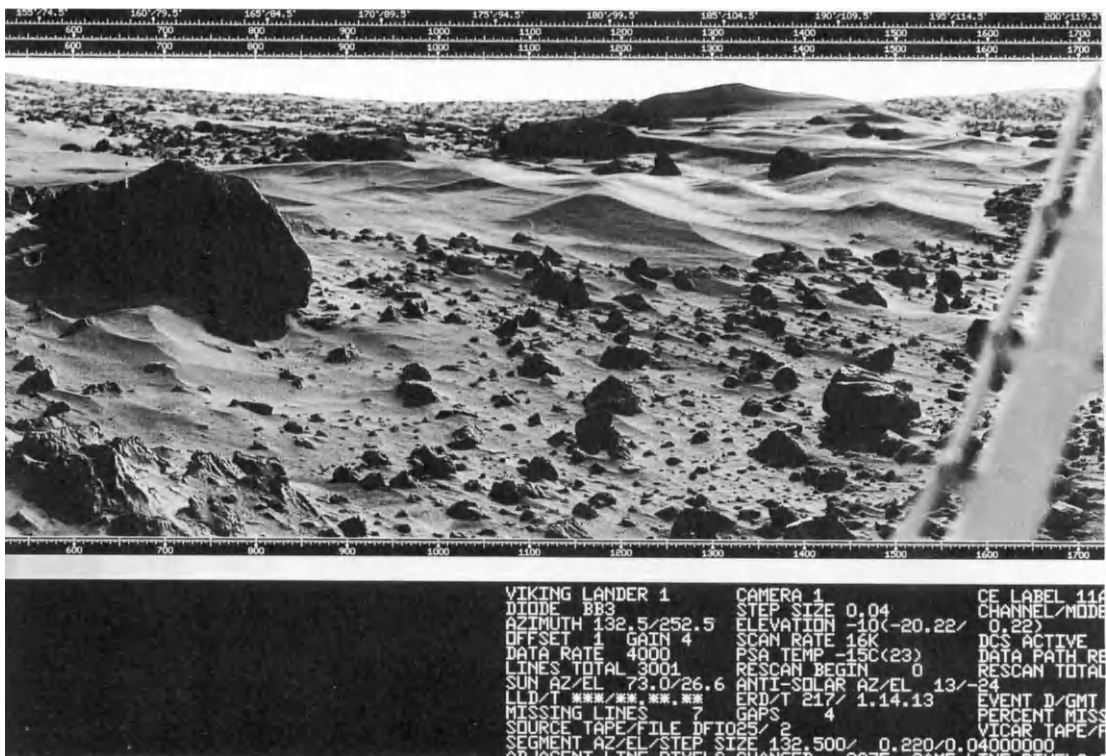


Figure 10  
BB3 Diode Image  
of 3m rock  
Lander I



Figure 11  
BB4 Diode  
Lander I



Figure 12  
Rescan Mode  
Footpad  
Lander I

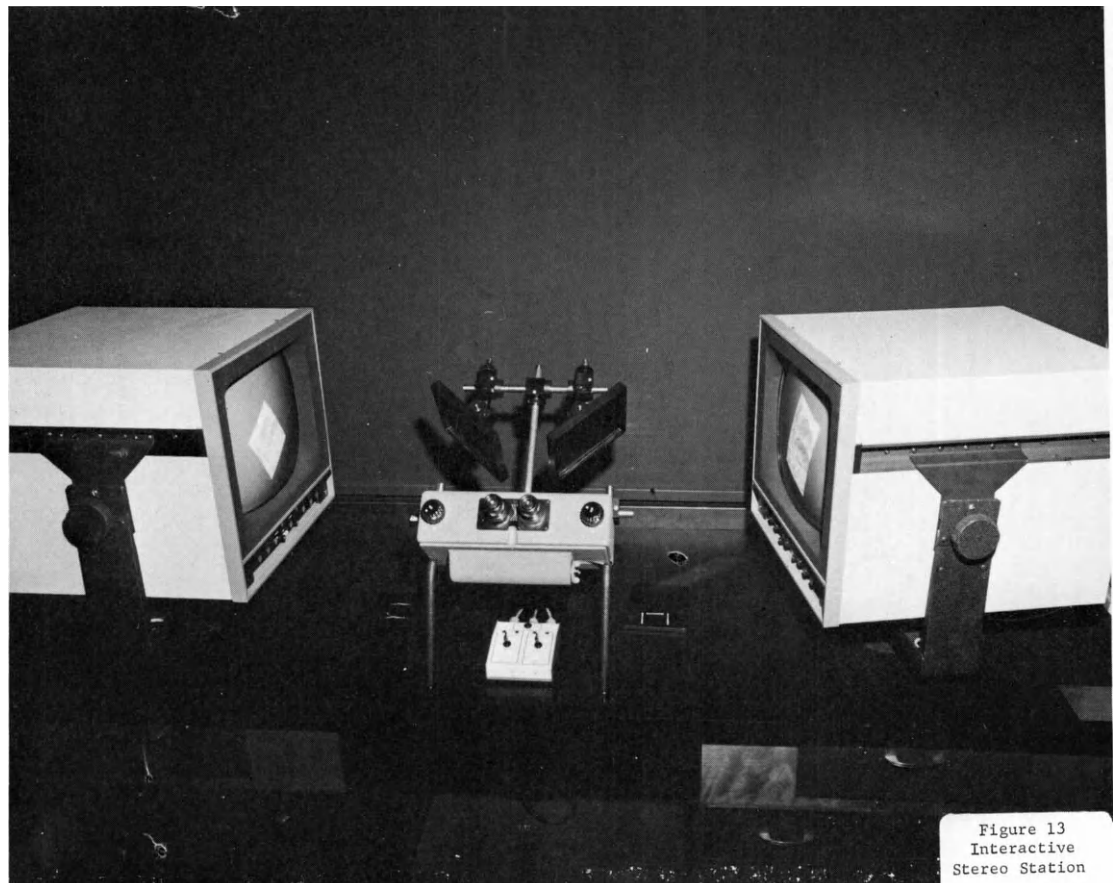


Figure 13  
Interactive  
Stereo Station

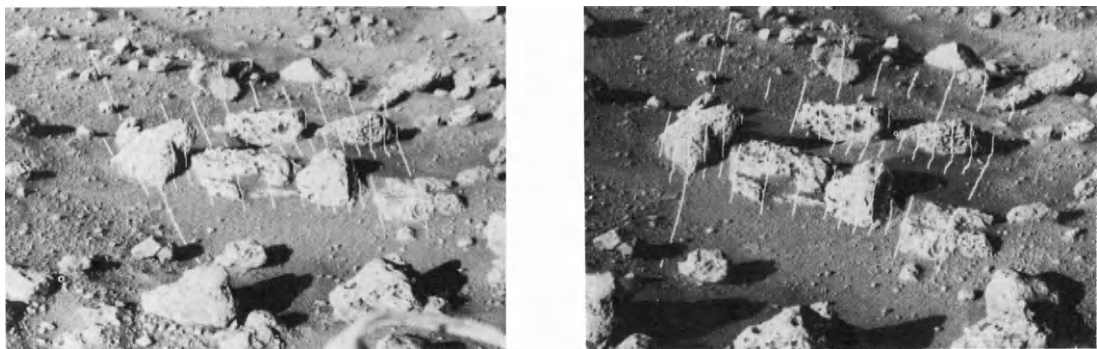
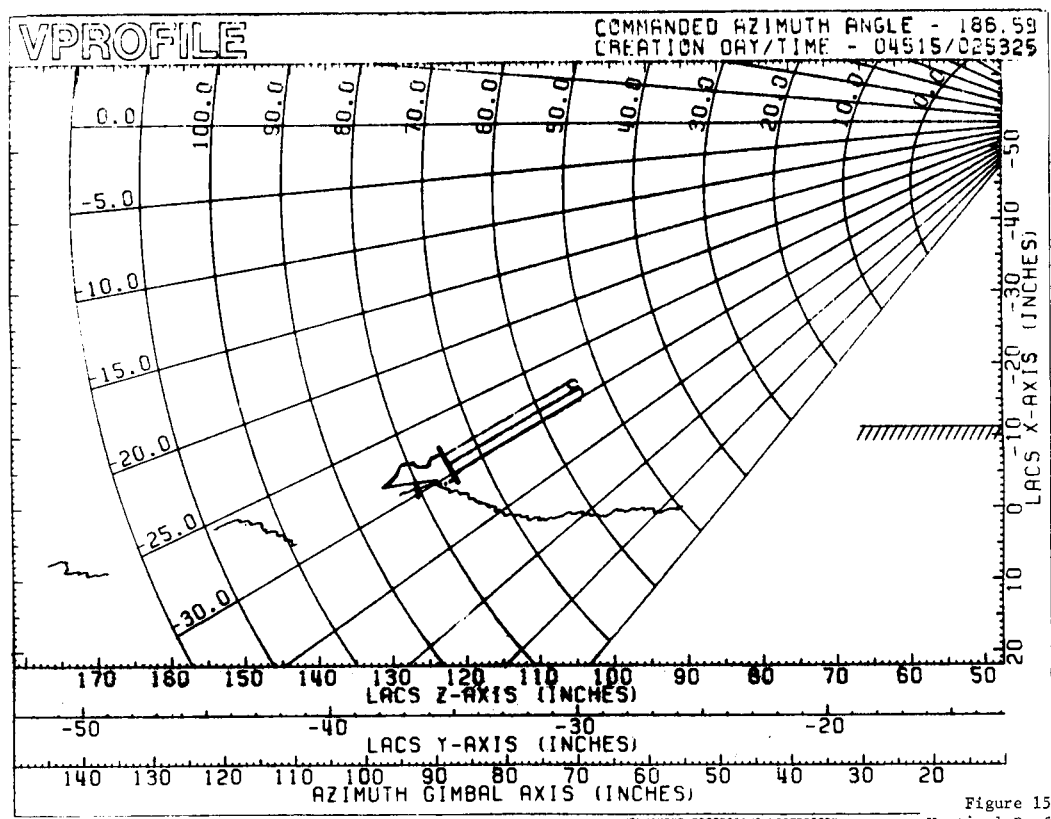


Figure 14  
Stereo Pair  
Vertical  
Profiling



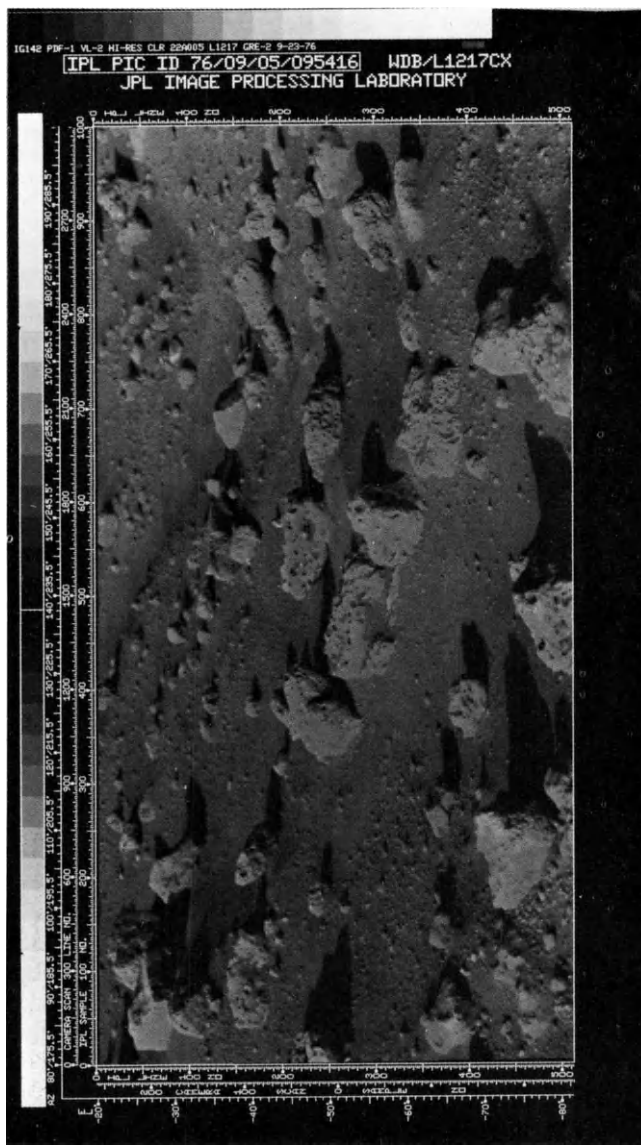


Figure 16  
Lander 2  
High Resolution-Color

# Apollo-Soyuz Experiments Summary

R. T. Giuli

ASTP Program Scientist, NASA Lyndon B. Johnson Space Center, Houston, Texas USA

## Abstract

The ASTP science and technology program conducted by the Apollo crew consisted of 28 separate experiments, including five conducted jointly with the Soyuz crew. Cosmic sources of extreme-ultraviolet and x-ray radiation were discovered. The interstellar medium in the vicinity of the solar system was investigated. The solar corona was photographed using spacecraft occultation of the solar disk. The radioactivation of potentially useful gamma-ray detectors by cosmic particle bombardment was measured, and the effects of cosmic particle impact upon living cells was investigated with three different techniques by three separate experiments. The concentrations of two atomic species and the aerosol component of the upper atmosphere were measured, respectively, by resonance absorption spectroscopy and solar extinction photometry. The Earth surface structure was investigated by photographic and visual observations, and the sub-surface structure was investigated by gravity-field measurements, employing highly precise space-craft-to-spacecraft tracking techniques. Zero-gravity effects upon the embryogenesis of fish vestibular systems and upon the rhythmicity of fungal growth patterns were investigated. Microbial growth and microbial transfer among crewmembers were measured. Mixtures of biological cells were separated into pure samples by two different electrophoresis techniques. Seven sets of solid materials were processed by high-temperature melting, and one set was processed by ambient-temperature diffusion.

## Introduction

The Apollo crew participated in 28 scientific and technological experiments during the joint Apollo-Soyuz mission of July 1975. These experiments included five which were conducted jointly with the Soviet crew and included two which were provided by the Federal Republic of Germany. In addition to these unilateral Apollo and joint Apollo-Soyuz experiments, a number of unilateral Soyuz experiments were performed. This report summarizes only the 28 experiments falling into the first two categories. All together the selected experiments formed a well integrated program of complementary scientific objectives. In several cases, related experiments employed different experimental techniques in pursuit of similar scientific objectives. A comparison of the scientific results and operational experiences from these experiments are being used to determine the best techniques to pursue in future space missions. The experiments are listed by discipline and topic in Table 1. The parentheses denote the joint-notation used for the jointly-conducted experiments.

The 28 experiments were selected from 161 proposals submitted to NASA from nine countries. Table 2 gives the numerical breakdown by country.

A complete description of the experiment concepts, instrumentation, operations, and preliminary analyses has been published.<sup>1</sup> A summary report containing more complete analyses is in preparation.<sup>2</sup> The following sections present a brief summary.

Table 1 American, \*German, and \*\*Joint American-Soviet Experiments

Space Sciences	
Astronomy	
MA-048	Soft X-ray Observations
MA-083	Extreme Ultraviolet Survey
MA-088	Helium Glow
MA-148	Artificial Solar Eclipse (AS-4)**
MA-151	Crystal Activation
Earth Studies	
MA-59	Ultraviolet Absorption (AS-5)**
MA-007	Stratospheric Aerosol Measurements
MA-136	Earth Observations and Photography
MA-089	Doppler Tracking
MA-128	Geodynamics
Life Sciences	
Particle	Radiation Effects on Living Cells
MA-106	Light Flash Observations
MA-107	Biostack III*
MA-147	Zone Forming Fungi (AS-1)**
Human Immune System	
AR-002	Microbial Exchange (AS-2)**
MA-031	Cellular Immune Response
MA-032	Polymorphonuclear Leukocyte Response
Vestibular System	
MA-161	Killifish Hatching and Orientation
Materials Processing	
Biological	
MA-011	Electrophoresis Technology
MA-014	Electrophoresis*
Solid	
MA-010	Multipurpose Furnace
MA-041	Surface Tension-Induced Convection
MA-044	Monotectic and Syntectic Alloys
MA-060	Interface Marking in Crystals
MA-070	Zero-G Processing of Magnets
MA-085	Crystal Growth from the Vapor Phase
MA-131	Halide Eutectic Growth
MA-150	Multiple Materials Melting (AS-3)**
MA-028	Crystal Growth

Table 2 Experiment Proposals Submitted to NASA

Origin	Number
USA	135
FRG	8
France	7
India	4
USSR	3
Ireland	1
Scotland	1
Sweden	1
Switzerland	1
TOTAL	161

## Astronomy

The astronomy experiments are listed in Table 1 in order of the distance away from the Earth that the objects of study lie. The soft x-ray objects lie deep in our galaxy and even beyond our galaxy. The extreme-ultraviolet objects lie within a few hundred light years from the solar system, while the portion of the interstellar medium investigated by the Helium Glow experiment lies within a few astronomical units from the solar system. The corona photographed during the Artificial Solar Eclipse experiment lay within approximately fifty solar radii from the Sun. Finally, two crystal detectors which have potential application for future gamma-ray astronomy payloads were carried onboard the Apollo spacecraft to measure their susceptibility to radioactivation by local cosmic particle bombardment.

### Concepts and Operations

The Soft X-ray Observations experiment was an attempt to obtain higher performance (*viz.*, higher angular resolution) from a rocket-class instrument by taking advantage of the longer observing time available with an Earth-orbiting stabilized platform. The instrument (Figure 1) was bolted into the scientific instruments bay of the Apollo service module. It was a gas proportional counter operated

which allowed the instrument to be used only for periods of two-minutes at a time. However, during those two-minute periods, the instrument performed well, and so new procedures were developed during the mission in near-real-time, employing the entire Apollo crew, to properly phase spacecraft pointing and instrument switching. The result was a cumulation of about one hour of high quality data which yielded successful achievements in all three objectives, especially in 1 and 3.

The Extreme Ultraviolet Survey experiment was an attempt to pioneer a new field of astronomy. Discrete sources of EUV radiation outside our solar system had never before been observed. The reason is that EUV radiation (defined here as radiation with wavelengths between 10 and 100 nm) is highly susceptible to absorption by the interstellar medium (ISM), which is mostly diffuse hydrogen gas. The previously supposed ISM density would not allow detectable amounts of EUV radiation to travel more than a few tens of light years, and few potential EUV sources exist within that distance of the solar system. Finally, the technology required for detecting faint EUV radiation was, to a large extent, undeveloped. In recent years, however, four favorable things occurred: the estimate of the ISM density went down, observations in other wavelengths suggested that many strong EUV sources may exist within a few hundred light years of the solar system, the requisite technology improved, and a suitable flight opportunity arrived. The instrument (Figure 2)

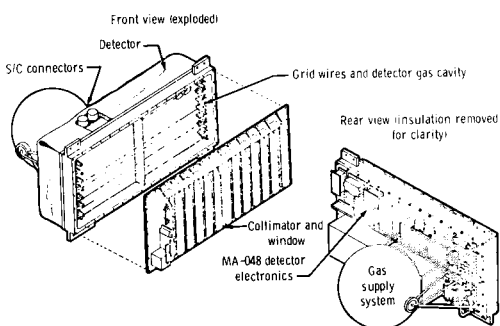


Fig. 1. MA-048 Soft X-ray Instrument

at 2700 volts with P10 gas (90% argon, 10% methane) at 1.1 atmosphere pressure across a 2 micron polycarbonate window. The aluminum honeycomb collimator provided a circular field of view with 4° FWHM and the effective detector area was 0.12 m<sup>2</sup>. Pointing of the instrument was accomplished by pointing of the spacecraft; there was no separate instrument pointing system. There were three main objectives of the experiment:

1. Scan the celestial sphere to determine the structure of the known, soft x-ray background and hence possibly the source(s) of this background.
2. Obtain the low-energy spectra of known x-ray sources for which higher energy spectra have been obtained, in order to derive distance estimates for these sources.
3. Obtain high time-resolution observations of discrete sources in order to discover x-ray pulsars.

Soon after initiating operation, the instrument developed a high-voltage-breakdown characteristic

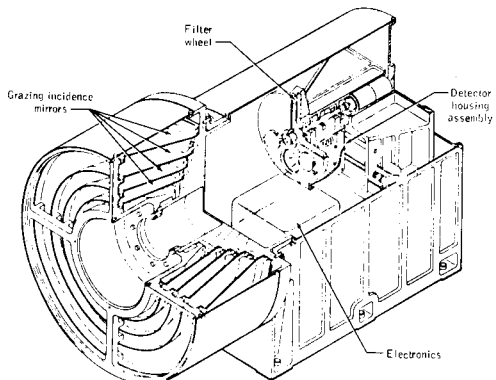


Fig. 2. MA-083 Extreme Ultraviolet Survey Instrument

consisted of collection optics, a filter wheel, and two channel electron multiplier detectors. The collection optics consisted of four concentrically mounted, paraboloidal, grazing incidence mirrors which focused the EUV radiation on the exposed position of a six-position, continuously rotating filter wheel. In back of the exposed position was one or the other detector, as selected by real-time command. The filter wheel had four EUV-transmitting filters, a UV-transmitting filter for inflight detector calibration, and an opaque position for continuous inflight monitoring of instrument background. The EUV instrument was bolted into the service module instruments bay along with the soft x-ray instrument, and instrument pointing was achieved by spacecraft pointing. An inflight pointing "raster scan" was performed to obtain precise definition of the instrument line-of-sight-direction

relative to the spacecraft axis. This exercise allowed the high resolution ( $2^{\circ}5$  FWHM) detector to be used exclusively during the flight, which maximized the instrument sensitivity and contributed in a major way to the outstanding achievements of this experiment.

The Helium Glow experiment was an attempt to determine unambiguously the temperature and density of the ISM in the vicinity of the solar system. A by-product of the investigation is the determination of the velocity of the local ISM relative to the Sun. The technique was to detect EUV radiation originating from the Sun which is resonantly back-scattered by the helium component of the ISM, specifically neutral helium ( $\text{HeI} - 58.4 \text{ nm}$ ) and once-ionized helium ( $\text{HeII} - 30.4 \text{ nm}$ ). Previous observations of the ultraviolet resonance line ( $\lambda = 121.6 \text{ nm}$ ) of the hydrogen component of the ISM have not yielded definitive results because it is not possible to separate the solar-scattered contribution of that radiation from the unknown contribution transmitted through the ISM from galactic sources. However, as we have discussed, there should be little EUV radiation transmitted from great distances, so the ambiguity is removed for the helium resonance radiation. Thus, we see that the property of EUV radiation which poses problems for EUV stellar astronomy (high susceptibility to absorption by the ISM) is the very property which makes the Helium Glow experiment feasible. The instrument (Figure 3)

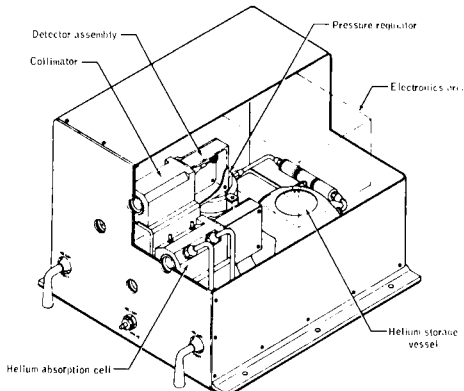


Fig. 3. MA-088 Helium Glow Instrument

consisted of two pair of redundant photometer systems. The "horizontal" pair incorporated thin metal transmission filters for isolation of the HeI ISM line and included cells of helium gas at  $130 \text{ Nm}^{-2}$  pressure which subtracted (absorbed) the helium geocorona contribution to the signal. The "vertical" pair used a thin metal transmission filter for isolation of the He II line. All four detectors were channel electron multipliers. The He II geocorona (magnetosphere) structure was investigated during orbital day, and the He II component of the ISM was investigated by pointing the instrument down the Earth-shadow during orbital night. The instrument was bolted into the service module instrument bay with the soft x-ray and EUV instruments, and the whole sky was scanned by a series of spacecraft roll maneuvers. The instrument functioned well, although one of the He II detectors failed part way through the

flight. A cumulative of ten hours of data were obtained.

The Artificial Solar Eclipse experiment was an attempt to demonstrate the feasibility of photographing the solar corona from one spacecraft by occulting the solar disk radiation with another spacecraft. The Apollo spacecraft backed away from the Soyuz spacecraft in the solar direction (Figure 4) until, at the separation of approximately 200 m, the

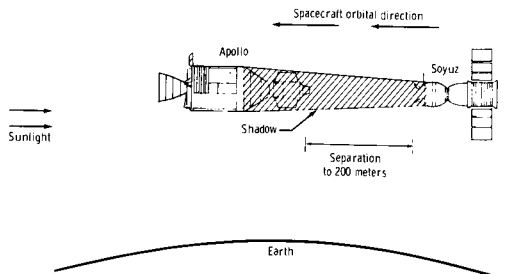


Fig. 4. MA-148 Artificial Solar Eclipse Spacecraft Orientation

Apollo subtended an angle of about two solar diameters, as seen from Soyuz. The Soyuz performed photography in the solar direction in white light (no filter) through a vignetting light baffle designed to block the bright sunlight reflected from the Earth beyond the terminator. All operations were performed successfully.

The Crystal Activation experiment was an attempt to learn more about the propensity of certain types of crystals to be radioactivated by particle bombardment in the Earth-orbital environment. The crystals (germanium and thallium-activated sodium iodide) are potentially important for use as detectors in future gamma-ray astronomy payloads. The problem is that cosmic ray particles such as high-energy protons (and secondary neutrons produced in spacecraft structure by these protons) can induce x-ray and gamma-ray activity via spallation interactions with the detector material. This detector background cannot be measured in flight, and hence it is difficult to account for the background contribution to the total signal when one attempts to measure the intensity of gamma-rays coming from astronomical sources. Consequently, one must investigate the background properties of the detectors separately, as in this experiment. The experiment consisted of carrying a sample of each of the crystals into orbit and then measuring the induced radioactivity after the mission. The measurements began on the recovery ship approximately 1.5 hours after atmospheric re-entry of the command module, in order to detect the short half-life species. Those and subsequent laboratory measurements were successful.

#### Results

The Soft X-ray Observations experiment made several important discoveries. For example, the previously known binary x-ray source in the Small Magellanic Cloud (a companion galaxy of our own galaxy), SMC X-1, was discovered to be an x-ray pulsar as well, thus identifying the compact component of the binary to be a rotating neutron

star. This is the first pulsar discovered outside our galaxy, and it has the shortest pulse-period (0.7157 sec) of any known x-ray binary pulsar. Two important observations of extended structure in the soft x-ray background were obtained. The first is associated with a known (optically) supernova remnant in the constellation Centaurus. The second is a previously known x-ray source in the constellation Cygnus hence has the name Cyg X-6. However, the ASTP observations, in conjunction with a rocket experiment by the same investigators, have shown for the first time that Cyg X-6 is an extended x-ray source and is not associated with any optical or radio object.

The Extreme Ultraviolet Survey experiment achieved the first detection of discrete sources of EUV radiation outside our solar system. To date, four such sources have been positively identified in the data. They are stars which were previously known optically to be the white dwarfs HZ43 and Feige 24, the dwarf nova SS Cygni, and the M-dwarf flare star Proxima Centauri. The two most intense sources are the white dwarfs, and this experiment determined that they are much hotter than was previously believed. In fact, they are now the hottest, most luminous white dwarfs known; the effective temperature of HZ43 is 110,000K, and it becomes the first white dwarf whose luminosity exceeds that of the Sun. The EUV data were also useful in providing more reliable estimates of the ISM mean densities in the directions of the white dwarfs: 0.01 to 0.02 H atoms cm<sup>-3</sup>. The dramatic new physical interpretation for the EUV objects establishes the importance of observing such objects at EUV wavelengths when their peak energy emission occurs at those wavelengths. Thus, this experiment has provided strong indication that the new field of EUV stellar astronomy may become an important one.

The Helium Glow experiment analysis is still underway. No definite conclusions have been obtained at this writing; no current theoretical model's fit the data in their present state of analysis.

The Artificial Solar Eclipse experiment was analyzed exclusively by the Soviet investigators, and they have submitted their results to NASA for publication in reference 2. They report the corona is detectable on 19 of the 55 exposures suitable for analysis, and they have obtained a coronal intensity distribution along the ecliptic westward from the Sun which extends almost to 50 solar radii.

The Crystal Activation experiment indicated that the induced activation was a factor of three less than that incurred on a similar experiment flown on the Apollo 17 lunar mission. The activation level of the ASTP crystals was expected to be much lower, however, due to the geomagnetic shielding of the low ASTP orbit. Regardless of the reason for this unexpected result, it is clear that such detectors used in gamma-ray astronomy experiments had best be placed far from heavy material.

#### Earth Studies

The Earth Studies experiments are listed in Table 1 in order of the distances above the Earth surface that the subjects of study are located. The Ultraviolet Absorption experiment investigated the atomic composition of the tenuous upper atmosphere at the spacecraft altitude, while the

Stratospheric Aerosol Measurements experiment measured the aerosols in the tropopause at about 20 km altitude. The Earth Observations and Photograpy experiment investigated a multitude of Earth surface features on land and in the oceans, and the Earth sub-surface structure was investigated by two variations of gravity-field measurements with two spacecraft-to-spacecraft tracking experiments.

#### Concepts and Operations

The Ultraviolet Absorption experiment was an attempt to apply a new technique, resonance absorption spectroscopy, to the investigation of the upper atmosphere. This technique had never before been applied in a space mission context, and at ASTP's relatively low orbital altitude of 220 km, it appeared feasible to measure the concentrations of neutral atomic oxygen and neutral atomic nitrogen. The former measurement would serve as a comparison with previous results from mass spectrometry experiments, and the latter measurement would constitute the first reliable measurement of N at such altitudes. Thus, this experiment could provide a first assessment of a technique which might be developed as a powerful method for measuring and monitoring the constituents of the upper atmosphere. The concept of the experiment was to produce collimated beams of 130.4 nm and 120.0 nm radiation (resonance for O and N), and 135.6 nm and 149.3 nm radiation (forbidden lines of O and N that are very weakly absorbed by these species). The forbidden line radiation originated in the same lamp sources as the resonant line radiation and hence defined the beam geometry, the reflectivity, and the transmission of the optical instrument for the resonance radiation independently of resonance absorption. The light was produced by radio-frequency-driven lamp sources and collimated by mirrors on the Apollo docking module. The light beams illuminated an array of corner reflectors mounted on the Soyuz spacecraft at a known distance from the Apollo. The portion of the beam striking the retroreflectors returned to a collecting mirror on the docking module and was focused on the entrance slit of a 0.75-meter Ebert-Eastie scanning spectrophotometer. The spectral range from 120.0 to 149.3 nm was scanned every 12 seconds through 1.5 nm ranges centered on 120.0, 130.4, 135.6, and 149.3 nm. The bandwidth of the spectrometer was approximately 1.15 nm. In order to prevent Doppler effects due to spacecraft orbital velocity from shifting the lamp frequency away from the atmospheric absorption frequency, it was necessary to maneuver the spacecraft such that the light beams travelled between the two spacecraft perpendicularly to their orbital velocity vectors. Primarily because of this requirement, the spacecraft maneuvers required for the three data runs (at approximate spacecraft separations of 150 m, 500 m, and 1000 m) became the most intricately planned maneuvers ever performed by an Apollo spacecraft during a scientific experiment. Figure 5 shows the planned maneuver schematic for the 500 m data run. Reflected signal (resonance absorption data) was obtained for this run, but not for the 150 m run, and only sporadically for the 1000 m run. An anomaly occurred during the 500 m run which has been interpreted as a degradation of the corner reflectors. Resonance fluorescence (resonance scattering) data were obtained during the 150 m data run.

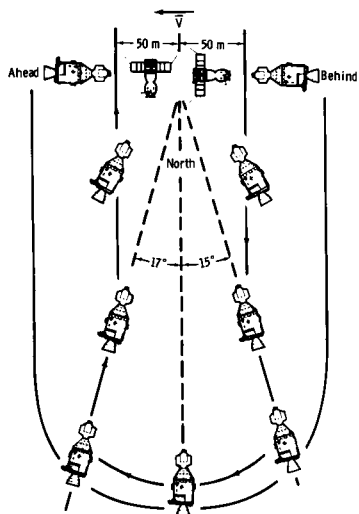


Fig. 5. MA-059 Ultraviolet Absorption Spacecraft Maneuver

The Stratospheric Aerosol Measurements experiment was an attempt to perform the first remote sensing of the atmospheric aerosol layers from an orbiting spacecraft, using solar extinction photometry. The concept was to monitor the extinction of direct sunlight at orbital sunrise and sunset, as the Sun-spacecraft line-of-sight traversed upward and downward through the lower 150 km of atmosphere (Figure 6). For this purpose a photometer sensitive

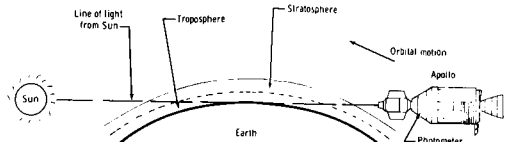


Fig. 6. MA-007 Stratospheric Aerosol Measurements Sunrise Orientation

to 1-micron radiation (the wavelength range most sensitive to aerosol extinction) was mounted in a command module window, and data were collected during two sunsets (Northern hemisphere) and two sunrises (Southern hemisphere). Concurrently, photography of the Sun with infra-red sensitive film was performed to obtain accurate Sun-shape and hence refined atmospheric refractivity models required for the analysis of the photometer data. Additionally, high altitude balloon sampling and ground-based LIDAR measurements were made near the site of the second sunset (Kansas City, MO) to provide "ground truth" comparison. High quality data were obtained.

The Earth Observations and Photography experiment was an attempt to utilize the recognition and interpretive capabilities of human observers to refine the selection of Earth surface features for photography and to provide in-situ contributions to analysis of these features. The phenomena to be observed were selected from the categories of geology, deserts, oceanography, hydrology, and

meteorology. The approach used for the ASTP effort was to have a Principal Investigator assemble a team of scientific investigators representing topics of special interest in fields mentioned above. An extensive crew training program involving classroom studies and aircraft fly-over exercises was conducted, and an extensive flight planning effort was expended to assure the acquisition of as much data as real-time cloud cover would allow. The plan then called for a post-mission data assessment in order to define a scientific analysis program. Many useful observations and photographs were obtained.

The Doppler Tracking experiment was one of two ASTP experiments which attempted to test the feasibility of performing refined measurements of the Earth gravity field structure with horizontal scale lengths of approximately 250-1000 km. Such measurements would be useful in describing the sub-surface structure of the Earth down to depths of several hundred kilometers, and it is anticipated that such information would have great importance for understanding tectonic plate processes. The problem is, surface gravimetry is useful only for gravity structure determinations of less than about 100 km scale size, and single-satellite orbit perturbation measurements are useful only for scale sizes greater than 2000 km. In principle, however, two spacecraft in orbit can recover the gravity field structure of the desired scale size by performing very-high-accuracy doppler measurements between them, while one of them is being accelerated by the gravity field anomaly. Roughly, the smallest anomaly scale size recoverable is about equal to the altitude of the lower spacecraft, and the largest scale size is comparable to the separation of the spacecraft. The spacecraft-to-spacecraft tracking technique employed in the Doppler Tracking experiment was the low-low technique, where the two spacecraft traveled in the same orbit at some suitable separation (Figure 7).

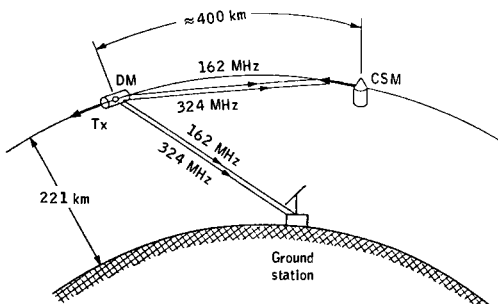


Fig. 7. MA-089 Doppler Tracking Low-Low Spacecraft Orientation

The two spacecraft were the Apollo CSM and the DM, which was jettisoned in a spin-stabilized mode (end-over-end) for the purpose of this experiment. A highly stable crystal oscillator ( $1.5 \text{ parts in } 10^{12}$ ) was located in the DM transmitter, which delivered 100 mW to the dual frequency monopole antenna at each of two phase-coherent frequencies: 162 MHz and 324 MHz. The antenna was mounted approximately coincident with the DM spin axis, which was perpendicular to the orbital plane. Thus, the antenna was continuously "visible" to the CSM. The purpose of the phase coherent dual frequency transmission was to be able to account for ionospheric effects in the doppler measurement. This feature introduced

the possibility of studying the horizontal scale of electron concentrations in the ionosphere and of detecting traveling ionospheric disturbances and boundaries of ionospheric turbulence. Consequently, ionospheric studies became a secondary objective of the experiment. After the DM was jettisoned, the CSM separated to an initial distance of 310 km which drifted to 430 km by the end of the data take (nine revs later, approximately 14 hours).

The Geodynamics experiment was the other ASTP experiment which attempted to detect and recover gravity field fine-structure, employing the high-low spacecraft-to-spacecraft tracking technique. For this experiment the low spacecraft was the Apollo, and the high was the geosynchronous ATS-6 satellite, located during the experiment over the Indian Ocean (Figure 8). The Geodynamics data link in Figure 8 was from the ATS ranging station in

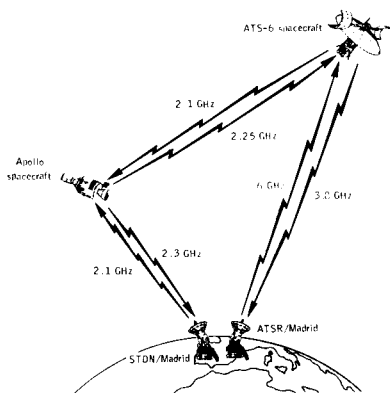


Fig. 8. MA-128 Geodynamics High-Low Spacecraft Orientation

Madrid to ATS-6 to Apollo, back to ATS-6 and to Madrid. The Apollo-STDR link was used for spacecraft orbit determination. The experiment involved no dedicated spacecraft hardware; the Apollo-ATS-6 communications link was developed for other reasons. The experiment acquired data on 108 passes under the ATS-6.

### Results

The Ultraviolet Absorption experiment successfully measured the concentrations of O and N at the ASTP altitude. The values were obtained by combining the resonance fluorescence data of the 150 m run with combined fluorescence and absorption data of the 500 m run. Preliminary values are  $[O] = 1.15 \times 10^9 \text{ cm}^{-3}$ ,  $[N] = 8.6 \times 10^6 \text{ cm}^{-3}$ . Continuing analysis is expected to refine these values, but already they are in good agreement with the oxygen measurements of the Atmospheric Explorer satellite extrapolated to the time and location of the ASTP measurements.

The Stratospheric Aerosol Measurements experiment yielded high quality photometer and photography results. The aerosol layer peaked at about 20 km altitude in the Northern hemisphere and somewhat lower in the Southern, and the peak concentration was about 50% higher in the Northern

hemisphere. These results, combined with balloon sampling measurements made in Australia prior to and after the ASTP mission, are consistent with seasonal, meridional transport of aerosols after the eruption of Volcan de Fuego in Guatemala, October 1974. The results are very encouraging for developing the solar extinction technique for long-term space-borne monitoring of the Earth atmosphere.

The Earth Observations and Photography experiment data have been reported<sup>1</sup>; their assessment is complete and an analysis program has been defined and is underway. Because of the inherent programmatic delay in undertaking the analysis (viz., the analysis program could not be defined until post-mission data assessment was complete), scientific results are, for the most part, not yet available at this writing.

The Doppler Tracking experiment was not able to achieve its prime objective of measuring gravity field anomalies. The data were degraded by a single-frequency noise level much higher than anticipated and too high to extract gravity field signature. The source of the noise is not known. The ionospheric investigation was highly successful. Analysis continues, but preliminary results are as follows:

1. Changes in the columnar electron content between the two spacecraft were accurately measured and yielded gradients as high as  $10^6 \text{ electrons/m}^3/\text{m}$  on both the day-side (typical density  $5 \times 10^{11} \text{ electrons/m}^3$ ) and night-side (typical density  $3 \times 10^9 \text{ electrons/m}^3$ ) ionosphere.

2. Traveling ionospheric disturbances were detected, the most noticeable one occurring off the coast of California. It was a nine-cycle wave with peak-to-peak electron density perturbation of 35%, with wavelength of 690 km (as would be seen from the ground), and with spatial extent of 7200 km along the Apollo orbital track.

The ionospheric results from the Doppler Tracking experiment are particularly noteworthy because they are the first such measurements of the ionosphere in the region of 200 km altitude.

The Geodynamics experiment successfully detected and recovered gravity field signatures with resolution within 10 m gal. Areas where such anomalies were recovered are the Indian Ocean Depression, the Himalayan Anomalous Region, an area in West-Central Africa near the Banqui magnetic anomaly, and the Zagros Thrust Zone which is at the juncture of the African and Eurasian tectonic plates. The high quality gravity measurements of the Geodynamics experiment were an extremely encouraging demonstration of the validity of the high-low spacecraft-to-spacecraft tracking technique. This technique may be developed to provide global coverage for gravity field measurements with future space projects. A bonus from the Geodynamics experiment was the use of the data for tropospheric studies. Analysis of the atmospheric refraction of the Apollo-ATS link near the horizon yielded refractivity, pressure, and temperature profiles which matched well with radiosonde determinations. This has important potential application for space-monitoring of meteorological properties of the troposphere.

### Particle Radiation Effects on Living Cells

With the advent of space flight, interest arose as to the effects upon humans and other living organisms of exposure to cosmic particle radiation. While the effects of protons are fairly well understood, recent interest has developed in understanding the implications of the HZE (highly charged and energetic) component of cosmic rays for long-duration space travel. Such particles can deposit energy in tissue at a linear rate exceeding  $1 \text{ GeV cm}^2 \text{ g}^{-1}$ , and such energy deposition is capable of killing a cell if the particle passes sufficiently close to the cell nucleus. The implications are particularly important for non-regenerative cells such as central nervous system cells. Three ASTP experiments investigated HZE impact effects on living cells. The Light Flash experiment measured visual effects produced by impact with the astronauts' eyes, the Biostack experiment measured mutations eventually produced in animals and plants which were flown in the dormant state (egg, seed), and the Zone Forming Fungi experiment attempted to observe the real-time mutations which might occur in a ring of fungal cells as they grew during the flight.

### Concepts and Operations

The Light Flash experiment was an attempt to record the "visual" sensations caused by impact of HZE particles on the dark-adapted retinae of two astronauts, and to correlate their "observations" of the intensities and shapes of the resulting flashes with measurements by particle detectors placed in close proximity to the astronauts' eyes. The objective was to determine quantitatively the frequency, character, latitudinal dependence, and identity of cosmic particles that cause the flash phenomena. The ultimate objective is to assess the radiation hazards for long-duration, Earth-orbiting and interplanetary missions. There were two detectors: a cadmium-doped silver-chloride crystal device which measured particle identity and energy transfer, and a silicon solid-state device which measured particle spectra (energies) and directions, and which also provided better time resolution than the silver-chloride crystals. The orientation of the retinae with respect to the Earth magnetic field was important (Figure 9) for interpreting the flashes. Two orbits of data were obtained, one of them using only the solid-state detector.

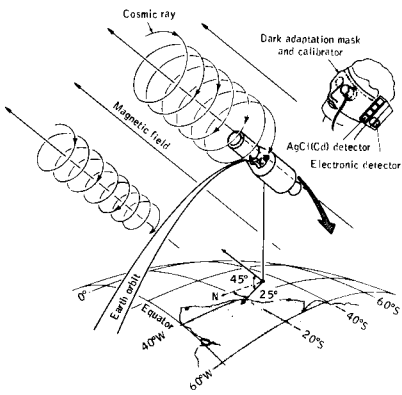


Fig. 9. MA-106 Light Flash Orientation

The Biostack III experiment was an attempt to confirm and extend the studies of HZE particle impact on biological systems, begun with Biostack I and II on Apollo 16 and 17. A feature of the ASTP mission is that the geomagnetic shielding yielded an order of magnitude lower radiation dose than the lunar missions. The experiment consisted of two cylindrical containers containing layers of dormant biological objects interleaved with sheets of particle detectors. The interleaving allowed accurate determination of the location of the hits on the biological objects, which consisted of plant seeds and eggs of lower animals such as brine shrimp. The biologicals were imbedded in layers of polyvinylalcohol, and the detectors consisted of sheets of cellulose nitrate, lexan, cellulose triacetate, Ilford K2 and K5 nuclear track emulsion, and (in one of the cylinders) silver chloride crystals with light-fixing capability. Figure 10 shows a representative section of one of the cylinders. The dip angle  $\delta$  helps locate the impacted biological object, the cone length  $L$ .

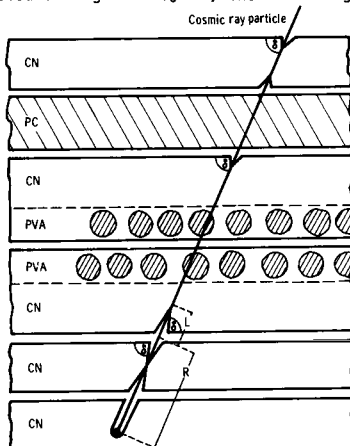


Fig. 10. MA-107 Biostack III Typical Sample/Detector Layers

determines energy loss, and the residual range  $R$  determines particle charge. PVA denotes polyvinylalcohol, CN denotes cellulose nitrate, and PC denotes a polycarbonate spacer. The cylinders were stored in the command module in a location of minimum shielding to ambient cosmic radiation.

The Zone Forming Fungi experiment had two objectives. One was to study radiation effects, especially HZE impact effects, upon the growth rates and development of growing cultures of Streptomyces (Actinomyces in the U.S.S.R.) levoris. Kras carried onboard the two spacecraft. The other was to ascertain the possible effect of space flight factors on the rhythmicity of the growth patterns exhibited in the cultures. The cultures were grown in Petri dishes, with sheets of lexan, cellulose nitrate, and cellulose triacetate placed above and below the dishes for determination of particle impact characteristics. Two such assemblies were packaged together in a device (Figure 11), and two such devices were launched in each spacecraft. The spore-zone-forming periodicity of the cultures prepared in Houston had been trained to be 12 hours out of phase with those prepared at the Baykonur Cosmodrome. During the docked portion of the flight, one device from each side was exchanged.

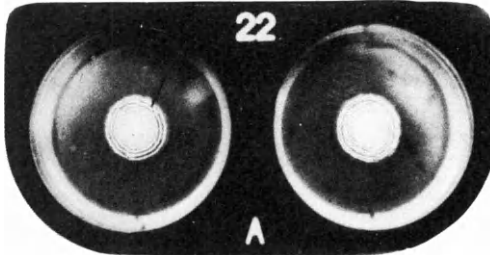


Fig. 11. MA-147 Zone Forming Fungi Culture Device

Photography of the zone formations was performed at approximately 12-hour intervals from the time the devices were loaded pre-mission until the experiment was terminated post-mission. Modifications to the photography schedule were made during flight to accommodate other flight activities.

### Results

The Light Flash experiment data for the silver-chloride crystals did not correlate well with either the astronaut event rate observations or the abundances calculated for the ASTP altitude. This was probably due to inadequate time-resolution for the crystals (viz., the decay time of unfixed heavy ion tracks was too long). The events observed in the South Atlantic Anomaly, when compared to similar observations performed on Skylab 4 (at an altitude of 440 km) suggest a physical interpretation for the mechanism of light flash production. This mechanism is inelastic collisions of protons with nuclei of carbon, nitrogen, or oxygen in the retina, and the arguments leading to this interpretation include the relative abundances of protons with energy loss  $> 15 \text{ GeV m}^{-1}$  at the two altitudes, the relative shielding of the spacecraft (Skylab shielding was much less than that of a command module), and the orientation of the retina with respect to the magnetic field in the South Atlantic Anomaly.

The Biostack III experiment analysis is partially completed. The biological objects which underwent impact have been identified. Objects adjacent to them are being used as controls. Growth and development studies and genetic studies are still in progress. Preliminary results are as follows: 1. Growth of *Bacillus subtilis* spores was significantly reduced for impacts which passed within four microns of the spore centers. 2. Seeds of *Zea mays* showed significant retardation in growth and development, and two impacted seeds failed to germinate. 3. No effects have yet been detected on the germination, growth and development of the impacted seeds of *Arabidopsis thaliana*. 4. Most of the impacted animal eggs showed serious damage during development. For example, the *Artemia salina* eggs displayed significantly reduced hatching rate, and development anomalies at the extremities and at the abdomen were evident. In comparison of the dosimetry results of Biostack III with those of Biostack I and II it was noted that, in spite of the much lower radiation dose for the ASTP mission, the frequency of nuclear disintegration stars was nearly twice that of Biostack II. Little is known

about their potential biological effects, but increased attention is being given them in the Biostack III analysis, especially since this radiation component reaches maximum intensity at altitudes of approximately 20 km, which is where SST's fly.

The Zone Forming Fungi experiment results showed that definite differences occurred in the zone growth rate and morphology, but the differences occurred non-uniformly among the various cultures. No specific property of spaceflight (for example, HZE radiation, weightlessness) can be correlated with any of the observed differences. Investigations are continuing to determine if the resulting abnormal spore morphology will appear in sub-culture.

### Human Immune System

The investigation of the effect of space flight factors on the infectious disease process has been a continuing one in both the U.S. and the U.S.S.R. since the advent of the space program. The Apollo-Soyuz mission offered a unique opportunity to study the process because of the large number of subjects (five crewmen and two spacecraft) which originated from widely separated environments and which were suddenly interfaced under space flight conditions. The Apollo-Soyuz investigation comprised three experiments. The Microbial Exchange experiment emphasized measurements of several microbial species, but also included measurements of species-specific antibodies. The Cellular Immune Response and Polymorphonuclear Leukocyte Response experiments investigated cell function.

### Concepts and Operations

The Microbial Exchange experiment was an attempt to monitor alterations in three factors: the composition of microbial populations inhabiting the Apollo and Soyuz crew members and spacecraft, the ability of each crew member to resist infection, and the ability of certain microorganisms to cause infection. The purpose was to address the overall problem of space flight effects on the balance between the immune system and infectious microorganisms. Because the two crews came from widely separated geographical and ecological areas, it was possible to identify specific marker microbes for study of cross-contamination patterns. The autoflora and immunocompetence levels of each crew member were established through repeated sampling and analyses before flight, so that flight changes could be measured and intercrew transfer of marker organisms could be identified. Likewise, certain immunological parameters of the blood and saliva of each crew member were studied to detect changes in the ability of the person to resist infection. This was the first space experiment to monitor species-specific antibodies. During flight, microbial samples were obtained by specially-designed swabs (Figure 12) from 15 areas in each spacecraft and from six locations on each crew member. The devices were launched and landed in the Soyuz, and initial laboratory studies were performed in Moscow by American and Soviet investigators.

The Cellular Immune Response and Polymorphonuclear Leukocyte Response experiments were laboratory investigations of immune system cell function as affected by spaceflight factors. They involved blood sample analysis before and after the mission; no inflight data were acquired. The

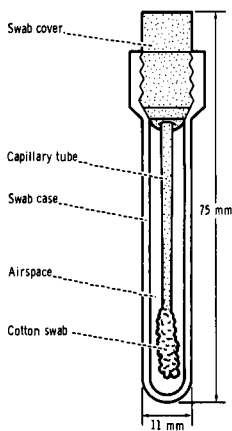


Fig. 12. AR-002 Microbial Exchange Collection Device

investigations pertained only to the Apollo crew members. In the former experiment the parameters studied were white blood cell concentrations, lymphocyte numbers, B- and T-lymphocyte distributions in peripheral blood, and lymphocyte responsiveness. In the latter experiment, the studies included total leukocyte count, differential count, measurement of leukocyte adhesion, evaluation of leukocyte migration and chemotaxis, and assessment of phagocytic ability.

#### Results

The Microbial Exchange experiment results were consistent with those of studies on previous missions and added results unique to the Apollo-Soyuz mission. A variety of potential pathogens was recovered from each of the prime and backup crew members before and after the flight, but no disease events occurred. The yeast Candida albicans and the bacteria Staphylococcus aureus transferred from one Apollo crew member to another, but no microbial transfer occurred between crews. No other medically significant changes in the microbial population occurred. The total load of aerobic bacteria inhabiting the skin and upper respiratory tract was essentially the same for all 10 crew members and was not significantly changed during flight. Likewise, no significant change in the presence of species-specific antibodies could be attributed to the mission.

The Cellular Immune Response analysis showed significant depression of the lymphocyte responsiveness from pre-mission levels, but the lymphocyte population remained essentially unchanged. The possibility that the immunosuppression was caused by inhalation of toxic gases rather than usual spaceflight factors cannot be assessed; no data are available on the effects of toxic gases on lymphocytic responses. Similar response depression was not observed on the various Apollo lunar missions, whereas it was observed on the much longer Skylab 3 and 4 missions.

The Polymorphonuclear Leukocyte Response analysis detected no substantial change in the leukocyte functions from pre-mission tests. It is noted, however, that the time scale for turnover

of the leukocytes, from insertion into the blood stream by the bone marrow to deposit in the tissues is only a few hours. Thus, the post-mission leukocytes tested were not the ones present during weightlessness, so it is not possible to describe the changes in leukocyte function as a function of time of exposure to spaceflight conditions. Thus, this study cannot draw conclusions on the possible effects of extended missions on leukocyte function.

#### Vestibular System

##### Concepts and Operations

The Killifish Hatching and Orientation experiment was the second in a series to determine the effects of spaceflight on certain portions of the life cycle of certain organisms. Emphasis was on the function and development of the vestibular system and on calcium metabolism as it relates to otolith development. A similar experiment in demonstration form was conducted on Skylab 3. It consisted of a plastic bag of synthetic sea water containing two juvenile Killifish (Fundulus heteroclitus) and another such bag containing 50 fertilized eggs. The juveniles exhibited looping swimming motion for several days, until gradually they adapted to visual cues for orientation. The orbit-hatched fry, however, exhibited no initial disorientation. They appeared to depend on visual cues for orientation in orbit, and those which were alive after recovery appeared to depend only on visual cues for orientation on the recovery ship, with no vestibular input. The animals died and were not preserved sufficiently to prevent deterioration. Typical otoliths were not visible in microscopic sections of these fish. The Apollo-Soyuz experiment was designed to extend the Skylab experiment, with emphasis on vestibular disturbance and embryonic development. Since otolith development is largely a matter of calcium metabolism, study of the otolith development was important not only for understanding the effects of spaceflight on the vestibular system, but possibly for using the otolith as a model for space research on calcium metabolism in general. The experiment consisted of two sets of five sea-water-filled plastic bags. One set contained immature fry (21 days old at launch) which had been reared from hatching in tanks presenting various visual environments. The other set contained numbers of fertilized eggs with different ages since fertilization. Figure 13 is a photo of the two sets. The data consisted of filming the swimming

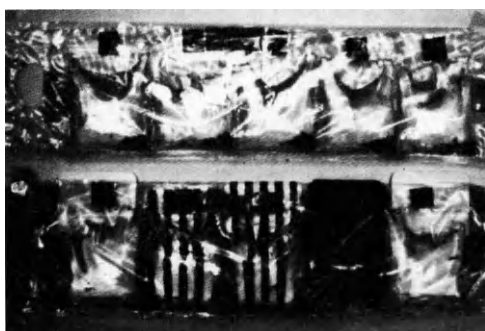


Fig. 13. MA-161 Killifish Egg and Fish Containers

behavior of the juveniles and orbit-hatchlings at various stages of the mission. Post-flight analysis included swimming-behavior testing, light- and electron-microscopy of the vestibular system, and continued zero-g-aircraft testing.

## Results

The Killifish Hatching and Orientation experiment analysis revealed that both the juveniles and hatchlings exhibited normal vestibular function upon return from flight. The juveniles' post-flight swimming patterns suggested abnormal swim bladders. Subsequent testing of maturing fish implied subtle changes in geotactic response and enhanced sensitization to environmental influences as compared with controls. Microscopy has revealed no significant effects on the development of the central nervous system, peripheral vestibular apparatus, the eye, or the cardiovascular system.

## Biological Materials Processing

For various types of biological research it is necessary to acquire pure samples of single-type live cells from a mixture of different types of live cells. The separation process is often not amenable to centrifuge or filter techniques because the different types of cells are not sufficiently dissimilar in size, shape, or mass, and the cells may be too fragile to survive in a viable form.

Electrophoresis is a separation method which utilizes the fact that live cells have a surface charge, the quantity of which is as unique to each type of cell as the cells' biological function. Thus, if a mixture of different types of cells is placed in an electrolytic buffer solution (the composition of which is compatible with the biological vitality of the cells), and if an electric field is applied, the different types of cells should separate into individual zones according to their individual electrophoretic mobilities. However, in ground-based laboratories the performance of the electrophoresis process is limited by effects which are mostly associated with a one-g environment. For example, the density difference between cell zones and buffer solution often causes sedimentation, and Joule heating of the electrophoretic column by the electric field often causes de-stabilizing convection currents. In principle these performance limitations can be eliminated in a zero-g or micro-g environment. On the Apollo-Soyuz mission two experiments successfully demonstrated, for the first time in a space environment, two types of electrophoresis. They were the Electrophoresis Technology experiment and the Electrophoresis experiment.

## Concepts and Operations

The Electrophoresis Technology experiment was an attempt to demonstrate the static column, or zonal, method by electrophoresing several sets of mixtures of cells. The method uses a static column of buffer solution (Figure 14) with the electric field aligned along the column. A sample of cell-mixture is introduced at one end, and the individual cell zones travel down the column at different speeds. Five different mixtures of cells were to be processed: a mixture of rabbit, human, and horse fixed-red-blood-cells, human peripheral blood lymphocytes, human fetal kidney cells, fixed rabbit

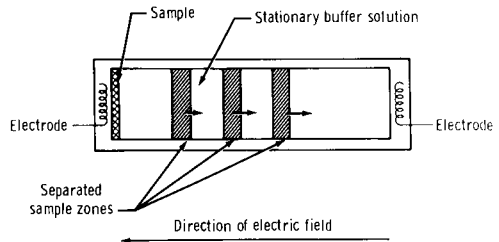


Fig. 14. MA-011 Electrophoresis Technology Static Column Concept

and human red blood cells, and fresh rabbit and human red blood cells. The latter two mixtures were processed by isotachophoresis, which is a self-sharpening-boundary type of zonal electrophoresis. The interest in processing fetal kidney cells was to assess the feasibility of isolating urokinase-producing cells. Urokinase is an enzyme which has the ability to dissolve blood clots, and there is much interest for eventual medical application. The supply is far too low to meet the demand, and although it is obtainable from cultures of fetal kidney cells, only 5% of the cells in the kidney cortex produce it. If the urokinase producing portion of the cells can be isolated, for example by space processing, the potential exists for increased rates of production. To assess this possibility, a pharmaceutical company participated in the kidney cell processing portion of this experiment. The various mixtures (eight in all, because the first three were duplicated) were launched in a cryogenic freezer to maintain cell viability. After the mixtures were processed, the columns were frozen with the cell zones in place, and they were stored and returned in the freezer for laboratory analysis. Thus, this experiment addressed the three technological requirements for eventual application of electrophoresis on space missions: preservation of cell viability prior to processing, processing, and post-processing preservation of viability.

The Electrophoresis experiment was an attempt to demonstrate improved performance of the free-flow method in a micro-g environment over that attainable on the ground. In this method the buffer solution flows continuously (Figure 15), and the cell mixture is continuously inserted into the flow. The electric field is aligned perpendicularly to the flow, so that the cells separate from each other laterally into streams. There were four mixtures processed in this experiment: rat bone marrow cells, fixed rabbit and human red blood cells, rat spleen cells, and rat lymph node cells with human red blood cells as markers. Except for the mixture of fixed cells, the mixtures were freshly prepared before launch in the Apollo command module. The rat lymph cells were frozen (stored in the cryogenic freezer of the Electrophoresis Technology experiment), the others were cooled until processing began approximately a day after launch. The separated streams were detected photo-optically, and the data were stored on magnetic tape; no attempt was made to preserve the cells after processing.

## Results

The Electrophoresis Technology experiment vividly demonstrated zonal electrophoresis with the fixed red blood cell mixture. This was the

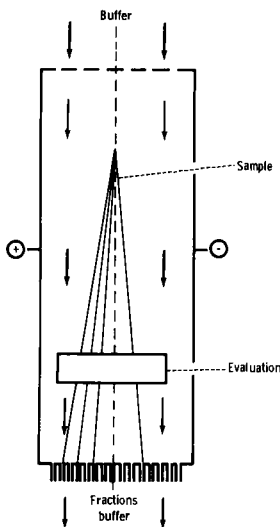


Fig. 15. MA-014 Electrophoresis Continuous Flow Concept

first successful demonstration of zonal electrophoresis in a space environment. The lymphocytes did not electrophorese successfully. The reason is probably that the cells lost viability; post-mission assessment revealed only 6% viability. The cause is not known. The isotachophoresis was partially successful, in that only front boundaries developed. No zone separation or rear boundaries were evident, possibly because the processing time was too low. The most significant result from a research application viewpoint was the kidney cell separation. Zones were formed and yielded concentrations of urokinase-producing cells, as demonstrated by subsequent laboratory culturing. Although the lymphocyte processing was not successful, sterilization techniques were developed in preparation for the experiment which may eventually allow family members of leukemia victims to donate blood years in advance of intended use, rather than the present requirement of donating with sometimes less than two days notice.

The Electrophoresis experiment encountered an anomaly in the photo-optical detection system. During flight the lamps were 42% brighter than their nominal values, resulting in saturation of the photodiode detector array. Consequently, only optical absorptions greater than 30% were detectable, and 30% was the upper limit expected for light absorption by the separated streams. However, absorption pulses did appear on the tape with a distribution similar to that expected for the separated streams. Subsequent ground tests revealed that the electrophoreses cells tend to aggregate irregularly in the regions of the electrophoretically separated streams, such that the pulse distributions do provide good representations of the separated cell-stream distributions. On the basis of this indirect evidence for successful electrophoresis, the result was that electrophoresis was accomplished with a ten-fold increase in the through-put rate and with at-least-as-sharp cell separation as is

achievable in one-g. The rat spleen cells gave the sharpest separation. The rat lymph node cells gave excellent separation and apparently exhibited the greatest tendency to form aggregations (viz., provided the greatest number of pulse-data). The rat bone marrow cells gave indication of good separation in spite of few data (viz., tended not to aggregate), and too few data were available for conclusions concerning the separation of human and rabbit red blood cells.

#### Solid Materials Processing

Two types of solid materials processing were conducted on the Apollo-Soyuz mission: high-temperature and low-temperature. The high-temperature effort consisted of melting and solidifying seven sets of materials samples for seven different experiments. All together, they investigated mechanical, optical, electrical, and/or magnetic properties of pure and mixed substances when they were processed by high temperature in a micro-g environment, i.e., in the absence of sedimentation and thermal convection effects in the liquid phases. Three of the experiments were extensions of furnace investigations begun on Skylab, three were entirely new investigations, and one was a jointly conducted experiment. The low temperature effort was an experiment which attempted to grow commercially important crystals in water at ambient Apollo cabin temperature. This was the first low-temperature processing experiment attempted in a space environment. The development and implementation of this experiment also incorporated the feature of cost-sharing between NASA and a commercial firm.

#### Concepts and Results

The Multipurpose Furnace experiment was actually a development effort to provide a facility for processing the seven high-temperature experiments during the mission. It was developed from a version flown on Skylab; it provided higher processing temperatures (nominally 1423 K) with no increase in power requirement. Also, circuitry was added to allow variable-rate controlled cooldown, and a helium injection rapid-cooldown system was developed to reduce the cool-to-touch time from 20 hours to as little as three hours. Thus, a greater number of experiments could be processed during the mission. Each experiment provided a set of three stainless steel cartridges (Figure 16), each of which contained between one and three ampoules of material to be processed. All three cartridges were processed

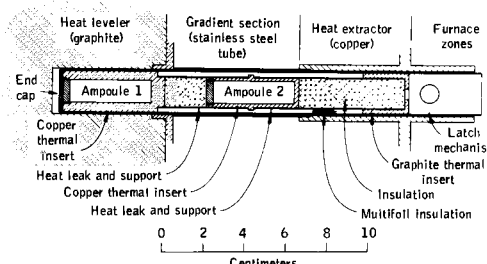


Fig. 16. MA-010 Multipurpose Furnace Typical Cartridge Assembly

simultaneously. The furnace operated extremely well

throughout the mission, except for the first use of the helium cooldown system. This anomaly resulted in a longer soak time for the first experiment with no notable degradation in the scientific results, and no further furnace anomalies occurred during the mission.

The Surface Tension Induced Convection experiment attempted to detect convective mixing in melted material in micro-g which might be due to surface tension gradients arising from compositional gradients. The material selected was pure lead interfaced to an alloy of lead and 0.05 atomic % gold, and samples were processed in both wetting and non-wetting ampoules. The processed samples revealed (incomplete) mixing occurred in a pattern not explainable by diffusion. The flow pattern occurred where the material contacted the non-wetting ampoule surface, and the best explanation appears to be that the flow was induced by interfacial tension gradients arising most likely from the compositional gradient. This conclusion is surprising because it requires that the well known hydrodynamic no-slip condition may not be valid in micro-g conditions.

The Monotectic and Syntectic Alloys experiment investigated the effects of micro-g melting and solidification of two materials, aluminum antimonide ( $\text{AlSb}$ ) and lead-zinc ( $\text{PbZn}$ ). Aluminum antimonide is potentially an efficient solar-cell material, perhaps 30% to 50% more efficient than silicon. The problem has been difficulty in obtaining stoichiometric homogeneity in the compound, and the material is highly reactive with moisture. This latter problem may be caused by EMF effects due to the presence of Al-rich and Sb-rich secondary phases that occur with the compound in one-g processing. The Apollo-Soyuz-processed samples revealed major improvements in macroscopic and microscopic homogeneity. They contain an average of four-times, and a maximum of 20-times, less of the undesirable secondary phase. Small amounts of the Al-rich phase are found only along parts of the grain boundaries, whereas one-g samples contain major grains of both the Al-rich and Sb-rich phases. The  $\text{PbZn}$  system was studied to investigate the phase segregation effects in micro-g for this immiscible system. Because of the large density differences between lead and zinc, it is difficult in one-g to prevent gravity separation during resolidification. It was hoped that the space-processed samples would result in a dispersion of fine particles of superconducting lead in a zinc-rich composition. However, the space processed samples failed to mix, even though the soak temperature was 40 K above the published miscibility gap. Although some Pb-particles were dispersed in the Zn matrix, the bulk of the lead remained in the same position as before melting.

The Interface Marking in Crystals experiment investigated the crystal growth and segregation characteristics in a directionally solidifying material. For this purpose gallium-doped germanium crystals growth on Earth were partially melted and resolidified as 55 ms current pulses ( $19.1 \text{ A cm}^{-2}$ ) were transmitted across the traveling solid-melt interface at

intervals of 4 s. The Peltier cooling by the current pulses at the interface caused time-identifiable demarcations which allowed growth rate determinations to be made. Many new results were revealed. No wetting of the ampoule by the material occurred, as opposed to ground-based processing. The possibility that wetting inversion in space is a phenomenon occurring for many systems has significant implications for materials processing technology in space applications. The growth rate was measured to increase rapidly from zero to  $7 \mu\text{m s}^{-1}$  at the onset of cooling. It then continued to increase over a distance of 2.5 cm and then reached a constant value of  $10.5 \mu\text{m s}^{-1}$ . The growth rate behavior was the same for the ground-processed samples, which indicates that the heat transfer was dominated by conduction (since laminar convection was present in the ground-based tests). All segregation theories assume a step-function jump from zero-to-constant growth rate, so these results require the development of a modified segregation theory. The segregation results show that, as expected, the dopant concentration increased in the bands as the interface traveled over approximately 1.5 cm. However, with continuing growth (at a rate which was still increasing) the dopant concentration decreased rather than reaching an expected steady-state value. It is most likely that this unexpected behavior is a feature of the geometry of the growth system rather than a characteristic of growth in micro-g conditions.

The Zero-G Processing of Magnets experiment investigated the possibility of enhancing the magnetic coercive strength of materials which may have important technological application in the future. The two magnetic materials tested were alloys of manganese bismuth and copper-cobalt cerium. The results were significant. Chemical homogeneity was substantially enhanced macroscopically and microscopically. Single-crystal matrices were grown, and primary crystal size exceeded that grown on Earth by a factor of ten (crystal size was limited by the ampoule dimensions). The  $\text{MnBi}$  samples yielded significantly improved coercive strength, exceeding previously reported values by 20% to 100%. In the unannealed state they achieved values exceeding  $15 \text{ MA m}^{-1}$ , and measurements are currently underway for the annealed state. The results for the  $\text{Cu-Co-Ce}$  samples did not show enhanced magnetic properties. The problem with the flight samples was similar to problems encountered with Earth-based processing of rare-earths. The material reacted with the crucible material of the ampoule to form an intermetallic reaction layer, which resulted in spurious nucleation of the magnetic phase ahead of the regrowth interface.

The Crystal Growth From the Vapor Phase experiment was an extension of a Skylab experiment in order to generalize and characterize the micro-g crystal growth of a class of compounds from the vapor phase. The Skylab experiment revealed that improved crystalline perfection and much-greater-than-expected mass transport rates occurred for  $\text{Ge Se}$  and  $\text{Ge Te}$  with  $\text{Ge I}_4$  as a transport agent. Crystal growth from the vapor phase for such compounds in the IV - VI class of materials is of major interest because their electronic properties are critically dependent on their degree of chemical homogeneity and crystalline perfection.

The Apollo-Soyuz experiment included new compounds and solid solutions transported with different transport agents in higher temperature gradients. The results confirm the Skylab results and extend the conclusions to more complex systems. They also provide experimental evidence for the cause of the enhanced transport rates over the theoretically predicted values. The homogeneity improvement in distribution of Te in the Ge Se Te starting sample is about a factor of 10. The corresponding improvement in distribution of Se in the Ge S Se sample is less pronounced. The transport rates were equal to or lower in micro-g conditions than on ground, but they were three-to-five-times greater than any diffusion theory would predict for micro-g conditions. Further, the enhanced rates cannot be explained solely on the basis of a diffusion process. The enhanced rates are most probably related to thermo-chemical effects of gas-phase reactions which have not been included in current vapor transport models.

The Halide Eutectic Growth experiment was an attempt to grow continuous fibers of lithium fluoride in a matrix of sodium chloride. The objective was to demonstrate the advantages of micro-g processing for obtaining infra-red-transmitting fiber optics. This experiment was an extension of a similar one on Skylab in which long fibers of sodium fluoride were grown in a matrix of sodium chloride. For the Apollo-Soyuz experiment, ingots of the LiF - NaCl eutectic were partially melted and directionally resolidified in micro-g conditions. Continuous LiF fibers were obtained, which yielded improved transmittance over a wider wavelength range with better image quality than for ground-processed samples.

The Multiple Materials Melting experiment had several objectives. This jointly-conducted experiment was analyzed exclusively by the Soviet investigators, and they have submitted their results for publication in reference 2. Three ampoules containing different materials were placed in each cartridge. One sample consisted of an aluminum rod with seven tungsten balls fused to one end and a rod of tungsten-rhenium alloy fused to the other. The objectives were to investigate formation of compounds with components of highly different specific weights, and diffusion and formation of intermetallic phases as a result of interaction of refractory inclusions in a meltable matrix. The inclusions were shifted during space processing, perhaps due to inflight spacecraft accelerations. The second ampoule contained an antimony-doped germanium-silicon solid solution. The purpose was to obtain monocrystals of homogeneous distribution of this semi-conductor material. Monocrystals were obtained with and without seeding by means of directional solidification, but with heterogeneous distribution of components due possibly to radial temperature gradients in the furnace. The third ampoule contained aluminum powder and small pieces of CuAl eutectic, to investigate, for example, sphere formation. The space-processed samples showed no significant difference from the ground-processed samples.

The Crystal Growth experiment was the first space attempt to demonstrate the possibility of growing commercially important crystals by diffusion of appropriate reactants toward each other through pure water at low temperature. Low

temperature methods avoid some of the complications associated with high-temperature processing such as phase transitions, component volatility, thermally induced strain, and contamination from the container. The most successful ground-based, low-temperature crystal growth process has been the gel method, in which reactants diffuse toward each other through a gel. The function of the gel is to support the growing crystals and suppress convection. The main problems are reduced diffusion rates through the gel and multiple nucleation of crystals in the gel, which combine to prevent large single crystals from being grown, and possible contamination of the crystals by the gel material. Since in micro-g the crystals presumably don't need convection suppression or crystal support, the gel can be replaced by pure water. The crystals were grown in reactors (Figure 17); compartment A contained the

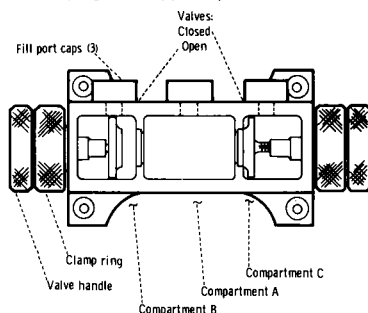


Fig. 17. MA-028 Crystal Growth Reactor

water, and the reactants were stored in compartments B and C. After the joint phase of the mission was completed and the Apollo had separated from the Soyuz, compartments B and C were opened and the reactants diffused toward each other. The reactants grown were calcium tartrate, calcium carbonate, and lead sulfide. The best crystals obtained were the calcium tartrate, with prismatic shapes as long as 2 mm and plate shapes as long as 5 mm. Many rhombohedral calcium carbonate crystals were formed as large as 1/2 mm on a side. The lead sulfide reaction was less successful, but it produced small crystals as large as 0.1 mm. However, the lead sulfide reaction was not complete at time of reentry. The need for temperature control was evident for all the reactions; the temperature in the command module ranged from 269 K to 297 K during the flight. The crystals obtained were of a size and quality comparable to the best obtainable in one-g in the same length of time.

#### References

1. Apollo-Soyuz Test Project Preliminary Science Report, NASA TM X-58173, U.S. Government Printing Office, February 1976.
2. Apollo-Soyuz Test Project Summary Science Report, NASA SP-412, U.S. Government Printing Office, in preparation.

# PLANNING FOR THE FUTURE INTELSAT SYSTEM

Harry L. Van Trees

Assistant Vice President, Advanced Systems, Communications Satellite Corporation,  
950 L'Enfant Plaza, South Washington, D.C. 20024

## 1. Introduction

In ref. 1, an initial description of the future INTELSAT system planning effort was given. The early objectives of the planning effort include: conducting a System Definition Study in order to identify and analyze several future system configurations; consideration of those transition paths (1979-1985) that could lead to future system alternatives; identifying key technologies that need to be developed for the future system and providing inputs to the INTELSAT R&D program; and in recognition of the fact that the future system will probably be significantly more complex than the current system, developing a methodology for effective planning and generating the necessary analysis and synthesis tools to carry out this methodology.

In this paper, some new results in the planning effort will be presented. In particular, a more detailed discussion of the methodology will be given. Familiarity with the contents of ref. [1] is assumed.

## 2. Methodology

This section describes the procedure leading to the formulation of composite systems which form the basis of the System Definition Study. To organize the process of formulation and evaluation of the composite systems, the design elements have been identified and grouped into five categories, as shown schematically in Figure 1.

a. Scenarios--included here are the major features of the user requirements which may be expected to be satisfied by the INTELSAT system in the study time frame. Different services included as part of the scenario are telephony traffic, occasional use service, leased transponder services, provision of specialized service, as well as considerations of route diversity and a model for TDMA access requirements.

b. System concepts--features defining a system concept consist of space segment, earth segment, and space segment configuration. Important factors in a system concept include the number of types of satellites and their roles, the earth segment equipments allowed (e.g., small antennas and TDMA/DSI), the traffic topology (or system connectivity) of the set of satellites, and whether or not the three-ocean region concept is retained.

c. Satellite concepts--the third major element in this process is the selection of the major properties of the satellite(s) to be considered. There are many alternatives for synthesizing spacecraft, each differing in terms of the number of uses of the various frequency bands, coverage capabilities, channelization, power requirements, mass, and cost.

d. Composite system design and evaluation--this stage of system planning pertains to the synthesis and evaluation of a composite system based on a scenario, a system concept, satellite designs, and earth station standards. The synthesis, i.e., determination of the earth and space segment requirements, will rely heavily on three system synthesis algorithms: automatic access, automatic assignment, and evolution, which are presently under development.

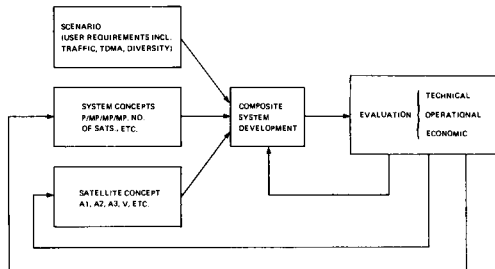


FIGURE 1  
COMPOSITE SYSTEM DEVELOPMENT PROCESS

e. Evaluation criteria--another major element in the planning process is the formulation of evaluation criteria which are generally agreed to and which can be applied in a relevant fashion to evaluate a particular composite system. The evaluation, which takes place after the systems have been defined in terms of space and earth segment requirements and their major features, serves in part as feedback for the optimization of a given approach. Further, the evaluation criteria may serve as decision elements in the system selections at the planning decision milestones. Each of the five elements in the formulation of a composite system is discussed briefly.

### 2.1. Scenarios

There is an inherent uncertainty as to INTELSAT user requirements for the period 1986-1993. This uncertainty relates to the telephony requirement and, perhaps more importantly from a system standpoint, to the requirement for non-telephony services. The problems that this uncertainty pose to the Future INTELSAT System Study can be addressed in two ways. First, an attempt can be made to improve the accuracy of user requirement forecasts, and thereby directly reduce the level of uncertainty. Alternatively, it is possible to generate a set of user requirement scenarios which encompass the likely range of growth uncertainty, and to develop various system concepts to satisfy these scenarios. The latter approach is being taken in this phase of the Study. A parallel forecasting effort is also being conducted.

In this subsection, the existing demand for each of the various INTELSAT services, and the factors affecting the future growth in demand for those services, will be discussed. A reasonably broad set of growth scenarios, each containing an explicitly stated set of assumptions concerning the future demand for the various services, will then be enumerated.

#### 2.1.1. Telephony Requirements

At the present time, fixed-service telephony requirements are the dominant factors in INTELSAT system planning.

##### 2.1.1.1. Pre-assigned Telephony

As of January 1976, the total pre-assigned telephony requirement was 13,370 channels. If the growth patterns presently foreseen for the period 1979-1988 continue beyond that period, the total telephony requirement will reach 296,000 channels by year-end 1993. A detailed summary of the present traffic forecast is shown in Table 2-1.

In addition to utilizing the current traffic forecast, a conservative and an optimistic telephony scenario have also been constructed. Other variations considered include non-uniform growth rates for various elements of the traffic matrix.

The growth in new links in the system and an increase in the number of countries with earth stations must also be included in the scenario.

##### 2.1.1.2. Demand-assigned Telephony Service

The demand-assigned service satisfies two types of traffic. First, it accommodates the overflow traffic between countries which are also interconnected by pre-assigned circuits, and second, it provides the only or most desirable interconnection for thin route traffic demands between some countries. The relative distribution of traffic between pre-assigned and demand-assigned circuits during the period 1986-1993 will depend very strongly on connectivity requirements and on economic issues, most importantly the relative charging for these two services.

The demand-assigned telephony service requirements are typically measured in terms of the total number of billable minutes per day. For planning the future INTELSAT system, however, a better measure of the demand-assignment multiple-access requirements appears to be the maximum DAMA loading during the system busy hour. This information in turn can be used, in the context of SPADE, to determine the number of 800-channel groups which the INTELSAT system will need to accommodate in the future.

Two issues are important for the planning of the DAMA service in the future INTELSAT system: the total number of DAMA users in a given ocean region; and the peak demand for channels during the system busy hours. The present SPADE system can accommodate a maximum of 49 countries, and a maximum of 800 DAMA channels. Both of these limits may well prove to be insufficient during the 1990's.

TABLE 2-1  
PRESENT TRAFFIC FORECASTS

	Actual Year-End Traffic	Projected Year-End Traffic*		
	1975	1979	1989	1993
Atlantic Region	8862	21998	102358	185334
Indian Ocean Region	2581	8954	42384	76742
Pacific Region	1926	3774	18116	33948
Global	13369	34726	162858	296024

\* INTELSAT BG-19-10 Traffic Data Base and Planning Committee Growth Rates Extended to 1993

Presently, a total of 32 countries have made commitments to introduce SPADE service in the Atlantic Region; in 19 of these countries, SPADE service is already in operation. Several countries are planning to expand their SPADE capabilities beyond 12 channels.

##### 2.1.2. Occasional Use Service

Occasional use service is presently provided by a global transponder in the Primary and Major Path satellites. Two services are provided: occasional use TV, and cable restoration. The growth of these services over the last four years shows that the total demand (in terms of minutes of use) has remained quite constant. To the extent that the demand for occasional use TV service is related to significant news and/or entertainment events, it is likely that such demand will not grow substantially. Cable restoration requirements, on the other hand, will probably grow with time.

##### 2.1.3. Leased Transponder Services

There has been a steady increase in leased transponder requirements during the past few years. While the majority of leases are pre-emptible in the event of satellite failure, most of them are also long term (typically five years).

In the future, it is likely that some of these requirements will grow to the point where the Signatories involved may opt for their own domestic or regional satellite systems. However, these decisions will be influenced by INTELSAT policies on availability and charging.

This suggests two possible scenarios. The first would be based upon the assumption that the demand for leased services would level off at 10 to 15 transponders, with some requirements ceasing as more regional domestic systems develop. The second scenario would be based upon the assumption that the demand for leased services would grow rapidly over the next four or five years to perhaps 20 to 25 transponders by 1980, and then at a nominal rate of 15 to 20 percent per year thereafter.

##### 2.1.4. Provision of Specialized Services in the 1985-1993 INTELSAT System

With feasibility proven and a substantial degree of maturity established, satellite communications has become the target of numerous applications studies aimed at exploiting the medium's

unique combination of capabilities in providing long-haul connections, multiple access, and substantial communications cross sections.

In analyzing the potential inclusion of any of the proposed specialized services for INTELSAT, the first crucial question is whether or not the provision of such services would impact on the system design, particularly the satellite design. Several of the new potential services reflect merely a traffic overlay upon the basic system and can, for initial planning purposes, be accommodated as an in-kind augmentation of the system's traffic level and connectivity even though they might require special treatment at an INTELSAT earth station. However, many of the proposed new services are predicated on or enhanced by unique access and/or processing capabilities which require specific system design efforts.

Some of these potential new services are:

a. Educational: Video and/or audio programs to the general public or individual institutions; national or international;

b. Entertainment: Video and/or audio programs to the general public; direct or through distribution; national or international;

c. Telecommunications (new users): Essentially private national or international data, voice or video communications not presently offered in the INTELSAT system;

d. Information: National or international mail, publications, news, or institutional information exchange;

e. Financial: Essentially private national or international transaction services (funds, credit card operations, reservation services, commodities exchange);

f. Ground Mobile: Public or private service to, from or between "small" users with mobile or temporary fixed earth stations; including maritime and aeronautical as well as vehicular stations;

g. Data Collection: Public or private environmental monitoring, status monitoring, location monitoring or housekeeping control services; some possibly requiring satellite sensor capability,

h. Data Relay: Collection, distribution or exchange of information, requiring special non-terrestrial coverage.

In addition to these services, several are of perhaps little volume, but conceivably of substantial public interest, viz: remote health service/consultations; emergency/disaster communications, time and frequency dissemination and specialized navigation services.

Some of these services could, in some form, be provided through the "nominal" INTELSAT network, but possibly at a cost disadvantage and, in most cases, requiring specialized earth segment interface provisions.

### 2.1.5. Diversity Requirements

The diversity requirement issue has two distinct aspects. The first relates to a desire for media diversity, i.e., diversity between cable and satellite paths. The second aspect of this problem relates to the need for route or path diversity within the satellite system.

It is assumed that at least three-path diversity will be required on the heavier Atlantic Region traffic routes during the period 1986-1993.

### 2.1.6. TDMA/DSI Introduction

The timing and rate of introduction of TDMA/DSI will be influenced by a number of factors. The major ones are as follows:

a. Experience gained during the field trials will affect the commencement of the operational use of TDMA. If the field trials are successful, the widespread introduction of TDMA/DSI could commence in 1982.

b. The cost of operational equipment will clearly play a key role.

c. The evolution of the terrestrial system may well be the critical factor influencing TDMA in the space segment. If the conversion of terrestrial systems to digital transmission proceeds at a reasonable pace during the 1980's, it is likely that space segment expansion will be predominately digital also.

d. If the traffic growth is such that there is a significant increase in connectivity requirements, the economic attractiveness of TDMA (relative to FDMA expansion) will increase even if there is no significant reduction in equipment costs.

These factors suggest two different ways of viewing the potential requirement for TDMA/DSI. First of all, TDMA can be viewed as one of several available design options to satisfy projected future traffic requirements. The rate of introduction of TDMA then becomes primarily a question of economic benefit to the system. This view permits, as an example, tradeoffs between the introduction of TDMA and the introduction of additional antennas. Alternatively, TDMA/DSI can be viewed as a requirement placed upon the system by terrestrial considerations. The basic thought here is that earth segment cost considerations play a dominant role insofar as individual Signatory decisions are concerned, i.e., near-term investment requirements are weighted more heavily than potential future space segment savings. These two alternative views of TDMA growth are complementary and lead to different approaches to the problem of scenario generation.

### 2.1.7. System Initial Boundary Conditions

The system's initial boundary conditions are those factors that are present in the system definition at the start of the study design period. They represent the initial set of constraints within which the system must operate. The systems being developed must be capable of transitioning from one form to another. In order to ensure this in the process of the system study, the initial boundary conditions must be specified.

The boundary conditions are comprised of the following elements: satellite type, configurations, spare, TDMA/DSI, FDMA/DSI, 14/11 GHz usage, 6/4 GHz usage, and traffic off-loading. Each of these can be specified for the three ocean regions.

#### 2.1.8. Initial Scenarios

Three scenarios have been hypothesized for the initial analyses. They represent a nominal, conservative, and optimistic forecast.

##### 2.1.8.1. Nominal Scenarios

Scenario Ia: This scenario is based on the premise that the growth patterns established in the recent past, i.e., during the last four to six years, will continue for the next eighteen years.

The principal features of this scenario are outlined in Table 2-2. In essence, it is assumed that the telephony requirement will grow as presently forecast to 296,000 channels by year-end 1993. At the same time, the number of user-to-user links is assumed to grow from the estimated 1979 level of 1,300 paths to 2,750 paths by year-end 1993, assuming that connectivity growth rate is equal to one-third of traffic growth rate. This scenario envisions somewhat limited conversion to TDMA/DSI. In particular, it is assumed that 20% of the system traffic will be converted to TDMA by year-end 1993. Leased service requirements are assumed to remain relatively stable at 10 40 MHz transponders. Occasional use/TV service requirements are assumed to increase from one 40 MHz transponder to a total of seven 40 MHz transponders, by year-end 1993. In addition, it is assumed that digital data services requirements, by year-end 1993, will be on the order of 10,000 equivalent voice channels.

Scenario Ib: This scenario is similar to scenario Ia in the sense that it is based on the premise that recently established growth patterns will continue for the next eighteen years. The sole difference between scenario Ia and Ib is that in the latter substantially greater conversion to TDMA/DSI (80%) is envisioned.

##### 2.1.8.2. Conservative Scenarios

Scenario IIa: The objective in formulating this scenario is to see what impact a somewhat slower rate of traffic growth would have upon the future evolution of the system when coupled with a hypothetical reduction in the cost of TDMA/DSI equipment.

The principal features of this scenario are also summarized in Table 2-2. It is assumed that telephony requirements at year-end 1979 will be 26,250 channels on 1200 links (25% and 8%, respectively, less than the corresponding figures for the nominal scenario). In addition, it is assumed that the traffic growth rate is 16% in 1980, that it decreases at 1% per year until 1986, and that it remains constant at 10% thereafter. These assumptions in traffic growth rate lead to 120,000 channels on 2030 links by year-end 1993. Once again, a connectivity growth rate equal to one-third of the traffic growth rate has been assumed.

In this scenario, it is assumed that by 1986 the cost of equipping an earth station for TDMA/DSI operation will be approximately half that experienced for the field trial equipment. TDMA introduction is assumed to proceed at whatever pace is economically advantageous to the system as a whole. In other words, for a given system/satellite concept, cost tradeoffs will be made between the various available means to satisfy traffic growth.

TABLE 2-2  
PHASE I ALTERNATIVE GROWTH SCENARIOS

	Telephony					Leased Services (Equiv. 40 MHz Trans.)	Occasional Use/TV (Equiv. 40 MHz Trans.)	Digital Data Services (Equivalent Voice Chs)
	Traffic Level	Connectivity (No. of Links)	Diversity Requirement	Demand Assigned Channels	Conversion to TDMA			
Scenario Ia (yr.-end 1993)	296,000	2750	Atlantic-3 paths Indian-2 paths Pacific-2 paths	AOR-800	20%	10	AOR-4 IOR-2 POR-1	10,000
Scenario Ib (yr.-end 1993)	296,000	2750	Atlantic-3 paths Indian-2 paths Pacific-2 paths	AOR-800	80%	10	AOR-4 IOR-2 POR-1	10,000
Scenario IIa (yr.-end 1993)	120,000	2030	Atlantic-3 paths Indian-2 paths Pacific-2 paths	AOR-800	Reduced cost assumption-introduced when advantageous.	10	AOR-4 IOR-2 POR-1	negligible
Scenario IIb (yr.-end 1993)	120,000	2030	Atlantic-3 paths Indian-2 paths Pacific-2 paths	AOR-800	80%	10	AOR-4 IOR-2 POR-1	negligible
Scenario III (yr.-end 1993)	375,000	3000	Atlantic-3 paths Indian-2 paths Pacific-2 paths	All Regions 2,400 -	50%	40	AOR-8 IOR-4 POR-2	50,000

The objective in this portion of the scenario is to determine the impact that a reduction in the cost of TDMA/DSI equipment would have upon the future evolution of the system.

In addition, this scenario assumes that leased services and occasional use/TV service requirements will be the same as those for the nominal scenario, and that digital data services will be negligible by year-end 1993.

Scenario IIb: This scenario is identical to scenario IIa insofar as telephony growth assumptions are concerned. In this scenario, however, TDMA/DSI introduction is treated as a user requirement imposed on the space segment by terrestrial considerations. It is assumed that TDMA/DSI introduction will commence in 1982 and proceed at a fairly rapid pace, i.e., by 1993 a total of 80% of the telephony traffic is assumed to be TDMA.

#### 2.1.8.3. Optimistic Scenario

Scenario III: The objective in formulating this scenario is to identify the potential impact of a substantial increase of growth in both telephony and non-telephony requirements on the evolution of the system.

It is assumed in this scenario that by 1993 the pre-assigned telephony requirement will reach 375,000 channels on 3000 links, starting with a 1979 traffic level of 34,500 channels on 1300 links and using a traffic growth rate of 18.5%, beginning in 1980, and a connectivity growth rate equal to one-third of the traffic growth rate. It is also assumed that there will be a digital data requirement equivalent to 50,000 voice channels by that time. Furthermore, it is assumed that there will be: a) a fourfold increase in leased service requirements; b) a threefold increase in the demand-assigned telephony requirement; and c) occasional use/TV service requirements of 14.40 MHz transponders.

#### 2.2. System Concepts

System concepts are composed of three basic elements: space segment, earth segment, and space segment configuration. The space segment in a specific year is comprised of N geosynchronous satellites at a particular orbital location. The earth segment associated with the global INTELSAT system in any specific year is composed of a set of system-user earth stations. The first important aspect of earth stations from a system design viewpoint is the types of earth stations that are allowed within the system. In the initial studies, Standard A and B stations will be assumed in the 6/4 GHz band and the Standard C station will be assumed in the 14/11 GHz band. The second aspect is the availability of TDMA equipment at the earth station.

The definition of a space segment configuration brings together the space segment and earth segment elements into a system concept. Space segment configuration includes:

- a. the number of satellite types allowed,
- b. a role for each of the N satellites,
- c. a gathering of the satellites into semi-independent operational groups, and

- d. a breakdown of the user requirements for assignment to each group of satellites.

Satellite type is equivalent to satellite design, and the number of types allowed impacts significantly on the system concept that can be developed. Beyond the continued use of previous generation satellites with residual in-orbit life, more than one type of satellite has major system cost, efficiency and modularity implications.

Satellite roles are either Primary (stand alone), distributed Primary, Major Path, trunk, spare, or special purpose.

The next two items, satellite grouping and user requirements breakdown, are closely related and deal essentially with the issue of continuing the firm breakdown of traffic and satellites according to the three-ocean region concept. While the three-ocean region concept has proved effective for INTELSAT purposes to date, continuing with this rigid structure is unnecessarily restrictive in the context of the future system study.

#### 2.2.1. Generic System Concepts

There are three basic system configurations possible within an ocean region:

- a. fully connected single Primary with multiple Major Paths,
- b. fully connected distributed Primary with multiple Major Paths, and
- c. limited connectivity systems.

Under concepts a and b, all system users in an ocean region can establish a communications link to each other via the primary satellite function, hence fully connected. In concept a, this primary satellite function is fulfilled by a single satellite, whereas in concept b, several satellites taken together combine to satisfy the full connectivity requirement. Concept c does not exhibit the full connectivity property and, in this case, not all communications links are feasible.

A slight generalization of that structure is necessary to handle the general multiple region case. Two inter-regional situations are possible:

- a. distinct ocean regions, and
- b. non-distinct ocean regions.

In the first case, the term "distinct ocean regions" is defined as the current three-ocean region concept with separate traffic data bases for each of the Atlantic, Indian and Pacific Ocean Regions. The non-distinct ocean region case, while perhaps not the best categorization, should be adequately descriptive to satisfy the current study needs. This case covers a wide range of possibilities from a single global traffic requirement to be somehow satisfied by a global collection of satellites to the case of a few channels of traffic from one ocean region being carried on a satellite in a different region.

#### 2.2.2. Initial System Concepts

With the system concept elements defined above, numerous specific system concepts can be formulated. Several system concepts have been selected for the initial studies.

Concept I: A fully connected single Primary with multiple Major Paths and distinct ocean regions; the concept is identified as

$$SC_I = \left\{ SP, FC; \left( N_{MP_i} - 1 \right) MP; U_i \right\}, i = 1, 2, 3$$

where the index denotes the ocean regions. Note that  $N_{MP_i}$  is a parameter within the concept.  $U_i$  denotes the user set in the  $i$ th ocean region.

Concept II: A fully connected distributed Primary with multiple Major Paths and distinct ocean regions; the concept is identified as

$$SC_{II} = \left\{ DP(N_{Pi}), FC; \left( N_{MPI} - N_{Pi} \right) MP; U_i \right\}, i = 1, 2, 3$$

$N_{pi}$  denotes the number of satellites in the distributed Primary in the  $i^{th}$  ocean region. Note that the means of achieving the full connectivity (e.g., ISL or cross-transmission) is not specified as part of the concept and is a degree of freedom available to the system designer.

Concept III: A fully connected single Primary in each distinct ocean region with multiple Major Paths and a joint usage of some satellites by users in different ocean regions; a specific example is satellite sharing by the Atlantic and Indian Ocean Regions; the concept is identified as

$$SC_{III} = \begin{cases} SP, FC; & \left( N_{MP_i} - 1 \right) MP; U_i \\ JP (N_j); & U_j \end{cases}, \quad i = 1, 2, 3$$

where  $U_j$  represents the joint user set and  $N_j$  represents the number of satellites accessed by this joint set.

Concept III retains the distinct ocean region nomenclature for the traffic topology within an ocean region.

### 2.3. Satellite Concepts

The satellite concepts represent the third element in the formulation of composite systems. Conceptually, it might be possible to formulate a generalized satellite model in which all salient features would be simply treated as variables. However, such an approach appears to be neither feasible nor necessary at this stage of the planning process.

However, a structure within which different satellite designs might be characterized is necessary. This structure is based on the most significant satellite features, namely: bandwidth, frequency, and coverage configuration. Within this categorization framework, the satellites defined in ref. 1 can be considered to form members of satellite classes. Thus, the satellites of system concepts A1, A2, A3, and B3 can be categorized for comparison with satellites of other INTELSAT designs, such as INTELSAT V, as well as satellites from other communications systems, such as the Japanese Broadcast Satellite Experiment and the Telesat spacecraft.

As the study progresses, other satellite designs will be considered as appropriate candidates for further development in the formulation of the composite systems. These could include upgraded or downgraded versions of the current satellites, as well as new satellite designs.

A gross classification of satellites is by total transponder available bandwidth. Considering directive satellite antenna beams and the use of both the 6/4 and 14/11 GHz frequency bands, total bandwidth ranging from 500 MHz (single use of one band) to over 5,000 MHz can be provided by a single spacecraft. The classification used here is as follows:

- a. Class I--up to 500 MHz
  - b. Class II--500 to 1,000 MHz
  - c. Class III--1,000 to 3,000 MHz
  - d. Class IV--3,000 to 5,000 MHz
  - e. Class V--greater than 5,000 MHz

The options for reusing the frequency spectrum in the 6/4 and/or 14/11 GHz bands are shown in the rows and columns, respectively, of the matrix in Table 2-3. Other, more detailed, classifications are also used in the study.

#### 2.4. Composite System Design and Evaluation

The basic elements of a composite system are:

- a. a scenario which specifies the user requirements in terms of types of services, amount of traffic, and diversity requirements;
  - b. a system concept which is composed of space segment configuration;
  - c. spacecraft requirements, a function of scenario and system concept under consideration; and
  - d. earth segment requirements which is a set of system-user earth station requirements.

The user requirements segment is the primary input to the general system planning process, and hence choice of a system concept, spacecraft, and earth station equipment will depend on the particular scenario under consideration.

TABLE 2-3  
SATELLITE BAND UTILIZATION MATRIX

The composite system design consists of choosing the most suitable system concept, satellite designs, and earth station standards for a given scenario, and determining the earth and space segment requirements

The initial system design procedure consists of two steps:

- a. determination of end-point (year-end 1993) earth and space segment requirements; and
- b. determination of system evolution between initial and final year.

#### 2.5. System Evaluation Criteria

The number of possible future systems for INTELSAT is large. Well-defined and generally accepted evaluation criteria by which these systems are compared are therefore essential.

The evaluation criteria have been divided into three categories: technical, operational, and economic. Some criteria are interrelated, and can tend to oppose each other; for example, as the system design is changed to improve the value of one criterion, the value of a second criterion might simultaneously decrease. For some criteria, a quantitative measure can be computed; in other cases, only a qualitative measure is practical.

No attempt has been made to define composite criteria, either within a category or across categories. The individual criterion will be used to explore system designs. These criteria serve two purposes:

- a. to conduct tradeoff studies and refine system designs; and
- b. to make decisions at various phases of the system planning and implementation.

The nature and usage of the evaluation criteria will vary as a function of, and are related to, the various milestones.

The initial set of criteria is:

##### Technical Criteria

- TC1 - Technical Risk
- TC2 - Reliability
- TC3 - Orbit Utilization
- TC4 - Spectral Utilization Efficiency
- TC5 - Spacecraft Physical Characteristics

##### Operational Criteria

Operational criteria are quantities which can be used to evaluate a system's performance during its operational life.

- OC1 - Transition from the INTELSAT V System
- OC2 - Multiregional Compatibility
- OC3 - Design Flexibility to Accommodate Changes in Traffic
- OC4 - Design Flexibility to Accommodate FDMA and TDMA

##### Economic Criteria

- EC1 - Total Space Segment Net Present Worth

- EC2 - Total Earth Segment Net Present Worth
- EC3 - System Cost Per Channel Year
- EC4 - Total and Per-channel Earth Segment Investment by Signatory
- EC5 - Average (Over Users) Per-channel Earth Segment Investment
- EC6 - Variance of Per-channel Earth Segment Investment

#### Analysis and Synthesis Procedures

It is necessary to develop various synthesis tools in order to carry out the planning methodology. Algorithms are being developed in three separate areas: system access, utilization, and evolution. At present, working algorithms have been developed in the first two areas.

##### 3.1. System Access Software

Determination of system accesses and traffic routing is one of the major steps in the synthesis of a multisatellite system configuration. Factors influencing each earth station's access and the traffic distribution over different satellites are:

- a. user traffic and diversity requirements;
- b. desired traffic distribution over the set of satellites;
- c. desired non-direct (ISL) traffic for the case of distributed/dual Primary;
- d. beam coverages and beam capacities for each satellite; and
- e. each satellite's orbital location, which implies the satellite's visibility by different earth stations.

A computer program that takes these requirements and constraints into account and automatically determines the "minimum" number of system accesses has been developed and tested. This computer program serves two major functions:

- a. access determination in a multisatellite system configuration; and
- b. formation of "communities of interest" on two satellites used in the distributed/dual Primary role.

This program can be used either for system synthesis or for system tradeoff studies.

Typical applications of this program are:

- a. determination of accesses for a multiple satellite system configuration with a distributed Primary and fixed capacity on the ISL to meet the 1993 traffic requirements in the Atlantic Region;
- b. tradeoff studies between ISL traffic and a number of second antennas for both a distributed Primary in the Atlantic Region and a distributed/dual Primary in the Indian Ocean Region;
- c. study of the impact of diversity requirements and desired traffic distribution over a set of satellites on the total number of system accesses; and

- d. study of the effect of traffic redistribution on a three-satellite system configuration in the Atlantic Region.

### 3.2. System Utilization Software

The system utilization software package is used to determine the earth segment requirements so that a given traffic matrix can be carried by a satellite of a particular design. Repeated application of the algorithm to each satellite in a system serving an ocean region yields the feasibility proof of the system design's capability to serve the user requirements in a specified year. The algorithm itself determines the utilization (that is, the setting of the satellite switches and the loading of each transponder) of a single satellite, given:

- a. the use mode of each transponder (FDMA or TDMA pre-assigned telephony, lease service, TV (occasional use), SPADE, or other);
- b. the access to the satellite with existing earth stations;
- c. the earth segment equipments that might be added to accommodate the user requirements; and
- d. the user requirements for this satellite (telephony and other services).

Other algorithms will be developed as the study progresses.

### 4. Summary

In ref. 1, an initial description of the future INTELSAT system planning model was given.

The purpose of this paper is to provide a more detailed discussion of the methodology that will be used in the study.

### Acknowledgement

The results reported here represent a collective effort by the staff of the Advanced Systems group, including H. Weiss, J. Fuenzalida, T. McGarty, W. Schnicke, M. Mohajeri, and R. Granger, with support from R. Davis, R. Fang, and L. Palmer of the COMSAT Laboratories staff.

### References

- 1. AIAA paper 76-233, H.L. Van Trees, COMSAT, Washington, D.C., Future INTELSAT System (1986-1993) Planning.

# ECS SATELLITE AND DERIVATIVES

P. J. Conchie

*Hawker Siddeley Dynamics Limited, Stevenage, Herts, England*

## Abstract

The requirements of the European Operational Communications Satellite (i.e. operation at 11-14 GHz for trunk telephony (CEPT) television (EBU) and communications with North Sea Oil Rigs) necessitated improvements in the payload capability of the OTS satellite.

These requirements enhance the capabilities of this modular design to meet the communication requirements of other regions of the world.

The work leading up to these improvements is described.

## I. Introduction

With the satisfactory completion of the development phase of the European OTS Satellite, attention has increasingly been directed to the operational vehicle to meet the requirements of the European Operational Communications Satellite (ECS) and regional communication satellites generally.

The overall philosophy of these developments was to improve the capability of the design by (i) small detail design improvements retaining essentially the developed design, (ii) taking advantage of new technology in limited areas, essentially in those areas requiring development to meet the higher demands of the mission. By this means the advantages of a proven design will be maintained with an up to date product.

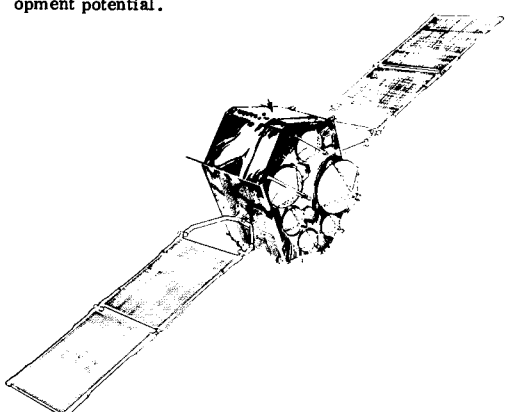
This programme has identified many improvements which will not be implemented in the short term either because the refinement is not required for the currently envisaged missions and/or has further development potential.

## II. Background

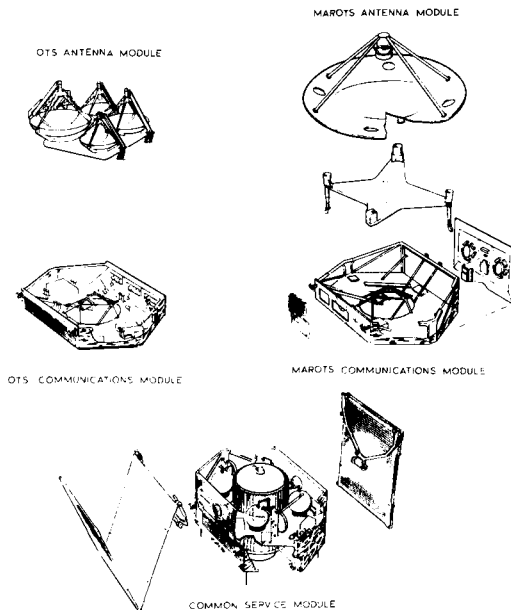
The OTS programme which forms the basis of the MESH proposals for Telecommunication Satellites has been described fully in various papers (ref. 1, 2, 3). In summary the OTS Orbital Test Programme came into being following a technology and feasibility programme which were implemented by the now European Space Agency in 1972.

The contract for the Orbital Test Satellite (OTS) (Figure 1) the experimental forerunner to the European Communications Satellite (ECS) was awarded to Hawker Siddeley Dynamics leading the MESH consortium AEG and Selenia by ESA at the end of 1973.

This satellite which will operate at 11 and 14 GHz is on schedule for launch in the summer of 1977 by a Thor Delta 3914. The design uses 3 axis stabilisation with sun following array panels and is modular (Figure 2) in concept to enable other communication missions to be accommodated in a cost effective manner.

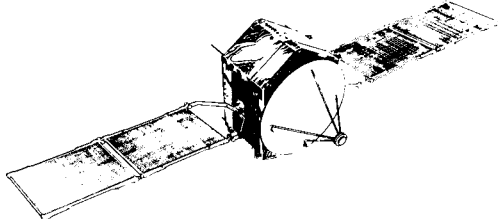


OTS IN-ORBIT VIEW FIG. 1



TRANSITION OF OTS TO MAROTS FIG. 2

The first mission to take advantage of this design concept is the European pre-optimal maritime communication satellite - MAROTS (Figure 3) which uses a service module identical to OTS, although also operating at 1.5GHz for communication with ships.



### MAROTS IN-ORBIT VIEW FIG. 3

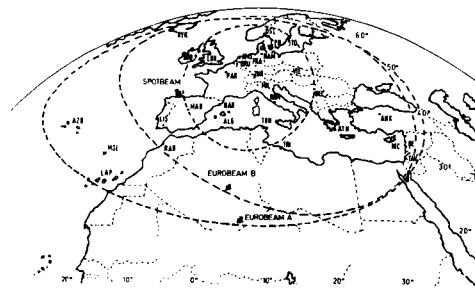
## OTS Payload

This payload consists of 2 modules A and B.

Module A is a reduced version of the intended operational payload for ECS and provides re-transmission of signals such as telephony in PSK/TDMA and television.

All major parameters, are basically the same as for the projected operational system.

Module A contains two chains of 40 MHz nominal bandwidth and two of 120 Hz bandwidth. Each pair is arranged in frequency re-use configuration employing orthogonal linear polarisations. The other module, called Module B, is intended for propagation experiments and narrow band transmission tests. It comprises two repeater chains of 5 MHz nominal bandwidth each with an associated on-board beacon signal generator and arranged in a frequency re-use configuration employing orthogonal circular polarisations. One repeater chain acts as a stand-in for the other but it is also possible to run both chains simultaneously for frequency re-use experiments. The two chains have substantially higher gain than those of Module A and as such they will permit access by small and relatively inexpensive earth stations. Table 1 summarises the performance characteristics and Figure 4 shows the coverage zones.



OTS ANTENNA COVERAGE FIG. 1

## MAROTS Payload

The MAROTS payload has been designed to exploit the OTS service module capability in terms of mass, power and other interfaces. The links between the satellite and the shore use frequencies in the 11-14 GHz band, and the links between the satellite and ships are in the 1.5-1.6 GHz band. Table 1 summarises the capacity of the system in terms of equivalent voice links.

The configuration is best described in terms of the various types of links. "Forward link" transmissions from a shore station are received on board the satellite by an Earth coverage 14 GHz horn antenna feeding redundant receivers.

Transmission to the ships is via a large 2 metre shaped reflector, which is designed to maximise gain at the edges of Earth coverage, where slant path and elevation angles are least favourable. The "return link" transmissions from the ships at 1.6 GHz are received using the same large reflector antenna upconverted to 11.7 GHz, amplified by a 20 watt travelling wave tube and transmitted for reception by the shore stations using a second earth coverage horn antenna.

A further channel of 0.5 MHz bandwidth for communications between shore stations is provided by cross-stapping the forward and return link transponders to allow satellite reception at 14 GHz and transmission at 11.7 GHz.

### III. Areas of Development

The basic requirements on the design for high reliability and for a modular design readily adaptable to various missions with minimum cost, remained the guiding principle in this work.

The ECS requirements differ (Table 1) from the more general requirements for a regional Satcom principally in the European requirements for 11-14 GHz operations due to frequency over-crowding problems in Europe and for the need of compatibility with the Ariane launch vehicle as well as the Thor Delta 3914.

The impact of the use of 11-14 GHz on the service module design is largely confined to the N/S station-keeping requirement. Since the ground stations for 11-14 GHz operations will have auto track, N/S station-keeping is not required; this releases some 60 kgs of mass for the payload.

Whilst it is desirable that all derivatives are compatible with the Ariane launch vehicle for future growth missions, it is only essential for the European mission. However, it is possible to achieve this compatibility by the use of alternative structure elements and maintain the commonality to a large extent. The major difference between these missions is therefore, as far as the service module is concerned, in the AOCS system, but even here a significant degree of commonality is maintained.

Table 1 Performance Summaries

Satellite	OTS	MAROTS	ECS	ARABSAT
Channels	6 x 20W (14/11 GHz)	1 x 60W (14/1.5GHz) 1 x 20W (1.6/11 GHz)	12 x 20W (14/11 GHz)	12 x 5W (6/4 GHz) 2 x 75W (6/2.5 GHz)
Capacity (One Way Links)	7200 + Module B	Up to 48 + 48	9 channels provide 10800 + 2TV + oil rig	Up to 1600 voice or 1 or 2 TV per <u>5 W channel.</u> 1 TV + 10 audio per 75W channel.
Eclipse Operation	1 channel	low power mode 6 voice channels	5 x 20W	12 x 5W
N-S Stationkeeping	Yes	No	No	Yes
Antenna Coverage	Spot Beam and Eurobeam 2.5° circular 4.9° x 8.6° ellipse	Earth 1.5/1.6 GHz 11 GHz 14 GHz	3 Spot Beams and Eurobeam 3.7° circular 5.2° x 8.9° ellipse	Arab League 2.5 GHz 6/4 GHz
Ground Stations	11 metre 3 metre	11 metre (shore) 1.5 metre (ship)	11-18 metre	10 metre (4/6 GHz) 3 metre (2.5 GHz)

#### AOCS

The AOCS for ECS is derived directly from that of OTS, modified to reflect the deletion of N/S station-keeping.

This requires:-

- o changes to the momentum (wheel) system
- o changes in normal mode control loops
- o deletion of two Hydrazine Propellant Tanks
- o optimisation of the mechanical design of Electronic units
- o deletion of 4 Roll/Yaw thrusters
- o deletion of Gyro package

#### Choice of Momentum System

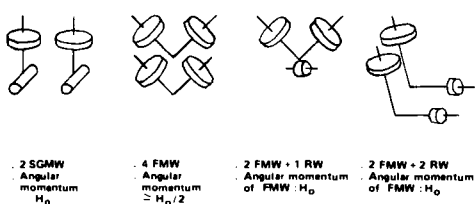
With the deletion of North/South Station-keeping, the capability for one degree of freedom controlled motion about the Roll axis is required to enable accurate antenna pointing over 7 years. The one degree of freedom system can be achieved in 4 ways as shown in Figure 5. These are (including redundancy):-

- 2 single gimballed Momentum Wheels (SGMW)
- 4 Skewed Fixed Momentum Wheels (FMW)
- 2 Skewed FMW + 1 transverse reaction wheel (RW)
- 2 Skewed FMW + 2 transverse reaction wheels

The solution with 2 skewed FMW's and 1 reaction wheel has great promise with the nominal operating configuration being one skewed FMW and one reaction wheel.

Redundancy is provided by either:-

- 2 Skewed FMW's (Reaction Wheel failure) or
- 1 Skewed FMW (No.2) and reaction wheel (skewed wheel (No.1) failure)



This one degree of freedom system also provides the capability for multi target missions with body fixed antenna, and results in a reduction in both the number of thrusters required, and number of pulses. The system provides high pointing accuracy in the presence of small orbit inclination.

The similarity between the electronics of OTS and ECS can be seen in Figure 6.

O.T.S.

PITCH AXIS



ROLL AXIS

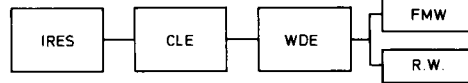


E.C.S.

PITCH AXIS



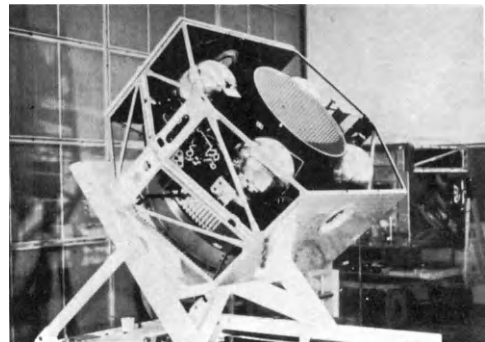
ROLL AXIS



OTS/ECS AOCS COMPARISON FIG. 6

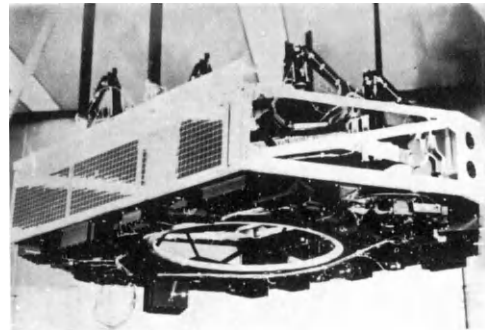
### Structure

The OTS structure concept is of two modules. The Service Module (Figure 7) comprises a central thrust cylinder which interfaces with, and transfers loads to the launch vehicle during launch, and a platform which carries the majority of the service subsystems; the Apogee Boost Motor within the central thrust cylinder, the Telemetry, Tracking and Command subsystem units, the Power subsystem units, the Attitude and Orbit Control subsystem units, including the Reaction Control Assembly and the Pyrotechnic subsystem elements. The North and South faces of the module are closed by sandwich panels which act as thermal control radiators, and which support the folded solar arrays and the array drive assemblies.



OTS SERVICE MODULE FIG. 7

The Payload Module (Figure 8) comprises a platform which supports the majority of the repeater units, North and South sidewalls which support the TWTs and their associated thermal radiators, and a second, angled platform which supports the various antennas, and directs them towards Europe.



OTS PAYLOAD MODULE FIG. 8

The extensive programme of testing on the structure has indicated margins which will allow the Service Module structure to be used essentially unchanged for ECS. The payload module is increased in height to accommodate the 12 instead of 6 TWT radiators.

Various detail improvements are possible and will be incorporated, e.g. the weight can be reduced by over 1 kg by the use of improved insert adhesives. In the longer term the use of carbon fibre material for the structure has been considered. However, the OTS structure is fabricated essentially of aluminium alloy, this material being the conventional lightweight, electrically and thermally conductive metal with adequate strength. The potential of carbon fibre as a structural material has long been recognised, and techniques of manufacture and its performance are now becoming well known. Preliminary estimates suggest that a total of 7 kg could be saved for the OTS structure. However, although this may be achievable from purely structural aspects, there are several impacts on other subsystems which require assessment.

Such impacts arise from the different thermal and electrical characteristics. While preliminary studies show that the carbon fibre laminates can be layered to provide thermal conductances similar to those of aluminium, the electrical characteristics cannot be achieved. Carbon fibre structure materials are likely to have a higher d.c. resistivity and RF loss than conventional materials. This may affect the satellite system in the following ways:- Box bonding - electrically isolated boxes or structure may acquire a static charge with subsequent discharges. The carbon fibre material resistivity is likely to be low enough to avoid this.

Box bonding:- EMC and harness impact. While OTS employs a single point grounding philosophy for d.c. and low frequency signals, the structure is used as a ground plane to which boxes and cable screens are bonded. The use of a comparatively high resistance structure would affect the grounding of boxes and cable screens and may lead to some increase in harness mass should EMC problems arise.

RF shielding - the poorer RF shielding properties of carbon fibre materials may lead to EMC problems and weight penalties in adding screening.

VHF antenna pattern - the VHF antenna pattern depends to some extent on the conductivity and bonding of the satellite outer skin.

For these reasons the projected use of carbon fibre in the near future has been limited to certain structural elements.

#### Thermal ECS

The ECS thermal control concept is based directly on that of OTS, in which the satellite acts essentially as an insulated box in which the equipments are mounted, heat being rejected from the North and South satellite faces. During transfer orbit, when heat dissipation within the satellite is low, the folded solar arrays and attached thermal fins limit the heat rejection from the control radiators, thus maintaining an acceptable internal environment.

The development for ECS in the thermal system is largely refinements or optimisations, (e.g. optimisations of the lightweight thermal insulation blankets) apart from those changes arising directly from the increased number of communication channels.

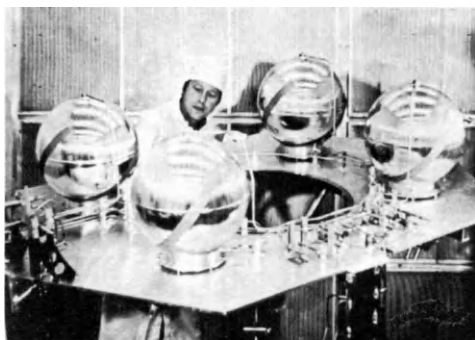
#### Reaction Control System (RCS)

The RCS used on ECS differs from that of OTS (Figure 9) in that:-

- two of the 4 propellant tanks are removed
- the 4 roll/yaw thrusters are removed
- the pipework is modified accordingly

Removal of two propellant tanks is possible following the deletion of the requirement for N-S station-keeping. The deletion of the 4 thrusters is possible

as the resulting is more mass effective for the single degree of freedom AOCS. Other improvements under consideration include the use of surface tension tanks and optimised flow control valves. Although diaphragm propellant tanks are used on OTS, surface tension tanks are now available which are lighter, have additional capacity and have a superior explosion efficiency, thus reducing residuals.



REACTION CONTROL SYSTEM FIG. 9

#### Augmented Electrothermal Hydrazine Thrusters

These devices are based on the electrothermal hydrazine thrusters which have a performance similar to that of the catalytic thrusters, but have an added device which allows heating of the exhaust products to temperatures of the order of 2000K. The additional heating causes further decomposition of the gases and the net performance of the thrusters in terms of propellant usage to thrust level is approximately 50% better than can be achieved by catalytic thrusters.

Use of these devices is thus extremely attractive for missions requiring north-south station-keeping, and up to 20kg or more propellant can be saved on 7 year missions. This mass saving is slightly offset by the mass of the thrusters and their electronic power control (approximately 3kg).

Thrust levels available are of the order 0.1N beginning of life for a heater power of the order 130 watts. Thus use of the thruster has an impact on the north-south station-keeping philosophy, power margins and yaw errors.

#### TT and C Subsystem

The demands of an experimental communications satellite on the TT and C subsystem are of course higher than those required by an operational system. Certain deletions and refinements and optimisations are therefore possible with attendant mass reductions.

### Electrical Power Subsystem

The electrical power subsystem of ECS retains the regulated bus concept of OTS with its attendant advantages, namely

- o a smooth transition between solar array and battery power at eclipse entry and exit
- o efficient utilisation of battery energy over a wide range of battery voltage
- o efficient utilisation of solar array power at end of life, and avoidance of solar array lock up problems.

Based on the OTS design experience, some simplifications and detailed circuit design improvements have been made to reduce the mass and improve the efficiency of the power conditioning and control, while extending the power level range and maintaining a modular system able to meet a range of requirements with the minimum of redesign.

Improvements have been made to the solar array regulator, the battery discharge regulators, the batteries and the battery protection and control circuits. These are described in more detail below.

#### Solar Array Regulator

The OTS employs a digital shunt regulator, comprising a redundant analogue full shunt of some 150W capability together with shunt dump switches on seven solar array sections each of some 100W capability, with control logic to clock the array sections in or out at a 20 kHz rate so as to maintain the analogue shunt working within its linear range.

The ECS employs a sequential switching shunt regulator, in which the analogue shunt is deleted. The solar array sections are switched in sequentially so that the array power equals the load current power while also maintaining the supply voltage within the specified range. Thus a number of array sections will be fully on, a number fully off and one continually switching to achieve the required current balance into the bus capacitor, resulting in a ripple voltage of some 100 mV p-p which is used to control the array section switches. The deletion of the analogue shunt yields a small mass saving and a large reduction in the thermal dissipation of the regulator.

The thermal dissipation is further reduced, and the circuit design simplified, by the use of non-redundant dump switches with series relays to clear possible short circuit failures via telecommand. Open circuit failures are acceptable as long as the load power exceeds the uncontrolled array power. The sequential switching shunt regulator has demonstrated an excellent transient response with good stability margins independent of uncontrolled circuit parameters. Analyses and tests on the OTS engineering model have proved that the voltage and current switching edges in the regulator and solar array circuits can be controlled to give adequate EMC margins even for a mission carrying a sensitive VHF payload.

### Battery Discharge Regulator

The OTS battery discharge regulator comprises 2 units each of 300W capability in active redundancy. The efficiency is about 0.9 at 100 watts output, but falls to about 0.8 at 300W. The units are mounted in the PCU and thermal constraints limit the total output to 300W. For ECS a modular approach has been adopted, with smaller units of 130W capability to give more flexibility in meeting a variety of output power and reliability requirements. The ECS battery discharge regulators operate in the light (unloading) mode with a common duty cycle to give inherent current sharing. This permits the efficient use of multiple batteries to feed the common power bus.

#### Batteries

ECS carries two batteries to meet the increased power demands. Each battery is mounted as a single pack, thus minimising the temperature differentials across the battery that could arise due to temperature differences across the spacecraft equipment mounting floor. A significant mass reduction is achieved by the use of thin walled battery cells, and a lightweight battery packaging technique.

#### Battery Protection and Control

OTS carries a battery protection unit (BPU) and a battery monitoring and control unit (BMCU). The BPU carries a transformer rectifier unit for each battery cell to prevent cell voltage reversal during discharge, in effect using the stronger cells to support the weak ones. The BMCU carries three separate functions namely:

- o an amp hour meter with a variable k factor to allow the battery charge to be terminated when the charge amp hours exceed the discharge amp hours by one of eight values between zero and 30%
- o a battery voltage comparator to give an output when the battery voltage rises above (on charge) or falls below (on discharge) a value preset by telecommand
- o a cell voltage monitor which measures each cell voltage in sequence, for telemetry to ground.

The BPU is most effective in prolonging battery life if one cell fails prematurely. With matched cells little extension of life is achieved, and protection against cell damage by voltage reversal can be achieved only by load shedding.

Thus for ECS the BPU is deleted, and a comparator added to the individual cell voltage monitor so that automatic load shedding may be initiated to avoid cell voltage reversal. A battery reconditioning facility is included so that battery performance may be recovered.

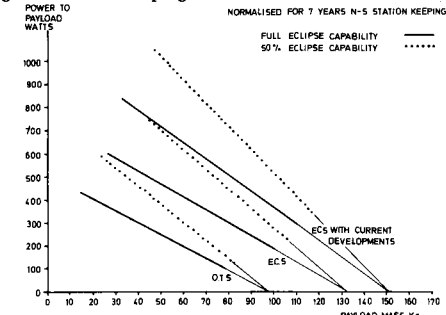
In addition the battery voltage comparator is retained, with the facility to adjust the selected trip voltage to take account of battery ageing or special operational requirements. The on-board amp hour meter is deleted, but telecommand override capability on all battery control operations permits this function to be carried out via telecommand, if desired.

Battery charging is from the 50V bus as on OTS, either via resistors or constant current regulators.

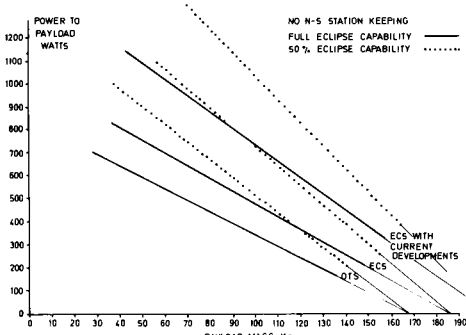
#### IV. System Capability

Table 1 shows the payload characteristics of OTS, MAROTS, ECS and ARABSAT, included as an example of a typical regional communication satellite.

Figures 10 and 11 summarise the effect of the developments to the basic OTS design, by showing the payload capabilities of OTS, ECS and OTS derivatives utilising the current technology developments. Figure 10 shows payload capability normalised to 7 years N-S station-keeping, for 100% and 50% eclipse capabilities. Figure 11 shows similar curves for missions not requiring N-S station-keeping.



PAYLOAD CAPABILITY NORMALISED FOR  
7 YEARS N-S STATION KEEPING FIG. 10



PAYLOAD CAPABILITY WITHOUT N-S  
STATION KEEPING FIG. 11

#### V. Conclusion

The developments described have significantly enhanced the performance of the basic OTS satellite without detracting from the advantages of the modular (bus) design approach. Continued emphasis has been applied

to reliability, especially the aspects of redundancy and the elimination of single point failure modes. With the developments described herein, the continued growth in launch vehicle capability, and the increasing mass efficiency of the communications units, there is good reason to believe that this design will meet the expanding market for future Regional Communication Satellites.

#### Acknowledgement

The author wishes to thank the European Space Agency and Hawker Siddeley Dynamics Limited, for permission to publish this paper and for the assistance and advice of their colleagues in its preparation.

#### References

1. The OTS Project - Basis of future European Space Communications System. AIAA paper No. 74-495 by R.C.Collectte and B.Stockwell European Space Research Organisation (ESRO)
2. The current status of the Orbital Test Satellite Programme - TELECOM 75. Geneva October 1975 by Colin Wearmouth, Hawker Siddeley Dynamics Limited
3. The Development of the Orbital Test Satellite. AIAA Paper No. 76-246 by C. Wearmouth and D. McLaurin, Hawker Siddeley Dynamics Limited.

#### Abbreviations (Including Figures)

CEPT	- Conference Europeenne Des Administrations Des Posts Et Telecommunications
EBU	- European Broadcasting Union
OTS	- Orbital Test Satellite
MESH	- MATRA, ERNO, SAAB, HSD, AERITALIA
ESA	- European Space Agency
MAROTS	- Maritime OTS
PSK/TDMA	- Phase Shift Key/Time Division Multiple Access
AOCS	- Attitude and Orbit Control Subsystem
RF	- Radio Frequency
TWT	- Travelling Wave Tube
EMC	- Electro-magnetic Compatibility
PCU	- Power Control Unit

# THE JAPANESE BROADCAST SATELLITE AND COMMUNICATIONS SATELLITE EXPERIMENTS

Ken-ichi Tsukamoto,<sup>\*</sup> Osamu Ogawa,<sup>\*\*</sup> Masayoshi Murotani,<sup>†</sup> Yoh Ichikawa,<sup>‡</sup>  
Hironobu Okamoto, Shoji Sonoda and Keigo Komuro<sup>‡</sup>

<sup>\*</sup>*Radio Research Laboratories, MOPT, Koganei-shi, Tokyo 184, Japan*

<sup>\*\*</sup>*Headquarters of Technical Administration and Construction, NHK, Jinnan, Shibuya-ku, Tokyo 150, Japan*

<sup>†</sup>*Yokosuka Electrical Communication Laboratory, NTT, Yokosuka-shi, Kanagawa 238-03, Japan*

<sup>‡</sup>*National Space Development Agency of Japan, Hamamatsu-cho, Minato-ku, Tokyo 105, Japan*

## Abstract

The Japanese Broadcasting Satellite (BSE) and Communications Satellite (CS) for experimental purposes will be launched in Feb. 1978 and Nov. 1977 respectively from the United States Eastern Test Range (ETR) by means of Delta 2914 launch vehicles. Various experiments will be conducted for three years in order to obtain necessary knowledges and techniques for establishing future operational domestic broadcasting and communications satellite systems in Japan. This paper will present the experimental schemes as well as the overall system configurations and characteristics including space-crafts and ground facilities.

## I. Introduction

(1) (2) The BSE and CS are two of the most important national space programs of which preparations are now under progressing in Japan. Both satellites are used in experimental basis for developing technologies necessary in future operational domestic broadcasting and communications satellite systems.

With the purposes of extending TV broadcasting service area to surrounding remote islands and dissolving difficulties of good quality TV signals reception in mountain districts and urban areas with massive buildings, BSE is launched in Feb. 1978, and put into a geostationary orbit of 110 degs. E. It is a medium-scale, three-axis stabilized spacecraft having two sets of 14/12 GHz transponders. CS is a medium-capacity, spin stabilized spacecraft having two sets of 6/4 GHz and six sets of 30/20 GHz transponders, and is launched into a geostationary orbit of 135 degs. E. in Nov. 1977. The purpose of introduction of domestic communications satellite systems in Japan is to get communication circuits to and from many surrounding remote islands and to secure flexibly applicable communication means in emergency cases such as terrestrial networks break down due to natural disasters as well as to provide effective solutions coping with rapid increase of general communication demands which could not be covered by the existing terrestrial networks.

Both of these space programs were initiated by Ministry of Posts and Telecommunications (MOPT), and the spacecrafts manufacturing, launching and stationing in orbits are carried out in responsibility of National Space Development Agency of Japan (NASDA). The spacecrafts launchings are supported by NASA, USA. The mission experiments will be conducted by Radio Research Laboratories (RRL) of

MOPT with cooperations of Japan Broadcasting Corporation (NHK) and Nippon Telegraph and Telephone Public Cooperation (NTT). Most distinguishing matters in these programs are utilization of higher frequency bands, quasi-millimeter waves, and high accurate performances in spacecraft position and attitude controls. Propagation experiments in these high frequency bands will be conducted with emphasis along with other broadcasting and communications experiments.

Various kinds of earth terminals are prepared for these mission experiments. Main Transmit and Receive Station (MTRS), Transportable Transmit and Receive Stations (TRRS), Receive Only Stations (ROS) and Simple Receive Equipments (SRB) are used in the BSE program, and Main Fixed Earth Station (MFES), Fixed Earth Stations (FES), Transportable Earth Stations (TES) and vehicle mounted type Small Transportable Earth Stations (STES) are used in the CS program.

Among these stations, MTRS and MFES belonging to RRL are key stations of respective space programs and used not only in broadcasting and communications experiments but also in spacecrafts controls through K-band and C-band Telemetry, Tracking and Command (TT & C) functions throughout their mission experiment periods.

## II. Spacecrafts

### (1) BSE Spacecraft

The BSE is a three-axis stabilized spacecraft weighing about 350 Kg in geo-stationary orbit, and has sun-oriented solar panels generating high power of about 1 Kw and K-band (14/12 GHz) direct conversion type transponders with three 100 watt TWT amplifiers for two channels color TV broadcasting. The 12 GHz down-link broadcasting carriers are efficiently radiated to cover whole Japan territory from the shaped-beam satellite parabolic antenna. The BSE system key parameters are summarized in Table 1.

The BSE will be launched from ETR by Delta 2914 launch vehicle into 95° flight azimuth. The BSE will be injected into transfer orbit having normal 166.7 Km x 35786 Km, 27.20° orbital inclination parameters.

The third apogee is selected for nominal orbit injection to allow time for precise orbit determination and spacecraft attitude maneuver. After attitude stabilization to the earth, orbit velocity corrections are made to correct injection errors and optimize the drift to the final geo-stationary location at 110° East longitude, normally 30 days after AKM burn.

On-station control is achieved by a zero-momentum

system through use of orthogonal reaction wheels.

The BSE orbital configuration on geo-stationary orbit and functional block diagram are shown in Figure 1 and 2.

Table 1 BSE system key parameters

Satellite location	110°E longitude
Experimental coverage	Japanese territory
Carrier frequency	
TT & C	
command/ranging	2110.8 MHz (1 MHz BW) 14.0125 GHz (ditto)
telemetry/ranging	2286.5 MHz (ditto) 11.7125 GHz (ditto)
Television up-link	14.250 - 14.300 GHz (25 MHz BW/TV channel) 14.350 - 14.430 GHz (ditto)
down-link	11.950 - 12.000 GHz (ditto) 12.050 - 12.130 GHz (ditto)
Channel capacity	2 - Color TV channels
Received quality	
TV-video	S/N = 45 dB at 1dB rain loss (TASO Grade 1)
TV-sound	S/N = 50 dB
Power flux density	
Japan mainlands	-108 dBW/m <sup>2</sup>
Remote territory	-117 dBW/m <sup>2</sup>
K-band antenna pointing accuracy	±0.2°(3σ)
On-orbit station-keeping accuracy	±0.1°(N/S and E/W, 3-years)
Initial solar array generated power	970 watts at worst case
Reliability	0.725
System design life	3-years
Launch vehicle	Delta 2914
Launch capability	675.8 Kg

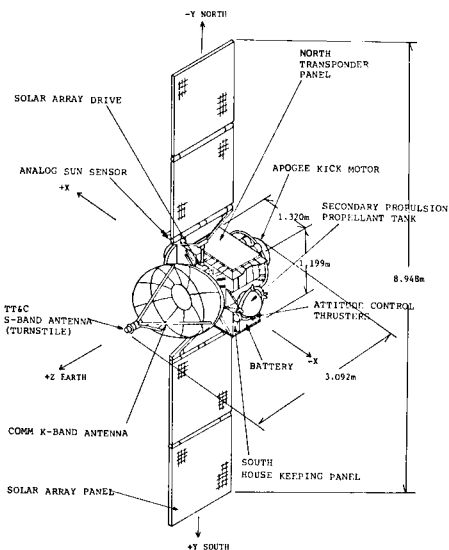


Fig. 1 BSE orbital configuration on geo-stationary orbit

The communication transponder design incorpora-

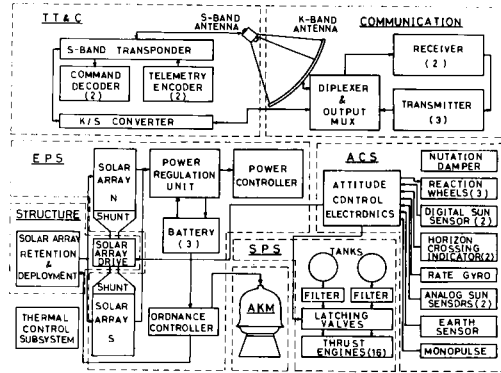


Fig. 2 Functional block diagram of BSE

tates two out of three transmit path and fully redundancy receive path. The input and output switch assemblies operate in conjunction to route the channel A and B (channelized) signals through their respective primary transmitters, or either channel through the redundant transmitter. The gain control circuit maintains the 100 watt TWT drive power at a constant level independent of received signal level component gains or frequency. The communication transponder performance characteristics are summarized in Table 2.

Table 2 Communication transponder performance characteristics

Power flux density at BSE	-82 to -96 dBW/m <sup>2</sup>
Gain control	over 16 dB range, automatically
100 W TWT drive level control	64 steps by command
Noise figure	less than 8.0 dB at receiver input point
Minimum RF output power	100 watts at output of 100 W TWT
Amplitude/Frequency response	± 1.0 dB/channel

The BSE K-band antenna is a center feed shaped-beam parabolic antenna which has three feed horns. It has adequate gain over the Japanese territory minimizing interference over neighboring countries.

The Tracking, Telemetry and Command (TT & C) Subsystem consists of a S-band antenna, dual S-band receiver-transmitters, telemetry encoders, command decoders, K/S and S/K converters to accept up-link commands and send BSE telemetry to the earth on the down-link carrier. The TT & C Subsystem also processes a tone modulated signal for BSE ranging information.

The S-band TT & C antenna, which provides approximately omni-directional coverage, is mounted forward of the K-band feed horns.

The Electrical Power Subsystem (EPS) provides the electrical power for all modes of BSE operation in launch, transfer orbit and three years geo-stationary satellite orbit phases. The EPS utilizes a solar array for power generation and batteries for energy storage. A solar array consists of four panels, two per spacecraft side, and batteries consist of three 4-AH sealed Nickel Cadmium batteries.

The Attitude Control Subsystem (ACS) stabilizes the attitude of the BSE during the transfer orbit,

drift orbit and geo-stationary orbit. An earth sensor, a monopulse RF sensor and solar array mounted sun sensors are used to derive roll, pitch and yaw error signals. Attitude information from any two of these three kinds of sensors is used in normal operation.

The Thermal Control Subsystem (TCS) is to maintain all BSE component temperatures and temperature gradients within design limits for all missions. The TCS consists of insulation blankets, thermal coatings, conduction spacers, heater/thermostat assemblies, and heat pipes to maintain the proper temperatures.

The Apogee kick Motor (AKM) is a solid propellant rocket motor ignited at the apogee of the elliptical transfer orbit to inject the BSE into a circular equatorial geo-stationary satellite orbit.

The Secondary Propulsion Subsystem (SPS) is a monopropellant hydrazine type propulsion system consisting of a propellant storage and expulsion section, and a rocket engine section.

The BSE weight distribution, power requirements and reliability prediction after 3-years are shown in Table 3.

Table 3 BSE Weight distribution/Power requirement/Reliability prediction

	Weight (Kg)	Average power (watts)	Reliability (after 3-yea) (%)
Structure/Mechanical	76.7	-	0.999
Communication	62.5	626.4	) 0.852
K-band antenna	7.0	-	
Tracking, Telemetry & Command	10.6	29.5	0.968
Electrical power	72.6	11.3	0.994
Attitude control	26.7	22.4	0.902
Thermal control	22.3	29.5	0.999
Apogee kick motor	344.4	-	0.996
Secondary propulsion	47.8	-	0.984
Ballast	2.5	-	-
Total	673.1	719.1	0.725

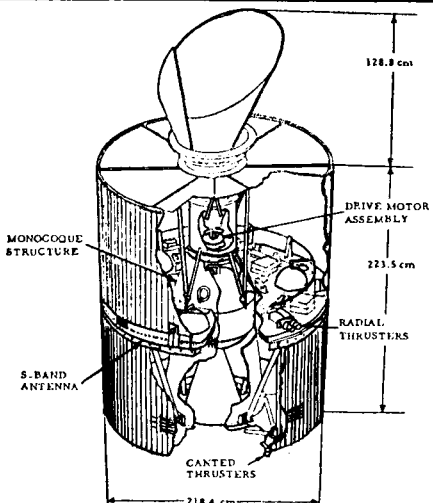


Fig. 3 Feature of the CS spacecraft

## (2) CS Spacecraft

The CS is a spin stabilized spacecraft weighing about 350 kg and has a mechanically despun communication antenna, as shown in Figure 3.

The communication subsystem consists of K- and C-band transponders, a communications control unit, and a high gain communication antenna. The block diagram of transponder group is shown in Figure 4. Each of six K-band transponders, with a frequency range of 27.7 - 30.0 GHz (uplink) and 17.7 - 21.2 GHz (downlink), and two C-band transponders of 5.9 - 6.4 GHz (uplink) and 3.7 - 4.2 GHz (downlink), has a 200 MHz bandwidth for telephone and color TV transmission and for PCM signals transmission up to 100 Mbps.

A composite K-band signal is received and separated into three bands designated F1, F2 and wide band signal which includes F3 through F6. Channel F1 contains a single channel receiver through TWT amplifier. Although all K-band channels have AGC, only F1 can be deactivated by ground command. F2 transponder also contains a single channel receiver and a TWT amplifier. F3 through F6 signals are directed to one of two redundant receivers where they are down-converted to an IF frequency and amplified. These four signals are separated by a hybrid and two diplexer/equalizers and directed to four individual transmitters. Each signal is again amplified and up-converted to the transmit frequency and fed to each TWT. The six output signals and a beacon signal generated by a separate transmitter, are recombined in the K-band output multiplexer.

Composite C-band signals from the despun antenna are separated into three signals, G1, G2 and the command signal. Transponder channel G1 contains a receiver with AGC, a transmitter, a TWT amplifier and an output isolator. Channel G2 contains a receiver, a bandpass filter, a switch attenuator, an auxiliary amplifier, a TWT amplifier and an output isolator. The switch attenuator provides signal level adjustment over 10.5 dB range in 1.5 dB increments upon ground command.

The C- to S-band down-converter converts C-band signals to S-band frequency. The signals are fed to the S-band receiver of the Telemetry, Tracking and Command (TT & C) subsystem for implementation. The S- to C-band up-converter accepts S-band

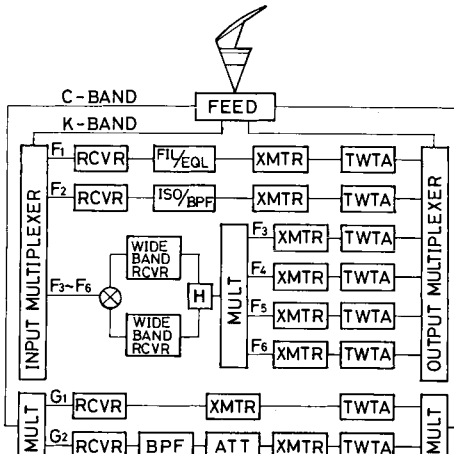


Fig. 4 Functional block diagram of CS transponders

telemetry signal from TT & C subsystem and converts them to the C-band telemetry signals. These C-band telemetry signals are combined with the communication signals of G1 and G2 channels in the C-band output multiplexer and fed to the antenna.

The performance of the transponder is summarized in Table 4.

Table 4 Transponder performance

	K-band	C-band
Frequency of operation	30/ 20 GHz	6/4 GHz
Number of channels	6	2
Channel bandwidth (3 dB)	200 MHz	200 MHz
Output power/channel	34 dBm	34.5 dBm
Input noise figure	13 dB	9 dB
Beacon output power	30 mW	25 mW

The mechanically despun communication antenna employs an unique shaped beam technology for K-band coverage. The antenna provides a 33 dB gain at K-band toward the Japanese mainlands. The shape of the reflector differs from the true paraboloid very little in terms of wavelength at C-band, and provides a 25 dB gain towards the main and remote islands.

The antenna system consists of a horn-reflector of graphite/epoxy, excited by networks specifically designed to produce circularly polarized radiation at C- and K-band frequencies, and transmission lines between the antenna and transponders. K-band signals are injected into and extracted from the feed horn assembly by an orthomode transducer separating receive and transmit signals on the basis of polarization and frequency. C-band signals are coupled to the feed horn by axial slots in the horn wall. The receiving and transmitting bands have four slots fed by rat race hybrids and separated by 90 degrees. Phase difference between adjacent slots produces circularly polarized waves. Filters at each coupling slot reject K-band energy. K-band antenna coverage is determined by a domestically developed computer program which predicts directive gain of the horn reflector antenna and shapes the reflector surface contour to optimize the coverage.

The telemetry, tracking and command (TT & C) subsystem uses dual S-band receivers and transmitters in the transponder. These units act redundantly with a C- to S-band converter to accept up-link commands/ranging signal and send telemetry data/ranging signal to ground control stations. The S-band antenna consists of a circular array of 64 cavity-backed cross-dipole elements and provides a tri-lobal pattern.

The attitude and antenna control subsystem provides azimuth pointing control in  $\pm 0.3^\circ$  accuracy for the communication antenna and also provides informations necessary to control satellite attitude.

The electrical power is supplied by a solar cell array which covers the outer CS cylindrical surface, and a 20 ampere-hour battery. The minimum array power during the 3 year mission life is 475 watts for the maximum spacecraft load of 378 watts.

The primary structure consists of a central cone and a horizontal equipment panel, and the drive motor assembly for despinning the antenna is mounted to the forward end of the central cone.

CS thermal control maintains the temperatures of spacecraft and components within  $10^\circ\text{C}$  upper and lower limits during all mission phases.

Thermal control is achieved passively and is augmented by heaters for the temperature sensitive equipments.

The apogee kick motor is a solid propellant SVM-6 motor, and the reccation control equipment is a monopropellant hydrazine system consisting of four axial and radial thrusters.

### III. Ground Facilities

The MTRS and MFES are installed as the key stations in both space programs at Kashima Branch of RRL which is located about 100 Km north-east of Tokyo. Other earth terminals are distributed throughout Japan territory and cooperate in the various mission experiments.

#### Earth Stations in the BSE Program

##### (1) Main Transmit and Receive Station (MTRS)

The MTRS is used for the 14/12 GHz TV broadcasting experiments and TT & C operations in the same frequency bands during the mission experiment period.

The antenna is a 13 meters dish near-field Cassegrain type of Az-El mount, and installed on the roof of the three stories main control building. Roughness of the main reflector surface is  $\pm 0.3 \text{ mm rms}$ , and four reflectors beam waveguide feeding system is adopted. The primary radiator of corrugated conical horn and duplexing waveguide assembly together with the transmitters and receivers are fixed in the buiding room separated from the rest parts of the antenna structure. In this configuration, feeding loss reduction and maintenance simplification are achieved. The feature of the antenna is shown in Photo 1 which was taken at the manufacturing company. The antenna is whole-sky steerable, and a higher modes type ( $\text{TM}_{01}$  &  $\text{TE}_{01}$ ) auto-tracking function is facilitated. A polarization plane auto-tracking mechanism is also equipped in the duplexing waveguide assembly. The typical electrical characteristics of this antenna system are as follows :

Receive system G/T (Spec.)	above 32.0 dB/ $^\circ\text{K}$ (12 GHz, $40^\circ\text{E1}$ )
Transmit EIRP (Spec.)	78.5 - 91.5 dBw(variable)
Frequency band	14.0 - 14.5 GHz for transmit 11.7 - 12.2 GHz for receive
Gain with feed loss	63.4 dB at 14.25 GHz 61.8 dB at 11.95 GHz
Noise temp. with feed loss	48°K (12 GHz, $40^\circ\text{E1}$ )
Cross-polarization discrimination	better than 30 dB (12 GHz, linear)
Tracking accuracy	0.01°rms at -125 dBm receiver input level

The antenna subsystem is followed by 14 GHz high power TWT amplifiers of which output power are continuously variable from 2 Kw to 100 watts, 140 MHz/14 GHz up-converters, 12 GHz/400 MHz low noise image compressed type down-converters of  $600^\circ\text{K}$  noise temperature, 400/140 MHz down-converters and 140 MHz IF switching board. A Dicke type 12 GHz radio meter working in and out of TV signal transmission band and 14/12 GHz loop-back test translator are also equipped. Wide band 140 MHz FM modulators and demodulators and various TV baseband signals test equipments are connected to the transmitters and receivers through the IF switching board. The TT & C subsystem consisting of command signal generator/modulator, telemetry signal

demodulator/decommutator, ranging equipment, on-line and off-line computing systems with various peripheral devices and spacecraft control softwares are prepared.

Photo 1  
Feature of K-band antenna for the MTRS



## (2) Other Ground Terminals

As a field transmitting and receiving terminal, Transportable Transmit and Receive Station (TTRS) will be applied. There are two kinds of TTRSSs, type A and B. The former is intended to access to the BSE from any place throughout Japan including the surrounding remote islands. This comprises 4.5 meters diameter antenna and a shelter where 2 Kw TV transmitter and 2 channel receivers are housed. It is capable of transmitting and receiving all of the types of signals envisaged for the BSE experimental program. It will provide a backup to the MTRS in case of a major failure.

Special features of this terminal are a high power, K-band klystron, low noise receivers and a simple automatic tracking mechanism to follow the motion of the BSE.

The K-band klystron is fully forced air cooled with high power gain 42 dB with maximum output power 2 Kw, and is being tunable to any of five pre-assigned TV channels between 14.0 and 14.5 GHz.

Unique SHF techniques of inserting mounted planer circuit into the waveguide have been applied for the low noise receiver with the system noise temperature 820°K.

As a simple tracking mechanism, the step track antenna pointing device is installed.

This terminal is intended to set up within 2 days or to disassemble in a day working three people.

Type B is fully mobile and equipped with 25 KVA power supply generator. The attached antenna has 2.5 meters diameter and its pointing is manually controlled. Other communication equipments and their functions are quite the same as those of type A.

This terminal is intended to access the BSE within two hours working three people from any place in the mainlands.

Receive Only Stations (ROS) will be used for the evaluation of community reception of broadcast TV signals throughout the country. They are intended for TV broadcasting to the communities in the remote islands or to those geographically isolated areas. For high quality TV receptions, ROSs of 4.5 meters diameter antenna and of 2.5 meters are used in the remote islands and in mainlands respectively.

The former has a program tracking device, whereas the latter is manually controlled.

ROS is capable of two TV channels reception with the system noise temperature lower than 550°K.

Simple Receive Equipments (SRE) are intended to verify the capabilities of the future satellite direct broadcast reception. Unique SHF techniques of inserting mounted planer circuit into the waveguide have been developed by NHK Technical Research Laboratories.

The receiver features 500°K system noise temperature over 180 MHz bandwidth, using a simplified down-converter as well as a simplified direct FM-AM modulation converter.

With this technical breakthrough, low cost, high sensitive 12 GHz receivers suitable for mass production and adaptable to the existing home TV set have been realized. photo 2 and 3 show the features of TTRS type B and SRE respectively.



Photo 2 Feature of the TTRS Type B

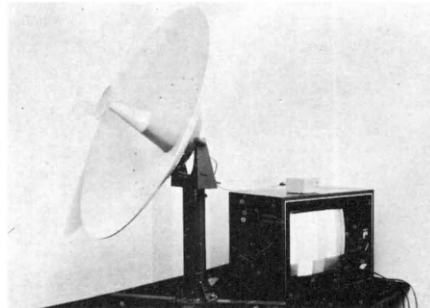


Photo 3 Feature of the SRE

## Earth Stations in the CS Program

### (1) Main Fixed Earth Station (MFES)

The MFES is used for K- and C-band communications experiments and C-band TT & C. It has K-band and C-band antenna systems. The structure of the K-band antenna is almost same as that of the BSE K-band antenna. Differences exist only in the primary radiator and duplexing waveguide assembly due to differences of operating frequencies and types of polarization. In the CS K-band antenna system, a higher mode ( $T_{M01}$ ) single channel type auto-tracking method is applied. The typical electrical characteristics of this antenna system are as follows ;

Receive system G/T (Spec.)	above 41.5 dB/°K (20 GHz) 50°El)
Transmit EIRP (Spec.)	about 90 dBw

Frequency band	27.5 - 31.0 GHz for transmit 17.7 - 21.2 GHz for receive
Gain with feed loss	69 dB at 30 GHz 66 dB at 20 GHz
Noise temp. with feed loss	71°K (20 GHz, 50°E1)
Cross-polarization discrimination	38.8 dB at 19.45 GHz
Tracking accuracy	0.01°rms at -125 dBm receiver input level

30 GHz high power TWT amplifiers of maximum 500 watts output power and a 20 GHz helium-gas cooled low noise parametric amplifier of 100°K noise temperature and 2.5 GHz bandwidth are used in the K-band system. The C-band antenna is a 10 meters dish transportable Cassegrain type, and installed on the ground near the main control building. 6 GHz high power TWT amplifiers of 300 watts output power and 4 GHz non-cooled parametric amplifiers of 55°K noise temperature are used in the C-band system. Radio meters and loop-back test frequency translators are equipped in both of K- and C-band systems. TT & C subsystem is installed completely separately from that of BSE.

The IF frequencies are selected as 1.7 GHz common for both of K- and C-band systems, and various types of communication test equipments and modulators/demodulators are used in common for both systems. Figure 5 is the block diagram of the communication test equipments.

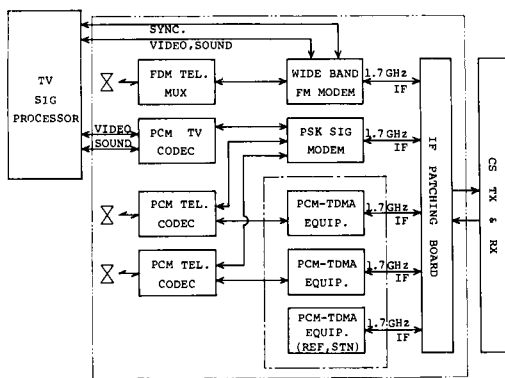


Fig. 5 Block diagram of communication test equipments at the MFES

The FM modulator/demodulator can process the baseband signals, such as FDM multiplexed telephony signals, color TV signals and others of 10 Hz to 15 MHz frequency band, with good modulating linearity of better than 1 dB over 100 MHz IF bandwidth.

The PSK signals test equipment is used for processing various kinds of digital signals such as TDM multiplexed PCM telephony signals, PCM TV signals and others with various modulation parameters. The modulation parameters can be selected as follows;

Clock frequency	6.3 MHz, 32 MHz, 64 MHz and External clock
Max. transmit capacity	96.768 Mbps
Modulation phase	2, 4 and 8 phases
Detection	Synch det.
Scrambling	Clock 6 MHz to 98 MHz, 7 or 17 stages shift-register

Test pattern gen.	Maximal length PN code with 6, 15 or 22 stages shift-register, Mark ratio 0, 1/16, 1/8, 1/4, 1/2, 3/4, 7/8 or 15/16
BER measurement	$10^{-1}$ to $10^{-8}$

The PCM TV signals are processed as shown in Figure 6, block diagram of PCM TV Codec. NTSC video signal and two channels sound signals are sampled in 10.752 MHz and 32 kHz clocks, and transformed to 10 parallel PCM signals of 5.376 MHz clock and a serial PCM signal of 768 kHz clock respectively. After multiplexing these signals, error correcting bits, R(12/11), are added in the Convolutional encoder and formed to a PCM TV signal of 64.512 Mbps.

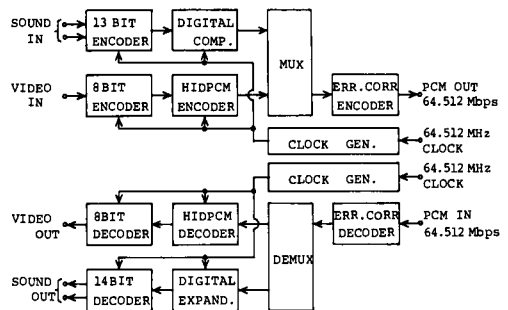


Fig. 6 Block diagram of PCM TV Codec at the MFES

The PCM-TDMA system developed by RRL is a system-clock non-coherent type and designed suitable for K-band multiple access communications considering potential instabilities of transmission path condition due to rainfall attenuation.

In this system, functions of reference station switchover and diversity station switchover at each ground terminal, in automatic or manual mode, are provided.

The main characteristics of this system are as follows;

Transmission rate	65.536 Mbs
Transmission capacity	960 telephone channels
Frame length	500 $\mu$ s
Frame structure	three steps superframes 210, 214, 217 bits
Modem	two phase DPSK, delay det.
System clock	non-coherent among bursts
Initial acquisition	low level PN codes
Baseband interface	30 channels PCM codecs
Rainfall protection	Switchover of reference station Switchover of diversity station

At NTT, another type of PCM-TDMA system has been developed and both types of PCM-TDMA systems will be examined in the CS program. Some other communications test equipments such as Spread Spectrum Random Access (SSRA) and Single Channel Per Carrier (SCPC) will be also connected to the K- or C-band transmitters and receivers through the IF switching board.

## (2) Other Ground Terminals

In addition to the MFES of RRL, various types of earth stations are being prepared for the CS experiment by NTT.

#### K-band Fixed Earth Station (K-FES)

An outline of Yosukawa Experimental Earth Station with a fully steerable 12.8 meters near-field Cassegrain antenna operating at both K and C bands was described in (2).

In addition to this earth station, a new K-band only earth station is now under construction. This K-FES has been designed as a model of future earth stations which will be constructed on the top of telephone exchange offices in the large cities in Japan. The antenna is a limited steerable Cassegrain antenna of 11.5 meters in diameter. The performance of this antenna is being measured using a test pedestal.

The features of this antenna are :

- The structure and feeder system are so designed that the antenna can be erected either on the top of a building or on the ground.
- The weight of the antenna is 24 tons. This can be compared with 50 tons of the existing 12.8 meters antenna.
- The antenna is of an X-Y mount. The steerability is  $\pm 12^\circ$  in Y-axis and  $47^\circ \pm 8^\circ$  in X-axis.

Other main characteristics of this antenna are shown in Table 5.

Table 5 Characteristics of K-FES antenna

Antenna type	Near-field, high efficiency shaped-beam Cassegrain antenna
Diameter	11.5 meters
Weight	23.9 tons
Wind velocity	70 m/s (survival) 20 m/s (operational)
Surface flatness of main reflector	0.17 mm r.m.s.
Bandwidth	17.7 - 21.2 GHz, 27.5 - 31.0 GHz
Antenna gain	66.0 dB 69.1 dB
Aperture efficiency	74 % 66 %
First sidelobe level	-15.2 dB -15.4 dB
Antenna noise temperature	25°K

One of other main equipment of K-FES is 30 GHz high power TWT amplifier (HPA). This HPA is an improved version of the existing water-cooled 100 W HPA(2). Main improvements are :

- Equipment output power of 200 W using a 300 W TWT, high efficiency and high gain (40 dB small signal gain) were achieved by means of collector-depression technique. The high gain of this equipment made it possible to employ a solid-state circuit as an exciter.
- The conventional water cooling is replaced by air cooling. This is expected to contribute to easier maintenance.
- Low loss in input circuits including high power circulators has been achieved.

#### Small Transportable Earth Station (STES)

Based on the measured characteristics of the C-band vehicle mounted transportable earth station(2), the design of a K-band vehicle mounted transportable earth station is under way.

#### IV. Experiments

Mission experiments of the BSE and the CS programs are described separately.

#### Experiments in the BSE Program

The experimental items are classified as follows.

1. Experiments on basic technologies in the broadcasting satellite system

- \* Evaluation of the broadcasting service area
- \* Experiments on TV transmission
- \* Experiments of radio wave propagation
- \* Experiments on frequency sharing
- \* Measurements of spacecraft on-board equipments characteristics
- \* Measurements of ground terminal equipments characteristics
- 2. Experiments on control and operation of satellite broadcasting system
- \* Experiments on spacecraft control technologies
- \* Experiments on satellite broadcasting operation technologies
- \* Experiments on accessing from multiple ground transmitting stations
- 3. Experiments on satellite broadcasting signal reception
- \* Evaluation of received TV signal qualities
- \* Improvement of broadcast signal receiving techniques

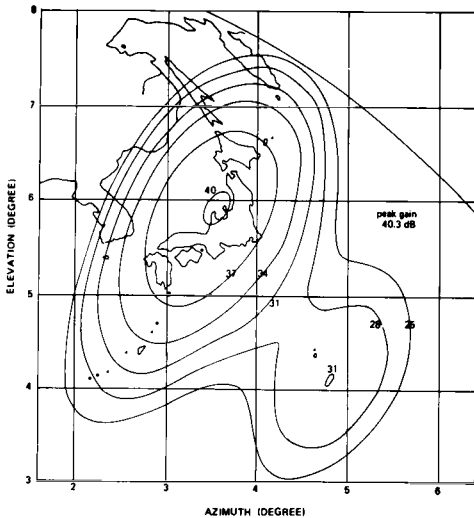


Fig. 7 Ground coverage footprint of the BSE antenna pattern

With the designed spacecraft antenna radiation pattern in 12 GHz down-link, shown in Figure 7, it is expected that high quality color TV of 45 dB S/N (TASO grade 1) could be received at any parts of Japan territory with reasonable rainfall attenuation margin when SREs of 1 to 1.6 meters antenna size are used in the mainlands or ROSSs of 2.5 to 4.5 meters antenna size are used in the surrounding remote islands. The link budgets are shown in Table 6. At various earth terminals distributed throughout Japan, field strength, C/N, TV signal quality and their variations will be measured during whole experimental period in order to evaluate effective service area. The spacecraft telemetry informations about transponder output power, attitude stability, etc. as well as ground weather data will be also used in these evaluations.

The standard of TV signal transmission parameters in the BSE program is taken as follows, considering compatibility with existing home TV sets.

System	NTSC Standard System M (525 lines, 30 frames/sec)
--------	---

Modulation	FM, Freq. dev. 12 MHz (p-p)
Sound subcarrier	
Frequency	4.5 MHz
Modulation	FM, Freq. dev. ±25 kHz (0-p)
Sound/Video ratio	1/6
Emphasis	CCIR Rec. 405-1

Table 6 Link budget of BSE program

Up Link (Kashima to BSE)			
TX power (dBw/ch)	20.0		
TX feeder loss (dB)	-3.5		
TX antenna gain (dB)	62.0		
Free space loss (dB)	-207.2		
RX antenna gain (dB)	39.5		
RX feeder loss (dB)	-0.5		
Noise power (dBw/25 MHz)	-122.6		
C/N	32.9		
Down Link			
Service area	Mainland	Remote	Ids
Antenna of RX	1.6mφ	4.5mφ	
TX power (dBw/ch)	20.0	20.0	
TX feeder loss (dB)	-1.7	-1.7	
TX antenna gain (dB)	37.0	28.0	
Free space loss (dB)	-205.8	-205.4	
RX antenna gain (dB)	43.5	52.5	
Received Carrier (dBw)	-109.7	-109.4	
Noise power (dBw/25 MHz)	-126.4	-126.4	
C/N	19.4	19.8	
Total C/N (dB)	19.2	19.6	
Threshold C/N (dB)	9.0	9.0	
Rain attenuation (dB) (99.9% of any month)	-7.0	-7.0	
Link margin (dB)	3.2	3.6	

System signal level diagram, up-and down-links path losses and their variations with time, C/N, frequency stabilities, etc. are measured in the spacecraft loop back circuits at the MTRS and/or TTRSSs. In the experiments, transmission parameters will be taken variable not only in the items listed above but also in modulation polarity, dispersal, AFC type and so forth. With the purposes of development of advanced TV broadcasting systems or of application technologies, various kinds of signals transmission experiments will be conducted such as multichannel sounds multiplexed TV signal, Y/C separated TV signal, digitalized TV signal and still pictures broadcasting. By means of VITS insertion, automatic monitoring and statistical analysis of TV signal transmission qualities will be made throughout the experimental period.

The radio wave propagation studies will be made in the BSE and the CS programs in parallel. Rainfall attenuation data of 12 GHz obtained at various earth terminals will be collected to Kashima in order to evaluate required link margins in domestic satellite systems in Japan. In addition to the statistical and regional rainfall attenuation studies regarding whole Japan territory, some special investigations of radio wave propagation will be made at Kashima. 12 GHz and 20 GHz radio meters attached to the respective 13 meters dish antenna, a separated 35 GHz radio meter, field strength measuring small terminals, rain gauges and specially designed weather radar will be worked in this study. The weather radar, working in 5.3 GHz with 250 Kw peak output power, is expected to provide rainfall rate distributions along the radio wave propagation paths from the satellites with spatial resolution of 250 meters x 1.5 degrees.

Data of 12 GHz and 20 GHz field strength, cross-polarization components, polarization plane angle of 12 GHz wave and their variations are measured by the 13 meters dish antenna systems. These data will be used in detailed studies of atmospheric absorption, rainfall attenuation, scintillation fading, depolarization and space diversity effects. Propagation studies in 14 GHz and 30 GHz satellites up-links will also be carried out by using the data of ground transmitting powers and satellites telemetry data.

Interference between the satellite and terrestrial broadcasting TV signals in 12 GHz will be measured for investigating frequency sharing problems. In this experiments, NHK's experimental station for 12 GHz terrestrial broadcasting will be used. From the terrestrial station, both of FM and VSB-AM TV signals will be broadcasted.

Through the K-band TT & C system, spacecraft control techniques such as position and attitude maneuvering, housekeeping and operation of on-board mission equipments, etc. will be studied. How to keep the position and attitude of the spacecraft precisely within the required accuracies of  $+0.1^\circ$  and  $\pm 0.2^\circ$  respectively for three years in minimum fuel consumption is the most interesting technical matters. Techniques of automatic or manual control of ground transmitter output power against the changes of rainfall attenuation for keeping the spacecraft receiver input level optimum, and the TV signal transmit timing control techniques among multiple ground transmitting stations for avoiding double illumination or signal intermittent break-off in TV signal source switchover time, will be developed in the experiment.

With ROSS and SREs installed throughout the country, satellite broadcast TV signal quality will be evaluated in various field conditions such as geographical features and weather conditions. Likewise, availability of high quality reception will be observed for long range of the satellite life time. The appropriate and reasonable configuration of satellite broadcast TV reception will be established both in urban and rural areas. For individual reception, selection of suitable antenna and its size taking account of satellite coverage patterns, installation, adjustment of antenna pointing and keeping, effects of circumstances, and capability of low cost receivers will be examined. For the isolated communities located in the remote islands and in mountainous surroundings, either cable TV systems or small output power rebroadcasting in VHF will be applied depending on the density of households.

And for metropolitan areas, to save the households shadowed by high buildings, cable TV system or small output power SHF rebroadcasting will be investigated.

#### Experiments in the CS Program

Intended experimental items in the CS program are as follows.

##### 1. Measurements of on-board equipments characteristics

- \* Characteristics of the on-board horn reflector mechanical despun antenna including antenna patterns, cross-polarization components and others by means of field strength measurements at many ground terminals or spacecraft antenna beam scanning
- \* Performance of antenna beam pointing during transient phases of spacecraft position and attitude maneuvering
- \* Characteristics of C- and K- bands mission

- transponders in the initial phase on orbit and their degradations with time
- 2. Experiments on signal transmission through the satellite communication system
  - \* Basic transmission characteristics of FM and PCM-PSK signals in various modulation parameters
  - \* Performance of multiple access communication systems of PCM-TDMA, SSRA (Spread Spectrum Random Access) and SCPC (Single Channel Per Carrier)
  - \* Frequency sharing between satellite and terrestrial systems and between two satellite systems
- 3. Measurements and evaluations of radio wave propagation characteristics
  - \* Statistical and regional rainfall attenuation studies in K-band satellite communication system covering whole Japan territory
  - \* Detailed investigations of K-band radio wave propagation in such items as rainfall attenuation, scintillation, depolarization and space diversity effects
- 4. Experiments on satellite communications system operation
  - \* Operation of multiple access communication systems such as PCM-TDMA, SSRA and SCPC
  - \* Remote control of satellite transponders, ground transmitter level control, site diversity switching according to rainfall attenuation conditions
  - \* Compatibility tests between satellite system and terrestrial networks especially in telephone exchanging function
  - \* Establishment of temporal circuits through the satellite by small earth terminals such as C- or K-band STESs
  - \* Establishment of satellite communication links to remote islands using the C-band TES
- 5. Experiments on spacecraft operation and control through C-band TT & C
  - \* Spacecraft position, attitude determination and maneuvering
  - \* Spacecraft antenna beam pointing control
  - \* Operation of mission transponders and house-keeping
  - \* Development of TT & C operation techniques and satellite operation softwares

The fundamental characteristics of the satellite communication system will be gathered from the following experiments. Modulation schemes are both frequency modulation and PCM-PSK.

In FM transmission, the noise loading characteristics, up- and down-path margin and stability will be evaluated. In PCM-PSK, the bit-error probability characteristics, up- and down-path margin and stability will be main points.

An experimental transmission of two broadcast quality television signals and 100 voice circuits using 100 Mb/s carrier is planned. Band compression and time division multiplex technique will be employed. The effects of satellite transmission on picture quality and synchronization will be evaluated. Multicarrier operation of a satellite transponder is another item in the experiment. The effects of AGC or limiting amplifier in the spacecraft will be examined on the TDMA signals and analog modulation signals.

Frequency sharing between satellite and terrestrial systems will also be studied in both C and K-bands. In this will be included an estimation on the interference reduction effect of energy dispersal and SSRA communication system.

The optimum operational parameters of transponders and earth stations for various types of satellite communication systems will be investigated.

Integration of the satellite system into the domestic terrestrial telecommunication network will also be studied.

A PCM-PSK JEMA experiment will be carried out among three K-band fixed earth stations. The information transmission rate will be 60 to 100 Mb/s. The following characteristics in both clock coherent and clock incoherent operation will be examined.

- Modulator to demodulator characteristics and carrier synchronization in burst mode operation.
- Bit error rate characteristics in burst mode operation.
- Burst synchronization characteristics in case of changeover of a reference station or time slot assignments.
- Acquisition characteristics in acquisition modem, acquisition signal detector and acquisition control process.
- Clock synchronization characteristics in clock regeneration and clock control process.

Another multiple access experiment on SSRA system will be carried out for the determination of the optimum operational points and for the evaluation of the synchronization characteristics and signal quality. Measuring items are as follows.

- Time required for initial acquisition
- Synchronization error
- Threshold of synchronization establishment
- Signal to noise ratio or bit error rate
- Baseband spectrum

Applicability of C-and K-band vehicle mounted transportable earth stations will also be studied. The objective of the stations is to establish temporarily 60 voice circuits or one CTV transmission.

Video conference and video telephone through the satellite are also included in the experiment plan.

The experiment concerning the integration of the satellite circuits into the terrestrial network aims at the survey of the effects of time delay on the existing telephone exchange and at the confirmation of speech quality, characteristics of new echo-suppressors etc.

Measurements of 30/20 GHz bands radio wave propagation characteristics are very important experimental items for evaluating required rainfall attenuation link margins and other propagation effects affecting to the transmission signal qualities. The experiments will be made in the way similar to that of the BSE case.

#### Acknowledgement

The authors wish to acknowledge the valuable discussions made by MOPT, NHK, NTT and NASDA staffs, and also the contributions of the spacecrafts and ground facilities manufacturing companies, Toshiba/GE, Mitsubishi/AFC and NEC.

#### References

- (1) T. ISHIDA et al., "Program of Medium-Scale Broadcasting Satellite for Experimental Purpose". AIAA Paper 76-255, April '76.
- (2) T. ISHIDA et al., "Program of Medium-Capacity Communication Satellite for Experimental Purpose". AIAA Paper 76-244, April '76.

# COOPERATION BETWEEN U.S. AND EUROPE IN TELECOMMUNICATIONS SATELLITE PROGRAMMES FOR MOBILE APPLICATIONS

W. Luksch\* and E. J. Martin\*\*

\*European Space Agency

\*\*COMSAT General Corporation

## Abstract

For a number of years, the European Space Agency (formerly ESRO) has been involved with U.S. entities, especially the COMSAT General Corporation, to collaborate in, and coordinate Telecommunications Satellite Programmes designed to enhance communications and related services for ships and aircraft. This paper provides a status report on the various programmes and cooperative efforts. In particular : the AEROSAT Programme (ESA, COMSAT General and the Government of Canada), the MARISAT system (MARISAT Consortium) and the MAROTS Programme (ESA).

ceived as a solution to communication problems for the Atlantic and Pacific Oceans, whilst the European MAROTS programme was aimed at improving communications in the Eastern Atlantic and the Indian Ocean, recent political developments are leading to the consideration of an integrated MARISAT/MAROTS system to provide an embryonic worldwide communications system network prior to the availability of satellites developed by the worldwide INMARSAT Organisation. The paper discusses in turn the MARISAT and MAROTS programmes before giving a synthesis of how they may provide the initial worldwide service.

## Introduction

The development of fixed service satellite communications has taken place at two distinct levels ; firstly that of intercontinental communications which has been the objective of the INTELSAT Organisation, and more recently the development of domestic service satellites such as those found in the U.S., Canada and now in other countries such as Indonesia, Brazil, etc. However, growth in fixed service communications is now taking place with the extension to regional systems such as that being planned within the framework of the European Space Agency in Europe (the so-called European Communications Satellite /ECS/) and such systems as ARABSAT. The development of mobile communications has been somewhat different and, in fact, has tended to be along bi-lateral or tri-lateral lines ; the most clear case of this which will be discussed first in this paper is that of AEROSAT, where the current programme foresees participation by the U.S., Europe, and Canada.

The situation for maritime satellite communications, although it has commenced in a somewhat different manner, is now taking on the aspect of transatlantic cooperation. Although initially, the American MARISAT system(\*) was con-

## The AEROSAT Programme

The AEROSAT programme has been established in the framework of a Memorandum of Understanding signed in the Summer of 1974, by the Federal Aviation Agency (FAA) for the United States, the Department of Transportation of Canada, and the European Space Agency (ESA) for Europe. The signatories have formed an Aeronautical Coordination Office (ACO) for the purpose of coordinating their experimental efforts (ground stations and avionics in particular).

This programme has been established to provide experience in technical, operational and managerial areas required in advance of establishing a fully operational capability ; to evaluate voice and data communications between ground and aircraft ; to permit the evaluation of dependent and independent surveillance capabilities and of navigational data derived by an aircraft utilising ground and satellite transmissions ; and to explore ways of using satellite capabilities to improve cost-effectiveness of oceanic route service. Thus far, there are 11 countries involved in this Joint Programme.

On the other hand, to take into account the U.S. policy that the Government will utilise commercial telecommunications facilities and services to the maximum extent feasible, the AEROSAT space segment will be developed and co-owned by a group consisting of COMSAT General, the Government of Canada and ESA. These entities have signed an Arrangement to that purpose in 1974 and jointly

(\*) The MARISAT system is jointly owned by four U.S. communications companies, COMSAT General, RCA Global Communications, ITT World Communications and Western Union International.

established, early in 1975, the AEROSAT Space Programme Office (SPO) as the integrated entity responsible for the day-to-day management of the space segment programme.

The AEROSAT system will permit experimentation and evaluation of :

- voice and digital data communications between suitably equipped aircraft and the ground ;
- dependent and independent air traffic control surveillance ;
- wideband techniques.

For the links between the satellite and the aircraft, the AEROSAT system will operate either in the aeronautical L-band (around 1.6 GHz) and in the aeronautical VHF band (around 130 MHz). For the links between the satellite and the ground it will operate in the aeronautical C-band (5.00 to 5.25 GHz).

The AEROSAT system will consist of two geostationary satellites positioned over the Atlantic Ocean nominally at 15 and 40 degrees West. Service coverage at L-band to aircraft will be provided in three zones corresponding approximately to :

- (a) the North and Central Atlantic,
- (b) Africa,
- (c) South America

as shown by Figure 1. Full earth coverage will be provided in the VHF band.

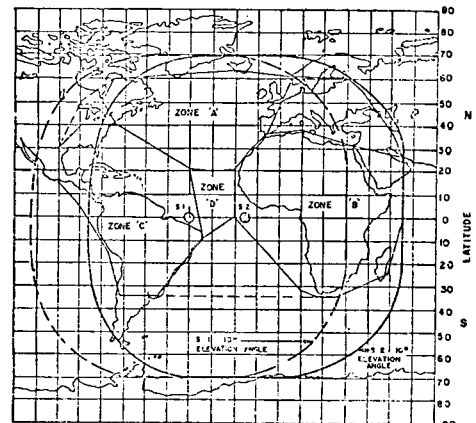


Figure 1 : Service coverage of AEROSAT

The AEROSAT system will be capable to provide during daylight several types of channels :

- communications channels for ground-to-air (5 L-band divided among the three zones, and 2 earth coverage VHF channels), air-to-ground (15 to 20 L-band and 4 VHF channels) and ground-to-ground (2 channels) voice and data signals ;
- surveillance channels for two satellites, two-way active ranging (through communication channels) ;
- experimental channels for wide-band two-way ranging and communication experiments (400 KHz or 10 MHz upon ground command : in this mode of operation the whole of the communication capacity needs not to be available).

During satellite eclipse, only one L-band ground-to-air and 8 L-band air-to-ground channels need to be provided.

The two satellites will be launched by the Delta 3914 launch vehicle from Kennedy Space Center. The first launch is planned during the second half of 1979 and the second launch a few months later.

A request for proposal (RFP) for the satellite was issued by the SPO in March of this year and three proposals were received in June. After detailed evaluation of these proposals, the co-owners have decided to initiate negotiations with an international industrial consortium led by the General Electric Company. An artist's concept of the satellite configuration proposed by this consortium is shown in Figure 2.

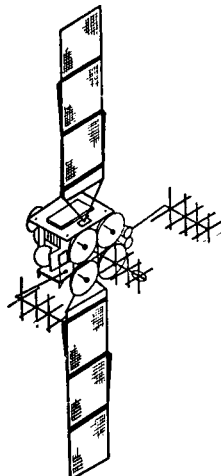


Figure 2 : Artist's concept of AEROSAT

It is expected that contract negotiations can be concluded and a contract awarded by mid-November which would maintain the schedule for a first AEROSAT launch by late 1979.

#### The MARISAT Programme

MARISAT, the U.S. Maritime Satellite Communications System, was conceived as a means to provide an early introduction of satellite communications services to ships and other marine platforms. This possibility arose as a result of a short term requirement by the U.S. Navy for communications services in the Atlantic and Pacific Ocean regions. An analysis of that requirement indicated that it could be satisfied by a common satellite platform shared with the commercial maritime services.

At the outset of the program, it was decided to procure three satellites, one each for service in the Atlantic and Pacific Ocean regions and an on-the-ground spare. As a result of an agreement recently concluded with the U.S. Navy, the spare satellite is scheduled for launch this month for service over the Indian Ocean region until such time as it may be required to replace a failed MARISAT satellite in the Atlantic or Pacific regions. At present, there are no plans for activating the commercial communications capability of the Indian Ocean MARISAT and its early operation, at least, will be confined to services for the U.S. Navy in the UHF frequency bands. Figure 3 shows the combined service coverage of the three MARISAT satellite configuration with existing satellite orbit locations of  $15^{\circ}\text{W}$  and  $176.5^{\circ}\text{E}$  and the planned service location of  $76^{\circ}\text{E}$  longitude.

The existing MARISAT system configuration is depicted in Figure 4. The Atlantic and Pacific regions are served through two essentially identical earth stations in the continental United States at Southbury, Connecticut and Santa Paula, California, respectively. The system is controlled and monitored at COMSAT General's Control Center in Washington, D.C. The two earth stations provide the connection with the terrestrial fixed telecommunications network for the relay of voice, data and telex messages between shore-based subscribers and appropriately equipped ships. These new satellite services became available in the Atlantic and Pacific service regions during the months of July and August, 1976, respectively.

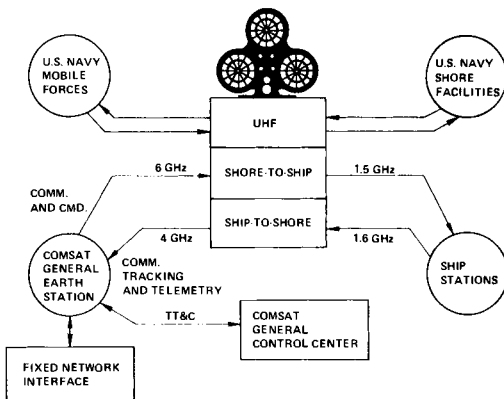


Figure 4 : MARISAT System Configuration

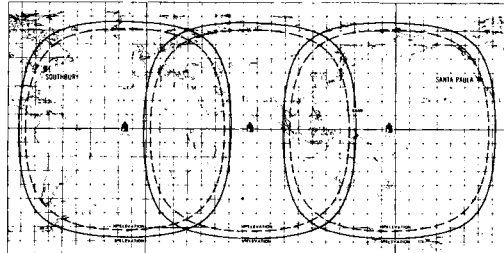


Figure 3 : Service coverage of MARISAT

Figure 5 is a photograph of the Southbury earth station. Each earth station has three antennas since the station also serves to control COMSAT General's domestic COMSTAR satellites.

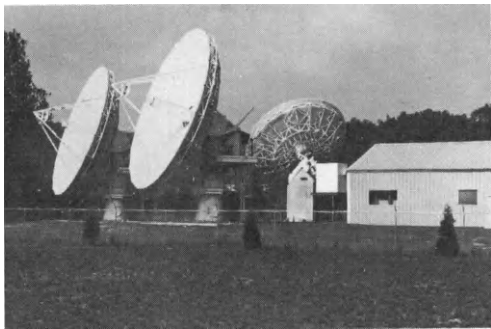


Figure 5 : Southbury Earth Station

With the launch of the third MARISAT, it will be necessary to establish an additional earth station facility for tracking, telemetry and command of the satellite at its Indian Ocean orbit position. An interim arrangement for this support is being negotiated involving the use of INTELSAT facilities until the new station is brought into service early next year. The new station is to be built at the existing facility of Fucino in Italy.

The MARISAT satellite, as shown in Figure 6, was developed by Hughes Aircraft, drawing heavily upon the spin-stabilized satellite technology employed so successfully for the early commercial satellite programs. However, a unique power sharing arrangement was incorporated into the satellite design so that its limited primary power can be traded between the UHF service for the U.S. Navy and the services to commercial shipping.

Each MARISAT satellite contains three communications repeaters. One of these operates in the UHF bands and contains three channels for the exclusive use of the U.S. Navy. Each of these channels may be activated or deactivated by ground command. In this manner, the power released from the UHF service becomes available for use by the commercial

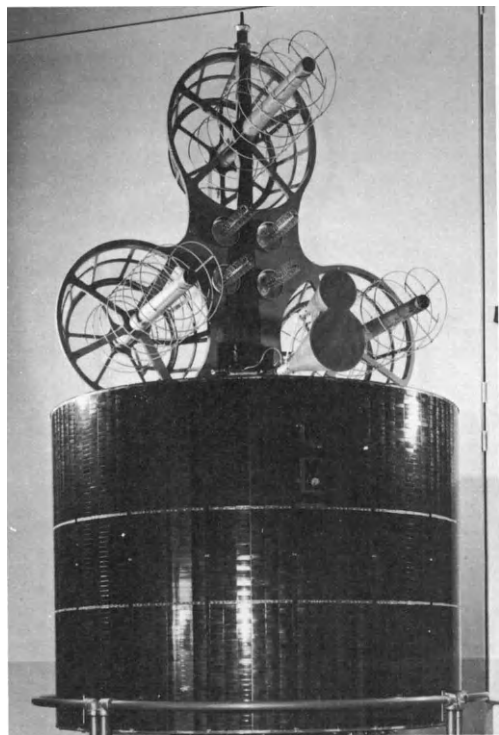


Figure 6 : MARISAT Satellite

maritime service. The other two repeaters are designed for civil maritime shore-to-ship and ship-to-ship communications, respectively. The shore-to-ship repeater translates 6 GHz emissions from the shore station to 1.5 GHz for retransmission to ships. The ship-to-ship repeater performs the reverse process, translating ship transmissions from 1.6 GHz to 4 GHz for relay to the shore stations. When the Navy uses all three of its UHF channels, as is presently the case in the Atlantic and Pacific satellites, the commercial maritime duplex communications capacity is one telephone and 44 telex channels per ocean region. With no use of the UHF channels, the commercial capacity will increase to the order of 14 telephone channels or an equivalent mix of telephone and telex channels. Sufficient energy storage is included in MARISAT's batteries to sustain all services available in sunlight through satellite eclipse.

The equipment on board ships required to complete the communications links with the shore station have been defined by the MARISAT system co-owners in the form of technical standards which have been distributed throughout the world. A typical implementation of this standard MARISAT mobile terminal utilizes an above-deck complement of equipment including a 1.3 meter radome-protected stabilized antenna, operating in the maritime satellite

frequency bands near 1.6 GHz, with a pointing system augmented by step-tracking. A typical below-decks equipment configuration is being produced in large quantities for COMSAT General by Scientific-Atlanta and is shown in Figure 7. It is of interest to note that a considerable number of the standards and operating principles of the MAROTS ship terminal have also been adopted in the MAROTS programme as discussed further below.

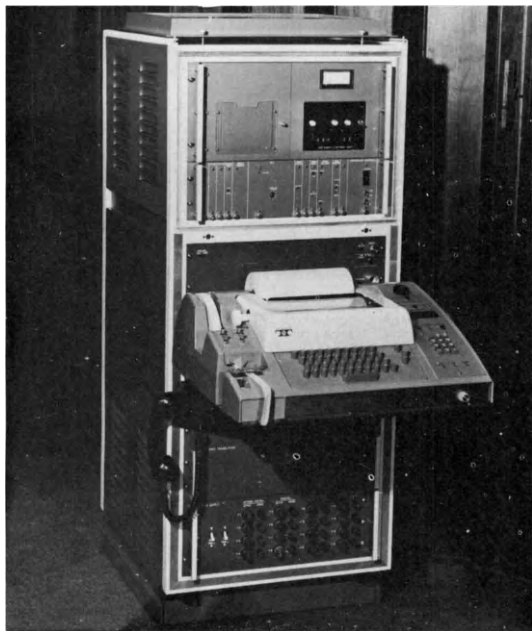


Figure 7 : A typical below-decks equipment configuration

#### The MAROTS Programme

In July 1973, the European Space Conference authorised ESA to undertake the development of a dedicated maritime communication satellite known as MAROTS (see Figure 8). In addition to 8 Member States of ESA which participate, Norway was an observer and now also takes part in the programme ; between them the participating states own about 36% of the world's shipping tonnage.

The initial programme was aimed at the launch of a single satellite early in 1978 although discussions are currently taking place with the Member States which would lead to the programme being enlarged such that it would be possible to launch up to three spacecraft of the MAROTS-type. It has been possible to construct a fairly economical programme by the reuse, almost without change, of the basic satellite module

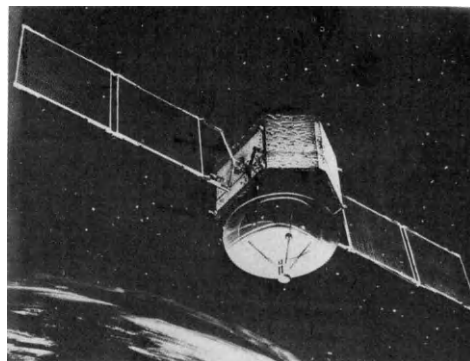


Figure 8: An artist's impression of MAROTS

of the Orbital Test Satellite (OTS) being developed in ESA's programme for a European telecommunications regional system. A demonstration of the interchangeability of the two spacecraft is shown in Figure 9. The original mission for MAROTS was to be an experimental and preoperational satellite in accordance with the guidelines for such satellites that had been discussed by the Intergovernmental Maritime Consultative Organisation (IMCO) under whose aegis discussions on a global maritime satellite system have been proceeding for some years and which led, at the beginning of September, to the intergovernmental decision to create the worldwide INMARSAT Organisation. At the intergovernmental Conference in February of this year, MAROTS was offered by the participating Member States to INMARSAT to form part of an embryonic maritime satellite system prior to the availability of INMARSAT's own satellites. MAROTS thereby, whilst retaining its experimental role, may be expected to give an operational function and this consideration has been a major facet in the discussion of an enlargement of the MAROTS programme to up to three satellites mentioned above. Thus, the mission of MAROTS may be characterised as the simultaneous acquisition of operational experience and experimental data in the field of maritime satellites; as far as the second facet of the mission is concerned it is hoped to perform a wide range of experimentation with promising techniques which are not yet sufficiently developed to be employed in the initial operational range but which could be important for follow-on maritime satellites.

Following the guidelines discussed in the IMCO forum, the satellite is intended to provide significant improvements when compared with the service currently provided on the MF/HF bands.

In particular, a comparatively large number of high quality channels will be made available and the speed at which calls are connected will greatly improve. These facilities will be uniformly available to users within the satellite coverage area. With the greatly increased quality and access speed, it will be possible to improve the safety and distress services whilst the advent of this alternative communications means will, hopefully, relieve congestion in the HF bands.

The links between the satellite and the ship will take place in the maritime mobile frequencies in L-band around 1.6 GHz whilst satellite and shore station will use portions service band around 11.7 and 14.5 GHz. During the injection of the satellite into geosynchronous orbit, telemetry, tracking and command functions will take place at VHF.

The satellite will, initially, be placed at 40°E longitude and it will provide coverage from the tip of South America in the East to Hong Kong and Western Australia.

In order to provide uniform service in the satellite coverage area, a large diameter, shaped L-band antenna is employed in this spacecraft design. A broadband transponder with a linear characteristic is employed, the bandwidth being 2.5 MHz.

The communications capability provided is 36 voice channels having a C/N<sub>0</sub> of 51 dB Hz when used with ship terminals similar to those employed in the MARISAT system (i.e., G/T = -4 dB/K). Employment of voice activation will increase the capacity to approximately 50 channels (the upper limit being bandwidth limited). It is also worthwhile noting a single voice channel can be replaced by a multiplex of 120 telex channels. Operation in eclipse is provided for and in this situation the capacity will be 6 voice channels.

These characteristics are summarised below, together with some of the physical characteristics of the satellite.

#### Summary of Characteristics

Launch Vehicle	Thor Delta 3914
Spacecraft Mass	462 kg in orbit
Payload Mass	80 kg
Dimensions	diameter: 2.18 m height: 1.95 m length: 8.60 m with deployed solar panels
Lifetime	7 years

#### Communications Capacity

Normal Operation	36 channels (50 with voice activation)
	3 shore-to-shore channels
Eclipse	6 channels
	3 shore-to-shore channels

Advantage was taken of the modularity which is illustrated in Figure 9 to use a service module design that is fully interchangeable with that of OTS and a communications module of nearly identical configuration. The two-meter shaped reflector for L-band transmissions is attached to the communications module and is pierced by four apertures, for the attitude sensors and for the satellite-to-shore communications antennas. The communications module incorporates the transponders and includes the linearised transistor power amplifier for L-band and a 20 watt TWTA, identical to that used in OTS operating at X-band.

The reutilisation of OTS designs led to an industrial situation under which two separate main contracts were placed, one with Hawker Siddeley Dynamics representing the MESH Consortium, for the platform efforts and a second for the payload work with Marconi Space and Defence Systems.

Development work proper commenced in December 1974 and as of today, testing of the payload breadboard and the thermal and mechanical models is complete with integration of the integration model about to commence.

Figure 10 indicates the coverage of MAROTS and also shows the coverage of the two MARISAT satellites. It may be seen from this figure that, except for a part of the South-East Pacific, the three satellites together will provide worldwide coverage, which suggests that a collaboration between the two systems could make available to the maritime community early communications services over all major routes.

It should be noted that it is the intention of the European States that use of MAROTS in an operational mode shall take place within an overall (international) INMARSAT framework. Notwithstanding this, in order to extend the commonality between the MAROTS and MARISAT systems, a commonality which already exists at the radio frequency level in terms of RF parameters of shipborne terminals, frequencies used for communications between the satellites and ships, etc., discussions are proceeding in order to examine how to maximise commonality at the level of operational procedures.

Should intersystem working prove possible, then as of the launch of the MAROTS satellite in 1978, an embryonic worldwide maritime satellite communications system will be available to users.

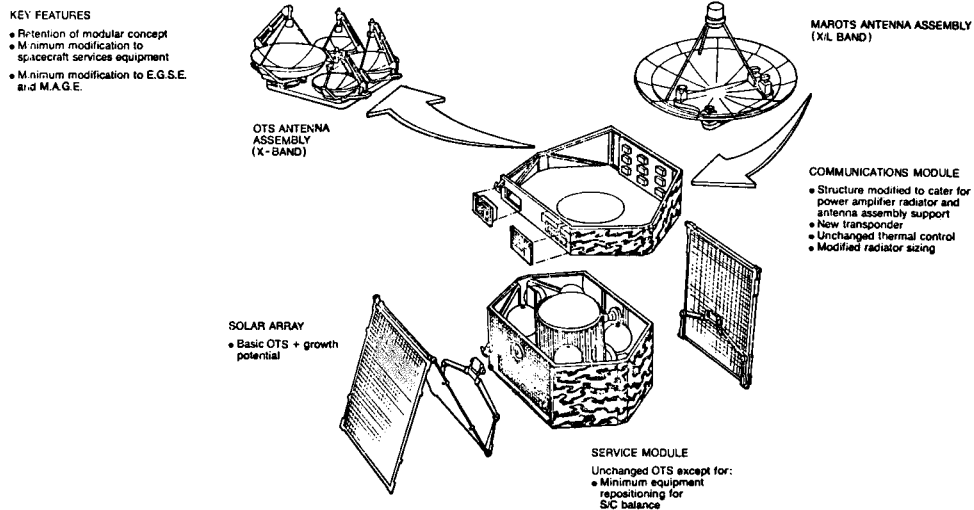


Figure 9 : OTS/MAROTS Service Module

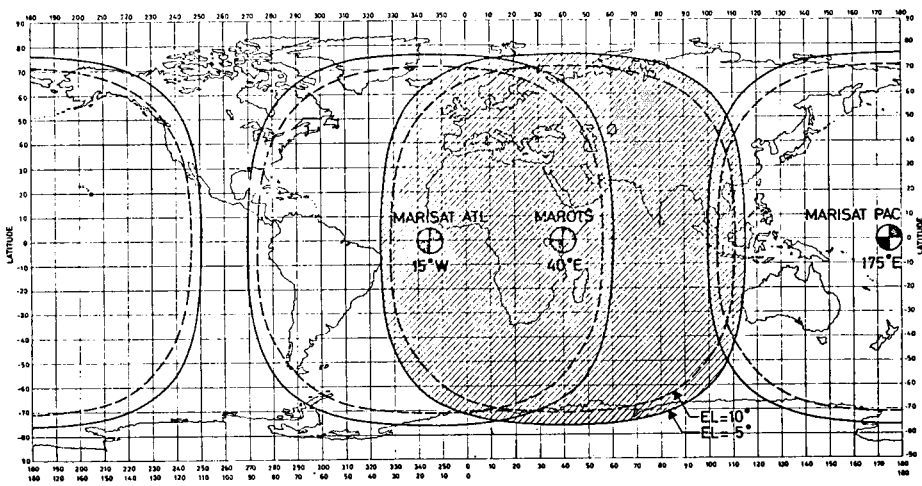


Figure 10 : COVERS PROVIDED BY MAROTS AND THE TWO MARISATS

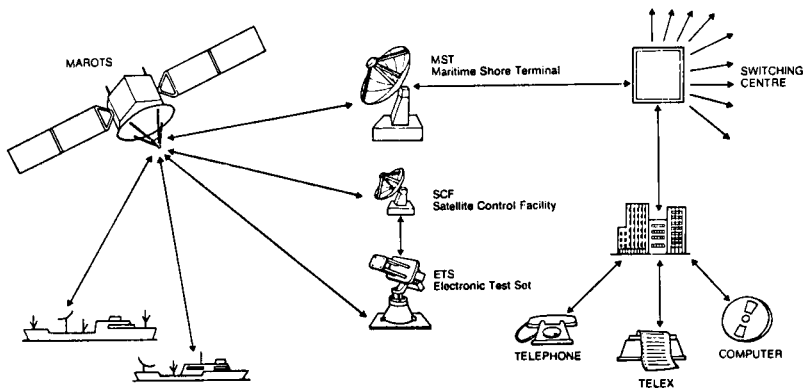


Figure 11 : Outline of the MAROTS System

# THE COMMUNICATIONS TECHNOLOGY SATELLITE FLIGHT PERFORMANCE

Harold R. Raine

*Communications Research Centre, Department of Communications,  
Ottawa, Ontario, Canada*

## Abstract

The Communications Technology Satellite (Hermes) was launched by NASA on 17 January 1976 as part of a joint U.S./Canadian program in which Canada designed, assembled and now operates the satellite. The satellite's primary features include a travelling wave tube (TWT) operating at a frequency of 12 Gigahertz with a power output of greater than 200 watts, extendible flexible solar arrays providing an initial power output of greater than 1300 watts, and a three axis stabilization system to maintain the satellite body pointing to within plus or minus 0.1 degrees about pitch and roll and 1.1 degrees about yaw. In this paper, highlights of the satellite operations are described. Significant areas of the performance of the main subsystems are reviewed to illustrate how mission objectives have been met. Where operational plans have been altered significantly, the changes are discussed. A brief status report of the Canadian communications experiments operations are presented.

## I. Introduction

The Communications Technology Satellite is an experimental geosynchronous communications satellite that was launched 17 January 1976 from Cape Canaveral, under an agreement<sup>1</sup> between Canada and the U.S. signed in 1971. The agreement provided for Canada to design and build the satellite and to control its operation after being placed on station by NASA.<sup>2</sup> NASA furnished the high-power (200 watts) travelling wave tube (TWT), its associated power conditioning and thermal control hardware, the 2914 Thor-Delta launch vehicle and environmental test and operational support. Subsequent to the original agreement, the European Space Agency (ESA) became a participant under an agreement with Canada. ESA provided certain space-craft components including a 20 watt TWT for 12 GHz operation, a parametric amplifier (paramp) and development of the deployable solar array blankets. Late in the satellite development, NASA also provided a Transient Event Counter to be added to the satellite baseline as an aid in studying space-craft charging phenomena.

The principal technological objectives of the CTS project are:

1. to develop and flight-test a travelling-wave tube having an efficiency greater than 50% and a saturated power output of 200 watts at a frequency of 12 GHz;
2. to develop and flight-test a light-weight extendible solar array with an initial power output greater than 1 KW;
3. to develop and flight-test a 3-axis stabilization system to maintain accurate antenna bore-sight positioning on a spacecraft having large flexible appendages; and

4. to conduct satellite communications experiments using the 12- and 14-GHz bands.

Hermes is the highest powered communications satellite launched to date (1976) (see Figure 1). It is regarded as a fore-runner of satellites that are expected to provide a wide range of expanded communications services in the next decade. While Hermes has a planned 2-year mission life, it has already been used over the past several months in experiments utilizing high-power television and other transmissions to small, earth stations (see Figure 2). All advanced-technology components within the satellite have performed well.

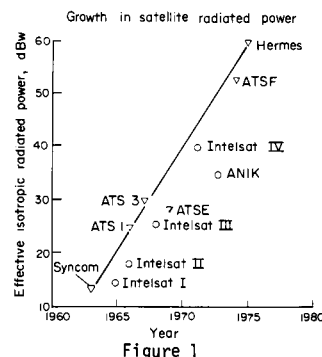


Figure 1



Figure 2 Earth Terminal

The purpose of this paper is to describe the operations to date and to provide an overall preliminary review of the satellite performance to the end of August 1976.

## II. Prime Operational Parameters

During the design phases and prelaunch planning, the following parameters were established:

- 2 year life
- orbit inclination less than  $0.65^{\circ}$  for as long as possible without North-South stationkeeping, beginning 3 to 6 months after launch
- $116.0^{\circ}\text{W} \pm 0.2^{\circ}$  longitude station at synchronous altitude
- SHF communications capability except during solar eclipses
- SHF antenna pointing accuracy within  $\pm 0.2^{\circ}$
- 12 days of SHF operation before the onset of the 1976 vernal equinox season
- solar eclipse seasons twice per year of about 48 days each with eclipse durations up to 72 minutes
- in a 3-axis stabilized mode, satellite body attitude maintained with an accuracy of  $\pm 0.1^{\circ}$  in roll and pitch and  $\pm 1.0^{\circ}$  in yaw.

### III. Prime Operational Constraints

During the satellite design and mission planning, the following operational constraints and nominal designs were established:

#### Transfer Orbit

- launch must not occur in or 30 days prior to synchronous orbit eclipse season
- the maximum continuous shadow condition must be less than 30 minutes
- transfer orbit 95 nautical miles minimum x 19624 nautical miles ( $185 \times 36344$  km) inclined at  $27.2^{\circ}$
- solar aspect angle must lie between  $65^{\circ}$  and  $115^{\circ}$  from the positive spin axis
- preparatory to apogee motor firing, the solar aspect angle must lie between  $65^{\circ}$  and  $82^{\circ}$  or  $98^{\circ}$  and  $115^{\circ}$  to allow an attitude determination of better than  $1^{\circ}$
- apogee motor firing must occur on or before the tenth apogee
- maximum continuous duration of radio silence should not exceed 90 minutes

#### Drift Orbit

- no solar eclipse permitted

#### Attitude Acquisition (transition phase from spinning body to 3-axis stabilized mode)

- satellite attitude under continuous control
- no solar eclipses
- maintain subsystem operation within design limits

#### On-Orbit (3-axis stabilized mode)

- maintain stabilization during sun and moon interference
- maintain stabilization during solar eclipses
- battery depth of discharge less than 60%
- maintain subsystem operation within design limits.

### IV. Satellite Description

An earlier publication<sup>3</sup> has already provided a comprehensive description of the Communications Technology Satellite. A brief outline is included to identify several changes introduced during the satellite development. The main operational modes will be described in the context of three main

mission phases; spinning phase, attitude-acquisition phase and on-orbit phase.

#### Major Development Modifications

During the spacecraft development, numerous weight-saving techniques were employed to meet the allowable lift-off weight. Finally the ion engine experiment, the liquid metal slip ring experiment, and the radio frequency interferometer were deleted from the original design. Significant changes were made in the SHF subsystem design<sup>4</sup> - in particular a low noise 14-GHz parametric amplifier and 12-GHz Gallium Arsenide Field Effect Transistor Amplifiers were introduced. A satisfactory lift-off weight of 1490.5 lbm (677 kg) was achieved.

Owing to an increasing concern in the potential hazards of spacecraft charging phenomena at synchronous altitudes, a transient-event counter was added. This counter senses electrical transients appearing in the attitude control subsystem cabling, the Deployable Solar Array (DSA) instrument cabling, and the DSA power cabling.

#### Satellite Description - Spin Stabilized Mode (Figure 3)

The satellite was separated from the Thor-Delta launch vehicle, spinning about the yaw axis at approximately 60 rpm. This nominal spin was maintained with only slight fluctuations throughout the transfer orbit, apogee injection and the station acquisition phases. Over this period the DSA was in a stowed condition. The east and west panels and the north and south jettisonable enclosures carried the body-mounted solar cells that, together with two 5.0 ampere-hour batteries, provided the satellite with power during spin-stabilized operations. Depending upon the solar aspect angle and temperatures, up to a nominal 100 watts were available from the body array during the sunlit periods.

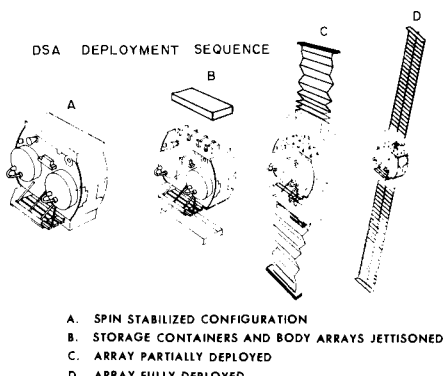


Figure 3

Commands were received by either a belt-array antenna on the thrust tube or beam antenna on the forward face. Telemetry was transmitted on either

a second belt antenna or a patch antenna on the forward face, the selection being made by ground command. The belt antenna was the prime antenna used during this phase. The S-band command/telemetry subsystem was used as a ranging transponder to provide range and range rate data for orbit determination.

Spinning sun sensors and earth sensors were used for attitude determination and to provide an onboard reference timing for the firing of the 5 lbf (22.4N) axial and radial hydrazine thrusters.

#### Satellite Description - Attitude Acquisition Phase

In this phase several of the sixteen Low Thrust Engines (LTE's) providing 0.15 lbf (0.67N) thrust were used to despin the satellite and perform reorientation manoeuvres. The most dramatic change in configuration started with the jettisoning of the north and south Jettisonable Body Solar Arrays (JBSA's) which lowered the satellite mass by 18.27 lbm (8.29 kg). Immediately after this activity, the DSA's were deployed.

Throughout this phase, spin rate and attitude of the satellite were controlled from the ground using data from the sun sensors and a rate gyro.

After array deployment, the momentum wheel was brought to its nominal operating speed of 3750 rpm, providing a momentum vector along the pitch axis. At the end of the sequence, the full on-board attitude control system was activated. In this mode, pitch errors detected by the Nonspinning (infrared) Earth Sensors (NESA's) are automatically corrected by momentum wheel speed changes. Roll error signals detected by the same earth sensors are corrected through the use of 0.15 lbf (0.67N) roll/yaw LTE's. The satellite is thus oriented with the positive yaw axis pointing toward the centre of the Earth, (see Figure 4). The long axis of the DSA's are pointed nominally perpendicular to the orbit plane along the pitch axis. The positive roll axis is in the direction of the satellite motion, i.e. Eastward.

#### Satellite Description - On-Orbit Phase (3-Axis Stabilized Mode)

Only highlights of the following subsystems are described, particularly where operational modes were changed from previous phases: Telemetry, Tracking and Command (TT&C), DSA, Thermal Control, Attitude Control Subsystem/Reaction Control Subsystem (ACS/RCS), Power, and SHF.

After on-orbit attitude was achieved, subsequent TT&C communications utilized the Earth-facing antennas.

After deployment, the arrays were temporarily placed in a sun-track mode until normal operation was confirmed. Array stepping control was then changed by command to a clock mode wherein each array is individually adjusted in 0.125° steps every 30 seconds to maintain approximate perpendicularity of the array plane to the sun line. Forty-six slip rings on each array are used to transfer power, data and various control signals between the array and the body of the satellite. Just prior to each solar eclipse, the array is adjusted to optimize the orientation at eclipse exit. Array stepping is stopped

throughout each eclipse period.

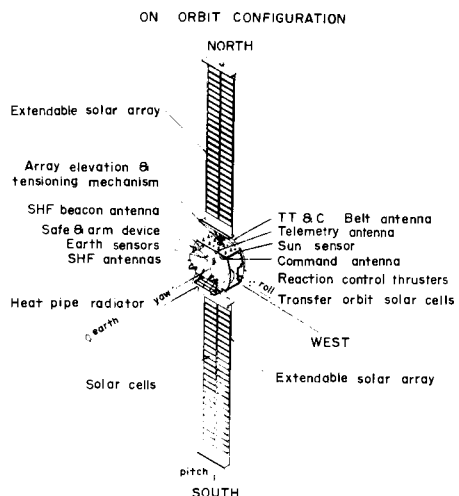


Figure 4

The thermal control subsystem hardware in the on-orbit phase consists of multilayer super insulation blankets, radiation areas of second surface mirrors, thermal coatings, variable conductance heat pipes and a radiator assembly, and electrical heaters. During the on-orbit phase, the satellite rotates once per day relative to the sun. This rotation results in significant diurnal temperature variations, particularly in components which are mounted externally. Low-power operational modes require the use of heaters to maintain favourable operating temperatures in the satellite.

From time to time, direct ground control of portions of the ACS/RCS subsystem is undertaken to perform two routine operations - East-West stationkeeping and momentum dumping. One of two LTE's are used to perform East-West stationkeeping. Another similar thruster is used to perform pitch wheel momentum dumping, i.e. to provide angular momentum in a direction which returns the speed of the momentum wheel to its nominal value after it has reached the limit of its operating range.

The power subsystem relies upon solar cells to generate electricity for the operation of the satellite. The experimental portion of this subsystem operates only while the array is illuminated by sunlight. All the SHF communications equipment and many of the thermal control heaters operate from the experiments bus. The house-keeping portion of the subsystem is powered either from the solar arrays or two rechargeable 5.0 ampere hour batteries when solar array power is unavailable.

The SHF subsystem consists of a single conversion communications transponder operating in 14-GHz uplink and 12-GHz downlink bands. Two channels can be used simultaneously utilizing two steerable spot beam antennas (See Figure 5). A

200 milliwatt beacon radiates a CW signal at 11.7 GHz from an earth coverage fixed horn antenna for propagation and satellite location purposes, as well as for monitoring the SHF local oscillator. All SHF equipment is switched off during solar eclipses.

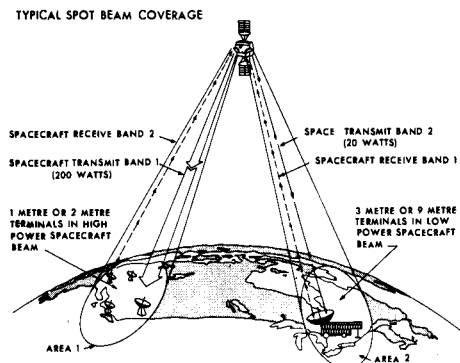


Figure 5

## V. Satellite Performance

Selected aspects of particular significance are highlighted in this section of the paper. Significant changes to operational plans are outlined. In some cases detailed performance has already been reported in other papers which are used as references.

### Performance - Spinning Phase

Since the main activities of this phase were aimed at putting the spacecraft on station, the apogee motor and ACS/RCS subsystems alone are addressed.

While it was planned to fire the apogee motor at the fifth apogee, this operation was postponed until the seventh apogee because of difficulties in the initial opening of the RCS latch valves. This problem arose from the presence of shock waves similar to a "water hammer" effect as the valves were opened initially and has been reported previously<sup>6</sup>. The shock destroyed one pressure transducer which in turn caused a malfunction in one reference power regulator causing the loss of several temperature sensors intended for use in subsequent control of the RCS thruster operation. These failures were overcome through revision of operational procedures.

The apogee motor provided a nominal velocity change of 1750.5 meters/second (1752 meters/second was desired). The apogee motor case temperature exceeded 140°C for approximately 30 hours providing soakback greater than expected. The components most affected by soakback were as follows:

Components	Temp. Reached	Design Temp.	Test Temp.
Battery B	+35°C	35°C	35°C
NESA (Base Temp)	+45°C	52°C	50°C
Telemetry Transmitter	+52°C	50°C	62°C

Since the peak temperatures were of short duration and the temperatures in the spacecraft test program were approximately the same or greater than those experienced during soakback, the soakback exposure was not regarded as a serious problem.

Following the apogee motor firing, a series of 5 lbf (22.4N) radial thruster firings established a drift profile (see Figure 6). Finally the satellite was located on station at 116.0°W (244.0°E). For comparison, the significant parameters prior to initiation of attitude acquisition are noted in Table 1. Two items are noteworthy - hydrazine consumption and orbit inclination.

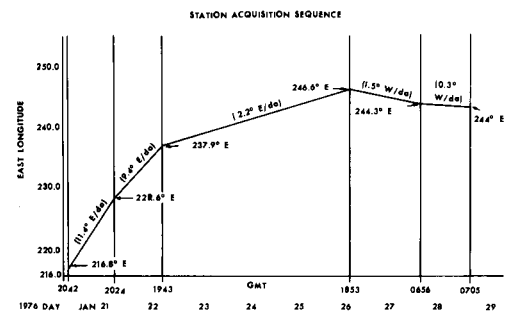


Figure 6

ATTITUDE ACQUISITION CRITERIA		Table 1
ITEM	GOAL	ACTUAL
Eccentricity	.0001	.000187
Hydrazine Consumed	<31.2 lbm (14.1 kg)	21.2 lbm (9.5 kg)
Longitude	116.0°W	116.00°W
Inclination	0.9°	0.655°
Spin Rate	54 - 66 rpm	59.9 rpm
Initial Node	270°	264.9°
Positive Spin Axis to Orbital Plane	-85 to -95°	-88.6°
Drift Rate	<0.02°/day	.003°/day Westward

The launch vehicle and apogee motor performances were nominal thus approximately 10 lbm (4.5 kg) of the hydrazine budgeted for dispersions was unused and remains available for future use. Misalignment of the apogee motor thrust vector, resulting from the 1° resolution of the satellite sun sensors led to the initial inclination being lower than planned. Without North-South Station-keeping, the inclination will exceed 0.9° before the end of the 2 year mission. Such inclination will have an undesirable, although tolerable effect on the operation of the SHF communication earth terminals. Figure 7 illustrates the actual inclination trend observed as well as the predicted trend.

### Performance - Attitude Acquisition Phases

The attitude acquisition task involved a series of paced activities with despin, DSA deployment and earth acquisition being the principal objectives. Owing to the criticality of the operation, the tasks were undertaken over the period 0300 GMT, 30 January through 1400 GMT, 1 February 1976 to allow time for calibration checks, checks of redundant equipment, battery charging, etc.

Only 1.5 lbm (0.68 kg) of hydrazine were required of the budgeted 2.1 lbm (0.95 kg). Table 2

illustrates the result of the final capture parameters compared with the specified limits.

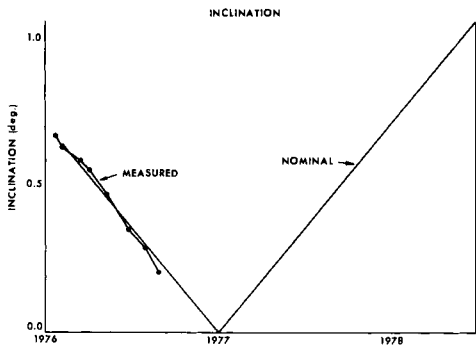


Figure 7

ACS CAPTURE PARAMETERS		<u>Table 2</u>
PARAMETER	SPECIFIED	ACTUAL
Pitch Position	$\pm 2.50^\circ$	$-1.400^\circ$
Pitch Rate	$\pm 0.10^\circ/\text{sec}$	$+0.029^\circ/\text{sec}$
Roll Position	$\pm 2.50^\circ$	$+0.188^\circ$
Roll Rate	$\pm 0.10^\circ/\text{sec}$	$+0.000^\circ/\text{sec}$
Yaw Position	$\pm 5.00^\circ$	$-0.900^\circ$
Yaw Rate	$\pm 0.10^\circ/\text{sec}$	$+0.001^\circ/\text{sec}$

The sequence was conducted nominally. Battery depth of discharge was maintained below 25%. The time from the zero rpm condition to availability of electrical power from the deployed solar array was less than one hour.

As a result of a slight unbalance, jettisoning of the JBSA's torqued the satellite slightly. Subsequently, the satellite required a  $160^\circ$  precession before final earth lock. This rather large precession caused the satellite orbital drift rate to increase from  $0.003^\circ/\text{day}$  to about  $0.034^\circ/\text{day}$ . As will be seen, a special E-W stationkeeping operation was subsequently performed to correct this drift rate.

#### Performance On Orbit - TT&C

In view of the advanced hardware being put into experimental service for the first time, the initial emphasis was aimed at gaining confidence in the operation before proceeding. Nearly continuous telemetry transmissions since 1 February to the control station at Ottawa have provided ample operational data for evaluation purposes. NASA personnel at the Lewis Research Center, Cleveland, Ohio have received this data also, for processing, primarily via land lines from Ottawa or the Goddard Space Flight Center, Greenbelt, Md.

Owing to the experimental nature of the satellite, several of the subsystems were designed to be operated in a partially "manual" mode rather than in an automatic mode. This approach has allowed operational modifications to be made as conditions change, for example "hands-on" control override of the high-power equipment. Although the normal daily operation of the on-

orbit attitude control is automatic, a command override capability is available if desired. As noted earlier, it was decided that SHF communications capability was not a requirement during solar eclipses. This particular relaxation, while saving considerable battery weight, introduced the requirement for a number of configuring commands before the entry and after the exit of each eclipse. In addition, the operational activity has been increased by the necessity to avoid sun interference effects on the NESAs caused by the sun/earth/satellite geometry which prevails during and near the eclipse seasons.

During each non-eclipse day, typically 40 configuring commands have been required unless special tests, momentum dumping or stationkeeping were performed. In contrast, during eclipse days when SHF communications were performed during the sunlit period, the number of commands averaged 100 command commands per day. This total dropped to about 50 commands per day while the satellite communications equipment was switched into a standby mode during eclipse days. The TT&C has been used routinely each week as a ranging transponder for orbit determination. Slant range accuracy of about  $\pm 5$  meters has been achieved using the ground control station at Ottawa.

#### Performance On Orbit - Thermal

The temperatures of the satellite components undergo wide variations relative to the temperatures experienced in the spinning phase. In Hermes the following factors play a predominant role in controlling these temperatures.

- unit electrical dissipation and operating mode
- placement in the satellite
- orbit slot (local satellite time)
- sun presence (or eclipse)
- heater control
- sun declination (time of year)

The main high dissipation units were installed on the inside of the North and South panels. Heat from these panels radiates to space via second surface mirrors. Therefore temperature in these areas are affected by the solar illumination on these panels during the summer and winter solstices, respectively. Electrical heaters are used to maintain adequate temperatures while the high power components are non operating.

In contrast, the temperature of equipment with large thermal mass such as the RCS tanks mounted in the centre of the satellite changes relatively little even between equinox and solstice conditions (see Figure 8).

Components mounted on the aft and forward platforms undergo significant daily temperature fluctuations. Equipment such as the NESAs mounted on the outside of the forward platform undergo even wider temperature variations (see Figure 9). The two earth sensors consistently exceed the design temperature during parts of each day in the summer solstice season. Component and spacecraft prelaunch testing provided confidence that these sensors can operate adequately at these elevated temperatures although some turn-on problems have been encountered since the launching.

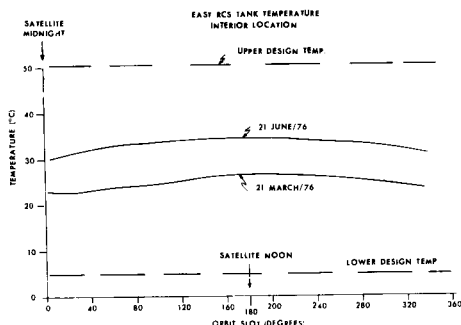


Figure 8

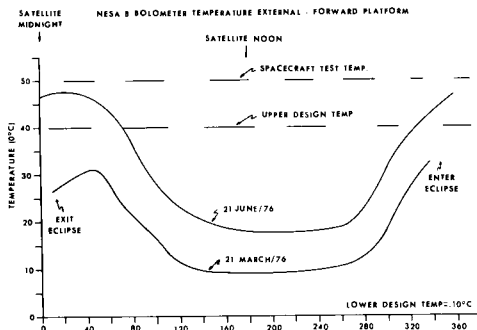


Figure 9

Heat from the SHF 200W TWT and its power processor is radiated to space after being conducted to the Heat Pipe Radiator via variable conductance heat pipes. Figure 10 illustrates the variation in heat pipe temperature over 24 hours with zero and saturated output power from the 200W TWT.

In general, temperatures of all components have been maintained within spacecraft prelaunch test limits and most are well within the design range. During sunlit operations with total satellite dissipation exceeding 600 watts, temperatures normally climb toward the upper portion of their operating range. During eclipses, satellite body temperatures begin to fall. This fall is arrested at the termination of each eclipse by heater control and resumption of normal operations.

#### Performance On Orbit - Power Subsystem

Total output power capability from the DSA at launch was approximately 1300 watts. Two raw bus voltages are supplied from the extendible array - an experiments bus nominally at 80-85 volts while delivering typically 7-8.5 amperes during SHF communications experiments, and a housekeeping bus at about 40V and typically delivering 3-4 amperes. Figure 11 shows predicted capability over the planned mission with a few data points for comparison.

An anomaly in the experiments bus array performance was observed on 8 June 1976. Analysis showed that 15% of the experiment array capability

was lost. While the exact cause cannot be determined, it is currently believed that a voltage breakdown in the array caused wiring damage leading to a loss of power from 6 panels. Since the experiments portion of the array had surplus power capability initially, this loss will not affect the mission. During the anomalous event, the Transient Event Counter (TEC) recorded numerous transients but there was no evidence of counts immediately before the anomaly. A temporary attitude disturbance coincided with the anomaly, possibly caused by expulsion of vapourized array material in the vicinity of the arc.

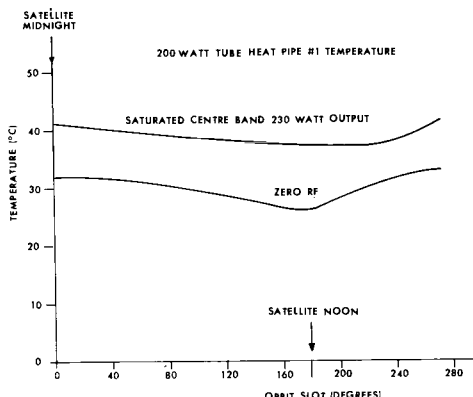


Figure 10

Unexplained transient events observed by the TEC for February, March and April were 42, 84 and 41 respectively. These events had no noticeable effect on satellite operation. The pattern of these and later events are being studied by investigators at the Lewis Research Center and the Communications Research Centre.

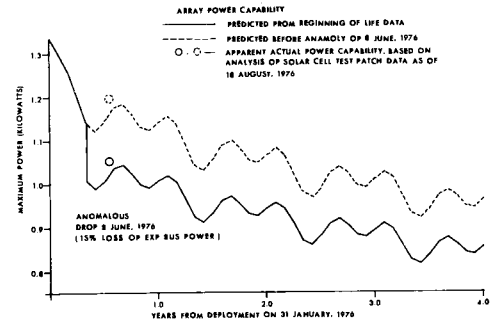


Figure 11

Initially, at the end of the array deployment on 1 February 1976, the extension system automatically terminated deployment with indication of 0.55 inch (1.4 cm) displacement of the negator spring. Relaxation and mechanical settling reduced the displacement by 0.14 inch (0.36 cm). On 4 February the arrays were retensioned, increasing the displacement by 0.13 inch (0.33 cm). Over the February/March time frame, relaxation again occurred until the values of 0.48 inch (1.22 cm)

and 0.42 inch (1.07 cm) were reached for the North and South arrays respectively. These displacements have remained sensibly constant over the past 6 months except for eclipses.

The most dramatic changes to the arrays occur during the eclipses (see Figure 12). During each eclipse when the array is cold, some relative motion takes place between the array blanket and the tubular BISTEM\* holding the array taut. Typically tension increases from about 8.9 lbf (39.6 N) to about 9.5 lbf (42.3 N) at the eclipse temperature extremes. During eclipses, there is a relative movement of approximately 1 inch (2.5 cm) between the blanket and the boom tip.

Studies<sup>7</sup> indicate the mechanical resonant frequencies of the arrays are much as expected, with excellent damping factors. Stepping of the arrays to maintain perpendicularity to the sun has been nominal - the plane of the arrays are typically  $89^\circ$  -  $91^\circ$  to the sun line about the pitch axis except for the small errors caused by array bending.

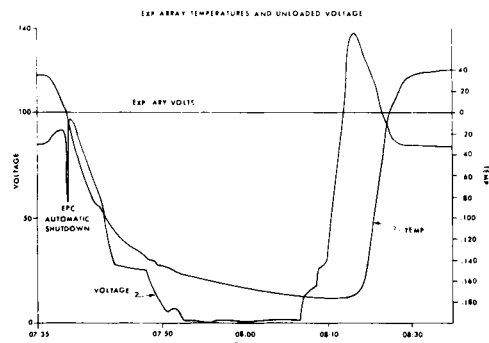


Figure 12

In Figure 13, analytical and computed solar torque effects caused by array dihedral are illustrated. Based on thruster torques and attitude behaviour during a 4 day test with the roll/yaw thrusters inhibited, it has been concluded that a  $3^\circ$  dihedral exists. This corresponds to an out of plane static bending of the array of 7 inches (18 cm) at the array tips.

Since the batteries perform a vital role during each eclipse, maintenance of the battery capacity is important. Battery charging routines and reconditioning exercises have been developed to ensure that the batteries will be capable of supplying the load during eclipses. Peak drain during the March eclipses was about 2.25 ampere-hours from each battery.

Battery capacity observed during the reconditioning exercises from before launch to August 1976 are shown in Table 3. Note that the improvement provided by a reconditioning can most easily be observed by performing a second cycle of reconditioning. A second cycle was not deemed necessary after the August reconditioning to determine the effect of the first cycle. While some degradation of capacity is evident, capacity continues to be

\* Registered Trademark of Spar Aerospace Products, Toronto, Ontario

adequate for eclipse operations.

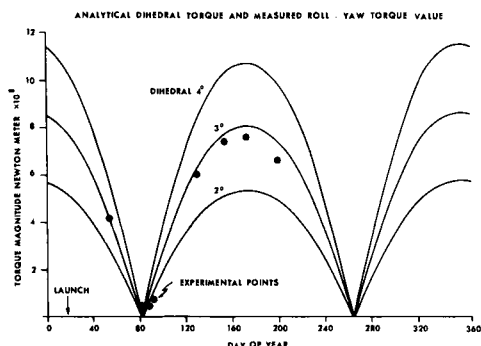


Figure 13

DATE	BATTERY RECONDITIONING HISTORY			
	CAPACITY TO 26.2V		CAPACITY TO 24V	
	BATT A	BATT B	BATT A	BATT B
1975				
27, 28 September	5.50	5.30	5.72	5.38
12, 13 December	4.95	4.62	5.32	5.00
16 December		4.82		5.00
1976				
8, 10 January	4.50	4.55		
16, 17 February	4.73	4.85	5.25	5.30
26, 29 April	4.46	4.15	4.90	
10 May	4.58		5.30	
13 May		4.60		5.18
15 August	4.06	4.45	5.14	5.33

One major anomaly has occurred in the power subsystem to date, causing a significant change in operational plans. On 4 March 1976, a high power relay in the experiments' bus power conditioner misbehaved, permanently damaging parts of the conditioner. Since the effects of switching this relay for each eclipse was suspected to be in some way connected with the anomaly, it was decided to refrain from switching to the redundant conditioner until the eclipse season ended. This decision therefore suspended SHF communications experiments until 20 April at which time the redundant conditioner was put into service. The same protective action was taken for the 1976 autumnal eclipse season, again suspending SHF communications experiments between 29 August and 19 October of this year.

#### Performance On Orbit - ACS/RCS

The ACS and RCS system operate together automatically to control the attitude of the satellite body. Figure 14 illustrates a typical indicated pointing variation well within  $\pm 0.1^\circ$ . Detailed studies of pitch and roll outputs from both (NESA's) indicate there may be a time-varying error of as much as  $0.16^\circ$ . Behaviour indicates the Momentum (wheel) vector may be misaligned with respect to the NESA-B by up to  $0.05^\circ$ .

Consequently antenna pointing uncertainty of  $\pm 0.08^\circ$  can be experienced in addition to the indicated body pointing errors. To date, this uncertainty has had no observable effect on the SHF communications experiments, since normal propagation

effects mask such small changes.

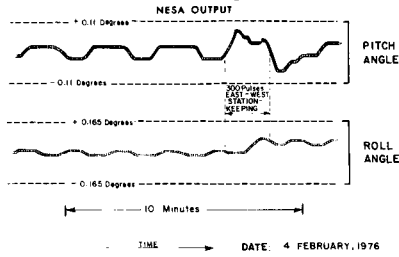


Figure 14

Momentum dumping, east-west stationkeeping and solar array slewing introduce short term pointing errors typically up to  $0.5^\circ$  mainly about the pitch axis. These operations have been scheduled at times when no SHF communications experimenters are operating near the edge of the SHF antenna patterns. There have been no beam-edge effects noticed by communications experimenters to date. Procedures could be adopted to reduce these transients if necessary.

While the attitude control normally has been quite stable, on a few occasions accurate control has degraded temporarily. Short transient disturbances about the pitch axis of nearly  $0.25^\circ$  peak amplitude have been observed. It is hypothesized that under certain combined momentum wheel speed and temperature conditions, drag torques fluctuate while temporary "channelling" of wheel bearing lubricants takes place. A change in wheel speed operating range has almost completely eliminated the phenomenon. Roll/yaw nutation cones of up to about  $+0.1^\circ$  with periods of 6 minutes were also observed regularly as the momentum wheel speed fell below 3700 rpm. It was discovered that the constants of the ACS subsystem were not completely suitable for a satellite body nutation period longer than 5 minutes. Again an increase of the momentum wheel speed range has raised the nutation frequency, allowing the roll rate controller to perform effectively.

Since the satellite was placed in a 3 axis stabilized mode, pitch axis control was lost only once on 9 April when NESA-A behaved abnormally. Subsequent investigations indicate that the scanning mirror in the NESA may have misbehaved at turn-on under relatively high temperature conditions. Procedures have been modified to minimize NESA switching and to choose switch on times when the NESA's are relatively cool. By inhibiting the offset thrusters during NESA-B sun or moon interference periods, the requirement for switching off NESA-B

has been eliminated.

Table 4 summarized the pitch momentum dumping since the satellite was placed in a 3 axis stabilized mode, to the end of August 1976. The effects of solar pressure torques have been in such a direction as always reduce the wheel speed - typically about 20 rpm  $\pm 2$  rpm per day. Consequently momentum dumps have only been required every 3 weeks. The prelaunch worst case analysis predicted momentum dumping could be required every  $3\frac{1}{2}$  days. Fuel consumption has been correspondingly lower than budgeted.

DATE	PITCH MOMENTUM DUMP SUMMARY 1976 - P1 THRUSTER						APPROX. NUMBER OF SLOTS
	TRANSIENT ROLL <sup>a</sup>	PEAK ANG. PITCH <sup>b</sup>	YAW <sup>c</sup>	WHEEL SPEED RPM START	WHEEL SPEED RPM FINISH	NUMBER OF 50msec PULSES	
8 Feb	-.065	-.440	-	3635	3744	15	.0010
8 Feb	-.012	-.370	-	3743	3794	7	.0005
19 Feb	-.076	-.373	-	3519	3795	27	.0019
26 Feb	+.056	+.385	-	3683	3813	20	.0014
26 Feb	+.046	-.359	-	3813	3901	12	.0008
26 Feb	+.065	+.331	-	3901	4003	51	.0035
11 Mar	-.036	+.351	-	3636	4003	51	.0016
26 Mar	-.076	-.428	-	3673	4099	58	.0040
26 Mar	-.021	+.452	-	4099	4132	59	.0018
12 Apr	-.076	-.485	-	3689	4132	59	.0041
12 Apr	-.024	+.474	-	4132	4172	59	.0018
3 May	-.076	-.588	-	3682	4132	59	.0041
3 May	-.024	+.520	-	4132	4172	59	.0018
21 May	-.376	-.600	-	3739	4124	48	.0033
21 May	+.064	+.685	-	4124	4172	57	.0015
11 June	-.076	-.438	-.28	3693	4128	57	.0039
11 June	+.0336	+.410	+.61	4128	4150	42	.0013
28 June	-.076	-.471	+.395	3832	4150	42	.0029
28 June	-.021	+.454	+.161	4150	4177	46	.0015
16 July	-.076	-.430	+.36	3827	4177	46	.0032
16 July	-.024	+.432	+.16	4177	4200	54	.0033
6 Aug	-.098	-.438	+.009	3793	4200	54	.0017
6 Aug	-.012	+.423	+.009	4200	4220	58	.0040
26 Aug	-.076	-.427	+.451	3787	4220	58	.0018
26 Aug	-.010	+.443	+.249	4220	4240	58	.0040

Table 5 summarizes the East-West Stationkeeping activity to the end of August 1976. After the initial use of the East thruster to correct for the disturbance introduced during the attitude acquisition, the West engine has always been utilized. Since the mission plans do not require correction of orbit eccentricity, stationkeeping is used only to keep the satellite within the  $116.0^\circ\text{W} \pm 0.2^\circ$  limit. As eccentricity increased during the summer of 1976, it has become difficult to meet this constraint consistently. It may be seen that stationkeeping has had varying effect on momentum wheel speed. This effect arises primarily because of a shift of the centre of mass due to relative solar array position at differing orbit slots.

Figure 15 illustrates the results of the E-W stationkeeping to the end of August 1976 and shows the predicted and measured eccentricity versus time. Extremes of the satellite longitude can be seen to fall within the operational goal except for short periods during peak orbit eccentricity.

Roll/yaw thruster activity varies according to the season primarily, modified by the dihedral effect noted earlier. A total of about 80-100 hydrazine thruster pulses (7 to 10 milliseconds each) were fired daily during the peak polar torque period. Typically about 60 of these are positive thruster pulses, with the remainder being negative pulses during the summer solstice period. Inasmuch as the solar pressure torque has been

DATE	EAST-WEST STATIONKEEPING SUMMARY 1976						CHANGE IN ECCENTRICITY PP/SEC	N/S
	TRANSIENT ROLL <sup>a</sup>	PEAK ANG. ERROR PITCH <sup>b</sup>	WHEEL SPEED RPM START	WHEEL SPEED RPM FINISH	NUMBER OF 50msec PULSES	LTE USED 1RM	HYDRAZINE SLOT <sup>c</sup>	
4 Feb	-.087	-.111	-	3653	3665	300	E .018 .008	.138 .042
7 Feb	-.076	-.175	-	3615	3666	400	E .024 .011	.184 .056
12 Mar	+.017	+.190	-	1982	3952	300	W .018 .008	.90 .136
12 Mar	-.016	-.175	-	3952	3952	300	W .018 .008	.90 .136
2 Apr	+.007	+.120	-	3971	3960	468	W .028 .013	.75 .213
2 Apr	-.065	-.137	-	3960	3960	468	W .028 .013	.75 .213
17 May	-.076	-.036	-	3839	3837	230	W .014 .006	.50 .106
17 May	-.076	-.112	-	3837	3837	230	W .014 .006	.50 .106
25 June	-.076	-.118	-.771	3872	3892	305	W .019 .009	.10 .141
25 June	-.043	+.091	+.107	3933	3950	275	W .0167 .008	2 .126
29 July	-.087	-.140	-.1070	3933	3950	275	W .0076 .003	348 .058
29 July	-.056	+.102	+.225	3950	3950	275	W .0076 .003	348 .058
26 Aug	-.087	-.159	-.1030	3781	3788	125	W .0076 .003	348 .058
26 Aug	-.021	+.091	+.1093	3788	3788	125	W .0076 .003	348 .058

typically only about 1/3 to 1/5 of the worst case predicted torque, offset thruster fuel consumption has been correspondingly lower. The number of daily offset pulses diminishes as the dihedral effect diminishes. The relative number of positive and negative pulses can be expected to reverse in the winter solstice if the satellite is symmetrical. Tentative indications are that offset thruster firings over 50-60 days may change the orbital velocity by the same amount as an East-West stationkeeping.

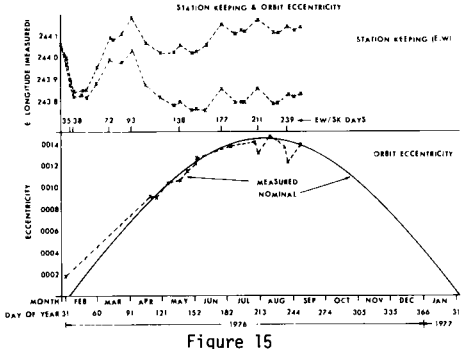


Figure 15

Table 6 summarizes the prelaunch hydrazine budget and a budget based upon actual fuel consumption. It may be noted that nearly nominal behaviour during both the spinning and nonspinning phases has resulted in a substantial uncommitted surplus of fuel. Its use is being considered for undertaking planned attitude experiments, extending the mission, and performing North-South Stationkeeping.

ITEM	HYDRAZINE FUEL BUDGET SUMMARY		Table 6	
	BUDGET	ACTUAL	lbm	Kg
Pre Apogee Fine Manoeuvre	5.0	2.3	5.0	2.3
Post Apogee Fine Manoeuvre	1.4	0.6	1.3	0.6
Station Acquisition Firing	24.8	11.2	14.9	6.7
Altitude Acquisition Sequence	2.1	1.0	1.5	0.7
On-Orbit Operations (2 years)	9.9	4.5	2.8*	1.3*
Uncommitted Surplus	10.7	4.8	28.4†	12.8†
Unusable Residual	0.8	0.4	0.8	0.4
TOTAL † Projected	54.7	24.8	54.7	24.8

#### Performance On Orbit - SHF Subsystem

Since the turn on of the SHF system, taking into account the shutdown during eclipse seasons, the SHF subsystem has operated for over 3000 hours. Periodic tests made of its performance have revealed no significant changes in the parameters. As an example, Table 7 lists the saturated gains at the two bands and the satellite system input noise temperature using the parametric amplifier. Figure 16 shows the saturated power output vs frequency from the 200W tube shortly after attitude acquisition, while sample test results obtained near the end of August are shown in Figure 17. Details of the 200W TWT performance are reported elsewhere<sup>8</sup>.

Protective circuitry in the TWT's power conditioners have occasionally turned off the power supplies. In some instances overdrive was established as the cause, while in others no direct cause

has been ascertained. SHF communications experiments were never disrupted by the shutdowns and each time the affected tube was quickly returned to normal service.

SHF TRANSPONDER PRE & POST LAUNCH TESTS		
PARAMETER	PRE LAUNCH	POST LAUNCH
TB1 Sat. Gain*	120.4	119.0 ± 0.89 dB
TB2 Sat. Gain	110.7 dB	109.6 ± 1 dB
Satellite Receiver System Noise Temp	1213° K	1349° K ± 300° K

\* Note: 5 dB attenuator is included.

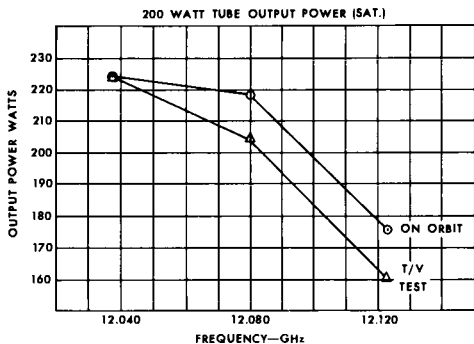


Figure 16

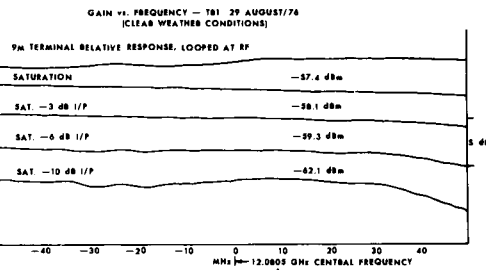


Figure 17

According to the experimental plan, the U.S. and Canada use alternate days for communications experiments in the respective countries. Typically each day the experiments tend to begin near the East Coast of North America and proceed westward with antenna steering required to follow the normal operations on Earth. Average antenna steering has been as follows:

$$\begin{aligned} \text{Antenna 1: } N-S &= 0.8^\circ/\text{day}, E-W = 3.8^\circ/\text{day} \\ \text{Antenna 2: } N-S &= 2.2^\circ/\text{day}, E-W = 7.6^\circ/\text{day} \end{aligned}$$

Though variable as different types of experiments are performed, these averages indicate the design life of 6500° for each axis will not be exceeded during the normal mission life.

Based upon a series of pattern measurements, there may be up to 0.1° maximum off-set in the actual North-South bore sighting of the SHF antennas. This discrepancy is still under investigation. It

has not caused any observable effects on the SHF communications experiments.

The U.S. experiments are reported elsewhere<sup>9</sup>. The types of Canadian communications experiments are listed in Table 8. In general, all communications experiments' phases planned for the 1976 summer solstice period have been completed. In particular, the FDMA Demand Assignment, High Data Rate, radio broadcast, special TV demonstrations are transportable telecommunications system experiments have been completed.

CANADIAN COMMUNICATIONS EXPERIMENTS (26) Table 8

CANADIAN COMMUNICATIONS EXPERIMENTS (26)	
12 Technical	14 Social
1 Terminal Evaluation +	5 Tele-education
3 Data/Modems +	3 Telemedicines
2 Multiple Access +	3 Community Interaction
2 Precision Measurements +	2 Radio/TV Broadcast*/+
1 Propagation +	1 Administration +
1 Computer Communications	
* Partially completed	* Complete

Link calculations<sup>10</sup> using a 1.2 metre terminal under normal conditions for a 6-MHz peak video deviation show Hermes will provide a maximum video S/N ratio (weighted peak to peak) of 50.6 dB with a 8.9 dB margin above threshold. This margin can be allocated to satellite antenna beam off-axis losses, propagation losses, etc. In practice, a 0.6 metre antenna with an image enhanced mixer has provided excellent television picture quality.

Terminals of various sizes will be operated on an experimental basis in several different parts of Canada (see Figure 18). Throughout the summer of 1976, terminals have been in use in Ontario, Quebec, Baffin Island and as far North as Resolute Bay.

## VI. Conclusions

The Communications Technology Satellite (Hermes) has demonstrated the successful operation of a number of advanced technology components in a space system. Transmissions to and from small earth stations has been demonstrated. During May through August, communications experiments have been virtually unaffected by satellite "housekeeping" operations. The SHF transponder has performed as specified. Attitude control has been adequate for communication purposes although minor disturbances occasionally exceed the specified pointing goal.

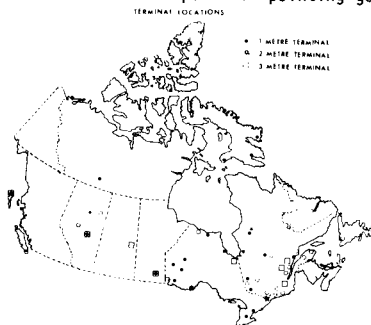


Figure 18

State of the art equipment has performed well although a reduction in solar array power capability has been experienced.

Based on the present information Hermes should be capable of fulfilling the mission objectives.

## Acknowledgements

Information for this paper has been gathered from many others working in the CTS project who are too numerous to mention. Their assistance and the help given by Mr. Cleon Holden in preparing this paper is greatly appreciated.

## References

1. J. Almond, Dr. C.A. Franklin and Dr. E.S. Warren, "A Perspective on the Canadian Satellite Program", Can. Elec. Eng. J. Vol. 1, No. 1 pp. 47-60, 1976.
2. B.C. Blevis and N.G. Davies, "Investigation of the Applications of Advanced Communications Satellite", Journal of the SMPTE, Vol. 84, pp 135-138, March 1975.
3. Dr. C.A. Franklin and E.H. Davidson, "A High Power Communications Technology Satellite for the 12 and 14 GHz Bands", AIAA 4th Communications Satellite Systems Conference, Paper 72-580, 24-26 April 1972.
4. Dr. L.D. Braun and V. O'Donovan, "Characteristics of a Communications Satellite Transponder", Microwave Journal, Vol. 17, pp. 45-47, December, 1974.
5. D.A. Bassett, "Ground Controlled Conversion of Communications Technology Satellite (CTS) From Spinning Mode to Three Axis Stabilized Mode", AIAA Guidance and Control Conference, San Diego, 16 August 1976.
6. V.J. Sansevero Jr., H. Garfinkel and S.F. Arch, "Flight Performance of the Hydrazine Reaction Control Subsystem for the Communications Technology Satellite", Joint AIAA/SAE 12th Propulsion Conference, Palo Alto, 26-28 July 1976.
7. T.D. Harrison, G.B. Long, Dr. V. Gore, Dr. F.R. Vigneron and E. Quittner, "In Orbit Characteristics of the Communications Technology Satellite Deployable Solar Array", Eleventh Intersociety Energy Conversion Engineering Conference, Las Vegas, 12-17 September 1976.
8. E.F. Millar, J.L. Fiala and I.G. Hansen, "Performance Characteristics of the 12 GHz, 200 Watt Transmitter Experiment Package for CTS", EASCON 75, pp. 202A-202G.
9. W.H. Robbins and P.L. Donoughe, "CTS United States Experiments - A Progress Report", Paper 76-228, IAF Conference, Anaheim, Calif., 10-16 October 1976.
10. B.C. Blevis and J.W.B. Day, "Canada/USA Experimental 12 GHz - CTS", CITEL InterAmerican Telecommunications Conference, Rio de Janeiro. 16 - 19 August 1976.

# ELECTRIC POWER SYSTEMS FOR FUTURE COMMUNICATIONS SATELLITES\*

F. H. Esch, W. J. Billerbeck and D. J. Curtin

COMSAT Laboratories, Clarksburg, Maryland 20734

## Abstract

To meet the capacity growth and added complexity of communications satellites, electric power systems have been improved significantly. Advanced development of all aspects of those systems and their effects are discussed. Details of lightweight deployed solar arrays, secondary batteries, and nuclear power approaches are provided. The various methods and devices, along with their advantages and disadvantages, are examined in terms of the parameters of interest. Attention is given to the interplay of different solar array and secondary power approaches with various power conditioning techniques. Finally, power system problem areas and the impact of this technology on communications capacity are discussed.

## Introduction

Satellites have become a routinely accepted means of relaying electronic communications. Although television is perhaps the form of communication which is most widely recognized by the general public, other forms, including teletype, facsimile and other data transmission, as well as voice communications, far exceed the traffic volume represented by television. In recent years much attention has been given to increasing satellite capacities through such means as clever modulation techniques, narrower antenna beams, and polarization diversity to allow frequency reuse, and through more efficient electronic devices. In addition, effort has been focused on increasing the electric power available for operating communications electronic devices. Many spacecraft subsystems typical of those aboard current communications satellites have fallen into design patterns in which changes are evolutionary, rather than revolutionary. The electric power systems for communications satellites, to a large degree, fit into this category.

In the early days of active repeater communications satellites, the considerations which had to be addressed were much more numerous than they are today. The rather modest mass and volume capability of early launch vehicles, elliptical versus circular orbit characteristics, and the various candidate means for power generation were among these considerations. At the present time, however, narrower limits have been established so that in almost all systems only geosynchronous orbits and photovoltaic conversion of solar energy by silicon cells are being given serious consideration. While it is possible to resort to other power generation means, including nuclear reactor systems, radio-isotope supplies, and conversion of solar heat through rotating machines, no near-future application of those alternate means is expected at this time.

Since the maturation of electric power systems for communications spacecraft, greater attention is being given to the efficiency of the various system elements and to the economic tradeoffs among the system concepts. Emphasis is being placed on reliability and longer operational lifetimes as exemplified by the INTELSAT series, for which design lifetimes have increased from 1.5 years to 10 years from INTELSAT I through INTELSAT V. In the power system, this imposes some particularly difficult requirements on energy storage for eclipse operation. Most secondary batteries simply have not been designed to live this long. This is an area which will require considerable attention over the next few years.

The requirements for DC primary power on typical commercial communications spacecraft continue to increase and are generally related to the communications traffic requirements. However, the relationship between DC power and communications channel capacity has become less direct because of the interplay of RF antenna gain and the use of time-division and other multiplexing schemes for piping more information through a channel with a given gain-bandwidth product.

An interesting example of the growth of DC power requirements is provided by the INTELSAT series of spacecraft. All of these use microwave-repeater-type devices in which the majority of the power goes to traveling wave tubes having a DC-to-RF conversion efficiency in the neighborhood of 30 percent. As shown in Fig. 1, the DC power requirement has increased with each new series of spacecraft. In fact, an interesting rule of thumb is that the power doubles with each major redesign. The relationship between DC load power and the number of telephonic half-circuits in these spacecraft is shown in Table 1.

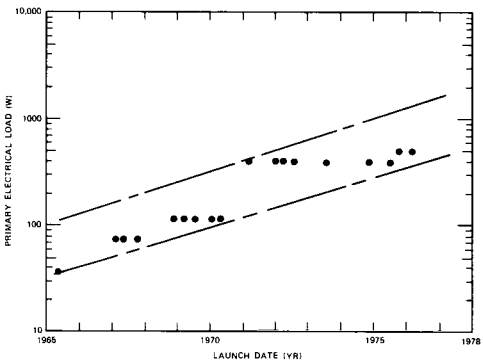


Fig. 1 Load Power Requirements for INTELSAT Communications Spacecraft

\*This paper is based upon work performed in COMSAT Laboratories under the sponsorship of the International Telecommunications Satellite Organization (INTELSAT) and the Communications Satellite Corporation. Views expressed in this paper are not necessarily those of INTELSAT.

Table 1. Technology Development, INTELSAT I-IVA

	INTELSAT Satellite				
	I	II	III	IV	IV-A
Year of 1st launch	1965	1967	1968	1971	1975
Dimensions (cm) { dia	72.1	142	142	238 <sup>a</sup>	238 <sup>a</sup>
height	59.6	67.3	104	282 <sup>b</sup>	282 <sup>b</sup>
Mass (kg) { at launch	68	162	293	1385	1469
in orbit	38	86	152	700	790
Primary power (W)	40	75	120	400	500
Transponders	2	1	2	12	20
No. of tel. circuits	240 <sup>c</sup>	240	1200	4000	6000
Design lifetime (yr)	1.5	3	5	7	7

<sup>a</sup>Drum.

<sup>b</sup>Overall.

<sup>c</sup>No multiple access.

In terms of electric power system development, there appear to be three areas which promise significant improvement in the next few years. These are a continued incremental upgrading of solar cell efficiency combined with a significant reduction in array structural weight, a reduction of life-limiting problems in energy storage devices, and the upgrading of power management in terms of increasing regulation precision and flexibility in DC/DC converters and associated devices. The current status and development direction of these areas will be discussed later in this paper.

#### Power Demands in a Communications Satellite

As mentioned earlier, the design of commercial communications spacecraft is beginning to stabilize and become an evolutionary process. A more detailed examination of the power system loads tends to reinforce this view. It is found that the ratio of power required by each of the subsystems is quite similar from one spacecraft to the next. Figure 2 shows the breakdown of power loads for a typical microwave repeater satellite.<sup>1</sup> It is interesting to note that these proportions are quite similar for either the drum spinner or the body-stabilized spacecraft, even though the various subsystems are quite different physically and functionally. It can be seen that the "housekeeping" equipment requires only about 13 percent of the total power, while almost 87 percent is allocated to the communications system. Of this, the majority (some 82 percent of the primary power) goes directly to the high-voltage power supplies for the traveling wave tube transmitters. Thus, it is observed that the spacecraft design is quite economical in terms of power required for functions subordinate to its central mission. Also, the dominance of the efficiency and weight of the high-voltage supplies becomes evident.

Economics has also become a very important aspect. As pointed out in an earlier paper,<sup>2</sup> the revenue potential of these satellites is quite large, since each one can handle a very large volume of communications traffic. Assuming that available weight saved in other subsystems can be effectively utilized by incorporating additional transponders and thus providing additional communications

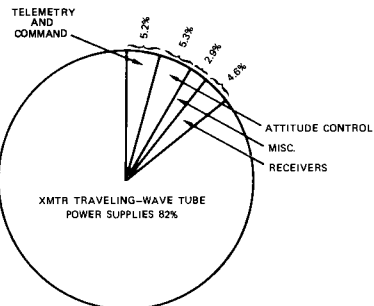


Fig. 2 Primary Power Distribution in a Typical Communications Spacecraft

channels, one analysis<sup>3</sup> shows that the revenue potential of one kilogram of satellite in-orbit weight is of the order of 1 to 2 million dollars.

Thus, in some cases, it becomes quite attractive to reduce the weight of the power system by increasing the power density of the various components. For example, in some of the early spacecraft the battery depth of discharge was restricted to about 20 to 30 percent of rated capacity, while in recent designs it may be about 55 percent of the total capacity, i.e., over 70 percent of the battery rated capacity. The gain in energy density, from the early values of about 8.0 Wh/kg up to the present levels of 13 to 15 Wh/kg, is nearly proportional.

#### Energy Conversion

##### Solar Power Systems

As commercial communications satellites have come of age, a number of new environmental and economic design considerations have become prominent in controlling new solar power system design. All of the commercial spacecraft have moved up to geosynchronous orbit, with its rather benign radiation environment. However, the sporadic unpredictable solar flare radiation which now contributes a significant portion of the degradation of photovoltaic cells imposes special requirements on the solar power system design. The less intense earth thermal inputs at these high altitudes tend to increase the severity of the temperature environment to which external components are exposed.

The major trends in solar power systems have been toward high reliability, high watts/kilogram, deployed solar arrays using high-efficiency silicon solar cells, new solar cell interconnect techniques, lighter structures, and novel deployment approaches. For communications satellites operating for 7-10 years at geostationary orbit, the end-of-life performance of these arrays is approaching 30 to 33 W/kg, including the weight of the orientation and power transfer assembly.

The silicon solar cell is not the only candidate for conversion of solar energy. Cadmium sulfide received considerable attention, particularly during the late 1960s, but has never overcome the penalties of poor efficiency and photodegradation during long sunlight exposure. Gallium arsenide, another candidate, continues to be attractive in that it has a

slightly higher theoretical efficiency and perhaps better radiation hardness than silicon. However, gallium arsenide cells must be developed to a practical configurative level before they can be considered for commercial use; the time scale required to accomplish such development is uncertain. An example of the work required is the development of a surface passivation dielectric for which high confidence in long-life stability, production uniformity, and reproducibility can be established.

During the latter part of the 1960s, the efficiency of silicon solar cells remained essentially constant, i.e., around 10 percent, or about 55 to 60 mW for a 2- x 2-cm cell. Considerable work was done on improving the solar cell stability under various environmental conditions, including humidity (i.e., soldered and Ti/PdAg contacts) and irradiation (i.e., use of n-p cells and 10- $\Omega$ -cm resistivity).

A major breakthrough in the efficiency of solar cells occurred with the development of the Violet solar cell.<sup>4</sup> This cell, shown in Fig. 3, represented a major advance in solar cell technology combining the use of very shallow diffused junctions (i.e., about 0.1  $\mu$ m), a new grid pattern for collecting the current from this shallow region, a new  $Ta_2O_5$  antireflective coating, and other innovations. For covered (2- x 2-cm) cells a peak power over 73 mW at 1 sun air mass zero conditions was observed in the laboratory. The particular importance of this development is that the performance gain occurred in the blue response of the cell and should therefore be radiation resistant. Early tests on laboratory-produced cells indicated that the cells retained most of their initial performance advantage under irradiation.<sup>5</sup> The cells degraded at a slightly higher rate than conventional (i.e., 10- $\Omega$ -cm) cells because they were made from low-resistivity 3- $\Omega$ -cm material.

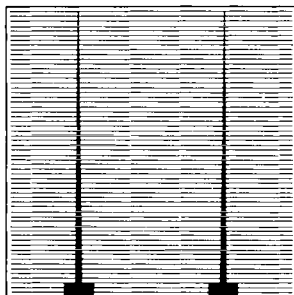


Fig. 3 COMSAT Violet Solar Cell

As mentioned above, the use of an improved optical system incorporating  $Ta_2O_5$  antireflective coatings ( $n \approx 2.3$ ) in these cells results in a performance gain when they are covered. This is in contrast to the usual losses experienced when cells with  $SiO_x$  coatings are covered. It is also expected that these  $Ta_2O_5$  coatings, if properly applied, should be stable under ultraviolet irradiation. Laboratory-produced cells have been tested<sup>6</sup> successfully under qualification-level tape peel, humidity, thermal soak, and thermal shock conditions. No peeling or color change has been noted in the  $Ta_2O_5$  coatings. This testing also included solar cell

modules fabricated using parallel gap resistance welding which have undergone 1,000 thermal shock cycles (-196°C to 100°C) without electrical or mechanical failure. The Violet solar cells have been flown successfully as experiments on the ATS-F and NTS-1 satellites. Cells with this type of performance are now being produced by several manufacturers and are being applied in several spacecraft programs.

The next step in improving solar cell efficiency occurred in 1974 with the development of the COMSAT Non-reflective (CNR) solar cell.<sup>7</sup> This solar cell is partially based on the Violet cell technology, but instead of using the normally flat front surface of the solar cell, it introduces a new surface structure that substantially reduces reflection losses from the cell surface. Selective chemical etching of the silicon produces multiple tetrahedra on the surface. These tetrahedra result in multiple interactions between the surface of the cell and the incoming light beam. The net effect of these interactions is that most of the incoming light is directed into the cell and very little is reflected off the surface.

The use of this antireflective surface and some other changes have led to 2- x 2-cm cells with a maximum power over 82 mW. An additional advantage of this cell is that the improvement achieved through the use of these new surfaces is not lost during irradiation so that the power advantage is maintained throughout life. Figure 4 compares the maximum power of a COMSAT CNR and Violet solar cells with that of conventional solar cells at the beginning of life and as they are irradiated.<sup>8</sup> It can be seen that the CNR cell initially has a power output which is about 56 percent higher than that of the conventional cell at 25°C, but after a dose of  $2 \times 10^{15}$  electrons/ $cm^2$ , its power output is over 58 percent higher. With other improvements in the stability of cover-slips and adhesives, the new space cells offer significant advantages over conventional cells. It is anticipated that cells of this type will reach production status in the near future.

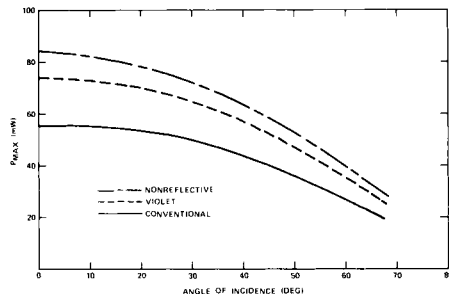


Fig. 4 Maximum Power Output of Non-reflective, Violet, and Conventional Cells as a Function of 1-MeV Electron Irradiation Fluence

One of the most severe problems in sun-oriented deployed solar arrays is the cumulative effect of thermal stress and strain applied to the solar cells interconnects, and adhesives during the mission. In geostationary orbit, the system experiences 700-1,000 eclipse cycles. Because of the low thermal

capacity of the array, coupled with the low earth albedo at this altitude, the arrays will cycle from approximately +55°C to -180°C (rigid substrate array) or -196°C (flexible substrate array). Furthermore, as shown in Fig. 5, the maximum rate of temperature change (i.e., thermal shock) for a lightweight flexible array is increased to more than six times that of a drum spinner array. In near-earth orbits, the thermal shock is not as significant, but the cycles are more frequent and may amount to several thousand in a mission of several years.

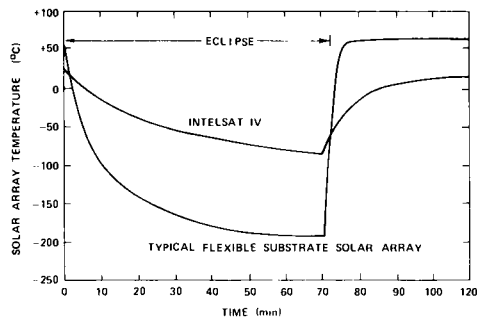


Fig. 5 Solar Array Temperature Profiles (longest eclipse) at Synchronous Orbit

The chief problems in reliability occur in the interconnects, the interconnect-to-solar-cell joint, and the solar-cell-to-substrate adhesives. Interconnect configurations and materials (e.g., silver-plated molybdenum or silver-plated Invar) which are relatively stress-free during thermal cycling are now used along with new solar cell interconnecting techniques such as parallel gap resistance welding, ultrasonic bonding, and thermal compression bonding. The advantages of these techniques are that they join the same metals (e.g., the silver contact on the solar cell to the silver-plated interconnect) without requiring an intermediate layer such as solder which can crack with repeated cycling, and that they are reproducible and readily adaptable to automation.<sup>9</sup> In addition, industry now uses silicone adhesives (e.g., RTV 566) that do not become brittle as quickly at low temperatures; consequently, unlike earlier materials, they do not overstress the cells, causing cell ruptures and breakage.

It has been shown that, with careful selection of interconnect materials, configurations, and interconnecting approach, followed by thorough testing, including thermal cycling to mission temperatures and durations, long-life interconnect systems can be achieved.<sup>10</sup>

Along with the dramatic improvements in solar cell performance and solar cell module technology, there have been major changes in solar array technology. These changes have occurred in all types of deployed solar arrays, including rigid and flexible substrate arrays and a new type of array that may be called semi-rigid. Since much of the weight of a typical solar array consists of structure and mechanisms, these advances have taken the form of new structural design concepts, coupled

with the application of lightweight materials having high stiffness.<sup>11</sup>

The best known type of deployed solar array is one which employs spring activation with some form of pantograph mechanism to deploy several panels of rigid substrates covered with solar cells. In the past, these arrays have typically used aluminum honeycomb substrates covered with either aluminum faceskins or an insulator. In more recent versions, a glass or carbon-fiber reinforced epoxy skin has been utilized. This type of array has several advantages, including stiffness, flat lay-down of solar cells, and flat packaging for a low stowage volume. It is also capable of providing transfer orbit power directly from the folded panels because the outer panel is folded with a portion of the cells facing outward during launch. A disadvantage of this type of array for some missions is that it usually cannot be retracted. However, this is typically not important on a communications satellite, for which retraction is unnecessary. The performance of the usual deployed rigid arrays using conventional solar cells is of the order of 10-12 W/kg at end of life.\*

In the newer types of rigid deployed arrays using less dense aluminum honeycomb and carbon-fiber faceskins with lightweight structural members (e.g., using beryllium or carbon fiber), power densities of 20-25 W/kg can be achieved under similar orbital conditions. Deployed rigid substrate arrays with an aluminum honeycomb core and carbon-fiber reinforced plastic faceskins will be used on the OTS and MAROTS satellites.

The next type of solar array is the deployed flexible substrate array. These are basically either rollout or foldout arrays. In the rollout type the array is stored on a drum during launch and deployed by a device such as a bi-stem boom. In the foldout concept, the array is folded and stored in some sort of box during launch and then deployed by a boom, a pantograph, or a pneumatic tube. A 14-kW rollout array, FRUSA, was flown successfully in 1971.<sup>12</sup> It utilized a single drum and two fiberglass reinforced Kapton blanket panels. Each blanket was deployed with a bi-stem boom on each side of the blanket.

A small flexible foldout array using pneumatic tube deployment was flown successfully on a satellite in 1974.<sup>13</sup> This array, developed by the Royal Aircraft Establishment, employed a pneumatically actuated tube to deploy a folded Kapton blanket. It is projected that a 1-kW version that has been designed but not yet fabricated will be able to deliver over 30 W/kg at end of life.

A large flexible foldout array is supplying the power for the 2-year mission of the Communications Technology Satellite (CTS) which was launched in 1976. This array employs a single bi-stem boom to deploy a folded substrate fabricated from glass-fiber reinforced Kapton.<sup>14,15</sup> The CTS solar array is a major achievement, since it is the first deployed flexible solar array to be flown at synchronous equatorial orbit. The successful

\*In this paper end of life refers to the end of seven years at synchronous equatorial orbit. The power density for a solar array includes the weight of the orientation and power transfer assembly. This approach is used because on a communications satellite the end-of-life power is most important.

performance of this array in orbit is the culmination of a significant development effort involving the European Space Agency, the Communications Research Center in Canada, and NASA; the blanket was developed in Europe and the deployment mechanism developed and integration performed in Canada. Although the array was designed to demonstrate technology rather than to represent the ultimate in power density, it would deliver close to 20 W/kg for a 7-year mission and could be optimized further with high-efficiency solar cells and lighter materials.

Another flexible foldout array, developed by Aerospatiale in France under the dual sponsorship of CNES and INTELSAT, uses a single pantograph to deploy a Kapton substrate solar array blanket for each wing of a 2-wing solar array.<sup>16</sup> This 1.1-kW/wing end-of-life system, shown in Fig. 6, can deliver almost 23 W/kg at end of life, while an optimized version using high-efficiency solar cells and lighter materials in the pantograph, yoke, etc., could achieve about 26 W/kg at end of life.

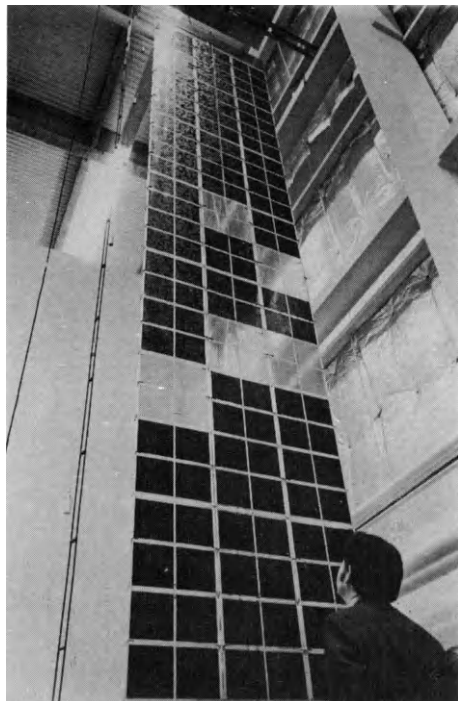


Fig. 6 High-Performance Flexible Foldout Solar Array

The chief disadvantage of the flexible solar systems has been their inability to provide reusable transfer orbit power. For example, on the CTS satellite the transfer orbit power was provided by two rigid solar panels mounted on top of the stowed deployable array. After synchronous orbit was

achieved, these two panels were jettisoned with a consequent loss of 50-100 W of additional power. For commercial communications satellites, this is not satisfactory since that additional power may well be required later in the mission. To overcome this deficiency, a so-called "hybrid" solar array using a rigid array for transfer orbit power is being developed. This rigid array is deployed at the same time as the flexible array and becomes part of the overall deployed array system so that it is reusable in synchronous orbit.

The third type of deployed array--the semi-rigid foldout array--combines a rigid and a flexible array by using a rigid frame and a pre-tensioned flexible substrate mounted within the frame. Some very early work along these lines was performed for the NASA/JPL-sponsored LASA project at Boeing. The present version of this concept,<sup>17</sup> known as the ultra-lightweight panel (ULP), is being developed at Messerschmitt-Bolkow Blohm (MBB) in Munich; AEG/Telefunken in Hamburg is a subcontractor for the solar array blanket. This work is being done under the sponsorship of INTELSAT and the DFVLR in West Germany.

The array blanket under development is a modified version of the solar array blanket developed by AEG/Telefunken for CTS. Because of the thermal mismatch between the carbon-fiber frame and the glass-fiber reinforced Kapton in the CTS-type blanket, the glass fiber in the blanket has been replaced by carbon fiber. The total array then utilizes a carbon-fiber reinforced Kapton blanket supported inside a carbon-fiber frame. Since both the frame and the blanket employ carbon fiber, there is no inherent mismatch in thermal properties. A model of one wing of this array is shown in Fig. 7. As designed, this array can deliver 30-33 W/kg at end of life.

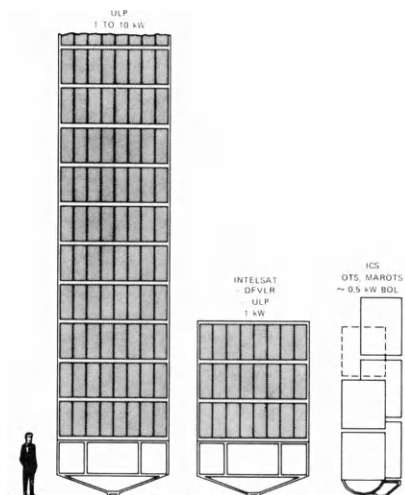


Fig. 7 MBB's Large Solar Array

### Nuclear Systems

All of the commercial communications satellites have used solar arrays for primary power and secondary battery systems for power during eclipse periods. However, coincident with the continued development of solar power/battery systems, nuclear isotope system developments have continued. It is important to compare the present and future characteristics of these latter systems to determine whether they should be considered for use on commercial communications systems.

All of the space radioisotope thermoelectric generators (RTGs) have utilized plutonium 238 radioisotope fuel with thermoelectric converters manufactured from doped lead-telluride or silicon-germanium. Since 1969, some 18 radioisotope thermoelectric generators have been launched and operated successfully in space on missions such as Triad, Pioneer 10 and 11, the Viking spacecraft, and LES 8 and 9.

The RTGs using lead-telluride have been under development for some time. In general these generators initially achieve not more than 3 W of electric power per kilogram, and somewhat less than 2.5 W/kg for a 5-year life. The Pioneer 10 was launched in March 1972 with four SNAP 19 RTGs, each weighing about 14 kg and together providing about 162.9 W or about 2.87 W/kg at beginning of life. However, at the end of three years in orbit, the power output had degraded almost 14 percent to about 135 W or 2.49 W/kg. Pioneer 11 was launched in April 1973, and the four SNAP 19 RTGs, with a total weight of about 55 kg, provided 158.7 W of electrical power or 2.93 W/kg. It is estimated that Pioneer 11 will encounter Saturn in October 1979 after 6.5 years in space and that at this point the power output will be about 104 W or 1.9 W/kg.<sup>18</sup>

Each of the two Viking spacecraft launched in 1975 consists of an orbiter and a lander. Each Viking lander, expected to soft land on Mars this year, contains two SNAP 19 RTGs providing the primary electrical power and thermal control.<sup>19</sup> These RTGs are predicted to produce about 38 W each, achieving about 2.56 W/kg at end of mission.

Of the newer developments, the multi-hundred-watt (MHW) generator is designed to produce 150 W of electrical power utilizing silicon-germanium thermoelectric converters and a high-temperature 2,400-thermal-watt plutonium 238 heat source. The initial system efficiency is slightly greater than 6 percent. It is predicted that after a 5-year life these systems should retain a power density over 3 W/kg.<sup>20</sup> Their first application was on LES 8 and 9, built by Lincoln Laboratories and launched in 1976.

The low watts/kilogram of these systems, coupled with the high cost of plutonium 238, resulting in overall system costs of more than \$20,000 per electrical watt versus about \$3,000 per watt for solar power/battery systems, have made radioisotope systems unattractive for commercial satellites. A development program is underway to improve the present converter initial efficiencies of 5-6 percent by replacing the older materials with selenide alloys having higher projected efficiencies.<sup>21</sup>

In addition, efforts are underway to reduce the costs of the plutonium below the present figure of about \$600 per thermal watt.

Along with the work on the selenide converters, work has been performed on Mini-Brayton dynamic cycles. Systems using radioisotope sources to power these heat engines have predicted power densities in the range of 4-6 W/kg. If these systems can be developed and proven and if the costs can be made competitive with those of future solar power/battery systems, they should again be analyzed for use on future commercial communications satellites. However, this does not appear fruitful at the present time.

During the 1960s and early 1970s, nuclear space power systems utilizing reactors were under development. However, this work has now been abandoned. Even if it is restarted, it is difficult to foresee any competitive system likely to be available until the late 1980s.

### Electric Energy Storage

The rechargeable nickel-cadmium (Ni-Cd) alkaline cell has been used to supply power during eclipse in a high percentage of all communications spacecraft flown to date. Its principal attractive features for this application have been the backlog of orbital experience, the high-rate deep-discharge capability, and the relatively long storage life.

A large number of Ni-Cd cells have been surveyed, as reported in Reference 22. This information has been updated to reflect the performance of recent cells that have been used in operational synchronous orbit missions. Figure 8 summarizes the present situation.

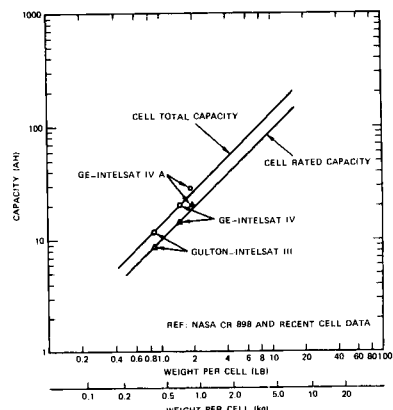


Fig. 8 Recent Ni-Cd Cells, Ampere-Hour Capacity versus Weight

Several important facts have come to light recently regarding performance characterization of the Ni-Cd cell and the philosophy of integrating it into a synchronous spacecraft power system. Most of

the available data, including those cited in Reference 23, indicate no loss, and actually a slight increase in total ampere-hour capacity to zero volts, with time and cycling in the synchronous orbit mode. On the other hand, it is known that cell terminal voltage, either on charge or on discharge, is quite variable and difficult to predict. It is a function of cell design, current, state of charge, temperature, contaminant levels, and previous temporal and cyclic history. Therefore, it appears logical to consider the cell as a circuit element which is a source of current or ampere-hours rather than as a constant voltage device.

Second, the importance of cell temperature should be recognized. The Ni-Cd battery is one of the most temperature-sensitive devices in a typical spacecraft. To operate to the deep depth of discharge which is essential to achieving high energy density, it is necessary to fully charge the cell. Since the charge efficiency drops off very rapidly at higher temperatures, the temperature of all the cells in a stack must be below 25°C. Low end temperatures during discharge are typically not a problem in synchronous satellites, since at the charge rates normally employed the battery temperature has usually returned to normal by the time the cell begins to evolve oxygen. Minimum temperatures of 0°C to 5°C have been experienced with quite satisfactory results, and lower temperatures can possibly be used if the charge rates are carefully controlled.

To construct a spacecraft battery by connecting a number of individual cells in series, several important factors must be considered. First, it appears desirable to perform a burn-in of about 30 cycles in order to reach a stabilized ampere-hour capacity before matching the cells. This allows a deep discharge without danger of reversing any of the cells. Matching to 5-percent capacity or better appears feasible at the present state-of-the-art.

To satisfy the thermal requirements outlined previously, and particularly to minimize cell-to-cell temperature variations in a large power system, designers have found it necessary to provide individual thermal paths to the structure for each cell. Alternatively, heat pipes can be used to provide uniform temperatures throughout the stack, as described in Reference 24.

Detailed battery component weights have been analyzed for several flight spacecraft. It has been determined that the average weight of the cells is about 82 percent of the total battery weight, with about 12 percent devoted to structure and the remaining 6 percent used for electronics and connectors. This information, together with the cell ampere-hours per kilogram, can be used to estimate the watt-hours per kilogram for complete batteries. The resultant curve plotted versus depth of discharge is shown in Fig. 9 as the "no redundancy" curve.

The reliability requirements for random failure of individual cells are quite stringent to ensure full operation for missions ranging up to 10 years. One approach that has been used to surmount this problem is to add one or two extra cells in series to the stack to accommodate shorted cells, and to use diodes or a transistor switch to bypass open-circuited cells. An alternative approach is to

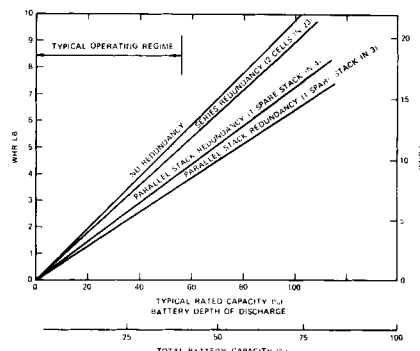


Fig. 9 Energy Density of Ni-Cd Batteries Packaged for Synchronous Orbit Application

provide a spare battery stack in parallel; this stack can then be switched in when needed. Both of these designs have been analyzed; the energy density curves versus depth of discharge are shown in Fig. 9.

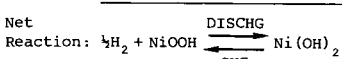
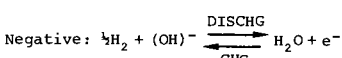
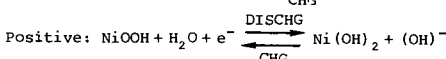
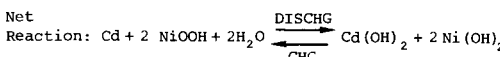
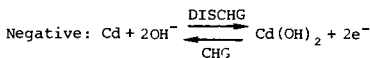
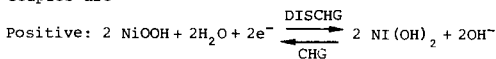
It is of interest to determine the battery depth of discharge which can be used in an operational satellite. The INTELSAT III program provided operational experience on spacecraft in synchronous orbit at a maximum depth of discharge of about 68 percent of rated capacity (=51 percent of total capacity). INTELSAT IV is operating at about 57 percent of rated capacity (=40 percent of total capacity), and a considerable amount of orbital operating data has been collected for mission times up to five years. Much has been learned in recent years about the necessary controls in cell processing and the control of contaminants required to produce a consistently good product. Also, the understanding of the chemical and electrochemical tests needed to adequately sample the manufactured lots of cells has been significantly improved.<sup>23</sup> Even with careful manufacturing using these controls and tests, the orbital experience data on existing cells indicate that operation beyond 5 to 7 years is quite problematic.

The shifting mission requirements mentioned earlier have led to requirements for improved energy density and much longer wear-out life which the battery industry is hard pressed to satisfy. The empirical curves of cycle life versus depth of discharge formerly used to predict cell life are simply not applicable to the long geosynchronous missions. Some useful data have been obtained from flight tests and from real-time ground tests in the NASA-sponsored NAD Crane facility, as well as at COMSAT Laboratories and from other real-time tests. However, this work is expensive, and the information feedback cycle is so long that it often does not keep up with cell manufacturing process changes and variations.

It has become clear that the need for improved wear-out life predictions for these longer missions requires R&D effort to develop an improved basic understanding of the various wear-out phenomena in the Ni-Cd cell, including separator oxidation, electrolyte redistribution, cadmium migration, and seal corrosion. Equally important is the development of

specific engineering tests which can be applied to rapidly evaluate the predicted wear-out life of sample cells in regard to each of these phenomena for life predictions and feedback into cell design and manufacturing processes. This type of approach has previously been taken by Bell Laboratories for long-life lead-acid cells for terrestrial use, and has resulted in many significant cell improvements.<sup>25</sup> It appears that there is an urgent need for this area to be vigorously developed for application to aerospace Ni-Cd cells.

Advanced electrochemical energy storage devices which offer improvements in energy density have been investigated for a number of years. Of the large number of possible systems, the low-temperature Ni-H<sub>2</sub> alkaline system presently appears to possess the best potential for synchronous orbit use.<sup>26</sup> These hermetically sealed secondary cells can be regenerated electrically, and require no pumps, valves, or other moving parts. In addition, they have the high-rate discharge capability needed for operation in synchronous orbit spacecraft. The electrolyte is an aqueous solution of 35-percent potassium hydroxide. The electrochemical equations governing the typical charge and discharge operation of the Ni-Cd and nickel-hydrogen (Ni-H<sub>2</sub>) couples are



respectively.

It can be seen that the nickel electrodes in both the Ni-Cd and the Ni-H<sub>2</sub> couples experience identical reactions; indeed, electrodes with similar physical characteristics can be used in either cell. The other half of this couple consists of a platinumized catalytic hydrogen electrode.

A typical physical arrangement of these new Ni-H<sub>2</sub> cells is shown in Fig. 10. A single cell design is being pursued in this work for a number of reasons. It offers a high energy density and is advantageous in terms of reliability, since leaks or electrical faults can be isolated to a single cell by using diode bypassing techniques. Some extensive analytical work has been conducted to evaluate the energy density that can be achieved in practical designs of these single cells. Specifically, computer models of the Ni-H<sub>2</sub> cells have been developed for parametric study. Further practical design and fabrication studies, including

structural and thermal aspects, have been done, including the appropriate testing.<sup>27</sup>

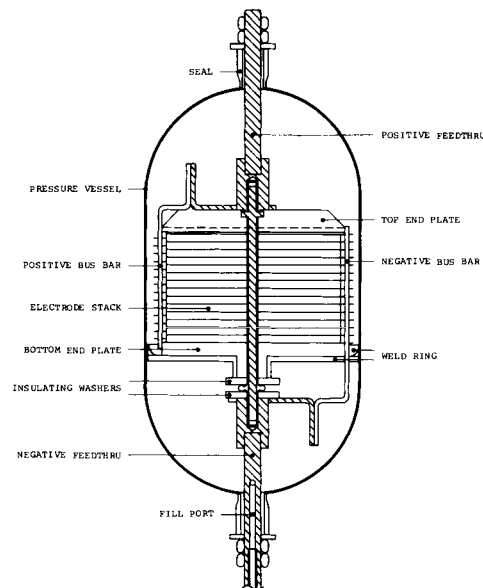


Fig. 10 Ni-H<sub>2</sub> Cell

The energy density which might be expected if Ni-H<sub>2</sub> cells were assembled into series strings for use as spacecraft batteries has been estimated. This estimate assumes the use of 35- to 50-Ah cells, since they are large enough to provide good cell energy density and have a capacity consistent with spacecraft designs in the kilowatt range.

Data in Reference 27 indicate that a cell energy density of about 44 Wh/kg was achieved for the 35-Ah design; estimates based on uprating it to 50 Ah indicate about 57 Wh/kg at 100-percent depth of discharge. When these cells were assembled into a 10-cell battery stack with the necessary structural and thermal arrangements and all the usual flight accessories such as bypass diodes, wiring, and connectors, the energy density of the 35-Ah unit was 39.2 Wh/kg. The 50-Ah unit was similarly estimated at 51.4 Wh/kg.

The depth of discharge which can ultimately be used with Ni-H<sub>2</sub> cells in operational missions is not yet completely clear. Extensive laboratory cycling testing has been done at 50- to 80-percent depth and the first flight experiment will be running at about 60-percent maximum depth. Figure 11 is a plot of energy density versus depth of discharge for these early design cells. If it is assumed that an 80-percent depth of discharge can eventually be used (which does not seem unreasonable in view of the known stability of the electrodes and the intrinsic reversal protection in the Ni-H<sub>2</sub> cell), these batteries will produce 31.4 and 41.1 Wh/kg, respectively. If a 2-in-20 series cell redundancy were used, the results would be 28.2 and 37 Wh/kg, respectively. Comparison with Fig. 9 indicates that these early design Ni-H<sub>2</sub> batteries

can achieve an energy density improvement of about 1.9 to 3.1 relative to the present Ni-Cd batteries. Undoubtedly, future development of the Ni-H<sub>2</sub> cell will continue to further improve this performance.

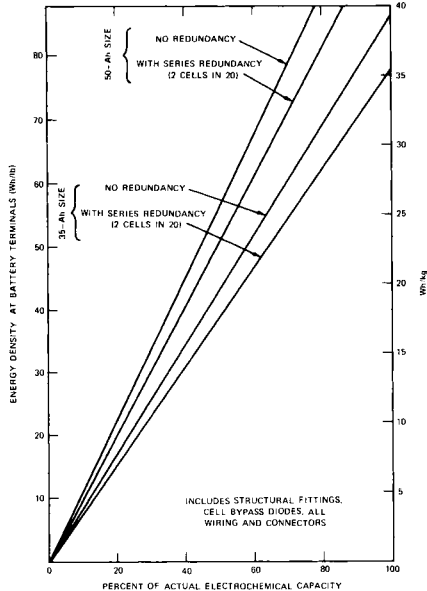


Fig. 11 Estimated Energy Density for a Present Technology Ni-H<sub>2</sub> Battery

Some flight prototype Ni-H<sub>2</sub> cells have now been built and put through extensive spacecraft qualification testing preparatory to a first flight test on the NTS-2 satellite in late 1976. The cell design is non-optimum in that a readily available 50-Ah case was used while the electrode capacities were adapted to 35 Ah for this experimental flight. Nonetheless, these cells produce an energy density of about 44 Wh/kg on discharge to 1 volt.<sup>28</sup> A rather heavy structural/thermal mounting arrangement and other auxiliary components contribute about 30 percent of the overall 7-cell battery weight, bringing the energy density of the battery down to 30.9 Wh/kg at 100-percent depth of discharge. At a conservative depth of discharge for nickel hydrogen of about 57 percent, this first complete battery in flight configuration produces a usable energy density of 17.6 Wh/kg.

In addition to the light weight of Ni-H<sub>2</sub> batteries, there are other perhaps more significant advantages. First, this couple is self-limiting in overcharge. The hydrogen pressure increases proportionally during charging, and once the nickel electrode is fully charged, the gas pressure stabilizes at that level. The primary problem associated with Ni-Cd operations, that of attempting long-term charging while skirting a dangerously close H<sub>2</sub> evolution potential, is simply nonexistent with this cell. Also, if a cell is reversed, hydrogen is generated at the nickel electrode according

to the same reaction as in normal charging. This gas is then consumed at the gas electrode. Thus, the cell is considerably more rugged than the Ni-Cd cell under both limiting conditions.

In terms of the mechanisms which are known to cause long-term cell degradation, a comparison of Ni-Cd and Ni-H<sub>2</sub> reveals that the seals in the Ni-H<sub>2</sub> cell must resist leakage against a higher pressure of H<sub>2</sub> rather than O<sub>2</sub> pressurant, the separator dry-out due to loss of electrolyte is probably similar, and, of course, the cadmium migration and nylon separator oxidation problems of the Ni-Cd cell are nonexistent in the Ni-H<sub>2</sub> cell. The experimental data presently available appear to support these suppositions and to indicate that indeed the life of these Ni-H<sub>2</sub> cells in geosynchronous orbit will considerably exceed that of Ni-Cd. However, additional laboratory investigation and flight operating experience will be needed to fully validate the wear-out life expectations.

#### Power Control and Conditioning

In the course of developing a number of commercial communications spacecraft, several design concepts or ground rules for power systems have evolved which are now being implemented in ongoing programs. These are primarily aimed at providing a very high probability of uninterrupted service for the full mission lifetime. They have a secondary goal, almost equally important, of ensuring that, when the spacecraft finally loses some of its capability, it degrades "gracefully," shedding channels without interrupting the remaining operational channels, and giving adequate time for replacement by other spacecraft. Some of these concepts are as follows:

a. Avoidance of catastrophic failure. No single component failure shall compromise full mission operation. This stems from the standard reliability considerations, but is especially important in any permanently connected portion of the primary power bus.

b. Protected bus concept. All power system loads must be designed to unload the main bus in case of a fault. This is arranged by means of overcurrent shutdown, fusing, or use of fusible components such as fusible resistors. In the latter two cases, it is essential to provide sufficient source current from the batteries to open the fusible component rapidly.

c. Multiple main buses. Whenever the design permits, the loads are grouped so that several completely independent primary buses can be used, each with its own separate solar generator and battery. The primary bus circuits must have redundant wiring.

d. Essential bus for critical functions. The command receiver with associated power switching and sometimes certain essential telemetry and attitude control functions are operated from a low-current bus which can draw power from several sources.

e. Automation at the earth end of the command and sensing links. When there is an even choice between hardware automation of sensing and power control functions in the spacecraft and software implementation at the earth station, the latter is

preferable to gain simplicity and associated reliability in the spacecraft.

f. Load contingency planning. In the design phase a load growth margin of 5 to 10 percent is carried for new equipment, tapering to 0 as all final flight hardware power requirements become measured values.

g. Adequate primary power sizing to provide the required end-of-mission power with high confidence. The design includes an allowance to account for component and process variations, measurement errors, and variability in long-term degradation estimates. Statistical probability analysis shows that this is typically 5 to 10 percent above the nominal end-of-mission power for 3 $\sigma$  confidence with contemporary solar array designs.

h. Reliability approach. A combined random failure and wear-out life analysis, tempered by previous experience, is used to evaluate power system designs. As mentioned earlier, the wear-out life aspect is particularly significant in the case of batteries. Of course, the usual flight-approved, high-reliability, burned-in components are used, and the equipment is put through a bench burn-in test, coupled with realistic environmental testing.

In terms of the hardware aspects, it appears that the spacecraft main bus voltages are increasing gradually as power levels increase. A number of the early commercial spacecraft operated at about 20 to 24 volts, while more recent designs have moved up to the 30- to 35-volt regions, and some experimental spacecraft operate at much higher voltages. For instance, the CTS main experiment bus runs at a nominal 76 volts DC.

The question of whether to use a regulated or unregulated main bus concept is still unresolved, and both designs are used. However, for spacecraft using a number of traveling wave tubes as the RF transmitters, detailed studies<sup>1</sup> have shown that the unregulated bus has a significant weight advantage. In that study, it became apparent that the weight and efficiency of the high-voltage electric power conditioners (EPCs) for these tubes dominated the power conditioning system in this type of spacecraft. For instance, in a typical design, the total EPC weight can be 1.5 to 3 times that of the other onboard power conditioning equipment.

Most of the early spacecraft used dissipative regulators in these EPCs. As in many other areas of power conditioning, these are now being replaced by switching regulators which offer efficiency and weight advantages. However, the situation is still quite fluid. The design of these units is quite difficult due to the high voltages and the precise output regulation and ripple requirements. Also, some of these requirements are changing as higher radio frequencies and output power levels require higher DC input voltages. The recent advent of the high-efficiency multicollector TWT handling digital modulation has also touched off a spate of new electric power conditioner designs to operate with these tubes.

#### Conclusions

Electric power system technology for communications satellites has been discussed and future

trends have been identified. From the design standpoint, constraints imposed by environment and operating conditions are quite well known, and emphasis is being placed on economic considerations, including higher reliability and mission lifetimes up to 10 years or more. It is anticipated that the end-of-mission power density for spacecraft power systems with solar arrays and secondary batteries will increase from the existing 3 to 5 W/kg up to about 10 to 12 W/kg in the next few years using equipment and technology which have already been proven on an experimental basis. These weight and life improvements are expected to be of even greater concern in the future, since communications satellites will be required to be more efficient in all respects.

Along with engineering development efforts aimed at such improvement, it is important to identify areas which require particular attention. Electrochemical energy storage devices need to be improved so that wear-out mechanisms can be reduced to the point at which high confidence levels can be established for the lifetimes desired in future communications satellites. This is expected to involve both design effort and process control. Another problem is that of establishing techniques for adequately inspecting solar cell interconnections, especially for lightweight long-life panels where welding or other non-solder bonding is employed. Also, there is a real need for innovation in developing simpler, high-efficiency power conditioning devices with high reliability, particularly those associated with the RF power amplifiers. With adequate progress in these problem areas and continued good engineering in efficient system design, future communications satellite power needs will be met with high confidence.

#### References

1. W. J. Billerbeck, "Electric Power for State-of-the-Art Communications Satellites," National Telecommunications Conference Record, NTC73, Vol. 1, pp. 19D-1-19D-12.
2. B. I. Edelson, H. W. Wood, and C. J. Reber, "Cost Effectiveness in Global Satellite Communications," *Raumfahrtforschung*, Vol. 20, Issue 2, March-April 1976.
3. B. Raab and S. Friedrich, "Design Optimization for Profit in Commercial Communications Satellites," AIAA 5th Communications Satellite Systems Conference, April 1974.
4. J. Lindmayer and J. Allison, "An Improved Silicon Solar Cell - the Violet Cell," *Proc. of the Ninth IEEE Photovoltaic Specialists Conference*, Silver Spring, Maryland, 1972, pp. 83-84; "The Violet Cell: An Improved Silicon Solar Cell," *COMSAT Technical Review*, Vol. 3, No. 1, Spring 1973, pp. 1-21.
5. R. Arndt, "Effects of Radiation on the Violet Solar Cell," *COMSAT Technical Review*, Vol. 4, No. 1, Spring 1974.
6. D. Curtin and R. Cool, "Qualification Testing of Laboratory Produced Violet Solar Cells," *Proc. of the Tenth IEEE Photovoltaic Specialists Conference*, Palo Alto, California, 1973, pp. 139-152.

7. J. Haynos et al., "The COMSAT Non-Reflective Solar Cell: A Second Generation Improved Cell," Proc. of the International Conference of Photovoltaic Power Generation, Hamburg, Germany, September 25-27, 1974, pp. 487-500.
8. J. F. Allison, R. Arndt, and A. Meulenberg, "A Comparison of the COMSAT Violet and Non-Reflective Solar Cells," COMSAT Technical Review, Vol. 5, No. 2, Fall 1975, p. 211-224.
9. R. Buhs, H. J. Durre, and H. W. Boller, "Welding of Solar Cells in a Production Line," Proc. of the Eleventh IEEE Photovoltaic Conference, Scottsdale, Arizona, 1975, pp. 126-133.
10. D. J. Curtin and W. J. Billerbeck, "Development of Advanced Interconnects for Solar Cells," COMSAT Technical Review, Vol. 4, No. 1, Spring 1974, pp. 53-68.
11. L. A. Harris, "Advanced Composites - An Assessment of the Future," Astronautics and Aeronautics, March 1976, pp. 22-35.
12. G. Wolff and A. Whitman, "The Flight of the FRUSA," Proc. of the Ninth IEEE Photovoltaic Specialists Conference, Silver Spring, Maryland, 1972, pp. 240-253.
13. B. Collins, "Power Generation for the X4 Spacecraft - A Step in the Development of a High Power/Mass Ratio Hybrid Solar Array System for Applications Spacecraft," Proc. of the International Conference on Photovoltaic Power Generation, Hamburg, Germany, September 1974, pp. 581-591.
14. R. Buhs, "Layout and Technology of the CTS Solar Array Blanket," Conference Record of the Tenth IEEE Photovoltaic Specialists Conference, Palo Alto, California, 1973, pp. 295-305.
15. J. S. Smith, S. S. Sachdev, and J. A. Hunter, "Testing of the Communications Technology Satellite Deployable Solar Array Subsystem," Proc. of the Eleventh IEEE Photovoltaic Specialists Conference, Scottsdale, Arizona, 1975, pp. 83-93.
16. G. Barkats, "Development of a Flexible Foldout Solar Array," Proc. of the International Congress, The Sun in the Service of Mankind, Paris, France, July 1973, pp. 251-259.
17. D. E. Koelle, "Advanced Lightweight Rigid Solar Arrays Based on Carbon Fiber Technology," International Astronautical Federation (IAF), XXVth Congress, Amsterdam 1974, Paper 74-085.
18. C. J. Goebel, "SNAP 19 Pioneer 10 and 11 RTG Deep Space Performance," Proc. of the Tenth International Energy Conversion Engineering Conference, Newark, Delaware, 1975, pp. 868-872.
19. W. M. Britain and S. T. Christenbury, "SNAP 19 Viking RTG Flight Configuration and Integration Testing," Proc. of the Ninth International Energy Conversion Engineering Conference, San Francisco, California, 1974.
20. R. L. Kerr and J. D. Reams, "Advances in Space Power Generation," International Astronautical Federation (IAF), XXVth Congress, Amsterdam, 1974, Paper 74-086.
21. P. J. Dick, "RTG Electrical Power for Spacecraft," Proc. of the 1974 IEEE Electronics and Aerospace Systems Convention, Washington, D. C., 1974, pp. 322-327.
22. "Study and Analysis of Satellite Power Systems Configurations for Maximum Utilization of Power," NASA CR-898, prepared by TRW Systems for GSFC, October 1967.
23. J. D. Dunlop and M. W. Earl, "Evaluation of INTELSAT IV Nickel-Cadmium Cells," Proc. 25th Power Sources Symposium, May 23, 1972, p. 40.
24. D. N. Stager and W. R. Scott, "Two Kilowatt Long Life Battery," TRW Report No. AFAPL-TR-71-43, June 1971.
25. "Lead-Acid Battery," Bell System Technical Journal, September 1970.
26. J. Stockel et al., "A Nickel-Hydrogen Secondary Cell for Synchronous Orbit Application," Proc. Seventh International Energy Conversion Engineering Conference, San Diego, California, 1972, pp. 87-94.
27. R. E. Patterson, W. Luft, and J. Dunlop, "Development of Spacecraft Power Systems Using Nickel-Hydrogen Battery Cells," 6th Communications Satellite Systems Conference, Montreal, Canada, April 5, 1976.
28. F. Betz, J. Stockel, and A. Gaudet, "Nickel-Hydrogen Storage Battery for Use on Navigation Technology Satellite-2," 11th International Energy Conversion Engineering Conference, September 1976.

# ANALYSIS OF THE SYMPHONIE EARTH SENSORS IN-FLIGHT OPERATION\* NEW EARTH SENSORS\*\*

F. Desvignes, F. X. Doitau, A. Juvigny\* and P. Vermande\*\*

\*Société Anonyme d'Etudes et Réalisations Nucléaires (SODERN),  
Limeil-Brévannes, France

\*\*Centre National d'Etudes Spatiales, Toulouse, France

## ABSTRACT

The paper starts by recalling the Symphonie spacecraft structure and attitude control system, a brief description of attitude acquisition and control procedures is given. The two types of Earth sensors are described, with emphasis on the model using thermopiles which measures roll and pitch misalignments in the spacecraft operational modes. A brief description of the sensors functional tests made prior to the integration on the spacecraft, and of the corresponding results, is given. The telemetry readouts available for the in-flight sensor tests are described. The interpretation of these data is explained and corresponding results are presented, which show a good agreement with predicted performance and functional tests made at ground with the simulators. These results permit to check the validity of some conventional hypotheses.

In a second part of the paper, the new infrared sensors developed for the current European and international spacecraft programmes are described, showing the accuracy and reliability improvements obtained.

## 1. INTRODUCTION

The first model of the French-German experimental telecommunications satellite has been launched on the 19th of December 1974. A second model has been launched on the 27th of August 1975. This is the first European three-axis stabilized geostationary spacecraft and, at our knowledge, the first in the world to use static horizon sensors - i.e. without moving parts - for the operational attitude control.

The relative merits of the "dithered" and static Earth sensors are subject to controversies in Europe as well as in the United States : the difficult problem of the zero drifts induced by the thermal constraints, due to the detection of the infrared radiation in d.c. mode, made questionable the feasibility of high accuracy Earth static sensors.

The first equipment made by SODERN on this principle has been designed by LEP and developed for the Symphonie spacecraft [1] ; careful tests made in simulators have shown a good agreement between the measured and the predicted characteristics, but the performance prediction and tests need some assumptions or conventions : the only real proof is on the observation and interpretation of the results obtained in flight. This report describes the telemetry data of the roll channels, and their interpretation.

## II. THE SYMPHONIE SPACECRAFT AND ITS ATTITUDE CONTROL SYSTEM

The Symphonie spacecraft has been built by the CIFAS, in which the Société Nationale Industrielle Aérospatiale (SNIAS, France) and Messerschmitt-Bölkow-Blohm (MBB, Federal Republic of Germany) had the responsibility for the system aspects and integration.

The spacecraft body (figure 2) is prism-shaped with an hexagonal base, 0.5 m in height (overall height : 2.0 m) and 1.7 m in outer diameter ; it is fitted with three solar panels giving an electrical power in the 200 to 300 W range (overall extension 6.8 m) ; the weight is 230 kg, when starting the operation in geostationary orbit.

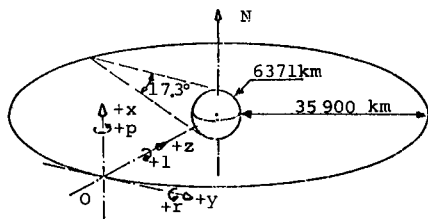


Figure 1. Symphonie spacecraft and orbit reference axes.

In operating configuration (figure 1), the prism axis (+x) corresponds to the pitch (p) axis : it is perpendicular to the equatorial orbit (parallel to the Earth poles axis, north N direction) ; the symmetry axis (+z) which corresponds to the infrared Earth static sensors line of sight points at the Earth centre, it corresponds to the yaw axis (l) ; the (+y) axis, which is perpendicular to the xOz plane, has to be the roll axis (r) which is parallel to

\* Analysis supported by the Consortium Industriel Franco-Allemand Symphonie (CIFAS).

\*\*Development supported by the European Space Agency (ESA) and by the Centre National d'Etudes Spatiales (CNES).

the spacecraft instantaneous speed (or momentum) vector.

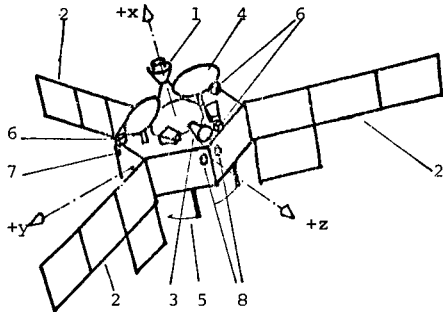


Figure 2. Symphonie spacecraft structure and reference axes

- 1 Apogee motor
- 2 Solar panels
- 3 Receiving antenna
- 4 Transmitting antennas
- 5 VHF antennas
- 6 Solar sensors
- 7 Earth horizon crossing sensor
- 8 Static Earth sensors

The attitude control system, which has been under the responsibility of MBB, comprises (figure 3) :

- one single narrow beam Earth horizon crossing sensor (SODERN, STR 01 type),
- three digital Sun sensors (Leitz-MBB), SS1, 2 and 3,
- two redundant two-axis infrared Earth static sensors (SODERN, STA 01 type), the sensitive axes oriented in the +z direction,
- one fixed momentum flywheel (Teldix) the momentum of which is oriented in the +x direction,
- eight cold gas thrusters (SNIAS), K 1 to 8,
- the associated electronics.

All along the transfer orbit (equatorial, altitudes : perigee 200 km, apogee 36.000 km), the spacecraft attitude is spin stabilized at about 120 rpm, with spin axis (x) parallel to the orbit minor axis. The actual spin characteristics (axis attitude, spin rate and phase) are determined at ground using the information given by the Earth crossing sensor (Earth phase), the Sun sensors (Sun phase and aspect angle) and the actual spacecraft orbit characteristics. The requirement for the Earth sensor accuracy was .15°, 1 stand. dev. including alignment errors, Earth radiance lack of uniformity (seasonal changes, North to South ratio in the range .5 to 2) and noise for a single measurement (occurrence rate 2 per second).

When the spacecraft is on the circular geosynchronous orbit, the solar panels are deployed, the spin rate is reduced to less than 0.7 rpm partly by the spin-up of the flywheel, its instantaneous attitude changes are observed with respect to the Sun, and to the Earth by the Earth static sensor. This last information is used to control the final three-axis Earth acquisition which is operated by the cold gas thrusters.

In normal mode of operation, the flywheel momentum (inertia momentum 0.064 kg.m<sup>2</sup>, spin rate 2700 to 3300 rpm, momentum from 18.1 to 22.1 N.m.s.) is controlled in close loop by the analog output of the pitch channel of the static horizon sensor ; when the flywheel spin rate reaches the above mentioned limits, a desaturation procedure is undertaken by the use of the cold gas thrusters (K5 to K8, thrust 1 N) ; to reach the nominal spin rate (3000 rpm), it requires less than 3mn. The expected frequency for this operation is less than once per month.

The flywheel stiffens the spacecraft attitude with respect to the y and z axes (roll and yaw). The natural torques applied to the spacecraft around these axes are such that the corresponding rates do not exceed 0.1 arc degree per day (20 nrd/s) but are usually much less (average 0.02°/day = 4 nrd/s). Due to the 24 hours orbit period, the yaw and roll misalignments commute four times a day (+ roll, + yaw → + yaw - roll → - roll - yaw → - yaw + roll → ...) in a sin-cos way : when roll maximizes, the yaw becomes nil ; when this maximum reaches a given maximum tolerance (0.3°), a limited duration torque (about 1 s) is applied round the z axis with the cold gas thrusters system (K2, K4) : this starts a spacecraft nutation movement the half angle of which is chosen such as, half a nutation period later

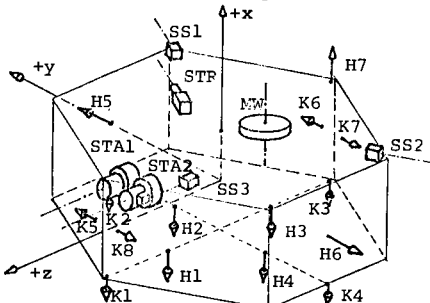


Figure 3. Symphonie spacecraft attitude and orbit control equipment

SS 1 to 3	: Solar sensors
STR	: Earth horizon crossing sensor
STA 1 and 2	: Static Earth sensors
MW	: Momentum wheel
H 1 to 7	: Hot gas thrusters
K 1 to 8	: Cold gas thrusters

(18.85 s), the roll misalignment is slightly over-corrected ; a second cold gas pulse (same magnitude and direction) is then applied to stop the nutation movement.

- The main requirements for the two-channel Earth static sensor were :
- Time constant less than 0.1 sec.,
  - Response field (geostationary orbit) :  $\pm 17^\circ$ ,
  - Linear field for acquisition  $\pm 2.6^\circ$
  - High linearity field (for fine pointing)  $\pm 0.5^\circ$
  - Zero accuracy (including alignment error, thermal constraints, Earth radiance lack of uniformity) :  $0.15^\circ$ , 1 stand. dev.

### III. THE EARTH SENSORS

#### The horizon crossing sensor

This equipment is of very classical design, it includes a germanium lens, an interference infrared bandpass filter, a bolometer and electronic circuits for bolometer supply, signal medium width bandpass amplification, peak amplitude relative level triggering circuits. The sensor delivers two square pulses, the medium occurrence time of which is related to the Earth centre crossing time in a way which is practically independant on the regular (seasonal) changes. The measured noise equivalent misalignment is  $0.05^\circ$  (1 stand. dev.), the error induced by the conventional seasonal changes in Earth radiance lack of uniformity as stated above do not exceed  $0.07^\circ$ . These values have been checked at ground with a self-calibrating simulator which permits the measurement of the sensor operational characteristics in a large range of temperatures, spin rates, chord lengths, Earth radiances lack of uniformity, with a  $0.003^\circ$  accuracy [5].

#### The static sensor (STA 01 type)

It is well known that the night and day attitude measurement with respect to the Earth by passive means require the sensing of the Earth emitted infrared radiation. For three-axis stabilized spacecraft, the main design and manufacturing problems come from the d.c. detection of the faint infrared signals corresponding to the small attitude changes, in presence of a large background, the magnitude of which changes with the sensor temperature [2].

There are two families of sensors [4] :

- "dithered" sensors, in which an oscillating mirror placed in front of a set of horizon crossing sensors produces an optical motion of the Earth image ;
- static (or radiation balance) sensors, in which the powers received by large area infrared sensitive detectors distributed around the Earth image are compared in d.c. mode : all changes in the spacecraft attitude with respect to the Earth introduce an image displacement, thus a change in the balance of the powers received by the various detectors. The only type of

uncooled long wavelength sensitive infrared detector which can be used in d.c. mode is the thermopile.

For reliability reasons, the use of this last concept has been recommended for Symphonie.

In the STA 01 sensor, eight identical thermopiles are distributed around an infrared image of the Earth focussed by a germanium lens and limited in wavelength range by a bandpass filter (13.5 - 17 microns). The field configuration of the sensitive areas is represented by figure 5.

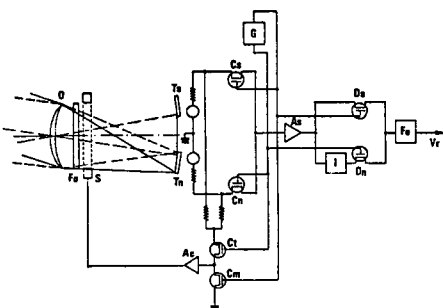


Figure 4. Static Earth sensor (SSA 01) basic configuration.

A	: a.c. amplifiers
C	: field-effect transistor choppers
D, I	: synchronous detector
Fe	: low-pass electrical filter
Fb	: bandpass infrared filter
G	: oscillator
O	: objective lens (germanium)
S	: cold space compensation source
T	: thermopiles
V	: analog output

The thermopiles are connected in opposition, two by two : this gives four channels, two for pitch ( $p_n$  and  $p_s$ ), two for roll ( $r_w$  and  $r_e$ ) ; the four d.c. outputs of the pairs of thermopiles are chopped by field effect transistors, a.c. amplified, reconverted in d.c. signals by synchronous detection, filtered, and d.c. amplified again (figure 4).

The use of redundant channels in pitch and roll is necessary if the attitude control is needed even when the Sun image is focussed on the thermopiles sensitive areas : the Sun radiation in the filtered wavelength range is not strong enough to damage the thermopiles but it remains much greater than the Earth one (100 times the Earth power change corresponding to a  $0.15^\circ$  misalignment [2]). Thus, the infrared sensor is fitted with a Sun sensor using silicon cells, the sensitive areas of which overlap the thermopiles ones in the front space : according to the Sun

position in the field, the Sun sensor switches automatically from one roll channel to the other and from one pitch channel to the other.

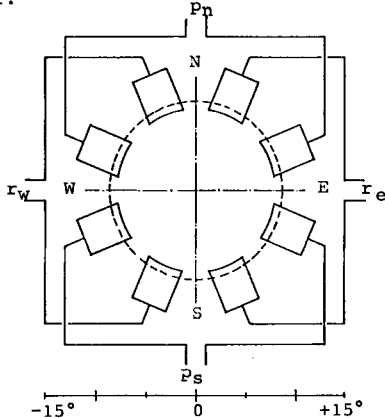


Figure 5. SODERN STA 01 static Earth sensor ; thermopile sensitive areas configuration in the field.

- These changes occur :
- for pitch from  $p_s$  to  $p_n$  close March 23, from  $p_n$  to  $p_s$  close September 24,
  - for roll, from  $r_w$  to  $r_e$  close 23:30, and from  $r_e$  to  $r_w$  close 00:05, solar local time on the next day, in short periods of the year, from February 17 to March 3, from April 10 to 25, from August 17 to September 3, and from October 9 to 23.

The redundancy of the channels is used too for increasing the sensor acquisition field when large cross misalignments occur. For this reason, switching from one channel to the other occurs during some attitude control operations.

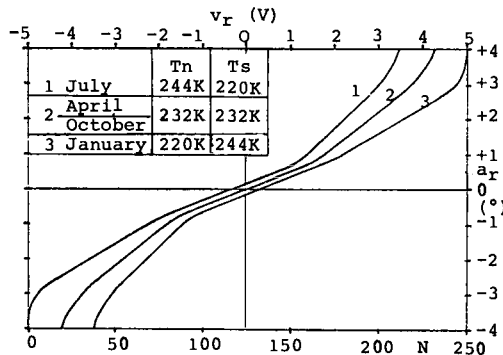


Figure 6. STA 01 sensor roll response functions (pitch at null) at four dates in the year. Analog output  $v_r$  and digital telemetry figure  $N$  versus misalignment  $a_r$ .

The main functional characteristics of this sensor are represented by figure 6 and in table 2.

Prior to their integration in the spacecraft, these sensors are tested in a simulator which comprises in a large vacuum bell-jar [5] :

- a liquid nitrogen cooled infrared collimator which simulates the Space and Earth radiation, thanks to a moderately cooled black disc placed in the front focal surface of a germanium lens ;
- a double gimballed platform on which the sensor is mounted. The attitude of the sensor on this platform is accurately measured by optical means ; the sensor temperature may be controlled according to predetermined programmes ;
- the front part of the sensor optical head may be irradiated with visible and near infrared radiation at air mass 0 level in order to simulate pre- and post-eclipse Sun irradiation constraint.

#### IV. THE RECEIVED DATA

##### Horizon crossing sensor

When the spacecraft approaches the transfer orbit apogee, the sensitive beam crosses the horizon (nominal period from 40 min prior to, to 40 min after the apogee) : the nominal conditions of operation are reached for a duration of about 60 min. The times elapsed between the Sun sensor pulse and the two Earth sensor pulses are measured and transmitted every two seconds in digital words ; the digitalization step corresponds to a time interval of 244  $\mu$ s or an angle of 0.176° at the nominal spin rate of 120 rpm.

##### Static sensor

- In nominal mode of operation :
- the pitch output is used for close-loop control of the flywheel, thus it is maintained nil ;
  - the roll output  $v_r$  (volts) of the channel (east or west) which is switched on is converted in an 8 bits digital word  $N$ , the decimal value of which is

$$N = 25 v_r + 124.3$$

This figure is also represented as abscissa scale for fig. 6.

In the telemetry format period (256 s) one gets :

- eight roll outputs (one each 32 sec.) (two times each for redundancy),
- one status word naming the operating channel (east or west),
- one status word naming the operating sensor (there are two redundant sensors on the satellite),
- one sensor head front temperature measurement.

For various reasons, a part only of these data is available but, thanks to the cooperation of the Centre d'Opérations Symphonie (Toulouse) and of the German Symphonie Operation Centre (Oberpfaffenhofen), we have got enough information to analyze all of the in-flight sensor behaviour which could be expected from the telemetry.

## V. DATA INTERPRETATION

### Horizon crossing sensor (STR 01)

This sensor is in operation for one single short period of time in the space-craft life. The telemetered data result of a combination of the Sun and Earth sensors outputs ; thus, it is difficult to separate the terms due to the two instruments. Furthermore, the digitalization step ( $0.17^\circ$ ) is much larger than the accuracy limits of the horizon sensor : the possibility to deduce some information on the in-flight sensor noise is doubtful.

The noise estimated from the telemetry readouts appears to be small with respect to the telemetry step.

Spin axis attitude corrections using the received data have been applied with good success, as well at the level of further check by the sensors system as at the level of the spacecraft injection on the geosynchronous orbit.

An attempt to deduce the spin axis attitude without use of the Sun aspect angle has been made. This requires the comparison of the remaining outputs at various orbit positions of the spacecraft close the apogee without attitude corrections : the result is in good agreement with the nominal method.

### Static sensor STA 01 : medium term zero drift

In a first series of analyses, the roll channel output available from the sensor in operation (MV 11) on the Symphonie I spacecraft has been recorded once each hour. It has been said that, if the fly-wheel momentum is not perpendicular to the orbit plane, the roll and yaw misalignments change continuously in a sinusoidal way with

- an amplitude equal to the perpendicularity defect and
- a one sidereal day period.

The readout versus time curves have been drawn, figure 7 is an example.

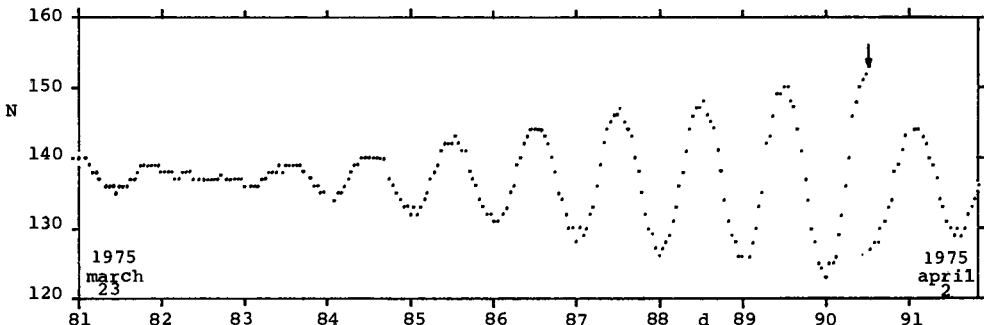


Figure 7. Symphonie I, MV 11 sensor roll east channel telemetry readouts N versus date d (example). The arrow indicates a roll correction on April 1, 12:10.

It appears that these curves shape usually differ from the perfect sinusoid. In spite of that, we have tried to determine the sensor digitalized output N corresponding to the time at which the roll misalignment is nil :

- using the medium values between peak readouts,
- using the readouts at which the half periods have the same duration.

The figure 8 represents typical results which show :

- irregular smooth changes with apparently no relation between the results obtained by the two methods,
- a discrepancy which never exceeds  $\Delta N = 3$ , i.e.  $0.06^\circ$ .

These short term changes have not been fully explained, they may be due for example to small extension local changes in Earth radiance.

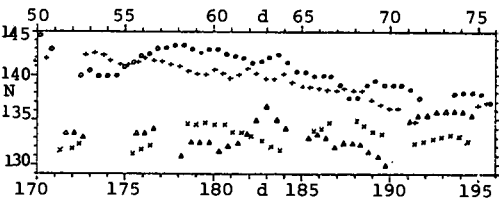


Figure 8. Symphonie I, sensor MV 11. Roll channels apparence medium term zero drift versus date d  
 + x middle of peak values, O Δ equal half period  
 O + roll east, from February 20 to March 16  
 Δ x roll west, from June 20 to July 14  
 (year 1975)

### STA 01 long term zero drift

The same type of curve has been drawn with all data available from a single sensor (MV 11 mounted on Symphonie I), in order to get an idea of the ageing of the sensor and of the actual seasonal Earth radiance effect.

The figure 9 represents this curve which covers more than one year operation, it shows :

- the medium term spread discussed above ;
- a seasonal change which may be evaluated to an amplitude of  $\pm (\delta N = 8)$  or  $\pm 0.16^\circ$  to be compared to the  $\pm 0.18^\circ$  predicted value,
- a  $\delta N = 3$  or  $0.06^\circ$  discrepancy between the zeros of the roll west and roll east channels. This result is in agreement with the one which was observed during the acceptance tests made by the manufacturer on this model.

It is still too soon for determining long term instrumental zero drifts which could be due to thermopile ageing in space or field effect transistor gate current changes.

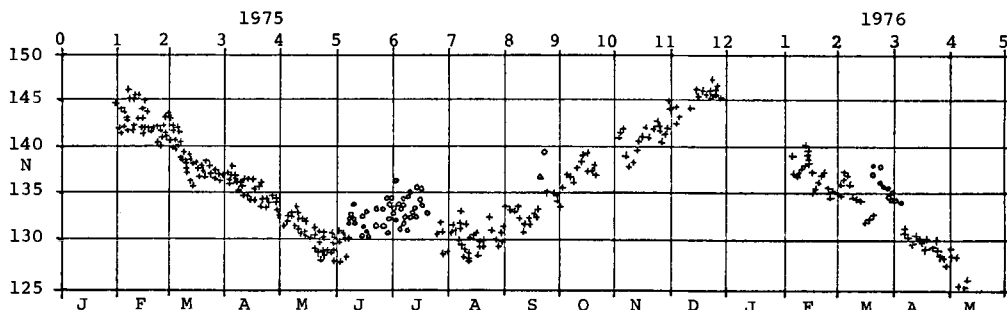


Figure 9. Symphonie I, MV 11 sensor, and Symphonie II, SP 01 sensor, roll channels long term apparent zero drift.

+ SI, MV 11 roll west  
O SI, MV 11 roll east  
Δ SII, SP 01 roll east

#### STA 01 noise

It may be seen from curves, such as figure 7, where unprocessed readouts are used, that the erratic changes do not exceed significantly 1 telemetry point, i.e.  $0.02^\circ$ . A detailed analysis of the noise, which would require the use of a large number of readouts in a short period of time, has not been done ; the estimation made by those who have carried out the data for all numerical calculations on the three sensors tested (MV 11, MV 12 on Symphonie I and SP 01 on Symphonie II) is that the erratic discrepancies with smooth curves are consistent with the  $0.010$  rms noise equivalent misalignment observed at ground on all models (12 models have been manufactured).

#### Temperature constraints on STA 01

According to the requirements, the sensors for the Symphonie spacecraft had to fulfil the zero accuracy requirement :

- all over a  $-20$  to  $+60^\circ\text{C}$  range
- a rate of change between - and  $+0.65^\circ\text{C}/\text{min.}$ , plus the direct effect of Sun eclipse.

Due to the detection of infrared radiation

in d.c mode, these constraints are very severe for this type of equipment : the functional-environmental tests made in simulator proved that the careful design of the optical head won the difficulty.

The figure 10 represents typical curves of the temperature changes occurring in 24-hour periods at the level of the front part of the optical head. The temperature range covers  $-3$  to  $+27^\circ\text{C}$  on this figure, the rate of change reaches  $8^\circ\text{C}/\text{h}$ . The temperature changes are conditioned by the sunrise from solar panels ( $\approx 19$  h GMT), the Sun is just in front at 0:40 GMT, the sunset due to solar panels occurs at about 6.

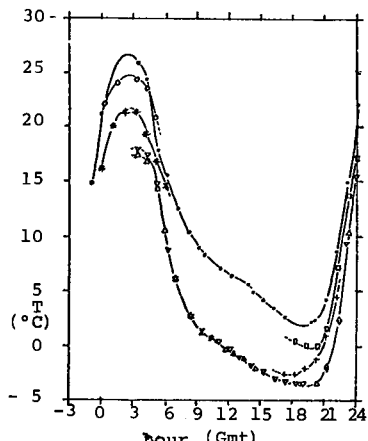


Figure 10. Symphonie I, MV 11 sensor optical head temperature T versus time (in 1975)

• March 2	Δ March 18
○ March 3	+ June 16
□ March 6	X June 17
▽ March 17	

Steeper temperature changes are observed during the periods when the Sun eclipses occur, i.e. between February 25 and April 12, and between September 1st and October 13. Figure 11 is a typical example which exhibits an amplitude of  $10^{\circ}\text{C}$  and peak rate of change from  $-0.63^{\circ}\text{C}/\text{mn}$  to  $+0.60^{\circ}\text{C}/\text{mn}$ .

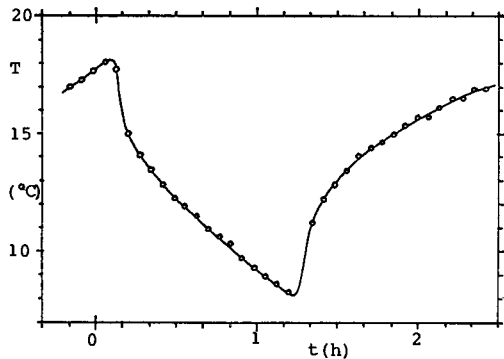


Figure 11. Symphonie II, SP 01 sensor Optical head (front top) Temperature  $T$  versus time  $t$  during the 1975 september 18-19 Sun eclipse.

The slow temperature changes with 24-hours period as represented by figure 10 do not introduce large enough drifts to be recognized from the roll oscillation. The figure 12 contains all available results on eclipse effects. For the SP 01 sensor, the readouts are collected once an hour but, during the eclipse (21:20 to 2:10), the rate is increased at two per 32 seconds (stairs on the curve). The comparison between these stairs and a sinusoidal curve fitted with the out-of-the-eclipse points show an average discrepancy of  $-1$  telemetry point, i.e.  $-0.02^{\circ}$ . The same test in simulator with a 1.5 times stronger temperature excursion led to a  $-0.04^{\circ}$  drift. For the MV 11 sensor, the figure is complicated by a switch which occurs at 1:66 from west to east roll channels : the eclipse occurs between 0:07 and 1:23. There, the eclipse observed on the roll west channel introduces a drift of  $\pm 3$  telemetry points or  $+0.04^{\circ}$  to  $+0.06^{\circ}$  which can be compared to the  $+0.05^{\circ}$  observed with the simulator. The  $\pm 7$  telemetry points shift ( $\pm 0.14^{\circ}$ ) for the same attitude when switching from the west to east channel is in rough agreement with the value observed in the simulator :  $+0.07^{\circ}$  and with the long term behaviour analysis figure (fig. 9).

#### The large misalignment experiment

The telemetered data in normal operation mode did not permit to answer two questions - the discrepancy between the observed annual average value for readout (fig. 9,

$N \leq 137$ ) and the expected one (fig. 6,  $N = 124.3$ ), i.e.  $0.25^{\circ}$ , - the response slope.

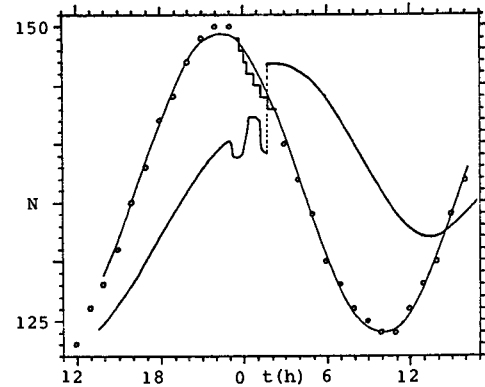


Figure 12. Symphonie I, MV 11 sensor and Symphonie II, SP 01 sensor roll channel outputs observed during September 1975 Sun eclipses. Telemetry readouts  $N$  versus time  $t$ . SP 01 roll east channel, Sept. 18-19, 0 and stairs = experimental data, light curve = sinusoidal best fit with 0.

MV 11 roll west and east channels Sept. 21-22 : bold curve = best fit with experimental data. Switch from west to east at 1:66.

The large misalignment experiment consists in introducing a large tilt angle between the flywheel momentum and the perpendicular to the orbit plane, in order to scan all the linear field of the sensor by the effect of the orbital motion around the Earth : the figure 13 represents the

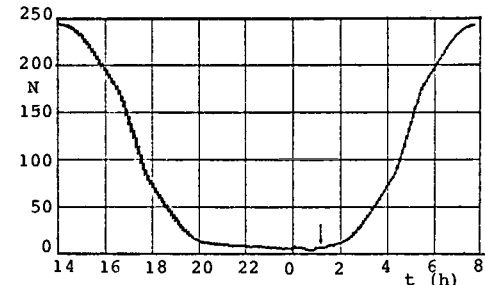


Figure 13. Symphonie I, MV 11 sensor. The large misalignment experiment roll channel output  $N$  versus time  $t$ ; 1975 October 22-23. Arrow indicates time of switch from east to west channel.

MV 11 roll channel output versus time from 1975/10/22 - 14:00 to 1975/10/23 - 8:00. In this period of the year, the seasonal component of the Earth radiance lack of uniformity is very small (fig. 9), thus the response function is expected to be symmetrical (fig. 6). Figure 13 represents the observed roll output versus time function ; the tilt angle between the flywheel momentum and the orbit plane is about 5°, the observed small oscillations with a 3.5 min. period are due to a beat between a nutation (period 38.85 sec.) and the sampling period (32 s).

From these results, the high slope part of the response function is located between  $N = 82$  and  $N = 170$ , values to be compared to the expected ones (fig. 6) :  $N = 85$  and  $N = 163$ .

The difference between the actual ( $N = 126$ ) and expected ( $N = 124.3$ ) values for the centre of the high slope region corresponds to about 0.04° : from this, it may be ascertained that the discrepancy (0.25°) observed between the average annual readout ( $N \approx 137$ ) and the expected value does not come from a sensor electrical drift.

The sensor structure is such as the angular length of the high slope field is certainly very stable : it must correspond to 1.60°. The expected corresponding output change is 3.20 V or  $\delta N = 80$ . A comparison between expected and observed values is given in table 1.

Sensor : MV 11  
Channel : roll east

Table 1

Nominal	Observed	
	simulator	flight 1975/10/22
High slope field (arc degree)	1.60	$m 1.62 \pm 0.08$
$\delta N$	80	$m 88 \pm 2$
Change in output (V)	3.20	$m 3.16$
Slope (V/°)	2.0	$d 2.17 \pm 0.05$

$h$  = hypothesis ;  $d$  = deduced by calculation ;  $m$  = measured.

The 10 % discrepancy may be attributed to various reasons such as an actual Earth radiance temperature higher than the expected one (236.5 K against 232 K), but also a change (increase) in sensor responsivity, gain drift in the telemetry analog to digital converter, ...

#### VI. NEW SODERN EARTH SENSORS

Since the Symphonie sensors design has been frozen, SODERN has participated to more recent programmes for which it has been led to improve the performance of the equipment.

In the field of Earth horizon crossing sensors, the main contribution has been

for Meteosat, for which a new type (STR 03) has been created, in order to fulfil new outer dimensions requirements and complementary functions. Design improvements led to a better accuracy and lower cost. The same type will be used on Intelsat V.

The main improvements have been introduced in the field of static Earth sensors. These SODERN design and development activities have been supported by the European Space Research and Technology Centre (ESTEC) and by the CNES, in the scope of the European Communications Satellite (ECS) and Aerosat projects [3].

A first improved model has been developed (STA 02) the zero accuracy of which is about 3 times better than the STA 01 (Symphonie) one.

Further improvements in the STA 02 design have been introduced in order to fit the Orbital Test Satellite (OTS) requirements : the improved sensor (STA 03) has been qualified and, presently (October 1976), two flight units have been delivered. The OTS first launch is planned for June 1977.

Table 2 summarizes the main characteristics of the three models. It must be said that these characteristics have been fully proven by the functional tests with equipment which simulates simultaneously all the environmental constraints the sensor has to withstand in operation.

These improvements are mostly due :  

- to the use of an active temperature control of the housing in which the detectors are mounted,
- to the use of thermopiles with compensating fields,

but many other tricks have also contributed to these progresses.

The analysis of the operation of these analog sensors shows that, now, the main source of errors remains the local irregular radiance uniformity defects of the Earth limb. This error, as well as the requirements on sensor housing thermal design and detectors responsitivity matching, are proportional to the linear field extension to residual error ratio.

Table 2

SODERN Earth static sensors characteristics  
(geosynchronous orbit operation, pitch and roll channels)

Sensor type	STA 01	STA 02	STA 03
<u>Field</u> (roll or pitch)			
<u>Acquisition</u>			
Overall (°)	14	15	14
Linear (positive slope) (°)	2.6	8	2
<u>Fine pointing</u>			
Linear (°)	2.6	2.4	2.0
High linearity range (°)	0.6	2.1	1.0
<u>Time constant</u> (s)	0.10	0.7	0.7
<u>Accuracy</u>			
Error budget at zero (3 stand. dev.)			
- Noise equivalent misalignment (°)	0.03	0.016	0.005
- Thermal constraints,			
- Temperature range (°C)	-20 to +60	0 to +40	-10 to +40
- Temperature rate of change (°C/h)	35	35	35
(+ Sun eclipse) : overall effect (°)	0.05	0.014	0.007
- Mechanical and optical alignment (with respect to reference mirrors) (°)	0.02	0.01	0.005
- Components ageing (°) for duration (years)	0.015	0.01	0.03
- Earth radiance lack of uniformity			
- assuming symmetrical distrib- ution of deviation with respect to equator			
pitch (°)	0.04	0.013	0.005
roll (°)	0.18	0.080	0.01
- extra term due to deviations with respect to this symmet- rical distribution (°)	0.03	0.03	0.028
<u>Power consumption</u>			
- at minimum temperature (W)	1.4	7.0	7.0
- at maximum temperature (W)	1.4	2.6	2.6
<u>Weight</u> (kg)	1.4	3.5	2.5

In order to increase this ratio and the accuracy at field edge, SODERN has undertaken the development of a digital static Earth sensor, a very promising concept. This work which is supported by CNES is still in progress.

#### VII. CONCLUSIONS

The telemetry readouts analysis of the Symphonie infrared sensors has shown a good agreement between the in-flight performance of these sensors and the predicted and ground measured ones ; these results are particularly important for the static Earth sensor which is the most original and critical equipment.

#### VIII. REFERENCES

- [1] Static horizon sensor. F. Desvignes, F.X. Doittau, H. Bourcier, H. Bacchi. 3èmes Journées d'Optique Spatiale, CNES Marseilles, 21-24 Sept. 1971.
- [2] Les senseurs d'horizon statiques. F. Desvignes, R. Zaharia. La Recherche Spatiale XIII(3), May-June 74, pp. 10-15.
- [3] IR horizon sensors for application satellites. F. Desvignes. European Space Days, ESTEC Noordwijk (Neth.), 17-29 May 1975.
- [4] Optical attitude sensors. A review. F. Desvignes. 7th IFAC Symposium : Automatic Control in Space. Rottach-Egern (F.R. Germany), 17-21 May 1976.
- [5] Earth simulators for IR horizon sensors testing. J. Bunel, F. Desvignes, JJ Hunzinger. 3èmes Journées d'Optique Spatiale, CNES Marseilles, 21-24 Sept. 1971.

# A SURVEY OF U.S. METEOROLOGICAL SATELLITE PROGRAMS

A. Schnapf

RCA Astro-Electronics Division, Princeton, New Jersey

## Abstract

This paper presents an overview of the USA's environmental satellite programs that have been evolving from 1958 to the present and reviews plans for the future meteorological and environmental satellite systems that are scheduled to be placed into service in the late '70's and early '80's. The development of the TIROS family of weather satellites, including TIROS, ESSA, ITOS/NOAA, and the future TIROS-N (the third-generation operational system) is summarized. The contribution of the Nimbus and ATS technology satellites to the development of the operational polar-orbiting and geostationary satellites is discussed. Included are descriptions of both the TIROS and the SMS/GOES future payloads currently under development to assure a continued and orderly growth of these systems into the 1980's. The effectiveness and benefits of the U.S. National Operational Meteorological Satellite System are also reviewed.

## Evolution of the U.S. Meteorological Satellite Programs

### TIROS

The TIROS (Television and Infra-Red Observation Satellite) system and its successor, the ITOS (Improved TIROS Operational System) system, have been the principal global operational meteorological satellite systems for the United States over the past 16 years. These systems matured from a research and development program, marked by the successful mission of TIROS-I in April 1960, to a semi-operational satellite system in which nine additional TIROS satellites were successfully launched in the period from 1960 to 1965. Each TIROS satellite carried a pair of miniature television cameras and in approximately half of the missions a scanning infrared radiometer was included with the instrument complement.

### ESSA

The commitment to provide routine daily worldwide observations without interruption in data was fulfilled by the introduction of the TIROS Operational System (TOS) in February 1966. This system employed a pair of ESSA (Environmental Science Services Administration) satellites, each configured for its specific mission. One of these satellites provided global weather data to the U.S. Department of Commerce's National Environmental Satellite Service at Suitland, Maryland, for processing and forwarding to the major forecasting centers of the United States and to nations overseas. The second satellite provided direct real-time readout of its APT (Automatic Picture Transmission) television pictures to simple stations located around the world. Nine ESSA satellites were successfully launched between 1966 and 1969. One of them, ESSA-8, remained in operation until March 1976. Larger television cameras (2.54-cm vidicon) developed for the Nimbus satellite program were adapted for use on the ESSA series, providing a significant increase in the quality of the cloud cover pictures over that obtained from the earlier TIROS cameras, which used a 1.27-cm vidicon.

### ITOS

The second decade of meteorological satellites was introduced by the successful orbiting on January 23, 1970, of ITOS-1\*, the second-generation operational weather satellite. This satellite dramatically surpassed the capabilities of the predecessor ESSA satellites, moving rapidly closer toward the objectives of the National Operational System. ITOS-1 provided in a single spacecraft the combined capability of two ESSA spacecraft -- the direct readout APT system, and the global stored images of the AVCS system. Additionally, ITOS-1 provided, for the first time, day-and-night radiometric data in real time or stored for later playback. Global observation of the earth's cloud cover was provided every 12 hours with the single ITOS spacecraft as compared to every 24 hours with two of the ESSA satellites. A second ITOS spacecraft, NOAA-1 (ITOS-A), was launched on December 11, 1970.

As the ITOS system evolved to become the ITOS-D system, the flexibility inherent in the spacecraft design permitted a broader and more sophisticated array of environmental sensors to be carried, with only minor changes to the spacecraft. This new sensor complement provided day-and-night imaging by means of Very High Resolution Radiometers (VHRR's) and medium resolution Scanning Radiometers (SR's). It included Vertical Temperature Profile Radiometers (VTPR's) for temperature soundings of the atmosphere and a Solar Proton Monitor (SPM) for measurements of proton and electron flux. Six spacecraft (ITOS-D, E-2, F, G, H, and I) were planned for the ITOS-D series. NOAA-2 (ITOS-D), the first satellite in this series, was successfully launched on October 15, 1972. Three additional satellites of this type (NOAA-3, NOAA-4, and NOAA-5) were placed into orbit in 1973, 1974, and 1976, respectively. Two more (ITOS-I and ITOS-E2) are available for later launching to assure the acquisition of global operational environmental data through 1978. The ITOS system, as it matures, brings closer the realization of the goals of the National Operational System.

The ITOS satellite system evolved from the proven technology of the TIROS and ESSA spacecraft. Many devices and techniques employed on the earlier series were enhanced, and the enhanced versions were used on the ITOS spacecraft. This orderly evolution permitted growth from a 3-axis spin-stabilized spacecraft to a 3-axis stabilized earth-oriented despin platform.

The principal objectives of this growth pattern during the evolution from an R&D satellite to a global operational system were improved performance, the provision for increased quality and more frequent acquisition of meteorological data, and more

\* This spacecraft was originally designated TIROS-M. After being placed into orbit, it was redesignated ITOS-1. Subsequent spacecraft in this series were named NOAA-1, NOAA-2, etc. by the National Oceanic and Atmospheric Administration, the successor to ESSA as operator of the system.

timely dissemination of the processed data to the users. The evolving system had to be compatible with the global ground network of local receiving stations as well as the two principal command-and-data acquisition sites. Finally, the operational system had to be cost-effective and have the capacity for future growth.

#### TIROS-N

The third-generation operational polar-orbiting environmental satellite system, designated TIROS-N, is currently under development and will be placed into operational service in 1978. Eight spacecraft in this series will provide global observational service from 1978 through 1984. This new series will have a new complement of data-gathering instruments. One of these instruments, the Advanced Very High Resolution Radiometer (AVHRR), will increase the amount of radiometric information for more accurate sea-surface temperature mapping and identification of snow and sea ice, in addition to day-and-night imaging in the visible and infrared bands. Other instruments, contained in a subsystem known as the TIROS Operational Vertical Sounder (TOVS), will provide improved vertical sounding of the atmosphere. These instruments are the Basic Sounding Unit (BSU), the Stratospheric Sounding Unit (SSU), and the Microwave Sounding Unit (MSU). A Data Collection System (DCS) will receive environmental data from fixed or moving platforms such as buoys or balloons and retain it for transmission to the ground stations. A Solar Environmental Monitor will be included to measure proton, electron, and alpha particle densities for solar disturbance prediction. The spacecraft bus is similar to that developed under the Defense Meteorological Satellite Program (DMSP)

of the United States Air Force. Figure 1 depicts the evolution of the TIROS-ESSA-ITOS-NOAA family of satellites.

The TIROS-ESSA-ITOS-NOAA spacecraft series was designed and built by the RCA Astro-Electronics Division under the technical management of the National Aeronautics and Space Administration, Goddard Space Flight Center, and procured (operational series) and operated by the U.S. Department of Commerce, National Oceanic and Atmospheric Administration.

#### Nimbus Technology Satellite

The Nimbus satellite program was initiated by the National Aeronautics and Space Administration in the early 1960's to develop an observational system capable of meeting the research and development needs of the nation's atmospheric and earth scientists.

The general objectives of the program were: (1) to develop advanced passive radiometric and spectrometric sensors for daily global surveillance of the earth's atmosphere and thereby provide a data base for long-range weather forecasting; (2) to develop and evaluate new active and passive sensors for sounding the earth's atmosphere and mapping surface characteristics; (3) to develop advanced space technology and ground techniques for meteorological and other earth-observational spacecraft; (4) to develop new techniques and knowledge useful for the exploration of other planetary atmospheres; (5) to participate in global observation programs (World Weather Watch) by expanding daily global weather observation capability; and (6) to provide a supplemental source of operational meteorological data.

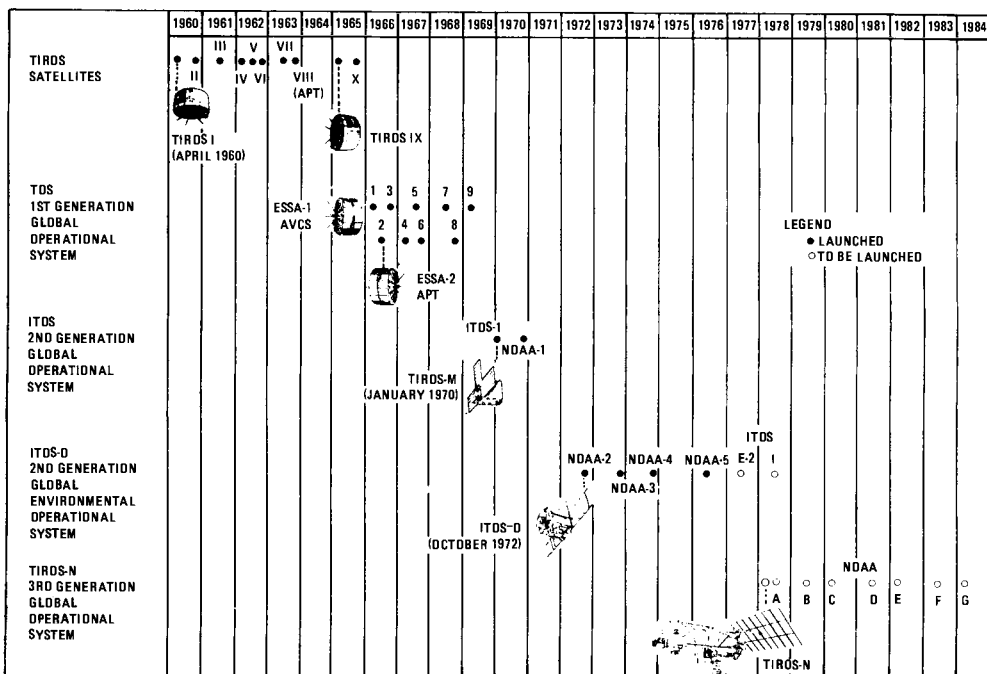


Figure 1. Evolution of TIROS-ESSA-ITOS-NOAA Meteorological Satellites

Originally, Nimbus was conceived as the operational system but was redirected to be (1) the test bed for advanced instruments for the future operational TIROS polar-orbiting satellites and (2) the research system for remote sensing and data collection. The Nimbus spacecraft system was developed under NASA/GSFC management, with the General Electric Company as the spacecraft integration contractor. The project has matured to become the nation's principal satellite program for remote-sensing research. Each new satellite in the Nimbus series has represented significant growth in sophistication, complexity, weight, capability, and performance.

A total of six Nimbus spacecraft was successfully placed into orbit from 1964 through 1975. The final spacecraft, Nimbus G, is scheduled for launch in 1978. This spacecraft will be instrumented with sensors to monitor the atmospheric pollutants. The Nimbus program has provided advanced television cameras, high-resolution radiometers, temperature sounding instruments, microwave sensors, a data collection system, and a data relay experiment. Figure 2 depicts the current Nimbus 6 spacecraft, which was launched on June 12, 1975.

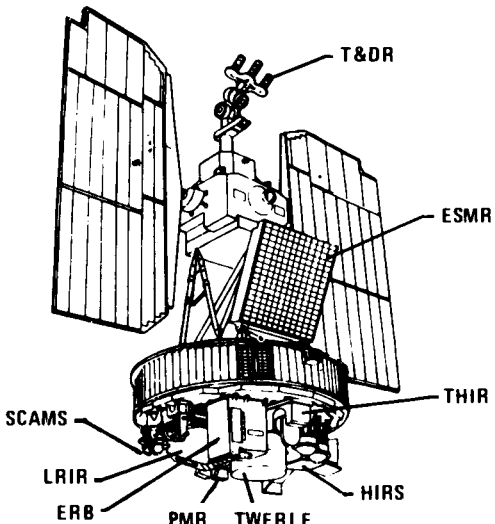


Figure 2. Nimbus 6 Spacecraft

#### ATS, Geostationary Technology Satellite

The increased launch vehicle capabilities available during the middle 1960's permitted satellites to be placed at geostationary altitudes and thus provided atmospheric scientists with a new dimension in observations, namely: continuous observations of almost one-third of the earth's surface. A NASA research program involving geostationary satellites was implemented in the Applications Technology Satellite (ATS) series. Although primarily designed to demonstrate communications satellite technology, several of the ATS series carried high-resolution cameras for atmospheric observation.

On December 7, 1966, ATS-1 was placed into geostationary orbit. One function of this technology satellite was to demonstrate the capability of providing a picture of the western hemisphere every 20

minutes through the use of a spin-scan camera. Useful data was provided from approximately 55°N to 55°S latitude. The ability to receive sequential photographs of the same area improved the possibility of early detection of severe storms and tornadoes, and provided real-time data of cloud and frontal movements.

A second technology satellite, ATS-3, was launched November 1967. This satellite, using a multi-spectral spin-scan camera, returned the first color images of the full earth disc. Copies of these pictures have been used for many applications in addition to meteorology. ATS-1 and ATS-3 were developed by NASA GSFC, with Hughes Aircraft as the prime contractor.

#### SMS/GOES, Operational Geostationary Satellite

The successful application of atmospheric observations from geostationary altitudes led to NASA's development of a satellite designed specifically for that purpose. This satellite, the SMS/GOES, was designed and integrated by the Aeronutronic Ford Corporation's Western Development Laboratories. NASA's prototype Synchronous Meteorological Satellite, SMS-1, was successfully launched in May 1974. Placed over the equator at 45°W longitude, it provided continuous hemispheric coverage. The principal instrument for SMS is a 16-inch aperture telescope for visible and infrared scanning. Built by Hughes Aircraft Company and called VISSR (Visible and Infrared Spin Scan Radiometer), this sensor permits day and night observation of clouds and the determination of temperatures, cloud heights, and wind fields.

The SMS also relays data received from remotely located data collection platforms such as river gauges, ocean buoys, ships, balloons, and aircraft. Its space environmental monitor (consisting of an X-ray sensor, an energetic particle sensor, and a magnetometer) detects unusual solar activity, such as flares, and measures the flow of electron and proton energy and the changes in the geomagnetic field. Observation and forecasting of atmospheric phenomena not specifically related to meteorology are thus possible on an operational basis.

Two additional satellites of the SMS design have been launched: SMS-2 on February 6, 1975 and the first operational version, GOES-1 (Geostationary Operational Environmental Satellite), on October 16, 1975.

After being positioned at 45°W longitude to support the international experiment called GATE off the west coast of Africa during the summer of 1974, SMS-1 was moved to 75°W, from where it provided routine images until replaced by GOES-1. SMS-2 is still in service at 135°W, providing coverage of the Pacific Ocean and the western United States.

#### National Operational Meteorological System

The U.S. National Operational Meteorological System has achieved full capability in the second decade of space operations. The system required, in addition to the polar-orbiting TIROS satellites, continuous viewing of the earth's cloud cover, a data relay for weather facsimile to users, and a capability for data collection from remote sensor platforms. The research and development that produced these current observational systems evolved out of the TIROS, Nimbus, and Advanced Technology Satellites. Table 1

TABLE 1. U.S. ENVIRONMENTAL SATELLITE PROGRAMS

Name	Launched	Period (Min)	Perigee (km)	Apogee (km)	Inclination (Deg)	Remarks
TIROS I	01APR60	99.2	796	867	48.3	1 Wide and 1 narrow camera
TIROS II	23NOV60	98.3	717	837	48.5	2 TV, passive & active IR scan
TIROS III	12JUL61	100.4	854	937	47.8	2 Wide-angle cameras, HB, 2 IR
TIROS IV	08FEB62	100.4	817	972	48.3	2 TV, 2 IR, HB
TIROS V	19JUN62	100.5	680	1119	58.1	2 TV
TIROS VI	18SEP62	98.7	783	822	58.2	2 TV
TIROS VII	19JUN63	97.4	713	743	58.2	2 TV, IR, ion probe, HB
TIROS VIII	21DEC63	99.3	796	878	58.5	1st APT TV direct readout & 1 TV
Nimbus I	28AUG64	98.3	487	1106	98.6	3 AVCS, 1 APT, HRIR "3 axis" stabil.
TIROS IX	22JAN65	119.2	806	2967	96.4	First "wheel"; 2 TV global coverage
TIROS X	02JUL65	100.6	848	957	98.6	Sun synchronous, 2 TV
ESSA 1	03FEB66	100.2	800	965	97.9	1st operational system, 2 TV, FPR
ESSA 2	28FEB66	113.3	1561	1639	101.0	2 APT, global TV coverage
Nimbus II	15MAY66	108.1	1248	1354	100.3	3 AVCS, HRIR, MRIR
ESSA 3	02OCT66	114.5	1593	1709	101.0	2 AVCS, FPR
ATS I	06DEC66	24 hr	41,257	42,447	0.2	Spin scan camera
ESSA 4	26JAN67	113.4	1522	1656	102.0	2 APT
ESSA 5	20APR67	113.5	1556	1635	101.9	2 AVCS, FPR
ATS III	05NOV67	24 hr	41,166	41,222	0.4	Color spin scan camera
ESSA 6	10NOV67	114.8	1622	1713	102.1	2 APT TV
ESSA 7	16AUG68	114.9	1646	1691	101.7	2 AVCS, FPR, S-Band
ESSA 8	15DEC68	114.7	1622	1682	101.8	2 APT TV
ESSA 9	26FEB69	115.3	1637	1730	101.9	2 AVCS, FPR, S-Band
Nimbus III	14APR69	107.3	1232	1302	101.1	SIRS A, IRIS, MRIR, IDCS, MUSE, IRLS
ITOS 1	23JAN70	115.1	1648	1700	102.0	2 APT, 2 AVCS, 2 SR, FPR, 3-axis stabil.
Nimbus IV	15APR70	107.1	1200	1280	99.9	SIRS B, IRIS, SCR, THIR, BUV, FWS, IDCS, IRLS, MUSE
NOAA 1	11DEC70	114.8	1422	1472	102.0	2 APT, 2 AVCS, 2 SR, FPR
NOAA 2	15OCT72	114.9	1451	1458	98.6	2 VHRR, 2 VTPR, 2 SR, SPM
Nimbus 5	11DEC72	107.1	1093	1105	99.9	SCMR, ITPR, NEMS, ESMR, THIR
NOAA 3	06NOV73	116.1	1502	1512	101.9	2 VHRR, 2 VTPR, 2 SR, SPM
SMS 1	17MAY74	1436.4	35,605	35,975	0.6	VISSR, DCS, WEFAK, SEM
NOAA 4	15NOV74	101.6	1447	1461	114.9	2 VHRR, 2 VTPR, 2 SR, SPM
SMS 2	06FEB75	1436.5	35,482	36,103	0.4	VISSR, DCS, WEFAK, SEM
Nimbus 6	12JUN75	107.4	1101	1115	99.9	ERB, ESMR, HIRS, LRIR, T&DR, SCAMS, TWERLE, PMR
GOES 1	16OCT75	1436.2	35,728	35,847	0.8	VISSR, DCS, WEFAK, SEM
NOAA 5	29JUL76	116.2	1504	1518	102.1	2 VHRR, 2 VTPR, 2 SR, SPM

APT - Automatic Picture Transmission TV  
 AVCS - Advance Vidicon Camera System  
 BUV - Backscatter Ultraviolet Spectrometer  
 DCS - Data Collection System  
 ERB - Earth Radiation Budget  
 ESMR - Electronic Scanning Microwave Radiometer  
 FPR - Flat Plate Radiometer  
 FWS - Filter Wedge Spectrometer  
 HB - Heat Budget Instrument  
 HIRS - High Resolution Infrared Sounder  
 HRIR - High Resolution Infrared Radiometer  
 IDCS - Infrared Disk Camera System  
 IRIS - Infrared Interferometer Spectrometer  
 IRSLS - Interrogation, Recording & Location SubSystem  
 ITPR - Infrared Temperature Profile Radiometer  
 LRIR - Limb Radiance Infrared Radiometer  
 MRIR - Medium Resolution Infrared Radiometer  
 MUSE - Monitor of Ultraviolet Solar Energy  
 NEMS - Nimbus E Microwave Spectrometer  
 PMR - Pressure Modulated Radiometer  
 SCAMS - Scanning Microwave Spectrometer  
 SCMR - Scatterometer, Cloud Mapping Radiometer  
 SCR - Selective Chopper Radiometer  
 SEM - Solar Environmental Monitor  
 SIRS - Satellite Infrared Spectrometer  
 SPM - Solar Proton Monitor  
 SR - Scanning Radiometer  
 THIR - Tropical High Resolution Infrared Radiometer  
 TDR - Tracking and Data Relay  
 TWERLE - Tropical Wind Energy Reference Experiment  
 VHRR - Very High Resolution Radiometer  
 VISSR - Visible Infrared Spin-Scan Radiometer  
 VTPR - Vertical Temperature Profile Radiometer  
 WEFAK - Weather Facsimile  
 TV - Television Cameras

summarizes the various satellites contributing to the R&D and operational phases of the U.S. meteorological programs.

#### Operational Systems Descriptions

##### Polar-Orbiting Satellites

###### a. The ITOS System

The ITOS satellites operate in a sun-synchronous near-polar circular orbit at an altitude of 1463 kilometers. During the satellite's 115-minute orbital period, the earth rotates 28.5 degrees. The sensor view angles assure contiguity of coverage between adjacent orbits as well as observation in the orbit track; hence, during the 12.5 orbits daily, global imaging is achieved.

The ITOS/NOAA system illustrated in Figure 3 provides both real-time direct data to APT-type receiving stations throughout the world and stored data to the two U.S.A. CDA\* stations for retransmission to NESS, the National Environmental Satellite Service, at Suitland, Maryland. Three types of real-time data are available worldwide to the local users: SR over the APT VHF link, VHRR over the S-band link, and VTPR over the beacon link. The SR data is provided to local users as 0.52 to 0.73-micrometer visible data and 10.5 to 12.5-micrometer IR data with a resolution of 3.7 and 7.4 km, respectively. The VHRR two-channel scanning radiometer provides data in two spectral regions to the local

user: 0.6 to 0.7-micrometer visible and 10.5 to 12.5-micrometer IR. The resolution at local vertical for the VHRR is 0.9 km, both in the IR and visible channels.

With respect to the stored data, the two-channel SR output is recorded continuously on the SR recorders for playback to the CDA stations and subsequent transmittal to NOAA's NESS at Suitland, Maryland for processing and dissemination. The stored SR data provides global coverage. The stored VHRR data is limited to 9 minutes of recorded data for a selected orbit and played back to a NOAA CDA station.

The VTPR provides sounding of the temperature profile from the surface of the earth to about 30,500 meters. These vertical soundings of the atmosphere are made on a global basis every 12 hours. The data recorded is stored on the SR recorders for later playback to the NOAA CDA station.

The SPM, by means of six solid-state detectors, continuously measures proton and electron flux at orbit altitude.

The ITOS system provides for continuous earth orientation of the spacecraft surface containing the primary sensors, and maintains three-axis orientation of the spacecraft to better than  $\pm 1$  degree at all times. The attitude control subsystem enables the satellite to align and maintain the roll, yaw, and pitch axes so that the earth-facing instrument panel is continuously aligned with the local vertical.

\* Command and Data Acquisition

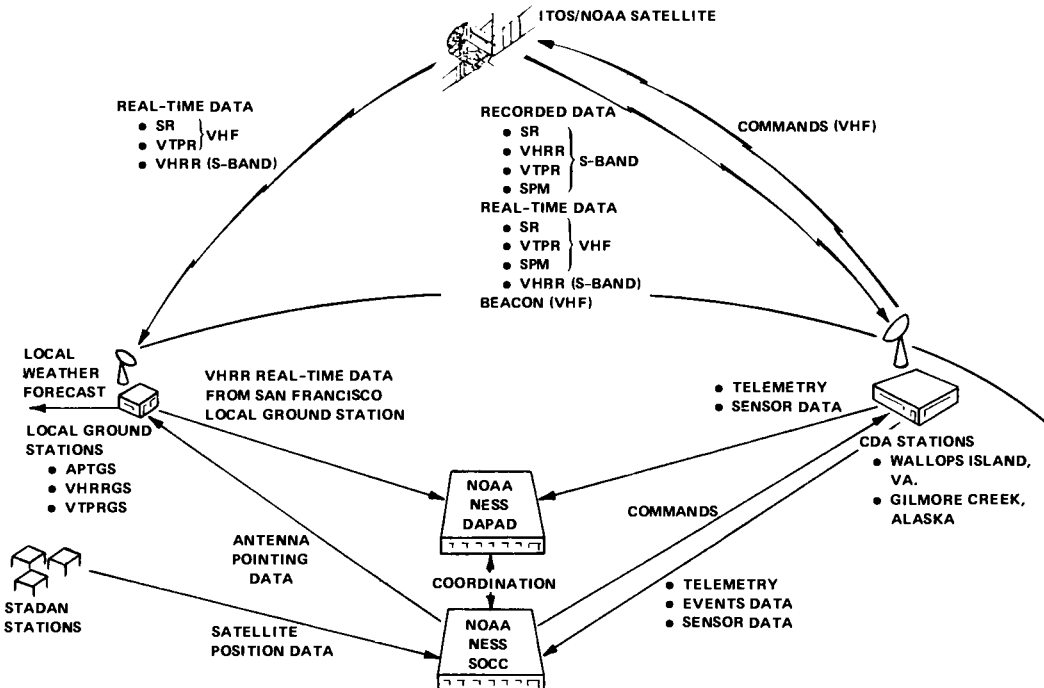


Figure 3. The ITOS/NOAA System

The general physical configuration of the ITOS satellite is shown in Figure 4. The satellite is a rectangular, box-shaped structure, approximately 101.6 cm by 101.6 cm by 121.9 cm long. On the bottom of the structure, a cylindrical transition section attaches to the 94-cm diameter adapter section of the launch vehicle. The ITOS-D series spacecraft weigh approximately 340 kg.

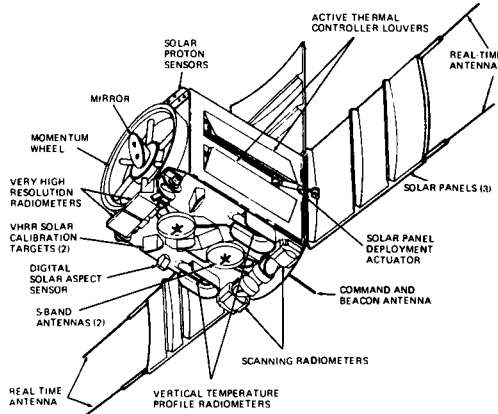


Figure 4. ITOS/NOAA Satellite

#### b. The TIROS-N System

In 1978, NASA and NOAA will introduce TIROS-N, the third-generation operational meteorological polar-orbiting satellite (Figure 5). This spacecraft will be equipped with improved sensors and instruments, and its data collection system will permit it to gather data from balloon and buoy platforms deployed about the planet. The TIROS-N satellite, in conjunction with two GOES satellites, will constitute the U.S.A.'s contribution to the World Weather Watch.

TIROS-N will provide NOAA with the global meteorological data required to support both the operational and the experimental portions of the World Weather Program. The data collected by the satellite's advanced instrument complement will be processed and stored on board for transmission to the central processing facility at Suitland, Maryland, via the CDA station. Data will also be transmitted in real time, at VHF and S-band frequencies, to remote stations distributed about the globe.

The TIROS-N satellite will operate in a near-polar circular sun-synchronous orbit with a nominal altitude of either 833 or 870 km. In the operational configuration, two satellites positioned with a nominal orbit plane separation of 90 degrees will be used.

The instrument payload for TIROS-N consists of:

- (1) The Advanced Very High Resolution Radiometer (AVHRR), a four-channel, cross-track scanning instrument providing image and radiometric data in the visible, near-infrared, and far-infrared portions of the spectrum.

- (2) The TIROS Operational Vertical Sounder (TOVS), a subsystem consisting of:
  - The Basic Sounding Unit (BSU), a 16-channel, step-scanned, far-infrared spectrometer, used to produce tropospheric temperature and moisture profiles.
  - The Stratospheric Sounding Unit (SSU), a 3-channel, pulse-modulated, step-scanned, far-infrared spectrometer, used to produce temperature profiles of the stratosphere.
  - The Microwave Sounding Unit (MSU), a 4-channel, step-scanned spectrometer with response in the 60-GHz O<sub>2</sub> band, used to produce temperature profiles of the atmosphere in the presence of clouds.
- (3) The Data Collection System (DCS), a random-access system for the collection of meteorological data from in-situ platforms, both movable and fixed, such as buoys, balloons, and remote weather stations.
- (4) The Space Environment Monitor (SEM), a multi-detector unit used to monitor solar particulate energies in the vicinity of the satellite.

In addition to this basic complement, a list of growth sensors anticipated for future requirements was used in developing the requirements for the spacecraft's support subsystem. This resulted in a satellite design with inherent growth capabilities for continued orderly evolution.

#### Geostationary Satellites

##### a. SMS/GOES

The capabilities of the SMS/GOES system include day-and-night earth imaging, retransmission of imaged data, data collection and relay from terrestrial data collection platforms, and space environment monitoring. However, the geostationary satellite's most important contribution may be its ability to show, in virtual real time, destructive natural events at several scales of size and motion.

The SMS/GOES system, as shown in Figure 6, consists of the spacecraft, ground stations, central data distribution system, and data collection platforms. The primary ground station is the Command and Data Acquisition (CDA) station located at Wallops Island, Virginia. The National Environmental Satellite Service (NESS) complex near Washington, DC receives the retransmitted VISSR data from the spacecraft and relays it to the Central Data Distribution Facility. Here it is processed digitally or "sectorized" and routed via high-quality telephone lines to regional stations for their own use and for further dissemination to Weather Service Forecast Offices located throughout the country.

The SMS/GOES spacecraft are launched from Cape Canaveral, Florida, by a three-stage Delta launch vehicle and are placed in circular orbits at an altitude of 35,800 km and with an orbit inclination of approximately 1.0 degree. At this altitude, the satellite remains continuously above the same point on earth and thus is termed geostationary, geosynchronous, or earth-synchronous.

Figure 7 shows the image coverage area and communications range of two GOES satellites stationed at

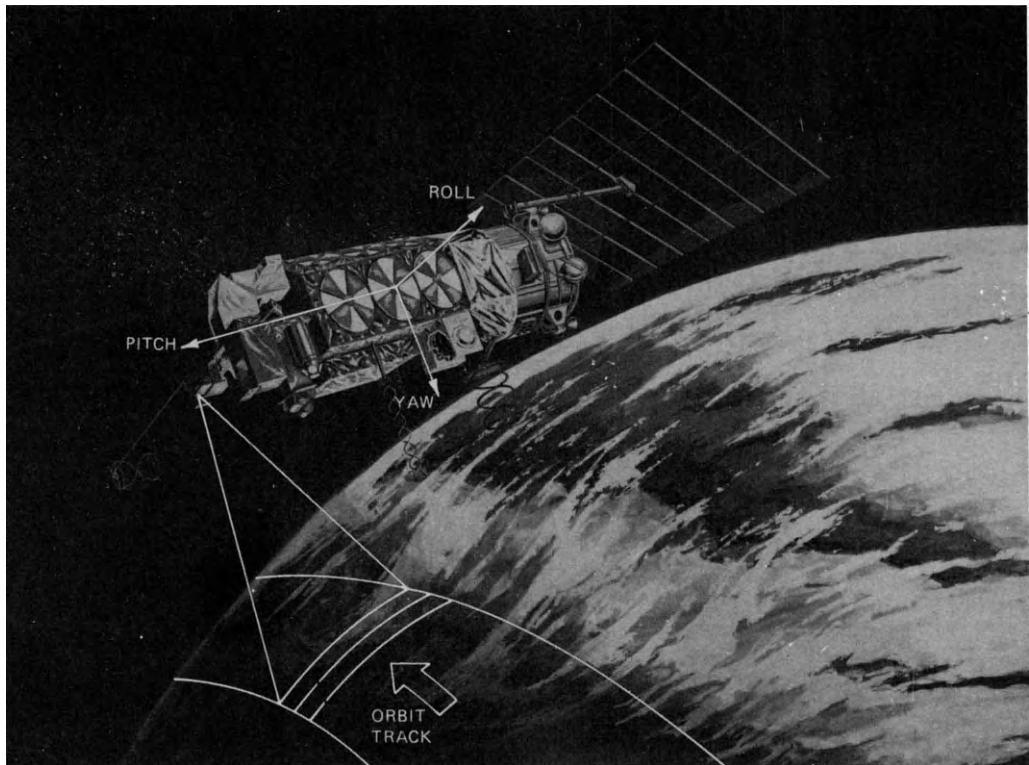


Figure 5. TIROS-N Environmental Operational Satellite

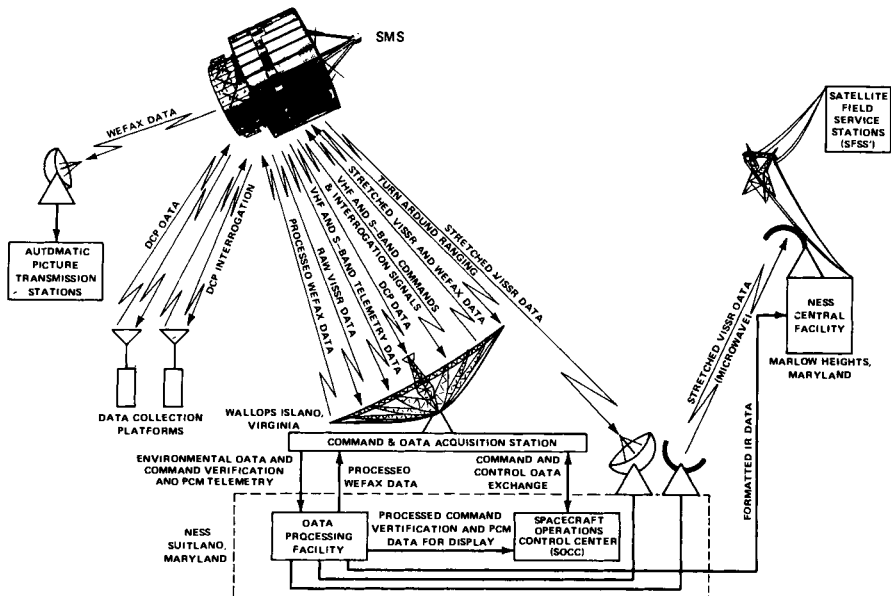


Figure 6. SMS/GOES System

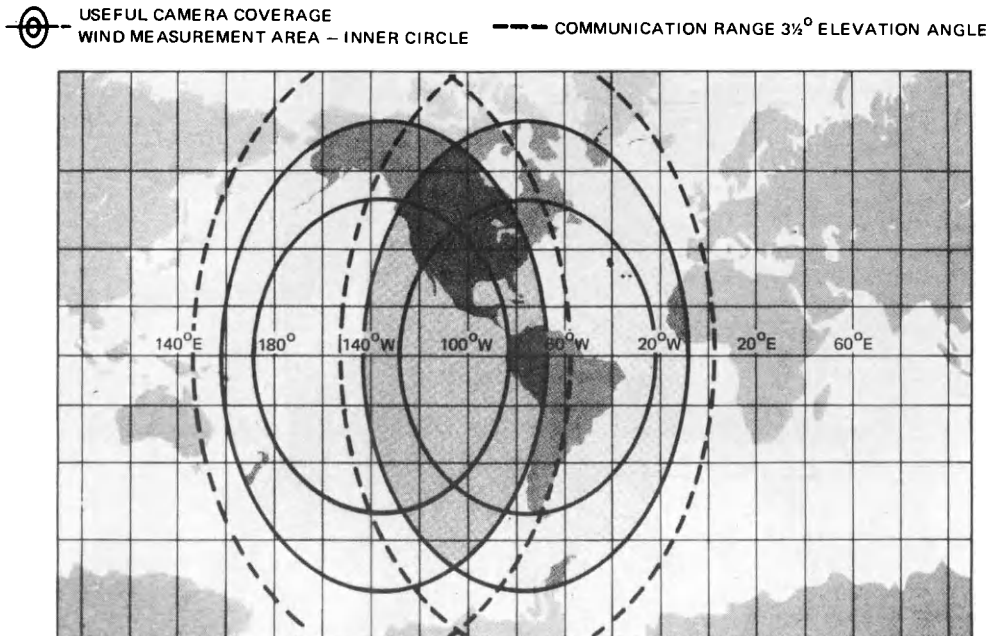


Figure 7. SMS/GOES Coverage Area (Two satellites: one located at 135°W longitude; the other at 75°W longitude).

approximately 75°W longitude and 135°W longitude. From these vantage points, they view all of North and South America and the adjacent ocean areas.

The SMS/GOES spacecraft shown in Figure 8 consists of a Visible and Infrared Spin-Scan Radiometer (VISSR) for high-resolution visible imagery and lower-resolution infrared imagery, a communications subsystem consisting of both S-band and UHF systems for data collection and relay, and a Space Environment Monitoring (SEM) subsystem. The spacecraft is spin-stabilized for proper earth imaging by an attitude control subsystem that aligns the spacecraft's spin axis parallel to the earth's polar axis and thus perpendicular to the orbital plane. The satellite rotates at 100 revolutions per minute, and the VISSR scanning mirror scans the earth for about one-twentieth of each complete 360-degree rotation. The VISSR scans from west to east in eight identical visible channels and two redundant infrared channels. While the spacecraft is completing its revolution, the mirror moves to the next southward step and acquires and transmits data again when it is looking at the earth. The radiometer accomplishes the 1821 scan steps required to provide a high-resolution image of nearly one quarter of the earth's surface within 18.2 minutes. The resulting visible images (0.55- to 0.70-micrometer band) contain 14,568 lines and have a resolution of nearly 0.8 km. The infrared images (10.5- to 12.6-micrometer band) have a total of 1821 lines with a 6.4-km resolution.

The spacecraft communications subsystem utilizes various S-band, UHF and VHF carrier frequencies for (1) the transmission of wideband VISSR video data to the CDA station; (2) the relay of reduced bandwidth

or "stretched" VISSR data from the CDA station, via spacecraft, to smaller data receiving stations; and (3) the transmission of weather facsimile (WEFAX) data to local ground stations equipped to receive S-band automatic picture-taking (APT) data. The WEFAX data is centrally produced on the NOAA computers in Suitland, Maryland, and then transmitted to the spacecraft from the CDA station.

The GOES data collection system collects and distributes environmental data acquired by remotely located, attended and unattended data collection platforms located on land, at sea, or in the atmosphere. The data collection platforms are environmental sensing devices with radio transmission and reception capabilities for relaying data as required. These platforms include instrumented buoys, river gauges, automatic weather stations, seismic and tsunami stations, and manned ships. Some examples of their uses are: (1) fixed stations in remote land areas send information on earthquakes, wind direction and velocity, humidity, and amount of rainfall; (2) river platforms measure currents, water levels, and temperatures; (3) marine platforms (either fixed or floating) measure tides, water and air temperatures, and provide tsunami warnings.

Many photographic and computer-generated products are derived from SMS/GOES images. One that is unique to the geostationary satellite data is derived from the ability to generate time-lapse movies from a series of registered GOES images (visible or infrared) of the full earth disc. By the use of both manual and computer techniques, selected cloud tracers are tracked in successive GOES images to determine wind speeds and directions.

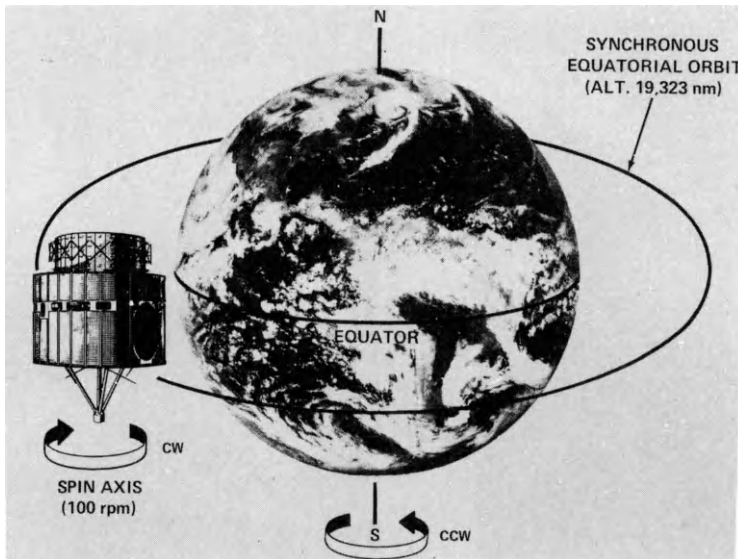


Figure 8. SMS/GOES Satellite in Orbit

b. GOES-D, E, and F

Three additional GOES satellites of more advanced design are planned. These satellites, GOES-D, E, and F, will employ a Visible-Infrared Spin-Scan Radiometer Atmospheric Sounder (VAS) to obtain simultaneous imaging in the visible and infrared portions of the spectrum, with a resolution of 0.9 km in the visible band and a resolution of 6.9 km in the infrared. Additionally, the VAS will obtain radiometric data in the earth's atmosphere water vapor and CO<sub>2</sub> absorption band and will thus provide the capability for determining the three-dimensional structure of the atmosphere with respect to temperature and humidity. The VAS, an advanced version of the VISSR developed for worldwide geostationary meteorological satellite systems, will:

- Preserve the capability of the SMS/GOES VISSR, i.e., simultaneous imaging in the visible and infrared portions of the spectrum, with a resolution of 0.9 km in the visible band and a resolution of 6.9 km in the infrared.
- Provide multispectral imaging simultaneously in five spectral bands, one visible and four selectable from the 12 infrared bands.
- Provide a dwell sounding mode from which moisture, temperature, and the vertical structure of the atmosphere may be determined.

The VAS represents an extension of the original VISSR imaging capability and includes additional thermal bands for the determination of atmospheric temperature at various altitude layers by spectral selection in the CO<sub>2</sub> absorption bands. Water content is also determined at several altitudes in the H<sub>2</sub>O absorption bands. In addition, cloud and earth-surface temperatures are measured in the 3.7-micrometer band for improved temperature values. Parameter flexibility, including spectral band selection,

spatial resolution, signal-to-noise ratio and geographic location, are incorporated into the sounding or multispectral imaging modes to provide measurements which best meet the needs of the research scientist. The capabilities of VAS will enable extensive research in atmospheric science from the geostationary vantage point.

Benefits

Over the past 16 years the quantity, quality, and reliability of satellite coverage has improved. Since 1966 the entire earth has been photographed at least once daily on a continuous basis. The photographs are not only used in real-time operations, but are also placed in archives from which they can be retrieved for use in research case studies. From its inception as a new research tool with its potential not fully realized, satellite data has steadily increased in importance. It is now being used by meteorologists and environmental scientists on a widespread basis in routine operations throughout the world, and is considered almost indispensable for analyses and short-range forecasts.

The meteorological data from around the earth is received at the National Environmental Satellite Service (NESS) in Washington, transformed into a broad variety of products and distributed throughout the world. Selected images from several satellites currently in use are shown in Figures 9 through 12. Although the processing necessary to reduce these images to the printed page results in the loss of detail, their scope and potential usefulness are readily apparent.

The satellite information has proven extremely useful in two broad types of situations. First, there are extensive areas of the earth from which conventional reports are sparse, namely: the oceanic regions of the northern and southern hemispheres, deserts, and the polar regions. Satellite information fills these voids by locating the large-scale

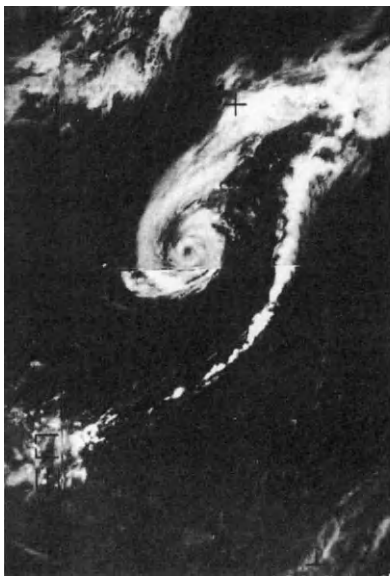


Figure 9. Tropical Storm Amy as Imaged by ESSA-8 APT Satellite on July 2, 1975 (Satellite in orbit more than 7½ years)

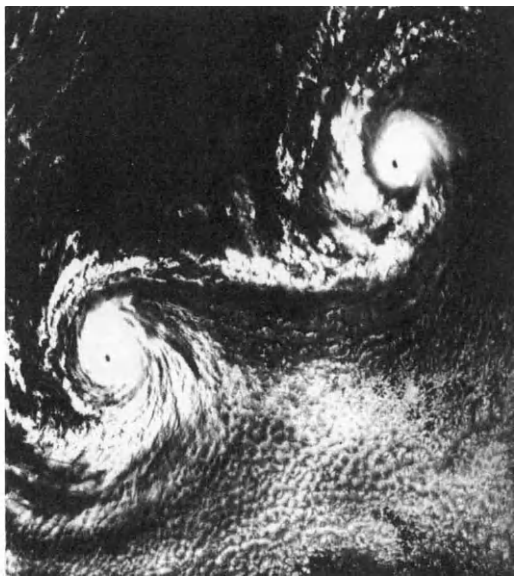


Figure 10. Hurricanes Ione and Kirsten, August 24, 1974; NOAA-3 VHRR Visible Spectrum Image



Figure 11. SMS-2 VISSR Visible-Spectrum Image of Western Hemisphere



Figure 12. Hurricane Candice (40.5°N by 59.0°W), August 21, 1976; NOAA-5 VHRR Infrared Image

features depicted by the cloud formations. These features include storm systems, fronts, upper level troughs and ridges, jet streams, fog, stratus, sea ice conditions, area of snow cover, and to some extent upper level wind directions and speeds. The satellite data is also used in conjunction with other data to provide quantitative heights of constant pressure surfaces as inputs to conventional analyses.

The second type of situation to which satellite data is usefully applied is the location and tracking of hurricanes, typhoons, and tropical storms. Coastal and island stations with little or no adjacent conventional weather information can make maximum use of APT data and the processed stored data from facsimile circuits. The satellite data provides information on the presence and position of frontal patterns, storms, and general cloud cover.

Satellite information has had a great impact on the routine surveillance and tracking of tropical storms. Since 1966, coverage of the world by the TIROS series satellites has been complete on a daily basis, and no tropical storm has escaped detection and daily tracking during the ensuing years. Storms are usually spotted in their developing stages, often beyond the normal range of weather reconnaissance aircraft from their bases of operation. The APT, direct readout infrared (DRIR), and processed stored visible and infrared data are available at most offices with tropical storm forecast responsibilities. All the tropical regions of the world are completely monitored through satellite data received by the National Environmental Satellite Service.

The infrared data from the ITOS/NOAA satellites can be used to produce charts showing the sea-surface temperature over a larger area and with more frequency than is possible from any other source. This information is useful to shipping interests and the fishing industry, and is a vital input to meteorological forecasts.

Satellite pictures display the extent and character of ice fields in the Arctic and Antarctic Seas, and on the Great Lakes, with a frequency and geographic coverage never before approached.

Worldwide atmospheric temperature soundings provided by the satellites result in more complete and accurate analyses for use in weather forecasts. Soundings by satellite provide coverage over oceans and remote areas not covered by conventional sounding instruments. Individual soundings from satellites aid in the interpretation of satellite picture data

by providing correlation at specific geographical locations. The continual soundings enable the location of atmospheric temperature gradients for use in studying atmospheric phenomena.

#### Future Expectations

The TIROS-ESSA-ITOS-NOAA polar-orbiting meteorological satellites have been the mainstay of the U.S. meteorological satellite programs; the forthcoming TIROS-N satellite series will assume this mission. The TIROS-ESSA-ITOS-NOAA family of satellites has fulfilled U.S.A. operational requirements by providing a reliable in-orbit system that transmits routine observations on a timely basis without interruption in service. Its evolutionary design has permitted a cost-effective approach in achieving program objectives and provided a gradual and effective improvement in service with existing worldwide receiving stations. With the advent of TIROS-N (the third-generation operational system), further improvements in observation and in the processing and dissemination of data will provide the polar-orbiting data required by the long-term goals of the National Operational System.

The complementary geostationary environmental satellites will be improved by the addition of an atmospheric sounding capability on the GOES-D, E, and F satellites. The soundings obtained will be used in investigations to identify conditions under which short-term severe storms are generated. Real-time temperature and thermal gradient data is expected to make significant contributions to the meteorologist's ability to understand these meso-scale phenomena and, in time, improve his ability to forecast the areas where severe thunderstorms and tornadoes are likely to occur.

As part of the international cooperation and participation within the World Meteorological Organization, Japan, the European Space Agency (ESA), and the U.S.S.R. are planning to launch their own geostationary environmental satellites within this decade. All except the U.S.S.R. satellite will be launched by the U.S., each aboard a NASA Delta launch vehicle from Cape Canaveral, Florida. These satellites will be spaced about 70 degrees apart around the equator. Japan plans to station their satellite over the western Pacific, ESA plans one over the eastern Atlantic, and the Soviet Union proposes to place one over the Indian Ocean. The polar-orbiting TIROS-N series will provide the global data, particularly filling in the data for the far polar regions.

# FUTURE ORBITAL ACTIVE IMAGING MICROWAVE EXPERIMENTS

J. W. Rouse, Jr.

*Texas A & M University, College Station, Texas*

## Abstract

Several major orbital active microwave experiments are now under study by the National Aeronautics and Space Administration. One of these, Seasat, has been approved for launch in 1978. Another, the TDS Soil Moisture System, may be launched during Shuttle Mission in 1981. The most advanced of these, the Spaceborne Imaging Radar (SIR) system, should be operational on the Shuttle after 1982. These systems activities demonstrate a new emphasis in earth observations which is attempting to capitalize on the unique advantages of active microwave remote sensing. Several studies show that multichannel active microwave image data rival multispectral scanner data for information value in several application areas.

## Introduction

Since the field of remote sensing began taking shape in 1964, the emphasis has been on the use of visible region sensors. From the simple camera to the sophisticated multispectral scanner, these sensors have dominated the attention of researchers in the field. Throughout these twelve years, however, active microwave imaging sensors have steadily progressed in importance until today their all-weather, day or night operational capability is viewed as the necessary next step in capitalizing

on the unique advantage of orbital earth resource monitoring. This paper outlines the reasons for the emergence of microwave sensors to the forefront of attention in the remote sensing field, and reviews the NASA program plans for incorporating this technology into future space missions.

## Application of Active Microwave Imaging Sensors

In 1974 the first comprehensive effort was made to examine the applications potential of active microwave sensors for earth observations. The 500 page text of the Active Microwave Workshop (1) is a thorough summary and analysis of the ten years of research and development in this area of remote sensing. The Workshop dealt with three major topic areas: land applications, ocean applications, and atmospheric applications. Table 1 is a listing of the applications identified in the land applications study.

A major effort of the active microwave working group was devoted to identifying the unique capability of active microwave sensors to establish clearly the advantages offered by these sensing techniques. The following list delineates the applications by discipline area, for which active microwave sensors provide the most practical, the most advantageous, or the exclusive means of obtaining the needed information.

Table 1 - Earth Applications of Active Microwave Sensors (1)

### Mineral resources and geologic applications:

- a. Landform identification and terrain analysis
- b. Mineral deposit location
- c. Petroleum exploration
- d. Ground water exploration
- e. Crustal motion
- f. Civil works
  - (1) Major construction site monitoring
  - (2) Construction material location

### Water resources applications:

- a. Lake ice monitoring
- b. Flood forecasting and monitoring
- c. Lake level determination and eutrophication
- d. Coastal wetlands mapping
- e. Water pollution monitoring
- f. Frozen water hydrologic observations
  - (1) Snowfields
  - (2) Glaciers
  - (3) Permafrost

### Agriculture, forestry, range, and soil applications:

- a. Crop identification
- b. Crop cover and condition
- c. Range inventory and biomass assessment
- d. Soil types and properties mapping
- e. Soil moisture determination
  - (1) Watershed management
  - (2) Crop yield prediction

### Land use, urban, regulatory, and cartographic applications:

- a. Disaster Monitoring
  - (1) Floodwater and coastal inundation
  - (2) Fire
  - (3) Wind damage
  - (4) Snowfall damage
  - (5) Earthquake damage
  - (6) Landslides
- b. Land use monitoring
  - (1) Existing land use
  - (2) Transportation networks
  - (3) Location of engineering materials
- c. Regulatory monitoring--oil spills
- d. Cartography

1. Earth/land:
  - a. Determine soil moisture for crop yield prediction
  - b. Map snowfields and glaciers
  - c. Monitor lake ice
  - d. Assess disasters for assistance and recovery
  - e. Perform landform identification and terrain analysis
  - f. Perform flood forecasting and watershed management
  
2. Oceans:
  - a. Determine sea state and surface winds
  - b. Map sea ice and iceberg locations
  - c. Monitor coastal processes
  - d. Monitor wave buildup in storm areas
  - e. Measure undulations of the geoid
  
3. Atmosphere:
  - a. Map freeze level height in rain clouds
  - b. Map rain intensity
  - c. Measure liquid water content
  - d. Map horizontal motion within cloud systems
  - e. Measure surface winds over the oceans
  - f. Map polar sea ice cover
  - g. Monitor maximum echo heights of storms

This listing contains an important message: there are several fundamental measurements required to achieve effective monitoring which can be obtained only with microwave sensors.

#### Status of Active Microwave Remote Sensing

The status of active microwave remote sensing can be summarized by noting that the oceanographic applications of altimeters and scatterometers are well established as a result of Skylab, but that few of the land and atmospheric applications have been satisfactorily verified. Of particular concern is the fact that imaging radar, which appears to offer the greatest potential, has not been tested in space and much of the aircraft data are of limited utility.

The Skylab missions supported the orbital testing of an altimeter for measurement of the geoid and a scatterometer for measurements of surface winds over the ocean. Both instruments provided data which confirmed the intended applications. The success of these experiments set the stage for the Seasat mission scheduled for launch in 1978.

Unfortunately, similar successes cannot be cited for the land and atmospheric applications. These applications have been studied using ground-based and aircraft sensors with varying degrees of success. With limited exceptions, these applications require two-dimensional image format data. Indeed, the precipitation mapping application requires three-dimensional measurements. The traditional PPI display of ground-based weather radar is a crude example of the type information required. In general, the main problem for both land and atmospheric applications, most particularly for land applications, is that of producing high-quality radar images.

There are available airborne imaging radar systems capable of producing high-quality images. Data from these sensors have been used to show the potential of space radar for ocean wave monitoring,

geologic mapping, land use delineations, surface water mapping, flood monitoring, and several other applications where "pictures" are the basic data need. However, none of these sensors are calibrated. Therefore, it is not possible at this time to acquire image data of use in applications requiring an accurate measure of return signal amplitudes. Such applications include soil moisture monitoring, crop identification, vegetation condition monitoring, freeze/thaw line monitoring, snow field equivalent moisture mapping, precipitation monitoring, etc.

The current background of information on the potential of active microwave sensors has been obtained from research projects employing ground-based sensors on experimental aircraft instruments. These have provided encouraging results, but confirmation of these applications must await the availability of calibrated, orbital imaging radar sensors.

#### The First Step: Seasat

The Seasat system to be launched in 1978 is a multiple sensor mission designed to monitor specific global characteristics of the oceans. It will carry three active microwave sensors: a precision altimeter, a surface windfield scatterometer, and a high-resolution imaging radar. The altimeter is expected to record average surface height variations over the ocean to within  $\pm 10$  cm. The scatterometer should be capable of surface wind velocity measurements accurate to within  $\pm 2$  m/sec and within a directional accuracy of  $\pm 10^\circ$ . The capability of these instruments is well understood and the utility of the measurements is well established.

The Seasat imaging radar is a synthetic aperture radar (SAR) and will be the first such device to be orbited for civilian uses. This sensor produces a 100 km wide image swath at a spatial resolution of 25 m. The images will be processed to a film and CECT format compatible with Landsat MSS data.

There are three features of the Seasat SAR system that limit its use: 1) the data are available on a real-time transmission basis only; 2) the telemetry bandwidth restricts the available radar signal dynamic range to a marginal 20 dB; and, 3) it is not calibrated. The first restriction means that data collection is possible only when the satellite is in sight of a suitable ground receiving station. This limits the total data available in any 24 hour period to less than 60 minutes. This problem is further compounded by the lack of adequate ground-data processing capability to handle these data. It is now estimated that during the first year of operation only 240 ten minute image records will be available. The second restriction means that the full dynamic range of land targets cannot be recorded. The calibration problem is restrictive, but since long-term system gain stability of  $\pm .5$  dB is expected, this issue may not be a severe limitation on the utility of the measurements. These limitations were the compromises required to fit the SAR within the size, weight, and power constants of the Seasat vehicle. Even so, this imaging radar is a significant advance and these data will prove invaluable in experiments to determine the value of orbital imaging radar for a wide range of ocean and land applications.

### Future Programs

The Seasat program is an approved NASA effort with a firm schedule. It is the only element of the NASA active microwave program plan with this distinction. There are several mission and support activities in various stages of planning, but all are still tentative. The most significant of the planned future program elements are:

- a. Shuttle OFT-2 Geology Mission,
- b. Shuttle TDS Hydrology Mission,
- c. Shuttle Multichannel Spaceborne Imaging Radar, and
- d. Shuttle Meteorological Radar

The recent acceleration of the microwave program planning is due to a large extent to the coming of Shuttle. The large payload capability of this vehicle coupled with the short sortie operational mode of the Shuttle make imaging radar systems operation both feasible and desirable.

The Shuttle OFT-2 (Orbital Flight Test #2) Geology Mission would employ a modified Seasat L-band SAR to obtain 55km swath width images at 40m spatial resolution. The images would be recorded at an incident angle of greater than 50° from nadir to obtain the low relief enhancement desired by mineral and petroleum exploration geologists. The OFT-2 mission is a 3-4 day duration shallow orbit (approximately ±30° from the equator) mission. The geology experiment would include radar and stereo camera coverage of select regions within the flight profile. It is a proof-of-concept mission. The sensors would be returned and refurbished for use on subsequent Shuttle flights. The Shuttle OFT-2 flight is planned for late 1979 or early 1980.

The Shuttle TDS Hydrology Mission would involve an L or C-band SAR mounted on the free-flying TDS (Technology Demonstration Satellite) for a 6-9 month flight. The orbit would permit coverage to about 72° north latitude. The TDS SAR may be an adaptation of the OFT-2 SAR; in fact, one plan calls for the use of the same hardware--a feat possible only in the Shuttle era. The TDS SAR would obtain 150km swath images at 100m resolution centered at about 10° from the nadir. The primary objective is to monitor hydrologic parameters such as surface water, flooding, ice, and soil moisture. The TDS mission is planned for the Shuttle OFT-5 flight in 1980 or early 1981.

The multichannel Spaceborne Imaging Radar (SIR) is the most sophisticated of the imaging radar systems being planned for future missions. This is the only one of these systems that would be calibrated. In addition, it would offer for the first time in orbit the capability to record images at wavelengths shorter than 3cm, which is especially significant for agricultural applications. Further, the SIR provides the only dual-polarization capability.

The SIR is a dual-frequency, dual-polarization, multiple incident angle imaging radar capable of 100km swath width at 25m spatial resolution. The on-board recording and subsequent digital processing assures retention of a large dynamic range (50dB) and high signal-to-noise ratio. This and the all-important calibration feature will move

orbital imaging radar out of the "picture-taking" mode, and finally make possible precision radar measurements on a two-dimensional scale.

The SIR is tentatively scheduled to begin operation on the Shuttle in 1982. It would provide an engineering and applications test bed during repeated flights on subsequent Shuttle missions. It is designed to address a wide range of land and ocean applications and is sufficiently flexible to permit modification of the system parameters as required in future applications studies.

The Shuttle Meteorological Radar (SMR) utilizes a unique antenna concept to achieve global measurements of precipitation. The SMR would provide a three-dimensional map of precipitation in 1km cells for a region 400km wide and 20km high along a path of the Shuttle. The SMR employs a large antenna to obtain multiple 1km diameter (on the surface) conical beams which move in a "push broom" pattern slightly forward of the Shuttle ground path. The vertical 1km high cells are formed by multiple range gates which slice the beam into twenty increments above the surface. The proposed system is a single frequency (X-band) unit which relies on established precipitation models to determine rain rates. A dual-frequency non-scanning version of this radar is presently being built for aircraft operations. The SMR is tentatively scheduled for launch about 1985.

### Conclusion

This brief overview to the NASA active microwave program plans has concentrated on the major orbital systems now under investigation. Behind these missions are a wide variety of aircraft, ground-based, and modeling research projects currently being supported or planned by NASA. These activities combine to establish a significant program effort and a notable acceleration of the microwave sensor development.

The goal is to achieve all-weather, day or night sensing capability to significantly improve the effectiveness of monitoring earth resources.

### References

1. R. E. Matthews (editor). Active Microwave Workshop Report. NASA SP-376, 1975.

# MULTIBAND SPACE IMAGERY—A CONTRIBUTION TO THE STUDY OF OCEANIC DYNAMICS\*

V. I. Kravtsova

*Moscow State University, Moscow, USSR*

It is quite evident when studying oceanic dynamics that the basic method should be a regular survey taken at various bands; to determine dynamics of transparency and colour (including turbidity, suspension content, plankton, etc.)—in the visible spectrum; to determine temperature and currents dynamics—in the heat infrared spectrum; to determine salinity and confusion dynamics—in the microwave spectrum. Though singular surveys supply data to study many dynamics characteristics, the multiband survey taken simultaneously in certain ranges (in comparison with black-and-white photographs) significantly expands the sphere of activity resulting from the experience perceived in the course of work with the photographs taken from the "Soyuz-12" spacecraft: they turned out to be especially effective in studying shallow-water areas and coastal regions.

Efficiency of the multiband photographs implementation to study water sites is based on two principles: (a) use of differences in spectral brightness of various coasts, surfaces, and submerged objects; (b) use of differences at a depth of penetration into water masses of light beams of various spectral bands.

Utilization of a "spectral signature" is essential, in the first place, in interpreting submerged objects. For instance, when the photographs of the northeastern sites of the Caspian Sea were being interpreted, it was realized that the use of images in the green and red spectral ranges permits the discrimination of underwater vegetation images in shallow waters from deep-water sea areas on space photographs (these objects are practically indistinguishable on ordinary panchromatic materials). Naturally, this fact is essential when dynamics of submerged vegetation are being studied.

The method of interpreting the underwater vegetation contours of northeastern Caspian subwater elevation of the Tyuleniy Archipelago among the Mangyshlak and Byzachi Peninsulas (Fig. 1). Survey of this area was accomplished from the "Soyuz-12" spacecraft in September 1973 by a multiband camera in the six spectral bands with the spectral sensitivity maximum: 0.47; 0.54; 0.58; 0.64; 0.66; 0.68 mkm (Khodarev *et al.*, 1975).

The dark image tone on the photographs in 0.64–0.68 mkm bands, usually corresponding to greater depths, is also found in the whole region around the Tyuleniy Archipelago Islands with depths of 1.5–3 m. The matter becomes clearer in an analysis of photographs taken in the blue and green bands with the

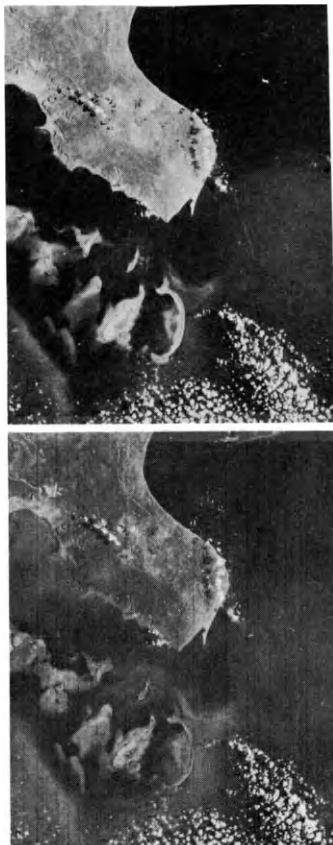


Fig. 1. Delineation of the northeastern Caspian region on the imagery from the "Soyuz-12" spacecraft, taken in the green (max. 0.54 mkm) I and red (max. 0.66 mkm) spectral bands.

sensitivity maximum within the range of 0.47 and 0.54 mkm. The sea deepwater sites in these bands are represented by an even gray tone and a section between the Tyuleniy Islands and along the coastline of the Byzachi Peninsula—by a more intense dark-gray tone. This dark-gray contour possesses rather clear boundaries. Its figured boundary is

\*Publication and distribution rights are reserved by the International Astronautic Federation, 250 Rue Saint-Jacques, 75005 Paris, France.

well distinguished, while inside the contour in separate sites, for example, between the Kulala and Morskoy Islands, the patched image structure is revealed which testifies that in this case we do not deal with deepwater images. This contour is interpreted as bottom vegetation, settling on the rocks of geological structure proceeding from the Byzachi Peninsula to the sea. It is interesting that bottom vegetation is definitely associated with certain depths—it does not spread deeper than 3 m and sandy shoals with depths of less than 1.5 m are free of it.

We shall note that the bottom vegetation image has a specific brownish colour, being discriminated from other shallow features on a coloured photograph, synthesized from the blue, green, and red bands photos.

The possibility of determining bottom vegetation using the multiband imagery and its discrimination from the delineation of the deep water sites is also confirmed by an instrumental interpretation of multiband photographs, based on measurements of D-negative optical densities. For instance, A- and B-objects (Fig. 2) look alike in the registrogram of the red band, but comparing it with the green band registrogram we can easily differentiate the A-object (depth section of 1.5-3 m with vegetation) from the B-object (deeper sites). The second very important dynamic bottom object is the relief forms of the sea bottom.

Relief forms of the sea bottom were presented on photographs only partially—the presence of bottom vegetation and a turbid water image, especially, causes interference. Nevertheless, careful analysis may help to differentiate several forms, reflected on a large-scale bathymetric map, observed during the subwater exploration (Andreyev *et al.*, 1971). An example: a system of parallel ridges and depressions at depths of 3-5 m, located north-west of the Kulala Island, and a sharp end south of this island

make part of it. Several bottom relief forms, reflected on space imagery, have not been formerly marked on this map. Thus, a series of coast-parallel bars are visible in the vicinity of part of the Mangyshlak Bay—a range relief of shoals formed by surge movements.

Forms of the bottom relief, vegetation, and other interpreted elements of shallow waters are shown in Fig. 3 in the interpretation scheme.

Results of interpretation are used to compile the northeastern Caspian shallow-water landscape scheme. It gives some idea of the main types of subwater natural-territorial complexes and regularities of their distribution. An aerial visual control has confirmed a high reliability of the similar schemes compiled on the basis of the multiband space imagery. Landscape exploration and mapping of sea shoals has recently been initiated, but we still lack materials, characterizing the coastal zone landscapes of vast water bodies (Guryeva *et al.*, 1968). An application of multiband space imagery enables us to take the first steps in solving these problems. The study of dynamic bottom objects—underwater vegetation and bottom relief forms—is only one of the trends of feasible multiband photographs applications to represent the "spectral signature" of the objects surveyed.

Another example of the "spectral signature" use is a study of coastal types and their dynamics in time. The relief formation process in the coastal zone is fixed in the area by the differences in territorial salinity—stagnancy of sea waters in lagoons, their drainage resulting in a formation of salty lakes, solonchaks, and solonetses. Salinization of the site is one of the characteristics being achieved by multiband photographs (Kravtsova, 1975). In particular, a comparison of the photographs taken in the blue and red spectral bands shows the image of sands and crust solonchaks to be similarly light on

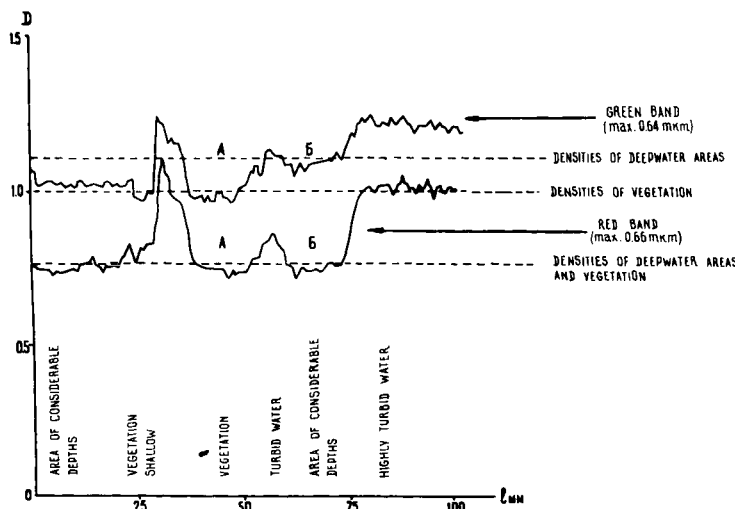


Fig. 2. Registrum of the shallow sites image's density measurement of the photographs, taken in the green (max. 0.54 mkm) and red (max. 0.66 mkm) spectral bands.

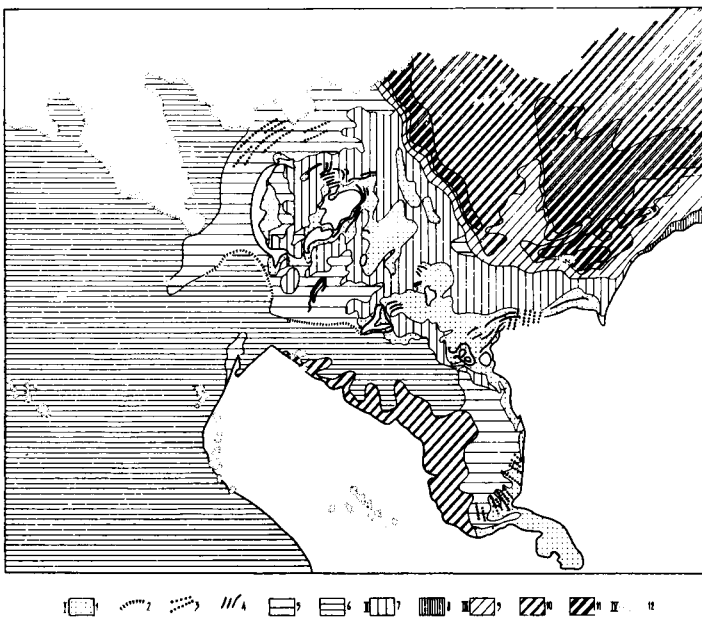


Fig. 3. The shallow site interpretation results of the northeastern Caspian region in the vicinity of the Tyuleniy Archipelago, based on multiband imagery. (I) Bottom relief forms: 1-sandy shallows with depths of up to 1.5 m; 2-ledges; 3-ranges (3-5 m) with hardly distinguishable bottom relief; (II) vegetation: 7-thickets of subwater vegetation; 8-thickets of subwater vegetation and mud deposits; (III) water pollution (sites of wave turbidity and outflow of solid sediments of temporal water bodies); 9-water pollution in the bottom side layer; 10-water pollution in the intermediate layer; 11-water pollution in the subsurface layer; (IV) clouds.

the photographs taken in a wide spectral band. It is extremely important when coastal dynamics are being studied since the barely visible chains of solonchaks among sands mark the location of ancient lagoons among accumulative forms—for instance, sandy bars.

Thus, the five ancient coastal bars, being nearest to the shore, can be seen on the photographs of the Mediterranean Sea coast in the vicinity of the Nile Delta taken in the red band, being the most informative one for the majority of objects. They are more definitely expressed on the surface like the bars with a height of 80–100 m with the Mariut Lake bays among them and a chain of closed depressions with crust solonchaks, solonchak meadows, and swamps. When the photographs taken in the blue and green bands ( $\lambda_{\max}=0.47$  and  $0.54 \text{ mkm}$ ) are used in an access to the red ones ( $\lambda_{\max}=0.66 \text{ mkm}$ ) four more ancient and less distinct bars remote from the coast can be seen. They are like denuded shafts with barely observable depressions among them. However, saline and swampy soils of these depressions, visible on the photographs taken in the blue and green bands, restore the whole set of ancient coastal bars containing nine shafts (Fig. 4).

The other side of the medal is the use of differences at a depth of penetration into water masses of light beams of various spectral bands. The top

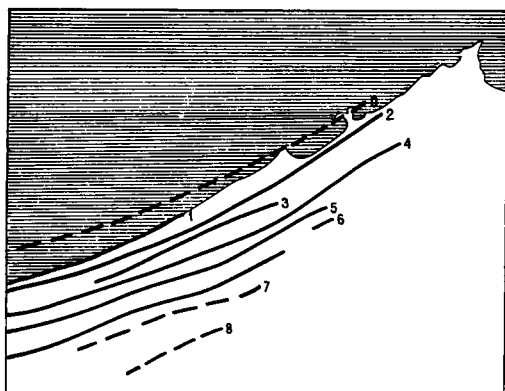


Fig. 4.

penetration is known (Charnell and Maulberge, 1973) to be observed for a short-wave range beam but the general reduction of the image contrast on space photographs due to the atmospheric effect does not

allow the photographs taken in this spectral range to be used effectively. The green band beam penetration is acknowledged to be the best for taking photos of water surface and underwater (Specht *et al.*, 1973); it reaches under clear water conditions above 20 m (in the band of 0.5-0.6 mkm). It comprises 12-15 m in the band of 0.6-0.7 mkm, 5-7 m in the band of 0.7-0.8 mkm. The beam penetration in the near infrared range (0.8-1.1 mkm) is measured in centimetres and submerged objects are not reproduced on the infrared spectral photographs; only surface water objects are visible. This feature allows multiband survey as a method of differentiated penetration into water masses at various depths to be used. We can get images corresponding to the cross-sections at various depths due to a set of multiband photographs. In the case of a coastal shallow-water zone with clear waters and a uniform bottom by the character of deposits and lack of vegetation, they will correspond to the bottom sections, i.e. isobars at various depths.

It is natural that such a drawing of isobars is extremely important when dynamics of bottom relief are being studied on a set of photographs taken at different times.

An analysis of the Mediterranean Sea coast photographs of the Nile Delta site can be used as an illustration. The light strip of the shallow-water zone is of various widths on spectral photographs; its boundaries correspond to the isobar of 20 m on the photographs taken in the 0.47-mkm maximum penetration band, isobar of 12-15 m in the 0.54 mkm maximum band, and isobar of 10 m in the bands of 0.66-0.68 mkm maximum (Fig. 5). This fact provides extensive aspects concerning the application of multiband photographs to the study of depths—the problem being extremely acute due to the shelf development. However, such a study of depths is possible only under clear-water conditions, with a uniform bottom geologically speaking, combined with a lack of water vegetation. In the case of a more complex bottom structure one can obtain a picture of bottom objects at various depths or a comparative picture at both surface and bottom. Thus, images in visible and near infrared bands are of a distinctly observable character on the multiband aerial photographs. Underwater spots are seen at the bottom on the photographs taken in the visible range, and an undulating structure and turbid streams on the surface in the infrared one. These photographs very vividly illustrate the opportunity of studying water areas at various depths by means of multiband survey.

It is very important to obtain cross-sections at various depths when water turbidity, suspensions in water mass, tendencies of suspension containing currents to migrate and distribute are being studied. The determination itself of the turbid water massifs sometimes were not successful.

In the presence of turbid waters, containing a large quantity of suspended material as a result of wave mixing of the bottom sediments of river accumulative discharge, great difficulties arise in the interpretation of photographs of shallows. We also observe this phenomenon in the Caspian images. Even the use of spectrally differentiated pictures cannot obtain the right answer in all cases, with the solution of the description of turbid water images from the light bottom features, e.g. shallows. Due to the predominantly dynamic character of water masses with high sediments content it is reasonable

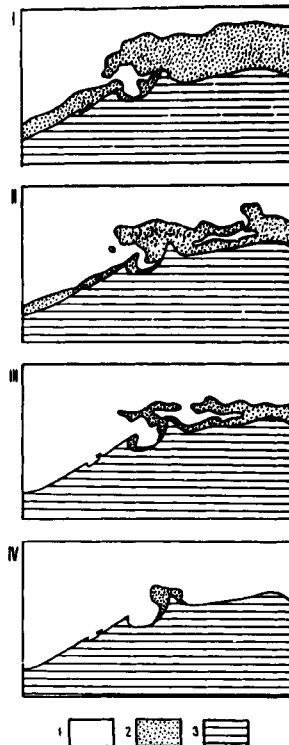


Fig. 5. Visual interpretation results of underwater relief on multiband photographs on the basis of image density discrimination: (I) band 4, 0.47 mkm max; (II) band 5, 0.54 mkm max; (III) band 1, 0.58 mkm max; (IV) band 6, 2.3-0.64, 0.66, 0.68 mkm max; 1—plots of deep sea water, 2—coastal shoal, 3—land surface.

for their determination to use photographs of different seasons of the year. In areas with alteration from one survey time to another by delineation, water turbidity and sediments movement are evident, while unvaried delineation presents a picture of depths, relief, and distribution of bottom objects (vegetation, bottom sediments). We have carried out the comparison of the Soyuz-12 SS imagery with ERTS's American resource satellite photographs. Delineation of the Uralskaya Borodina depression region, which was distinguished on the Soyuz-12 imagery by its light colours, suffered considerable changes during the period between surveys. Mixing streams of water bodies, discharging the river sediments of the Volga and Ural Rivers into the northern part of the Caspian Sea up to its eastern coast, are clearly visible. Two small light contours of prolonged form only stayed immutable confirming that shoal waters are depicted here. It is also confirmed by bathymetric map, with the help of which contours of shallows can be fixed very schematically while they are perfectly distinct on space imagery.

Multiband images, which could not be used for separation of turbid waters, were found to be very useful for their investigation after the determination of an object. Thus, applying the statement of different beam penetration depths in the water media in various spectral ranges, we tried to define the "relief" of turbid cloud on multiband imagery or boundaries of its dissemination at different depths, reviewing every zonal image as a horizontal cross-section of the turbid cloud at certain depths. Results of this determination are given in Fig. 3. The possibility of fixing deep-water turbid tails in river estuaries is of especial significance. It will help to study the tendencies of the material washed out from river run-off. In this respect a vivid example is presented by the photographs of the Danube Delta obtained from the ERTS satellite taken in four spectral ranges. In the photographs taken in a near infrared band of 0.8-1.1 mkm the coastal line, river bed, and land surface lakes are distinctly visible but we failed to obtain any characteristics of water masses within clearly distinguishable water areas. Separate contours of washout extending at a distance of 3-5 km from the coast are traced facing the Danube beds on the photographs taken in the zone of 0.7-0.8 mkm. These contours noticeably expand and unite into a single strip of 10 km wide on the photographs in the visible spectrum where objects of the upper water layer and of deep water masses are presented. In the photographs taken in the green band of 0.5-0.6 mkm one more less expressive strip extending at a distance of 25 km from the coast is visible, besides the former primary strip of aggradations of 10 km wide (Fig. 6). This photograph shows a significantly larger width of a turbid water zone in the deep-water layers than on the surface. This example illustrates an interesting peculiarity of suspended material distribution with its tendency to subside to the bottom layer in the immediate vicinity of the river mouth and a comparatively small volume of material transportation in the upper layer previously observed when multiband aerial photographs were being analysed.

Therefore, even a single photograph provides sufficient information on suspended material dynamics. These possibilities will increase when a set of multiband photographs taken at different times are being used.



Fig. 6. Interpretative results of suspensions discharge in the Danube Estuary in the photographs from ERTS satellite taken in four spectral bands. Contour of suspension cloud: 1-on the photographs of the 0.5-0.6 mkm band; 2-the 0.6-0.7 mkm band photographs; 3-the 0.7-0.8 mkm band photographs; 4-clear water sea surface; 5-rivers and lakes on the land surface.

#### REFERENCES

1. Andreyev, V. V., Dobrynina, T. A., Ignatov, E. I., Maev, E. G. and Shiryaev, V. N. (1971) Relief dna i donnye otlozheniya Mangyshlakskogo poroga. V kn.: *Kompleksye issledovaniya Kaspiyskogo morya*, Moscow, izd. MGU.
2. Charnell, R. L. and Maulberge, A. Oceanic observation of New York Bight by ERTS-1. *Nature*, 242, No. 5399, pp. 451-452.
3. Guryeva, Z. I., Petrov, K. M., Ramm, N. S. and Sharkov, V. V. (1968) *Geologo-geomorfologicheskoye izuchenie morskikh melkovodiy i beregov po materialam aerofotosyemki*, Leningrad, izd. Nauka.
4. Khodarev, Yu., Dunaev, B., Zeyeman, Yu., Knishnikov, Yu., Kotzov, V., Kravtsova, V., Lebedev, V., Makarov, O., Fivensky, Yu. and Tcheshov, Yu. (1975) *Multiband photography from the Soyuz-12 and Soyuz-13 spacecraf*ts; its application in Earth resources studies. Space Research Institute, AS USSR, Moscow.
5. Kravtsova, V. I. (1975) Primenenie mnogozonalnoi kosmicheskoi syemki v geograficheskikh issledovaniyah i tematicheskem kartografirovaniyu. V kn. *Issledovaniya zemnykh resursov kosmicheeskimi sredstvami. II Metody interpretatsii i ispolzovaniya informatsii*. AN USSR, Moscow.
6. Kravtsova, V. I. and Antonova, C. Yu. (1974) Primenenie mnogozonalnoi syemki dlya izucheniya i kartografirovaniya melkovodiy (na primere severo-vostochnogo Kaspiya). *Izvestiya VUZov, seriya geologiya i razvedka*, No. 12.
7. Specht, M. R., Needler, D. and Fritz, N. L. (1973) New color film for water photography penetration. *Photogr. Eng.*, 39, No. 4, pp. 359-369.

# THE RULES OF CLASSIFICATION OF WATER SURFACE CONDITIONS IN REMOTE SOUNDING FROM SPACE

Yu. E. Sidorov and S. V. Solonin

Leningrad Hydrometeorological Institute, 98 Malookhtinsky pr., 195196 Leningrad, USSR

## Abstract

The problem of statistical synthesis of rules of classification of ocean surface conditions under conditions of absence of complete *a priori* information on parameters of data distributions of multifrequency measurements of outgoing microwave radiation of the "ocean-atmosphere" system in remote sounding from space is considered. Diverse values of parameters of linear equation connecting radiobrightness temperatures  $T_R$  of ocean surface on two wavelengths,  $\lambda_1$  and  $\lambda_2$ , for non-polluted and polluted, for steady and troubled surface and so on, serve as a physical basis for classification. For the rules synthesis principles of non-biasness and invariance in the theory of checking of complicated statistical hypotheses are used to which the considered problem is reduced. Probability characteristics of obtained rules, block diagrams of corresponding devices are determined and their practically important properties which make possible utilization of these devices in automated digital systems of space data handling are mentioned.

In the report at the 26th Congress of the International Astronautical Federation [1] as an illustration of fruitfulness of application of methods of *a priori* uncertainty overcoming were considered the problems of synthesis of data classification rules of remote sounding of atmosphere over the ocean and of ocean depths. However, the problem of ocean surface condition objective classification was not touched upon. The problem's urgency is caused by the fact that knowledge of water surface conditions is necessary for solution of diverse scientific and applied problems. In particular, successful solution of water surface conditions classification problems is essential for reduction of estimate error of diverse oceanographic parameters (temperature, salinity of the sea, etc.), for navigation and fishery, and also for solution of hydrosphere pollution problem.

The aim of the present report is to remedy this flaw and to obtain the rules of classification of water surface conditions, in parametrical *a priori* uncertainty [1], when functional appearance of the law of observed data distribution is known and *a priori* uncertainty is expressed by ignorance of this law's parameters.

For the synthesis of classification rules of water surface conditions we shall use data of multifrequency measurements in microwave range in the "ocean-atmosphere" system in remote sounding from space. This is connected with perspectiveness of microwave range application for estimation of characteristics of sea, sea ice, oil pollutants. Therefore let us assume that water surface conditions classification is conducted using data of

radiobrightness temperature of the surface  $T_R(\lambda_i)$ ,  $i = 1, 2, \dots$  ( $\lambda$  - wavelength). Various values of parameters in the linear equation connecting radiobrightness temperatures on various wavelengths and under various conditions of ocean surface may serve as a physical basis for classification.

Thus, mathematically the problem of classification may be formulated as a problem of estimation of these parameters in terms of the theory of checking complicated statistical hypotheses [2].

As a zero hypothesis  $H_0$  we shall take the hypothesis that, for example, parameter  $b$  is equal to  $b_o$ . The alternative to  $H_0$  is the complicated hypothesis  $H_1 : b \neq b_o$ .

To formulate the rules of checking hypotheses  $H_0$  and  $H_1$  we shall use the following assumptions. Let us assume that values  $T_R(\lambda_1)$  and  $T_R(\lambda_2)$  are described by normal distribution with dispersion  $\sigma^2$  and average  $\bar{T}_R(\lambda_i)$ ,  $i = 1, 2$ , where averages are connected by equations of linear regression [2].

With these assumptions the rule of checking hypothesis  $H_0$  may be obtained by using both principle of non-biasness and invariance [2].

In the first case the rule of checking of regression hypothesis  $H_0$  is uniformly the most powerful (UMP) non-biased with region of form acceptance

$$W = \frac{\left| \frac{\sum v_i y_i}{\sqrt{\sum (x_j - \bar{x})^2}} - b_o \right|}{\sqrt{\frac{1}{\sum (y_i - \bar{y})^2 - \sum (v_i y_i)^2} / (n-2)}} \leq C' \quad (1)$$

where  $v_i = (x_i - \bar{x}) / \sqrt{\sum (x_j - \bar{x})^2}$ ,  $\bar{x} = \sum x_i / n$ ,  $y = \sum y_i / n$ , and  $\bar{y}$  are independent measurements of radiobrightness of investigated ocean part surface at wavelengths  $\lambda_1$  and  $\lambda_2$  respectively. A threshold  $C'$  is determined by given probability  $\alpha$  of the first kind error from equation

$$\int_{-C'}^{C'} t_{n-1}(w) dw = 1-\alpha, \quad (2)$$

where  $t_{n-1}(w)$  distribution of statistics of  $W$  at  $H_0$ , being central  $t$ -distribution with  $(n-1)$ st degree of freedom.

Having conducted corresponding algebraic transformations, eqn. (1) may be written in following equivalent form:

$$C'_1 A^2 - C'_2 A + C'_3 \sum x_j^2 - C'_4 (\sum x_j)^2 - C'^2 \sum y_i^2 + C'_5 (\sum y_i)^2 + C'^2 A^2 \leq 0, \quad (3)$$

where  $A = \sum y_i \frac{x_i - \bar{x}}{\sqrt{\sum (x_j - \bar{x})^2}}$ ,  $C'_1 = n-2$ ,  $C'_2 = 2(n-2)b'_0$ ,  
 $C'_3 = (n-2)b'_0$ ,  $C'_4 = \frac{n-2}{n} b'_0$ ,  $C'_5 = \frac{C'^2}{n}$ .

Condition (3) determines the block diagram of classification device, which one can clearly see—has to be composed of units of evaluation of constant  $C'$ , variable  $A$ , accumulators, multiplier units, squaring units, subtraction and comparison with zero units (of digital comparator). Interaction of these units is determined completely by inequality (3).

Output of the rules (1), (2) may be expressed by non-central  $t$ -distribution,  $t_{n-1}(w, \delta)$  in the form

$$\beta = 1 - \int_{-C'}^{C'} t_{n-1}(w, \delta) dw, \quad (4)$$

where parameter of non-centrality  $\delta$  depends only on differences  $b - b'_0$ . Curves, calculated by formula (4), taking into account (2) by means of tables [3] for various values  $\alpha$ ,  $\delta$  and  $d = n-1$  are presented in Fig. 1. From the analysis of those it is clearly seen that probability (4) grows with increase of sample  $d$  and parameter  $\delta$  what is clearly explainable from the physical point of view: the higher the quantity of observations and "contrast"  $b - b'_0$  the easier the achievement of correct classification.

Classification of ocean surface conditions using the rule (1) is conducted as follows: If (1) is correct hypothesis  $H_0$  is accepted (indicating, for example, that the sea is quiet, oil pollutants are absent, ice is one year old, etc.), and if  $W > C'$  alternative  $H_1$  is accepted (the sea is troubled, oil skin exists, ice is many years old, etc.).

In the second case the rule of checking of regression hypothesis  $H_0$  will be UMP invariant with the region of rejection  $H_0$  of the form

$$W^* = \frac{|\hat{b} - b'_0| \sqrt{\sum (x_j - \bar{x})^2}}{\sum (y_i - \hat{y} - \hat{b}x_i)^2 / (n-2)} > C'', \quad (5)$$

where  $\hat{b} = \sum (y_i - \bar{y})(x_i - \bar{x}) / \sum (x_j - \bar{x})^2$ ,  $\hat{a} = \bar{y} - \hat{b}\bar{x}$ , and the threshold  $C''$  is determined from equation

$$\alpha = 2 \int_{-C'}^{\infty} t_{n-1}(w^*) dw^*. \quad (6)$$

The block diagram of invariant classification device comes from inequality equal to (5)

$$C'' \hat{b} \sum x_j^2 - C'_2 b^2 (\sum x_j)^2 - 2C'_1 b'_0 \hat{b} \sum x_j^2 + 2C'_2 b'_0 \hat{b} (\sum x_j)^2 \\ + C'_1 b'_0 \sum x_j^2 - C'_2 b'_0 (\sum x_j)^2 - C''^2 \sum y_i^2 + 2C''^2 \sum y_i \bar{y} \quad (7)$$

$$- 2C''^2 \sum y_i \hat{b} \bar{x} - 2C''^2 \sum y_i \hat{b} x_i - C''^2 \sum (\bar{y} - \hat{b} \bar{x} + \hat{b} x_i) > 0,$$

where  $C'_1 = n-2$ ,  $C'_2 = (n-2)/n$ ,  $\bar{y} = \sum y_i/n$ ,  $\bar{x} = \sum x_i/n$ ,  $\delta = \sum (y_i - \bar{y})(x_i - \bar{x}) / \sum (x_j - \bar{x})^2$ . This diagram is more complicated than previous because of bigger quantity of interacting units and their linkages.

The power of the rules (5) and (6) depends only on  $b - b'_0$ , it may be expressed in terms of non-central  $t$ -distribution

$$\beta(\psi) = \int_{-C''}^{\infty} t_{n-1}(w^*, \psi) dw^*, \quad (8)$$

where  $\psi$  is a parameter of non-centrality, and is calculated by means of tables [3]. The character of curves of probability (8) will be the same as in the first case (Fig. 1).

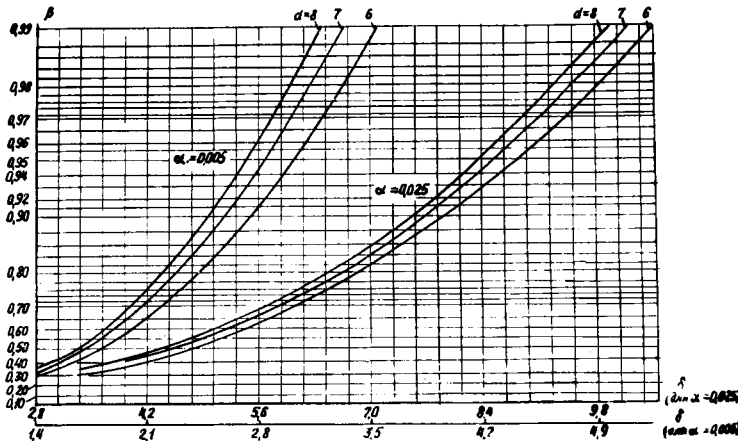


Fig. 1. Efficiency of non-biased rule of water surface conditions classification.

The rule (5), (6) is invariant to systematical errors of measurements in both channels, what is especially valuable for microwave range because of difficulties of absolute calibration of instruments.

Thus, the rules (1), (2) and (5), (6) are obtained, which have a number of practically important properties, namely: (a) they do not depend on *a priori* unknown parameters ( $\sigma^2$  and b) of normal distribution of the observed data; (b) they have permanent probability of the error of first kind (probability of false classification); (c) they have the greatest probability of correct solution in classes of non-biased and invariant rules, respectively, and (d) they are convenient for realization by means of digital equipment.

The emphasized qualities of classification rules make possible their utilization in automated digital

systems of space data handling under conditions of *a priori* uncertainty-usual conditions of space observations.

#### REFERENCES

1. Mitnik, L. M., Sidorov, Yu. E. and Solonin, S. V. Remote investigations of the environment from space and problems of space data handling. International Astronautical Federation (I.A.F.) XXVIth Congress, Lisbon, 1975, 36 pp. (preprint).
2. Lehmann, E. L. *Testing Statistical Hypotheses*. John Wiley & Sons, Inc., New York, 1959.
3. Bolshev, L. N. and Smirnov, N. V. *Mathematical Statistics Tables*. Moscow, published by Computer Center of the USSR Academy of Sciences, 1968.

# MATERIALS PROCESSING IN SPACE: A SCIENTIFIC OVERVIEW

R. A. Lefever

*Director of Materials Preparation, School of Engineering, University of Southern California,  
Los Angeles, California*

The influence of gravity on the properties and behavior of materials is discussed in general terms, within the broad categories of physical deformation, sedimentation, convection in liquids and gases, and containerless processing, and illustrated with the results of selected space processing experiments. The relevance of theoretical studies, ground-based experiments, and zero-gravity simulation to space processing are outlined and opportunities provided by sounding rocket flights and early Spacelab missions are briefly described.

## I. Introduction

More than fifty materials processing experiments have been conducted aboard Skylab, Apollo Soyuz and more recent sounding rocket flights. Post-flight analyses of experimental data and materials, combined with ground-based studies, have provided new insights into important physical principles and processes and reveal areas in which further space processing endeavors may be of substantial value both scientifically and commercially (1,2).

The majority of the materials space processing experiments have been designed to evaluate the effects of gravity on convection and density segregation in processes involving liquid and gas phases, to utilize the unique zero-gravity environment to produce materials of exceptional purity, compositional homogeneity or microstructural perfection and to prepare multi-component solids with unique structures and novel properties. While post-flight analyses are still in progress in many cases, the results of Skylab and Apollo Soyuz experiments have been reported in some detail (3,4) and reviews have been published (1,2). Previous review papers have generally emphasized the experimental results. In the present paper, the co-ordinating theme is physical properties, treated in a descriptive manner, with the results of selected space processing experiments serving as instructive examples. While the subject matter is divided into several broad categories for ease of discussion, dividing lines are not always clearly defined and most processes involve more than one physical effect.

## II. Gravitational Field Effects

### Deformation

One of the most obvious effects of gravity is simple deformation. In a gravitational field, supported liquid drops flatten, levitated drops are not spherical and liquids supported by pedestals (as in vapor-liquid-solid and Verneuil crystal growth techniques) or supported between vertical rods (as in floating zones) may sag to the point of detachment, with the magnitude of the effect depending on size and surface tension.

Typical melt sagging is illustrated in Figure 1a for the vertical floating zone configuration. The zone diameter is limited by the volume of liquid

that can be supported by the bottom pedestal and surface tension effects. Large zone diameters generally require that the zone be thin in order to minimize liquid volume. As a result, problems are encountered with thermal geometry, liquid-solid interface shape and system stability. These problems can be eliminated to some extent by proper coil shaping to provide melt levitation and silicon melts in the range of 7.5-10 cm in diameter can be supported in this manner.

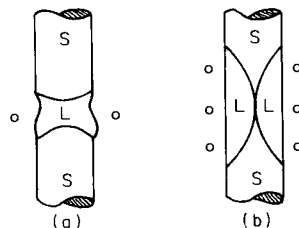


Figure 1. Floating zones in (a) earth gravity and (b) zero gravity. From Ref. (5).

The maximum stable zone length at zero-gravity is equal to zone circumference regardless of surface tension (5,6). Thus, zone lengths to 32 cm may be stable without special support requirements for zone diameters of the order of 10 cm. This is illustrated in Figure 1b, which also shows the change in liquid-solid interface shape that results from the loss of buoyancy-driven convection and the corresponding convective heat transfer, a subject that is discussed further in the section on convection. Whether the zone free surface curves inward or outward depends primarily on melt volume relative to diameter of the solid supports, and the results of calculations on the diameters and configurations of stable zones have been published (6,7) for various conditions of size and rotation rate.

In the course of pulling single crystals from the melt (Czochralski method), small diameter seed rods are normally employed. In order to achieve single crystal growth from polycrystalline seed rods or to minimize propagation of defects from single crystal seeds, the diameter may be further reduced during the early stages of growth. The weight of large crystals grown subsequently can cause dislocation and slip plane generation in these regions and propagation of these defects into the bulk crystal in the course of further growth.

### Sedimentation

A large area of phenomena that involve gravitational effects is that of separation as a result of density differences. Systems in which gravity separation plays an important role include miscible liquids, immiscible liquids and liquids containing

dispersed solids, all of which produce dispersions or composites of solid particles in a solid matrix on solidification, or solids in which the dispersed phase is a liquid or gas (e.g., foams).

Immiscible liquids and liquids containing dispersed solids constitute a large class of systems of interest in space processing. From such systems, multiphase solids with unique properties can be prepared providing that uniform and controlled dispersions are achieved. Since the various constituents of a multicomponent system are almost always of different density, the problem on earth is one of preventing phase separation prior to and during solidification.

Several types of interesting space processing experiments have been conducted with multiphase systems. A series of simple experiments conducted aboard Skylab 4 (8) illustrate the value of being able to visually observe the behavior of oil-water dispersions in the absence of gravity. While the emulsions separated completely in ten seconds on earth, they were stable for ten hours in space. With stability of this magnitude, it is possible to study in detail the properties of such systems and, in combination with ground-based studies, predict the behavior of, for example, opaque immiscible alloys at high temperatures. Also, since surface tension gradients cause vapor bubbles in a liquid to move in a temperature gradient and such bubbles are very buoyant, zero-gravity experiments provide an excellent environment for the study of liquid-vapor interface energies.

Two alloy systems, lead-zinc and aluminum-antimony were examined in experiments conducted aboard Apollo Soyuz (Ref. (4), p. 24-1). The PbZn system is characterized by a large liquid immiscibility gap and a large density difference between Pb ( $11.7 \text{ g/cm}^3$ ) and Zn ( $7.14 \text{ g/cm}^3$ ). While preventing separation between Pb and Zn is difficult on earth, it was expected that space processing would result in intimate mixing of the two liquids and a solid in which fine particles of superconducting Pb are dispersed in a Zn matrix. Although complete homogenization was not achieved, preliminary studies have demonstrated the presence of dispersed fine Pb particles.

AlSb, a semiconducting compound with an energy gap of 1.62 ev, solidifies by a syntetic transformation of two molten constituents to a constant-composition compound. Again, large density differences ( $2.7 \text{ g/cm}^3$  for Al and  $6.62 \text{ g/cm}^3$  for Sb) prevent formation of a homogeneous melt and lead to segregation during solidification on earth. A comparison of ground- and space-processed samples of AlSb reveals significant improvements in homogeneity in the material solidified in space. The ground-based experiments produced samples with individual grains of Al- and Sb-rich phases, while an Al-rich phase was found only as a minor intergranular constituent in the space-processed samples.

Results with the gallium-bismuth liquid immiscibility system, investigated in drop-tower free-fall experiments, are particularly interesting (9). Dispersions of fine particles of Ga in a Bi matrix were produced, resulting in samples with a temperature-dependence of electrical properties much different from those of a sample prepared on earth under identical conditions. While the latter sample

exhibits increasing resistivity with increasing temperature to 280 K, with a  $d\rho/dT$  slope similar to that of pure (semimetallic) Bi, the zero-gravity sample with the smallest particle size ( $1-2 \mu\text{m}$ ) exhibits the negative  $d\rho/dT$  slope characteristic of an intrinsic semiconductor at temperatures above about 100 K. In addition, the space-processed samples have somewhat higher superconducting transition temperatures (Ref. (3), p. 1043). Similar experiments were conducted aboard Skylab on the immiscible liquid and solid systems gold-germanium, lead-zinc-antimony and lead-tin-indium. While none of the earth-processed samples of AuGe dispersions exhibited superconductivity, the zero-gravity samples were weakly superconducting at 1.5 K (Ref. (3), p. 135). The space-processed PbZnSb samples exhibited not only the 7.2 K superconducting transition temperature of the samples prepared on earth but an additional transition at 9.2 K (higher than that of any component element) as well (Ref. (3), p. 136). All of the space-processed samples were much finer and more uniform dispersions than their earth-processed counterparts.

Composites that are formed by solidification of a liquid containing a dispersed solid phase that is elongate in form (e.g., whiskers) are of interest from the standpoints of enhancement and anisotropy of strength. Samples of a typical composite, containing silicon carbide whiskers in a silver matrix were prepared on earth and aboard Skylab by holding a sintered mechanical mixture of silicon carbide whiskers (2, 5 and 10 volume %) and powdered Ag above the melting point of Ag for several hours and then cooling in the furnace (Ref. (3), p. 203). While whisker floating and coagulation occurred in the ground-based studies, whisker distribution was relatively uniform in the Skylab experiments, resulting in samples with somewhat higher and considerably more uniform microhardness values. Directionally solidified eutectics also fall in the category of composites and eutectics of copper-aluminum (Ref. (3), pp. 457 and 953), and of NaCl-NaF and NaCl-LiF (Refs. (3), p. 469, (4), p. 28-1, and (10)), with improved physical properties, and lead-antimony (first sounding rocket flight, December 11, 1975, analysis in progress), have been prepared in zero-gravity experiments. The NaCl-LiF eutectics are discussed further in the section on the mechanical effects of convection.

#### Convection

Convective stirring in liquids can play an important role in determining not only the concentration and distribution of impurities in polycrystalline solids and single crystals produced by solidification of melts and solutions, but bulk composition as well. Furthermore, changes in the nature and degree of convection during solidification, a common occurrence in practice, can introduce marked fluctuations in composition and microstructure. Such variations frequently have adverse effects on physical properties and device performance, and many schemes, including forced convection, have been devised to minimize these effects.

#### Buoyancy-driven

A common cause of natural convection on earth is

the buoyancy effect of density differences associated with temperature and concentration gradients. Temperature gradients are often imposed by system geometry but they also result from heat effects associated with the solidification process. Concentration gradients frequently result from crystallization processes, in the course of which solution density in the immediate vicinity of the solid-liquid interface differs from that of the bulk solution.

Figure 2 illustrates the effect of liquid mixing on solid composition, for distribution of an impurity for which the ratio of the concentration between the solid and liquid is less than one.

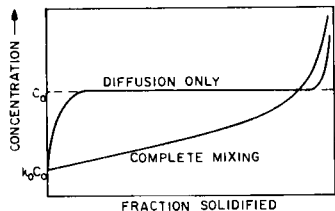


Figure 2. Concentration of solute after solidification under conditions of complete liquid mixing and diffusion transport only. From Ref. (11), p. 17.

The solute in this case is less soluble in the solid than in the liquid and the distribution coefficient,  $k_0$ , is less than one. As solidification proceeds, solute is rejected into the solution at the solid-liquid interface. In the ideal case of complete mixing in the liquid, the rejected solute is uniformly distributed through the remaining liquid and solute concentration in the solid increases uniformly with fraction solidified. In the absence of mixing, a liquid layer containing a high concentration of solute rapidly develops at the solid-liquid interface. Under conditions of dynamic equilibrium, the concentration at the interface is such that the concentration in the solid is identical to that of the liquid, giving an effective distribution coefficient of unity. This situation is illustrated in Figure 3.

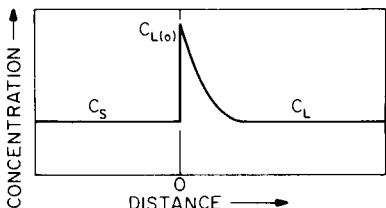


Figure 3. Solute concentration at the interface under conditions of diffusion transport in the liquid.

It can be readily seen that, from the standpoint of compositional uniformity, a diffusion-controlled solidification process is very desirable. However, the condition illustrated in Figure 3 is highly sensitive to fluctuations in solidification conditions. A sudden increase in solidification rate caused, for example, by a change in thermal conditions, can lead to a marked increase in solute

concentration or complete incorporation of the solute-rich interface. Furthermore, a system in this condition is predisposed to constitutional supercooling (see below). In practice, the situation usually lies between the two extremes of diffusion-only and complete mixing in the liquid phase and forced convection is frequently employed to override buoyancy-driven natural convection.

The advantages of eliminating buoyancy-driven convection by zero-gravity processing are illustrated in Figure 4, the results of experiments conducted on Skylab on the growth of tellurium-doped crystals of indium antimonide (Ref. (3), p. 275).

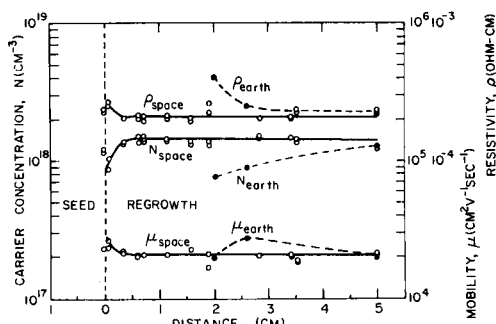


Figure 4. Carrier concentrations and mobilities for Te-doped InSb crystals grown on earth and aboard Skylab. From Ref. (3), p. 296.

The ability of diffusion-controlled solidification to produce material with uniform electrical properties is apparent from the data.

The concepts outlined above can be extended to the more general case of binary solid solutions, in which the "impurity" is one of the components and is present in relatively high concentrations. The results of atomic absorption analyses on InSb-GaSb solid solutions solidified aboard Skylab and in two experimental configurations on earth are shown in Figure 5. The compositions of the original ingots were  $In_{0.3}Ga_{0.7}Sb$ . The distribution coefficient of indium at this initial composition is about 0.05.

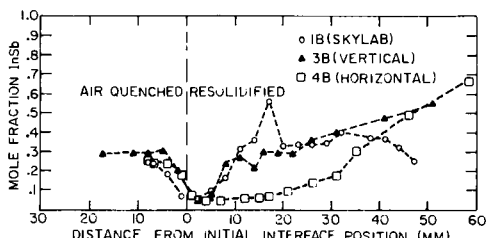


Figure 5. Compositions of InSb-GaSb samples solidified aboard Skylab and on earth. From Ref. (12), p. 41.

The temperature gradients present during horizontal Bridgman solidification on earth result in convective mixing of the liquid, leading to the gradual increase in indium concentration in the ingot with increasing fraction solidified. In the

case of melts solidified vertically on earth, the temperature gradient was such that the melt temperature increased from bottom to top, suppressing buoyancy-driven convection. Likewise, aboard Skylab the lack of gravity inhibited buoyancy-driven convection. In both cases, the indium concentration in the solid increases rapidly with fraction solidified and then becomes relatively constant, indicating diffusion-controlled materials transport in the liquid.

Seed and crystal rotation are frequently used in crystal growth processes to reduce thermal asymmetry that may be present in the liquid and the magnitude of concentration gradients at the solid-liquid interface. The forced convection that results from rotation can interact with natural convection to produce complex liquid behavior during growth. An interesting example of this is illustrated in Figure 6. In the early stages of growth, buoyancy-driven convection dominates, with melt flowing upward along the crucible walls and downward in the cooler central region in a spiral pattern driven by crystal rotation. As the diameter of the crystal increases, the surface becomes increasingly effective in driving convection until it overrides natural convection. At that point, an abrupt turnover in melt flow occurs, with melt then reaching the growing surface from the cool bottom center of the crucible rather than from the hotter sides, resulting in a sudden change in growth condition. Such effects can cause undesirable changes in composition and generate defects. Zero-gravity experiments provide a means for removal of buoyancy effects in studies of convection from other sources.

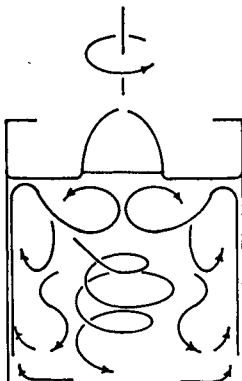


Figure 6. Effect of rotating crystal surface on buoyancy-driven convection in growth from the melt. See Acknowledgements.

Convection also influences the rate of removal of the heat of fusion and crystallization in melt solidification and solution-crystallization processes, respectively, a fact that is not always fully appreciated. Heat evolved during the growth of a single crystal, for example, accumulates at the solid-liquid interface and must be dissipated. In the absence of heat removal by the effective process of convection (and in the absence of radiative heat loss), heat is removed by the relatively slow process of diffusion, and crystal growth rates must be decreased substantially in order to

maintain stable growth conditions. Too rapid a growth rate under conditions of poor heat removal can lead to interface instability, cellular growth and the formation of dendrites.

The presence of composition gradients near the solid-liquid interface of a melt in the process of solidification can lead to constitutional supercooling, illustrated in Figure 7. In the case of the pseudobinary InSb-GaSb system, for example, the increase in InSb at the interface (see Figure 3) lowers the freezing point of the liquid in this region. In order to maintain the solidification process, heat removal from the solid must be increased which, in turn, decreases the liquid temperature near the interface. As a result, a temperature gradient may be established such that the temperature of the liquid a short distance from the interface is less than the freezing point.

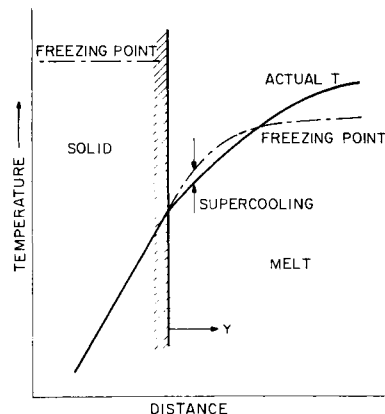


Figure 7. Constitutional supercooling during solidification. From Ref. (13), p. 127.

Problems associated with constitutional supercooling are compounded by inadequate removal of heat in the absence of convection. Under the conditions of reduced natural convection in space processing, it is necessary to maintain temperature gradients that are relatively high in order to prevent excessive supercooling, which can lead to compositional inhomogeneities and changes in microstructure through interface breakdown.

Convection is, of course, important in processes involving vapor transport. Indeed, many schemes for the growth of crystals from the vapor phase are designed to provide convective materials transport. The vapor phase growth of germanium-tellurium and germanium-selenium crystals was investigated in a variety of conditions, using GeI<sub>4</sub> as the transport agent, aboard Skylab (Ref. (3), p. 235) and Apollo Soyuz (Ref. (4), p. 27-1) and in corresponding experiments on earth. While the space-grown crystals were structurally more homogeneous and contained lower defect concentrations than the crystals grown on earth, the most interesting result is the fact that transport rates in both the Skylab and Apollo Soyuz experiments were significantly higher than predicted.

Convection also influences nucleation processes.

Crystals of relatively insoluble materials can be grown in aqueous systems by reacting appropriate solutions. However, convective mixing results in high supersaturations that lead to the formation of large numbers of nuclei, resulting in many small crystals. This problem has been successfully circumvented in some cases by incorporating the reactant solutions in gels. Slow diffusion through the gels results in nucleation control and the formation of crystals that are smaller in number and larger in size. However, the use of gels imposes restrictions on solution pH and concentration and usually results in incorporation of gel components into the crystals. Experiments with three materials frequently grown in gels were conducted in a similar geometry but without gels aboard Apollo Soyuz. Crystals of calcium tartrate, calcium carbonate and lead sulfide were prepared by bringing reactant solutions into contact with opposite sides of a volume of solvent during flight and allowing nucleation and growth to occur by diffusion (Ref. (4), p. 30-1). Excessive nucleation occurred in all cases, but the resulting crystals were about the same in size and at least as good in quality as those obtained by gel methods on earth in the same length of time.

#### Surface tension-driven

Convection can also be driven by surface tension gradients. Interfacial tension gradients in vapor-liquid interfaces can result from temperature or composition gradients and generate tangential stresses which, in turn, induce fluid motion. Convection driven in this manner is commonly referred to as thermocapillary flow or the Marangoni effect. Since solidification processes on earth are usually conducted in containers or with melts in contact with surfaces and buoyancy-driven flow tends to be the dominant cause of natural convection, the effects of surface tension gradients are observed only under special circumstances.

The floating zone process employed for materials purification and crystal growth involves containerless melts in a configuration that lends itself to mathematical analysis. Extensive studies of the nature and magnitude of surface tension-driven flow in the floating zone process have been conducted, particularly for silicon (14,15,16). Figure 8 shows the calculated flow streamlines for a silicon floating zone at zero gravity, where  $\psi$  is a dimensionless stream function defined by  $V_r = \partial\psi/\partial z$  and  $V_z = -\partial\psi/\partial r$ , and  $V_r$  and  $V_z$  are the dimensionless radial and axial velocity components of the liquid, respectively.

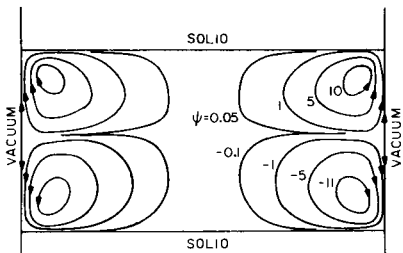


Figure 8. Computed streamlines for surface tension-driven flow at zero gravity with a parabolic temperature profile on the free melt surface. From Ref. (16), p. 14.

Figure 9 shows the impurity concentration fields in the melt at steady state for the convection conditions shown in Figure 8 and an impurity with a distribution coefficient of 0.1. The impurity variations in the melt result in corresponding concentration variations in the solid. Studies of the comparative effects of buoyancy- and surface tension-driven flow have shown that, for floating zones of silicon on earth, surface tension-driven convection dominates at zone diameters of less than about 0.8 cm (16).

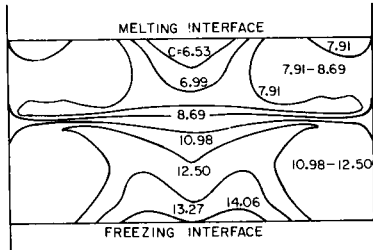


Figure 9. Computed impurity concentration fields at steady state in a silicon melt, for flow conditions shown in Figure 8 and impurity  $k_0 = 0.1$ . From Ref. (16), p. 15.

Experiments designed to look for convection driven by surface tension gradients have been conducted at zero gravity and Bénard cells were generated by surface tension-driven convection in experiments conducted aboard Apollo 14 (17). In several Skylab experiments conditions favorable for surface tension-driven flow were present (in some instances, inadvertently), but in most cases evidence for convection from this source was not revealed by post-flight analyses (Refs. (3), pp. 235, 275 and 301, and (18), p. v). However, more recent studies on InSb-GaSb ingots prepared by directional solidification in a series of experiments conducted aboard Skylab 3 reveal large composition variations attributed to bulk convection driven by surface tension gradients (19). In these experiments, substantial regions of the melts were not in contact with the container walls during solidification. Figure 10 shows the indium concentrations, determined by electron microprobe analysis, across the diameters of transverse sections taken from two regions of an ingot solidified from a melt of initial composition  $In_{0.1}Ga_{0.9}Sb$ . While the composition is uniform across the section taken from a region solidified from melt in contact with the container walls (1C-16), a substantial radially-symmetric variation in In concentration is present in the region solidified from melt not in contact with the container walls (1C-32). Using the system geometry and the most likely values for physical properties, calculations of surface tension-driven convection give a symmetrical two-vortex pattern, shown in Figure 11, that is compatible with the microprobe data. As bulk melt is swept across the surface by convection, indium is rejected from the solid resulting in a melt that is increasingly rich in indium and a corresponding continual increase in indium content of the solid, in a configuration corresponding to geometry of the convection pattern. This result illustrates the importance of avoiding conditions that may lead to convection driven by surface tension gradients in containerless zero-gravity

experiments (see section on containerless processing) and suggests that the use of containers in space processing may have advantages over and above simple containment in some cases.

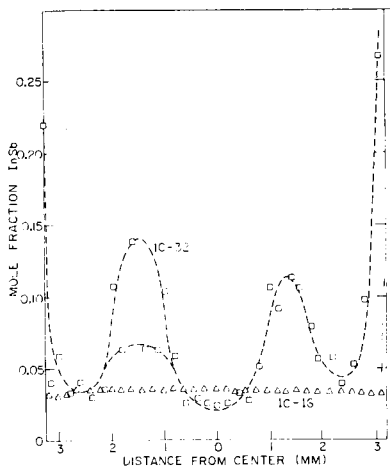


Figure 10. Radial distribution of indium in InSb-GaSb ingot directionally solidified aboard Skylab 3.

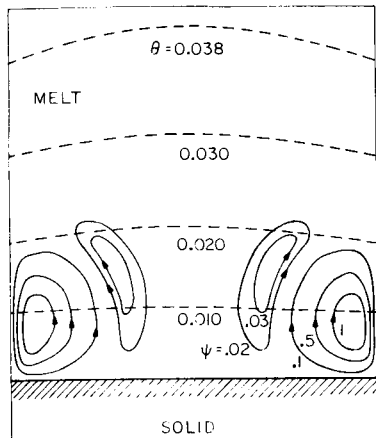


Figure 11. Computed streamlines for surface tension-driven convection in Skylab 3 InSb-GaSb solidification experiments.

#### Mechanical effects

Convection can, of course, have effects on materials that are primarily mechanical in nature. Such effects, normally observed only in the case of relatively fragile materials, may be important, for example, in the preparation of fiber eutectics. Figures 12 and 13 show NaF fibers in an NaCl matrix prepared by eutectic solidification on earth and aboard Skylab, respectively (Refs. (3), p. 469 and (10)). The enhanced alignment and increased fiber length in the samples solidified in space,

which lead to improved optical transmission along the fiber axis, are attributed to the absence of vibrational and convective disturbances. Similar results were obtained with NaCl-LiF eutectics aboard Apollo Soyuz (Ref. (4), p. 28-1).

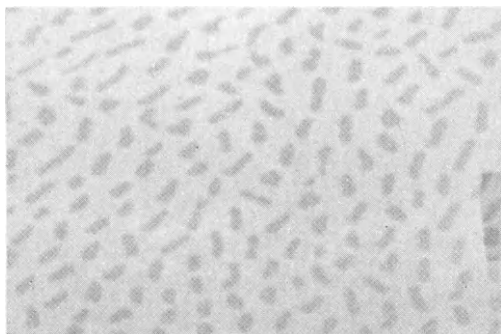


Figure 12. Longitudinal section of NaCl-NaF eutectic showing discontinuous NaF fibers. (1500X before reduction).

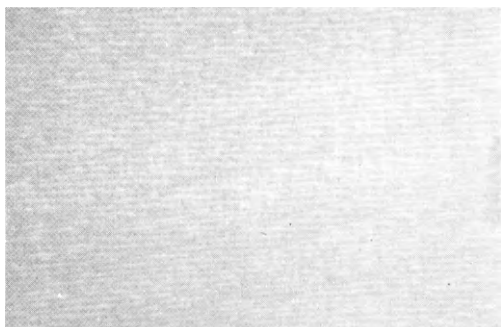


Figure 13. Longitudinal section of NaCl-NaF eutectic showing continuous NaF fibers. (135X before reduction).

Convection can break fragile dendrites, producing randomly-oriented nuclei that alter the structures of cast alloys, for example, during solidification. Dendrites frequently form during the early stages of crystal growth from flux systems (20). Subsequent backfilling between dendrite branches during the later stages of reduced growth rate results in physically sound, equidimensional crystals. Misalignment between dendrite branches during the backfilling process results in dislocations that are subsequently propagated throughout the crystal. It is highly likely that the degree of dendrite misalignment is influenced by the magnitude and nature of convection currents during the early stages of crystal growth from flux systems.

#### Electrophoresis

Electrophoresis, which involves the transport of electrically charged ions or particles in an electric field, is the most useful technique available for the separation of complex mixtures of proteins. Most electrophoretic separations are conducted on an analytical or micropreparative scale and involve various schemes, including the use of

gels or porous solid media, steep solute gradients, or thin fluid films to reduce the effects of convection associated with temperature gradients and solute-solvent density gradients and inhibit sedimentation of large particles (e.g., living cells). A source of convection resulting from temperature gradients is the solution heating caused by passage of an electric current. Electrophoresis in a free solution was first demonstrated aboard Apollo 14, using deoxyribonucleic acid, hemoglobin and soluble dyes. Further experiments were conducted aboard Apollo 16 with polystyrene latex as models for living cells (21). While equipment problems were encountered in the Apollo 14 experiments and backflow occurred as a result of electro-osmosis in the Apollo 16 experiments, the studies demonstrated that the effects of gravity-induced sedimentation and thermal convection were eliminated in zero gravity.

Experiments on the separation of the proteins ferritin and hemoglobin in one case and a suspension of human red blood cells in the other were conducted aboard Skylab (Ref. (3), p. 729). Simple equipment of the isotachophoresis type, a process characterized by self-restoring boundaries between compartments and in which the sample is introduced at the interface between two homogeneous buffers, was employed. While sharp boundaries were observed in the blood cell experiments, they were curved. Nevertheless, the Skylab experiments, in combination with corresponding ground-based studies, demonstrated that isotachophoresis can be employed for the separation of living cells.

In a series of experiments on Apollo Soyuz, electrophoresis and isotachophoresis columns were used to examine the separation of three species of fixed red blood cells (rabbit, human and horse), fresh rabbit and human red blood cells, human peripheral blood lymphocytes and human fetal kidney cells (Ref. (4), p. 20-1). Separation of human lymphocytes was not achieved, but separation of the three types of fixed red blood cells was obtained and frozen live cells were transported into space, electrophoretically processed and returned as viable cells. The electro-osmosis effect, encountered in the Apollo 16 experiments, was reduced by coating the insides of the electrophoresis columns with a biocompatible material with a zeta potential close to zero.

The successful separation of human kidney cells is particularly interesting from the standpoint of space processing economics and commercialization. The important enzyme urokinase, which is capable of producing blood clot lysis by conversion of plasminogen to plasmin, can currently be produced only by inefficient procedures involving cultures of cells from human fetal kidneys and demand far exceeds current capacity (Ref. (4), p. 20-5). The ability to isolate the approximately 5 percent of the cells in the cortex of the kidney that produce urokinase by zero-gravity electrophoresis, followed by culturing of the isolated "producing" cells on earth, is an example of the way in which space processing of relatively small quantities of material could support a large ground-based operation.

A study of free-flow electrophoresis, a method capable of large flow rates but particularly susceptible to convection and sedimentation problems on earth, was also conducted aboard Apollo Soyuz (Ref. (4), p. 21-1). Good separations were achieved with rat lymph node cells containing human

erythrocytes as markers, rat spleen cells and rat bone marrow cells. A comparison of ground-based and zero-gravity separation for rat bone marrow is shown in Figure 14.

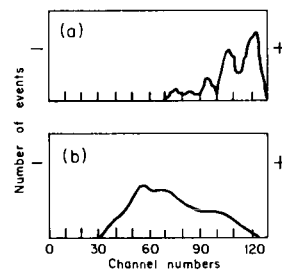


Figure 14. Separation of bone marrow cells under zero-gravity (a) and one-gravity (b) conditions. From Ref. (4), p. 21-16.

### III. Containerless Processing

An attractive feature of zero-gravity processing of materials is the ability to handle a reactive liquid, for example, without the requirement of a container for confinement. Containers are frequently a source of contamination in melt processing, particularly at high temperatures. In some cases, for example the high-melting-point rare earth oxides, containers that do not react substantially have not been found. In many cases, even small concentrations of impurities can adversely affect optical and electrical properties, decreasing, for example, optical transmission or carrier lifetimes.

Such processes as vapor-liquid-solid, Verneuil, floating zone and skull melting have been developed for the growth of crystals in the absence of foreign-material containers. To some degree, all of these methods have thermal mass problems, thermal conductivity problems associated with large solid supports or containers and/or large-melt support problems. In floating zone and pedestal techniques, melt support and shaping have been achieved to some extent by melt levitation but this involves establishing dynamic equilibrium between the supporting force and the pull of gravity under thermal and geometry conditions that frequently change with time.

Various methods exist for positioning melts in space. The same zone and pedestal techniques used on earth are applicable and modifications, in which small uniformly-spaced support (and materials feed) rods of the same composition as the melt serve for positioning, are possible and can be arranged in such a manner as to improve thermal symmetry. Acoustic and electromagnetic fields can be used at lower power levels and to support larger masses than on earth. However, such techniques can cause convection and oscillations in the melt, reducing other potential benefits of zero-gravity processing. Questions arise concerning the best methods for heating large suspended melts in ways that will not distort the positioning fields and cause impedance mismatch. Techniques involving absorption of radiant energy will probably play an important role.

Containerless materials processing experiments

have been conducted in space and relevant ground-based studies have been made on electromagnetic (Ref. (3), p. 603) and acoustic (Ref. (3), pp. 647 and 679) positioning of containerless liquids. The ends of cylindrical single crystal rods were melted during Skylab missions 3 and 4 to form large drops supported at one end by the solid rod (Ref. (3), p. 257). Directional solidification from the interface with the support crystal resulted in material with a continual reduction in dislocation density with fraction crystallized from values approximating those of the seed crystal to concentrations reduced by a factor of about 6 after growth of 1 cm. In a sample doped with selenium, the material solidified last exhibited distinct periodic banding when examined by x-ray topography and chemical etching. The banding is attributed to growth rate variations associated with a cyclic increase in dopant concentration at the solid-liquid interface followed by removal by diffusion (22).

The behavior and stable sizes of floating zones of water were determined in a series of experiments conducted on Skylab 4 (Ref. (3), p. 837). Rotational instabilities of the type shown in Figure 15 were observed. The C-mode (right side of Figure 15), which had not been previously observed, could be eliminated by increasing the water viscosity, using a soap solution-air emulsion. The relative stabilities of the axisymmetric and C-mode configurations as functions of rotation rate and zone length were found to generally agree with Plateau simulation studies (6,7), discussed further in the section below on zero-gravity simulation.

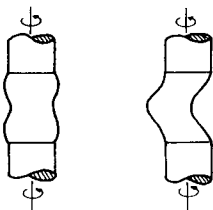


Figure 15. Axisymmetric (left) and C-mode (right) shapes of rotating liquid zones. From Ref. (5), p. 189.

While floating zone configurations are attractive for space processing, convection can occur as a result of surface tension gradients (14,15,16) and undesirable liquid-solid interface shapes may be present (Figure 1b). For these reasons, and on the basis of the results from the InSb-GaSb directional solidification experiments discussed above, it may be desirable not to eliminate entirely from consideration for zero-gravity materials processing some of the more conventional container techniques.

Container surfaces also serve as favorable sites for heterogeneous nucleation. Calcium aluminum silicate glass doped with neodymium is a commercial laser material. Increasing the calcium content relative to aluminum would increase laser efficiency but causes crystallization as a result of nucleation at the container walls. The use of zero-gravity processing might allow preparation of the desired calcium-rich glass (23). It might also be possible to produce laser glasses in the desired final forms in orbit, eliminating the necessity for wasteful and expensive machining operations.

#### IV. Zero-gravity Simulation

There are various ways in which zero-gravity conditions can be simulated on earth. Buoyancy-driven convection and the effects of convection can be minimized by proper selection of liquids and gases with favorable values of such physical properties as density, viscosity, heat capacity and surface tension and, in particular, the temperature dependence of these properties. Buoyancy-driven convection can be eliminated by use of proper temperature gradients or, in the case of electrically-conductive liquids, by application of a magnetic field, or can be overridden by forced convection. However, the use of such techniques imposes, in many cases, undesirable system and/or geometry restrictions. The following examples illustrate some of the work that has been conducted on relatively-direct simulation of zero-gravity conditions and problems that are encountered.

Zero-gravity floating zones can be approximated by the Plateau method (5,6,7), in which one liquid is suspended in a second liquid with which it is immiscible but equal in density. The technique produces excellent simulation of zero-gravity conditions and results concerning zone size and rotational stability are in good agreement with Skylab experiments (Ref. (3), p. 837). However, the Plateau method possess an inherent limitation in its ability to model zero-gravity zones because of the presence of an outer liquid surrounding the zone, which influences the rotational and vibrational instability modes of the zone and the form of flow patterns in the zone (Ref. (3), p. 842).

Studies have been conducted on zero-gravity simulation in the growth of crystals from solutions, by examining systems for which the change in solution density with concentration and the heat of crystallization are both very small. When other necessary constraints are imposed, including the ability to produce equidimensional crystals, low solvent volatility to minimize the tendency for crystal formation at the surface, and favorable solubility relationships, the number of possible systems becomes relatively small. Experiments with a candidate system thymol-diethyl carbonate (using schlieren observation techniques) gave unusual results, including an abrupt transition from equidimensional to dendritic growth and, in a sphere dissolution experiment, the formation of a very stable plume that wound through the experimental cell (24). It became apparent in the course of these studies that reducing the Grashoff number, the ratio of buoyant to viscous forces, to values approximating those obtainable with a gravitational acceleration on the order of  $10^{-6}g$ , is very difficult on earth.

While it is difficult on earth to accurately simulate zero gravity conditions in materials processing, behavior at zero gravity can be predicted in many cases on the basis of properly designed experiments conducted on earth. Many ground-based experiments were conducted in support of the Skylab and Apollo Soyuz experiments and broader studies, both theoretical and experimental, with the objectives of understanding and predicting the behavior of materials at zero gravity have been conducted and are in progress (3,4,25). It is anticipated that considerably more theoretical and experimental work will be conducted in support of the forthcoming Spacelab missions.

## V. Future Opportunities

The Apollo Soyuz mission was the last manned space flight with Apollo-derived systems designed to be used only once and to return only a fraction of the original payload to earth. The next manned orbital system suitable for extensive space processing of materials will be the Space Transportation System (STS), which will be reusable and able to return large payloads. Equipment costs will be minimized by the use of flexible general-purpose designs that will allow a variety of experiments to be conducted with minor apparatus modifications. A shuttle vehicle system, consisting of a non-retrievable external propellant tank, reusable solid rocket boosters and a reusable orbiter, will be periodically placed in orbit and remain there for a period of about 7 days before returning to earth. The orbiter cargo bay will be capable of carrying a variety of payloads, including the Spacelab unit being developed by the European Space Agency. Various Spacelab configurations are planned, some of which will have pressurized modules that can be manned by technically trained personnel capable of conducting in-flight materials processing experiments. The first STS flight is scheduled for 1979.

Recent requests from the technical community to identify significant experiments and requirements for future space processing missions resulted in over 100 responses from the U.S. and abroad. Studies of these suggestions and of other promising materials experiments are being conducted by working groups under NASA sponsorship and by contractors in order to identify facilities and power requirements and scientific areas requiring further theoretical and ground-based experimental studies.

Interim opportunities for zero-gravity materials processing experiments are being provided by sounding rocket flights that began in December of 1975 and are planned to continue at a rate of about three per year through 1980. Approximately 5-6 minutes of near-weightlessness are available during each flight, with as much as 10 minutes per flight projected for the later stages of the program when larger sounding rockets become available. Flight characteristics and vehicle resource information are available and an inventory of general purpose equipment has been developed, including a furnace, temperature control unit, devices for electromagnetic and acoustic levitation, specialized furnaces and an electrophoretic separator.

## VI. Summary

It is not possible to treat the scientific principles that underlie materials processing in space in any depth in an overview such as this. Likewise, it is not possible to review all of the space processing experiments conducted to date. I have attempted to focus on those physical processes and properties that are strongly influenced by gravity and to briefly describe the results of pertinent zero-gravity experiments. Many good experiments were not mentioned and the detailed mission reports (3,4) should be consulted for additional information.

## VII. Acknowledgements

I would like to thank Dr. James H. Bredt, NASA Headquarters, for the opportunity to present this

material and express appreciation to Mr. E. C. McKinnan, Dr. R. S. Snyder and Dr. R. E. Allen, NASA Marshall Space Flight Center, for recent data and valuable discussions. I am indebted to Dr. A. S. Yue, University of California at Los Angeles, for providing photographic originals for Figures 12 and 13, and to Dr. C. D. Brandle, Union Carbide Crystal Products Department, for Figure 6 and related information.

## References

1. Stuhlinger, E., "Materials Processing in Space, A Look Toward the Future," Astronautics and Aeronautics, Vol. 13, No. 5, 1975, pp. 20-41.
2. Aviation Week and Space Technology, January 26, 1976, pp. 46-64.
3. Proceedings of the Third Space Processing Symposium - Skylab Results, NASA TM X-70252, 1974.
4. Apollo-Soyuz Test Project, Preliminary Science Report, NASA TM X-58173, 1976.
5. Carruthers, J. R., "The Application of Drops and Bubbles to the Science of Space Processing of Materials," Proceedings of the International Colloquium on Drops and Bubbles, California Institute of Technology, 1974, pp. 161-193.
6. Carruthers, J. R. and Grasso, M., J. Appl. Phys., Vol. 43, No. 2, 1972, pp. 436-445.
7. Carruthers, J. R. and Grasso, M., J. Cryst. Growth, Vol. 13/14, 1972, pp. 611-614.
8. Lacy, L. L. and Otto, G. H., AIAA/AGU Conference on Scientific Experiments of Skylab, Huntsville, Alabama, AIAA Paper No. 74-1242, 1974.
9. Lacy, L. L. and Otto, G. H., AIAA Journal, Vol. 13, No. 2, 1975, pp. 219-220.
10. Yue, A. S. and Yu, J. G., AIAA/ASME 1974 Thermophysics and Heat Transfer Conference, Boston, Massachusetts, AIAA Paper No. 74-646, 1974.
11. Pfann, W. G., Zone Melting, Wiley, New York, 1958.
12. Wilcox, W. R., et al., "Directional Solidification of InSb-GaSb Alloys," Skylab Science Experiments, Vol. 38, Science and Technology, 1975, pp. 27-41.
13. Wilcox, W. R., "The Role of Mass Transfer in Crystallization Processes," Preparation and Properties of Solid State Materials, Vol. 1, R. A. Lefever, ed., Dekker, New York, 1971, pp. 37-182.
14. Chang, C. E. and Wilcox, W. R., Int. J. Heat Mass Transfer, Vol. 19, No. 4, 1976, pp. 355-366.
15. Chang, C. E. and Wilcox, W. R. "Thermocapillary Flow in a Cylindrical Liquid Drop at Zero Gravity," Proceedings of the International Colloquium on Drops and Bubbles, California Institute of Technology, 1974, pp. 194-207.

16. Chang, C. E., Lefever, R. A. and Wilcox, W. R., "Analytics of Crystal Growth in Space," Final Report, NASA Contract No. NAS8-29847, 1975.
17. Grodzka, P. G. and Bannister, T. C., Science, Vol. 176, No. 4034, 1972, pp. 506-508.
18. Gatos, H. C. and Witt, A. F., "Indium Antimonide Crystal Growth, Experiment M562," Final Report, NASA CR-120558, 1974.
19. Lefever, R. A. and Chang, C. E., Bull. Am. Phys. Soc., Vol. 20, Series II, 1975, p. 1511.
20. Chase, A. B., "Exploratory Flux Crystal Growth," Preparation and Properties of Solid State Materials, Vol. I, R. A. Lefever, ed., Dekker, New York, 1971, pp. 183-264.
21. Snyder, R. S., et al., Separation and Purification Methods, Vol. 2, No. 2, 1973, pp. 259-282.
22. Wiedemeier, H., et al., Third American Conference on Crystal Growth, Stanford, California, 1975, Abstracts, p. 108.
23. Aviation Week and Space Technology, January 26 1976, p. 53.
24. Wilcox, W. R., et al., "Analytics of Crystal Growth in Space," Annual Report, NASA Contract NAS8-29847, 4 June 1974, pp. 103-106.
25. Passaglia, E. and Parker, R. L., NBS Space Processing Research, NBSIR 76-980, National Bureau of Standards, February 1976, NASA Contract W-13,475, Mod. 4.

# METHODS UTILIZED IN EVALUATING THE PROFITABILITY OF COMMERCIAL SPACE PROCESSING

H. L. Bloom\* and P. T. Schmitt\*\*

*General Electric Company, Valley Forge, Pa.*

## Abstract

Paper reports on NASA-funded studies which 1) identify potential commercial space processing products 2) derive technical and programmatic process development data and 3) evaluate potential profitability of manufacturing the products. Paper focuses on Profitability Analysis. Initially, groundwork is laid for Business Concept Definition and Assessment, and the ties among ground and space functions. Subsequently, Throughput Analysis is demonstrated by analysis of processing Surface Acoustic Wave Devices. Paper documents a mathematical financial analysis model, "INVEST", and provides key profitability measures for space processed isoenzymes.

## Introduction

Recent studies (1, 2, 3) carried out under NASA aegis have stepped back from the analysis of Space Pro-

cessing techniques and experimental investigations to focus on a more mundane, but real, problem---commercial practicality.

Typically, at the General Electric Company, we have completed a three-phase study "Identification of Beneficial Uses of Space" (Figure 1) under contract NAS8-28179 from NASA's Marshall Space Flight Center. This effort identified a community of potential Space Processing Users, defined plans for specific technical steps and administrative processes required in carrying out specific commercial Space Processes, and realistically assessed

- (1) the resources required to carry out the plans,
- (2) the potential returns from such ventures, and
- (3) resultant profitability.

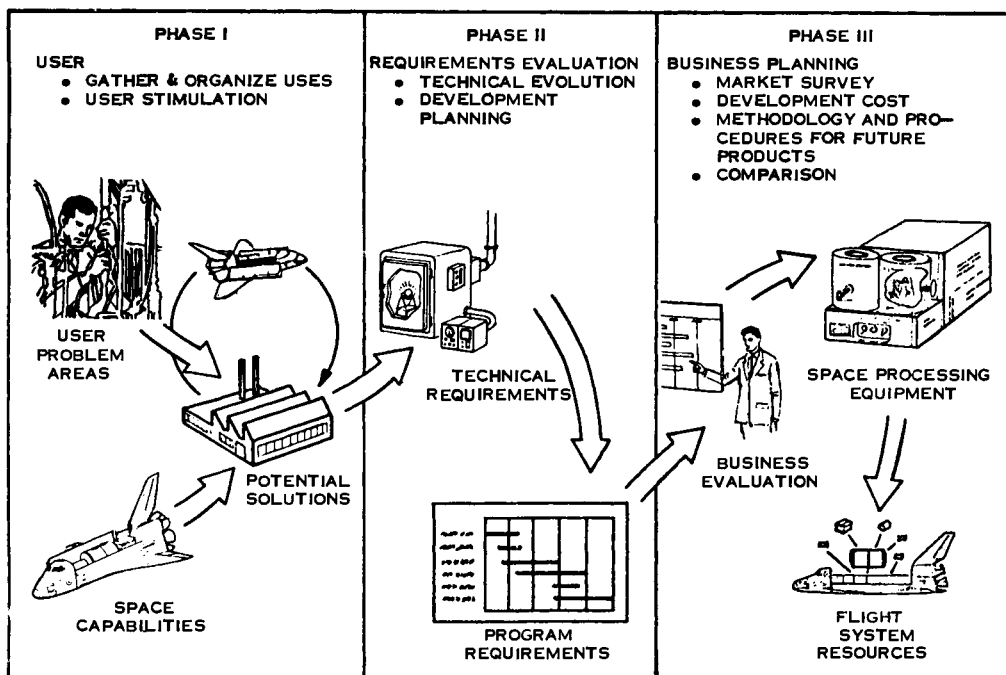


Figure 1. Beneficial Uses of Space Phases I, II, and III Relationships

\* Manager of Advanced Space Processing Programs

\*\*Program Development Engineer

Table 1, from Phase 1 of this Study, is an early list of those products which were estimated to be of the highest potential value. Subsequent Phases of that Study concentrated on the four products listed in Figure 2.

ing the visibility of needed development and production resources, in organizing cost data, and in maintaining communications between the Aerospace and non-Aerospace participants.

Table 1. High Value Products

Products	Basic Space Processes Required
High purity vaccines	Electrophoresis
High specificity viral insecticides	Electrophoresis (free flow)
Multi-gigahertz frequency surface acoustic wave electronic components	Large crystal growth and vibration-free lithography
Single crystal and/or eutectic high temperature turbine buckets	Large crystal growth and/or convectionless solidification
High purity, ductile tungsten x-ray targets	Levitation melting and supercooling
High purity radioisotopes	Particle manipulation by small forces
Large, uniform silicon single crystals	Large crystal growth and/or convectionless solidification
Uniform garnet single crystal films	Convectionless epitaxial crystal growth
Transparent metal oxides	Levitation melting and uniform supercooling
High specificity isoenzymes	Electrophoresis (large pore gel) or isoelectric focussing

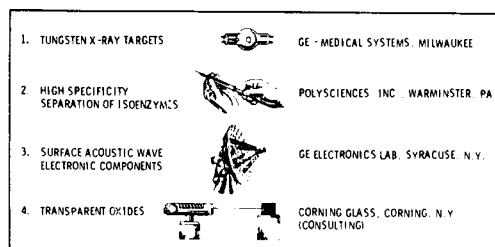


Figure 2. Products Analyzed in Phase III Study

In similar efforts, Reference 2 addresses commercial aspects of space manufacturing single crystal silicon ribbon for use in integrated circuit substrates, while Reference 3 develops data for space manufacturing single crystals used in computer memories. A review of factors involved in commercialization of space processing (Fig. 3) identifies the engineering and economic factors (left side of figure) developed in the aforementioned studies, and the legal/political factors (right side of figure) which have been left for later consideration. As demonstrated in this figure, analysis of the engineering/economic factors involves a mix of Aerospace and non-Aerospace contributions. For the study discussed in Reference 1, a key step in blending Aerospace and non-Aerospace methods is the construction of Work Breakdown Structures (Figure 4) for programs to develop and produce the products under study.

While such structuring of tasks and documenting of a related glossary of aerospace terms are not common to commercial industry, they are valuable in maintain-

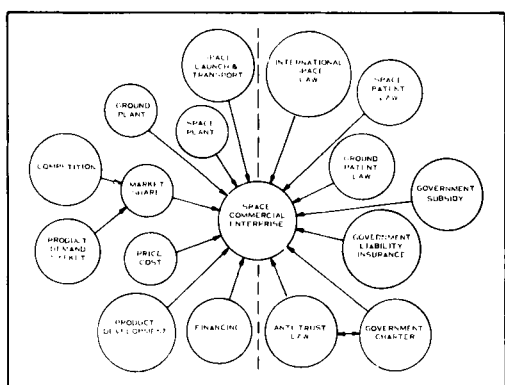


Figure 3. Factors Involved in Space Commercial Enterprise

It is important to note that, to foster such communications, each Work Element in the Work Breakdown Structure is backed by a description of the task involved in the Work Element, a list of the resources required to accomplish the task, and estimates of the costs of such resources.

#### Key Methodology

Definition and assessment of the business aspects of Space Processing requires a thorough understanding of the interactions among Technical, Resources Planning, and Market Analysis activities. An overview of a method of accounting for such interactions is shown in Figure 5. As utilized in the Study of Reference 1, this

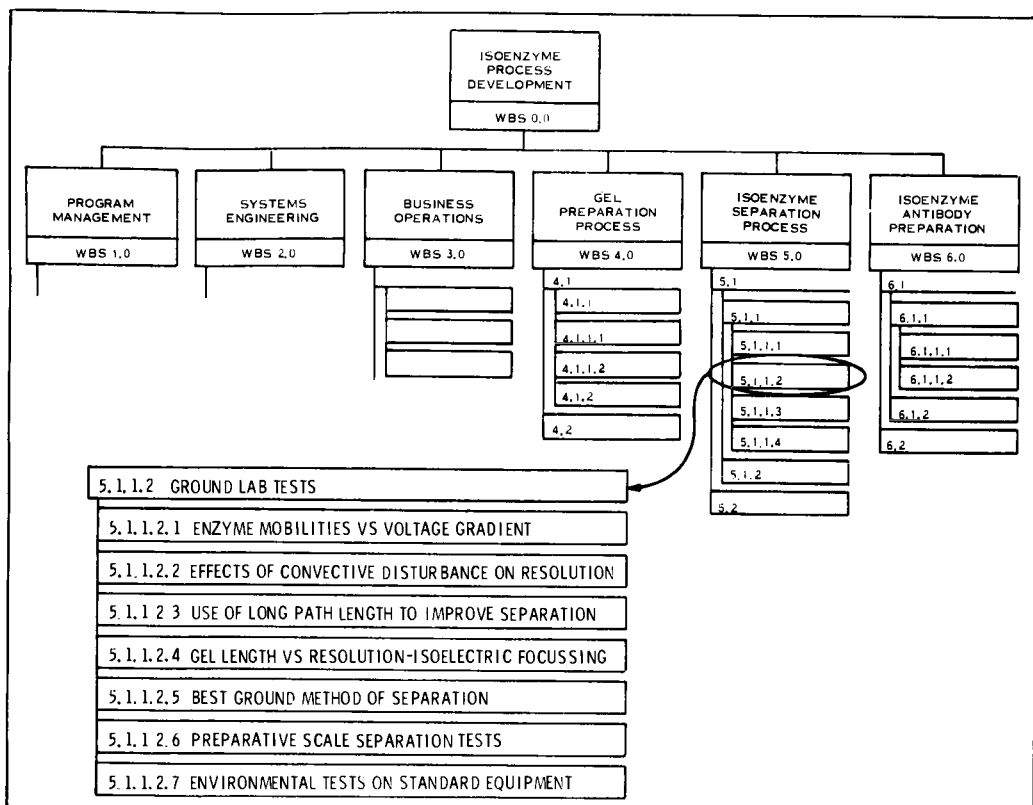


Figure 4. Typical Work Breakdown Structure

methodology includes, for example, analyses of such source materials as national and corporate requirements and planning documents; dialogs with representatives from industrial organizations to identify pro-

ducts of interest, the associated implementation problems and potential benefits, as well as to forecast the business climate for the products. In addition, the

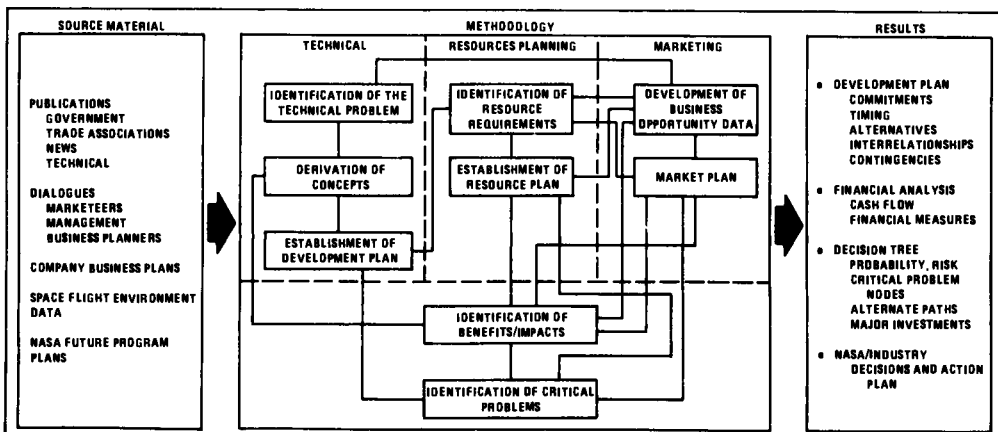


Figure 5. Future Business Planning Methodology

methodology includes detailed analyses of NASA's plans for space experimentation and development of pertinent space systems, such as the Space Shuttle and Spacelab. Finally, the methodology provides such results as definition of key research and development programmatic elements, critical technical and administrative problems, and associated decisions required of NASA and Industry.

Although details of the content of each of the steps depicted in Figure 5 and criteria for analyzing the key tradeoffs are beyond the scope of this paper, typical such information is to be found in Reference 1. This paper, however, does address several key areas involved in producing Financial Analysis data.

### Throughput Analysis

Throughput Analysis answers the question "How much resource (material, labor, power, etc.) must be put into a given process step in order to extract a given output?" When carried out for each sequential process step, over a total process, working back from the final required output to the starting raw material, we obtain the total set of utilized resources, which enable the determination of Product Unit Cost, quantity of raw material, required capacity of processing equipment, energy consumed in process, process duration, etc. necessary for Financial Analysis.

The driving requirement for "Throughput" depends upon understanding of the quantity of final product required, which, in turn, is derived from the market forecast.

Other criteria affecting "throughput" include shrinkage (due to fabrication waste and defect losses), process time and power (impacting energy needs), degree of automation (impacting labor hours), etc. A typical example of "throughput" for one step in the process of manufacturing Surface Acoustic Wave Devices (1) is given in Figure 6.

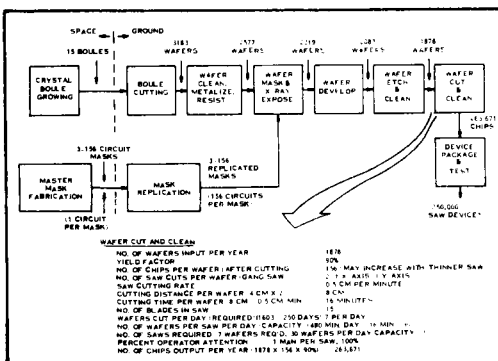


Figure 6. Sample Throughput Analysis Summary (For Surface Acoustic Wave Devices) (Throughput Per Year)

Reference 2, utilizing a unique crystal growing technique, has carried out a comparison of "throughput" of that space-based technique with that of the usual ground-based method. Results are depicted in Table 2. Since "throughput" has such a profound effect on Unit Product Cost, the improvement noted in the Table has contributed considerably to the profitability results in Reference 2.

Table 2. Silicon Crystal IC Processing (From Reference 2)

Operation	Earth Production			Space Production		
	Avg. Yield	Cum. Yield	Equiv. Chip Quantity	Avg. Yield	Cum. Yield	Equiv. Chip Quantity
1. Start (equivalent material)	100%	100%	375	100%	100%	325
2. Wafer cutting	59	54	221	(100)	100%	325
3. Wafer Polishing	63	37	139	(100)	100%	325
4. Geometric Layout	81	40	113	(97)	97	363
5. Channel Diffusion	93	29	107	95	92	346
6. Base Diffusion	90	26	92	(98)	90	319
7. Emitter Diffusion	45	22	87	85	77	288
8. Metallization	90	20	71	(96)	74	276
9. Wafer Test	25	15	55	25	55	207
10. Wafer Scribing	95	11	47	(94)	52	195
11. Tie & Wire Bond	95	11	40	(94)	49	183
12. Packaging	95	10	38	95	46	174
13. Final Test	75	8	28	75	35	130

( ) Denotes Change Total Improvement factor =  $\frac{130}{28} = 5.6$

### Cost of Operations in Space

For specific products investigated in Reference 1, the cost of operations in space is a significant portion (40% to 70%) of Unit Production Cost. In that reference, some operations costs account for launch to orbit; in-orbit utilization of crew time, electrical power and data management systems; as well as pre-and post-flight launch site operations - calculated for both developmental and full-scale manufacturing phases. While Reference 2 lists "Transportation Costs" at 12% to 26% of Unit Production Cost, such items as power and data management costs have been accounted for under other headings.

Thus, we can expect the cost of utilizing space as a manufacturing milieu---that is, use of the Space Shuttle and its resources, to be a significant portion of the costs of commercial Space Processing. Such a circumstance dictates the need for a method to calculate User Costs for the Space Shuttle. While both References 1 and 2 have developed User Cost Models, since their publication, NASA has generated preliminary User Charge Policy which will, eventually, develop into the official policy. When available, the official policy should be used by interested parties. In the interim, for relative comparisons of various processes, the Models of either Reference 1 or 2 may be utilized. Table 3 summarizes the space operations cost factors of Reference 1 - where up-transport refers to the phase of flight in which each particular Space Shuttle resource (payload weight and

volume, energy, data handling and communications capacity) are utilized.

Table 3. Recommended User Cost Allocation Rates for Shuttle/Spacelab Utilization

SHUTTLE RESOURCE UTILIZED	RATES UTILIZED IN STUDY*
Up-Transport Volume	\$13.780/cubic meter
Up-Transport Weight	\$108.81/kg
On-Orbit Energy	\$1721/kWh
On-Orbit Crew	\$8448/man hr
On-Orbit Data Transmission	\$4286/MHz of RF Bandwidth
On-Orbit Data Processing	\$2.38/word of Experiment Computer Storage
Down-Transport Weight	\$184.44/kg.
Ground Operations, Mechanical Handling	\$1.278/cubic meter
Ground Operations, Electronic Handling	\$20.89/word of Experiment Computer Storage

\*Based on  $C_M$ . Average per-mission Operational Cost =  $\$10.7 \times 10^6$ .

### Financial Analysis Model

The "proof of the pudding" for commercial Space Processing is the analysis that assembles all the costs and their timing, the product selling price with its market and timing, and determines the potential profitability of specific products. Figure 7 depicts the Financial Analysis Model utilized in Reference 1. Starting with the six basic inputs listed on the left, the model generates the four basic measures of profitability commonly utilized in assessing commercial ventures. In addition, the model allows determination of another key measure - break-even point, which for Reference 1 is defined by Figure 8. This model has been programmed for computer operation under the name "INVEST", and is enhanced in value by providing interactive capability, as shown in Figure 9. Details of the elements pictured in Figure 7 are too voluminous to include in this paper, and will be found in the Phase III report of Reference 1.

While the Financial Analysis Model for Reference 2 is structured somewhat differently from that in Figure 9, and also accounts for inflation, the measures

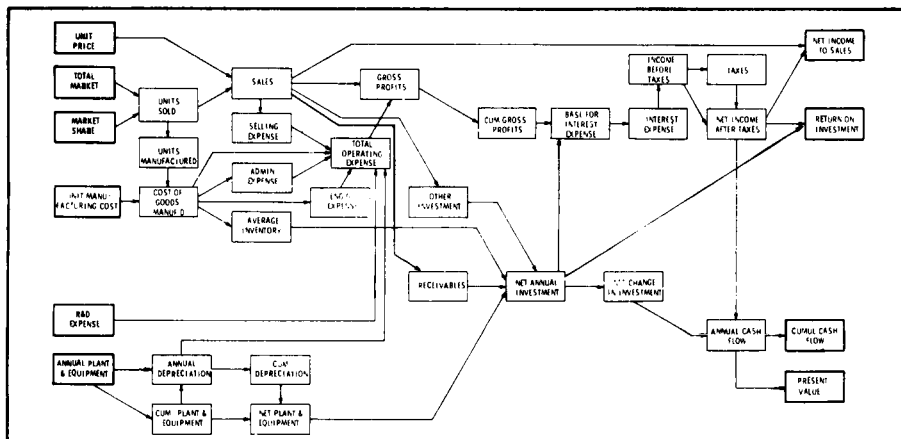


Figure 7. Financial Analysis Method for Assessment of Space Processing Opportunities

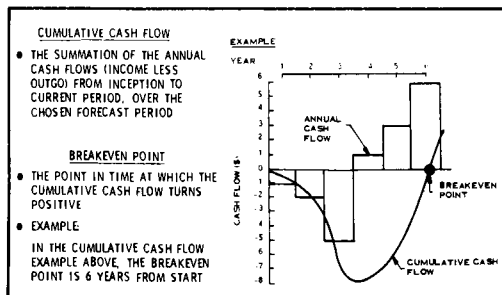


Figure 8. Definitions of Key Financial Measures

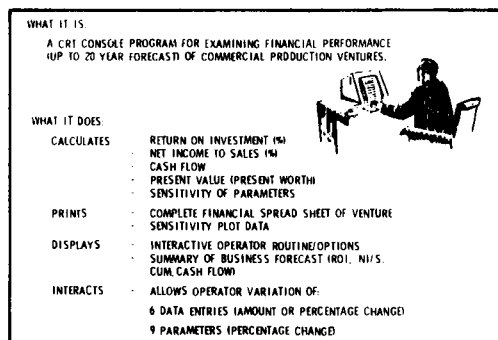


Figure 9. "INVEST" Program - Interactive New Venture Examination & Sensitivity Test

of profitability are essentially the same. Both models enable ready evaluation of the sensitivity of profitability with variations in input factors or such constants as interest or tax rates.

Financial analysis of a typical space processed product is demonstrated in Figure 10. Using the INVEST program, the financial measures of profitability have been calculated for two cases. In case A, all the Research and Development for gel electrophoresis is the burden of the User, despite its potential applicability to other biologicals and/or pharmaceuticals. In case B, it is assumed that the general research in space-based gel electrophoresis is carried out by NASA (or other source) and only that directly involved in separation of isoenzymes is borne by the User. While other measures show relatively little change, the breakeven point is shortened considerably in Case B.

#### Conclusions

The potential profitability of Space Processed products has been analyzed in several Studies. In general, such products appear to offer potentially better capabilities than their present ground processed counterparts. Even though expected capabilities range as high as several times better than those of present ground-processed products, market analyses indicate that potential commercial Users are reluctant to pay an equivalent increase in price for the better product. This, coupled with the fact that Space-processed products tend to higher production costs than present ground-processed products, makes for comparatively late breakeven points.

The derived profitability analysis methods can be utilized, at this stage of development, to improve the potential profitability. This can be done by analyzing

the sensitivity of profitability to various factors, and operating upon those variables that impact Cash Flow most. For example, Research and Development costs may be shared or otherwise reduced. On-orbit Production equipment concepts may be improved to reduce weight, size or power requirements.

Further interaction with market analysts may be required to determine the acceptability of more advantageous life cycle/price relationships.

In any case, Profitability Analysis appears to offer another set of criteria for selection from among the many experiments identified in the Space Processing disciplines.

Finally, while pure research in Space Processing must always remain a key stone in future programs, the enthusiastic support of industry will be more easily obtained if their technical needs are supported by favorable economics.

#### References

1. Study for Identification of Beneficial Uses of Space (Phases I, II, III) Final Report, Contract NAS 8-28179, GE Documents No. 73SD4259, 73SD4281, 75SDS4281 December 10, 1972 - November 30, 1975
2. Feasibility Study of Commercial Space Manufacturing, Contract NAS 8-31353, McDonnell Douglas Document, MDC E 1400, December 1975.
3. Ulrich, D., Chung, A., Yan, C. and McCreight, L., Economic Analysis of Crystal Growth in Space, Contract NAS 8-27942, Document DCN-1-1-50-13668 (1F), July 1972.

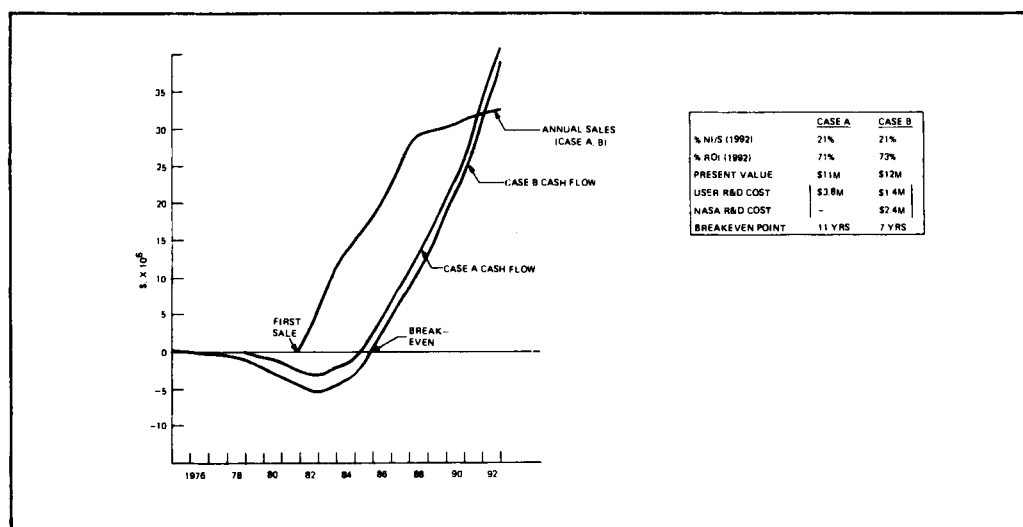


Figure 10. Isoenzymes Cash Flow

# CONTRIBUTION OF THE SPACELAB DATA MANAGEMENT SYSTEM TO LOWER COST SPACE RESEARCH

J. J. Burger\* and E. R. Tanner\*\*

## Abstract

This paper reviews the design and operation of the Spacelab data management system as it has evolved. Significant improvements and extensions of the original baseline system have been incorporated and will be discussed. They include the capability for the remote control of Spacelab subsystems, improved remote data acquisition units, a high-rate digital data multiplexer, and an improved high-rate digital recorder. Emphasis will be placed on the overall system aspects, including considerations on the use of minicomputers as an adjunct to the basic Spacelab data system. The approach for experiment related software production and integration will be addressed as well. The paper focuses on the contributions of the data management system in reducing the cost of research in Spacelab.

## I. Introduction

Past experience has clearly demonstrated the benefits and scientific returns from space research. The view of the Earth with a global coverage, unobscured viewing to the Sun and space, access to the space plasmas, and finally cancellation of the effects of gravity represent features of space which are unique for research in many disciplines. To provide a more cost-effective access to space for exploiting these features with the increasingly more ambitious equipment foreseen, NASA is developing the Space Transportation System. At the same time it is recognized that on the ground one of the basic drives for cost effective progress in science and technology is provided by laboratory research. Here, the competent investigators are provided with adequate equipment to carry out their experiments in a favorable environment, operating with their instruments and observational data in a closed feedback loop. To allow this laboratory approach to take place in space is the prime aim of the Spacelab, which ESA is developing for augmenting the capability of the Space Transportation System.

The Spacelab is designed as a modular, reusable, general purpose laboratory which will be flown to and from space in the cargo-bay of the Orbiter. It comprises two basic elements, a habitable pressurized compartment (module) and unpressurized equipment mounting platforms (pallets), which can be flown separately or in various combinations. The general features of the external configuration are shown in Fig. 1.

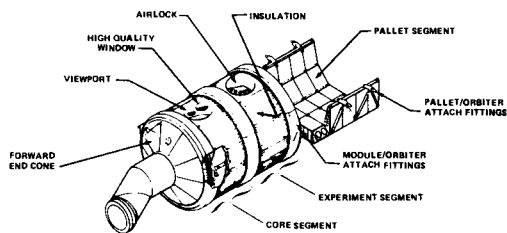


Fig. 1 Spacelab external configuration.

Spacelab offers all general type support which is usual for ground laboratories (e.g. structural support, power conditioning and distribution, air conditioning, etc.) with standard, but flexible interfaces, allowing easy integration of a multitude of experiments.<sup>1</sup> In addition to this general support, the Spacelab provides several needed support items, which are not yet common as a standard for ground laboratories, but which will contribute significantly to lower costs for space experiments. Among these is the command and data management system (CDMS) which is the subject of this paper.

## II. The Overall Spacelab Data Handling Concept

Spacelab missions will serve simultaneously a large number of experiments, nearly all of which will require some degree of control as a function of the mission profile and will acquire data which have to be processed further by electronic means. The main functions of Spacelab data handling are summarized as follows:

- (1) Control and management of Spacelab subsystems
- (2) Control of experiment operations by means of subsystem resources allocation
- (3) Acquisition of experiment data and associated experiment data processing
- (4) Formatting and merging of experiment data for down-link transmission
- (5) Up- and down-link communications with the ground operations center.

\*ESA Space Science Department, ESTEC, Noordwijk, The Netherlands.

\*\*Systems Requirements and Analysis Branch, NASA/MSFC, Huntsville, USA.

The basic ground rule for designing the system responsive to these functions has been to minimize duplications while maintaining an easy integration of both experiments into Spacelab, and Spacelab with the Orbiter. This has led to the decision to use the Orbiter system for communications, and to provide in Spacelab a sophisticated computer system for management and processing of the data of subsystems and experiments. Since several Spacelab experiments are foreseen whose data acquisition rates will exceed the capabilities of the Spacelab computer system, a high rate digital multiplexer system is provided together with a digital recorder to cover periods when ground communication is not available. In addition it is recognized that some experiments will require data processing capabilities in excess of what the Spacelab computer system offers so that experiment specific data handling equipment should be considered as part of the overall system. A final major element of the Spacelab CDMS is the associated software. The five building blocks thus forming the Spacelab data handling systems are schematically shown in Fig. 2 and will be addressed in some detail in the following paragraph.

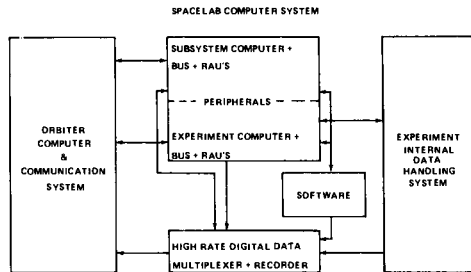


Fig. 2 Overall Spacelab data handling block diagram.

### III. The Orbiter Computer and Communication System

Like any space experiment, Spacelab payloads will require commands from and data transmission to the ground. For these functions Spacelab utilizes the available Orbiter system, shown schematically in Fig. 3. Figure 3 shows that a wide range of data rates can be accommodated by s-band and ku-band links, the details of which can be found in Reference 2.

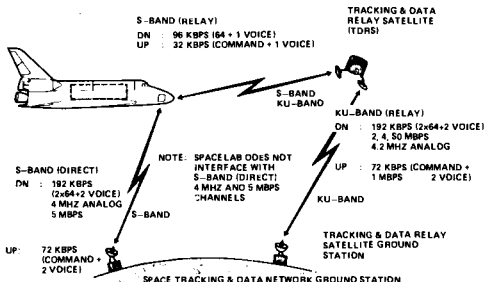


Fig. 3 Orbital communication links.

The interface between the Spacelab data and the Orbiter communication system is two-fold. First, for Spacelab system management and low rate experiment housekeeping data, a link is provided between the Spacelab CDMS computers and the 192 KBPS telemetry channel. The second interface connects the output of the high rate data multiplexer with the wide band ku-link. The capability of this link can be selected by the Orbiter ku-band signal processor according to mission needs, up to 50 MBPS.

The ground coverage for communications will vary according to the mission profile between 50 to 85 percent. The noncoverage periods are bridged by the Spacelab high rate digital recorder and by the Orbiter payload recorder for the lower data rates.

In addition to the Spacelab to Orbiter data communication links, Spacelab routes to the Orbiter caution and warning data to identify potential safety critical situations which may require corrective actions. The Orbiter provides the Spacelab CDMS system with guidance, navigation, control, timing, and ground commands. The Orbiter will also send the commands for initiating the Spacelab subsystem operations and for remote control of the Spacelab during checkout.

### IV. The Spacelab Computer System

The CDMS block diagram in Fig. 4 shows that the nucleus of the Spacelab data handling system is formed by three identical CII MITRA 125 S general purpose computers, the characteristics of which are summarized in Table 1. One computer is devoted to subsystems management and control, the second is reserved for experiment operations, and the third one serves as a back-up for the two others in case a malfunction should occur.

All communications between the computers and the rest of the CDMS are handled by input-output units, which control the transfer of external data into the computer core memory and from the memory to all peripherals on a priority basis and using direct memory access. The standard peripherals are shared by the two operating computers. In this way a mass memory unit is used for storage of all basic and flight application software for subsystems and experiments. It can be used for overlay of software programmes which exceed the 64 K core computer memory size. Other peripherals include three data display units with associated keyboards (two in the Spacelab module and one in the Orbiter aft flight deck) for communications with the two computers at the discretion of the payload specialists.

The Spacelab subsystem equipment is controlled during normal operations by the subsystem computer via the subsystem I/O unit, the subsystem bus, and remote acquisition units (RAU's), which can issue on/off and serial command words as well as receive analog and digital monitoring signals. These signals are processed and analyzed by the S/S computer to identify

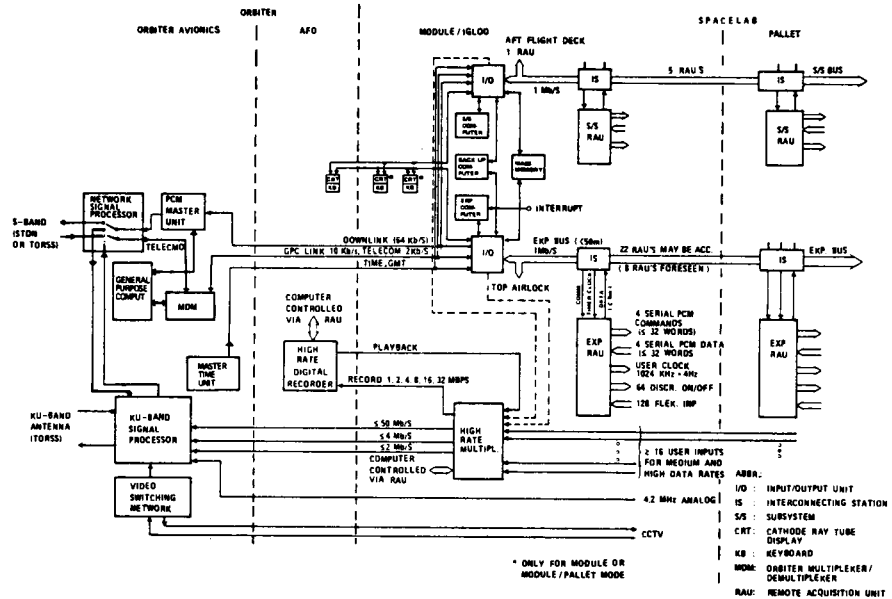


Fig. 4 CDMS block diagram.

Table 1 Computer characteristics

FORMATS	FLOATING POINT 32 BITS (24 + 8)		
OPERANDS: INSTRUCTIONS:	8,16,32 AND 24 + 8 (FLOATING POINTS) BITS 16 BITS		
CONTROL UNIT	MICRO-PROGRAMMED CONTROL UNIT		
CYCLE TIME 300 nS	MICRO-INTERRUPT CAPABILITY		
MICRO-INSTRUCTIONS 4 K WORDS OF 16 OR 20 BITS	GIBSON MIX $3.5 \times 10^5$ OPERATIONS/SECOND		
INSTRUCTION SET	<ul style="list-style-type: none"> <li>NUMBER OF INSTRUCTIONS 128</li> <li>FORMAT 16 BITS</li> <li>IMMEDIATE 8 BITS</li> <li>ADDRESSING CAPABILITY</li> <li>DIRECT 256 BYTES</li> <li>INDIRECT MEMORY DOUBLE WORD</li> <li>RELATIVE 512 BYTES</li> <li>BASED 256 BYTES</li> <li>INDEXED 64 K BYTES</li> <li>TYPE</li> <li>CALL AND STORE</li> <li>LOGIC AND COMPARISON OPERATIONS</li> <li>SHIFT OPERATIONS</li> <li>FIXED-TO-FLOATING AND FLOATING-TO-FIXED CONVERSIONS</li> <li>CONDITIONAL AND UNCONDITIONAL JUMPS</li> </ul>		
ADDRESSING MODES	<ul style="list-style-type: none"> <li>IMMEDIATE, DIRECT, INDIRECT,</li> <li>RELATIVE TO CURRENT ADDRESS, RELATIVE TO A PROGRAM COUNTER, HALF WORD,</li> <li>WORD, CHARACTER, DOUBLE WORD</li> <li>ADDRESSING CAPABILITY</li> <li>BYTE, WORD, DOUBLE WORD</li> </ul>		
NUMBER OF ADDRESSABLE REGISTERS	4 SPECIALIZED REGISTERS 62 DEDICATED REGISTERS 7 BASE REGISTERS		
COMPUTING SPEED	<b>FIXED POINT 16 BITS</b> ADD/SUB DIRECT 2 $\mu$ s INDIRECT 3 $\mu$ s MUL/DIV DIRECT 4 $\mu$ s INDIRECT 5 $\mu$ s		
	<b>FIXED POINT 32 BITS</b> ADD/SUB DIRECT 5.5 $\mu$ s INDIRECT 6.5 $\mu$ s MUL/DIV DIRECT 8.3 $\mu$ s INDIRECT 9.3 $\mu$ s		
INPUT/OUTPUT	<ul style="list-style-type: none"> <li>INTERRUPTS           <ul style="list-style-type: none"> <li>NUMBER OF EXTERNAL</li> <li>NUMBER OF INTERNAL</li> <li>NUMBER OF SOFTWARE</li> <li>INTERRUPT CONTROL</li> <li>PRIORITY SCHEDULER</li> </ul> </li> <li>DATA TRANSFER MODE           <ul style="list-style-type: none"> <li>PROGRAM CONTROLLED               <ul style="list-style-type: none"> <li>DATA RATE</li> <li>ND OF ADDRESSABLE PERIPHERALS</li> </ul> </li> <li>DIRECT MEMORY ACCESS               <ul style="list-style-type: none"> <li>DATA RATE</li> <li>CONTROL</li> </ul> </li> </ul> </li> <li>WORD LENGTH</li> <li>DISCRETE</li> <li>REAL TIME WORK</li> </ul>		
MEMORY	<ul style="list-style-type: none"> <li>TYPE: 18 MIL FERRIT CORES, 2 1/2 D CONFIGURATION</li> <li>CAPACITY: 64K 16-BIT WORDS (PLUS 1 PARITY BIT AND 1 PROTECTION BIT) EXTENDIBLE TO 512 K 16-BIT WORDS</li> <li>MDODULE: 16 K WORDS</li> <li>CYCLE TIME: 920 ns</li> <li>ADDRESSING:</li> <li>QUANTUM: BYTE, WORD</li> <li>ACCESS TIME: 420 ns</li> <li>PORTS: p</li> </ul>		
KEYBOARD	8 LEVELS		
MODEM	5 LEVELS		
DISPLAY	PROGRAM DEPENDENT		
RAU	MICROPROGRAM + SOFTWARE SOFTWARE		
RAU	INPUT/OUTPUT UNIT		
IS	INTERCONNECTING STATION		
S/S	SUBSYSTEM		
CRT	CATHODE RAY TUBE		
KB	DISPLAY		
MDM	KEYBOARD		
RAU	ORBITER MULTIPLEXER/ DEMULTIPLEXER		
RAU	REMOTE ACQUISITION UNIT		

the actions which are required for the correct performance of the subsystem. In this way, for example, the Spacelab instrument pointing system, which provides arc second pointing accuracy and stability, is operated. Those functions which require control prior to activation of the subsystem computer, i.e. the environment control liquid and air cooling loops, are initiated via the Orbiter. For Spacelab remote control and checkout purposes, the Orbiter computers can transmit on/off commands to the Spacelab subsystem equipment and receive the required monitoring signals.

Experiments interface with the CDMS for control, monitoring, data acquisition, and processing primarily through experiment RAU's which can be located in all module racks and on the pallets. They offer bidirectional links for acquisition of digital and analog data and for commands. The data exchange between RAU's and the I/O unit is performed via a bit serial bus with a 1 MBPS clock rate. A schematic diagram of the RAU is presented in Fig. 5. A modular design has been selected. The smallest unit available is the mini-RAU, consisting of the power supply module and the core module. Extensions with the so-called interface module and the core module and user time clock module can be incorporated to adapt the channel numbers to the experiments requirements. In this way the RAU can provide up to 64 on/off commands, and 4 PCM commands. Under software control, a maximum block size of thirty-two 16-bit words can thus be transferred.

to accept either discrete (i.e. one bit of parallel digital data) or analog input signals. For discrete inputs, groups of 16 channels are addressable, and during one scan cycle up to eight 16-bit groups can be transmitted under software control. In the case of the analog data acquisition, either 2 or 16 adjacent input channels can be addressed. The RAU digitizes the analog data with 8 bit resolution and thus converts the data from two channels into 16 bit words for transmission to the I/O unit. Four channels are available for transfer of serial digital data per RAU. A maximum of thirty-two 16-bit words can be accepted per read-out cycle per channel.

Up to 22 experiment RAU's can be accommodated by the CDMS. The data acquisition and commanding is controlled by software. For subsystem control, the Spacelab software system scans the subsystem RAU's periodically with periods of 10, 100 or 1000 ms. According to mission needs, the experimenters can incorporate software to generate additional measurement cycles using the operating system task scheduler. This scheduler accepts priority levels and queues experiment software requests for data and command transmission. In addition it will be possible in exceptional cases that an experiment which requires very fast response of the CDMS to particular events is directly connected with one of the hardware interrupts of this experiment computer.

The experiment computer system previously described will be utilized for several main tasks. First, it will manage the overall experiment operations, in particular for those aspects which involve a correlation between the Spacelab status (e.g. attitude, available power, etc.) and the experiments measurements. This also includes the confirmation and control of the proper experiment functioning, by either automatic checks incorporated in the experiment software or the usage of the data display units and keyboards by the payload specialists. Secondly, the computer can and will be used for processing of experiment data as required for either experiment control or data compression. Thirdly, the experiment computer system will output the data from the multitude of simultaneously operating experiments as acquired through the RAU's and processed as required into an integrated single data stream for transfer to the Orbiter's communication system.

The Spacelab computer system finds its limitations in the data transfer rates of the data bus and, possibly, the processing capability of the computer. It is anticipated that continuous analysis and reduction of data can be accomplished for data rates up to roughly 50 KBPS, while merging of experiment data up to several hundred KBPS will be achieved.

## V. The Multiplexer System

The Spacelab high rate digital multiplexer (HRDM) system has been added as part of the CDMS to collect and merge the data of those experiments whose data rates exceed the capabilities of the computer

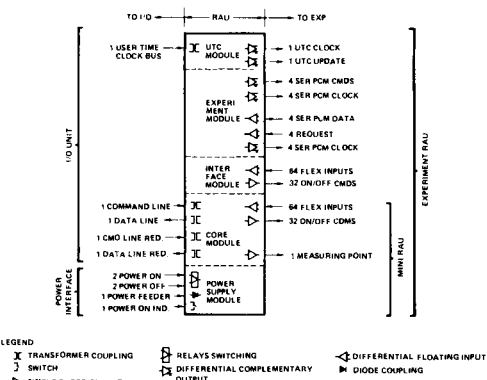


Fig. 5 Remote acquisition unit block diagram.

By using the user time clock module, the experiment will be provided with a 1024 kHz clock and a 4 Hz update output, which are derived from the Orbiter master time unit and are therefore synchronized with CMT. It is expected that this system will achieve an absolute time accuracy of 1 ms and a relative accuracy of 10  $\mu$ s.

For data transmission to the RAU, the experimenter can select "flexible inputs" or transfer PCM serial data. The flexible inputs can be programmed

system, i.e. above say several hundred KBPS. It includes the HRDM and a high rate digital data recorder (HRDR) as indicated in Fig. 4.

The HRDM, which is presently being defined in detail, is expected to provide up to 16 experiment input channels with allocated bit rates which are consistent with the Orbiter wide band operating modes. In addition several dedicated input channels are foreseen for data acquisition from the subsystem and experiment I/O units, from the HRDR and to provide direct access to the ku-band signal processor. The output rate of the HRDM is independently variable and can be selected to match the down-link channel in use. The HRDM output can be switched either directly to the Orbiter ku-band signal processor or to the HRDR.

The HRDR provides an intermediate storage for the experiment data as merged by the HRDM. The HRDR is used during interruption of the communications ground link or during periods that the ku-band mode does not match the HRDM output rates. During playback, the recorder data are interleaved into the real time data stream through a recorder dedicated input channel of the HRDM according to the schematics shown in Fig. 4. Table 2 summarizes the characteristics of the HRDR, the most salient ones being the tape exchange capability and the possibility to select the input and output data rates according to the mission needs between 1 and 32 MBPS.

Table 2 High rate digital recorder characteristics

RECORD TECHNIQUE	LONGITUDINAL, 28 TRACKS
DATA TRACKS	26
DATA STORAGE	$3.8 \times 10^{10}$ BITS
BIT DENSITY/TRACK	12.5 Kb/inch
DATA RATE INPUT	1.2, 4, 8, 16, 32 Mb/s
DATA RATE OUTPUT	2.4, 8, 16, 32 Mb/s
TOTAL RECORD TIME	600, 300, 150, 75, 37.5, 18.75 MIN
DATA TYPE	SERIAL IN, SERIAL OUT, NRZ-L + CLOCK
BIT ERROR RATE	$1 \times 10^{-6}$
START TIME	5 s
STOP TIME	2.5 s
TAPE HANDLING	TAPE CARTRIDGE, AUTOMATIC THREADING
TAPE LOADING TIME	0.4 MIN.
REWIND TIME	4.8 MIN.
TAPE WIDTH/REEL DIAMETER	1" / 14"
TAPE REEL WITH TAPE AND CARTRIDGE	4.8 kg

The operation of the HRDM/ HRDR system is controlled by the CDMS computer according to the requirements of the mission phase, regarding the allocation of input channels, input rates, and output rate. The control of experiments which have to transfer their data to the HRDM is similar to those whose data are acquired through RAU's in that these high rate experiments will also be controlled through RAU's. The proper functioning of the high rate experiments can be checked by taking data samples through the RAU's and data bus to the computer for further processing.

The multiplexer system includes a ground segment which splits the composite data stream into the original experiment data streams. Splitting of the HRDR playback output channel will require a subsequent second stage demultiplexing. In this way the multiplexer system will be completely transparent, i.e. the experiment data will be available on ground as it was presented to the multiplexer on board Spacelab.

#### VI. The Usage of Experiment Minicomputers

The vast majority, if not all, of the experiments on Spacelab will include electronic data handling equipment, which will be required to:

(1) Internally control the experiment modes

(2) Accept and process external inputs required for the experiment operation

(3) Acquire and process the experiment sensor signals into the form desired by the experimenters

(4) Transmit the experiment data for further processing or routing to the ground.

The complexity of these functions varies largely from experiment to experiment and it will depend on this complexity whether an experiment would normally include: a) only specially designed electronics, b) specially designed electronics plus one or more microcomputers, or c) would incorporate in addition a mini-computer. With the availability of the Spacelab CDMS system with its flexible, versatile I/O structure and powerful computing capabilities, it is expected that a significant reduction in experiment specific data handling hardware can be achieved.

However, for some exceptionally complex experiments it will still be most efficient to include in the experiment a minicomputer and to accept the associated penalties on experiment weight, volume, and power usage. Nevertheless, in these cases an interface between the CDMS and the experiment computer is required to 1) enable merging of the experiment data into the overall Spacelab data stream, 2) provide the experiments with the required information on Spacelab and Orbiter status, and 3) permit the utilization of the CDMS peripherals (digital display units, keyboards, and mass memory unit) for experiment functional checks, payload specialists interaction when required, and software storage.

The RAU interface will offer sufficient capabilities for the communication between the CDMS and the experiment minicomputer; the data transfer in this case is controlled by software at both sides of the interface, rather than only at the CDMS side.

## VII. Software

The software system completes the CDMS and provides to the users the versatility which is inherently available in the hardware design, i.e. to adapt by simple means the functioning of the hardware to the special needs of a particular set of experiments joined together into one Spacelab payload.

The Spacelab computer software comprises all software needed for subsystem testing, integration, checkout, onboard data handling for subsystems, onboard data handling support for experiments, and checkout of the CDMS part of the experiment interfaces. It is designed in a modular way to allow for good testability and maximum use of common functional units. Thus commonality can be achieved between the subsystem and experiment computers concerning the operating system and general facilities such as operation interface, fault isolation, subroutine library, etc. The experiment specific application software packages running in the experiment computer under the Experiment Computer Operating System (ECOS) must be provided by the experimenter and/or the payload integrator.

The ECOS allows for synchronous as well as asynchronous tasks to be performed. The executive performs initialization, scheduling, and termination of tasks. It assures memory allocation and overlays as needed, and it controls the allocation of peripherals, telemetry channels, and data bus. In addition the executive initializes the operating system and provides recovery after soft system failures. It also periodically performs a self check providing appropriate messages in case of malfunctions. The I/O functions provide all services necessary to operate the RAU's. They format and transmit data as needed for the displays and for all communication between the Orbiter and the CDMS. Functions which are common to many application programmes, e.g. a library of mathematical functions, are included in the general facilities.

The experiment application software may be written in higher order languages HAL/S (which is a real-time programming language allowing the scheduling and synchronization of programmes) or GOAL (which permits a convenient specification of checkout procedures). It may also be written in the MITRA 125 S assembler language. Inclusion or support to FORTRAN is under consideration.

## VIII. Experiment Integration

Simple and easy integration of experiments is a major objective of Spacelab and has been a major influence in the hardware and software design.

The principle hardware interface between experiments and the CDMS, i.e. the RAU, is well defined and sufficiently versatile to accommodate a wide range of experiment requirements. Consequently the production of the experiment part of the interface as well as the

integration and test are expected to be straightforward and cost-effective. An ESA study has demonstrated that the CDMS hardware has sufficient inherent capabilities to accommodate electronic standard interfaces other than those provided by the RAU. For example, it has been shown to be feasible to interface equipment which is based on the existing CAMAC standards either with the RAU's (if a data rate below 1 MBPS is acceptable) or directly with the experiment computer minibus. The design of the CAMAC controller interface, which is required in both cases, appears to be quite feasible and could be considered by user groups who apply CAMAC at present for their ground or balloon experiments.

The details of the experiment to multiplexer hardware interface are still under discussion, but again the simplicity of experiment integration will be a decisive factor.

Since experiment application software can be developed in high order languages with well defined mnemonics, syntax rules, I/O routines and other general facilities, experiment software production will be straightforward. The interfaces between the experiment software and the ECOS are embedded in the high order language specifications and the hardware resources (e.g. core size, CPU time, and peripheral usage, etc.) assigned to each experiment. The test and integration of the experiment software will be supported by the Spacelab developed operating system and other software aids.

## IX. Summary and Conclusions

The tasks for Spacelab data handling outlined in Section II appear to be effectively realized by the overall system presented. The Orbiter and ground system provide an adequate and efficient communication link as required. The CDMS computer system is capable of providing an overall effective data management, data acquisition, and data processing capability for all experiment data rates which do not exceed approximately 100 KBPS; still at higher data rates, the multiplexer system will assure the appropriate data acquisition. If for some experiments the requirements for onboard data processing exceed the capability of the CDMS, an adequate interface with minicomputers incorporated in the experiments can be provided. Finally, standard but flexible experiment to CDMS interfaces, regarding hardware and software, contribute towards an easy and simple integration. It is believed that the approach taken strikes the right balance between central and experiment specific hardware, where for the vast majority of experiments the usage of central Spacelab CDMS provisions will result in reduced complexity, weight, and cost, while permitting an optimal utilization of on-orbit observation time.

References

1. Spacelab Payload Accommodation Handbook, ESA ref. no. SLP/2104, May 1976.
2. Space Shuttle System Payload Accommodation, NASA ref. no. JSC-07700, Vol. XIV, November 1975.